Filogenia y biogeografía del Clado *Antillattus* (Araneae: Salticidae: Euophryini)

Franklyn Cala Riquelme

Universidad Nacional de Colombia
Facultad de Ciencias
Departamento de biología Bogotá
Colombia, 2020

Filogenia y biogeografía del Clado *Antillattus* (Araneae: Salticidae: Euophryini)

Franklyn Cala Riquelme

Tesis o trabajo de investigación presentado como requisito para optar al título de:

Doctor en ciencias-biología

Director

Dr. EDUARDO FLOREZ-DAZA
Instituto de Ciencias Naturales
Universidad Nacional de Colombia
Sede Bogotá
Colombia

Codirector

PhD. INGI AGNARSSON
Department of Biology
120 A, Marsh Life Science Building
Burlinton
VT 05405-0086 USA

Universidad Nacional de Colombia
Facultad de Ciencias
Departamento de biología Bogotá
Colombia, 2020

"EMPLEARSE EN LO ESTÉRIL CUANDO SE PUEDE HACER LO ÚTIL, OCUPARSE EN LO FÁCIL CUANDO SE TIENE BRÍOS PARA INTENTAR LO DIFÍCIL, ES DESPOJAR DE DIGNIDAD EL TALENTO"

José Martí

A MI FAMILIA

A MI HIJO AMAURY

A MI ESPOSA

A LA SISTEMÁTICA

Agradecimientos

Un sincero agradecimiento a mi director de tesis Eduardo Florez Daza por sus oportunos y sabios consejos, así como por permitirme el acceso al material depositado en el Instituto de Ciencias Naturales. Especial agradecimiento además a Ingi Agnarsson y Greta Binford por permitirme ser parte del proyecto de biogeografía de islas, el apoyo financiero, y la realización de investigaciones en conjunto. A Abel Perez, Alexander Sánchez, Giraldo Alayón, David Ortíz, Robert Anderson, Andrew Smith, Gavin Guanyang Zhang, Martin Fikáček, Yoandri Suarez Megna, Jairo Moreno, Albert Deler-Hernández y al Grupo CarBio por su apoyo en salidas de campos, consejos y donación de material del Caribe insular.

Un agradecimiento especial a Wayne Maddison y Gustavo Ruiz por invitarme en el 2014 al curso de saltícidos del neotropico. A Abel Bustamante, Alexandre Salgado, Jairo Moreno, Alexander Sabogal, Sarah Crews, David Ortiz, Alexander Sánchez, Giraldo Alayón, Wayne Maddison, Ivan L. F. Magalhaes, y William Galvis por propiciar un espacio de debate de varios enfoques en el campo de la aracnología. A Abel Bustamante y Alexandre Salgado por su ayuda en la toma de imagens SEM y fotografías de material tipo. A Nadine Dupérré por la por la donación de literatura y las primeras enseñanzas en ilustración.

A profesor Carlos Suriel y al colectivo de trabajo del Museo de Santo Domingo por su ayuda desintersada y préstamo de material. A todos los profesores del Programa de Doctorado por sus interesantes conferencias.

A todas las personas del Centro Oriental de Ecosistemas y Biodiversidad (BIOECO) que de una forma u otra han contribuido con que este trabajo por fin esté concluyendo. Especial agradecimiento a cada una de las personas del Museo Nacional de Historia Natural de Santo Domingo (MNHNSD) y en especial a Carlos Suriel por su valiosa ayuda durante los trabajos desarrollados en esa institución. Tambien a los colegas del Instituto de Ciencias Naturales, por su colaboración en estos años.

Finalmente, agradezco de manera especial a las fuentes financiadoras que han permitido desarrollar mi trabajo (IdeaWILD, PeoplesTrust, WWF, Rufford, CITMA). A todos y todas muchas gracias.

Resumen

La tribu Euophryini resulta en la actualidad, una de las más diversas dentro de la familia salticidae. Dentro de este grupo, los representantes neotropicales conforman 11 clados, de los cuales, el clado Antillattus (*Antillattus* 13 spp, *Truncattus* 5 spp, *Petemathis* 5 spp, posiblemente *Allodecta* 1 spp, *Caribatus* 1 spp) resulta exclusivo del Caribe insular. Para aclarar la filogenia y biogeografía del clado Antillattus, amplificamos y secuenciamos tres genes (nuclear: 28S rDNA; mitocondrial: 16S, COI) correspondientes a especies pertenecientes al grupo de estudio y a grupos hermanos (68 terminales en total) dentro de gran parte del Caribe biogeográfico. Además, se utilizó un total de 125 caracteres morfológicos, que en combinación con la evidencia molecular, ayudó a aclarar las relaciones entre los géneros y especies. Se estudió en mayor detalle los caracteres morfológicos de los géneros y especies del clado Antillattus así como de sus grupos relacionados con el objetivo de profundizar en la comprensión de filogenética desde una panorámica morfológica. Adicionalmente, para comprender el origen y el momento de la colonización del grupo, se pone a prueba la hipótesis de GAARlandia y la hipotesis no-GAARlandia como posibles vías de colonización y diversificación del cladoAntillattus en las Antillas Mayores. La hipotesis combinada (ADN+morfología) de trabajo, apoya la monofilia del clado Antillattus. Los resultados indican que el género Antillattus sensus Zhang y Maddison (2015), no es monofilético, y para el presente estudio se divide en los géneros *Pensacolatus*, *Antillattus* y *Bryanattus* **gen. nov.**. La filogenia combinada de datos morfológicos y moleculares, también apoyó la transferencia de especies a los géneros *Truncattus*, *Bryanattus*, *Cobanus*, *Compsodecta* y la descripción del género *Paracobanus* **gen. nov.**. La revisión detallada proporciona nuevos limites de géneros y especies, 19 **comb. nov.**, 2 **gen. nov.**, 11 **sp. nov.**. Finalmente, los resultados también sugieren que la radiación del grupo tuvo lugar en el último periodo de GAARlandia y que la diversificación dentro del Caribe insular, es el resultado de vicarianza y eventos fundadores. Adicionalmente, se encontró evidencia que sugiere que La Española jugó un papel como punto de distribución hacia Cuba y Puerto Rico.

Palabras claves: filogénia; evidencia total; Salticidae; Caribe insular; evento-fundador; sistemática.

Abstrac

The Euophryini tribe is currently one of the most diverse groups of salticidae. Within this group, the neotropic is represented by 11 clades, included the Antillattus clade (*Antillattus* 13 spp, *Truncattus* 5 spp, *Petemathis* 5 spp, possibly *Allodecta* 1 spp and *Caribatus* 1 spp). To clarify the phylogeny and biogeography of the Antillattus clade, we amplified and sequenced three genes (nuclear: 28S rDNA; mitochondrial: 16S, COI) corresponding to species belonging to the study group and outgroups (68 terminals). In addition, a total of 125 morphological characters were used, which in combination with the molecular evidence, helped to clarify the relationships between genera and species. Additionally, the GAARlandia hypothesis and the non-GAARlandia hypothesis are tested as possible routes of colonization and diversification of the Antillattus clade. The combined working hypothesis (DNA + morphology) supports the monophyly of the Antillattus clade. The results indicate that the genus *Antillattus* sensus Zhang and Maddison (2015), is not monophyletic, and it is divided into the genus *Pensacolatus*, *Antillattus* and *Bryanattus* **gen. nov.**. The results also supported the transferences of species to the genera *Truncattus*, *Bryanattus* **gen. nov.**, *Cobanus*, *Compsodecta*, and the description of the genus *Paracobanus* **gen. nov.**. The detailed review provides new limits of genera and species, 19 **comb. nov.**, 2 **gen. nov.**, 11 **sp. nov.**. Finally, the results also suggest that the radiation of the group occurred in the last period of GAARlandia and that diversification within the Greate Antilles is the result of vicariance and founder-event. Additionally, evidence suggest that Hispaniola played a role as a point of dispersion to other Antillean islands.

Key words: phylogeny; total evidence; Salticidae; insular caribbean; founder-event; systematic.

Contenido

Pág.

1- INTRODUCCIÓN……..…….....23
1.0 Características e importancia de las arañas ……..…….....….24
1.1 Origen y evolución de las arañas…….……..…….....….25
1.2 Estructura del orden araneae…….…….....….....27
1.3 La familia Salticidae……..…….……28
1.3.1 Clasificación…….……..…….....28
1.4 Subfamilia Salticinae Blackwall, 1841…….…..…….……...30
1.4.1 Caracteres de la subfamilia Salticinae …….....31
1.5 Clado Salticoida Maddison y Hedin (2003)……..…..31
1.6 Clado Saltafresia Bodner y Maddison (2012)……..……...31
1.6.1 Subclado Simonida Maddison (2015)……..31
1.6.2 La tribu Euophryini …….....….32
1.6.2.0 Clasificación …….……...32
1.6.2.1 Caracteres morfológicos …….…….33
1.7. La fauna de arañas del caribe insular …….…...33
1.7.1. Euofrinidos del caribe insular …….……...35
1.7.2 Clado Antillattus …….…....35
1.7.2.0 Clasificación ……...….35
1.8 Problema de investigación …….…….36
1.9 Hipótesis ……...….37
1.10. Objetivo general ……..…37
1.10.0 Objetivos específicos ……....37
1.11 Bibliografía ……...…...38
2- PHYLOGENY, MORPHOLOGY AND EVOLUTION OF JUMPING SPIDER CLADE ANTILLATTUS AND THEIR SISTER GROUPS (SALTICOIDA: EUOPHRYINI)-……44
2.0. Introduction …….....45
2.1. Material and methods ……..……..…..47
2.1.0. Taxon sample……...…..……..47
2.1.0.1. Outgroups ……..48
2.1.0.2. Ingroups ……..…..49
2.1.1. Specimen preparation ……..……..…..49

2.1.2. Character sampling ……..……..……..51
2.1.3. Synapomorphies and character trait evolution ……..51
2.1.4. Morphological phylogenetic signal …….…….....52
2.1.5. Molecular analyses ……..…….....52
2.1.5.0. Sequencing …….……..…...……..53
2.1.5.1. Alignment and substitution model ……..……..53
2.1.5.2. Phylogenetic inference ……....54
2.1.5.3. Parsimony …….……..…..55
2.1.5.4. Maximum likelihood ……..…...55
2.1.5.5. Bayesian inference ……..…...56
2.1.6. Topology tests …….……....56
2.1.7. Character descriptions and definitions …….……..…..57
2.1.7.0 Cephalothorax, legs and chelicerae …….…..57
2.1.7.1. Abdomen ……..……....63
2.1.7.2. Male palp ……..……..…..64
2.1.7.3. Female genitalia ……....72
2.2. Result ……..……..…..95
2.2.0. Morphological reconstruction and phylogenetic signal ……95
2.2.1. COI ……..……...…..96
2.2.2. 16S ……..……....96
2.2.3. 28S …….…..……..…..96
2.2.4. All genes combined (COI, 16S, 28S) and topology test ……97
2.2.5. DNA and morphology total evidence …….……..97
2.3.0. Phylogenetic inference ……...112
2.3.1. Chelicerae teeth evolution ……..113
2.3.2. Palp evolution ……..……..115
2.3.3. Receptacle in copulatory duct evolution ……..……...117
2.3.4 Taxonomy ……...…...…..126
2.3.4.0. *Allodecta* is a *Compsodecta* ……..…...126
2.3.4.1. *Caribattus* is not a member of the Antillattus clade ……..……...126
2.3.4.2. *Cobanus* is a different genus of *Sidusa* ……127
2.3.4.3 Antillattus Clade ……..……....134
2.4. References ……158
3.- NEW GENERA AND SPECIES REVEALED BY PHYLOGENETIC ANALYSES OF

ANTILLATTUS (SALTICIDAE: EUOPHRYINI)-……...…...171
3.0. Introduction ……..….173
3.1. Material and methods ……...……174
3.1.0. Taxon sampling……..…….174
3.1.1. Morphology……..……...….175
3.1.1.0 Morphological characters……..……..…..175
3.1.2 Molecular methods…….…….....176
3.1.3 Phylogenetic analyses…….……...….....177
3.1.4 Species delimitation…..…….……...…….....179
3.1.5 Topology tests…….……...…….....180
3.2 Results …….……...….....181
3.2.0 Specimen sampling and phylogenetic inference…….……...…..181
3.2.1 Combined molecular and morphology results……...181
3.2.2 *Antillattus*, *Pensacolatus*, and *Bryanattus* species delimitation……....182
3.3 Discussion …...…….……...……189
3.3.0 Phylogenetic inference ….……..…….....189
3.3.1 Delimitation……...…...193
3.3.2 Taxonomy…….....…...193
3.4 Conclusion…….……..…….…...242
3.5 References…….…….....243
4. - ISLAND-TO-ISLAND VICAREANCE, FOUNDER-EVENT AND WITHIN-AREA SPECIATION, THE BIOGEOGRAPHY OF THE ANTILLATTUS CLADE (SALTICIDAE: EUOPHRYINI)-…….……...……253
4.0 Introduction ……..……..…….255
4.1 Material and methods …….……..…….259
4.1.0 Taxon sample..…….……...…….259
4.1.1 DNA extraction, PCR amplification and sequencing…….……259
4.1.2 Sequence alignment……...……...260
4.1.3 Phylogenetic inference ……..……...……...260
4.1.4 Time calibration……..……...260
4.1.5 Divergence estimation……...……..….261
4.1.6 Biogeographical reconstruction……262
4.2. Results…….....….263

4.2.0. Phylogeny and divergence time……..……...…..263
4.2.1. Biogeographic analysis……...……264
4.2.2. Estimation of biogeographical events……...……..……..264
4.2.3. GAARlanida hypothesis……..……..……..…265
4.2.4. Founder-event hypothesis……...…….265
4.3. Discussion……..……....265
4.3.0. GAARlandia……...……265
4.3.1. Inter-island biogeographical history…….……..…266
4.3.3 From Hispaniola to Cuba and Puerto Rico…….……..267
4.4 Conclusion……...……268
4.5 References……...……276
5.0 Concuiciones generales……..….287
Supplementary……..…..……..289

Lista de figuras

Pág.

1- INTRODUCCIÓN

Figure. 1.0. A-C. Esquema general de la morfología externa de una araña (Salticidae). A) Vista dorsal B) Vista ventral C) Vista lateral. Abreviaturas: ALE = ojos anterolaterales; AME = ojos anteromediales; Ch = quelicero; Cox = coxa; Ed = enditos; Ep = epiginio; Lb = Labium; PLE = ojos posteriores laterales; PME = ojos medios posteriores; Pp = pedipalpo; Spi = hilandera; Str = Esternón……...……....….25

Figure. 1.1. Resumen de la filogenia molecular de Salticidae de Maddison 2015..……..….30

2- PHYLOGENY, MORPHOLOGY AND EVOLUTION OF JUMPING SPIDER CLADE ANTILLATTUS AND THEIR SISTER GROUPS (SALTICOIDA: EUOPHRYINI)-

Figure. 2.0. Male carapace, frontal view. A, *Compsodecta festiva*. B, *Agobardus*. C, *Bryanattus keyserlingi* **comb. nov.**. D, *Cobanus mandibularis* **comb. nov.**. E, *Antillattus cambridgei*. F, *Sidusa*……..…...77

Figure. 2.1. Male habitus, lateral and frontal view. A-B, unknown euophryine. C-D, *Antillattus cambridgei*. E-F, *Truncattus martii* **sp. nov.**. G-H, *Bryanattus keyserlingi* **comb. nov.**..……...……....78

Figure. 2.2. Male carapace, dorsal view. A, *Truncattus flavus*. B, *Pensacola signata*. C, *Corticattus latus*. D, *Agobardus anormalis montanus*. G. *Cobanus mandibularis* **comb. nov.**. E, *Sidusa* sp. F, *Antillattus gracilis*. H, *Petemathis portoricensis*. I. *Mexigonus arizonensis*……..…..79

Figure. 2.3. Male chelicerae, frontal view. A, *Bryanattus keyserlingi* **comb. nov.**. B, *Compsodecta darlingtoni*. C, *Antillattus cubensis*..……..……...80

Figure. 2.4. Scanning electron micrographs of chelicerae. A, Female of *Anasaitis*, promarginal view. B, Male of unknown euophrine, retromarginal view. C, Female of *Sidusa*, retromarginal view. D-E, Male of *Antillattus cambridgei*, promarginal view. F and I, *Bryanattus keyserlingi* **comb. nov.**, promarginal view. G-H, Male of *Cobanus manidibularis* **comb. nov.**, retromarginal view.……...……..81

Figure. 2.5. Tibia and metatarsus leg spination, ventral view. A-B, *Corticattus latus*. C, *Popcornella yunque*. D, *Agobardus anormalis montanus*. E, *Compsodecta maxillaris* **comb. nov.**. F. *Cobanus extensus*……..……...……..82

Figure. 2.6. Scanning electron micrographs of the epigynum (A-E), and male pre-spiracular bump and pre-spiracular hairs (F-I). A, Female of *Anasaitis*, ventral view. B-C,

Female of *Sidusa*. D-E, Female of *Chapoda*. F-G, Male of *Bryanattus keyserlingi* **comb. nov.**. H-I, Male of *Cobanus mandibularis* **comb. nov.**……..…..……..83
Figure. 2.7. Structures of left male palps (A-C) and female genitalia (C-D). A, *Agobardus* sp. male palp, ventral view. B, *Agobardus* sp., male palp, retrolateral view. C, *Agobardus* sp., RTA. D, *Chapoda* sp., female genitalia, dorsal view. E, *Chapoda* sp., secondary spermathechae, dorsal view……...84
Figure. 2.8. Scanning electron micrographs of the male endites. A, *Cobanus mandibularis* **comb. nov.**. B, unknown euophrine. C, *Chapoda*. D, *Sidusa*. E, *Antillattus cambridgei*. F, *Bryanattus keyserlingi* **comb. nov.**.……..……..……...85
Figure. 2.9. Scanning electron micrographs of the male palp. A, *Anasaitis*. B, *Agobardus*. C, *Cobanus mandibularis* **comb. nov.**. D, *Sidusa*. D, *Compsodecta*. E, *Bryanattus keyserlingi* **comb. nov.**. F, *Antillattus cambridgei*.……..……..……..86
Figure. 2.10. Scanning electron micrographs of the male palp. A, *Anasaitis*. B, *Cobanus mandibularis* **comb. nov.**. C, *Compsodecta darlingtoni*. D, *Bryanattus keyserlingi* **comb. nov.**. E, *Truncattus flavus*. F, *Antillattus cambridgei*. G, *Chapoda sanlorenzo*. H, *Sidusa* sp. I, *Popcornella* sp.……..……..……...87
Figure. 2.11. Bulb of the male palp, ventral view. A, *Marma*. B, *Sidusa*. C, *Pensacolatus darlingtoni* **comb.nov.**. D, *Petemathis portoricensis*. E, *Truncattus flavus*. F, *Pensacola signata*. G. *Agobardus*. H, *Cobanus multidentatis* **sp. nov.**. I, *Antillattus cubensis*……..88
Figure. 2.12. Scanning electron micrographs of the male palp. A and D, *Corythalia*. B *Agobardus*. C, *Antillattus cambridgei*. E, *Chapoda*. F, *Compsodecta*……...89
Figure. 2.13. Scanning electron micrographs of the male palp. A, *Popcornella*. B-C, *Cobanus*. D, *Antillattus cambridgei*. E, *Chapoda*. F, *Bryanattus keyserlingi* **comb. nov.**. G, unknown euophrine. H, *Sidusa*. I, *Agobardus*……..…..90
Figure. 2.14. Scanning electron micrographs of the embolus. A-B, *Cobanus*. C, *Popcornella*. D-E, *Corithalia*. F, *Chapoda*. G, unknown euophrine. H, *Antillattus cambridgei*. I, *Anasaitis*……...…..91
Figure. 2.15. Male embolus. A, *Compsodecta*. B, *Pensacola signata*. C, *Bryanattus* **gen. nov**.. D, *Agobardus*. E-F, *Cobanus*.……..…..92
Figure. 2.16. Scanning electron microscopy images of the internal epigynum. A and H, *Popcornella*. B and E, *Sidusa*. C, G and I, *Chapoda*. D-F, *Corythalia*……...93
Figure. 2.17. Female internal genitalia, dorsal view. A, *Agobardus*. B, *Bryanattus*. C, *Truncattus*. D, *Cobanus*. E, *Sidusa*. F, unknown euophrine.……..……..94
Figure. 2.18. Strict consensus (Morphology) of the most parsimonious trees obtained under

equal weights (CI=0.37, RI=0.83).……..……..102
Figure. 2.19. Topology (Morphology) obtained under *k* = 17. Filled and open squares represent the sensitivity analysis under different implied weighting values (*k*=3-25). Numbers are Goodman- Bremer support, Jackknife percentages and symmetric resampling values, respectively.……..…..……..103
Figure 2.20. Summary of ML and MP analyses on the COI tree from the ML analysis.……..……..104
Figure 2.21. Summary of ML and MP analyses for 16S. Tree shown is the best tree from the ML analysis.…….…..105
Figure 2.22. Summary of ML and MP analyses on the 28S tree from the ML analysis.……..……..106
Figure 2.23. Summary of ML, MP and BI analyses of all genes combined (COI, 16S, 28S) using the constraint tree from the ML analysis.…….……107
Figure 2.24. The best tree from Bayesian analysis on the combined morphological and molecular datasets (morphology, 28S, 16S and COI)……...108
Figure 2.25. ML tree from the combined morphological and molecular datasets (morphology, 28S, 16S and COI).…….…..……..109
Figure 2.26. Strict consensus (unconstrained analysis) from MP analysis on the combined morphological and molecular datasets (morphology, 28S, 16S and COI)…..……..110
Figure 2.27. Strict consensus (constrained analysis) from MP and summary of ML and BI analyses on the combined morphology and DNA datasets (morphology, 28S, 16S and COI).…….……111
Figure 2.28. The evolution of female retromarginal tooth fusion (char. 21-22). Char 21, which can be absent (state 0) or present (state 1). Char 22, which can be bicuspid (state 0) or multicuspid (state 1). The character is unambiguous optimized on our preferred tree (MP).……..……..119
Figure 2.29. The evolution of the male retromarginal tooth II (char. 32), which can be absent (state 0) or present (state 1). The character is unambiguous optimized on our preferred tree (MP).……..120
Figure 2.30. The evolution of anterior-lateral cusp of the male endite (char. 71), which can be reduced (state 0) or developed (state 1). The character is unambiguous optimized on our preferred tree (MP).……..121
Figure 2.31. The evolution of the ventral tibial apophysis (char. 80), which can be absent (state 0) or present (state 1). The character is unambiguous optimized on our preferred tree

(MP)……..……..122
Figure 2.32. The evolution of the proximal tegular lobe (char. 86), which can be absent (state 0) or present (state 1). The character is unambiguous optimized on our preferred tree (MP).……123
Figure 2.33. The evolution of the prolateral sperm duct loop (char. 91), which can be absent (state 0) or present (state 1). The character is unambiguous optimized on our preferred tree (MP).……...……...…..124
Figure 2.34. The evolution of the female copulatory duct receptacle (char. 118), which can be reduced (state 0) or developed (state 1). The character is unambiguous optimized on our preferred tree (MP).……..125
Figure 2.35. Endites, ventral view. A, *Compsodecta darlingtonia***.** B, G, *Compsodecta gratiosa*. C, *Compsodecta grisea*. D-E, *Compsodecta festiva*. F, *Compsodecta peckhami*. ……..……....140
Figure 2.36. *Compsodecta maxillaris* **comb. nov.** A and C, Male (holotype MCZ-IZ 22099), habitus, dorsal view. B, Male (holotype MCZ-IZ 22099), habitus, ventral view. D, Male left palp, ventral view..……...…….141
Figure 2.37. *Caribattus inutilis*. A, male (holotype MCZ-IZ 21697), habitus. B, male (holotype MCZ-IZ 21697), habitus, prosoma lateral view. C, femur. D, Male habitus, prosoma frontal view……..……..142
Figure 2.38. Male palp and epigynum of *Sidusa* and *Cobanus*. A, *Cobanus bifurcata* **comb. nov.**, male palp, ventral view. B *Cobanus mandibularis* **comb. nov.**, male palp, ventral view. C-D, *Sidusa,* male palp, ventral view. E, *Sidusa,* female internal epigynum, dorsal view. F, *Cobanus cambridgei* **comb. nov.***,* female epigynum, ventral view.……...……..143
Figure 2.39. Holotype of *Cobanus electus*. A, male (holotype MCZ-IZ 21179) habitus, dorsal view. B, male (holotype MCZ-IZ 21179) habitus, ventral view. C, female habitus, ventral view. D, female (allotype MCZ-IZ 26056) habitus, dorsal view. E, male (holotype MCZ-IZ 21179 palp*,* ventral view. F and H, male (holotype MCZ-IZ 21179 palp, retrolateral view. G, epigynum (allotype MCZ-IZ 26056), ventral view..……...144
Figure 2.40. Holotype of *Cobanus bifurcata* **comb. nov.** A, female (allotype MCZ-IZ 26055) habitus, dorsal view. B, female (allotype MCZ-IZ 26055) habitus, ventral view. C, male (holotype MCZ-IZ 20508) palp, ventral view. D, male (holotype MCZ-IZ 20508) palp, retrolateral view. E, epigynum (allotype MCZ-IZ 26055), ventral view... ……..……..…..145

Figure 2.41. *Cobanus mandibularis* **comb. nov.** from Colombia. A, male, habitus. B-C, male, habitus, prosoma lateral view. D, male abdomen, ventral view.……..146
Figure 2.42. *Cobanus mandibularis* **comb. nov.** A, male (holotype MCZ-IZ 21971), habitus. B-C, male (holotype MCZ-IZ 21971), habitus, prosoma lateral view. C, male palp (holotype MCZ-IZ 21971), prolateral view. D, male palp (holotype MCZ-IZ 21971), retrolateral view. E-F, male (holotype MCZ-IZ 21971) palp, ventral view...……..147
Figure 2.43. *Cobanus multidentatis* **sp. nov.** A, male, habitus, dorsal view. B, female, habitus, dorsal view. C, male chelicerae, retromarginal view. D, male palp, ventral view. E, female, internal genitalia, ventral view.……..……..148
Figure 2.44. *Cobanus multidentatis* **sp. nov.** A, male, habitus, dorsal view. B, female, habitus, dorsal view. C, male chelicerae, retromarginal view. D, male palp, ventral view. E, female, internal genitalia, ventral view...……..149
Figure 2.45. *Paracobanus* [Ecuador]. A, male, habitus, dorsal view. B, female, habitus, dorsal view. C, male palp, ventral view. D, male chelicerae, retromarginal view. E, female, internal genitalia, ventral view. Images by Wayne Maddison, released under a Creative Commons Attribution (CC-BY) 3.0 license...……..150
Figure 2.46. *Paracobanus boteroi* **sp. nov.** A, male, habitus, dorsal view. B, female, habitus, dorsal view. C, male chelicerae, retromarginal view. D, male palp, ventral view. E, female, internal genitalia, ventral view....……..151
Figure 2.47. *Truncattus turquinensis* **comb. nov.** A, male (holotype MCZ-IZ 23381), habitus, dorsal view. B, male (holotype MCZ-IZ 23381), habitus, ventral view. C, female (allotype MCZ-IZ 25848), habitus, dorsal view. D, female (allotype MCZ-IZ 25848), habitus, ventral view. E, male palp, ventral view. F, male (holotype MCZ-IZ 23381) palp, prolateral view. G, male (holotype MCZ-IZ 23381) palp, retrolateral view. H, female (allotype MCZ-IZ 25848), genitalia, ventral view.....……..152
Figure 2.48. *Truncattus martii* **sp. nov.** A, male, habitus, dorsal view. B, female, habitus, dorsal view. C, male chelicerae, retromarginal view. D, male palp, ventral view. E, female, internal genitalia, ventral view.....……..……..153
Figure 2.49. *Truncattus platnicki* **sp. nov.** A, male, habitus, dorsal view. B, female, habitus, dorsal view. C, male chelicerae, retromarginal view. D, male endite, ventral view. E, male palp, ventral view. F, male palp, retrolateral view. G, female, internal genitalia, ventral view.....……..…...154
Figure 2.50. A-B, *Agobardus anormalis montanus*, male and female habitus. C-D, *Agobardus bahoruco* male, male and female habitus. E-F, *Bytocrottus crypticus*, male and

female habitus. Images by Wayne Maddison, released under a Creative Commons Attribution (CC-BY) 3.0 license.....155

Figure 2.51. A-B, *Compsodecta peckhami*, male and female habitus. C-D, *Compsodecta haitiensis* male, male and female habitus. E-F, *Corticattus latus*, male and female habitus. Images by Wayne Maddison, released under a Creative Commons Attribution (CC-BY) 3.0 license.....156

Figure 2.52. A-B, *Pensacola signata*, male and female habitus. C-D, *Petemathis sp.* male, male and female habitus. E-F, *Cobanus sp.*, male and female habitus. Images by Wayne Maddison, released under a Creative Commons Attribution (CC-BY) 3.0 license.....157

3.- NEW GENERA AND SPECIES REVEALED BY PHYLOGENETIC ANALYSES OF ANTILLATTUS (SALTICIDAE: EUOPHRYINI)-

Figure 3.0. Both ML and BI constrained and unconstrained analyses of molecular data (COI, 16S, 28S). ……186

Figure 3.1 Topology obtained under *k* =17. Filled (presence) and open (absence) squares represent the clade under equal weights and different implied weighting schemes. Numbers are Goodman-Bremer support, Jackknife percentages, and symmetric resampling values.……187

Figure 3.2. Summary of MP total evidence analysis of all genes combined (COI, 16S, 28S), morphology, BI total evidence, and ML total evidence.……...188

Figure 3.3. Concatenated COI and morphological species delimitation of *Antillattus*, *Pensacolatus*, and *Bryanattus*. The tree fragment corresponds to the BI tree. 1-2: Generalized Mixed Yule Coalescent (GMYC) analyses of Yule, simple (1) and multiple (2), for all genes combined. 3: Poisson Tree Process (bPTP) highest supported solution for combined genes. 4: Automatic Barcode Gap Discovery (ABGD) consistently recovered groupings for the COI gene. 5: Hard-Gap barcoding for the COI gene. 6: Morphology-based delimitation.……...189

Figure 3.4. General distribution of the *Bryanattus*, *Pensacolatus*, and *Antillattus* new species.……...213

Figure 3.5. *Antillattus gracilis*, *Antillattus placidus*. A, *A. gracilis*, male holotype (MCZ-IZ 21477), habitus, dorsal view. B, *A. placidus*, male holotype (MCZ-IZ 22690), habitus, dorsal view. C, *A. gracilis* (MCZ-IZ 21477), male chelicerae, retromarginal view. D, *A. gracilis*, female chelicerae, retromarginal view. E, *A. placidus* (MCZ-IZ 22690), male chelicerae, retromarginal view. F, *A. gracilis*, male left palp, clove oil digested bulb, ventral view. G, *A. placidus* (MCZ-IZ 22690), male left palp, ventral view. *A. gracilis*. H-I, female

of *A. gracilis*, genitalia, (H) ventral view, (I) clove oil digested internal genitalia, dorsal view.……...…....214

Figure 3.6. Scanning electron microscopy images. *Antillattus cambridgei*. A-B, male chelicerae, promarginal view. C, male endite, ventral view. F-H, male palp, (F), cymbium, ventral view, (G) bulb, ventral view, (H) embolic tip, ventral view. *Antillattus cubensis*. D-E, male palp, (D) ventral view, (E) retrolateral view. I, female genitalia, ventral view.…..…..215

Figure 3.7. Female internal genitalia. A-B, *Antillattus cambridgei* (A) dorsal view, (B) ventral view. C, *Antillattus cubensis*, ventral view.……....216

Figure 3.8. *Antillattus cambridgei*. A, male, habitus, dorsal view. B, female, habitus, ventral view C, male left palp, clove oil digested bulb, ventral view. D, male, chelicerae, retromarginal view. E, female, clove oil digested internal genitalia, ventral view. F, female, clove oil digested internal genitalia, dorsal view.…….……....217

Figure 3.9. *Antillattus cubensis*. A, male, habitus, dorsal view. B, female, habitus, ventral view C, Male left palp, clove oil digested bulb, ventral view. D, male, endite, ventral view. E, Female, clove oil digested internal genitalia, ventral view. F, female, clove oil digested internal genitalia, dorsal view.……..…218

Figure 3.10. *Antillattus ocultus* **sp. nov.** A, male, habitus, dorsal view. B, male chelicerae, retromarginal view. C, male endite, ventral view. D, male left palp, clove oil digested bulb, ventral view. D, female, clove oil digested internal genitalia, ventral view.……....219

Figure 3.11. *Pensacolatus maxillosus* **comb. nov.** A, male (holotype MCZ-IZ 22010), habitus, dorsal view. B, male (holotype MCZ-IZ 22010), habitus, ventral view. C, female (allotype MCZ-IZ 25833), habitus, dorsal view. D, female (allotype MCZ-IZ 25833), habitus, ventral view. E-F, male, habitus, ventral view. G, male left palp, ventral view. H, female genitalia, ventral view.……...……...220

Figure 3.12. *Pensacolatus maxillosus* **comb. nov.** A, male chelicera, retromarginal view. B, female chelicerae, retromarginal view. C, male palp, ventral view. D, female genitalia, ventral view.……...……..221

Figure 3.13. Female internal genitalia. A, *Pensacolatus naranjoi* **sp. nov.**, dorsal view. B, *Pensacola montanus* **comb. nov.**, ventral view. C, *Pensacolatus darlingtonia* **comb. nov.**, ventral view.……..…….…….....222

Figure 3.14. *Pensacolatus darlingtoni* **comb. nov.** A, male, habitus, frontal view. B, male palpal tibia, retrolateral view. C, male palp, ventral view. D, female internal genitalia, ventral view.……....223

Figure 3.15. *Pensacolatus montanus* **comb. nov.** A and F, male (holotype MCZ-IZ 22169), habitus, dorsal view. B, male (holotype MCZ-IZ 22169), habitus, ventral view. C, female (allotype MCZ-IZ 25834), habitus, dorsal view. D, female (allotype MCZ-IZ 25834), habitus, ventral view. E, male, habitus, ventral view. G, female genitalia, ventral view. H, locality data.……224
Figure 3.16. *Pensacolatus montanus* **comb. nov.** A and F, male (holotype MCZ-IZ 22169), habitus, dorsal view. B, male (holotype MCZ-IZ 22169), habitus, ventral view. C, female (allotype MCZ-IZ 25834), habitus, dorsal view. D, female (allotype MCZ-IZ 25834), habitus, ventral view. E, male, habitus, ventral view. G, female genitalia, ventral view. H, locality data.……225
Figure 3.17. *Pensacolatus scutiformis* **comb. nov.** A, female (allotype MCZ-IZ 25849), habitus, dorsal view. B, male (holotype MCZ-IZ 21177), habitus, dorsal view. C, male palp, ventral view. D, female genitalia, ventral view……226
Figure 3.18. *Pensacolatus scutiformis* **comb. nov.** A, male, chelicerae, retromarginal view. B, male palp, ventral view. C, male palp, retrolateral view. D, male palp, prolateral view.……227
Figure 3.19. *Pensacolatus naranjoi* **sp. nov.** A, male, habitus, dorsal view. B, female, habitus, dorsal view. C, male, habitus, frontal view. D, male. left palp, clove oil digested bulb ventral view. E, male palp, retrolateral view. F, Female, clove oil digested internal genitalia, ventral view..……228
Figure 3.20. *Pensacolatus surieli* **sp. nov.** A, male, habitus, dorsal view. B, female, habitus, dorsal view. C, male chelicerae, retromarginal view. D, female chelicerae, retromarginal view. E, male left palp, clove oil digested bulb, ventral view. G, female, clove oil digested internal genitalia, ventral view. F, female genitalia, ventral view..…229
Figure 3.21. Scanning electron microscopy images. *Bryanattus keyserlingi* **comb. nov.**. A-B, male chelicerae, promarginal view. C, male endite, ventral view. D-F, male prespiracular bump. G, male palpal cymbium, ventral view. (H) male palpal bulb, ventral view. I, male embolic disc..……230
Figure 3.22. Scanning electron microscopy images. *Bryanattus orientalis* **sp. nov.** A-B, male, habitus (A) dorsal view, (B) lateral view. C, male endite, ventral view. D, male leg I. F, female chelicerae, retromarginal view. *Bryanattus keyserlingi* **comb. nov.**. E, male leg I…….....231

Figure 3.23. Scanning electron microscopy images. *Bryanattus orientalis* **sp. nov.** A-B, male chelicerae (A) promarginal view, (B) retromarginal view. C, male palp, ventral view. D, female genitalia, ventral view, arrow indicate the slit like a "pocket"……..…..232
Figure 3.24. Female internal genitalia. A-B, *Bryanattus thanos* **sp. nov.**, (A) ventral view, (B) dorsal view. C-D, *Bryanattus sanchezi* **sp. nov.**, (C) ventral view, (D) dorsal view. E-F, *Bryanattus orientalis* **sp. nov.**, (E) ventral view, (F) dorsal view.…….…….233
Figure 3.25. *Bryanattus mandibulatus* **comb. nov.** A, male (holotype MCZ-IZ 21974), habitus, dorsal view. B, male (holotype MCZ-IZ 21974), habitus, ventral view. C, female (allotype MCZ-IZ 21974), habitus, dorsal view. D-E, female (allotype MCZ-IZ 21974), habitus, ventral view. F, male left palp, ventral view. G, male left palp, retrolateral view…….234
Figure 3.26. *Bryanattus mandibulatus* **comb. nov.** A, male chelicerae, retromarginal view. B, male left palp, clove oil digested bulb, ventral view. C, female, genitalia, clove oil digested internal genitalia, dorsal view. D, female, genitalia, ventral view. E, female of *Bryanattus keyserlingi* **comb. nov.**, ventral view.……..……..…235
Figure 3.27. *Bryanattus keyserlingi* **comb. nov.** A-B, male (holotype MCZ-IZ 21748), habitus, dorsal view. B-C, female from Pico Turquino, dorsal view. E-H, male from Pico Turquino, dorsal view……..……..…236
Figure 3.28. *Bryanattus orientalis* **sp. nov.** A, male, habitus, dorsal view. B, female, habitus, dorsal view. C, male, left palp, clove oil digested bulb, ventral view. D, female, clove oil digested internal genitalia, ventral view. E, female, clove oil digested internal genitalia, dorsal view.…….…237
Figure 3.29. *Bryanattus thanos* **sp. nov.** A, male, habitus, dorsal view. B, female, habitus, dorsal view. C, male, chelicerae, retromarginal view. D, left palp, clove oil digested bulb, ventral view. E, female, clove oil digested internal genitalia, dorsal view.……..…238
Figure 3.30. *Bryanattus sanchezi* **sp. nov.** A, male, habitus, dorsal view. B, female, habitus, dorsal view. C-D male chelicerae, (C) frontal view, (D) retromarginal view. E, male, left palp, clove oil digested bulb, ventral view. D, male, endite, ventral view. F, female, clove oil digested internal genitalia, dorsal view.……..…239
Figure 2.31. A-B, *Antillattus cambridgei*, male and female habitus. C-D, *Antillattus gracilis* male, male and female habitus. E-F, *Antillattus placidus*, male and female habitus. Images by Wayne Maddison, released under a Creative Commons Attribution (CC-BY) 3.0 license.…….…….…240

Figure 2.32. A-B, *Pensacolatus applanatus* **comb. nov.**, male and female habitus. C-D, *Pensacolatus darlingtoni* **comb. nov.,** male, male and female habitus. E-F, *Pensacolatus maxilosus* **comb. nov.**, male and female habitus. Images by Wayne Maddison, released under a Creative Commons Attribution (CC-BY) 3.0 license.……241

4. - ISLAND-TO-ISLAND VICAREANCE, FOUNDER-EVENT AND WITHIN-AREA SPECIATION, THE BIOGEOGRAPHY OF THE ANTILLATTUS CLADE (SALTICIDAE: EUOPHRYINI)-

Figure 4.0. Diagrams of different biogeographical events assumed by the different models tested in this study [adapted from Matzke (2015)]. Cladogenetic events include within-area speciation, vicariance and founder events. Anagenetic events include range expansion and range contraction.……..……...…….256

Figure 4.1. Maps (A–D) show simplified continent and island positions in the respective time window used for the time-stratified analysis. A – Hispaniola; B – Cuba; C – Puerto Rico; D – South America; E –North America…….…….…..261

Figure. 4.2. Beast divergence time estimations of all genes (COI, 16S, 28S) using a Bayesian relaxed molecular clock. Scale in in millions of years. Bars show 95% HDP……...…….271

Figure 4.3. Results of the ancestral range estimation using time-stratified DEC model of BioGeoBEARS. Phylogram corresponding to the time-stratified DEC model. Pie charts represent the probabilities of each possible geographic area pre- and post-split. The tree on the right shows the most probable geographic range pre and post-split; are the events from stochastic mapping.……...……...272

Figure 4.4. Results of the ancestral range estimation using time-stratified DEC+j model of BioGeoBEARS. Phylogram corresponding to the time-stratified DEC+j model. Pie charts represent the probabilities of each possible geographic area pre- and post-split. The tree on the right shows the most probable geographic range pre and post-split; are the events from stochastic mapping.……...…..….273

Figure 4.5. Histograms of the counts of different kinds of events found in each of the 50 BSMs. The x-axis gives the number of events, the y-axis gives the number of BSMs in which a specific number of events was observed. The models are a non-time-stratified and time-stratified DEC models.……..……..…..274

Figure 4.6. Histograms of the counts of different kinds of events found in each of the 50 BSMs. The x-axis gives the number of events, the y-axis gives the number of BSMs in

which a specific number of events was observed. The models are a non-time-stratified and time-stratified DEC+j models……..…276

Lista de tablas

Pag.

2- PHYLOGENY, MORPHOLOGY AND EVOLUTION OF JUMPING SPIDER CLADE ANTILLATTUS AND THEIR SISTER GROUPS (SALTICOIDA: EUOPHRYINI)-

Table. 2.0. Known diversity of the antillattus clade and sampled diversity ……....49

Table 2.1. Substitution models selected by jModeltest for each individual gene region and partition.……...……..54

Table 2.2. MP (*k=17* and equal weights) morphological synapomorphies and mapping of morphological character changes on DNA+ morphology MP, ML and BI trees.…….....98

Table 2.3. MP total evidence morphological synapomorphies under ACCTRAN and DELTRAN optimization.……..99

Table 2.4. Summary statistics from the equal weights and implied weighting analyses. k: concavity constant, N: number of most parsimonious trees, L: tree length, CI: consistency index, RI: retention index.…….……...…….....100

Table 2.5. Likelihood heterogeneity test (LHT) results and Bayes factors (BF) are from tests against the unconstrained topology. Positive values indicate greater support for the hypothesis (constrained topology). For BF, values between 0–2 indicate no evidence of a difference, 2–6 indicate substantial evidence for a difference, 6–10 indicates strong evidence for a difference and >10 indicates decisive evidence for a difference in the likelihood of the topologies (Kass and Raftery, 1995). Asterisks indicate a monophyletic grouping that is not rejected.……..……..…..101

Table. **2.6.** Relative fit difference (RFD) of alternative phylogenetic hypotheses found using constrained searches. *C* = sum of fit of characters contradicting most parsimonious tree; *F* = sum of fit of characters favoring most parsimonious tree.……..101

3.- NEW GENERA AND SPECIES REVEALED BY PHYLOGENETIC ANALYSES OF ANTILLATTUS (SALTICIDAE: EUOPHRYINI)-……..……....171

Table 3.0. Substitution models selected by jModelTest for each individual gene region and partition.……...……...….177

Table 3.1 Likelihood heterogeneity test (LHT) and Bayes Factors (BF) from tests against the unconstrained topology. Positive values indicate greater support for the hypothesis (constrained topology). For BF, values between 0–2 indicate no evidence of a difference, 2–6 indicate substantial evidence for a difference, 6–10 indicated strong evidence for a difference and >10 indicated decisive evidence for a difference in the likelihood of the

topologies (Kass and Raftery, 1995). Asterisks indicate a monophyletic grouping that is not rejected.…….……183

Table 3.2 MP (*k=17* and equal weights) morphological synapomorphies and mapping of morphological character changes on the MP-total evidence tree.……..……..183

Table 3.3 MP total evidence morphological synapomorphies under ACCTRAN and DELTRAN optimization.…….…...184

Table 3.4 Summary statistics from the equal weights and implied weighting analyses. k: concavity constant, N: number of most parsimonious trees, L: tree length, CI: consistency index, RI: retention index.…….....….…...184

Table 3.5 Relative fit difference (RFD) of alternative phylogenetic hypotheses found using constrained searches. C = sum of fit of characters contradicting most parsimonious tree, F = sum of fit of characters favoring most parsimonious tree.…….....…...185

Table 3.6 Genetic distances (Kimura 2-parameter) within and between the molecular operational taxonomic units (MOTUs) which were identified by molecular species delimitation methods. (1) *Pensacolatus darlingtoni*, (2) *Pensacolatus maxillosus*, (3) *Pensacolatus applanatus*, (4) *Bryanattus sanchezi* **sp. nov.**, (5) *Bryanattus orientalis* **sp. nov.**, (6) *Bryanattus* sp. [Cuba1], (7) *Bryanattus thanos* **sp. nov.**, (8) *Bryanattus keyserlingi*, (9) *Antillattus cubensis*, (10) *Antillattus gracilis*, (11) *Antillattus placidus*, (12) *Antillattus ocultus* **sp. nov.**, (13) *Antillattus cambridgei*…….…....185

4. - ISLAND-TO-ISLAND VICAREANCE, FOUNDER-EVENT AND WITHIN-AREA SPECIATION, THE BIOGEOGRAPHY OF THE ANTILLATTUS CLADE (SALTICIDAE: EUOPHRYINI)-

Table 4.0. Substitution models selected by jModelTest for each individual gene region and partition.……..…….……260

Table 4.1. Results of the molecular clock tests: analyses of 75 terminal...…….262

Table 4.2. BioGeoBEARS' relative model probabilities (just put DEC + J, DIVALIKE + J etc. don't need to mention it again here) for non-time-stratified and time-stratified analyses. Best performing model is marked by asterisk for groups of analyses. LnL = log likelihood; n par = number of parameters in the analysis; d, e, j = parameres of the model (d = dispersal, e = extinction, j = founder event); AIC = Aikake information criterion; AICc = size-corrected AIC.…….…269

Table 4.3. Statistical chi-squared comparasion between with and without founder-event (j) BioGeoBEARS model.……...…….....….....269

Table 4.4. Summary count of non-time-constrained BSMs. DEC= dispersal-extinction-cladogenesis; DEC + j= dispersal-extinction-cladogenesis + jump dispersal. Abbreviations: a, range-switching dispersal; d, range-expansion dispersal; e, extinction; y, sympatric range-copying speciation; s, sympatric-subset speciation; v, vicariance; j, jump dispersal or founder-event speciation; Ÿd, allopatric dispersal; ad, anagenetic dispersal; Ÿa: allopatric anagenetic; Ÿc: allopatric cladogenetic; sums, adds up all of the events across the stochastic maps.……..……...270

Table 4.5. Summary count of time-constrained BSMs. DEC= dispersal-extinction-cladogenesis; DEC+ j= dispersal-extinction-cladogenesis and founder event. Abbreviations: a, range-switching dispersal; d, range-expansion dispersal; e, extinction; y, sympatric range-copying speciation; s, sympatric-subset speciation; v, vicariance; j, jump dispersal or founder-event speciation; Ÿd, allopatric dispersal; ad, anagenetic dispersal; Ÿa: allopatric anagenetic; Ÿc: allopatric cladogenetic; sums, adds up all of the events across the stochastic maps.……..…….…..270

CAPÍTULO 1

1.0 Características e importancia de las arañas

Como ocurre para otros grupos en las zonas tropicales y subtropicales del planeta, las arañas exhiben una especial diversidad en áreas de rica vegetación. Sin embargo, también están presentes en ambientes áridos, zonas de marea, cimas de montañas, conquistando incluso algunos ambientes dulceacuícolas (Foelix 2011; Ubick *et al*. 2017; World Spider Catalog 2020).

A diferencia de otros arácnidos, las arañas presentan el cuerpo dividido en dos partes unidas por un pedicelo. La parte anterior se denomina prosoma o cefalotórax y la parte posterior es el opistosoma o abdomen (fig.1.0 A-C). El prosoma dorsalmente tiene el carapacho y en la parte ventral se encuentran el esternón, los enditos y el labio (fig. 1B). El abdomen en su parte posterior posee glándulas sericígenas que segregan un líquido, que, al ponerse en contacto con el aire mediante unas estructuras llamadas hilanderas, se solidifica inmediatamente y produce la seda de araña (Foelix 2011). En la parte ventral del abdomen se localizan las aberturas genitales y las aberturas respiratorias (estigmas o espiráculos). Las arañas, al igual que el resto de los arácnidos, tienen seis pares de apéndices articulados que se insertan en el prosoma, estos están formados por: un par de quelíceros, un par de pedipalpos y cuatro pares de patas locomotoras.

Por último, mientras que el enorme éxito evolutivo de otros grupos se explica, en parte, por una gran diversidad de estrategias tróficas, Araneae es el único taxón compuesto en su totalidad por animales depredadores (Coddington y Levi 1991). Su alimentación se basa por lo general en artrópodos (incluyendo a otras arañas como presas) y pequeños vertebrados como peces, lagartos y ranas (Foelix 2011). Esta característica sumada a su abundancia, les atribuye la particular condición de ser depredadores intermedios en las cadenas tróficas de varios grupos de invertebrados, reguladores biológicos, y elementos claves para la autorregulación de los ecosistemas y agro-ecosistemas (Aguilar 1974-1977; Clausen 1986; Marc *et al*. 1999; Metcalf y Flint 1974).

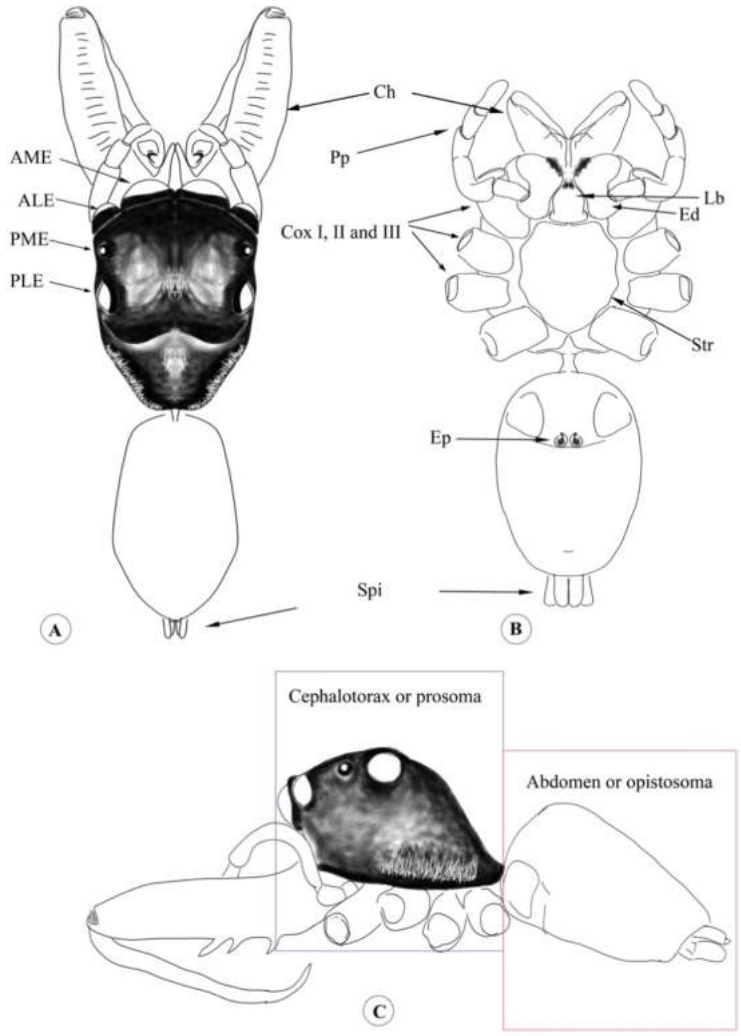

Figure. 1.0. A-C. Esquema general de la morfología externa de una araña (Salticidae). A) Vista dorsal B) Vista ventral C) Vista lateral. Abreviaturas: ALE = ojos anterolaterales; AME = ojos anteromediales; Ch = quelicero; Cox = coxa; Ed = enditos; Ep = epiginio; Lb = Labium; PLE = ojos posteriores laterales; PME = ojos medios posteriores; Pp = pedipalpo; Spi = hilandera; Str = Esternón.

1.1 Origen y evolución de la familia Salticidae

Los antepasados de las arañas se encuentran entre los primeros grupos de animales que poblaron las tierras emergidas, al menos se conocen desde hace 380 millones de años, unos 200 millones de años antes que los primeros dinosaurios aparecieran. Los fósiles más antiguos atribuibles a arañas, provienen del Carbonífero (Dunlop *et al*. 2012; Penney *et al*. 2012; Selden

y Penney 2010) y el devónico medio siendo *Palaeothele montceauensis* el único representante hasta la fecha. En aquellos tiempos eran muy abundantes los trigonotárbidos (Trigonotarbi), un orden extinto de arácnidos cuyo registro fósil se extiende desde el Silúrico hasta el Pérmico inferior, los cuales se consideran muy cercanos al antecesor común de todas las arañas (Shear *et al.* 1987). Se cree que los trigonotárbidos carecían de hileras y, por tanto, no producían seda. También tenían un opistosoma marcadamente segmentado, exoesqueleto quitinoso y no poseían pedicelo. Otro orden fósil del Devónico muy cercano a las arañas es Uraraneida, recientemente descrito con base a restos inicialmente interpretados como pertenecientes a arañas. Reestudiando el material se llegó a la conclusión de que esos animales –si bien producían seda- tenían un flagelo caudal semejante al del actual orden Telyphonida (Selden *et al*. 2008b). Cabe mencionar, finalmente, a la famosa *Megarachne servinei* Hunicken, hallada en estratos Permo-Carboníferos de San Luis, considerada durante mucho tiempo como la araña más grande conocida de todas las que vivieron en la Tierra. El enorme fósil de una longitud de alrededor de 33 cm fue reinterpretado como perteneciente a Eurypterida (Selden *et al*. 2005).

Si bien no existe una teoría universalmente aceptada sobre las relaciones dentro de Arachnida, casi todos los análisis filogenéticos aceptan que Araneae se encuentra en el mismo clado que los restantes órdenes de arácnidos "tetrapulmonados": junto con los órdenes Amblypygi, Thelyphonida y Schizomida (Dunlop 1999; Coddington *et al*. 2004). Actualmente se conocen más de 1.100 especies fósiles de arañas (Dunlop *et al*. 2012).

La edad mínima de divergencia de la familia Salticidae está fijada en 44 Mya (fósil del ámbar del Báltico) (Weitschat y Wichard 2002) con un estimado de 44-49 Mya según se cita en Penney (2008), y están compuestos por miembros de la subfamilia viviente Hisponinae (referido como Gorgopsininae en Petrunkevitch 1950, 1958; Wunderlich 2004) y otros saltícidos basales (Wunderlich 2004). Dado que actualmente no existe un registro fósil datado a partir del período Cretácico (Penney 2008), Zhang y Maddison (2013) plantean la hipótesis de que la divergencia de la familia Salticidae sea de 100 Mya.

En la región Caribe, los saltícidos resultan abundantes en el ámbar dominicano (16 Mya; Penney 2008). Seis especies de euofrinidos fósiles han sido registradas para el ámbar dominicano: *Corythalia ocululiter; C. pilosa; C. scissa; Pensacolatus coxalis; P. spinipes; P. tibialis* (véase Penney 2008). Entre ellos, los holotipos de *Pensacolatus coxalis* (SMF Be 938) y *P. spinipes* (SMF Be 930) depositados en el Instituto de Investigación y Museo de Historia Natural Senckenberg (Alemania). Basado en estos datos Zhang y Maddison (2013) establecen la edad mínima para los grupos hermanos de euofrinidos en 16 Mya.

1.2 Estructura del orden Aranae

Araneae es el único orden de Arachnida que tiene los quelíceros asociados con glándulas venenosas, apéndices abdominales (hilanderas) conectados a glándulas sericígenas, ausencia del músculo depresor trocánter-fémur y pedipalpos de los machos modificados como órganos de transferencia de esperma (Coddington *et al*. 2004). El Orden Araneae se subdivide en dos Subórdenes: Mesothele (Liphistiomorphae) y Opisthothele (Coddington y Levi 1991; Platnick y Gertsch 1976; Wheeler *et al*. 2016).

Platnick y Gertsch (1976) sentaron las bases de la actual clasificación, estableciendo la división basal entre las plesiomórficas Mesothelae (con rastros de segmentación abdominal) y las derivadas Opistothelae (el resto de las arañas, en las que los rastros de segmentación opistosómica han desaparecido). Según Raven (1985a) pueden ser separados también atendiendo a la forma del esternón: 1) tan estrecho como el labio en Mesothele; 2) mucho más ancho que el labio en Opisthothele. Mesothele se encuentra representadas por tres familias de las cuales los representantes de dos de ellas (Arthrolycosidae y Arthromygalidae) ya están extintos siendo la familia Liphistiidae con especies de Asia Oriental la única viviente (World Spider Catalog 2020). Opistothelae por su parte, se encuentra conformada por dos infraórdenes: Mygalomorphae y Araneomorphae.

Mygalomorphae conservan parte de los caracteres basales exhibidos en las mesotelas, como son los quelíceros ortognatos y dos pares de pulmones. Fue revisado por Raven (1985) y por primera vez propone una cladograma para familias, subfamilias y agrupaciones genéricas. El trabajo de Raven (1985) se convirtió entonces en un punto de partida para el estudio de la sistemática de alto nivel de Mygalomorphae.

Araneomorphae es el grupo más diverso de Araneae (más del 90% de las especies) con una diversidad morfológica y de hábitos sustancialmente mayor. Se diferencia, básicamente por la disposición labidognata de los quelíceros. Según la más reciente clasificación (ver Wheeler *et al*. 2016), Araneomorphae se compone por tres grandes clados (Synspermiata, Palpimanoidea y Entelegynae) y varios clados menores. Los Entelegynae se distinguen por tener palpos especialmente desarrollados y complejos, con numerosos escleritos accesorios embólicos, y que se activa por fuerzas hidráulicas (más que musculares, como en las haploginas); las hembras, en correspondencia, tienen un verdadero epigino, usualmente elaborado.

Los enteleginos a su vez comprenden al clado RTA (apófisis tibial retrolateral del palpo) con una clara tendencia a la pérdida del cribelo y a la adopción de un estilo de caza activa con es el caso de las errantes asechadoras (e.g. Salticidae, Lycosidae, Thomisidae, Anyphaenidae) (ver Wheeler *et al*. 2016).

1.3 La familia Salticidae

Las arañas saltarinas (Araneae: Salticidae) comprenden un gran grupo de organismos vivientes con 6 170 especies descritas, 645 géneros (13% de la riqueza total de especies y el 15% de los géneros) (World Spider Catalog 2020). El grupo de las saltícidos o arañas saltadoras (jumping spiders en ingles) se caracteriza por tener un sistema visual de alta resolución (Jackson and Li 2001; Jackson *et al*. 1998), un elaborado comportamiento de cortejo (Jackson 1989; Foelix 2011), y una gran diversidad de formas (Simon, 1901, 1902; Maddison 2015; Ubick *et al*. 2017).

1.3.1 Clasificación

La familia Salticidae, puede ser confundida con algunos representantes de familias como Coriniidae, Oxyopidae, y Thomisidae (Ubick *et al*. 2017). En general son arácnidos que varían en tamaño pudiéndose encontrar individuos desde unos pocos milímetros (e.g *Popcornella*, *Maeotha*) hasta varios centímetros (e.g. *Phydippus*). Atendiendo a la morfología, son agrupadas dentro de los ecribelados, enteleginos con dos uñas tarsales y ocho ojos (Ubick *et al*. 2017). En general, los salticidos son diferenciables del resto de las familias por la disposición de los ojos (generalmente formando tres hileras de ojos 4-2-2 aunque en *Lyssomanes* encontramos cuatro hileras 2-2-2-2). El prosoma usualmente es más largo que ancho en especial en las formas que resultan miméticas de hormigas (e.g. *Synemosyna*, *Fluda*, *Peckhamia*), mientras que, en las formas miméticas de escarabajos, el prosoma es más ancho que largo (e.g. *Rhetenor*). El quelícero exhibe una rica variabilidad de formas que van desde pequeños a largos, robustos o delgados, proyectados y desarrollados, ornamentados o sin ornamentaciones, a dimórficos o similares entre hembras y machos.

Eugène Simon de 1901–1903 estableció lo que se conocería como la clasificación histórica de Salticidae. Atendiendo a la dentición de los queliceros Eugène Simon separa a la familia Salticidae en tres grandes secciones (Pluridentati, Fissidentati, Unidentati). Sin embargo, esta agrupación artificial, resultó ser no acertada al agrupar especies que en la actualidad se reconocen no están relacionadas (Madisson 2015). Petrunkevitch (1928) y

Roewer (1954) respetaron la propuesta establecida por Eugène Simon y mantuvieron sustancialmente su clasificación artificial.

Prószyński (1976), realiza una nueva clasificación por medio de caracteres genitales del macho y la hembra. Esta clasificación reorienta lo hasta entonces conocido como Salticidae y es considerada más natural que la propuesta por Eugène Simon. Sin embargo, incluyó solo una pequeña fracción de los géneros de la familia. Trabajos recientes (e.g. Maddison y Hedin 2003a; Bodner 2009; Maddison 2015; Zhang y Maddison 2013, 2015) han mostrado que la forma básica de varias de las estructuras genitales masculinas i.e. la forma del embolo, y la forma del tegulum- resultan frecuentemente en convergencias.

Wanless (1980c, 1981a), aplicó razonamiento cladístico con la finalidad de resolver y/o aclarar varias de las relaciones entre los saltícidos y sus grupos hermanos. A pesar de esta panorámica de análisis, la mayoría de los géneros de Salticidae continuaron siendo poco claros.

Recientemente, Maddison (2015) establece una nueva clasificación para la familia teniendo como base la información molecular y la morfológica de la mayoría de las especies conocidas hasta la fecha. Basado en esta propuesta de Maddison (2015), la familia Salticidae se compone de siete subfamilias (Fig. 1.1), cuatro grandes clados (Amicoida, Salticoida, Marpissoida, Saltafresia), 30 tribus y 13 subtribus. Dentro del clado Saltafresia (ver Bodner y Maddison 2012; Maddison *et. al*. 2014), se incluyen las tribus Plexippini, Aelurillini, Euophryini, Chrysillini, Leptorchestini, Hasariini, Salticini y el género *Nannenus* (ver, Madisson 2015).

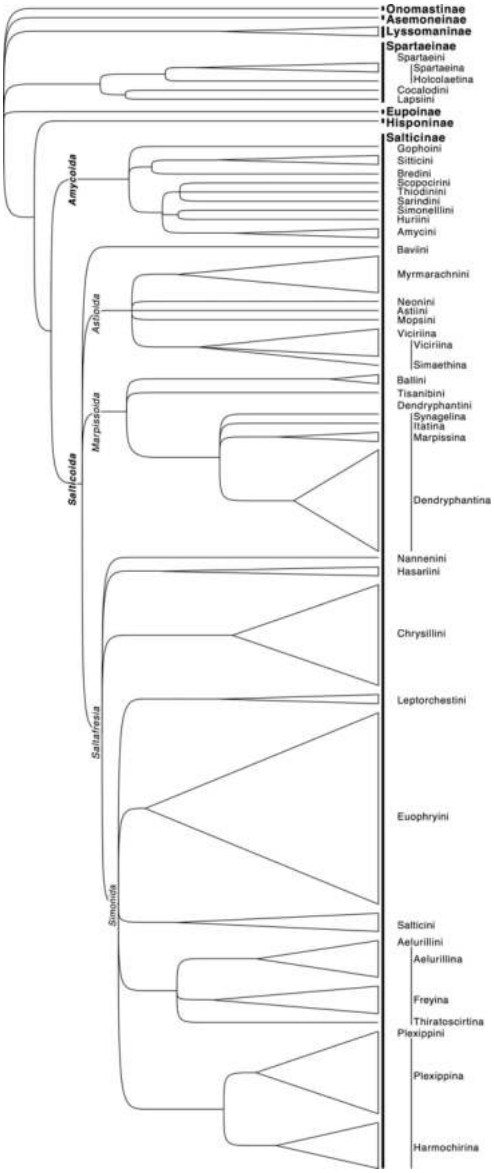

Figure. 1.1. Resumen de la filogenia molecular de Salticidae de Maddison 2015.

1.4 Subfamilia Salticinae Blackwall, 1841

Originalmente creada por Blackwall (1841) como Salticidae, ha sido considerada con anterioridad como una "división" dentro de Salticidae (ver Maddison 1996) o un clado mayor "Salticoida" (Maddison y Hedin 2003a) con aproximadamente cerca del 93% de las especies conocidas (Maddison 2015). Salticinae está dividida en dos clados mayores: Amycida y Salticoida. La monofilia de la subfamilia ha sido puesta a prueba por caracteres morfológicos (Maddison 1996; Ramírez 2014) y moleculares (Bodner y Maddison 2012; Maddison *et al*. 2014)

1.4.1 Caracteres de la subfamilia Salticinae

La subfamilia Salticinae puede delimitarse teniendo en cuenta la combinación de los siguientes caracteres: (1) garra del tarso ausente en el palpo de la hembra (Maddison 1996; Ramírez 2014); (2) apófisis mediana ausente en el palpo masculino (este carácter también resulta ausente en Spartaeinae, Hisponinae, y Lyssomaninae (ver Maddison 2015); (3) esclerito inter-quelicerales reducido (Maddison 1996; Ramírez 2014); (4) sistema traqueal más complejo (Galiano 1976b; Wanless 1980c, 1981a; Ramírez 2014); y (5) cymbium constrictor en la articulación tibial, generalmente con una muesca distintiva ubicada prolateralmente (Maddison 2015).

1.5 Clado Salticoida Maddison y Hedin (2003)

El clado salticoida es el grupo hermano de los amycoidas neotropicales que incluye la mayoría de las especies descritas para la subfamilia Salticinae (Maddison 2015). Las relaciones entre los subgrupos de Salticoida son ambiguas, pero algunos análisis (Bodner y Maddison 2012) sugieren que los baviines, los marpissoides y los astiodes podrian formar un clado hermano de Saltafresia. Maddison *et al.* (2014) reconocen al clado salticoida pero no le dan un nombre. Un año más tarde, Maddison (2015) le reasigna el nombre Salticoida basado en evidencia molecular de fragmentos de genes (28S rRNA, 18S rRNA, wingless, myosin HC).

1.6 Clado Saltafresia Bodner y Maddison (2012)

Saltafresia es el más grande de los tres clados de Salticoida *sensus stricto* con más de 3000 especies descritas hasta la fecha. A pesar del notable gran número de especies del grupo, la forma corporal de las especies es bastante conservadora habiendo solamente unos pocos grupos mirmecomorfos o escarabeiformes (Maddison 2015). Saltafresia es en gran parte afro-eurasiática, con la excepción de varios euofrinidos y freyinos del nuevo mundo. Hasta el presente no se conocen sinapomorfias para Saltafresia, pero el grupo está bien apoyado por datos moleculares (Bodner y Maddison 2012; Maddison *et al*. 2014).

1.6.1 Subcaldo Simonida Maddison (2015)

Simonida contiene a Plexippini, Aelurillini, Leptorchestini, Salticini y Euophryini (Bodner y Maddison 2012; Maddison *et al.* 2014). Es formalmente considerado como el clado más pequeño incluyendo los géneros tipo de los cinco grupos antes mencionados. Entre las características que definen al clado Simonida se encuentran: (1) patas relativamente robustas (e.g. *Cytaea*, *Aelurillus*, *Freya*, *Pellenes*, *Evarcha*); (2) tercer par de patas más largas,

posiblemente acompañadas de cambios que modifican la mecánica del salto (Otto y Hill 2012b).

1.6.2 La tribu Euophryini

Peckham, Peckham y Wheeler, 1889: Athamii; Simon, 1901: Bythocroteae, Chalcoscirteae, Coccorchesteae, Diolenieae, Evophrydeae, Saitideae, Sobasineae, Thianieae, Zenodoreae; *Simon, 1903*: Athameae, Bellieneae, Cytaeae, Emathideae, Laufeieae, Servaeae, Spilargeae; *Petrunkevitch, 1928*: Coccorchestinae, Cytaeinae, Spilarginae; *Roewer, 1954*: Coccorchestinae, Cytaeinae, Spilarginae; Athameae, Bellieneae, Bythocroteae, Chalcoscirteae, Cytaeeae, Diolenieae, Ematheae, Euophryeae, Laufeieae, Pensacoleae, Saiteae, Serveae, Sobasineae, Spilargeae, Thianieae, Zenodoreae. *Prószyński, 1976*: Euophrydinae; *Wanless, 1988*: Euophryinae. *Zhang and Maddison, 2013*: Euophryinae. *Maddison, 2015*: Euophryini.

La tribu Euophryini se encuentra conformada por más de 1000 especies y se encuentra ampliamente distribuida en los trópicos del viejo y nuevo mundo (Maddison y Hedin 2003a; Prószyński 1976; Zhang y Maddison 2015). No obstante, y a pesar de la elevada radiación de este grupo, algunas especies y géneros de euofrinos son notablemente uniformes, con la excepción de los representantes del trópico Autraliano *Diolenius*, *Sobasina*, *Paraharmochirus*, *Athamas* y *Coccorchestes* (Zhang y Maddison 2012b, 2015).

1.6.2.0 Clasificación

Creada inicialmente como una subfamilia por Eugène Simon en 1901, la Euophryinae fue considerada como un grupo dentro de la clasificación de Eugène Simon (ver Simon 1901; 1903). Inicialmente comprendía a los géneros *Akela*, *Euophrys* y *Rhyphelia*. Sin embargo, la clasificación propuesta por Eugène Simon tendría la problemática de agrupar géneros que en la actualidad comprendemos no están relacionados (Maddison 2015; Zhang y Maddison 2015).

Luego de casi 80 años, Jerzy Prószyski (1976) aclaró los límites de la subfamilia Euophryinae por primera vez al delimitarla como un grupo de especies con la presencia de un émbolo enrollado en el extremo distal del tegulum. Trece géneros fueron incluidos como Euophryinae, aunque dos de estos son actualmente considerados como *Marpissoida* (Maddison y Hedin 2003a) y *Heliofanina* (Maddison 1987).

Maddison y Hedin (2003a) consideraron 34 géneros dentro de la subfamilia, revisando nuevamente la delimitación con el objetivo de especificar la forma particular de los genitales. Estos autores determinaron que los integrantes de la subfamilia Euophryinae presentan (1) el embolo libre y enrollado posicionado en el extremo distal de tegulum con el plano de la espiral

del émbolo más o menos paralelo al eje longitudinal del palpo; (2) ducto espermático formando una proyección retrolateral hacia el centro del tegulum, (3) y epiginio generalmente en forma de "ventana".

Maddison y Hedin (2003a) proponen que Euophryinae es un clado dentro de Salticoida y sugieren que podría ser hermana de Plexippoida. Sin embargo, Maddison *et al.* (2008) sugieren que Euophryinae es un grupo hermano de Plexippoida + *Philaeus* y *Salticus*. Bodner (2009), encuentra que Euophryinae cae dentro de un gran clado con algunos grupos de Salticoida como son Plexippoida, Aelurilloida, Heliophaninae, y el grupo *Philaeus*.

Zhang y Maddison (2013, 2015) por medio de una extensa filogenia molecular y datos morfológicos, apoyan la condición monofilética de Euophryinae, e incorporan 85 géneros al grupo y más de 1000 especies convirtiéndose en una de las subfamilias más grandes. Zhang y Maddison (2013, 2015) encontraron una estructuración similar a la obtenida por Bodner (2009), con Euophryinae dentro de un clado mayor compuesto por varios Salticoida que incluyen a los géneros no agrupados *Nannenus*, *"Bathippus"pahang*, *Bristowia*, *Cheliceroides*, *Salticus*, y los reagrupados *Chinattus* (Hasarieae), *Heliophanus* (Heliophaninae), *Yllenus* (Leptorchesteae), *Aelurillus* y *Freya* (Aelurilloida), *Philaeus* (*Philaeus* group), *Plexippus*, *Habronattus* y *Havaika* (Plexippoida). En ese mismo año, Maddison (2015) establece a Euophryinae como la tribu Euoprhryini y la incluye dentro de la subfamilia Salticinae, Salticoida: Saltafresia: Simonida (ver Maddison 2015).

1.6.2.1 Caracteres morfológicos

Generalmente, el palpo de los euofrinidos tiene una espiral embolica simple que se diferencia del resto al ser una espiral abierta orientada ventralmente (Prószyński 1976; Zhang y Maddison 2015), con el eje de la espiral perpendicular al resto del palpo (Maddison y Hedin 2003a). El SDL (sperm duct loop) del tegulum del palpo del macho, resulta en cierta manera distintivo del grupo (Zhang y Maddison 2015), sin embrago también se puede ver en dendrifantinos como *Phanias* y *Rhene* (ver Maddison 1996). Finalmente, algunas especies poseen un epiginio en forma de "ventana" que guía al embolo (Maddison y Hedin 2003a; Zhang y Maddison 2015).

1.7 La fauna de arañas del caribe insular

Las arañas también representan uno de los grupos mayoritarios dentro de la biota de artrópodos del Caribe insular (Alayon 2000). Los valores de endemismos para muchos grupos

pueden llegar a ser de 100 % (Alayon 2001, 2006) y la ocurrencia de endemismos asociadas a islas resulta muy frecuente (Bloom *et al*. 2014; McHugh *et al*. 2014; Zhang and Maddison 2013).

La mayor riqueza de especies de la fauna de arañas actuales de las Antillas corresponde al archipiélago de Cuba (World Spider Catalog 2020). Un elemento a destacar en la fauna de arañas de las Antillas es la extrema rareza (probablemente por el efecto de los métodos de colecta) de muchas de sus especies, condicionada posiblemente por la restringida distribución geográfica y la dependencia de condiciones ecológicas particulares que caracterizan a algunas de ellas. El notable endemismo, sumado a la extrema rareza de algunas de las especies, convierte a las arañas del caribe insular en un grupo particularmente interesante para estudiarlas en esta área geográfica, considerada como uno de los 25 lugares de mayor biodiversidad en el planeta (Mittermeier *et al.* 2005).

Hasta el 2017, han sido publicado solamente 220 trabajos en los últimos 173 años, tomando como inicio los trabajos de Walckenaer (1837). La mayor parte de los estudios resultan referentes a descripción de especies. Sin embargo, estudios referentes a la biogeografía y relaciones filogenéticas solo han sido recientemente tenidos en cuenta (e.g. Čandek *et al.* 2019; Chamberland *et al*. 2018; McHugh *et al*. 2014; Tong *et al*. 2019; Zhang and Maddison 2013).

Entre las principales problemáticas identificadas para el estudio de las arañas de las Antillas se encuentra la ausencia de especialistas locales, lo cual a llevado a que los principales estudios sean realizados por aracnólogos europeos y norteamericanos. Por otra parte, el interés que despiertan los arácnidos es muy bajo si lo comparamos con otros grupos mucho más carismáticos (aves, mamíferos, reptiles, mariposas) lo cual ha dificultado en gran medida la obtención de recursos para las investigaciones.

Los vacíos de conocimientos y las problemáticas identificadas dan una idea de que todavía queda mucho por hacer y para lograr incrementar el nivel de conocimientos y llenar estos vacíos, posiblemente se necesitaría más de un milenio al ritmo actual de catalogación. Esto no sería un problema si la biodiversidad del planeta no estuviera en peligro y las especies no estuvieran desapareciendo a un ritmo acelerado cada año (Wilson 1992).

Los programas de conservación actuales no toman en consideración el papel fundamental de las arañas en el funcionamiento de los ecosistemas naturales, ni siquiera el estatus de especies concretas de invertebrados, excepto en unos pocos casos. Si bien no podemos conservar lo que no conocemos, tampoco podremos conocer aquello que no puede conservarse el tiempo suficiente para ser conocido. Esta paradoja propuesta por el aracnólogo español Antonio Melic (2000) nos hace reflexionar sobre la importancia de invertir mayores

esfuerzos en el estudio y conservación de los arácnidos y en general de los artrópodos de nuestro planeta.

Llenando parte de los vacíos de conocimiento existentes en el estudio de las arañas del Caribe, podríamos contribuir a identificar las principales amenazas y la vulnerabilidad de algunas de las especies, para poder establecer las prioridades de conservación de estos singulares animales en esta región especifica o al menos dirigir nuestros esfuerzos de conservación a áreas con altos valores de diversidad y endemismos.

1.7.1 Euofrinidos del caribe insular

Los euofrínidos resultan abundantes y megadiversos dentro del caribe insular (World Spider Catalog 2020). Según Zhang y Maddison (2013), los euofrinidos caribeños están agrupados dentro de dos grandes clados, representados por al menos cinco radiaciones independientes probablemente con origen suramericano (Zhang y Maddison 2013). Estas radiaciones datan del Eoceno-tardío al Mioceno-medio durante parte del periodo de conexión entre las islas del mar caribe con el continente (Iturralde-Vinent 2006). En el caribe insular se encuentran los clados Antillattus, *Naphrys*-*Corticattus*, Agobardus, *Anasaitis*-*Corythalia* y el género *Popcornella* (Zhang y Maddison 2013, 2015).

1.7.2 Clado Antillattus

El clado Antillattus se encuentra conformado por los géneros *Antillattus* Bryant (1943)*, Truncattus* Zhang y Maddison*, Petemathis* Prószyński y Reinhold y posiblemente los géneros monotípicos *Allodecta* Bryant y *Caribattus* Bryant (Zhang y Maddison 2013, 2015). Según Zhang y Maddison (2015) puede ser vagamente definido por la presencia de dos dientes promarginales en el quelícero, machos con embolo enrollado no más de la mitad de un círculo, el epiginio en las hembras con un septum medio relativamente ancho, opérculo genital usualmente en la zona intermedia, y el ducto de copulación relativamente corto (Bryant 1940, 1943, 1950; Zhang y Maddison 2012a, 2015).

1.7.2.0 Clasificación

Los primeros estudios correspondientes a los géneros y especies que conforman al clado Antillattus, tienen lugar en los trabajos de Franganillo (1930, 1935) y Bryant (1940, 1943, 1950). Franganillo (1930, 1935) describe a *Emathis unispina*, material tipo que posteriormente es extraviado de la colección. Años después, Bryant (1940) en su monografía sobre las especies de arañas de Cuba, describe a *Agobardus keyserlingi*, *A. mandibulatus* y transfiere a *Emathis*

cubensis (Franganillo 1935) a *Agobardus*. Bryant (1943) describe para La Española al género *Antillattus* junto con las especies *Antillattus gracilis* y *A. placidus*. En este mismo estudio, Bryant describe a *Amycus cambridgei* [transferida a *Cobanus* por Galiano (1968c)], *Pensacola darlingtoni*, *P. electa*, *P. maxillosa*, *P. montana*, *P. peckhami* y *Siloca electa*. En 1950, Bryant realiza su última contribución sobre saltícidos del caribe insular al describir a los géneros monotípicos *Allodectta* (*A. maxillaris*) y *Caribattus* (*C. inutilis*, antiguamente *Saitis inutilis* Peckham y Peckham (1901) para Jamaica.

Varias años después, Prószyński y Deeleman-Reinhold (2012) describen al género *Petemathis*, y establecen como especie tipo a *Emathis portoricensis =Petemathis portoricensis* (Petrunkevitch 1930) y transfieren a *Emathis luteopunctata* Petrunkevitch, *E. minuta* Petrunkevitch, *E. tetuani* Petrunkevitch y *E. unispina* Franganillo. La mas reciente contribución al grupo corresponde a Zhang y Maddison (2012a) donde se describe a *Antillattus applanatus* y al género *Truncattus* (*Truncattus cachotensis*, *T. dominicanus* y *T. flavus*).

1.8 Problema de investigación

La mayoría de los trabajos publicados sobre euofrinidos neotropicales continúan resultando de tipo taxonómico, mientras que unos pocos hacen referencia a la filogenia y biogeografía. Para el Caribe, la información existente resulta sesgada e insuficiente. Las principales problemáticas se encuentran en el poco conocimiento de la fauna, la pérdida o la complejidad para la detección del material tipo, y la insuficiente información de las descripciones originales.

Aunque se realizó una aproximación a la filogenia y evolución del clado Antillattus en el trabajo de Zhang y Maddison (2013, 2015), su comprensión resulta aún lejos de ser completada. Los resultados obtenidos por Zhang y Maddison (2013, 2015) proporcionan un marco filogenético básico, pero las relaciones correspondientes a los géneros y especies dentro del clado, continúa sin ser solucionadas. En este sentido, es necesario proporcionar una filogenia robusta dentro del clado Antillattus lo cual permita obtener un mejor acercamiento a la biogeografía histórica y la evolución de caracteres.

Zhang y Maddison (2015) encuentran elementos que soporta la monofília del clado Antillattus. Sin embargo, algunos aspectos resultan intrigantes. Primero, varias de las especies incluidas dentro de los géneros que componen al clado no resultaron analizadas (deficiencia de taxon sampling) (por ejemplo, *Antillattus cubensis* (Franganillo), *A. keyserlingi* (Bryant), *A. mandibulatus* (Bryant) y los géneros *Caribattus* Bryant y *Allodectta* Bryant. Sumado a esto, algunas especies están asignadas a géneros con los cuales no comparten los caracteres

diagnósticos y posiblemente pertenezcan a otros géneros conocidos o aún por describir. En segunda instancia, muchas de las especies de euofrinidos del Caribe resultan muy parecidas en su morfología y aún no se han identificado caracteres diagnósticos para separarlas. Esto hace necesario la obtención de información molecular y morfológica que brinde evidencia para comprobar la inclusión o no de éstos dentro del clado Antillattus.

Por otra parte, la divergencia temporal del clado Antillattus arroja ciertas aproximaciones sobre la biogeografía. Sin embargo, cuestiones relacionadas con el origen caribeño de los géneros y especies y la inferencia de los posibles eventos de dispersiones y / o vicarianza que expliquen los patrones de distribución actual de las especies del clado Antillattus permanecen inciertos. Finalmente, estudios comparativos exhaustivos de ciertos rasgos morfológicos, tales como los bulbos copuladores de los palpos masculinos, los quelíceros en hembras y machos y la genitalia de la hembra bajo la microscopia de barrido (SEM), podrían revelar características más confiables para delimitar morfológicamente al clado Antillattus y al género *Antillattus*.

Con base a lo anterior se plantean las siguientes preguntas de investigación: ¿Cuál es la relación filogenética entre los géneros y especies que componen el clado Antillattus? ¿Pertenecen los géneros *Allodecta* y *Caribattus* al clado Antillattus? ¿Corresponden *A. cubensis* (Franganillo), *A. keyserlingi* Bryant, *A. mandibulatus* Bryant al género *Antillattus*? ¿Cuál es la historia biogeográfica de las especies del clado Antillattus? ¿cuáles son los caracteres morfológicos que definen a los géneros que conforman al clado Antillattus?

1.9 HIPÓTESIS

El análisis de marcadores moleculares y caracteres morfológicos de las especies que componen al clado Antillattus, podría aclarar las relaciones filogenéticas entre los géneros y especies, ayudando a obtener una aproximación de la historia evolutiva, biogeográfica y finalmente a definir caracteres morfológicos que sean de utilidad en el esclarecimiento de los grupos.

1.10 Objetivo general

Proponer una hipótesis de relación filogenética para los géneros y especies del clado Antillattus utilizando caracteres morfológicos y moleculares.

1.10.0 Objetivos específicos

- Evaluar la validez de los géneros y especies que componen el clado Antillattus con base en el criterio de monofilia
- Identificar y evaluar los caracteres morfológicos que presenten utilidad filogenética en el marco de las especies estudiadas.
- Delimitar los géneros y especies del clado Antillattus utilizando caracteres morfológicos y moleculares.
- Comprobar si los géneros *Caribattus* Bryant y *Allodectta* Bryant, y las especies *A. cubensis* (Franganillo), *A. keyserlingi* Bryant, *A. mandibulatus* Bryant pertenecen al clado Antillattus.
- Describir la variación intra- e inter-especifica de los quelíceros, el bulbo copulador del palpo del macho y de la genitalia de las hembras, de las especies que conforman al clado Antillattus.
- Analizar el patrón biogeográfico de las especies que componen al clado Antillattus, evaluando los posibles procesos que expliquen el patrón de distribución y compararlos con propuestas biogeográficas previas para la región.

1.11 BIBLIOGRAFÍA

Aguilar, F. P. G. (1974). Arañas del campo cultivado I: Población de araneidos en algodonales de Cañete, Huaura y Rímac. *Revista peruana de entomología* **17**(1), 21-27.

Aguilar, F. P. G. (1975). Arañas del campo cultivado II: Fluctuación de las familias de araneidos en algodonales de la Costa Central. *Revista peruana de entomología* **18**(1), 25-28.

Aguilar, F. P. G. (1976). Arañas del campo cultivado III: Araneidos en algodonales del Valle de Lurín, Lima. *Revista peruana de entomología* **19**(1), 71-72.

Aguilar, F. P. G. (1977). Las arañas en el agroecosistema algodonero de la Costa Peruana. *Anales Científicos* UNA, XV (1-4): 109-121.

Alayón, G. G. (2000). Las arañas endémicas de Cuba (Arachnida: Araneae). *Revista Ibérica de Aracnología* **2**, 1-48.

Alayón, G. G. (2001a). Especie nueva de *Selenops* (Araneae: Selenopidae) de Curazao, Antillas Holandesas. *Solenodon* **1**: 17-20.

Alayón, G. G. (2006). Endemicidad y relaciones de las arañas (Araneae) de las Antillas mayores. *Cocuyo* **16**, 63-68.

Blackwall, J. (1841). The difference in the number of eyes with which spiders are provided proposed as the basis of their distribution into tribes; with descriptions of newly

discovered species and the characters of a new family and three new genera of spiders. *Transactions of the Linnean Society of London* **18**, 601-670.

Bloom, T., Binford, G., Esposito, L. A., Alayón G., G., Peterson, I., Nishida, A., Loubet-Senear, K. and Agnarsson, I. (2014). Discovery of two new species of eyeless spiders within a single Hispaniola cave. *Journal of Arachnology* **42**, 148-154. doi:10.1636/k13-84.1

Bodner, M. R., and Maddison, W. P. (2012). The biogeography and age of salticid spider radiations (Araneae: Salticidae). *Molecular Phylogenetics and Evolution* **65**: 213-240.

Bodner, M. R. (2009) MS Thesis: The Biogeography and Age of Salticid Spider Radiations with the Introduction of a New African Group (Araneae: Salticidae). 108pp.

Bryant, E. B. (1940). Cuban spiders in the Museum of Comparative Zoology. *Bulletin of the Museum of Comparative Zoology* **86**, 247-554.

Bryant EB. (1943) The salticid spiders of Hispaniola. *Bulletin of the Museum of Comparative Zoology* 92, 445-529.

Bryant EB. (1950) The salticid spiders of Jamaica. *Bulletin of the Museum of Comparative Zoology* 103, 163-209.

Candek K, Agnarsson I, Binford G, Kuntner M. 2019. Biogeographic history of *Cyrtognatha* spiders reveals a single mid-Miocene owerwater colonization of the Caribbean archipelago. *Scientific Reports* **9**, 397.

Chamberland, L., McHugh, A., Kechejian, S., Binford, G. J., Bond, J. A., Coddiongton, J. A., Dolman, G., Hamliton, C., Harvey, M. S., Kuntner and M, Agnarsson I. (2018). From Gondwana to GAARlandia: global biogeography of ogre-faced spiders (Deinopidae) mirrors geologic history. *Journal of Biogeography* **45**, 2442-2457.

Clausen, I. H. S. (1986). The use of spiders as ecological indicators. *Bulletin of the British Arachnological Society* **7**, 83-86.

Coddington, J. A., Giribet, G., Harvey, S. M., Prendini, L., Walter, E. D. (2004). Arachnida. Pages 296-318. In: Cracraft J, Donoghue JM. (eds.), *Assembling the Tree of Life*. Oxford University Press, New York.

Coddington, J. A., Levi, H. W. (1991). Systematics and Evolution of Spiders (Araneae). *Annual Review of Ecology and Systematics* **22**(1), 565–592. doi:10.1146/annurev.es.22.110191.003025

Dunlop, J. A., Penney, D., Jekel, D. (2012). A summary list of fossil spiders and their relatives. In: Platnick NI (2012) The World Spider Catalog, version 12.5. *American Museum of Natural History*, online at http://research.amnh.org/entomology/spiders/catalog/index.html

Dunlop, J. A. (1999). Pasando revista a la evolución de los quelicerados. In: Melic A, De Haro JJ, Mendez M, Ribera I. (eds.), Evolución y filogenia de Arthropoda. *Boletin de la Sociedad Entomologica Aragonesa* **26**, 255-272.

Foelix, R. (2011). Biology of spiders, 3rd ed. Oxford: Oxford University Press.

Franganillo, B. P. (1930). Arácnidos de Cuba: Mas arácnidos nuevos de la Isla de Cuba. *Memorias del Instituto Nacional de Investigaciones Cientificas* **1**, 47-99. [reprinted separately, pp. 1-55; only reprint seen and cited]

Franganillo, B. P. (1935c). Estudio de los arácnidos recogidos durante el verano de 1934. *Estudios de "Belen"* 1935(?55-56), 23-30.

Franganillo, B. P. (1936). *Los arácnidos de Cuba hasta 1936*. Cultural La Habana, 183 pp.

Galiano, M. E. (1976b). Comentarios sobre la categoria sistematica del taxon Lyssomanidae (Araneae). *Revista del Museo Argentino de Ciencias Naturales Bernardino Rivadavia* (Ent.) **5**, 59-70.

Galiano, M. E. (1968c). Revision de los géneros *Acragas*, *Amycus*, *Encolpius*, *Hypaeus*, *Mago* y *Noegus* (Salticidae, Araneae). *Revista del Museo Argentino de Ciencias Naturales Bernardino Rivadavia* (Ent.) **2**, 267-360.

Iturralde-Vinent, M. A. (2006). Meso-Cenozoic Caribbean paleogeography: implications for the historical biogeography of the region. *International Geology Review* **48**, 791–827.

Jackson, R. R., Li, D., Barrion, A. T., Edwards, G. B. (1998) Prey-capture techniques and prey preferences of nine species of ant-eating jumping spiders (Araneae: Salticidae) from the Philippines. *New Zealand of Zoology* **25**, 249-272.

Jackson, R. R, Li D. (2001) Prey-capture techniques and prey preferences of Zenodorus durvillei, *Z. metallescens* and *Z. orbiculatus*, tropical ant-eating jumping spiders (Araneae: Salticidae) from Australia. *New Zealand Journal of Zoology* **28**, 299-341.

Jackson, R. R. (1989) The biology of *Cobanus mandibularis*, a jumping spider (Araneae: Salticidae) from Costa Rica: intraspecific interactions, predatory behaviour, and silk utilization. *New Zealand Journal of Zoology* **16**, 383-392.

Maddison, W. (1987). *Marchena* and other jumping spiders with an apparent leg-carapace stridulatory mechanism (Araneae: Salticidae: Heliophaninae and Thiodinae). *Bulletin of the British Arachnological Society* **7**, 101-106.

Maddison, W. P., Li, D. Q., Bodner, M., Zhang, J. X., Xu, X., Liu, Q. Q., and Liu, F, X. (2014). The deep phylogeny of jumping spiders (Araneae, Salticidae). *ZooKeys* **440**, 57-87. doi:10.3897/zookeys.440.7891

Maddison, W. P. (1996). *Pelegrina* Franganillo and other jumping spiders formerly placed in the genus *Metaphidippus* (Araneae: Salticidae). *Bulletin of the Museum of Comparative Zoology* **154**, 215-368.

Maddison, W. P. (2015). A phylogenetic classification of jumping spiders (Araneae: Salticidae). *Journal Arachnology* **43**, 231-292.

Maddison, W. P., and Hedin, M.C. (2003a). Jumping spider phylogeny (Araneae: Salticidae). *Invertebrate Systematics* **17**,529-549.

Marc, P., Canard, A., and Ysnel, F. (1999). Spiders (Araneae) useful for pest limitation and bioindication. *Agriculture, Ecosystems and Environment* **74**: 229-273.

Mchugh, A., Yablonsky, C., Binford, G., and Agnarsson I., (2014). Molecular phylogenetics of Caribbean *Micrathena* (Araneae: Araneidae) suggests multiple colonization events and single island endemism. *Invertebrate Systematics* **28**, 337-349

Metcalf, C. L., and Flint, W. P. (1974). *Insectos destructivos e insectos útiles. Sus Costumbres y su Control*. Cía. Editorial Continental. Barcelona. 1208 p.

Mittermeier, R. A., Robles-Gil, P., Hoffman, M., Pilgrim, J., Brooks, T., Mittermeier, C.G., Lamoreux, J., and da Fonseca, G.A.B. (2005). Hotspots revisited: earth's biologically richest and most endangered terrestrial ecoregions. Mexico: Agrupación Sierra Madre, 1–392 pp.

Otto, J. C., Hill, D. E. (2012b). Two new Australian peacock spiders that display inflated and extended spinnerets (Araneae: Salticidae: Euophryinae: *Maratus* Karsch 1878). *Peckhamia* **104.1**: 1-28.

Penney, D., Dunlop, J., and Marusik, Y. (2012). *Summary statistics for fossil spider species taxonomy. ZooKeys* **192**, 1–13.doi:10.3897/zookeys.192.3093

Penney, D. (2008) Dominican Amber Spiders: A comparative palaeontological-neontological approach to identification, faunistics, ecology and biogeography. Siri Scientific Press.

Petrunkevitch, A. (1950) Baltic amber spiders in the Museum of Comparative Zoology. *Bulletin of the Museum of Comparative Zoology at Harvard College*. Cambridge, Massachusetts, USA, 326-263.

Petrunkevitch, A. (1958) Amber spiders in European collections. *Transactions of the Connecticut Academy of Arts and Sciences*. Yale University Press. New Haven Connecticut, USA, (41), 97-400.

Platnick, N. I., Coddington, A. J., Forster, R. R., Griswold, E. C. (1991). Spinneret morphology and the phylogeny of haplogyne spiders (Araneae, Araneomorphae). *American Museum Novitates*. **3016**: 1-73.

Platnick, N. I, and Gertsch, J. W. (1976). The suborders of spiders: A cladistic analysis (Arachnida, Araneae). *American Museum Novitates* **2607**, 1-15.

Prószyński, J., and Deeleman-Reinhold, C. L. (2012). Description of some Salticidae (Aranei) from the Malay Archipelago. II. Salticidae of Java and Sumatra, with comments on related species. *Arthropoda Selecta* **21** (1), 29-60.

Prószyński, J. (1976) Studium systematyczno-zoogeograficzne nad rodzina Salticidae (Aranei) Regionow Palearktycznego i Nearktycznego. *Rozprawy Wyzszej Szkoly Pedagogicznej* **6**, 1- 260.

Ramírez, M. J. (2014). The morphology and phylogeny of dionychan spiders (Araneae: Araneomorphae). *Bulletin of the American Museum of Natural History* **390**, 1-374. Link doi:10.1206/821.1

Raven, R. J. (1985a). The spider infraorder Mygalomorphae (Araneae): Cladistics and systematics. *Bulletin of the American Museum of Natural History* **182**, 1-180.

Selden, P. A., Corronca, J. A., and Hünicken, M. A. (2005). *The true identity of the supposed giant fossil spider Megarachne. Biology Letters* **1**(1), 44–48.doi:10.1098/rsbl.2004.0272

Selden, P. A., and Penney, D. (2010). Fossil spiders. Biological Reviews **85**, 171–206. doi: 10.1111/j.1469-185X.2009.00099.x

Selden, P. A., Shear, W. A., and Sutton, M. A., (2008b). Fossil evidence for the origin of spider spinnerets, and a proposed arachnid order. *Proceedings of the National Academy of Sciences*, U. S. A. **105**, 20781–20785.

Shear, W. A., Selden, P. A., Rolfe, W. D. I., Bonamo, P. M., and Grierson, J. D. (1987). New terrestrial arachnids from the Devonian of Gilboa, New York (Arachnida: Trigonotarbida). American Museum Novitates **2901**, 1–74.

Simon, E. (1902). Description d'arachnides nouveaux de la famille des Salticidae (Attidae) (suite). *Annales de la Société Entomologique de Belgique* **46**, 24-56, 363-406.

Simon, E. (190l). *Histoire naturelle des Araignees.* Tome 2, Fascicule 3. Seconde edition. Paris, Librairie encyclopedique de Roret. 381-668pp.

Tong, Y., Binford, G., Agnarsson, I. (2019). Huntsmen of the Caribbean: multiple tests of the GAARlandia hypothesis. *Molecular Phylogenetics and Evolution* **130**, 259-268.

Ubick, D., Paquin, P., Cushing, P. E., and Roth, V. (2017). *Spiders of North America: an identification manual*. 2nd Edition. American Arachnological Society. Keene, New Hampshire, USA.

Walckenaer, C. A. (1837). *Histoire naturelle des insectes. Aptères*. Paris 1, 1-682. doi:10.5962/bhl.title.61095

Wanless, F. R. (1980c). A revision of the spider genus *Onomastus* (Araneae: Salticidae). *Bulletin of the British Museum of Natural History* (Zool.) **39**, 179-188.

Wanless, F. R. (1981a). A revision of the spider genus *Hispo* (Araneae: Salticidae). *Bulletin of the British Museum of Natural History* (Zool.) **41**, 179-198.

Weitschat, W., and Wichard, W. (2002) Atlas of plants and animals in Baltic amber. *Geological Magazine* **139** (5), 597.

Wheeler, W. C., Coddington, J. A., Crowley, L. M., Dimitrov, D., Goloboff, P. A., Griswold, C. E., and Zhang, J. (2016). The spider tree of life: phylogeny of Araneae based on target-gene analyses from an extensive taxon sampling. *Cladistics*, **33**(6), 574–616.doi:10.1111/cla.12182

Wilson, E. O. (1992). The diversity of life. Cambridge, Mass., Harvard University. Press. 424 pp.

World Spider Catalog (2020). World Spider Catalog. Natural History Museum Bern, online at http://wsc.nmbe.ch, version 21.0, accessed on February 1th. doi: 10.24436/2

Wunderlich, J. (2004) Fossil spiders in amber and copal. *Beiträge zur Araneologie*, **3ab**, 1-1908.

Zhang, J. X., and Maddison, W. P. (2012a). New euophryine jumping spiders from the Dominican Republic and Puerto Rico (Araneae: Salticidae: Euophryinae). *Zootaxa.* **3476**,1-54.

Zhang, J. X, Maddison, W. P. (2012b). New euophryine jumping spiders from Papua New Guinea (Araneae: Salticidae: Euophryinae). *Zootaxa* **3491**, 1-74.

Zhang, J. X., Maddison, W. P. (2013). Molecular phylogeny, divergence times and biogeography of spiders of the subfamily Euophryinae (Araneae: Salticidae). *Molecular Phylogenetics and Evolution* **68**,81-92.

Zhang, J. X., Maddison, W. P. (2015). Genera of euophryine jumping spiders (Araneae: Salticidae), with a combined molecular-morphological phylogeny. *Zootaxa*. **3938**, 1-147.

CAPÍTULO 2

PHYLOGENY, MORPHOLOGY AND EVOLUTION OF JUMPING SPIDER CLADE ANTILLATTUS (SALTICOIDA: EUOPHRIINI)

Phylogeny, morphology and evolution of the jumping spider clade Antillattus and its sister groups (Salticoida: Euophryini)

Abstract

Most studies of salticid phylogenies have focused on molecular data, but few phylogenies based on morphological work have been published to date. Here, tests the validity of the Antillattus clade, the phylogenetic relationships of its various lineages, the exact placement of the genera *Caribattus* and *Allodecta* and closely study the morphological traits of the Antillattus clade and its sister groups to clarify generic limits. To address these issues, we combine morphological and molecular data, including 125 morphological characters, data from the nuclear gene 28S, and data from the mitochondrial genes 16S and COI, totaling 3,218 characters scored for 25 Antillattus clade species, 42 sister groups and one outgroup taxon. These data were analyzed using likelihood, parsimony and Bayesian methods. *Pensacolatus* and *Bryanattus* **gen. nov.** are recovered within the Antillattus clade, while *Caribattus* and *Allodecta* are excluded. The limits of *Sidusa* and *Cobanus* are strongly supported by both morphological and total evidence (molecular+morphology) analyses. We transfer *S. bifurcata* (Chickering, 1946), *S. cambridgei*, (Chickering, 1946), *S. electa* (Chickering, 1946), *S. mandibularis* (Peckham and Peckham, 1895) and *S. unicolor* (F.O. Pickard-Cambridge, 1900) to *Cobanus*. We also transfer *Petemathis unispina* to *Bryanattus*, *Sidusa turquinensis* and *S. inconspicua* to *Truncattus* and consider *Allodecta* a junior synonym of *Compsodecta*. *Paracobanus* **gen. nov.** is described to include the type species *Paracobanus botero* **sp. nov.** Finally, we describe the *Cobanus* species *C. multidentatis* **sp. nov.** and *C. chocquibtown* **sp. nov.** from Colombia and the *Truncattus* species *T. martii* **sp. nov.** and *T. platnicki* **sp. nov.** from Cuba.

Keywords: Salticidae, Euophryines, Caribbean, generic review, total evidence, new synonym.

2.0 Introduction

The way we conduct systematic studies is strongly influenced by the questions we want to answer. In general, there are two aims: (1) to identify and define species, and 2) to determine the relationships between these species. Obtaining a strongly supported species tree (or phylogenetic hypothesis) forms the basis for all subsequent studies, including taxonomy, systematics.

In the past several decades, the remarkable growth of molecular phylogenetics has diminished scientific interest in morphological data (Giribet 2015; Lee and Palci 2015; Pagel 1999). The focus on molecular data has been fueled by observations that molecular and morphological phylogenies often seem to be at odds with each other (Benton 1999; Easteal 1999; Jenner 2004; Scotland *et al*. 2003; Wiens 2004). However, the use of morphological characters for phylogenetic inference has returned within the scientific community (Cabra-García and Hormiga 2019; de S. *et al*. 2014; Martin *et al.* 2018; Mirande 2017; Sánchez-Pacheco *et al*. 2018). One of the main reasons for this shift is the use of total evidence methods that allow analysis of a combination of morphological and molecular datasets (de Sá *et al*. 2014; Mirande 2017; Sánchez-Pacheco *et al*. 2018). Furthermore, phenotypic data are the basis for the formulation of initial phylogenetic hypotheses and guide appropriate taxon sampling (Cabra-García and Hormiga 2019; Chakrabarty *et al*. 2017; Koch and Gauthier 2018). Like Cabra-García and Hormiga (2019), it should also be considered that even in a case of overwhelming disproportionality, morphological characters continue to be indispensable to include extinct lineages within phylogenies (Edgecombe 2017; Giribet 2015; Goloboff *et al*. 2019; Huang *et al*. 2018; Lee and Palci 2015; Pyron 2015; Wang *et al*. 2018; Wanninger 2015) and to propose phenotypic to delimit clades (e.g. Martin *et al*. 2018). Because of the beneficial aspects of both molecular (e.g. extent of the dataset,) and morphological (e.g. applicability to museum specimens, old samples, fossil, ontogenetic information) data, we integrate both in our overall dataset.

Of the more than 48,000 known spider species, 6080 are jumping spiders (Salticidae) (World Spider Catalog 2020). The large bulk of the diversity within the family consists of a well-delimited clade, the Salticoida (Maddison 2015; Ruiz and Maddison 2012). The phylogeny of Salticoida has been recovered by molecular data (e.g. Maddison *et al*. 2007; Maddison and Hedin 2003) and has been supported by several apomorphic features, such as the loss of the female palpal claw and characters concerning internal eye structures (e.g. cell bodies of ALE photoreceptors displaced to side) (Maddison 2015; Maddison and Hedin 2003).

Currently, Salticoida is composed of Agoriini, Astioida, Marpissoida and Saltafresia (Maddison 2015). Saltafresia is the third and largest (more than 3000 species) of the four major clades of the Salticoida *sensu stricto* (see Maddison 2015). With the exception of some euophryines and freyines, the majority of Saltafresia are Afro-Eurasian (World Spider Catalog 2020; Maddison 2015). Euophryini was originally created by Eugène Simon (1901) as "Evophrydeae" to group the unidentate genera *Akela*, *Euophrys* and *Rhyphelia*. After several decades, Prószyński (1976) clarified the delimitation and considered the tribe as Euophryinae.

The composition of Euophryinae was considerably extended by Maddison and Hedin (2003a) (34 genera) and posteriorly by Zhang and Maddison (2015) (83 genera). That same year, Maddison (2015) transferred Euophryinae to the tribe Euophryini. Despite the high diversity of this group, euophryines all have a palp with the typical spiral embolus (Prószyński 1976; Zhang and Maddison 2015) and an epigynum with a circular window (Maddison 2015). Recently, Zhang and Maddison (2015) resolved the relationships among a worldwide representation of the euophryine lineages. They present evidence of high levels of euophryine diversity in the Caribbean region and identify several groups, including the Antillattus clade.

In an attempt to find synapomorphies for euophryine clades, Zhang and Maddison (2015) constructed molecular and morphological phylogenies (Zhang and Maddison 2015). Unfortunately, these phylogenies did not completely resolve the taxonomic problems. The main issues are the limited number of species sampled and sequenced, too few morphological characters, and the lack of morphological support for some of the proposed groups. These factors can influence the delimitation genera and the clades into which they fall. For example, *Cobanus* species were transferred to *Sidusa* despite notable differences in morphology.

The Antillattus clade includes the genera *Antillattus* Bryant (1943), *Truncattus* Zhang and Maddison (2012) *Petemathis* Prószyński and Deeleman-Reinhold (2012), and probably *Allodecta* Bryant (1950) and *Caribattus* Bryant (1950) (Zhang and Maddison 2015). This clade is defined by having two promarginal cheliceral teeth, a male palp with a coiled embolus no more than half a circle, and by females with a middle septum of the epigynum, a copulating operculum typically found in the intermediate area of the vulva and relatively short copulatory ducts (Bryant 1940, 1943, 1950; Zhang and Maddison 2012, 2015). Zhang and Maddison (2015) transferred the species of *Pensacola* from the Dominican Republic (see Bryant 1943) to *Antillattus*. This decision is not supported by unambiguous synapomorphies. Additionally, *Allodecta* and *Caribattus* were proposed as members of the Antillattus clade, but their phylogenetic positions were not tested with morphological data. The goals of this study are to review the phylogeny considering both morphological and molecular data, and to test the monophyly of Antillattus clade, the monophyly of the genera in this clade and their relationships to one another using a total evidence approach.

2.1 Material and methods

2.1.0 Taxon sample

Specimens were collected using methods in Cuba, Puerto Rico, Jamaica, Hispaniola, Lesser Antilles, Mexico and Colombia as part of the Caribbean biogeographic project

(http://www.islandbiogeography.org) (supplementary figure 1, table 1). The material collected was fixed in 95% ethanol. Voucher specimens will be deposited in the University of Vermont's Natural History Museum and the Smithsonian Institute (**USNM**, J. Coddington), Instituto de Ciencias Naturales-Universidad Nacional de Colombia, Bogotá (**ICN**, E. Flórez); Museo Argentino de Ciencias Naturales Bernardino Rivadavia, Buenos Aires (**MACN**, C. L. Scioscia); Museo de Zoología Comparativa, Universidad de Harvard, Cambridge (**MCZ**, G. Giribet, L. Leibensperger); Museo Nacional de Historia Natural "Felipe Poey", La Habana, Cuba (**MNHN**, G. Alayon). Type species and additional material were examined from the following collections: Museum of Comparative Zoology, Harvard University (**MCZ**); Museo Nacional de Historia Natural, Santo Domingo (**MNHNSD**).

2.1.0.1 Outgroups

The outgroups were selected to sample the lineages of Caribbean species of the Agobardus clade (*Compsodecta*, *Agobardus* and *Bythocrotus*), *Popcornella*, *Corticathus*, the continental *Sidusa-Cobanus* and *Mexigonus-Pensacola* clades, the latter of which includes the sister group of the Antillattus clade according Zhang and Maddison (2013, fig:1). The *Sidusa-Cobanus* clade is the sister group to all euophryines, including the Antillattus clade. Here, the *Sidusa-Cobanus* clade is represented by *Sidusa gratiosa*, *S. electus*, *S. cambridgei*, *S. mandibularis*, *S. unicolor*, *Cobanus extensus* and the undescribed *Sidusa* sp. French Guiana 1, *S.* sp. French Guiana 2 (see Zhang and Maddison 2015) and *S.* sp. Colombia 1, *S.* sp. Colombia 2, *S.* sp. Colombia 3, *Cobanus* sp. Colombia 1, and *C.* sp. Colombia 2. *Mexigonus cf. minutus*, *M. arizonensis*, *M. morosus*, *Pensacola signata* and *P. sylvestri* represent the *Pensacola-Mexigonus* clade, which is sister to Antillattus clade +(*Corticattus*+(*Popcornella*+(Agobardus clade)). The genus *Popcornella* is represented by *Popcornella furcata*, *P. spiniformis* and *P. yunque*. The genus *Corticattus* is composed of *Corticattus guajataca* and *C. latus* and the Agobardus clade by the species *Compsodecta festiva*, *C. haytiensis*, *C. peckhami*, *C. gratiosa*, *C. grisea*, *C. valida*, *Bythocrotus crypticus*, *B. cf. crypticus* (see Zhang and Maddison 2015), *Agobardus gramineus*, *A. anormalis montanus*, *A. brevitarsus*, *A. oviedo*, *A. phylladiphilus*, *A. cordiformis* and *A. bahoruco*. Marpissoida [*Ghelna canadiensis*] was chosen to root the resulting cladograms.

The "*Sidusa*" species of Cuba and the monotypic genera *Allodecta* and *Caribattus* were sampled more extensively than other genera to test whether they are members of the Antillattus clade. Monotypic genera are problematic theoretically, taxonomically and practically (Agnarsson 2004).

The Antillattus clade intergeneric relationships and their outgroup structure are poorly known (see Zhang and Maddison 2015). The relationships of the Antillattus clade with its outgroups has been tested with molecular data (see Zhang and Maddison 2013, 2015). Using these results, we based taxon sampling towards the ingroup (the unknown) and their sister groups rather than excessively testing the structure of euophryines inferred in previous phylogenies. We do not intend to solve the aforementioned problems of euophryine phylogeny. Rather, we rely on the assumption that the outgroup composition allows a good test of Antillattus clade monophyly and genera relationships.

2.1.0.2 Ingroups

Taxa were chosen to represent the Antillattus clade, including the morphological variation (see table 2.0 and supplementary table 1). Whenever possible, ingroups included all species of the Antillattus clade to test the monophyly of the genera and because competent comparative morphology is difficult if only a few specimens are available (Agnarsson 2004). We included *Antillattus gracilis*, *A. placidus*, *A. applanatus*, *A. darlingtoni*, *A. maxillosus*, *A. cambridgei*, *A. cubensis*, *A. keyserlingi* and *A. scutiformis*. Undescribed species morphologically close to *A. keyserlingi* also are included. The species *Truncattus cachotensis, T. dominicanus* and *T. flavus* represent the genus *Truncattus*. We also included undescribed Cuban species to test whether they correspond to the genus *Truncattus*. The focus on *Antillattus* and *Truncattus* allows us to test the monophyly (or rather the demonstration of its likely polyphyly, see Forster *et al.* 1990) and serves as a platform for revision of the genera (Cala-Riquelme *et al.* in rev.). Finally, *Petemathis* is represented by *Petemathis portoricensis* and *P. tetuani*.

Table. 2.0. Known diversity of the antillattus clade and sampled diversity

	Diversity	Molecular Sample	%	Taxonomy Sample	%
Antillattus	13	9	69	12	92
Truncattus	5	4	80	4	80
Petemathis	5	2	40	4	80
Caribattus	1	1	-	1	100
Allodecta	1	1	-	1	100
	25	17	68	22	88

2.1.1 Specimen preparation

Morphology was studied in detail by means of microscopy and SEM photography (Álvares-Padilla and Hormiga 2008). Because we did not sample all species, we obtained SEM images of a representative of each genus. When we could not obtain SEM images due to missing

or poorly preserved specimens, character scoring was complemented by light microscopy and/or SEM images from the literature of the same or closely related species. SEM photographs were taken using the QUANTA-200-FEI Microscope from the Scanning Electron Microscopy Laboratory at the Universidad Nacional de Colombia and with a Mira3 Tescan Laboratório Institucional de Microscopia Eletrônica de Varredura of the Museu Paraense Emílio Goeldi, Belém, Brazil Universidad de Para, Belem, Brazil.

Samples were examined and illustrated using an AIMscope stereomicroscope with a built-in camera. The left palp was used for all imaging. Female genitalia were dissected and cleared with clove oil. Male genitalia were expanded with KOH according to Shear (1967). Both male and female genitalia were examined in clove oil. All drawings were made digitally by means of a WACOM in the Autodesk SketchBook program (https://sketchbook.com). All measurements (in millimeters) were taken using a scale grid. In this study, we use terminology standardized by Zhang and Maddison (2015) and Ramírez (2014). This standardization allowed us to propose a hypothesis of homology between structures.

Anatomical abbreviations:

ALE= anterior lateral eye
AME= anterior median eye
Bf=fang base
BG= Bennett's gland
BH=basal hematodochae
C=conductor
Cb=cymbium
CD=copulatory duct
CDR=copulatory duct receptacle
Co= copulatory opening
DH= distal hematodochae
dTL=distal tegular lobe
E = embolus
ECP= epigynal coupling pockets
ED= embolic disc
Edc= endite cusp
FD= fertilization duct
Fe= femur
Fg = fang groove
Fu= fundus
PB= pre-spiracular bump
PH=pre-spiracular hairs
PLE= posterior lateral
PLEsR= posterior lateral eyes row
PME= posterior median eye
PPA= patella apophysis
PS = primary spermathecae
pSDL= prolateral sperm duct loop
pT=promarginal tooth
PTA= prolateral tibial apophysis
pTL = proximal tegulat lobe
rSDL= retrolateral sperm duct loop
rT= retrolateral tooth
RTA= retrolateral tibial apophysis
S= spermophorae
Sh=shaft
SR= salticid radix
SS = secondary spermathecae
ST= subtegulum
T =tegulum

La= lamella
Ms=mastidion
OQ=ocular guadrangle
VTA= ventral tibial apophysis
WE= window of the epigynum

2.1.2 Character sampling

Many of the characters (66 characters) used in this study were obtained or adapted from previous phylogenetic studies of Entelegynae and Salticidae (e.g. Álvarez-Padilla *et al*. 2009; Azevedo *et al*. 2018; Ramirez 2014; Zhang and Maddison 2015) as well as from diagnoses and description of genera in these clades (Bryant 1940, 1943, 1950; Zhang and Maddison 2012, 2015).

The interpretation of secondary spermathecal homologies in this paper differs from that of Zhang and Maddison (2015) and instead follows the proposed by Ramírez (2014). The retromarginal and promarginal tooth count follows Azevedo *et. al.* (2018), with topological modification.

The dataset for the phylogenetic analysis comprised 125 characters (59 new characters, 40 binary, 19 multistate ordered, 66 multistate unordered, 0.92 applicable and not missing, 515 internal gaps). Characters were placed into four groups: male palp, female genitalia, cephalothorax (including the legs and chelicerae) and abdomen. To discretize continuous characters in valid states, we followed Ramírez (2003) and Scharanschkin and Doyle (2006) as follows: Measurements of up to five specimens per species were obtained, covering the known distributional range. All measurements were corrected for size by dividing each measurement by the length of the carapace. The codification and/or adaptation of characters involves the interpretation of homology statements, the separation of sexually dimorphic characters and the separation of one mixed character into two or more neomorphic and transformational characters (*sensu* Sereno 2007). For the codification of characters, we follow the logical structure proposed by Sereno (2007). Twenty-three characters (1, 8-9, 11-13, 15-16, 23-24, 26-28, 30, 58, 60-61, 89, 96-97, 107, 110-111) are parsimony uninformative in the present context but are included because of their likely relevance to future studies of Salticidae. Character descriptions and definitions are detailed later.

2.1.3 Synapomorphies and character trait evolution

Mesquite v. 3.6 (Maddison and Maddison 2018b) was used to visualize synapomorphies and to conduct ancestral character state reconstruction using parsimony. Winclada 1.00.08 (Nixon 2002) and TNT v.1.5 (Goloboff *et al*. 2008; Goloboff and Catalano

2016) were used to identify and plot unambiguously optimized synapomorphies (see Ramírez 2014) shared across optimal trees of equal weights, implied weights and total evidence under MP, ML and BI.

We are aware that character optimization under the criterion of parsimony on topologies resulting from Bayesian and/or likelihood analyses contradicts the functional structure of cladistics and should not be used to explain the character evolution (Assias 2017, 2015; Franz 2005a, 2014). However, we consider that character optimization in model-based analyses can be used to visualize congruent synapomorphies from the parsimony analysis. The congruent synapomorphies are indicated in bold and presented in table 2.2.

Additionally, within our morphological dataset, ACCTRAN or DELTRAN (table 2.3) commands were used as necessary, favoring the preservation of the homology of complex structures and avoiding illogical optimizations. In accelerated transformation (ACCTRAN), changes are assigned along branches as quickly as possible (passing up); in delayed transformation (DELTRAN), they are assigned as late as possible. However, in some instances ACCTRAN results in illogical optimization for taxa coded as inapplicable for that character, and thus DELTRAN is necessary to avoid illogical optimization, although only a single gain is inferred (see Agnarsson 2004; Ramírez 2014).

2.1.4 Morphological phylogenetic signal

To compare phylogenetic signals, we used different morphological character sets (cephalothorax, palp and epigynum). These character sets may be susceptible to different selection pressures. For example, genitalia may be subject to sexual selection. Separate and combined phylogenetic analyses were conducted. Phylogenetic signals for each character set were analyzed with the retention index of each tree (Farris 1989a; Farris 1989b; Kitching *et al*. 1998; Klingenberg and Gidaszewski 2010). Finally, the informativeness of each character set was quantified by recording the percentages of characters with a retention of 100 compared to the total number of characters in both partitioned and combined analyses.

2.1.5 Molecular analyses

DNA was isolated with the Qiagen DNeasy Tissue Kit (Qiagen, Valencia, CA, USA). We sequenced fragments of cytochrome-c-oxidase subunit 1 (COI), 16S and 28S. We amplified COI with LCO1490 (GGTCAACAAATCATAAAGATATTGG) (Folmer *et al*. 1994) and C1-N-2776 (GGATAATCAGAATATCGTCGAGG) (Hedin and Maddison 2001). The partial fragment of the 16S gene was amplified with 16SA/12261 (CGCCTGTTTACCAAAAACAT)

(Folmer *et al.* 1994) and 16SB (CCGGTTTGAACTCAGATC) (Hedin and Maddison 2001). The 28S gene was amplified with 28SO (TCGGAAGGAACCAGCTACTA) and 28SC (GAAACTGCTCAAAGGTAAACGG). For COI and 28S, the polymerase chain reaction (PCR) was performed with an initial denaturation at 94ºC for 2 min, followed by 40 cycles of denaturation at 94 ºC for 25 sec, annealing at 50ºC (first round)/ 44.5ºC (second round) for 25 sec and extension at 65ºC for 2 min (first round)/ 1 min (second round); with a final extension at 72ºC for 10 min. The PCR conditions to amplify 16S-ND1 were: initial denaturation at 94°C for 2 min; followed by 35 cycles of 35 sec at 94°C, annealing at 48 ºC for 35 sec, and extension at at 65ºC for 2 min (first round)/ 1 min (second round); with a final extension at 72ºC for 10 min. Amplified fragments were sequenced in both directions using Sanger sequencing at GENEWIZ's New Jersey facility. The forward and reverse reads were interpreted with Phred and Phrap (Green 1999; Green and Ewing 2002) via Chromaseq v. 1.31 (Maddison and Maddison 2018a) in Mesquite v. 3.6 (Maddison and Maddison 2018b) using default parameters.

2.1.5.0 Sequencing

Amplified fragments were sequenced in both directions using Sanger sequencing at GENEWIZ's New Jersey facility. The forward and reverse reads were interpreted with Phred and Phrap (Green 1999; Green and Ewing 2002) via Chromaseq v. 1.31 (Maddison and Maddison 2018a) in Mesquite v. 3.6 (Maddison and Maddison 2018b) using default parameters.

2.1.5.1 Alignment and substitution model

The data were aligned using the online version of MAFFT (https://mafft.cbrc.jp/alignment/server/) (Katoh and Standley 2013). Structural genes can be difficult to assign as there are often insertions and deletions, particularly in the loops. Therefore we tested the sensitivity of the of the 28S and 16S alignments, we used different combinations of strategies under a progressive method (FFT-NS-1; FFT-NS-2, G-INS-1) and an interactive refinement method (FFT-NS-I, E-INS-I, L-INS-I, G-INS-I, Q-INS-I), with the parameters 1PAM, 20PAM and 200 PAM, and a gap opening penalty (1.53, 1.60, 1.65, 1.70, 1.75, 1.80, 1.85, 2.00, 3.00, 4.00). To obtain a better sequence alignment, we followed the method proposed by Zhang and Maddison (2013, 2015) using the complete genome of *Habronattus oregonensis* (Peckham and Peckham) (GenBank AY571145; see Masta and Boore 2004; Zhang and Maddison 2015) to base our alignment. The data resulting from the alignments were manually reviewed in Mesquite 3.6 (Maddison and Maddison 2018b) with reference to the

translation of amino acids using the "Color Nucleotide by Amino Acid" option. To test the quality of the alignment, we performed maximum likelihood (ML) searches with different alignments and with the concatenation of all the alignments using = RAxMLHPC v8.2.12 = (Stamatakis 2006) with 10 search repetitions and under the assumptions of the GTRGAMMAI model. Finally, the selected alignment was one that provided the topologically congruent tree in the concatenated alignments. We decided to use the alignment resulted of strategy L-INS-I with a parameter 1PAM / k = 200, a penalty of opening GAPs of 1.53 and a configuration of 100. The appropriate substitution model by codon position was selected with jModeltest 2.1.10 (Darriba *et al*. 2012) using the Akaike information criterion (AIC) (Posada and Buckley 2004) to select among the 24 models that can be implemented in MrBayes (see Table 2.1).

Table 2.1. Substitution models selected by jModeltest for each individual gene region and partition.

	substitution model		
	AIC	AICc	BIG
16S	GTR+I+G (012345)	GTR+I+G (012345)	GTR+I+G (012345)
COI 1-2nd codon	GTR+I+G (012345)	GTR+I+G (012345)	GTR+I+G (012345)
COI 3rd codon	TrN+I+G (010020)	TrN+I+G (010020)	TrN+I+G (010020)
28S	GTR+I+G (012345)	GTR+I+G (012345)	TrN+I+G (010020

2.1.5.2 Phylogenetic inference

Phylogenetic analyses were performed for the individual matrices (morphological, 28S, 16S and COI) and a combined dataset containing all three concatenated genes and the morphological data. In the combined matrix, the data were divided into six partitions: morphological, 28S, 16S, COI 1st+2nd codon and 3rd codon. GAPS were treated as missing characters. In spite of the strengths and weaknesses from philosophical and statistical points of view, we preferred the topology obtained under Parsimony (Baker 2003; Felsenstein 1978; Goloboff and Pol 2005; Goloboff *et al*. 2018; Grant and Kluge 2008a; Kluge 2001; Kluge and Grant 2006; Kolaczkowski and Thornton 2004; Ospina-Sarria and Cabra-García 2018; Sansom *et al*. 2018) over the topology obtained under Bayesian inference (Barker 2015; Goloboff and Pol 2005; Holder *et al*. 2008; Kolaczkowski and Thornton 2009; Nylander *et al*. 2004; O'Reilly *et al*. 2016; Schrago *et al*. 2018; Wright and Hillis 2014) and Maximum likelihood (Pol and Siddall 2001; Siddall 1998; Steel and Penny 2000; Swofford *et al*. 2001; Tuffley and Steel

1997; Wright and Hillis 2014; Zhou *et al*. 2018), for discussing the phylogenetic relationships. Nevertheless, we take a partially eclectic position following a notion of support, where the clades recovered with multiple analytical approaches are considered to be better supported than those obtained with fewer approaches (see, Parry *et al*. 2017; Ward *et al*. 2015; Whelan *et al*. 2015). We consider having an overview under the idea that the choice of optimum criterion should be assessed critically in any phylogenetic analysis (Rindal and Brower 2011; Padial *et al*. 2014; Goicoechea *et al*. 2016; Cabra-Garcías and Hormiga 2019). FIGTREE and Adobe Illustrator were used to edit our trees.

2.1.5.3 Parsimony

Parsimony analysis was conducted on the morphological and combined (molecular and morphology) datasets using TNT 1.5 (Goloboff *et al*. 2008; Goloboff and Catalano 2016). Random Sectorial Searches (RSS) + consensus Sectorial Searches (CSS) + Ratchet (ratchet 1000 rounds) + Drift (drift 20 rounds) + Tree Fusing (fuse 20 rounds) with 5000 random addition sequences was used under equal weights following of TBR+SPR (commandline: *rseed[; hold 10000; xinact; xmult: rss css fuse 20 drift 20 ratchet 1000 replic 5000*; *sec: slack 20; bbreak: tbr spr safe fillonly; xmult; bbreak)*. The search with implied weights (Goloboff, 1993; Goloboff et al. 2008b) was run using 10 different values of the concavity constant (k = 3, 5, 7, 9, 11, 17, 20, 25, 50, 100) (Giribet 2003; Goloboff 1993; Goloboff et al. 2008b) (commandline: *piwe=;).* Finally, group frequencies under jackknifing (JK) (commandline: *mult: noratchet replic 100 tbr hold 10; resample jak replic 5000 freq from 0 [mult]; mult;*) for morphology only, Bootstrap (BT) (commandline: *resample boot replic 2000 [mult]; mult;*), symmetrical resampling (SR) (commandline: *resample = [mu1=ho1;] sym rep 10000 prob 33 freq*) (Goloboff *et al.* 2003) and Bremer support (BS) (commandline: *mult: tbr spr replic 2000; mult; sub 1; sub 2; sub 3; sub 4; sub 5; sub 6; sub 7; sub 100; bsupport!!+0;*) values (Bremer 1988; Goodman *et al*. 1982; Grant and Kluge 2008a; Mendes 2011; Ramírez 2014) were estimated as support measures.

2.1.5.4 Maximum likelihood

RAxMLHPC v8.2.12 (Stamatakis 2006, 2014) was used to perform maximum likelihood analysis for the individual and combined gene matrices, each with 500 replicates under the assumptions of the GTRGAMMAI model (raxmlHPC-PTHREADS.exe -T 2 -f a -x 897 -m GTRGAMMAI -p 335 -N 500 -o Ghelna_canadensis -s MLDNA.phy -n MLDNA.tre -O -w). Bootstrap analyses were also carried out to calculate the support of the clades in a

separate execution of RAxML with 1000 replicates. ML total evidence was carried out using IQ-TREE v.2.0 (Nguyen *et al*. 2015). ModelFinder (Kalyaanamoorthy *et al*. 2017), as implemented in IQ-TREE v.2.0 (Nguyen *et al*. 2015), was used to select the optimal partitioning scheme and substitution models for the DNA and morphological characters (iqtree -s dataMatrix.nex --runs 100 -m TESTMERGEONLY -spp setsBlock.nex -pre iqtreeAnalysis -nt AUTO).

2.1.5.5 Bayesian inference

The Bayesian analysis was carried out using MrBayes v. 3.2.7a (Altekar *et al*. 2004; Huelsenbeck and Ronquist 2001; Ronquist and Huelsenbeck 2003) through the online portal CIPRES (https://www.phylo.org/portal2) (Miller *et al.* 2010) for the combined matrix considering five partitions (morphology, 28S, 16S, COI 1st-2nd codon and 3rd codon). For phenotypic characters, the *MKv+Γ* model was used. The analysis was run under the following parameters (command: "mcmcp ngen = 200,000,000 printfreq = 1000 samplefreq = 1000 nchains = 8 savebrlens = yes"). The results were imported into Tracer v1.7 (Rambaut and Drummond 2007) to determine the stabilization of the probability. The stationary phase was checked using the standard deviation of split frequencies and with the plot of likelihood by generation. The consensus tree and the posterior probabilities were generated by discarding a "burn-in" of 25% of the resulting trees.

2.1.6 Topology tests

Constrained topologies were used to evaluate alternative evolutionary hypotheses. This was done using both likelihood heterogeneity tests (LHT) and Bayes Factors (BF) for ML and BI (Azevedo *et al*. 2018; Huelsenbeck and Bull 1996; Kass and Raftery 1995). The likelihood heterogeneity test (LHT) (Huelsenbeck and Bull 1996) was developed to evaluate the hypothesis that differences in phylogenetic estimates can be explained by stochastic variation. The likelihood heterogeneity test compares the likelihood L_1 obtained under the constraint that the same phylogeny underlies all of the data sets with the L_0 as the unconstrained hypothesis. The likelihood ratio test statistic is $LHT=2(lnL_1 - InL_0)$, where *lnL* is the likelihood, and L_0 and L_1 are the hypotheses being compared calculated as a X^2 distribution with *n* degrees of freedom. H_0 is accepted if $L_0=L_1$ and rejected if L_0/L_1. The *BF* is calculated through the equation $BF = 2\ ln\ f(D|H_1) - 2\ ln\ f(D|H_0)$, where $f(D|H)$ is the marginal model likelihood, *D* is the data and H_0 and H_1 are the hypotheses being compared (in this case, the unconstrained and constrained topology, respectively). In the standard test, we calculated the marginal

likelihood of H_0 by using an unconstrained analysis with an uninformative prior across topology space, whereas the marginal likelihood of H_1 was calculated from an absolute monophyly constraint on *Pensacolatus* as an informed topology prior. Values between 0–2 indicate no evidence of a difference between the two hypotheses, 2–6 indicate substantial evidence, 6–10 indicate strong evidence for a difference and >10 indicates decisive evidence for a difference in the likelihood of the topologies (Kass and Raftery 1995). The lower the BF, the lower the support for the unconstrained tree. Marginal likelihoods were estimated through the harmonic means in MrBayes 3.2.7a, and likelihoods were estimated in RAxMLHPC v8.2.12 (Stamatakis 2006, 2014).

Finally, Relative Fit Difference (RFD) (Goloboff and Farris 2001) for parsimony analysis was also implemented. RFD is calculated through the formula *1-(C /F)*, where *C* is the sum of fits of characters increasing their fit in the constrained hypothesis (contradicting the most parsimonious tree), and F represents the characters that decrease their fits in constraints (favoring the most parsimonious tree). Therefore, the lower the RFD, the lower the support for the most parsimonious (unconstrained) tree in relation to the constrained topology. *C* and *F* for each constrained analysis were calculated using TNT.

2.1.7 Character descriptions and definitions

Characters taken from Zhang and Maddison (2015), whether modified or not, are marked ZM15, followed by the character number [e.g. ZM15-1 is character 1 in Zhang and Maddison (2015)]. Other character takes are marked as follows: Ramírez (2014) as R14; Azevedo *et al*. (2018) as AZ18; and Álvarez-Padilla *et al.* (2009) AP09.

2.1.7.0 *Cephalothorax, legs and chelicerae*

For the prosoma, we encoded characters of the cephalothorax, eyes, chelicerae and legs (fig. 1.1 A-C). The anterior part bearing the eyes is the cephalic area. The thoracic area is delimited by a thoracic furrow. Salticidae have a basic pattern of eight eyes in three rows (*Lyssomanes* have four rows) and follow the general nomenclature of Araneae: anterior median (**AME**), anterior lateral (**ALE**), posterior median (**PME**) and posterior lateral (**PLE**) eyes (figs. 1.1A-C). The clypeus is the stretch of carapace between the eyes and the anterior margin of carapace (see, Ramírez 2014).

Salticid chelicerae have a thick basal article, the paturon, and a pointed articulated fang. The paturons articulate against each other on a median line at the posterior end of which there is a single, small intercheliceral sclerite (see Ramirez 2014). Over the furrow (promargin

and retromargin) there are usually teeth and specialized setae (figs. 2.3). The fang articulates on two strong condyles. In the mesal articular membrane between the fang and the paturon, there is a small sclerite, the plagula ventralis, where the fang flexor tendon attaches. The fang has two sections, a smooth base, and a shaft, usually with longitudinal striae and a posterior internal serrula (figs. 2.3). The generalities of legs joint articulations are summarized in Ramírez (2014).

Cephalothorax

Character 1: Male cephalothorax, cheek expanded laterally: (0) absent (figs. 2.2A-C, E-I). (1) present (FIG. 2.2D). (ZM15-6. Fig 38) COMMENTS: In *Agobardus anormales montanus* and some species of *Corythalia*, the male carapace is cheek behind rather ALEs. This feature is also found in males of *Ascyltus* and *Aruattus* (Karsch 1878; Berry *et al*. 1997; Logunov and Azarkina 2008; Zhang and Maddison 2015). Outside of euophryines, the character is also scored 1 within the tribe Plexippini (e.g. *Afrobeata*).

Character 2: Male cephalothorax, white scales at edge of the carapace: (0) absent (fig. 2.1A-B). (1) present (fig. 2.1 C-F). In many salticids groups, white scales are common on the prosoma, but establishing homology is complex. We refer to the white band of scales observed at the edge of the carapace in lateral and anterior position as a homolog. This band can be thin or wide. We do not encode this state here, but it could be included in future studies. We define three additional characters according to the region where the scales were found, and the area they occupy (char. 3-5). COMMENTS: In Euophryini, the genera *Anasaitis*, *Corythalia*, *Agobardus*, *Antillattus*, *Bryanattus*, *Pensacolatus*, *Compsodecta*, *Tylogonus* and *Thorelliola* have white scales on the edge of the carapace. More commonly, these scales are located on the lateral edges of the carapace and frontally between the AME and the clypeus (figs 2.1, C-F). The character is also observed within the basal subfamily Spartaeinae (e.g. *Tabuina*, *Yamangalea*); the Salticoida clade (e.g. *Bavia*); the clade Marpissoida [e.g. *Hentzia*, *Metaphidippus*); and the tribe Aelurillini [e.g. *Phlegra*, *Chira, Eustiromastix*).

Character 3: Male cephalothorax, white scales at edge of the carapace in anterior position: (0) absent (fig. 2.1B). (1) present (fig. 2.1F). COMMENTS: *Pensacola, Caribattus inutilis*, *Paracobanus* **gen. nov.**, *Petemathis*, *Agobardus*, *Bythocrotus*,

Compsodecta (including *Allodecta*), *Pensacolatus*, *Antillattus*, *Truncattus* and *Bryanattus* (scored 1).

Character 4: Male cephalothorax, white scales at edge of the carapace in lateral position: (0) absent (fig. 2.1A). (1) present (fig. 2.1C and E). COMMENTS: *Pensacola* (scored 1); *Caribattus* (scored 1); *Agobardus* (scored 1); *Bythocrotus* (scored 1); *Compsodecta* (including *Allodecta*), (scored 1); *Pensacolatus Antillattus* (scored 1); *Truncattus* (scored 1); and *Bryanattus* **gen. nov.** (scored 1).

Character 5: Male cephalothorax, white scales at edge of the carapace in lateral position occupying: (0) only the half the carapace (fig. 2.1C); (1) the entire carapace (fig. 2.1E). COMMENTS: *Pensacola* (scored 1); *Caribattus* (scored 1); *Agobardus* (scored 1); *Bythocrotus* (scored 1); *Pensacolatus* (scored 1); and *Truncattus* (scored 1).

Character 6: Cephalothorax, ocular quadrangle (**OQ**) length to carapace total length ratio: (0) between 30% and 45% (fig. 2.2I). (1) >45% (fig. 2.1A-H). The ocular quadrangle (**OQ**) is widely used in spiders to describe the total area occupied by the eyes. COMMENTS: In Salticidae, species with an OQ occupying ≤ 45% of the total length of the prosoma can be found along of the phylogeny (e.g. *Phlegra*, *Ghelna, Mexigonus, Mogrus*).

Character 7: Cephalothorax, posterior lateral eyes row (**PLEsR**): (0) shorter than carapace width (fig. 2.1C, D, I). (1) as long as carapace width (fig. 2.1A-B, E, H). COMMENTS: In *Corticattus*, the PLEs row is shorter than the carapace width, and usually the carapace is flattened. In species of *Corythalia*, *Mexigonus* and *Furculattus*, this character is particularly conspicuous (see, Zhang and Maddison, 2012, 2015). The PLEsR shorter than the carapace width is also found within the basal genera *Onomastus, Asemonea*, *Goleba, Chinoscopus*, *Lyssomanes* and the tribe Lapsiini.

Chelicerae

Character 8: Female paturon, promarginal tooth I: (0) absent. (1) present. (AZ18-73). COMMENTS: We follow the proposal of Azevedo *et al.* (2018) and teeth were separated into serially homologous structures. We considered tooth I the furthest awayfrom the base of the fang. In the cases that we found more than four retromarginal teeth or three promarginal teeth, they were lumped into one character "extra teeth" (Fig. 2.2). Like Azevedo *et al*. (2018), we attempted to

establish homology among each individual tooth based on topological equivalence criteria.

Character 9: Female paturon, promarginal tooth II: (0) absent. (1) present.

Character 10: Female paturon, promarginal tooth III: (0) absent. (1) present.

Character 11: Female paturon, promarginal tooth distal: (0) absent. (1) present.

Character 12: Female paturon, promarginal tooth medial: (0) absent. (1) present.

Character 13: Female paturon, promarginal tooth proximal: (0) absent. (1) present.

Character 14: Female paturon, promarginal tooth fused: (0) absent. (1) present. COMMENTS: In many Salticidae groups, teeth may appear fused at the base, forming bicuspids or multicuspids (see, Ramírez 2014; Simon 1903; Zhang and Maddison 2015). We considered the fusion of the teeth at the base a neomorphic character (Sereno 2007).

Character 15: Female paturon, promarginal tooth fused: (0) bicuspid. (1) multicuspid.

Character 16: Female paturon, retromarginal tooth I: (0) absent. (1) present.

Character 17: Female paturon, retromarginal tooth II: (0) absent. (1) present.

Character 18: Female paturon, retromarginal tooth III: (0) absent. (1) present.

Character 19: Female paturon, retromarginal tooth IV: (0) absent. (1) present.

Character 20: Female paturon, retromarginal extra teeth: (0) absent. (1) present.

Character 21: Female paturon, retromarginal tooth fused: (0) absent. (1) present.

Character 22: Female paturon, retromarginal tooth fused: (0) bicuspid. (1) multicuspid.

Character 23: Male paturon, promarginal tooth I: (0) absent. (1) present.

Character 24: Male paturon, promarginal tooth II: (0) absent. (1) present.

Character 25: Male paturon, promarginal tooth III: (0) absent. (1) present.

Character 26: Male paturon, promarginal tooth distal: (0) absent. (1) present.

Character 27: Male paturon, promarginal tooth medial: (0) absent. (1) present.

Character 28: Male paturon, promarginal tooth proximal: (0) absent. (1) present.

Character 29: Male paturon, promarginal tooth fused: (0) absent. (1) present.

Character 30: Male paturon, promarginal tooth fused: (0) bicuspids. (1) multicuspids.

Character 31: Male paturon, retromarginal tooth I: (0) absent. (1) present.

Character 32: Male paturon, retromarginal tooth II: (0) absent. (1) present.

Character 33: Male paturon, retromarginal tooth III: (0) absent. (1) present.

Character 34: Male paturon, retromarginal tooth IV: (0) absent. (1) present.

Character 35: Male paturon, retromarginal extra teeth: (0) absent. (1) present.

Character 36: Male paturon, retromarginal tooth distal: (0) absent. (1) present.

Character 37: Male paturon, retromarginal tooth medial: (0) absent. (1) present.

Character 38: Male paturon, retromarginal tooth proximal: (0) absent. (1) present.

Character 39: Male paturon, retromarginal tooth fused: (0) absent. (1) present.

Character 40: Male paturon, retromarginal tooth fused: (0) bicuspids. (1) multicuspids.

Character 41: Male paturon, retromarginal teeth: (0) inconspicuo (fig. 2.4A). (1) evident (fig. 2.4B). (2) different size (fig. 2.4I). COMMENTS: The character is scored (0) in some species of *Anasaitis* (e.g. *A. venatoria*, *A. arcuata*), within *Corticattus* and in some species of *Agobardus* (e.g. *A. gramineus*, *A. bahoruco*, *A. phylladiphilus*). The character is scored (1) in *Pensacola*, *Caribattus, Mexigonus*, *Pensacolatus* and *Cobanus*. The character is scored (2) in *Antillattus* and *Agobardus*.

Character 42: Male paturon, posterior surface depression: (0) absent. (1) present (ZM15-26; figs 88, 94). COMMENTS: *Heliophanus* (scored 1); *Ghelna* (scored 1); *Bythocrotus* (scored 1); *Petemathis* (scored 1); *Colyttus* (scored 1); *Lagnus* (scored 1); *Soesilarishius* (scored 1); and *Truncattus* (scored 1).

Character 43: Male paturon, mesal margin concave: (0) absent. (1) present (ZM15-29, figs 65–66). COMMENTS: *Pensacolatus*, (scored 1); *Anasaitis*, (scored 01); *Chapoda,* (scored 01); *Corythalia*, (scored 01); *Mexigonus*, (scored 01); *Omoedus*, (scored 1); *Pseudeuophrys*, (scored 1); *Servaea*, (scored 1); and *Tylogonus*, (scored 1).

Character 44: Male paturon, mesal cuticle: (0) similar to the rest. (1) rugose (fig. 2.4A). (AP09-113). COMMENTS: *Pensacolatus*, (scored 1), *Bryanattus*, (scored 1) and *Antillattus*, (scored 1) show differentiation between the mesal cuticle at the base of paturon to the rest of the paturon.

Character 45: Male paturon, fang groove length to base of paturon width ratio. (0) less longer than wide (fig. 2.4A). (1) as longer as wide or slightly longer than wide (usually 0.2x to 0.5x longer than wide) (fig. 2.4B). (2) 1.0x-2.0x or longer than wide (fig. 2.4D, F-G). States ordered. COMMENTS: The fang groove is a furrow-shaped space of the chelicera into which fits the fang (see Ubick *et al*. 2017). The fang groove can be reduced or developed, depending on fang size. *Corticattus*, (scored 0); *Compsodecta,* (scored 1); *Bythocrotus*, (scored 1); *Pensacola*, (scored 1); *Antillattus*, (scored 2); *Cobanus*, (scored 2); *Chalcolecta*, (scored 2); and *Parabathippus*, (scored 2).

Character 46: Male paturon, length to clypeus width ratio: (0) half of the clypeus (fig. 2.1B). (1) more than half or almost as long as clypeus (fig. 2.4F). (2) longer than clypeus (fig. 2.4D). (AP09-108). States ordered. COMMENTS: *Corticattus*, (scored 0); *Compsodecta,* (scored 1); *Bythocrotus*, (scored 1); *Pensacola*, (scored 1); *Antillattus*, (scored 2); *Cobanus*, (scored 2); *Chalcolecta*, (scored 2); and *Parabathippus*, (scored 2).

Character 47: Male paturon, projecting: (0) downwards (fig. 2.1A, E). (1) obtuse angle (fig. 2.1 G-H). (2) forwards (fig. 2.1C). The projection of the chelicerae refers to the angle (90º, approximately 100º, and 180º) that this forms in relationship to the carapace. COMMENTS: *Cobanus,* (scored 2); *Antillattus,* (scored 2); *Bryanattus mandibularis* **comb. nov.**, (scored 1); *B. keyserlingi* **comb. nov.**, (scored 1); and *Truncattus,* (scored 0).

Character 48: Male paturon, sexual dimorphism: (0) absent. (1) present. (AP09-118). COMMENTS: Álvarez-Padilla *et al*. 2009 referred to the paturon length as sexually dimorphic. However, the length is not the only way in which sexual dimorphism can be demonstrated. We also included as sexual differences the shape of the paturon and the presence or absence of a mastidion. *Antillattus*, (scored 1): males with long paturon and mastidion; *Bryanattus,* (scored 1): males with long paturon and mastidion or with short paturon and mastidion; *Parabathippus,* (scored 1); and *Cobanus,* (scored 1): males with long paturon.

Character 49: Male paturon, anteromesal mastidion: (0) absent. (1) present. (fig. 2.3A-C) (ZM15-27). COMMENTS: Zhang and Maddison (2015) encode the character as presence or absence of an anterior surface projection. The anterior surface projection is known as a mastidion in the literature (Ubick *et al*. 2017). The mastidion is observed within Amicoida and *Saltafresia*. Like the tooth homology proposal in Azevedo *et al*. (2018), mastidion were separated into serially homologous structures. We wanted to establish homology among each individual tooth based on topological equivalence criteria. The paturon was divided into three topological regions (anterior, mesal and posterior), and two views (ectal and mesal). Anterior: between base of fang and first third of the fang groove. Mesal: close to the end of fang groove. Posterior: close to the base of the paturon.

Character 50: Male paturon, mediomesal mastidion: (0) absent. (1) present.

Character 51: Male paturon, posteromesal mastidion: (0) absent. (1) present.

Character 52: Male paturon, anteroectal mastidion: (0) absent. (1) present.

Character 53: Male paturon, medioectal mastidion: (0) absent. (1) present.

Character 54: Male paturon, posteroectal mastidion: (0) absent. (1) present.

Character 55: Paturon, cuticle sexual dimorphism: (0) same texture in male and females. (1) different. (AP09-117).

Character 56: Male fang, base length to shaft length ratio: 0) shaft longer than fang base. (1) shaft as long as fang base; (2) fang base longer than shaft. States ordered. COMMENTS: Usually, the shaft is longer than the fang base or approximately equal in size (see Ramírez 2014); however, in species with long fangs, the base of the fang is longer than the shaft. *Bryanattus,* (scored 2); *Antillattus,* (scored 2); and *Cobanus,* (scored 2).

Legs and spines

Character 57: Male leg: (0) 1st longer than 4st. (1) 4st longer than 1st. (ZM15-32).

Character 58: Male leg I, femur modified: (0) absent. (1) present. COMMENTS: Within our dataset, the character is scored (1) in some species of *Bryanattus*.

Character 59: Male leg I, fringe: (0) absent. (1) present (ZM15-34).

Character 60: Male leg II, fringe: (0) absent. (1) present (ZM15-35).

Character 61: Male leg III, fringe: (0) absent. (1) present (ZM15-36).

Character 62: Female leg, tibia I ventral macroseta number (fig. 2.5): (0) 2-2. (1) 2-2-2. (2) 2-2-2-2 or more. States ordered. (ZM15-38)

Character 63: Male leg, tibia I ventral macroseta number (fig. 2.5): (0) 0. (1) 2-2. (2) 2-2-2. (3) 2-2-2-2 or more. States ordered. (ZM15-39)

Character 64: Female leg, metatarsus I ventral macroseta number (fig. 2.5): (0) 2-2. (1) 2-2-2. (2) 2-2-2-2. States ordered. (ZM15-40)

Character 65: Male leg, metatarsus I ventral macroseta number (fig. 2.5): (0) 2-2. (1) 2-2-2. (2) 2-2-2-2. States ordered. (ZM15-41)

2.1.7.1 *Abdomen*

A generalized abdominal segment is delimited posteriorly by a ventral furrow, which extends to a pair of apodemes with dorsoventral and longitudinal segmental muscles (see Purcell 1910). The epigastric area corresponds with the second abdominal segment, between the pedicel and the epigastric furrow (See Ramírez (2014), fig. 98D). This region bears the anterior book lungs,

the female genitalia and the male epiandrum. The third abdominal segment, here referred to as the postepigastrium, extends between the epigastric furrow and the spiracles of the posterior respiratory system (See Ramírez 2014, fig. 98C). It contains the posterior book lungs or transformations thereof. The fourth and fifth segments bear the spinnerets.

Character 66: Postepigastrium, male pre-spiracular bump: (0) absent. (1) present (fig. 2.6F-G). (ZM15-44). COMMENTS: The pre-spiracular bump was first documented by Zhang and Maddison (2015), but those observations were not reliable for documenting variation (e.g. hair tufts and bump shape). The bump is easy to detect with transmitted light. This character is reliably scored and separates the genera *Antillattus* and *Pensacolatus*. *Bryanattus,* (scored 1); *Antillattus,* (scored 1); *Cobanus,* (scored 1); *Sidusa,* (scored 1); and *Petemathis,* (scored 1).

Character 67: Postepigastrium, male pre-spiracular bump width/ ALS width: (0) as wide as ALS (fig. 2.6, F). (1) approximately 2x wider than ALS. COMMENTS: *Antillattus,* (scored 1); *Cobanus,* (scored 1); and *Petemathis,* (scored 1), *Bryanattus,* (scored 0); and *Sidusa,* (scored 0).

Character 68: Postepigastrium, male pre-spiracular hair tufts: (0) absent. (1) present (fig. 2.6, H-I). COMMENTS: *Antillattus,* (scored 1); *Cobanus,* (scored 1); *Petemathis,* (scored 1); and *Sidusa,* (scored 1).

2.1.7.2 *Male palp* (fig. 2.7, A-C)

The palpal coxae are expanded, forming the endites which bear a distal-lateral serrula (see Ramírez 2014). For many species, the femur and patella may have one or more processes, of which the most commonly found are the ventral basal, the ventral median and the ventral apical (fig. 2.9; 2.10) processes. The tibiae have a retrolateral process (retrolateral tibial apophysis, **RTA**). Other apophyses included the prolateral process (**PTA**), the ventral apical, the middle or the basal (**VaTA**, **VmTA** and **VbTA**).

In the Antillattus clade as well as in other jumping spiders (see Edwards, 2015), the basal hematodochae (**BH**) originates in the alveolus of the cymbium; it is large, coiled and connected to the subtegulum. At its distal end, the basal hematodochae attaches among the transverse ridges of the subtegulum. The middle hematodochae (**MH**) wraps around the subtegulum through which the spermophora passes. The distal hematodochae (**DH**) are pleated and may expand considerably (see Maddison 1996; Edwards 2015; Zhang and Maddison 2015).

The spermophorae (**S**) emerge from the fundus (**Fu**) in the subtegulum (see Bodner and Maddison 2012; Edwards, 2015). They extend from the middle of the tegulum and form a

loop before reaching the proximal edge of the tegulum. The spermophorae continue as a retrolateral sperm duct loop (**rSDL**) that turns before reaching the distal edge to cross to the prolateral side of the tegulum, then turns distally along the prolateral side, all along the edge of (or in some cases, across the middle of) the embolic hematodochae. In some species, it is possible to see a prolateral sperm duct loop (**pSDL**). Finally, the spermophorae make a right angle turn into the embolus.

The salticid radix (**SR**) is usually well-developed. As in Edwards (2015), we argue that the term has not been correctly defined (see Ramírez 2014; Coddington 1990). The spermophorae surrounds it while passing through the embolic hematodochae. The "salticid radix" is more like a sclerite that surrounds the hematodochae just before the base of the embolus, and it is completely visible when the distal hematodochae (**DH**) are expanded. The tegulum (**T**) has a distal tegular lobe (**dTL**), and in some cases a proximal tegular lobe (**pTL**).

The embolic disc (**ED**) is an expanded basal region of the embolus commonly with an external sclerotized surface and an internal membranous surface. The embolic disc is not fused to the tegulum. The embolus (**E**) is moderately elongate to short, curved and arises from an embolic disc. The embolus is elongate in some genera (e.g. *Agobardus*) and usually curved in opposite direction from RTA (e.g. *Chapoda*) (fig. 2.8).

Character 69: Male palp, endite anterolateral cusp: (0) absent. (1) present (fig. 2.8, C, E-F). (ZM15-9). COMMENTS: The “cusp” is on the anterior-lateral edge of the endite. The character was originally coded to consider the smaller cusp; however, some species have a more developed cusp that is conspicuous (e.g. *Pensacola*). The re-coding of the character allowed us to establish a primary homology between the small cusp presented by Zhang and Maddison (2015) and the developed “cusp” observed in *Pensacolatus*. We also found that sometimes the “cusp” is only visible under a microscope. We divide the character proposed by Zhang and Maddison (2015) into two separate characters. The first codes only the presence or absence of the “cusp”, while the second codes its level of development (char. 70). *Corticattus* (scored 1); *Pensacola* (scored 1); *Antillattus* (scored 1); *Truncattus* (scored 1); *Bryanattus* (scored 1); *Amphidraus* (scored 1); *Coccorchestes* (scored 1); *Coryphasia* (scored 1); *Corythalia* (scored 1); *Ilargus* (scored 1); *Laufeia* (scored 1); *Leptathamas* (scored 1); *Maeota* (scored 1); *Mopiopia* (scored 1); *Naphrys* (scored 1); *Pseudeuophrys* (scored 1); *Saitis* (scored 1); *Saphrys* (scored 1); *Thyenula* (scored 1); *Viribestus* (scored 1); and *Zabkattus* (scored 1).

Character 70: Male palp, endite anterior-lateral cusp: (0) reduced (fig. 2.8, C). (1) developed (fig. 3.16, B). COMMENTS: *Corticattus* (scored 0); *Antillattus* (scored 0); *Truncattus* (scored 0); *Bryanattus* (scored 0); *Amphidraus* (scored 0); *Coccorchestes* (scored 0); *Coryphasia* (scored 0); *Corythalia* (scored 1); *Ilargus* (scored 0); *Laufeia,* (scored 0); *Leptathamas* (scored 0); *Maeota* (scored 0); *Mopiopia* (scored 0); *Naphrys* (scored 0); *Pseudeuophrys* (scored 0); *Saitis* (scored 0); *Saphrys* (scored 0); *Thyenula* (scored 0); *Viribestus* (scored 0); *Zabkattus* (scored 1); *Pensacola* (scored 1); and *Pensacolatus* (scored 1).

Character 71: Male palp, endites lateroanterior projection: (0) absent (fig. 2.8, B). (1) present (fig. 2.8, F). COMMENTS: The proximal lobe of the endite projects outwards and is wider than base (Fig 2.5, F). This projection is usually observed in males and should not be confused with the projection observed in *Compsodecta* (char. 72). *Antillattus* (scored 1); *Pensacola* (scored 1); and *Pensacolatus* (scored 1).

Character 72: Male palp, endites with a ventral bump: (0) absent. (1) present. COMMENTS: *Compsodecta* (scored 01).

Character 73: Palp, endite sexual dimorphism: (0) absent. (1) present (fig. 2.8, C, F).

Character 74: Male palp, femur: (0) straight (fig. 2.9, A-B). (1) slightly curved (Fig. 2.8, D). (2) curved (Fig. 2.8, F). (ZM15-50). COMMENTS: Zhang and Maddison (2015) coded the shape variation of the femur and considered two states (2014): 0) straight and (1) curved. These authors noted that in the lineages with long, developed male chelicerae, the palpal femora are usually also elongate and very curved (e.g. *Bathippus*, *Parabathippus, Canama*). However, the curvature of the femur can also be less pronounced (e.g. *Pensacola*, *Pensacolatus*, *Compsodecta*, *Sidusa*) or straight (e.g. *Corticattus, Truncattus*, *Popcornella*, *Agobardus*).

Character 75: Male palp, femur dorsal macrosetae: (0) no macrosetae. (1) 1 macroseta. (2) 2 macrosetae. (3) 3 macrosetae. (4) 4 macrosetae. (5) 5 macrosetae. (6) 6 macrosetae. (7) ≥ 8 macrosetae. (ZM15-51). States ordered.

Character 76: Male palp, patella and tibia length dorsally: (0) patella longer than tibia (fig. 2.9, D). (1) patella shorter or equal to tibia (fig. 2.9, C). (ZM15-53).

Character 77: Male palp, patellar apophysis (**PPA**): (0) absent. (1) present (fig. 2.10, C). (ZM15-60). COMMENTS: The patellar apophysis was used previously used as a character by Ramírez (2014: char. 310, figs. 140G, 157D, 163G). Zhang

and Madison (2015) refer to a protrusion on the prolateral side of the palpal patella that is sometimes armed with a large macroseta like in some species of *Thorelliola*. *Compsodecta* (scored 1); *Thorelliola* (scored 1); e.g. *Onomastus* (scored 1); *Aelurillus* (scored 1); and *Amycus* (scored 1).

Character 78: Male palp, tibia: (0) unmodified, the tibia is uniformly cylindrical or slightly wider distally (fig. 2.10, F). (1) modified, the tibia having keels or is expanded (fig. 2.10, C). COMMENTS: *Compsodecta* (scored 1); *Bythocrotus* (scored 1).

Character 79: Palp, tibia with modifications in addition to the RTA, VTA and PTA: (0) absent. (1) present (fig. 2.10, C, G).

Character 80: Male palp, tibia ventral apophysis (**VTA**): (0) absent. (1) present (fig. 2.10, A, C, E, G). (ZM15-48). The ventral apophysis character was originally proposed as a ventral bump by Zhang and Maddison (2015); however, we prefer to use the apophysis terminology following Ramírez (2014). According to the topological position, the lateral and ventral tibia apophyses can be separated into PTA, PvTA (topological variation of the PTA), RTA, RvTA (topological variation of the RTA), VTA, VdTA (topological variation of the VTA) and VpTA (topological variation of the VTA). We only consider the presence/absence of the VTA and any of its topological variations. Future studies should consider separating the different topological variants of the tibial apophysis. COMMENTS: *Compsodecta*, (scored 1) present VpTA and VdTA in addition to VTA; *Chapoda* (1896), (scored 1) the VTA is strongly modified and developed; *Pensacolatus*, (scored 01).

Character 81: Male palp, prolateral tibial apophysis (**PTA**): (0) absent. (1) present (fig. 2.10, C). (ZM15-61). COMMENTS: *Compsodecta*, (scored 1) present PvTA in addition to PTA; *Anasaitis*, (scored 01); *Bulolia*, (scored 1) slightly shorter than RTA; *Bythocrotus*, (scored 1) reduced; *Maeota*, (scored 01); *Popcornella*, (scored 01); *Soesilarishius*, (scored 01); *Thorelliola*, (scored 01).

Character 82: Male palp, retrolateral tibial apophysis (**RTA**): (0) long, finger-like (fig. 2.10, A, B, H). (1) short (fig. 2.10, E, I). (ZM15-55).

Character 83: Male palp, RTA: (0) direct ventrally (fig. 2.10, H). (1) straight (fig. 2.10, B). (2) direct dorsally (fig. 2.10, E). COMMENTS: *Pensacolatus*, (scored 1); *Popcornella*, (scored 0); *Caribattus*, (scored 1); *Mexigonus*, (scored 1); *Petemathis*, (scored 1); *Agobardus*, (scored 1); *Truncattus,* (scored 2).

Character 84: Hematodochae, distal hematodochae: (0) reduced (ZM-15, fig. 655). (1) developed (ZM-15, fig. 648-651). In jumping spiders, as in other groups, the copulatory bulb is formed by several sclerites articulated to each other via flexible or inflatable hematodochae (R14: fig. 139, C). The level of development of an unexpanded distal hematodochae in species without an embolic disc (e.g. *Popcornella*) is usually reduced compared to species with an embolic disc (e.g. *Agobardus* 1885). COMMENTS: *Pensacolatus*, (scored 1); *Popcornella*, (scored 0); *Caribattus*, (scored 1); *Mexigonus*, (scored 1); *Petemathis*, (scored 1); *Agobardus*, (scored 1); *Truncattus,* (scored 1).

Character 85: Tegulum, tegular reduction: (0) absent, the tegulum includes the spermophorae and articulates internally to the terminal hematodochae (fig. 2.11, G, H, I). (1) present, this character describes the articulation of the hematodochae with the tegulum outside of the sclerite (fig. 2.11, F). COMMENT: *Pensacola,* (scored 1).

Character 86: Tegulum, proximal tegular lobe (**pTL**): (0) absent (fig. 2.12, A-B, H). (1) present (fig. 2.12, C, E). (ZM15-47). COMMENTS: *Pensacolatus*, (scored 1); *Popcornella*, (scored 1); *Caribattus*, (scored 0); *Mexigonus*, (scored 1); *Petemathis*, (scored 1); *Agobardus*, (scored 0); *Truncattus*, (scored 1); *Compsodecta*, (scored 0); *Anasaitis*, (scored 01); *Bythocrotus*, (scored 0).

Character 87: Tegulum, tegular lobe over tibia (**pTL**): (0) less than half the tegulum width. (1) half the tegulum width (2) more than half the tegulum width. States ordered. COMMENTS: *Pensacolatus*, (scored 01); *Popcornella*, (scored 2); *Mexigonus*, (scored 0); *Petemathis*, (scored 1); *Truncattus*, (scored 2).

Character 88: Tegulum, proximal tegular lobe (**pTL**): (0) inconspicuo. (1) evident (fig. 2.12, C). (2) developed (fig. 2.12, E). States ordered. COMMENTS: *Pensacolatus*, (scored 01); *Popcornella*, (scored 1); *Mexigonus*, (scored 1); *Petemathis*, (scored 1); and *Truncattus*, (scored 2).

Character 89: Tegulum, distal tegular lobe (**dTL**): (0) absent (fig. 2.13, A). (1) present (fig. 2.13, G, I). The dPT was previously defined as a tegular shoulder by Zhang and Madison (2015) and referred to the small distal process at the retrolateral shoulder of the tegulum that is common in the Saitis clade. The “anterior tegular bulge” (Waldock 1995), “tegular shoulder” (Maddison, 1996), “anterior lamella” (Żabka and Pollard 2002) and “distal tegular lobe” (Richardson and Żabka 2007) have all been used for this character in the literature. According

to Edwards (2015), the tegular lobe within the TBD can be divided into the proximal prolateral lobe (pPL) and the proximal retrolateral lobe (pRL). Richardson and Żabka (2007) named three tegular processes: (1) the prolateral distal tegular lobe; (2) the dorsal distal tegular lobe; and (3) the ventral distal tegular lobe. We consider both the dorsal distal tegular lobe and the distal tegular lobe as dTL. In future studies, these characters should be coded separately. COMMENTS: *Pensacolatus*, (scored 1) without ventral distal tegular lobe; *Popcornella*, (scored 01); *Petemathis*, (scored 1) without ventral distal tegular lobe; *Truncattus*, (scored 1), without ventral distal tegular lobe; *Caribattus*, (scored 1); *Mexigonus*, (scored 1), without ventral distal tegular lobe; *Agobardus*, (scored 1), like a conductor; *Compsodecta*, (scored 1), like a conductor.

Character 90: Tegulum, distal tegular lobe (**dTL**) width/ tegulum width ratio: (0) a quarter. (1) half or more than half. COMMENTS: *Pensacolatus*, (scored 1); *Popcornella*, (scored 01); *Mexigonus*, (scored 0); *Petemathis*, (scored 1); *Truncattus*, (scored 1); *Caribattus*, (scored 0); *Agobardus*, (scored 1); *Compsodecta*, (scored 1).

Character 91: Spermophorae, prolateral sperm duct loop (**pSDL**): (0) absent. (1) present (fig. 2.11B). (ZM15-57). COMMENTS: *Amphidraus*, (scored 1); *Bulolia*, (scored 1); *Coccorchestes*, (scored 1) *Corticattus*, (scored 1); *Leptathamas*, (scored 1); *Neonella*, (scored 1); *Pensacola*, (scored 1); and *Xenocytaea*, (scored 1).

Character 92: Spermophorae, sperm duct loop on retrolateral side of bulb (**rSDL**): (0) absent. (1) present (fig. 2.11). (ZM15-56). Zhang and Maddison (2015) presented the sperm duct loop on the retrolateral side of the palp. Maddison and Hedin (2003) considered the rSDL an important character to distinguish euophryines from other Salticoida; however, a similar sperm duct loop is also present within Amycini, Dendryphantini and Ballini. Zhang and Maddison (2015) concluded that this could be the result of convergent evolution. COMMENTS: *Agobardus*, (scored 1), *Amphidraus*, (scored 1); *Bulolia*, (scored 0); *Coccorchestes*, (scored 0); *Corticattus*, (scored 0); *Leptathamas*, (scored 1); *Neonella*, (scored 0); *Pensacola*, (scored 1); and *Xenocytaea*, (scored 0).

Character 93: Spermophorae, retrolateral sperm duct loop width (**rSDL**): (0) less than half of bulb width (fig. 2.11, B). (1) about half of bulb width (fig. 2.11, F). (2) more than half of bulb width (fig. 2.11, G-I). (ZM15-58). States ordered.

COMMENTS: *Agobardus*, (scored 12); *Caribattus*, (scored 2); *Compsodecta*, (scored 12); *Pensacola*, (scored 1); *Mexigonus*, (scored 12); and *Sidusa*, (scored 0).

Character 94: Spermophorae, retrolateral sperm duct loop shape (**rSDL**): (0) open S-like (fig. 2.11, C). (1) closed S-like (fig. 2.11, B). COMMENTS: *Pensacolatus*, (scored 1).

Character 95: Spermophorae, coiled near the embolic division: (0) absent. (1) present (fig. 2.11, B, F). COMMENTS: *Coryphasia*, (scored 1); *Corticattus*, (scored 1) *Pensacola*, (scored 1); and *Sidusa*, (scored 1).

Character 96: Embolic division, salticid radix: (0) absent. (1) present. (ZM15-71). Zhang and Maddison (2015) defined the salticid radix as a separate from sclerite on the distal hematodochae between the embolic disc and the tegulum. The region was previously called the radix by Logunov and Cutler (1999) and the distal division of the tegulum by Edwards (2015). Ramírez (2014) defined the radix as an intermediate sclerite between the embolus and tegulum, with the spermaphor passing through it. We use the term salticid radix proposed by Logunov and Cutler (1999) and re-coded the character proposed by Zhang and Maddison (2015) following Sereno (2007). COMMENTS: *Agobardus*, scored (1); *Amphidraus*, (scored 0); *Anasaitis*, scored (1); *Bathippus*, (scored 1); *Bulolia*, (scored 1); *Corticattus*, (scored 1); and *Pensacola*, (scored 1).

Character 97: Embolic division, salticid radix: (0) fused (fig. 2.13, A). (1) free (fig. 2.13, B). (ZM15-71). COMMENTS: COMMENTS: *Heliophanus*, (scored 0); and *Tylogonus*, (scored 0).

Character 98: Embolic division, embolus coil: (0) absent. (1) present (fig. 2.13, B-I). (ZM15-46). Prószyński (1976) suggested that a curved or coiled embolus is an important character to define euophryines (see, Maddison 2015; Maddison and Hedin 2003; Zhang and Maddison 2015). However, some genera in this group do not have a curved embolus (e.g. *Anasaitis*, *Tylogonus, Popcornella*). We re-coded the character proposed by Zhang and Maddison (2015) as two different characters following Sereno (2007). COMMENTS: *Agobardus*, (scored 1); *Amphidraus*, (scored 1); *Anasaitis*, (scored 0); *Antillattus*, (scored 1); *Bathippus*, (scored 1); *Bulolia*, (scored 1); *Bythocrotus*, (scored 1); *Caribattus*, (scored 1); *Chalcoscirtus*, (scored 1); *Chapoda*, (scored 1); *Compsodecta*, (scored 1); *Corticattus*, (scored 1); and *Popcornella*, (scored 0).

Character 99: Embolic division, embolus coil: (0) equal or less than half a circle (fig. 2.13, B). (1) more than half a circle but no more than one and a half circles (fig. 2.13, E); (2) more than one and a half circles (fig. 2.13, H). (ZM15-46). States ordered. COMMENTS: *Agobardus*, (scored 1); *Pensacola*, (scored 0); *Caribattus*, (scored 0); *Mexigonus*, (scored 0); *Bythocrotus*, (scored 0); *Compsodecta*, (scored 0); *Corticattus*, (scored 1); *Coryphasia*, (scored 01); and *Sidusa*, (scored 2).

Character 100: Embolic division, embolus: (0) close to the tegulum (fig. 2.13, D). (1) distant from the tegulum (fig. 2.13, F). Within the salticids that have a coiled embolus, some lineages have an embolus close to the tegulum (e.g. *Agobardus*; *Corythalia*, *Antillattus*, *Corticattus*, *Coryphasia*), while other lineages have embolus further from the embolus (e.g. *Bryanattus*; *Truncattus*, *Pensacola*, *Pensacolatus*, *Petemathis*).

Character 101: Embolic division, plane of spiral of embolus: (0) parallel to longitudinal axis of the bulb (fig. 2.13, D, H). (1) perpendicular to longitudinal axis of the bulb (fig. 2.13, G). (ZM15-64). COMMENTS: *Agobardus*, (scored 1); *Bythocrotus*, (scored 0); and *Antillattus*, (scored 0).

Character 102: Embolic division, embolus origin: (0) 12 o'clock. (1) 2 and ≤3 o' clock. (2) >4 and <5 o' clock. (3) >5 and ≤8 o'clock. (4) >8 and 12 o'clock. COMMENTS: *Agobardus*, (scored 3); *Pensacola*, (scored 2); *Caribattus*, (scored 2); *Mexigonus*, (scored 2); *Bythocrotus*, (scored 1); *Compsodecta*, (scored 23); *Corticattus*, (scored 1); and *Sidusa*, (scored 0).

Character 103: Embolic division, embolus length: (0) as long as embolic disc or 1.1x longer than embolic disc. (1) 1.5x longer than embolic disc. States ordered. COMMENTS: *Agobardus*, (scored 1); *Antillattus*, (scored 0); *Pensacola*, (scored 2); *Caribattus*, (scored 1); *Mexigonus*, (scored 1); *Bythocrotus*, (scored 0); *Compsodecta*, (scored 1); *Corticattus*, (scored 2); and *Sidusa*, (scored 2).

Character 104: Embolic division, embolic disc (**ED**): (0) absent (fig. 2.13, A). (1) present (fig. 2.13, B-1). (ZM15-66) (fig. 2.8; fig. 2.9). Zhang and Maddison (2015) referred to the embolic disc as expanded sclerite at the end of the distal hematodochae where the embolus usually originates (e.g. *Antillattus*). Ramírez (2014) encoded the embolic disc as the embolar basal process (char: 352) to refer to a sclerotized process that is continuous with the embolus. Within euophryines, the embolic disc is very reduced or even completely lost (e.g. *Anasaitis*,

Popcornella). COMMENTS: *Amphidraus*, (scored 1); *Bulolia*, (scored 1); *Corticattus*, (scored 1); *Pensacola*, (scored 1); and *Popcornella*, (scored 0).

Character 105: Embolic division, embolic disc (**ED**) width: (0) less than half of the tegulum. (1) half of the tegulum. (2) more than half of the tegulum. States ordered. COMMENTS: *Antillattus*, (scored 1); *Corticattus*, (scored 2); *Pensacola* (1885), (scored 0); and *Petemathis*, (scored 0).

Character 106: Embolic division, lamella: (0) absent. (1) present (fig. fig. 2.13, B-C). (ZM15-65). Zhang and Maddison (2015) referred to an independent process along the embolus found in several lineages. The lamella proposed by Zhang and Maddison (2015) has been previously called a "conductor" in the literature (Davies and Żabka 1989; Bodner 2002). However, conductor is a term that refers to a non-homologous structure (see Coddington 1990; Ramírez 2014). Ramírez (2014) defined the conductor as a typically semi-membranous sclerite, which may be partially or totally sclerotized or hyaline, often with a canal or depression fitting part of the embolus. He concluded that the conductor is a tegular sclerite that is occasionally associated with the embolus. Edwards (2015) stated that the conductor within freyines is a distal palpal apophysis, ventral to the embolus. This seems to refer to the same thing as in Zhang and Maddison (2015) and clearly contradicts Ramírez (2014). Here, we use the term lamella proposed by Zhang and Maddison (2015) to avoid confusion. COMMENTS: *Colyttus*, (scored 1); *Coryphasia*, (scored 01); *Neonella*, (scored 1); *Pristobaeus*, (scored 1); *Saitis*, (scored 1); *Saphrys*, (scored 1); *Cobanus,* (scored 1); and *Viribestus*, (scored 1).

Character 107: Embolic division, **ED** bump: 0) absent. 1) present. COMMENTS: *Bryanattus*, (scored 01).

2.1.7.3 *Female genitalia* (fig. 2.7, E-D)

Zhang and Maddison (2015) introduced the term 'window of the epigynum' (**WE**) to define the membranous space that connects the copulatory openings (**Co**). The window of the epigynum likely evolved as an adaptation of the embolic disc (**ED**) or embolic base (**EB**). The WE is usually accompanied by a spiral guide that can be long (e.g. *Sidusa*) or short (e.g. *Cobanus*). Additionally, species with a ventral tibial apophysis (**VTA**) have epigynal coupling pockets (**ECP**) (e.g. *Chapoda*, *Cobanus*).

The copulatory opening (**CO**) is followed by a stretch of copulatory duct (**CD1**). The secondary spermathecae (**SS**) or accessory gland (**AG**) follows the first section of the duct and may or may not be developed. Between the secondary spermathecae (**SS**) and the primary spermathecae (**PS**), there is a second section of the copulatory duct (**CD2**) that may or may not be developed. The fertilization ducts (**FD**) connects the primary spermathecae to the uterus externus (see Ramírez 2014, fig. 169A). Bennett's gland (**BG**) is found in the fertilization duct and extends internally into the primary spermathecae.

Character 112: Epigynum, copulatory opening as a pocket: (0) absent. (1) present (fig. 2.38, F; 2.39, G; 2.40, E; 2.43, E; 2.44, E). Some Old-World taxa, such as the genera *Chinattus*, *Habrocestoides* and *Heliophanus*, have a dorsally-opening coupling pocket (Maddison et al. 2008; Edwards, 2015). The pocket is also present within freyines and euophryines (Edwards, 2015; Bodner, 2002). COMMENTS: *Cobanus*, (scored 1).

Character 113: Epigynum, copulatory opening with spiral guide: (0) absent (fig. 2.6, A). (1) present (fig. 2.6, B-E). (ZM15-77). The spiral guide is observed in species with a WE. This character appears in the euophryines and some freyines (Edwards 2015; Maddison 2015; Zhang and Maddison 2015). Zhang and Maddison (2015) encoded the character for the first time as present or absent. We add a new character related to the development of the spiral guide (char. 114). COMMENTS: *Agobardus*, (scored 1); and *Popcornella*, (scored 0).

Character 114: Epigynum, spiral guide: (0) reduced (fig. 2.6, D-E). (1) developed (fig. 2.6, B-C). The development of the spiral guide is a character correlated with the length of the embolus and its number of turns. Species with a short embolus have a reduced spiral (e.g. *Pensacolatus*, *Compsodecta*, *Naphrys*). COMMENTS: *Corticattus*, (scored 1); *Pensacola*, (scored 1); and *Sidusa*, (scored 1).

Character 115: Epigynum, position of copulatory opening (**CO**) in relationship to vulva: (0) anterior; (1) median. (2) posterior. (ZM15-72). States ordered. COMMENTS: *Agobardus*, (scored 01); *Cobanus*, (scored 2); *Pensacola*, (scored 12); and *Sidusa*, (scored 1).

Character 116: Epigynum, CD1: (0) less than CD2 length (fig. 2.16, A, D). (1) as long as CD2 length (fig. 2.16, C). (2) longer than CD2 length (fig. 2.16, B). States ordered. Within entelegyne spiders, the copulatory duct is usually divided into two sections: (1) copulatory opening/secondary spermathecae; (2) secondary

spermathecae/primary spermathecae. The first section of the copulatory duct (CD1) begins at the copulatory opening and is usually flexible, unsclerotized and correlated in shape and length with the embolus (Ramírez 2014). We code the length of CD1 as a neomorphic character (Sereno 2007). COMMENTS: *Agobardus*, (scored 01); *Corticattus*, (scored 1); *Pensacola*, (scored 1); *Popcornella*, (scored 0); and *Sidusa*, (1895), (scored 2).

Character 117: Epigynum, secondary spermathecae, size, relative to primary spermathecae: (0) less than half of primary spermathecae. (1) about half of primary spermathecae; (2) more than half of primary spermathecae. (R14-373). States ordered. Ramírez (2014) considered the character applicable when the secondary spermathecae have a lumen distinguishable from the copulatory duct or primary spermatheca. Within Salticidae, Ramírez scored (1) in *Lyssomanes*, *Hispo* and *Plexippus*. COMMENTS: *Agobardus*, (scored 0); *Corticattus*, (scored 2); *Pensacola*, (scored 1); *Popcornella*, (scored 0); and *Sidusa*, (scored 1).

Character 118: Epigynum, copulatory duct receptacle: (0) None, copulatory duct lumen not expanded in a receptacle separate from the primary and secondary spermathecae (fig, 2.16, A and C; fig. 2.17, A, B and E). (1) copulatory duct widened, forming a defined chamber between the copulatory opening and the primary spermathecae that differs from the secondary spermathecae (fig, 2.16, D; fig. 2.17, C, D and F). (R14-374). Within euophryines and other related groups, the secondary spermathecae and copulatory duct receptacle may be contiguous; however, both are clearly distinguished with conventional microscopy and SEM. COMMENTS: *Agobardus*, (scored 0); *Antillattus*, (scored 1) *Mexigonus*, (scored 0); *Compsodecta*, (scored 1); *Cobanus*, (scored 1); and *Pensacolatus*, scored (1).

Character 119: Epigynum, copulatory duct receptacle: (0) narrower than the primary spermathecae (fig 2.17, D). (1) as wide as the primary spermathecae (fig 2.17, C). COMMENTS: *Antillattus*, (scored 1); *Compsodecta*, (scored 0); *Cobanus*, (scored 0); and *Pensacolatus*, scored (1).

Character 120: Epigynum, copulatory duct receptacle: (0) developed anteriorly the primary spermathecae (fig. 2.16, D). (1) developed in front of the primary spermathecae (fig. 2.17, C). (2) developed lateral of the primary spermathecae (fig. 2.17, D). COMMENTS: *Antillattus*, (scored 1); *Bythocrotus*, (scored 2); *Caribattus*,

(scored 0); *Compsodecta*, (scored 0); *Cobanus*, (scored 0); and *Pensacolatus*, scored (1).

Character 121: Epigynum, copulatory duct / primary spermathecae connection: (0) internal position relative to primary spermathecae. (1) anteriorly primary spermathecae. (2) external position relative to primary spermathecae. States ordered. COMMENTS: *Agobardus*, (scored 0); *Antillattus*, (scored 1); *Bythocrotus*, (scored 1); *Caribattus*, (scored 1); *Compsodecta*, (scored 12); *Cobanus*, (scored 0); *Pensacolatus*, (scored 01); and *Popcornella*, (scored 01).

Character 122: Epigynum, primary spermathecae shape: (0) spherical or ovoid. (1) kidney-shaped. (2) narrow coil. (ZM15-81).

Character 123: Epigynum, primary spermathecae: (0) near one another (fig. 2.16, D). (1) slightly separated (fig. 2.17, D). (2) separated by approximately one diameter of a spermatheca. COMMENTS: *Ghelna*, (scored 0); *Agobardus*, (scored 01); *Antillattus*, (scored 1); *Bythocrotus*, (scored 2); *Bryanattus*, (scored 012) *Caribattus*, (scored 0); *Compsodecta*, (scored 0); *Cobanus*, (scored 1); *Pensacola*, (scored 0); *Pensacolatus*, (scored 01); *Popcornella*, (scored 1); and *Mexigonus*, (scored 0).

Character 124: Epigynum, fertilization duct at the base of the copulatory duct: (0) absent. (1) present. (ZM15-73). The position of the copulatory duct was used by Álvarez-Padilla *et al.* (2009), Álvarez-Padilla and Hormiga (2011), Ramírez (2014), Zhang and Maddison (2015) and Azevedo *et al.* (2018). Álvarez-Padilla et al. (2009) and Álvarez-Padilla and Hormiga (2011) coded the position of the copulatory duct as (0) posterior; (1) anterior. Ramírez (2014) encodes it as (0) posterior, close to the epigastric furrow, and (1) far away from the epigastric furrow. Both are similar to the definition proposed by Zhang and Maddison (2015). We prefer to use the proposal of Zhang and Maddison (2015). COMMENTS: *Lyssomanes* (scored 1); *Hispo* (scored 0); *Ghelna* (scored 1); *Agobardus*, (scored 1); *Antillattus*, (scored 1); *Bythocrotus*, (scored 1); *Caribattus*, (scored 1); *Compsodecta*, (scored 1); *Cobanus*, (scored 01); *Pensacolatus*, (scored 1); and *Popcornella*, (scored 1).

Character 125: Epigynum, Bennett's gland insertion: (0) depressed or superficial (fig. 2.17, A-E). (1) everted (fig. 2.17, F). Bennett's gland was encoded by Ramírez (2014) to refer to the pores documented by Bennett (1992) and referred by Forster (1970). COMMENTS: *Hispo* (scored 0); *Ghelna* (scored 0);

Agobardus, (scored 01); *Antillattus*, (scored 0); *Bythocrotus*, (scored 0); *Compsodecta*, (scored 0); *Cobanus*, (scored 0); *Pensacolatus*, (scored 1); and *Popcornella*, (scored 0).

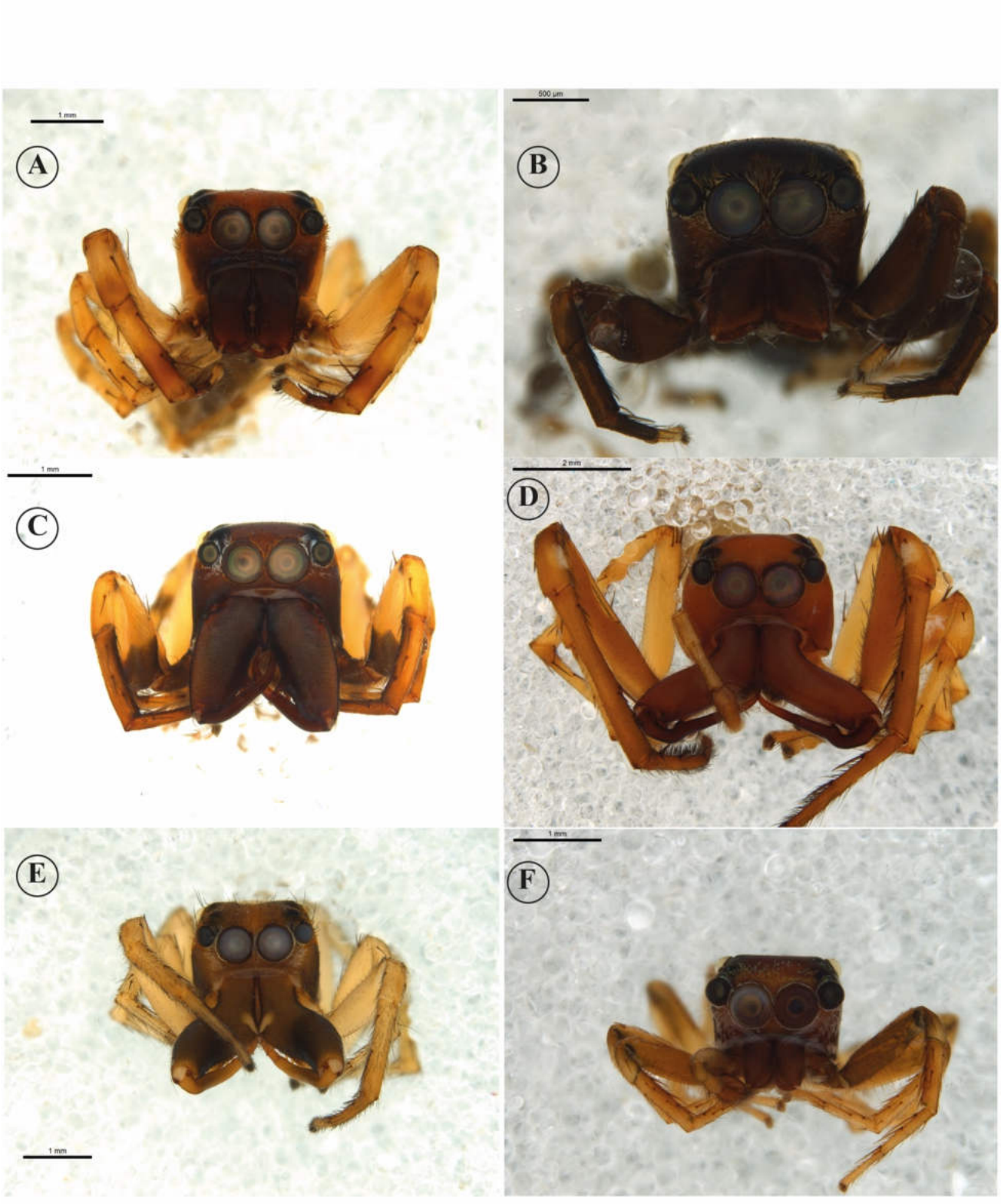

Figure. 2.0. Male carapace, frontal view. A, *Compsodecta festiva*. B, *Agobardus*. C, *Bryanattus keyserlingi* **comb. nov.**. D, *Cobanus mandibularis* **comb. nov.**. E, *Antillattus cambridgei*. F, *Sidusa*.

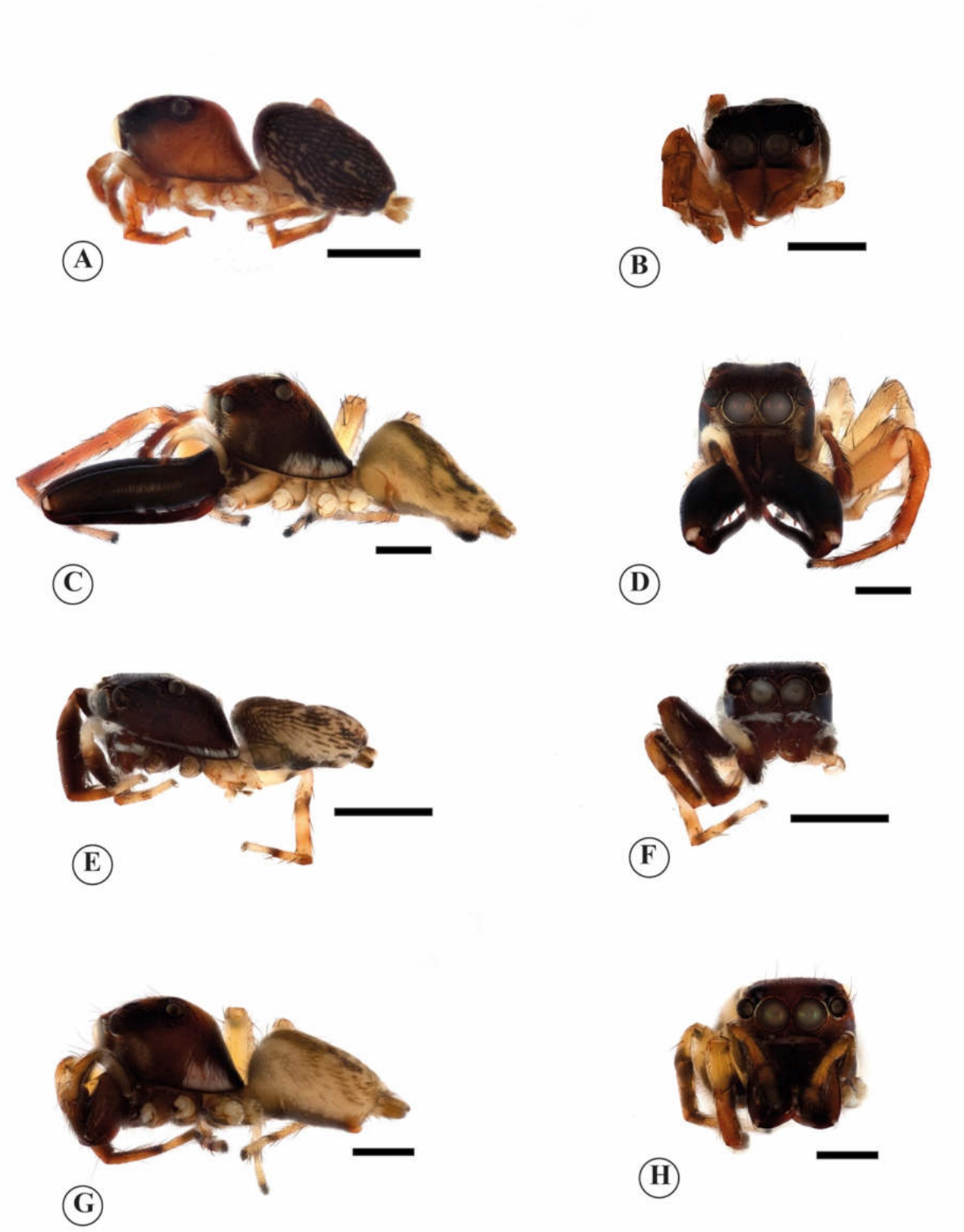

Figure. 2.1. Male habitus, lateral and frontal view. A-B, unknown euophryine. C-D, *Antillattus cambridgei*. E-F, *Truncattus martii* **sp. nov.**. G-H, *Bryanattus keyserlingi* **comb. nov.**.

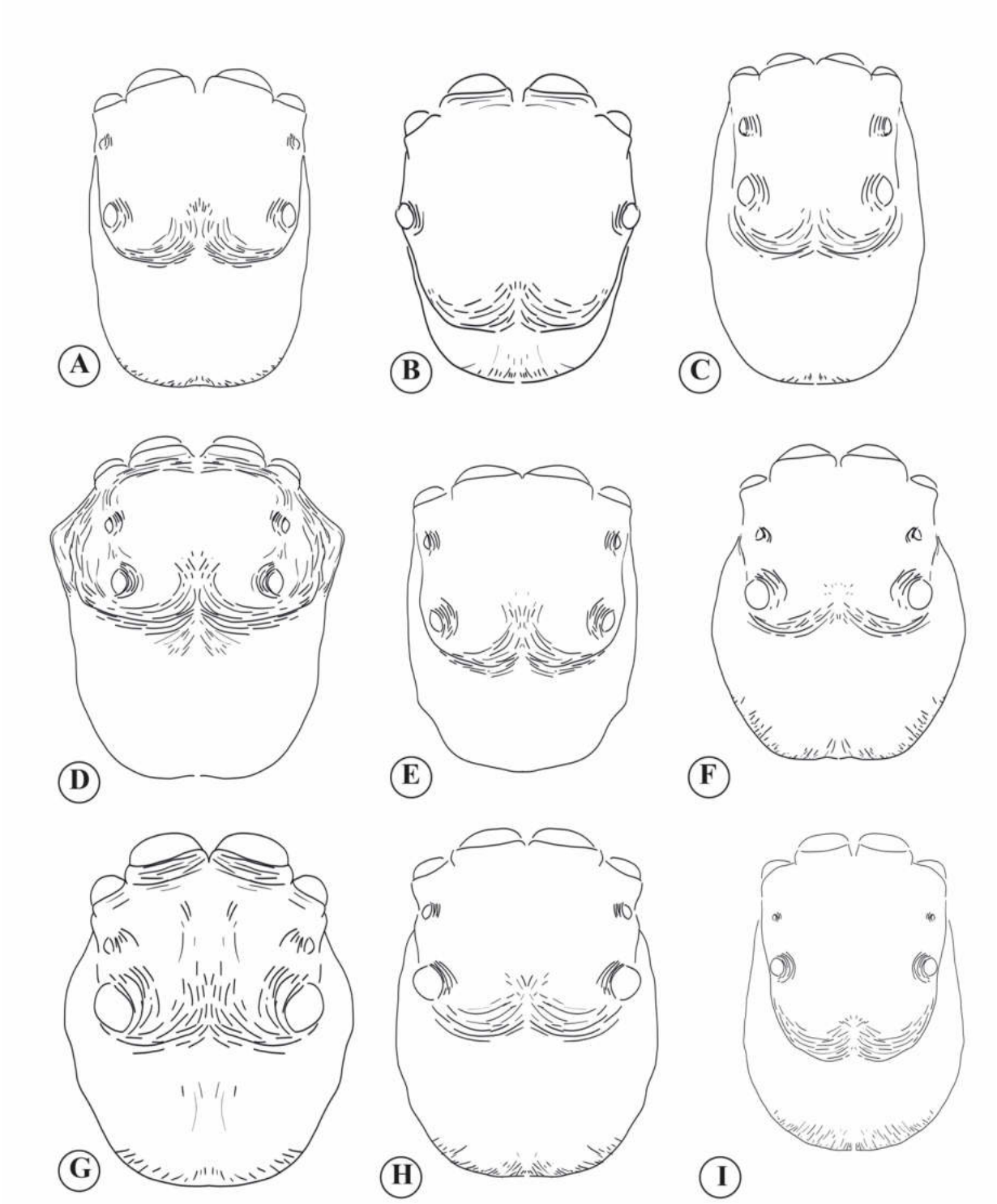

Figure. 2.2. Male carapace, dorsal view. A, *Truncattus flavus*. B, *Pensacola signata*. C, *Corticattus latus*. D, *Agobardus anormalis montanus*. G. *Cobanus mandibularis* **comb. nov.**. E, *Sidusa* sp. F, *Antillattus gracilis*. H, *Petemathis portoricensis*. I. *Mexigonus arizonensis*.

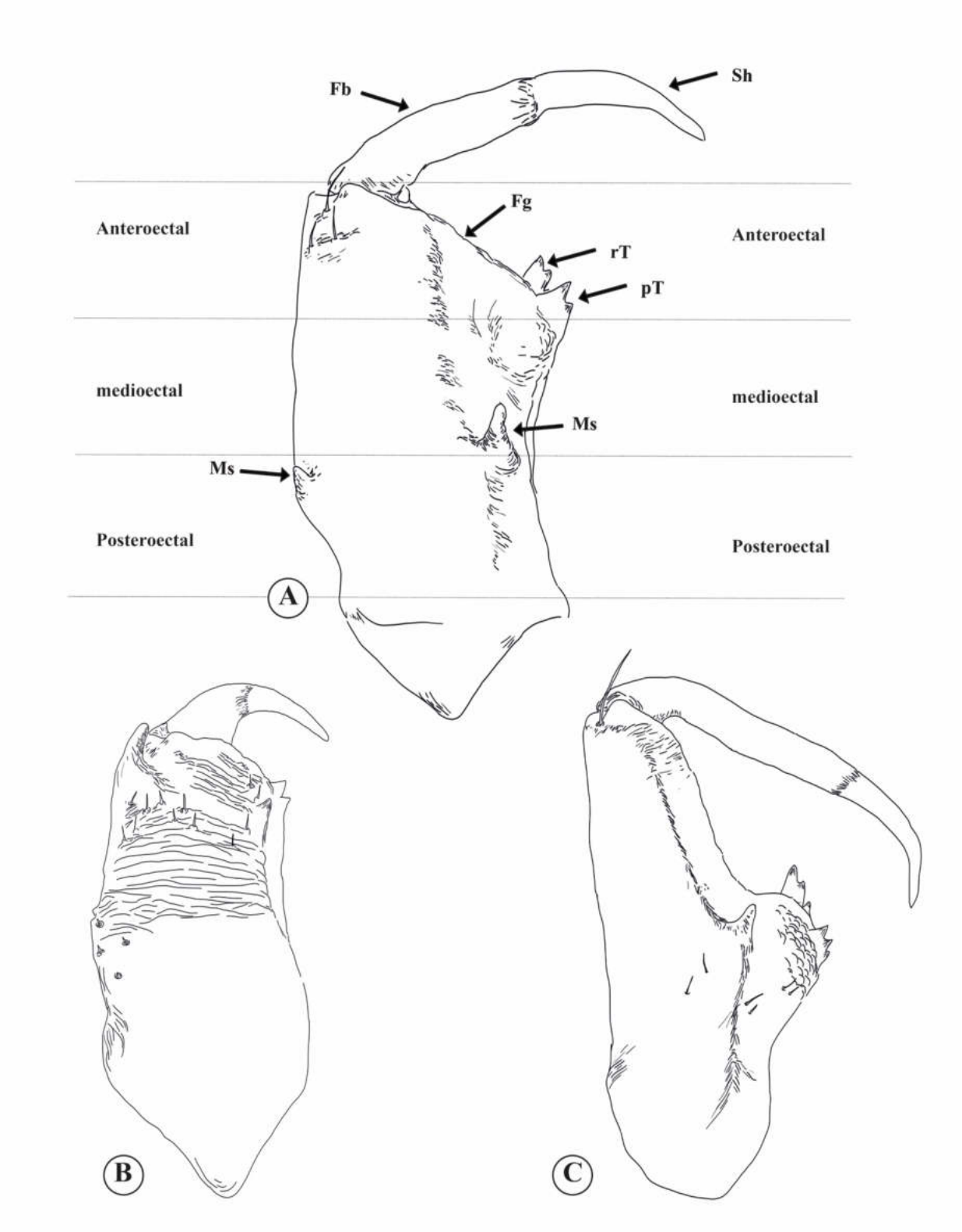

Figure. 2.3. Male chelicerae, frontal view. A, *Bryanattus keyserlingi* **comb. nov.**. B, *Compsodecta darlingtoni*. C, *Antillattus cubensis*.

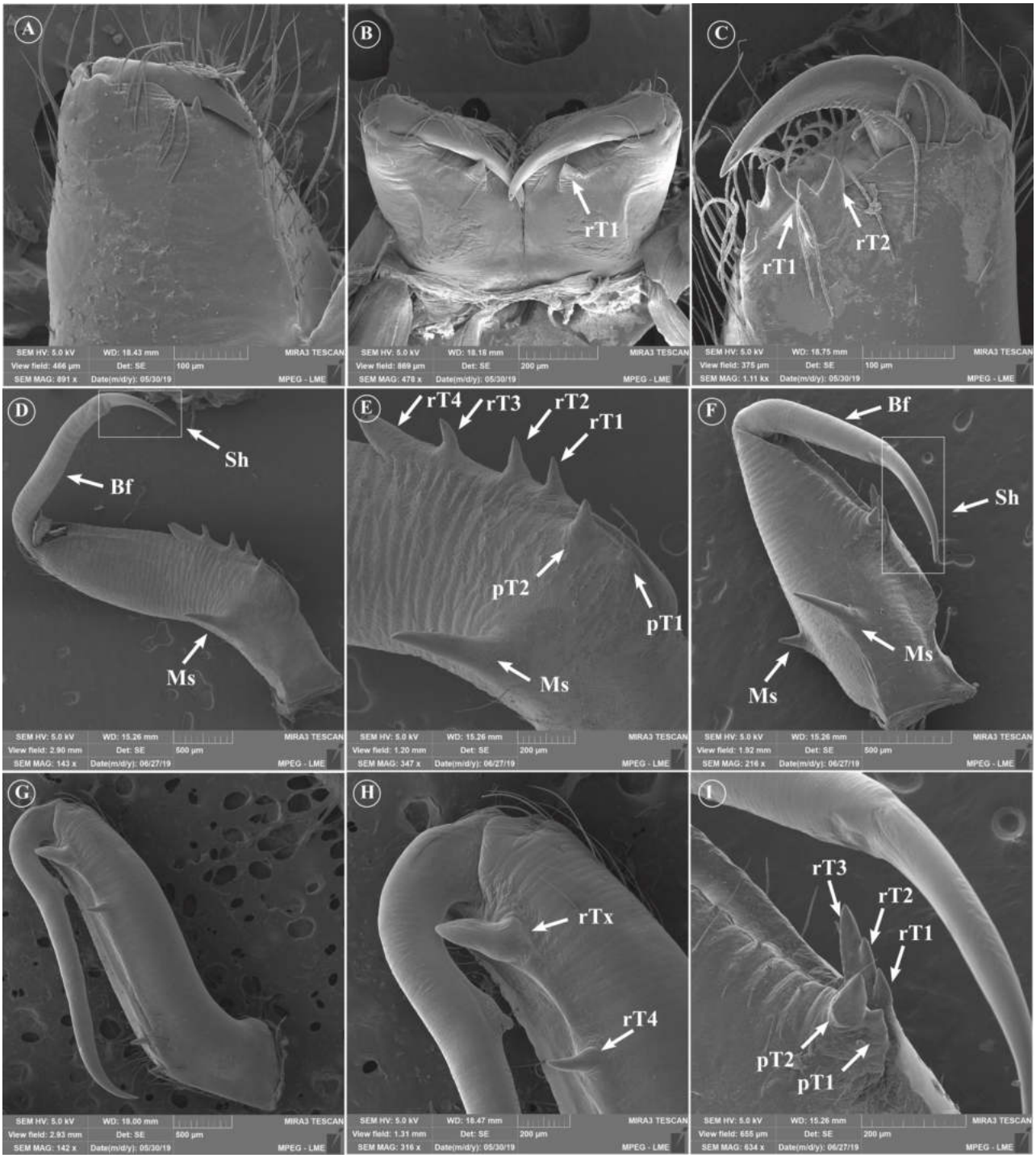

Figure. 2.4. Scanning electron micrographs of chelicerae. A, Female of *Anasaitis*, promarginal view. B, Male of unknown euophrine, retromarginal view. C, Female of *Sidusa*, retromarginal view. D-E, Male of *Antillattus cambridgei*, promarginal view. F and I, *Bryanattus keyserlingi* **comb. nov.**, promarginal view. G-H, Male of *Cobanus manidibularis* **comb. nov.**, retromarginal view.

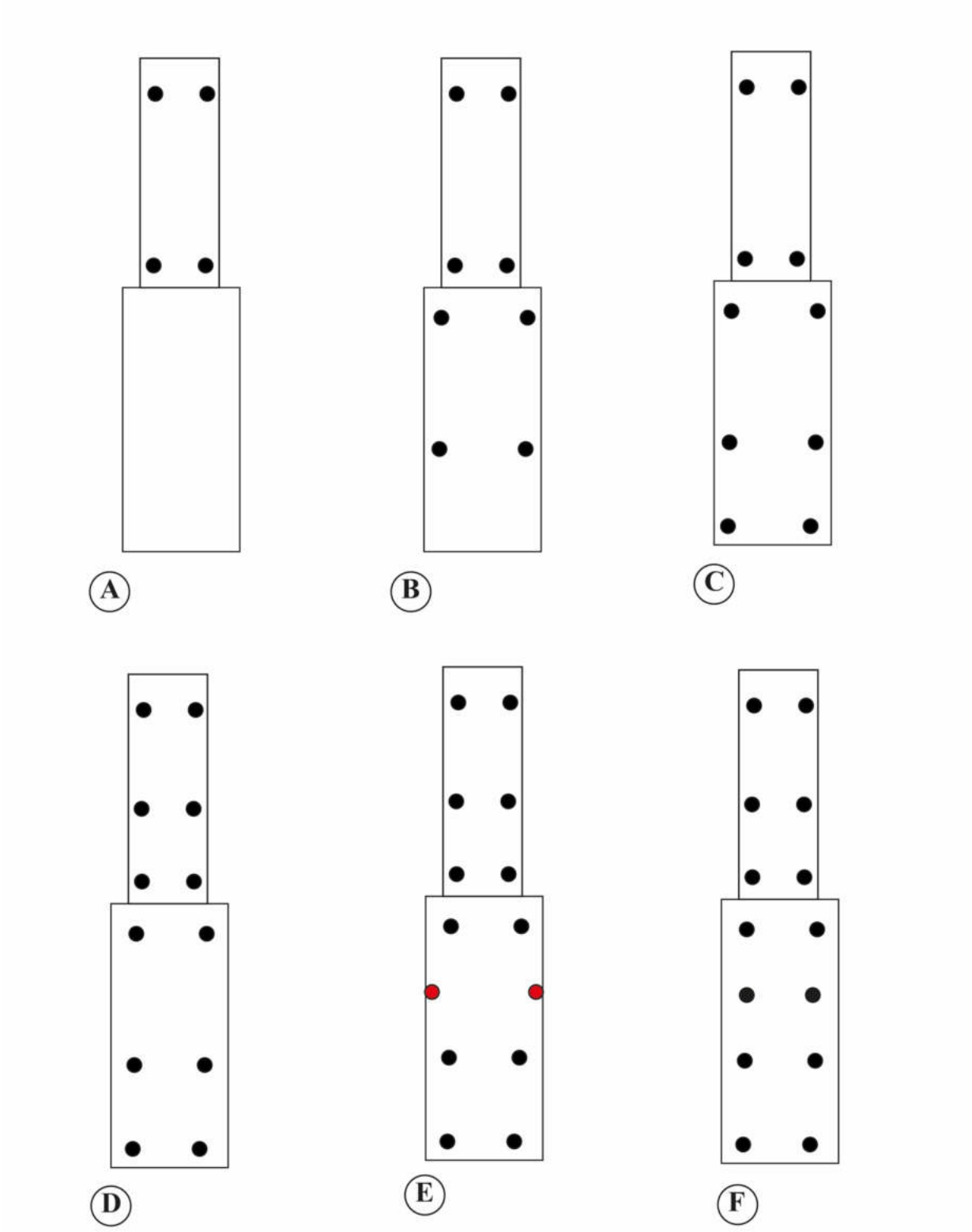

Figure. 2.5. Tibia and metatarsus leg spination, ventral view. A-B, *Corticattus latus*. C, *Popcornella yunque*. D, *Agobardus anormalis montanus*. E, *Compsodecta darlingtoni*. F. *Cobanus extensus*.

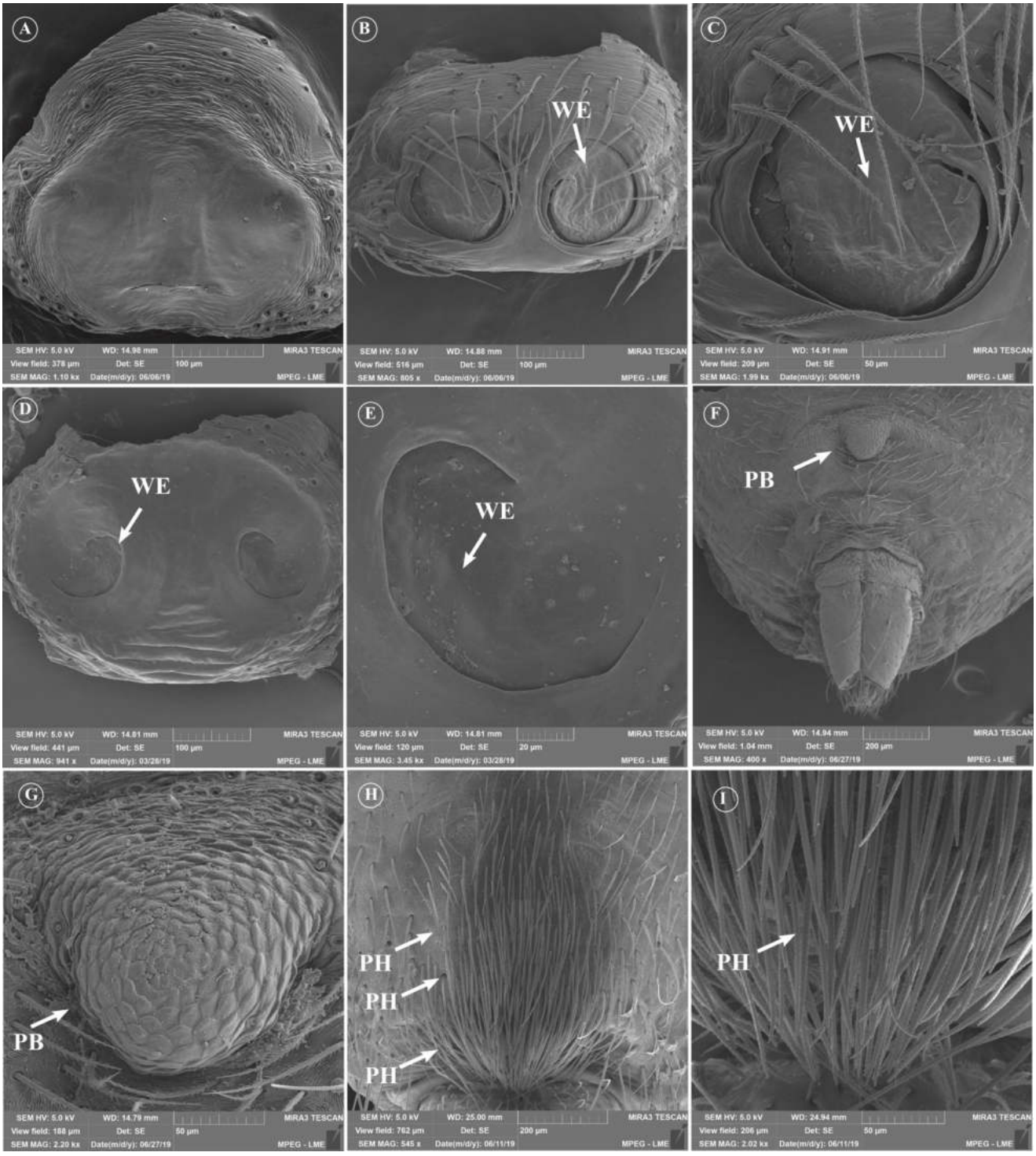

Figure. 2.6. Scanning electron micrographs of the epigynum (A-E), and male pre-spiracular bump and pre-spiracular hairs (F-I). A, Female of *Anasaitis*, ventral view. B-C, Female of *Sidusa*. D-E, Female of *Chapoda*. F-G, Male of *Bryanattus keyserlingi* **comb. nov.**. H-I, Male of *Cobanus mandibularis* **comb. nov.**.

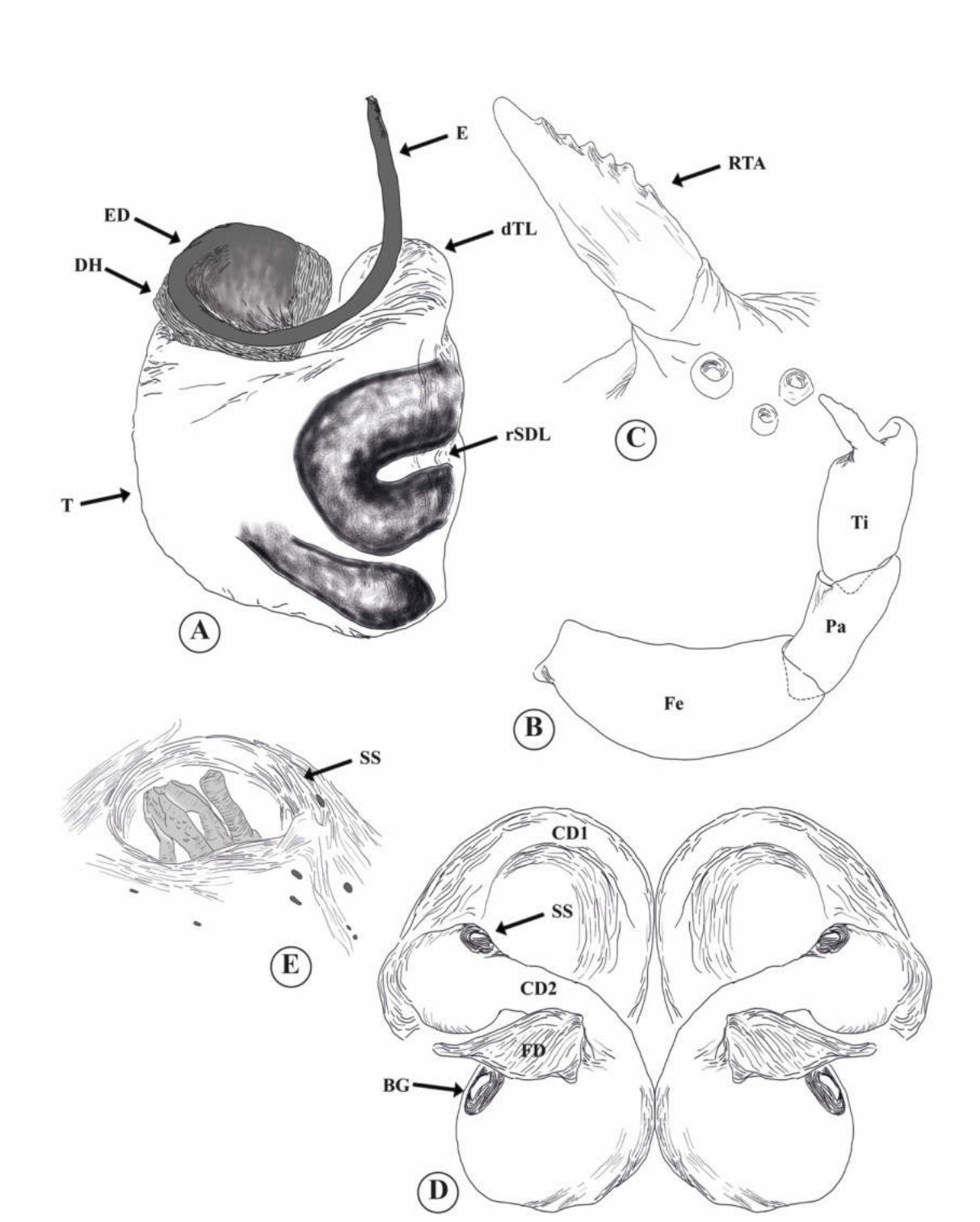

Figure. 2.7. Structures of left male palps (A-C) and female genitalia (C-D). A, *Agobardus* sp. male palp, ventral view. B, *Agobardus* sp., male palp, retrolateral view. C, *Agobardus* sp., RTA. D, *Chapoda* sp., female genitalia, dorsal view. E, *Chapoda* sp., secondary spermathechae, dorsal view.

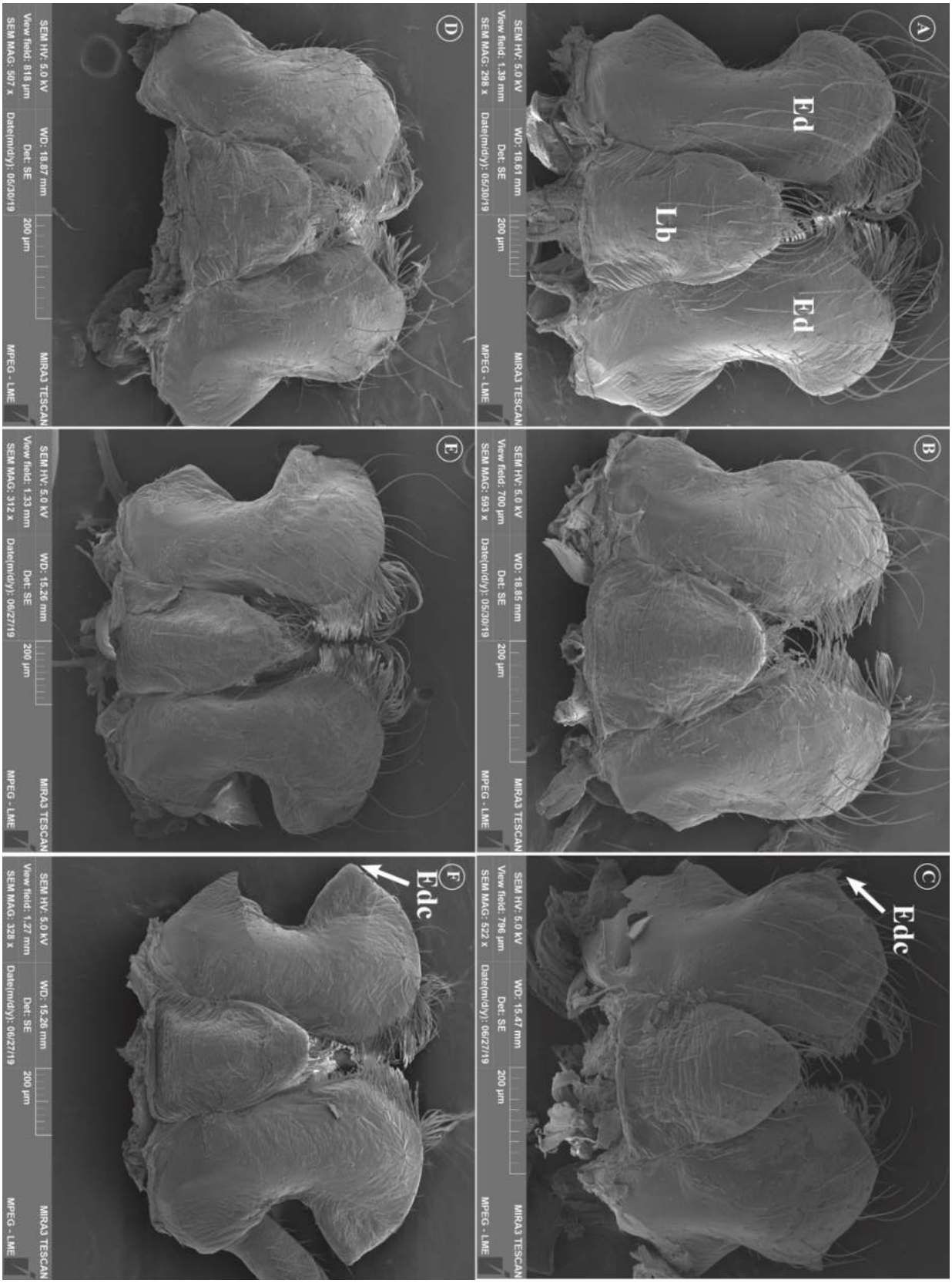

Figure. 2.8. Scanning electron micrographs of the male endites. A, *Cobanus mandibularis* **comb. nov.**. B, unknown euophrine. C, *Chapoda*. D, *Sidusa*. E, *Antillattus cambridgei*. F, *Bryanattus keyserlingi* **comb. nov.**.

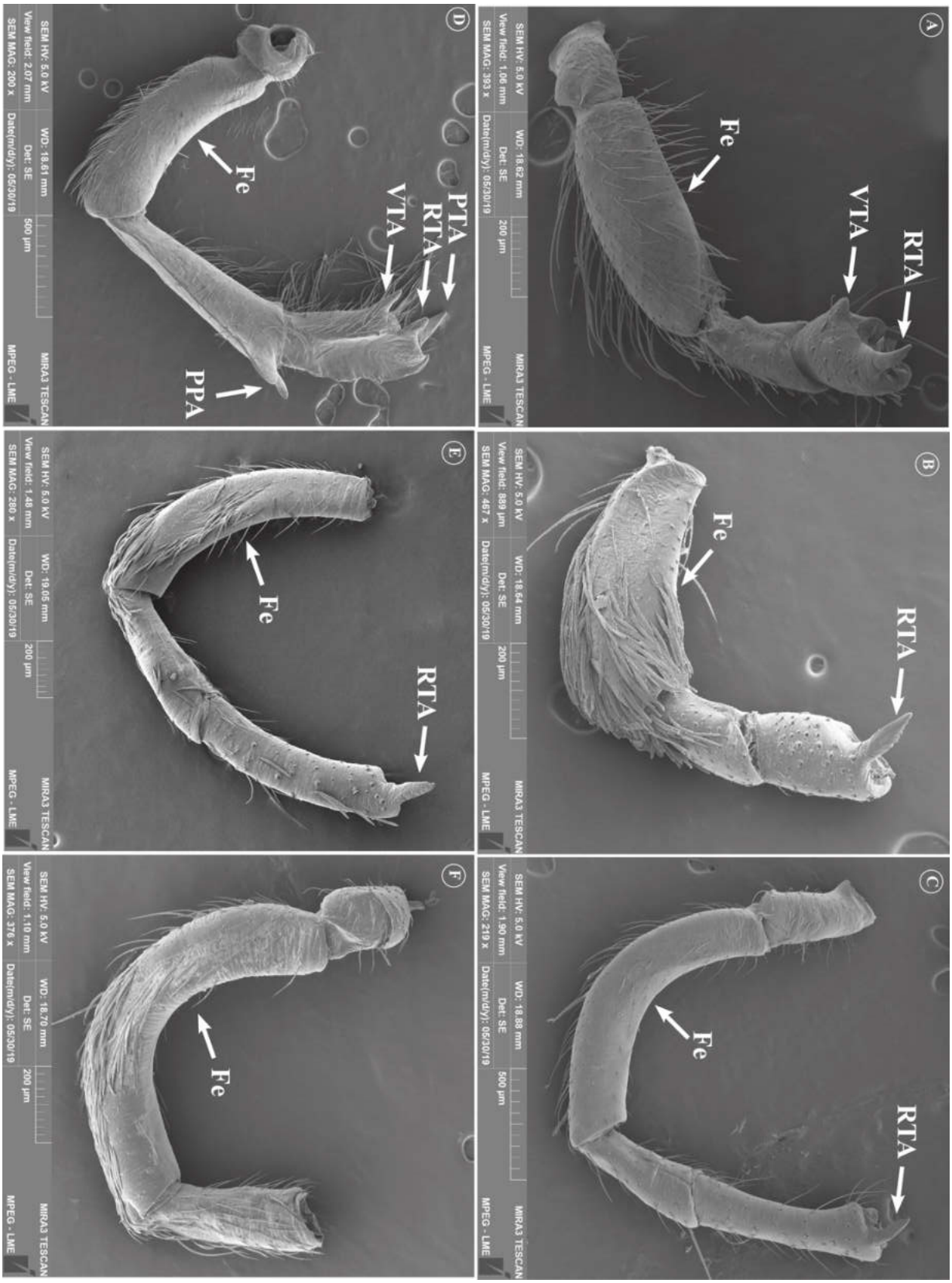

Figure. 2.9. Scanning electron micrographs of the male palp. A, *Anasaitis*. B, *Agobardus*. C, *Cobanus mandibularis* **comb. nov.**. D, *Sidusa*. D, *Compsodecta*. E, *Bryanattus keyserlingi* **comb. nov.**. F, *Antillattus cambridgei*.

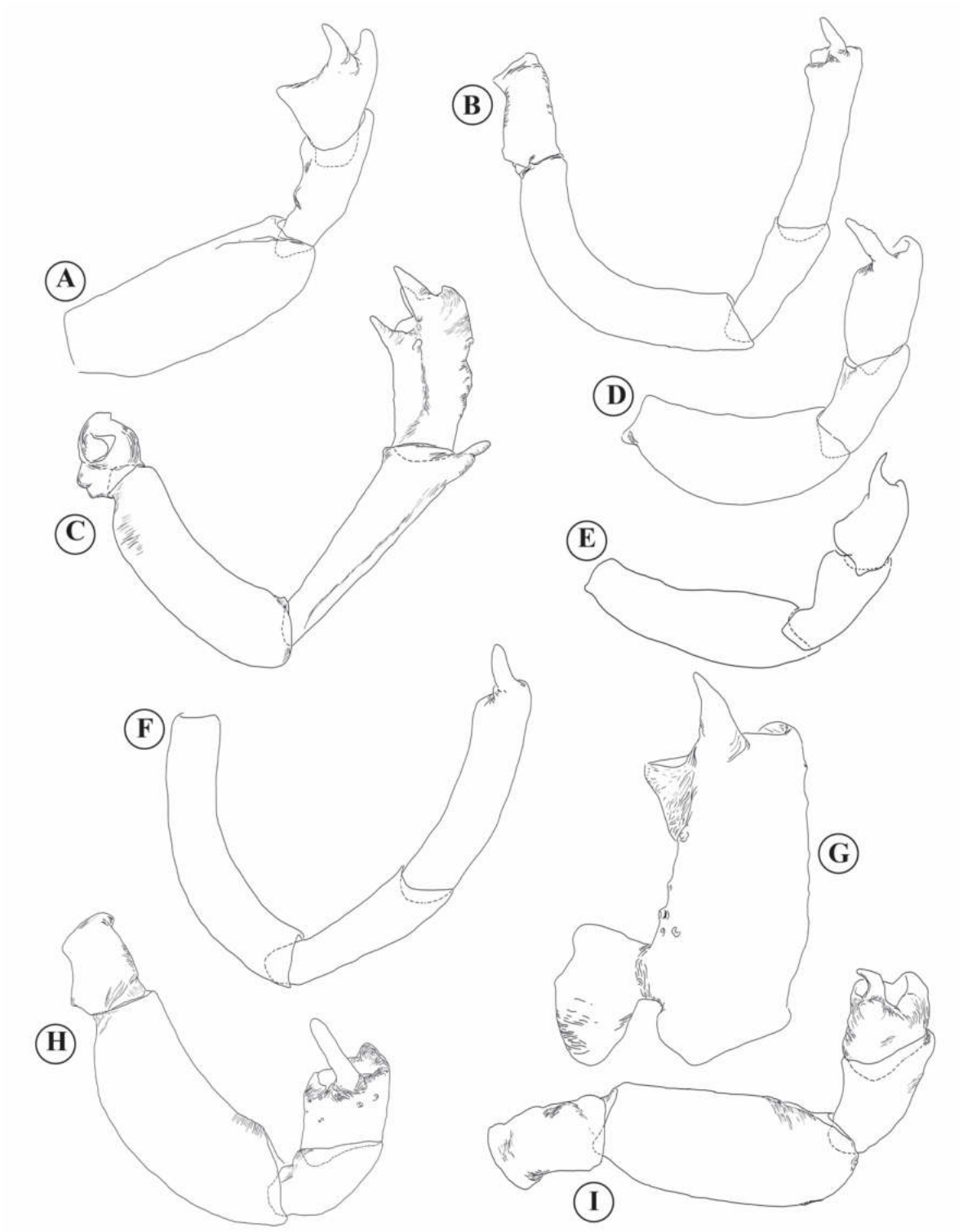

Figure. 2.10. Scanning electron micrographs of the male palp. A, *Anasaitis*. B, *Cobanus mandibularis* **comb. nov.**. C, *Compsodecta darlingtoni*. D, *Bryanattus keyserlingi* **comb. nov.**. E, *Truncattus flavus*. F, *Antillattus cambridgei*. G, *Chapoda sanlorenzo*. H, *Sidusa* sp. I, *Popcornella* sp.

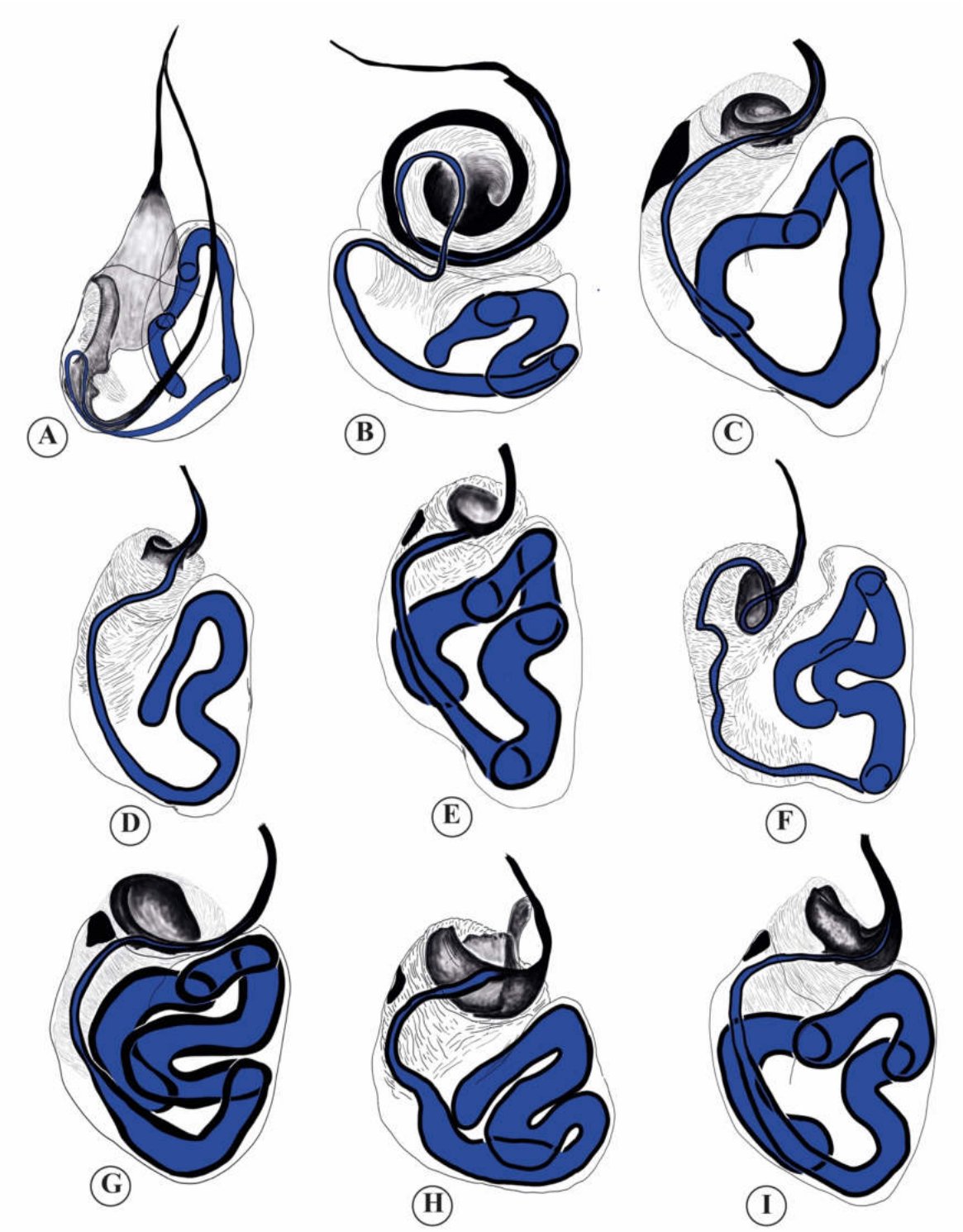

Figure. 2.11. Bulb of the male palp, ventral view. A, *Marma*. B, *Sidusa*. C, *Pensacolatus darlingtoni* **comb.nov.**. D, *Petemathis portoricensis*. E, *Truncattus flavus*. F, *Pensacola signata*. G. *Agobardus*. H, *Cobanus multidentatis* **sp. nov.**. I, *Antillattus cubensis*.

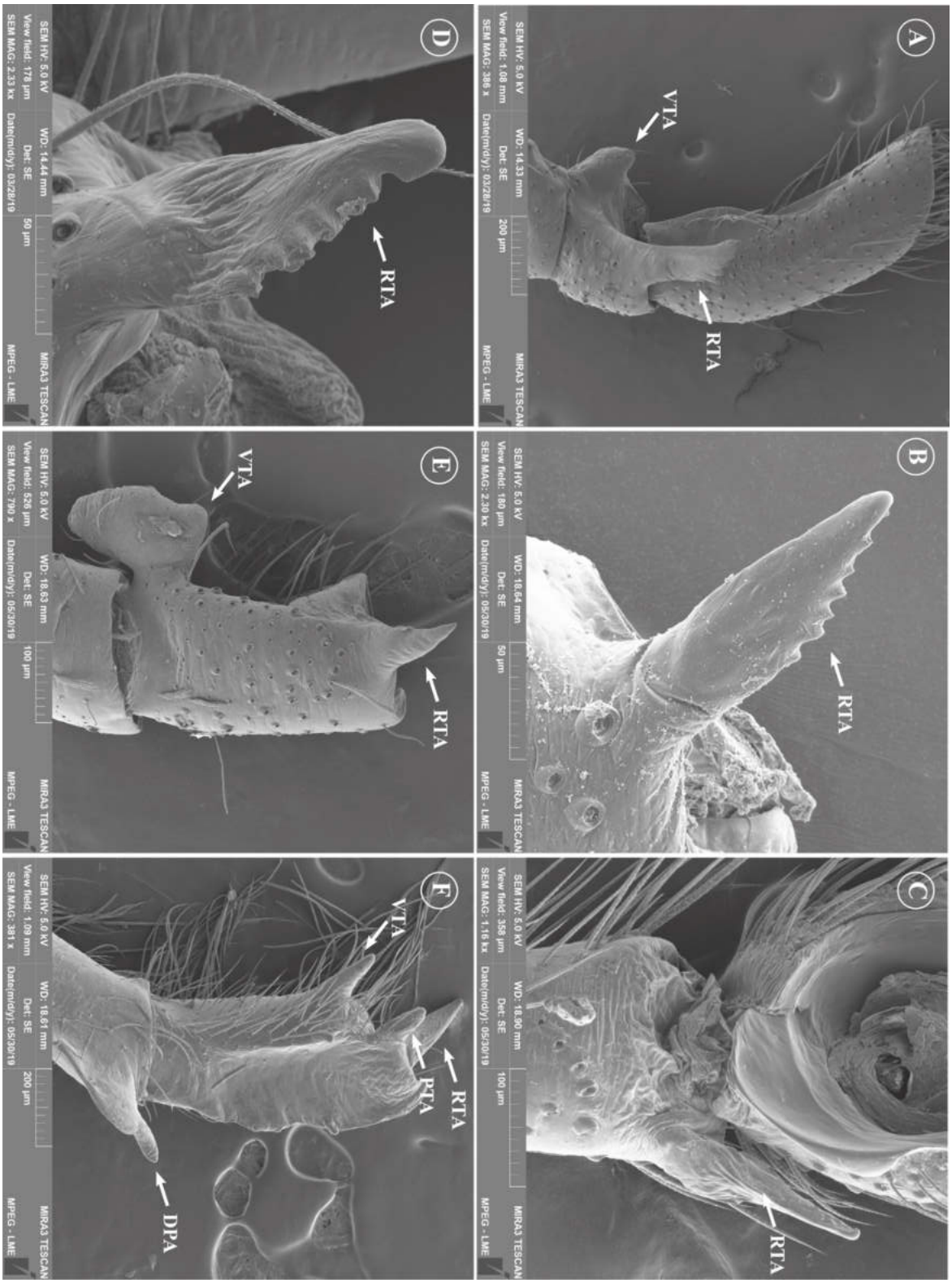

Figure. 2.12. Scanning electron micrographs of the male palp. A and D, *Corythalia*. B *Agobardus*. C, *Antillattus cambridgei*. E, *Chapoda*. F, *Compsodecta*.

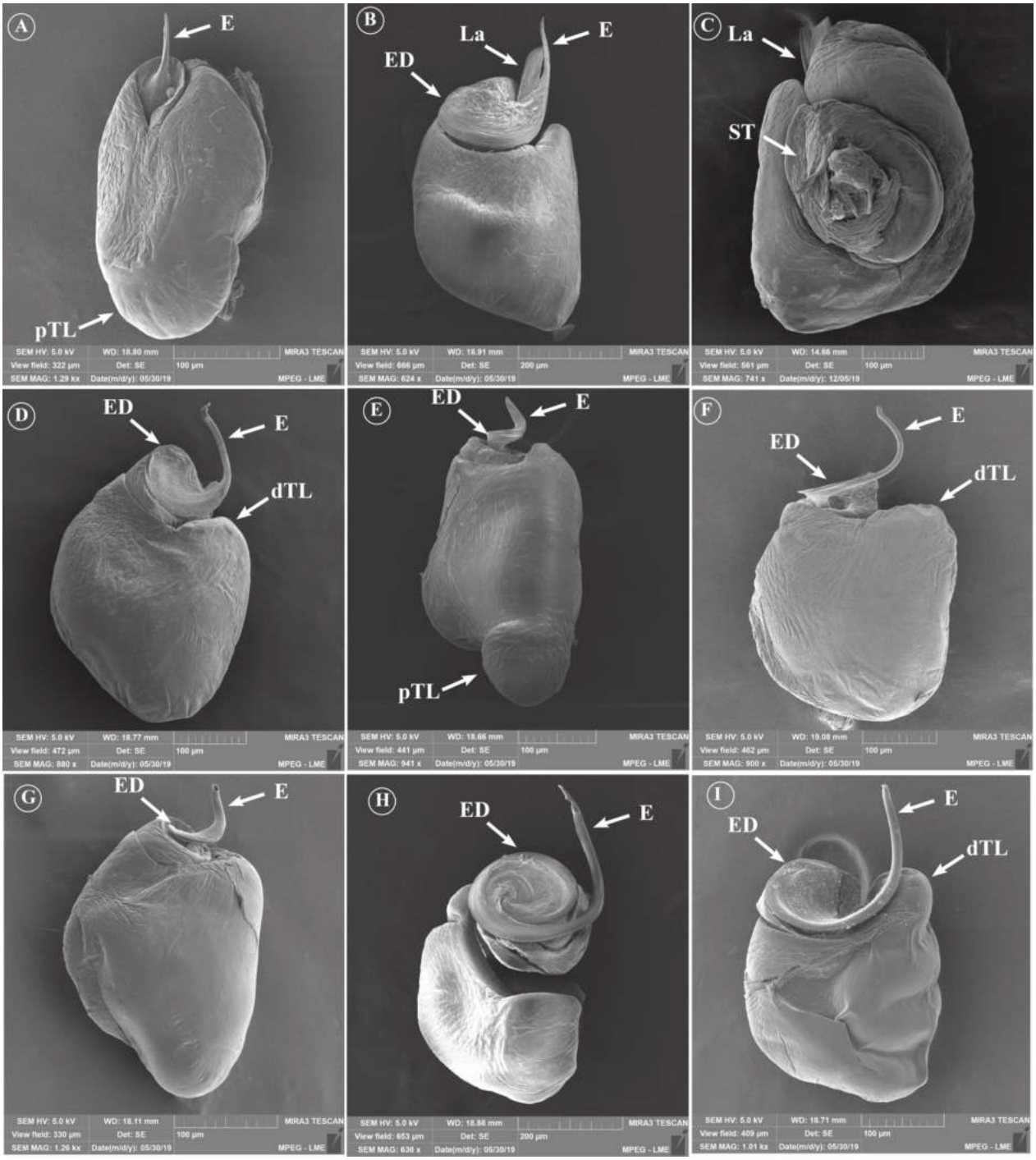

Figure. 2.13. Scanning electron micrographs of the male palp. A, *Popcornella*. B-C, *Cobanus*. D, *Antillattus cambridgei*. E, *Chapoda*. F, *Bryanattus keyserlingi* **comb. nov.**. G, unknown euophrine. H, *Sidusa*. I, *Agobardus*.

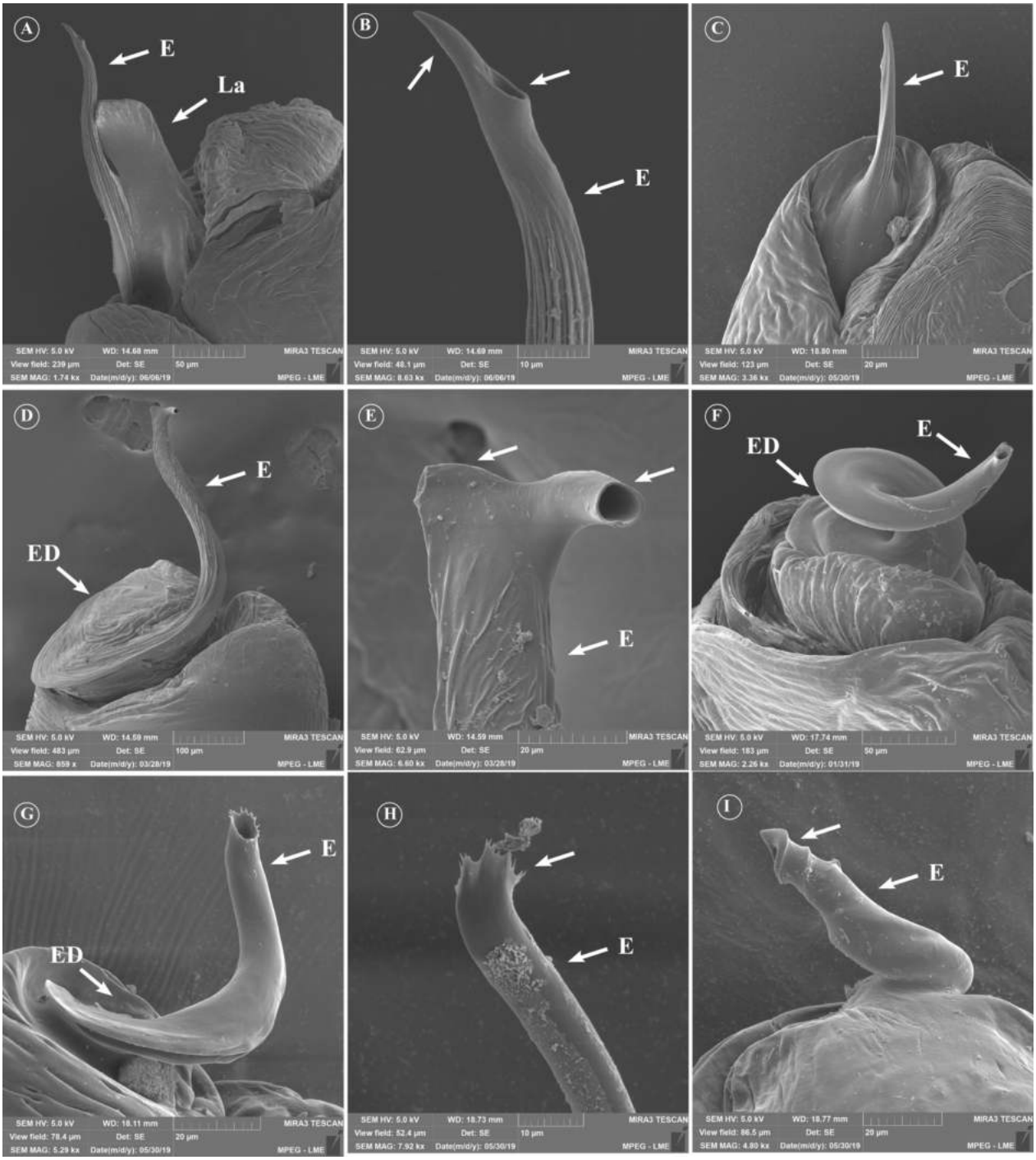

Figure. 2.14. Scanning electron micrographs of the embolus. A-B, *Cobanus*. C, *Popcornella*. D-E, *Corithalia*. F, *Chapoda*. G, unknown euophrine. H, *Antillattus cambridgei*. I, *Anasaitis*.

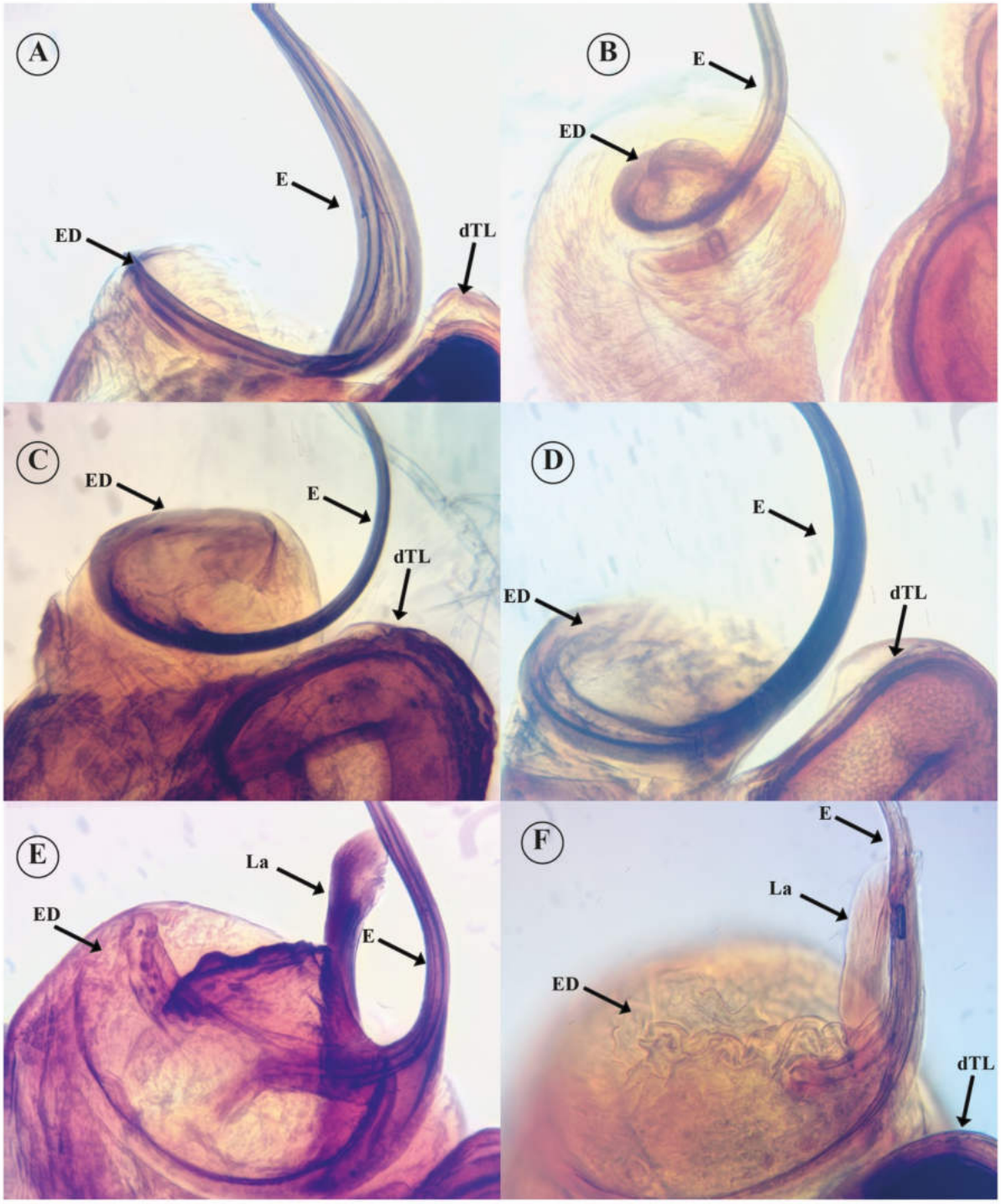

Figure. 2.15. Male embolus. A, *Compsodecta*. B, *Pensacola signata*. C, *Bryanattus* **gen. nov**.. D, *Agobardus*. E-F, *Cobanus*.

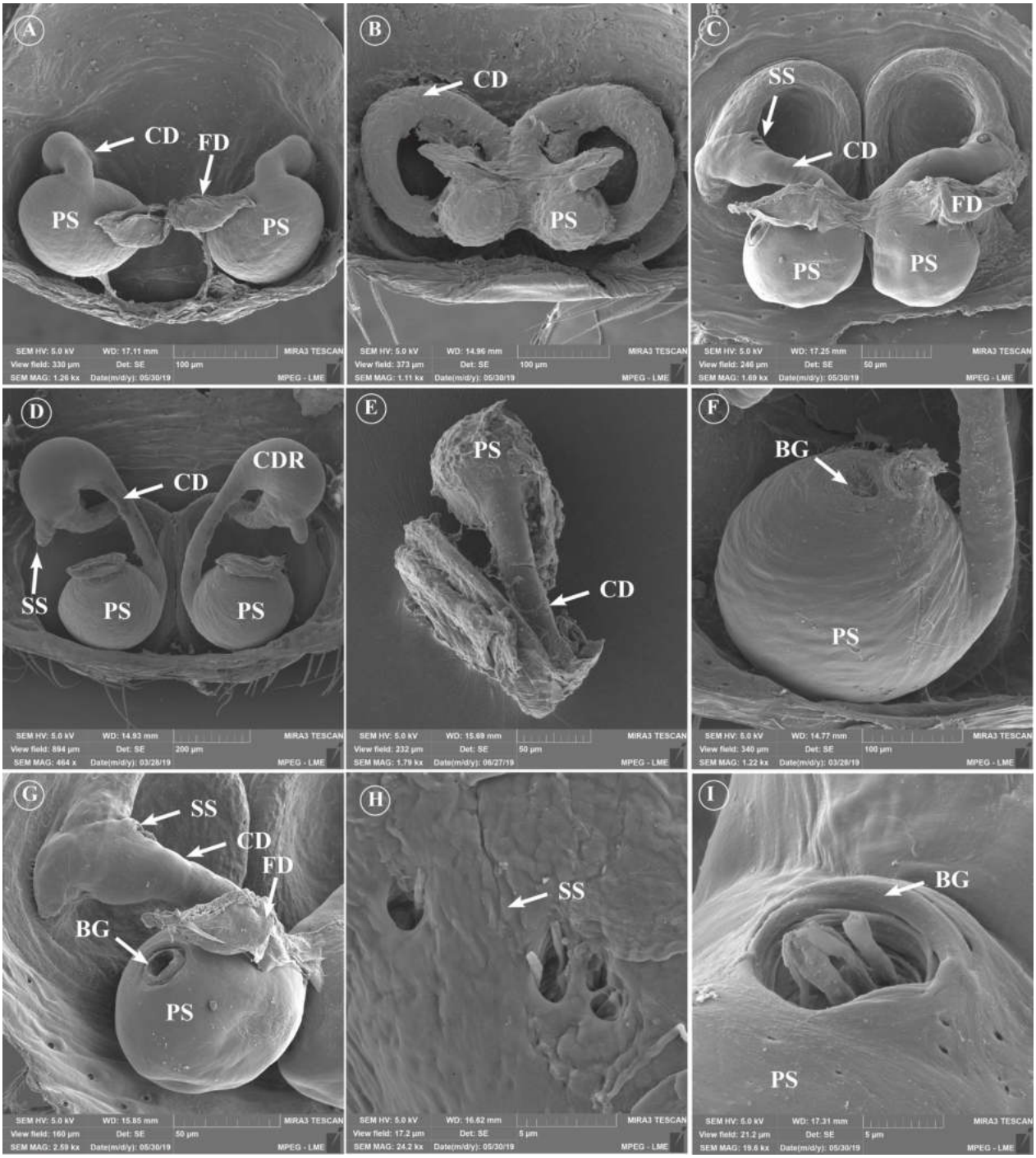

Figure. 2.16. Scanning electron microscopy images of the internal epigynum. A and H, *Popcornella*. B and E, *Sidusa*. C, G and I, *Chapoda*. D-F, *Corythalia*.

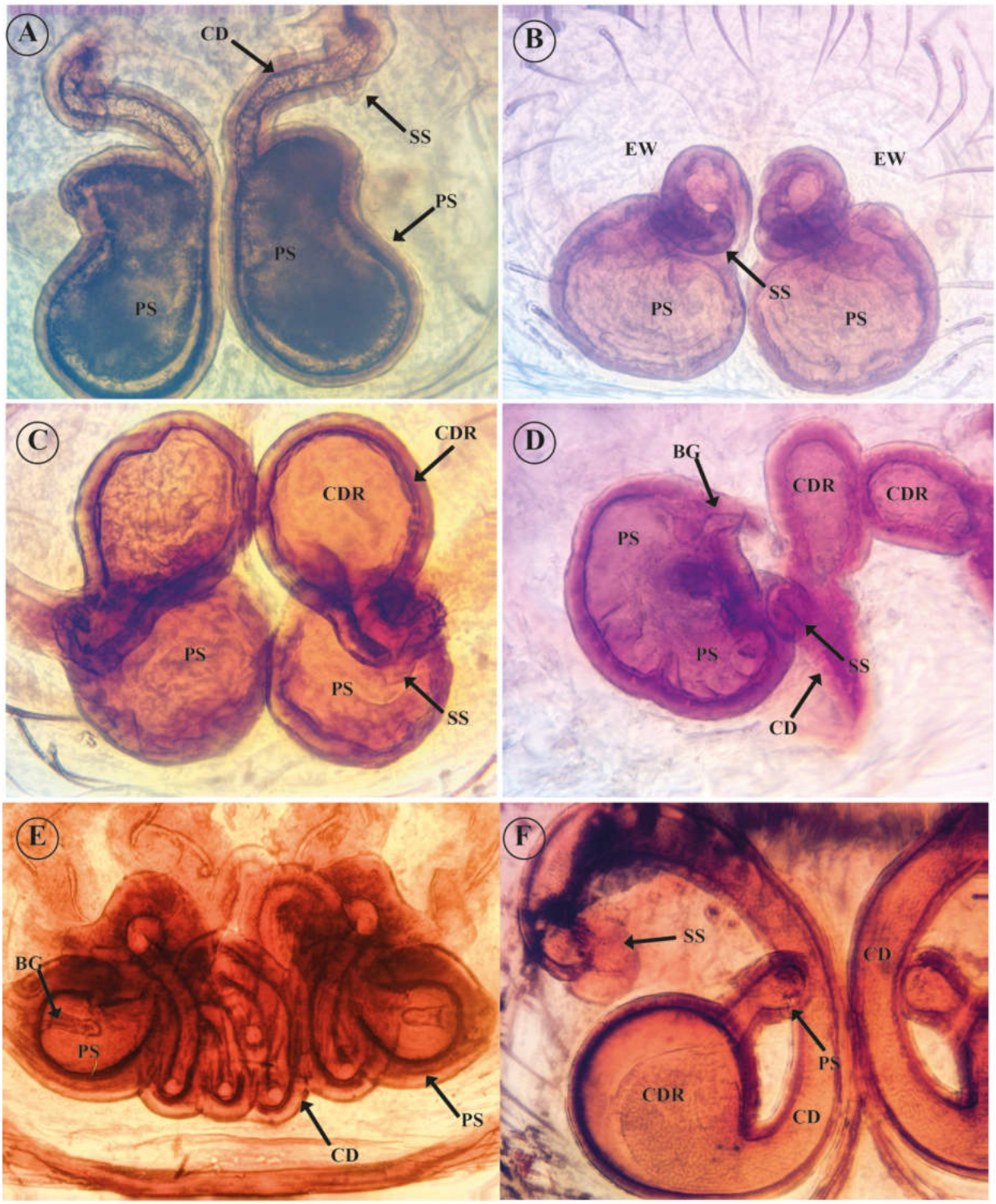

Figure. 2.17. Female internal genitalia, dorsal view. A, *Agobardus*. B, *Bryanattus*. C, *Truncattus*. D, *Cobanus*. E, *Sidusa*. F, unknown euophrine.

2.2 Results

2.2.0 Morphological reconstruction and phylogenetic signal

The final dataset resulted in a matrix with 125 characters (23 uninformative) scored for 68 taxa. We surveyed 18 characters from the female genitalia (2 uninformative), 39 from the male genitalia (4 uninformative), and 68 from the prosoma+abdomen (17 uninformative). The equal weights analysis resulted in 47 most parsimonious trees with 377 steps [consistency index (CI) = 0.37, retention index (RI) = 0.83]. The strict consensus of the 47 most parsimonious trees recovers the monophyly of: *Popcornella*, *Bythocrotus*, *Corticattus*, *Sidusa*, *Paracobanus*, *Cobanus*, *Mexigonus*, *Agobardus*, *Petemathis*, *Caribattus*, *Compsodecta* (including *Allodecta*), *Pensacola*, *Pensacolatus*, *Antillattus*, *Truncattus* and *Bryanattus* **gen. nov.** (Fig. 2.18). Additionally, the strict consensus recovered the Antillattus clade, although with poor resolution, and included *Pensacola*. *Antillattus* (*sensu* Zhang and Maddison, 2015) comprises three groups of species. We will call them the *Antillattus* group, *Bryanattus* **gen. nov.** group and *Pensacolatus* group and they will be discussed in detail in the next chapter.

The parsimonious trees obtained under the implied weights (*k*) analysis also recovered the Antillattus clade to include the genus *Pensacola* (see figure 2.19). Considering the stability of the results, the trees obtained in the implied weights analyses with different values of *k* showed some differences in topological positions and steps in contrast to the tree from the equal weights analysis (table 2.4). The genus *Caribattus* is recovered with poor resolution as a sister group of the genera *Bythocrotus* and *Compsodecta*, while *Agobardus* and *Corticattus* are also recovered with poor resolution as a sister group to *Mexigonus* and the *Sidusa*-*Cobanus* clade. The trees found under other concavity values and under equal weights are used to discuss the robustness of the genera and clades. All genera are strongly supported by jackknife, resampling analysis and Bremer support values (Fig. 2.19). The sensitivity to weighting regimes is summarized in the working hypothesis tree (Fig. 2.19).

The analyses using the prosoma+abdomen and the palp character subset resulted in 102 [146 steps; consistency index (CI) = 0.45, retention index (RI) = 0.88] and 107 [122 steps; consistency index (CI) = 0.41, retention index (RI) = 0.85] parsimonious trees. The prosoma+abdomen subset consensus tree strongly recovers the monophyly of: *Bythocrotus*, *Corticattus*, *Cobanus*, *Mexigonus*, *Bryanattus, Agobardus, Pensacola* and *Antillattus*. The consensus trees from the palp and prosoma+abdomen character subsets differ in topology. The palp character subset strongly recovers the monophyly of: *Popcornella*, *Bythocrotus*, *Corticattus*, *Sidusa*, *Truncattus*, *Petemathis*, *Pensacola*, *Pensacolatus* and *Antillattus*. The genus *Compsodecta* (without *Allodecta*) is recovered with low support. Thirteen characters with

a retention of 100 appeared on the prosoma+abdomen subset tree, and eleven appeared in the palp subset character tree.

Finally, the epigynum character subset resulted in 126 parsimonious trees with 55 steps [consistency index (CI) = 0.45, retention index (RI) = 0.85] and only recovered the monophyly of the genera *Sidusa* and *Paracobanus* **gen. nov**. Six characters with a retention of 100 appeared on the epigynum subset tree.

2.2.1 *COI*

For COI, the alignment resulted in 1270 sites. The results from the ML analyses are summarized in figure 2.20. The best ML tree found has an lnL -9843.776262. The genera *Bythocrotus*, Mexigonus*, Petemathis, Bryanattus* **gen. nov.** and the *Sidusa-Cobanus* clade are recovered with high bootstrap support (> 70%). The genera *Agobardus*, *Compsodecta*, *Truncattus* and *Antillattus* are recovered with low bootstrap support (≤70%). The Antillattus clade is recovered with low bootstrap support, and the genus *Pensacolatus* is not monophyletic. The TNT analysis found 54 equally parsimonious trees (Tree length=2026, CI: 0.32, RI: 0.38). The strict consensus tree recovered the genera *Bythocrotus, Petemathis, Mexigonus, Bryanattus, Antillattus* and the clade *Sidusa-Cobanus* with high levels of support (bootstrap > 70%). As in the ML analysis, the genera *Agobardus*, *Compsodecta* and the Antillattus clade were all recovered with low support (≤70%), but *Truncattus* and *Pensacolatus* are not monophyletic.

2.2.2 *16S*

For 16S, the sequence alignment resulted in 641 sites (2069 internal gaps). The results from the ML analyses are summarized in figure. 2.21. The best ML tree found has an lnL -6792.384803. The genera *Corticattus*, *Agobardus*, *Bythocrotus*, *Petemathis*, *Truncattus*, *Bryanattus* and the *Sidusa-Cobanus* clade are strongly supported (> 75%) by the ML bootstrap analysis. The TNT analysis found 8 equally parsimonious trees (Tree length=1471, CI: 0.33, RI: 0.42). The strict consensus tree recovers the genera *Agobardus*, *Bythocrotus*, *Mexigonus*, *Truncattus*, and *Bryanattus,* and the *Sidusa-Cobanus* clade as monophyletic with high levels of support (bootstrap > 70%).

2.2.3 *28S*

For 28S, the alignment resulted in 1180 sites (2302 internal gaps). The results from the ML and MP analyses are summarized in figure. 2.22. The best ML tree has an lnL of -

8077.010867. The analysis recovered the monophyly of *Mexigonus*, *Popcornella*, *Compsodecta*, *Bythocrotus*, *Agobardus, Bryanattus, Petemathis* and the *Sidusa-Cobanus* clade with high levels of clade support (bootstrap < 70%). *Pensacolatus*, *Truncattus*, *Cobanus*, *Antillattus* and *Corticattus* are paraphyletic. The TNT analysis found 1 parsimonious tree (Tree length=1395, CI: 0.43, RI: 0.58). The monophyly of *Bythocrotus*, *Petemathis, Popcornella*, *Bryanattus*, *Compsodecta*, *Agobardus* and the Sidusa-Cobanus clade are recovered with strong support (bootstrap >70%). As in the ML analysis, *Pensacolatus*, *Truncattus*, *Cobanus*, *Antillattus* and *Corticattus* are paraphyletic.

2.2.4 All genes combined (COI, 16S, 28S)

The combined molecular dataset consisted of 3089 sites (17955 internal gaps). The results of the hypothesis tests of constrained vs unconstrained trees are given in table 2.5. The unconstrained tree (fig. 2.23) displays a more likely topology than the constrained tree, unsupporting the monophyly of *Pensacolatus*. From here on we refer to the trees resulting from the unconstrained topology. The Antillatus clade is recovered as monophyletic and this is strongly supported (ML, bootstrap > 70%). The phylogeny suggests that the Antillattus clade is sister to other Caribbean (e.g. *Agobardus*, *Compsodecta*, *Popcornella*) and continental clades (e.g. *Cobanus*, *Sidusa*), but these nodes are poorly supported. Within the Antillattus clade, the relationships between genera are poorly supported (ML, bootstrap ≤ 70%). For example, *Petemathis* is resolved as sister to *Truncattus* (*Bryanattus* (*Pensacolatus*+*Antillattus*) with low support (ML, bootstrap ≤ 70%). *Antillattus* (*Pensacolatus*+*Bryanattus*) is recovered with low support (ML, bootstrap ≤ 70%). The consensus tree of unconstrained BI analysis differed from the ML tree. All genera were recovered as monophyletic except *Cobanus*. The deeper nodes had stronger support via BI than by ML. For example, the genus *Bryanattus* is resolved as the sister taxon of (*Pensacolatus*+*Antillattus*), and this relationship is strongly supported (pp > 0.95). Similarly, *Petemathis* is resolved as the sister taxon of *Truncattus* (*Bryanattus* (*Pensacolatus*+*Antillattus*) with low support (pp ≤ 0.95). The result of the BI analysis also strongly supports the Agobardus clade and their internal relationships (pp > 0.95).

2.2.5 Total evidence

Our combined evidence (total evidence) resulted in 3217 sites (41646 internal gaps) that produced consistent phylogenetic estimates. In contrast with the trees inferred separately from morphological and molecular datasets (combined and individual loci), the total evidence tree has consistently strong nodal support and recovered both genera and clades as

monophyletic. The MP, BI and ML trees were mostly congruent and recovered the genera *Popcornella*, *Corticattus*, *Agobardus*, *Bythocrotus*, *Caribattus*, *Paracobanus* **gen. nov**., *Cobanus*, *Sidusa*, *Pensacola*, *Mexigonus, Petemathis*, *Truncattus*, *Bryanattus*, and *Antillattus* and the *Sidusa-Cobanus* clade with high support (see, figs. 2.24-2.26). Nevertheless, some differences were observed between trees. The monophyly of the genus *Pensacolatus* was support by BI and ML. From the MP analysis, the constrained hypothesis (a cost of 2 steps) seems to have evidence that is almost as good as the most parsimonious hypothesis, supporting the monophyly of *Pensacolatus* (fig. 2.27). The low RFD value supports forcing *Pensacolatus* to be monophyletic as the most parsimonious hypothesis (see table 2.6). From here on, in addition to the MP consensus tree resulting from the constrained topology. Both ML and MP recovered the Agobardus clade, but little support, while the BI analysis recovered the same clade with strong support. The genus *Caribattus* changed position within the phylogeny depending on the type of analysis. Both ML and BI positioned *Caribattus* close to *Mexigonus*, *Pensacola* and the *Sidusa-Cobanus* clade (figs. 2.24, 2.25), whereas MP positioned *Caribattus* close to the Agobardus clade. However, the position of *Caribattus* within all phylogenies lacks strong support.

Table 2.2. MP (*k=17* and equal weights) morphological synapomorphies and mapping of morphological character changes on DNA+ morphology MP, ML and BI trees.

	Morphology		DNA+ Morphology		
	equal weights	*k*=17	ML	BI	MP
Caribattus	**29-1**, **59-1**, 93-2	**29-1**, **59-1**, 93-2	**29-1**, **59-1**, 93-2	**29-1**, **59-1**	**29-1**, **59-1**
Corticattus	3-0, 4-0, 7-0, 21-1, **29-1**, 41-0, **46-0**, 57-2, 62-0, 63-0, 65-0, 69-1, 76-0, 80-1, 87-0, 91-1, 92-0, 95-1, 99-1, 101-0, 102-4, 103-2, 105-2, 114-1, 115-0, 116-1, **117-2**	7-0, 21-1, **29-1**, **46-0**, 62-0, 63-0, 65-0, 69-1, 80-1, 91-1, 92-0, 95-1, 101-0, 102-4, 114-1, **117-2**	3-0, 7-0, **29-1**, 41-0, **46-0**, 76-0, 80-1, 92-0, 99-1, 102-4, 115-0, 116-1, **117-2**	7-0, 21-1, **29-1**, 41-0, **46-0**, 57-2, 62-0, 63-0, 65-0, 80-1, 87-0, 91-1, 95-1, 116-1, **117-2**	7-0, **29-1**, 41-0, **46-0**, 57-2, 62-0, 63-0, 65-0, 80-1, 87-0, 91-1, 95-1, 116-1, **117-2**
Mexigonus	2-0, **6-0**, **7-0**, **75-1**, **80-1**, 109-2	**6-0**, 7-0, **75-1**, **80-1**	2-0, **6-0**, **7-0**, **75-1, 80-1**	**6-0**, **7-0**, **75-1**, **80-1**, 86-1	2-0, **6-0**, **7-0**, **75-1**, **80-1**, 86-1
Pensacola	**53-1**, **56-2**, **85-1**, 90-0, 91-1, **95-1**, 103-2, 105-0	**53-1**, **56-2**, **85-1**, **91-1**, **95-1**, 103-2, 105-0	44-1, 48-1, 50-1, **53-1**, **56-2**, 69-1, 71-1, 73-1, 74-1, **85-1**, **91-1**, **95-1**, 100-1, 103-2, 105-0	44-1, 45-1, 48-1, 50-1, **53-1**, **56-2**, **85-1**, 90-0, **91-1**, **95-1**, 103-2	44-1, 45-1, 48-1, 50-1, **53-1**, **56-2**, 59-1, 69-1, 71-1, 73-1, 74-1, **85-1**, **91-1**, **95-1**, 100-1, 105-0
Popcornella	**2-0**, **84-0**, **87-2**, **123-1**	**2-0**, **84-0**, **87-2**, **123-1**	**2-0**, **84-0**, **87-2**, **123-1**	**2-0**, **84-0**, **87-2**, **123-1**	**2-0**, **84-0**, **87-2**, **123-1**
Agobardus clade	NON	NON	86-0	NON	56-0, 102-3

Agobardus	32-1, 39-1, 41-2, 45-1, 57-2, **64-1**, **65-2**, 99-1, 102-3, 116-1, **121-0**	4-1, 32-1, 39-1, 45-1, **64-1**, **65-2**, **121-0**, 125-1	17, 32-1, 39-1, 41-0, 57-2, **64-1**, **65-2**, 99-1, **121-0,** 125-1	32-1, 39-1, 41-2, **64-1**, **65-2**, 99-1, **121-0**	41-0, **64-1**, **65-2**, 99-1, 117-0, **121-0**
Bythocrotus	**14-1**, **29-1**, **42-1**, 75-1, 76-0, **101-0**, **102-1**, **103-0**, **123-2**	**14-1**, **29-1**, **42-1**, 75-1, 76-0, **101-0**, **102-1**, **103-0**, **123-2**	**14-1**, **29-1**, **42-1**, **101-0**, **102-1**, **103-0**, 120-2, **123-2**	**14-1**, **29-1**, **42-1**, 76-0, 80-1, **101-0**, **102-1**, **103-0**, 120-2, **123-2**	**14-1**, **29-1**, **42-1**, 90-0, **101-0**, **102-1**, **103-0**, 120-2, **123-2**
Compsodecta	**5-0**, **48-1**, **72-1**, **73-1**, 74-1, 90-1	**5-0**, **48-1**, **72-1**, **73-1**	**5-0**, **48-1**, **72-1**, **73-1**, 74-1, 90-1	**5-0**, **48-1**, **72-1**, **73-1**, 74-1	**5-0**, **48-1**, **72-1**, **73-1**, 74-1, 90-1
Antillattus clade	21-1, 32-1, 39-1, 45-1, 69-1, 74-1, 90-1, **100-1**, 118-1, 119-1	69-1, **100-1**, 119-1	90-1, **100-1**, 118-1	**100-1**	**100-1**
Antillattus	41-2, **46-2**, **47-2**, **51-1**, **56-2**, **68-1**, **74-2**, **100-0**, **103-0**, **109-2**	**46-2**, **47-2**, **51-1**, **56-2**, **68-1**, **74-2**, **100-0**, **103-0**, **109-2**	41-2, **46-2**, **47-2**, **51-1**, **56-2**, **68-1**, **74-2**, **100-0**, 101-0, **103-0**, **109-2**	41-2, **46-2**, **47-2**, **51-1**, **56-2**, **68-1**, **74-2**, **100-0**, 101-0, **103-0**, **109-2**	29-0, 41-2, 43-0, **46-2**, **47-2**, **51-1**, **56-2**, **68-1**, **74-2**, **100-0**, **103-0**, **109-2**
Bryanattus	29-1, 43-1, 50-1, 93-2, **115-0**, **118-0**	29-1, 43-1, 50-1, 93-2, **115-0**, **118-0**	**115-0**, **118-0**, 121-0	67-1, **115-0**, **118-0**, 121-0	67-1, **115-0**, **118-0,** 121-0
Pensacolatus	29-1, 43-1, 55-1, **94-0**	29-1, 43-1, 55-1, **94-0**	17-0, 21-0, 59-1, 70-1, 86-1, **94-0**	59-1, 70-1, **94-0**	59-1, 70-1, **94-0**
Petemathis	**4-0**, 18-1, 19-1, 33-1, 34-1, 41-1, 42-0, 69-0, 75-1, 76-0, 105-0, 119-0, **120-1**, 121-0	**4-0**, 42-0, 69-0, 75-1, 76-0, 105-0, 119-0, **120-1**	**4-0**, 18-1, 19-1, 33-1, 34-1, 76-0, **120-0**, 121-0	**4-0**, 18-1, 19-1, 33-1, 34-1, 75-1, **120-0**, 121-0	**4-0**, 18-1, 19-1, 33-1, 34-1, 76-0, **120-0**, 121-0
Truncattus	22-0, 41-0, 42-0, 57-2, 74-0, 80-1, **83-2**, **87-2**, **88-2**	57-2, **83-2**, **87-2**, **88-2**	22-0, **83-2**, **87-2**, **88-2**	22-0, **83-2**, **87-2**, **88-2**	22-0, **83-2**, **87-2**, **88-2**
Sidusa-Cobanus Clade	21-1, 22-0, 62-2, 63-3, **64-1**, 65-2, **66-1**, 101-0, 109-2	17-1, 21-1, 32-1, 62-2, 63-3, **64-1**, 65-2, **66-1**, 101-0	22-0, **64-1**, **66-1**	17-1, 21-1, 62-2, 63-3, **64-1**, 65-2, **66-1**, 101-0	62-2, 63-3, **64-1**, 65-2, **66-1**
Cobanus	31-0, **34-1**, **35-1**, **36-0**, **37-1**, **38-1**, **45-2**, **46-2**, **47-2**, **48-1**, **56-2**, **75-2**, 103-0, **121-0**, **123-1**	**34-1**, **35-1**, **36-0**, **37-1**, **38-1**, **45-2**, **46-2**, **47-2**, **48-1**, **56-2**, **75-2**, 103-0, **121-0**, **123-1**	**34-1**, **35-1**, **36-0**, **37-1**, **38-1**, **45-2**, **46-2**, **47-2**, **48-1**, **56-2**, 74-2, **75-2**, **121-0**, **123-1**	31-0, **34-1**, **35-1**, **36-0**, **37-1**, **38-1**, **45-2**, **46-2**, **47-2**, **48-1**, **56-2**, 74-2, **75-2**, 103-0, **121-0**, **123-1**	**34-1**, **35-1**, **36-0**, **37-1**, **38-1**, **45-2**, **46-2**, **47-2**, **48-1**, **56-2**, **75-2**, 103-0, **121-0**, **123-1**
Paracobanus	**59-1**, **71-1**, **90-1**, **117-1**	2-1, **59-1**, **71-1**, **90-1**, **117-1**	**59-1**, **71-1**, **90-1**, **117-1**	**59-1**, **71-1**, 74-0, **90-1**, **117-1**	2-1, **59-1**, **71-1**, 74-0, **90-1**, **117-1**
Sidusa	91-1, 93-0, 95-1, **99-2**, **102-4,** 103-2, 105-0, **114-1**, **116-2**	39-1, 91-1, 93-0, 95-1, **99-2**, **102-4**, 103-2, 105-0, **114-1**, **116-2**	39-1, **99-2**, **102-0**, **105-0**, **116-2**	91-1, 93-0, 95-1, **99-2**, **102-4**, 103-2, **105-0**, 114-1, **116-2**	91-1, 93-0, 95-1, **99-2**, **102-4**, 105-0, **114-1**, **116-2**

Table 2.3. MP total evidence morphological synapomorphies under ACCTRAN and DELTRAN optimization.

	ACCTRAN	***DELTRAN***
Caribattus	29-1, 59-1, 125-1	29-1, 59-1, 93-2

Corticattus	7-0, 29-1, 41-0, 46-0, 57-2, 62-0, 63-0, 65-0, 69-1, 76-0, 80-1, 87-0, 91-1, 92-0, 95-1, 102-4, 114-1, 116-1, 117-2	7-0, 17-1, 21-1, 29-1, 41-0, 46-0, 57-2, 62-0, 63-0, 65-0, 69-1, 80-1, 87-0, 91-1, 95-1, 102-4, 103-2, 114-1, 116-1, 117-2
Mexigonus	2-0, 6-0, 7-0, 75-1, 80-1, 86-1	2-0, 6-0, 7-0, 75-1, 80-1, 86-1
Pensacola	44-1, 45-1, 48-1, 50-1, 53-1, 56-2, 59-1, 69-1, 71-1, 73-1, 85-1, 91-1, 93-1, 95-1, 100-1, 103-2, 104-0, 114-1, 116-1, 124-0	44-1, 45-1, 48-1, 50-1, 53-1, 56-2, 59-1, 69-1, 71-1, 73-1, 74-1, 85-1, 91-1, 95-1, 100-1, 103-2, 105-0
Popcornella	2-0, 81-1, 84-0, 87-2, 121-1, 123-1	2-0, 84-0, 87-2, 92-1, 123-1
Agobardus clade	56-0, 102-3	56-0, 102-3
Agobardus	41-0, 47-1, 64-1, 65-2, 115-0, 118-0, 121-0	17-1, 32-1, 39-1, 41-0, 64-1, 65-2, 93-2, 99-1, 118-0, 121-0
Bythocrotus	14-1, 29-1, 42-1, 48-0, 90-0, 101-0, 102-1, 103-0, 120-2, 123-2	14-1, 29-1, 42-1, 76-0, 90-0, 101-0, 102-1, 120-2, 123-2
Compsodecta	5-0, 49-1, 72-1, 73-1, 104-0	5-0, 48-1, 72-1, 73-1, 74-1
Antillattus clade	21-1, 40-1, 69-1, 74-1, 86-1, 93-0, 100-1, 119-1	100-1
Antillattus	29-0, 41-2, 43-0, 46-2, 47-2, 51-1, 56-2, 68-1, 74-2, 100-0, 101-0, 103-0, 109-2	41-2, 46-2, 47-2, 51-1, 56-2, 68-1, 74-2, 100-0, 101-0, 109-2
Bryanattus	67-1, 93-2, 115-0, 118-0, 121-0	29-1, 43-1, 50-1, 67-1, 93-2, 115-0, 118-0, 121-0
Pensacolatus	17-0, 21-0, 32-0, 39-0, 59-1, 70-1, 94-0, 120-1	29-1, 42-1, 59-1, 70-1, 86-1, 93-0, 94-0
Petemathis	4-0, 18-1, 19-1, 33-1, 34-1, 69-0, 75-1, 76-0, 119-0, 120-1, 121-0	4-0, 18-1, 19-1, 33-1, 34-1, 40-1, 74-1, 75-1, 76-0, 105-0, 120-1, 121-0
Truncattus	22-0, 40-0, 74-0, 83-2, 87-2, 88-2	22-0, 69-1, 83-2, 87-2, 88-2, 119-1
Sidusa-Cobanus Clade	2-0, 21-1, 32-1, 62-2, 63-3, 64-1, 65-2, 66-1, 68-1, 106-1, 112-1, 115-2, 120-2	16-1, 21-1, 62-2, 63-3, 64-1, 65-2, 66-1, 115-2, 120-2
Cobanus	34-1, 35-1, 36-0, 37-1 ,38-1, 45-2, 46-2, 47-2, 48-1, 56-2, 74-2, 75-2, 103-0, 121-0, 123-1	2-0, 34-1, 35-1, 36-0, 37-1 ,38-1, 45-2, 46-2, 47-2, 48-1, 56-2, 68-1, 74-2, 75-2, 103-0, 106-1, 112-1, 118-1, 121-0, 123-1
Paracobanus	2-1, 59-1, 68-0, 71-1, 74-1, 90-1, 117-1	59-1, 71-1, 74-1, 90-1, 106-1, 112-1, 117-1, 118-1
Sidusa	91-1, 93-0, 95-1, 99-2, 102-4, 103-2, 105-0, 112-0, 114-1, 115-1, 116-2, 118-0	2-0, 68-1, 91-1, 93-0, 95-1, 99-2, 102-4, 103-2, 105-0, 114-1, 116-2

Table 2.4. Summary statistics from the equal weights and implied weighting analyses. k: concavity constant, N: number of most parsimonious trees, L: tree length, CI: consistency index, RI: retention index.

	tree	steps	CI	RI
equal weights	47	377	0.37	0.83
k=3	1	382	0.37	0.83
k=5	1	380	0.37	0.83
k=7	1	380	0.37	0.83
k=9	1	378	0.37	0.83
k=11	1	378	0.37	0.83
k=15	1	378	0.37	0.83
k=17	1	377	0.37	0.83

k=25	1	377	0.37	0.83
k=100	1	377	0.37	0.83

Table 2.5. Likelihood heterogeneity test (LHT) results and Bayes factors (BF) are from tests against the unconstrained topology. Positive values indicate greater support for the hypothesis (constrained topology). For BF, values between 0–2 indicate no evidence of a difference, 2–6 indicate substantial evidence for a difference, 6–10 indicates strong evidence for a difference and >10 indicates decisive evidence for a difference in the likelihood of the topologies (Kass and Raftery, 1995). Asterisks indicate a monophyletic grouping that is not rejected.

	Marg. Log Lik.		**Evidence against constraint**
ML Unconstrained H_0	-26072.460786		
Pensacolatus* Constrained H_1	-26077.942041	10.94*	df=1, P=0.001
BI Unconstrained H_0	-24981.08		
Pensacolatus* Constrained H_1	-24988.65	**BF**=15.14*	substantial evidence

Table. **2.6.** Relative fit difference (RFD) of alternative phylogenetic hypotheses found using constrained searches. *C* = sum of fit of characters contradicting most parsimonious tree; *F* = sum of fit of characters favoring most parsimonious tree.

Constrained	**Fit**	**C**	**F**	**C/F**	**RFD**
Pensacolatus	50156462	7321898	7412924	0. 987720	0. 0122793
Unconstrained	50110949	-	-	-	-

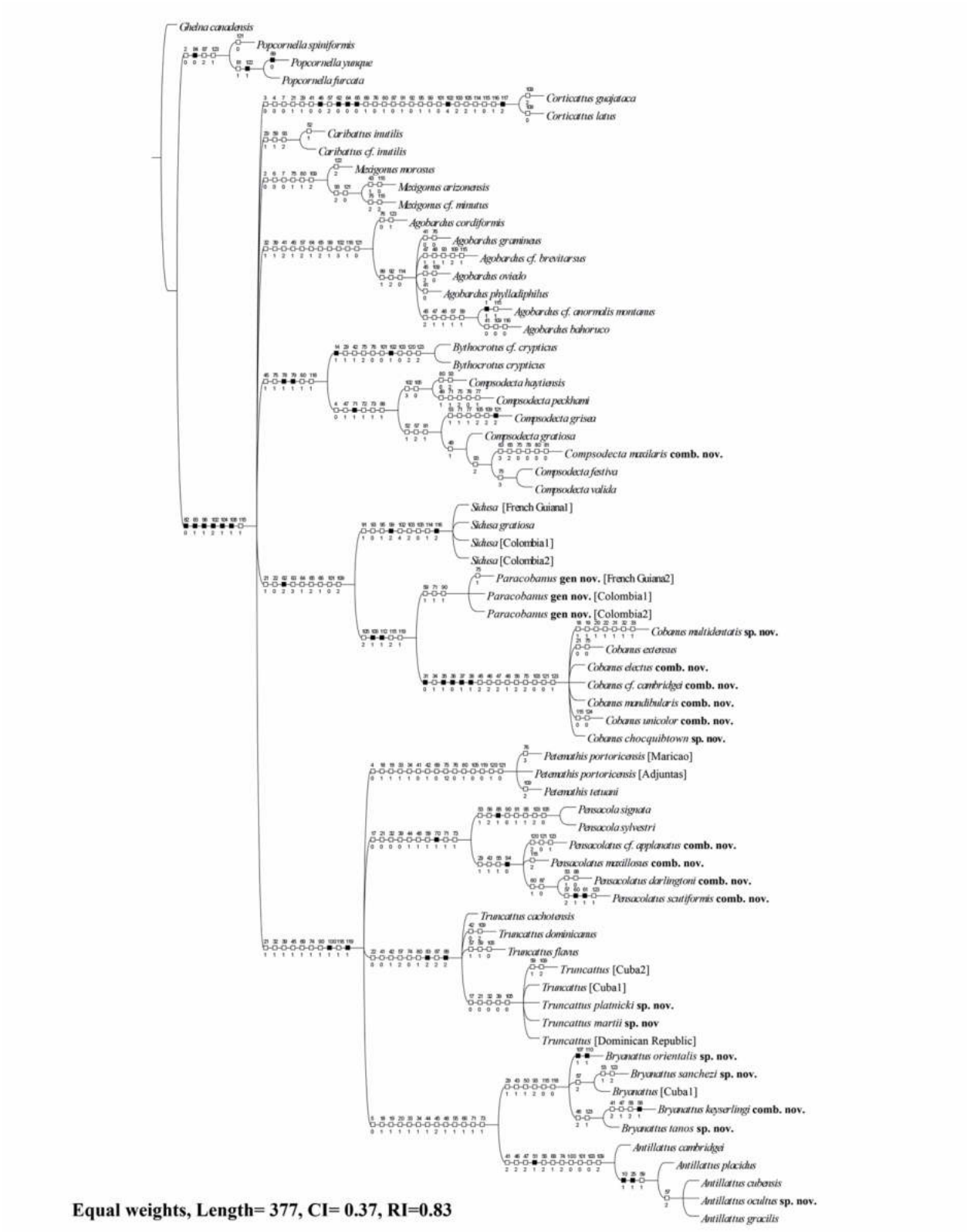

Figure. 2.18. Strict consensus (morphology) of the most parsimonious trees obtained under equal weights (CI=0.37, RI=0.83).

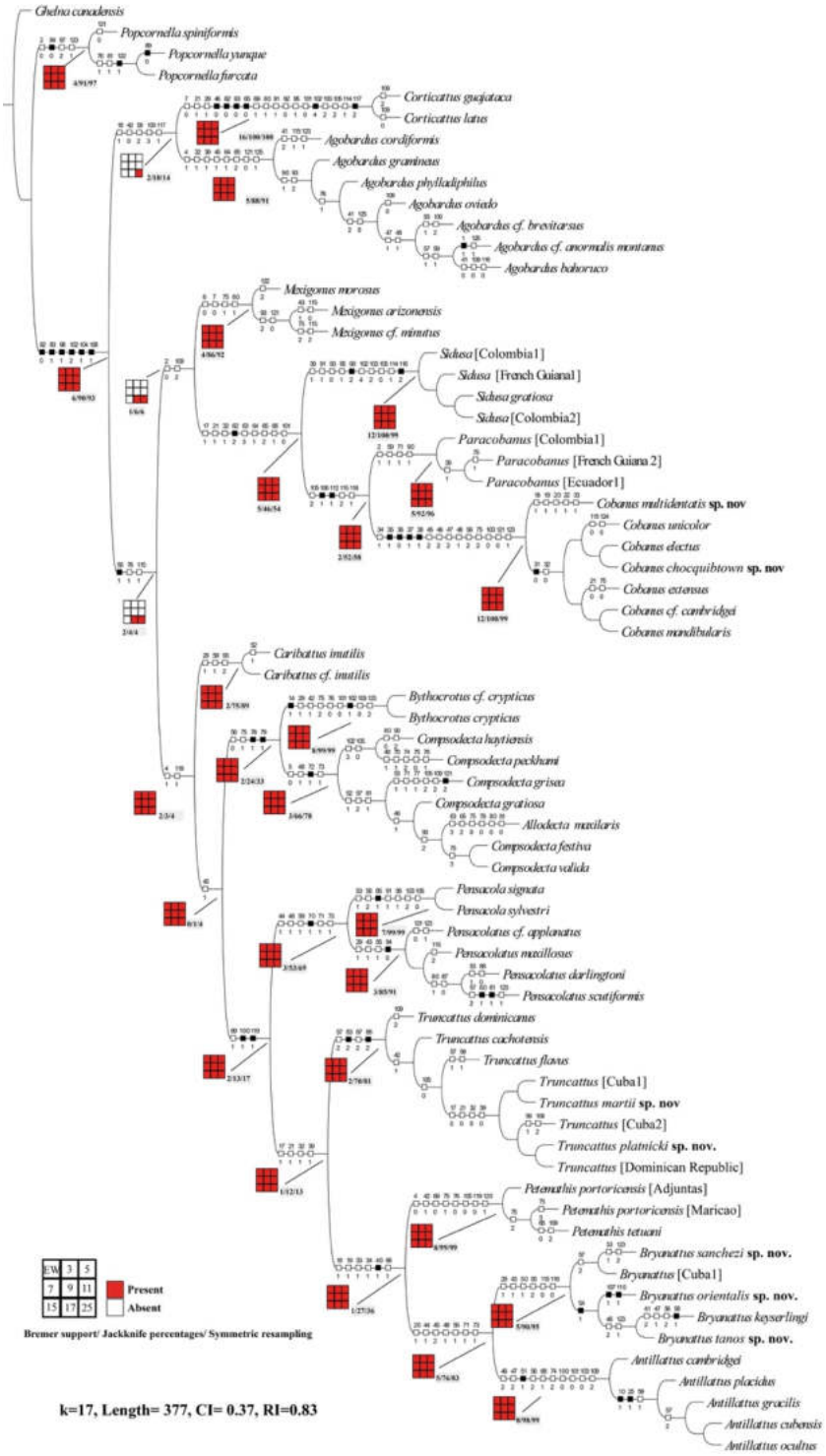

Figure. 2.19. Topology (Morphology) obtained under $k = 17$. Filled and open squares represent the sensitivity analysis under different implied weighting values (k=3-25). Numbers are Goodman- Bremer support, Jackknife percentages and symmetric resampling values, respectively.

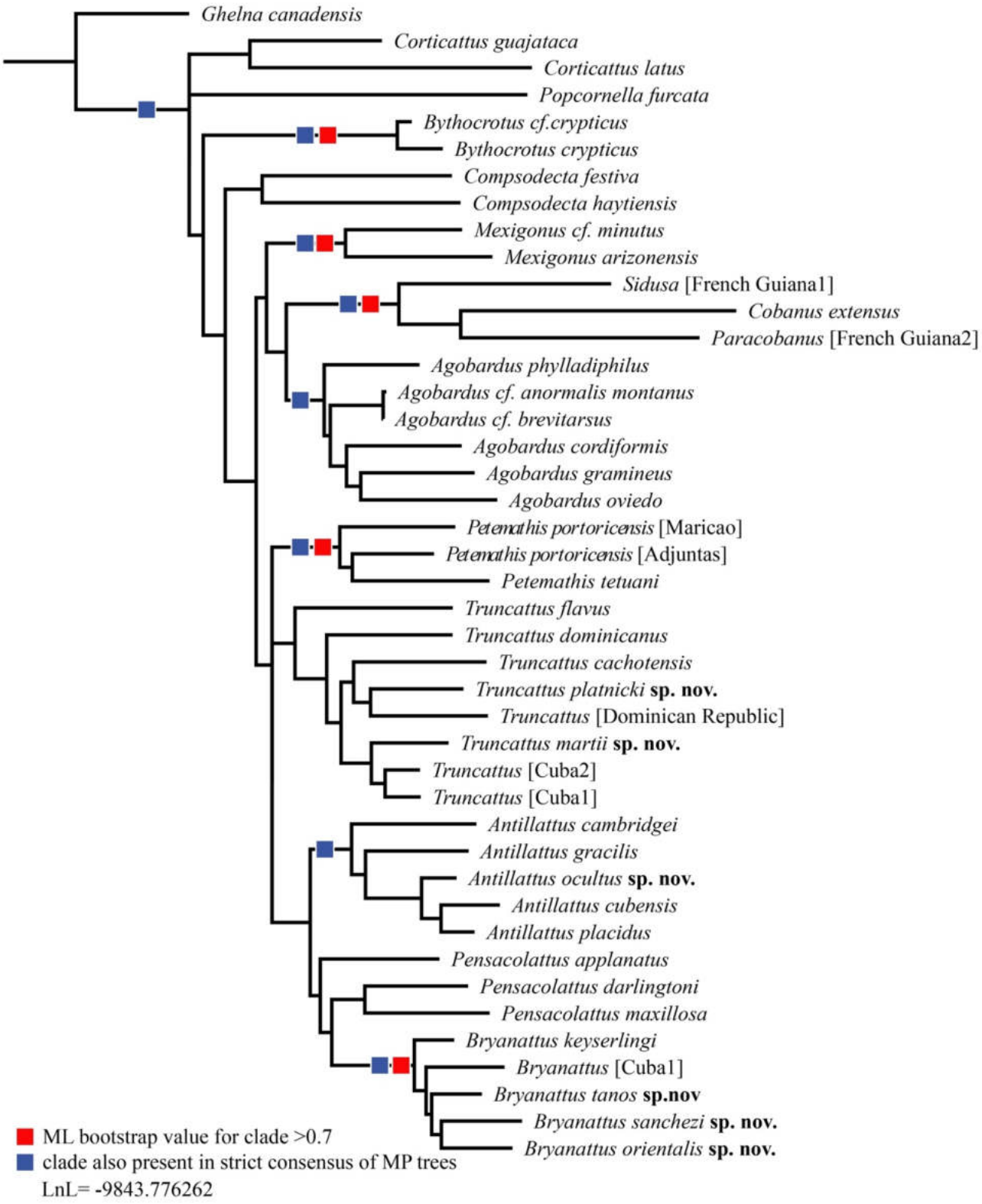

Figure 2.20. Summary of ML and MP analyses on the COI tree from the ML analysis.

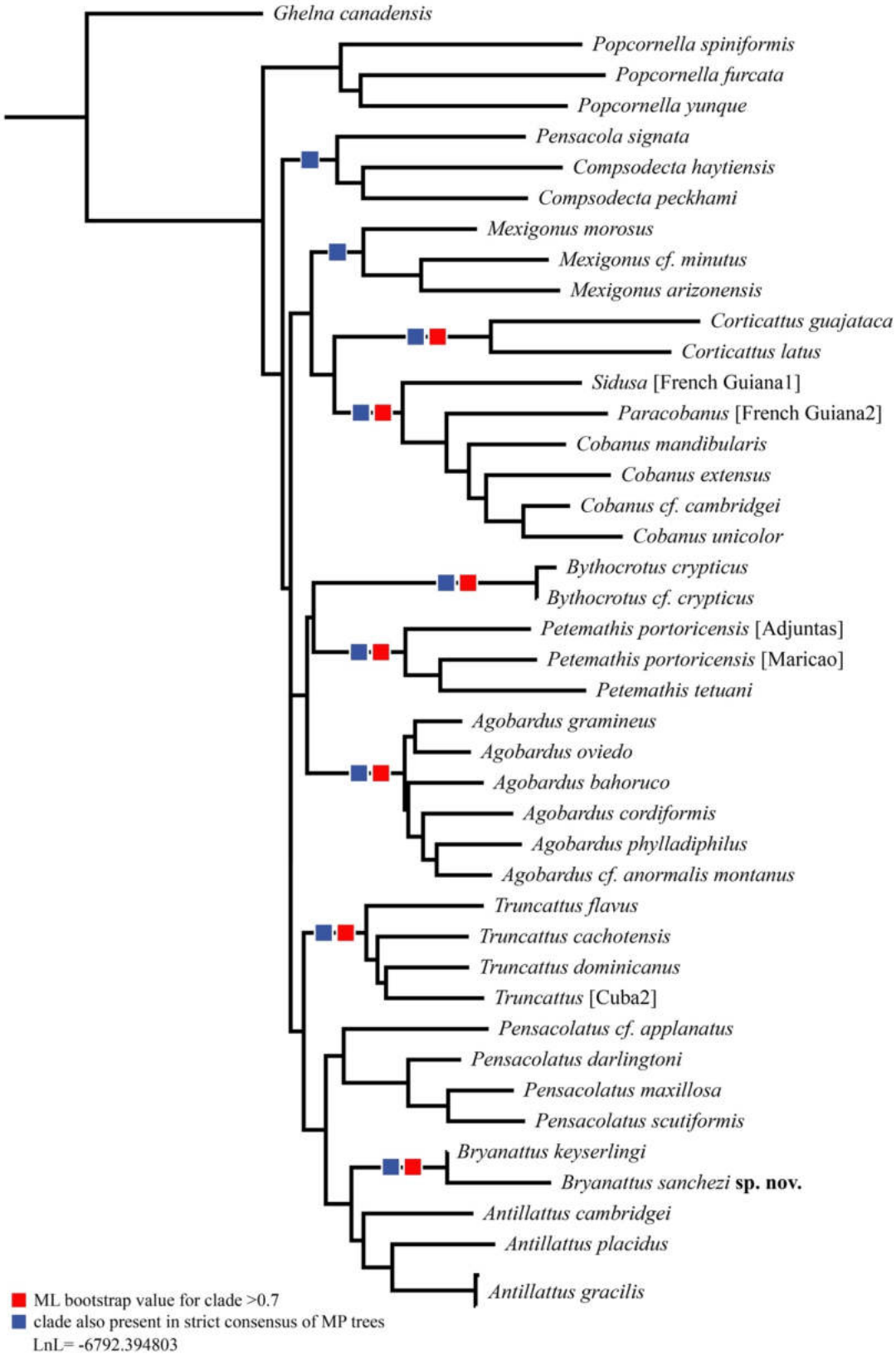

Figure 2.21. Summary of ML and MP analyses for 16S. Tree shown is the best tree from the ML analysis.

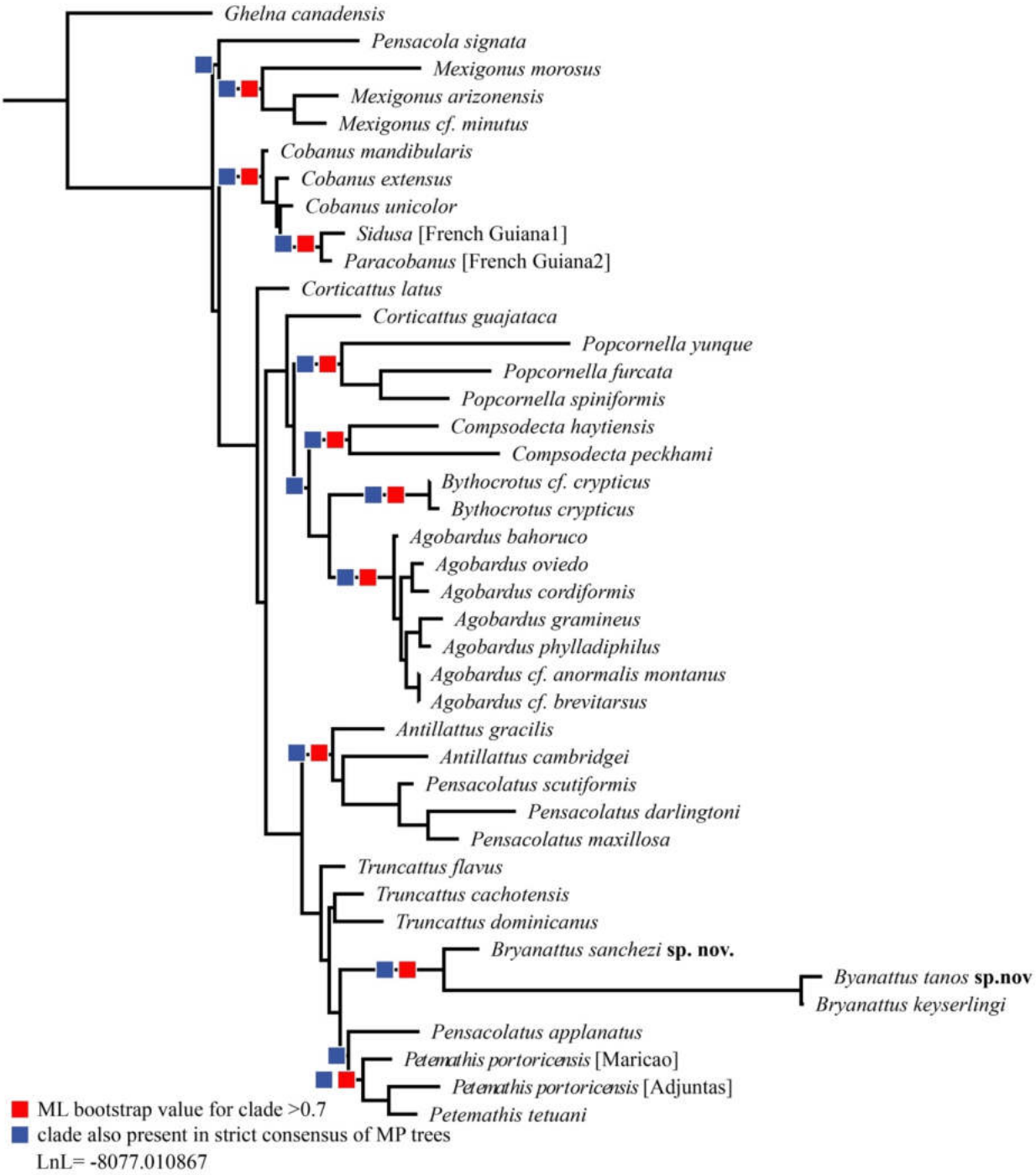

Figure 2.22. Summary of ML and MP analyses on the 28S tree from the ML analysis.

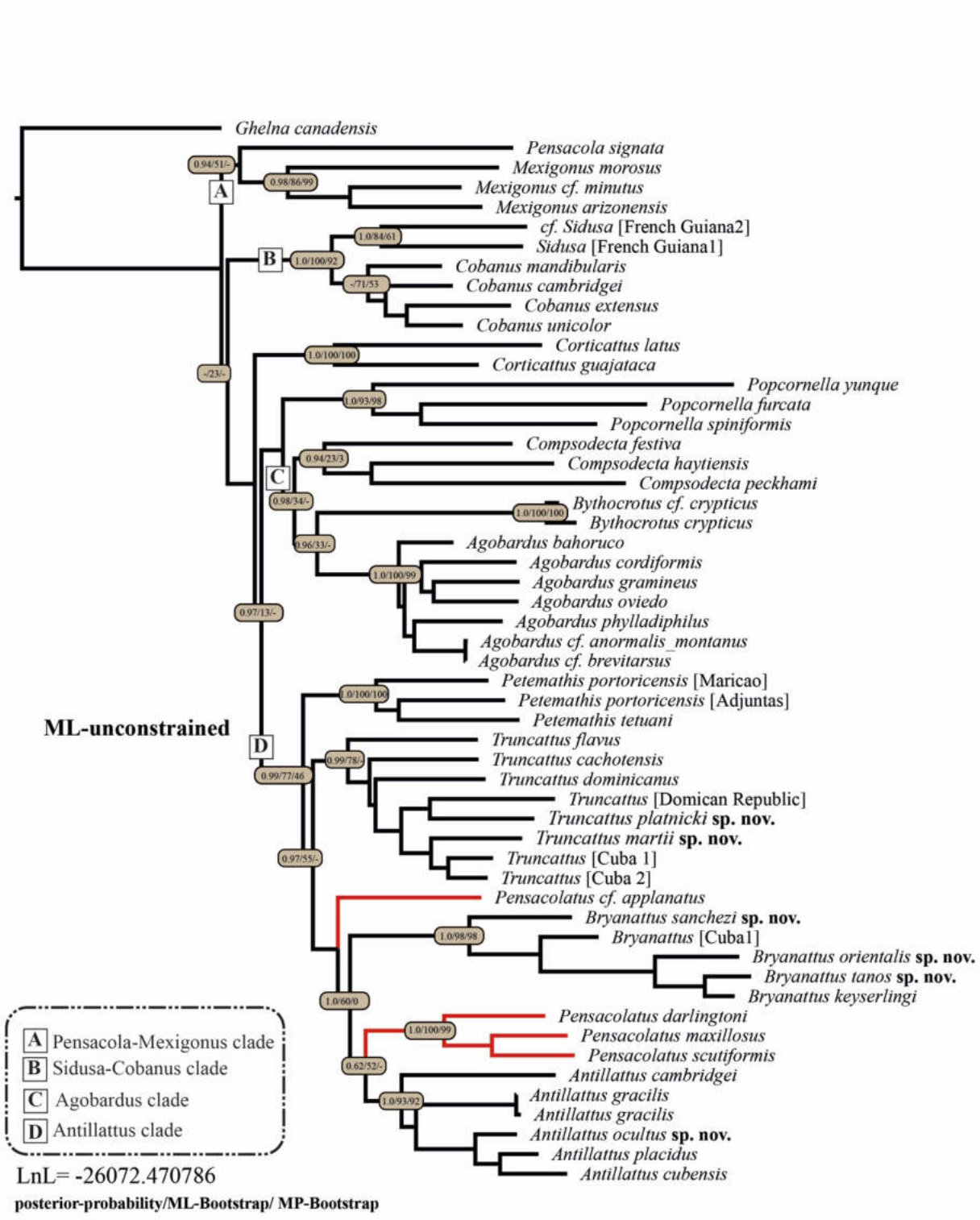

Figure 2.23. Summary of ML, MP and BI analyses of all genes combined (COI, 16S, 28S) using the constraint tree from the ML analysis.

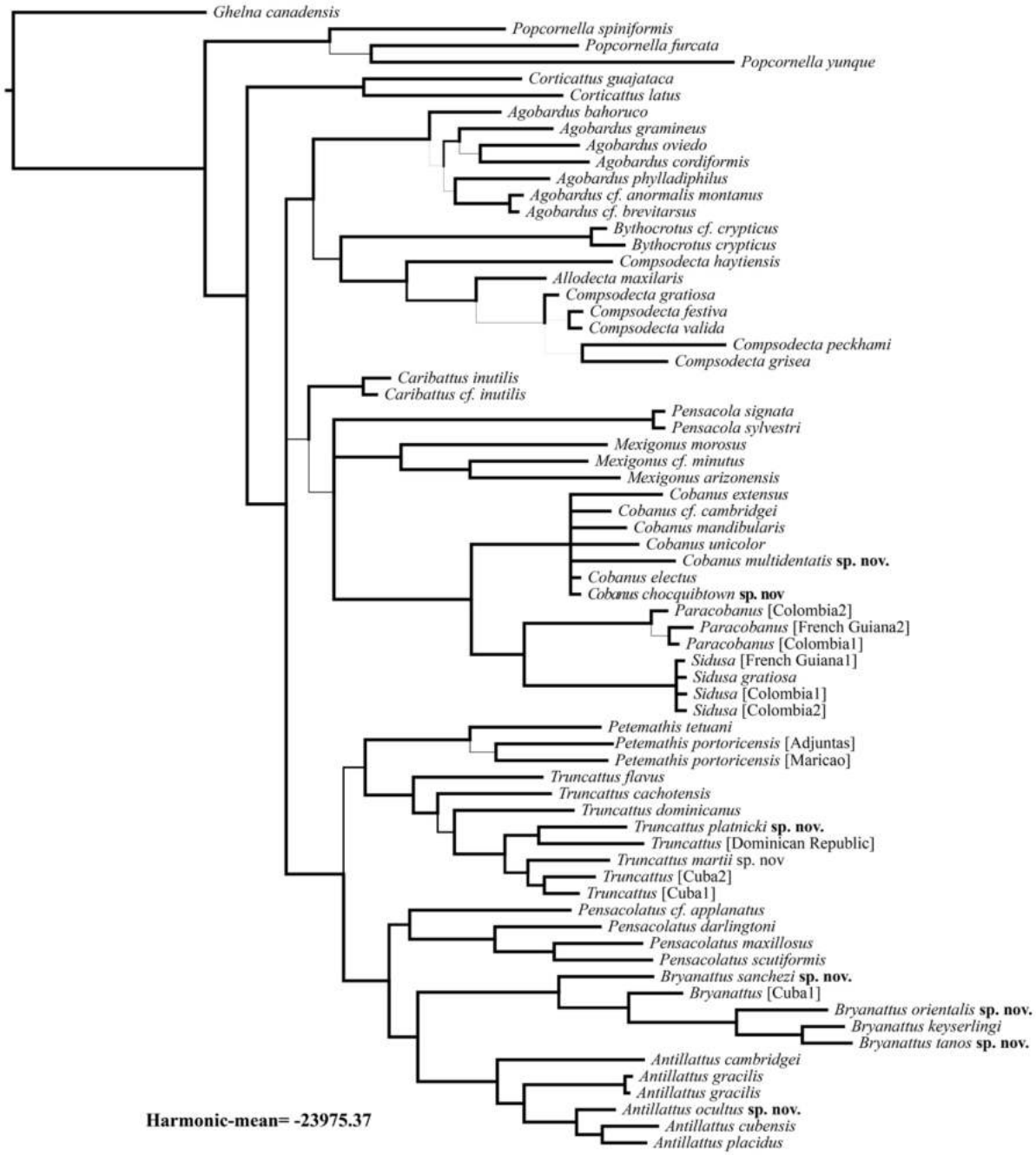

Figure 2.24. The best tree from Bayesian analysis on the combined morphological and molecular datasets (morphology, 28S, 16S and COI).

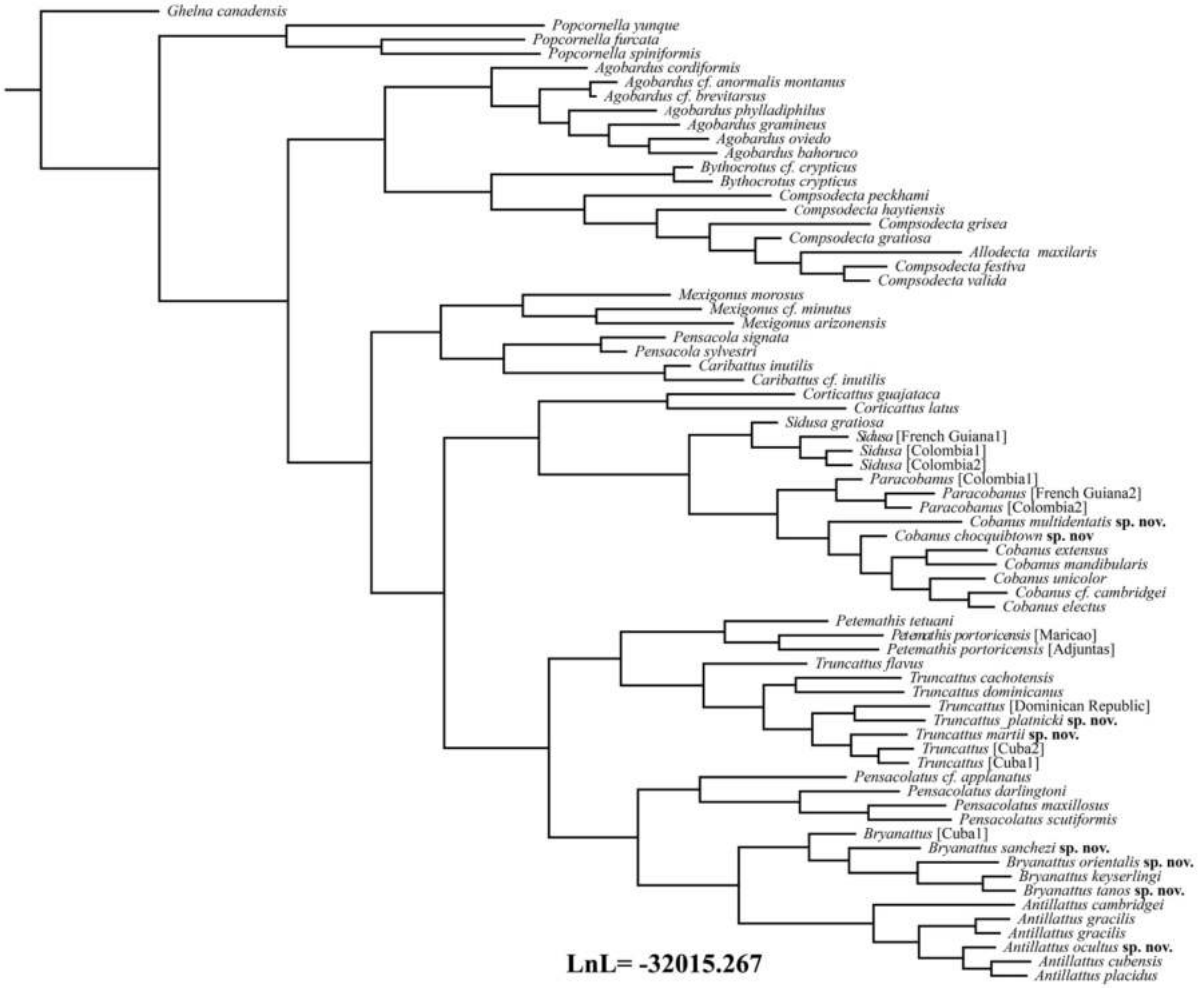

Figure 2.25. ML tree from the combined morphological and molecular datasets (morphology, 28S, 16S and COI).

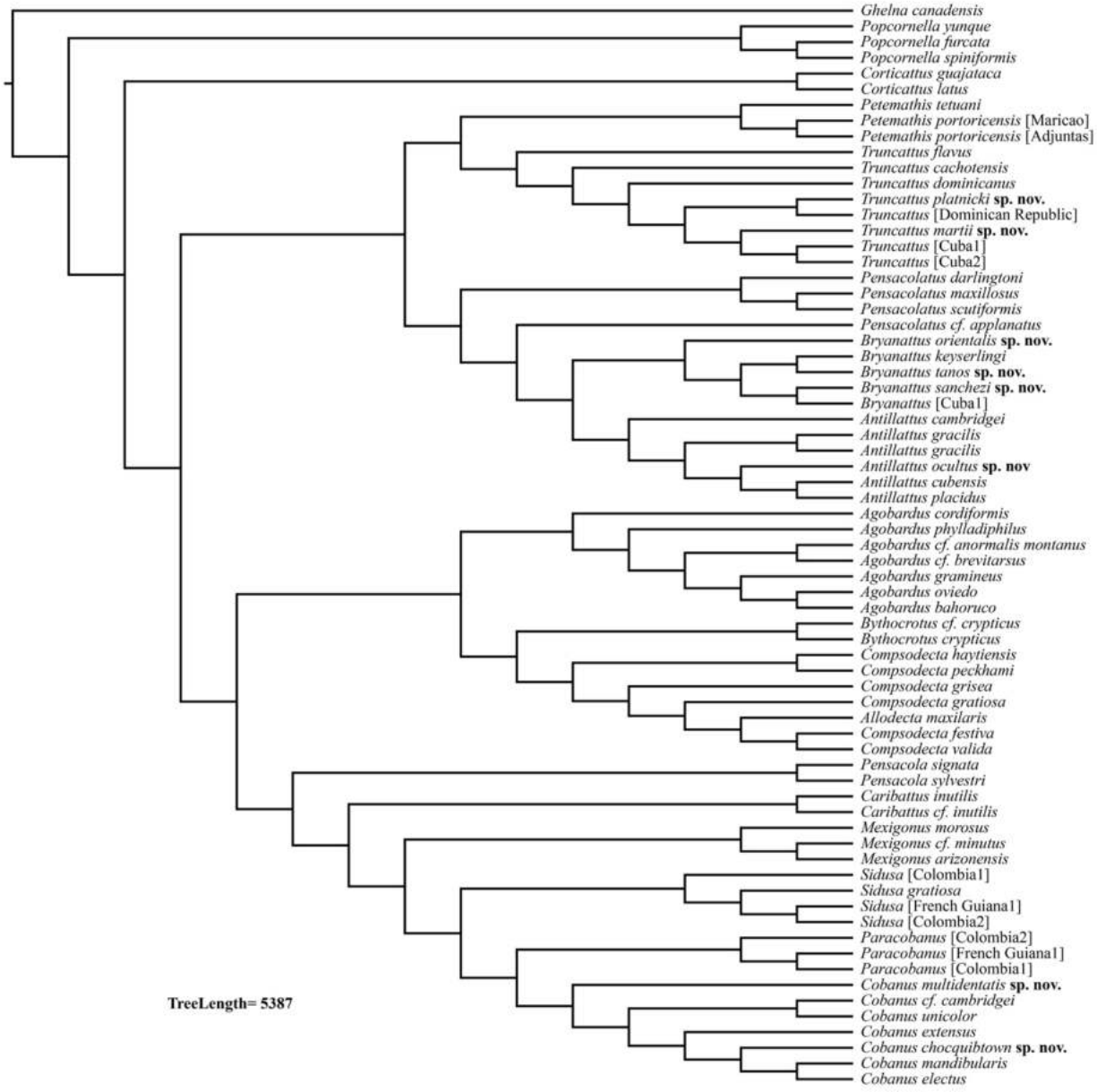

Figure 2.26. Strict consensus (unconstrained analysis) from MP analysis on the combined morphological and molecular datasets (morphology, 28S, 16S and COI).

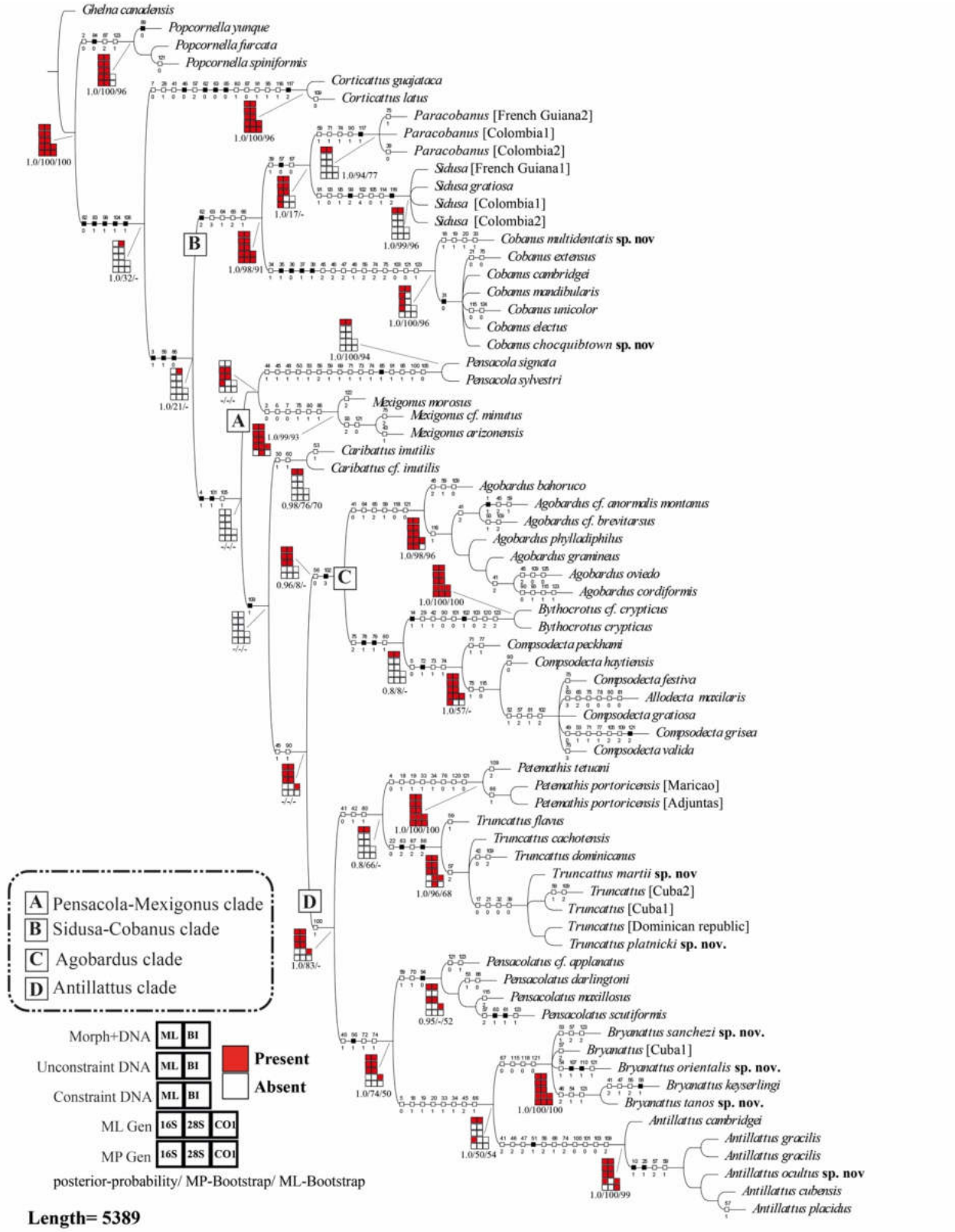

Figure 2.27. Strict consensus (constrained analysis) from MP and summary of ML and BI analyses on the combined morphology and DNA datasets (morphology, 28S, 16S and COI).

2.3 Discussion

2.3.0 Phylogenetic inference

Our study was designed to evaluate the monophyly of the Antillattus clade and explore the relationship between its genera. Nevertheless, we are aware that limited sampling leads to sensitive topologies (Cabra-Garcías and Hormiga 2020) and that the inclusion of more species and data will affect the structure of our phylogeny.

In addition, the exclusive use of molecular characters can result in a lack of morphological sense to general groups with morphologically different taxa (Cabra-Garcías and Hormiga 2019; Kluge 2004 2009). Although morphological characters were dramatically outnumbered by DNA data, they were phylogenetically informative and resolved the relationships between taxa quite well. Zhang and Maddison (2015) also included morphological evidence, but their morphology tree poorly resolved. Based on retention index value, our character subset analysis shows a good phylogenetic signal from our morphological characters.

Previously, the only morphological phylogeny that included the genera *Caribattus* Bryant (1950) and *Allodecta* Bryant (1950) was the PhD thesis of G. Bodner (2002). Their preferred cladogram recovered *Caribattus* as sister to *Euryattus bleekeri* (Doleschall 1859), and *Allodecta* is nested with *Bathippus* Thorell (1892) and *Cobanus* F. O. Pickard-Cambridge (1900). In our study, the genus *Caribattus* appears to be more closely related to the Agobardus clade, and *Allodecta* is nested within *Compsodecta*. We believe that the instability of *Caribattus* is a product of missing data (Kearney 2002), search heuristics (Zhou *et al*. 2018) and a lack of molecular data.

Zhang and Maddison (2015) found two possibilities of the relationship of the Antillatus clade to the [whatever group you want to use here]: 1) the Agobardus clade is sister to the Antillattus clade; 2) the Pensacola-Mexigonus clade is sister to the Antillattus clade. Our favored hypothesis shows the Agobardus clade as sister to the Antillattus clade and the Pensacola-Mexigonus clade as sister to the Agobardus clade + Antillattus clade.

The results obtained under ML, BI and MP total evidence analytical approaches show some congruence with one another. Our analyses recover the Sidusa-Cobanus clade, contradicting more recent hypotheses, resulting in the transfer of *Cobanus* to *Sidusa*. We found that the Sidusa-Cobanus clade is recovered based on two unambiguous synapomorphies: metatarsus with 2-2-2 macrosetae (char. 64-2 and pre-spiracular bump present (char. 66-1).

The Antillattus clade is recovered to include the genera *Petemathis*, *Truncattus*, *Pensacolatus* and *Bryanattus* **gen. nov**. Within our dataset, the Antillattus clade is supported by one homoplasious synapomorphy (table 2.2), the development of the embolus in relation to

the distal tegular lobe. However, the addition of new taxa may preclude this character from being a synapomorphy of the Antillattus clade.

Our analysis of total evidence and all genes combined differed in the placement of *Truncattus* and *Petemathis*. In the molecular phylogeny and the total evidence phylogeny of Zhang and Maddison (2013, 2015), *Truncattus* is recovered as a sister group of Antillattus, while *Petemathis* is recovered as a sister group of *Truncattus* + *Antillattus*. Our combined molecular analysis yielded similar results to those obtained by Zhang and Maddison (2013, 2015) and recovered *Truncattus* as a sister group of *Antillattus* with strong support (pp = 0.99). The working hypothesis considering all of the evidence contradicts these results and recovers *Truncattus* as the sister taxon of *Petemathis* with low support values (MP-bootstrap = 0.66; pp = 0.8).

We believe that the recovery of the *Petemathis+Truncattus* clade is a product of combining the morphological and molecular data. Previous studies have shown that morphological characters can have a disproportionately large effect on total evidence phylogenetic analyses, changing both topology and support, thus affecting concomitant taxonomic decisions (de Sá *et al*. 2014; Mirande 2017; Sánchez-Pacheco *et al*. 2018; Cabra-García and Hormiga 2019). The phylogenetic hypothesis obtained from our data are inconclusive; however, they minimize the number of transformation events required to explain the character states as hypotheses of homology (Cabra-García and Hormiga 2019; Farris 2008; Freudenstein 2005).

Finally, we have provided evidence and a preconceived idea that the genus *Pensacolatus* is monophyletic. We acknowledge that broader molecular sampling is necessary for subsequent studies. The molecular and total evidence phylogenetic reconstructions proposed by Zhang and Maddison (2013, 2015) recovered *Antillattus applanatus* (here transferred to *Pensacolatus*) as closely related to *Antillattus gracilis* and *A. cambridgei*, away from its presumed sister species *Antillattus darlingtoni*, *A. maxillosus* and *A. scutiformis*. The monophyly of *Pensacolatus* is not recovered in the tree inferred from the unconstrained combined molecular dataset and the unconstrained MP total evidence analysis (fig. 2.27), and our constrained ML and BI molecular are less likely than unconstrained. However, our analyzes of total evidence found that *Pensacolatus* is monophyletic.

2.3.1 Cheliceral teeth evolution

The chelicerae are one of the most used structures in phylogenetic analysis and taxonomy of spiders (Azevedo *et al*. 2018; Cabra-Garcia and Brescovit 2016; Ramírez 2014;

Zhang and Maddison 2015). In salticids, the morphological characters typically involve a retromarginal and promarginal tooth count; cheliceral size; stridulatory organs and presence or absence of ornamentations (Bryant 1940, 1943, 1950; Simon 1903; Zhang and Maddison 2015). We coded and mapped these characters within the molecular phylogeny and total evidence tree and found that they can be very informative.

Simon (1903) introduced the pluridentati, unidentati and fissidentati based on the retromarginal teeth. This classification system was the basis for the elaboration of the characters used to date to refer to the dentition of the promarginal and the retromarginal teeth i.e. 1 tooth; 1 bicuspid tooth; multiple cusps. However, a character can be more informative if analyzed independently (Sereno 2007). We separated the teeth into serially homologous structures under a topological equivalence criterion.

Azevedo *et al.* (2018) also used this approach with much more informative results. Ramírez (2014) showed that coding only the number of teeth (regardless of homology of each tooth) was 'highly incongruent with the phylogenetic tree'. An overview of the cheliceral teeth within euophryines is given in figure 2.2. We found that the female and male paturon promarginal tooth III first appears within *Antillattus* (char. 10 [state 1], char. 25 [state 1]). The presence of three or more promarginal teeth is scored as present in basal groups of Salticidae (e.g. Lyssomaninae). This condition can also be scored as present within Amycoida, Marpissoida and Saltafresia. This indicates that it is a plesiomorphic state that has arisen and been lost several times during the evolution of Salticidae.

The male retromarginal tooth II appears at least four or six times independently. Within the Agobardus clade, retromarginal tooth II appears in *Agobardus*, and is then lost in *Compsodecta* and *Bythocrotus* (fig. 2.29). Similarly, in the Antillattus clade, the retromarginal tooth II appears in *Petemathis* and Dominican Republic *Truncattus*, is lost in Cuban *Truncattus* and *Pensacolatus*, and returns in *Bryanattus* and *Antillattus* (fig. 2.29). For example, basal groups, such as *Onomastus*, *Asemonea*, and *Lyssomanes* are pluridentati, indicating that this is a pleisomorphic trait, but within Amicoida and Saltafresia, the character state is present in some groups and lost in others.

Another character we examine is whether the teeth are fused on a common base or are independent (char. 21 and char. 29), or bicuspid or multicuspid (char. 22 and char. 30) (fig. 2.28). The fusion of the teeth appears to be a condition that has evolved within *Amycoida* and Saltafresia, appearing and disappearing many times within Euophriyni. We found that teeth appeared fused distally in relation to the base of the fang. This suggests that there may have

been a migration of the retromarginal teeth post-fusing. The genus *Antillattus* supports this hypothesis. *A. cambridgei* presents what we call incomplete fusion of the retromarginal teeth.

A loss of teeth has occurred in a different sense within *Cobanus*. The retromarginal teeth I, II and III (char. 31-0, 32-0, 33-0) have been lost among *Cobanus* species including *C. extensus*, and only teeth IV and V, closest to the base of the fang, are present. The loss of some retromarginal teeth is observed in other groups within Salticidae. For example, within *Hentzia*, teeth I, II and III are lost. The taxonomic distribution of retromarginal tooth count, retromarginal tooth fusion and their topological position indicates that we should expect high levels of homoplasy in that character system. However, the system still retains strong phylogenetic signal (RI between 0.70 and 100).

2.3.2 Palp evolution

The male palp morphology provides the largest suite of characters for study and traditional description in Salticidae. The taxonomic history for these character sets can be divided into before and after Prószyński (1976). Although male genitalia are commonly used in spider phylogenetic systematics, it can be extremely difficult to establish homologies of the palpal sclerites across diverse taxa (Azevedo *et al*. 2018; Hormiga 1994ab; Ramírez 2014). For example, Ramírez (2014) does not discern separate homology correspondences for a dorsal apical tibial apophysis, an RTA displaced to a dorsal position, or a dorsal subprocesses of a complex RTA. The same happens when establishing a homology of the conductor within spiders (Ramírez 2014).

We collected an extensive number of palpal characters (39 characters). One of these is an apomorphy in Salticoida, the endite having an anterior-lateral cusp (fig. 2.30). Our analysis shows that it has independently evolved at least four times. We focus the remaining discussion on the tibia and the palpal bulb. The reader should refer to Ramírez (2014) for further discussion on the ontogeny and homology of palpal elements. An overview of the palp within euophryines and its landmarks is given in figure 2.7 A-C.

Tibia and VTA: Within euophryines, the male palpal tibia is usually quasi-cylindrical and generally with an RTA, although in some species it has a VTA and/or PTA. In *Compsodecta* and *Bytocrottus*, the tibia is modified to have a globose appearance, ridges or has a subtriangular appearance. The tibiae of the members of the Antillattus clade are characteristically cylindrical, without a PTA and with simple RTA, ranging from short to long. A VTA (fig. 2.31) appears in *Truncattus* and *Petemathis* and then is lost in some *Pensacolatus* species and re-appears in

others, to finally be lost in *Antillattus* and *Bryanattus*. As in Zhang and Maddison (2015), the VTA can arise and be lost within some clades e.g. Anasaitis-Corythalia and the Antillattus clade.

pTL: Ramírez (2014) considers the tegular lobe a locking mechanism that can fits an opposing lobe on a subtegulum (see Griswold *et al*. 2005: char. 116; Ramírez 2014, fig. 143A, B). In Salticidae, the tegular lobe (according to Ramírez 2014) is scored as present in the basal genus *Portia* and absent in *Plexippus*. The tegular lobe proposed by Zhang and Maddison (2015) is not homologous to the structure proposed by Ramírez (2014). For Zhang and Maddison (2015), the tegular lobe is a proximal projection of the tegulum onto the tibia that not locked with the subtegulum. Edwards (2015), following Galiano (1994), divided the tegular lobe into a proximal prolateral lobe and a proximal retrolateral lobe. However, it is complicated to consider proximal prolateral lobe and a proximal retrolateral lobe in groups where this structure is as wide as the tegulum (e.g. *Truncattus*, *Popcornella*) or where the lobe is more toward the medial area of the tegulum (e.g. *Corythalia*). Here, we refer to the tegular lobe as the proximal tegular lobe (pTL).

The pTL is found in basal Salticidae. In *Onomastus*, the tegulum ends in a thin and curved tegular apophysis. Within Spartaeinae, the pTL is present in some species (e.g. *Portia fimbriata*). In Salticoida, the character is scored as present some groups. For example, within Agoriini, the pTL appears in *Agorius*. Within the tribe Baviini, the character appears within *Bavia* and *Stagetillus*. *Piranthus* likely has a pTL, but there are no known male specimens. The pTL also appears within the tribe Neonini. The pTL has appeared at least five times throughout our dataset (fig. 2.32).

Edwards (2015) mentioned a relationship between the pTL and VTA that appears to restrict the rotation of the lobe. Functionally, this would be similar to what Ramírez (2014) describes; however, this must be tested. We also found that not all species with a pTL had a VTA. For example, several species of *Plexippus*, *Freya decorata*, *Chinattus parvulus*, *Chapoda gitae*, *Coryphasia fasciiventris* and *Naphrys pulex* have a pTL but do not have a VTA. By contrast, *Anasaitis placida*, *Bythocrottus crypticus*, *Chapoda peckhami* and *Omoedus brevis* have a VTA but do not have pTL.

pSDL and rTDL: The pSDL and the rSDL are plesiomorphic characters that have been lost and reappeared multiple times throughout the evolutionary history of Salticidae. In basal genera like *Asemonea*, both conditions occur. Most euophryines have a sperm duct loop on the

retrolateral side of the palpal bulb, and this has been considered an important character to distinguish euophryines from other Salticoida (Maddison and Hedin 2003; Zhang and Maddison 2015). Within Euophryini, *Amphidraus complexus*, *Pensacola signata*, *Varinatina minuta* and *Sidusa* species all have both a pSDL and an rSDL. However, the rSDL is missing in some genera, such as *Bulolia*, *Coccorchestes*, *Sobasina*, *Marma* and *Neonella*, while the pSDL is present in a few lineages, including *Coccorchestes*, *Bulolia*, *Leptathamas* and *Corticattus*. Within *Antillattus*, *Truncattus*, *Petemathis* and *Pensacolatus*, the rSDL occupies less than half of the bulb width, while in *Bryanattus* the rSDL occupies more than half of the bulb width (fig. 2.33).

Embolic disc: The term embolic disc was proposed by Zhang and Maddison (2015) to refer to the disc-shaped element of the embolus basal process. Ramírez (2014) defines the embolic basal process as a sclerotized process, continuous with the embolus (Ramírez 2014; figs. 144A, 156E, 162D, 166D). Throughout Salticidae, the presence of this process is plesiomorphic and present in basal groups, such as Lyssomaninae and Spartaeinae (Ramírez, 2014). Edwards (2015) defined the embolus base as an expanded basal region of the embolus that is often different from the tegulum and usually more heavily sclerotized than the embolus which may or may not be fused to the tegulum. The embolic disc and its characteristic rotation appear within Euophryini, in some Dendryphantini and Freyina (Zhang and Maddison, 2015; Edwards, 2015). Unlike other processes, the embolic disc is completely free, which allows it to rotate on its axis when the embolic hematodochae expands. Evolutionarily, the embolic disc could be associated with the female window of epigynum. For example, males with embolic disc have females with window of epigynum. These window of epigynum are designed so that the embolic disc fits perfectly (e.g. *Agobardus*, *Antillattus*, *Cobanus*, *Sidusa*). This may be evidence of genital coevolution, including sexual selection (Eberhard 1985; Hosken and Stockley 2004), for mechanically feasible copulation and a lock-and-key mechanism to prevent hybridization (Eberhard 1985; Shapiro and Porter 1989).

2.3.3 Receptacle in copulatory duct evolution

According to Ramírez (2014), entelegynes usually have two pairs of ball-shaped receptacles, the primary and secondary spermathecae. The primary spermathecae connect to the fertilization duct and contain Bennett's gland (see Sierwald 1989, Ramírez 2014). The secondary spermathecae are blind receptacles with large glandular pores and ducts (Sierwald 1989; Carico and Holt 1964, and Ramírez 2003). Zhang and Maddison (2015) used the term

“accessory gland” to refer to the same structure that Ramírez (2014) describes as secondary spermathecae. The accessory gland is widely used in Salticidae taxonomy (e.g. Kanesharatnam and Benjamin 2016; Rubio *et al*. 2016; Żabka 1987, 1994). The argument for recognizing these structures as spermathecae is the homology between the gland ducts and the gland duct found on spermathecae and ducts of many haplogynes (Ramírez 2014, fig. 168B; Cala-Riquelme *et al*. 2015, figs 6-7) and Mygalomorphae (Michalik *et al*. 2005). By this reasoning, character secondary spermathecae (ch-76) proposed by Zhang and Maddison (2015) does not make sense because in Salticidae, the secondary spermathecae according to Ramirez (2014) it would be the accessory gland. We refer to the secondary spermathecae proposed by Zhang and Maddison (2015) as a receptacle in the copulatory duct according to Ramirez (2014). The receptacle in the copulatory duct is an expansion of the copulatory duct between the primary and secondary spermathecae (Ramírez 2014, figs. 173B, 178E, 180A, B, F, 181E, F). Within Salticidae, the character state is plesiomorphic (*Hispo*, score 1), and appears in several groups throughout the phylogeny.

In euophryines, the copulatory duct between the secondary spermathecae and the copulatory duct receptacle is generally very short. Our results indicate that the copulatory duct receptacle has appeared at least five times (fig. 2.34). The size of the copulatory duct receptacle and its position in relation to the primary spermathecae seem to be related: The larger copulatory duct receptacles are developed over the primary spermathecae or in front of them, while the smaller ones evolved laterally.

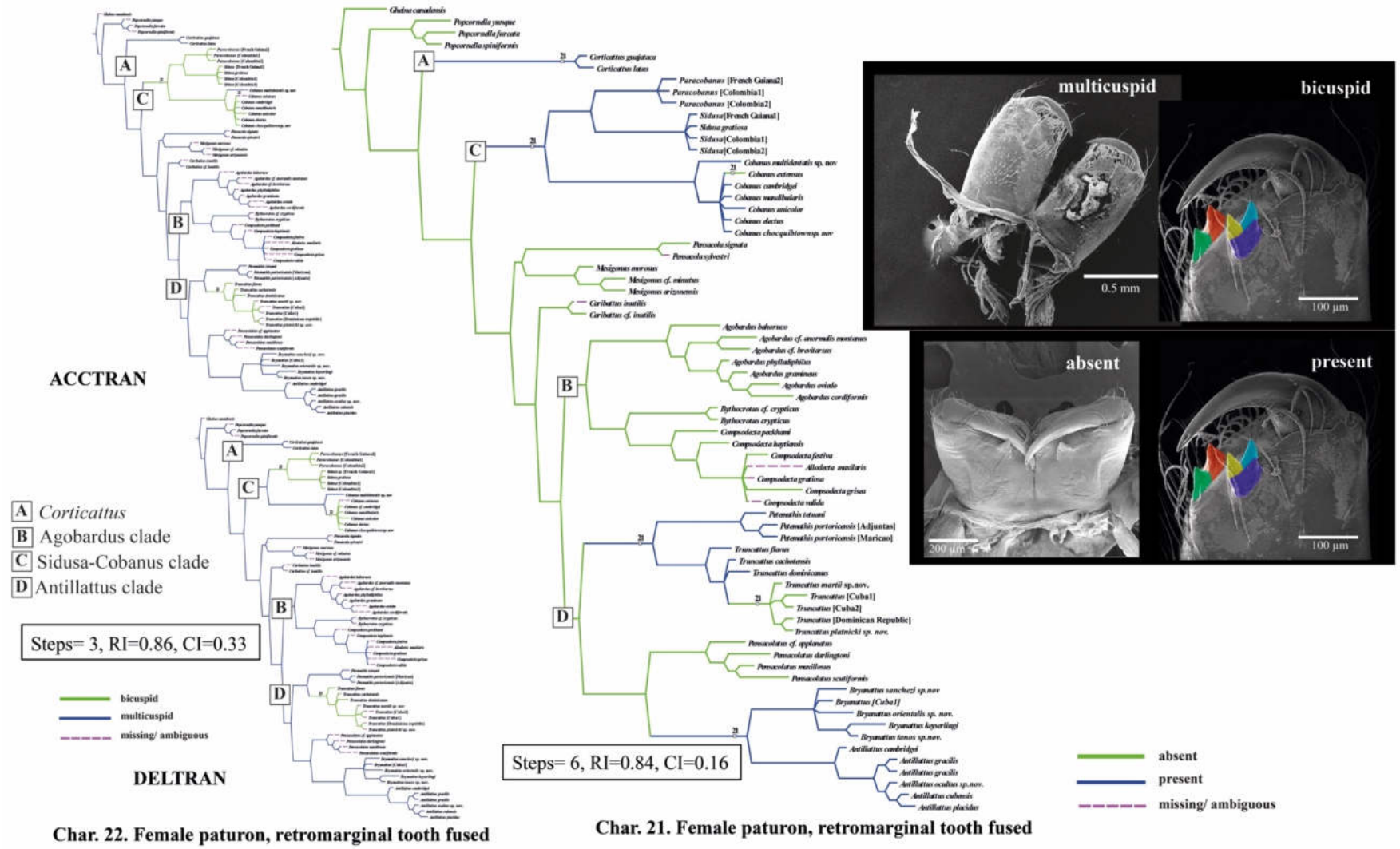

Figure 2.28. The evolution of female retromarginal tooth fusion (char. 21-22). Char 21, which can be absent (state 0) or present (state 1). Char 22, which can be bicuspid (state 0) or multicuspid (state 1). The character is unambiguous optimized on our preferred tree (MP).

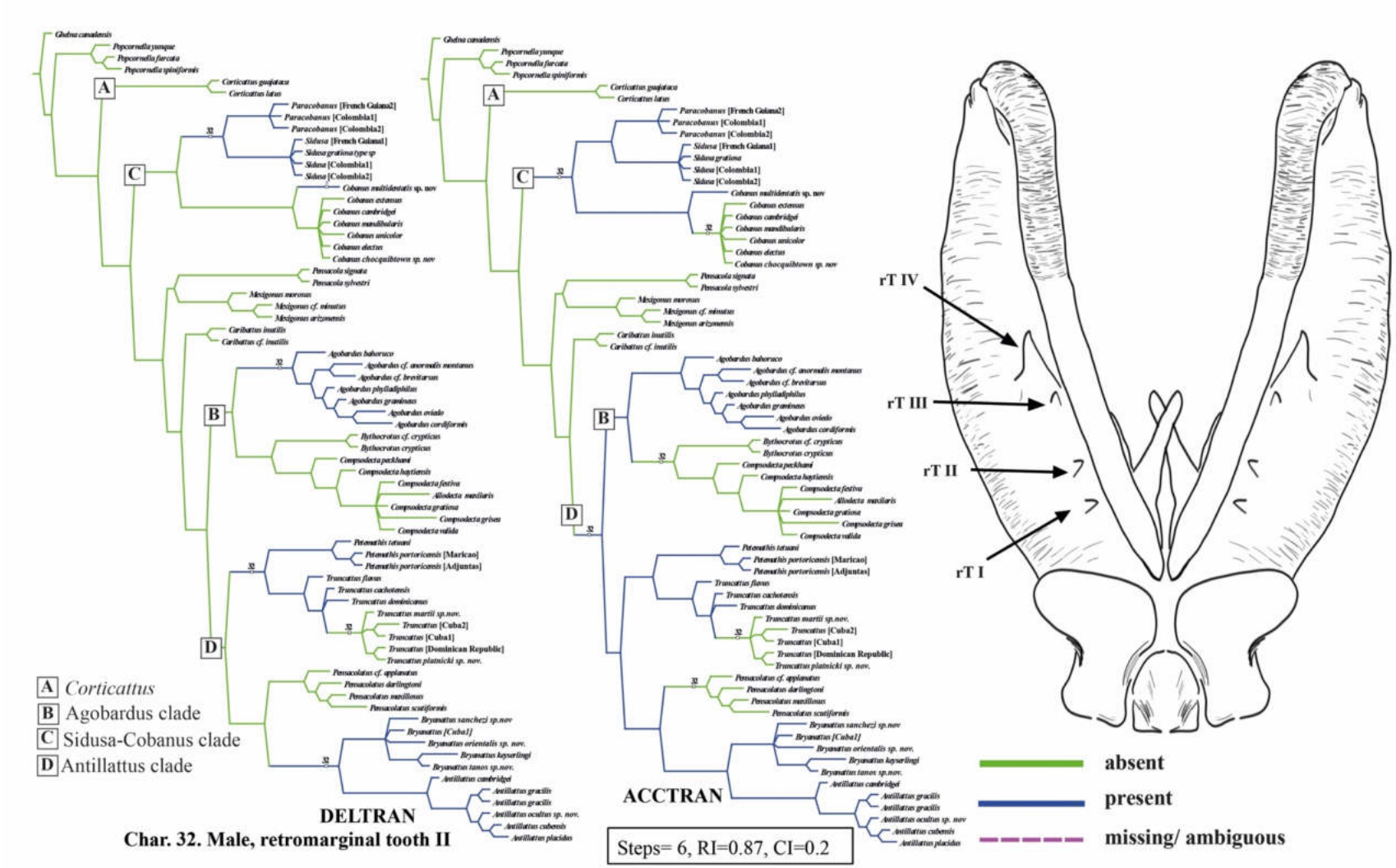

Figure 2.29. The evolution of the male retromarginal tooth II (char. 32), which can be absent (state 0) or present (state 1). The character is unambiguous optimized on our preferred tree (MP).

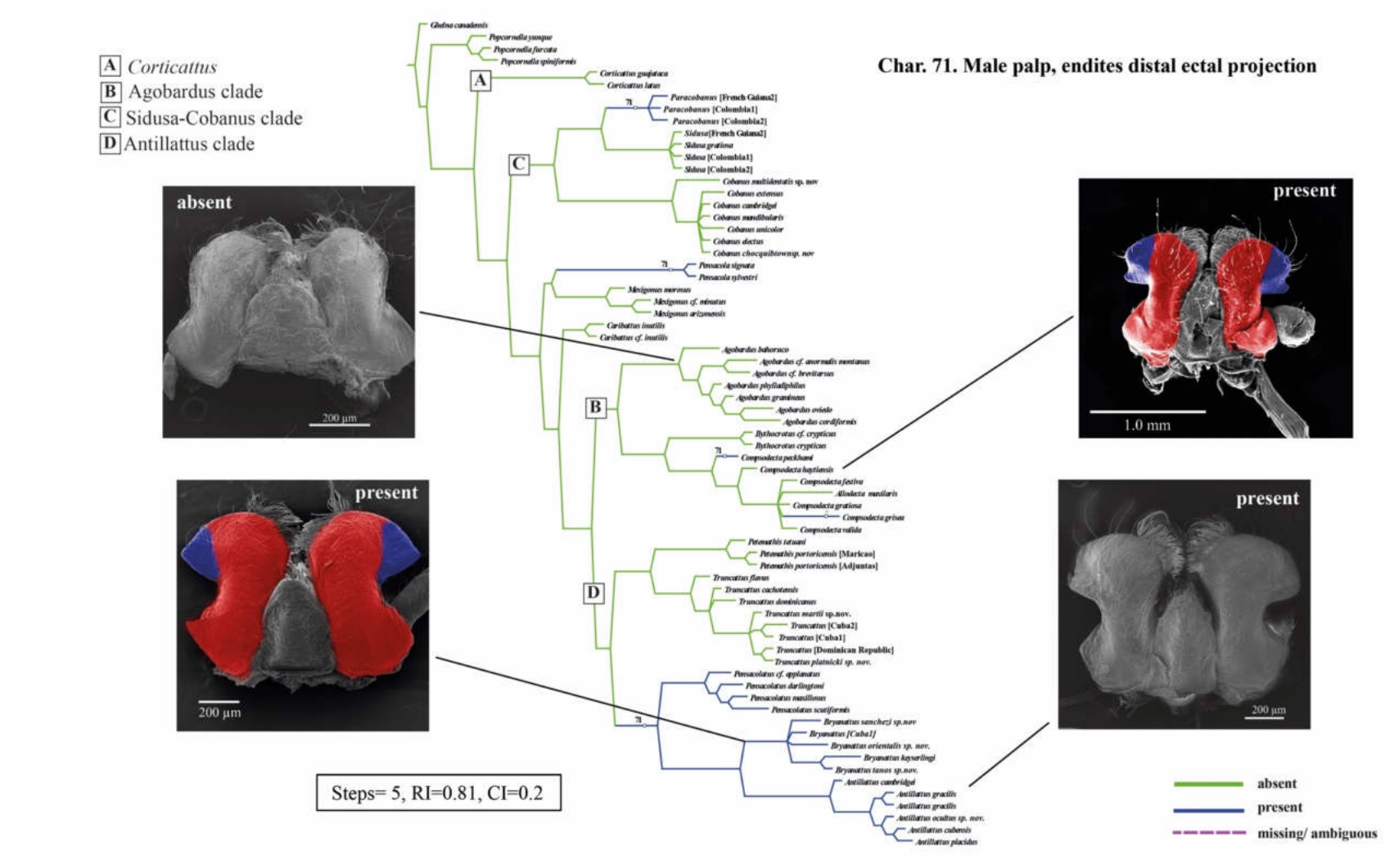

Figure 2.30. The evolution of anterior-lateral cusp of the male endite (char. 71), which can be reduced (state 0) or developed (state 1). The character is unambiguous optimized on our preferred tree (MP).

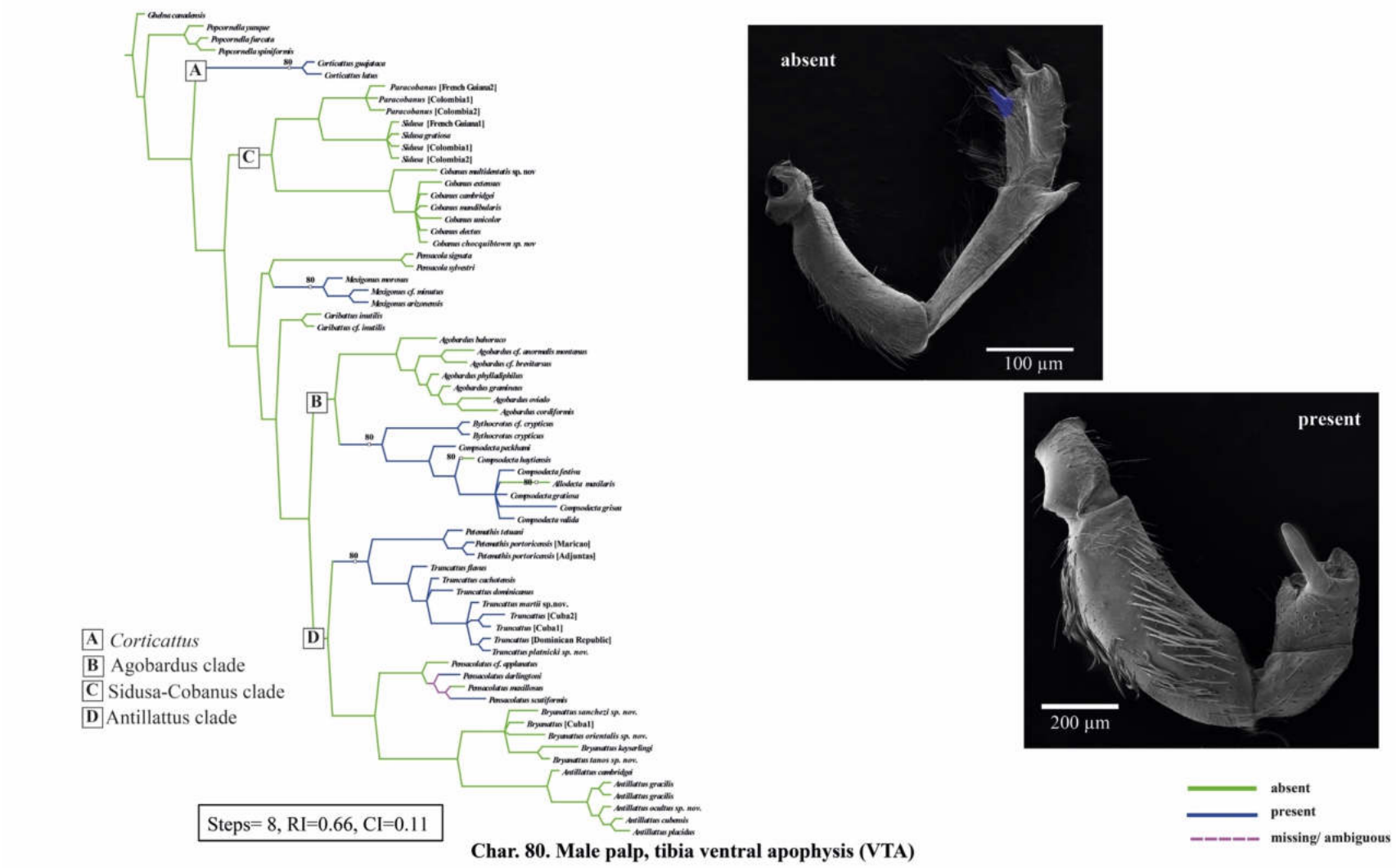

Figure 2.31. The evolution of the ventral tibial apophysis (char. 80), which can be absent (state 0) or present (state 1). The character is unambiguous optimized on our preferred tree (MP).

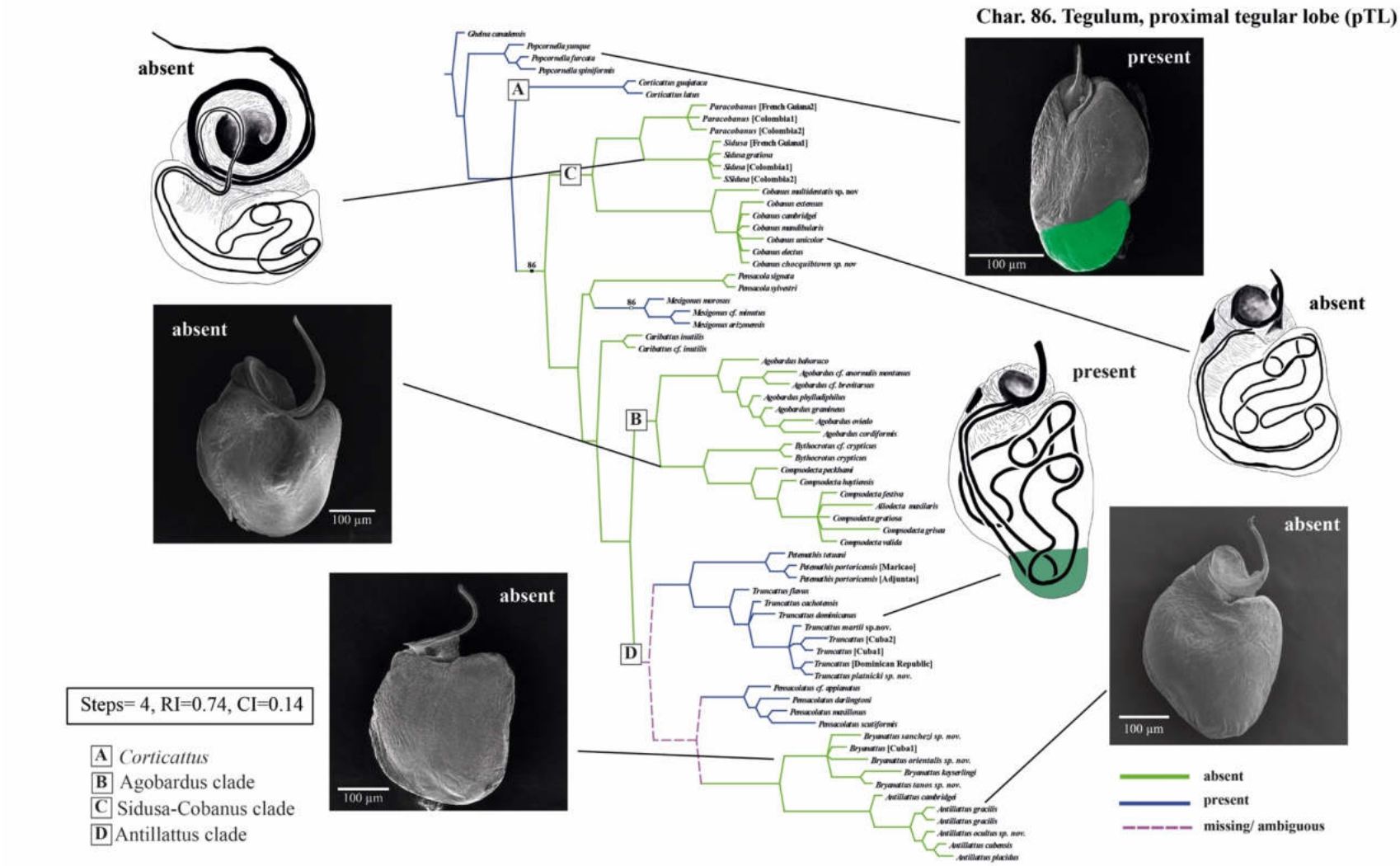

Figure 2.32. The evolution of the proximal tegular lobe (char. 86), which can be absent (state 0) or present (state 1). The character is unambiguous optimized on our preferred tree (MP).

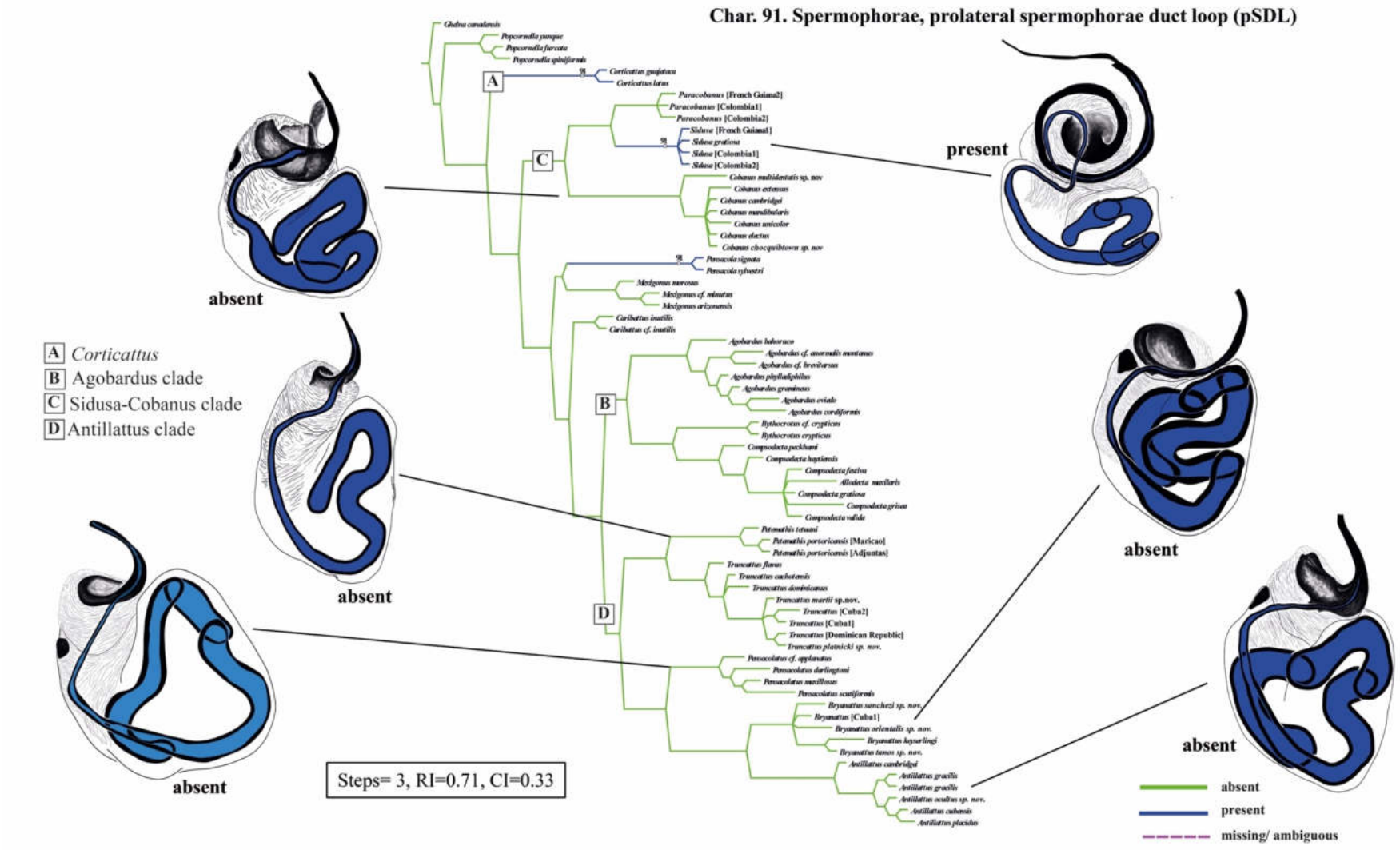

Figure 2.33. The evolution of the prolateral sperm duct loop (char. 91), which can be absent (state 0) or present (state 1). The character is unambiguous optimized on our preferred tree (MP).

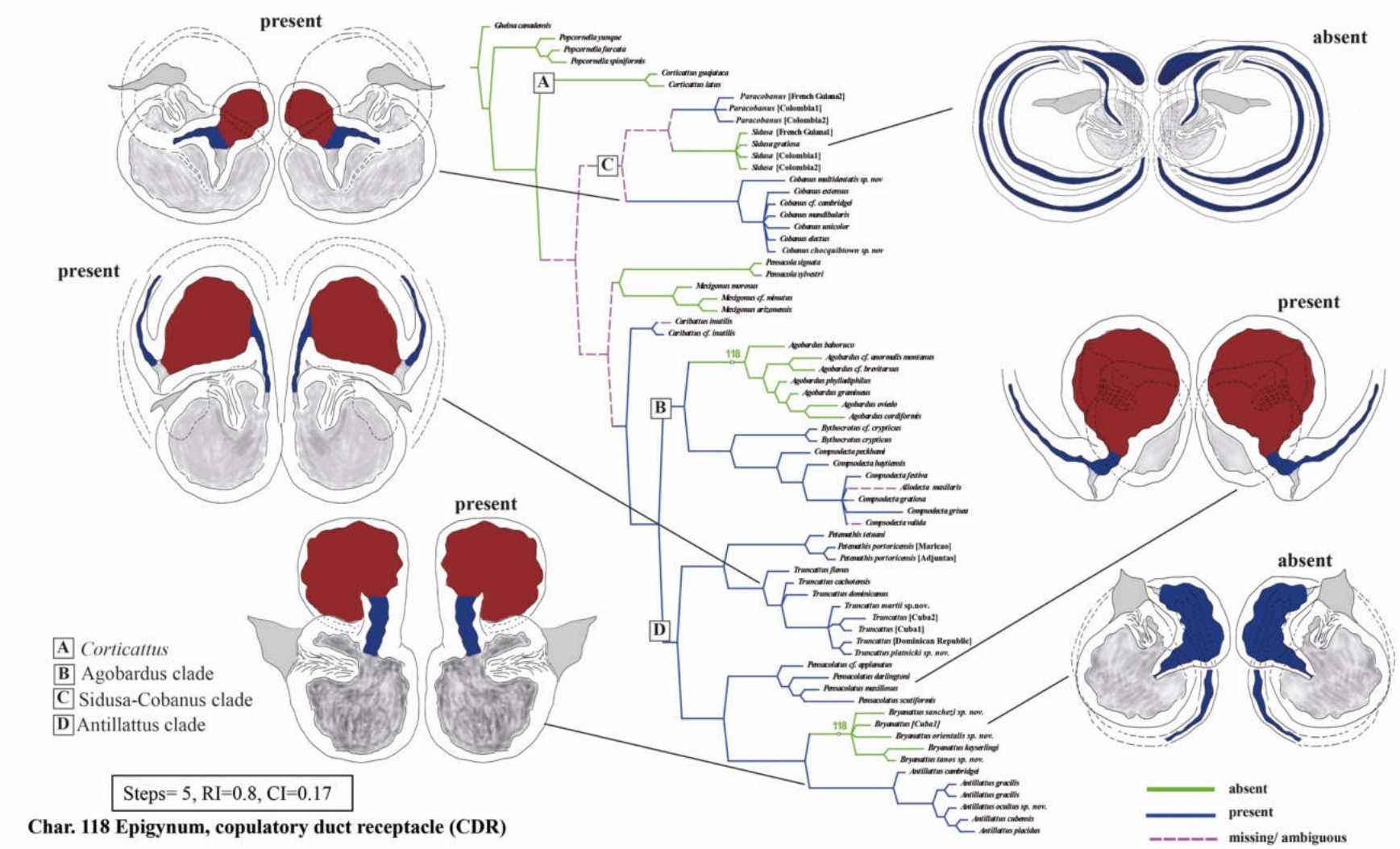

Figure 2.34. The evolution of the female copulatory duct receptacle (char. 118), which can be reduced (state 0) or developed (state 1). The character is unambiguous optimized on our preferred tree (MP).

2.3.4 Taxonomy

2.3.4.0 *Allodecta* is synonymous with *Compsodecta*

Allodecta (fig. 2.36) was originally described by Bryant (1950) as endemic to Jamaica. She described *Paradecta* and included *P. festiva*, *P. darlingtoni*, *P. gratiosa* and *P. valida*; however, *Allodecta maxillaris* was considered to belong to a different genus. Zhang and Maddison (2015) transferred *Paradecta* to *Compsodecta* based on modifications to the enlarged male endites (parallel transverse ridges or flat surfaces or projections), the anterior surface of the chelicerae and the male palpal tibia, patella and/or femur (small projection, wide extension or flat surface). The authors also considered *Allodecta* as a possible Antillattus clade member. Our analyses are consistent with results of Zhang and Maddison (2015) by recovering *Paradecta* as a junior synonym of Compsodecta; however, they contradict the position of *Allodecta* as a memer of the Antillattus clade.

We found molecular and morphological evidence that supports *Allodecta* as a junior synonym of *Compsodecta*. The tibia with 2-2-2-2v and the metatarsus with 2-2-2 macrosetae, are an atypical condition within the Antillattus clade and *Compsodecta*. However, this did not prevent the species from being placed within *Compsodecta* with strong support. Six unambiguous synapomorphies support the inclusion of *Allodecta* within *Compsodecta*: The male cephalothorax has lateral white scales extending across half of the carapace (char. 5[state 0] homoplasious); a paturon that is sexually dimorphic (char. 48[state 1] homoplasious); the palpal endite is globose and sexually dimorphic (char. 72 and 73[state 1] homoplasious) (fig. 2.35); the palpal femur, slightly curved (char. 74 [state 1] homoplasious); and the distal tegular lobe occuping a half or more than half of tegulum width.

2.3.4.1 *Caribattus* is not a member of the Antillattus clade

Like *Allodecta*, *Caribattus* (fig. 2.37) is a monotypic genus described by Bryant (1950). Bryant (1950) considered the main difference between *Caribattus* and other genera the male cheliceral tooth count (1 retromarginal tooth and four promarginal teeth distributed on 1 bicuspid and two independent teeth). Unfortunately, the type material is in poor condition and the palps are lost. Bodner (2002) managed to review the type material of *Caribattus* and encoded the palp and other somatic characters including the cheliceral teeth, finding that the promargin has only two teeth. We viewed the type material and congruent with Bodner 2002, we found only 2 teeth on the promargin. In addition, we observed a small anteroectal mastidion.

We were able to collect some additional specimens in Jamaica that we consider *Caribattus*, and we used these for the coding of morphological characters. *Caribattus* was considered by Zhang and Maddison (2015) to be included within the Antillattus clade. Our findings indicate that *Caribattus* can be distinguished from species in the Antillattus clade by the following character combinations: male palpal endite without anterolateral cusp (char. 69 [state 0], homoplasious); embolus developed close to the tegulum (char. 100 [state 0], homoplasious); female with copulatory duct receptacle narrower than the primary spermathecae (char. 119 [state 0], homoplasious). Thus, we conclude that *Caribattus* not is a member of the Antillattus clade. Morphological evidence indicates that *Caribattus* may be closer to representatives of the Agobardus clade or other Caribbean clades, but this should be evaluated further with the inclusion of molecular data.

2.3.4.2 *Cobanus* and *Sidusa* are different genera (fig. 2.38-2.44)

Zhang and Maddison (2015) included eight probable *Cobanus* species in their molecular phylogeny and two probable *Sidusa* species. We examined their figures and taxonomically, some species were misidentified as *Cobanus*, and one of the species was erroneously included within *Sidusa*. *Sidusa* was described by Peckham and Peckham (1895) to include *S. gratiosa* and currently comprises 33 accepted species. Sidusa was described by Peckham and Peckham (1895) to include S. gratiosa and currently comprises 33 accepted species. A revisition of original descripcion, figures, and some type species, makes us believe that many of this species are misdescribed as *Sidusa* and should be transferred or described as new genera. We also uncovered strong evidence to consider *Sidusa* and *Cobanus* as two separates but closely related genera.

Zhang and Maddison (2015) transferred 19 species to *Sidusa*, including all *Cobanus* species. Based on our results, many of these species are misplaced within *Sidusa*. Our molecular and morphological results support that *Sidusa* and *Cobanus* are different genera and recover the monophyly of the *Sidusa-Cobanus* clade.

Five unambiguous synapomorphies strongly support the monophyly of the *Sidusa-Cobanus* clade: female and male tibia with 2-2-2-2 ventral macrosetae (char. 62[state 2], non-homoplasious; char. 63[state 3], homoplasious); metatarsus with 2-2-2 macrosetae (char. 64[state 1], non-homoplasious; char. 65[state 2], homoplasious); and male pre-spiracular bump, present (char. 66[state 1], homoplasious). One morphological character that has been used to distinguish *Sidusa* and *Cobanus* is the male chelicerae, which are elongated in *Cobanus* but are not elongated in *Sidusa* (Bodner 2002, Zhang and Maddison 2015). The length of male

chelicerae is quite variable (Bodner 2002, Zhang and Maddison 2015), and other characters are more informative.

The genus *Sidusa* (fig. 2.31 C, D and E) is strongly supported as monophyletic by seven unambiguous synapomorphies: male palp with prolateral spermophorae duct loop (char. 91 [state 1] homoplasious); retrolateral sperm duct loop occupying less than half of bulb width (char. 93 [state 0] homoplasious); spermophorae coil before entering the embolic disc (char. 95 [state 1] homoplasious); embolus coils more than one and a half times (char. 99 [state 2] non-homoplasious); embolic disc occupying less than half of the tegulum (char. 105 [state 0] homoplasious); epigynum with spiral guide developed (char. 114 [state 1] homoplasious); copulatory duct with longer between copulatory opening and secondary spermathecae (char. 116 [state 2] non-homoplasious). Based on these characteristics, the genus *Sidusa* contains the continental species: *S. angulitarsis* Simon (1902), *S. viridiaurea* Simon (1902) and the type species *S. gratiosa* Peckham and Peckham (1895).

Our data indicate that *S. cambridgei*, (Chickering 1946), *S. electa* (Chickering 1946), and *S. mandibularis* (Peckham and Peckham 1895) are misplaced in *Sidusa*. They differ from the type species *S. gratiosa* in many key characteristics, such as male retromarginal teeth IV (char. 34 [state 1] homoplasious) and V, present (char. 35 [state 1] non-homoplasious) medially and proximally (char. 36 and 37 [state 1] non-homoplasious), paturon elongated and projected forwards, with a developed fang groove (char. 45, 46 and 47 [state 2] homoplasious); fang with the base longer than shaft (char. 56 [state 2] homoplasious); pre-spiracular hair tufts, present (char. 68 [state 1] homoplasious); embolus with lamella (char. 106 [state 1] homoplasious); and epigynum with pocket (char. 112 [state 1] homoplasious) and receptacle in copulatory duct in addition to primary and secondary spermathecae (char. 118 [state 1] homoplasious). We propose to transfer *S. bifurcata* (Chickering 1946), *S. cambridgei*, (Chickering 1946), *S. electa* (Chickering 1946), *S. mandibularis* (Peckham and Peckham 1895) and *S. unicolor* (F.O. Pickard-Cambridge 1900) to *Cobanus*.

Cobanus multidentatis **sp. nov.**

Fig. 2.43, A-E

Type material: Male holotype (ICN-Ar 12817), COLOMBIA, Risaralda, Santuario-La Celia, Verdum, 2.11.2010, rainforest leaf litter, Col: Guzmán-Ruiz, C. Paratype 1 female (ICN-Ar 12818) same data as holotype. (ICN-Ar 12819, 3 males, 10 females) same data as holotype.

Other Material: COLOMBIA: Quindio, Filandia, Estación Bremen, 14-20.iv.1998, Col: unknown (ICN-Ar 12820, 2 males). Risaralda, Correg. La Florida, Vda. La Suiza, SFF. Otún, Quinbaya, Qda. Palo Blanco, 4.7278333N, -75.5801083W, 1.i-31.xii.2005, Col: A. Sabogal (ICN-Ar 7710, 1 male, 2 females). Risaralda, Correg. La Florida, Vda. La Suiza, SFF. Otún, Quinbaya, Qda. Palo Blanco, 4.7278333N, -75.5801083W, 6.vi.2005, Col: A. Sabogal (ICN-Ar 7706, 1 male, 4 females). Risaralda, Correg. La Florida, Vda. La Suiza, SFF. Otún, Quinbaya, Qda. Palo Blanco, 4.7278333N, -75.5801083W, 6.vi.2005, Col: A. Sabogal (ICN-Ar 7750, 4 males, 5 females). Risaralda, Correg. La Florida, Vda. La Suiza, SFF. Otún, Quinbaya, Qda. Palo Blanco, 4.7278333N, -75.5801083W, 6.vi.2005, Col: A. Sabogal (ICN-Ar 7751, 7 males, 1 females). Risaralda, Correg. La Florida, Vda. La Suiza, SFF. Otún, Quinbaya, Qda. Palo Blanco, 4.7278333N, -75.5801083W, 6.vi.2005, Col: A. Sabogal (ICN-Ar 7753, 1 female). Risaralda, Correg. La Florida, Vda. La Suiza, SFF. Otún, Quinbaya, Qda. Palo Blanco, 4.7278333N, -75.5801083W, 6.vi.2005, Col: A. Sabogal (ICN-Ar 7742, 1 male). Risaralda, Correg. La Florida, Vda. La Suiza, SFF. Otún, Quinbaya, Qda. Palo Blanco, 4.7278333N, -75.5801083W, 6.vi.2005, Col: A. Sabogal (ICN-Ar 7817, 4 males, 6 females). Risaralda, Correg. La Florida, Vda. La Suiza, SFF. Otún, Quinbaya, Qda. Palo Blanco, 4.7278333N, -75.5801083W, 6.vi.2005, Col: A. Sabogal (ICN-Ar 7810, 1 male, 1 female). Risaralda, Correg. La Florida, Vda. La Suiza, SFF. Otún, Quinbaya, Qda. Palo Blanco, 4.7278333N, -75.5801083W, 6th July 2005, Col: A. Sabogal (ICN-Ar 7748, 1 male). Risaralda, Correg. La Florida, Vda. La Suiza, SFF. Otún, Quinbaya, Qda. Palo Blanco, 4.7278333N, -75.5801083W, 6.vi.2005, Col: A. Sabogal (ICN-Ar 7808, 1 male). Risaralda, Correg. La Florida, Vda. La Suiza, SFF. Otún, Quinbaya, Qda. Palo Blanco, 4.7278333N, -75.5801083W, 6.vi.2005, Col: A. Sabogal (ICN-Ar 7754, 1 female).

Diagnosis: Male palp of *Cobanus multidentatis* **sp. nov.** can be distinguished of other species of *Cobanus* by having the chelicerae with a multicuspid retromarginal teeth (fig. 2.43, C); the lamella wider towards the tip (fig 2.43, D) curved and separated of embolus path. Female of *Cobanus multidentatis* **sp. nov.** can be distinguished of other species of *Cobanus* by having a multicuspid retromarginal teeth. Aditionally, female of *Cobanus multidentatis* **sp. nov.** can be distinguished of *C. mandibularis* **comb. nov.**, *C. electus* **comb. nov.** and *C. unicolor* **comb. nov.** by having the PS 2x wider than CDR; and can be distinguished of *Cobanus cambridgei* **comb. nov.**, and *C. bifurcata* **comb. nov.** by having the CO posteriorly, and a mesal CDR.

Etymology: The species epithet is a noun in apposition referring to the retromarginal dentition (*multi*=many, *dentatis*= toothed, L.).

Description: Male (holotype: ICN-Ar 12817): Carapace, yellow to reddish, black at base of eyes, with white hairs under the LE and the fovea. Chelicerae, endites, and labium, reddish; sternum, yellow. Legs I yellow to reddish; legs II to IV, yellow. Abdomen, ventrally gray to light yellow; dorsally, gray to yellow with two dark bands. Total length 6.55. Carapace 3.0 long, 2.3 wide, 1.4 high. Clypeus 0.3 high. AER 2.0 wide, PER 1.9 wide. OQ length 1.45. Chelicerae 2.3, with two promarginal teeth, and nine retromarginal teeth. Abdomen 3.3 long, longer than wide. Leg measurements: I– coxae 1.0, trochanter 0.4, femur 2.3, patella 1.2, tibia 2.7, metatarsus 2.0, tarsus 1.0; II– 0.8, 0.4, 2.0, 1.1, 1.6, 1.2, 0.7; III–0.7, 0.35, 1.7, 0.9, 1.65, 1.5, 0.9; IV–0.8, 0.4, 2.0, 0.7, 1.6, 1.7, 0.8. *Leg spination*, I– femur drd1, d1-1-1, dpd1, dp1; patella p1, d1; tibia p1-0-0-0, r1-0-1-0, v2-2-2-2; metatarsus p0-0-1, r0-0-1, v2-2-2. II– femur drd1, d1-1-1, dpd1, dp1; patella p1, d1; tibia p1-1-0, dpv1, r1-1-0, drv1, v2-2-2; metatarsus p1-1, r1-1, v2-2. III– femur drd1, d1-1-1, drp1, dp1; patella p1, r1; tibia r1-1-1, p1-1-1, v1-0-2; metatarsus r1-0-1, d2-2-2, p1-0-1, v2-0-2. IV– femur drd1, d1-1-1, drp1, dp1; patella p1, r1; tibia r1-1-1, p1-1-1, v1-0-2; metatarsus r1-0-1, d2-2-2, p1-0-1, v2-0-2. Palp (fig. 2.43 D); VTA, absent; RTA, long, finger-like; pTL, absent; RSDL occupying half of bulb width; ED occupying half of bulb width; embolus as long as embolic disc width; lamella, developed, separated at base of embolus, and converges at a slightly wide tip.

Female (Paratype: ICN-Ar ICN-Ar 12818): Carapace, pale yellow reddish. Chelicerae, endites, labium, sternum and legs yellow to light reddish. Abdomen, ventrally gray; dorsally, gray with two dark bands. Total length 6.55. Carapace 2.2 long, 1.8 wide, 1.4 high. Clypeus 0.15 high. AER 1.6 wide, PER 1.5 wide. OQ length 1.5. Chelicerae 0.8 long, with two promarginal teeth and a retromarginal multicuspid tooth. *Abdomen*, 4.5 long, longer than wide. Leg measurements: I– coxae 0.7, trochanter 0.4, femur 1.2, patella 0.6, tibia 1.3, metatarsus 0.8, tarsus 0.5; II– 0.7, 0.4, 1.5, 0.6, 1.05, 0.7, 0.5 III–0.7, 0.4, 1.8, 0.5, 1.2, 0.75, 0.5; IV–0.7, 0.4, 1.6, 0.5, 1.3, 1.25, 0.5. *Leg spination*, I– femur drd1, d1-1-1, dpd1, dp1; patella p1, d1; tibia p1-0-0-0, r1-0-1-0, v2-2-2-2; metatarsus p0-0-1, r0-0-1, v2-2-2. II– femur drd1, d1-1-1, dpd1, dp1; patella p1, d1; tibia p1-1-0, dpv1, r1-1-0, drv1, v2-2-2; metatarsus p1-1, r1-1, v2-2. III– femur drd1, d1-1-1, drp1, dp1; patella p1, r1; tibia r1-1-1, p1-1-1, v1-0-2; metatarsus r1-0-1, d2-2-2, p1-0-1, v2-0-2. IV– femur drd1, d1-1-1, drp1, dp1; patella p1, r1; tibia r1-1-1, p1-1-1, v1-0-2; metatarsus r1-0-1, d2-2-2, p1-0-1, v2-0-2. *Epigynum*, (fig.2.43, E), WE occupying more than 1/2 of epigynal plate; CO posteromesal; pocket, present; CDR mesal in relation to PS; PS spherical, close to one another; FD, distant from the CD; BG, depressed or superficial.

Cobanus chocquibtown **sp. nov.**

Fig. 2.44A-F

Type material: Male holotype (ICN-Ar 12821), COLOMBIA, Chocó, Lloró, Centro de practica e investigación de la Universidad Tecnologica del Chocó "Diego Luis Cordoba", 5.51467N, -76.55271W, 22-27.i.2018, rainforest, Col: F. Cala-Riquleme, W. Galvis, S. Galvis, F. Vasquez, F. G. Firiontino, A. Novoa. Paratype 1 male, 1 female (ICN-Ar 12822) same data as holotype. (ICN-Ar 11018, 5 males, 11 females) same data as holotype. (ICN-Ar 12823, 1 male, 1 female) same data as holotype. (ICN-Ar 12824, 4 males), Risaralda, Santuario-La Celia, Verdum, 2.xi.2010, rainforest leaf litter, Col: Guzmán-Ruiz, C.

Diagnosis: Male chelicerae of *Cobanus chocquibtown* **sp. nov.** resemble those of *Cobanus mandibularis* **comb. nov.**, but can be distinguished by having robust chelicerae without a distal tooth at the base of the fang (fig. 2.44, C); and the fang without the tooth. Male of *Cobanus chocquibtown* **sp. nov.** also, can be separated from other *Cobanus* by the male lamella almost as long as the embolus (fig. 2.44, E). Female of of *Cobanus chocquibtown* **sp. nov.** can be distinguished from *Cobanus mandibularis* **comb. nov.***,* and others *Cobanus* by having the CDR anteriorly to the PS; and the PS outside of EW (fig. 2.44, F).

Etymology: The species epithet is a noun in apposition referring to the popular group ChocQuibTown. ChocQuibTown is a hip-hop group from Chocó, Colombia. The band's music draws influence from a wide variety of modern genres including hip-hop and electronica, combined with traditional Colombian genres including salsa, Latin jazz, and Afro-Latin rhythms.

Description: Male (holotype: ICN-Ar 12821**)**: Carapace, reddish, black at base of eyes. Chelicerae, endites, and labium, reddish; sternum, gray to yellow. Legs pale gray to black. Abdomen, ventrally gray to black; dorsally, gray to black with iridescent scales. Total length 5.2. Carapace 2.3 long, 2.1 wide, 1.8 high. Clypeus 0.1 high. AER 2.0 wide, PER 1.8 wide. OQ 1.6 long. Chelicerae 2.44, with two basal promarginal teeth, and two distal retromarginal teeth. Abdomen 2.95 long, longer than wide. Leg measurements: I– coxae 0.8, trochanter 0.4, femur 2.1, patella 1.0, tibia 1.9, metatarsus 1.4, tarsus 0.6; II– 0.6, 0.35, 1.9, 0.8, 1.3, 1.2, 0.6; III–0.6, 0.35, 2.15, 0.9, 1.4, 1.6, 0.6; IV–0.6, 0.35, 1.9, 0.7, 1.5, 1.65, 0.7. *Leg spination*, I– femur drd1, d1-1-1, dpd1, dp1; patella p1, d1; tibia p1-0-1-0, r1-0-1-0, v2-2-2-2; metatarsus p0-0-1, r0-0-1, v2-2-2. II– femur drd1, d1-1-1, dpd1, dp1; patella p1, d1; tibia p1-1-0, dpv1, r1-1-0, drv1, v2-2-2; metatarsus p1-1, r1-1, v2-2. III– femur drd1, d1-1-1, drp1, dp1; patella p1, r1; tibia r1-1-1, p1-1-1, v1-0-2; metatarsus r1-0-1, d2-2-2, p1-0-1, v2-0-2. IV– femur drd1, d1-1-1, drp1, dp1; patella p1, r1; tibia r1-1-1, p1-1-1, v1-0-2; metatarsus r1-0-1, d2-2-2, p1-0-1, v2-0-2. Palp (Fig. 2.44, E); VTA, absent; RTA long finger-like; rSDL occupying more than half of bulb width;

ED occupying the half of the bulb wide; embolus as long as embolic disc wide; lamella, almost as long as the embolus, near the path of the embolus, tip slightly wide and curved.

Female (Paratype: ICN-Ar 12822**)**: Carapace, yellow to reddish, black at base of eyes. Chelicerae, endites and labium, light reddish; sternum and legs, yellow. Abdomen, ventrally gray to light black; dorsally, gray with black spots. Total length 5.0. Carapace 2.2 long, 1.6 wide, 1.2 high. Clypeus 0.1 high. AER 1.65 wide, PER 1.55 wide. OQ 1.4 long. Chelicerae 0.8 long, with two promarginal teeth, and a retromarginal biscuspid. *Abdomen*, 2.6 long, longer than wide. Leg measurements: I– coxae 0.5, trochanter 0.3, femur 1.3, patella 0.75, tibia 0.9, metatarsus 0.65, tarsus 0.5; II– 0.5, 0.3, 1.3, 0.6, 0.9, 0.6, 0.5; III–0.5, 0.3, 1.6, 0.7, 1.0, 1.2, 0.5; IV–0.6, 0.3, 1.6, 0.6, 1.1, 1.2, 0.5. *Leg spination*, I– femur drd1, d1-1-1, dpd1, dp1; patella p1, d1; tibia p1-0-1-0, r1-0-1-0, v2-2-2-2; metatarsus p0-0-1, r0-0-1, v2-2-2. II– femur drd1, d1-1-1, dpd1, dp1; patella p1, d1; tibia p1-1-0, dpv1, r1-1-0, drv1, v2-2-2; metatarsus p1-1, r1-1, v2-2. III– femur drd1, d1-1-1, drp1, dp1; patella p1, r1; tibia r1-1-1, p1-1-1, v1-0-2; metatarsus r1-0-1, d2-2-2, p1-0-1, v2-0-2. IV– femur drd1, d1-1-1, drp1, dp1; patella p1, r1; tibia r1-1-1, p1-1-1, v1-0-2; metatarsus r1-0-1, d2-2-2, p1-0-1, v2-0-2. *Epigynum*, (Fig.2.44, F), WE, occupying 1/2 of epigynal plate; CO, posteroectal; SS developed; CDR, internal in relation to PS; PS spherical, close to one another; FD, distant from the CD; BG, depressed or superficial.

Genus *Paracobanus* **gen. nov.**

Fig. 2.45A-E; Fig. 2.46A-E

Type species: *Paracobanus boteroi* **sp. nov.**

Other undescribed species: *Paracobanus* sp. Ecuador, 1 male, 1 female (ECU11-4930 WPM#11-046), ECUADOR, Orellana, Yasuní Res. Stn. area, Napo Trail W0.6767, W76.4018, Col: W. Maddison. *Paracobanus* sp. French Guiana, 1 male, 1 female (JXZ100). FRENCH GUIANA, Commune Règina, les Nourages Field Station, 4.069N, -52.669W, Coll: J. X. Zhang, W. Maddison.

Diagnosis: *Paracobanus* **gen. nov.** is recovered as sister of *Sidusa* and within the mayor group *Cobanus* + (*Sidusa*+*Paracobanus*). The genus *Paracobanus* **gen. nov.** resemble *Sidusa* and *Cobanus* by males and females with 2-2-2 metatarsus I ventral macroseta, 2-2-2-2 tibia I ventral macroseta, and males with pre-spiracular bump. Male of *Paracobanus* **gen. nov** resembles *Sidusa* in the paturon with the retromarginal teeth fused (bicuspids) (fig. 2.46, C), the leg I longer than legs II, III and IV, and the pre-spiracular as wide as one of the anterolateral spinnerets; but, can be distinguished by having the leg I with fringe; the endites with the

lateroanterio projection; the palpal femur slightly curved; and the bulb with the following characteristic: dTL occupying the half or more than half of tegulum width, pSDL absent, SD without the coil near the embolic division, the embolus coil not more equal or less than half a circle and with a lamella. Female of *Paracobanus* **gen. nov.** can be distinguished from *Sidusa* by having the ECP; the EW without a long spiral guide; a short CD and a CDR. Male of *Paracobanus* **gen. nov** also resembles *Cobanus* by having the embolus coil not more of half a circle, the presence of a lamella; and the pSDL absent; but, can be distinguished by having the paturon projected downward; the retromarginal teeth fused (bicuspids), and with retromarginal tooth distal in relation to fang base; the fang groove as longer as base of paturon wide, and the shaft as long as fang base; the paturon more than half or almost as long as clypeus width; the palpal femur slightly curved and without macrosetae; and the palpal tibia as long as patella. Female of *Paracobanus* **gen. nov** also resembles *Cobanus* by having an ECP (fig. 2.45, E; 2.46, E); the lack of spiral guide; the CD short; and the precense of a CDR; but, can be distinguished by having the ECP open downward.

Etymology: The generic name is similar to *Cobanus* as the two genera are similar; however, "para" as been added to differentiate the genera; masculine in gender.

Paracobanus boteroi **sp. nov.**

Fig. 2.46A-E

Type material: Male holotype (ICN-Ar 12825), COLOMBIA, Nariño, Barbacoas, Vda. Altaquer, Reserva Natural Rio Ñambí, 1.4666N, -78.1166W, 2-6.vii.2017, rainforest, Col: D. Martinez, F. Cala-Riquelme, W. Galvis, S. Galvis. Paratype 1 female (ICN-Ar 12825), same data as holotype.

Etymology: The species epithet is a noun in apposition referring to Fernando Botero Angulo, a Colombian figurative artist and sculptor.

Description: Male (holotype: ICN-Ar 12825): Carapace, reddish, eyes ringed with black. Chelicerae, endites, and labium dark reddish; sternum, gray to light reddish. Legs I-II dark gray to dark reddish, patella and tarsus light yellow; Legs III-IV, light yellow. Abdomen, ventrally gray to drak grey; dorsally, gray to black spots and with iridescent scales. Total length 4.2. Carapace 2.0 long, 1.5 wide, 1.1 high. Clypeus 0.1 high. AER 1.5 wide, PER 1.4 wide. OQ 1.2 long. Chelicerae 0.65, with two promarginal teeth, and a retromarginal bicuspid tooth. Abdomen 2.05 long, longer than wide. Leg measurements: I– coxae 0.4, trochanter 0.25, femur 1.4, patella 0.5, tibia 0.9, metatarsus 0.7, tarsus 0.5. II– 0.4, 0.25, 1.2, 0.5, 0.8, 0.6, 0.45. III– 0.4, 0.25, 1.4, 0.5, 0.8, 0.6, 0.5. IV–0.4, 0.25, 1.4, 0.5, 0.85, 0.95, 0.5. *Leg spination*, I– femur

drd1, d1-1-1, dpd1, dp1; patella p1, d1; tibia p1-0-1-0, r1-0-1-0, v2-2-2-2; metatarsus p0-0-1, r0-0-1, v2-2-2. II– femur drd1, d1-1-1, dpd1, dp1; patella p1, d1; tibia p1-1-0, dpv1, r1-1-0, drv1, v2-2-2; metatarsus p1-1, r1-1, v2-2. III– femur drd1, d1-1-1, drp1, dp1; patella p1, r1; tibia r1-1-1, p1-1-1, v1-0-2; metatarsus r1-0-1, d2-2-2, p1-0-1, v2-0-2. IV– femur drd1, d1-1-1, drp1, dp1; patella p1, r1; tibia r1-1-1, p1-1-1, v1-0-2; metatarsus r1-0-1, d2-2-2, p1-0-1, v2-0-2. Palp (Fig. 2.46, D); VTA absent; RTA long, finger-like; rSDL occupying the half of bulb width; ED occupying the half of the bulb wide; embolus as long as embolic disc width; lamella, as long as the embolus, curved and thin, developed far the path of the embolus, tip thinner.

Female (Paratype: ICN-Ar 12825): Carapace, yellow to reddish, black at base of eyes. Chelicerae, endites and labium, light reddish; sternum and legs, yellow. Abdomen, ventrally pale gray; dorsally, gray with black spots. Total length 4.7. Carapace 2.0 long, 1.4 wide, 1.2 high. Clypeus 0.1 high. AER 1.5 wide, PER 1.4 wide. OQ 1.2 long. Chelicerae 0.55 long, with two promarginal teeth, and a retromarginal biscuspid. *Abdomen*, 2.4 long, longer than wide. Leg measurements: I– coxae 0.4, trochanter 0.3, femur 1.1, patella 0.5, tibia 0.8, metatarsus 0.6, tarsus 0.55. II– 0.4, 0.2, 1.1, 0.45, 0.65, 0.6, 0.5. III–0.4, 0.2, 1.4, 0.5, 0.8, 0.85, 0.55. IV–0.4, 0.2, 1.4, 0.5, 1.0, 0.95, 0.55. *Leg spination*, I– femur drd1, d1-1-1, dpd1, dp1; patella p1, d1; tibia p1-0-1-0, r1-0-1-0, v2-2-2-2; metatarsus p0-0-1, r0-0-1, v2-2-2. II– femur drd1, d1-1-1, dpd1, dp1; patella p1, d1; tibia p1-1-0, dpv1, r1-1-0, drv1, v2-2-2; metatarsus p1-1, r1-1, v2-2. III– femur drd1, d1-1-1, drp1, dp1; patella p1, r1; tibia r1-1-1, p1-1-1, v1-0-2; metatarsus r1-0-1, d2-2-2, p1-0-1, v2-0-2. IV– femur drd1, d1-1-1, drp1, dp1; patella p1, r1; tibia r1-1-1, p1-1-1, v1-0-2; metatarsus r1-0-1, d2-2-2, p1-0-1, v2-0-2. *Epigynum*, (Fig. 2.46, E), WE, occupying 1/2 of epigynal plate; CO posteromesal; SS, reduced; CDR, mesal in relation to PS; PS spherical, separated to one another; FD, distant from the CD; BG depressed or superficial.

2.3.4.3 Antillattus Clade

As reported in Zhang and Maddison (2015), our study found that the Antillattus clade is well-supported and is restricted to the Caribbean Islands. We found morphological evidence for the Antillattus clade but the support is poor. This clade comprises *Antillattus*, *Pensacolatus*, *Bryanattus*, *Petemathis* and *Truncattus*. All genera are strongly supported as monophyletic by DNA, morphology and total evidence. *Antillattus*, *Pensacolatus* and *Bryanattus* will be discussed in detail in chapter 3. Here, we only focus on *Petemathis* and *Truncattus*.

Petemathis are small to medium-sized spiders usually found on foliage, branches or tree trunks (Zhang and Maddison, 2015). The genus is only known from Puerto Rico. Simon (1899) described the genus *Emathis* to include *E. weyersi*. According to Simon (1899), *Emathis*

have a promargin with two teeth and a retromargin with a multicuspid fissident tooth. Based on this, Petrunkevitch (1930) described some Caribbean species within *Emathis*. The type species *Emathis weyersi* has an embolus that is coiled many times (Bryant 1940, Prószyński 1984, Prószyński and Deeleman-Reinhold 2012). Bryant (1940) discussed the misidentification and inclusion of some Caribbean species within the genus *Emathis*. Based on strong differences in genital organs, Prószyński and Deeleman-Reinhold (2012) described *Petemathis* to include *Emathis portoricensis* Petrunkevitch (1930), *Emathis luteopunctata* Petrunkevitch (1930), *Emathis minuta* Petrunkevitch (1930), *Emathis tetuani* Petrunkevitch (1930) and *Emathis unispina* Franganillo, 1930. Based on the description by Franganillo (1936), *Petemathis unispina* has all the characters to be considered a member of *Bryanattus*. These characters are: males with large and divergent chelicerae; two pair of mastidion (one internal and one external); four retromarginal teeth with a common base; the female with five retromarginal teeth with a common base. Our data support the transfer of *Petemathis unispina* to *Bryanattus*. Eight unambiguous synapomorphies strongly support the monophyly of *Petemathis*: Male cephalothorax without lateral white scales (char. 4 [state 0] homoplasious); female and male with the retromarginal tooth III and IV (char. 18 [state 1]; char. 19 [state 1]; char. 33 [state 1]; char. 34 [state 1] homoplasious); male palpal patella longer than tibia (char. 76 [state 0] homoplasious); and female with the copulatory duct receptacle developed distal in relation to primary spermathecae (char. 120 [state 0] homoplasious); and copulatory duct connected internally in relation to primary spermathecae (char. 121 [state 0] homoplasious).

Based on our results, we transfer *S. turquinensis* and *S. inconspicua* to *Truncattus*. Most erroneous taxonomic placements occur by making decisions without reviewing the type material and/or original descriptions. Salticidae are no exception. In the case of *Sidusa*, F.O.P. Cambridge (1901; p. 196) makes a series of taxonomic decisions based on the morphology of *S. recondita* (transferred to *Chapoda* by Zhang and Maddison 2015). O.P. Cambridge (1901; p. 196) designation permit the inclusion of Antillean species within *Sidusa* (See Bryant, 1940; Petrunkevitch 1914). Bryant (1940) described *S. turquinensis* and *S. inconspicua* as based on the definition provided by F.O.P. Cambridge (1901). Our molecular and morphological data indicate that *S. turquinensis* is misplaced in *Sidusa* and should be transferred to *Truncattus*. Additionally, we reviewed the description of *S. inconspicua*. Our analyses placed the Cuban species (including *S. turquinensis*) within *Truncattus*. *Truncattus* was described by Zhang and Maddison (2012) based on molecular and morphological data obtained from the type species, *T. flavus* Zhang and Maddison, as well as *T. cachotensis* and *T. dominicanus*. Salgado and Ruiz (2017) transferred the *Nebridia* species *N. mendica* and *N. manni*, described by Bryant (1943),

to *Truncattus* based on one bicuspid retromarginal tooth and a retrolateral depression on the chelicerae, and the male palp with a large, proximal tegular lobe. However, the retromarginal bicuspid tooth is lost within the Cuban species. Our morphological data show that the proximal tegular lobe is the most important character to consider: the proximal tegular lobe occupying more than half of the tegulum width (char. 87 [state 2] homoplasious) and developed (char. 88 [state 2] non-homoplasious).

Genus *Truncattus* Zhang and Maddison 2012

Truncattus turquinensis **comb. nov.**

Fig. 2.47A-G

Sidusa turquinensis Bryant, 1940: 461, pl. 18, f. 240, 248 (Dmf).

Type material: Male holotype (MCZ-IZ 23381), CUBA, Pico Turquino, 6000 ft, 16-21 June 1936, Coll: Philip J. Darlington, Jr. Female same date as holotype (MCZ-IZ 25848).
Other material: CUBA, Granma prov.: Bartolome Massó, RE "Pico Caraca", Alto de Meriño, 19.9690811N, -77.0082209W, 5.iii.2013, beating in rainforest Col: F. Cala-Riquelme, (ICN-Ar 12826, 1 male, 4 females). Guisa, Buey arriba, National Park "Pico la Bayamesa", 20.049798N, -76.584254W, 23.v.2003, beating in rainforest Col: A. Sanchez-Ruiz, (ICN-Ar 12827, 1 female). Bartolome Maso, National Park "Pico Turquino", Pico Joaquin, 20.013022N, -76.833858W, 25.iii.2012, beating in rainforest Col: F. Cala-Riquelme, A. Deler-Hernández, (ICN-Ar 12828, 3 males, 3 females). Bartolome Maso, National Park "Pico Turquino", Pico Joaquin, 20.013022N, -76.833858W, 5.ii.2012, beating in rainforest Col: F. Cala-Riquelme, A. Deler-Hernández, R. Anderson. (ICN-Ar 12829, 1 male, 2 females).

Truncattus inconspicua **comb. nov.**

Type material: Female Allotype (MCZ-IZ 21627), CUBA, Trinidad Mts., Buenos Aires, 2500-3500 ft, 9 May 1936, Col: Philip J. Darlington, Jr. **Note**: The correct locality is Cuba, Cienfuegos Prov., Cumanayagua, Buenos Aires, 21.966155 N, - 80.131007 W.

Truncattus martii **sp. nov.**

Fig. 2.48A-E

Type material: Male holotype (ICN-Ar 12830), CUBA, Granma, Bartolome Maso, National Park "Pico Turquino", Pico Joaquin, 20.013022N, -76.833858W, 28.ix.2014, beating in rainforest Col: F. Cala-Riquelme, A. Deler-Hernández. Paratype (ICN-Ar 12831 male, 3

females) CUBA, Granma, Bartolome Maso, National Park "Pico Turquino", Pico Joaquin, 20.013022N, -76.833858W, 28.iii.2012, beating in rainforest Col: F. Cala-Riquelme, A. Deler-Hernández.

Diagnosis: Males of *Truncattus martii* **sp. nov.** resemble *Truncattus cachotensis* in the habitus and abdominal pattern, but can be distinguished of this and other hispaniolan known *Truncattus* by having one retromarginal tooth (fig. 2.48, E). Female of *Truncattus martii* **sp. nov.** also resemble *Truncattus cachotensis* in the habitus and abdominal pattern, but can be distinguished of this and other *Truncattus* by having the CO posteromesal; and the CDR as wide as PS (fig. 2.48 E).

Etymology: The species epithet is a noun in apposition referring to the Cuban national hero José Martí.

Description: Male (holotype: ICN-Ar 12830): Carapace, dark reddish to black, with a light area posterior to the fovea. Chelicerae, endites, labium and sternum yellow to reddish. Legs I and II, yellow to reddish, darker than legs III and IV; femur I with a prolateral dark area. Legs III and IV, gray to light reddish. Abdomen, ventrally gray to dark; dorsally, gray to black. Total length 3.2. Carapace 1.5 long, 1.1 wide, 0.95 high. Clypeus 0.1 high. AER 1.1 wide, PER 1.1 wide. OQ 0.8 long. Chelicerae 0.55, with two promarginal teeth, and one retromarginal tooth. Abdomen 1.7 long, longer than wide. Leg I with fringes. Leg measurements: I– coxae 0.3, trochanter 0.2, femur 0.85, patella 0.45, tibia 0.65, metatarsus 0.45, tarsus 0.3. II– 0.3, 0.25, 0.8, 0.4, 0.55, 0.4, 0.3. III–0.25, 0.15, 0.8, 0.4, 0.55, 0.4, 0.25. IV–0.5, 0.22, 0.95, 0.3, 0.75, 0.7, 0.45. *Leg spination*, I– femur drd1, d1-1-1, dpd1, dp1; patella p1, d1; tibia p1-1-0, v2-2-2; metatarsus p1-1, v2-2. II– femur drd1, d1-1-1, dpd1, dp1; patella p1, d1; tibia p1-1-0, v2-2-2; metatarsus p1-1, v2-2. III– femur drd1, d1-1-1, drp1, dp1; patella p1, r1; tibia r1-1-1, d2-2-0, p1-1-1, v1-0-2; metatarsus r1-1, d2-2, p1-1, v2-2. IV– femur drd1, d1-1-1, drp1, dp1; patella p1, r1; tibia r1-1-1, d2-2-0, p1-1-1, v1-0-2; metatarsus r1-1, d2-2-2, p1-1, v2-2. Palp (Fig. 2.48, D); VTA, present; RTA long, finger-like, slightly curved dorsally; pTL developed, almost as wide as bulb; rSDL occupying more than half of bulb width; ED occupying the half of bulb width; embolus as long as ED wide.

Female (Paratype: ICN-Ar 12831): Carapace reddish brown to black, with a light area posterior to the fovea. Chelicerae, endites, sternum and labium reddish. Legs gray to pale reddish. Abdomen, ventrally gray to yellow with sparse black spots; dorsally, pale yellow with black pattern. Total length 4.0. Carapace 1.4 long, 1.0 wide, 0.7 high. Clypeus 0.1 high. Anterior eye row 1.1 wide, posterior eye row 1.1 wide. Ocular quadrangle length 0.75. Chelicerae 0.3 long, with two promarginal teeth, and one retromarginal tooth. *Abdomen*, 2.2 long, longer than wide.

Leg measurements: I– coxae 0.3, trochanter 0.2, femur 0.75, patella 0.45, tibia 0.55, metatarsus 0.4, tarsus 0.3. II– 0.3, 0.2, 0.75, 0.3, 0.45, 0.35, 0.3. III–0.3, 0.15, 0.85, 0.3, 0.5, 0.55, 0.35. IV–0.35, 0.2, 1.0, 0.45, 0.65, 0.6, 0.5. *Leg spination*, I– femur drd1, d1-1-1, dpd1, dp1; patella p1, d1; tibia p1-1-0, v2-2-2; metatarsus p1-1, v2-2. II– femur drd1, d1-1-1, dpd1, dp1; patella p1, d1; tibia p1-1-0, v2-2-2; metatarsus p1-1, v2-2. III– femur drd1, d1-1-1, drp1, dp1; patella p1, r1; tibia r1-1-1, d2-2-0, p1-1-1, v1-0-2; metatarsus r1-1, d2-2, p1-1, v2-2. IV– femur drd1, d1-1-1, drp1, dp1; patella p1, r1; tibia r1-1-1, d2-2-0, p1-1-1, v1-0-2; metatarsus r1-1, d2-2-2, p1-1, v2-2. *Epigynum*, (Fig. 2.48, E), WE occupying more of 1/2 of epigynal plate; CO anteromesal; CD straight, in anterior position in relation to PS; PS spherical, close to each other; FD distant from the CD; BG depressed or superficial.

Truncattus platnicki **sp. nov.**

Fig. 2.49A-E

Type material: Male holotype (ICN-Ar 12832), CUBA, Granma, Bartolome Maso, National Park "Pico Turquino", Pico Joaquin, 20.013022N, -76.833858W, September 2014, rainforest leaf litter, Col: F. Cala-Riquelme, A. Deler-Hernández. Paratype (ICN-Ar 12832, 1 male, 4 females) same data as holotype.

Diagnosis: Like *Truncattus martii* **sp. nov.**, male of *Truncattus platnicki* **sp. nov.** can be distinguished from other other hispaniolan known *Truncattus Truncattus* by having one retromarginal tooth (fig. 2.49C). Male of *Truncattus platnicki* **sp. nov.** can be distinguished from *Truncattus martii* **sp. nov.** by having the prosoma dark reddish to black and the abdomen with the dense black patron (fig. 2.49A). Female of *Truncattus platnicki* **sp. nov.** can be distinguished from other Truncattus by having the CO anteroectal (fig. 2.49G).

Etymology: The species epithet is a noun in apposition referring to the late Dr. Norman Platnick, Curator Emeritus of Invertebrate Zoology at the American Museum of Natural History.

Description: Male (holotype: ICN-Ar 12832): Carapace, dark reddish to black, with a light area posterior to the fovea and white hairs. Chelicerae, endites, labium, and sternum, dark reddish to brown. Legs light reddish to dark red. Abdomen, ventrally light yellow to black; dorsally, black with yellow spots. Total length 3.1. Carapace 1.55 long, 1.15 wide, 0.95 high. Clypeus 0.1 high. AER 1.1 wide, PER 1.1 wide. OQ 0.8 long. Chelicerae 0.6, with two promarginal teeth, and one retromarginal tooth. Abdomen 1.65 long, longer than wide. Legs I with fringes. Leg measurements: I– coxae 0.35, trochanter 0.2, femur 1.0, patella 0.5, tibia 0.75, metatarsus 0.55, tarsus 0.4. II– 0.35, 0.2, 0.85, 0.5, 0.6, 0.5, 0.3. III–0.3, 0.2, 0.95, 0.4, 0.8, 0.6, 0.45. IV–

0.4, 0.25, 1.25, 0.35, 0.8, 0.75, 0.5. *Leg spination*, I– femur drd1, d1-1-1, dpd1, dp1; patella p1, d1; tibia p0-0-1, v2-2-2; metatarsus p1-1, v2-2. II– femur drd1, d1-1-1, dpd1, dp1; patella p1, d1; tibia p0-1-1, db1, v2-2-2; metatarsus p1-1, v2-2. III– femur drd1, d1-1-1, drp1, dp1; patella p1, r1; tibia r0-1-1, db2, p0-1-1, v1-0-2; metatarsus r1-1, d2-2, p1-1, v2-2. IV– femur drd1, d1-1-1, drp1, dp1; patella p1, r1; tibia r0-1-1, d2-2-0, p0-1-1, v1-0-2; metatarsus r1-1, d2-2-2, p1-1, v2-2. Palp (fig. 2.49, E-F); VTA, present; RTA long, finger-like, slightly curved dorsally; pTL developed, almost as wide as bulb; rSDL occupying 1/2 of the bulb width; ED occupying 1/2 of the bulb width; embolus as long as ED width.

Female (Paratype: ICN-Ar 12832): Carapace, reddish to black. Chelicerae, endites, labium, sternum and legs, light reddish. Abdomen, ventrally gray to black; dorsally, pale yellow to black. Total length 3.2. Carapace 1.5 long, 1.15 wide, 0.75 high. Clypeus 0.1 high. Anterior eye row 1.15 wide, PER 1.15 wide. OQ 0.85 long. Chelicerae 0.5 long, with two promarginal teeth, and one retromarginal tooth. *Abdomen*, 1.8 long, longer than wide. Leg measurements: I– coxae 0.4, trochanter 0.2, femur 0.85, patella 0.55, tibia 0.65, metatarsus 0.5, tarsus 0.45. II– 0.3, 0.2, 0.8, 0.45, 0.55, 0.55, 0.3. III–0.3, 0.15, 0.8, 0.4, 0.5, 0.55, 0.4. IV–0.45, 0.2, 1.05, 0.45, 0.8, 0.8, 0.5. *Leg spination*, I– femur drd1, d1-1-1, dpd1, dp1; patella p1, d1; tibia p0-0-1, v2-2-2; metatarsus p1-1, v2-2. II– femur drd1, d1-1-1, dpd1, dp1; patella p1, d1; tibia p0-1-1, db1, v2-2-2; metatarsus p1-1, v2-2. III– femur drd1, d1-1-1, drp1, dp1; patella p1, r1; tibia r0-1-1, db2, p0-1-1, v1-0-2; metatarsus r1-1, d2-2, p1-1, v2-2. IV– femur drd1, d1-1-1, drp1, dp1; patella p1, r1; tibia r0-1-1, d2-2-0, p0-1-1, v1-0-2; metatarsus r1-1, d2-2-2, p1-1, v2-2. *Epigynum*, (fig.2.49, G), EW occupying 1/2 of epigynal plate; CO, medioectal; CD straight, and anterior in relation to PS; PS spherical, close to one another; FD distant from the CD; BG depressed or superficial.

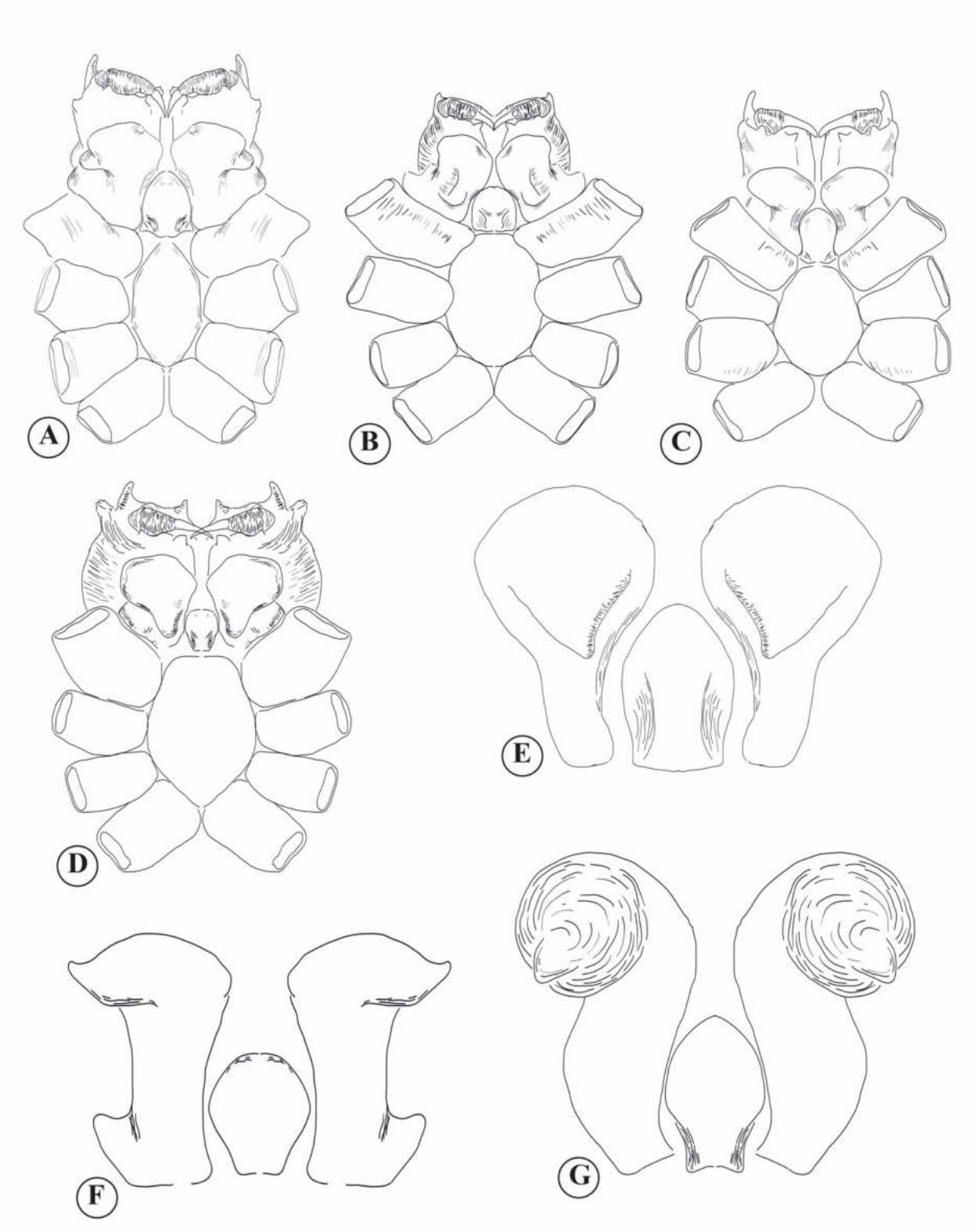

Figure 2.35. Endites, ventral view. A, *Compsodecta darlingtonia***.** B, G, *Compsodecta gratiosa*. C, *Compsodecta grisea*. D-E, *Compsodecta festiva*. F, *Compsodecta peckhami*.

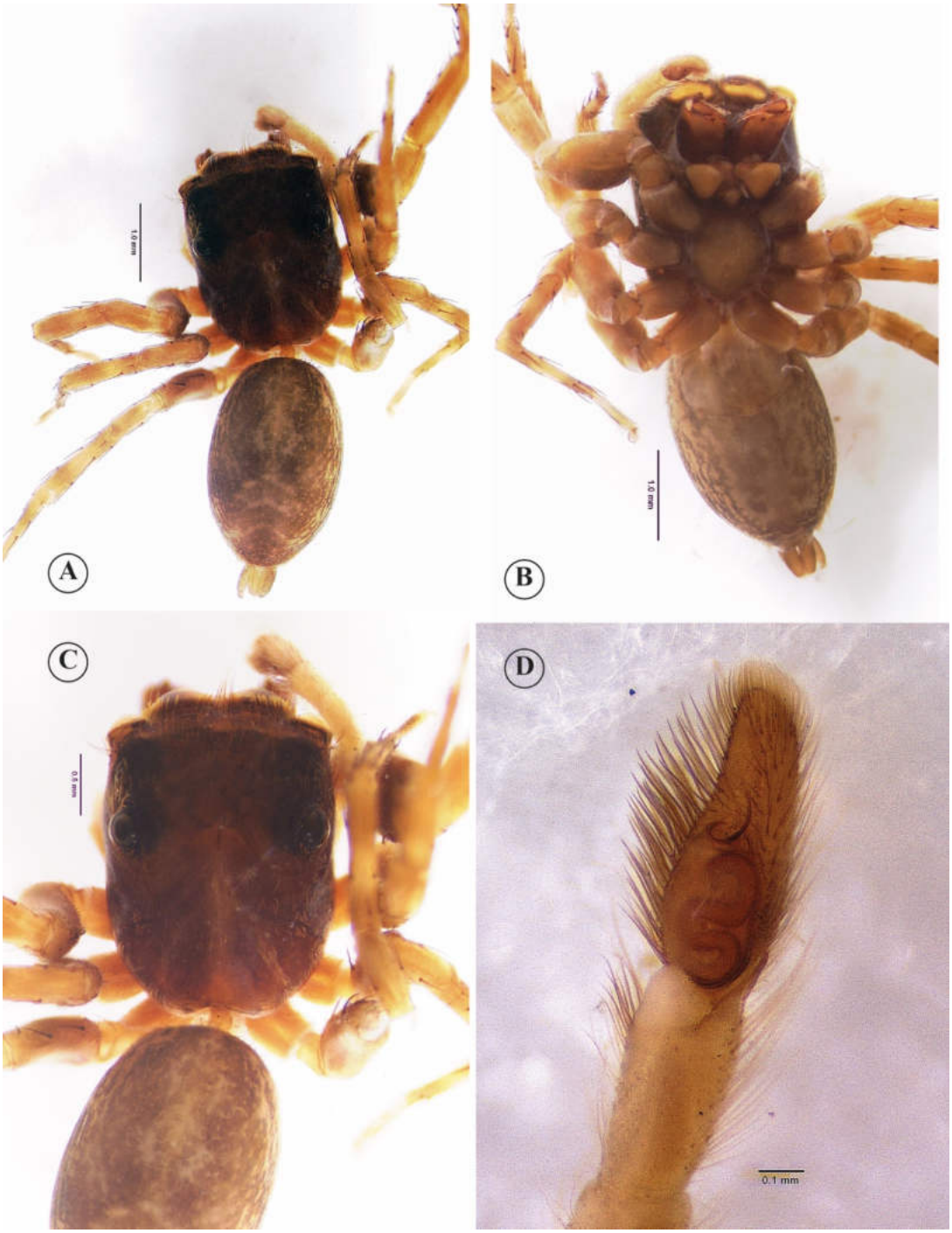

Figure 2.36. *Compsodecta maxillaris* **comb. nov.** A and C, Male (holotype MCZ-IZ 22099), habitus, dorsal view. B, Male (holotype MCZ-IZ 22099), habitus, ventral view. D, Male left palp, ventral view.

Figure 2.37. *Caribattus inutilis*. A, male (holotype MCZ-IZ 21697), habitus. B, male (holotype MCZ-IZ 21697), habitus, prosoma lateral view. C, femur. D, Male habitus, prosoma frontal view.

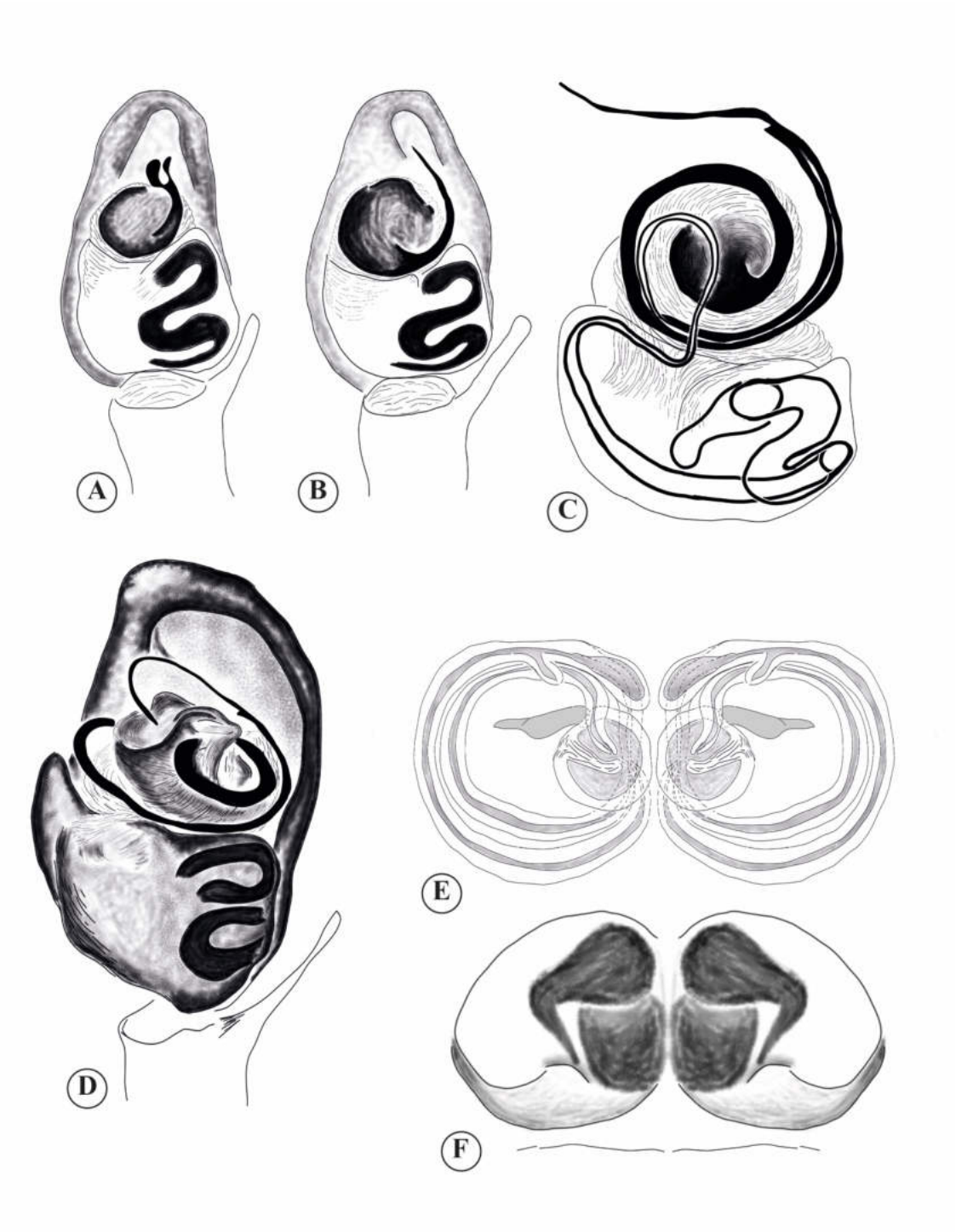

Figure 2.38. Male palp and epigynum of *Sidusa* and *Cobanus*. A, *Cobanus bifurcata* **comb. nov.**, male palp, ventral view. B *Cobanus mandibularis* **comb. nov.**, male palp, ventral view. C-D, *Sidusa,* male palp, ventral view. E, *Sidusa,* female internal epigynum, dorsal view. F, *Cobanus cambridgei* **comb. nov.**, female epigynum, ventral view.

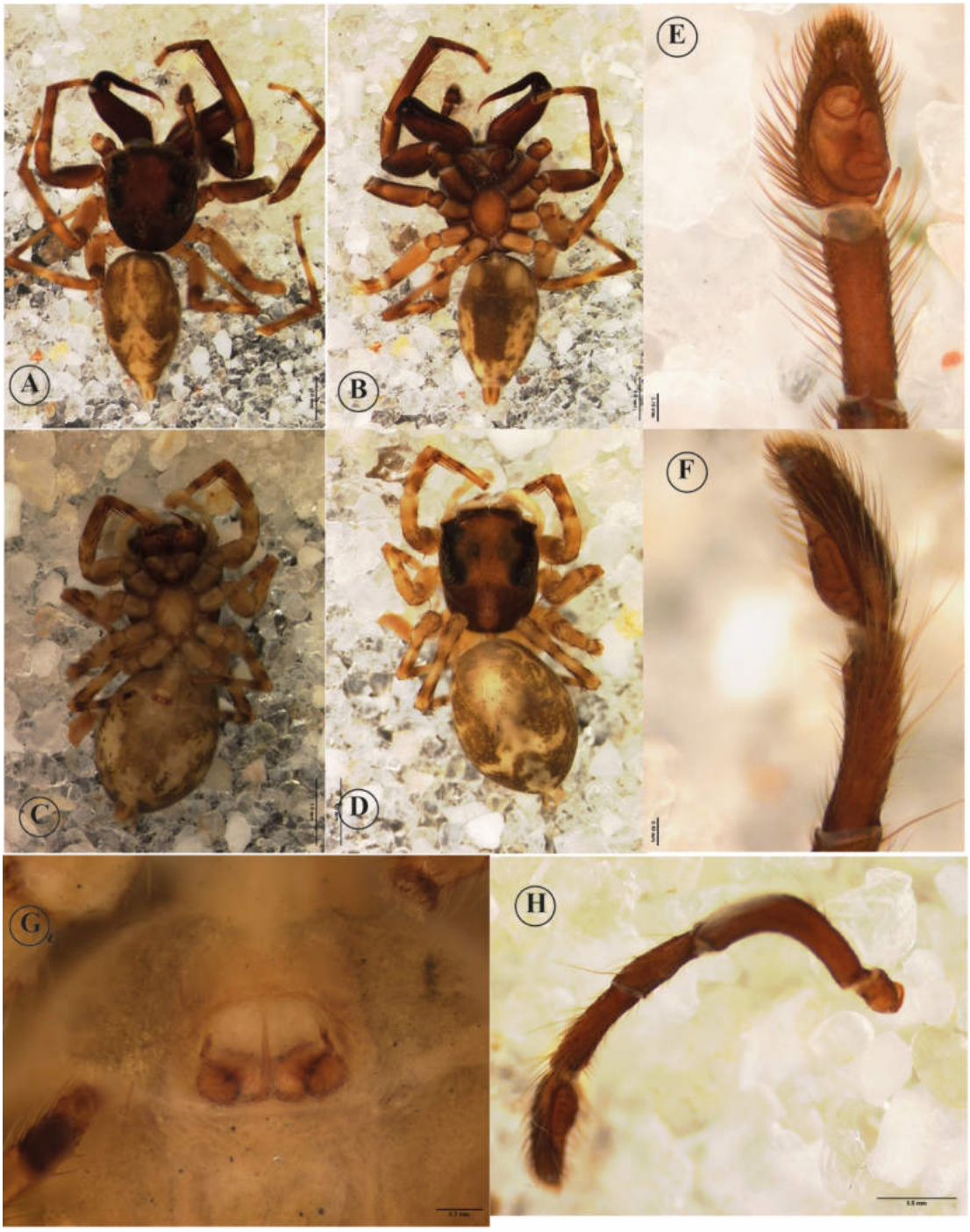

Figure 2.39. Holotype of *Cobanus electus*. A, male (holotype MCZ-IZ 21179) habitus, dorsal view. B, male (holotype MCZ-IZ 21179) habitus, ventral view. C, female habitus, ventral view. D, female (allotype MCZ-IZ 26056) habitus, dorsal view. E, male (holotype MCZ-IZ 21179 palp, ventral view. F and H, male (holotype MCZ-IZ 21179 palp, retrolateral view. G, epigynum (allotype MCZ-IZ 26056), ventral view.

Figure 2.40. Holotype of *Cobanus bifurcata* **comb. nov.** A, female (allotype MCZ-IZ 26055) habitus, dorsal view. B, female (allotype MCZ-IZ 26055) habitus, ventral view. C, male (holotype MCZ-IZ 20508) palp, ventral view. D, male (holotype MCZ-IZ 20508) palp, retrolateral view. E, epigynum (allotype MCZ-IZ 26055), ventral view.

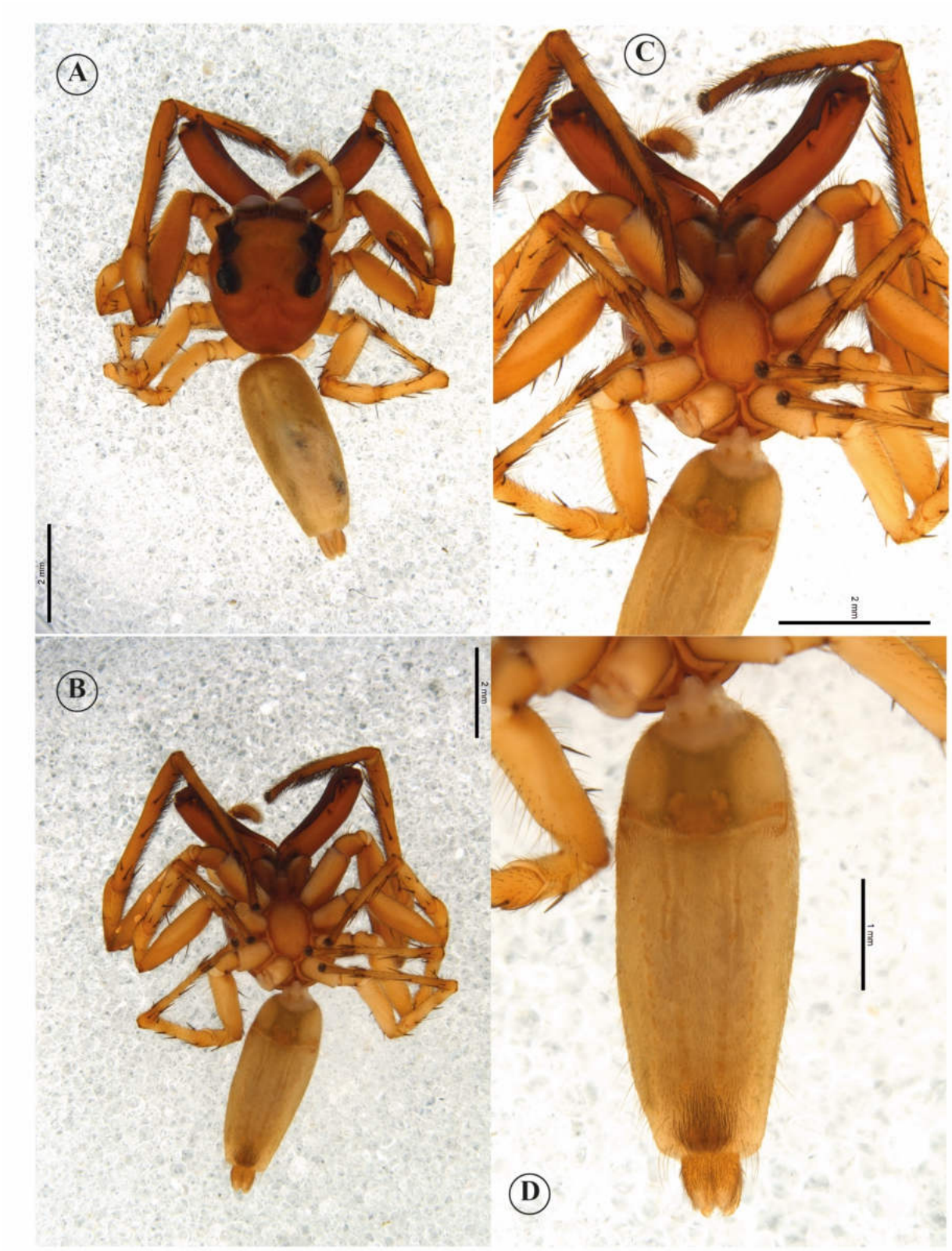

Figure 2.41. *Cobanus mandibularis* **comb. nov.** from Colombia. A, male, habitus. B-C, male, habitus, prosoma lateral view. D, male abdomen, ventral view.

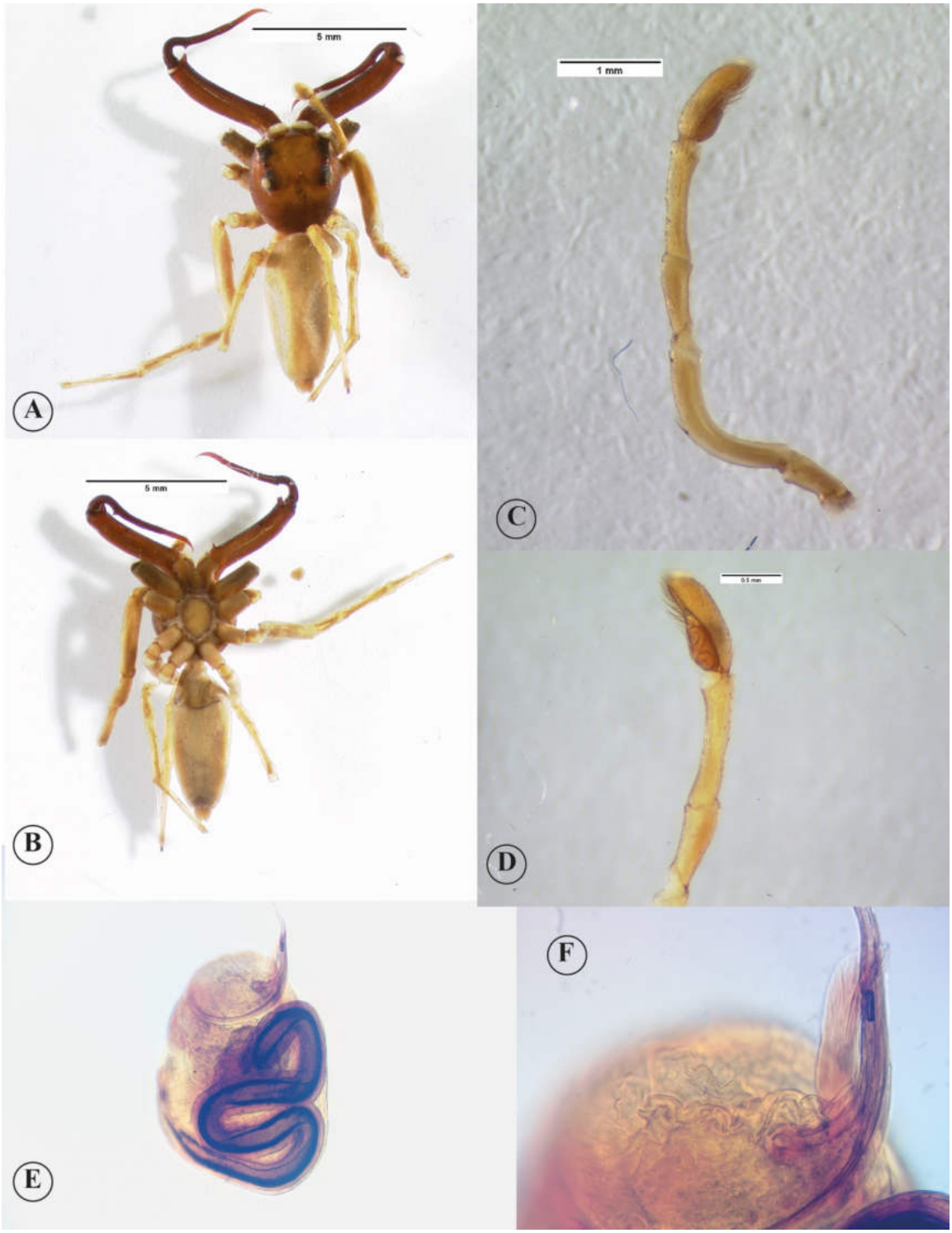

Figure 2.42. *Cobanus mandibularis* **comb. nov.** A, male (holotype MCZ-IZ 21971), habitus. B-C, male (holotype MCZ-IZ 21971), habitus, prosoma lateral view. C, male palp (holotype MCZ-IZ 21971), prolateral view. D, male palp (holotype MCZ-IZ 21971), retrolateral view. E-F, male (holotype MCZ-IZ 21971) palp, ventral view.

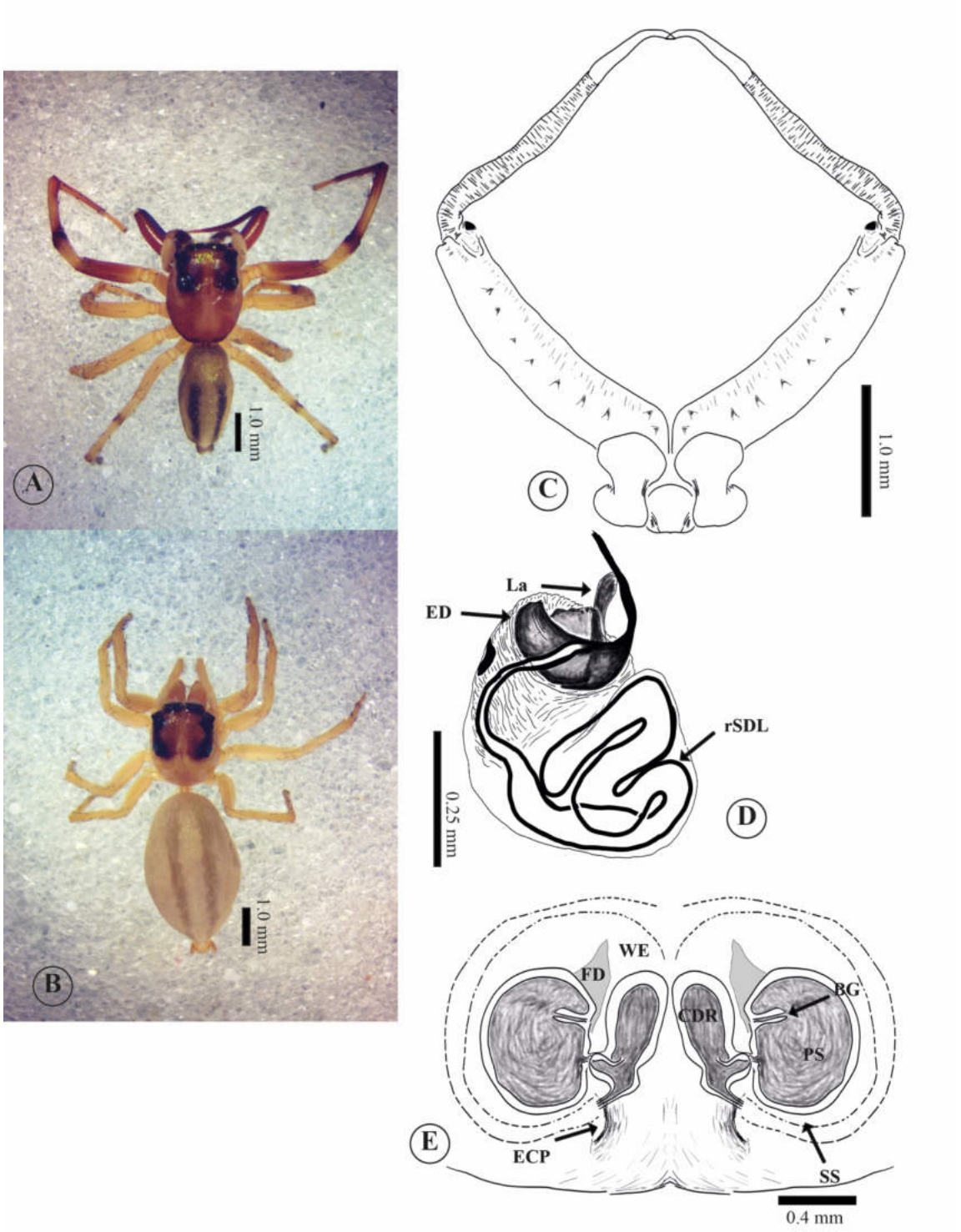

Figure 2.43. *Cobanus multidentatis* **sp. nov.** A, male, habitus, dorsal view. B, female, habitus, dorsal view. C, male chelicerae, retromarginal view. D, male palp, ventral view. E, female, internal genitalia, ventral view.

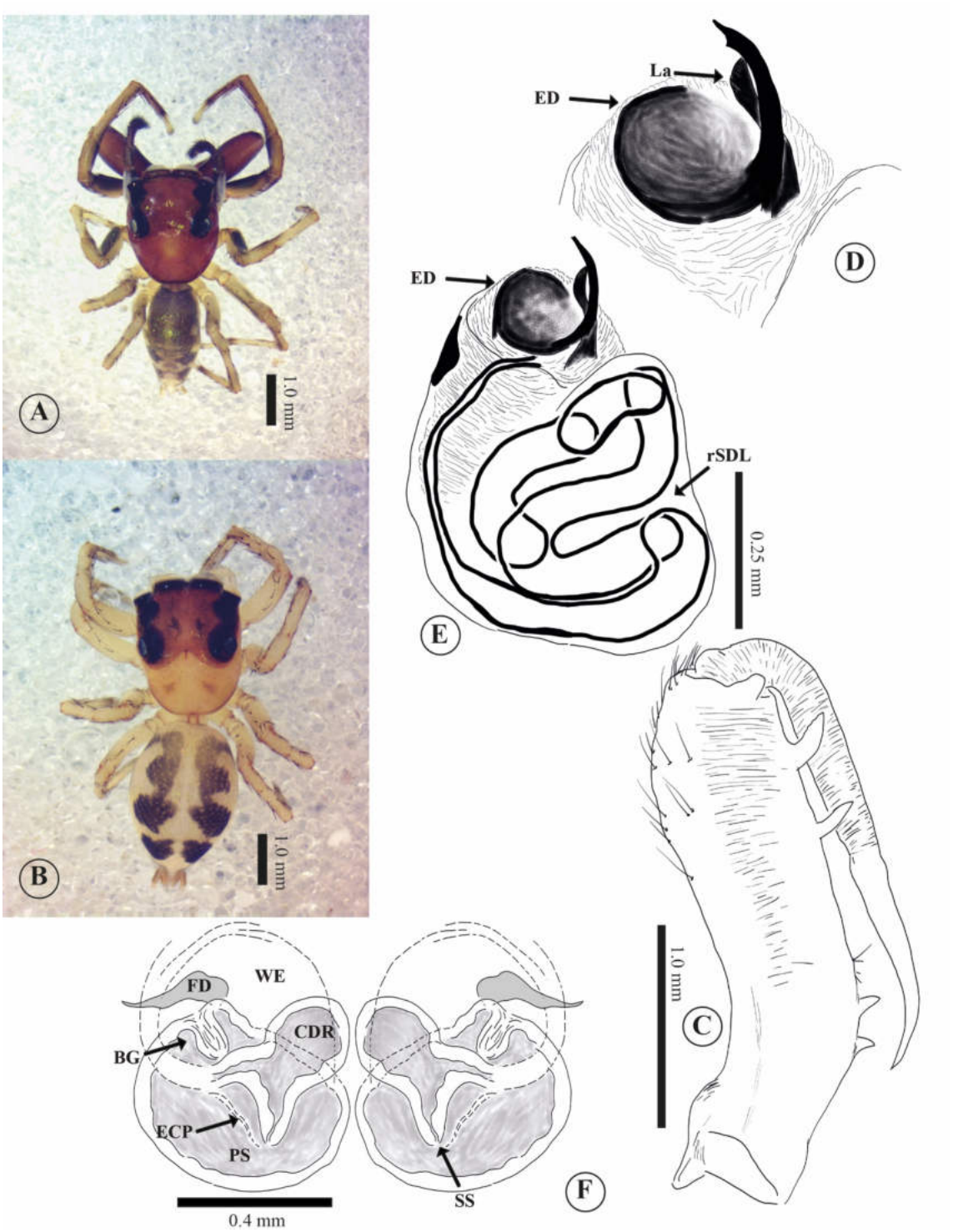

Figure 2.44. *Cobanus multidentatis* **sp. nov.** A, male, habitus, dorsal view. B, female, habitus, dorsal view. C, male chelicerae, retromarginal view. D, male palp, ventral view. E, female, internal genitalia, ventral view.

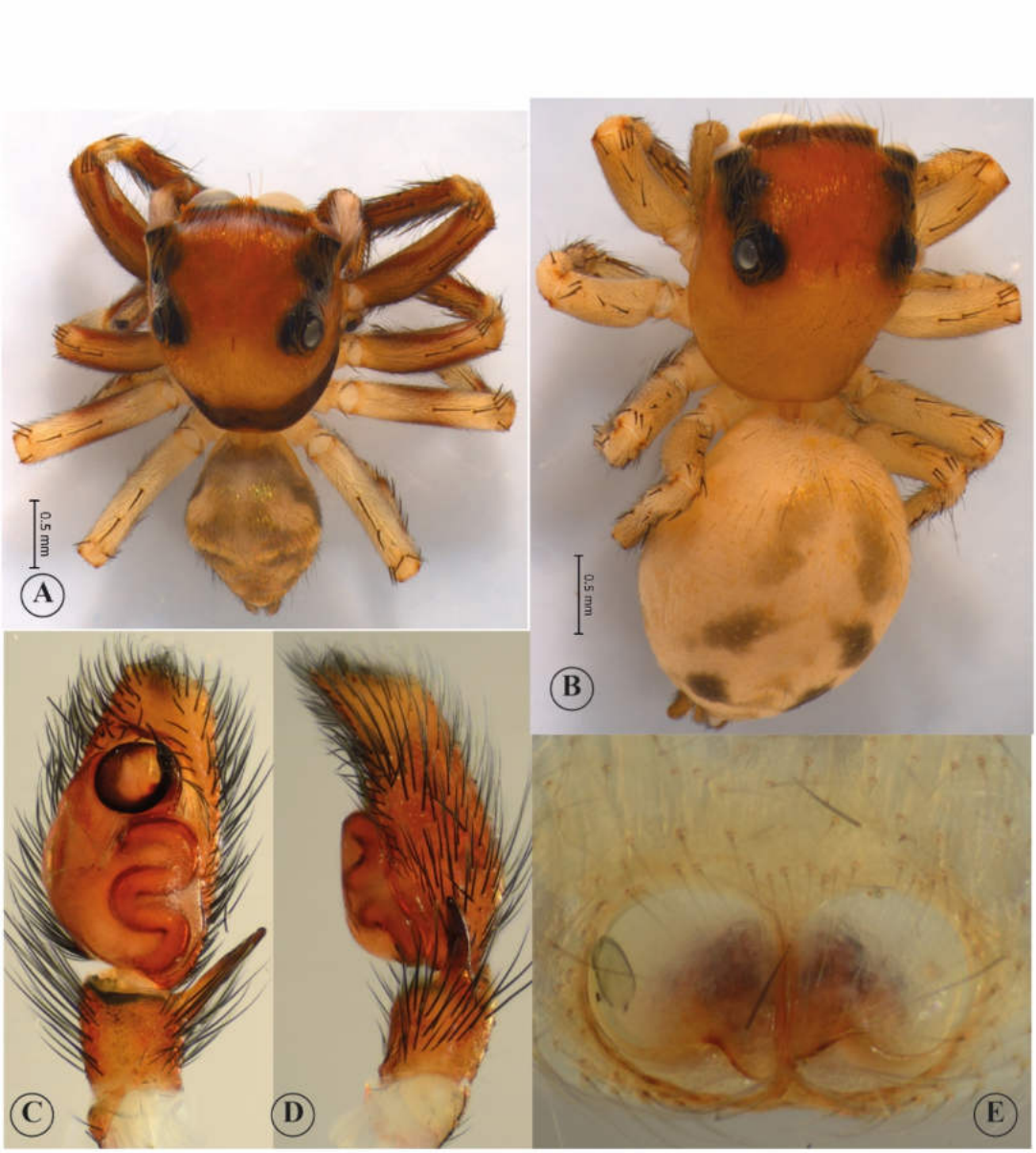

Figure 2.45. *Paracobanus* [Ecuador]. A, male, habitus, dorsal view. B, female, habitus, dorsal view. C, male palp, ventral view. D, male chelicerae, retromarginal view. E, female, internal genitalia, ventral view. Images by Wayne Maddison, released under a Creative Commons Attribution (CC-BY) 3.0 license.

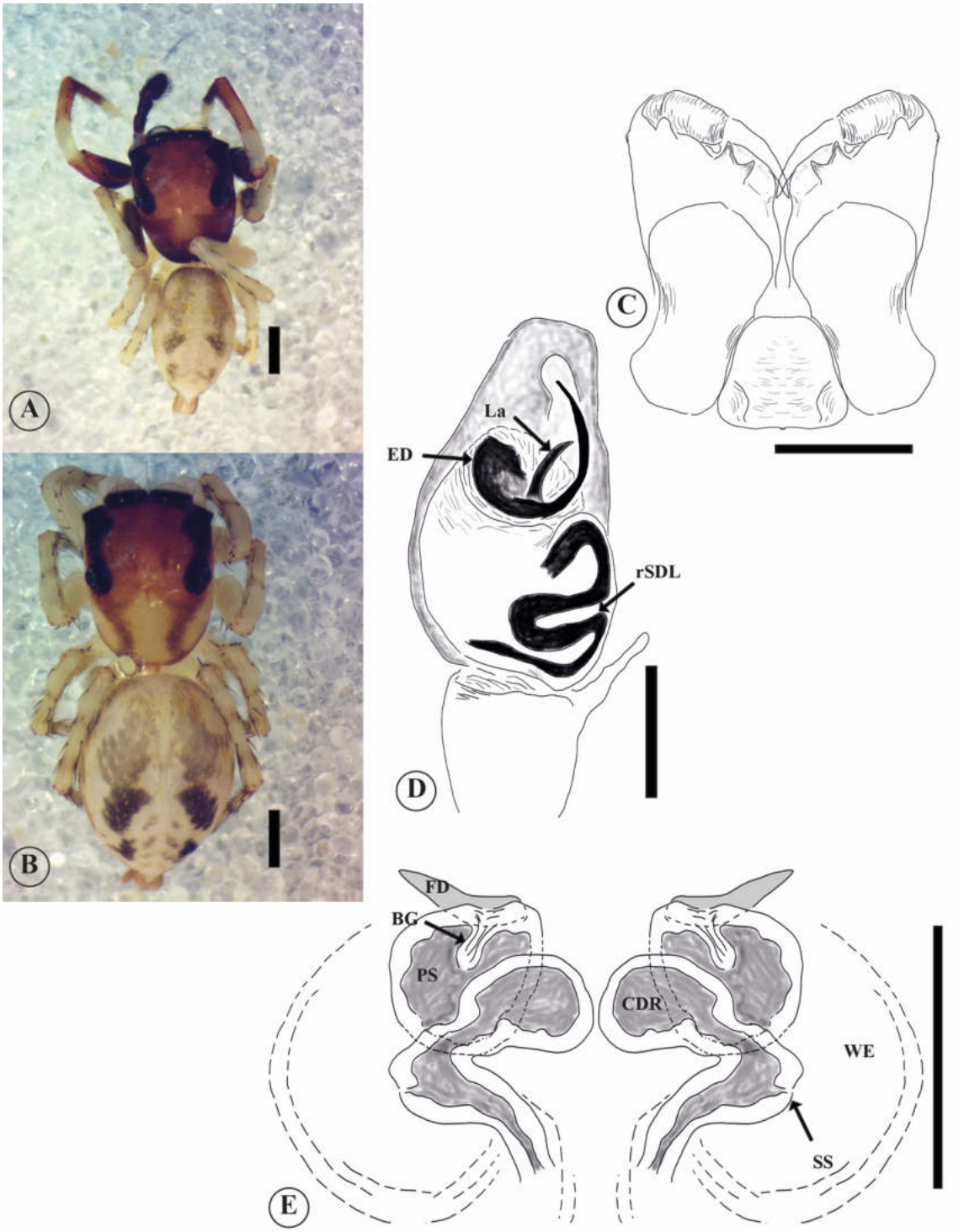

Figure 2.46. *Paracobanus boteroi* **sp. nov.** A, male, habitus, dorsal view. B, female, habitus, dorsal view. C, male chelicerae, retromarginal view. D, male palp, ventral view. E, female, internal genitalia, ventral view.

Figure 2.47. *Truncattus turquinensis* **comb. nov.** A, male (holotype MCZ-IZ 23381), habitus, dorsal view. B, male (holotype MCZ-IZ 23381), habitus, ventral view. C, female (allotype MCZ-IZ 25848), habitus, dorsal view. D, female (allotype MCZ-IZ 25848), habitus, ventral view. E, male palp, ventral view. F, male (holotype MCZ-IZ 23381) palp, prolateral view. G, male (holotype MCZ-IZ 23381) palp, retrolateral view. H, female (allotype MCZ-IZ 25848), genitalia, ventral view.

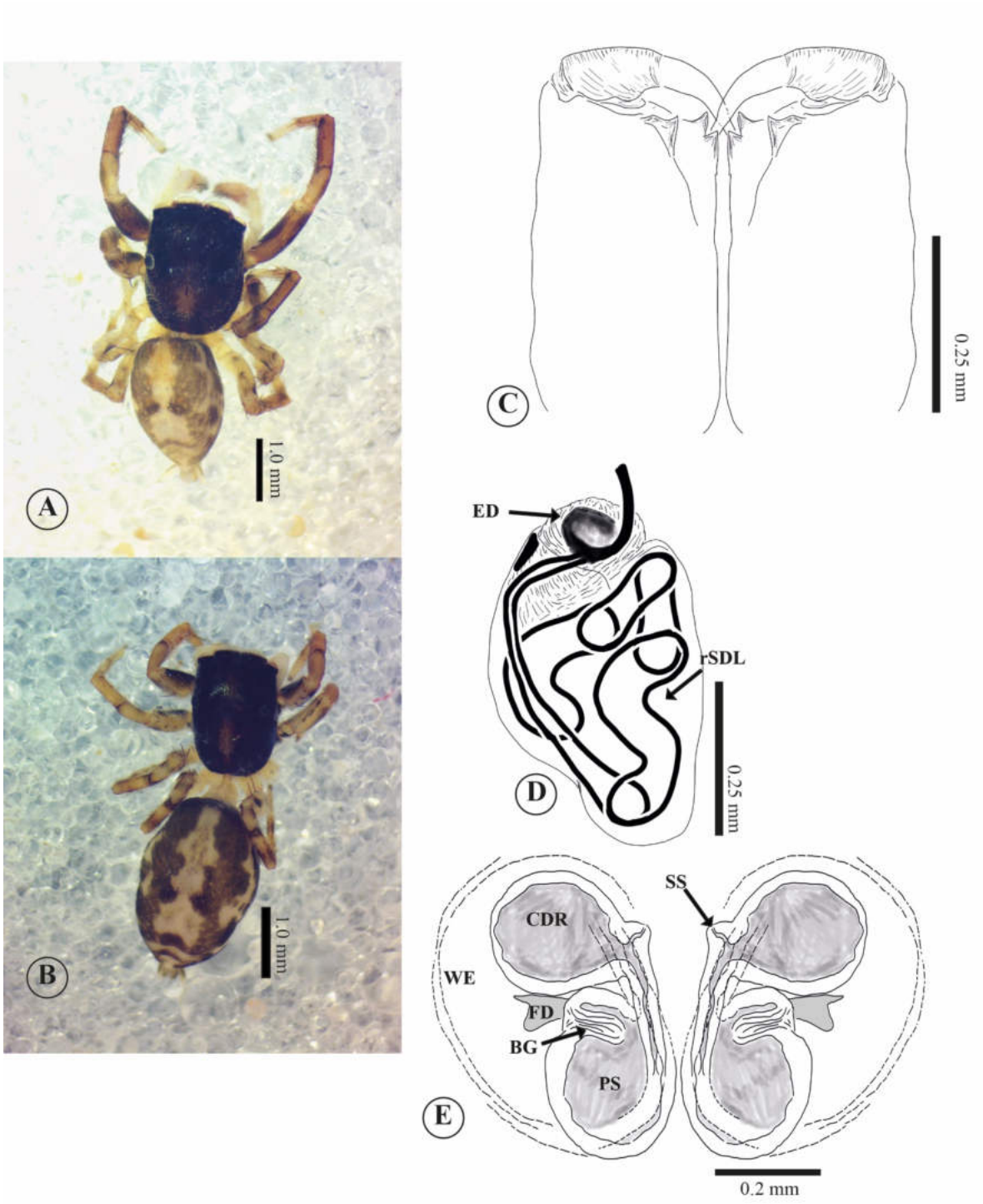

Figure 2.48. *Truncattus martii* **sp. nov.** A, male, habitus, dorsal view. B, female, habitus, dorsal view. C, male chelicerae, retromarginal view. D, male palp, ventral view. E, female, internal genitalia, ventral view.

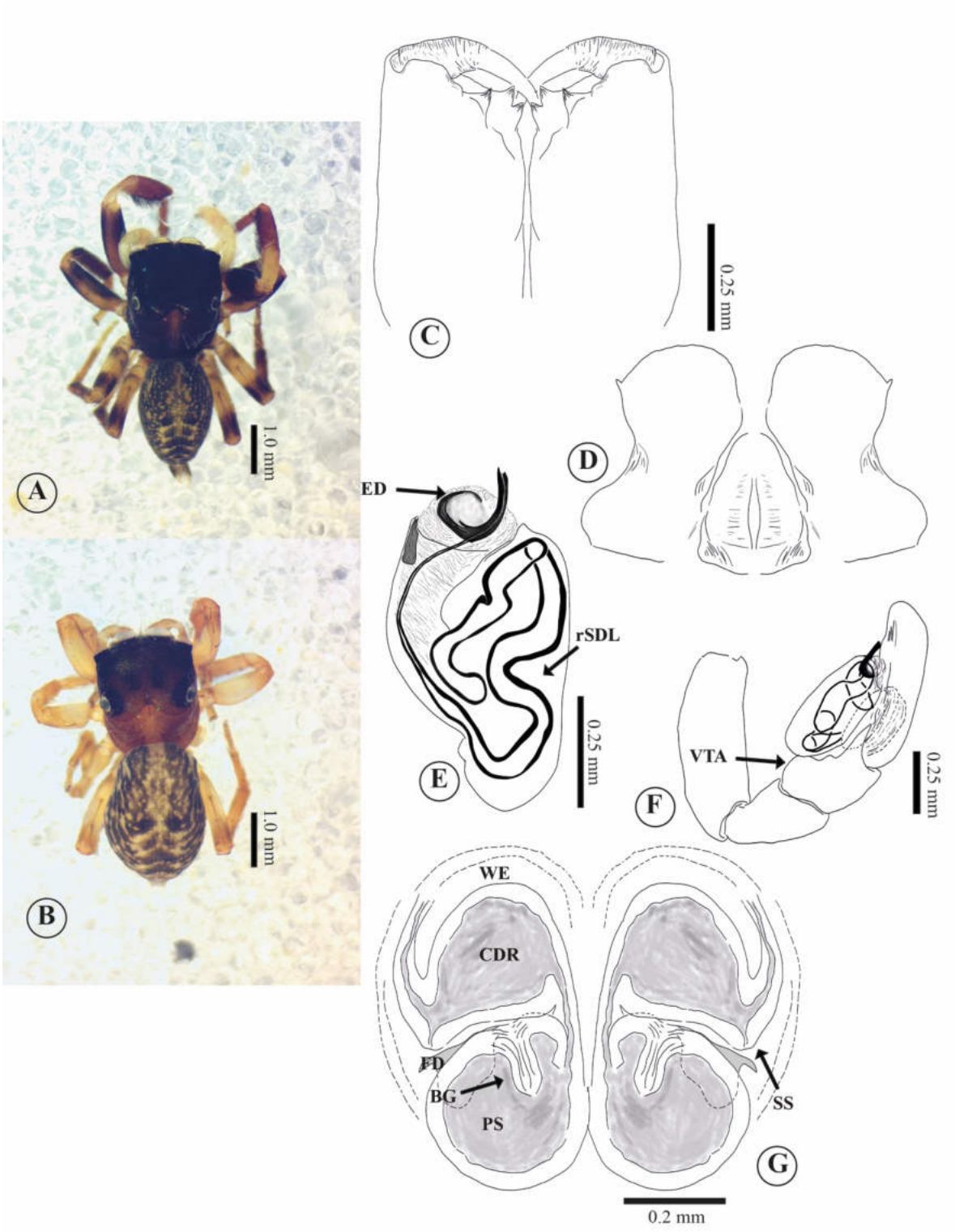

Figure 2.49. *Truncattus platnicki* **sp. nov.** A, male, habitus, dorsal view. B, female, habitus, dorsal view. C, male chelicerae, retromarginal view. D, male endite, ventral view. E, male palp, ventral view. F, male palp, retrolateral view. G, female, internal genitalia, ventral view.

Figure 2.50. A-B, *Agobardus anormalis montanus*, male and female habitus. C-D, *Agobardus bahoruco* male, male and female habitus. E-F, *Bytocrottus crypticus*, male and female habitus. Images by Wayne Maddison, released under a Creative Commons Attribution (CC-BY) 3.0 license.

Figure 2.51. A-B, *Compsodecta peckhami*, male and female habitus. C-D, *Compsodecta haitiensis* male, male and female habitus. E-F, *Corticattus latus*, male and female habitus. Images by Wayne Maddison, released under a Creative Commons Attribution (CC-BY) 3.0 license.

Figure 2.52. A-B, *Pensacola signata*, male and female habitus. C-D, *Petemathis sp.* male, male and female habitus. E-F, *Cobanus sp.*, male and female habitus. Images by Wayne Maddison, released under a Creative Commons Attribution (CC-BY) 3.0 license.

2.4 References

Agnarsson, I. (2004) Morphological phylogeny of cobweb spiders and their relatives (Araneae, Araneoidea, Theridiidae). *Zoological Journal of the Linnean Society* **141** (4), 447–626.

Altekar, G., Dwarkadas, S., Huelsenbeck, J. P., and Ronquist, F. (2004). Parallel Metropolis coupled Markov chain Monte Carlo for Bayesian phylogenetic inference. *Bioinformatics* **20**, 407–415. doi:10.1093/bio informatics/btg427

Álvarez-Padilla, F., Dimitrov, D., Giribet, G., and Hormiga, G. (2009). Phylogenetic relationships of the spider family Tetragnathidae (Araneae, Araneoidea) based on morphological and DNA sequence data. *Cladistics* **25**, 109-146. doi:10.1111/j.1096-0031.2008.00242.x

Álvarez-Padilla, F., and Hormiga, G. (2008). A protocol for digesting internal soft tissues and mounting spiders for scanning electron microscopy. *Journal of Arachnology* **35**, 538-542.

Álvarez-Padilla, F., and Hormig, G. (2011). Morphological and phylogenetic atlas of the orb-weaving spider family Tetragnathidae (Araneae: Araneoidea). *Zoological Journal of the Linnean Society* **162**, 713-879.

Azevedo, G. H. F., Griswold, C. E., and Santos, A. J. (2018a). To complicate or to simplify? Phylogenetic tests of complexity trends and genital evolution in ground spiders (Araneae: Dionycha: Gnaphosidae). *Zoological Journal of the Linnean Society* **84**(3): 673-694. doi:10.1093/zoolinnean/zly016

Baker, A. (2003). Quantitative parsimony and explanatory power. *British Journal for the Philosophy of Science* **54**, 245–259.

Barker, D. (2015). Seeing the wood for the trees: philosophical aspects of classical, Bayesian and likelihood approaches in statistical inference and some implications for phylogenetic analysis. *Biology and Philosophy* **30**, 505–525.

Bennett, R. G. (1992). The spermathecal pores of spiders with special reference to dictynoids and amaurobioids (Araneae, Araneomorphae, Araneoclada). *Proceedings of the Entomological Society of Ontario* **123**, 1-21.

Benton, M. J. (1999) Early origins of modern birds and mammals: molecules vs. morphology. *BioEssays* **21**, 1043–1051

Berry, J. W., Beatty, J. A., and Prószyński, J. (1997). Salticidae of the Pacific Islands. II. Distribution of nine genera, with descriptions of eleven new species. *Journal of Arachnology* **25**, 109-136.

Bodner, G. S. S. (2002) PhD Thesis: Biodiversity assessment and systematics of Neotropical jumping spiders (Araneae: Salticidae). 450pp.

Bösenberg, W., and Strand, E. (1906). Japanische Spinnen. *Abhandlungen der Senckenbergischen Naturforschenden Gesellschaft* **30**, 93-422.

Bremer, K. (1988) The limits of aminoacid sequence data in angiosperm phylogenetic reconstruction. *Evolution* **42** (4), 795– 803.

Bryant, E. B. (1940). Cuban spiders in the Museum of Comparative Zoology. *Bulletin of the Museum of Comparative Zoology* **86**, 247-554.

Bryant, E. B. (1943) The salticid spiders of Hispaniola. *Bulletin of the Museum of Comparative Zoology* **92**, 445-529.

Bryant, E. B. (1950) The salticid spiders of Jamaica. *Bulletin of the Museum of Comparative Zoology* **103**, 163-209.

Cabra-García, J., Brescovit, A. D. (2016). Revision and phylogenetic analysis of the orb-weaving spider genus *Glenognatha* Simon, 1887 (Araneae, Tetragnathidae). *Zootaxa* **4069**(1), 1-183. doi:10.11646/zootaxa.4069.1.1

Cabra-García, J., and Hormiga, G. (2019). Exploring the impact of morphology, multiple sequence alignment and choice of optimality criteria in phylogenetic inference: a case study with the Neotropical orb-weaving spider genus *Wagneriana* (Araneae: Araneidae), *Zoological Journal of the Linnean Society* **XX**, 1–176. DOI: 10.1093/zoolinnean/zlz088

Cala-Riquelme, F., Gutiérrez-Estrada, M. A., and Flórez-Daza, E. (2015). The genus *Loxosceles* Heineken and Lowe 1832 (Araneae: Sicariidae) in Colombia, with description of new cave-dwelling species. *Zootaxa* **4012**(2), 396-400. doi:10.11646/zootaxa.4012.2.12

Carico, J. E., and Holt, P. C. (1964). A comparative study of the female copulatory apparatus of certain species in the spider genus Dolomedes. *Technical Bulletin* VA 5–27. Blacksburg: Virginia Agricultural Experiment Station.

Chakrabarty, P., Faircloth, B. C., Alda, F., Ludt, W. B., Mcmahan, C. D., Near, T. J., Dornburg, A., Albert, J. S., Arroyave, J., Stiassny, M. L. J., Sorenson, L., and Alfaro, M. E. (2017). Phylogenomic systematics of ostariophysan fishes: ultraconserved elements support the surprising nonmonophyly of characiformes. *Systematic Biology* **66**, 881–895.

Chickering, A. M. (1946). The Salticidae of Panama. *Bulletin of the Museum of Comparative Zoology* **97**, 1-474.

Coddington, J. A. (1990). Ontogeny and homology in the male palpus of orb-weaving spiders and their relatives, with comments on phylogeny (Araneoclada: Araneoidea, Deinopoidea). *Smithsonian Contributions to Zoology* **496**, 1-52.

Darriba, D., Taboada, G. L., Doallo, R., and Posada, D. (2012). jModelTest 2: more models, new heuristics and parallel computing. *Nature Methods* **9**, 772. doi:10.1038/nmeth.2109

Davies, V. T, and Żabka, M. (1989). Illustrated keys to the genera of jumping spiders (Araneae: Salticidae) in Australia. *Memoirs of the Queensland Museum* **27**, 189-266.

de S. R. O, Grant, T., Camargo, A., Heyer, W. R., Ponssa, M. L., and Stanley, E. (2014). Systematics of the Neotropical genus Leptodactylus Fitzinger, 1826 (Anura: Leptodactylidae): phylogeny, the relevance of non-molecular evidence, and species accounts. *South American Journal of Herpetology* **9**, S1–S128.

Doleschall, L. (1859). Tweede Bijdrage tot de kennis der Arachniden van den Indischen Archipel. *Acta Societatis Scientiarum Indica-Neerlandica* **5**, 1-60.

Easteal, S. (1999). Molecular evidence far the early divergence of placental mammals. *BioEssays* **21**,1052– 1058

Edgecombe, G. D. (2017). Inferring arthropod phylogeny: fossils and their interaction with other data sources. *Integrative and Comparative Biology* **57**, 467–476.

Edwards, G. B. (2015). Freyinae, a major new subfamily of Neotropical jumping spiders (Araneae: Salticidae). *Zootaxa* **4036**(1): 1-87. doi:10.11646/zootaxa.4036.1.1

Farris, J. S. (1989a). The retention index and homoplasy excess. *Systematic Zoology* **38**, 406-407.

Farris, J. S. (1989b). The retention index and the rescaled consistency index. *Cladistics* **5**: 417–419.

Farris, J. S. (2008). Parsimony and explanatory power. *Cladistics* **24**, 825-847. doi:10.1111/j.1096-0031.2008.00214.x

Felsenstein, J. (1978). Cases in which parsimony or compatibility methods will be positively misleading. *Systematic Zoology* **27**, 401–410.

Folmer, O., Black, M., Hoeh, W., Lutz, R., and Vrijenhoek, R. (1994). DNA primers for amplification of mitochondrial cytochrome oxidase subunit I from diverse metazoan invertebrates. *Molecular Marine Biology and Biotechnology* **3**, 294–299.

Forster, R. R., Platnick, I. N., and Coddington, A. J. (1990). A proposal and review of the spider family Synotaxidae (Araneae, Araneoidea), with notes on theridiid interrelationships. *Bulletin of the American Museum of Natural History* **193**, 1–116.

Forster, R. R. (1970). The spiders of New Zealand. Part III. *Otago Museum Bulletin* **3**, 1-184.

Franganillo, B. P. (1936). *Los arácnidos de Cuba hasta 1936*. Cultural La Habana, 183 pp.

Freudenstein, J.V. (2005) Characters, States and Homology, *Systematic Biology* **54** (6), 965–973, https://doi.org/10.1080/10635150500354654

Galiano, M. E. (1994a). Revision of the genus *Pachomius* (Araneae, Salticidae). *Bulletin of the British Arachnological Society* **9**, 214-220.

Giribet, G. (2015). Morphology should not be forgotten in the era of genomics–a phylogenetic perspective. Zoologischer Anzeiger **256**, 96-103.

Goicoechea, N., Frost, D. R., De la Riva, I., Pellegrino, K., Sites, J., Rodrigues, M. T., and Padial, J. M. (2016). Molecular systematics of teioid lizards (Teioidea/Gymnophthalmoidea: Squamata) based on the analysis of 48 loci under tree-alignment and similarity-alignment. *Cladistics* **32**, 624–671.

Goloboff, P. A., and Catalano, S. A. (2016). TNT version 1.5, including a full implementation of phylogenetic morphometrics. *Cladistics* **32**, 221–238.

Goloboff, P. A., Farris, J. S., Nixon, K. C. (2008a). TNT, a free program for phylogenetic analysis. *Cladistics* **24** (5), 774–786. http://dx.doi.org/10.1111/j.1096-0031.2008.00217.x

Goloboff, P. A., Farris, J. S. (2001). Methods for quick consensus estimation. *Cladistics* **17**, S26–S34. https://doi.org/10.1111/j.1096-0031.2001.tb00102.x

Goloboff, P. A, Pittman, M., Pol, D., and Xu, X. (2019). Morphological datasets fit a common mechanism much more poorly than DNA sequences and call into question the Mkv model. *Systematic Biology* **68**, 494–504.

Goloboff, P. A., and Pol, D. (2005). Parsimony and Bayesian phylogenetics. In: Albert V, ed. Parsimony, phylogeny, and genomics. London: Oxford University, 148–159.

Goloboff, P. A., Torres, A., and Arias, J. S. (2018a). Weighted parsimony outperforms other methods of phylogenetic inference under models appropriate for morphology. *Cladistics* **34**, 407–437.

Goodman, M., Olson, C. B., Beeber, J. E., and Czelusniak, J. (1982) New perspectives in the molecular biological analysis of mammalian phylogeny. *Acta Zoologica Fennica* **169**, 19–35.

Grant, T., and Kluge, A. (2008a) Credit where credit is due: The Goodman-Bremer support metric. *Molecular Phylogenetics and Evolution* **49** (1), 405–406.

Green, P., and Ewing, B. (2002). Phred, version 0.020425 c. Distributed by the authors. Available via: http://phrap.org.

Green, P. (1999). Phrap, version 0.990329. Distributed by the author. Available from http://www.phrap.org.

Griswold, C. E., and Ramírez, M. J., Coddington, J. A., and Platnick, N. I. (2005). Atlas of phylogenetic data for entelegyne spiders (Araneae: Araneomorphae: Entelegynae) with

comments on their phylogeny. *Proceedings of the California Academy of Sciences* **56** (Suppl. II), 1-324.

Hedin, M. C., and Maddison, W. P. (2001). Acombined molecular approach to phylogeny of the jumping spider subfamily Dendryphantinae (Araneae: Salticidae). *Molecular Phylogenetics and Evolution* **18**, 386–403. doi:10. 1006/mpev.2000.0883

Hoff, M., Orf, S., Riehm, B., Darriba, D., and Stamatakis, A. (2016). Does the choice of nucleotide substitution models matter topologically? *BMC Bioinformatics* **17**, 143.

Holder, M. T., Sukumaran, J., and Lewis, P. O. (2008). A justification for reporting the majority-rule consensus tree in Bayesian phylogenetics. *Systematic Biology* **57**, 814–821.

Hormiga, G. (1994a). A revision and cladistic analysis of the spider family Pimoidae (Araneoidea: Araneae). *Smithsonian Contributions to Zoology* **549**, 1-104.

Hormiga, G. (1994b). Cladistics and the comparative morphology of linyphiid spiders and their relatives (Araneae, Araneoidea, Linyphiidae). *Zoological Journal of the Linnean Society* **111**, 1-71.

Huang, D., Hormiga, G., Cai, C., Su, Y., Yin, Z., Xia, F., and Giribet, G. (2018). Origin of spiders and their spinning organs illuminated by mid-Cretaceous amber fossils. *Nature Ecology and Evolution* **2**, 623–627.

Huelsenbeck, J. P., and Bull, J. J. (1996). A likelihood ratio test to detect conflicting phylogenetic signal. *Systematic Biology* **45**, 92–98. DOI: 10.1093/sysbio/45.1.92

Huelsenbeck, J. P., and Ronquist, F. (2001). MRBAYES: Bayesian inference of phylogenetic trees. *Bioinformatics* **17**, 754–755. doi: 10.1093/bioinformatics/17.8.754

Jenner, R. A. (2004) Accepting partnership by submission? Morphological phylogenetics in a molecular millennium. *Systematic Biology* **53**, 333–342

Kainer, D., and Lanfear, R. (2015). The effects of partitioning on phylogenetic inference. *Molecular Biology and Evolution* **32**, 1611–1627.

Kalyaanamoorthy, S., Minh, B. Q., Wong, T. F. K., von Haeseler, A., and Jermiin, L. S. (2017). ModelFinder: fast model selection for accurate phylogenetic estimates. *Nature Methods* 14: 587–589.

Kanesharatnam, N., and Benjamin, S. P. (2016). Three new generic records and descriptions of four new species of jumping spiders (Araneae, Salticidae) from Sri Lanka. *European Journal of Taxonomy* **228**, 1-23. doi:10.5852/ejt.2016.228

Karsch, F. (1878a). Übersicht der von Peters in Mossambique gesammelten Arachniden. *Monatsberichte der Königlich Preussischen Akademie der Wissenschaften zu Berlin* **1878**, 314-338.

Kass, R. E., and Raftery, A. E., (1995). Bayes factors. *Journal of the American Statistical Association* **90**, 773–795.

Katoh, K., Standley, D. M. (2013). MAFFT multiple sequence alignment software version 7: improvements in performance and usability. *Molecular Biology and Evolution* **30**, 772–780.

Kearney, M. (2002). Fragmentary taxa, missing data, and ambiguity: mistaken assumptions and conclusions. *Systematic Biology* **51**, 369–381.

Kitching, I. J., Forey, P. L., Humphries, C. J., and Williams, D. M. (1998). Cladistics: the theory and practice of parsimony analysis. 2nd ed. Oxford: Oxford University Press.

Klingenberg, C., and Gidaszewski N. (2010). Testing and Quantifying Phylogenetic Signals and Homoplasy in Morphometric Data. *Systematic Biology* **59**(3), 245-261.

Kluge, A., and Grant, T. (2006). From conviction to anti-superfluity: old and new justifications of parsimony in phylogenetic inference. *Cladistics* **22**, 276–288.

Kluge, A. (2001b). Parsimony with and without scientific justification. Cladistics 17: 199–210.

Kluge, A. (2004). On total evidence: for the record. *Cladistics* **20**, 205–207.

Kluge, A. (2009). Explanation and falsification in phylogenetic inference: exercises in Popperian philosophy. *Acta Biotheoretica* **57**, 171–186.

Koch, N. M., and Gauthier J. A. (2018). Noise and biases in genomic data may underlie radically different hypotheses for the position of *Iguania* within Squamata. *PLoS ONE* **13**, e0202729.

Kolaczkowski, B., and Thornton, J. W. (2004). Performance of maximum parsimony and likelihood phylogenetics when evolution is heterogeneous. *Nature* **431**, 980–984.

Kolaczkowski, B., and Thornton, J.W. (2009). Long-branch attraction bias and inconsistency in Bayesian phylogenetics. *PLoS ONE* **4**, e7891.

Lee, M. S. Y., and Palci, A. (2015). Morphological Phylogenetics in the Genomic Age. *Current Biology* **25**, R922-R929.

Logunov, D. V., and Azarkina, G. N. (2008b). Two new genera and species of Euophryinae (Aranei: Salticidae) from SE Asia. *Arthropoda Selecta* **17**, 111-115.

Logunov, D. V., and Cutler, B. (1999). Revision of the genus *Paramarpissa* F. O. P.-Cambridge, 1901 (Araneae, Salticidae). *Journal of Natural History* **33**(8), 1217-1236. doi:10.1080/002229399299996

Maddison, D.R., and Maddison, W.P. (2018a). Chromaseq: a Mesquite package for analyzing sequence chromatograms. Version 1.31. http://chromaseq.mesquiteproject.org

Maddison, W. P. (1996). *Pelegrina* Franganillo and other jumping spiders formerly placed in the genus *Metaphidippus* (Araneae: Salticidae). *Bulletin of the Museum of Comparative Zoology* **154**, 215-368.

Maddison, W. P. (2015). A phylogenetic classification of jumping spiders (Araneae: Salticidae). *Journal Arachnology* **43**, 231-292.

Maddison, W. P., and Maddison, D.R. (2018b). Mesquite: a modular system for evolutionary analysis. Version 3.6 http://mesquiteproject.org

Maddison, W. P., Bodner, M. R., and Needham, K. M. (2008). Salticid spider phylogeny revisited, with the discovery of a large Australasian clade (Araneae: Salticidae). *Zootaxa*, **1893**, 46-64.

Maddison, W. P., Zhang, J. X., and Bodner, M. R. (2007). A basal phylogenetic placement for the salticid spider Eupoa, with descriptions of two new species (Araneae: Salticidae). *Zootaxa* **1432**: 23-33.

Maddison, W.P., and Hedin, M.C. (2003). Jumping spider phylogeny (Araneae: Salticidae). *Invertebrate Systematics* **17**, 529-549.

Martin, R. P., Olson, E. E., Girard, M. G., Smith, W. L., and Davis, M. P. (2018). Light in the darkness: new perspective on lanternfish relationships and classification using genomic and morphological data. *Molecular Phylogenetics and Evolution* **121**, 71–85.

Masta, S. E., and Boore, J. L. (2004) The complete mitochondrial genome sequence of the spider Habronattus oregonensis reveals rearranged and extremely truncated tRNAs. *Molecular Biology and Evolution* **21** (5), 893-902.

Michalik, P., Reiher, W., Tintelnot-Suhm, M., Coyle, F. A. and Alberti, G. (2005). Female genital system of the folding-trapdoor spider *Antrodiaetus unicolor* (Hentz, 1842) (Antrodiaetidae, Araneae): ultrastructural study of form and function with notes on reproductive biology of spiders. *Journal of Morphology* **263**, 284-309.

Miller, M. A., Pfeiffer, W., and Schwartz, T. (2010) "Creating the CIPRES Science Gateway for inference of large phylogenetic trees" in Proceedings of the Gateway Computing Environments Workshop (GCE), 14 Nov. 2010, New Orleans, LA pp 1 - 8.

Mirande, J. M. (2017). Combined phylogeny of ray-finned fishes (Actinopterygii) and the use of morphological characters in large-scale analyses. *Cladistics* **33**, 333–350.

Nguyen, L.T., Schmidt, H. A., von Haeseler, A., and Minh, B. Q. (2015). IQ-TREE: a fast and effective stochastic algorithm for estimating maximum-likelihood phylogenies. *Molecular Biology and Evolution* **32**, 268–274.

Nixon, K. (2002). WinClada. Version 1.00.08. Available at: http://www.cladistics.com/

Nylander, J. A., Ronquist, F., Huelsenbeck, J. P., and Nieves-Aldrey, J. (2004). Bayesian phylogenetic analysis of combined data. *Systematic Biology* **53**, 47–67.

O'Reilly, J., Puttick, M., Parry, L., Tanner, A., Tarver, J., Fleming, J., Pisani, D., and Donoghue, P. (2016). Bayesian methods outperform parsimony but at the expense of precision in the estimation of phylogeny from discrete morphological data. *Biology Letters* **12**, 20160081.

Ospina-Sarria, J. J., and Cabra-García, J. 2018. Parsimony analysis of unaligned sequence data: some clarifications. *Cladistics* **34**, 574–577.

Padial, J. M., Grant, T., and Frost, D. R. (2014). Molecular systematics of terraranas (Anura: Brachycephaloidea) with an assessment of the effects of alignment and optimality criteria. *Zootaxa* **3825**, 001–132.

Pagel, M. (1999). Inferring the historical patterns of biological evolution. *Nature* **401**, 877–884.

Parry, L. A., Baron, M. G., and Vinter, J. (2017). Multiple optimality criteria support Ornithoscelida. *Royal Society Open Science* **4**: 170833.

Peckham, G. W. and Peckham, E. G. (1895). Spiders of the *Homalattus* group of the family Attidae. *Occasional Papers of the Natural History Society of Wisconsin* **2**, 159-183.

Petrunkevitch, A. (1914b). Attidae of the Yale Dominica Expedition. *Journal of The New York Entomological Society* **22**, 329-331.

Petrunkevitch, A. (1930a). The spiders of Porto Rico. Part two. *Transactions of the Connecticut Academy of Arts and Sciences* **30**, 159-356.

Pickard-Cambridge, F. O. (1900). Arachnida - Araneida and Opiliones. In: *Biologia Centrali-Americana*, Zoology. London **2**, 89-192.

Pickard-Cambridge, F. O. (1901a). Arachnida - Araneida and Opiliones. In: *Biologia Centrali-Americana*, Zoology. London **2**, 193-312.

Pol, D., and Siddall, M. E. (2001). Biases in maximum likelihood and parsimony, a simulation approach to a 10-taxon case. *Cladistics* **17**, 266–281.

Posada, D., and Buckley, T. R. (2004). Model selection and model averaging in phylogenetics: advantages of Akaike Information Criterion and Bayesian Approaches over Likelihood Ratio Tests. *Systematic Biology* **53**, 793–808.

Prószyński, J. (1976) Studium systematyczno-zoogeograficzne nad rodzina Salticidae (Aranei) Regionow Palearktycznego i Nearktycznego. *Rozprawy Wyzszej Szkoly Pedagogicznej* **6**, 1- 260.

Prószyński, J. (1984a). Atlas rysunków diagnostycznych mniej znanych Salticidae (Araneae). *Wyższa Szkola Rolniczo-Pedagogiczna, Siedlcach* **2**, 1-177.

Prószyński, J., and Deeleman-Reinhold, C. L. (2012). Description of some Salticidae (Aranei) from the Malay Archipelago. II. Salticidae of Java and Sumatra, with comments on related species. *Arthropoda Selecta* **21** (1), 29-60.

Purcell, W. F. (1910). The phylogeny of the tracheae in Araneae. *Quarterly Journal of Microscopical Science* **54**, 519-564.

Pyron, R. A. (2015). Post-molecular systematics and the future of phylogenetics. *Trends in Ecology and Evolution* **30**, 384–389.

Rambaut, A., Suchard, M.A., Xie, D., and Drummond, A.J. (2014). Tracer v1.6. Available at: <http://beast.bio.ed.ac.uk/Tracer>.

Ramírez, M. J. 2014. The morphology and phylogeny of dionychan spiders (Araneae: Araneomorphae). *Bulletin of the American Museum of Natural History* **390**, 1–374.

Ramírez, M. J. (2003) The spider subfamily amaurobioidinae (Araneae: Anyphaenidae): A phylogenetic revision at generic level. *Bulletin of the Museum of Natural History* **277**, 1–262.

Richardson, B. J., and Żabka, M. (2007). A revision of the Australian jumping spider genus *Prostheclina* Keyserling, 1892 (Araneae: Salticidae). *Records of the Australian Museum* **59**, 79-96.

Rindal, E., and Brower, A. V. (2011). Do model-based phylogenetic analyses perform better than parsimony? A test with empirical data. *Cladistics* **27**, 331–334.

Ronquist, F., and Huelsenbeck, J. P. (2003). Mrbayes 3: Bayesian phylogenetic inference under mixed models. *Bioinformatics* **19**, 1572–1574.

Rubio, G. D., Baigorria, J. E. and Edwards, G. B. (2016). First description of the female of the jumping spider *Balmaceda nigrosecta* Mello-Leitão (Salticidae, Dendryphantini, Marpissina). *ZooKeys* **563**, 11-19. doi:10.3897/zookeys.563.6705

Ruiz, G. R. S., and Maddison, W. P. (2012). DNA sequences corroborate Soesiladeepakius as a non-salticoid genus of jumping spiders: placement with lapsiines, phylogeny, and description of six new species (Araneae, Salticidae). *Zoological Journal of the Linnean Society* **165**, 274-295.

Salgado, A., and Ruiz, G. R. S. (2017). Ten new species of *Amphidraus* Simon, 1900 (Araneae: Salticidae: Euophryini) and three new combinations. *Zootaxa* **4312**(3), 401-437. doi:10.11646/zootaxa.4312.3.1

Sánchez-Pacheco, S. J., Torres -Carvajal, O., Aguirre-Peñafiel, V., Nunes, P. M., Verrastro, L., Rivas, G. A., Rodrigues, M. T., Grant, T., and Murphy, R. W. (2018). Phylogeny of Riama (Squamata: Gymnophthalmidae), impact of phenotypic evidence on molecular

datasets, and the origin of the Sierra Nevada de Santa Marta endemic fauna. *Cladistics* **34**, 260–291.

Sansom, R. S., Choate, P. G., Keating, J. N., and Randle, E. (2018). Parsimony, not Bayesian analysis, recovers more stratigraphically congruent phylogenetic trees. *Biology Letters* **14**, 20180263.

Scharaschkin, T., and Doyle, J.A. (2006) Character evolution in Anaxagorea (Annonaceae). *The American Journal of Botany* **93** (1), 36–54.

Schrago, C. G, Aguiar, B. O, Mello, B. (2018). Comparative evaluation of maximum parsimony and Bayesian phylogenetic reconstruction using empirical morphological data. *Journal of Evolutionary Biology* **31**, 1477–1484.

Scotland, R. W, Olmstead, R. G., Bennett, J. R. (2003) Phylogeny reconstruction: the role of morphology. *Systematic Biology* **52**, 539–548.

Sereno, P. C. (2007). Logical basis for morphological characters in phylogenetics. *Cladistics* **23**, 565–587.

Shear, W. A. (1967). Expanding the palpi of male spiders. *Breviora* **259**, 1–27.

Siddall, M. E. (1998). Success of parsimony in the four-taxon case, long-branch repulsion by likelihood in the Farris Zone. *Cladistics* **14**, 209–220.

Sierwald, P. (1989). Morphology and ontogeny of female copulatory organs in American Pisauridae, with special reference to homologous features (Arachnida, Araneae). *Smithsonian Contributions to Zoology* **484**, 1–24.

Simon, E. (1877b). Etudes arachnologiques. 5e Mémoire. IX. Arachnides recueillis aux îles Phillipines par MM. G. A. Baer et Laglaise. *Annales de la Société Entomologique de France* (5) **7**, 53-96.

Simon, E. (1885a). Arachnides recueillis par M. Weyers à Sumatra. Premier envoi. *Annales de la Société Entomologique de Belgique* **29** (C.R.), 30-39.

Simon, E. (1899a). Contribution à la faune de Sumatra. Arachnides recueillis par M. J. L. Weyers, à Sumatra. (Deuxiéme mémoire). *Annales de la Société Entomologique de Belgique* **43**, 78-125.

Simon, E. (1902). Description d'arachnides nouveaux de la famille des Salticidae (Attidae) (suite). *Annales de la Société Entomologique de Belgique* **46**, 24-56, 363-406.

Simon, E. (190l). *Histoire naturelle des Araignees.* Tome 2, Fascicule 3. Seconde edition. Paris, Librairie encyclopedique de Roret. 381-668pp.

Stamatakis A. (2014). RAxML version 8: a tool for phylogenetic analysis and post-analysis of large phylogenies. *Bioinformatics* **30**, 1312–1313.

Stamatakis, A. (2006). RAxML-VI-HPC: Maximum Likelihood-based Phylogenetic Analyses with Thousands of Taxa and Mixed Models. *In Bioinformatics* **22**(21), 2688-2690.

Steel, M., and Penny, D. (2000). Parsimony, likelihood, and the role of models in molecular phylogenetics. *Molecular Biology and Evolution* **17**, 839–850.

Swofford, D. L., Waddell, P. J., Huelsenbeck, J. P., Foster, P. G., Lewis, P. O., and Rogers, J. S. (2001). Bias in phylogenetic estimation and its relevance to the choice between parsimony and likelihood methods. *Systematic Biology* **50**, 525–539.

Thorell, T. (1877b). Studi sui Ragni Malesi e Papuani. I. Ragni di Selebes raccolti nel 1874 dal Dott. O. Beccari. *Annali del Museo Civico di Storia Naturale di Genova* **10**, 341-637.

Thorell, T. (1892). Studi sui ragni Malesi e Papuani. IV, 2. *Annali del Museo Civico di Storia Naturale di Genova* **31**, 1-490.

Tuffley, C., and Steel, M. (1997). Links between maximum likelihood and maximum parsimony under a simple model of substitution. *Bulletin of Mathematical Biology* **59**, 581–607.

Ubick, D., Paquin, P., Cushing, P. E., and Roth, V. 2017. *Spiders of North America: an identification manual*. 2nd Edition. American Arachnological Society. Keene, New Hampshire, USA.

Waldock, J. M. (1995). A new species of *Maratus* from southwestern Australia (Araneae: Salticidae). *Records of the Western Australian Museum, Supplement* **52**, 165-169.

Wang, B., Dunlop, J. A., Selden, P. A., Garwood, R. J., Shear, W. A., Müller, P., and Lei, X. 2018. Cretaceous arachnid Chimerarachne yingi gen. et sp. nov. illuminates spider origins. *Nature Ecology and Evolution* **2**, 614–622.

Wanninger, A. (2015). Morphology is dead – long live morphology! Integrating MorphoEvoDevo into molecular EvoDevo and phylogenomics. *Frontiers in Ecology and Evolution* **3**, 54.

Ward PS, Brady SG, Fisher BL, Schultz TR. 2015. The evolution of myrmicine ants: phylogeny and biogeography of a hyperdiverse ant clade (Hymenoptera: Formicidae). *Systematic Entomology* **40**, 61–81.

Whelan, N. V., Kocot, K. M., Moroz, L. L., and Halanych, K. M. (2015). Error, signal, and the placement of Ctenophora sister to all other animals. *Proceedings of the National Academy of Sciences of the United States of America* **112**, 5773–5778.

Wiens JJ (2004) The role of morphological data in phylogeny reconstruction. Systematic Biology **53**, 653–661.

World Spider Catalog (2020). World Spider Catalog. Natural History Museum Bern, online at http://wsc.nmbe.ch, version 21.0, accessed on February 1th. doi: 10.24436/2

Wright, A., and Hillis, D. (2014). Bayesian analysis using a simple likelihood model outperforms parsimony for estimation of phylogeny from discrete morphological data. *PLoS ONE* **9**, e109210.

Wright, A., and Hillis, D. (2014). Bayesian analysis using a simple likelihood model outperforms parsimony for estimation of phylogeny from discrete morphological data. *PLoS ONE* **9**, e109210.

Żabka, M. (1987). Salticidae (Araneae) of Oriental, Australian and Pacific Regions, II. Genera *Lycidas* and *Maratus*. *Annales Zoologici, Warszawa* **40**, 451-482.

Żabka, M. (1994). Salticidae (Arachnida: Araneae) of Oriental, Australian and Pacific regions, X. Genus *Simaetha* Thorell. *Records of the Western Australian Museum* **16**, 499-534.

Żabka, M. and Pollard, S. (2002). Salticidae (Arachnida: Araneae) of New Zealand: genus *Hypoblemum* Peckham and Peckham, 1886. *Records of the Canterbury Museum* **16**, 64-72.

Zhang, J.X., and Maddison, W.P. (2012). New euophryine jumping spiders from the Dominican Republic and Puerto Rico (Araneae: Salticidae: Euophryinae). *Zootaxa* **3476**, 1-54.

Zhang, J.X., and Maddison, W.P. (2013). Molecular phylogeny, divergence times and biogeography of spiders of the subfamily Euophryinae (Araneae: Salticidae). *Molecular Phylogenetics and Evolution* **68**, 81-92.

Zhang, J.X., and Maddison, W.P. (2015). Genera of euophryine jumping spiders (Araneae: Salticidae), with a combined molecular-morphological phylogeny. *Zootaxa* **3938**,1-147.

Zhou X, Shen X, Hittinger CT, Rokas A. 2018. Evaluating fast maximum likelihood-based phylogenetic programs using empirical phylogenomic data sets. *Molecular Biology and Evolution* **35**, 486–503.

CAPÍTULO 3

NEW GENERA AND SPECIES REVEALED BY PHYLOGENETIC ANALYSES OF ANTILLATTUS (SALTICIDAE: EUOPHRYINI)

New genus and species revealed by phylogenetic analyses of *Antillattus* (Salticidae: Euophryini)

Cala-Riquelme, Franklyn; Programa de Doctorado en Ciencias-Biología, Universidad Nacional de Colombia, Bogotá, Colombia. Email: franklyncalariquelme@gmail.com

May-Collado, Laura J.; Department of Biology, 120 A, Marsh Life Science Building, Burlington, VT 05405-0086 USA. E-mail: lmaycollado@gmail.com

Binford, Greta; Department of Biology, Lewis and Clark College, Portland, OR, USA. E-mail: binford@lclark.edu

Wiencek, Patrick; Department of Biology, 120 A, Marsh Life Science Building, Burlington, VT 05405-0086 USA. Email: wiencek.patrick@gmail.com

Florez-Daza., Eduardo; Grupo de estudio de arácnidos & Miriápodos, Instituto de Ciencias Naturales, Universidad Nacional de Colombia, Bogotá, Colombia. E-mail: aeflorezd@unal.edu.co

Agnarsson, Ingi; Department of Biology, 120 A, Marsh Life Science Building, Burlington, VT 05405-0086 USA. E-mail: iagnarsson@gmail.com

Abstract

An extensive ongoing survey of Caribbean arachnids continues to uncover, across multiple genera and families, greater species richness than hitherto appreciated. Here, we focus on a clade of jumping spiders endemic to the Caribbean, currently all placed in the genus *Antillattus*. Phylogenetic analyses were conducted on *Antillattus* s. l., and the group was revised based on the analyses. These analyses are based on molecular and morphological data, and include Cuban species, which were absent from previous analyses. A total of 125 morphological characters were scored for the group. Additionally, these data were used for species delimitation and identification. Our results indicate indicate that several species formerly placed in *Antillattus* are misplaced in this genus and a new placement is proposed. One morphological synapomorphies and molecular data support the monophyly of the Antillattus clade and indicate that the genus as currently circumscribed actually comprises three divergent clades (*Antillattus*, *Pensacolatus* and *Bryanattus* **gen. nov.**). The monophyly of *Antillattus* (new circumscription) is supported by twelve morphological synapomorphies and is revised to include *A. gracilis*, *A.*

placidus, *A. cambridgei*, *A. cubensis*, and *A. ocultus* **sp. nov.** *Antillattus ocultus* **sp. nov.** is genetically distinct from the other species but is morphologically cryptic. The genus *Pensacolatus* is revised to include *P. darlingtonia* **comb. nov.**, *P. electus* **comb. nov.**, *P. maxillosus* **comb. nov.**, *P. montanus* **comb. nov.**, *P. peckhami* **comb. nov.** *P. scutiformis* **comb. nov.**, *P. surieli* **sp. nov**., and *P. naranjoi* **sp. nov**. Finally, *Bryanattus* **gen. nov.** is proposed to include the type species *Bryanattus keyserlingi* **comb. nov.**, *B. mandibulatus* **comb. nov.**, *B. unispina* **comb. nov.**, *B. orientalis* **sp. nov.**, *B. thanos* **sp. nov.** and *B. sanchezi* **sp. nov.**

Keywords: taxonomy, morphology, jumping spiders, Caribbean

3.0 Introduction

The Caribbean region is known for its high levels of species diversity and endemism, and is considered a biodiversity hotspot (Mittermeier *et al*. 2005, Ricklefs and Birmingham 2008). The magnitude and structure of this diversity is an active area of discovery, particularly for terrestrial arthropods. Molecular phylogenetic studies have recently centered on Caribbean invertebrates (Agnarsson *et al*. 2016; Čandek *et al*. 2019; Čandek and Kuntner 2015; Ceccarelli and Zaldívar-Riverón 2013; Chamberland *et al*. 2018; Crews and Gillespie 2010; Deler *et al*. 2017; Dziki *et al*. 2015; Esposito *et al*. 2015; Lewis *et al*. 2015; Matos-Maraví *et al.* 2014; McHugh *et al*. 2014; Rodriguez Pitts and von Dohlen 2015; Tong *et al*. 2019; Wahlberg 2006; Wahlberg and Freitas 2007; Zhang and Maddison 2013, 2015; Zhang *et al*. 2017). Nevertheless, there has been a resurgence of morphological data in the form of integrative data sets (Cabra-García and Hormiga 2019; Chakrabarty *et al*. 2017, Koch and Gauthier 2018).

Of the nearly 48,300 known spider species (Arthropoda: Chelicerate: Arachnida: Araneae), 6182 are jumping spiders (Salticidae) (World Spider Catalog 2020), making this the most species rich spider family. Recent phylogenetic analyses have indicated the potential of some salticids as models for biogeographical and molecular evolutionary studies (Maddison 2015). Because of this, the focus of the current study is the genus *Antillattus* Bryant 1943, which is nested within the tribe Euophryini Simon 1901, in the clade Saltafresia Bodner and Maddison 2012 (see Maddison *et al*. 2014, Maddison 2015). The tribe Euophryini is comprised of more than 1000 species that are widely distributied across both the Old and New World tropics (Maddison 2015; Maddison and Hedin 2003; Prószyński 1976; Zhang and Maddison 2015). Phylogenetic research has revealed that New and Old-World euophryines are reciprocally monophyletic (Bodner and Maddison 2012; Maddison and Hedin 2003; Maddison *et al*. 2008),

indicating that most euophryine diversification occurred intra-continentally (Zhang and Maddison 2013).

Recently, Zhang and Maddison (2013, 2015) resolved Euophryine relationships using a worldwide dataset. They presented evidence of high levels of euophryine diversity in the Caribbean region and identified the Antillattus clade as one of three salticid clades represent in the Caribbean. The Antillattus clade includes *Antillattus* Bryant 1943, *Truncattus* Zhang and Maddison 2012, *Petemathis* Prószyński and Deeleman-Reinhold 2012, and probably *Allodecta* Bryant 1950 and *Caribattus* Bryant 1950 (Zhang and Maddison 2015). This clade is diagnosed by having 1) two promarginal cheliceral teeth, 2) male palp with the embolus coiled less than 180°, 3) females with a wide median septum on the epigynum, 4) a copulating operculum typically found in the intermediate area of the vulva, and 5) relatively short copulatory ducts (Bryant 1940, 1943, 1950; Zhang and Maddison 2012, 2015).

The genus *Antillattus* Bryant 1943 contains 13 species described from Cuba, Hispaniola, and Puerto Rico (Bryant 1940, 1943; Galiano 1968; Zhang and Maddison 2012, 2015). In this work, we add depth to the sampling of Zhang and Maddison (2013, 2015) in the euophryine lineage, which includes the Antillattus clade.

Based on morphological characteristics, the genus *Antillattus* as currently circumscribed (supplementary figure 1) actually contains more than one genus, and several Cuban species that have not yet been described. As previously stated, the goal of this study is to review the species of *Antillattus* and their relatives distributed in the Greater Antilles, considering both morphological and molecular evidence. We provide characters that are useful for genera delimitation and describe new genera and species. Finally, we present evidence for a possible morphologically 'cryptic' species and employ DNA tree-based methods, barcode gap analysis, and morphology to explore species delimitation.

3.1 Material and methods

3.1.0 Taxon sampling

Specimens were collected diurnally in 2012 and 2013 by beating vegetation across Cuba and the Dominican Republic (supplementary figure 1, supplementary table 1). Taxa represented in our collection included *Antillattus cubensis*, *A. placidus*, *A. keyserlingi*, *A. cambridgei*, *A. gracilis, A. maxillosa*, and *A. darlingtoni* as well as potentially new species (see below). Specimens were fixed in 95% ethanol. Additional data from *Antillattus* and outgroup specimens

were obtained from GenBank (Zhang and Maddison 2013, 2015) for use in molecular analyses. Caribbean voucher specimens will be deposited in the University of Vermont's Natural History Museum and the Smithsonian Institute. Type species were examined and additional material was reviewed from the following collections: Museum of Comparative Zoology, Harvard University (**MCZ**); University of Vermont's Natural History Museum (**USNM-ENT**), and Museo Nacional de Historia Natural, Santo Domingo (**MNHNSD**).

3.1.1 Morphology

Dissected female genitalia were examined after digestion in potassium hydroxide (KOH) to remove soft tissues. Female and male genitalia were examined using a NIKON 4024913 microscope. Material for scanning electronic microscopy was prepared following the methods of Álvarez-Padilla and Hormiga (2008): specimens were dried under an incandescent light bulb, attached to metallic stubs using either adhesive copper tape or carbon stickers, and sputter coated with 10nm of gold using a sputter-Q150R. Images were made with a QUANTA-200-FEI microscope at Laboratorio de microscopia electronica de Barrido, Universidad Nacional de Colombia. Photographs were taken using the Visionary Digital BK laboratory system equipped with a Canon 5D and 65-mm macro zoom lens. Images were stacked with Helicon Focus 5.3 and processed with Photoshop CS6. Measurements are expressed in millimeters.

We use standard terminology for Araneae, employing general abbreviations following Ramirez (2014) and Zhang and Maddison (2015): *Prosoma*: anterior lateral eye (ALE); anterior median eye (AME); mastidion (Ms); ocular quadrangle (OQ); posterior lateral eye (PLE); posterior median eye (PME); promarginal tooth (pT); retrolateral tooth (rT). *Abdomen*: pre-spiracular bump (PB). *Epigynum*: Bennett's gland (BG); copulatory duct (CD); copulatory duct with receptacle (CDR); copulatory opening (Co); fertilization duct (FD); median septum (MS); primary spermathecae (PS); secondary spermathecae (SS); window of the epigynum (WE). *Palp*: distal tegular lobe (dTL); embolic disc (ED); embolus (E); fundus (Fu); proximal tegular lobe (pTL); retrolateral sperm duct loop (rSDL); retrolateral tibial apophysis (RTA); salticid radix (SR); spermophorae (S); spermophorae reduction (SR); tegulum (T); ventral tibial apophysis (VTA).

3.1.1.0 Morphological characters

The phylogenetic dataset is comprised of 125 characters. Characters were grouped by: male palp, female genitalia, cephalothorax (including the legs and chelicerae), and abdomen.

Continuous characters were graphically visualized to discretize them into valid states (Ramírez 2003; Scharanschkin and Doyle 2006; Cabra-García and Brescovit 2016). Mesquite v. 3.6 (Maddison and Maddison 2018b) was used to visualize synapomorphies and to conduct ancestral character state reconstructions using parsimony. Winclada 1.00.08 (Nixon 2002) and TNT v.1.5 (Goloboff *et al.* 2008a; Goloboff and Catalano 2016) were used to identify and plot unambiguously optimized synapomorphies (see Ramírez 2014) shared across optimal trees of equal weights, implied weights, and total evidence under Parsimony (MP). The synapomorphies are presented in table 3.2.

Additionally, within our morphological dataset, ACCTRAN or DELTRAN (table 3.3) commands were used as necessary, favoring the preservation of the homology of complex structures and avoiding illogical optimizations (Agnarsson and Miller 2008). In accelerated transformation (ACCTRAN), changes are assigned along branches as quickly as possible (passing up), and in delayed transformation (DELTRAN), as late as possible. However, in some instances ACCTRAN results in illogical optimization for taxa coded as inapplicable for that character, and DELTRAN is necessary to avoid illogical optimization, although only a single gain is inferred (see Agnarsson 2004; Agnarsson and Miller 2008; Ramírez 2014).

3.1.2 Molecular methods

DNA was isolated with the Qiagen DNeasy Tissue Kit (Qiagen, Valencia, CA, USA). We sequenced fragments of COI, 16S, and 28S. We amplified COI with LCO1490 (GGTCAACAAATCATAAAGATATTGG) (Folmer *et al.* 1994) and C1-N-2776 (GGATAATCAGAATATCGTCGAGG) (Hedin and Maddison 2001). The rDNA gene 16S was amplified with 16SA/12261 (CGCCTGTTTACCAAAAACAT) (Folmer *et al.* 1994) and 16SB (CCGGTTTGAACTCAGATC) (Hedin and Maddison 2001). The 28S gene was amplified with 28SO (TCGGAAGGAACCAGCTACTA) and 28SC (GAAACTGCTCAAAGGTAAACGG). For COI and 28S, the polymerase chain reaction (PCR) was performed with an initial denaturation at 94ºC for 2 min, followed by 40 cycles of denaturation at 94 ºC for 25 sec, annealing at 50ºC (first round)/ 44.5ºC (second round) for 25 sec and extension at 65ºC for 2 min (first round)/ 1 min (second round); with a final extension at 72ºC for 10 min. The PCR conditions to amplify 16S-ND1 were: initial denaturation at 94°C for 2 min; followed by 35 cycles of 35 sec at 94°C, annealing at 48 ºC for 35 sec, and extension at at 65ºC for 2 min (first round)/ 1 min (second round); with a final extension at 72ºC for 10 min. Amplified fragments were sequenced in both directions using Sanger sequencing at

GENEWIZ's New Jersey facility. The forward and reverse reads were interpreted with Phred and Phrap (Green 1999; Green and Ewing 2002) via Chromaseq v. 1.31 (Maddison and Maddison 2018a) in Mesquite v. 3.6 (Maddison and Maddison 2018b) using default parameters.

3.1.3 Phylogenetic analyses

Outgroup selection was based on the phylogeny proposed by Zhang and Maddison (2013). As primary outgroups, we included COI sequences for the following taxa: *Ghelna canadience*, *Brythocrotus* (*B. crypticus*, *B. cf. crypticus*), *Compsodecta* (*C. festiva*, *C. haytiensis*, *C. peckhami*), *Agobardus* (*A. gramineus*, *A. anormalis montanus*, *A. brevitarsus*, *A. oviedo*, *A. phylladiphilus*, *A. cordiformis*, *A. bahoruco*), *Cobanus* (*C. extensus*, *C. unicolor, C. mandibularis*), *Sidusa* (*S.* sp. French Guiana1 and *S.* sp. French Guiana2) (Zhang and Maddison 2015). Additionally, COI data for nine ingroup taxa of the *Antillattus* clade (species from *Petemathis*, *Truncattus*, and *Antillattus*) from Zhang and Maddison (2015) were downloaded from GenBank (supplementary table 1).

Alignments were performed in MAFFT (Katoh and Standley 2013) using L-INS-I with a parameter 1PAM / k = 200, a GAPs opening penalty of 1.53, and a configuration of 100. Gaps were treated as missing characters. The dataset was partitioned by gene (in the case of COI by codon), and the appropriate substitution model for each partition was selected with jModeltest 2.1.10 (Darriba *et al.* 2012) using the Akaike information criterion (Posada and Buckley 2004) to select among the 24 models that can be implemented in MrBayes (table 3.0).

Table 3.0 Substitution models selected by jModelTest for each individual gene region and partition.

Partition	Substitution model
16S	TIM3+G (012032)
COI 1st -2nd codons	GTR+I+G (012345)
COI 3rd codon	TVM+I+G (012314)
28S	GTR+G (012345)

The selection of the "correct" optimality criterion is a critical point in any phylogenetic analysis and (Cabra-García and Hormiga 2019; Goicoechea *et al*. 2016; Padial *et al*. 2014; Rindal and Brower 2011). Usually, parsimony, maximum likelihood and Bayesian methods are considered to provide the main types of optimality criteria for phylogenetic inference, and the selection of any of them generates a point of discussion over strengths and weaknesses from philosophical and statistical points of view (Cabra-García and Hormiga 2019; Felsenstein,

2004; Lemey *et al*. 2009; Patané *et al*. 2018; Swofford *et al*. 1996; Wheeler, 2012; Whelan and Morrison 2017; Yang and Rannala 2012; Yang, 2006, 2014). An approach we agree with is focusing on clades that are congruent across methodologies as the strongholds of the phylogeny (Parry *et al*. 2017; Ward *et al*. 2015; Whelan *et al*. 2015).

The morphological dataset and concatenated total evidence dataset were analyzed using parsimony in TNT 1.5 (Goloboff *et al.* 2008a; Goloboff and Catalano 2016). A random Sectorial Searches (RSS) + consensus Sectorial Searches (CSS) + Ratchet (ratchet 40 rounds) + Drift (drift 20 rounds) + Tree Fusing (fuse 20 rounds) with 3000 random addition sequences was conducted under equal weights following with TBR+SPR. The search with implied weights (Goloboff 1993; Goloboff *et al*. 2008b) was run using 10 different values of the concavity constant (k = 3, 5, 7, 9, 11, 17, 27, 37, 47) (Goloboff *et al*. 2008b; Giribet 2003; Goloboff 1993). Finally, group frequencies under jackknifing (JK), symmetrical resampling (SR) (Goloboff *et al*. 2003), and Bremer support (BS) values (Goodman *et al*. 1982; Bremer 1988; Grant and Kluge 2008a; Ramírez 2014) were estimated as support measures.

RAxMLHPC v8.2.12 (Stamatakis 2006, 2014) was used to perform maximum likelihood analysis for the individual and combined gene matrices, each with 500 replicates under the assumptions of the GTRGAMMAI model (raxmlHPC-PTHREADS.exe -T 2 -f a -x 897 -m GTRGAMMAI -p 335 -N 500 -o Ghelna_canadensis -s MLDNA.phy -n MLDNA.tre -O -w). Bootstrap analyses were also carried out to calculate the replicability of the clades in a separate execution of RAxML with 1000 replicates. ML total evidence was conducted in IQ-TREE v.2.0 (Nguyen *et al*. 2015). ModelFinder (Kalyaanamoorthy *et al*. 2017), as implemented in IQ-TREE v.2.0 (Nguyen *et al*. 2015), was used to select the optimal partition scheme and substitution models for the molecular and morphological characters (iqtree -s dataMatrix.nex --runs 100 -m TESTMERGEONLY -spp setsBlock.nex -pre iqtreeAnalysis -nt AUTO).

Finally, we used the CIPRES online portal (Altekar *et al.* 2004; Miller *et al.* 2010) to run a DNA and a combined data (molecular and morphology) Bayesian analysis with MrBayes v. 3.2.6 (Huelsenbeck and Ronquist 2001; Ronquist and Huelsenbeck 2003). For phenotypic characters, the *MKv+Γ* model was used. We ran the Markov chain Monte Carlo (MCMC) with four chains for 25,000,000 generations, sampling every 1000 generations, with a sampling frequency of 100 and a burn-in of 25%. The results were examined in Tracer v.1.6 (Rambaut *et al.* 2014) to verify proper mixing of chains, that stationarity had been reached, and to determine adequate burn-in. All resulting trees were interpreted in FIGTREE v.1.4.2 and edited in Adobe Illustrator CS6.

3.1.4 Species delimitation

For species delimitation we used a combination of tree-based species delimitation methods, genetic distances, and morphology. For delimitation using morphology, a traditional morphological survey was conducted based on somatic and sexual characters of adult specimens. Additionally, subtle and quantitative differences were considered when they could be matched in at least three specimens of each morph and no overlap in variation was found.

The General Mixed Yule-Coalescent model (GMYC) with single and multiple thresholds (Pons *et al.* 2006; Fujisawa and Barraclough 2013) was applied to our calibrated ultrametric tree in R 3.0.2 (R_Core_Team 2014) with the Splits package (http://splits.r-forge.r-project.org/) (Ezard *et al.* 2009). Phylogenetic analyses were run in BEAST v. 1.8.4 under a lognormal relaxed clock model (Drummond *et al.* 2012) with a COI substitution rate parameter (ucld.mean) as a normal prior (mean=0.0112 and s.d.=0.001) (Bidegaray-Batista and Arnedo 2011). The analysis ran for 25,000,000 generations using a birth-death speciation model with best fit substitution models and default options for all other settings. The results were examined in Tracer 1.6 (Rambaut *et al.* 2014) to determine burn-in and to check for stationarity. Logcombiner 1.8.4 (BEAST package) was used to merge the tree files of the replicates of each scheme. Finally, LogCombiner v. 1.8.4 (BEAST package) was used to build maximum clade credibility trees after discarding the first 25% of trees. The consensus tree was produced in TreeAnnotator v1.8.4 (BEASTpackage).

The Bayesian implementation of the Poisson tree processes model (bPTP) (Zhang *et al*. 2013) was run on the RAxML gene trees. The analysis was run as a rooted tree with outgroups removed for 100,000 generations with 10% burn-in. The Hard-Gap DNA (ABGD) barcode procedure sorted the terminals into hypothetical species with calculated p-values based on the barcode gap. We used MEGA6 (Tamura *et al*. 2013) to calculate genetic distance via the Kimura 2-parameter (K2P) model (Table 2). Finally, we also carried out automatic barcode gap (ABGD) analyses online (http://wwwabi.snv.jussieu.fr/public/abgd/), employing K2P. We analyzed the data using two different values for the Pmin (0.0001 and 0.001), Pmax (0.1 and 0.2), and relative gap width (X = 0.5, 1 or 1.5) parameters with the other parameters set to default values.

3.1.5 Topology tests

Constrained topologies were used to evaluate alternate evolutionary hypotheses. This was done using both likelihood heterogeneity tests (LHT) and Bayes Factors (BF) for ML and BI (Azevedo *et al*. 2018; Kass and Raftery 1995; Huelsenbeck and Bull 1996). The likelihood heterogeneity test (LHT) (Huelsenbeck and Bull 1996) was developed to evaluate the hypothesis that differences in phylogenetic estimates can be explained by stochastic variation. The likelihood heterogeneity test compares the likelihood L_1 obtained under the constraint that the same phylogeny underlies all of the data sets with the L_0 as the unconstrained hypothesis. The likelihood ratio test statistic is $LHT=2(lnL_1 - InL_0)$, where lnL is the likelihood, and L_0 and L_1 are the hypotheses being compared, calculated as an X^2 distribution with n degrees of freedom. H_0 is accepted if $L_0=L_1$ and rejected if L_0/L_1. The BF is calculated through the equation $BF = 2\ ln\ f(D|H_1) - 2\ ln\ f(D|H_0)$, where $f(D|H)$ is the marginal model likelihood, D is the data and H_0 and H_1 are the hypotheses being compared (in this case, the unconstrained and constrained topology, respectively). In the standard test, we calculated the marginal likelihood of H_0 by using an unconstrained analysis with an uninformative prior across topology space, whereas the marginal likelihood of H_1 was calculated from an absolute monophyly constraint on *Pensacolatus* as an informed topology prior. Values between 0–2 indicated no evidence of a difference between the two hypotheses, 2–6 indicated substantial evidence, 6–10 indicated strong evidence for a difference and >10 indicated decisive evidence for a difference in the likelihood of the topologies (Kass and Raftery 1995). The lower the BF, the lower the support for the unconstrained tree. Marginal likelihoods were estimated through the harmonic means in MrBayes 3.2.7a, and likelihoods were estimated in RAxMLHPC v8.2.12 (Stamatakis 2006, 2014).

Finally, Relative Fit Difference (RFD) (Goloboff and Farris 2001) for parsimony analysis was also implemented. RFD is calculated through the formula $1-(C/F)$, where C is the sum of fits of characters increasing their fit in the constrained hypothesis (contradicting the most parsimonious tree), and F represents the characters that decrease their fits in constraints (favoring the most parsimonious tree). Therefore, the lower the RFD, the lower the support for the most parsimonious (unconstrained) tree in relation to the constrained topology. C and F for each constrained analysis were calculated using TNT.

3.2 Results

3.2.0 Specimen sampling and phylogenetic inference

Molecular Results: Our concatenated matrix contains 3,089 bp (COI: 1,270 bp from 43 terminals, 16S: 641 bp from 43 terminals, 28S: 1,180 bp from 41 terminals) from 54 terminals. The phylogeny is well supported at the species level; however, some deeper nodes are weakly supported (fig. 3.0). Our results indicated that *Pensacolatus* is not monophyletic. We ran an analysis constraining the monophyly of *Pensacolatus* and compared the values (-lnls) of both trees. The results of the hypothesis tests are given in table 3.1. The table shows both the likelihood heterogeneity test (LHT) results and the Bayes factors (BF) calculated from the unconstrained tree (where *Pensacolatus* is not monophyletic) and the constrained topology (where *Pensacolatus* is monophyletic). The results indicate that the constrained tree and the unconstrained tree are not equiprobable; thus, the monophyly of *Pensacolatus* is rejected. The unconstrained tree supports the monophyly of *Antillattus* and *Bryanattus* (ML, bootstrap > 70%, pp > 0.95).

Morphological phylogeny: The final matrix contained 125 characters (23 uninformative) scored for 68 taxa. We surveyed 18 characters from the female genitalia, 39 from the male genitalia, 3 from the male abdomen, and 65 from other body parts. The equal weights analysis yielded 47 equally parsimonious trees with 377 steps [consistency index (CI) = 37, retention index (RI) = 83]. The strict consensus of these trees recovered the relationships within genera with good resolution and showed a close relationship between *Pensacola* and *Pensacolatus* (BS=3, JK=53, SR=69). The most parsimonious tree obtained for k=17 also recovered the relationships of *Pensacolatus*+*Pensacola* and *Antillattus*+*Bryanattus* and supported the placement of the genera within the Antillattus clade. These genera were strongly supported in both equal weights and implied weights analyses. The trees found under other concavity values and under equal weights are used to discuss the robustness of genera and clades. All genera were strongly supported by the jackknife, resampling analysis, and Bremer support values. The equal weights analysis, the sensitivity to weighting regimes, and support values are summarized in the working hypothesis tree (fig. 3.1, table 3.2 and 3.4).

3.2.1 Combined molecular and morphology results

Our concatenated total evidence matrix contained 3,218 characters and provided support for some nodes that conflicted between our morphological and molecular data. The MP, BI, and ML trees generated were congruent and recovered strong support values for *Petemathis,*

Truncattus, Antillattus, and *Bryanattus* **gen. nov.** Both BI and ML strongly supported the monophyly of the genus *Pensacolatus* (see figure 3.2); and the MP hypothesis in which *Pensacolatus* is constrained to be monophyletic is almost as well-supported as the most parsimonious hypothesis (see table 3.5).

Generally, our analyses agree that *Pensacolatus*, containing *P. applanatus, P. darlingtoni*, *P. maxillosa,* and *P. montanus,* is a morphologically coherent group that is sister to *Antillattus*. *Antillattus* contains the type species *A. gracilis* along with *A. cambridgei*, *A. placidus*, and *A. cubensis*. Finally, the genus *Bryanattus* **gen. nov.** includes the type species *B. keyserlingi*, in addition to *B. mandibularis* and three new species described here.

Three unambiguous synapomorphies supporting *Pensacolatus* are: male legs I with fringes (char. 59[state 1]); male endites with the anterolateral cusp usually developed (char. 70 [state 1], homoplasious); and an inconspicuous retrolateral sperm duct loop (char. 94 [state 1], non-homoplasious). The monophyly of the genus *Bryanattus* is strongly supported by four unambiguous synapomorphies: male pre-spiracular bumps are as wide as ALS (char. 67 [state 1]); female copulatory openings are anteriorly positioned positioned relative to the vulva (char. 115 [state 0]); primary and secondary spermathecae receptacles are absent (char. 118 [state 0]), and the copulatory duct usually connect at an internal position relative to the primary spermathecae (char. 121 [state 0]). Finally, *Antillattus* is supported by the followed unambiguous synapomorphies: fused male promarginal teeth (char. 29[state 0]); male paturons with differently sized retromarginal teeth (char. 41[state 2]; char. 43[state 0]); male paturons that are longer than clypeus width (char. 46[state 2], homoplasious), and project forwards (char. 47[state 2]); male paturons with a posteromesal mastidion (char. 51[state 2], non-homoplasious); fang bases longer than fang shafts (char. 56[state 2], homoplasious); pre-spiracular hair tufts are present (char. 68[state 1]); curved palpal femur (char. 74[state 2]); embolus path that are close to the tegulum (char. 100[state 2]), with embolus as long as the embolic disc (char. 103[state 0]); and females with the epigynal window occupying more than half of the epigynal plate (char. 109[state 2]). The unambiguous synapomorphies are presented in table 3.3. The ACCTRAN and DELTRAN optimizations are shown in table 3.3.

3.2.2 *Antillattus*, *Pensacolatus*, and *Bryanattus* species delimitation

DNA: Bayesian inference based on GMYC delimited between 17 and 20 lineages as putative species. Based on the concatenated molecular tree in bPTP, *Bryanattus thanos* **sp. nov.** and *Bryanattus keyserlingi* were considered the same species. Hard-Gaps and ABGD analyses supported 13 species hypotheses, while the Bayesian tree based on GMYC simple delimitation

supported nine, the Bayesian tree based on GMYC multiple delimitation supported eight, and bPTP for the concatenated molecular dataset supported 11. The morphological delimitation was 100% congruent with the Hard-Gaps and ABGD delimitation, and 86% consistent with bPTP. Interspecific distances for all species were >4 % (fig. 3.3, table 3.6).

Morphology: Nine species and three putative species were identified (figs. 3.3). Key characters that were useful for group delimitation are related to spermatheca shape, copulatory duct position, epigynal window length, male endite shape, mastidion number and position, chelicerae shape, tegular lobe presence, and embolus shape. Continuous or morphometric differences observed were not consistent within populations e.g. the relative size of chelicera.

Table 3.1 Likelihood heterogeneity test (LHT) and Bayes Factors (BF) from tests against the unconstrained topology. Positive values indicate greater support for the hypothesis (constrained topology). For BF, values between 0–2 indicate no evidence of a difference, 2–6 indicate substantial evidence for a difference, 6–10 indicated strong evidence for a difference and >10 indicated decisive evidence for a difference in the likelihood of the topologies (Kass and Raftery, 1995). Asterisks indicate a monophyletic grouping that is not rejected.

	Marg. Log Lik.		**Evidence against constraint**
ML Unconstraint H_0	-26072.460786		
Pensacolatus* Constraint H_1	-26077.942041	10.94*	df=1, P=0.001
BI Unconstraint H_0	-24981.08		
Pensacolatus* Constraint H_1	-24988.65	**BF**=15.14*	substantial evidence

Table 3.2 MP (*k=17* and equal weights) morphological synapomorphies and mapping of morphological character changes on the MP-total evidence tree.

DNA+ Morphology	DNA+ Morphology		DNA+ Morphology
	equal weights	*k*=17	MP
Pensacolatus *Antillattus* *Bryanattus*	NON	NON	44-1, 55-1, 71-1, 73-1.
Antillattus *Bryanattus*	5-0, 18-1, 19-1, 20-1, 33-1, 34-1, 39-1, 44-1, 45-2, 48-1, 55-1, 66-1, 71-1, 73-1,	20-1, 44-1, 45-2, 48-1, 66-1, 55-1, 71-1, 73-1	5-0, 18-1, 19-1, 20-1, 33-1, 34-1, 45-2, 66-1

Antillattus	41-2, 46-2, 47-2, 51-1, 56-2, 68-1, 74-2, 100-0, 103-0, 109-2	46-2, 47-2, 51-1, 56-2, 68-1, 74-2, 100-0, 103-0, 109-2	29-0, 41-2, 43-0, 46-2, 47-2, 51-1, 56-2, 68-1, 74-2, 100-0, 103-0, 109-2
Bryanattus	29-1, 43-1, 50-1, 93-2, 115-0, 118-0	29-1, 43-1, 50-1, 93-2, 115-0, 118-0	67-1, 115-0, 118-0, 121-0
Pensacolatus	29-1, 43-1, 55-1, 94-0	29-1, 43-1, 55-1, 94-0	59-1, 70-1, 94-0

Table 3.3 MP total evidence morphological synapomorphies under ACCTRAN and DELTRAN optimization.

	ACCTRAN	***DELTRAN***
Antillattus clade	21-1, 40-1, 69-1, 74-1, 86-1, 93-0, 100-1, 119-1	100-1
Antillattus	29-0, 41-2, 43-0, 46-2, 47-2, 51-1, 56-2, 68-1, 74-2, 100-0, 101-0, 103-0, 109-2	41-2, 46-2, 47-2, 51-1, 56-2, 68-1, 74-2, 100-0, 101-0, 109-2
Bryanattus	67-1, 93-2, 115-0, 118-0, 121-0	29-1, 43-1, 50-1, 67-1, 93-2, 115-0, 118-0, 121-0
Pensacolatus	17-0, 21-0, 32-0, 39-0, 59-1, 70-1, 94-0, 120-1	29-1, 42-1, 59-1, 70-1, 86-1, 93-0, 94-0

Table 3.4 Summary statistics from the equal weights and implied weighting analyses. k: concavity constant, N: number of most parsimonious trees, L: tree length, CI: consistency index, RI: retention index.

	tree	**steps**	**CI**	**RI**
equal weights	47	377	0.37	0.83
k=3	1	382	0.37	0.83
k=5	1	380	0.37	0.83
k=7	1	380	0.37	0.83
k=9	1	378	0.37	0.83
k=11	1	378	0.37	0.83
k=15	1	378	0.37	0.83
k=17	1	377	0.37	0.83
k=25	1	377	0.37	0.83
k=100	1	377	0.37	0.83

Table 3.5 Relative fit difference (RFD) of alternative phylogenetic hypotheses found using constrained searches. C = sum of fit of characters contradicting most parsimonious tree, F = sum of fit of characters favoring most parsimonious tree.

Constrained	Fit	C	F	C/F	RFD
Pensacolatus	50, 156462	73, 21898	74, 12924	0.987720	0,0122793
Unconstrained	50, 110949	-	-	-	-

Table 3.6 Genetic distances (Kimura 2-parameter) within and between the molecular operational taxonomic units (MOTUs) which were identified by molecular species delimitation methods. (1) *Pensacolatus darlingtoni*, (2) *Pensacolatus maxillosus*, (3) *Pensacolatus applanatus*, (4) *Bryanattus sanchezi* **sp. nov.**, (5) *Bryanattus orientalis* **sp. nov.**, (6) *Bryanattus* sp. [Cuba1], (7) *Bryanattus thanos* **sp. nov.**, (8) *Bryanattus keyserlingi*, (9) *Antillattus cubensis*, (10) *Antillattus gracilis*, (11) *Antillattus placidus*, (12) *Antillattus ocultus* **sp. nov.**, (13) *Antillattus cambridgei*

MOTUs	1	2	3	4	5	6	7	8	9	10	11	12	13
1	0.005	0.103	0.094	0.115	0.115	0.115	0.103	0.106	0.124	0.112	0.106	0.118	0.121
2		0.015	0.103	0.112	0.115	0.112	0.100	0.115	0.131	0.118	0.124	0.109	0.106
3			0.00	0.100	0.097	0.100	0.100	0.112	0.106	0.094	0.112	0.106	0.110
4				0.003	0.075	0.068	0.079	0.068	0.137	0.141	0.147	0.134	0.140
5					0.001	0.061	0.064	0.061	0.131	0.118	0.131	0.109	0.128
6						0.003	0.068	0.065	0.140	0.131	0.150	0.124	0.127
7							0.003	0.053	0.128	0.112	0.124	0.109	0.118
8								0.025	0.141	0.141	0.144	0.121	0.133
9									0.005	0.097	0.044	0.053	0.097
10										0.003	0.076	0.079	0.088
11											0.003	0.047	0.106
12												0.003	0.091
13													0.016

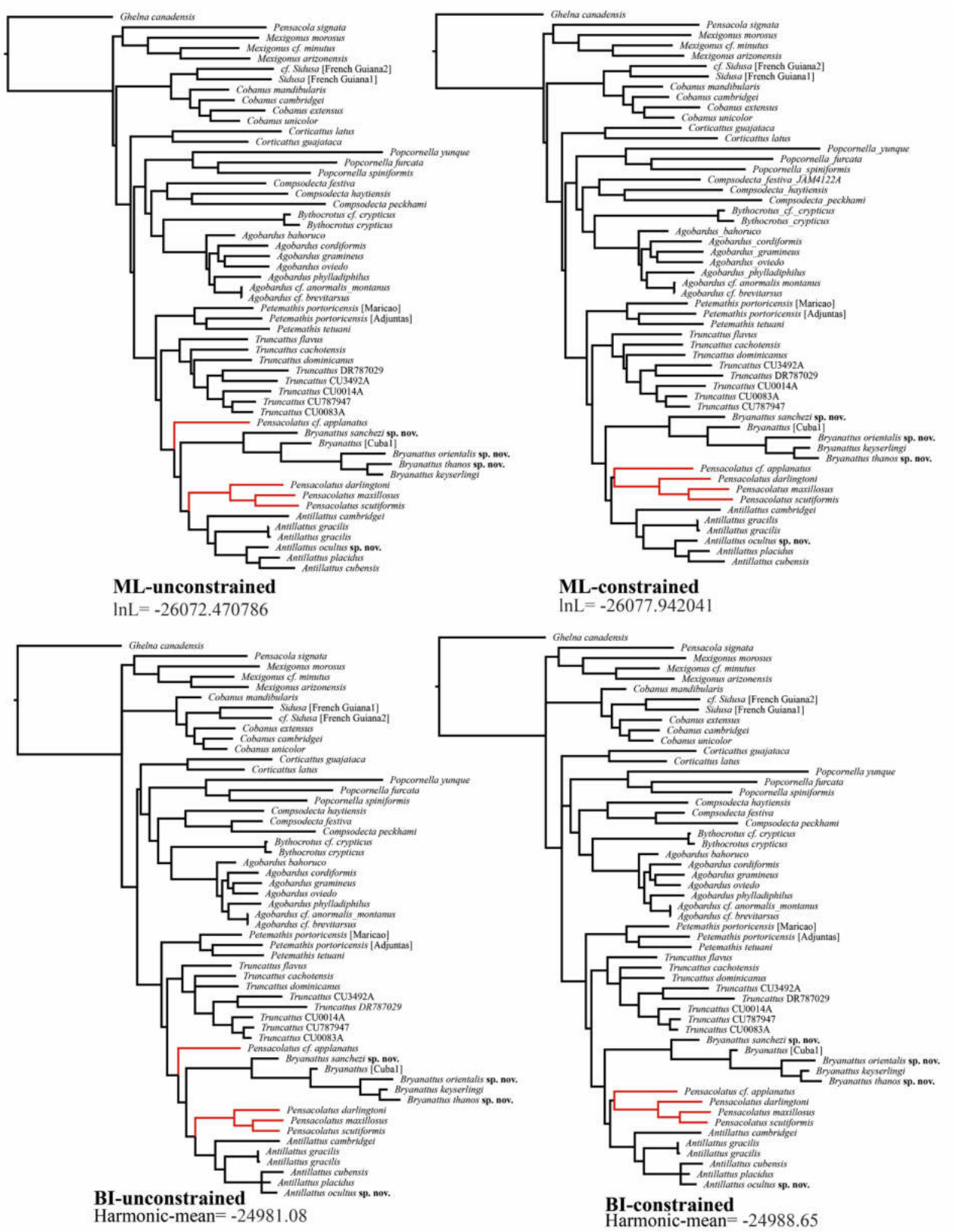

Figure 3.0. Both ML and BI constrained and unconstrained analyses of molecular data (COI, 16S, 28S).

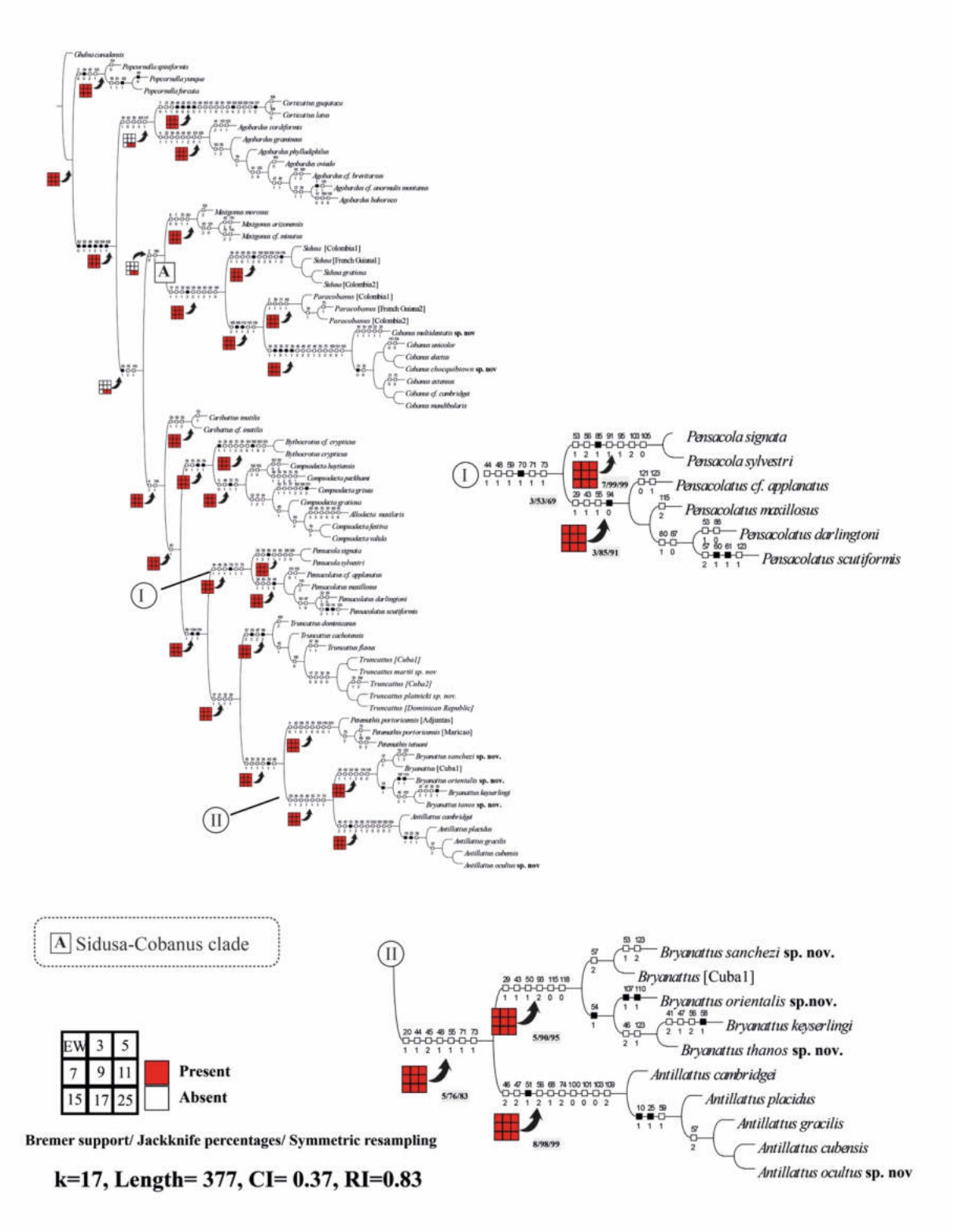

Figure 3.1. Topology obtained under k =17. Filled (presence) and open (absence) squares represent the clade under equal weights and different implied weighting schemes. Numbers are Goodman-Bremer support, Jackknife percentages, and symmetric resampling values.

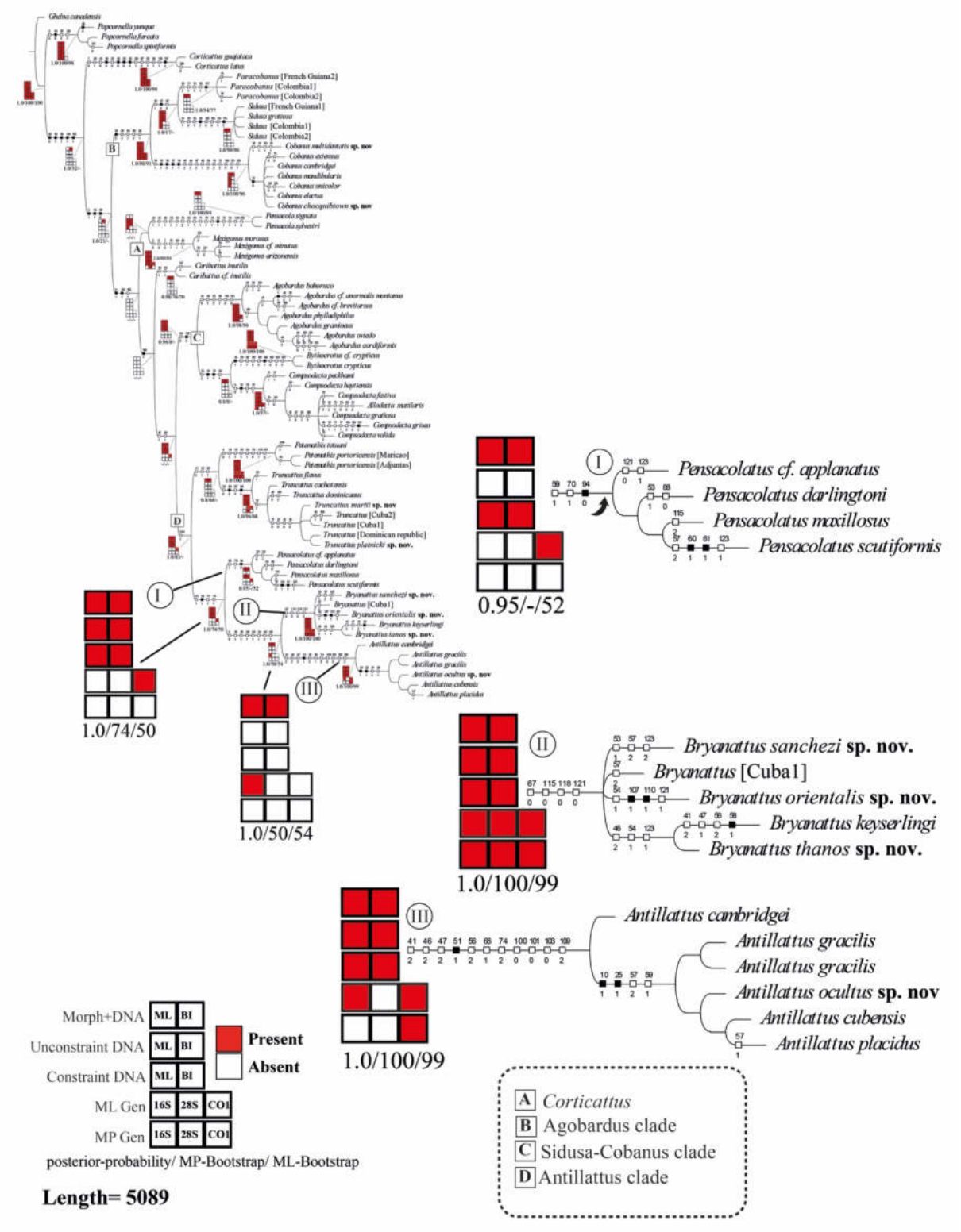

Figure 3.2. Summary of MP total evidence analysis of all genes combined (COI, 16S, 28S), morphology, BI total evidence, and ML total evidence.

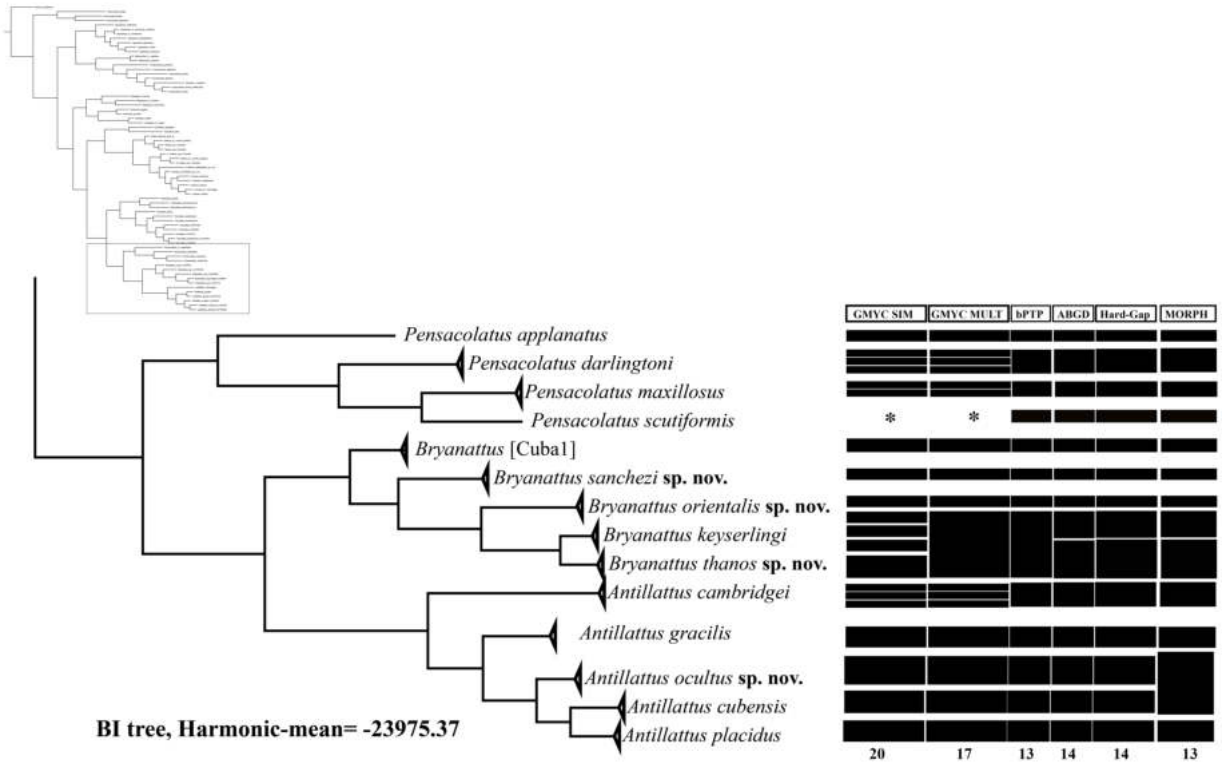

Figure 3.3. Concatenated COI and morphological species delimitation of *Antillattus*, *Pensacolatus*, and *Bryanattus*. The tree fragment corresponds to the BI tree. 1-2: Generalized Mixed Yule Coalescent (GMYC) analyses of Yule, simple (1) and multiple (2), for all genes combined. 3: Poisson Tree Process (bPTP) highest supported solution for combined genes. 4: Automatic Barcode Gap Discovery (ABGD) consistently recovered groupings for the COI gene. 5: Hard-Gap barcoding for the COI gene. 6: Morphology-based delimitation.

3.3 Discussion

3.3.0 Phylogenetic inference

In the past few years, the phylogeny and taxonomy of Caribbean euophryines has received renewed attention (Zhang and Maddison 2012, 2013, 2015). Nevertheless, these questions are far from being resolved (Alayón 2000). The present study was designed to test the monophyly of the genus *Antillattus* sensu Zhang and Maddison (2015). As expected, the inclusion of Cuban species improved the phylogenetic resolution of our analyses, and the total evidence analyses provided robust results. Additionally, our data yielded new results for the structure of the genus *Antillattus* sensu Zhang and Maddison (2015). The new evidence indicates that *Antillattus* (see Zhang and Maddison 2015), as currently described, is comprised

of three separate monophyletic groups (fig 3.2). Using morphological and molecular evidence together, we propose three genera and discuss their relationships to one another below.

Antillattus applanatus, *A. darlingtoni*, *A. maxillosus*, and *A. montanus* form a morphologically coherent clade that we consider as *Pensacolatus*. The type species of *Antillattus—A. gracilis*—forms a clade with *A. cambridgei*, *A. placidus*, and *A. cubensis*. A third morphologically coherent clade is formed by *A. keyserlingi*, *A. mandibularis*, and three new species and are here placed in the new genus *Bryanattus* **gen. nov.**

Four unambiguous synapomorphies support *Pensacolatus* (*Antillattus*+*Bryanattus*) (fig. 3.2, table 3.2): male paturons with sexually dimorphic and rugose mesal cuticles (char. 44 and char. 55); dimorphic endites, with distal ectal projections (char. 71 and 73).

Wunderlich (1988) described *Pensacolatus* based on a Dominican amber fossil (20-15 Mya). According to Wunderlich (1988), *Pensacolatus* is characterized by normal, non-divergent chelicerae, apparently without a mastidion; with endites widened distally and with small cusps; tibia I with 3 pairs of macrosetae; male palps with retrolateral and ventral apophysis; elongated bulbs with tegular lobes; spiraled embolus' with embolic discs; and epigynum with the receptacle in the copulatory duct, in addition to primary and secondary spermathecae (see Wunderlich 1988, 2004). Wunderlich (1988) also mentions the similarity and possible close relation of the fossil species with the species described by Bryant (1943) as *Pensacola* (Peckham and Peckham 1885).

The euophryine phylogeny proposed by Zhang and Maddison (2013, 2015) shows the Pensacola-Mexigonus clade as the sister group of the Antillattus clade. Our morphological data show a close relationship between the genera *Pensacola* and *Pensacolatus* which may suggest a common ancestor. We also find morphological characters to differentiate both genera. *Pensacola signata* differs from other species by the unambiguous character: males with reduced tegulum (char. 104) (fig 2.11, F).

In addition to the morphological similarity between the species proposed by Wunderlich (1988, 2004) and Bryant (1943), molecular dating (Zhang and Maddison 2013) puts the radiation of the Antillattus clade between 25.49-14.79 Mya. This geological range encompasses the proposed age of Dominican amber (see Iturralde-Vinent and MacPhee 1996) and is consistent with the conclusions of Wunderlich.

Our data indicate that seven species currently placed in *Antillattus* belong in *Pensacolatus*. They differ from the type species *Antillattus gracilis* in key characteristics, including the number of retromarginal and promarginal teeth, tegular lobe absence/presence, the shape of the retrolateral sperm duct loop, and the presence of a pre-spiracular bump. The

genus *Pensacolatus* is supported by the number of retromarginal teeth; absence of the pre-spiracular area; and inconspicuous retrolateral sperm ducts. We propose the transfer of *Antillattus darlingtoni, A. electus, A. maxillosus, A. montanus, A. peckhami, A. scutiformis*, and *A. applanatus* to *Pensacolatus*.

The sister relationship between *Bryanattus* **gen. nov.** and *Antillattus* is supported by eight unambiguous synapomorphies (table 3.2). Bryant (1943) described the genus *Antillattus* based on the morphological characters of *A. gracilis* and *A. placidus*. *Antillattus cambridgei* has had a taxonomic history full of erroneous identifications. Bryant (1943), described *Amycus cambridgei* despite its evident dissimilarity with this genus. Galiano (1968) transferred *Amycus cambridgei* to *Cobanus*; however, its placement here was inconclusive. We found that *Cobanus* can be distinguished from *Antillattus* by the presence of a lamella on the embolus (char. 106), legs with different numbers of macrosetae on the metatarsus and tibia (char. 62 to 65), and an epigynum with a pocket (char. 112). Zhang and Maddison (2015) placed *Cobanus cambridgei* in *Antillattus* based on molecular evidence. Here, we found morphological synapomorphies that support the placement of *A. cambridgei* at a basal position within *Antillattus*. The synapomorphies are: males with developed, forward projecting paturons; the presence of a posteromesal mastidion; fangs with longer bases than shafts; a wide pre-spiracular bumb; a curved palpal femur; an absent proximal tegular lobe; the retrolateral sperm duct loop occupying about half of the bulb width; females with retromarginal multicuspid teeth; the window of the epigynum occupying about half of plate; and copulatory duct receptacles developed distal to primary spermathecae.

Antillattus cubensis had also been previously placed within the genera *Emathis* and *Agobardus*. Franganillo (1935) described *Emathis cubensis* based on a female and an immature male from Santiago de Cuba. Unfortunately, Franganillo's description of the species is poor. Bryant (1943) considered the genera *Emathis* and *Commoris* as junior synonyms of *Agobardus* and transferred *Emathis cubensis* to *Agobardus*. In the same work, Bryant (1943) redescribed *Agobardus cubensis* and mentioned that this species may not belong in this genus but made no taxonomic changes. Zhang and Maddison (2015) transferred *Agobardus cubensis* to *Antillattus*. Our molecular and morphological results also support the inclusion of *Antillattus cubensis* within *Antillattus*.

Antillattus can be clearly differentiated from *Pensacolatus* and *Bryanattus* as described above in the diagnoses, and no other proposed species currently seem to belong to this genus. Retromarginal multicuspid teeth, the absence of a tegular lobe, and the shape of the retrolateral sperm duct loop and pre-spiracular bump are some of the characters that differentiate *Antillattus*

from other genera and support it as a genus (fig. 3.2). We propose the following species belong to *Antillattus*: *A. gracilis*, *A. cubensis*, *A. placidus*, and *A. cambridgei*.

Additionally, we propose the new genus *Bryanattus* based on morphology, DNA, and total evidence analyses. Initially, two of the species (*B. keyserlingi* and *B. mandibulatus*) were described as *Agobardus*. The genus *Agobardus* Keyserling (1885) was monotypic when first described as *Agobardus anormalis*. Bryant (1940) noted some characteristics of the genus: high cephalothoraxes; a large paturon that is divergent in some males and vertical in females and small males; retromargins with a divided tooth; long and sinuous fangs; male endites that are often elongated into a lobe on the anterolateral side; enlarged femurs of leg I in males, modified with a ventral spur or carina; and palpuses as long as or longer than the cephalothorax, without a tegular lobe. However, many of these characters are ambiguous and homoplasious. Under the proposed characters and morphological similarity, Bryant (1940) included *A, keyserlingi* and *A. mandibulatus* in *Agobardus*. Zhang and Maddison (2015), based on the illustration and description proposed by Bryant (1940), transferred *A. keyserlingi* and *A. mandibulatus* to *Antillattus*. Our results indicate that *Agobardus keyserlingi* and *Agobardus mandibulatus* belong to the Antillattus clade but in *Bryanattus* **gen. nov.** rather than *Antillattus*. This is supported by our molecular and morphological phylogenies.

As is typical in many euophryines, some characters exhibit wide variation within a genus e.g. small chelicerae in *Agobardus cordiformis* or large divergent chelicerae in *Agobardus anormalis*. *Bryanattus* **gen. nov.** differs in many key characteristics from the type species *Agobardus anormalis*, such as the presence of a pre-spiracular bump (fig. 3.21, D-E); retromarginal multicuspid teeth in both sexes and a promarginal bicuspid tooth in the male (fig. 3.21, B); paturons with concave mesal margins and mesomesal mastidion (fig. 3.21, A); fang bases as long as, or longer than, the fang shaft (fig. 3.21, A); male endites that are often elongated into a lobe lobe anterolaterally; slightly curved femurs of the male palp; emboluses that are coiled into a circle or semi-circle; reduced ducts between the copulatory opening and the secondary spermathecae; and and anteriorly located fertilization ducts.

Additionally, Franganillo (1936) described the species *Emathis unispina* based on a male from Sierra Maestra, Cuba. Bryant (1940) discussed the misidentification and inclusion of some Caribbean species within the genus *Emathis*. Based on strong differences in genital organs, Prószyński and Deeleman-Reinhold (2012) described the genus *Petemathis* to include *Emathis portoricensis*, *E. luteopunctata*, *E. minuta*, *E. tetuani*, and *E. unispina*. However, the transfer of *E. unispina* to *Petemathis* is incorrect. Based on the description by Franganillo (1936), *P. unispina* has all the characters to be considered a member of *Bryanattus*. These

characters are males with large and divergent chelicerae; with two pair of mastidions (one internal and one external); four retromarginal teeth with a common base and females with five retromarginal teeth that have a common base. We also transferred the species *P. unispina* to *Bryanattus*. Below we describe additional species of *Bryanattus* **gen. nov**.

3.3.1 Delimitation

We found consistency results between morphological, hard-gaps, and ABGD delimitation methods. Most distance-based barcoding methodologies have been criticized for the artificiality and doubtful universality of the applied threshold. We avoided such problems in Hard-Gap barcoding by looking for the intra- and inter-specific variability thresholds in our own datasets. Using this method, we obtained robust results with COI because an unambiguous gap was found, allowing us to use single-marker delimitation (table 3.6). The average minimum interspecific distance of congeners was 4.0%. Previous studies of diverse animal groups have reported a minimum interspecific distance for sister species of >2% (Hebert *et al*. 2004a; Hebert *et al*. 2004b; Johns and Avise 1998; Klicka and Zink 1997; Ward *et al*. 2005). In spiders, arbitrary thresholds of 2%-6% have been proposed (Agnarsson *et al*. 2016; Cao *et al*. 2016; Ortiz and Francke 2016). Hard-Gap barcoding recovered all the known species and also some morphologically cryptic lineages. GMYC suggest a higher number of morphologically cryptic lineages, but should not be overinterpreted as evidence for additional species (Fernández and Giribet 2014; Opatova *et al*. 2013; Satler *et al*. 2013). The single locus bPTP approach (Zhang *et al*. 2013) performed well with our dataset in relation to morphology by recovering all but one species. More conservatively, looking at the consistency among all employed methods, they are all congruent in suggesting at least fourteen species (fig 3.4). Thus, our combined molecular and morphological analyses contribute to a growing body of evidence of high diversity in the Caribbean region and indicate evidence of cryptic species.

3.3.2 Taxonomy

Our phylogenetic results show that species of *Antillattus, Bryanattus*, and *Pensacolatus* are monophyletic. Additionally, the genera are strongly supported by morphological and molecular evidence. Based on these results, the following genera and species are proposed:

Antillattus Bryant (1943)

Fig. 3.5-3.10

Antillattus Bryant, 1943: 461, type species: *Antillattus gracilis* Bryant, 1943: p. 461-462, fig. 14, 18, 20. Male holotype (MCZ-IZ 21477), Haití, Dame-Marie, 1941 (between 1 January and 31 December), Col: A. Audant.

Material examined: *Antillattus cambridgei*: (3 males, 3 females, ICN-Ar 12839), Dominican Republic, Santiago Rodriguez prov., Mata Grande, PN Armando Bermúdez, 19.1896893N, -71.0012313W, 7.vii.2012, Col: A. Deler-Hernández. (2 males, 2 females, ICN-Ar 12840), Dominican Republic, Santiago Rodriguez prov., Mata Grande, PN Armando Bermúdez, 19.1896893N, -71.0012313W, 7.vii.2012, Col: A. Deler-Hernández. *Antillattus cubensis*: Cuba, Cienfuegos prov., Soledad, Jardín Botanico, 20.v.2013, Col: Cala-Riquelme, F; Deler-Hernández, A; Andersson, R (4 males, 3 females, ICN-Ar 12834). (4 males, 4 females, ICN-Ar 12835), Cuba, Holguin Prov., Moa, National Park Humboldt, Sector La Melba, La Melba, 20.549898N, -74.838108W, 1.xi.1997, Col: A. Sánchez. (2 males, 3 females, ICN-Ar 12836), Cuba, Granma Prov., Bartolome Masó, National Park Pico Turquino, La Platica, 20.0129376N, -76.8901133W, 29.ix.2014, beating vegetation in rainforest Col: F. Cala-Riquelme. (3 males, 3 females, ICN-Ar 12837), Cuba, Cienfuegos Prov., Soledad, Jardín Botánico de Cienfuegos, 22.1273241N, -80.3306984W, 20.v.2013, Col: F. Cala-Riquelme, A. Deler-Hernández. (3 males, 3 females, ICN-Ar 12838) Cuba, Guantánamo Prov., Baracoa, Ecological Reserve "Yunque-Quibijan-Duaba", Turey, Las Delicias, 20.332078N, - 74.568672W, 6.iv.2012, Col: F. Cala-Riquelme, A. Deler-Hernández. *Antillattus gracilis*: (1 male, 1 female, MNHNSD-09794) Republica Dominicana, Loma del Pichon, 27-30.vi.1998. *Antillattus placidus*: (1 male, MCZ-IZ 22690) Haití, Ennery, 19.483333N, -72.483333W, 7.viii.1934, wild caught, Col: Philip J. Darlington, Jr. (1 male, USNM-ENT 00784586), Dominican Republic, La Vega prov., Constanza, Cachote, 18.984742N, -70.727953W, 7.vii.2012, Col: CarBIO Team.

Composition: We include the following species in *Antillattus*: *Antillattus gracilis* Bryant; *Antillattus cambridgei* (Bryant); *Antillattus cubensis* (Franganillo); and *Antillattus placidus* Bryant.

Diagnosis: The genus *Antillattus* resembles *Truncattus*, *Petemathis, Pensacolatus*, and *Bryanattus* by the males having a developed distal hematodochae, and the presence of the sperm duct loop on the retrolateral side of the bulb (figs 2.11, A-I; 3.5, F-G; 3.8, C; 3.9, C; 3.10, D; 3.12, C; 3.14, C; 3.16, C; 3.18, B-C; 3.19 D-E; 3.20, E; 3.26, B; 3.28, C; 3.29, D; 3.30, E). Additionally, *Antillattus* shares several characteristics with *Pensacolatus* and *Bryanattus*, including: male paturons with differences between the mesal cuticle and the rest of the paturon

cuticle (figs. 3.12, A; 3.14, A; 3.21, A; 3.22, F; 3.26, A); sexually dimorphic paturons; sexually dimorphic endites that are expanded laterally (fig. 3.6, C; 3.9, D; 3.10, C; 3.12, A; 3.16, B; 3.21, C); and palps with patella that are shorter than or equal to the tibia (fig. 2.9, E-F; 2.10, D, F; 3.11, G; 3.12, C; 3.15, F; 3.16, D; 3.17, C); however, *Antillattus* can be differentiated from congeners by the male paturon projecting forwards, with a posteromesal mastidion (figs. 3.5, A-B, E; 3.8, A; 3.9, A; 3.10, A); fang bases that are longer than the shaft (with the exception of *Bryanattus keyserlingi* and *B. mandibularis*) (fig. 3.6, B; 3.8, D; 3.10, B); post-epigastrium with pre-spiracular hair tufts; palps with curved femurs (fig. 3.6, E); embolus as long as the embolic disc (fig. 3.6, G; 3.8, C; 3.9, C; 3.10, D); and epigynum windows occupying much more than half of the epigynal plate (fig. 3.6, I; 3.7, C). *Antillattus* can be differentiated from *Pensacolatus* by males having retromarginal teeth II, III, and IV present (fig. 3.5, C, E; 3.6, A-B; 3.8, D; 3.10, B); retromarginal teeth being fused to each other (fig. 3.5, C, E; 3.6, A-B; 3.8, D; 3.10, B); and the absence of anterolateral cusps on their endites (fig. 3.6, C; 3.9, D; 3.10, C). Finally, *Antillattus* can be differentiated from *Bryanattus* by male post-epigastrium having a pre-spiracular bump 2x wider than one of the ALS; epigynum with the copulatory opening located mesoposteriorly relative to the vulva (fig. 3.6, I; 3.7, A-C; 3.8, E-F; 3.9, E-F; 3.10, E); and copulatory ducts with a receptacle in addition to the primary and secondary spermathecae (fig. 3.5, H-I; 3.7 A-C; 3.8, E-F).

Description: Small spiders ranging from 4.0 to 4.8 mm in length. Sexually dimorphic in chelicerae size, and endite shape. The carapace in males is approximately as long as the abdomen; usually dark, with a lighter dorsal area, and white scales at front and lateral edges of carapace. The anterior row of eyes is wider than the others in both sexes; the second row is midway between ALE and PLE; the OQ is approximately 48-55% of carapace length. The clypeus is lower than AME radius. Chelicerae in both sexes with three promarginal teeth (with the exception of *A. cambridgei*), and the retromargin with a multicuspid. The male chelicerae are longer than the clypeus width, and projects forwards. Aditonally, males have a posteromesal mastidion and fang bases that are longer than shafts. Endites are sexually dimorphic and in males project to the prolaterodistal side. Labium are subtriangular, shorter than endites, with two laterobasal concavities. The abdomen is longer than it is wide, pale gray to yellow with black and/or dark reddish pattern and spots. Leg spination has the following pattern: (from *Antillattus gracilis*) male, I– femur rd1, d1-1-1, drd1, dd1, patella p1, tibia p1-1-0, r0-0-1, v2-2-2, metatarsus p1-1, r1-1, v2-2; II– femur r1, rd1, d1-1-1, drd1, dd1, patella p1, r1, tibia p1-1-0, r1-1-0, v2-2-2, metatarsus p1-1, r1-1, v2-2; III– femur rd1, d1-1-1, drd1, dd1, patella p1, r1, tibia p1-1-1, d1-0-0, r1-1-1, v1-0-2, metatarsus p1-1, d2-2, r1-1, v2-2; IV– femur rd1, d1-1-1,

drd1, dd1, patella p1, r1, tibia p1-1-0, d1-0-0, r1-1-0, v1-0-2, metatarsus p1-1, d2-2, r1-1, v2-2; female, I– femur rd1, d1-1-1, drd1, dd1, patella p1, tibia p1-1-0, r0-0-1, v2-2-2, metatarsus p1-1, r1-1, v2-2; II– femur r1, rd1, d1-1-1, drd1, dd1, patella p1, tibia p1-1-0, r1-1-0, v2-2-2, metatarsus p1-1, r1-1, v2-2; III– femur rd1, d1-1-1, drd1, dd1, patella p1, tibia p1-1-1, d1-0-0, r1-1-1, v1-0-2, metatarsus p1-1, d2-2, r1-1, v2-2; IV– femur rd1, d1-1-1, drd1, dd1, patella p1, r1, tibia p1-1-0, d1-0-0, r1-1-0, v1-0-2, metatarsus p1-1, d2-2, r1-1, v2-2. The male palp, with the femur curved, usually as long as the patella+tibia. Tibia have finger-like RTA, and spermophorae have a rSDL. The tegulum has a dTL and not a pTL, and the ED is both parallel to the bulb and as long as its width. The WE occupy more than half of the epigynal plate. The CO has a reduced spiral guide, and is followed by a short stretch of CD1. The CD2 has a receptacle in addition to the PS and small SS, and is as wide as the PS. The PS are spherical and near one another. The FD is relatively close to the CD, and BG is depressed or superficial.

Antillattus ocultus **sp. nov.**

Figs. 3.10A-E

Type material: Male holotype (ICN-Ar 12841), CUBA, Pinar del Rio prov., National Park Maravillas de Viñales, 22.65364N, - 83.69967W, 19-21.iv.2012, Col: CarBIO Team, beating vegetation in tropical forest. Paratype (ICN-Ar 12841), 4 females, 13 males, same data as holotype.

Diagnosis: Males of *Antillattus ocultus* **sp. nov.** can be separated from other *Antillattus* species (except *A. cubensis*) by the sub-square and slightly divergent shape of the chelicerae (Fig. 3.10, A-B), and by the shape of the embolic disc (Fig. 3.10, D). *Antillattus ocultus* **sp. nov.** can be differentiated from all other *Antillattus*, including *A. cubensis*, by the following unique mtDNA nucleotide substitutions of the standard DNA barcode (see, Agnarsson *et al.* 2015): A (50), G (125), G (299), A (440), A (449), G (458), G (572), T (647).

Etymology: The species epithet refers to the absence of morphological characters to differentiate the species from *Antillattus cubensis*.

Description: Male (holotype: ICN-Ar 12841): Carapace, dark yellow to reddish, with white scales and black around the eyes. Chelicerae, endites, labium, and leg I are all reddish to brown. Abdomen gray to yellow, with reddish and dark bands. Total length 5.3. Carapace 2.5 long, 1.8 wide, 1.2 high. Clypeus 0.2 high. Anterior eye row 1.5 wide, posterior eye row 1.4 wide. OQ length 1.3. Chelicerae 1.3, with tricuspid promarginal teeth, and multicuspid retromarginal teeth (from three to five); one mediomesal mastidion. Abdomen, 2.7 long, longer than wide. Leg measurements, I– coxae 0.9, trochanter 0.6, femur 1.8, patella 0.7, tibia 1.4, metatarsus 0.8,

tarsus 0.5; II– 0.6, 0.3, 1.6, 0.7, 1.2, 0.6, 0.5; III–0.6, 0.3, 1.8, 0.8, 1.1, 0.9, 0.5; IV–0.7, 0.4, 1.8, 1.0, 1.2, 1.1, 0.7. Leg spination, I– femur rd1, d1-1-1, drd1, dd1, patella p1, tibia p1-1-1, r1-0-1, v2-2-2, metatarsus p1-1, r1-1, v2-2; II– femur r1, rd1, d1-1-1, drd1, patella p1, r1, tibia p1-1-1, r1-0-1, v2-2-2, metatarsus p1-1, r1-1, v2-2; III– femur rd1, d1-1-1, drd1, dd1, patella p1, r1, tibia p1-1-1, d1-0-0, r1-1-1, v1-0-2, metatarsus p1-1, d2-2, r1-1, v2-2; IV– femur rd1, d1-1-1, drd1, dd1, patella p1, r1, tibia p1-1-0, d1-0-0, r1-1-0, v1-0-2, metatarsus p1-1, d2-2, r1-1, v2-2. Palp (fig. 3.10, D), RTA long and finger-like. Embolus, distally striated, and as long as the ED wide.

Female (Paratype: ICN-Ar 12841): Carapace gray to reddish, with black around eyes. Chelicerae, endites and labium are all yellow. Legs yellow with black spots on tibia, tarsus, and metatarsus of legs III and IV. Abdomen gray, with four black bands of spots. Total length 5.8. Carapace 1.6 long, 1.7 wide, 1.2 high. Clypeus 0.2 high. Anterior eye row 1.5 wide, posterior eye row 1.4 wide. OQ length 1.3. Chelicerae 0.9 long, with three promarginal teeth, and multicuspid retromarginal teeth. Abdomen 3.3 long, longer than wide. Leg measurements, I– coxae 0.6, trochanter 0.4, femur 1.4, patella 0.7, tibia 1.1, metatarsus 0.5, tarsus 0.4; II– 0.5, 0.3, 1.3, 0.7, 0.8, 0.6, 0.3; III–0.5, 0.3, 1.3, 0.6, 0.9, 0.8, 0.4; IV–0.5, 0.3, 1.7, 0.8, 1.3, 0.8, 0.4. Leg spination, I– femur rd1, d1-1-1, drd1, dd1, patella p1, tibia p1-1-1, r1-0-1, v2-2-2, metatarsus p1-1, r1-1, v2-2; II– femur r1, rd1, d1-1-1, drd1, patella p1, r1 tibia p1-1-1, r1-0-1, v2-2-2, metatarsus p1-1, r1-1, v2-2; III– femur rd1, d1-1-1, drd1, dd1, patella p1, r1, tibia p1-1-1, d1-0-0, r1-1-1, v1-0-2, metatarsus p1-1, d2-2, r1-1, v2-2; IV– femur rd1, d1-1-1, drd1, dd1, patella p1, r1, tibia p1-1-0, d1-0-0, r1-1-0, v1-0-2, metatarsus p1-1, d2-2, r1-1, v2-2. Genitalia (Fig. 3.10, E), very similar to other species of the genus; WE occupying more than half of the epigynal plate; CO at median position; CDR in addition to PS and SS as wide as the PS; PS spherical and close to one another; FD relatively close to the CD2; BG depressed or superficial.

Pensacolatus Wunderlich, 1988

Figs. 3.11 - 3.20

Type species: *Pensacolatus coxalis* Wunderlich, 1988

Material examined: *Pensacolatus peckhami* (3 females, MNHNSD09.808) Republica Dominicana, San Juan prov., Valle de Bao, bajada de Pico Duarte, 9.vi.1992, beating rainforest vegetation, Col: K. Guerrero, M. Ivie. *Pensacolatus darlingtoni* (4 males, 2 females, MNHNSD09.1602) Republica Dominicana, La Vega prov., Constanza, La Neverita, PN Valle Nuevo, 18.6969722N, -70.591138W, 17.x.2011, Col: G. de los Santos. *Pensacolatus montanus* (2 males, 4 females, MNHNSD09.1602) Republica Dominicana, San Juan prov., Sabana

Nueva, PN José del Carmen Ramirez, 19.1206828N, -70.6422089W, 17.xi.2011, Col: G. de los Santos, C. Marte, C. Suriel. (1 male, 6 juveniles, MNHNSD09.1598) Republica Dominicana, La Vega prov., Constanza, Sabana Quéliz, PN José del Carmen Ramirez, 18.8070203N, -70.6752405W, 15.i.2011, Col: S. Carrero, G. de los Santos. (1 male, 3 females, MNHNSD09.1604) Republica Dominicana, San Juan prov., Sabana Nueva, PN José del Carmen Ramirez, 19.1206828N, -70.6422089 W, 19.x.2011, Col: G. de los Santos, C. Marte, C. Suriel. (1 male, MNHNSD09.1600) Republica Dominicana, San Juan de la Maguana prov., Sabana vieja, PN José del Carmen Ramirez, 9.i.2011, Col: A. Sánchez, R. Rodriguez. (1 male, 1 juvenil, MNHNSD09.1599) Republica Dominicana, San Juan de la Maguana prov., Sabana vieja, PN José del Carmen Ramirez, 9.i.2011, Col: A. Sánchez, R. Rodriguez. (1 male, 2 females, MNHNSD 09.1603) Republica Dominicana, San Juan de la Maguana prov., Sabana vieja, PN José del Carmen Ramirez, 10.i.2008, Col: G. de los Santos, R. Rodriguez. *Pensacolatus electus* (2 males, MNHNSD 09.1597) Republica Dominicana, La Vega prov., Constanza, La Piramide, PN Valle Nuevo, 18.9063646N, - 70.7444894W, 17.i.2011, Col: S. Carrero, G. de los Santos. *Pensacolatus scutiformis* (1 males MCZ-IZ 21177) Dominican Republic, rainforest near Valle Nuevo, Cord. Cent., 6000 to 6000 ft, 8/1938 (1938-08-01 - 1938-08-31), wild caught, Col: Philip J. Darlington, Jr. (1 female MCZ-IZ 25849) Dominican Republic, Loma Rucilla Mts., Cord. Cent., 1-30.vi.1938, wild caught, Col: Philip J. Darlington, Jr. (1 male, 1 female, MNHNSD 09.1601), La Vega prov., Constanza, La Piramide, PN Valle Nuevo, 18.9063646N, - 70.7444894W, 19.i.2011, Col: S. Carrero, G. de los Santos.

Diagnosis: The genus *Pensacolatus* was originally described based on a Dominican amber fossil. Wunderlich (1988) noted the morphological similarity to species described by Bryant (1943) as *Pensacola*, suggesting that the species described by her could correspond to this same genus. The evolutionary dating of the Antillattus clade (see Zhang and Maddison 2013) is consistent with the age of Dominican amber. Here, we revise the original description, provide illustrations and photos of the species, and conclude that the species described as *Pensacola* by Bryant (1943) correspond to *Pensacolatus.* The males of *Pensacolatus* can be distinguished from *Antillattus* and *Bryanattus* by the chelicerae with one retromarginal tooth (figs. 3.11 B, C, E, F; 3.12A-B; 3.14 B; 3.18 A; 3.20 C), usually as wide as tall; post-epigastrium without a pre-spiracular bump and pre-spiracular hair tufts (figs. 3.11 B; 3.15 B); endite with a anterolateral cusp (figs. 3.11 B, E, F; 3.12 A; 3.14 A; 3.15 B, 3.16 B; 3.18 A); tegulum with a pTL (figs. 3.11 G; 3.12 C; 3.14 C; 3.15 E; 3.16 C; 3.17 C; 3.18 B, D; 3.19 D); and rSDL that occupy less than half of the bulb width, with the loop being inconspicuous (figs. 3.11 G; 3.12 C; 3.14 C; 3.15 E; 3.16 C; 3.17 C; 3.18 B, D; 3.19 D; 3.20 E). The female of *Pensacolatus* resemble

Antillattus by the presence of a CDR in addition to the SS and PS, but can be distinguished by the CDR having developed ventrally to the PS (figs. 3.11 H; 3.12 D; 3.13 A-C; 3.14 D; 3.15 G; 3.16 E; 3.17 D; 3.19 F; 3.20, G). Finally, *Pensacolatus* can be differentiated from *Bryanattus* by the presentse of a CDR (Figs. 3.10 H; 3.11 D; 3.12 D; 3.13 G; 3.14 E; 3.17 F; 3.18 G).

Description: *Pensacolatus* are small spiders ranging from about 4.3 to 6.0 mm in length, and are sexually dimorphic in chelicerae and endite shape. The carapace in males is shorter than the abdomen, and is usually reddish to dark brown with white scales at the front and lateral edges. The anterior row of eyes is wider than the others in both sexes. The second row of eyes is midway between the ALE and PLE, and the OQ is approximately 44-48% of carapace length. The clypeus is lower than the AME radius, and is reddish to dark brown in males. Chelicerae in a bicuspid promarginal tooth in the male and two teeth in the female, and the retromargin with a single tooth in both sexes. Male chelicerae are as long as the clypeus' width, project downwards, and have a concave mesal margin. Aditonally, males have a mediomesal mastidion as well as a medioectal mastidion in some species; and the fang base as long as shaft. Endites are sexually dimorphic and in males are projected on the prolaterodistal side, and have an anterolateral cusp. Labium is subtriangular, shorter than endites, and with two laterobasal concavities. The abdomen is suboval and longer than it is wide, pale gray to black with patterns and spots; ventrally, the post-epigastrium lacks the pre-spiracular bump and pre-spiracular hairs-tufts. Leg spination has the following pattern: (from *Pensacolatus maxillosus*), male, I– femur d1-1-1, drd1, dd1, patella p1, d1, tibia p1-1-1, v2-2-2, metatarsus p1-1, r1-1, v2-2; II– femur r1, rd1, d1-1-1, drd1, d1, patella p1, r1, tibia p1-1-1, v2-2-2, metatarsus p1-1, r1-1, v2-2; III– femur dr1, drd1, d1-1-1, drp1, dp1, patella p1, r1, tibia p1-1-1, d1, r1-1-1, v1-0-2, metatarsus p1-1, d2-2, r1-1, v2-2; IV– femur dr1, drd1, d1-1-1, drp1, dp1, patella p1, r1, tibia p1-1-1, d1, r1-1-1, v1-0-2, metatarsus p1-1, d2-2, r1-1, v2-2; female, I– femur d1-1-1, drd1, dd1, patella p1, d1, tibia p1-1-1, v2-2-2, metatarsus p1-1, r1-1, v2-2; II– femur r1, rd1, d1-1-1, drd1, d1, patella p1, r1; tibia p1-1-1, v2-2-2, metatarsus p1-1, r1-1, v2-2; III– femur dr1, drd1, d1-1-1, drp1, dp1, patella p1, r1, tibia p1-1-1, d1, r1-1-1, v1-0-2, metatarsus p1-1, d2-2, r1-1, v2-2; IV– femur dr1, drd1, d1-1-1, drp1, dp1, patella p1, r1, tibia p1-1-1, d1, r1-1-1, v1-0-2, metatarsus p1-1, d2-2, r1-1, v2-2. The male palp, with the femur straight, is usually as long as patella+tibia. Tibia with a finger-like RTA. The rSDL is inconspicuous, and the tegulum has both a dTL and pTL. The embolic disc is at an acute angle to the longitudinal axis of the bulb and is longer than it is wide. The WE occupy more than half of the epigynal plate. The CO is in a median position relative to the vulva, with a reduced spiral guide, followed by a short stretch of CD1. The CD2 has a receptacle in addition to the PS and small SS, and is as wide as

the PS. The PS are spherical and near one another. The FD is relatively close to the CD2, and BG is depressed or superficial.

Composition: We include the following species in *Pensacolatus*: *Antillattus darlingtoni, A. electus, A. maxillosus, A. montanus, A. peckhami, A. scutiformis*, and *A. applanatus*.

Pensacolatus naranjoi **sp. nov.**

Fig. 3.19A-F

Type material: Male holotype (ICN-Ar 12842), CUBA, Santiago de Cuba, Protected Natural Landscape "Gran Piedra", La Isabelica, 20.005769N, -75.617843W, 27-29.i.2012, beating rainforest vegetation, Col: F. Cala-Riquelme, A. Deler-Hernández. Paratype (ICN-Ar 12842, 1 female) same data as holotype.

Diagnosis: *Pensacolatus naranjoi* **sp. nov.** resembles *P. applanatus* in the posterior placement of the female CO, and the PS being placed outside the WE, but the two can be distinguished by *P. naranjoi* not having a mediomesal mastidion, *P. naranjoi* palps having VTA, and the female CD2 of *P. naranjoi* connecting anteriorly with the PS. *P. naranjoi* **sp. nov.** also resembles *P. maxilosus* and *P. scutiformis* in the male paturons lacking mastidions (fig. 3.19, C), but can be distinguished by *P. naranjoi* having unmodified retromarginal teeth and concave paturons. Finally, *P. naranjoi* **sp. nov.** can be distinguished from other conspecifics by the male paturons that lack a mastidion, the inconspicuous endite cusps, and females having PS developed outside the WE (fig. 3.19, F).

Etymology: The species epithet is a noun in apposition referring to Dr. Carlos Naranjo, professor and investigator of Invertebreate Zoology in the Department of of the Centro Oriental de Ecosistemas y Biodiversidad (BIOECO).

Description: Male (holotype: ICN-Ar 12842): Carapace, reddish to black, white scales at edge of carapace. Chelicerae, endites, labium, and sternum, pale yellow to reddish. Legs I, pale yellow to reddish; legs II to IV, gray to light reddish. Abdomen, ventrally gray to black; dorsally, gray to black. Total length 3.5. Carapace 1.6 long, 1.1 wide, 0.9 high. Clypeus 0.1 high. Anterior eye row 1.1 wide, posterior eye row 1.1 wide. OQ length 0.75. Chelicerae 1.1, with two promarginal teeth and one retromarginal tooth. Abdomen 1.65 long, longer than wide. Leg measurements: I– coxae 0.45, trochanter 0.25, femur 0.95, patella 0.5, tibia 0.8, metatarsus 0.55, tarsus 0.45; II– 0.3, 0.2, 0.65, 0.3, 0.55, 0.4, 0.35; III–0.35, 0.2, 1.0, 0.4, 0.65, 0.7, 0.45; IV–0.45, 0.25, 1.15, 0.5, 0.75, 0.75, 0.5; Leg spination, I– femur drd1, d1-1-1, dpd1, dp1, patella p1, d1, tibia p1-1-1, v2-2-2, metatarsus p1-1, v2-2; II– femur drd1, d1-1-1, dpd1, dp1, patella p1, d1, tibia p1-1-1, v2-2-2, metatarsus p1-1, v2-2; III– femur drd1, d1-1-1, drp1, dp1, patella

p1, r1, tibia r1-1-0, d1-2, p1-0-1, v1-0-2, metatarsus r1-1, d2-2, p1-1, v2-2; IV– femur drd1, d1-1-1, drp1, dp1, patella p1, r1, tibia r0-1-1, d2-2-0, p0-1-1, v1-0-2, metatarsus r1-1, d2-2-2, p1-1, v2-2. Palp (Fig. 3.19, D-E), VTA, present; RTA long, finger-like, straight; pTL, present, inconspicuous, occupying less than of half of bulb width; rSDL occupying less than half of bulb width; embolus as long as embolic disc width.

Female (Paratype: ICN-Ar 12842): Carapace, reddish to black, with white scales at edge of carapace. Chelicerae, endites, labium, and sternum gray to yellow. Legs pale yellow to dark, with black spots. Abdomen, ventrally gray to black; dorsally, gray to black. Total length 3.8. Carapace 1.6 long, 1.1 wide, 0.75 high. Clypeus 0.1 high. Anterior eye row 1.1 wide, posterior eye row 1.05 wide. OQ length 0.8. Chelicerae 0.75 long, with two promarginal teeth and one retromarginal tooth. *Abdomen*, 1.9 long, longer than wide. Leg measurements: I– coxae 0.3, trochanter 0.25, femur 0.75, patella 0.5, tibia 0.65, metatarsus 0.55, tarsus 0.45; II– 0.45, 0.25, 0.75, 0.5, 0.6, 0.45, 0.3; III–0.45, 0.2, 1.0, 0.5, 0.55, 0.6, 0.35; IV–0.5, 0.25, 1.1, 0.5, 0.7, 0.75, 0.5. *Leg spination*, I– femur drd1, d1-1-1, dpd1, dp1, patella p1, d1, tibia p1-1-1, v2-2-2, metatarsus p1-1, v2-2; II– femur drd1, d1-1-1, dpd1, dp1, patella p1, d1; tibia p1-1-1, v2-2-2, metatarsus p1-1, v2-2; III– femur drd1, d1-1-1, drp1, dp1, patella p1, r1, tibia r0-1-1, rd 1-1-0, d1-1-0, pd 1-1-0, p0-1-1, v1-0-2, metatarsus r1-1, d2-2, p1-1, v2-2; IV– femur drd1, d1-1-1, drp1, dp1, patella p1, r1, tibia r0-1-1, rd 1-1-0, d1-1-0, pd 1-1-0, p0-1-1, v1-0-2, metatarsus r1-1, d2-2-2, p1-1, v2-2. Epigynum, (Fig. 3.19, F), WE, occupying half of epigynal plate; CO, external, at middle position relative to spermathecae; CD2, short and curved, developed anteriorly of PS; PS, ovoid, close to one another; FD, distant from the CD2; BG, depressed or superficial.

Pensacolatus surieli **sp. nov.**

Fig. 3.20A-F

Type material: Male holotype (MNHNSD 09.1608), Republica Dominicana, Elias Piña prov., Hondo Valle, El Hoyazo, Sabana del silencio, PN Sierra de Neiba, 18.65229N, -71.56707W, 19-22.vi.2015, beating rainforest vegetation, Col: G. De los Santos, C. Marte, A. Sánchez. Paratype, (MNHNSD 09.1608) 3 females, same data as holotype. (1 male, 4 females, MNHNSD 09.1609).

Other material examined: Republica Dominicana, Elias Piña Prov., Hondo Valle, El Hoyazo, Sabana del silencio, PN Sierra de Neiba, 18.65229N, -71.56707W, 19-22.vi.2015, beating rainforest vegetation, Col: G. De los Santos, C. Marte, A. Sánchez. (1 male, 4 females, MNHNSD 09.1607) Republica Dominicana, Elias Piña Prov., Hondo Valle, El Hoyazo, Sabana

del silencio, PN Sierra de Neiba, 18.65229N, -71.56707W, 19-22.vii.2015, beating rainforest vegetation, Col: G. De los Santos, C. Marte, A. Sánchez.

Diagnosis: The male palps of *Pensacolatus surieli* **sp. nov** resemble those of other *Pensacolatus* species, but can be distinguished from *Pensacolatus darlingtoni, P. montanus, P. peckhami,* and *P. applanatus* by their chelicerae lacking mastidions, and their endites lacking endite cusps. The male palps of *Pensacolatus surieli* **sp. nov** can be distinguished from *P. electus, P. maxillosus, P. scutiformis* by the male promarginal teeth being modified into a large tooth resembling a mastidion, the retromarginal tooth being highly developed and approximately half the length of the promarginal tooth, and a truncated tooth on the fang (fig. 3.20, C). The female epigynum of *Pensacolatus surieli* **sp. nov** resemble the epigynum of *Pensacolatus darlingtoni, P. montanus, P. peckhami, P. maxillosus,* and *P. scutiformis*, but can be distinguished from these species by the retromarginal tooth having a wide base (fig. 3.20, D). The female epigynum of *Pensacolatus surieli* **sp. nov** can also be distinguished from *P. applanatus* by the CDR being as wide as the primary spermathecae, and the CD2 being connected distally with the PS (fig. 3.20).

Etymology: The species epithet is a noun in apposition referring to Carlos Suriel, investigator at the Museo Nacional de Historia Natural de Santo Domingo (MNHNSD).

Description: Male (holotype: MNHNSD 09.1608): Carapace, reddish, with white scales at edge of carapace. Chelicerae, endites, labium, and sternum, reddish to dark. Legs I to II, yellow to reddish; legs III to IV, light yellow. Abdomen, ventrally gray to black; dorsally, gray to black with a light reddish scutum. Total length 5.8. Carapace 2.6 long, 2.0 wide, 1.2 high. Clypeus 0.1 high. Anterior eye row 1.9 wide, posterior eye row 1.8. wide. OQ length 1.45. Chelicerae 1.4, with one big promarginal tooth, one big retromarginal tooth, and fang with a truncated tooth. Abdomen 3.3 long, longer than wide. Legs I with fringes. Leg measurements: I– coxae 1.0, trochanter 0.7, femur 2.4, patella 0.7, tibia 2.1, metatarsus 1.3, tarsus 0.8; II– 0.8, 0.4, 1.6, 1.0, 1.2, 0.9, 0.6; III–0.8, 0.4, 1.9, 1.0, 1.2, 1.0, 0.7; IV–0.8, 0.4, 1.9, 0.85, 1.3, 1.4, 0.7. Leg spination, I– femur d1-1-1, dpd1, dp1, patella p1, d1, tibia p1-1-0, dpv 1, v2-2-2, drv 1, metatarsus p1-1, v2-2; II– femur rd1, drd1, d1-1-1, dpd1, dp1, patella p1, d1, tibia p1-1-0, dpv 1, v2-2-2, drv 1, metatarsus p1-1, v2-2; III– femur rd1, drd1, d1-1-1, drp1, dp1, patella p1, r1, tibia r1-1-1, d1, p1-1-1, v1-0-2, metatarsus r1-1, d2-2, p1-1, v2-2; IV– femur rd1, drd1, d1-1-1, drp1, dp1, patella p1, r1, tibia r1-1-1, d1, p1-1-1, v1-0-2, metatarsus r1-1, d2-2, p1-1, v2-2. Palp (fig. 3.20, E), VTA, absent; RTA long, finger-like, straight; pTL, present, slightly obvious, occupying less half of bulb width; rSDL occupying less than half of bulb width; embolus as long as embolic disc width.

Female (Paratype: MNHNSD 09.1608): Carapace, yellow to dark reddish, with white scales at edge of carapace. Chelicerae, endites, labium, and sternum, yellow to reddish. Legs pale yellow to light reddish. Abdomen, ventrally gray with black spots; dorsally, gray to dark. Total length 6.0. Carapace 2.6 long, 1.8 wide, 1.1 high. Clypeus 0.1 high. Anterior eye row 1.7 wide, posterior eye row 1.65 wide. OQ length 1.35. Chelicerae 0.95 long, with two promarginal teeth, and one retromarginal tooth; retromarginal tooth wide at base. Abdomen, 3.35 long, longer than wide. Legs I without fringes. Leg measurements: I– coxae 0.7, trochanter 0.4, femur 1.55, patella 1.0, tibia 1.1, metatarsus 0.8, tarsus 0.55; II– 0.6, 0.4, 1.3, 0.5, 0.9, 0.45, 0.6; III–0.6, 0.3, 1.6, 0.8, 1.0, 1.1, 0.8; IV–0.8, 0.4, 1.65, 0.8, 1.2, 1.2, 0.8. Leg spination, I– femur d1-1-1, dpd1, dp1, patella p1, d1, tibia p1-1-0, dpv 1, v2-2-2, drv 1, metatarsus p1-1, v2-2; II– femur rd1, drd1, d1-1-1, dpd1, dp1, patella p1, d1, tibia p1-1-0, dpv 1, v2-2-2, drv 1, metatarsus p1-1, v2-2; III– femur rd1, drd1, d1-1-1, drp1, dp1, patella p1, r1, tibia r1-1-1, d1, p1-1-1, v1-0-2, metatarsus r1-1, d2-2, p1-1, v2-2; IV– femur rd1, drd1, d1-1-1, drp1, dp1, patella p1, r1, tibia r1-1-1, d1, p1-1-1, v1-0-2, metatarsus r1-1, d2-2, p1-1, v2-2. Epigynum, (fig.3.20, G-F), WE, occupying more of half of epigynal plate; CO, external, at posterior position in relation to spermathecae; CDR, developed at front of PS; PS, ovoid, close to one another; FD, distant from the CD2; BG, depressed or superficial.

Bryanattus **gen. nov.**

Fig. 3.21 - 3.30

Type species: *Bryanattus keyserlingi* Bryant (1940) (from *Antillattus*, **comb. nov.**)

Diagnosis: The genus *Bryanattus* **gen. nov.** is similar to *Antillattus* and *Pensacolatus*, all of which are restricted to the Caribbean Islands (see Zhang and Maddison 2015). The species of this clade usually have sexually dimorphic male paturons with rugose mesal cuticles (fig. 3.21, A, 3.22, F; 3.23, B). They also typically have sexually dimorphic endites with anterolateral projections, and an embolus that is coiled no more than half of a circle (fig. 3.21, H; 3.23, C; 3.25, F; 3.26, B; 3.28, C; 3.29, D; 3.30, E). Nevertheless, species of the genus *Bryanattus* **gen. nov.** can be differentiated from the genera *Antillattus* and *Pensacolatus* by several characteristics: the male pre-spiracular bumps as wide as one of ALS (fig. 3.21, D); the rSDL occupying more than half of the bulb width (fig. 3.26, B; 3.28, C; 3.29, D; 3.30, E); in females, CO that are in an anterior position relative to the vulva; and lack of a CDR in addition to the PS and SS (fig. 3.26, C, E; 3.28, D-E; 3.29, E; 3.30, F).

Etymology: The generic epithet is a patronym in honour of Dr. Elizabeth Bangs Bryant (April 7, 1875 – January 6, 1953), American arachnologist of the Museum of Comparative Zoology (MCZ). The generic name is from the combination of *Bryan* (referring to Elizabeth Bryant) and *-attus* (a common ending for salticid genera).

Description: Small spiders ranging from about 4.0 to 5.2 mm in length. They display sexual dimorphism in their chelicerae and endites. The carapace in male is approximately as long as abdomen; usually dark yellow to reddish brown, with white scales at front and lateral edges of carapace. The anterior row of eyes is wider than others in both sexes; the second row midway between ALE and PLE; the OQ approximately 58-63% of carapace length. The clypeus, is lower than AME radius, and reddish to dark brown in male, yellow in female. Chelicerae with a bicuspid promarginal tooth in male, and two teeth in female; retromargin with multicuspid teeth in both sexes. The male chelicerae are usually as long as clypeus' width, projected downwards or forming an obtuse angle, and with the mesal margin concave. Aditionally, males have a mediomesal mastidion as well as a posteroectal mastidion in some species, and the fang base as long as shaft or longer than shaft. Endite are sexualle dimorphic and in males are projected prolaterodistally. Labium is subtriangular, shorter than endites, and with two laterobasal concavities. The abdomen is suboval and longer that it is wide, yellow to dark with patterns and spots. Leg spination has the following pattern: (from *Bryanattus keyserlingi*), male, I– femur drd1, d1-1-1, dpd1, dp1, patella p1, d1, tibia r1-0-1, p1-1-1, v2-2-2, metatarsus r1-1, p1-1, v2-2; II– femur drd1, d1-1-1, drp1, dp1, patella r1, p1, tibia r1-1-1, p1-1-1, v2-2-2, metatarsus r1-1, p1-1, v2-2; III– femur drd1, d1-1-1, drp1, dp1, patella p1, r1, tibia r1-1-1, d1, p1-1-1, v2-0-2, metatarsus r1-1, d2-2, p1-1, v2-2; IV– femur drd1, d1-1-1, drp1, dp1, patella p1, r1, tibia r1-1-1, d1, p1-1-1, v2-0-2, metatarsus r1-1, d2-2, p1-1, v2-2; female, I– femur drd1, d1-1-1, dpd1, dp1, patella p1, d1, tibia r1-0-1, p1-1-1, v2-2-2, metatarsus r1-1, p1-1, v2-2; II– femur drd1, d1-1-1, drp1, dp1, patella r1, p1, tibia r1-1-1, p1-1-1, v2-2-2, metatarsus r1-1, p1-1, v2-2; III– femur drd1, d1-1-1, drp1, dp1, patella p1, r1, tibia r1-1-1, d1, p1-1-1, v2-0-2; metatarsus r1-1, d2-2, p1-1, v2-2. IV– femur drd1, d1-1-1, drp1, dp1, patella p1, r1, tibia r1-1-1, d1, p1-1-1, v2-0-2, metatarsus r1-1, d2-2, p1-1, v2-2. The male palp with the femur straight, as long as patella+tibia. Tibia have finger-like RTA, and the rSDL occupying more than half of bulb width. The tegulum have a dTL and not pTL, and the ED is both forms an acute angle to the longitudinal axis of the bulb and longer than ED width. The WE in *Bryanattus* occupies about half of the epigynal plate. The CO is in an anterior position relative to the vulva, and has a reduced spiral guide followed by a short stretch of CD1. The SS are slightly developed, but

lack a CDR in addition to the PS and SS. The PS are spherical. The FD are relatively close to the CD2, and BG are depressed or superficial.

Composition: We include the following species in *Bryanattus*: *Antillattus keyserlingi, A. mandibulatus,* and *Petemathis unispira*.

Bryanattus keyserlingi **comb. nov.** (Bryant, 1940)

Figs 3.26 E – 3.21 A-H

Type material: Male holotype (MCZ-IZ 21748), CUBA, Oriente (historical province), Prov. Guantanamo, Boniato Range, Rio Frio, 20.091111 N -75.856944 W, 5th September 1936, Col: Philip J. Darlington, Jr. **Note**: The locality of the type material is unclear. The Boniato Range and Rio Frio (Sierra de Canasta Range) are geographically distant from each other. The correct location is probably the Boniato Range, Santiago de Cuba.

Other material examined: CUBA: **Santiago de Cuba prov**., Santiago, Paisaje Natural protejido "Gran Piedra", 20.0113204 N, -75.6270849 W, 27-29.i.2012, beating vegetation in rainforest Col: F. Cala-Riquelme (ICN-Ar 12848, 2 males, 5 females). **Granma prov.**, Bartolomé Maso, Parque Nacional Pico Turquino, La Platica, Bosque de Majagua, 20.0129376N, -76.8901133W, 29.ix.2014, beating vegetation in rainforest Col: F. Cala-Riquelme (ICN-Ar 12849, 4 males, 1 female). Bartolomé Maso, Parque Nacional Pico Turquino, La Platica, 20.0129376N, -76.8901133W, 29.ix.2014, beating vegetation in rainforest Col: F. Cala-Riquelme (ICN-Ar 12850, 3 males, 3 females). Bartolomé Maso, Reserva Ecológica Pico Caraca, Alto de Meriño, 19.9690811N, -77.0082209W, 8.iii.2013, beating vegetation in rainforest Col: F. Cala-Riquelme, A. Deler-Hernández (ICN-Ar 12851, 6 males, 5 females). Bartolomé Maso, Reserva Ecológica Pico Caracas, Alto de Meriño, 19.9690811N, -77.0082209W, 5.iii.2013, beating vegetation in rainforest Col: F. Cala-Riquelme, A. Deler-Hernández (ICN-Ar 12852, 1 male). **Camaguey prov.**, Sierra de Cubitas, Reserva Ecológica "Limones Tuabaquey", 21.5892145N, -77.7536364W, 3.iv.2012, beating vegetation in dry forest Col: CarBioTeam (ICN-Ar 12853, 2 males). Sierra de Cubitas, Reserva Ecológica "Limones Tuabaquey", 21.5892145 N, -77.7536364W, 14.iv.2012, beating vegetation in dry forest Col: F. Cala-Riquelme, A. Deler-Hernández (ICN-Ar 12854, 1 male, 1 female). Sierra de Cubitas, Reserva Ecológica "Limones Tuabaquey", 21.5892145N, -77.7536364W, 15.v.2013, beating vegetation in dry forest Col: F. Cala-Riquelme (ICN-Ar 12855, 1 male, 1 female subadult). **Holguín prov.**, Moa, Parque Nacional Humboldt, Sector La Melba, La Melba, 20.549898 N, -74.838108 W, 6.vi.2004, beating vegetation in rainforest Col: J. Delgado (ICN-Ar 12856, 1 male). Moa, Parque Nacional Humboldt, Sector La Melba, La Melba, 20.549898N, -74.838108W, 1.ix.1997, beating

vegetation in rainforest Col: A. Sánchez (ICN-Ar 12857, 1 male). **Guantánamo prov.**, Baracoa, Reserva Ecológica "Yunque-Quibijan-Duaba", subida al Yunque, 20.3485039N, -74.5727877W, 3.iv.2012, beating vegetation in rainforest Col: CarBioTeam (ICN-Ar 12858, 2 males). Baracoa, Reserva Ecológica "Yunque-Quibijan-Duaba", subida al Yunque, 20.3485039N, -74.5727877W, 30.i.2010, beating vegetation in dry forest Col: F. Cala-Riquelme (ICN-Ar 12859, 1 male). Baracoa, Reserva Ecológica "Yunque-Quibijan-Duaba", Turey, Las Delicias, 20.332078N, - 74.568672W, 3.iv.2012, beating vegetation in rainforest Col: F. Cala-Riquelme, A. Deler-Hernández (ICN-Ar 12860, 8 males, 2 females). Baracoa, Parque Nacional Humboldt, Sector Baracoa, Santa María, 20.521130N, -74.702268W, beating vegetation in secondary forest Col: F. Cala-Riquelme (ICN-Ar 12861, 1 male, 1 female).

Diagnosis: Males of *Bryanattus keyserlingi* **comb. nov.** resemble those of *Bryanattus mandibulatus* **comb. nov.** in the 135º angle of chelicerae projection (fig. 3.27, A-B), and the presence of a ventrally developed keel on femur I (fig. 3.22, E; fig. 3.27, B), but can be distinguished by having an ectal mastidion (fig. 3.21, A). The females of *Bryanattus keyserlingi* **comb. nov.** can be distinguished from those of *Bryanattus mandibulatus* **comb. nov.** by the anterior positioning of the CO relative to the WE, the presence of a developed and curved CD2; and the PS being developing inside the WE (fig. 3.26, E). *Bryanattus keyserlingi* **comb. nov.** resemble *Bryanattus thanos* **sp. nov.** and *Bryanattus orientalis* **sp. nov.** in the presence of both ectal and mesal mastidion, but can be distinguished from them by the fang base being longer than the shaft (fig. 3.21, A); and the chelicerae being projected 135º (fig. 3.27, B). The females of *Bryanattus keyserlingi* **comb. nov.** can be distinguished from thpose of *Bryanattus thanos* **sp. nov.** by the development of the SS in an anterodistal position and the WE lacking a "pocket". The females of *Bryanattus keyserlingi* **comb. nov.** can also be distinguished from those of *Bryanattus orientalis* **sp. nov.** by the CD2 connecting anteriorly with the PS. Finally, *Bryanattus keyserlingi* **comb. nov.** can be distinguished from *Bryanattus sanchezi* **sp. nov.** by the presence of mastidion on male chelicera, the chelicerae being projected 135º, fang bases that are longer than the shaft, and the female shape of the epigynum.

Bryanattus mandibulatus **comb. nov.** (Bryant, 1940)

Figs. 3.25A-G, 3.26 A-D

Type material: Male holotype (MCZ: IZ:21974), CUBA, Trinidad Mts., Buenos Aires, 9.v.1936, Col: Philip J. Darlington, Jr. Female, same date as holotype. **Note**: The correct placement of this locality is Cuba, Cienfuegos Prov., Cumanayagua, Buenos Aires, 21.966155N, - 80.131007W.

Other material: CUBA: **Santi spiritus prov.**, Trinidad, PN Topes de Collantes, camino a el salto de Caburní, 21.918120N, -80.01049W, 12.vii.2015, beating vegetation in rainforest Col: F. Cala-Riquelme, A. Deler-Hernández (2 male, 1 female, ICN-Ar 12843). Trinidad, PN Topes de Collantes, camino a el salto de Caburní, 21.918120N, -80.01049W, 11.vii.2015, beating vegetation in rainforest Col: F. Cala-Riquelme, A. Deler-Hernández (1 male, 1 female, ICN-Ar 12843). Trinidad, PN Topes de Collantes, camino a el salto de Caburní, 21.918120N, -80.01049W, 13.vii.2015, beating vegetation in rainforest Col: F. Cala-Riquelme, A. Deler-Hernández (2 males, 3 females, ICN-Ar 12843). **Cienfuego prov.**, Soledad, Jardín Botánico de Cienfuegos, 22.1273241N, -80.3306984W, 20.v.2013, Col: F. Cala-Riquelme, A. Deler-Hernández (1 male, ICN-Ar 12843).

Diagnosis: Males of *Bryanattus mandibulatus* **comb. nov.** can be distinguished from *Bryanattus thanos* **sp. nov.** and *Bryanattus orientalis* **sp. nov.** by their chelicerae lacking ectal mastidion; fang bases that are longer than the shafts; and chelicerae that are projected 135º (fig. 3.25, A-B; 3.26, A). Females of *Bryanattus mandibulatus* **comb. nov.** can be distinguished by those from *Bryanattus thanos* **sp. nov.** and *Bryanattus orientalis* **sp. nov.** by the CO being posterior in relation to de WE; and the SS being positioned mesally (fig. 3.26, C). Males of *Bryanattus mandibulatus* **comb. nov.** can be distinguished from males of *Bryanattus sanchezi* **sp. nov** by their mesal mastidion; fang bases longer than their shafts; and the chelicerae being projected 135º. Finally, females of *Bryanattus mandibulatus* **comb. nov.** resemble the females of *Bryanattus sanchezi* **sp. nov.** in the general configuration of the epigynum (fig. 3.26, C), but can be distinguished by the WE being smaller than the PS, the SS being opposite the CO, and the PS being close to each other (fig. 3.26, C).

Bryanattus orientalis **sp. nov.**

Fig. 3.22, A-F; 3.23; 2.24, E-F; 3.28

Type material: Male holotype (ENT-CU0090A), CUBA, Granma prov., Bartolome Maso, Parque Nacional "Pico Turquino", km10 Pico Joaquin, 20.013022N, -76.833858W, 28.iii.2012, beating vegetation in rainforest Col: F. Cala-Riquelme, A. Deler-Hernández. Paratype (ENT-CU0090A), 1 female, same date as holotype. Granma prov., Bartolome Maso, Parque Nacional "Pico Turquino", La platica, 20.012938N, -76.8901133W, 29.xi.2014, beating vegetation in rainforest Col: F. Cala-Riquelme, A. Deler-Hernández, R. Anderson (ICN-Ar 12862, 2 males, 1 female). Santiago de Cuba, Santiago, Paisaje Natural protejido "Gran Piedra", 20.0113204N,

-75.6270849W, 4-8.v.2012, beating vegetation in rainforest Col: F. Cala-Riquelme, A. Deler-Hernández (ICN-Ar 12863; 1 male, 5 females).

Diagnosis: The males of *Bryanattus orientalis* **sp. nov.** resemble *Bryanattus thanos* **sp. nov.** and *Bryanattus sanchezis* **sp. nov.** by the downward projection of the chelicerae, chelicerae that are smaller than the clypeus, and the fang bases that are as long as the shaft, but can be distinguished from *Bryanattus sanchezis* **sp. nov.** by having the ectal and mesal mastidion (fig. 3.23, A-B); and can be distinguished of *Bryanattus thanos* **sp. nov.** by the presence of a bump in the embolic disc (fig 3.23, C). Females of *Bryanattus orientalis* **sp. nov.** can be distinguished from other *Bryanattus* species including *Bryanattus thanos* **sp. nov.** and *Bryanattus sanchezis* **sp. nov.** by the anteroposterior positioning of the SS, and the CD2 being both straight and connected anteriorly to PS (fig. 3.24, E-F; 3.28, D-E).

Etymology: The species epithet refers to Oriental region of Cuba.

Description: Male (holotype: ENT-CU0090A): Carapace, dark yellow to reddish with white scales and black around the eyes. Chelicerae, endites, and labium yellow to light reddish. Legs gray to yellow, legs I and II darker than others. Abdomen gray to yellow, with two longitudinal black bands. Total length 3.4. Carapace 2.2 long, 1.2 wide, 1.0 high. Clypeus 0.1 high. Anterior eye row 1.2 wide, posterior eye row 1.2 wide. OQ length 1.0. Chelicerae 0.7, with bicuspid promarginal teeth and multicuspid retromarginal teeth; mesal margin concave; male with mediomesal and posteroectal mastidion. Abdomen 1.8 long, longer than wide. Leg, femur I ventral projection, absent. Leg measurements: I– coxae 0.5, trochanter 0.25, femur 1.2, patella 0.6, tibia 0.8, metatarsus 0.6, tarsus 0.5; II– 0.5, 0.3, 1.1, 0.6, 0.8, 0.6, 0.4; III–0.4, 0.2, 1.2, 0.6, 0.9, 0.6, 0.3. IV–0.5, 0.2, 1.2, 0.5, 0.8, 0.8, 0.4; Leg spination, I– femur drd1, d1-1-1, dpd1, dp1, patella p1, d1, tibia r0-0-1, p1-1-0, v2-2-2, metatarsus r1-1, p1-1, v2-2; II– femur drd1, d1-1-1, drp1, dp1, patella r1, p1, tibia r1-1-0, d1-0-0, p1-1-1, v2-2-2, metatarsus r1-1, p1-1, v2-2; III– femur drd1, d1-1-1, drp1, dp1, patella p1, r1, tibia r1-1-1, d1, p1-1-1, v1-0-2, metatarsus r1-1, d2-2, p1-1, v2-2; IV– femur drd1, d1-1-1, drp1, dp1, patella p1, r1, tibia r1-1-0, d1-0-0, p1-1-1, v2-2-2; metatarsus r1-1, d2-2, p1-1, v2-2. Palp (fig. 3.23, C; 3.28, C), RTA long, finger-like; embolus as long as ED is wide; ED ovoid, with a bump.

Female (Paratype: ENT-CU0090A): Carapace gray to pale reddish, black around eyes. Chelicerae, endites, labium, and legs gray to pale yellow. Abdomen gray to pale yellow and reddish with black pattern. Total length 4.5. Carapace 2.3 long, 1.4 wide, 1.2 high. Clypeus 0.2 high. Anterior eye row 1.4 wide, posterior eye row 1.4 wide. OQ length 1.3. Chelicerae 0.9 long, with bicuspid promarginal teeth and multicuspid retromarginal teeth. Abdomen 2.4 long, longer than wide. Leg measurements: I– coxae 0.5, trochanter 0.4, femur 1.2, patella 0.6, tibia

1.0, metatarsus 0.5, tarsus 0.4; II– 0.5, 0.3, 1.2, 0.7, 0.6, 0.5, 0.3; III–0.5, 0.2, 1.5, 0.6, 0.8, 0.8, 0.5; IV–0.6, 0.3, 1.6, 0.7, 0.9, 0.8, 0.5. Leg spination, I– femur drd1, d1-1-1, dpd1, dp1, patella p1, d1, tibia r0-0-1, p1-1-0, v2-2-2, metatarsus r1-1, p1-1, v2-2; II– femur drd1, d1-1-1, drp1, dp1, patella r1, p1, tibia r1-1-0, d1-0-0, p1-1-1, v2-2-2; metatarsus r1-1, p1-1, v2-2; III– femur drd1, d1-1-1, drp1, dp1, patella p1, r1, tibia r1-1-1, d1, p1-1-1, v1-0-2, metatarsus r1-1, d2-2, p1-1, v2-2, IV– femur drd1, d1-1-1, drp1, dp1, patella p1, r1, tibia r1-1-0, d1-0-0, p1-1-1, v2-2-2, metatarsus r1-1, d2-2, p1-1, v2-2. Genitalia (fig. 3.23, D; 3.24, E-F; 3.28, D-E), WE occupying much more than half of the epigynal plate, with a median "pocket"; CO at anterior position; CD2 at anterior position in relation to PS, slightly curved; SS at anteroectal position; PS, spherical and close to one another; FD relatively close to the CD2; BG depressed or superficial.

Bryanattus thanos **sp. nov.**

Fig. 3.24, A-B; 3.29

Type material: Male holotype (ICN-Ar 12864), CUBA, Holguin prov., Moa, Parque Nacional "Humboldt", La Melba, 20.44433N, -74.80699W, 20.vii.2014, beating vegetation in rainforest Col: F. Cala-Riquelme, A. Deler-Hernández, R. Anderson. Paratype (ICN-Ar 12864), 1 female, 2 males, same date as holotype.

Other material examined: **Guantanamo prov.**, Baracoa, PNP "Yara-Majayara", Cueva del Agua, 20.340971N, -74.470463W, 16.vii.2012, beating vegetation in rainforest Col: F. Cala-Riquelme, A. Deler-Hernández, M. Frikaček (ICN-Ar 12865, 3 females). Baracoa, RE "Yunque-Duaba-Quibijan", Subida al Yunque, 20.343796N, -74.574847W, 11.vii.2012, beating vegetation in rainforest Col: F. Cala-Riquelme, A. Deler-Hernández, M. Frikaček (ICN-Ar 12866, 2 females). Baracoa, RE "Yunque-Duaba-Quibijan", Subida al Yunque, 20.343796N, -74.574847W, 2.ii.2012, beating vegetation in rainforest Col: F. Cala-Riquelme, A. Deler-Hernández, R. Anderson (ICN-Ar 12867, 2 females, 3 males). Baracoa, RE "Yunque-Duaba-Quibijan", Las Delicias, 20.3310253N, -74.5651038W, 3.iv.2012, beating vegetation rainforest Col: F. Cala-Riquelme, A. Deler-Hernández (ICN-Ar 12868, 1 female, 1 male). Baracoa, RE "Yunque-Duaba-Quibijan", Subida al Yunque, 20.343796N, -74.574847W, 30.ii.2010, beating vegetation in rainforest Col: F. Cala-Riquelme, A. Deler-Hernández (ICN-Ar 12869, 1 male). **Holguin prov.**, Moa, Parque Nacional "Humboldt", La Melba, 20.44433N, -74.80699W, 20.vii.2014, beating vegetation in rainforest Col: F. Cala-Riquelme, A. Deler-Hernández, R. Anderson (ICN-Ar 12870, 2 males). Moa, Parque Nacional "Humboldt", La Melba, 20.44433N, -74.80699W, 1.ix.1997, beating vegetation in rainforest Col: A. Sanchez

(ICN-Ar 12871, 1 male). Moa, Parque Nacional "Humboldt", La Melba, 20.44433N, -74.80699W, 25.ix.1998, beating vegetation in rainforest Col: R. Teruel (ICN-Ar 12872, 1 male, 1 female). Moa, Parque Nacional "Humboldt", La Melba, 20.44433N, -74.80699W, 24.ix.2014, beating vegetation in rainforest Col: A. Deler (ICN-Ar 12873, 1 male).

Diagnosis: The males of *Bryanattus thanos* **sp. nov.** can be distinguished from *Bryanattus sanchezi* **sp. nov.** by having both an ectal and a mesal mastidion. Females of *B. thanos* **sp. nov.** can be distinguished from other *Bryanattu*s species by their wide, curved CD2 that are connected anterolaterally to the PS.

Etymology: The species epithet refers to Thanos, a fictional supervillain published by Marvel Comics. His name is partly a play on words that refers to the Greek term Θάνατωσ = *Thánatos*, which means death.

Description: Male (holotype: ICN-Ar 12864): Carapace, reddish to brown with black area around the eyes, and lateral white bands at edge of carapace. Chelicerae, endites, labium and sternum reddish. Legs gray to dark reddish, legs I and II darker at coxa, metatarsus and tarsus; femur I with a prolateral dark area. Abdomen gray to yellow, with a dark pattern. Total length 3.5. Carapace 2.0 long, 1.6 wide, 1.4 high. Clypeus 0.1 high. Anterior eye row 1.4 wide, posterior eye row 1.5 wide. OQ length 1.2. Chelicerae 1.05, with bicuspid promarginal teeth and multicuspid retromarginal teeth; mesal margin concave; male with mediomesal and posteroectal mastidion. Abdomen 1.7 long, longer than wide. Leg measurements: I– coxae 0.45, trochanter 0.3, femur 1.05, patella 0.6, tibia 0.85, metatarsus 0.75, tarsus 0.5; II– 0.45, 0.25, 1.0, 0.55, 0.75, 0.6, 0.5; III–0.45, 0.25, 1.25, 0.6, 0.75, 0.6, 0.35; IV–0.45, 0.25, 1.25, 0.5, 0.75, 0.85, 0.5. Leg spination, I– femur drd1, d1-1-1, dpd1, dp1, patella p1, d1, tibia r0-1-1, p1-1-1, v2-2-2, metatarsus r1-1, p1-1, v2-2; II– femur drd1, d1-1-1, drp1, dp1, patella r1, p1, tibia r1-1-0, d1-1-1, p1-1-1, v2-2-2, metatarsus r1-1, p1-1, v2-2; III– femur drd1, d1-1-1, drp1, dp1, patella p1, r1, tibia r1-1-1, d1, p1-1-1, v1-0-2, metatarsus r1-1, d2-2, p1-1, v2-2; IV– femur drd1, d1-1-1, drp1, dp1, patella p1, r1, tibia r1-1-0, d1-0-0, p1-1-1, v2-2-2, metatarsus r1-1, d2-2, p1-1, v2-2. Palp (fig. 3.29 D), RTA long, finger-like, embolus as long as embolic disc is wide; ED ovoid and without a bump.

Female (Paratype: ICN-Ar 12864): Carapace gray to pale reddish, black around eyes. Chelicerae, endites, labium, and legs gray to pale yellow. Abdomen gray to pale yellow with black pattern. Total length 4.2. Carapace 1.9 long, 1.5 wide, 1.2 high. Clypeus 0.1 high. Anterior eye row 1.3 wide, posterior eye row 1.4 wide. OQ length 1.2. Chelicerae 0.8 long, with bicuspid promarginal teeth and multicuspid retromarginal teeth. Abdomen 2.5 long, longer than wide. Leg measurements: I– coxae 0.5, trochanter 0.25, femur 1.0, patella 0.55, tibia 0.6, metatarsus

0.5, tarsus 0.5; II– 0.4, 0.25, 1.0, 0.5, 0.7, 0.45, 0.3; III–0.4, 0.25, 1.25, 0.55, 0.7, 0.75, 0.5; IV– 0.5, 0.25, 1.25, 0.5, 0.75, 0.7, 0.5. Leg spination, I– femur drd1, d1-1-1, dpd1, dp1, patella p1, d1, tibia r1-1-0, p1-1-1, v2-2-2, metatarsus r1-1, p1-1, v2-2; II– femur drd1, d1-1-1, drp1, dp1, patella r1, p1, tibia r1-1-0, d1-0-0, p1-1-1, v2-2-2, metatarsus r1-1, p1-1, v2-2; III– femur drd1, d1-1-1, drp1, dp1, patella p1, r1, tibia r1-1-1, d1, p1-1-1, v1-0-2, metatarsus r1-1, d2-2, p1-1, v2-2; IV– femur drd1, d1-1-1, drp1, dp1, patella p1, r1, tibia r1-1-0, d1-0-0, p1-1-1, v2-2-2, metatarsus r1-1, d2-2, p1-1, v2-2. Genitalia (fig. 3.24, A-B; 3.29 E), WE occupying much more than half of epigynal plate; CO at anterior position; CD2 slightly anterolateromesal to PS, curved; PS, spherical and separated by their diameter; FD relatively close to the CD2; BG depressed or superficial.

Bryanattus sanchezi **sp. nov.**

Fig. 3.24, C-D; 3.30

Type material: Male holotype (ICN-Ar 12847), CUBA, Sancti Spíritus, Trinidad, PN Topes de Collantes, camino a el salto de Caburní, 21.918120N, -80.01049W, 12.vii.2015, beating vegetation in rainforest Col: F. Cala-Riquelme, A. Deler-Hernández. Paratype (ICN-Ar 12847), 1 female, same date as holotype.

Diagnosis: The males of *Bryanattus sanchezi* **sp. nov.** can be distinguished from other members of *Bryanattus* by their chelicerae, which lack both ectal and mesal mastidion (fig. 3.30, C). The females of *Bryanattus sanchezi* **sp. nov.** resemble those of *Bryanattus mandibulatus* **comb. nov.** (see diagnosis of *B. mandibulatus* **comb. nov.**) in their small CD1 and CD2 and their PS outside of the WE. These two species can be distinguished by the SS being directed posteroectally and close to BG, and the PS being separated by their radius (fig. 3.30, F). The females of *Bryanattus sanchezi* **sp. nov.** can also be distinguished from the other females of *Bryanattus* by the same characteristics they share with *Bryanattus mandibulatus* **comb. nov.**.

Etymology: The specific epithet is a patronym in honour of Dr. Alexander Sánchez-Ruiz, one of the most important arachnology research scientists of the Caribbean region.

Description: Male (holotype: ICN-Ar 12847): Carapace, dark yellow to reddish with white scales and black area around the eyes. Chelicerae, endites and labium reddish. Legs I and II yellow to reddish, legs III and IV gray to yellow. Abdomen gray to yellow with two black bands. Total length 3.3. Carapace 1.8 long, 1.2 wide, 1.05 high. Clypeus 0.1 high. Anterior eye row 1.2 wide, posterior eye row 1.2 wide. OQ length 1.1. Chelicerae 0.7, downwards, with bicuspid promarginal teeth and multicuspid retromarginal teeth; mesal margin concave; male with mediomesal and posteroectal mastidion. Abdomen 1.5 long, longer than wide. Leg

measurements, I– coxae 0.3, trochanter 0.2, femur 1.05, patella 0.55, tibia 0.8, metatarsus 0.45, tarsus 0.4; II– 0.3, 0.2, 0.9, 0.45, 0.55, 0.45, 0.35; III–0.3, 0.25, 1.1, 0.55, 0.6, 0.6, 0.4; IV–0.35, 0.2, 1.05, 0.35, 0.6, 0.6, 0.4. Leg spination, I– femur drd1, d1-1-1, dpd1, dp1, patella p1, d1, tibia r1-1-0, p1-1-1, v2-2-2, metatarsus r1-1, p1-1, v2-2; II– femur drd1, d1-1-1, drp1, dp1, patella r1, p1, tibia r1-1-0, p1-1-1, v2-2-2, metatarsus r1-1, p1-1, v2-2; III– femur drd1, d1-1-1, drp1, dp1, patella p1, r1, tibia r1-1-1, d1-0-0, p1-1-1, v1-0-2, metatarsus r1-1, d2-2, p1-1, v2-2; IV– femur drd1, d1-1-1, drp1, dp1, patella p1, r1, tibia r0-1-1, dr1-1-0, dp1-1-0, p0-1-1, v0-0-2, metatarsus r1-1, d2-2, p1-1, v2-2. Palp (fig. 3.30, E), RTA long, finger-like; embolus as long as ED width; ED ovoid, without a bump.

Female (Paratype: ICN-Ar 12847): Carapace gray to pale reddish, black around eyes. Chelicerae, endites, labium, and legs gray to yellow. Abdomen gray to pale yellow with black pattern. Total length 3.6. Carapace 1.7 long, 1.4 wide, 1.1 high. Clypeus 0.1 high. Anterior eye row 1.3 wide, posterior eye row 1.3 wide. OQ length 1.0. Chelicerae 0.6 long, with bicuspid promarginal teeth, and multicuspid retromarginal teeth. Abdomen 1.9 long, longer than wide. Leg measurements, I– coxae 0.35, trochanter 0.2, femur 1.0, patella 0.55, tibia 0.65, metatarsus 0.6, tarsus 0.4; II– 0.35, 0.25, 0.85, 0.55, 0.6, 0.55, 0.35; III–0.4, 0.25, 1.1, 0.45, 0.7, 0.8, 0.45; IV–0.5, 0.2, 1.2, 0.5, 0.8, 0.75, 0.45. Leg spination, I– femur drd1, d1-1-1, dpd1, dp1, patella p1, d1, tibia r0-0-1, p1-1-1, v2-2-2, metatarsus r1-1, p1-1, v2-2; II– femur drd1, d1-1-1, drp1, dp1, patella r1, p1, tibia r1-1-0, p1-1-1, v2-2-2, metatarsus r1-1, p1-1, v2-2; III– femur drd1, d1-1-1, drp1, dp1, patella p1, r1, tibia r1-1-1, d1, p1-1-1, v1-0-2, metatarsus r1-1, d2-2, p1-1, v2-2; IV– femur drd1, d1-1-1, drp1, dp1, patella p1, r1, tibia r1-1-0, d1-0-0, p1-1-1, v2-2-2, metatarsus r1-1, d2-2, p1-1, v2-2. Genitalia (fig. 3.30, F), WE occupying much more than half of epigynal plate; CO at medial position; CD2 lateromesal to PS, short; PS, spherical, separated by their diameter, and partially inside the WE; FD relatively close to the CD2; BG, depressed or superficial.

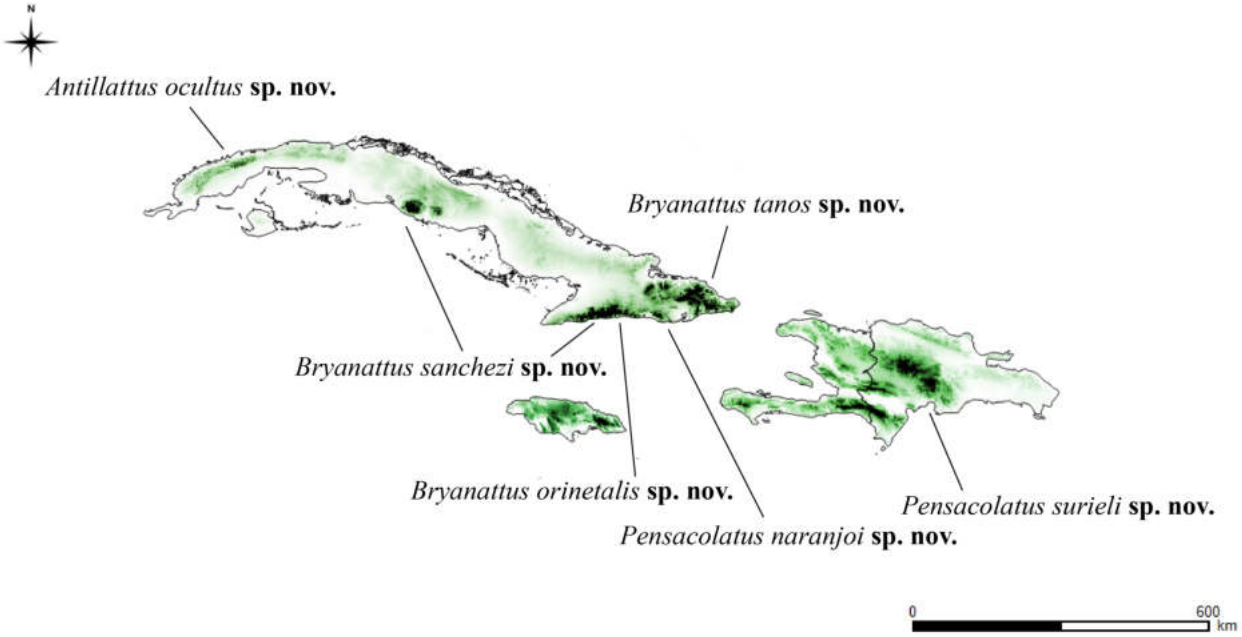

Figure 3.4. General distribution of the *Bryanattus*, *Pensacolatus*, and *Antillattus* new species.

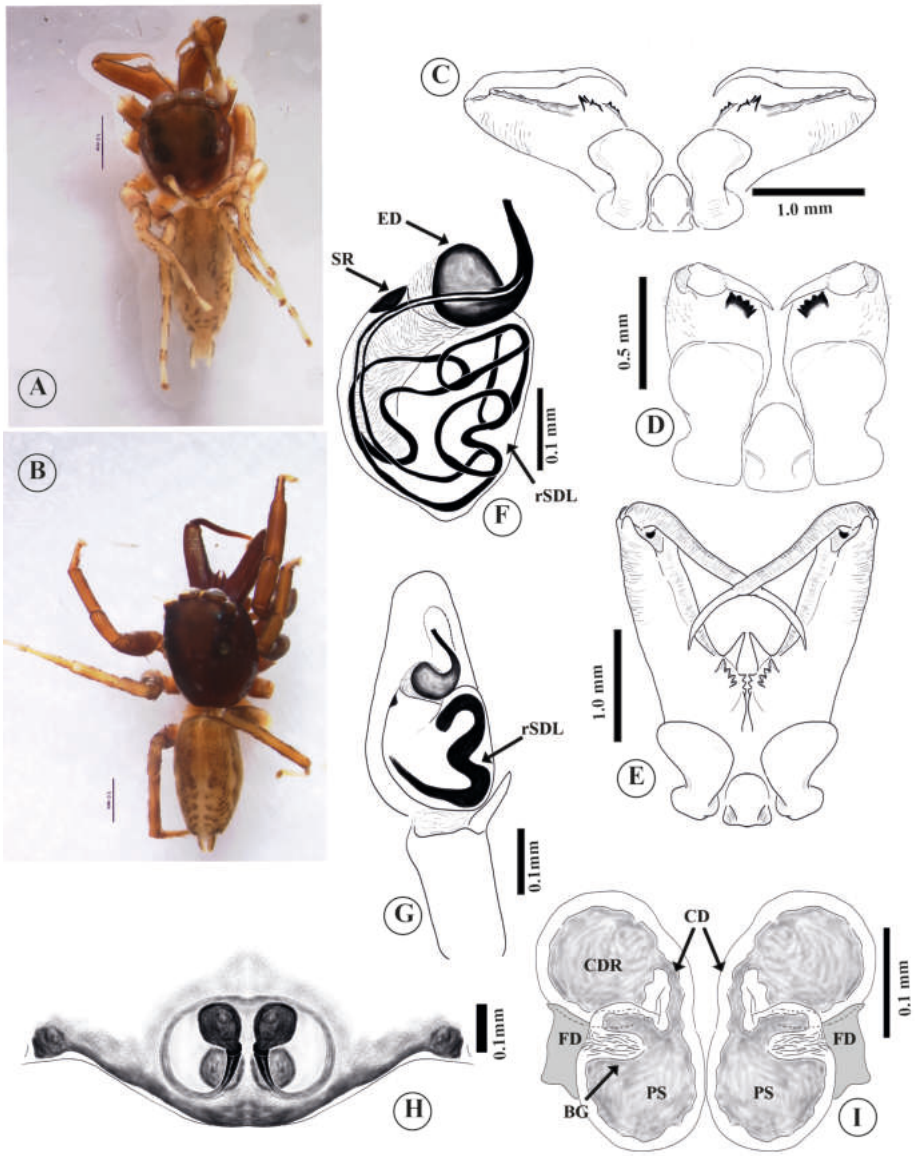

Figure 3.5. *Antillattus gracilis*, *Antillattus placidus*. A, *A. gracilis*, male holotype (MCZ-IZ 21477), habitus, dorsal view. B, *A. placidus*, male holotype (MCZ-IZ 22690), habitus, dorsal view. C, *A. gracilis* (MCZ-IZ 21477), male chelicerae, retromarginal view. D, *A. gracilis*, female chelicerae, retromarginal view. E, *A. placidus* (MCZ-IZ 22690), male chelicerae, retromarginal view. F, *A. gracilis*, male left palp, clove oil digested bulb, ventral view. G, *A. placidus* (MCZ-IZ 22690), male left palp, ventral view. *A. gracilis*. H-I, female of *A. gracilis*, genitalia, (H) ventral view, (I) clove oil digested internal genitalia, dorsal view.

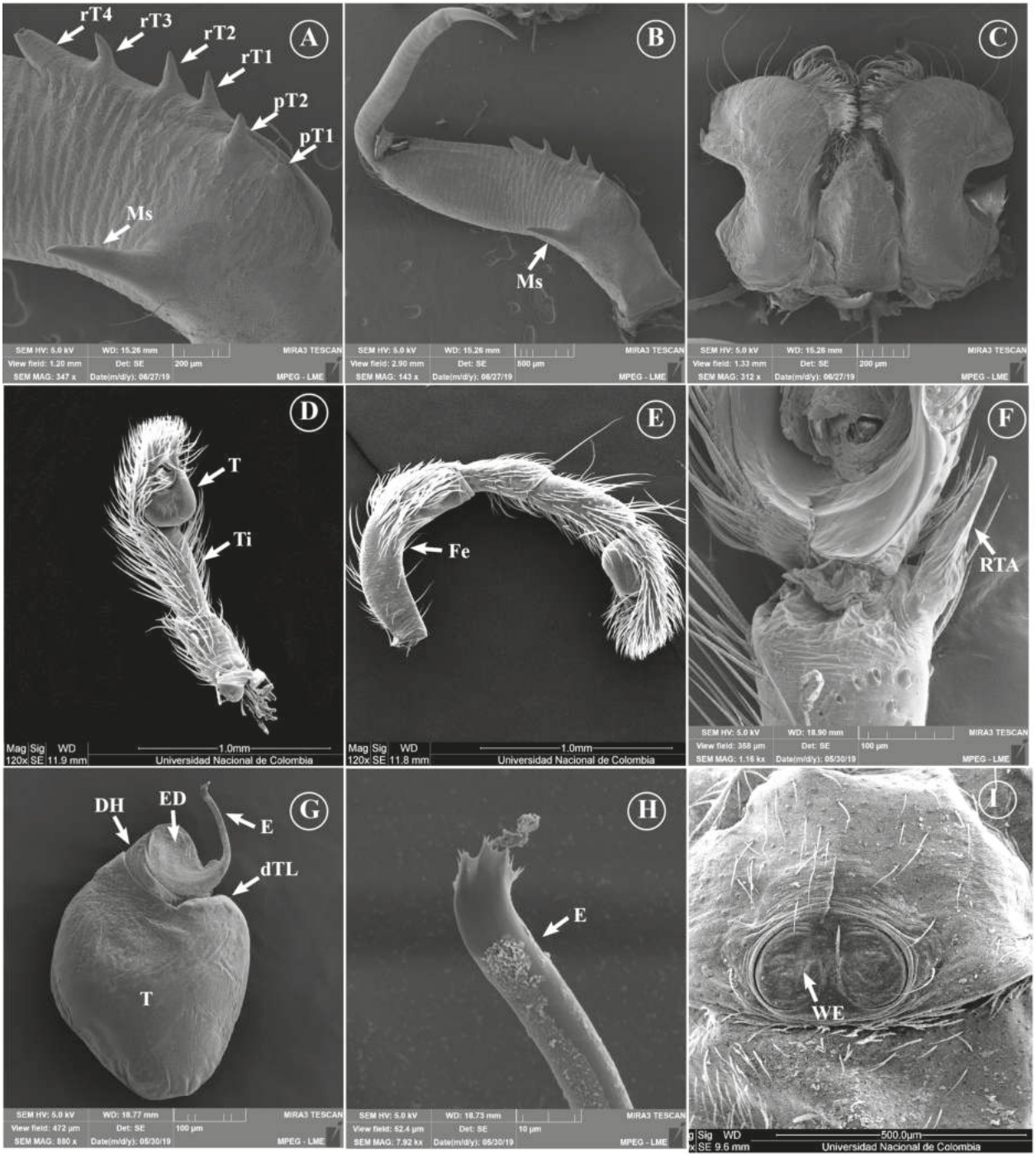

Figure 3.6. Scanning electron microscopy images. *Antillattus cambridgei*. A-B, male chelicerae, promarginal view. C, male endite, ventral view. F-H, male palp, (F), cymbium, ventral view, (G) bulb, ventral view, (H) embolic tip, ventral view. *Antillattus cubensis*. D-E, male palp, (D) ventral view, (E) retrolateral view. I, female genitalia, ventral view.

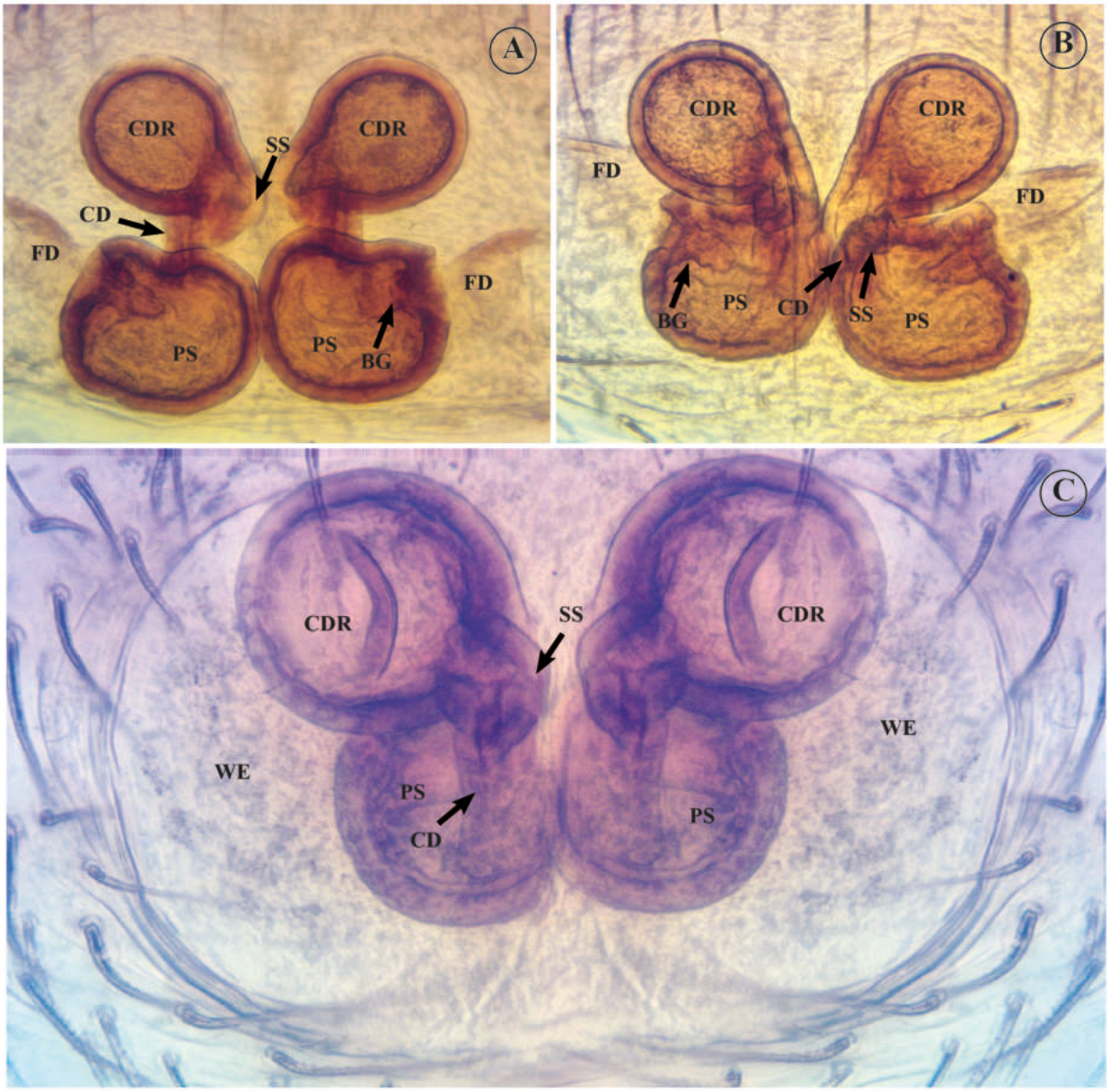

Figure 3.7. Female internal genitalia. A-B, *Antillattus cambridgei* (A) dorsal view, (B) ventral view. C, *Antillattus cubensis*, ventral view.

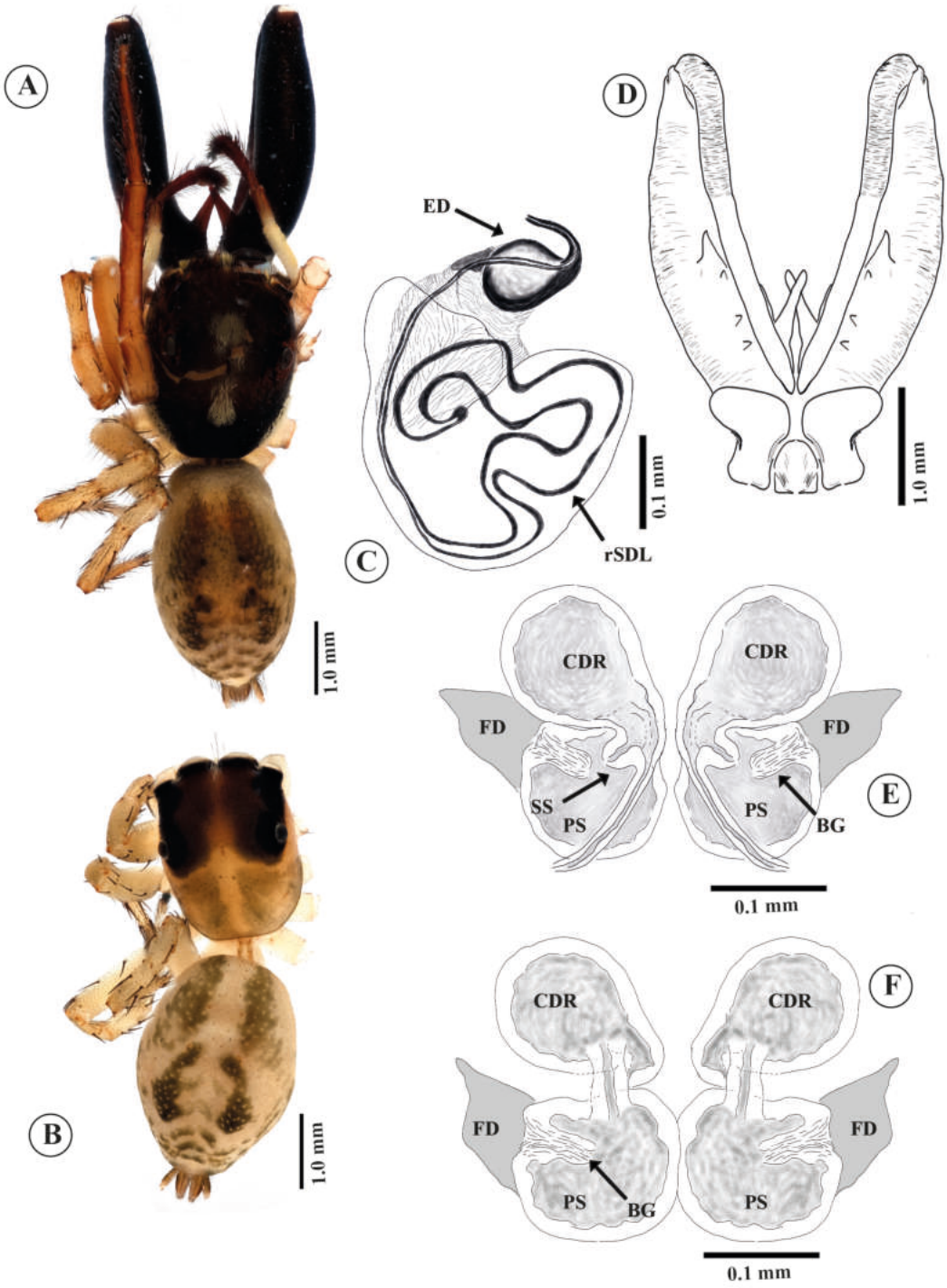

Figure 3.8. *Antillattus cambridgei*. A, male, habitus, dorsal view. B, female, habitus, ventral view C, male left palp, clove oil digested bulb, ventral view. D, male, chelicerae, retromarginal view. E, female, clove oil digested internal genitalia, ventral view. F, female, clove oil digested internal genitalia, dorsal view.

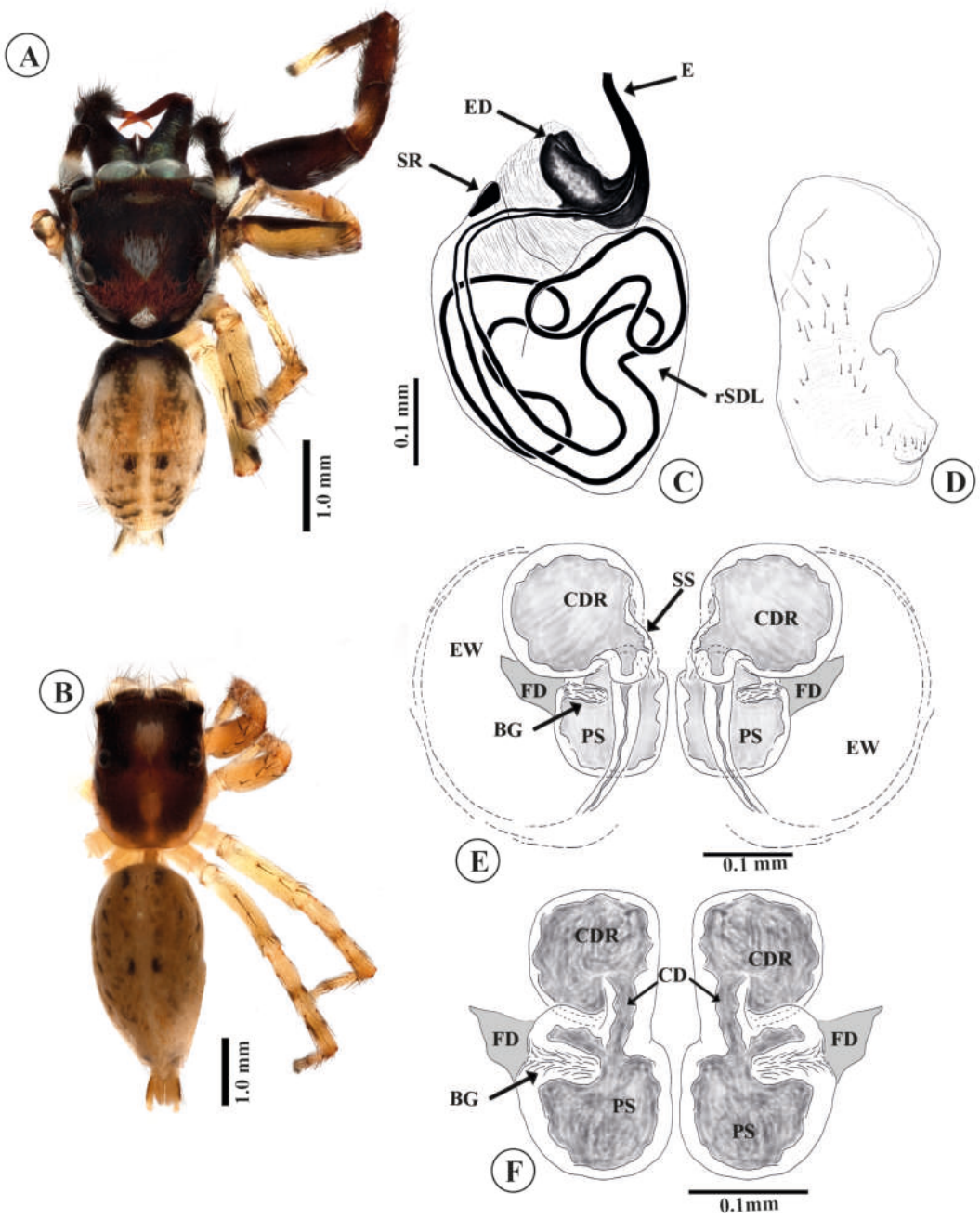

Figure 3.9. *Antillattus cubensis*. A, male, habitus, dorsal view. B, female, habitus, ventral view C, Male left palp, clove oil digested bulb, ventral view. D, male, endite, ventral view. E, Female, clove oil digested internal genitalia, ventral view. F, female, clove oil digested internal genitalia, dorsal view.

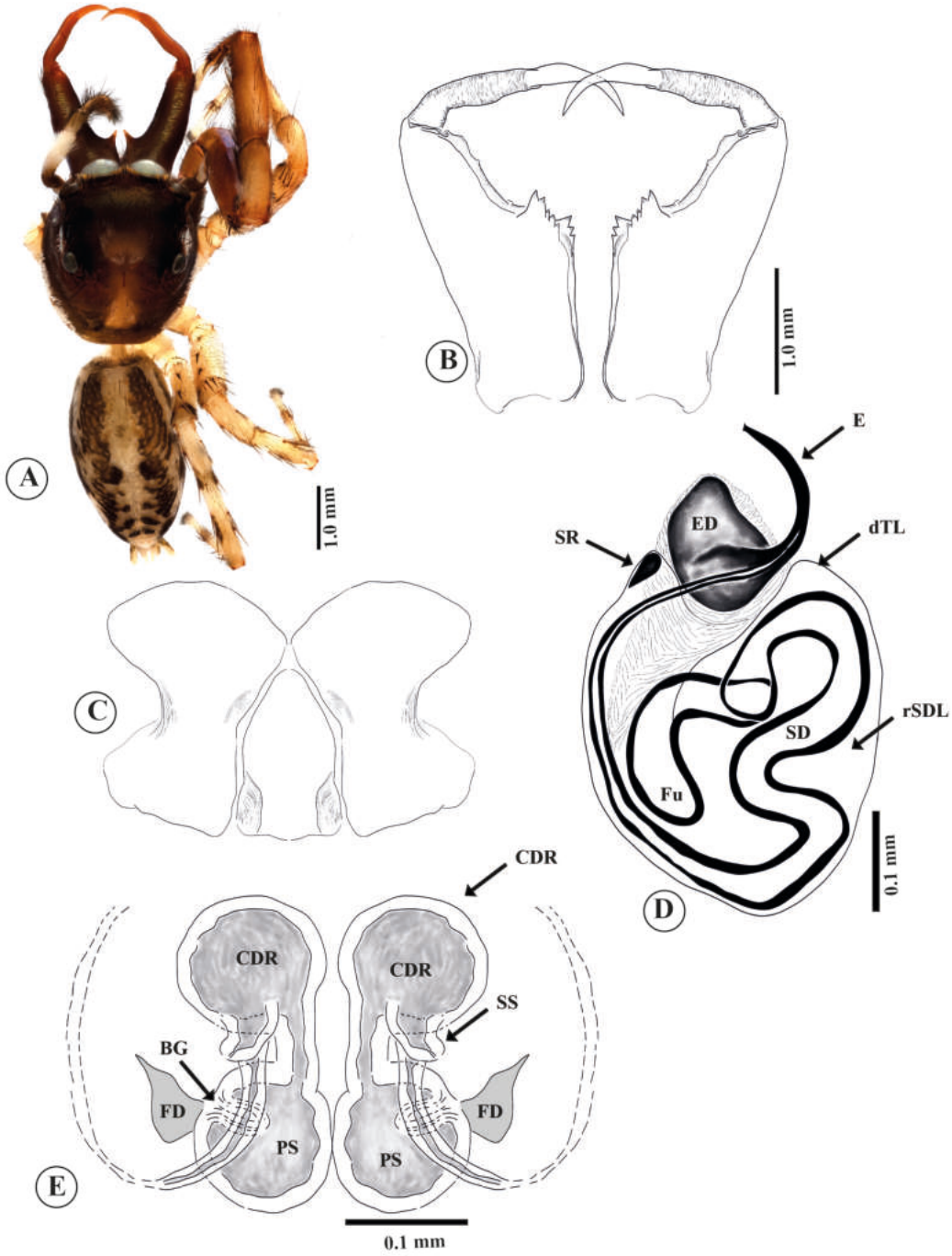

Figure 3.10. *Antillattus ocultus* **sp. nov.** A, male, habitus, dorsal view. B, male chelicerae, retromarginal view. C, male endite, ventral view. D, male left palp, clove oil digested bulb, ventral view. D, female, clove oil digested internal genitalia, ventral view.

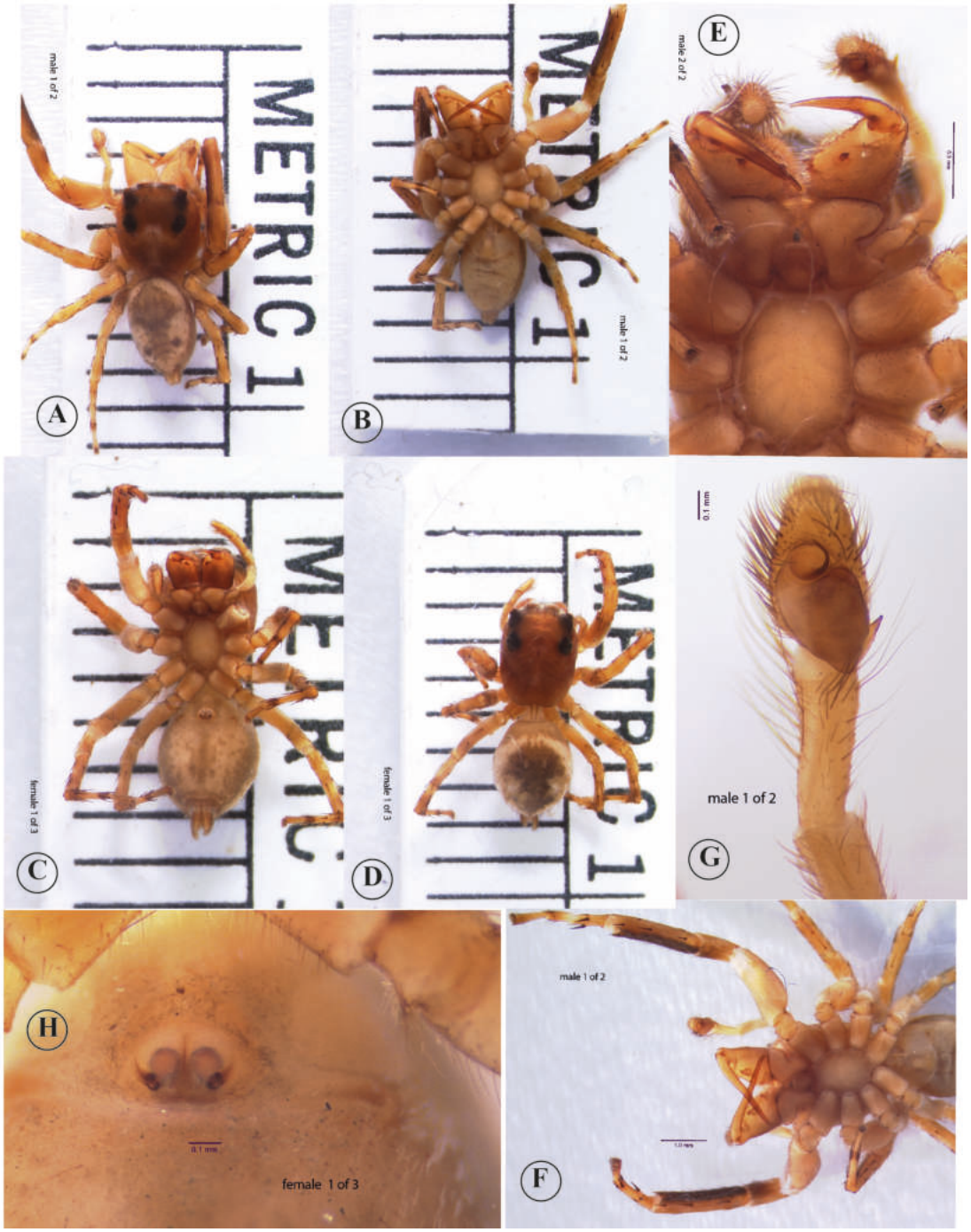

Figure 3.11. *Pensacolatus maxillosus* **comb. nov.** A, male (holotype MCZ-IZ 22010), habitus, dorsal view. B, male (holotype MCZ-IZ 22010), habitus, ventral view. C, female (allotype MCZ-IZ 25833), habitus, dorsal view. D, female (allotype MCZ-IZ 25833), habitus, ventral view. E-F, male, habitus, ventral view. G, male left palp, ventral view. H, female genitalia, ventral view.

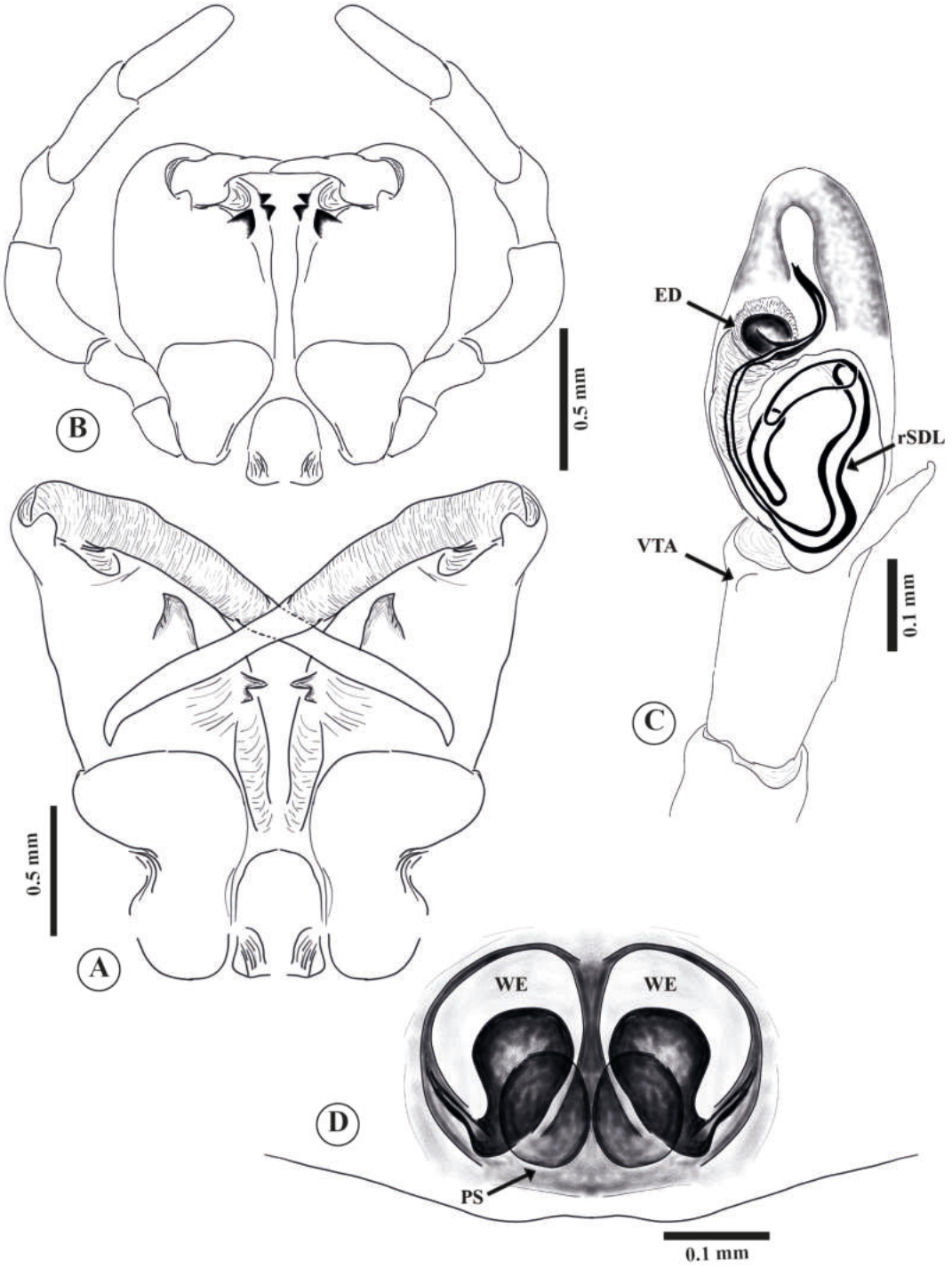

Figure 3.12. *Pensacolatus maxillosus* **comb. nov.** A, male chelicera, retromarginal view. B, female chelicerae, retromarginal view. C, male palp, ventral view. D, female genitalia, ventral view.

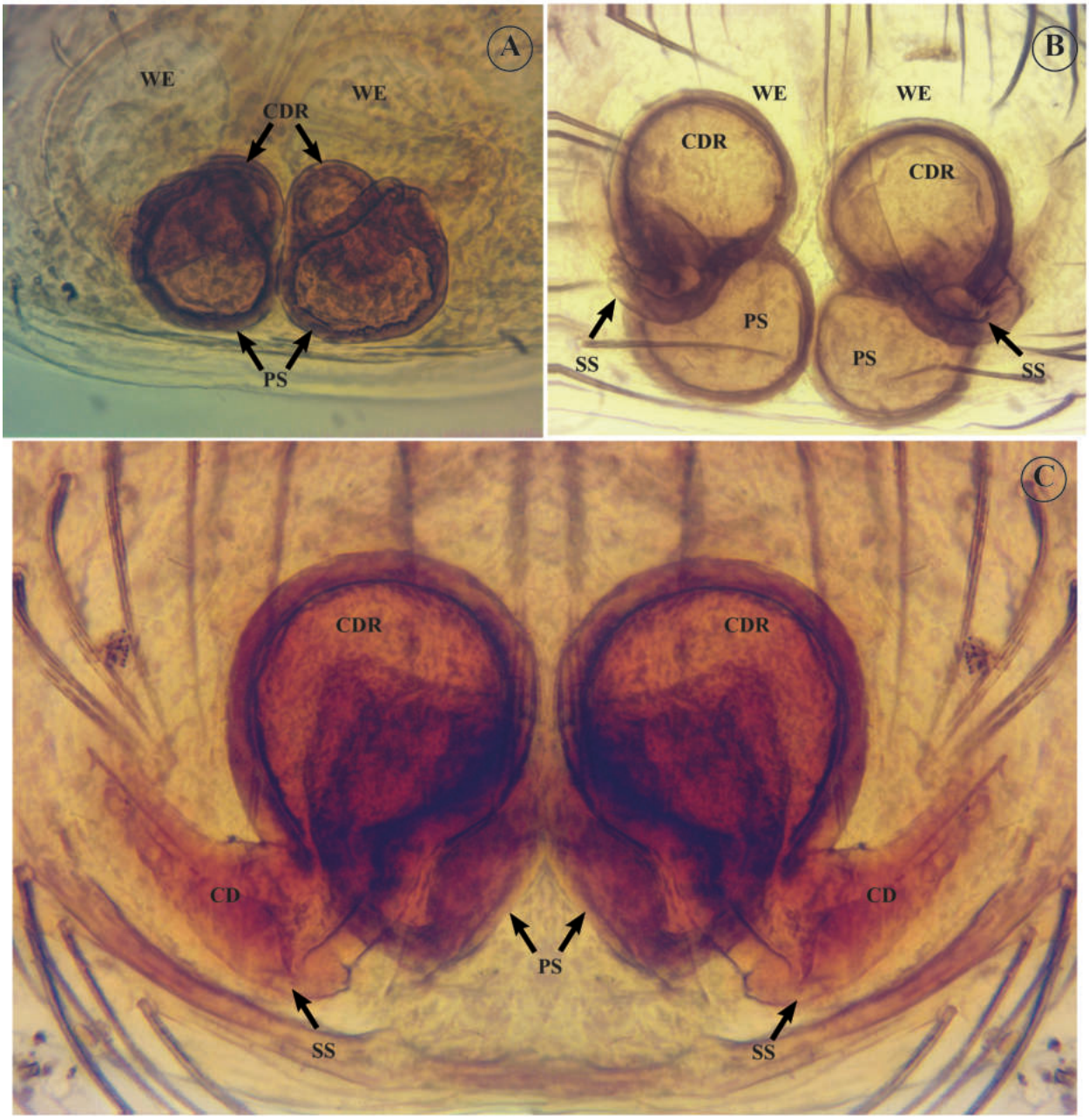

Figure 3.13. Female internal genitalia. A, *Pensacolatus naranjoi* **sp. nov.**, dorsal view. B, *Pensacola montanus* **comb. nov.**, ventral view. C, *Pensacolatus darlingtonia* **comb. nov.**, ventral view.

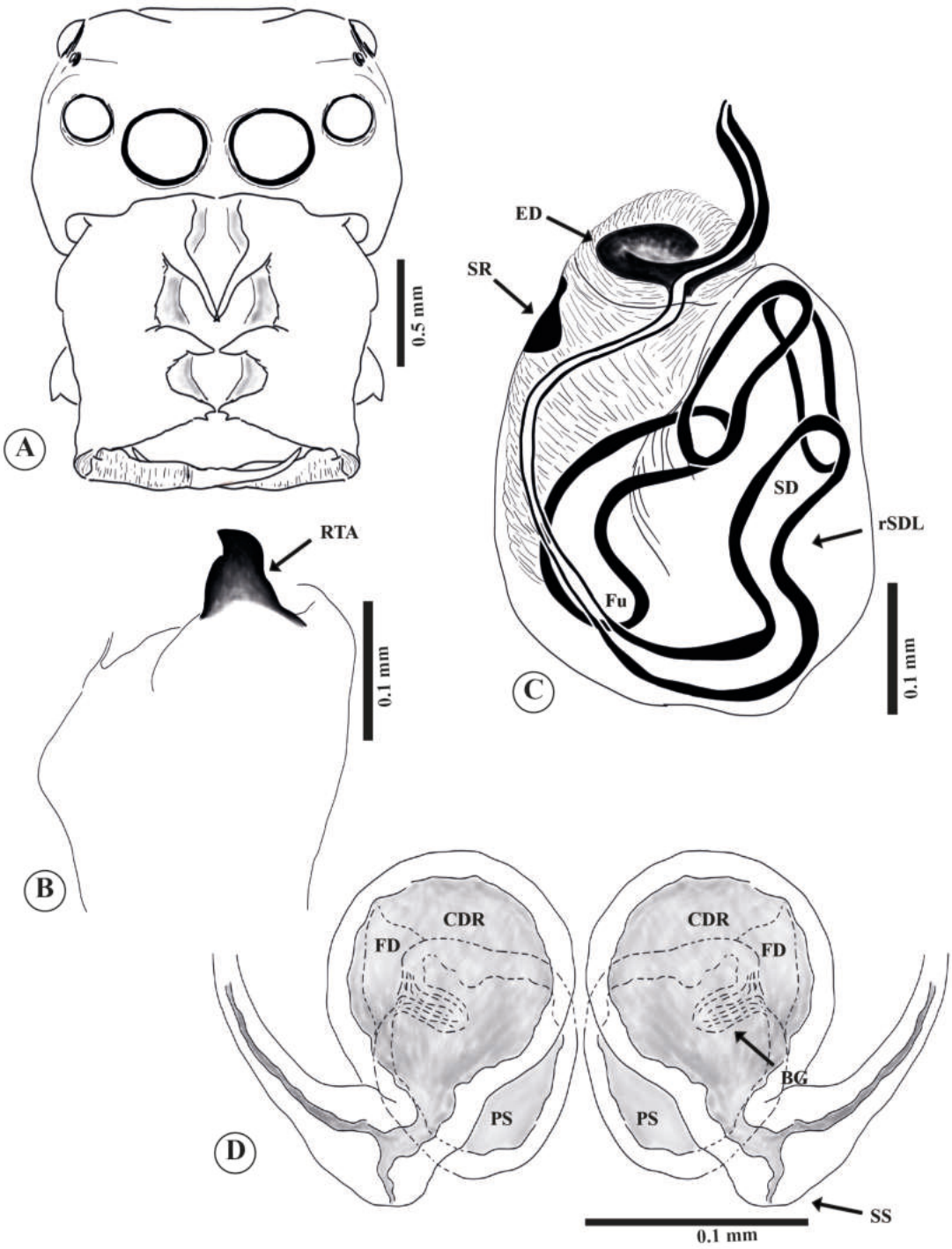

Figure 3.14. *Pensacolatus darlingtoni* **comb. nov.** A, male, habitus, frontal view. B, male palpal tibia, retrolateral view. C, male palp, ventral view. D, female internal genitalia, ventral view.

Figure 3.15. *Pensacolatus montanus* **comb. nov.** A and F, male (holotype MCZ-IZ 22169), habitus, dorsal view. B, male (holotype MCZ-IZ 22169), habitus, ventral view. C, female (allotype MCZ-IZ 25834), habitus, dorsal view. D, female (allotype MCZ-IZ 25834), habitus, ventral view. E, male, habitus, ventral view. G, female genitalia, ventral view. H, locality data.

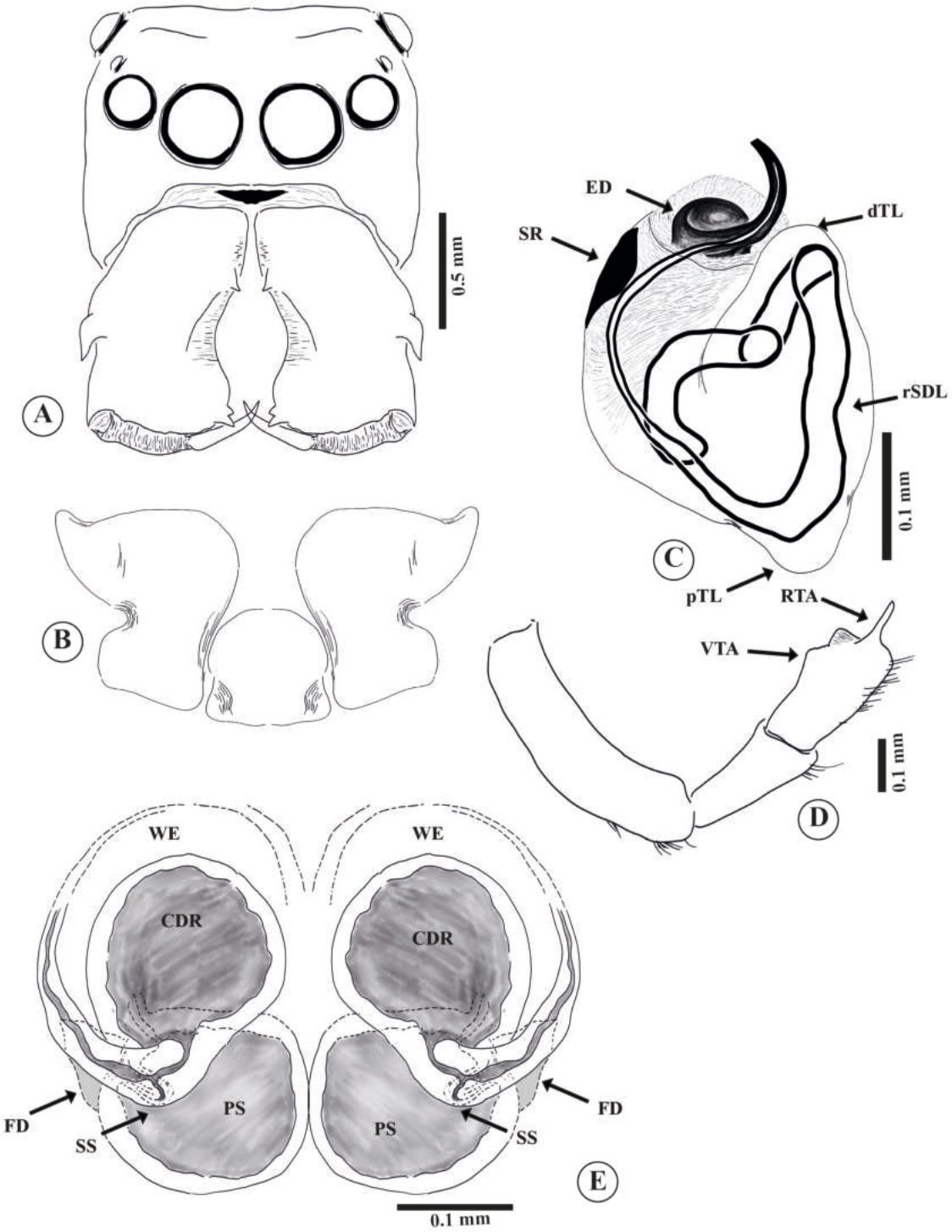

Figure 3.16. *Pensacolatus montanus* **comb. nov.** A, male, habitus, frontal view. B, male endites, ventral view. C, male palp, ventral view. D, male palp, retrolateral view. E, female internal genitalia, ventral view.

Figure 3.17. *Pensacolatus scutiformis* **comb. nov.** A, female (allotype MCZ-IZ 25849), habitus, dorsal view. B, male (holotype MCZ-IZ 21177), habitus, dorsal view. C, male palp, ventral view. D, female genitalia, ventral view.

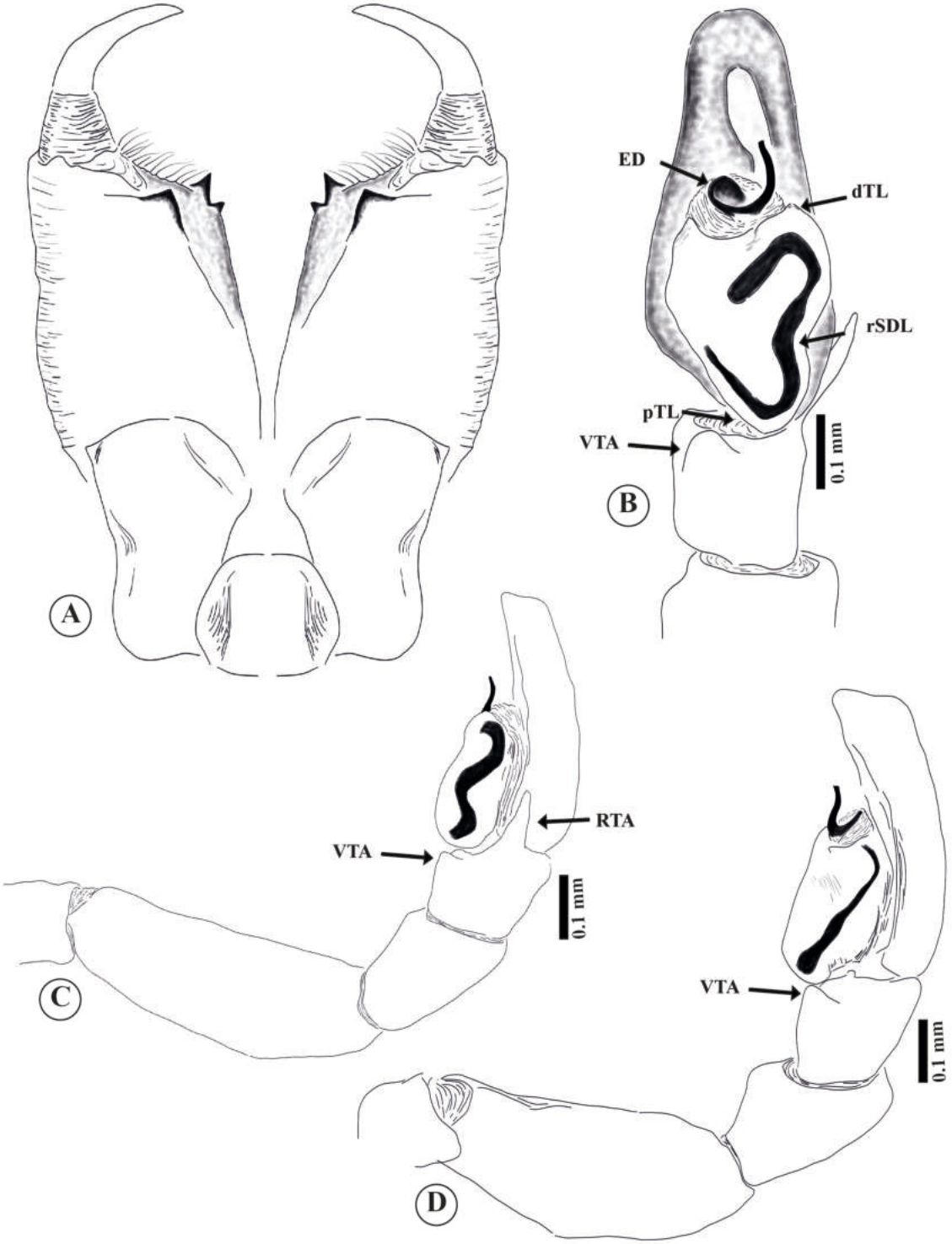

Figure 3.18. *Pensacolatus scutiformis* **comb. nov.** A, male, chelicerae, retromarginal view. B, male palp, ventral view. C, male palp, retrolateral view. D, male palp, prolateral view.

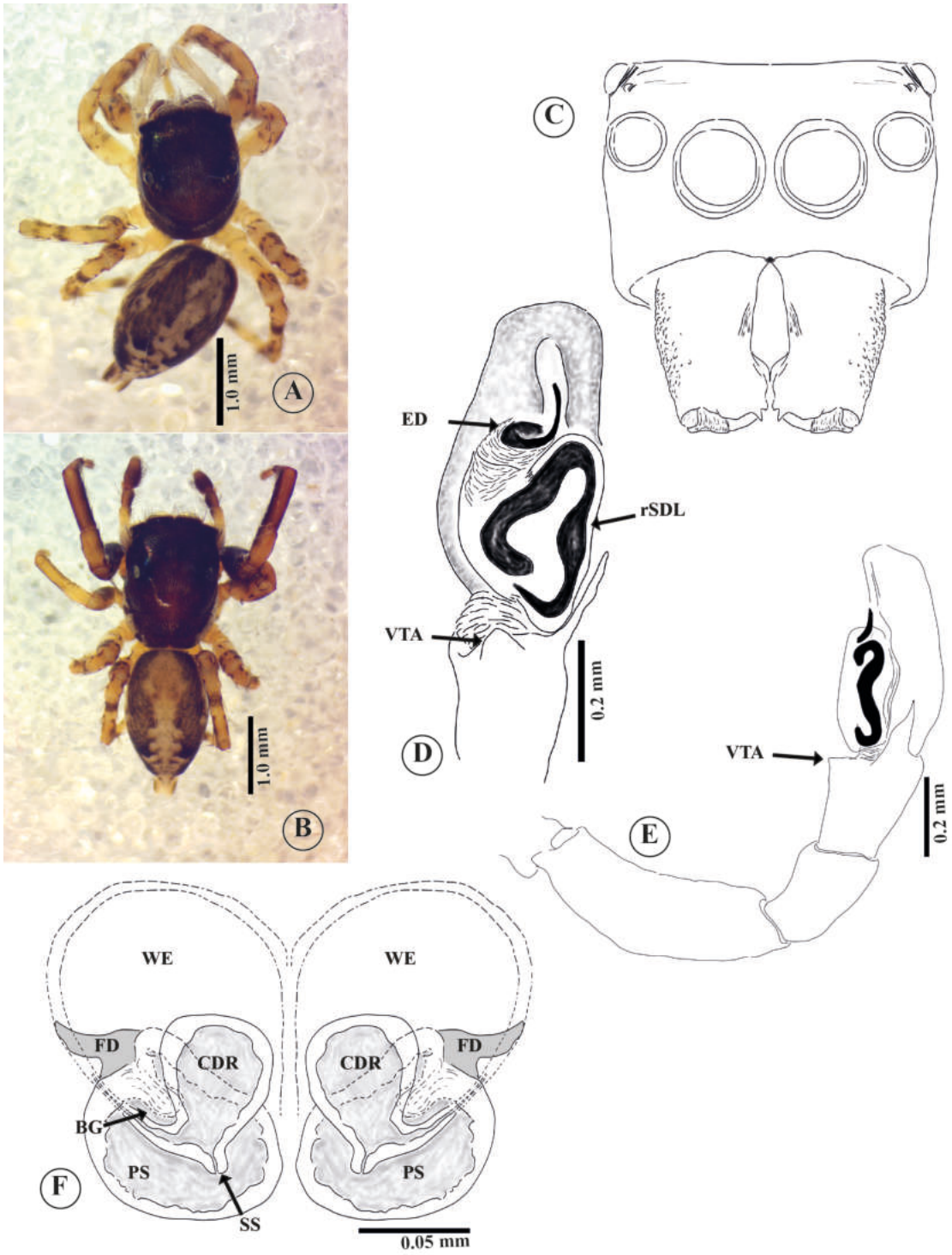

Figure 3.19. *Pensacolatus naranjoi* **sp. nov.** A, male, habitus, dorsal view. B, female, habitus, dorsal view. C, male, habitus, frontal view. D, male. left palp, clove oil digested bulb ventral view. E, male palp, retrolateral view. F, Female, clove oil digested internal genitalia, ventral view.

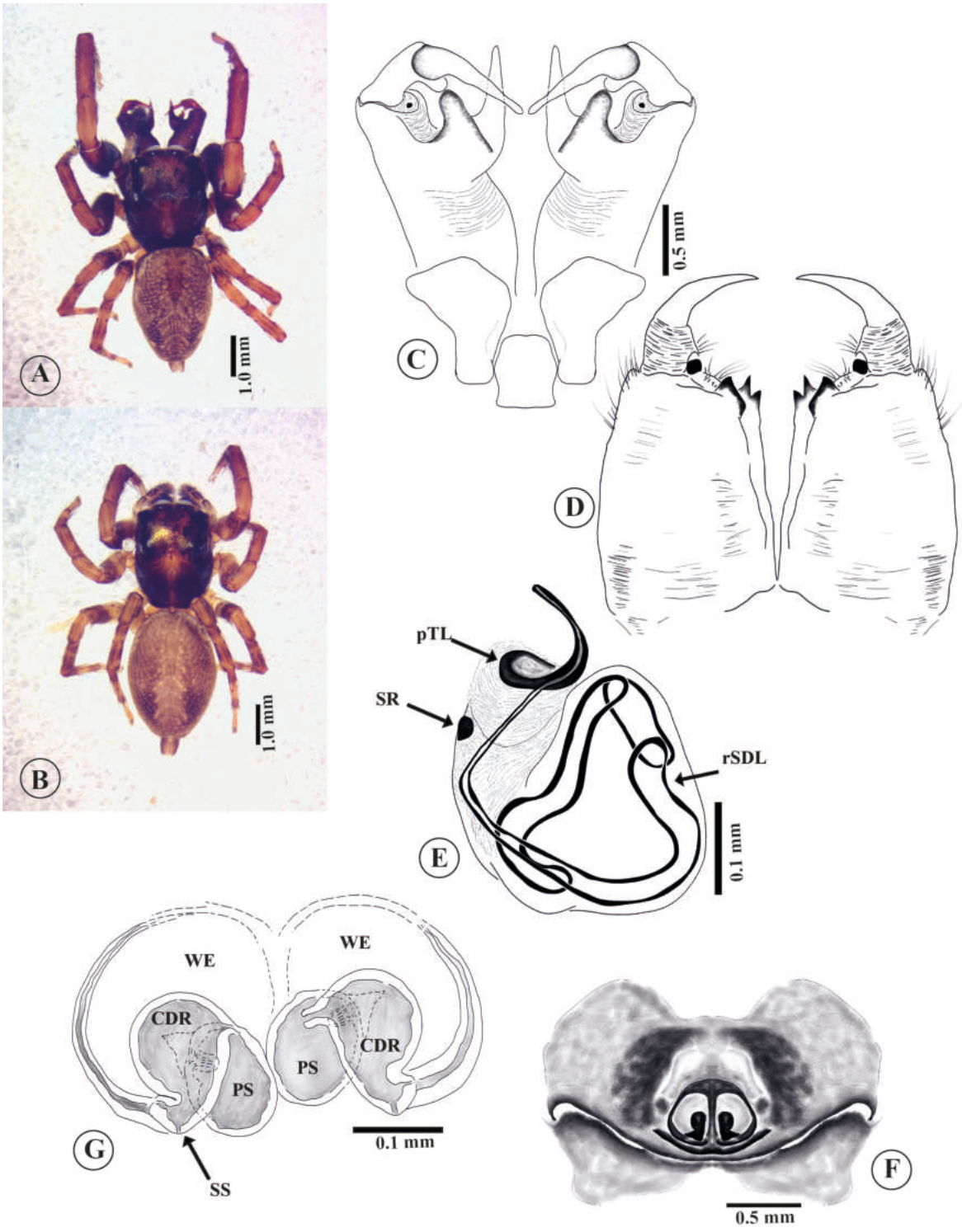

Figure 3.20. *Pensacolatus surieli* **sp. nov.** A, male, habitus, dorsal view. B, female, habitus, dorsal view. C, male chelicerae, retromarginal view. D, female chelicerae, retromarginal view. E, male left palp, clove oil digested bulb, ventral view. G, female, clove oil digested internal genitalia, ventral view. F, female genitalia, ventral view.

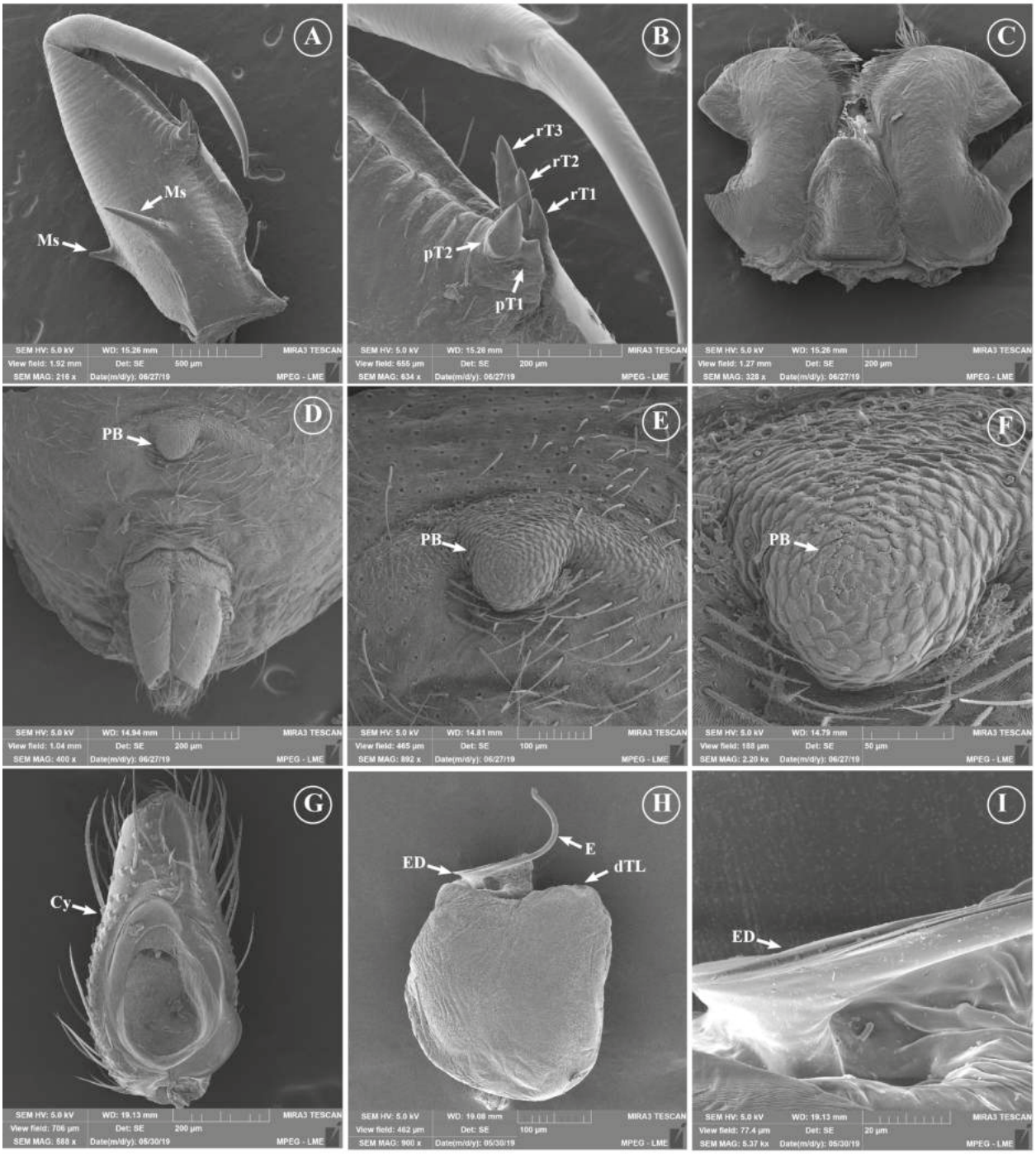

Figure 3.21. Scanning electron microscopy images. *Bryanattus keyserlingi* **comb. nov.**. A-B, male chelicerae, promarginal view. C, male endite, ventral view. D-F, male prespiracular bump. G, male palpal cymbium, ventral view. (H) male palpal bulb, ventral view. I, male embolic disc.

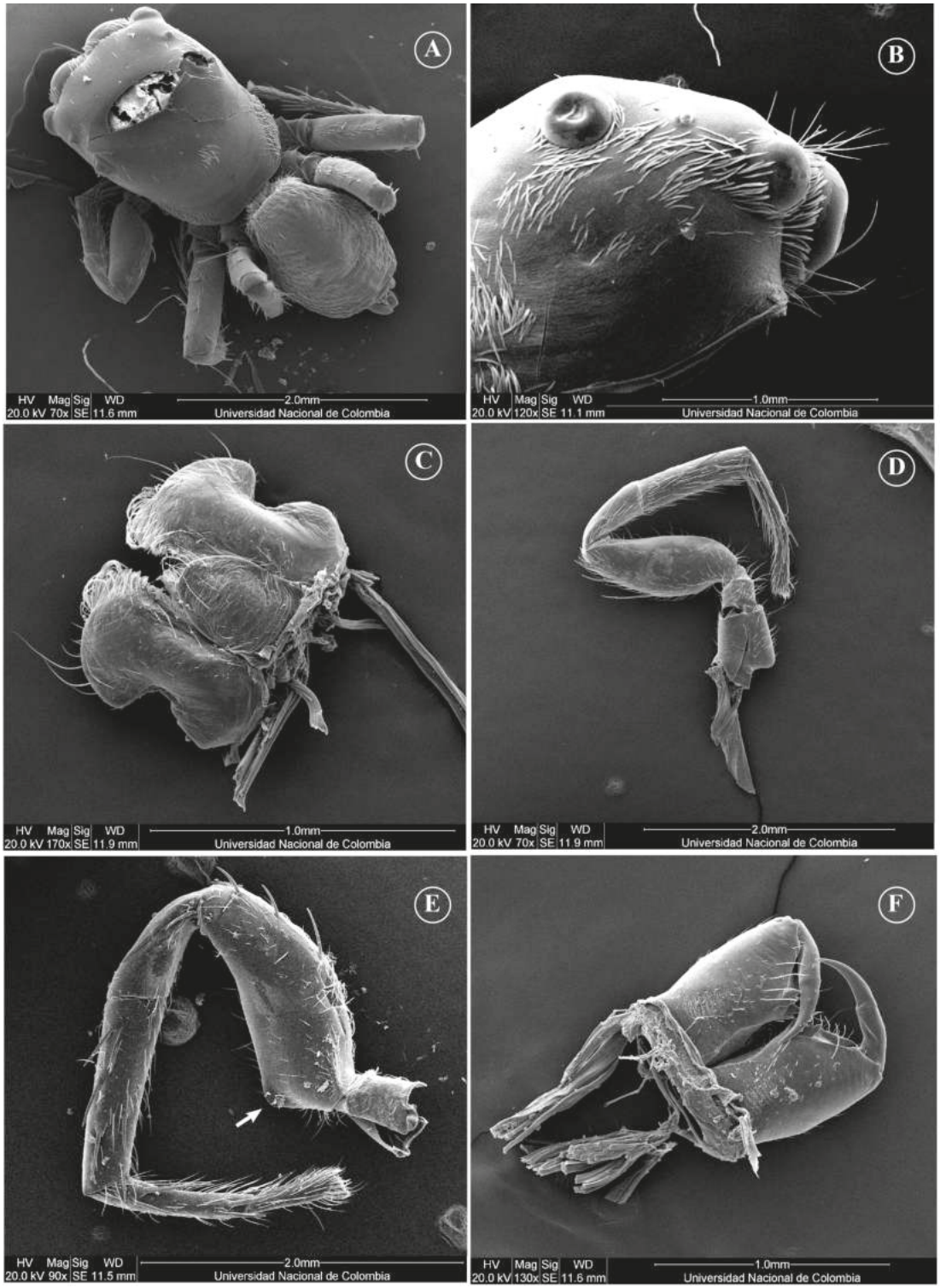

Figure 3.22. Scanning electron microscopy images. *Bryanattus orientalis* **sp. nov.** A-B, male, habitus (A) dorsal view, (B) lateral view. C, male endite, ventral view. D, male leg I. F, female chelicerae, retromarginal view. *Bryanattus keyserlingi* **comb. nov.**. E, male leg I.

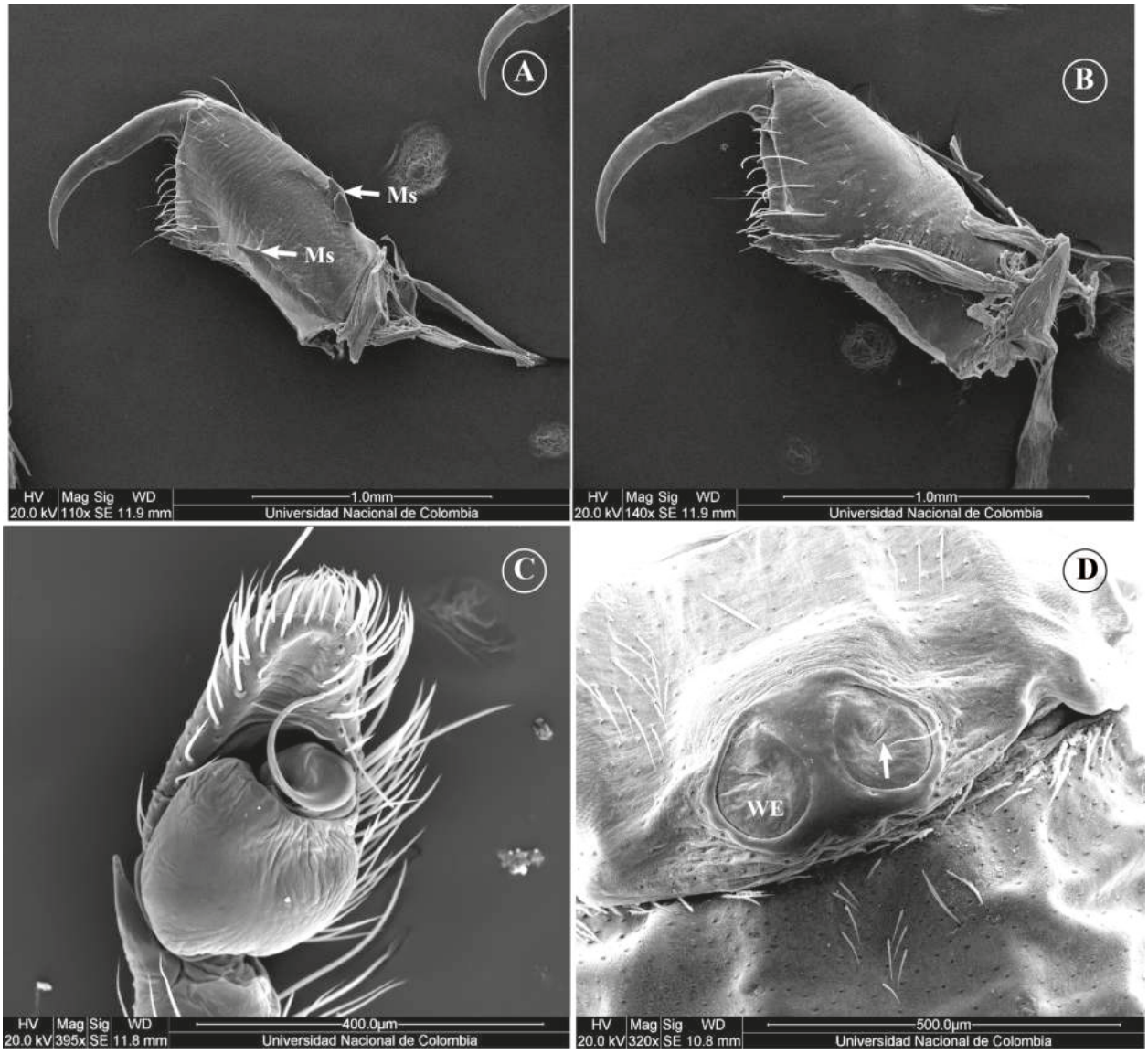

Figure 3.23. Scanning electron microscopy images. *Bryanattus orientalis* **sp. nov.** A-B, male chelicerae (A) promarginal view, (B) retromarginal view. C, male palp, ventral view. D, female genitalia, ventral view, arrow indicate the slit like a "pocket".

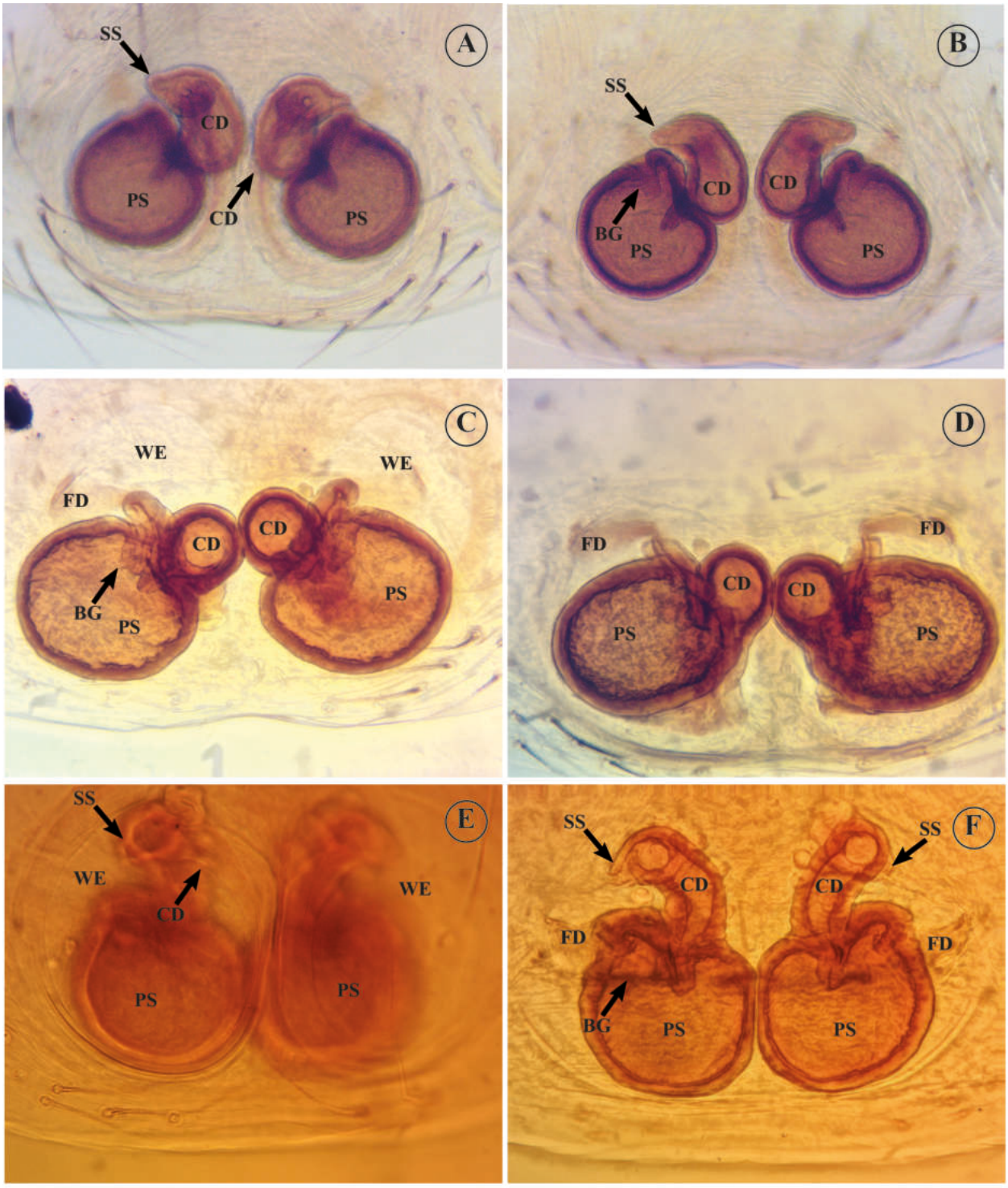

Figure 3.24. Female internal genitalia. A-B, *Bryanattus thanos* **sp. nov.**, (A) ventral view, (B) dorsal view. C-D, *Bryanattus sanchezi* **sp. nov.**, (C) ventral view, (D) dorsal view. E-F, *Bryanattus orientalis* **sp. nov.**, (E) ventral view, (F) dorsal view.

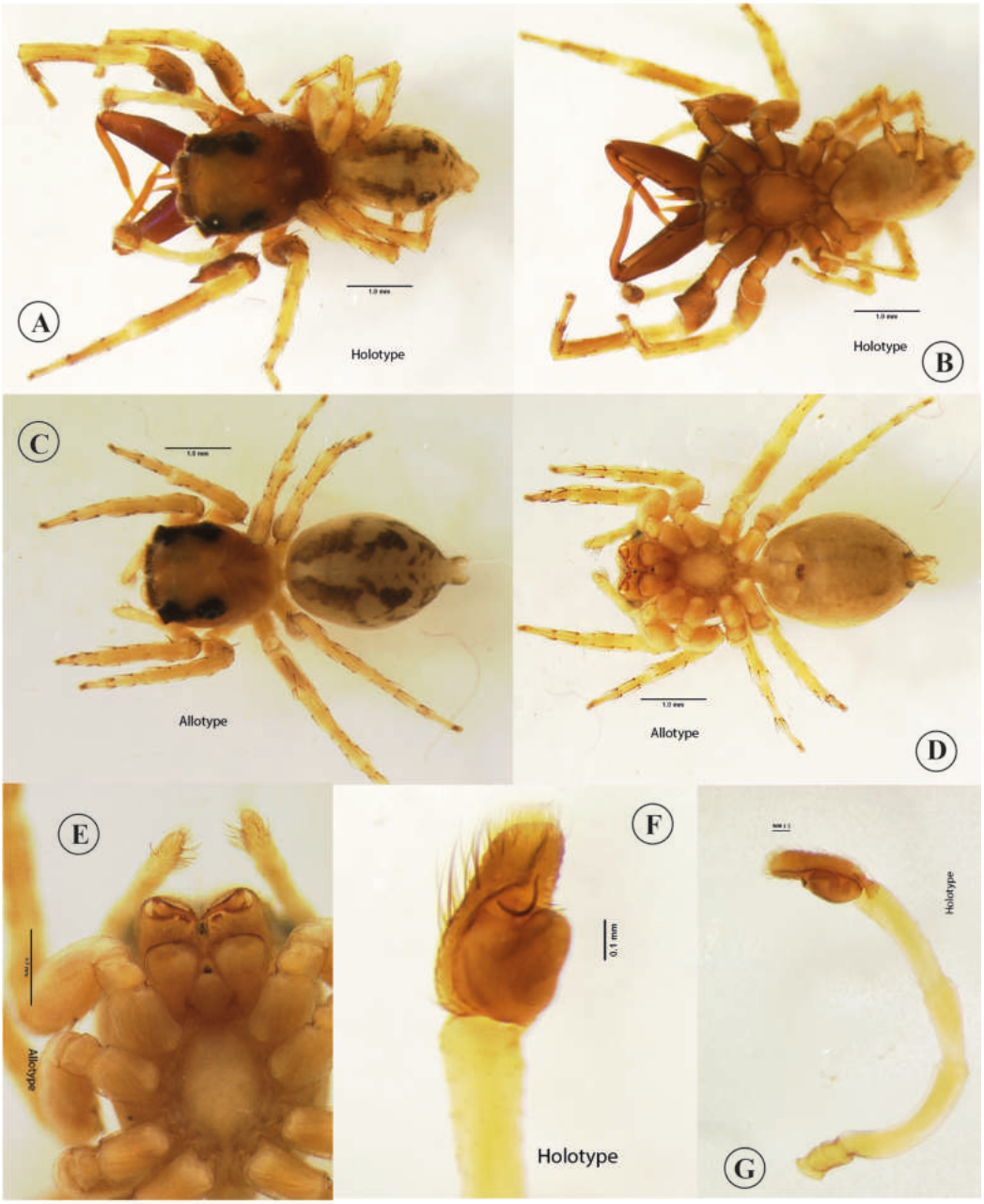

Figure 3.25. *Bryanattus mandibulatus* **comb. nov.** A, male (holotype MCZ-IZ 21974), habitus, dorsal view. B, male (holotype MCZ-IZ 21974), habitus, ventral view. C, female (allotype MCZ-IZ 21974), habitus, dorsal view. D-E, female (allotype MCZ-IZ 21974), habitus, ventral view. F, male left palp, ventral view. G, male left palp, retrolateral view

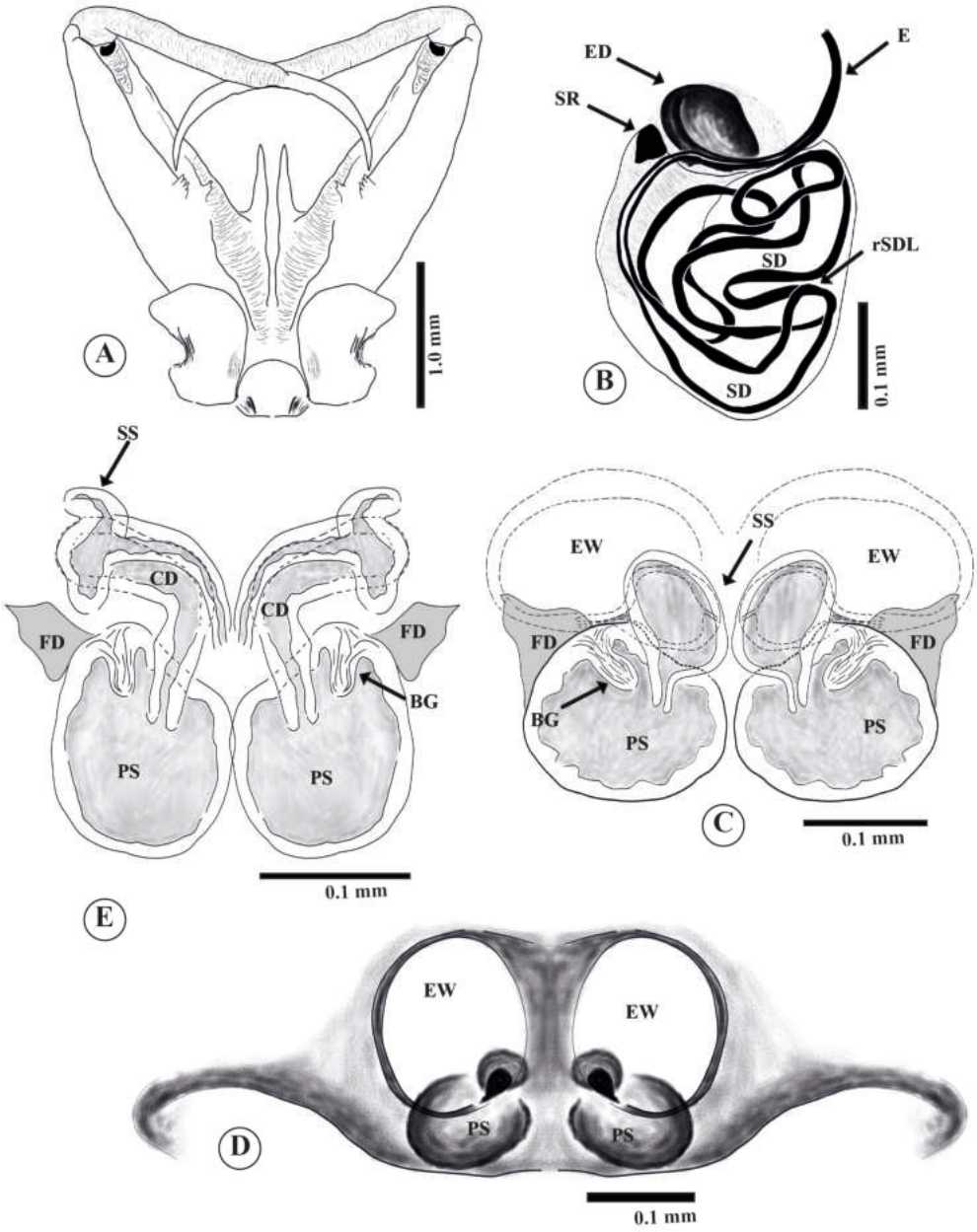

Figure 3.26. *Bryanattus mandibulatus* **comb. nov.** A, male chelicerae, retromarginal view. B, male left palp, clove oil digested bulb, ventral view. C, female, genitalia, clove oil digested internal genitalia, dorsal view. D, female, genitalia, ventral view. E, female of *Bryanattus keyserlingi* **comb. nov.**, ventral view.

Figure 3.27. *Bryanattus keyserlingi* **comb. nov.** A-B, male (holotype MCZ-IZ 21748), habitus, dorsal view. B-C, female from Pico Turquino, dorsal view. E-H, male from Pico Turquino, dorsal view.

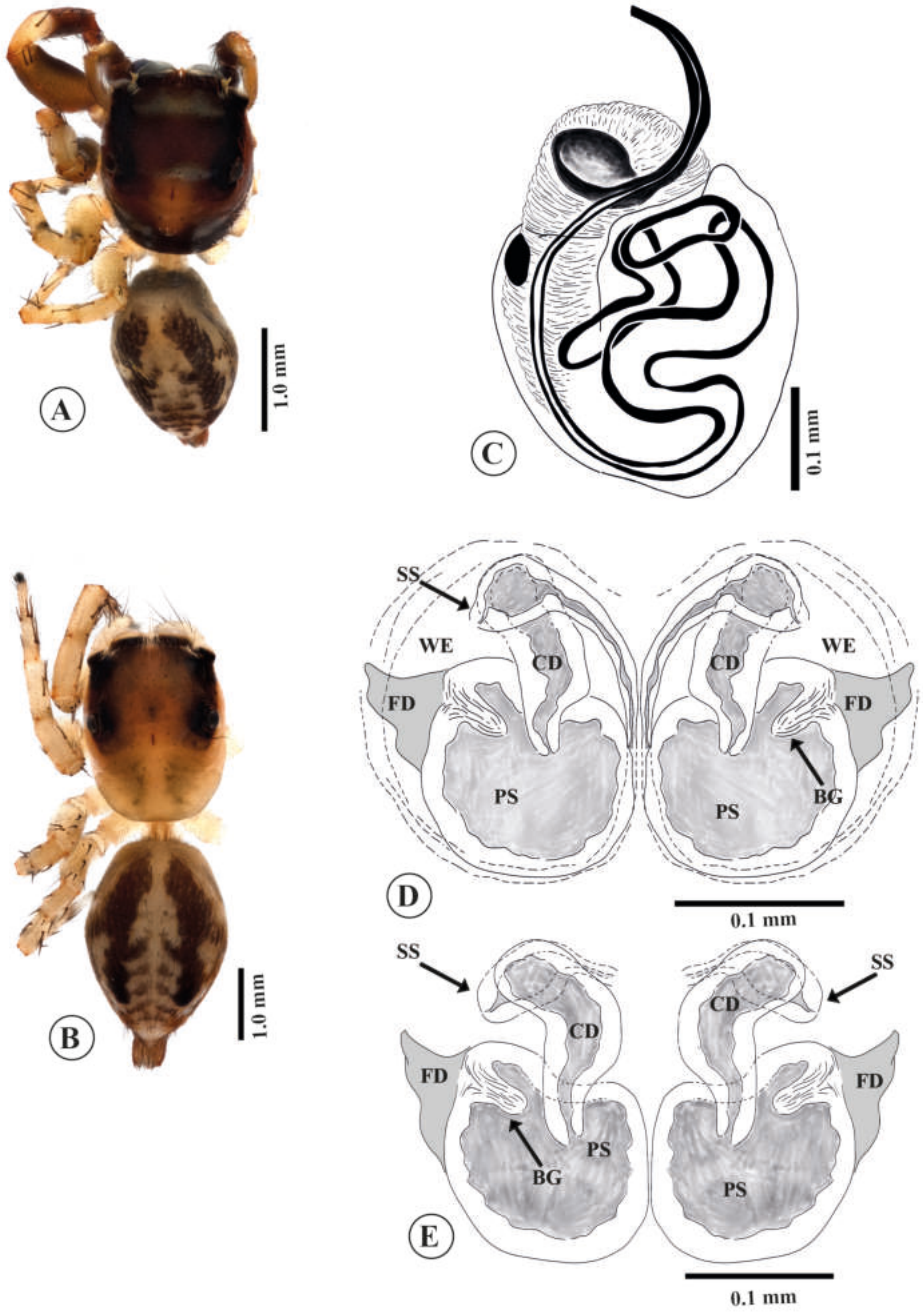

Figure 3.28. *Bryanattus orientalis* **sp. nov.** A, male, habitus, dorsal view. B, female, habitus, dorsal view. C, male, left palp, clove oil digested bulb, ventral view. D, female, clove oil digested internal genitalia, ventral view. E, female, clove oil digested internal genitalia, dorsal view.

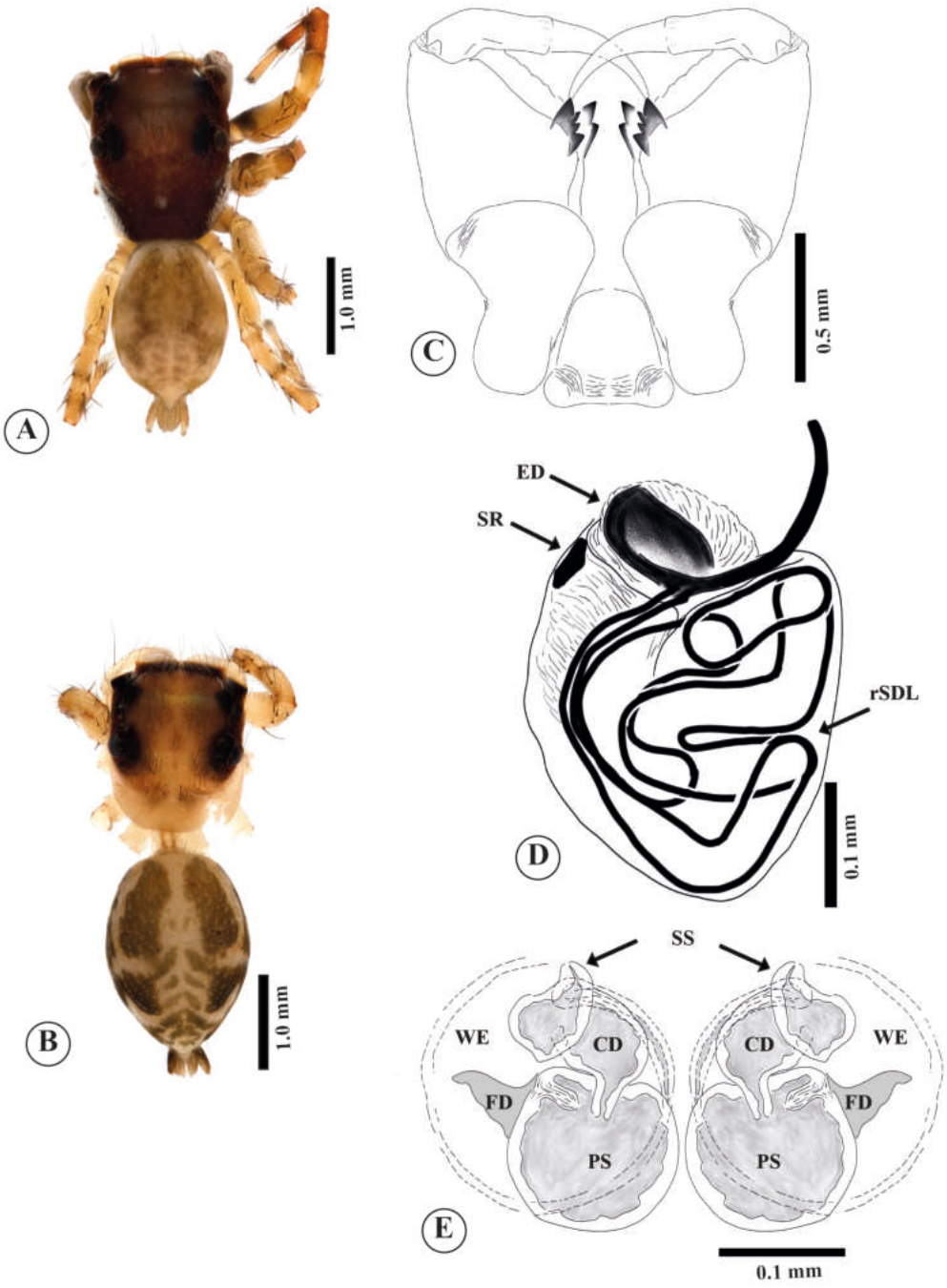

Figure 3.29. *Bryanattus thanos* **sp. nov.** A, male, habitus, dorsal view. B, female, habitus, dorsal view. C, male, chelicerae, retromarginal view. D, left palp, clove oil digested bulb, ventral view. E, female, clove oil digested internal genitalia, dorsal view.

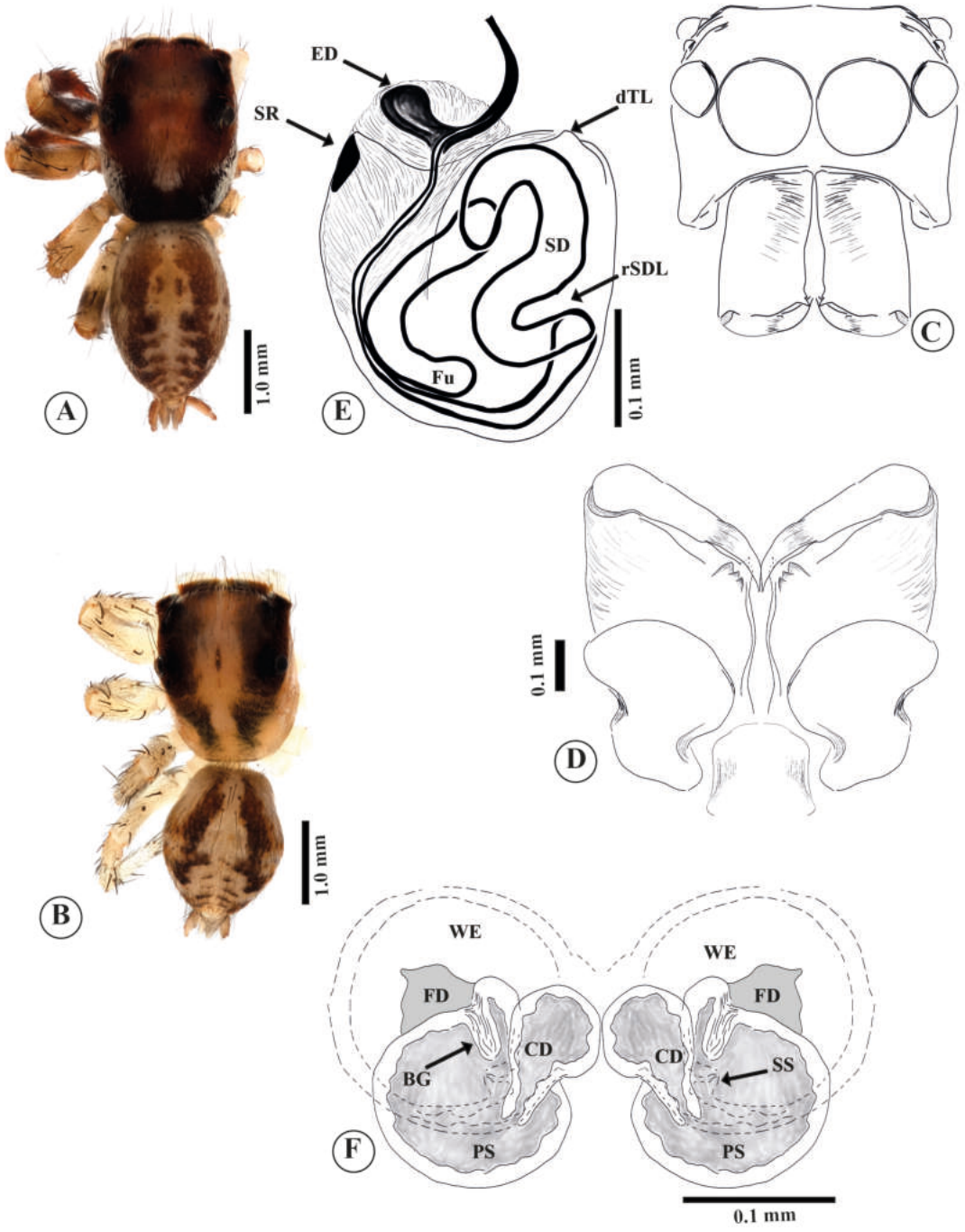

Figure 3.30. *Bryanattus sanchezi* **sp. nov.** A, male, habitus, dorsal view. B, female, habitus, dorsal view. C-D male chelicerae, (C) frontal view, (D) retromarginal view. E, male, left palp, clove oil digested bulb, ventral view. D, male, endite, ventral view. F, female, clove oil digested internal genitalia, dorsal view.

Figure 2.31. A-B, *Antillattus cambridgei*, male and female habitus. C-D, *Antillattus gracilis* male, male and female habitus. E-F, *Antillattus placidus*, male and female habitus. Images by Wayne Maddison, released under a Creative Commons Attribution (CC-BY) 3.0 license.

Figure 2.32. A-B, *Pensacolatus applanatus* **comb. nov.**, male and female habitus. C-D, *Pensacolatus darlingtoni* **comb. nov.,** male, male and female habitus. E-F, *Pensacolatus maxilosus* **comb. nov.**, male and female habitus. Images by Wayne Maddison, released under a Creative Commons Attribution (CC-BY) 3.0 license.

3.4 Conclusion

Our study contributes to understanding the diversity of *Antillattus*, *Pensacolatus*, and *Bryanattus* **gen. nov.** jumping spiders using expanded taxon sampling and both morphological and molecular data. As currently defined, the genus *Antillattus* is resolved into three divergent clades that can each be distinguished morphologically. Thus, we have constructed two additional genera, *Pensacolatus* and *Bryanattus*, to encompass the diversity. We transferred *A. darlingtoni, A. electus, A. maxillosus, A. montanus, A. peckhami*, and *A. scutiformis* to *Pensacolatus* and consider *Antillattus gracilis*, *A. placidus*, *A. cubensis*, and *A. cambridgei* as true *Antillattus*. Both *Pensacolatus* and *Antillattus* are strongly supported by molecular and morphological data. The other species previously included within *Antillattus* are described here as *Bryanattus* **gen. nov.** and *Pensacolatus*. Additionally, genetic distances, gene-trees, morphology, and species delimitation analyses (Fig. 3.4, table 3.6) support the existence of multiple species and cryptic species. Future research will be directed toward examining the biogeography of the Antillattus clade, adding more data to the growing body of arthropod evolutionary research in the Caribbean biodiversity hotspot.

Acknowledgements

Many thanks to all the members of the CarBio team and our collaborators for their tireless effort in the field over the last six years. Many thanks to Robert Anderson, Martín Fikáček, Andrew Smith and Guanyang Zhang Rodrigo for their important help in the field. Special thanks to our collaborators in Cuba: Alexander Sanchez, Giraldo Alayón, Albert Deler-Hernandez and rangers of "Pico Turquino National Park, "Maravillas de Viñales" National Park, "Sierra de Cubitas" Ecological Reserve, "Topes de Collantes" National Park, "Duaba-Yunque-Quibijan" Ecological Reserve and "Soledad" Botanical Garden. In Hispaniola: Solanlly Carrero Jiménez and Gabriel de los Santos for their invaluable help with the organization and execution of logistically complex expeditions and ongoing collaboration. We also want to give special thanks to Laura Leibensperger (MCZ-IZ), and Carlos Suriel (MNHNSD) for their valuable help with images and loan of material. We especially acknowledge the comments and critique of Jairo Moreno, Alexandre Sargado, Sarah Crews, Abel Bustamante and anonymous reviewers. We are grateful to the authorities and personnel of the Cuban Ministry of Science, Technology and Environment (CICA-CITMA), and the Empresa Nacional para la Protección de la Flora y la Fauna (ENPFF) for providing access to protected areas under their control. Funding for this work came from NSF DEB-1050187-1050253- 1314749 to IA and GB.

Conflicts of interest

The authors declare no conflicts of interest

3.5 References

Agnarsson, I. (2004) Morphological phylogeny of cobweb spiders and their relatives (Araneae, Araneoidea, Theridiidae). *Zoological Journal of the Linnean Society* **141** (4), 447–626.

Agnarsson, I., LeQuier, S. M., Kuntner, M., Cheng, R.-C., Coddington, J.A., and Binford, G. (2016). Phylogeography of a good Caribbean disperser: *Argiope argentata* (Araneae, Araneidae) and a new 'cryptic' species from Cuba. *ZooKeys* **625**, 25–44. 10.3897/zookeys.625.8729

Alayón, G. G. (2000). Las arañas endémicas de Cuba (Arachnida: Araneae). *Revista Ibérica Aracnología* **2**: 1-48.

Altekar, G., Dwarkadas, S., Huelsenbeck, J. P., and Ronquist, F. (2004). Parallel Metropolis coupled Markov chain Monte Carlo for Bayesian phylogenetic inference. *Bioinformatics* **20**, 407–415. doi:10.1093/bio informatics/btg427

Álvarez-Padilla, F., and Hormiga, G. (2008). A protocol for digesting internal soft tissues and mounting spiders for scanning electron microscopy. *Journal of Arachnology* **35**, 538-542.

Baker, A. (2003). Quantitative parsimony and explanatory power. *British Journal for the Philosophy of Science* **54**, 245–259.

Barker, D. (2015). Seeing the wood for the trees: philosophical aspects of classical, Bayesian and likelihood approaches in statistical inference and some implications for phylogenetic analysis. *Biology and Philosophy* **30**, 505–525.

Bidegaray-Batista, L., and Arnedo, M. A. (2011). Gone with the plate: the opening of the Western Mediterranean basin drove the diversification of ground-dweller spiders. *BMC Evolutionary Biology*, **11**, 317.

Bodner, M. R., and Maddison, W. P. (2012). The biogeography and age of salticid spider radiations (Araneae: Salticidae). *Molecular Phylogenetics and Evolution* **65,** 213–240.

Bremer, K. (1988) The limits of amino acid sequence data in angiosperm phylogenetic reconstruction. *Evolution* **42** (4), 795– 803.

Bryant, E. B. (1940). Cuban spiders in the Museum of Comparative Zoology. *Bulletin of the Museum of Comparative Zoology* **86**, 247-554.

Bryant, E. B. (1943) The salticid spiders of Hispaniola. *Bulletin of the Museum of Comparative Zoology* **92**, 445-529.

Bryant, E. B. (1950) The salticid spiders of Jamaica. *Bulletin of the Museum of Comparative Zoology* **103**, 163-209.

Cabra-García, J., and Brescovit, A. D. (2016). Revision and phylogenetic analysis of the orb-weaving spider genus *Glenognatha* Simon, 1887 (Araneae, Tetragnathidae). *Zootaxa* **4069** (1), 1-183. doi:10.11646/zootaxa.4069.1.1

Cabra-García, J., and Hormiga, G. (2019). Exploring the impact of morphology, multiple sequence alignment and choice of optimality criteria in phylogenetic inference: a case study with the Neotropical orb-weaving spider genus *Wagneriana* (Araneae: Araneidae), *Zoological Journal of the Linnean Society* **XX**, 1–176. doi: 10.1093/zoolinnean/zlz088

Čandek, K., Agnarsson, I., Binford, G. J., and Kuntner, M. (2019). Biogeography of the Caribbean *Cyrtognatha* spiders. *Scientific Reports* **9**: 397. doi:10.1038/s41598-018-36590-y

Čandek, K., and Kuntner, M. (2015). DNA barcoding gap: reliable species identification over morphological and geographical scales. *Molecular Ecology Resources* **15**, 268–277. doi: https://doi.org/10.1111/1755-0998.12304.

Cao, X.W., Liu, J., Chen, J., Zheng, G., Kuntner, M., and Agnarsson, I. (2016). Rapid dissemination of taxonomic discoveries based on DNA barcoding and morphology. *Scientific Reports*, **6**:1-13.

Ceccarelli, F.S., and Zaldívar-Riverón, A. 2013. Broad polyphyly and historical biogeography of the Neotropical wasp genus *Notiospathius* (Braconidae: Doryctinae). *Molecular Phylogenetics and Evolution*, **69**, 142–152.

Chakrabarty, P., Faircloth, B. C., Alda, F., Ludt, W. B., Mcmahan, C. D., Near, T. J., Dornburg, A., Albert, J. S., Arroyave, J., Stiassny, M. L. J., Sorenson, L., and Alfaro, M. E. (2017). Phylogenomic systematics of ostariophysan fishes: ultraconserved elements support the surprising nonmonophyly of characiformes. *Systematic Biology* **66**, 881–895.

Chamberland, L., McHugh, A., Kechejian, S., Binford, J. G., Bond J. E., Coddington, J., Dolman, G., Hamilton C. A., Harvey M. S., Kuntner, M., and Agnarsson, I. (2018). From Gondwana to GAARlandia: Evolutionary history and biogeography of ogre-faced spiders (*Deinopis*). *Journal of* Biogeography **45**, 2442–2457. https://doi.org/10.1111/jbi.13431

Crews, S.C., and Gillespie, R.G. (2010). Molecular systematics of *Selenops* spiders (Araneae: Selenopidae) from North and Central America: implications for Caribbean biogeography. *Biological Journal of the Linnean Society* **101**, 288–322.

Darriba, D., Taboada, G. L., Doallo, R., and Posada, D. (2012). jModelTest 2: more models, new heuristics and parallel computing. *Nature Methods* **9**, 772. doi:10.1038/nmeth.2109

Deler-Hernández, A., Sýkora, V., Seidel, M., Cala-Riquelme, F., and Fikáček, M. (2017). Multiple origins of the *Phaenonotum* beetles in the Greater Antilles (Coleoptera: Hydrophilidae): phylogeny, biogeography and systematics, *Zoological Journal of the Linnean Society*, **183**, 97–120, https://doi.org/10.1093/zoolinnean/zlx071

Dziki, A., Binford, G.J., Coddington, J.A., and Agnarsson, I. (2015). *Spintharus flavidus* in the Caribbean – a 30 million year biogeographical history and radiation of a 'widespread species'. *PeerJ* **3**, e1422.

Esposito, L.A., Bloom, T., Caicedo, L., Alicia-Serrano, A., Sanchez-Ruiz, J., May-Collado, L.J., Binford, G., Agnarsson, I. (2015). Islands within islands: diversification of tailless whip spiders (Amblypygi, Phrynus) in Caribbean caves. *Molecular Phylogenetics and Evolution* **93**, 107–117.

Ezard, T., Fujisawa, T., and Barraclough, T. (2009). SPLITS: species' Limits by Threshold Statistics. R Packag. version 1.0-14/r31. Available at: http://R-Forge.R-project.org/projects/splits/

Felsenstein J. (1978). Cases in which parsimony or compatibility methods will be positively misleading. *Systematic Zoology* **27**, 401–410.

Fernández, R., and Giribet, G. (2014). Phylogeography and species delimitation in the New Zealand endemic, genetically hypervariable harvestman species, *Aoraki denticulata* (Arachnida, Opiliones, Cyphophthalmi). *Invertebrate Systematic* **28**, 401–414. doi: http://dx.doi.org/10.1071/IS14009.

Folmer, O., Black, M., Hoeh, W., Lutz, R., and Vrijenhoek, R. (1994). DNA primers for amplification of mitochondrial cytochrome oxidase subunit I from diverse metazoan invertebrates. *Molecular Marine Biology and Biotechnology* **3**, 294–299.

Franganillo B., P. (1936)**.** Los arácnidos de Cuba hasta 1936. *Cultural La Habana*, 183 pp.

Fujisawa, T., and Barraclough, T.G. (2013). Delimiting species using single-locus data and the Generalized Mixed Yule Coalescent approach: a revised method and evaluation on simulated data sets. *Systematic Biology* **62**, 707–724.

Galiano, M. E. (1968). Revisión de los géneros *Acragas, Amycus, Encolpius, Hypaeus, Mago* y *Noegus* (Salticidae, Araneae). *Revista del Museo Argentino de Ciencias Naturales "Bernardino Rivadavia"* **2**, 267-360.

Giribet, G. (2003) Stability in phylogenetic formulations and its relationship to nodal support. *Systematic Biology* 52 (4), 554– 564.

Goicoechea, N., Frost, D.R., De la Riva. I., Pellegrino, K., Sites, J., Rodrigues, M.T., and Padial, J.M. (2016). Molecular systematics of teioid lizards (Teioidea/Gymnophthalmoidea:

Squamata) based on the analysis of 48 loci under tree-alignment and similarity-alignment. *Cladistics* **32**, 624–671.

Goloboff, P.A., and Pol, D. (2005). Parsimony and Bayesian phylogenetics. In "Parsimony, phylogeny, and genomics". (Ed V. Albert) pp. 148–159. (Oxford University Press: London, UK.)

Goloboff PA, Torres A, Arias JS. (2018a). Weighted parsimony outperforms other methods of phylogenetic inference under models appropriate for morphology. *Cladistics* **34**, 407–437.

Goloboff, P. A., and Catalano, S.A. (2016). TNT version 1.5, including a full implementation of phylogenetic morphometrics. *Cladistics* **32**, 221–238.

Goloboff, P.A, Farris, J.S. and Nixon, K.C. (2008a) TNT, a free program for phylogenetic analysis. *Cladistics* **24** (5), 774–786. http://dx.doi.org/10.1111/j.1096-0031.2008.00217.x

Goloboff, P.A. (1993) Estimating character weights during tree search. *Cladistics* **9** (1), 93–91. http://dx.doi.org/10.1111/j.1096-0031.1993.tb00209.x

Goloboff, P.A., Carpenter, J.M., Arias, J.S. and Miranda Esquivel, D.R. (2008b) Weighting against homoplasy improves phylogenetic analysis of morphological data sets. *Cladistics*, **24** (5), 758–773. http://dx.doi.org/10.1111/j.1096-0031.2008.00209.x

Goloboff, P.A., Farris, J.S., Källesjö, M., Oxelman, B., Ramírez, M.J. and Szumik, C.A. (2003) Improvements to resampling measures of group support. *Cladistics* **19** (4), 324–332.

Goodman, M., Olson, C. B., Beeber, J. E. and Czelusniak, J. (1982) New perspectives in the molecular biological analysis of mammalian phylogeny. *Acta Zoologica Fennica* **169**, 19–35.

Grant, T. and Kluge, A. (2008a) Credit where credit is due: The Goodman-Bremer support metric. *Molecular Phylogenetics and Evolution* **49** (1), 405–406.

Green, P. (1999). Phrap, version 0.990329. Distributed by the author. Available at http://www.phrap.org.

Green, P., and Ewing, B. (2002). Phred, version 0.020425 c. Distributed by the authors. Available at http://phrap.org.

Hebert, P. D. N., Cywinska, A., Ball, S. L., and Dewaard, J. R. (2003). Biological identifications through DNA barcodes. *Proceedings Biological Sciences* **270**, 313-321.

Hebert, P. D. N., Penton, E. H., Burns, J. M., Janzen, D. H. and Hallwachs, W. (2004b). Ten species in one: DNA barcoding reveals cryptic species in the neotropical skipper butterfly

Astraptes fulgerator. *Proceedings of the National Academy of Sciences of the United States of America* **101**, 14812-14817.

Hedin, M. C., and Maddison, W. P. (2001). A combined molecular approach to phylogeny of the jumping spider subfamily Dendryphantinae (Araneae: Salticidae). *Molecular Phylogenetics and Evolution* **18**, 386–403. doi:10. 1006/mpev.2000.0883

Holder, M. T., Sukumaran, J., and Lewis, P. O. (2008). A justification for reporting the majority-rule consensus tree in Bayesian phylogenetics. *Systematic Biology* **57**, 814–821.

Huelsenbeck, J. P., and Ronquist, F. (2001). MRBAYES: Bayesian inference of phylogenetic trees. *Bioinformatics* **17**, 754–755. doi: 10.1093/bioinformatics/17.8.754

Iturralde-Vinent, M. A., and MacPhee, E. D. R. (1996). Age and paleogeographical origin of Dominican amber. *Science* **273**, 1850– 1852.

Johns, G. C., and Avise, J. C. (1998). A comparative summary of genetic distances in the vertebrates from the mitochondrial cytochrome b gene. *Molecular Biology and Evolution*. **15**, 1481−1490.

Kalyaanamoorthy, S., Minh, B. Q., Wong, T. F. K., von Haeseler, A., and Jermiin, L. S. (2017). ModelFinder: fast model selection for accurate phylogenetic estimates. *Nature Methods* **14**, 587–589.

Katoh, K., and Standley, D.M. (2013). MAFFT multiple sequence alignment software version 7: improvements in performance and usability. *Molecular Biology and Evolution* **30**, 772–780.

Keyserling, E. (1885). Neue Spinnen aus America. VI. *Verhandlungen der Kaiserlich-Königlichen Zoologisch-Botanischen Gesellschaft in Wien* **34**, 489-534.

Kitching, I. J., Forey, P. L., Humphries, C. J., Williams, D. M. (1998). Cladistics: the theory and practice of parsimony analysis. 2nd ed. Oxford: Oxford University Press.

Klicka, J., and Zink, R. M. (1997) The importance of recent ice ages in speciation: A failed paradigm. *Science* **277**, 1666− 1669.

Kluge A. (2001b). Parsimony with and without scientific justification. Cladistics 17: 199–210.

Koch, N. M., and Gauthier J. A. (2018). Noise and biases in genomic data may underlie radically different hypotheses for the position of *Iguania* within Squamata. *PLoS ONE* **13**: e0202729.

Kolaczkowski B, Thornton JW. (2004). Performance of maximum parsimony and likelihood phylogenetics when evolution is heterogeneous. *Nature* **431**, 980–984.

Kolaczkowski, B., and Thornton J.W. (2009). Long-branch attraction bias and inconsistency in Bayesian phylogenetics. *PLoS ONE* **4**, e7891.

Lewis, D. S., Sperling, F. A. H., Nakahara, S., Cotton, A. M., Kawahara, A. Y., and Condamine, F. L. (2015). Role of Caribbean Islands in the diversification and biogeography of Neotropical *Heraclides swallowtails*. *Cladistics* **31**, 291–314.

Maddison, D. R., and Maddison, W. P. (2018a). Chromaseq: a Mesquite package for analyzing sequence chromatograms. Version 1.31. Available at http://chromaseq.mesquiteproject.org

Maddison, W. P. and Maddison, D.R. (2018b). Mesquite: a modular system for evolutionary analysis. Version 3.6. Available at http://mesquiteproject.org

Maddison, W. P., Bodner, M. R., and Needham, K. M. (2008). Salticid spider phylogeny revisited, with the discovery of a large Australasian clade (Araneae: Salticidae). *Zootaxa* **1893**, 46-64.

Maddison, W. P. (2015). A phylogenetic classification of jumping spiders (Araneae: Salticidae). *Journal Arachnology* **43**, 231-292.

Maddison, W.P., and Hedin, M.C. (2003). Jumping spider phylogeny (Araneae: Salticidae). *Invertebrate Systematics* **17**, 529-549.

Maddison, W.P., Evans, S. C., Hamilton, C. A., Bond, J. E., Lemmon, A. R., and Lemmon, E. M. (2014). The deep phylogeny of jumping spiders (Araneae, Salticidae). *ZooKeys* **440**, 57–87.

Matos-Maraví, P., Núñez Águila, R., Peña, C., Miller, J.Y., Sourakov, A., Wahlberg, N. (2014). Causes of endemic radiation in the Caribbean: evidence from the historical biogeography and diversification of the butterfly genus *Calisto* (Nymphalidae: Satyrinae: Satyrini). *BMC Evolutionary Biology* **14**, 199.

Mchugh A., Yablonsky C., Binford G., and Agnarsson I., (2014). Molecular phylogenetics of Caribbean *Micrathena* (Araneae: Araneidae) suggests multiple colonization events and single island endemism. *Invertebrate Systematics* **28**, 337-349

Miller, M. A., Pfeiffer, W., and Schwartz, T. (2010). Creating the CIPRES Science Gateway for inference of large phylogenetic trees. In 'Proceedings of the Gateway Computing Environments Workshop (GCE)'. pp. 1–8. (New Orleans, LA.)

Mittermeier, R. A., Robles-Gil, P., Hoffman, M., Pilgrim, J., Brooks, T., Mittermeier, C. G., Lamoreux, J., and da Fonseca, G. A. B. (2005). Hotspots revisited: earth's biologically richest and most endangered terrestrial ecoregions. (Agrupación Sierra Madre: Mexico).

Nguyen, L. T., Schmidt, H. A., von Haeseler, A., Minh, B. Q. (2015). IQ-TREE: a fast and effective stochastic algorithm for estimating maximum-likelihood phylogenies. *Molecular Biology and Evolution* **32**, 268–274.

Nixon, K. (2002). WinClada. Version 1.00.08. Available at http://www.cladistics.com/

Nylander, J. A., Ronquist, F., Huelsenbeck, J. P., Nieves-Aldrey, J. (2004). Bayesian phylogenetic analysis of combined data. *Systematic Biology* **53**, 47–67.

O'Reilly, J., Puttick, M., Parry, L., Tanner, A., Tarver, J., Fleming, J., Pisani, D., and Donoghue, P. (2016). Bayesian methods outperform parsimony but at the expense of precision in the estimation of phylogeny from discrete morphological data. *Biology Letters* **12**, 20160081.

Opatova, V., Bond, J. E., and Arnedo, M. A., (2013). Ancient origins of the Mediterranean trap-door spiders of the family Ctenizidae (Araneae, Mygalomorphae). *Molecular Phylogenetics and Evolution* **69**, 1135–1145. doi: http://dx.doi.org/10.1016/j.ympev.2013.08.002.

Ortiz D., and Francke O. F. (2016). Two DNA barcodes and morphology for multi-method species delimitation in *Bonnetina* tarantulas (Araneae: Theraphosidae). *Molecular Phylogenetics and Evolution* **101**, 176-193.

Padial, J. M., Grant, T., and Frost, D. R. (2014). Molecular systematics of terraranas (Anura: Brachycephaloidea) with an assessment of the effects of alignment and optimality criteria. *Zootaxa* **3825**, 001–132.

Peckham, G. W. and Peckham, E. G. (1885b). On some new genera and species of Attidae from the eastern part of Guatemala. *Proceedings of the Natural History Society of Wisconsin* **1885**, 62-86.

Petrunkevitch, A. (1930b). The spiders of Porto Rico. Part three. *Transactions of the Connecticut Academy of Arts and Sciences* **31**, 1-191.

Pons, J., Barraclough, T., Gomez-Zurita, J., Cardoso, A., Duran, D., Hazell, S., Kamoun, S., Sumlin, W., and Vogler, A. (2006). Sequence-based species delimitation for the DNA taxonomy of undescribed insects. *Systematics Biology* **55**, 595-609.

Posada, D., and Buckley, T. R. (2004). Model selection and model averaging in phylogenetics: advantages of Akaike Information Criterion and Bayesian Approaches over Likelihood Ratio Tests. *Systematic Biology* **53**, 793–808.

Prószyński, J. (1976) Studium systematyczno-zoogeograficzne nad rodzina Salticidae (Aranei) Regionow Palearktycznego i Nearktycznego. *Rozprawy Wyzszej Szkoly Pedagogicznej* **6**, 1- 260.

Prószyński, J., and Deeleman-Reinhold, C. L. (2012). Description of some Salticidae (Aranei) from the Malay Archipelago. II. Salticidae of Java and Sumatra, with comments on related species. *Arthropoda Selecta*, **21** (1), 29-60.

Rambaut, A., Suchard, M. A., Xie, D., and Drummond, A. J. (2014). Tracer v1.6. Available at http://beast.bio.ed.ac.uk/Tracer.

Ramírez, M. J. (2014). The morphology and phylogeny of dionychan spiders (Araneae: Araneomorphae). *Bulletin of the American Museum of Natural History* **390**, 1–374.

Ramírez, M. J. (2003) The spider subfamily amaurobioidinae (Araneae: Anyphaenidae): A phylogenetic revision at generic level. *Bulletin of the Museum of Natural History* **277**, 1–262.

Ricklefs, R., and Bermingham, E. (2008). The West Indies as a laboratory of biogeography and evolution. *Revue de zoologie et de botanique africaines* **2393**, 413. https://doi.org/10.1098/rstb.2007.2068.

Rindal, E., and Brower, A. V. (2011). Do model-based phylogenetic analyses perform better than parsimony? A test with empirical data. *Cladistics* **27**, 331–334.

Rodriguez, J., Pitts, J. P., von Dohlen, C. D. (2015). Historical biogeography of the widespread spider wasp tribe Aporini (Hymenoptera: Pompilidae). *Journal of Biogeography* **42**, 495–506.

Ronquist, F., and Huelsenbeck, J. P. (2003). MrBayes 3: Bayesian phylogenetic inference under mixed models. *Bioinformatics* **19**, 1572–1574.

Satler, J. D., Carstens, B. C., and Hedin, M. (2013). Multilocus species delimitation in a complex of morphologically conserved trapdoor spiders (Mygalomorphae, Antrodiaetidae, Aliatypus). *Systematic Biology* **62**, 805–823. http://dx.doi.org/10.1093/sysbio/syt041.

Scharaschkin, T. and Doyle, J. A. (2006) Character evolution in Anaxagorea (Annonaceae). *The American Journal of Botany* **93** (1), 36–54.

Schrago, C. G., Aguiar, B. O., Mello, B. (2018). Comparative evaluation of maximum parsimony and Bayesian phylogenetic reconstruction using empirical morphological data. *Journal of Evolutionary Biology* **31**, 1477–1484.

Simon, E. (1901a)**.** *Histoire naturelle des araignées. Deuxième édition, tome second*. Roret Paris, 381-668. doi:10.5962/bhl.title.51973

Stamatakis, A. (2014). RAxML version 8: a tool for phylogenetic analysis and post-analysis of large phylogenies. *Bioinformatics* **30**, 1312–1313.

Stamatakis, A. (2006). RAxML-VI-HPC: Maximum Likelihood-based Phylogenetic Analyses with Thousands of Taxa and Mixed Models. *In Bioinformatics* **22** (21), 2688-2690.

Tamura K., Stecher G., Peterson D., Filipski A., and Kumar S. (2013). MEGA6: Molecular Evolutionary Genetics Analysis version 6.0. *Molecular Biology and Evolution* **30**, 2725-2729.

Tong, Y., Binford G. J., Rheims C. A., Kuntner, M., Liu, J., and Agnarsson, I. (2019). Huntsmen of the Caribbean: Multiple tests of the GAARlandia hypothesis. *Molecular Phylogenetics and Evolution* **130**, 259-268. doi: 10.1016/j.ympev.2018.09.017.

Wahlberg, N. (2006). That awkward age for butterflies: insights from the age of the butterfly subfamily Nymphalinae (Lepidoptera: Nymphalidae). *Systematic Biology* **55**, 703–714.

Wahlberg, N., and Freitas, A.V. (2007). Colonization of and radiation in South America by butterflies in the subtribe Phyciodina (Lepidoptera: Nymphalidae). *Molecular Phylogenetics and Evolution* **44**, 1257–1272.

Ward, R.D., Zemlak, T.S., Innes, B.H., Last, P.R., and Hebert P.D.N. (2005). DNA Barcoding Australia´s Fish Species. *Philosophical Transactions of the Royal Society of London. Serie B: Biological Science* **360**,1847-1857.

Whelan, N. V., Kocot, K. M., Moroz, L. L., and Halanych, K. M. (2015). Error, signal, and the placement of *Ctenophora* sister to all other animals. *Proceedings of the National Academy of Sciences of the United States of America* **112**, 5773–5778.

World Spider Catalog (2020). "World Spider Catalog", version 21.0 (Natural History Museum Bern). Available at http://wsc.nmbe.ch. doi: 10.24436/2

Wright, A., and Hillis, D. (2014). Bayesian analysis using a simple likelihood model outperforms parsimony for estimation of phylogeny from discrete morphological data. *PLoS ONE* **9**, e109210.

Wunderlich, J. (1988). "Die fossilen Spinnen im Dominikanischen Bernstein". (Published by the author Straubenhardt: Germany).

Wunderlich, J. (2004). Fossil jumping spiders (Araneae: Salticidae) in Baltic and Dominican amber, with remarks on Salticidae subfamilies. In "Fossil spiders in Amber and Copal - Fossile Spinnen in Bernstein und Kopal". (Ed. J. Wunderlich) 3 (A), pp. 1761-1819 (Beiträge zur Araneologie: Hirschberg, Leutershausen.)

Zhang, G., Basharat, U., Matzke, N., and Franz, N.M. (2017). Model selection in statistical historical biogeography of Neotropical insects – the Exophthalmus genus complex (Curculionidae: Entiminae). *Molecular Phylogenetics and Evolution* **109**, 226–239.

Zhang, J., Kapli, P., Pavlidis, P., and Stamatakis, A., (2013). A general species delimitation method with applications to phylogenetic placements. *Bioinformatics* **29** (22), 2869–2876.

Zhang, J. X., and Maddison, W. P. (2012). New euophryine jumping spiders from the Dominican Republic and Puerto Rico (Araneae: Salticidae: Euophryinae). *Zootaxa.* **3476**,1-54.

Zhang, J. X., and Maddison, W. P. (2013). Molecular phylogeny, divergence times and biogeography of spiders of the subfamily Euophryinae (Araneae: Salticidae). *Molecular Phylogenetics and Evolution* **68**, 81-92.

Zhang, J.X., and Maddison, W.P. (2015). Genera of euophryine jumping spiders (Araneae: Salticidae), with a combined molecular-morphological phylogeny. *Zootaxa*. **3938**, 1-147.

CAPÍTULO 4

ISLAND-TO-ISLAND VICAREANCE, FOUDER-EVENT, AND WITHIN-AREA SPECIATION, THE BIOGEOGRAPHY OF THE ANTILLATTUS CLADE (SALTICIDAE: EUOPHRYINI)

Island-to-island vicariance, founder-event and within-area speciation, the biogeographal history of the Antillattus clade (Salticidae: Euophryini)

Cala-Riquelme, Franklyn; Programa de Postgrado Doctorado en Ciencias-Biología, Universidad Nacional de Colombia, Bogotá, Colombia. Email: franklyncalariquelme@gmail.com

Wiencek, Patrick; Department of Biology, 120 A, Marsh Life Science Building, Burlington, VT 05405-0086 USA. Email: wiencek.patrick@gmail.com

Flores-Daza, Eduardo; Grupo de estudios de Arácnidos & Miriápodos, Instituto de Ciencias Naturales, Universidad Nacional de Colombia, Bogotá, Colombia. Email: aeflorezd@unal.edu.co

Binford, Greta; Department of Biology, Lewis and Clark College, Portland, OR, USA. Email: binford@lclark.edu

Agnarsson, Ingi; Department of Biology, 120 A, Marsh Life Science Building, Burlington, VT 05405-0086 USA. Email: iagnarsson@gmail.com

Abstract

The Caribbean Archipelago is a biodiversity hotspot that plays a key role in developing our understanding of how dispersal ability affects species formation. In island systems, species with intermediate dispersal abilities tend to exhibit greater diversity, as may be the case for many of the salticid lineages of the insular Caribbean. Here, we examine patterns of diversification in the Antillattus clade and their diversification within and among islands of the Caribbean Archipelago. We used three markers (COI, 16S and 28S) and Bayesian approaches (Mr. Bayes, BEAST, BioGeoBEARS) to infer phylogenetic relationships and biogeographic history of the Antillattus clade. To understand the origin and the timing of colonization of the group, we tested the hypotheses that connections via a landbridge (GAARlandia) and post-GAARlandia overwater dispersal events explain the Antillattus clade's diversity in the Greater Antilles. The ancestor of the Antillattus clade appears to have colonized the Caribbean via GAARlandia, while the diversification between taxa from Cuba, Hispaniola and Puerto Rico appears to have originated by vicariance, founder-events and within-island speciation. Hispaniola was colonized from the N.S. America, and in turn seems to be the nucleus from where Cuba and Puerto Rico were colonized. Time tree analysis and model-based BioGeoBEARS analyses of ancestral ranges estimated that the clade, diverged c. 18 Mya,

probably from the Hispaniola ancestor that subsequently colonized Cuba via the Windward Passage. Finally, multiple dispersal events (founder-events) between Cuba and Hispaniola during the Middle-Miocene and the Late-Miocene occurred in *Antillattus* and *Truncattus* species.

Keywords. Caribbean biogeography, molecular dating, ancestral range analysis, endemics, founder-event, intermediate dispersion model.

4.0 Introduction

Biological diversity is expressed geographically as a complex mosaic of species distributions that are the product of geological history and speciation (Gittenberger 1991; Kozak *et al*. 2006; Rundell and Price 2009). An ancestral species might find itself in the presence of an ecological opportunity by: 1) colonization of isolated areas, such as *de novo* islands or newly formedlakes or mountaintops; 2) emergence of a new resource; or the 3) the development of a feature that provides the species with access to newly available resources (Carlquist 1974; Leigh *et al*. 2007; Losos and Ricklefs 2009; Schluter 2000; Simpson 1953), each of which could lead to speciation (Coyne and Orr 2004; Nosil 2012; Schluter 2009; Stroud and Losos 2016).

Since Darwin and Wallace, evolutionary biologists have been fascinated by the extraordinary diversity and richness of islands. This interest has increased due to the use of molecular methods in phylogenetics and biogeography (Agnarsson and Kuntner 2012; Dávalos 2004; McHugh et al. 2014; Ricklefs and Bermingham 2008) and theories like long-distance dispersal, vicariance and intermediate dispersal models being used to explain speciation events (Agnarsson, *et al*. 2014; Cowie and Holland 2006; De Queiroz 2005; Gillespie and Roderick 2002; Gillespie *et al*. 2012; Weaver *et al*. 2016).

The Greater Antilles are one of the planet's recognized biodiversity hotspots (Mittermeier *et al.* 2005; Ricklefs and Bermingham 2008). The area is complex both geologically (e.g. landbridge islands, volcanics, uplifted coral shelves) and geographically, make it an important model system for studying dispersal/colonization, and vicariance as mechanisms for the origin of diversity, both between and within-islands (Agnarsson, *et al*. 2014; Claramunt *et al*. 2012; Crews and Gillespie 2010; Deler-Hernandez *et al*. 2017; Diamond *et al*. 1976; Dziki *et al*. 2015; Esposito *et al*. 2015; Iturralde-Vinent 2006; McHugh *et al*. 2014; Zhang and Maddison 2013) (fig. 4.0).

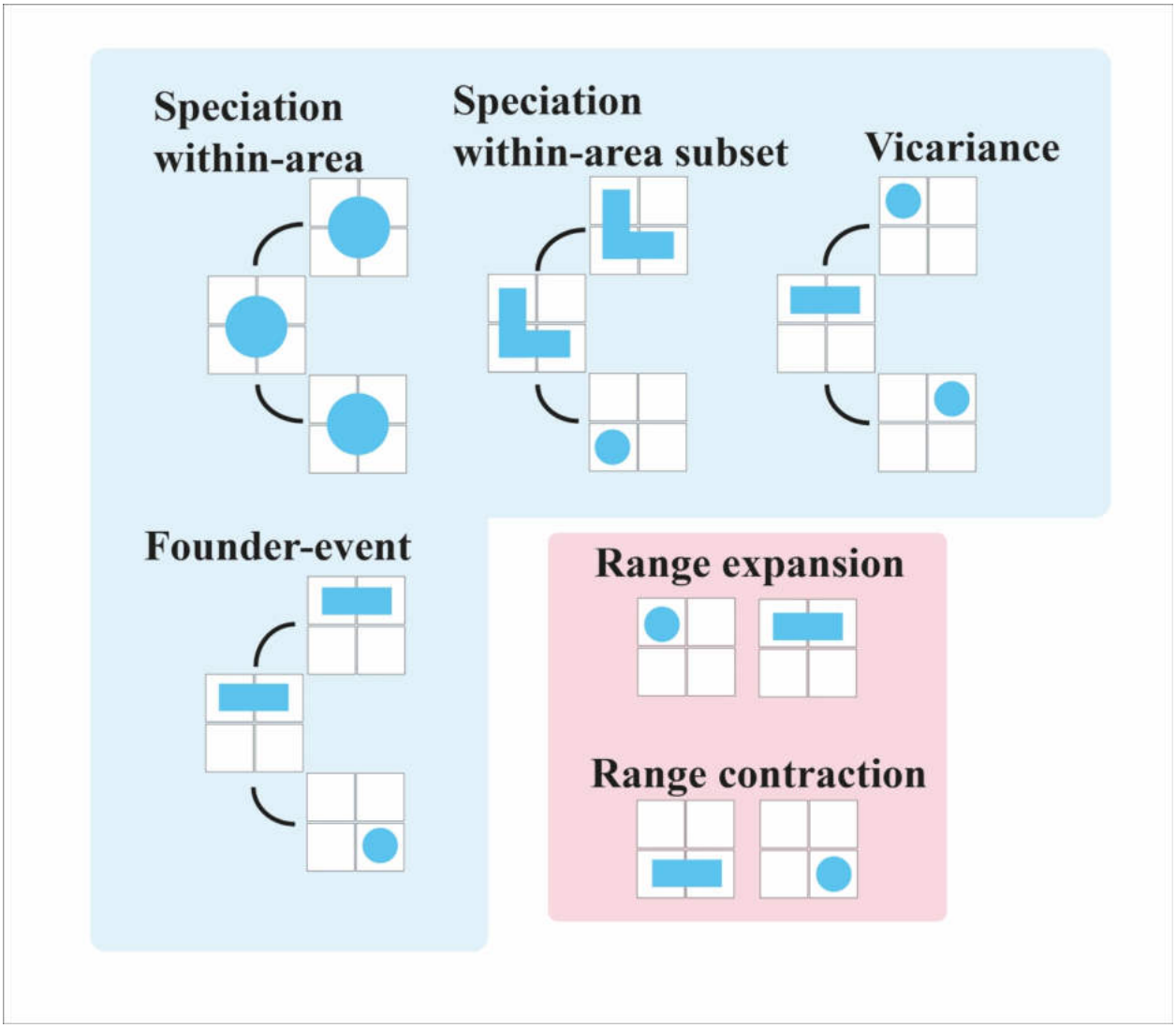

Figure 4.0. Diagrams of different biogeographical events assumed by the different models tested in this study [adapted from Matzke (2015)]. Cladogenetic events include within-area speciation, vicariance and founder events. Anagenetic events include range expansion and range contraction.

The proto-Antilles emerged as a volcanic arc during the Cretaceous-Early Eocene (*c*. 65-55 Mya) on the eastward moving Caribbean Plate in a period of maximum land and minimum sea. (Iturralde-Vinent and MacPhee 1999; Iturralde-Vinent 1982, 2006; MacPhee and Iturralde-Vinent 1994, 1995, 2000; Mann *et al*. 1990; Pindell and Barrett 1990; White and MacPhee 2001). Durante el Eoceno Cretácico-Temprano (c. 65-55 Mya), plataformas, crestas, tierras bajas, pozos y archipiélagos de islas volcánicas (Iturralde-Vinent y MacPhee, 1999).

The uplift of the core Greater Antilles began during the Middle Eocene (*c*. 48-37 Mya) and reached its maximum land area at the Eocene-Oligocene (*c*. 40-30 Mya) boundary. Island

area was reduced when sea level was higher in the Late-Oligocene to Middle-Miocene (c. 28-15 Mya), but the islands remained exposed, possibly with exception of parts of present-day Jamaica and Hispaniola which are believed to have emerged permanently during the Neogene (Iturralde-Vinent and MacPhee 1999; Iturralde-Vinent 2006). According to Iturralde-Vinent and MacPhee (1999), GAARlandia connected the northern portion of South America with the Caribbean islands.

The origin of the present-day terrestrial biota of the Greater Antilles has been explained by three possible hypotheses. The first hypothesis assumes that ancestral lineages colonized the Caribbean volcanic arc (closely spaced islands on the leading edge of the Caribbean) during the Upper Cretaceous and the Early Paleocene (*c*. 100-65 Mya), and survived there as relics until the present (Iturralde-Vinent 1982; Iturralde-Vinent and MacPhee 1999; Rosen 1975 1985; Tada *et al.* 2003). The second hypothesis assumes long-distance over-water dispersal events between land masses during the Cenozoic (*c*. 55-3 Mya) (Hedges 2001, 2006; Hedges *et al*. 1992) as occurred in *Solenodons* (Sato *et al*. 2016), Urocoptid snails (Uit de Weerd *et al*. 2016), or *Micrathena* spiders (Crews and Esposito 2020; McHugh *et al*. 2014). A third hypothesis assumes the existence of the GAARlandia (GAAR = Greater Antilles Aves Ridge) a landbridge hypothesized to have existed 35 to 32 Mya, briefly connecting the Greater Antilles and continental South America during the Eocene-Oligocene transition (Iturralde-Vinent and MacPhee 1999; MacPhee and Ituralde- Vinent 2000). This geologic hypothesis predicts the near-simultaneous colonization of multiple lineages over a relatively short time (Alonso *et al*. 2012; Říčan *et al*. 2013; Weaver *et al*. 2016) as occurred in Peltophryne toads (Alonso *et al*. 2012), poecilid fishes (Weaver *et al*. 2016), cichlids (Říčan *et al*. 2013), or deinopis/spintharus/ sparassid spiders (Chamberland *et al*. 2018; Dziki *et al*. 2015; Tong *et al*. 2019). According to MacPhee and Ituralde- Vincent (2000), a two-part GAARlandia (combining dispersal-vicariance model) landspan model of is consistent with most aspects of Antillean land-mammal biogeography as currently known. In brief, the GAARlandia hypothesis (c. 35-32) allows for a brief phase of dispersal c.30-32 Ma from northern South America into the future northern Greater Antilles via a landspan. This form of vicariance (described as "island-to-island" vicariance, in contradistinction to the "continent-island" vicariance of Rosen) is a parsimonious explanation for the astounding similarity in post-Miocene land-mammal faunas across the northern Greater Antilles (MacPhee and Ituralde-Vinent 2000).

Greater Antilles colonization is not always explained by the GAARlandia, vicariance or long-distance-dispersal (Iturralde-Vinent 2006; Iturralde-Vinent and MacPhee 1999) and remain in active debate (Ali 2012; Hedges 2006; MacPhee and Iturralde-Vinent 2005). Rare overwater dispersal (and founder-events) (Agnarsson *et al*. 2016; Censky *et al*. 1998; Cowie and Holland 2006, Dávalos 2004; Gillespie *et al*. 2012; Hedges 2001; McHugh *et al*. 2014) may better explain the timing of arrival and pattern of some taxa and their speciation.

The above scenarios have been tested by phylogenetic studies. In the last decade there has been an increase in phylogeographic studies with insects (Ceccarelli and Zaldívar-Riverón 2013; Deler-Hernández *et al*. 2017; Lewis *et al*. 2015; Matos-Maravi *et al*. 2014; Rodriguez *et al*. 2015; Wahlberg 2006; Wahlberg and Freitas 2007; Zhang *et al*. 2017) and arachnids (Agnarsson *et al*. 2016; Čandek *et al*. 2019; Chamberland *et al*. 2018; Crews and Gillespie 2010; Dziki *et al*. 2015; Esposito *et al*. 2015; McHugh *et al*. 2014; Tong *et al*. 2019, Zhang and Maddison 2013)

Jumping spiders (Salticidae) constitute a diverse, globally distributed group of species (*c*. 6080 total species) (World Spider Catalog 2020). Within Salticidae, euophryines are a relatively young group (*c*. 33-30 Mya) (Zhang and Maddison 2013). Phylogenetic reconstruction shows that much like other salticid lineages (Bodner and Maddison 2012; Maddison and Hedin 2003; Maddison *et al*. 2008), New and Old-World euophryines are grouped into separate clades, indicating that most euophryine diversification occurred intra-continentally (Zhang and Maddison 2013). In revisionary work focused on euophryines, Zhang and Maddison (2013) highlighted the Antillattus clade as one of several salticid clades represented in the Caribbean. The Antillattus clade includes the genera *Antillattus* Bryant (1943), *Truncattus* Zhang and Maddison (2012) and *Petemathis* Prószyński and Deeleman-Reinhold (2012) (Zhang and Maddison 2013, 2015).

Here, we examine the biogeographic history of Antillattus clade. We test the GAARlandia hypothesis as the colonization route to the Greater Antilles. We also aim to reconstruct the historical biogeography of the Antillattus clade´s genera, and we test hypotheses of 1) overwater dispersal (founder-event), and 2) within-island speciation as possible explanations for the diversity observed in the Greater Antilles. We infer the ancestral ranges of the Antillattus clade species based on a newly constructed, time-calibrated molecular phylogeny. The analysis is based on three gene fragments and includes sixty-three ingroup terminals. Using BioGeoBEARS, we use probabilistic inference to test the relative fit of three biogeographic models with and without a jump dispersal parameter ‘‘j”.

4.1 Materials and methods

4.1.0 Taxon sample

One-hundred-ten specimens were collected using beating methods in Cuba, Puerto Rico and Hispaniola (supplementary figure 1, table 1). The material collected was fixed in 95% ethanol. Caribbean voucher specimens will be deposited in the University of Vermont's Natural History Museum and Smithsonian Institute.

4.1.1 DNA extraction, amplification and sequencing

Outgroup selection was based on the phylogeny proposed by Zhang and Maddison (2013). As primary outgroups, we added the DNA barcodes from *Cobanus*, *Mexigonus*, *Sidusa*, *Brythocrotus*, *Compsodecta* and *Agobardus* and from the Antillattus clade (*Petemathis*, *Truncattus* and *Antillattus*) (Zhang and Maddison 2013, 2015). Taxon sample information is included in supplementary table 1.

DNA was isolated with the Qiagen DNeasy Tissue Kit (Qiagen, Valencia, CA, USA). We sequenced fragments of COI, 16S and 28S. We amplified COI with LCO1490 (GGTCAACAAATCATAAAGATATTGG) (Folmer *et al*. 1994) and C1-N-2776 (GGATAATCAGAATATCGTCGAGG) (Hedin and Maddison 2001). The fragment of 16S was amplified with 16SA/12261 (CGCCTGTTTACCAAAAACAT) (Folmer *et al*. 1994) and 16SB (CCGGTTTGAACTCAGATC) (Hedin and Maddison 2001). The 28S fragment was amplified with 28SO (TCGGAAGGAACCAGCTACTA) and 28SC (GAAACTGCTCAAAGGTAAACGG). For COI, 16S and 28S, the polymerase chain reaction (PCR) was performed with an initial denaturation at 94ºC for 2 min, followed by 40 cycles of denaturation at 94 ºC for 25 sec, annealing at 50ºC (first round)/ 44.5ºC (second round) for 25 sec and extension at 65ºC for 2 min (first round)/ 1 min (second round); with a final extension at 72ºC for 10 min. Amplified fragments were sequenced in both directions using Sanger sequencing at GENEWIZ's New Jersey facility. The forward and reverse reads were interpreted with Phred and Phrap (Green 1999; Green and Ewing 2002) via Chromaseq v. 1.31 (Maddison and Maddison 2018a) in Mesquite v. 3.6 (Maddison and Maddison 2018b) using default parameters.

4.1.2 Sequence alignment

Alignments were performed in MAFFT (Katoh and Standley 2013) using L-INS-I with a parameter 1PAM / k = 200, a GAPs opening penalty of 1.53, and a configuration of 100. Gaps were treated as missing characters. The dataset was partitioned by gene (in the case of COI by codon), and the appropriate substitution model for each partition was selected with jModeltest 2.1.10 (Darriba *et al.* 2012) using the Akaike information criterion (Posada and Buckley 2004) to select among the 24 models that can be implemented in MrBayes (table 4.0).

Table 4.0. Substitution models selected by jModelTest for each individual gene region and partition.

Partition	Substitution model
16S	TIM3+G (012032)
COI 1st -2nd codons	GTR+I+G (012345)
COI 3rd codon	TVM+I+G (012314)
28S	GTR+G (012345)

4.1.3 Phylogenetic inference

RAxMLHPC v8.2.12 (Stamatakis 2006, 2014) was used to perform maximum likelihood analysis for the individual and combined gene matrices, each with 500 replicates under the assumptions of the GTRGAMMAI model (raxmlHPC-PTHREADS.exe -T 2 -f a -x 897 -m GTRGAMMAI -p 335 -N 500 -o Ghelna_canadensis -s MLDNA.phy -n MLDNA.tre -O -w). Bootstrap analyses were also carried out to calculate the replicability of the clades in a separate execution of RAxML with 1000 replicates. Finally, we used the CIPRES online portal (Altekar *et al.* 2004; Miller *et al.* 2010) to run a DNA and combined (molecular and morphology) Bayesian analysis with MrBayes v. 3.2.6 (Huelsenbeck and Ronquist 2001; Ronquist and Huelsenbeck 2003). We ran the Markov chain Monte Carlo (MCMC) with four chains for 25,000,000 generations, sampling every 1000 generations, with a sampling frequency of 100 and a burn-in of 25%. The results were examined in Tracer v.1.6 (Rambaut *et al.* 2014) to verify proper mixing of chains, that stationarity had been reached, and to determine adequate burn-in. All resulting trees were interpreted in FIGTREE v.1.4.2 and edited in Adobe Illustrator CS6.

4.1.4 Time calibration

The age of Euophryini (between 30.19 Mya [95% highest posterior density (confidence interval): 37.84–28.93 Mya] and 33.84 Mya [95% highest posterior density (confidence interval): 55.52–23.10 Mya].) and the age of the Antillattus clade (between 19.74

Mya [95% highest posterior density (confidence interval): 25.49–14.79 Mya] and 22.34 Mya [95% highest posterior density (confidence interval): 36.83–14.77 Mya]) were constrained following the results of the time tree analysis of Euophryini performed by Zhang and Maddison (2013) based on a wide spectrum of fossil calibrations. We used Bayes Factors (table 4.1) to test alternative clock models (non-clock, strict clock, relaxed clock) using a stepping-stone method (Xie *et al.* 2011) as implemented in MrBayes 3.2.7a (Ronquist and Huelsenbeck 2003; Ronquist *et al*. 2012).

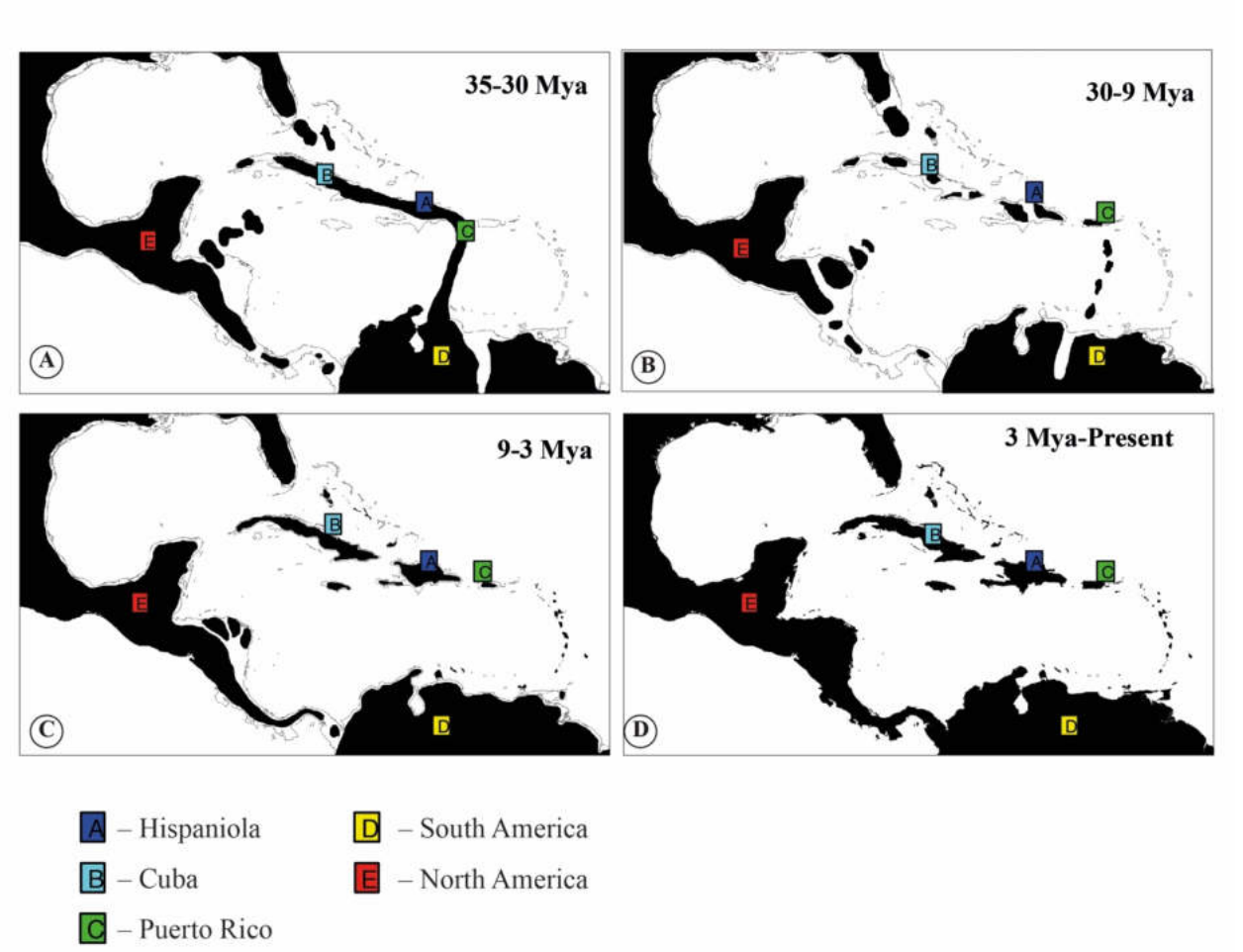

Figure 4.1. Maps (A–D) show simplified continent and island positions in the respective time window used for the time-stratified analysis. A – Hispaniola; B – Cuba; C – Puerto Rico; D – South America; E –North America

4.1.5 Divergence estimation

Node ages were estimated with BEAST 1.8.4 (Drummond *et al*. 2012) under a lognormal relaxed clock model (Battistuzzi *et al*. 2011) with a COI substitution rate parameter (ucld.mean) as a normal prior (mean=0.0112 and s.d.=0.001) (Bidegaray-Batista and Arnedo

2011) and estimated substitution rate parameter for 28S and 16S. The analysis ran for 10,000,000 generations with a birth-death process (Gernhard 2008) under a GTR+G+I model, with default options for all other prior and operator settings. The results were examined in Tracer 1.7 (Rambaut *et al*. 2014) to determine burn-in and to check for stationarity. The final consensus tree was produced in TreeAnnotator v1.8.4, with 25% burn-in.

Table 4.1. Results of the molecular clock tests: analyses of 75 terminal

	non-clock	strict	relaxed	relaxed_birthDeath
1	22601.4	22580.5	22460.1	22416.3563
2	22570.9	22522.7	22424.4	22339.4587
mean	22586.15	22551.6	22442.25	**22373.6891**

4.1.6 Biogeographical reconstruction

For ancestral range estimation of the Antillattus clade, we used the tree resulting from the divergence dating analysis as the input tree. As inter-island divergences are present in our phylogeny, we coded the Caribbean islands in their past shape, considering their historical composition of multiple paleo-islands (Iturralde-Vinent and MacPhee 1999). The distribution ranges were divided into the following five areas: A – Hispaniola; B – Cuba; C – Puerto Rico; D – South America; E –North America (fig. 4.1, A-D). We carried out the ancestral range estimation in the R package BioGeoBEARS (Matzke 2014) to test different time periods and infer which are more likely with base of the model's configuration. This package tests three models in a maximum likelihood framework with various parameters that can be altered to test specific scenarios: a DEC model (Ree and Smith 2008), a DIVALIKE model (likelihood version of the DIVA model: Ronquist 1997) and a BAYAREALIKE model (likelihood version of the BayArea model: Landis *et al*. 2013). Moreover, each model is available in its original version and with an additional parameter *+j* representing jump dispersal, or a founder event, which is speciation following long-distance dispersal; six base models are available in total.

We conducted non-time-stratified and time-stratified analyses to estimate ancestral range distribution on given nodes. Unconstrained non-stratified analyses were done using default parameter values. For time-stratified analyses, time periods were defined as follows to reflect the paleogeography of the area in each period (Deler-Hernández *et al*. 2017; Iturralde-Vinent 2006; Matos-Maraví *et al*. 2014; O'Dea *et al.* 2016): (1) 9 My-present: Plio-Pleitosene to present configuration; (2) 15-9 Mya: the Greater Antilles significantly reduced in area and widely separated from South America by deep sea (3) 23-15 Mya: Windward Passage (4) 28-23 Mya: Mona Passage (5) 32-30: GAARlandia hypothesis allows for a brief phase of dispersal

from northern South America into the future northern Greater Antilles via a landspan (MacPhee and Iturralde-Vinent 2000).

Finally, dispersal probabilities were set to reflect paleogeography as follows: they were set to 0.8 when two areas were adjacent, to 0.5 when two areas were weakly separated by a geographical barrier, to 0.2 when two areas were separated by water over a distance less than 200 km, to 0.05 for connection by island chain (e.g. Lesser Antilles) or intermediate island (e.g. Hispaniola between Cuba and Puerto Rico), 0.001 for long-distance dispersal (areas separated by more than 200 km from sea), and to 0.0001 when dispersal was not possible by the lack area availability (we followed the BioGeoBEARS manual in setting extremely low rather than zero probabilities). Models of both non-time-stratified and time-stratified analyses were compared using likelihood values and the Akaike information criterion corrected for small sample sizes (AICc) (Matzke 2013).

4.2 Results

4.2.0 Phylogeny and divergence time

Our Bayesian phylogeny supports the Antillattus clade (fig. 4.2). The phylogeny recovered *Bryanattus*, *Pensacolatus* and *Petemathis* as single island monophyly. The lineages of *Antillattus* and *Truncattus* are shared between Hispaniola and Cuba. The genetic structure reflects patterns consistent with historical island connectivity. Like the The BI phylogeny also recovered the Puerto Rican species as sister to Hispaniola and Cuban Antillattus clade members and the close relationships of *Pensacolatus*, *Bryanattus* and *Antillattus*.

The chronogram of the Antillattus clade is presented in figure 4.2, with branch lengths as the median estimated age. This reconstruction is supported by the birth-death process derived chronogram with a relaxed clock model as the best-fitting clock model. BEAST indicates that the first divergence between the Antillatus clade and others happened in the Oligocene (*c*. 31 Mya); and most of the subsequent divergences happened in the Oligocene to Pliocene (*c*. 27-3 Mya). The lineage leading to *Petemathis* diverged during the late Oligocene (*c.* 24 Mya). The divergence of the lineages leading to *Truncattus*, *Antillattus* and *Pensacolattus* were dated to the early Miocene (*c.* 22 Mya, *c.* 20 Mya and *c.* 18 Mya respectively) and the lineage leading to *Bryanattus* appears in the middle Miocene (*c.* 13 Mya). The *Antillattus* and *Truncattus* species of Cuba and Hispaniola share a common ancestor during the Middle Miocene (*c.* 12 Mya). In our BEAST analysis, the maximum credibility tree is similar to the MLtree from the

RAxML analysis and the BI tree from the MrBayes analysis. The posterior probability values from our BEAST analyses are similar to those in the unconstrained MrBayes analysis.

4.2.1 Biogeographic analysis

The estimation of ancestral ranges suggests that the most recent common ancestor of Antillattus clade in our dataset most likely resided in Northern South America (fig. 4.2). The Antillattus clade seems to have originated in Hispaniola (fig. 4.2) and colonized Puerto Rico and Cuba. The Antillattus clade likely diverged from an ancestor from Northern South America (fig. 4.3). We implemented the basic models (DEC, DIVALIKE and BAYAREALIKE) plus the founder-event parameter j and tested whether vicariance, or overwater dispersal (founder-events), better explained the colonization of the Greater Antilles. According to the best-fitting model, the ancestor to the Antillattus clade dispersed to the Caribbean from mainland South America = during the existence of the GAARlandia land bridge, but the radiation of Antillattus clade (Fig. 4.3) occurred after the subsidence of the GAARlandia land bridge. The biogeographical hypothesis testing in BioGeoBears identified differences between the basic models and founder-event models (Table 4.1). Models that incorporated the j parameter fit the data better than those that didn't allowing for jump dispersal (Table 4.0). The favored model was the stratified DEC+j among all tested models (log likelihood: LnL = -44.20; parameter estimates: d = 0, e = 0 and j = 0.0153) (Table 4.0). but this was not statistically different from the non-time-stratified DIVALIKE+ j (log likelihood: LnL = -44.55; parameter estimates: d = 0, e = 0 and j = 0.018) models were equally probable.

4.2.2 Estimation of biogeographical events

The BioGeoBEARS stochastic map (BSM) based on 50 stochastic historical map estimates between 74 and 78.62 biogeographic events (fig. 4.4 and fig. 4.5). Of those, between 4.62 and 4.72 were exclusively anagenetic events, and 74 were cladogenetic events representing within-area speciation (84%), within-area speciation subset (2%), founder-event (11%) and vicariance (3%) (tables 4.2 and 4.3).

Evidence suggests that the ancestor of the Antillattus clade could have come from Northern South America to the Greater Antilles, followed by a Caribbean radiation. Focusing on dispersal events, we found that the patterns in the Greater Antilles reflect a core in Hispaniola. According to BSM, the principal dispersal events must have taken place as follows: a major movement from Hispaniola to Cuba (range expansion: 2.84, founder-event: 4.62), Cuba to Hispaniola (0.64, 1.08), Hispaniola to Puerto Rico (0.26, 0.54), Puerto Rico to Hispaniola

(0.08, 0), and Cuba to Puerto Rico (0.02, 0.04). Overall, Hispaniola was the source for 67% of the estimated dispersal events (Fig. 4.3).

4.2.3 GAARlandia hypothesis

We tested if the GAARlandia hypothesis could explain the colonization of the Caribbean. The results suggest that the fauna of the Greater Antilles and South America (fig. 4.3) were separated as a result of vicariance (*c.* 31 Mya). This is consistent with the ancestors of the Antillattus clade colonizing the Greater Antilles from South America during or just before the proposed time-frame of GAARlandia (see, Iturralde-Vinent and MacPhee 1999). Consequently, our results reject the vicariance hypothesis of Rosen.

4.2.4 Founder-event hypothesis

Our analyses indicate that between *c.* 27-13 Mya a series of founder-events (+ j) occurred followed by within-island speciation. We also found evidence of founder-events in Puerto Rico, Cuba and Hispaniola, including recent events between Cuba and Hispaniola (*c.* 12 Mya) (fig. 4.3).

4.3 Discussion

4.3.0 GAARlandia

The proximity of some Caribbean islands to nearby South America has facilitated the biotic exchange between these regions. The GAARlandia hypothesis (Iturralde-Vinent and MacPhee 1999) (Greater Antilles + Aves Ridge) as an available colonization route has been a point of debate in recent decades (Ali 2012; Hedges 1996, 2006). The main discussion focuses on the timeframe of the connection between the Antilles and Northern South America, the lack of geologic evidence, and the lack of South American representatives for many groups in the Caribbean (Ali 2012; Hedges 1996, 2006).

Our data suggest that the Antillattus clade colonized the Greater Antilles once (fig. 4.2) and support

the South American origin via GAARlandia. This is incongruent with the vicariance hypothesis of Rosen (1975, 1985), which assumes that Caribbean lineages originated by the colonization of the proto-Antillean volcanic arc in the Late Cretaceous (c. 65.5 Mya) and survived the K-Pg boundary.

Other studies have found the GAARlandia hypothesis valid as a route of colonization to the Antilles with estimated times between *c.* 35 and *c.* 32 Mya (spiders (Binford *et al*. 2008;

Crews and Gillespie 2010; Chamberland *et al*. 2018; McHugh *et al*. 2014), scorpions (Esposito and Prendini 2019), beetles (Deler-Hernández *et al*. 2018; Zhang *et al.* 2018) frogs (Alonso *et al*. 2012) and freshwater fish (Říčan et al. 2013; Weaver *et al*. 2016). The two-part GAARlandia landspan model of MacPhee and Iturralde-Vinent (2000) is consistent with most biogeographic aspects. 1) a brief phase of dispersal c.32-30 Mya from northern South America into the future northern Greater Antilles via a landspan; accompanied of a strong filter, permitting only a few lineages to successfully cross and establish themselves, followed by a radical reduction in dispersal opportunity as the landmass subsided; and finally, 2) by island-to-island vicariance event. We consider the combined dispersal-vicariance hypothesis of GAARlandia (MacPhee and Iturralde-Vinent 2000) as the most parsimonious explanation about the origin of the Antillattus clade.

4.3.1 Inter-island biogeographical history

Founder-events are increasingly recognized as mechanisms that shape the distribution of organisms on islands (e.g. Gillespie *et al*. 2012; de Queiroz 2005; Schönhofer *et al*. 2013; Toussaint *et al*. 2016). In our analyses, jump dispersal was more likely than island-island vicariance. However, the explanation of dispersal by founder-event is consistent when vicariance is not supported by geological history (e.g. *Calisto*: Matos-Maraví *et al*. 2014). We believe, given the paleogeographic scenario in correlation with our dating estimations, that the most plausible explanation on the origin of *Petemathis*, *Bryanattus* and *Pensacolatus* is the island-to-island vicariance, while the most plausible explanation for the genera *Truncattus* and *Antillattus* is the over-water dispersal (founder-event).

The Antillattus clade diverged c. 27 Mya, and the Puerto Rican genus *Petemathis* was the first to diverge (c. 24 Mya), around the time of opening of the Mona passage. The rest of the genera are endemic to Hispaniola and Cuba, some shared between both (*Truncattus* c. 22 Mya, *Antillattus* c. 20 Mya, *Pensacolatus* c. 18 Mya, and *Bryanattus* c. 13 Mya). The divergence of *Petemathis* (c. 24 Mya), *Pensacolatus* (c. 18 Mya) and *Bryanattus* (c. 18 Mya) around the time of opening of the Mona passage and Windward passage can be explained by vicariance. Similar studies show the occurrence of dispersal/colonization processes during the period of connection between Hispaniola, Cuba, and Puerto Rico (c. 22 Mya in tree frogs of *Osteopilus*: Moen and Wiens, 2009; c. 20 Mya, in weevils *Exophthalmus*: Zhang *et al.* 2017; c. 15 Mya and in butterflies genus *Calisto*: Matos-Maraví *et al*. 2014). Island-to-island vicariance is consistent with the period of the Mona Passage (Puerto Rico-Hispaniola, c. 30-20 Mya) (Iturralde- Vinent and MacPhee 1999; Matos-Maraví *et al*. 2014), and the Windward Passage (Hispaniola-Eastern

Cuba, *c*. 17-14 Mya) (Iturralde-Vinent and MacPhee 1999; Matos-Maraví *et al*. 2014). Furthermore, *Petemathis*, *Bryanattus* and *Pensacolatus* are single-island endemic and sister-island lineages, as predicted by the island-to-island vicariant model.

Additionally, the divergence of *Truncattus* (c. 22 Mya) and *Antillattus* (c. 20 Mya) occurred around the time of opening of the Mona passage and Windward passage. However, the occurrence of both *Antillattus* and *Truncattus* in Cuba and Hispaniola and the recent colorizations events (*c.* 13-8 Mya), are most consistent with a scenario of colonization by overwater dispersal (founder-event).

Given the biology of spiders, dispersal by ballooning is entirely possible. Jumping spiders use silk for dispersal by using a behavior known as "ballooning" (Bell *et al*. 2005; Eberhard 1987; Foelix 2011), in which atmospheric conditions play an important role. Spiders have been observed ballooning distances ranging from a few hundred meters (Vollrath 1982; Coyle 1983, 1985; Coyle *et al*. 1985; Morse 1993; Follner and Klarenberg 1995; Schneider *et al*. 2001) up to 900 km (Bristowe 1930; Darwin 1839, 1879; Harrell and Yoshimoto 1964; Okuma and Kisimoto 1981; Yoshimoto and Gressitt 1961 1963; Yoshimoto *et al*. 1962a,b). The ability to balloon could be one of the ways that favored inter-island colonization of *Micrathena* (Crews and Esposito 2020; McHugh *et al*. 2014), *Spintharus* (Dziki *et al*. 2015), *Cyrtognatha* (Čandek *et al.* 2019), and *Argiope* (Agnarsson *et al.* 2016) when there are no connections between islands (Crews and Esposito, 2020).

4.3.3 From Hispaniola to Cuba and Puerto Rico

Our study indicates Hispaniola as a potential source for subsequent radiations throughout the Greater Antilles, with multiple exchanges between Cuba and Hispaniola. Other studies also support Hispaniola as a point of dispersion to other Antillean islands (Hedges and Woods 1993; Woods *et al*. 2001). Fabre *et al*. (2014) found evidence in Caribbean Capromyidae (hutias) supporting Hispaniola as a potential source of colonization to other Greater Antilles islands and the Bahamas. In their study they suggest either (i) a vicariant event between eastern (Hispaniola) and western (Bahamas, Cuba, Jamaica) hutias or (ii) stepping-stone colonization from east to west. Čandek *et al*. 2019 found for *Cyrthognata* spiders that dispersal from Hispaniola explains the colonization of the rest of the islands. The BioGeoBEARS ancestral range estimation of the GAARlandia DEC+j model for *Deinopis* (see, Chamberland *et al*. 2018) also supports the hypothesis of pivotal dispersal role of Hispaniola. McHugh *et al*. (2014) suggested that Caribbean *Micrathena* are not monophyletic and therefore must have colonized the region multiple times, and find evidence of multiple interchanges between Cuba, Hispaniola

and Puerto Rico. We are unsure whether Hispaniola played a fundamental role in our case, but for now, the evidence seems to indicate that it does. Further studies of Caribbean biota will be required to solidify the exact role of Hispaniola and the overall biogeographical complexity of the Greater Antilles.

4.4 Conclusion

Our study sheds new light on the biogeography of the Antillattus clade, their radiation. The phylogenetic and biogeographical evidence presented in this study agrees with the Caribbean paleogeographical model of colonization. The ancestor of the Antillattus clade appears to have colonized the Caribbean via GAARlandia. Our results suggest that the evolution of the Antillattus clade included both vicariant processes and founder-events. Jumping spiders once again show their potential for biogeographical study, and offer great promise for further, more detailed studies related to colonization and founder-events mechanism for different lineages. Among other insights, we have uncovered the importance of Hispaniola in the Antillattus clade's colonization of the Caribbean, thereby providing further evidence that islands can function as sources of settlers. Finally, we show that richness in single-island endemism is largely the outcome of in-situ diversification. Future research should be directed to understanding the within-island speciation.

Table 4.2. BioGeoBEARS' relative model probabilities (just put DEC + J, DIVALIKE + J etc. don't need to mention it again here) for non-time-stratified and time-stratified analyses. Best performing model is marked by asterisk for groups of analyses. LnL = log likelihood; n par = number of parameters in the analysis; d, e, j = parameres of the model (d = dispersal, e = extinction, j = founder event); AIC = Aikake information criterion; AICc = size-corrected AIC.

Non-time-constrained									
	LnL	**npar**	**D**	**e**	**j**	**AIC**	**AICc**	**AIC-WT**	**AICc-WT**
DEC	-50.93	2	0.0017	<0.0001	0	105.9	106.025	0.0019	0.002
DEC J*	-44.20	3	<0.0001	<0.0001	0.0153	94.4	94.741	0.58	0.576
DIVALIKE	-57.11	2	0.0033	<0.0001	0	118.2	118.391	3.90E-06	4.21E-06
DIVALIKE J	-44.55	3	<0.0001	<0.0001	0.0180	95.1	95.436	0.41	0.407
BAYAREALIKE	-65.23	2	<0.0001	0.0372	0	134.5	134.625	1.20E-09	1.26E-09
BAYAREALIKE J	-47.80	3	<0.0001	<0.0001	0.0197	101.6	101.928	0.016	0.016
Time-constrained									
DEC	-50.93	2	0.0017	<0.0001	0	105.9	106	0.0032	0.0034
DEC J*	-44.20	3	<0.0001	<0.0001	0.015	94.4	94.74	0.97	0.97
DIVALIKE	-57.11	2	0.0033	<0.0001	0	118.2	118.4	6.50E-06	7.10E-06
DIVALIKE J	-61.19	3	0.0033	0.01	0.0001	128.4	128.7	4.10E-08	4.10E-08
BAYAREALIKE	-65.23	2	<0.0001	0.037	0	134.5	134.6	1.90E-09	2.10E-09
BAYAREALIKE J	-47.79	3	<0.0001	<0.0001	0.02	101.6	101.9	0.027	0.027

Table 4.3. Statistical chi-squared comparasion between with and without founder-event (j) BioGeoBEARS model.

Non-time- stratified									
alt	Null	LnLalt	LnLnull	DFalt	DFnull	DF	Dstatistic	pval	test
DEC J	DEC	-44.2	-50.93	3	2	1	13.46	<0.001	chi-squared
DIVALIKE J	DIVALIKE	-44.55	-57.11	3	2	1	25.13	<0.001	chi-squared
BAYAREALIKE J	BAYAREALIKE	-47.79	-65.23	3	2	1	34.87	<0.001	chi-squared
Time- stratified									
DEC J	DEC	-44.2	-50.93	3	2	1	13.46	<0.001	chi-squared
DIVALIKE J	DIVALIKE	-61.19	-57.11	3	2	1	-8.15	<0.001	chi-squared
BAYAREALIKE J	BAYAREALIKE	-47.79	-65.23	3	2	1	34.87	<0.001	chi-squared

Table 4.4. Summary count of non-time-constrained BSMs. DEC= dispersal-extinction-cladogenesis; DEC + j= dispersal-extinction-cladogenesis + jump dispersal. Abbreviations: a, range-switching dispersal; d, range-expansion dispersal; e, extinction; y, sympatric range-copying speciation; s, sympatric-subset speciation; v, vicariance; j, jump dispersal or founder-event speciation; Ÿd, allopatric dispersal; ad, anagenetic dispersal; Ÿa: allopatric anagenetic; Ÿc: allopatric cladogenetic; sums, adds up all of the events across the stochastic maps.

DEC												
	j	*a*	*d*	*e*	*s*	*v*	*y*	*Ÿd*	*ad*	*Ÿa*	*Ÿc*	*Total events*
means	0	0	4.72	0	7.7	7.18	59.12	4.72	4.72	4.72	74	78.72
stdevs	0	0	0.64	0	1.62	0.39	1.48	0.64	0.64	0.64	0	0.64
sums	0	0	236	0	385	359	2956	236	236	236	3700	3936
DEC+j												
	j	*a*	*d*	*e*	*s*	*v*	*y*	*Ÿd*	*ad*	*Ÿa*	*Ÿc*	*Total events*
means	7.94	0	0	0	1.8	1.96	62.3	7.94	0	0	74	74
stdevs	0.84	0	0	0	1.5	0.64	1.31	0.84	0	0	0	0
sums	397	0	0	0	90	98	3115	397	0	0	3700	3700

Table 4.5. Summary count of time-constrained BSMs. DEC= dispersal-extinction-cladogenesis; DEC+ j= dispersal-extinction-cladogenesis and founder event. Abbreviations: a, range-switching dispersal; d, range-expansion dispersal; e, extinction; y, sympatric range-copying speciation; s, sympatric-subset speciation; v, vicariance; j, jump dispersal or founder-event speciation; Ÿd, allopatric dispersal; ad, anagenetic dispersal; Ÿa: allopatric anagenetic; Ÿc: allopatric cladogenetic; sums, adds up all of the events across the stochastic maps.

DEC												
	j	*a*	*d*	*e*	*s*	*v*	*y*	*Ÿd*	*ad*	*Ÿa*	*Ÿc*	*Total events*
means	0	0	4.62	0	7.78	7.08	59.14	4.62	4.62	4.62	74	78.62
stdevs	0	0	0.6	0	1.54	0.27	1.53	0.6	0.6	0.6	0	0.6
sums	0	0	231	0	389	354	2957	231	231	231	3700	3931
DEC+j												
	j	*a*	*d*	*e*	*s*	*v*	*y*	*Ÿd*	*ad*	*Ÿa*	*Ÿc*	*Total events*
means	7.72	0	0	0	1.94	1.96	62.37	7.72	0	0	74	74
stdevs	0.9	0	0	0	1.38	0.64	1.07	0.9	0	0	0	0
sums	386	0	0	0	97	98	3119	386	0	0	3700	3700

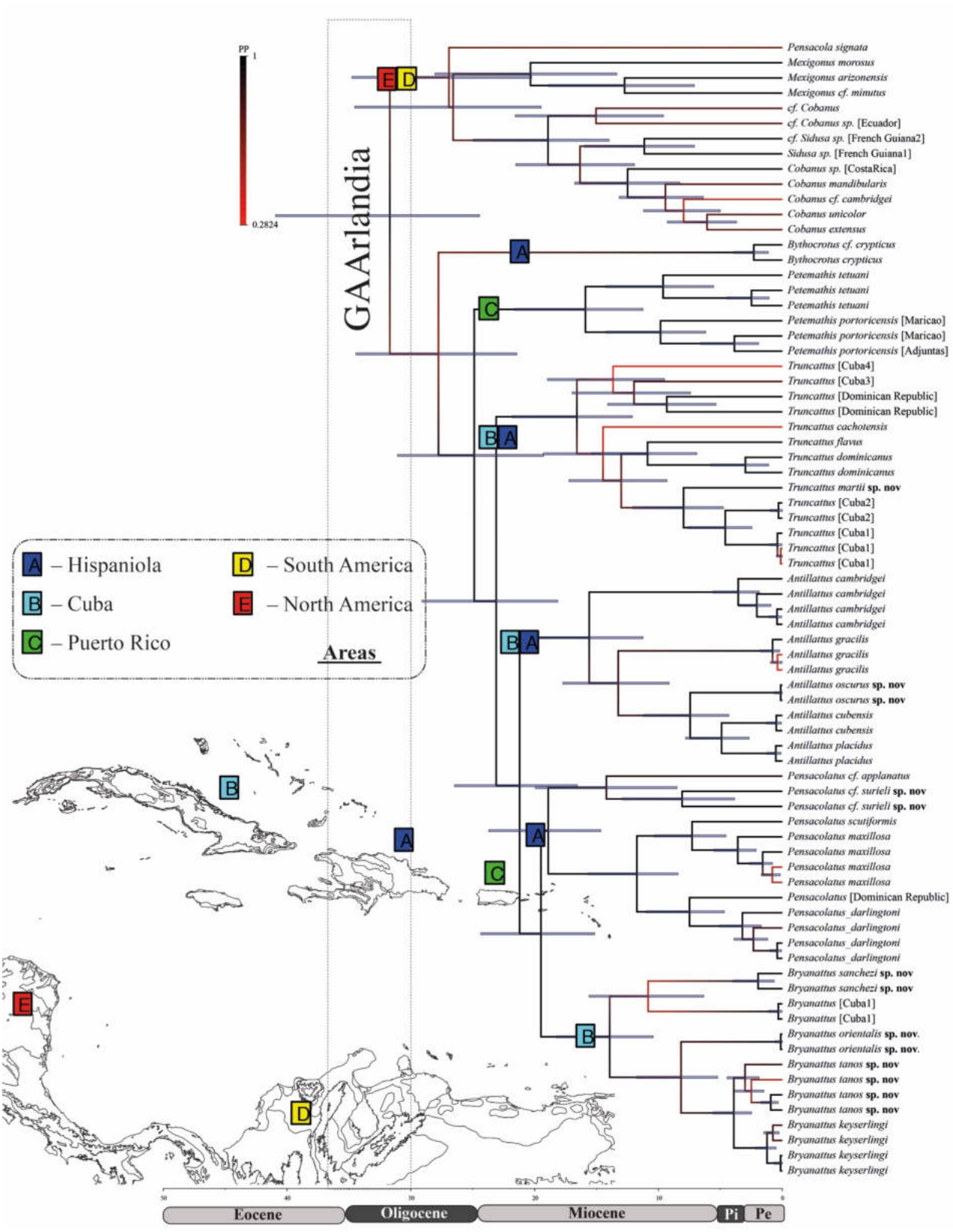

Figure. 4.2. Beast divergence time estimations of all genes (COI, 16S, 28S) using a Bayesian relaxed molecular clock. Scale in in millions of years. Bars show 95% HDP.

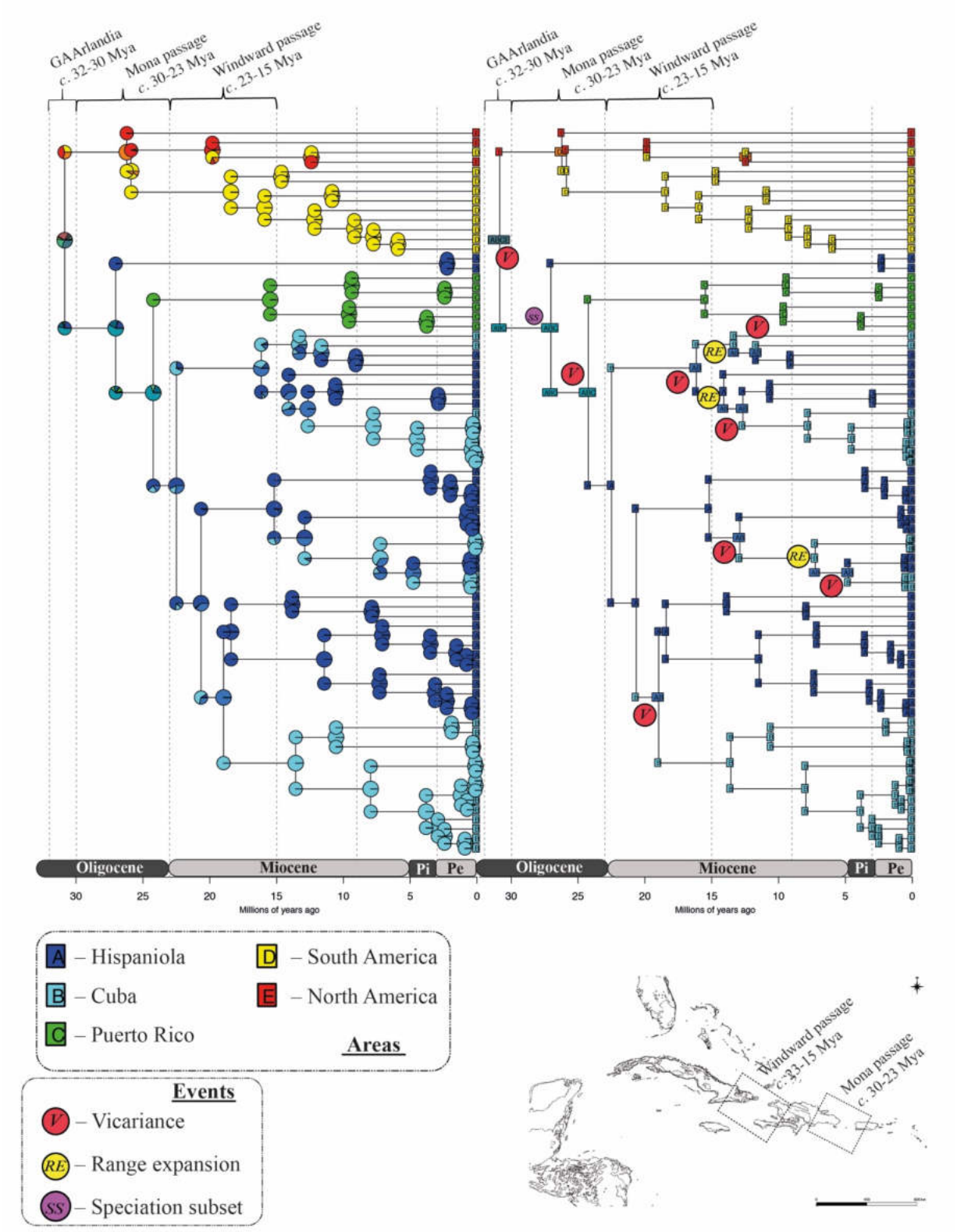

Figure 4.3. Results of the ancestral range estimation using time-stratified DEC model of BioGeoBEARS. Phylogram corresponding to the time-stratified DEC model. Pie charts represent the probabilities of each possible geographic area pre- and post-split. The tree on the right shows the most probable geographic range pre and post-split; are the events from stochastic mapping.

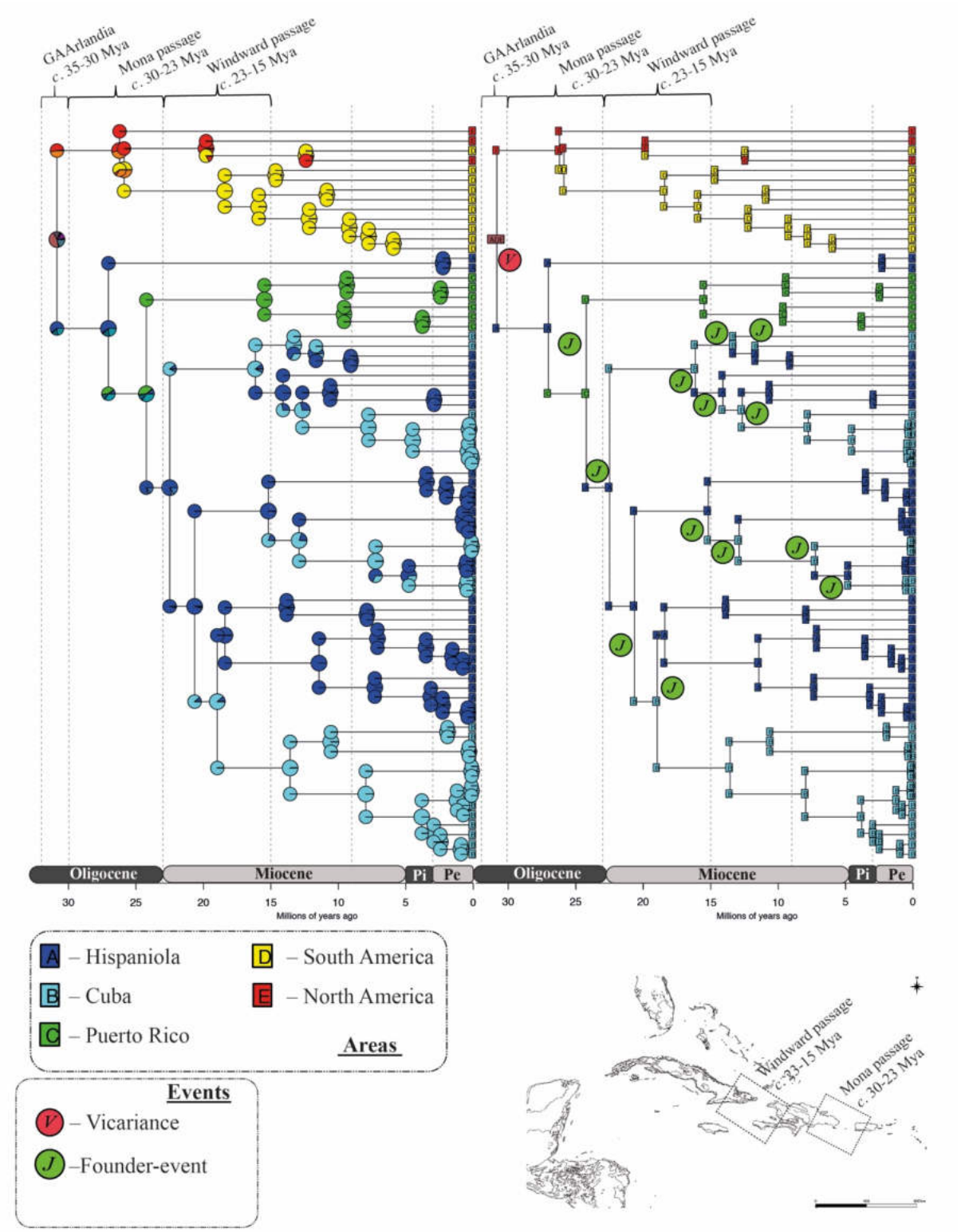

Figure 4.4. Results of the ancestral range estimation using time-stratified DEC+j model of BioGeoBEARS. Phylogram corresponding to the time-stratified DEC+j model. Pie charts represent the probabilities of each possible geographic area pre- and post-split. The tree on the right shows the most probable geographic range pre and post-split; are the events from stochastic mapping.

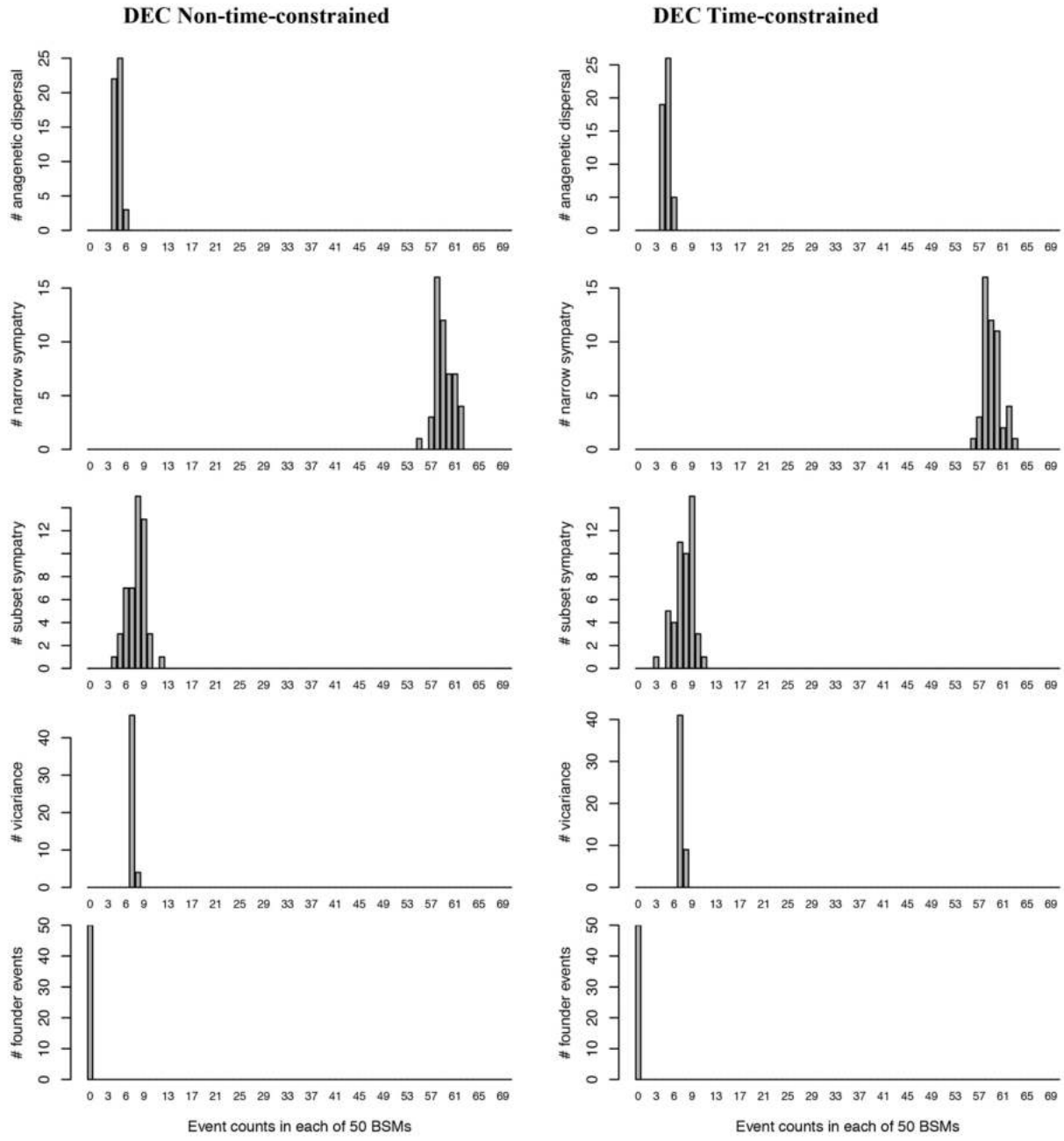

Figure 4.5. Histograms of the counts of different kinds of events found in each of the 50 BSMs. The x-axis gives the number of events, the y-axis gives the number of BSMs in which a specific number of events was observed. The models are a non-time-stratified and time-stratified DEC models.

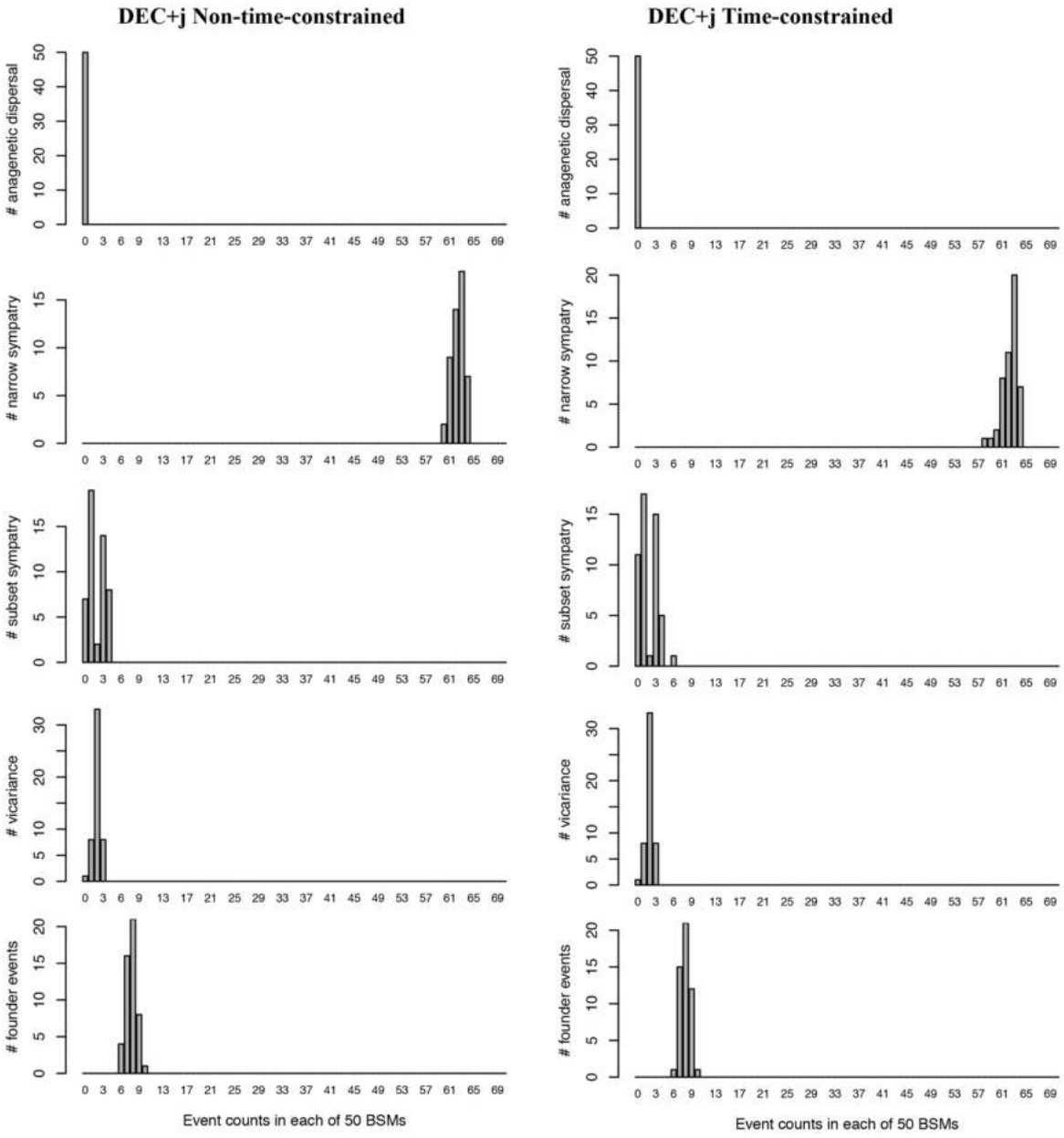

Figure 4.6. Histograms of the counts of different kinds of events found in each of the 50 BSMs. The x-axis gives the number of events, the y-axis gives the number of BSMs in which a specific number of events was observed. The models are a non-time-stratified and time-stratified DEC+j models.

4.5 References

Agnarsson, I., and Kuntner, M. (2012). The generation of a biodiversity hotspot: biogeography and phylogeography of the western Indian Ocean islands. In ´Current Topics in Phylogenetics and Phylogeography of Terrestrial and Aquatic Systems´. (Ed. K. Anamthawat-Jonsson). pp. 33–82. (Tech Publishers: Rijeka). doi: 10.5772/38958

Agnarsson, I., Cheng, R. C., Kuntner, M. (2014). A Multi-Clade Test Supports the Intermediate Dispersal Model of Biogeography. *PlosOne* **91**, e86780. doi: 10.1371/journal.pone.0086780.

Agnarsson, I., LeQuier, S. M., Kuntner, M., Cheng, R-C., Coddington, J. A., and Binford, G. (2016). Phylogeography of a good Caribbean disperser: *Argiope argentata* (Araneae, Araneidae) and a new 'cryptic' species from Cuba. *ZooKeys* **2016**, 25–44. doi: https://doi.org/10.3897/zookeys.625.8729.

Ali, J. R. (2012). Colonizing the Caribbean: is the GAARlandia land-bridge hypothesis gaining a foothold? *Journal of Biogeography* **39**, 431–433.

Alonso, R., Crawford, A. J., and Bermingham, E. (2012). Molecular phylogeny of an endemic radiation of Cuban toads (Bufonidae: Peltophryne) based on mitochondrial and nuclear genes. *Journal of Biogeography* **39**, 434–451.

Barel, C. J. A. (1973) Studies on dispersal of *Adoxophyes orana* F.V.R. in relation to the population sterilization technique. *Mededelingen Landbhoogesch, Wageningen* **73**, 1–107.

Battistuzzi, F. U., Billing-Ross, P., Paliwal, A., and Kumar, S. (2011). Fast and slow implementations of relaxed-clock methods show similar patterns of accuracy in estimating divergence times. *Molecular Biology and Evolution* **28**(9), 2439–2442. doi: https://doi.org/10.1093/molbev/msr100

Bell, J. R., Bohan, D. A., Shaw E. M., Weyman, G. S. (2005). Ballooning dispersal using silk: world fauna, phylogenies, genetics and models. *Bulletin of Entomological Research* **95**, 69–114. doi: 10.1079/BER2004350.

Berger B. A., Kriebel R., Spalink D., and Sytsma K.J. (2016) Divergence times, historical biogeography, and shifts in speciation rates of Myrtales. *Molecular Phylogenetics and Evolution* **95**, 116–136.

Binford, G. J., Callahan, M. S., Bodner, M. R., Rynerson, M. R., Nunez, P. B., Ellison, C. E., and Duncan, R. P. (2008). Phylogenetic relationships of Loxosceles and Sicarius spiders

are consistent with Western Gondwanan vicariance. *Molecular Phylogenetics and Evolution* **49**, 538–553. doi:10.1016/j.ympev.2008.08.003

Bodner, M. R., and Maddison, W. P. (2012). The biogeography and age of salticid spider radiations (Araneae: Salticidae). *Molecular Phylogenetics and Evolution* **65**, 213–240.

Bristowe, W.S. (1958) The world of spiders. (Collins: London).

Čandek, K., Agnarsson, I., Binford, G. J., and Kuntner, M. (2019). Biogeography of the Caribbean *Cyrtognatha* spiders. *Scientific Reports*, **9**, 397. doi:10.1038/s41598-018-36590-y

Carlquist, S. (1974). Island Biology. (Columbia Univ. Press: New York/London)

Carson, H. L. (1983) Chromosomal sequences and interisland colonizations in Hawaiian *Drosophila*. *Genetics* **103**, 465–482.

Censky, E. J., Hodge, K., and Dudley, J. (1998). Over-water dispersal of lizards due to hurricanes. Nature **395**(6702), 556. doi: https://doi.org/10.1038/26886

Claramunt, S., Derryberry, E.P., Remsen Jr., J.V., Brumfield, R.T. (2012). High dispersal ability inhibits speciation in a continental radiation of passerine birds. *Proceedings of the Royal Society B-Biological Sciences* **279**, 1567–1574. doi: 10.1098/rspb.2011.1922

Cowie, R. H., and Holland, B. S. (2006). Dispersal is fundamental to biogeography and the evolution of biodiversity on oceanic islands. *Journal of Biogeography* **33**(2), 193–198. https://doi.org/10.1111/j.1365-2699.2005.01383.x

Coyle, F.A. (1983) Aerial dispersal by mygalomorph spiderlings (Araneae, Mygalomorphae). *Journal of Arachnology* **11**, 283–286.

Coyle, F.A. (1985) Ballooning behavior of Ummidia spiderlings (Araneae, Ctenizidae). *Journal of Arachnology* **13**, 137–138.

Coyle, F. A., Greenstone, M. H., Hulsch, A. L. and Morgan, C. L. (1985) Ballooning mygalomorphs: estimates of the masses of *Sphodros* and *Ummidia* ballooners (Araeneae: Atypidae, Ctenizidae). *Journal of Arachnology* **13**, 291–296.

Coyne, J. A., and Orr, H. A. (2004). Speciation. (Sinauer: Sunderland, MA)

Crews, S. C., and Gillespie, R. G. (2010). Molecular systematics of *Selenops* spiders (Araneae: Selenopidae) from North and Central America: implications for Caribbean biogeography. *Biological Journal of the Linnean Society* **101**, 288–322.

Darriba, D., Taboada, G. L., Doallo, R., and Posada, D. (2012). jModelTest 2: more models, new heuristics and parallel computing. *Nature Methods* **9**, 772. doi:10.1038/nmeth.2109

Darwin, C. (1839) Journal of researches into the geology and natural history of the various countries visited by H.M.S. Beagle under the command of Captain Fitzroy R.N. from 1832 to 1836. London, Henry Colburn.

Darwin, C. (1879) A naturalist's voyage. (John Murray: London).

Dávalos, L. M. (2004). Phylogeny and biogeography of Caribbean mammals. *Biological Journal of the Linnean Society* **81**, 373–394.

De Queiroz, K. (2005). A unified species concept and its consequences for the future of taxonomy. *Proceedings of the California Academy of Sciences* **56**, 196-215.

Deler-Hernández, A., Sýkora, V., Seidel, M., Cala-Riquelme, F., and Fikáček, M. (2017). Multiple origins of the *Phaenonotum* beetles in the Greater Antilles (Coleoptera: Hydrophilidae): phylogeny, biogeography and systematics, *Zoological Journal of the Linnean Society* **183**, 97–120. doi: https://doi.org/10.1093/zoolinnean/zlx071

Diamond, J. M., Gilpin, M. E., and Mayr, E. (1976). Species-Distance Relation for Birds of Solomon Archipelago, and Paradox of Great Speciators. *Proceedings of the National Academy of Sciences of the United States of America* **73**, 2160–2164. doi: 10.1073/pnas.73.6.2160

Drummond, A. J., Suchard, M. A., Xie, D. and Rambaut, A. (2012). Bayesian phylogenetics with BEAUti and the BEAST 1.7. *Molecular Biology and Evolution* **29**, 1969–1973.

Dziki, A., Binford, G.J., Coddington, J.A., and Agnarsson, I. (2015). *Spintharus flavidus* in the Caribbean – a 30 million year biogeographical history and radiation of a 'widespread species'. *PeerJ* **3**, e1422.

Eberhard, W. G. (1987). How spiders initiate airborne lines. *Journal of Arachnology* **15**, 1–9.

Esposito, L. A., Prendini, L. (2019). Island ancestors and New World biogeography: A case study from the scorpions (Buthidae: Rhopalurusinae). *Scientific Reports* 1–11. doi: https://doi.org/10.1038/s41598-018-33754-8.

Esposito, L. A., Bloom, T., Caicedo, L., Alicia-Serrano, A., Sanchez-Ruiz, J., May-Collado, L. J., Binford, G., Agnarsson, I. (2015). Islands within islands: diversification of tailless whip spiders (Amblypygi, Phrynus) in Caribbean caves. *Molecular Phylogenetics and Evolution* **93**, 107–117.

Fabre, P.-H., Vilstrup, J. T., Raghavan, M., Der Sarkissian, C., Willerslev, E., Douzery, E. J. P., and Orlando, L. (2014). Rodents of the Caribbean: origin and diversification of hutias unravelled by next-generation museomics. *Biology Letters* **10**(7), 20140266–20140266.doi:10.1098/rsbl.2014.0266

Foelix, R. (2011). Biology of spiders. 3rd ed. (Oxford University Press: Oxford).

Follner, K., and Klarenberg, A. J. (1995) Aeronautic behaviour in the wasp-like spider *Argiope bruennichi* (Scopoli) (Araneae. Argiopidae). pp. 66–72 In `Proceedings of the 15th European Colloquium of Arachnology`. (Budejovice: Czech Republic).

Folmer, O., Black, M., Hoeh, W., Lutz, R., and Vrijenhoek, R. (1994). DNA primers for amplification of mitochondrial cytochrome oxidase subunit I from diverse metazoan invertebrates. *Molecular Marine Biology and Biotechnology* **3**, 294–299.

Gernhard T. 2008. The conditioned reconstructed process. J. Theor. Biol. 253(4):769–778.

Gillespie, R. G., and Roderick, G. K. (2002). Arthropods on islands: Colonization, speciation, and conservation. *Annual Review of Entomology* **47**(1), 595–632. https://doi.org/10.1146/annurev.ento.47.091201.145244

Gillespie, R. G., Baldwin, B. G., Waters, J. M., Fraser, C. I., Nikula, R., and Roderick, G. K. (2012). Long-distance dispersal: A framework for hypothesis testing. Trends in Ecology and Evolution, 27(1), 47–55. https://doi.org/10.1016/j.tree.2011.08.009

Gittenberger, E. (1991) What about non-adaptive radiation? *Biological Journal of the Linnean Society* **43**, 263–272

Green, P. (1999). Phrap, version 0.990329. Distributed by the author. Available from http://www.phrap.org.

Green, P., and Ewing, B. (2002). Phred, version 0.020425 c. Distributed by the authors. Available via: http://phrap.org.

Harrell, J.C., and Yoshimoto, C.M. (1964) Trapping of air-borne insects on ships in the Pacific. Part 5. *Pacific Insects* **6**, 274–282.

Hedges, S. B. (2001). Biogeography of the West Indies: an overview. In ´Biogeography of the West Indies: Patterns and Perspectives´. (Eds C. A. Woods and F.E Sergile) pp15-33. (CRC Press. Baton Rouge, LA).

Hedges, S. B. (2006). Paleogeography of the Antilles and origin of West Indian terrestrial vertebrates. *Annals of the Missouri Botanical Garden* **93**(2), 231–244. https://doi.org/10.3417/0026-6493(2006)93[231:POTAAO]2.0.CO;2

Hedges, S.B., Hass, C. and Maxson, L., (1992). Caribbean biogeography: molecular evidence for dispersal in West Indian terrestrial vertebrates. P*roceedings of National Academy of Sciences* **89**: 1909-1913.

Hedges, S.B., Woods, C.A. (1993): Caribbean hot spot. *Nature* **364**: 375.

Hill, D.E. (2009). Salticidae ofthe Antarctic land bridge. *Peckhamia* **76**(1),1–14.

Iturralde-Vinent MA. (2006). Meso-Cenozoic Caribbean paleogeography: implications for the historical biogeography of the region. *International Geology Review* **48**, 791–827.

Iturralde-Vinent, M.A., and MacPhee, R. D. E. (1999). Paleogeography of the Caribbean region: implications for Cenozoic biogeography. *Bulletin of the American Museum of Natural History* **238**, 1-95.

Iturralde-Vinent, M. A. (1982). Aspectos geológicos de la biogeografía de Cuba. *Ciencias de la Tierra y del Espacio* **5**, 85-100.

Katoh, K., and Standley, D.M. (2013). MAFFT multiple sequence alignment software version 7: improvements in performance and usability. *Molecular Biology and Evolution* **30**, 772–780.

Kennedy, G.G., and Smitley, D.R. (1985) Dispersal. pp. 233–242 in Helle, W. and Sabelis, M.W. (Eds) Spider mites. Their biology, natural enemies and control. Volume 1A. The Tetranychidae. Oxford, Elsevier.

Kozak, K. H., Weisrock D. W., and Larson, A. (2006) Rapid lineage accumulation in a non-adaptive radiation: phylogenetic analysis of diversification rates in Eastern North American woodland salamanders (Plethodontidae: Plethodon). *Proceedings of the Royal Society B: Biological Sciences* **273**, 539–546.

Landis, M. J., Matzke, N. J., Moore, B. R., and Huelsenbeck, J. P. (2013). Bayesian analysis of biogeography when the number of áreas is large. *Systematic Biology* **62**, 789–804.

Leigh, E. G. Jr., Hladik, A., Hladik, C. M., and Jolly, A. (2007). The biogeography of large islands, or how does the size of the ecological theater affect the evolutionary play? *Revue d''ecologie* **62**,105–68

Lomolino, M. V., Riddle, B. R., Whittaker, R. J., and Brown, J. H. (2010) Biogeography, 4th edn. Sinauer Associated Inc, Sun- derland, MA.

Losos, J. B., Parent, C. E. (20099. The speciation-area relationship. In The Theory of Island Biogeography Revisited, ed. J. B. Losos, R. E. Ricklefs, pp. 415–38. Princeton, NJ: Princeton Univ. Press

MacPhee, R.D.E., and Iturralde-Vinent, M.A. 2000. A short history of Greater Antillean land mammals: Biogeography, paleogeography, radiation, and extinctions. *Tropics* **10**(1), 145-154.

MacPhee, R.D.E., and Iturralde-Vinent, M.A. (1994). First Tertiary land mammal fossils from Greater Antilles: an Early Miocene sloth (Xenarhra, Megalonychidae) from Cuba. *American Museum Novitates* **3094**, 1-13.

MacPhee, R. D. E., and Iturralde-Vinent, M.A. (1995). Origin of the Greater Antilles land mammal fauna 1: New Tertiary land mammals from Cuba and Puerto Rico. *American Museum* Novitates **314**, 1-31.

Maddison, D.R., and Maddison, W.P. (2018a). Chromaseq: a Mesquite package for analyzing sequence chromatograms. Version 1.31. http://chromaseq.mesquiteproject.org

Maddison, W. P. (2015). A phylogenetic classification of jumping spiders (Araneae: Salticidae). *Journal Arachnology* **43**, 231-292.

Maddison, W. P., and Maddison, D.R. (2018b). Mesquite: a modular system for evolutionary analysis. Version 3.6 http://mesquiteproject.org

Maddison, W. P., Bodner, M. R., and Needham, K. M. (2008). Salticid spider phylogeny revisited, with the discovery of a large Australasian clade (Araneae: Salticidae). *Zootaxa*, **1893**, 46-64.

Maddison, W.P., and Hedin, M.C. (2003). Jumping spider phylogeny (Araneae: Salticidae). *Invertebrate Systematics* **17**, 529-549.

Mann, P., Schubert, C., and Burke, K. (1990). Review of Caribbean neotectonics. In The geology of North America. Vol. H-The Caribbean region. Boulder, CO: Geological Society of America, Vol. 1990, 307–338. Research supported by University of Texas, CONICIT, and Universidad de Los Andes.

Masta, S. E., and Boore, J. L. (2004) The complete mitochondrial genome sequence of the spider Habronattus oregonensis reveals rearranged and extremely truncated tRNAs. *Molecular Biology and Evolution* **21** (5), 893-902.

Matos-Maraví P., Águila R.N., Peña C., Miller J.Y., Sourakov A., and Wahlberg N. (2014) Causes of endemic radiation in the Caribbean: evidence from the historical biogeography and diversification of the butterfly genus *Calisto* (Nymphalidae: Satyrinae: Satyrini). *BMC Evolutionary Biology* **14**, 199.

Matzke, N. J. (2013). Probabilistic historical biogeography: new models for founder-event speciation, imperfect detection, and fossils allow improved accuracy and model-testing. *Frontiers of Biogeography* **5**, 242–248.

Matzke, N. J. (2014). Model selection in historical biogeography reveals that founder-event speciation is a crucial process in Island Clades. *Systematic Biology* **63**, 951–970.

Mchugh, A., Yablonsky, C., Binford, G., and Agnarsson, I., (2014). Molecular phylogenetics of Caribbean *Micrathena* (Araneae: Araneidae) suggests multiple colonization events and single island endemism. *Invertebrate Systematics* **28**, 337-349

Mittermeier, R.A., Robles-Gil, P., Hoffman, M., Pilgrim, J., Brooks, T., Mittermeier, C.G., Lamoreux, J., and da Fonseca, G.A.B. (2005). Hotspots revisited: earth's biologically richest and most endangered terrestrial ecoregions. (Agrupación Sierra Madre: Mexico).

Morse, D.H. (1993) Some determinants of dispersal by crab spiderlings. *Ecology* **74**, 427–432.

Nosil, P. (2012). Ecological Speciation. (Oxford University Press: Oxford, UK).

O'Dea, A., Lessios, H. A., Coates, A. G., Eytan, R. I., Restrepo-Moreno, S. A., Cione, A. L., Collins, L. S., de Queiroz, A., Farris, D. W., Norris, R. D., Stallard, R. F., Woodburne, M. O., Aguilera, O., Aubry, M. P. P., Berggren, W. A., Budd, A. F., Cozzuol, M. A., Coppard, S. E., Duque-Caro, H., Finnegan, S., Gasparini, G. M. M., Grossman, E. L., Johnson, K. G., Keigwin, L. D., Knowlton, N., Leigh, E. G., Leonard-Pingel, J. S., Marko, P. B., Pyenson, N. D., Rachello-Dolmen, P. G., Soibelzon, E., Soibelzon, L., Todd, J. A., Vermeij, G. J., Jackson, J. B. (2016). Formation of the Isthmus of Panama. *Science Advances* **2**, e1600883.

Okuma, C., and Kisimoto, R. (1981) Air borne spiders collected over the East China Sea. *Japanese Journal of Applied Entomology and Zoology* **25**, 296–298.

Paulay, G., and Meyer, C. (2002) Diversification in the tropical pacific: comparisons between marine and terrestrial systems and the importance of founder speciation. *Integrative and Comparative Biology*, **42**, 922–934.

Pindell, J. L., and Barrett, S. F. (1990). Geological evolution of the Caribbean region: A plate tectonic perspective. In `The Caribbean Region: Geological society of America`. (Eds. G. Dengo and J. E. Case). pp. 405–432. (The Geology of North America:)

Platnick, N. I. (1976a) Concepts of dispersal in historical biogeography. *Systematic Zoology* **25**, 294–295.

Posada, D., and Buckley, T. R. (2004). Model selection and model averaging in phylogenetics: advantages of Akaike Information Criterion and Bayesian Approaches over Likelihood Ratio Tests. *Systematic Biology* **53**, 793–808.

Pregill, G. K., and Olson, S. L. (1981). Zoogeography of West Indian Vertebrates in Relation to Pleistocene Climatic Cycles. *Annual Review of Ecology and Systematics* **12**(1), 75–98. doi:10.1146/annurev.es.12.110181.000451

Prószyński, J., and Deeleman-Reinhold, C. L. (2012). Description of some Salticidae (Aranei) from the Malay Archipelago. II. Salticidae of Java and Sumatra, with comments on related species. *Arthropoda Selecta* **21** (1), 29-60.

Rambaut, A., Suchard, M. A., Xie, D., and Drummond, A. J. (2014). Tracer v1.6. Available at http://beast.bio.ed.ac.uk/Tracer.

Ree, R. H, Smith, S. A. (2008). Maximum likelihood inference of geographic range evolution by dispersal, local extinction, and cladogenesis. *Systematic Biology* **57**, 4–14.

Říčan, O., Piálek, L., Zardoya, R., Doadrio, I., Zrzavý, J. (2013). Biogeography of the Mesoamerican Cichlidae (Teleostei: Heroini): colonization through the GAARlandia land bridge and early diversification. *Journal of Biogeography* **40**, 579–593.

Ricklefs, R. and Bermingham, E. (2008). The West Indies as a laboratory of biogeography and evolution. *Philosophical Transactions of the Royal Society of London, Series B, Biological Sciences* **363**, 2393-2413.

Rodriguez, J., Pitts, J. P., von Dohlen, C. D. (2015). Historical biogeography of the widespread spider wasp tribe Aporini (Hymenoptera: Pompilidae). *Journal of Biogeography* **42**, 495–506.

Ronquist, F., Teslenko, M., van der Mark, P., Ayres, D. L., Darling, A., Höhna, S., Larget, B., Liu, L., Suchard, M. A., Huelsenbeck, J. P. (2012). MrBayes 3.2: efficient Bayesian phylogenetic inference and model choice across a large model space. *Systematic Biology* **61**(3), 539-42. doi: 10.1093/sysbio/sys029.

Ronquist, F. (1997). Dispersal-vicariance analysis: a new approach to the quantification of historical biogeography. *Systematic Biology* **46**, 195–203.

Rosen, D.E. (1975). A vicariance model of Caribbean biogeography. *Systematic Zoology* **24**, 431-464.

Rosen, D. E., (1985). Geological hierarchies and biogeographical congruence in the Caribbean. *Annals of the Missouri Botanical Garden* **72**, 636-659.

Rundell, R. J., and Price, T. D. (2009). Adaptive radiation, nonadaptive radiation, ecological speciation and nonecological speciation. *Trends in Ecology and Evolution* **24**(7), 394–399.doi:10.1016/j.tree.2009.02.007

Sato, J. J., Ohdachi, S. D., Echenique-Diaz, L. M., Borroto-Páez, R., Begué-Quiala, G., Delgado-Labañino, L. J., Gámez-Díez, J., Álbarez-Lemus, J., Nguyen, T. S., Yamaguchi, N., and Kita, M. (2016). Molecular phylogenetic analysis of nuclear genes suggests a Cenozoic overwater dispersal origin for the Cuban solenodon. *Scientific Report* **6**, 31173. doi: https://doi.org/10.1038/srep31173

Schluter, D. (2000). The Ecology of Adaptive Radiation. (Oxford University Press: Oxford, UK)

Schluter, D. (2009). Evidence for ecological speciation and its alternative. *Science* **323**(5915), 737–41

Schneider, J. M., Roos, J., Lubin, Y., and Henschel, J. R. (2001) Dispersal of *Stegodyphus dumicola* (Araneae, Eresidae): they do balloon after all! *Journal of Arachnology* **29**, 114–116.

Schönhofer, A. L., McCormack, M., Tsurusaki, N., Martens, J., and Hedin, M. (2013). Molecular phylogeny of the harvestmen genus Sabacon (Arachnida: Opiliones: Dyspnoi) reveals multiple Eocene–Oligocene intercontinental dispersal events in the Holarctic. *Molecular Phylogenetics and Evolution* **66**(1), 303–315. doi:10.1016/j.ympev.2012.10.001

Shaw, A. J., Shaw, B., Johnson, M. G., Devos N., Stenøien, H. K., Flatberg, K. I., and Carter, B. E. (2015) Phylogenetic structure and biogeography of the Pacific Rim clade of *Sphagnum* subgen. *Subsecunda*: haploid and allodiploid taxa. *Biological Journal of the Linnean Society* **116**, 295–311.

Simpson, G. G. (1953). The Major Features of Evolution. (Columbia University Press: New York)

Stamatakis, A. (2014). RAxML version 8: a tool for phylogenetic analysis and post-analysis of large phylogenies. *Bioinformatics* **30**, 1312–1313.

Stamatakis, A. (2006). RAxML-VI-HPC: Maximum Likelihood-based Phylogenetic Analyses with Thousands of Taxa and Mixed Models. *In Bioinformatics* **22**(21), 2688-2690.

Stuart, Y. E., and Losos, J. B. (2013). Ecological character displacement: glass half full or half empty? *Trends in Ecology and Evolution* **28**(7), 402–8.

Tada, R., Iturralde-Vinent, M., Matsui, T., Tajika, E., Oji, T., Goto, K., Nakano, Y., Takayama, H., Yamamoto, S., Toyoda, K., García-Delgado, D., Díaz-Otero, C., and Rojas Consuegra, R. (2003). K/T Boundary deposits in the Paleo-western Caribbean basin. AAPG Mem. Chapter 26. 23 p.

Tänzler, R., Dam, M. H. V., Toussaint, E. F. A., Suhardjono, Y. R., Balke, M., and Riedel, A. (2016). Macroevolution of hyperdiverse flightless beetles reflects the complex geological history of the Sunda Arc. *Scientific Reports* **6**, 18793.

Templeton, A. R. (2008). The reality and importance of founder speciation in evolution. *BioEssays* **30**, 470-479.

Toft, S. (1995) Two functions of gossamer dispersal in spiders? *Acta Jutlandica* **70**, 257–268.

Tong, Y., Binford, G., Rheims, A. R., Kuntner, M., Liu, J., and Agnarsson, I. (2019). Huntsmen of the Caribbean: Multiple tests of the GAARlandia hypothesis. *Molecular Phylogenetics and Evolution* **130**, 259-268. doi: https://doi.org/10.1016/j.ympev.2018.09.017

Toussaint, E. F. A., Fikacek, M. and Short, A. E. Z. (2016) India-Madagascar vicariance explains cascade beetle bio- geography. *Biological Journal of the Linnean Society* **118**, 982–991.

Uit de Weerd, D. R., Robinson, D. G., and Rosenberg, G. (2016). Evolutionary and biogeographical history of the land snail family Urocoptidae (Gastropoda: Pulmonata) across the Caribbean region. *Journal of Biogeography* **43**, 763–777.

Voelker, G., Peñalba, J. V., Huntley J. W., and Bowie R. C. K. (2014) Diversification in an Afro- Asian songbird clade (*Erythropygia–Copsychus*) reveals founder-event speciation via trans-oceanic dispersals and a southern to northern colonization pattern in Africa. *Molecular Phylogenetics and Evolution* **73**, 97–105.

Vollrath, F. (1982) Colony formation in a social spider. *Zeitschrift fu ̈r Tierpyschologie* **60**, 313–324.

Wahlberg, N. (2006). That awkward age for butterflies: insights from the age of the butterfly subfamily Nymphalinae (Lepidoptera: Nymphalidae). *Systematic Biology* **55**, 703–714.

Wahlberg, N., and Freitas, A.V. (2007). Colonization of and radiation in South America by butterflies in the subtribe Phyciodina (Lepidoptera: Nymphalidae). *Molecular Phylogenetics and Evolution* **44**, 1257–1272.

Weaver, P. F., Cruz, A., Johnson, S., Dupin, J., and Weaver, K. F. (2016). Colonizing the Caribbean: Biogeography and evolution of livebearing fishes of the genus Limia (Poeciliidae). *Journal of Biogeography* **43**(9), 1808–1819. doi: https://doi.org/10.1111/jbi.12798

White, J. L. and MacPhee, R. D. E. (2001). The sloths of the West Indies: a systematic and phylogenetic review. In: `Biogeography of the West Indies: Patterns and perspectives`. (Eds. C.A. Woods and F.E. Sergile). pp201-235. (CRC Press: Boca Raton, FL).

Woods, C., Borroto P. R., and Kilpatrick C. (2001) Insular patterns and radiation of West Indian rodents. In: `Biogeography of the West Indies: Patterns and perspectives`. (Eds. C.A. Woods and F.E. Sergile). pp. 333–351. (CRC Press: Boca Raton, FL).

World Spider Catalog (2020). World Spider Catalog, version 21.0. (Natural History Museum Bern: Washington, DC). Available at http://wsc.nmbe.ch. doi: 10.24436/2

Xie, W., Lewis, P. O., Fan, Y., Kuo, L., Chen, M. H. (2011). Improving marginal likelihood estimation for Bayesian phylogenetic model selection. *Systematic Biology* **60**, 150–160.

Yoshimoto, C. M. and Gressitt, J. C. (1961) Trapping of air borne insects on ships in the Pacific (part 4). *Pacific Insects* **3**, 556–558.

Yoshimoto, C. M. and Gressitt, J. C. (1963) Trapping of air borne insects in the Pacific-Antarctic Area. 2. *Pacific Insects* **5**, 873–883.

Yoshimoto, C. M., Gressitt, J. C. and Mitchell, C. J. (1962a) Trapping of air borne insects in the Pacific-Antarctic Area. 1. *Pacific Insects* **4**, 847–858.

Yoshimoto, C. M., Gressitt, J. C. and Wolff, T. (1962b) Airborne insects Galathea expedition. *Pacific Insects* **4**, 269–291.

Zhang, G., Basharat, U., Matzke, N., and Franz, N. M. (2017). Model selection in statistical historical biogeography of Neotropical insects – the *Exophthalmus* genus complex (Curculionidae: Entiminae). *Molecular Phylogenetics and Evolution* **109**, 226–239.

Zhang, J. X., and Maddison, W. P. (2012). New euophryine jumping spiders from the Dominican Republic and Puerto Rico (Araneae: Salticidae: Euophryinae). *Zootaxa.* **3476**,1-54.

Zhang, J. X., and Maddison, W. P. (2013). Molecular phylogeny, divergence times and biogeography of spiders of the subfamily Euophryinae (Araneae: Salticidae). *Molecular Phylogenetics and Evolution* **68**, 81-92.

Zhang, J. X., and Maddison, W. P. (2015). Genera of euophryine jumping spiders (Araneae: Salticidae), with a combined molecular-morphological phylogeny. *Zootaxa*. **3938**, 1-147.

5.0 Concluciones generales

El presente estudio contribuyó a comprender la diversidad de las arañas saltarinas del clado Antillattus utilizando un muestreo de taxones ampliado y datos morfológicos y moleculares ADN. Sin embargo, somos conscientes una futura inclusión de más especies y datos podría cambiar las topologías resultantes en el presente estudio.

- El principal objetivo de esta tesis es proporcionar un marco filogenético para los géneros y especies que componen al clado Antillattus. La filogenia del clado Antillattus se reconstruye utilizando datos moleculares y morfológicos. La monofília del clado Antillattus y sus grupos hermanos, resultó respaldada por la filogenia molecular y la evidencia total (molecular + morfología). El clado Antillattus se recupera para incluir los géneros *Petemathis*, *Truncattus*, *Pensacolatus* y *Bryanattus*. **gen. nov.**, mientras que *Caribattus* y *Allodecta* no forman parte del clado Antillattus. *Allodecta* es un sinónimo menor de *Compsodecta* y *Caribattus* se encuentra relacionado con el clado Agobardus.
- El estudio detallado de caracteres morfológicos permitió profundizar en la morfología de los géneros y especies del clado Antillattus. Los caracteres morfológicos mostraron una mejor señal filogenética [(ver Zhang y Maddison (2015)] al recuperar con buen soporte la monofília de todos los géneros y algunas de las relaciones mas profundas. Los caracteres morfológicos en la filogenia proporcionaron una mejor comprensión de los géneros y sus delimitaciones. Algunos de los caracteres y sus estados, especialmente en el palpo del macho y la genitalia de la hembra, como la forma del lóbulo tegular proximal y la presencia y ausencia del receptáculo en los genitales femeninos, mostraron gran valor informativo en la delimitación. En este mismo sentido, el recuento de dientes de quelíceros, resultó ser más informativo al ser separado cada diente como un carácter y considerado según su ubicación.
- Un hallazgo interesante de la filogenia molecular y morfológica es que el género *Antillattus* se resuelve en tres clados (*Pensacolatus*, *Antillattus* y *Bryanattus* **gen. nov.**). Se consideran como representantes del género *Antillattus* a las especies *Antillattus gracilis*, *A. placidus*, *A. cubensis, A. Cambridgei* y se describe a la especie *A. ocultus* **sp. nov**.. Se transfieren al género *Pensacolatus* a las especies de *Pensacolas* de Bryant (1943), a *Antillattus scutiformis* y a *A. Applanatus,* y se describen las especies *Pensacolatus naranjoi* **sp. nov.** para cuba, y *Pensacolatus surieli* **sp. nov.** para Republica Dominicana. *Petemathis unispina*, Antillattus *keyserlingi* y *A. mandubulata*

son transferidas a *Bryanattus* **gen. nov.,** y *Bryanattus orientalis* **sp. nov.**, *Bryanattus thanos* **sp. nov.,** *Bryanattus sanchezi* **sp. nov..**

- Las especies *Sidusa turquinensis* y *S. inconspicua* son tranferidas a el género *Truncattus* y se escriben las especies *Truncattus martii* **sp. nov.**, T. *platnicki* **sp. nov..**
- Los géneros *Sidusa* y *Cobanus* son recuperados por la evidencia morfológica, molecular y combinada (molecular + morfología). Las especies *Sidusa bifurcata*, *S cambridgei*, *S. electa*, *S. mandibularis* y *S. unicolor* son transferidas a *Cobanus* y se describen las nuevas especies *Cobanus multidentatis* **sp. nov.**, *C. chocquibtown* **sp. nov.** y el género y *Paracobanus* **gen. nov.**. con la especie *P. Boteroi* **sp. nov.**.
- Las arañas saltarinas muestran una vez más su potencial para el estudio biogeográfico, y ofrecen una gran promesa para futuros estudios más detallados. La evidencia filogenética y biogeográfica presentada en este estudio concuerda con el modelo paleogeográfico de colonización del Caribe (GAARlandia). Los resultados sugieren que la evolución del clado Antillattus y su diversificación entre las islas de las Antillas mayores, incluyó tanto procesos de vicarianza entre islas como eventos-fundadores por dispersión sobre el agua. Adicionalmente, se plantea importancia de La Española en la colonización de las diferentes islas del caribe, y se proporciona evidencia de que La Española estaria funcionando como una fuente de colonos.

Supplementary

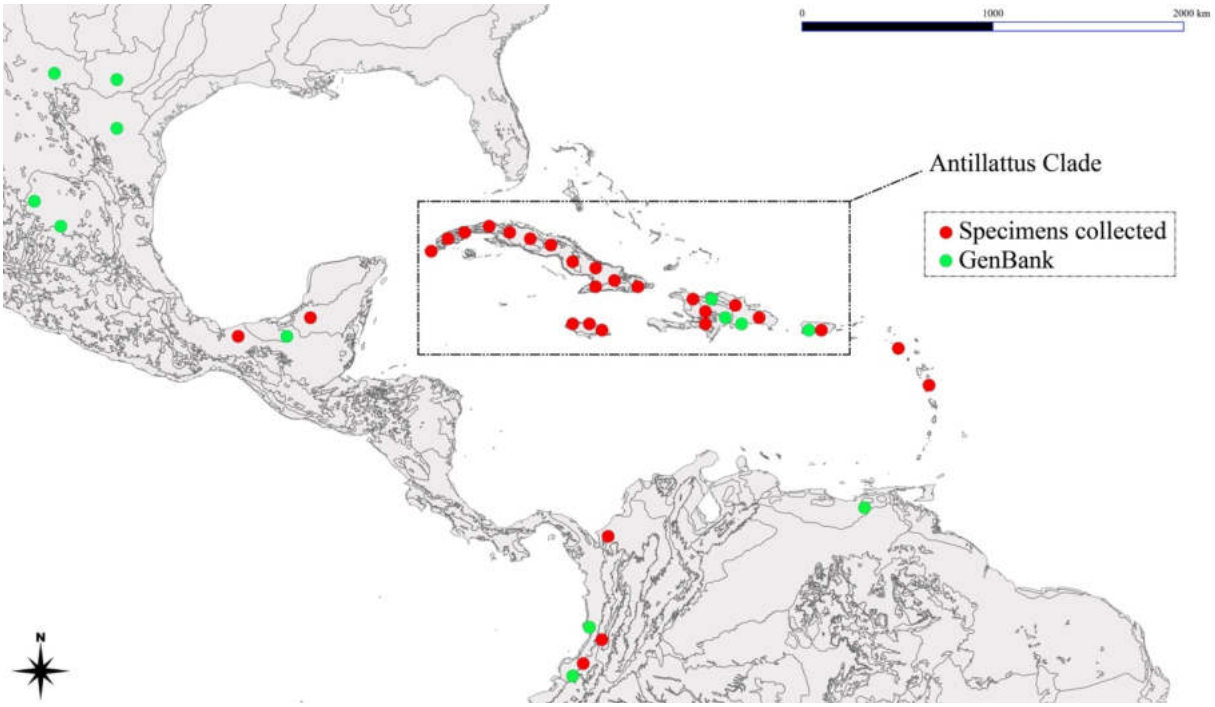

Supplementary figure 1 Map of specimens collected and samples obtained of Genbank (Zhang and Maddison 2013) for this study.

Supplementary table 1 Taxon sample with specific collection information and accession numbers.

Specie	Voucher CarBio	Locality	COI	16S	28S
Agobardus bahoruco	JXZ324	DOMINICAN REPUBLIC: Pedernales: P.N.Sierra de Bahoruco (N18.128 W71.558)		Zhang and Maddison 2013	Zhang and Maddison 2013
Agobardus cf. anormalis Montanus	JXZ357	DOMINICAN REPUBLIC: Pedernales: P.N.Sierra de Bahoruco (N18.128 W71.558)	Zhang and Maddison 2013	Zhang and Maddison 2013	Zhang and Maddison 2013
Agobardus cf. brevitarsus	JXZ311	DOMINICAN REPUBLIC: Pedernales: P.N.Sierra de Bahoruco (N18.128 W71.558)	Zhang and Maddison 2013	Zhang and Maddison 2013	Zhang and Maddison 2013
Agobardus cordiformis	JXZ358	DOMINICAN REPUBLIC: Pedernales: east of Pedernales (N17.965 W71.635)	Zhang and Maddison 2013	Zhang and Maddison 2013	Zhang and Maddison 2013
Agobardus gramineus	JXZ314	DOMINICAN REPUBLIC: Pedernales: east of Pedernales (N17.965 W71.635)	Zhang and Maddison 2013	Zhang and Maddison 2013	Zhang and Maddison 2013
Agobardus oviedo	JXZ312	DOMINICAN REPUBLIC: Pedernales: Laguna de Oviedo (N17.802 W71.349)	Zhang and Maddison 2013	Zhang and Maddison 2013	Zhang and Maddison 2013
Antillattus cambridgei	JXZ321	DOMINICAN REPUBLIC: La Vega: Reserva Científica Ébano Verde (N19.033 W70.543)	Zhang and Maddison 2013	Zhang and Maddison 2013	Zhang and Maddison 2013
Antillattus cambridgei	DR784676 DR785410 DR785798 DR782454	DOMINICAN REPUBLIC: La Alta Gracia, San Rafael de Yuma, National Park Los Haitises, Sendero de Bosque Húmedo (19.06707, -69.4635W), 12/VI/ 2012, Col. CarBioTEAM	X	X	
Antillattus cambridgei	DR785494 DR782541	DOMINICAN REPUBLIC: La Alta Gracia, San Rafael de Yuma, El Morro East of Ranger	X	X	

		Station Monte Cristi (19.893421N, -71.653395W), 23/VI/ 2012, Col. CarBioTEAM			
Antillattus cambridgei	DR782541 DR785783 DR785508	DOMINICAN REPUBLIC: La Alta Gracia, San Rafael de Yuma, Loma Quita Espuela (19.35504N, -070.111W), 14/VI/ 2012, Col. CarBioTEAM	X	X	
Antillattus cambridgei	DR782598	DOMINICAN REPUBLIC: La Alta Gracia, San Rafael de Yuma, Loma Quita Espuela (19.35504N, -070.111W), 14/VI/ 2012, Col. CarBioTEAM	X	X	X
Antillattus cambridgei	DR784852 DR785098 DR785696 DR785438 DR787296	DOMINICAN REPUBLIC: La Alta Gracia, San Rafael de Yuma, National Park Los Haitises, Sendero de Bosque Húmedo (19.06707, -69.46355W), 12/VI/ 2012, Col. CarBioTEAM	X	X	
Antillattus cambridgei	DR787296 DR787293 DR787254 DR787223	DOMINICAN REPUBLIC: La Vega, Jarabacoa, Scientific Reserve Ebano Verde (19.03627N, -70.54337W), 27/VI/ 2012, Col. CarBioTEAM	X	X	
Antillattus cambridgei	DR787328 DR787252 DR787285 DR787207 DR787327 DR787319 DR787324	DOMINICAN REPUBLIC: Santo Domingo, Los Tablones (19.05116 N, - 70.88866W), 28/VI/ 2012, Col. CarBioTEAM	X	X	
Antillattus cambridgei	DR787105	DOMINICAN REPUBLIC: San Juan, National Park Armando Bermudez, La Cienaga (19.1758974 N, - 71.049948W), 28/VI/ 2012, Col. CarBioTEAM	X	X	
Antillattus cf. applanatus	JXZ336	DOMINICAN REPUBLIC: Barahona: Cachote (N18.101 W71.194)	Zhang and Maddison 2013	Zhang and Maddison 2013	Zhang and Maddison 2013
Antillattus cubensis	CU003076 CU002975 CU003097 CU003360 CU002456 CU003486 CU02560A CU02975A CU03033A CU03076A CU03097A CU03360A	CUBA: Cienfuegos, Soledad, Jardín Botanico de Cienfuegos (22.1249512N, -80.32548859W), 21/IV/ 2013, Col. F. Cala-Riquelme, A Deler-Hernández, R. Anderson, G. Y. Zhang, A. Smith.	X		
Antillattus cubensis	CU03417A CU03488A	CUBA: Santiago de Cuba, San Luis, Dos Caminos de San Luis (20.17929190N, -75.78350636W), 21/IV/ 2013, Col. F. Cala-Riquelme, A Deler-Hernández.	X		
Antillattus cubensis	CU3075A	CUBA: Santiago de Cuba, Santiago de Cuba, Loma del Gato (20.01063N, -76.0370899W), 21/IV/ 2013, Col. F. Cala-Riquelme, A Deler-Hernández.	X		
Antillattus cubensis	CU02583A	CUBA: Guantánamo, Baracoa, Ecological Reserve Yunque-Duaba-Quibijan, El Yunque (20.33178N - 74.56919W), 04/IV/2012, Col. CarBioTEAM.	X		
Antillattus cubensis	CU787598 CU783280 CU787621 CU787283 CU787277	CUBA: Granma, Bartolomé Maso, National Park Pico Turquino, Subida a Palma Mocha km 2.5 (20.00939N - 76.89402W), 26/III/ 2012, Col. CarBioTEAM.	X		
Antillattus gracilis	JXZ320	DOMINICAN REPUBLIC: La Vega: P.N.Armando Bermúdez (N19.06 W70.86)		Zhang and Maddison 2013	Zhang and Maddison 2013
Antillattus gracilis	DR782845 DR787278	DOMINICAN REPUBLIC: Santo Domingo, Los Tablones (19.05116 N, - 70.88866W), 28/VI/ 2012, Col. CarBioTEAM	X	X	
Antillattus ocultus	CU03373A CU03396A CU03539A CU03534A	CUBA: Pinar del Rio, Viñales, Natural Park Maravillas de Viñales (22.65364 N, - 83.69967 W), 19-21/IV/ 2012, CarBioTEAM	X		
Antillattus placidus	DR787249	DOMINICAN REPUBLIC: La Vega, Jarabacoa, Scientific Reserve Ebano Verde (19.03627N, -70.54337W), 27/VI/ 2012, Col. CarBioTEAM	X	X	

Antillattus placidus	DR782502 DR785683 DR785081	DOMINICAN REPUBLIC: La Alta Gracia, San Rafael de Yuma, Loma Quita Espuela (19.35504N, -070.111W), 14/VI/ 2012, Col. CarBioTEAM	X	X	
Bryanattus keyserlingi	CU02985A	CUBA: Granma, Bartolomé Maso, National Park Pico Turquino (20.05269N -76.502926W), 03/IV/ 2012, Col. CarBioTEAM.	X		
Bryanattus keyserlingi	CU03135A	CUBA: Holguin, Frank Pais, National Park Mesura-Piloto (20.529N -75.768), 10-12/V/ 2013, Col. F. Cala-Riquelme, A Deler-Hernández, R. Anderson, G. Y. Zhang, A. Smith.	X		
Bryanattus keyserlingi	CU02571A	CUBA: Santiago de Cuba, Natural Park La Gran Piedra, La Isabelica (20.01161329N, -75.62379927W), 26/I/ 2012, Col. F. Cala-Riquelme, A Deler-Hernández, R. Anderson, N. Frank.	X		
Bryanattus keyserlingi	CU787312	CUBA: Guantánamo, Baracoa, Ecological Reserve Yunque-Duaba-Quibijan, El Yunque (20.33178N - 74.56919W), 04/IV/2012, Col. CarBioTEAM.	X		
Bryanattus keyserlingi	CU783425 CU03043A CU783232 CU783187 CU783404 CU783281 CU783245 CU02951A CU00088A CU787433 CU00081A	CUBA: Granma, Bartolomé Maso, National Park Pico Turquino (20.05269N -76.502926W), 24-25/III/ 2012, Col. CarBioTEAM.	X		
Bryanattus keyserlingi	CU787625	CUBA: Granma, Bartolomé Maso, National Park Pico Turquino (20.05269N -76.502926W), 24-25/III/ 2012, Col. CarBioTEAM.	X		X
Bryanattus keyserlingi	CU787302	CUBA: Granma, Bartolomé Maso, National Park Pico Turquino (20.05269N -76.502926W), 24-25/III/ 2012, Col. CarBioTEAM.	X	X	X
Bryanattus keyserlingi	CU782822	CUBA: Granma, Bartolomé Maso, National Park Pico Turquino (20.05269N -76.502926W), 24-25/III/ 2012, Col. CarBioTEAM.	X	X	X
Bryanattus keyserlingi	CU03538A CU02467A	CUBA: Holguin, Frank Pais, National Park Mesura-Piloto (20.529N -75.768), 10-12/IV/ 2012, Col. F. Cala-Riquelme, A Deler-Hernández, R. Anderson, G. Y. Zhang, A. Smith.	X		
Bryanattus keyserlingi	CU03395A	CUBA: Holguin, Frank Pais, National Park Mesura-Piloto (20.529N -75.768), 10-12/IV/ 2012, Col. F. Cala-Riquelme, A Deler-Hernández, R. Anderson, G. Y. Zhang, A. Smith.	X	X	X
Bryanattus keyserlingi	CU03036A CU03274A	CUBA: Granma, Bartolomé Maso, National Park Pico Turquino, sendero de la Mariposa (20.015N -76.8399W), 3/II/ 2012, Col. Col. F. Cala-Riquelme, A Deler-Hernández.	X		
Bryanattus orientalis **sp. nov.**	CU00025A CU00086A	CUBA: Granma, Bartolomé Maso, National Park Pico Turquino, Aguada de Joaquin (20.01309N - 76.83400W), 28/III/ 2012, Col. CarBioTEAM.	X		
Bryanattus orientalis **sp. nov.**	CU00090A	CUBA: Granma, Bartolomé Maso, National Park Pico Turquino, Aguada de Joaquin (20.01309N - 76.83400W), 28/III/ 2012, Col. CarBioTEAM.	X	X	
Bryanattus orientalis **sp. nov.**	CU00004A CU00016A	CUBA: Granma, Bartolomé Maso, National Park Pico Turquino (20.05269N -76.502926W), 24-25/III/ 2012, Col. CarBioTEAM.	X		
Bryanattus sanchezi **sp. nov.**	CU787945	CUBA: Granma, Bartolomé Maso, National Park Pico Turquino, Subida a Palma Mocha km 2.5 (20.00939N - 76.89402W), 26/III/ 2012, Col. CarBioTEAM.	X	X	X
Bryanattus sanchezi **sp. nov.**	CU00107A	CUBA: Granma, Bartolomé Maso, National Park Pico Turquino, Subida a Palma Mocha km 2.5 (20.00939N - 76.89402W), 26/III/ 2012, Col. CarBioTEAM.	X		

Bryanattus [Cuba1]	CU787957 CU03506A	CUBA: Pinar del Rio, Viñales, National Park Viñales, (22.65707N - 83.70161W), 20-21/IV/ 2012, Col. CarBioTEAM.	X		
Bryanattus thanos **sp.nov**	CU00100A CU03361A	CUBA: Guantánamo, Baracoa, Ecological Reserve Yunque-Duaba-Quibijan, El Yunque (20.33178N - 74.56919W), 04/IV/2012, Col. CarBioTEAM.	X		
Bryanattus thanos **sp.nov**	CU03317A	CUBA: Guantánamo, Baracoa, Ecological Reserve Yunque-Duaba-Quibijan, El Yunque (20.33178N - 74.56919W), 04/IV/2012, Col. CarBioTEAM.	X		X
Bryanattus thanos **sp.nov**	CU03121A	CUBA: Guantánamo, Nibujón, National Park Humbolt, Santa Maria del Loreto (20.05269N - 76.502926W), 1-5/II/ 2012, Col. F. Cala-Riquelme, A. Deler-Hernández Martin Fikacek	X		
Bythocrotus cf. crypticus	JXZ323	DOMINICAN REPUBLIC: El Seibo: Pedro Sanchez (N18.86 W69.11)	Zhang and Maddison 2013	Zhang and Maddison 2013	
Bythocrotus crypticus	JXZ322	DOMINICAN REPUBLIC: Barahona: Parque Nacional Sierra Martín García (N18.424 W71.112)	Zhang and Maddison 2013	Zhang and Maddison 2013	
Cobanus cambridgei	JXZ122	COSTA RICA: Prov. San José: Aprox. 10km from Santa Maria de Dota towards Naranjillo Village (N9.65 W83.97)		Zhang and Maddison 2013	Zhang and Maddison 2013
Cobanus extensus	JXZ122	ECUADOR: Pichincha: near El Cisne (N0.1493 W79.0317)		Zhang and Maddison 2013	Zhang and Maddison 2013
Cobanus mandibularis	JXZ245	PANAMA: Panamá: Gamboa, Pipeline Road (N9.15840 W79.74252)		Zhang and Maddison 2013	Zhang and Maddison 2013
Cobanus unicolor	JXZ244	PANAMA: Chiriqui: Fortuna, Quebrada Samudio (N8.73464 W82.24839)		Zhang and Maddison 2013	Zhang and Maddison 2013
Compsodecta festiva	JAM4122A	JAMAICA: Portland, Millbank (N18.013361, W76.37975)	X		
Compsodecta haytiensis	JXZ325	DOMINICAN REPUBLIC: Barahona: Highway 44 south of Barahona (N18.138 W71.070)	Zhang and Maddison 2013	Zhang and Maddison 2013	Zhang and Maddison 2013
Compsodecta peckhami	JXZ327	DOMINICAN REPUBLIC: Pedernales: Rio Mulito (N18.155 W71.758)		Zhang and Maddison 2013	Zhang and Maddison 2013
Corticattus guajataca	JXZ305	PUERTO RICO: Isabela: Bosque de Guajataca (N18.421 W66.966)	Zhang and Maddison 2013	Zhang and Maddison 2013	Zhang and Maddison 2013
Corticattus latus	JXZ337	DOMINICAN REPUBLIC: Pedernales: Laguna de Oviedo (N17.802 W 71.349)	Zhang and Maddison 2013	Zhang and Maddison 2013	Zhang and Maddison 2013
Mexigonus arizonenzis	JXZ163	USA: Arizona: Yavapai Co., Iron Springs (N34.58476 W112.57071)	Zhang and Maddison 2013	Zhang and Maddison 2013	Zhang and Maddison 2013
Mexigonus cf. minuta	d117	ECUADOR: Pichincha: Quito	X	X	X
Mexigonus morosus	JXZ362	USA: California: San Mate Co. (N37.434 W122.311)		Zhang and Maddison 2013	Zhang and Maddison 2013
Paracobanus [French guiana2]	JXZ100	FRENCH GUIANA: Commune Règina, les Nourages Field Station (N4.069 W52.669)	Zhang and Maddison 2013	Zhang and Maddison 2013	Zhang and Maddison 2013
Pensacola signata	JXZ371	GUATEMALA: Depto. Petén: Reserva Natural Ixpanpajul		Zhang and Maddison 2013	Zhang and Maddison 2013
Pensacolatus darlingtoni	JXZ341	DOMINICAN REPUBLIC: La Vega: Reserva Científica Ébano Verde (N19.033 W70.543)	Zhang and Maddison 2013	Zhang and Maddison 2013	Zhang and Maddison 2013
Pensacolatus darlingtoni	787120	DOMINICAN REPUBLIC: San Juan: Pico Duarte	X	X	
Pensacolatus darlingtoni	786937 784873	DOMINICAN REPUBLIC: Valle nuevo	X	X	
Pensacolatus darlingtoni	784828 784873	DOMINICAN REPUBLIC: Ebano Verde: Midtrail (N19.02645-19.02645)	X	X	
Pensacolatus maxillosus	JXZ335	DOMINICAN REPUBLIC: La Vega: road Constanza to Ocoa, Valle Nuevo (N18.700 W70.606)	Zhang and Maddison 2013	Zhang and Maddison 2013	Zhang and Maddison 2013

Pensacolatus scutiformis	JXZ326	DOMINICAN REPUBLIC: La Vega: road Constanza to Ocoa, Valle Nuevo (N18.848 W70.720)		Zhang and Maddison 2013	Zhang and Maddison 2013
Pensacolatus. maxillosus	DR786952 DR786992 DR786981	DOMINICAN REPUBLIC: Valle nuevo, Villa Pajón (N18.82208, W070.6838)	X	X	
Petemathis portoricensis	PR782206	PUERTO RICO: Villalba: Toro negro, El Bolo Trail (N18.1777401, W66.488319)	X	X	
Petemathis portoricensis [Adjuntas]	JXZ306	PUERTO RICO: Adjuntas: HWY143 to Cerro Punta (N18.167 W66.576)	Zhang and Maddison 2013	Zhang and Maddison 2013	Zhang and Maddison 2013
Petemathis portoricensis [Maricao]	JXZ303	PUERTO RICO: Maricao: Bosque de Maricao (N18.150 W66.994)	Zhang and Maddison 2013	Zhang and Maddison 2013	Zhang and Maddison 2013
Petemathis tetuani	JXZ303	PUERTO RICO: Maricao: Bosque de Maricao (N18.150 W66.994)	Zhang and Maddison 2013	Zhang and Maddison 2013	Zhang and Maddison 2013
Petemathis tetuani	PR782277	PUERTO RICO: Villalba: Toro negro, El Bolo Trail (N18.1777401, W66.488319)	X	X	
Petemathis tetuani	PR392859	PUERTO RICO: Rio Grande: El Yunque, Mt. Britton (N18.295744, W65.790649)	X	X	
Popcornella furcata	JXZ334	DOMINICAN REPUBLIC: La Vega: Reserva Científica Ébano Verde (N19.04 W70.518)	Zhang and Maddison 2013	Zhang and Maddison 2013	Zhang and Maddison 2013
Popcornella spiniformis	JXZ339	DOMINICAN REPUBLIC: Barahona: Cachote (N18.098 W71.187)		Zhang and Maddison 2013	Zhang and Maddison 2013
Popcornella yunque	JXZ309	PUERTO RICO: Río Grande: El Yunque Nat. Forest (N18.3174 W65.8314)		Zhang and Maddison 2013	Zhang and Maddison 2013
Sidusa [French guiana1]	JXZ128	FRENCH GUIANA: Commune Règina, les Nourages Field Station (N4.069 W52.669)	Zhang and Maddison 2013	Zhang and Maddison 2013	Zhang and Maddison 2013
Truncattus martii **sp. nov**	CU00014A	CUBA: Granma, Bartolomé Maso, National Park Pico Turquino (20.05269N -76.502926W)	X		
Truncattus [Cuba2]	CU787947 CU03405A	CUBA: Granma, Bartolomé Maso, National Park Pico Turquino (20.05269N -76.502926W)	X	X	X
Truncattus [Cuba1]	CU787949 CU00083A CU03065A	CUBA: Granma, Bartolomé Maso, National Park Pico Turquino (20.05269N -76.502926W)	X		
Truncattus platnicki **sp. nov.**	CU3492A	CUBA: Granma, Bartolomé Maso, National Park Pico Turquino (20.05269N -76.502926W)	X		
Truncattus [Dominican Republic]	DR787029	DOMINICAN REPUBLIC: Valle nuevo, Villa Pajón (N18.82208, W070.6838)	X		
Truncattus cachotensis	JXZ338	DOMINICAN REPUBLIC: Barahona: Cachote (N18.101 W71.194)	Zhang and Maddison 2013	Zhang and Maddison 2013	Zhang and Maddison 2013
Truncattus dominicanus	JXZ340	DOMINICAN REPUBLIC: La Vega: P.N.Armando Bermúdez (N19.06 W70.86)	Zhang and Maddison 2013	Zhang and Maddison 2013	Zhang and Maddison 2013
Truncattus dominicanus	DR787325	DOMINICAN REPUBLIC: San Juan, Los tablones (19.05116N, -70.88866 W)	X	X	
Truncattus flavus	JXZ332	DOMINICAN REPUBLIC: La Vega: P.N.Armando Bermúdez (N19.06 W70.86)	Zhang and Maddison 2013	Zhang and Maddison 2013	Zhang and Maddison 2013
Ghelna canadensis	JQ312080.1	USA: North Carolina (N35.70446 W82.36339)	EF201651	X	KT462689.1

Supplementary table 2 Scored morphological matrix. "-" indicates the character is not applicable in the species; "?" indicates the character state is ambiguous in the species or not known.

	char.1	char.2	char.3	char.4	char.5	char.6	char.7	char.8	char.9	char.10	char.11	char.12	char.13	char.14	char.15	char.16	char.17	char.18	char.19	char.20	char.21	char.22	char.23	char.24	char.25	char.26	char.27	char.28	char.29	char.30	char.31	char.32	char.33	char.34	char.35	char.36	char.37	char.38	char.39	char.40	char.41	char.42	char.43	char.44	char.45	char.46	char.47	char.48	char.49	char.50	char.51	char.52	char.53	char.54	char.55	char.56	char.57	char.58	char.59	char.60	char.61	char.62	char.63
Ghelna canadensis	0	1	0	0	-	0	1	1	1	0	1	0	0	0	-	1	0	0	0	0	0	-	1	1	0	1	0	0	0	-	1	0	0	0	0	1	0	0	0	-	1	1	0	0	1	1	0	0	0	0	0	0	0	0	0	0	?	0	0	0	0	1	2
Pensacola signata	0	1	1	1	1	1	1	1	1	0	1	0	0	0	-	1	0	0	0	0	0	-	1	1	0	1	0	0	0	-	1	0	0	0	0	1	0	0	0	-	1	0	0	1	1	1	0	1	0	1	0	0	1	0	0	2	1	0	1	0	0	1	2
Pensacola sylvestri	0	1	1	1	1	1	1	?	?	?	?	?	?	?	?	?	?	?	?	?	?	?	1	1	0	1	0	0	0	-	1	0	0	0	0	1	0	0	0	-	1	0	0	1	1	1	0	1	0	1	0	0	1	0	0	2	1	0	1	0	0	?	2
Caribattus inutilis	0	1	1	1	1	1	1	?	?	?	?	?	?	?	?	?	?	?	?	?	?	?	1	1	0	1	0	0	1	0	1	0	0	0	0	1	0	0	0	-	1	0	0	0	0	1	0	0	0	0	0	1	0	0	0	1	1	0	1	0	0	1	2
Caribattus cf. inutilis	0	1	1	1	1	1	1	1	1	0	1	0	0	0	-	1	0	0	0	0	0	-	1	1	0	1	0	0	1	0	1	0	0	0	0	1	0	0	0	-	1	0	0	0	0	1	0	0	0	0	0	0	0	0	0	1	1	0	1	0	0	1	2
Sidusa sp. French Guiana2	0	1	1	0	-	1	1	1	1	0	1	0	0	0	-	1	1	0	0	0	1	0	1	1	0	1	0	0	0	-	1	1	0	0	0	1	0	0	1	0	1	0	0	0	0	1	0	0	0	0	0	0	0	0	0	1	0	0	1	0	0	2	3
cf. Sidusa sp1 Colombia	0	1	1	0	-	1	1	1	1	0	1	0	0	0	-	1	1	0	0	0	1	0	1	1	0	1	0	0	0	-	1	1	0	0	0	1	0	0	1	0	1	0	0	0	0	1	0	0	0	0	0	0	0	0	0	1	0	0	1	0	0	2	3
cf. Sidusa sp2 Colombia	0	1	1	0	-	1	1	1	1	0	1	0	0	0	-	1	1	0	0	0	1	0	1	1	0	1	0	0	0	-	1	1	0	0	0	1	0	0	0	-	1	0	0	0	0	1	0	0	0	0	0	0	0	0	0	1	0	0	1	0	0	2	3
Mexigonus arizonensis	0	0	-	-	-	0	0	1	1	0	1	0	0	0	-	1	0	0	0	0	0	-	1	1	0	1	0	0	0	-	1	0	0	0	0	1	0	0	0	-	1	0	1	0	0	1	0	0	0	0	0	0	0	0	0	1	1	0	0	0	0	1	2
Mexigonus cf. minutus	0	0	-	-	-	0	0	1	1	0	1	0	0	0	-	1	0	0	0	0	0	-	1	1	0	1	0	0	0	-	1	0	0	0	0	1	0	0	0	-	1	0	0	0	0	1	0	0	0	0	0	0	0	0	0	1	1	0	0	0	0	1	2
Mexigonus morosus	0	0	-	-	-	0	0	1	1	0	1	0	0	0	-	1	0	0	0	0	0	-	1	1	0	1	0	0	0	-	1	0	0	0	0	1	0	0	0	-	1	0	0	0	0	1	0	0	0	0	0	0	0	0	0	1	1	0	0	0	0	1	2
Popcornella spiniformis	0	0	-	-	-	1	1	1	1	0	1	0	0	0	-	1	0	0	0	0	0	-	1	1	0	1	0	0	0	-	1	0	0	0	0	1	0	0	0	-	1	0	0	0	0	1	0	0	0	0	0	0	0	0	0	0	1	0	0	0	0	1	2
Popcornella yunque	0	0	-	-	-	1	1	1	1	0	1	0	0	0	-	1	0	0	0	0	0	-	1	1	0	1	0	0	0	-	1	0	0	0	0	1	0	0	0	-	1	0	0	0	0	1	0	0	0	0	0	0	0	0	0	0	1	0	0	0	0	1	2
Popcornella furcata	0	0	-	-	-	1	1	1	1	0	1	0	0	0	-	1	0	0	0	0	0	-	1	1	0	1	0	0	0	-	1	0	0	0	0	1	0	0	0	-	1	0	0	0	0	1	0	0	0	0	0	0	0	0	0	0	1	0	0	0	0	1	2
Agobardus gramineus	0	1	1	1	1	1	1	1	1	0	1	0	0	0	-	1	1	0	0	0	0	-	1	1	0	1	0	0	0	-	1	1	0	0	0	1	0	0	1	0	0	0	0	0	1	1	0	0	0	0	0	0	0	0	0	0	2	0	0	0	0	1	2
Agobardus cf. anormalis montanus	1	1	1	1	1	1	1	1	1	0	1	0	0	0	-	1	1	0	0	0	0	-	1	1	0	1	0	0	0	-	1	1	0	0	0	1	0	0	1	0	2	0	0	0	2	1	1	1	0	0	0	0	0	0	0	0	1	0	1	0	0	1	2
Agobardus bahoruco	0	1	1	1	1	1	1	1	1	0	1	0	0	0	-	1	1	0	0	0	0	-	1	1	0	1	0	0	0	-	1	1	0	0	0	1	0	0	1	0	0	0	0	0	2	1	1	1	0	0	0	0	0	0	0	0	1	0	1	0	0	1	2
Agobardus cf. brevitarsus	0	1	1	1	1	1	1	1	1	0	1	0	0	0	-	1	1	0	0	0	0	-	1	1	0	1	0	0	0	-	1	1	0	0	0	1	0	0	1	0	2	0	0	0	1	1	1	1	0	0	0	0	0	0	0	0	2	0	0	0	0	1	2
Agobardus oviedo	0	1	1	1	1	1	1	1	1	0	1	0	0	0	-	1	1	0	0	0	0	-	1	1	0	1	0	0	0	-	1	1	0	0	0	1	0	0	1	0	2	0	0	0	2	1	0	0	0	0	0	0	0	0	0	0	2	0	0	0	0	1	2
Agobardus phylladiphilus	0	1	1	1	1	1	1	1	1	0	1	0	0	0	-	1	1	0	0	0	0	-	1	1	0	1	0	0	0	-	1	1	0	0	0	1	0	0	1	0	0	0	0	0	1	1	0	0	0	0	0	0	0	0	0	0	2	0	0	0	0	1	2
Agobardus cordiformis	0	1	1	1	1	1	1	1	1	0	1	0	0	0	-	1	1	0	0	0	0	-	1	1	0	1	0	0	0	-	1	1	0	0	0	1	0	0	1	0	2	0	0	0	1	1	0	0	0	0	0	0	0	0	0	0	2	0	0	0	0	1	2
Bythocrotus cf. crypticus	0	1	1	1	1	1	1	1	1	0	1	0	0	1	0	1	0	0	0	0	0	-	1	1	0	1	0	0	1	0	1	0	0	0	0	1	0	0	0	-	1	1	0	0	1	1	0	0	0	0	0	0	0	0	0	0	1	0	0	0	0	1	2
Bythocrotus crypticus	0	1	1	1	1	1	1	1	1	0	1	0	0	1	0	1	0	0	0	0	0	-	1	1	0	1	0	0	1	0	1	0	0	0	0	1	0	0	0	-	1	1	0	0	1	1	0	0	0	0	0	0	0	0	0	0	1	0	0	0	0	1	2
Compsodecta haytiensis	0	1	1	1	0	1	1	1	1	0	1	0	0	0	-	1	0	0	0	0	0	-	1	1	0	1	0	0	0	-	1	0	0	0	0	1	0	0	0	-	1	0	0	0	1	1	0	1	0	0	0	0	0	0	0	0	1	0	0	0	0	1	2
Compsodecta peckhami	0	1	1	1	0	1	1	1	1	0	1	0	0	0	-	1	0	0	0	0	0	-	1	1	0	1	0	0	0	-	1	0	0	0	0	1	0	0	0	-	1	0	0	0	1	1	0	1	1	0	0	0	0	0	0	0	1	0	0	0	0	1	2
Compsodecta festiva JAM4122A	0	1	1	1	0	1	1	1	1	0	1	0	0	0	-	1	0	0	0	0	0	-	1	1	0	1	0	0	0	-	1	0	0	0	0	1	0	0	0	-	1	0	0	0	1	1	0	1	1	0	0	1	0	0	0	0	2	0	0	0	0	1	2
Allodecta maxilaris	0	1	1	1	0	1	1	?	?	?	?	?	?	?	-	1	?	?	?	?	?	?	1	1	0	1	0	0	0	-	1	0	0	0	0	1	0	0	0	-	1	0	0	0	1	1	0	1	1	0	0	1	0	0	0	0	2	0	0	0	0	?	3
Compsodecta gratiosa	0	1	1	1	0	1	1	?	?	?	?	?	?	?	?	?	?	?	?	?	?	?	1	1	0	1	0	0	0	-	1	0	0	0	0	1	0	0	0	-	1	0	0	0	1	1	0	1	1	0	0	1	0	0	0	0	2	0	0	0	0	?	2
Compsodecta grisea	0	1	1	1	0	1	1	1	1	0	1	0	0	0	-	1	0	0	0	0	0	-	1	1	0	1	0	0	0	-	1	0	0	0	0	1	0	0	0	-	1	0	0	0	1	1	0	1	0	0	0	1	1	0	0	0	2	0	0	0	0	1	2
Compsodecta valida	0	1	1	1	0	1	1	?	?	?	?	?	?	?	-	1	?	?	?	?	?	?	1	1	0	1	0	0	0	-	1	0	0	0	0	1	0	0	0	-	1	0	0	0	1	1	0	1	1	0	0	1	0	0	0	0	2	0	0	0	0	?	2
Corticattus guajataca	0	1	0	0	-	1	0	1	1	0	1	0	0	0	-	1	1	0	0	0	1	1	1	1	0	1	0	0	1	0	1	0	0	0	0	1	0	0	0	-	0	0	0	0	0	0	0	0	0	0	0	0	0	0	0	0	2	0	0	0	0	0	0
Corticattus latus	0	1	0	0	-	1	0	1	1	0	1	0	0	0	-	1	1	0	0	0	1	1	1	1	0	1	0	0	1	0	1	0	0	0	0	1	0	0	0	-	0	0	0	0	0	0	0	0	0	0	0	0	0	0	0	0	2	0	0	0	0	0	0
Pensacolatus cf. applanatus	0	1	1	1	1	1	1	1	1	0	1	0	0	0	-	1	0	0	0	0	0	-	1	1	0	1	0	0	1	0	1	0	0	0	0	1	0	0	0	-	1	0	1	1	1	1	0	1	0	1	0	0	0	0	1	1	1	0	1	0	0	1	2
Pensacolatus darlingtoni	0	1	1	1	1	1	1	1	1	0	1	0	0	0	-	1	0	0	0	0	0	-	1	1	0	1	0	0	1	0	1	0	0	0	0	1	0	0	0	-	1	0	1	1	1	1	0	1	0	1	0	0	1	0	1	1	1	0	1	0	0	1	2
Pensacolatus maxillosus	0	1	1	1	1	1	1	1	1	0	1	0	0	0	-	1	0	0	0	0	0	-	1	1	0	1	0	0	1	0	1	0	0	0	0	1	0	0	0	-	1	0	1	1	1	1	0	1	0	0	0	0	0	0	1	1	1	0	1	0	0	1	2
Pensacolatus scutiformis	0	1	1	1	1	1	1	1	1	0	1	0	0	0	-	1	0	0	0	0	0	-	1	1	0	1	0	0	1	0	1	0	0	0	0	1	0	0	0	-	1	0	1	1	1	1	0	1	0	0	0	0	0	0	1	1	2	0	1	1	1	1	2
Antillattus cambridgei	0	1	1	1	0	1	1	1	1	0	1	0	0	0	-	1	1	1	1	1	1	1	1	1	0	1	0	0	0	-	1	1	1	1	0	1	0	0	1	1	2	0	0	1	2	2	2	1	0	0	1	0	0	0	1	2	1	0	0	0	0	1	2
Antillattus cubensis CU3075A	0	1	1	1	0	1	1	1	1	1	1	0	0	0	-	1	1	1	1	1	1	1	1	1	1	1	0	0	0	-	1	1	1	1	0	1	0	0	1	1	2	0	0	1	2	2	2	1	0	0	1	0	0	0	1	2	2	0	1	0	0	1	2
Antillattus placidus DR782502	0	1	1	1	0	1	1	1	1	1	1	0	0	0	-	1	1	1	1	1	1	1	1	1	1	1	0	0	0	-	1	1	1	1	0	1	0	0	1	1	2	0	0	1	2	2	2	1	0	0	1	0	0	0	1	2	1	0	1	0	0	1	2
Petemathis portoricensis M	0	1	1	0	-	1	1	1	1	0	1	0	0	0	-	1	1	1	1	0	1	1	1	1	0	1	0	0	0	-	1	1	1	1	0	1	0	0	1	1	0	1	0	0	1	1	0	0	0	0	0	0	0	0	0	1	1	0	0	0	0	1	2
Petemathis portoricensis A	0	1	1	0	-	1	1	1	1	0	1	0	0	0	-	1	1	1	1	0	1	1	1	1	0	1	0	0	0	-	1	1	1	1	0	1	0	0	1	1	0	1	0	0	1	1	0	0	0	0	0	0	0	0	0	1	1	0	0	0	0	1	2
Petemathis tetuani	0	1	1	0	-	1	1	1	1	0	1	0	0	0	-	1	1	1	1	0	1	1	1	1	0	1	0	0	0	-	1	1	1	1	0	1	0	0	1	1	0	1	0	0	1	1	0	0	0	0	0	0	0	0	0	1	1	0	0	0	0	1	2
Truncattus cachotensis	0	1	1	1	1	1	1	1	1	0	1	0	0	0	-	1	1	0	0	0	1	0	1	1	0	1	0	0	0	-	1	1	0	0	0	1	0	0	1	0	0	1	0	0	1	1	0	0	0	0	0	0	0	0	0	1	2	0	0	0	0	1	2
Truncattus dominicanus	0	1	1	1	1	1	1	1	1	0	1	0	0	0	-	1	1	0	0	0	1	0	1	1	0	1	0	0	0	-	1	1	0	0	0	1	0	0	1	0	0	0	0	0	1	1	0	0	0	0	0	0	0	0	0	1	2	0	0	0	0	1	2
Truncattus flavus	0	1	1	1	1	1	1	1	1	0	1	0	0	0	-	1	1	0	0	0	1	0	1	1	0	1	0	0	0	-	1	1	0	0	0	1	0	0	1	0	0	1	0	0	1	1	0	0	0	0	0	0	0	0	0	1	1	0	1	0	0	1	2
Truncattus turquinencis CU787947	0	1	1	1	1	1	1	1	1	0	1	0	0	0	-	1	0	0	0	0	0	-	1	1	0	1	0	0	0	-	1	0	0	0	0	1	0	0	0	-	0	1	0	0	1	1	0	0	0	0	0	0	0	0	0	1	2	0	1	0	0	1	2
Truncattus CU3492A	0	1	1	1	1	1	1	1	1	0	1	0	0	0	-	1	0	0	0	0	0	-	1	1	0	1	0	0	0	-	1	0	0	0	0	1	0	0	0	-	0	1	0	0	1	1	0	0	0	0	0	0	0	0	0	1	2	0	0	0	0	1	2
Truncattus CU0083A	0	1	1	1	1	1	1	1	1	0	1	0	0	0	-	1	0	0	0	0	0	-	1	1	0	1	0	0	0	-	1	0	0	0	0	1	0	0	0	-	0	1	0	0	1	1	0	0	0	0	0	0	0	0	0	1	2	0	0	0	0	1	2
Truncattus CU0014A	0	1	1	1	1	1	1	1	1	0	1	0	0	0	-	1	0	0	0	0	0	-	1	1	0	1	0	0	0	-	1	0	0	0	0	1	0	0	0	-	0	1	0	0	1	1	0	0	0	0	0	0	0	0	0	1	2	0	0	0	0	1	2
Truncattus DR787029	0	1	1	1	1	1	1	1	1	0	1	0	0	0	-	1	0	0	0	0	0	-	1	1	0	1	0	0	0	-	1	0	0	0	0	1	0	0	0	-	0	1	0	0	1	1	0	0	0	0	0	0	0	0	0	1	2	0	0	0	0	1	2
Antillattus ocultus CU3534A	0	1	1	1	0	1	1	1	1	1	1	0	0	0	-	1	1	1	1	1	1	1	1	1	1	1	0	0	0	-	1	1	1	1	0	1	0	0	1	1	2	0	0	1	2	2	2	1	0	0	1	0	0	0	1	2	2	0	1	0	0	1	2
Antillattus gracilis	0	1	1	1	0	1	1	1	1	1	1	0	0	0	-	1	1	1	1	1	1	1	1	1	1	1	0	0	0	-	1	1	1	1	0	1	0	0	1	1	2	0	0	1	2	2	2	1	0	0	1	0	0	0	1	2	2	0	1	0	0	1	2
Bryanattus keyserlingi CU3395A	0	1	1	1	0	1	1	1	1	0	1	0	0	0	-	1	1	1	1	1	1	1	1	1	0	1	0	0	1	0	1	1	1	1	0	1	0	0	1	1	2	0	1	1	2	2	1	1	0	1	0	0	0	1	1	2	1	1	0	0	0	1	2
Bryanattus sp4 CU3317A	0	1	1	1	0	1	1	1	1	0	1	0	0	0	-	1	1	1	1	1	1	1	1	1	0	1	0	0	1	0	1	1	1	1	0	1	0	0	1	1	1	0	1	1	2	2	0	1	0	1	0	0	0	1	1	1	1	0	0	0	0	1	2
Bryanattus sp1 CU787945	0	1	1	1	0	1	1	1	1	0	1	0	0	0	-	1	1	1	1	1	1	1	1	1	0	1	0	0	1	0	1	1	1	1	0	1	0	0	1	1	1	0	1	1	2	1	0	1	0	1	0	0	1	0	1	1	2	0	0	0	0	1	2
Bryanattus sp3 CU787957	0	1	1	1	0	1	1	1	1	0	1	0	0	0	-	1	1	1	1	1	1	1	1	1	0	1	0	0	1	0	1	1	1	1	0	1	0	0	1	1	1	0	1	1	2	1	0	1	0	1	0	0	0	0	1	1	2	0	0	0	0	1	2
Bryanattus sp2 CU00090A	0	1	1	1	0	1	1	1	1	0	1	0	0	0	-	1	1	1	1	1	1	1	1	1	0	1	0	0	1	0	1	1	1	1	0	1	0	0	1	1	1	0	1	1	2	1	0	1	0	1	0	0	0	1	1	1	1	0	0	0	0	1	2
Cobanus multidentatis sp. nov	0	0	-	-	-	1	1	1	1	0	1	0	0	0	-	1	1	1	1	1	1	1	1	1	0	1	0	0	0	-	1	1	1	1	1	0	1	1	0	-	1	0	0	0	2	2	2	1	0	0	0	0	0	0	0	2	1	0	0	0	0	2	3
Cobanus extensus	0	0	-	-	-	1	1	1	1	0	1	0	0	0	-	1	1	0	0	0	0	-	1	1	0	1	0	0	0	-	0	0	0	1	1	0	1	1	0	-	1	0	0	0	2	2	2	1	0	0	0	0	0	0	0	2	1	0	0	0	0	2	3
Cobanus electus	0	0	-	-	-	1	1	1	1	0	1	0	0	0	-	1	1	0	0	0	1	0	1	1	0	1	0	0	0	-	0	0	0	1	1	0	1	1	0	-	1	0	0	0	2	2	2	1	0	0	0	0	0	0	0	2	1	0	0	0	0	2	3
Cobanus cf. cambridgei	0	0	-	-	-	1	1	1	1	0	1	0	0	0	-	1	1	0	0	0	1	0	1	1	0	1	0	0	0	-	0	0	0	1	1	0	1	1	0	-	1	0	0	0	2	2	2	1	0	0	0	0	0	0	0	2	1	0	0	0	0	2	3
Cobanus mandibularis	0	0	-	-	-	1	1	1	1	0	1	0	0	0	-	1	1	0	0	0	1	0	1	1	0	1	0	0	0	-	0	0	0	1	1	0	1	1	0	-	1	0	0	0	2	2	2	1	0	0	0	0	0	0	0	2	1	0	0	0	0	2	3
Cobanus unicolor	0	0	-	-	-	1	1	1	1	0	1	0	0	0	-	1	1	0	0	0	1	0	1	1	0	1	0	0	0	-	0	0	0	1	1	0	1	1	0	-	1	0	0	0	2	2	2	1	0	0	0	0	0	0	0	2	1	0	0	0	0	2	3
Cobanus colombiano sp. nov	0	0	-	-	-	1	1	1	1	0	1	0	0	0	-	1	1	0	0	0	1	0	1	1	0	1	0	0	0	-	0	0	0	1	1	0	1	1	0	-	1	0	0	0	2	2	2	1	0	0	0	0	0	0	0	2	1	0	0	0	0	2	3
Sidusa sp. French Guiana1	0	0	-	-	-	1	1	1	1	0	1	0	0	0	-	1	1	0	0	0	1	0	1	1	0	1	0	0	0	-	1	1	0	0	0	1	0	0	1	0	1	0	0	0	0	1	0	0	0	0	0	0	0	0	0	1	?	0	0	0	0	2	3
Sidusa gratiosa type sp	0	0	-	-	-	1	1	1	1	0	1	0	0	0	-	1	1	0	0	0	1	0	1	1	0	1	0	0	0	-	1	1	0	0	0	1	0	0	1	0	1	0	0	0	0	1	0	0	0	0	0	0	0	0	0	1	?	0	0	0	0	2	3
Sidusa sp1 colombia	0	0	-	-	-	1	1	1	1	0	1	0	0	0	-	1	1	0	0	0	1	0	1	1	0	1	0	0	0	-	1	1	0	0	0	1	0	0	1	0	1	0	0	0	0	1	0	0	0	0	0	0	0	0	0	1	0	0	0	0	0	2	3
Sidusa sp2 Colombia	0	0	-	-	-	1	1	1	1	0	1	0	0	0	-	1	1	0	0	0	1	0	1	1	0	1	0	0	0	-	1	1	0	0	0	1	0	0	1	0	1	0	0	0	0	1	0	0	0	0	0	0	0	0	0	1	0	0	0	0	0	2	3

Taxon	char.64	char.65	char.66	char.67	char.68	char.69	char.70	char.71	char.72	char.73	char.74	char.75	char.76	char.77	char.78	char.79	char.80	char.81	char.82	char.83	char.84	char.85	char.86	char.87	char.88	char.89	char.90	char.91	char.92	char.93	char.94
Ghelna canadensis	0	1	0	-	0	1	0	0	0	0	0	2	0	0	0	0	0	0	1	0	1	0	1	1	0	1	0	0	0	-	-
Pensacola signata	0	1	0	-	0	1	1	1	0	1	1	0	1	0	0	0	0	0	0	1	1	1	0	-	-	1	0	1	1	1	1
Pensacola sylvestri	?	1	0	-	0	1	1	1	0	1	1	0	1	0	0	0	0	0	0	1	1	1	0	-	-	1	0	1	1	1	1
Caribattus inutilis	0	1	0	-	0	0	-	0	0	0	0	0	1	0	0	0	0	0	0	1	1	0	0	-	-	1	0	0	1	2	1
Caribattus cf. inutilis	0	1	0	-	0	0	-	0	0	0	0	0	1	0	0	0	0	0	0	1	1	0	0	-	-	1	0	0	1	2	1
Sidusa sp. French Guiana2	1	2	1	0	0	0	-	1	0	0	1	1	1	0	0	0	0	0	0	1	1	0	0	-	-	1	1	0	1	1	1
cf. Sidusa sp1 Colombia	1	2	1	0	0	0	-	1	0	0	1	0	1	0	0	0	0	0	0	1	1	0	0	-	-	1	1	0	1	1	1
cf. Sidusa sp2 Colombia	1	2	1	0	0	0	-	1	0	0	1	0	1	0	0	0	0	0	0	1	1	0	0	-	-	1	1	0	1	1	1
Mexigonus arizonensis	0	1	0	-	0	0	-	0	0	0	0	1	1	0	0	0	1	0	0	1	1	0	1	1	1	1	0	0	1	2	1
Mexigonus cf. minutus	0	1	0	-	0	0	-	0	0	0	0	2	1	0	0	0	1	0	0	1	1	0	1	1	1	1	0	0	1	2	1
Mexigonus morosus	0	1	0	-	0	0	-	0	0	0	0	1	1	0	0	0	1	0	0	1	1	0	1	1	1	1	0	0	1	1	1
Popcornella spiniformis	0	1	0	-	0	0	-	0	0	0	0	0	0	0	0	0	0	0	1	0	0	0	1	2	1	1	0	0	1	1	1
Popcornella yunque	0	1	0	-	0	0	-	0	0	0	0	0	1	0	0	0	0	1	1	0	0	0	1	2	1	0	-	0	1	1	1
Popcornella furcata	0	1	0	-	0	0	-	0	0	0	0	0	1	0	0	0	0	1	1	0	0	0	1	2	1	1	0	0	1	1	1
Agobardus gramineus	1	2	0	-	0	0	-	0	0	0	0	0	0	0	0	0	0	0	0	1	1	0	0	-	-	1	1	0	1	2	1
Agobardus cf. anormalis montanus	1	2	0	-	0	0	-	0	0	0	0	0	1	0	0	0	0	0	0	1	1	0	0	-	-	1	1	0	1	2	1
Agobardus bahoruco	1	2	0	-	0	0	-	0	0	0	0	0	1	0	0	0	0	0	0	1	1	0	0	-	-	1	1	0	1	2	1
Agobardus cf. brevitarsus	1	2	0	-	0	0	-	0	0	0	0	0	1	0	0	0	0	0	0	1	1	0	0	-	-	1	1	0	1	1	1
Agobardus oviedo	1	2	0	-	0	0	-	0	0	0	0	0	1	0	0	0	0	0	0	1	1	0	0	-	-	1	1	0	1	2	1
Agobardus phylladiphilus	1	2	0	-	0	0	-	0	0	0	0	0	1	0	0	0	0	0	0	1	1	0	0	-	-	1	1	0	1	2	1
Agobardus cordiformis	1	2	0	-	0	0	-	0	0	0	0	0	0	0	0	0	0	0	0	1	1	0	0	-	-	1	0	0	1	1	1
Bythocrotus cf. crypticus	0	1	0	-	0	0	-	0	0	0	0	2	0	0	1	1	1	0	0	1	1	0	0	-	-	1	0	0	1	1	1
Bythocrotus crypticus	0	1	0	-	0	0	-	0	0	0	0	2	0	0	1	1	1	0	0	1	1	0	0	-	-	1	0	0	1	1	1
Compsodecta haytiensis	0	1	0	-	0	0	-	0	1	1	1	1	1	0	1	1	0	0	0	1	1	0	0	-	-	1	1	0	1	2	1
Compsodecta peckhami	0	1	0	-	0	0	-	1	1	1	1	2	0	1	1	1	1	0	0	1	1	0	0	-	-	1	1	0	1	1	1
Compsodecta festiva JAM4122A	0	1	0	-	0	0	-	0	1	1	1	3	1	0	1	1	1	1	0	1	1	0	0	-	-	1	1	0	1	2	1
Allodecta maxilaris	?	2	0	-	0	0	-	0	1	?	1	0	1	0	0	?	0	0	0	1	1	0	0	-	-	1	1	0	1	2	1
Compsodecta gratiosa	?	1	0	-	0	0	-	0	1	?	1	1	1	0	1	1	1	1	0	1	1	0	0	-	-	1	1	0	1	1	1
Compsodecta grisea	0	1	0	-	0	0	-	1	1	1	1	1	1	1	1	1	1	1	0	1	1	0	0	-	-	1	1	0	1	1	1
Compsodecta valida	?	1	0	-	0	0	-	0	1	?	1	3	1	0	1	?	1	1	0	1	1	0	0	-	-	1	1	0	1	?	1
Corticattus guajataca	0	0	0	-	0	1	0	0	0	0	0	0	0	0	0	0	1	0	0	1	1	0	1	0	1	1	0	1	0	-	-
Corticattus latus	0	0	0	-	0	1	0	0	0	0	0	0	0	0	0	0	1	0	0	1	1	0	1	0	1	1	0	1	0	-	-
Pensacolatus cf. applanatus	0	1	0	-	0	1	1	1	0	1	1	0	1	0	0	0	0	0	0	1	1	0	1	1	1	1	1	0	1	0	0
Pensacolatus darlingtoni	0	1	0	-	0	1	1	1	0	1	1	0	1	0	0	0	1	0	0	1	1	0	1	0	0	1	1	0	1	0	0
Pensacolatus maxillosus	0	1	0	-	0	1	1	1	0	1	1	0	1	0	0	0	0	0	0	1	1	0	1	1	1	1	1	0	1	0	0
Pensacolatus scutiformis	0	1	0	-	0	1	1	1	0	1	1	0	1	0	0	0	1	0	0	1	1	0	1	0	1	1	1	0	1	0	0
Antillattus cambridgei	0	1	1	1	1	1	0	1	0	1	2	0	1	0	0	0	0	0	0	1	1	0	0	-	-	1	1	0	1	1	1
Antillattus cubensis CU3075A	0	1	1	1	1	1	0	1	0	1	2	0	1	0	0	0	0	0	0	1	1	0	0	-	-	1	1	0	1	1	1
Antillattus placidus DR782502	0	1	1	1	1	1	0	1	0	1	2	0	1	0	0	0	0	0	0	1	1	0	0	-	-	1	1	0	1	1	1
Petemathis portoricensis M	0	1	1	1	0	0	-	0	0	0	1	3	0	0	0	0	1	0	0	1	1	0	1	1	1	1	1	0	1	0	1
Petemathis portoricensis A	0	1	1	1	0	0	-	0	0	0	1	1	0	0	0	0	1	0	0	1	1	0	1	1	1	1	1	0	1	0	1
Petemathis tetuani	0	1	0	-	0	0	-	0	0	0	1	2	0	0	0	0	1	0	0	1	1	0	1	1	1	1	1	0	1	0	1
Truncattus cachotensis	0	1	0	-	0	1	0	0	0	0	0	0	1	0	0	0	1	0	0	2	1	0	1	2	2	1	1	0	1	0	1
Truncattus dominicanus	0	1	0	-	0	1	0	0	0	0	0	0	1	0	0	0	1	0	0	2	1	0	1	2	2	1	1	0	1	0	1
Truncattus flavus	0	1	0	-	0	1	0	0	0	0	0	0	1	0	0	0	1	0	0	2	1	0	1	2	2	1	1	0	1	0	1
Truncattus turquinencis CU787947	0	1	0	-	0	1	0	0	0	0	0	0	1	0	0	0	1	0	0	2	1	0	1	2	2	1	1	0	1	0	1
Truncattus CU3492A	0	1	0	-	0	1	0	0	0	0	0	0	1	0	0	0	1	0	0	2	1	0	1	2	2	1	1	0	1	0	1
Truncattus CU0083A	0	1	0	-	0	1	0	0	0	0	0	0	1	0	0	0	1	0	0	2	1	0	1	2	2	1	1	0	1	0	1
Truncattus CU0014A	0	1	0	-	0	1	0	0	0	0	0	0	1	0	0	0	1	0	0	2	1	0	1	2	2	1	1	0	1	0	1
Truncattus DR787029	0	1	0	-	0	1	0	0	0	0	0	0	1	0	0	0	1	0	0	2	1	0	1	2	2	1	1	0	1	0	1
Antillattus ocultus CU3534A	0	1	1	1	1	1	0	1	0	1	2	0	1	0	0	0	0	0	0	1	1	0	0	-	-	1	1	0	1	1	1
Antillattus gracilis	0	1	1	1	1	1	0	1	0	1	2	0	1	0	0	0	0	0	0	1	1	0	0	-	-	1	1	0	1	1	1
Bryanattus keyserlingi CU3395A	0	1	1	0	0	1	0	1	0	1	1	0	1	0	0	0	0	0	0	1	1	0	0	-	-	1	1	0	1	2	1
Bryanattus sp4 CU3317A	0	1	1	0	0	1	0	1	0	1	1	0	1	0	0	0	0	0	0	1	1	0	0	-	-	1	1	0	1	2	1
Bryanattus sp1 CU787945	0	1	1	0	0	1	0	1	0	1	1	0	1	0	0	0	0	0	0	1	1	0	0	-	-	1	1	0	1	2	1
Bryanattus sp3 CU787957	0	1	1	0	0	1	0	1	0	1	1	0	1	0	0	0	0	0	0	1	1	0	0	-	-	1	1	0	1	2	1
Bryanattus sp2 CU00090A	0	1	1	0	0	1	0	1	0	1	1	0	1	0	0	0	0	0	0	1	1	0	0	-	-	1	1	0	1	2	1
Cobanus multidentatis sp. nov	1	2	1	1	1	0	-	0	0	0	2	2	1	0	0	0	0	0	0	1	1	0	0	-	-	1	0	0	1	1	1
Cobanus extensus	1	2	1	1	1	0	-	0	0	0	2	0	1	0	0	0	0	0	0	1	1	0	0	-	-	1	0	0	1	1	1
Cobanus electus	1	2	1	1	1	0	-	0	0	0	2	?	1	0	0	0	0	0	0	1	1	0	0	-	-	1	0	0	1	1	1
Cobanus cf. cambridgei	1	2	1	1	1	0	-	0	0	0	2	?	1	0	0	0	0	0	0	1	1	0	0	-	-	1	0	0	1	1	1
Cobanus mandibularis	1	2	1	1	1	0	-	0	0	0	2	2	1	0	0	0	0	0	0	1	1	0	0	-	-	1	0	0	1	1	1
Cobanus unicolor	1	2	1	1	1	0	-	0	0	0	2	2	1	0	0	0	0	0	0	1	1	0	0	-	-	1	0	0	1	1	1
Cobanus colombiano sp. nov	1	2	1	1	1	0	-	0	0	0	2	2	1	0	0	0	0	0	0	1	1	0	0	-	-	1	0	0	1	1	1
Sidusa sp. French Guiana1	1	2	1	0	1	0	-	0	0	0	0	0	1	0	0	0	0	0	0	1	1	0	0	-	-	1	0	1	1	0	1
Sidusa gratiosa type sp	1	2	1	0	1	0	-	0	0	0	0	0	1	0	0	0	0	0	0	1	1	0	0	-	-	1	0	1	1	0	1
Sidusa sp1 colombia	1	2	1	0	1	0	-	0	0	0	0	0	1	0	0	0	0	0	0	1	1	0	0	-	-	1	0	1	1	0	1
Sidusa sp2 Colombia	1	2	1	0	1	0	-	0	0	0	0	0	1	0	0	0	0	0	0	1	1	0	0	-	-	1	0	1	1	0	1

Taxon	char.95	char.96	char.97	char.98	char.99	char.100	char.101	char.102	char.103	char.104	char.105	char.106	char.107	char.108	char.109	char.110	char.111	char.112	char.113	char.114	char.115	char.116	char.117	char.118	char.119	char.120	char.121	char.122	char.123	char.124	char.125
Ghelna canadensis	0	1	1	0	-	-	-	0	-	0	-	0	-	0	-	-	-	0	-	-	0	0	0	0	-	-	1	2	0	1	?
Pensacola signata	1	1	1	1	0	1	1	2	2	1	0	0	0	1	2	0	1	0	1	1	1	1	0	0	-	-	1	0	0	0	0
Pensacola sylvestri	1	1	1	1	0	1	1	2	2	1	0	0	0	?	?	?	?	?	?	?	?	?	?	?	?	?	?	?	?	?	?
Caribattus inutilis	0	?	?	1	0	0	1	2	1	1	1	0	0	?	?	?	?	?	?	?	?	?	?	?	?	?	?	?	?	?	?
Caribattus cf. inutilis	0	1	1	1	0	0	1	2	1	1	1	0	0	1	1	0	1	0	1	0	1	0	0	1	0	0	1	0	0	1	1
Sidusa sp. French Guiana2	0	1	1	1	0	0	0	2	1	1	2	1	0	1	2	0	1	1	1	0	2	0	1	1	0	2	1	0	0	1	0
cf. Sidusa sp1 Colombia	0	1	1	1	0	0	0	2	1	1	2	1	0	1	2	0	1	1	1	0	2	0	1	1	0	2	1	0	0	1	0
cf. Sidusa sp2 Colombia	0	1	1	1	0	0	0	2	1	1	2	1	0	1	2	0	1	1	1	0	2	0	1	1	0	2	1	0	0	1	0
Mexigonus arizonensis	0	1	1	1	0	0	1	2	1	1	1	0	0	1	2	0	1	0	1	0	0	0	0	0	-	-	0	0	0	1	0
Mexigonus cf. minutus	0	1	1	1	0	0	1	2	1	1	1	0	0	1	2	0	1	0	1	0	2	0	0	0	-	-	0	0	0	1	0
Mexigonus morosus	0	1	1	1	0	0	1	2	1	1	1	0	0	1	2	0	1	0	1	0	1	0	0	0	-	-	1	2	0	1	0
Popcornella spiniformis	0	1	1	0	-	-	-	0	-	0	-	0	0	0	-	-	-	0	0	-	0	0	0	0	-	-	0	0	1	1	0
Popcornella yunque	0	1	1	0	-	-	-	0	-	0	-	0	0	0	-	-	-	0	0	-	0	0	0	0	-	-	1	1	1	1	0
Popcornella furcata	0	1	1	0	-	-	-	0	-	0	-	0	0	0	-	-	-	0	0	-	0	0	0	0	-	-	1	1	1	1	0
Agobardus gramineus	0	1	1	1	1	0	1	3	1	1	1	0	0	1	1	0	1	0	1	0	0	1	0	0	-	-	0	0	0	1	1
Agobardus cf. anormalis montanus	0	1	1	1	1	0	1	3	1	1	1	0	0	1	1	0	1	0	1	0	1	1	0	0	-	-	0	0	0	1	1
Agobardus bahoruco	0	1	1	1	1	0	1	3	1	1	1	0	0	1	0	0	1	0	1	0	0	0	0	0	-	-	0	0	0	1	0
Agobardus cf. brevitarsus	0	1	1	1	1	0	1	3	1	1	1	0	0	1	2	0	1	0	1	0	1	1	?	0	-	-	0	0	0	1	0
Agobardus oviedo	0	1	1	1	1	0	1	3	1	1	1	0	0	1	0	0	1	0	1	0	0	1	0	0	-	-	0	0	0	1	0
Agobardus phylladiphilus	0	1	1	1	1	0	1	3	1	1	1	0	0	1	1	0	1	0	1	0	0	1	0	0	-	-	0	0	0	1	1
Agobardus cordiformis	0	1	1	1	1	0	1	3	1	1	1	0	0	1	1	0	1	0	1	0	1	1	0	0	-	-	0	0	1	1	1
Bythocrotus cf. crypticus	0	1	1	1	0	0	0	1	0	1	1	0	0	1	1	0	1	0	1	0	1	0	0	1	0	2	1	0	2	1	0
Bythocrotus crypticus	0	1	1	1	0	0	0	1	0	1	1	0	0	1	1	0	1	0	1	0	1	0	0	1	0	2	1	0	2	1	0
Compsodecta haytiensis	0	1	1	1	0	0	1	3	1	1	0	0	0	1	1	0	1	0	1	0	0	0	0	1	0	0	1	0	0	1	0
Compsodecta peckhami	0	1	1	1	0	0	1	3	1	1	0	0	0	1	1	0	1	0	1	0	1	0	0	1	0	0	1	0	0	1	0
Compsodecta festiva JAM4122A	0	1	1	1	0	0	1	2	1	1	1	0	0	1	1	0	1	0	1	0	0	0	0	1	0	0	1	0	0	1	0
Allodecta maxilaris	0	1	1	1	0	0	1	2	1	1	1	0	0	?	?	?	?	?	?	?	?	?	?	?	?	?	?	?	?	?	?
Compsodecta gratiosa	0	1	1	1	0	0	1	2	1	1	1	0	0	?	?	?	?	?	?	?	?	?	?	?	?	?	?	?	?	?	?
Compsodecta grisea	0	1	1	1	0	0	1	2	1	1	2	0	0	1	2	0	1	0	1	0	0	0	0	1	0	0	2	0	0	1	0
Compsodecta valida	0	1	1	1	0	0	1	2	1	1	1	0	0	?	?	?	?	?	?	?	?	?	?	?	?	?	?	?	?	?	?
Corticattus guajataca	1	1	1	1	1	0	0	4	2	1	2	0	0	1	2	0	1	0	1	1	0	1	2	0	-	-	1	0	0	1	0
Corticattus latus	1	1	1	1	1	0	0	4	2	1	2	0	0	1	0	0	1	0	1	1	0	1	2	0	-	-	1	0	0	1	0
Pensacolatus cf. applanatus	0	1	1	1	0	1	1	2	1	1	1	0	0	1	1	0	1	0	1	0	1	0	0	1	1	2	0	0	1	1	0
Pensacolatus darlingtoni	0	1	1	1	0	1	1	2	1	1	1	0	0	1	1	0	1	0	1	0	1	0	0	1	1	1	1	0	0	1	0
Pensacolatus maxillosus	0	1	1	1	0	1	1	2	1	1	1	0	0	1	1	0	1	0	1	0	2	0	0	1	1	1	1	0	0	1	0
Pensacolatus scutiformis	0	1	1	1	0	1	1	2	1	1	1	0	0	1	1	0	1	0	1	0	1	0	0	1	1	1	1	0	1	1	0
Antillattus cambridgei	0	1	1	1	0	0	0	2	0	1	1	0	0	1	2	0	1	0	1	0	1	0	0	1	1	0	1	0	0	1	0
Antillattus cubensis CU3075A	0	1	1	1	0	0	0	2	0	1	1	0	0	1	2	0	1	0	1	0	1	0	0	1	1	0	1	0	0	1	0
Antillattus placidus DR782502	0	1	1	1	0	0	0	2	0	1	1	0	0	1	2	0	?	0	1	0	1	0	0	1	1	0	1	0	0	1	0
Petemathis portoricensis M	0	1	1	1	0	1	1	2	1	1	0	0	0	1	1	0	1	0	1	0	1	0	0	1	0	1	0	0	0	1	0
Petemathis portoricensis A	0	1	1	1	0	1	1	2	1	1	0	0	0	1	1	0	1	0	1	0	1	0	0	1	0	1	0	0	0	1	0
Petemathis tetuani	0	1	1	1	0	1	1	2	1	1	0	0	0	1	2	0	1	0	1	0	1	0	0	1	0	1	0	0	0	1	0
Truncattus cachotensis	0	1	1	1	0	1	1	2	1	1	1	0	0	1	1	0	1	0	1	0	1	0	0	1	1	0	1	0	0	1	0
Truncattus dominicanus	0	1	1	1	0	1	1	2	1	1	1	0	0	1	2	0	1	0	1	0	1	0	0	1	1	0	1	0	0	1	0
Truncattus flavus	0	1	1	1	0	1	1	2	1	1	0	0	0	1	1	0	1	0	1	0	1	0	0	1	1	0	1	0	0	1	0
Truncattus turquinencis CU787947	0	1	1	1	0	1	1	2	1	1	0	0	0	1	2	0	1	0	1	0	1	0	0	1	1	0	1	0	0	1	0
Truncattus CU3492A	0	1	1	1	0	1	1	2	1	1	0	0	0	1	1	0	1	0	1	0	1	0	0	1	1	0	1	0	0	1	0
Truncattus CU0083A	0	1	1	1	0	1	1	2	1	1	0	0	0	1	1	0	1	0	1	0	1	0	0	1	1	0	1	0	0	1	0
Truncattus CU0014A	0	1	1	1	0	1	1	2	1	1	0	0	0	1	1	0	1	0	1	0	1	0	0	1	1	0	1	0	0	1	0
Truncattus DR787029	0	1	1	1	0	1	1	2	1	1	0	0	0	1	1	0	1	0	1	0	1	0	0	1	1	0	1	0	0	1	0
Antillattus ocultus CU3534A	0	1	1	1	0	0	0	2	0	1	1	0	0	1	2	0	1	0	1	0	1	0	0	1	1	0	1	0	0	1	0
Antillattus gracilis	0	1	1	1	0	0	0	2	0	1	1	0	0	1	2	0	1	0	1	0	1	0	0	1	1	0	1	0	0	1	0
Bryanattus keyserlingi CU3395A	0	1	1	1	0	1	1	2	1	1	1	0	0	1	1	0	1	0	1	0	0	0	0	0	-	-	0	0	1	1	0
Bryanattus sp4 CU3317A	0	1	1	1	0	1	1	2	1	1	1	0	0	1	1	0	1	0	1	0	0	0	0	0	-	-	0	0	1	1	0
Bryanattus sp1 CU787945	0	1	1	1	0	1	1	2	1	1	1	0	0	1	1	0	1	0	1	0	0	0	0	0	-	-	0	0	2	1	0
Bryanattus sp3 CU787957	0	1	1	1	0	1	1	2	1	1	1	0	0	1	1	0	1	0	1	0	0	0	0	0	-	-	0	0	0	1	0
Bryanattus sp2 CU00090A	0	1	1	1	0	1	1	2	1	1	1	0	1	1	1	1	1	0	1	0	0	0	0	0	-	-	1	0	0	1	0
Cobanus multidentatis sp. nov	0	1	1	1	0	0	0	2	0	1	2	1	0	1	2	0	1	1	1	0	2	0	0	1	0	2	0	0	1	1	0
Cobanus extensus	0	1	1	1	0	0	0	2	0	1	2	1	0	1	2	0	1	1	1	0	2	0	0	1	0	2	0	0	1	1	0
Cobanus electus	0	1	1	1	0	0	0	2	0	1	2	1	0	1	2	0	1	1	1	0	2	0	0	1	0	2	0	0	1	1	0
Cobanus cf. cambridgei	0	1	1	1	0	0	0	2	0	1	2	1	0	1	2	0	1	1	1	0	2	0	0	1	0	2	0	0	1	1	0
Cobanus mandibularis	0	1	1	1	0	0	0	2	0	1	2	1	0	1	2	0	1	1	1	0	2	0	0	1	0	2	0	0	1	1	0
Cobanus unicolor	0	1	1	1	0	0	0	2	0	1	2	1	0	1	2	0	1	1	1	0	0	0	0	1	0	2	0	0	1	0	0
Cobanus colombiano sp. nov	0	1	1	1	0	0	0	2	0	1	2	1	0	1	2	0	1	1	1	0	2	0	0	1	0	2	0	0	1	1	0
Sidusa sp. French Guiana1	1	1	1	1	2	0	0	3	2	1	0	0	0	1	2	0	1	0	1	1	1	2	0	0	-	-	1	0	0	1	0
Sidusa gratiosa type sp	1	1	1	1	2	0	0	3	2	1	0	0	0	1	2	0	1	0	1	1	1	2	0	0	-	-	1	0	0	1	0
Sidusa sp1 colombia	1	1	1	1	2	0	0	3	2	1	0	0	0	1	2	0	1	0	1	1	1	2	0	0	-	-	1	0	0	1	0
Sidusa sp2 Colombia	1	1	1	1	2	0	0	3	2	1	0	0	0	1	2	0	1	0	1	1	1	2	0	0	-	-	1	0	0	1	0

Supplementary Species delimitation

ABGD Web results using K80 Kimura mesure of distance

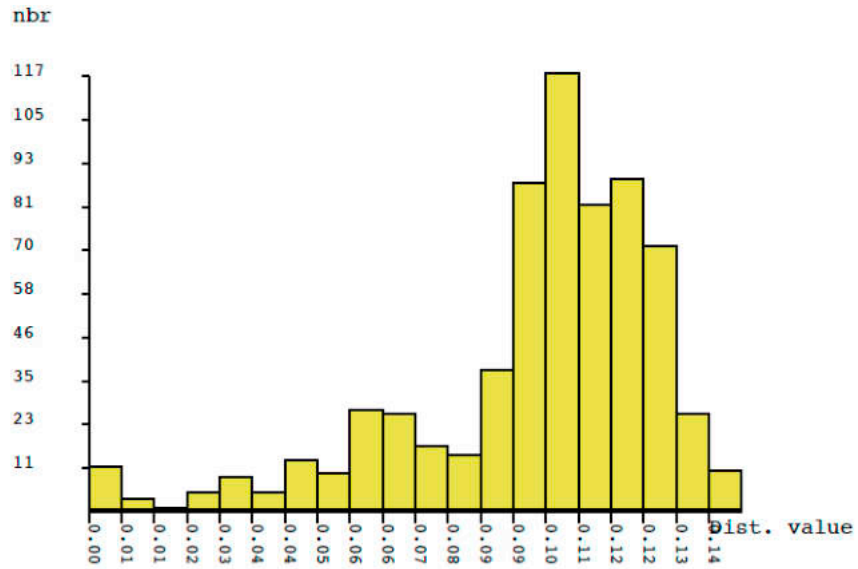

Histogram of distances

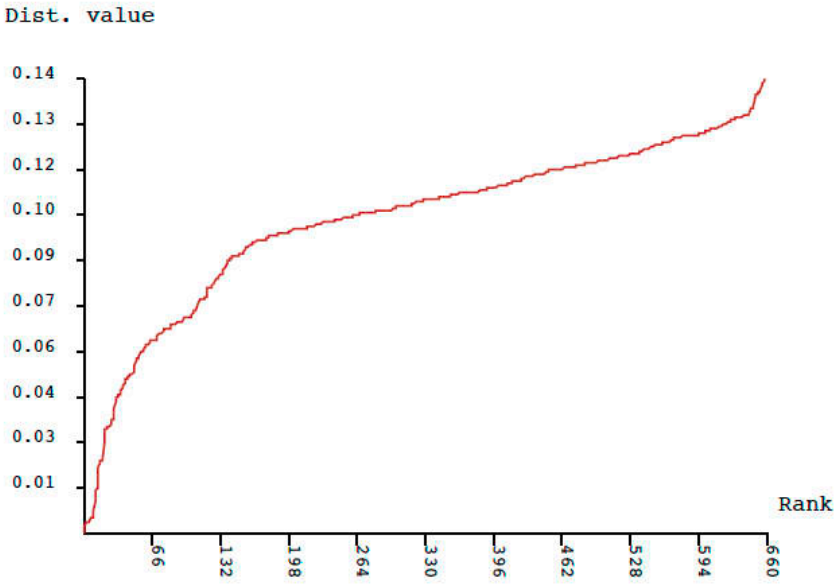

Ranked distances

Bayesian poisson tree processes (bPTP) (COI)

Acceptance rate: 0.071080000000000004

Merge: 49883

Split: 50117

Estimated number of species is between 38 and 51

Mean: 47.05

Bayesian poisson tree processes (bPTP) (all genes)
Accptance rate: 0.29411999999999999

Merge: 49891

Split: 50109

Estimated number of species is between 44 and 62

Mean: 52.44

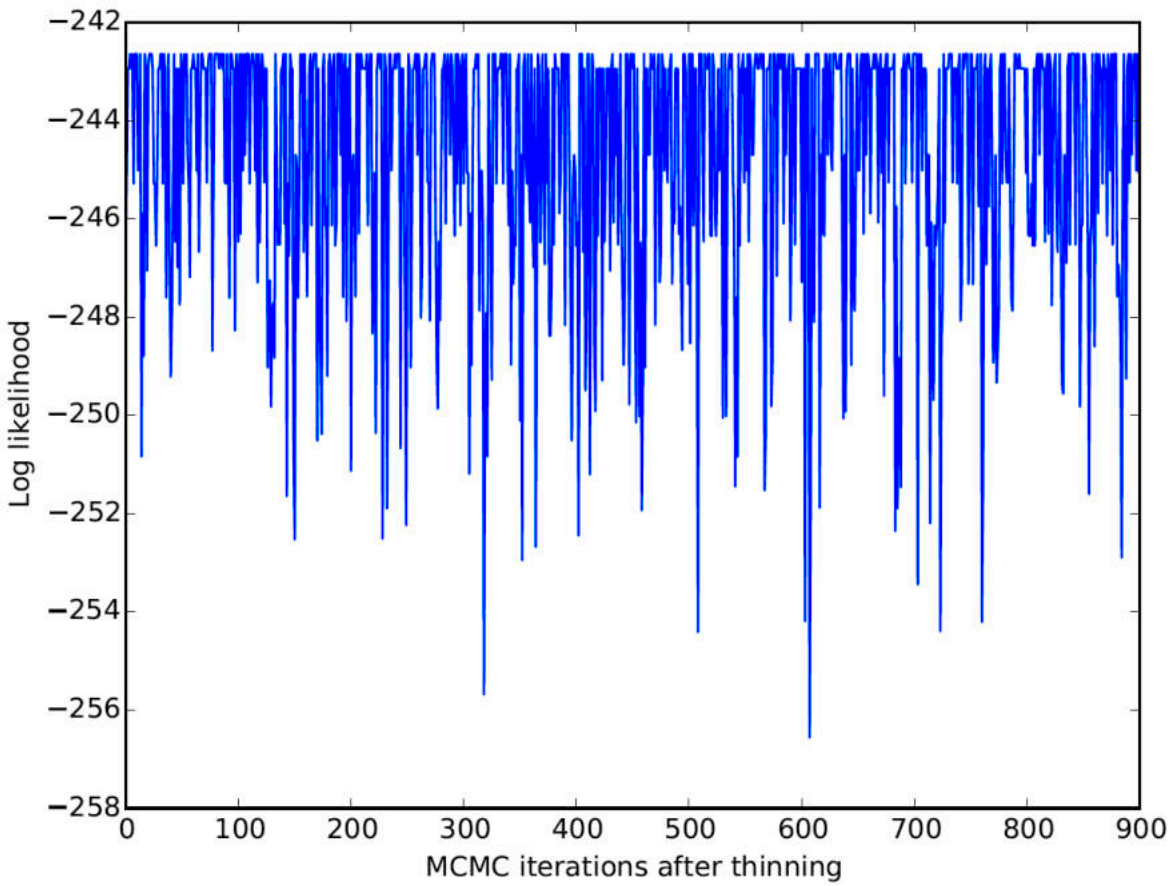

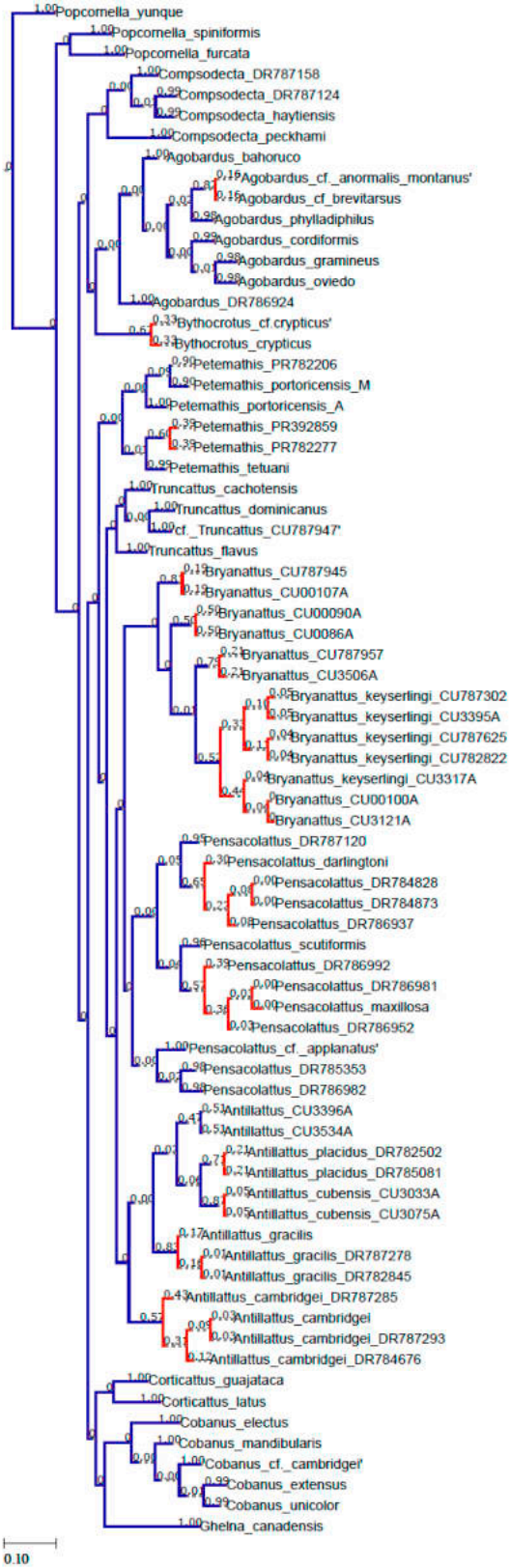

Maximum likelihood solution

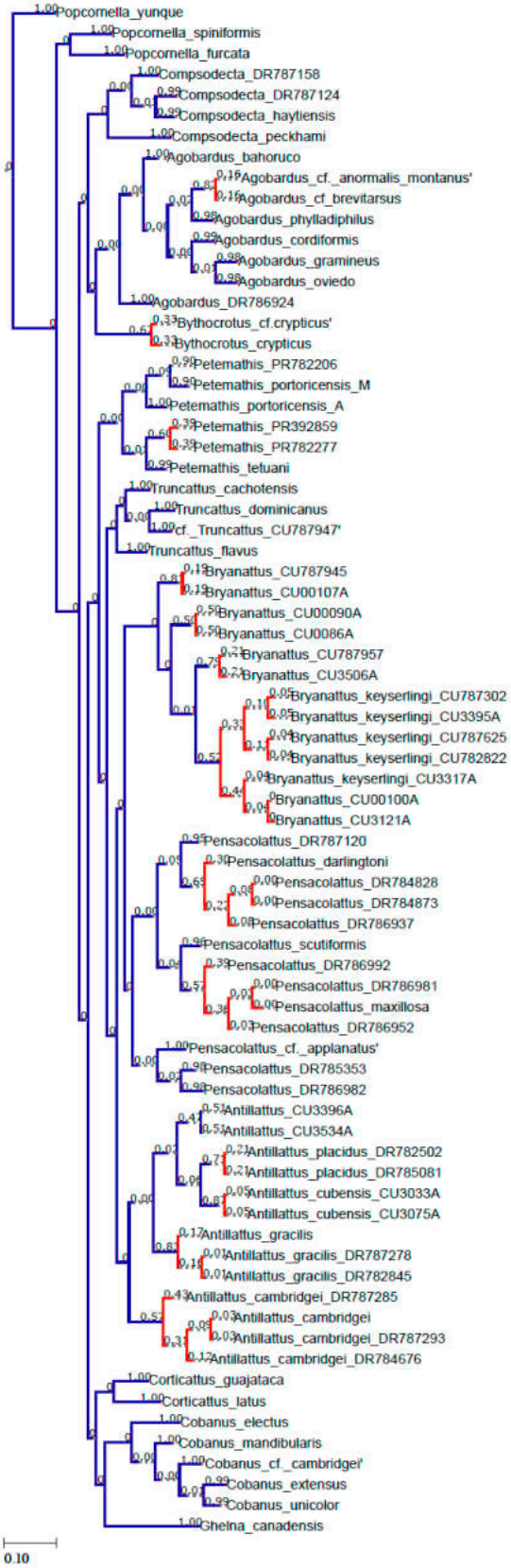

Highest Bayesian supported solution

GMYC species delimitation

method: single
likelihood of null model: 7.33336
maximum likelihood of GMYC model: 16.87764
likelihood ratio: 19.08856
result of LR test: 7.160964e-05***
number of ML clusters: 14
confidence interval: 13-17
number of ML entities: 47
confidence interval: 35-50
threshold time: -0.8203354

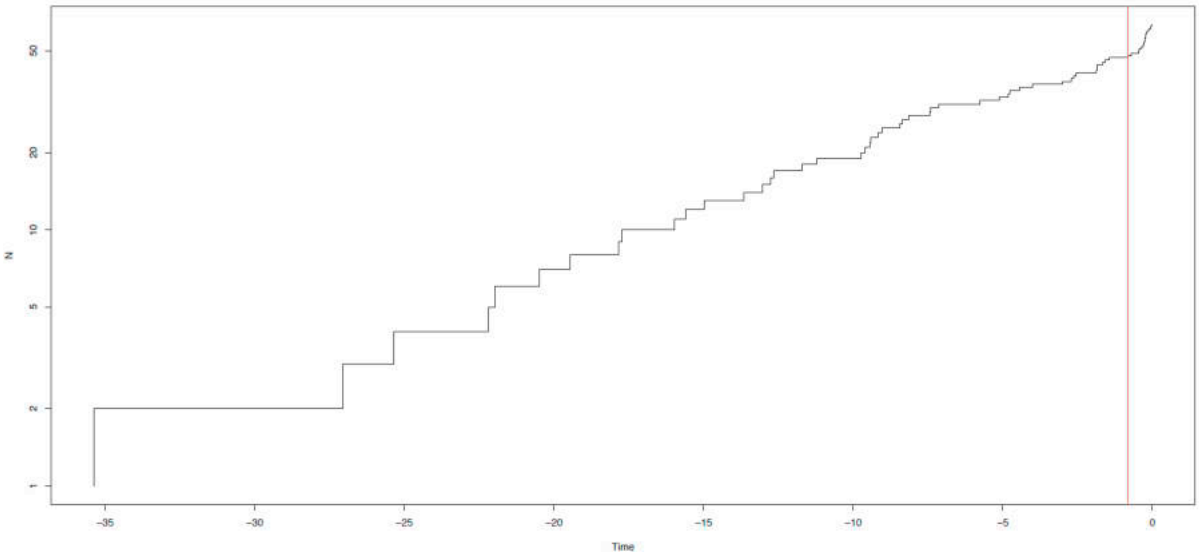

method: multiple
likelihood of null model: 7.33336
maximum likelihood of GMYC model: 17.79928
likelihood ratio: 20.93185
result of LR test: 2.849095e-05***
number of ML clusters: 20
confidence interval: 14-20
number of ML entities: 32
confidence interval: 26-43
threshold time: -22.177 -9.031479 -4.447873 -1.566529 -0.2500227

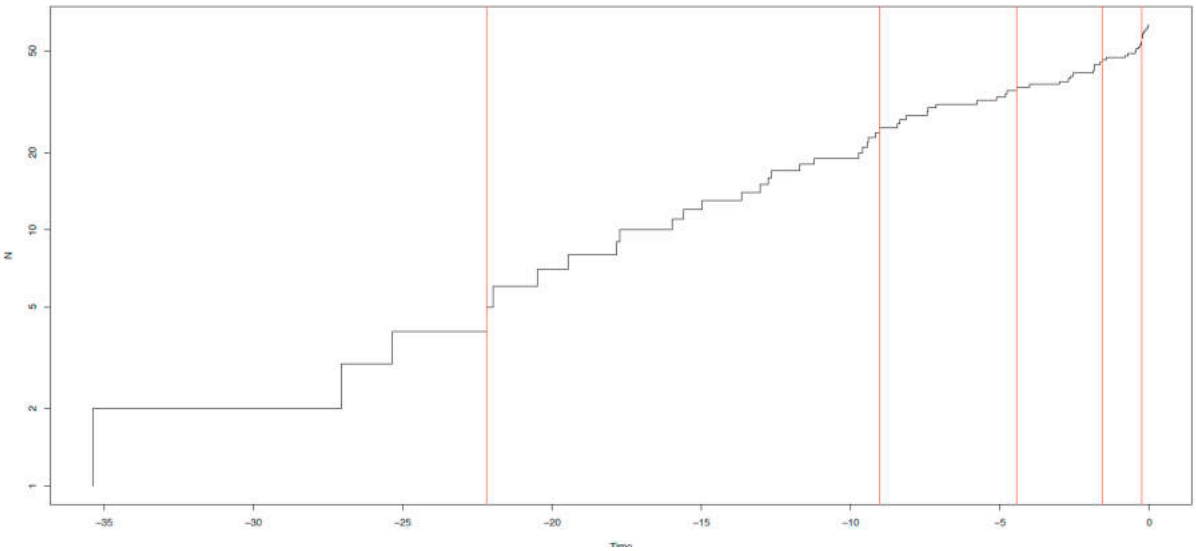

Supplementary phylogenetic Analyses
Parsimony
equal weights
rseed[;
hold 50000;
xinact;
ratchet: iter 1000;
xmult: rss css fuse 20 drift 20 ratchet 40 replic 3000; xmult;
mult: tbr spr replic 2000;
sec: slack 20;
bbreak: tbr safe fillonly;
mult;
xmult;
bbreak;
nelsen*;

implied weights
rseed[;
hold 50000;
xinact;
piwe: 3;
piwe=;
ratchet: iter 1000;
xmult: rss css fuse 20 drift 20 ratchet 40 replic 3000; xmult;
mult: tbr spr replic 2000;
sec: slack 20;
bbreak: tbr safe fillonly;
mult;
xmult;
bbreak;
nelsen*;

constrain
force=(1 2 3 4 5 6 7 37 38 58 59 60 61 62 63 64 65);
constrain=;
force;

Bremer support
sub 1; sub 2; sub 3; sub 4; sub 5; sub 6; sub 7; sub 8; sub 100; bsupport!!+0;

Jackknifing
rseed[; mult: noratchet replic 100 tbr hold 10; resample jak replic 1000 freq from 0 [mult];
mult;

Symmetrical resampling
resample = [mu1=ho1;] sym rep 10000 prob 33 freq from 0;

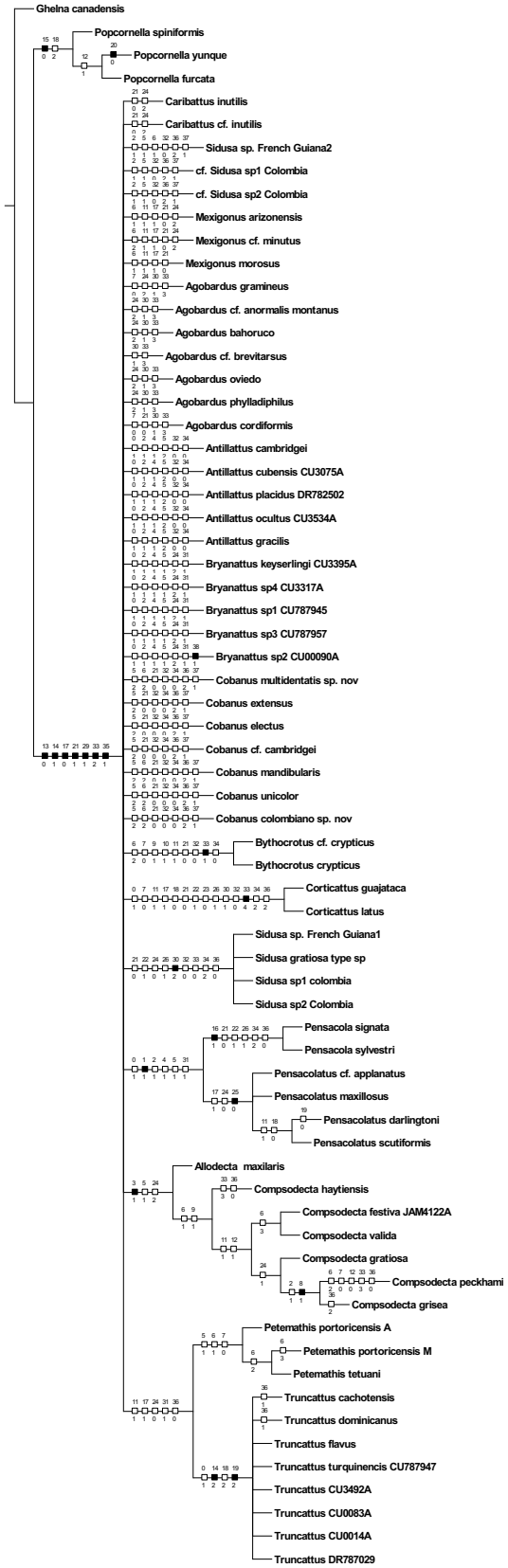

Figure. Strict consensus (palp subset) of the 107 parsimonious trees obtained under equal weights (122 steps; CI = 0.41, RI = 0.85)

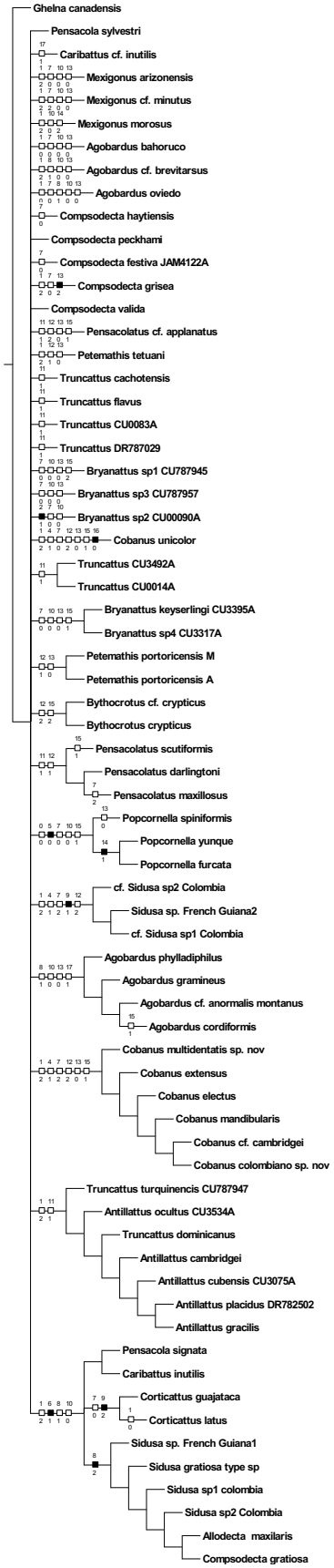

Figure. Strict consensus (epigynum subset) of the 126 parsimonious trees obtained under equal weights (55 steps; CI = 0.45, RI = 0.85)

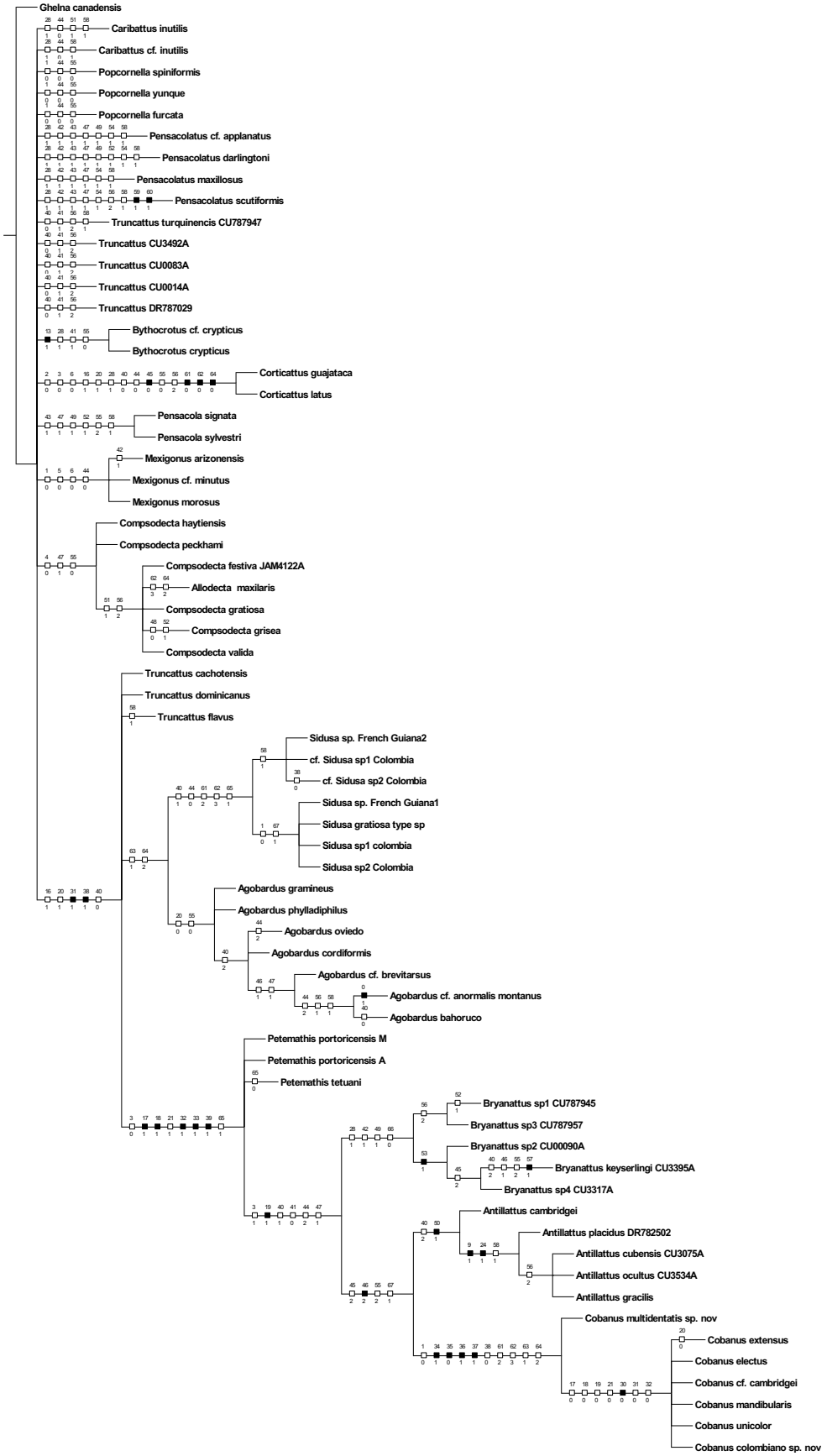

Figure. Strict consensus (prosoma+abdomen subset) of the 102 parsimonious trees obtained under equal weights (146 steps; CI = 0.45, RI = 0.88)

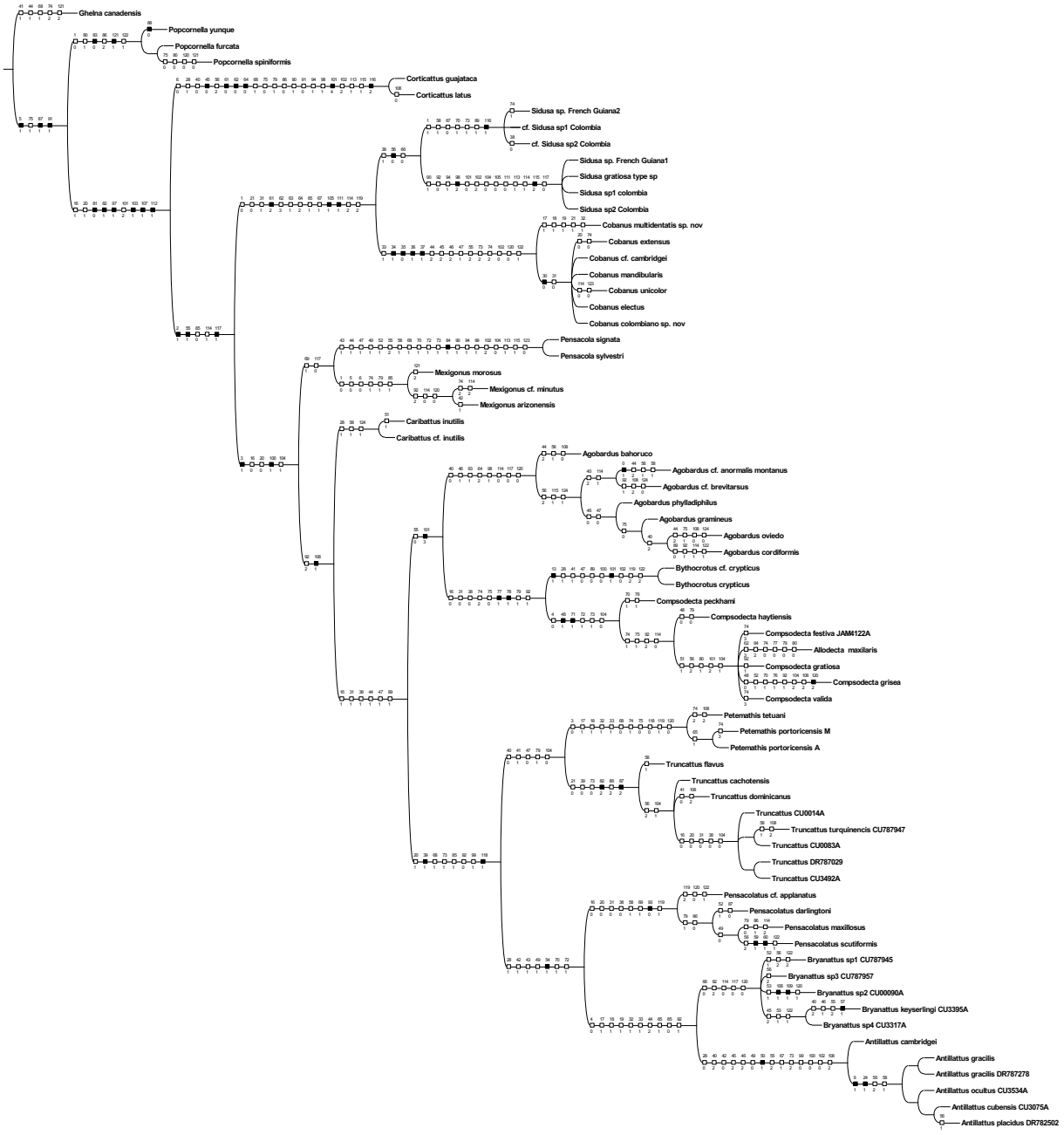

Figure. Strict consensus (morphology) of the most parsimonious trees obtained under equal weights (CI=0.37, RI=0.83). ACCTRAN

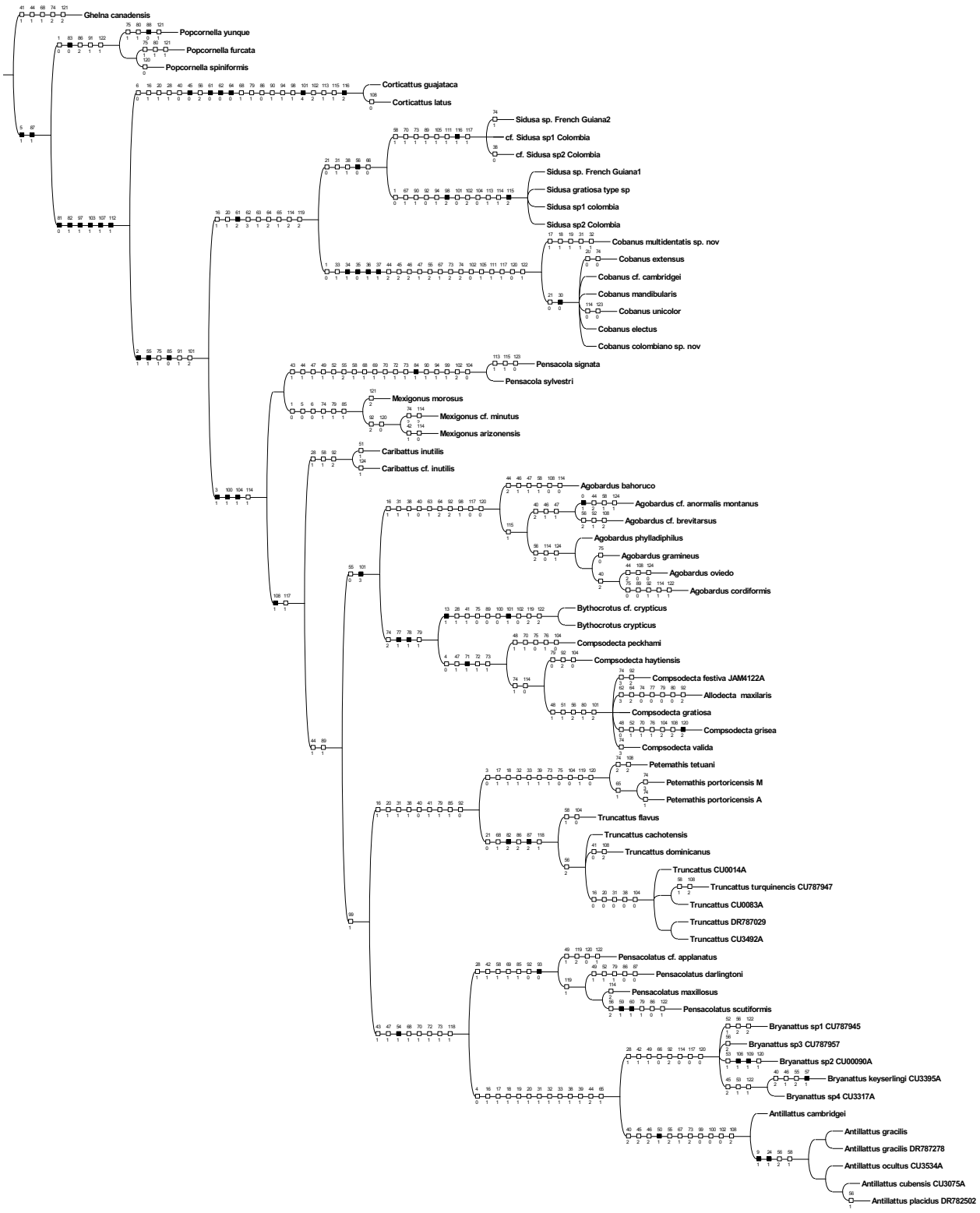

Figure. Strict consensus (morphology) of the most parsimonious trees obtained under equal weights (CI=0.37, RI=0.83). DELTRAN

Table. Dispersal probabilities and time periods

35-30 Mya					
	A	B	C	D	E
A	1	0.8	0.8	0.5	0.05
B	0.8	1	0.8	0.2	0.05
C	0.8	0.8	1	0.5	0.05
D	0.5	0.2	0.5	1	0.8
E	0.05	0.05	0.05	0.8	1

30-23 Mya					
	A	B	C	D	E
A	1	0.2	0.2	0.00001	0.00001
B	0.2	1	0.05	0.00001	0.00001
C	0.2	0.05	1	0.00001	0.00001
D	0.05	0.00001	0.00001	1	0.8
E	0.00001	0.00001	0.00001	0.8	1

23-15 Mya					
	A	B	C	D	E
A	1	0.05	0.05	0.00001	0.00001
B	0.05	1	0.00001	0.00001	0.00001
C	0.05	0.00001	1	0.00001	0.00001
D	0.05	0.00001	0.00001	1	0.8
E	0.00001	0.00001	0.00001	0.8	1

15-9 Mya					
	A	B	C	D	E
A	1	0.05	0.05	0.00001	0.00001
B	0.05	1	0.00001	0.00001	0.00001
C	0.05	0.00001	1	0.00001	0.00001
D	0.05	0.00001	0.00001	1	0.8
E	0.00001	0.00001	0.00001	0.8	1

9-3 Mya					
	A	B	C	D	E
A	1	0.05	0.05	0.00001	0.00001
B	0.05	1	0.00001	0.00001	0.00001
C	0.05	0.00001	1	0.00001	0.00001
D	0.05	0.00001	0.00001	1	0.8
E	0.00001	0.00001	0.00001	0.8	1

BioGeoBEARS BAYAREALIKE on Psychotria M0_unconstrained
ancstates: global optim, 5 areas max. d=0; e=0.0372; j=0; LnL=−65.23

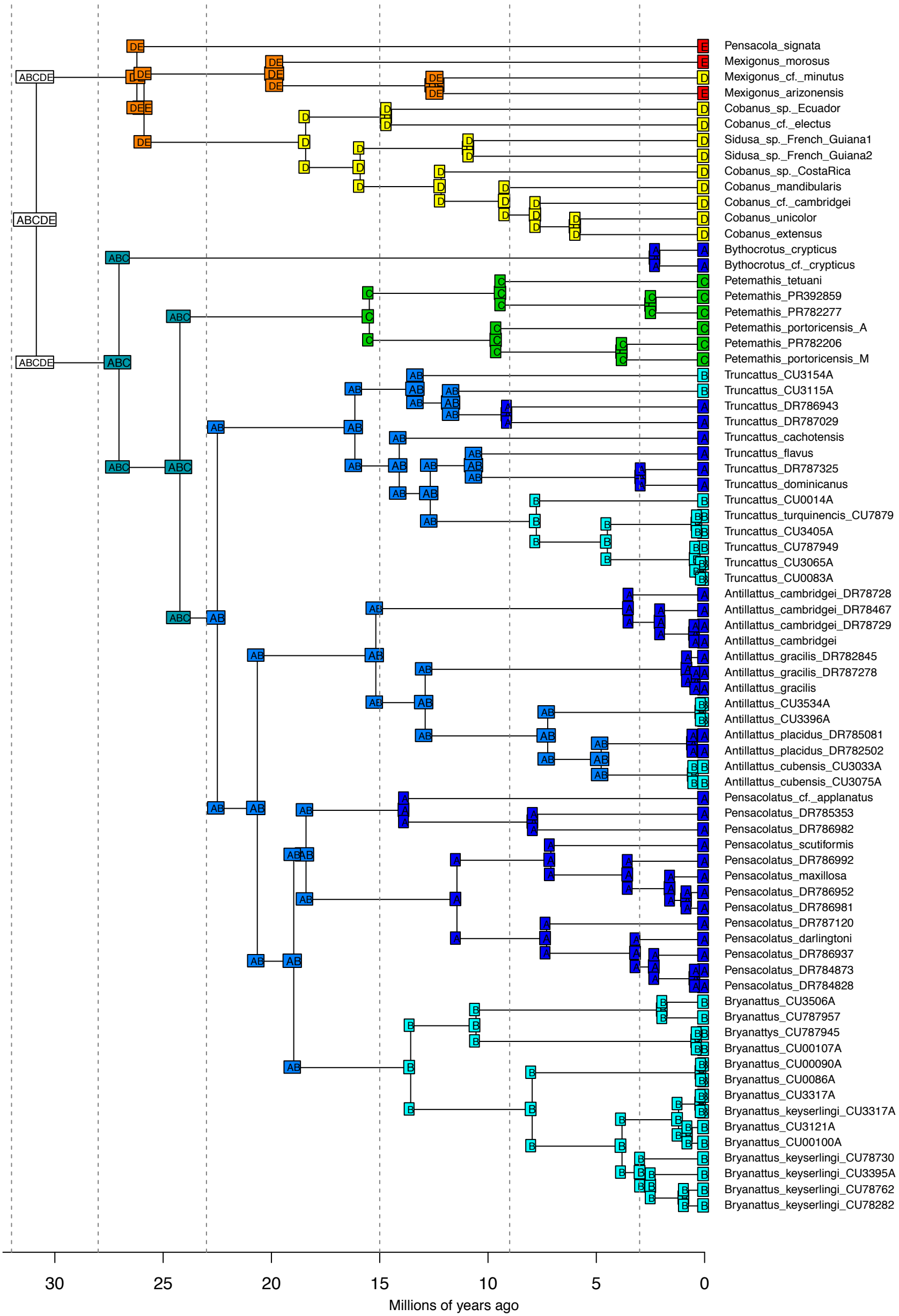

BioGeoBEARS BAYAREALIKE on Psychotria M0_unconstrained
ancstates: global optim, 5 areas max. d=0; e=0.0372; j=0; LnL=−65.23

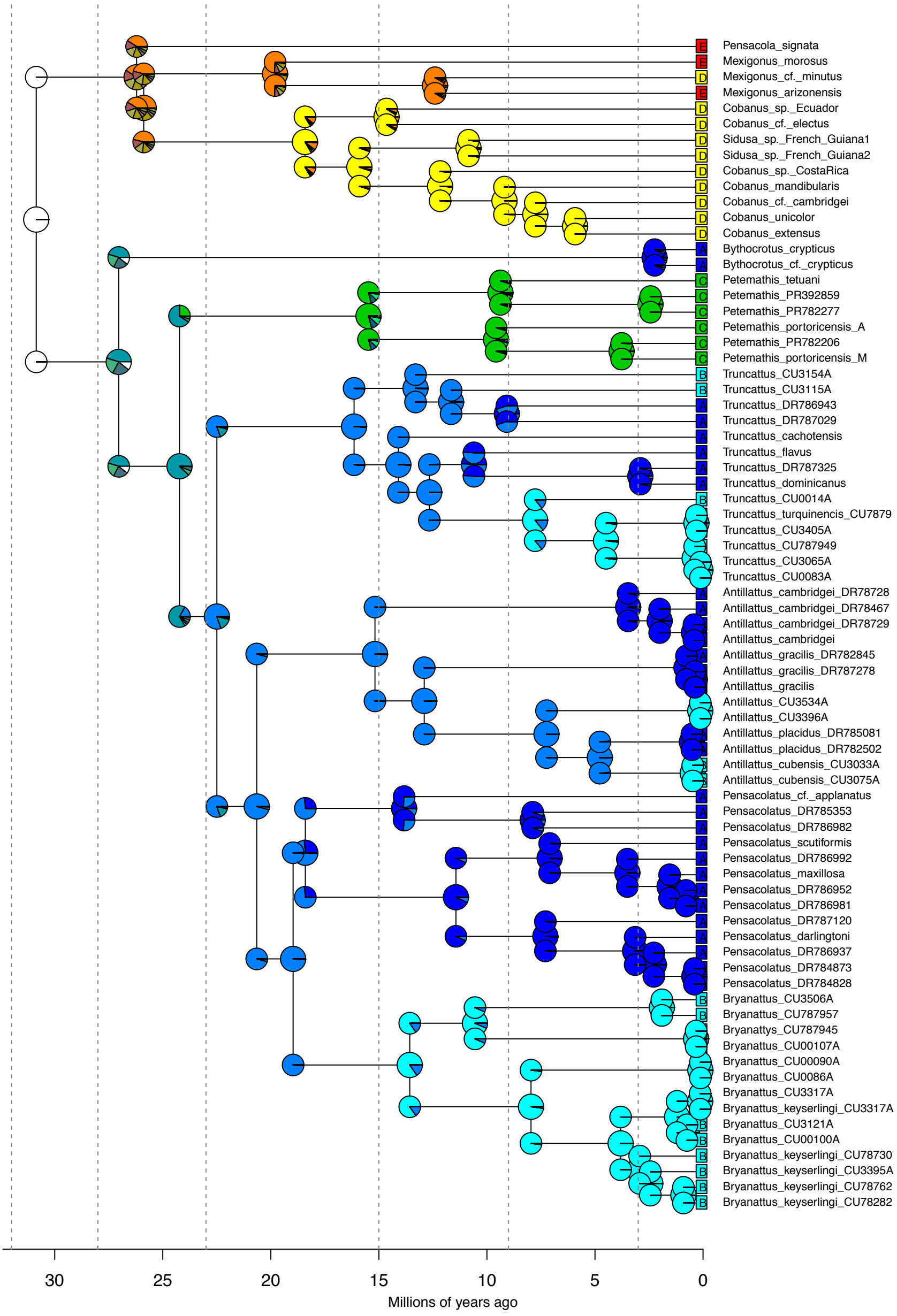

BioGeoBEARS BAYAREALIKE+J on Psychotria M0_unconstrained
ancstates: global optim, 5 areas max. d=0; e=0; j=0.0197; LnL=−47.79

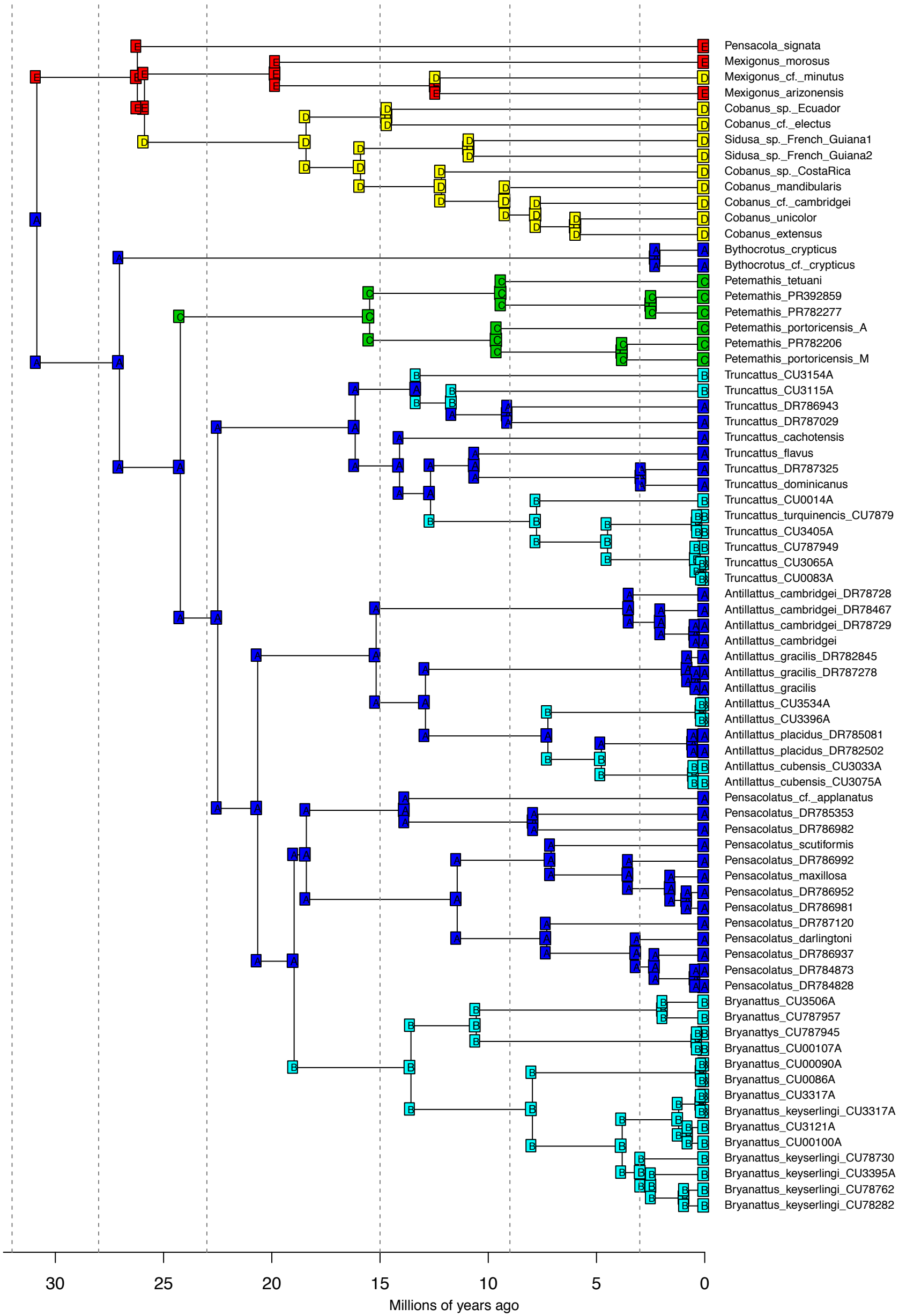

BioGeoBEARS BAYAREALIKE+J on Psychotria M0_unconstrained
ancstates: global optim, 5 areas max. d=0; e=0; j=0.0197; LnL=−47.79

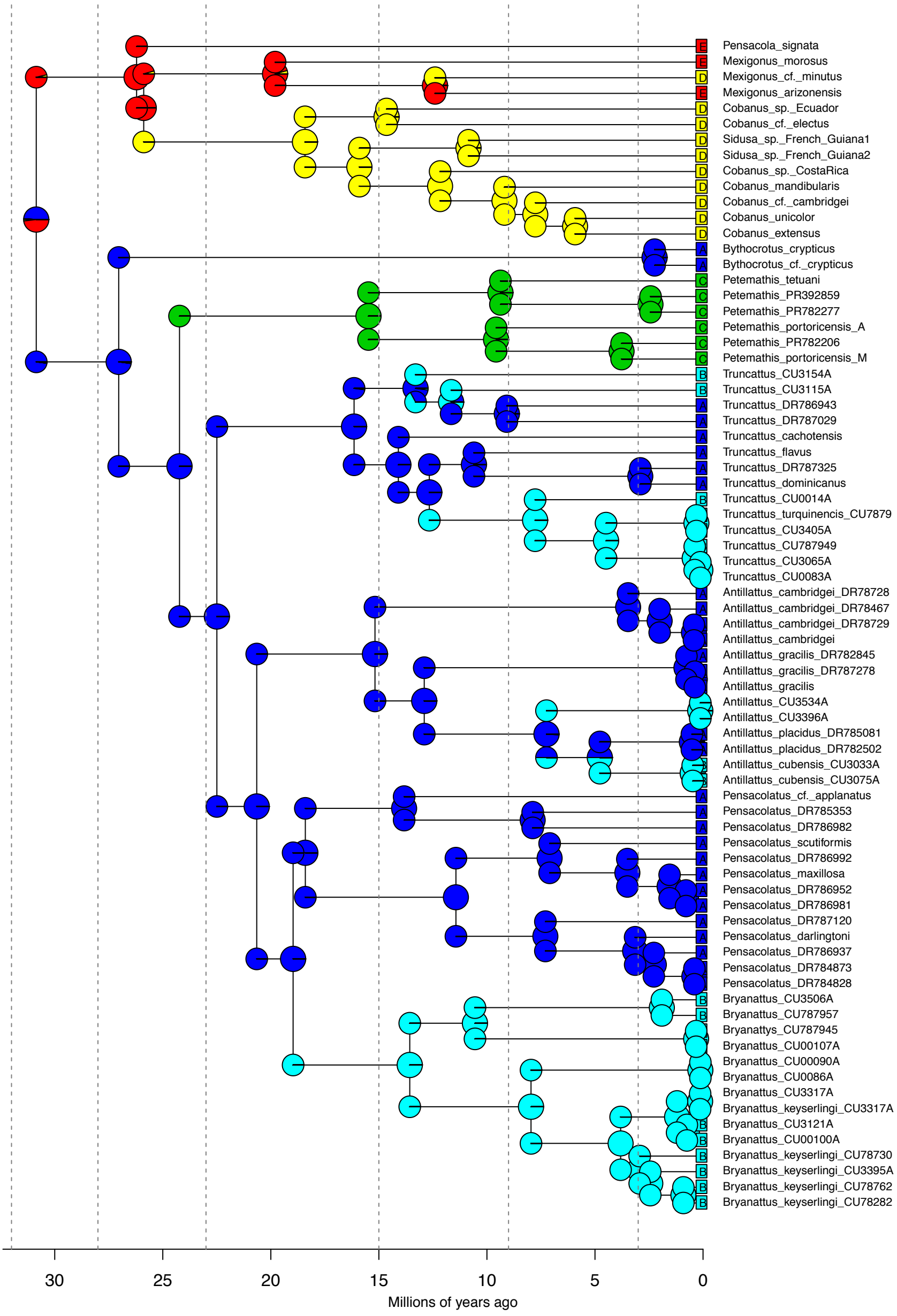

BioGeoBEARS DIVALIKE on Psychotria M0_unconstrained
ancstates: global optim, 5 areas max. d=0.0033; e=0; j=0; LnL=−57.11

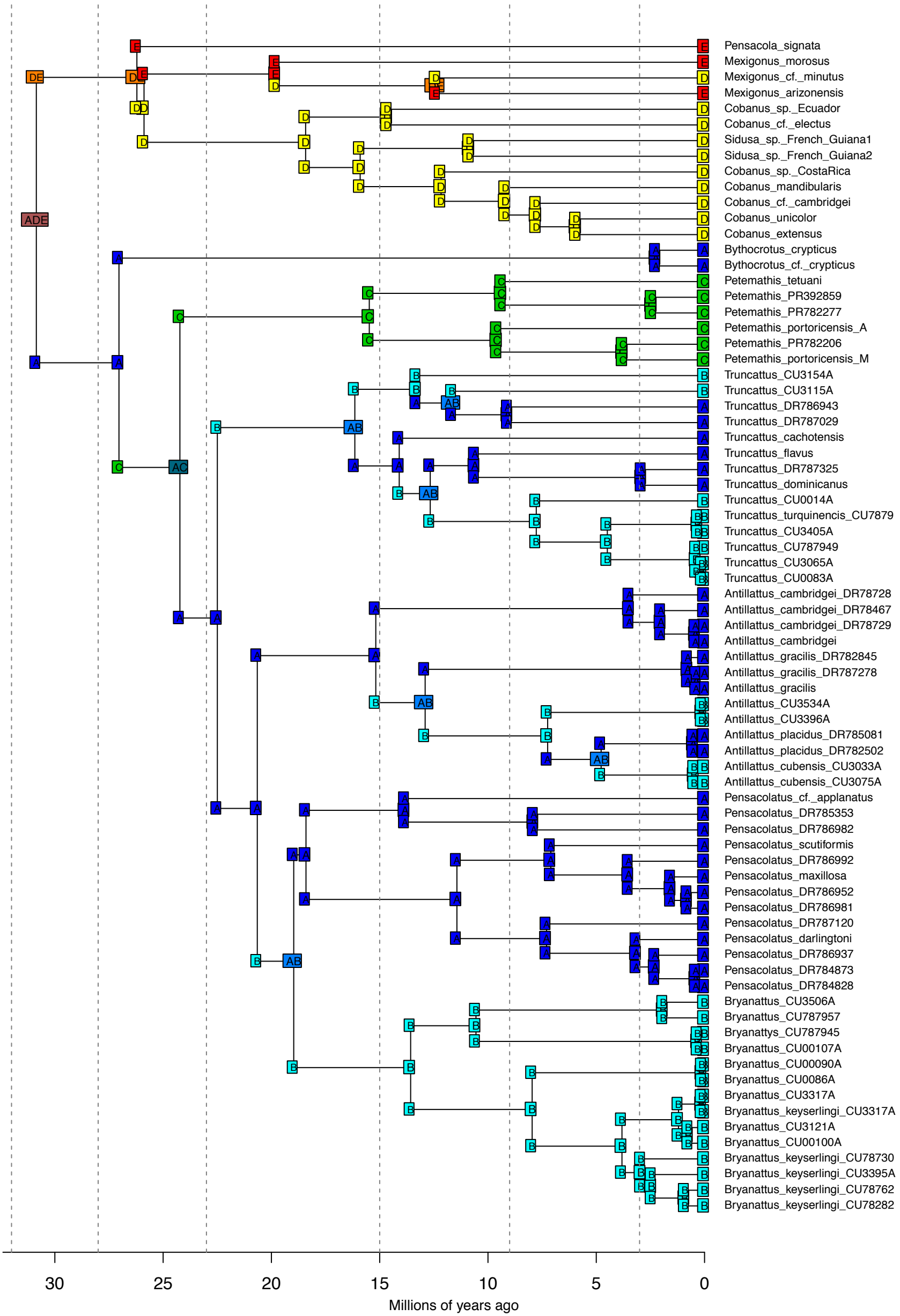

BioGeoBEARS DIVALIKE on Psychotria M0_unconstrained
ancstates: global optim, 5 areas max. d=0.0033; e=0; j=0; LnL=−57.11

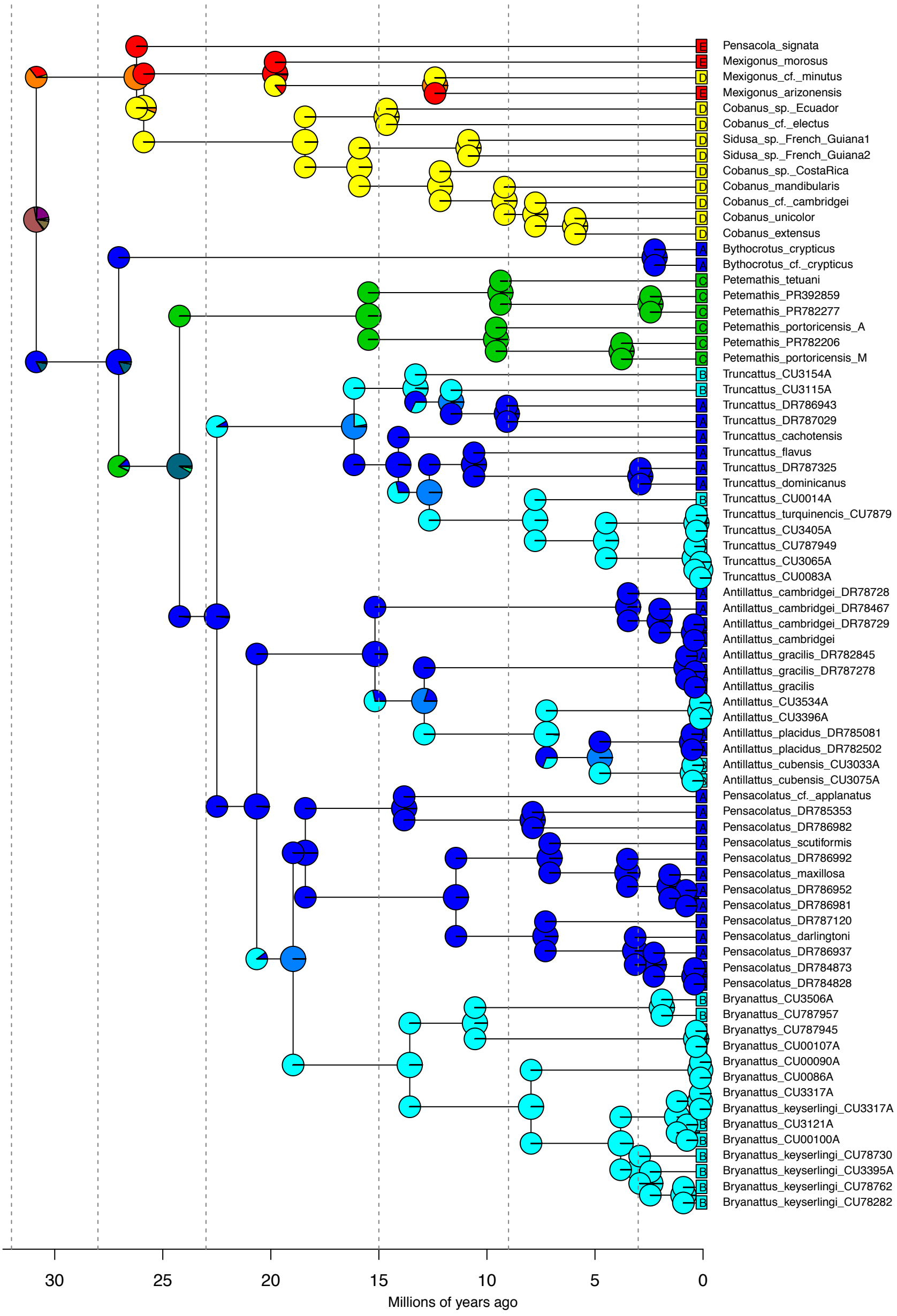

BioGeoBEARS DIVALIKE+J on Psychotria M0_unconstrained
ancstates: global optim, 5 areas max. d=0.0033; e=0.01; j=1e−04; LnL=−61.19

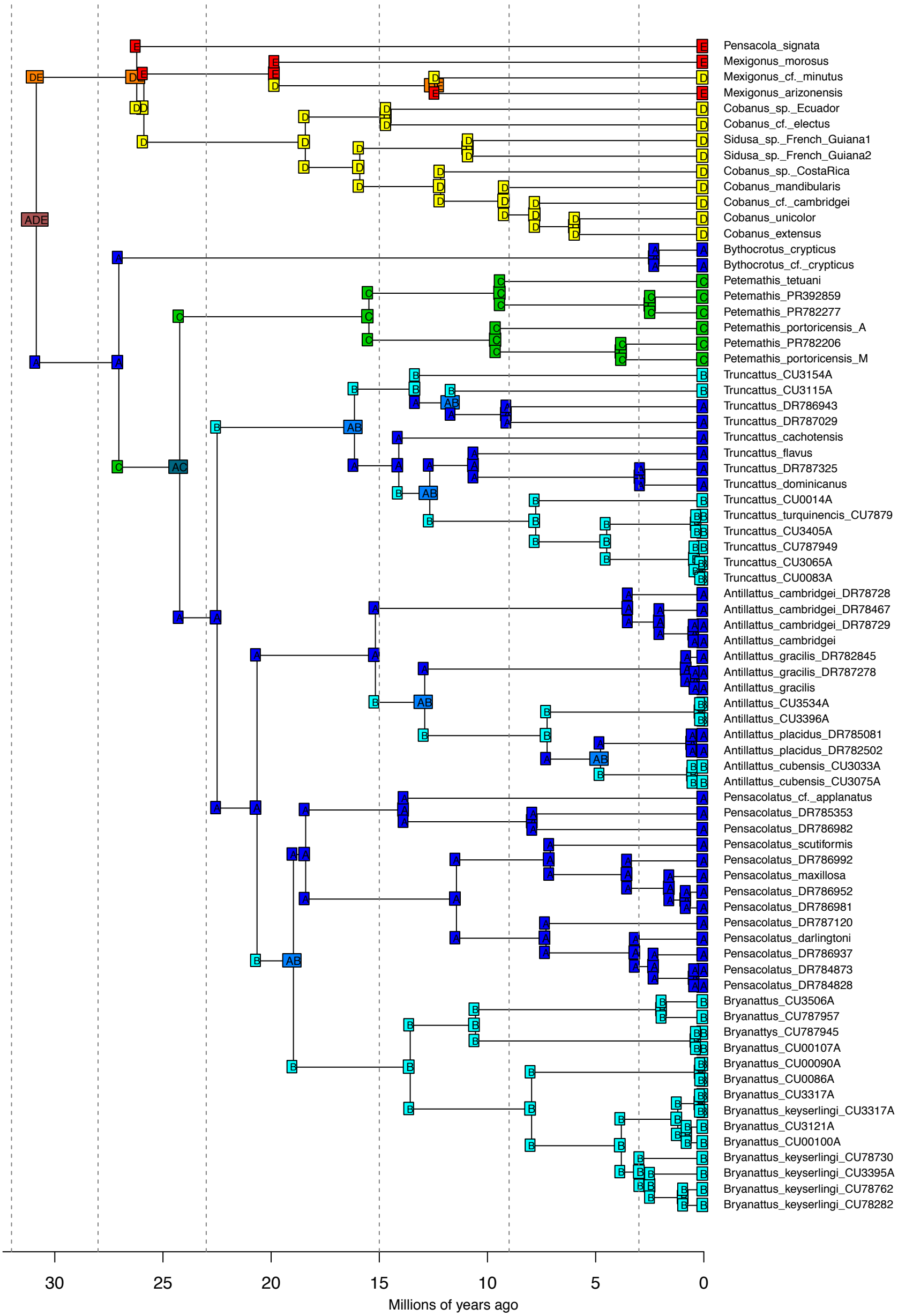

BioGeoBEARS DIVALIKE+J on Psychotria M0_unconstrained
ancstates: global optim, 5 areas max. d=0.0033; e=0.01; j=1e−04; LnL=−61.19

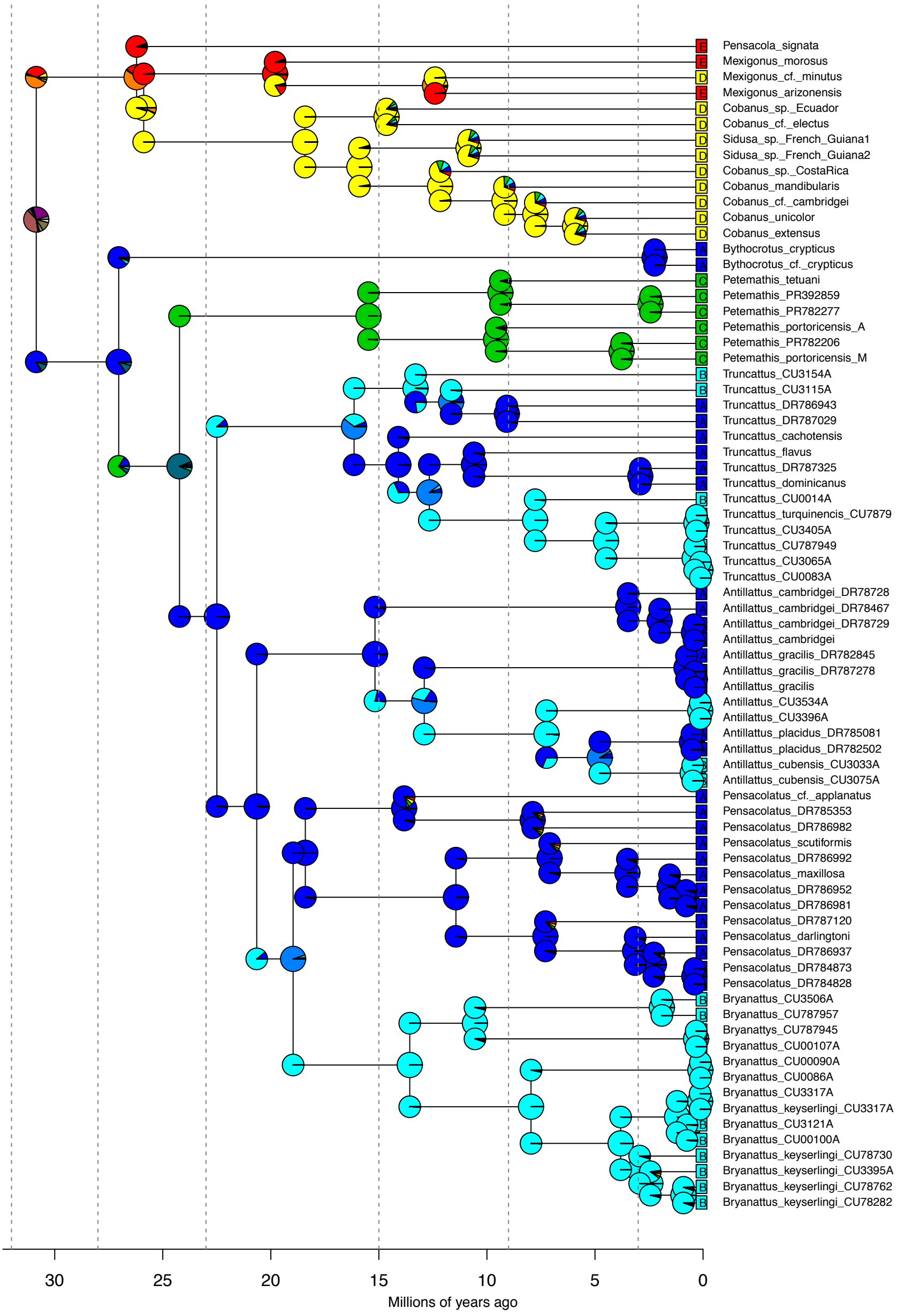

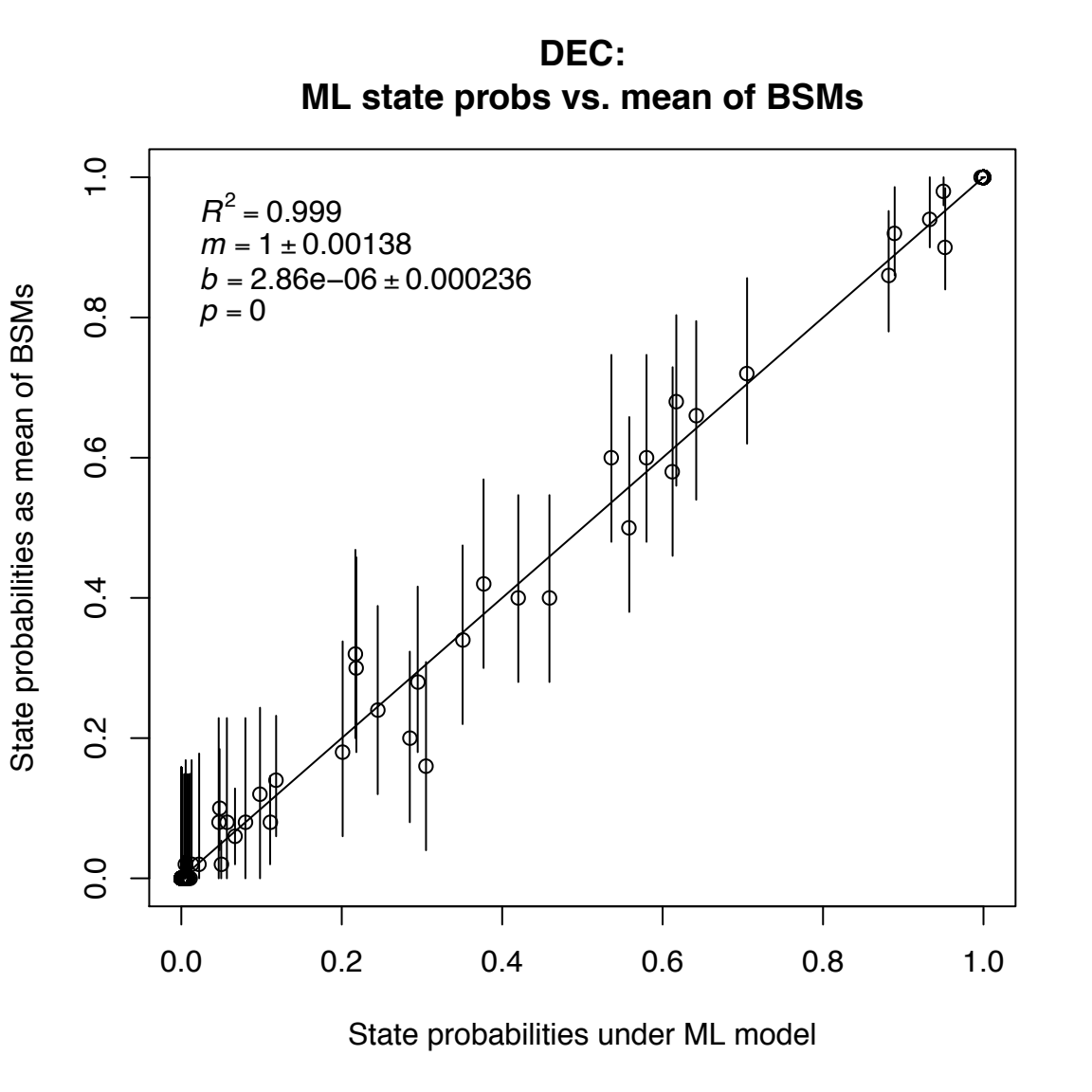
DEC:
ML state probs vs. mean of BSMs
$R^2 = 0.999$
$m = 1 \pm 0.00138$
$b = 2.86e{-}06 \pm 0.000236$
$p = 0$
State probabilities as mean of BSMs
State probabilities under ML model
0.0
0.2
0.4
0.6
0.8
1.0

DEC – Stochastic Map #1/50
ancstates: global optim, 5 areas max. d=0.0017; e=0; j=0; LnL=–50.93

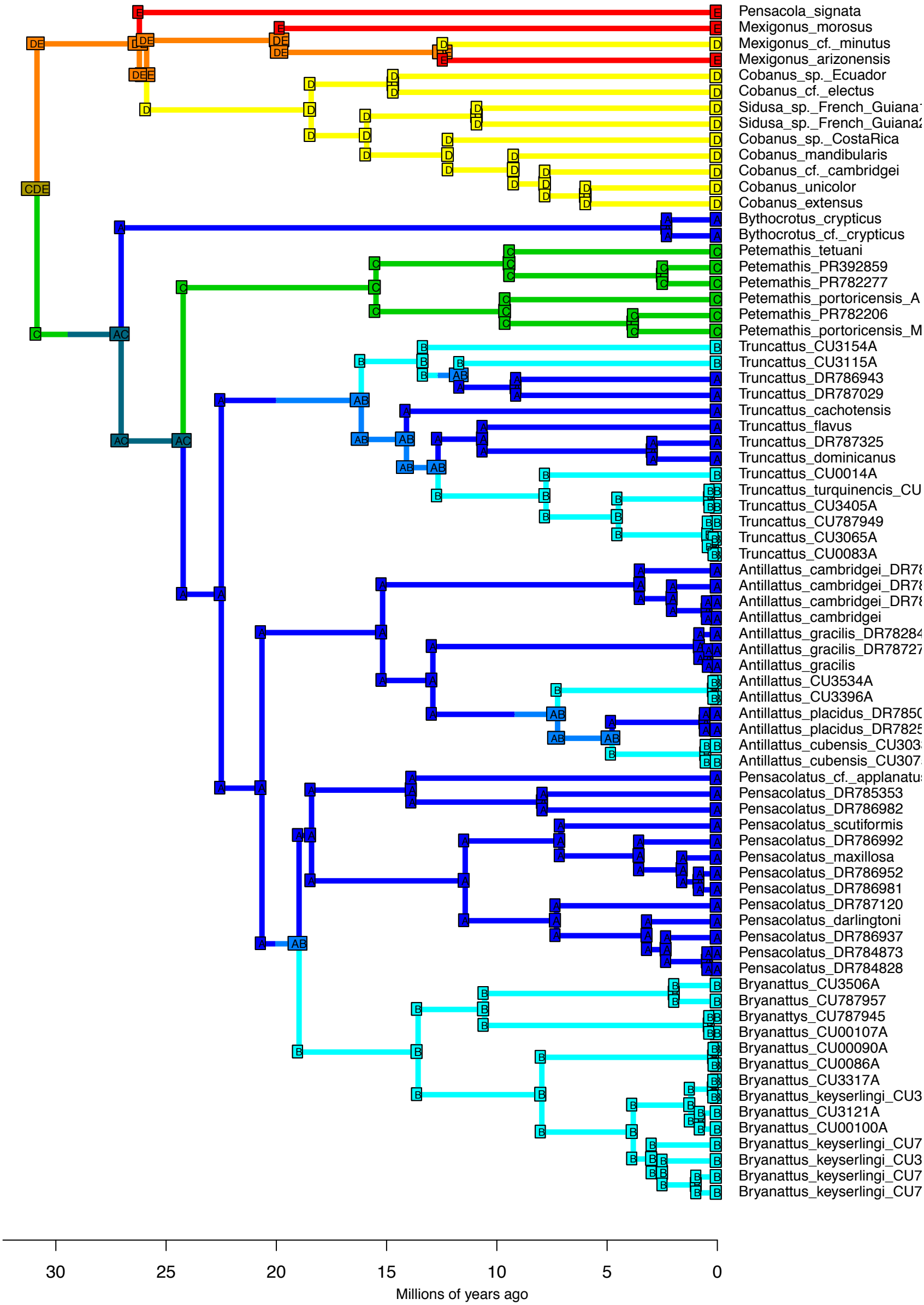

DEC – Stochastic Map #2/50
ancstates: global optim, 5 areas max. d=0.0017; e=0; j=0; LnL=–50.93

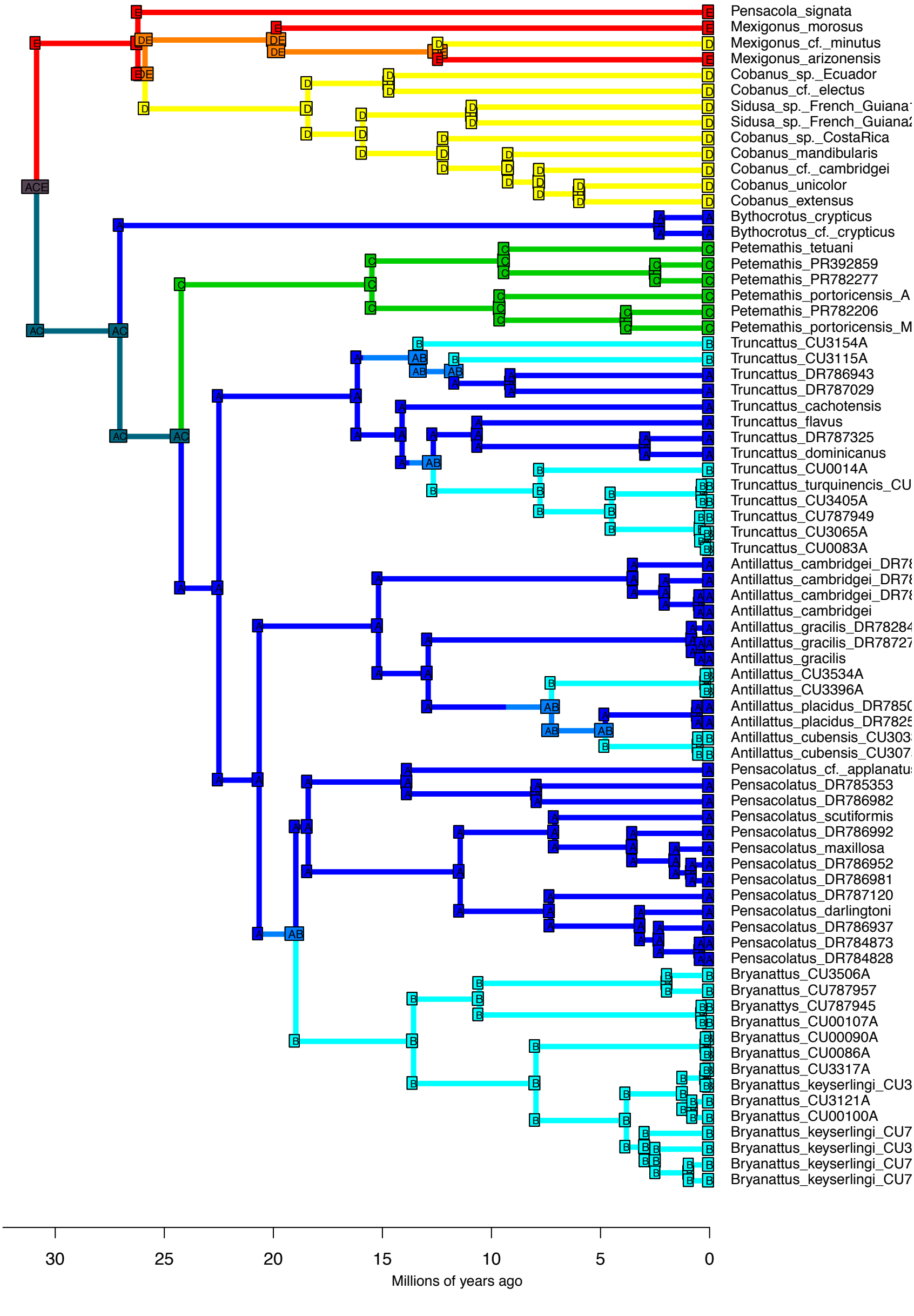

DEC – Stochastic Map #3/50
ancstates: global optim, 5 areas max. d=0.0017; e=0; j=0; LnL=–50.93

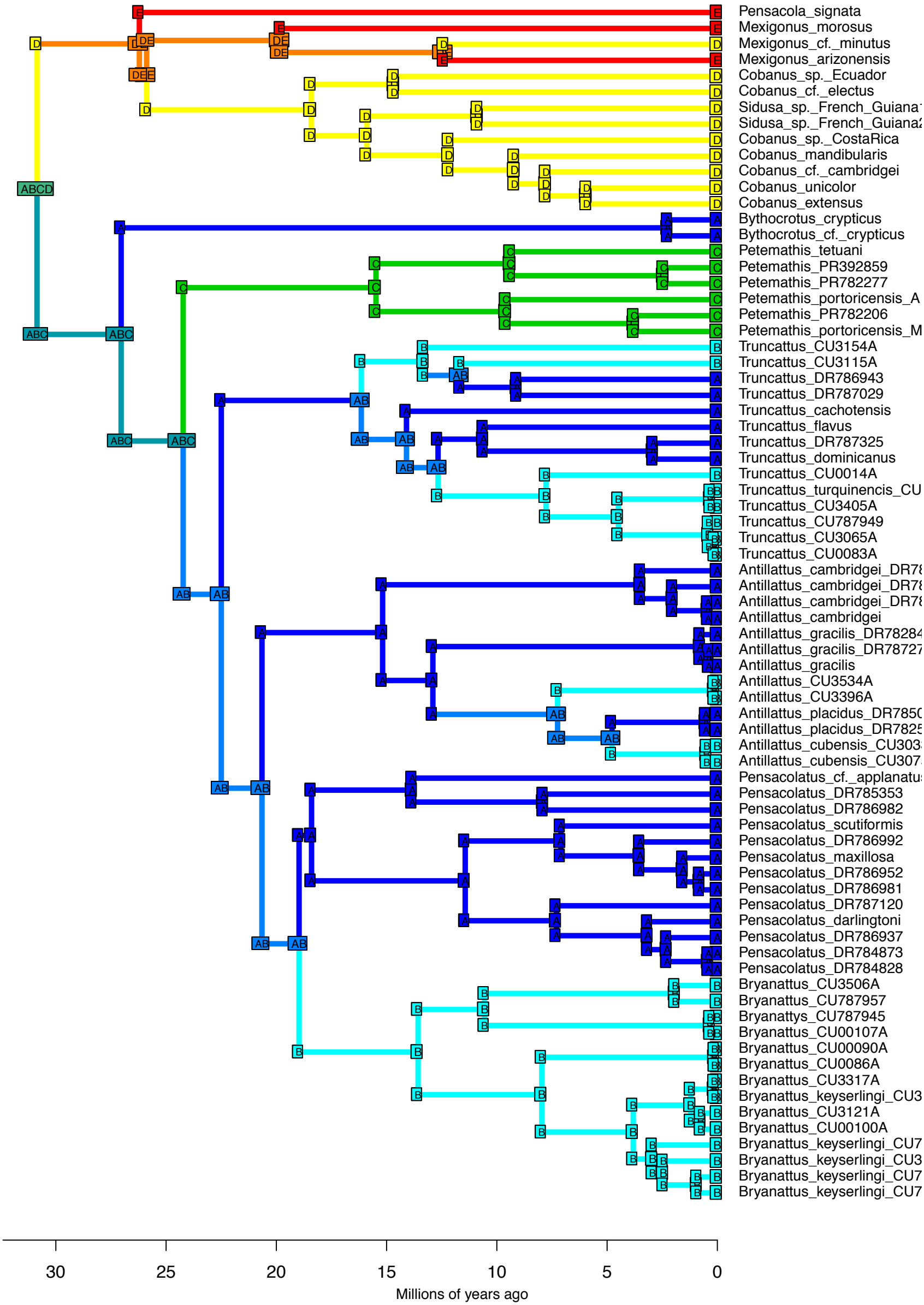

DEC – Stochastic Map #4/50
ancstates: global optim, 5 areas max. d=0.0017; e=0; j=0; LnL=–50.93

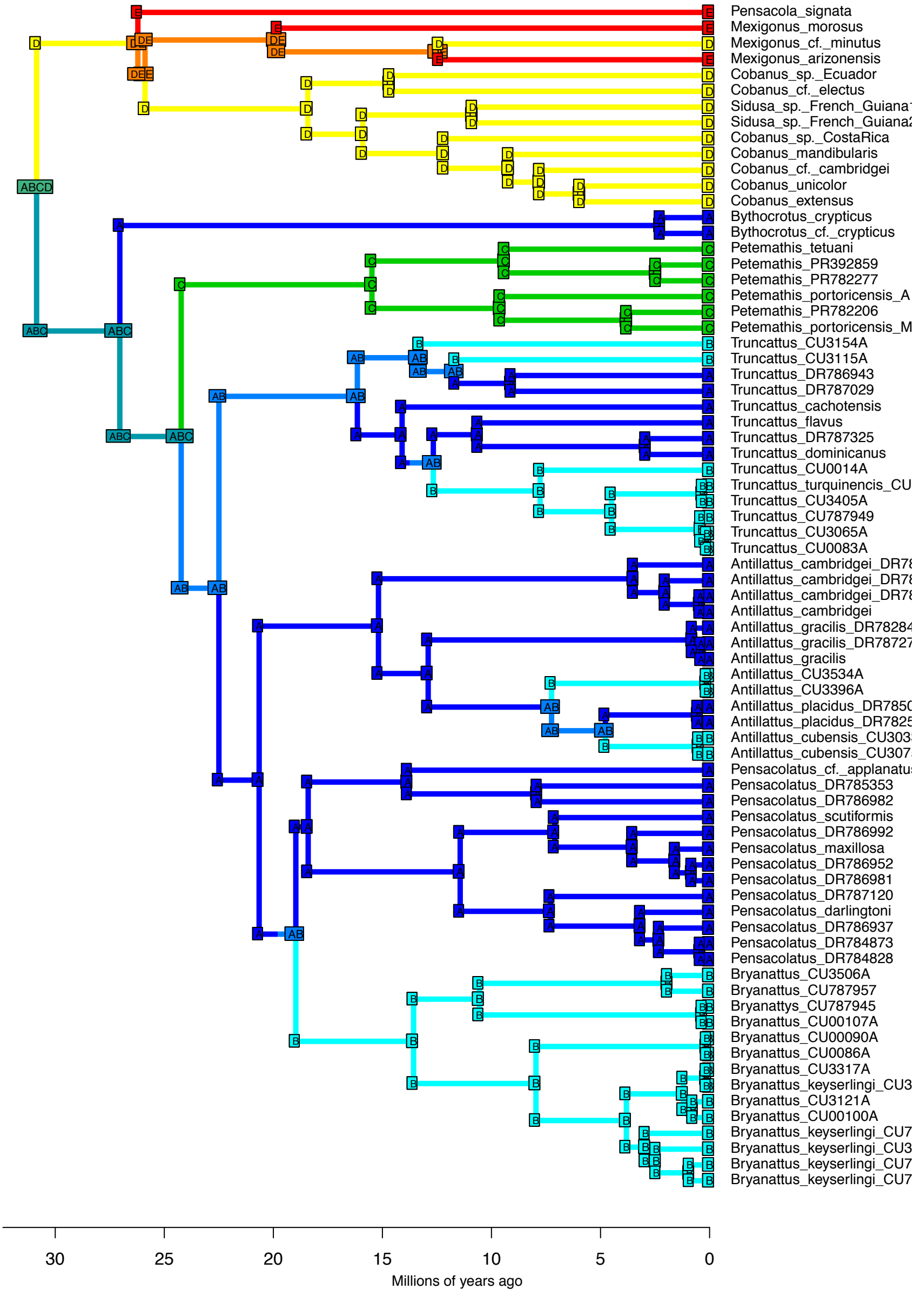

DEC – Stochastic Map #5/50
ancstates: global optim, 5 areas max. d=0.0017; e=0; j=0; LnL=–50.93

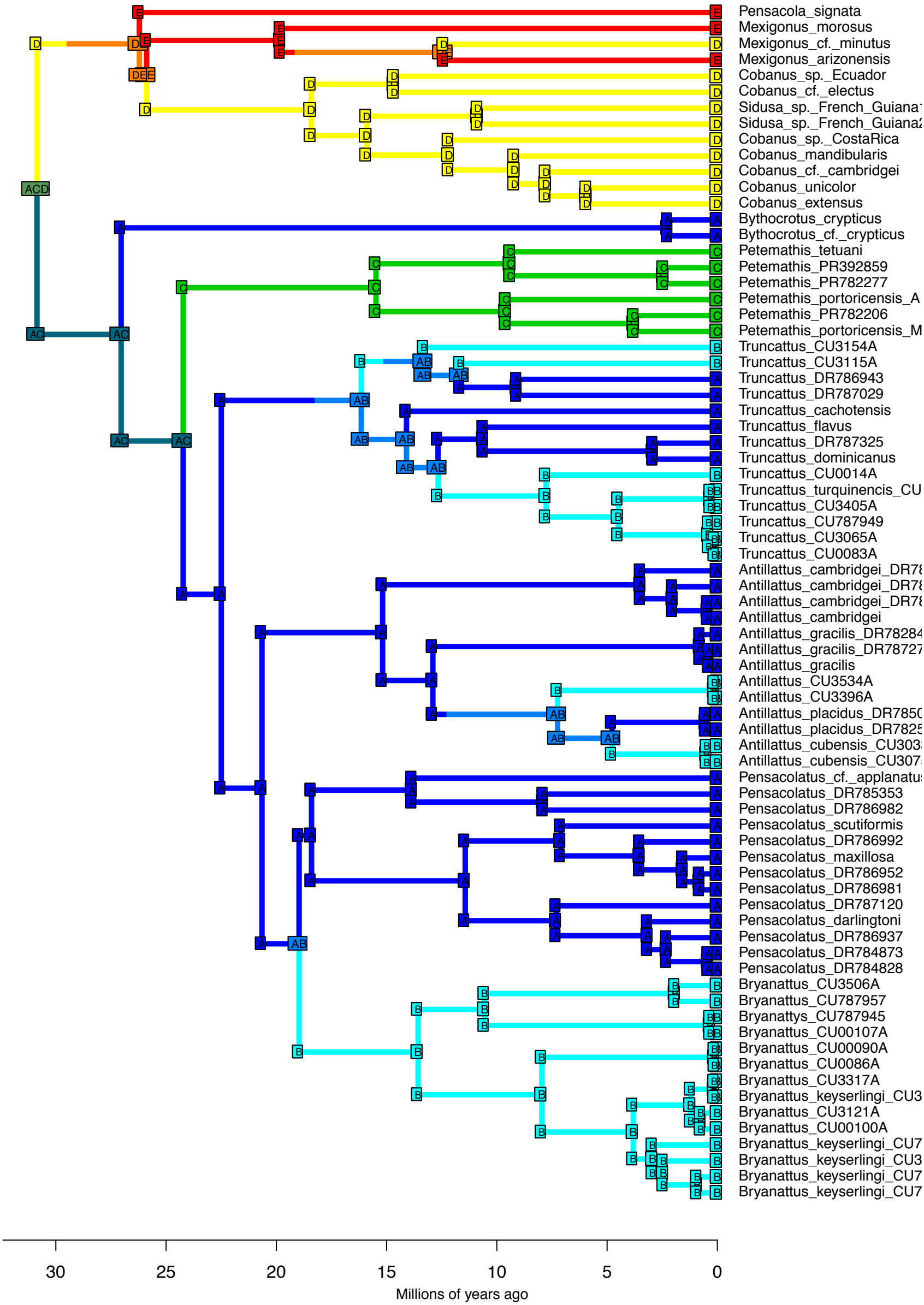

DEC – Stochastic Map #6/50
ancstates: global optim, 5 areas max. d=0.0017; e=0; j=0; LnL=–50.93

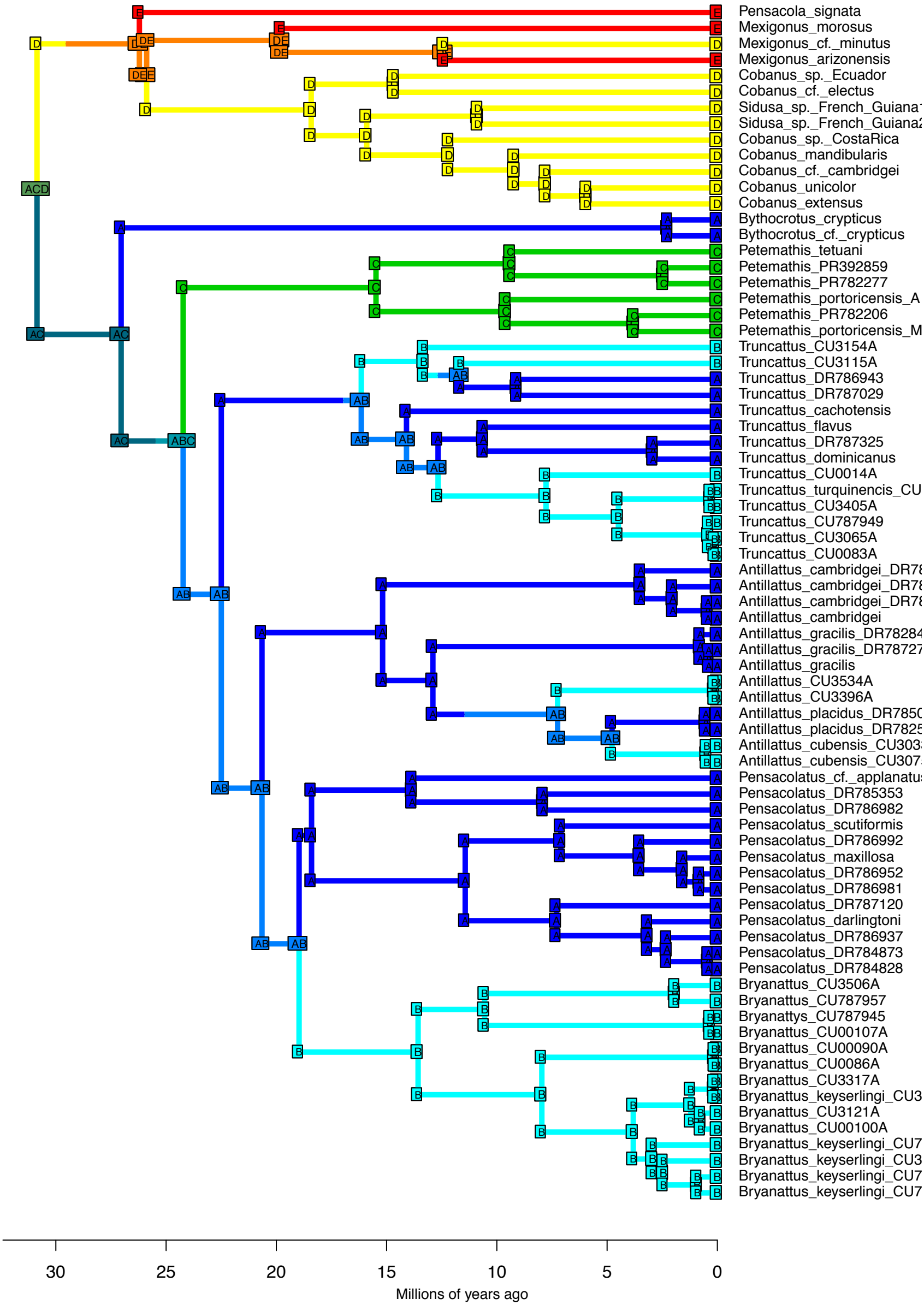

DEC – Stochastic Map #7/50
ancstates: global optim, 5 areas max. d=0.0017; e=0; j=0; LnL=–50.93

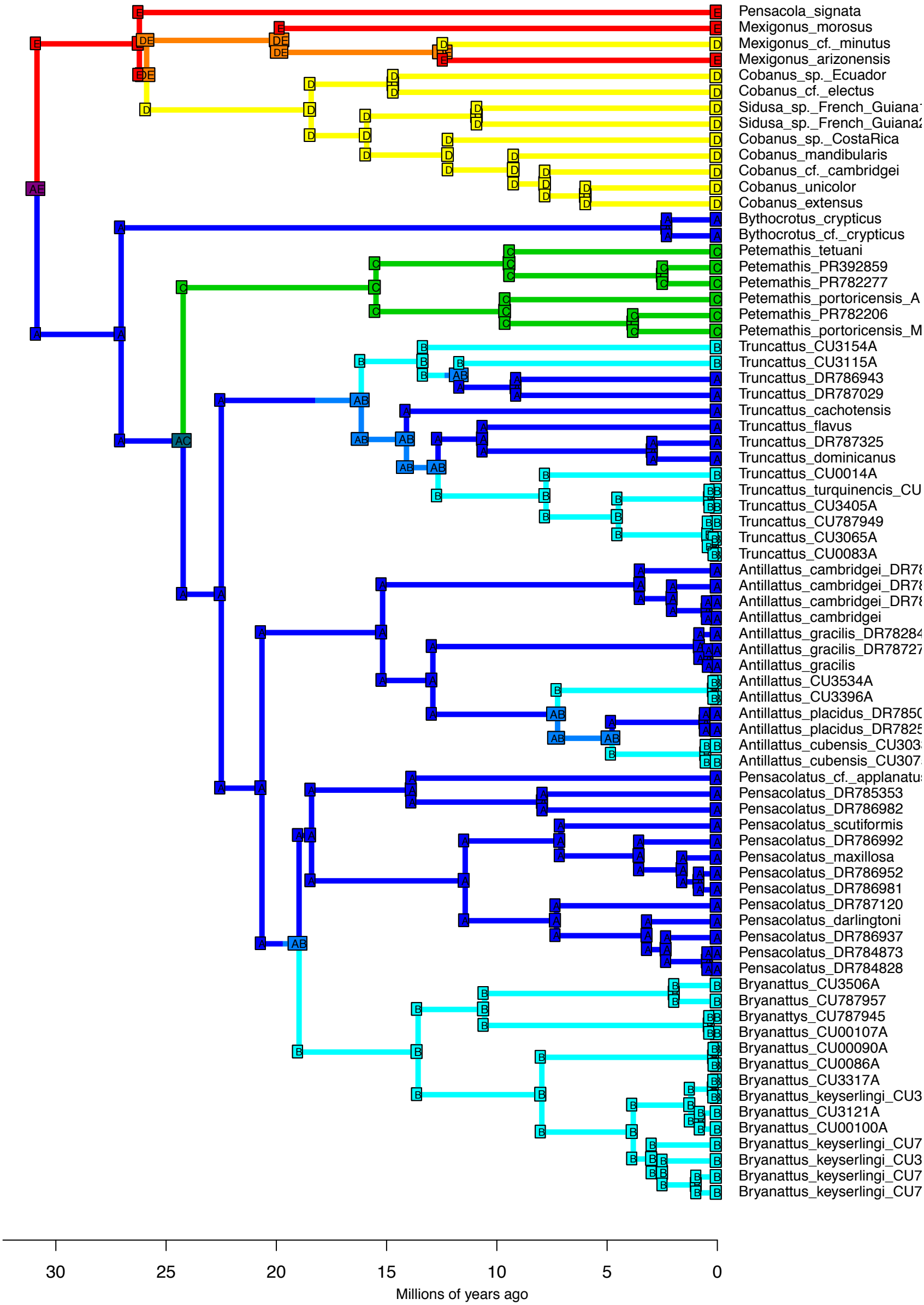

DEC – Stochastic Map #8/50
ancstates: global optim, 5 areas max. d=0.0017; e=0; j=0; LnL=–50.93

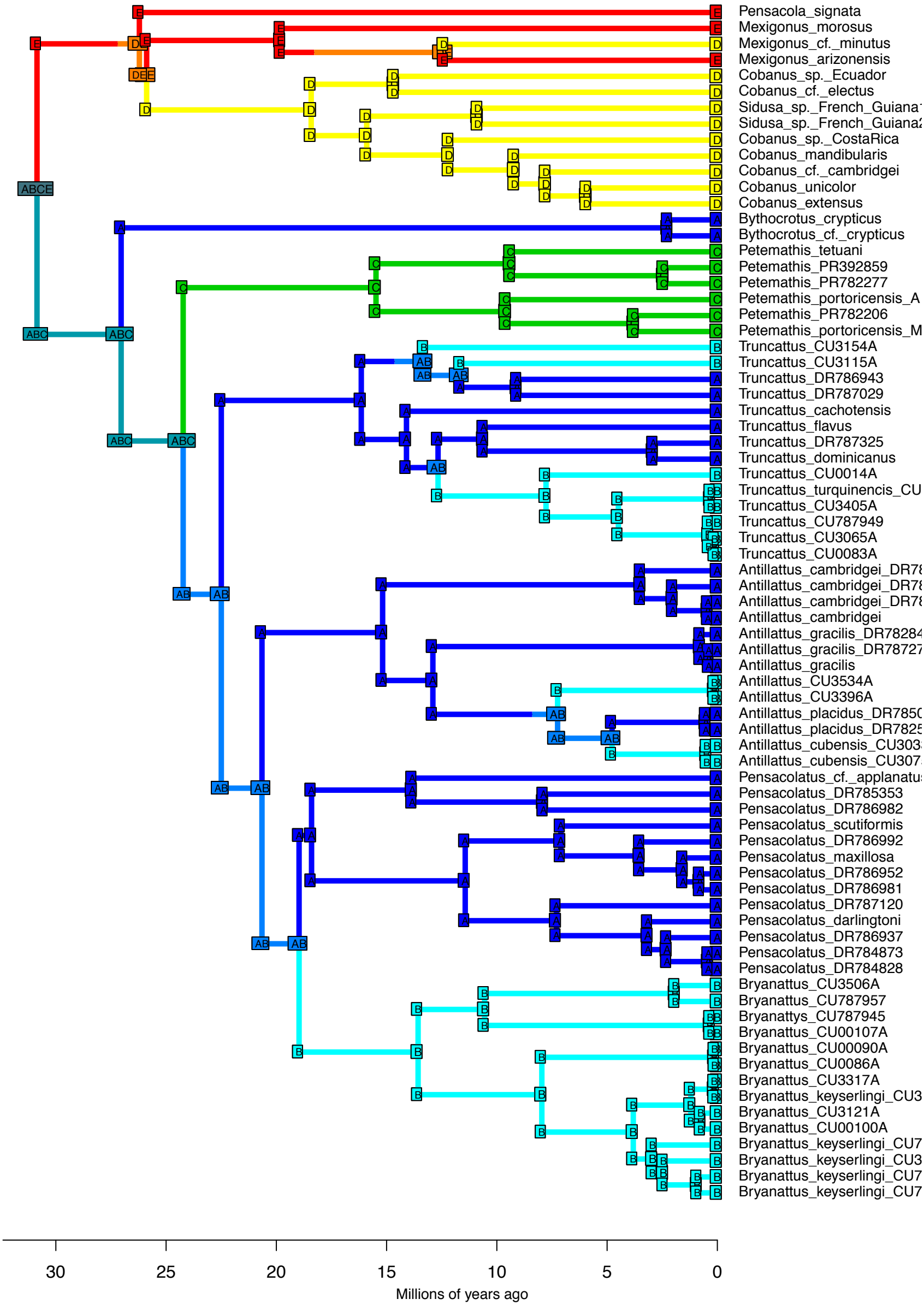

DEC – Stochastic Map #9/50
ancstates: global optim, 5 areas max. d=0.0017; e=0; j=0; LnL=–50.93

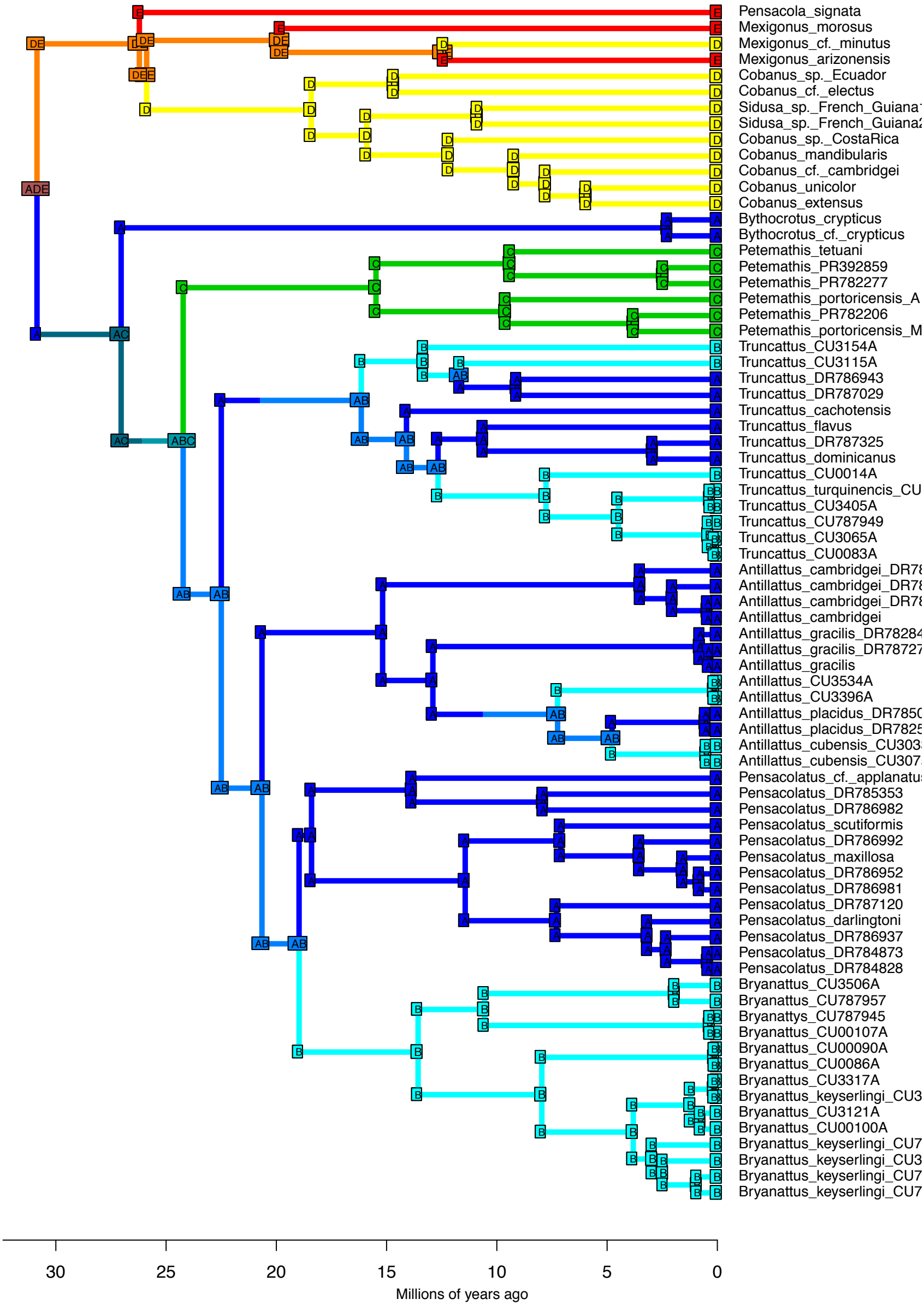

DEC – Stochastic Map #10/50
ancstates: global optim, 5 areas max. d=0.0017; e=0; j=0; LnL=–50.93

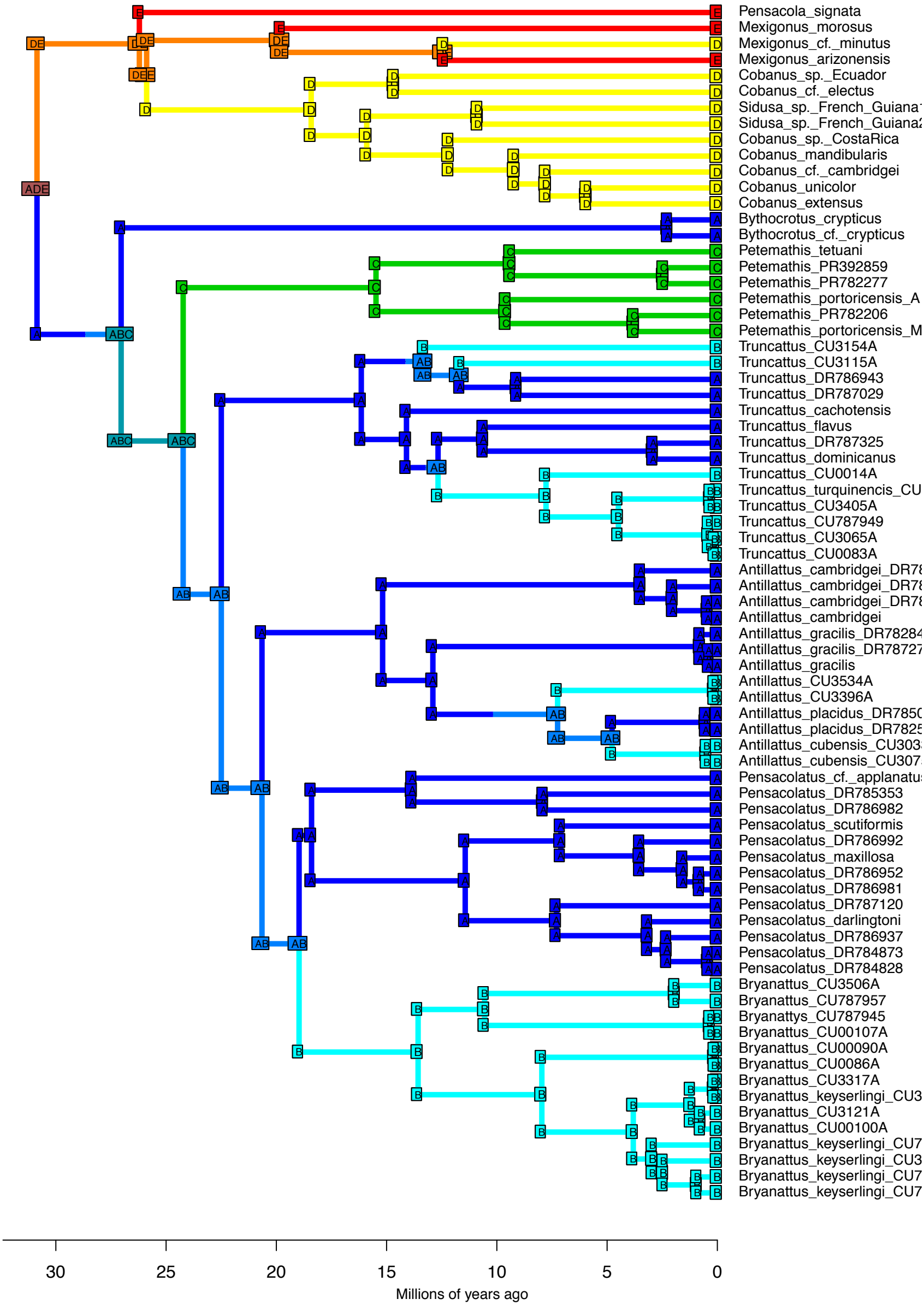

DEC – Stochastic Map #11/50
ancstates: global optim, 5 areas max. d=0.0017; e=0; j=0; LnL=–50.93

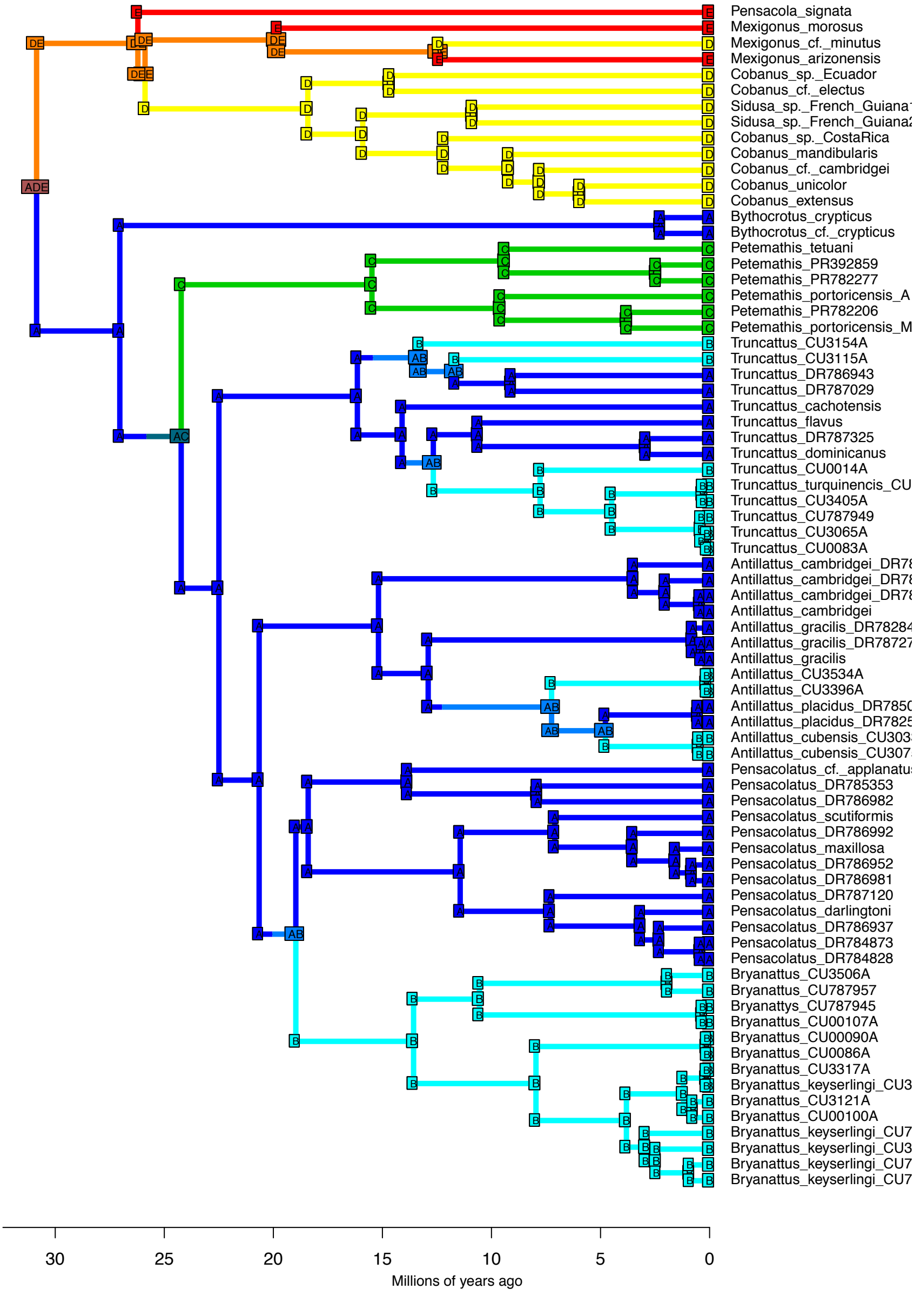

DEC – Stochastic Map #12/50
ancstates: global optim, 5 areas max. d=0.0017; e=0; j=0; LnL=–50.93

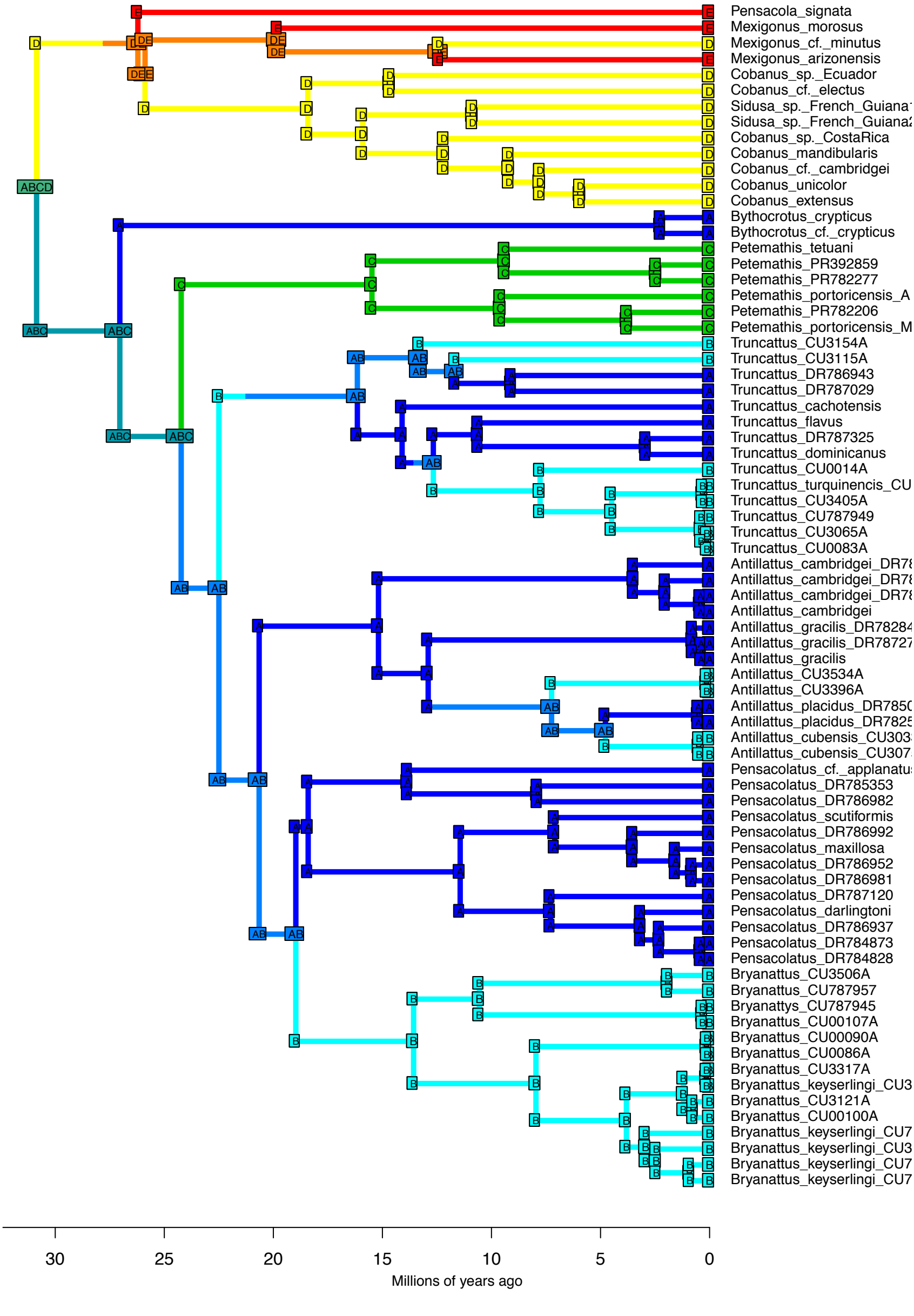

DEC – Stochastic Map #13/50
ancstates: global optim, 5 areas max. d=0.0017; e=0; j=0; LnL=–50.93

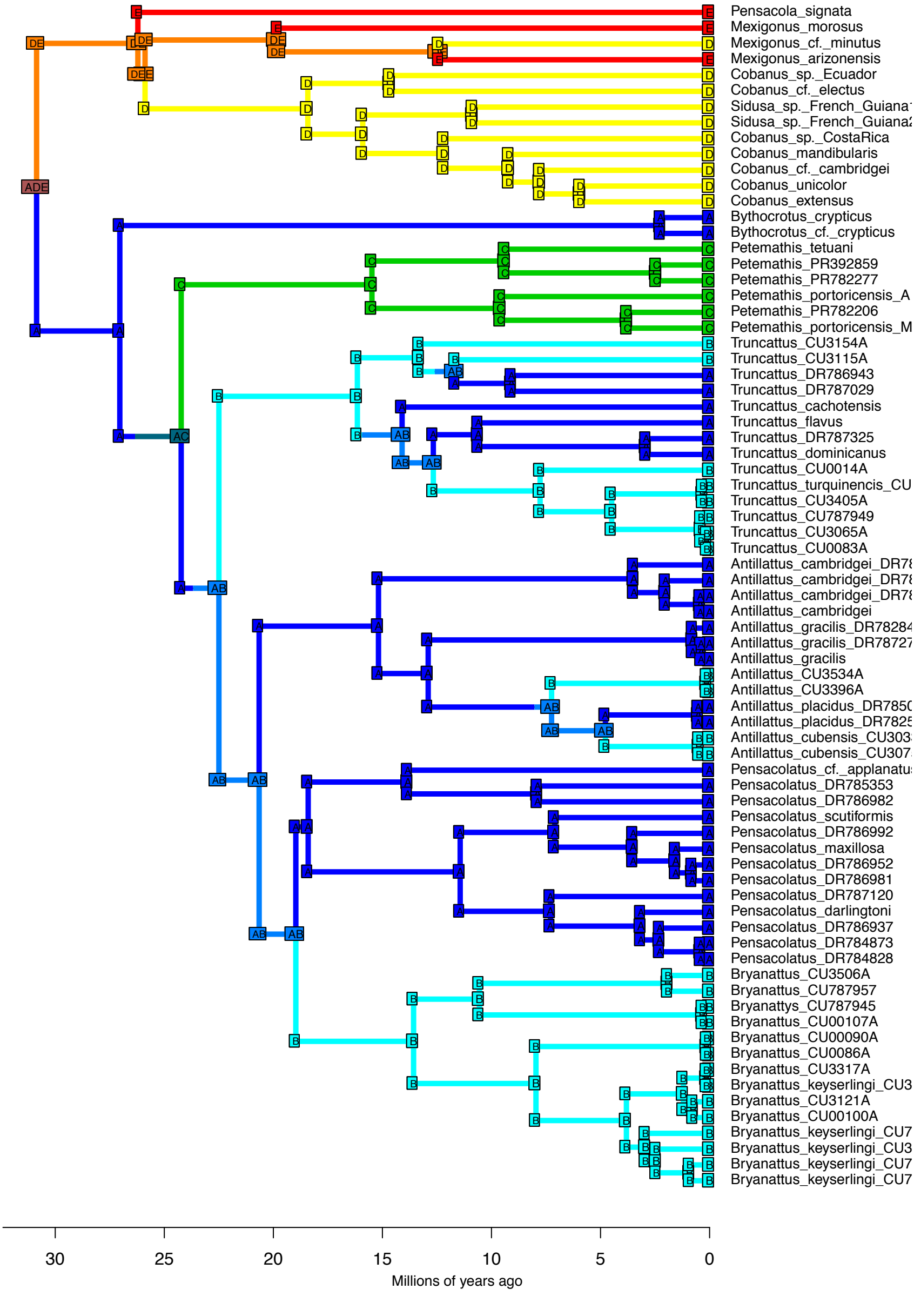

DEC – Stochastic Map #14/50
ancstates: global optim, 5 areas max. d=0.0017; e=0; j=0; LnL=–50.93

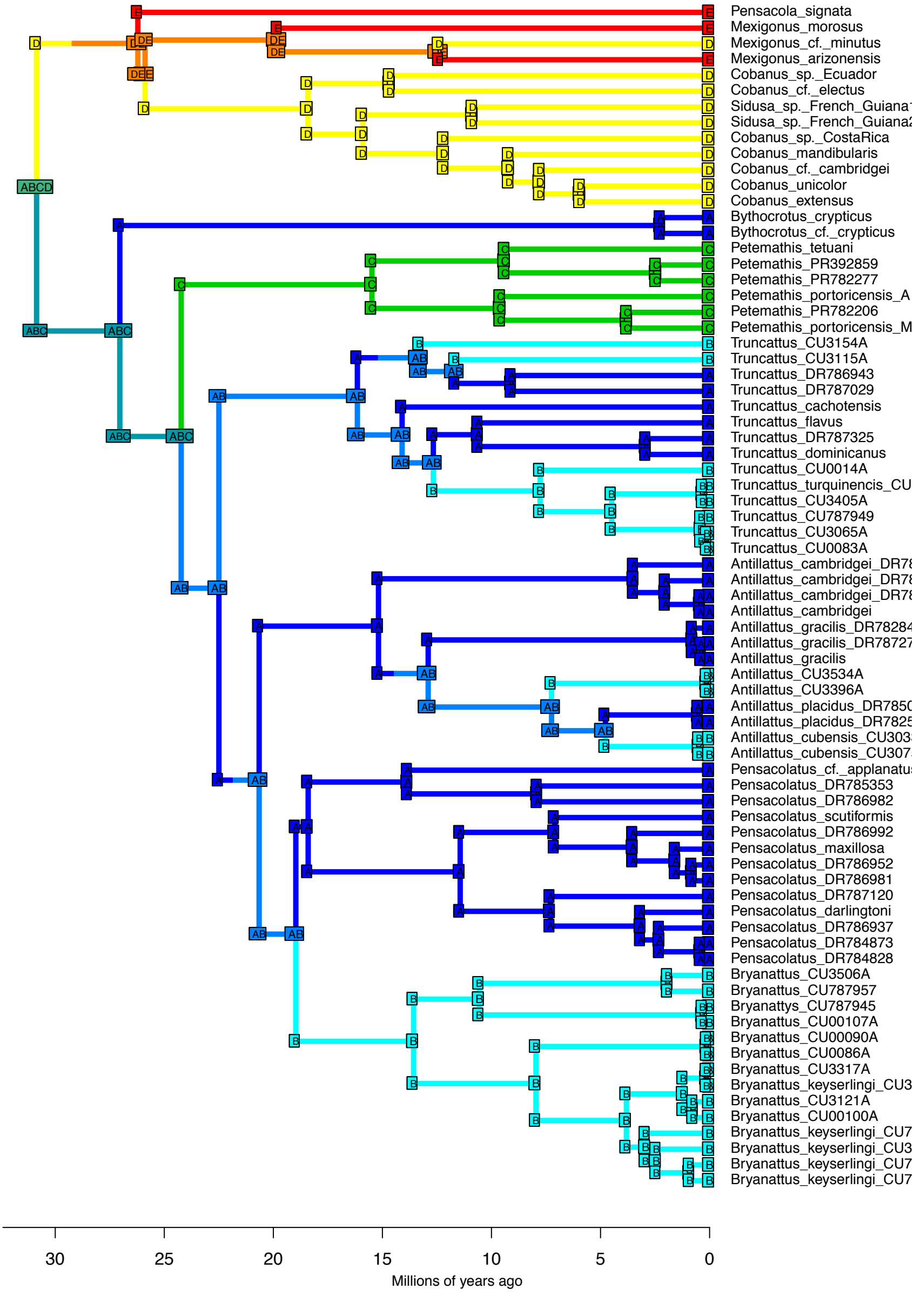

DEC – Stochastic Map #15/50
ancstates: global optim, 5 areas max. d=0.0017; e=0; j=0; LnL=–50.93

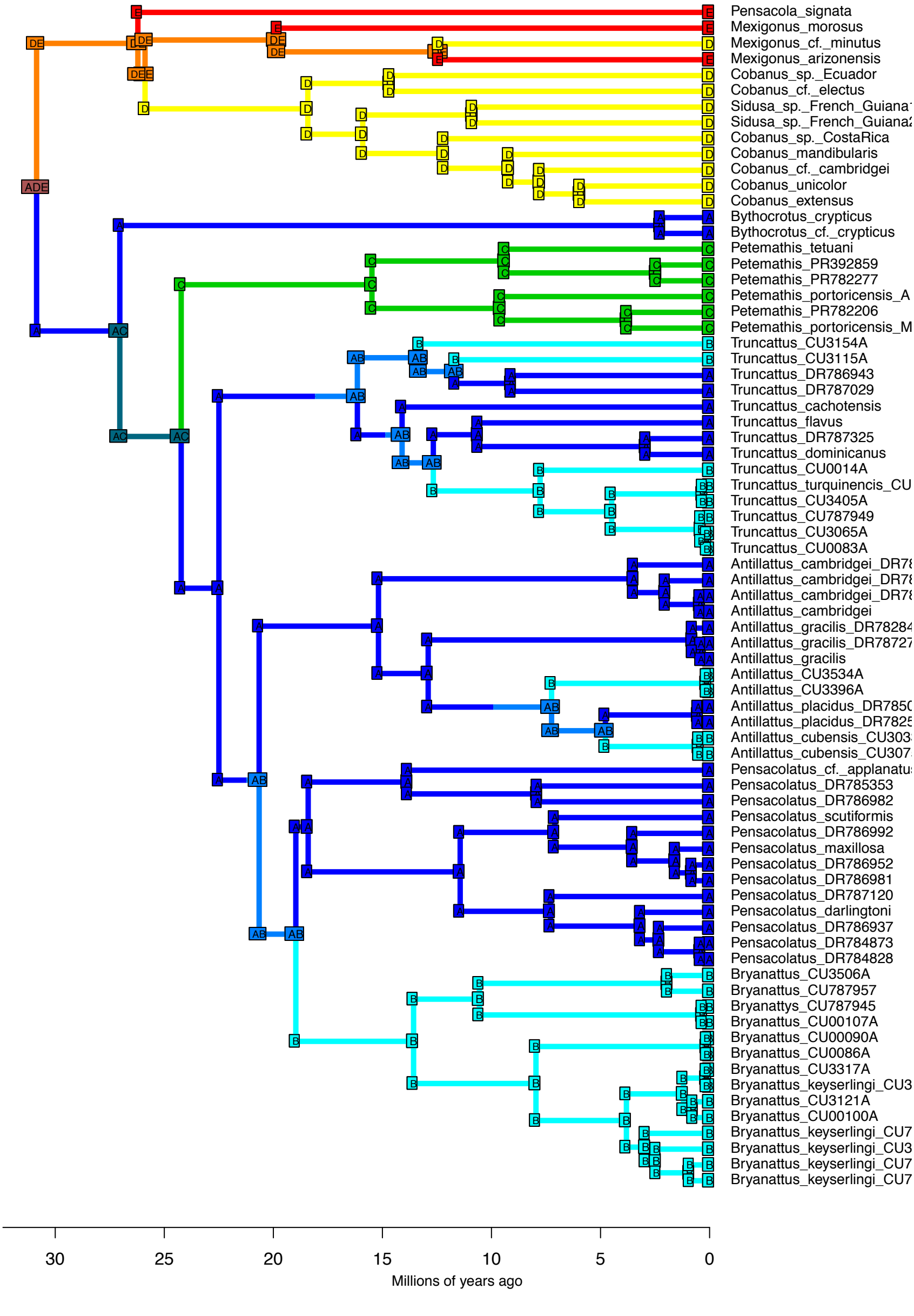

DEC – Stochastic Map #16/50
ancstates: global optim, 5 areas max. d=0.0017; e=0; j=0; LnL=–50.93

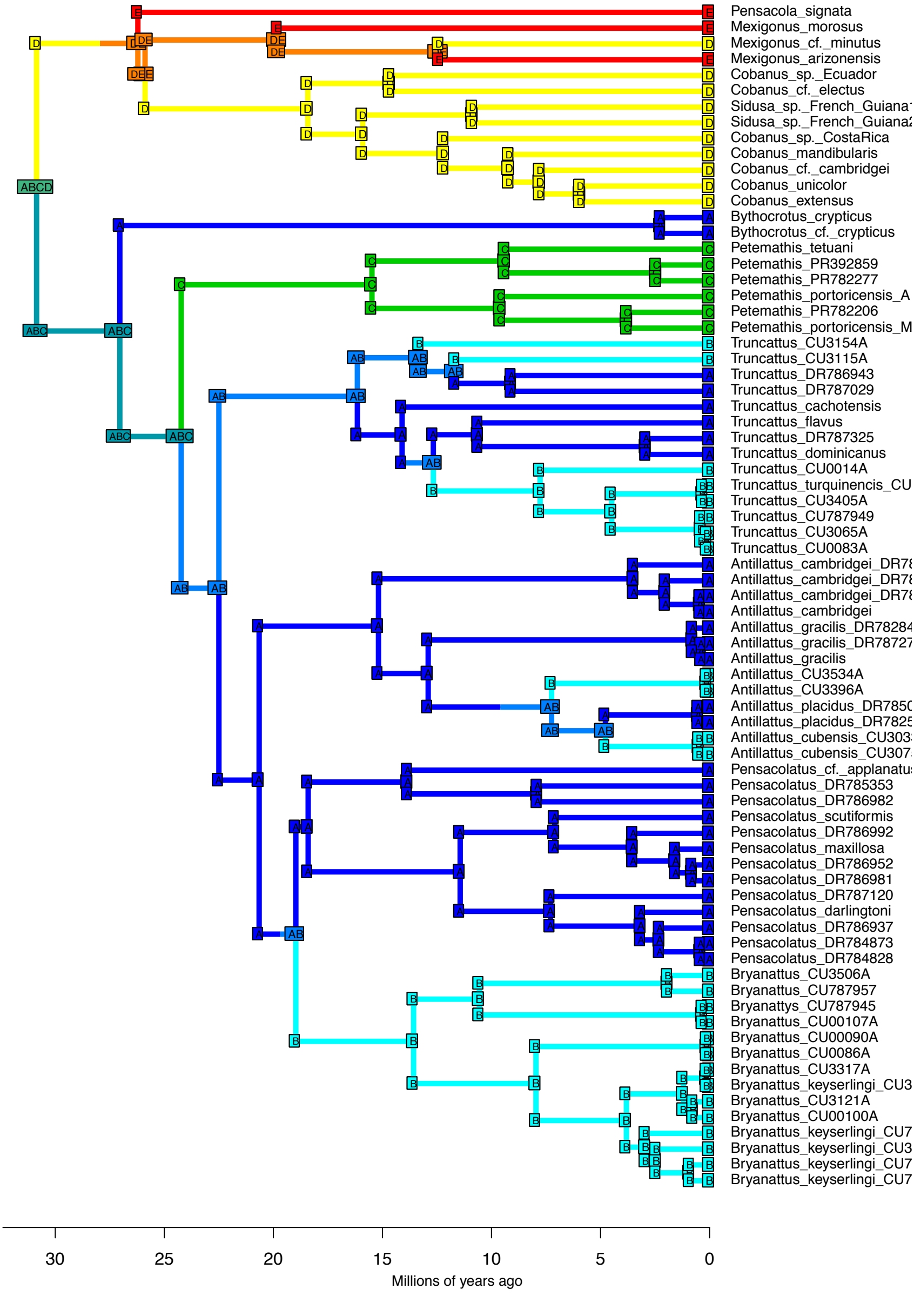

DEC – Stochastic Map #17/50
ancstates: global optim, 5 areas max. d=0.0017; e=0; j=0; LnL=–50.93

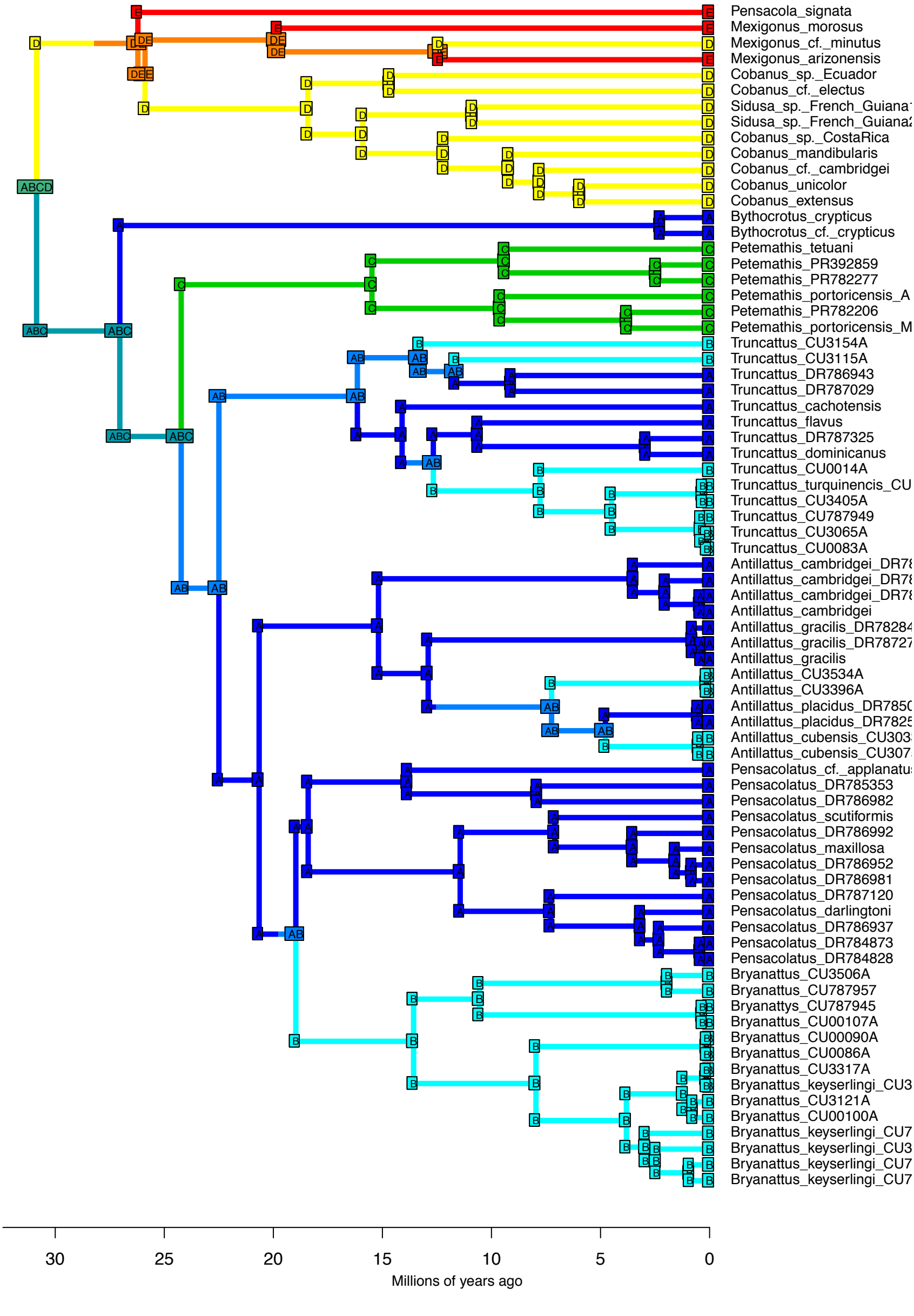

DEC – Stochastic Map #18/50
ancstates: global optim, 5 areas max. d=0.0017; e=0; j=0; LnL=–50.93

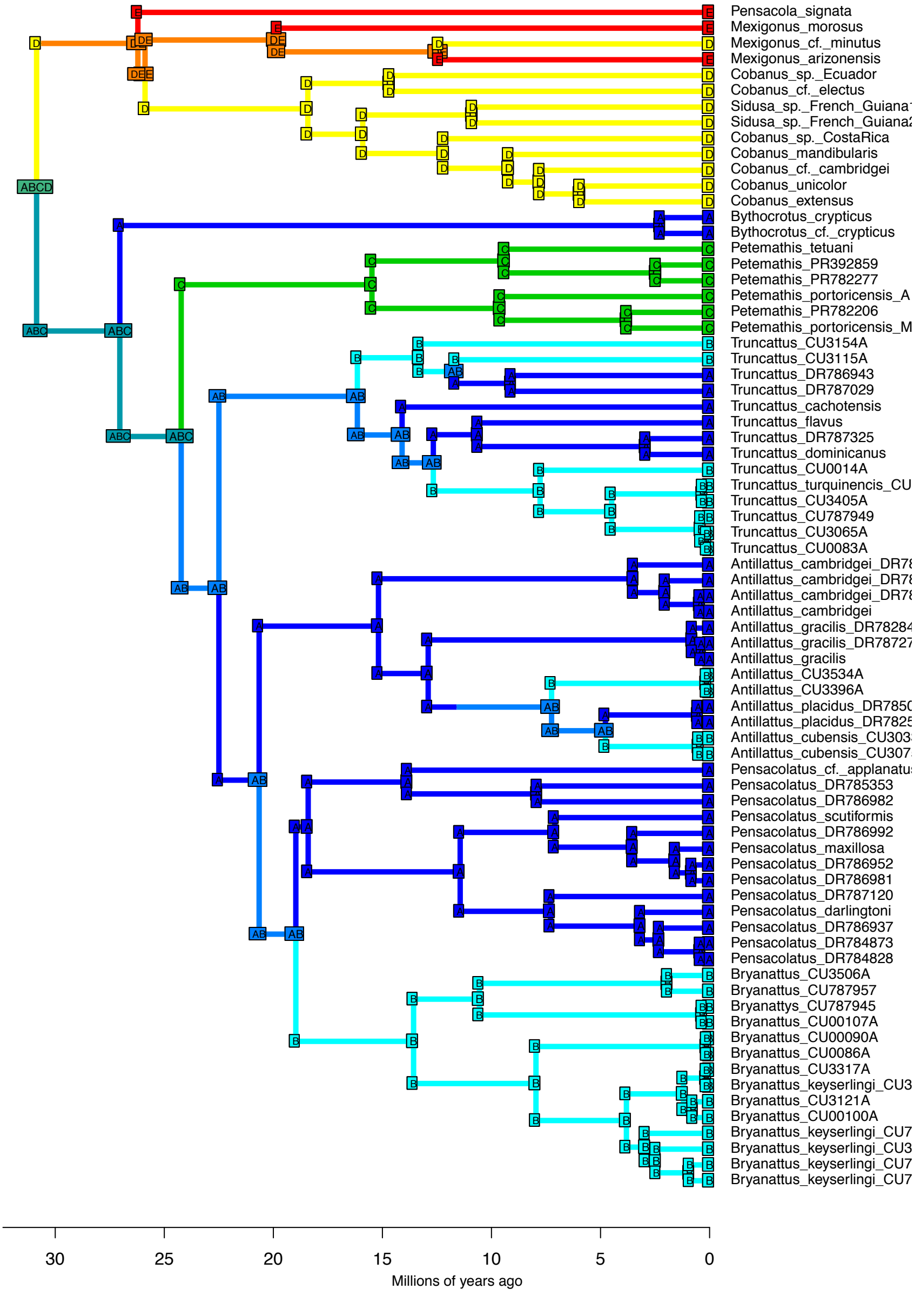

DEC – Stochastic Map #19/50
ancstates: global optim, 5 areas max. d=0.0017; e=0; j=0; LnL=–50.93

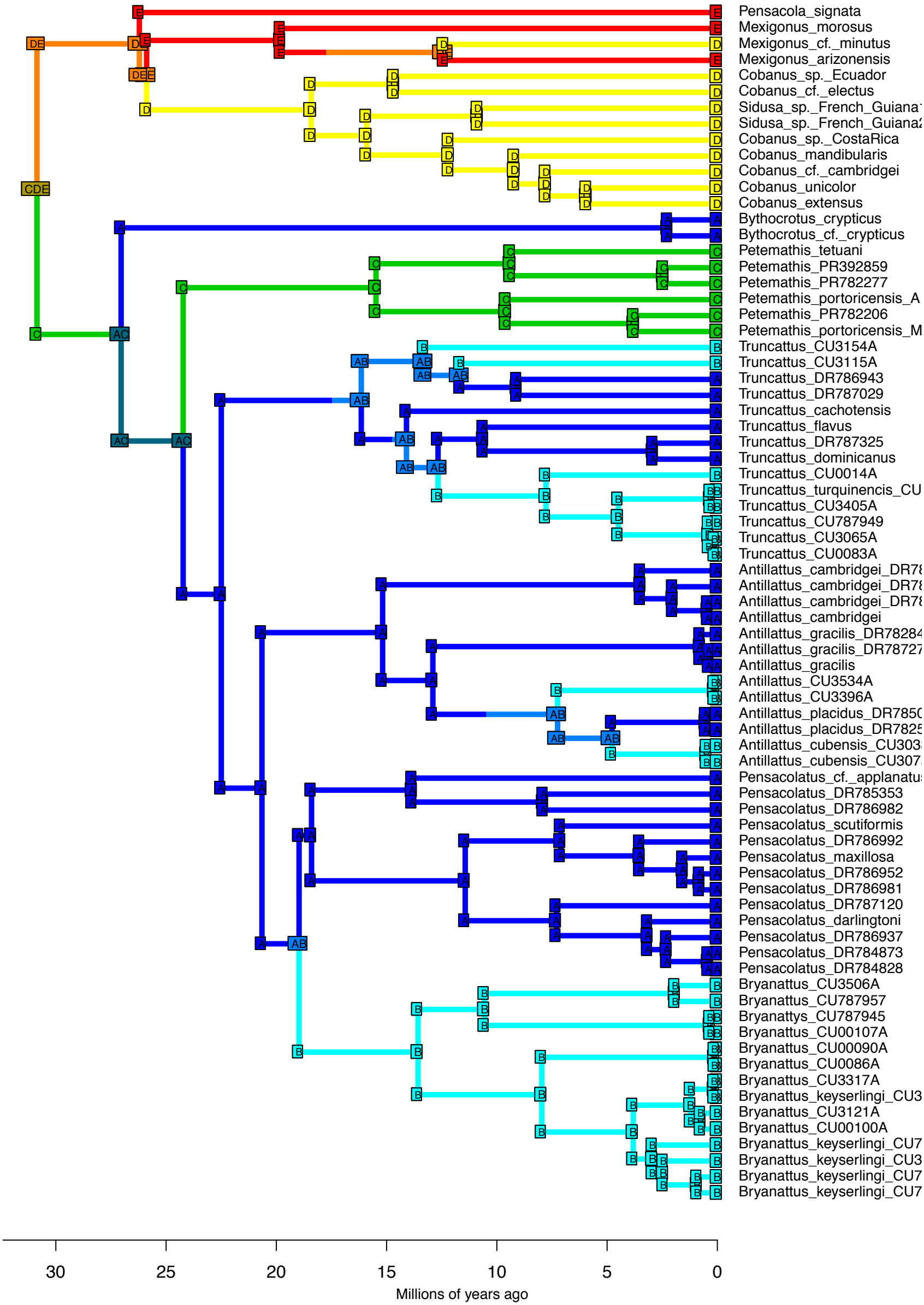

DEC – Stochastic Map #20/50
ancstates: global optim, 5 areas max. d=0.0017; e=0; j=0; LnL=–50.93

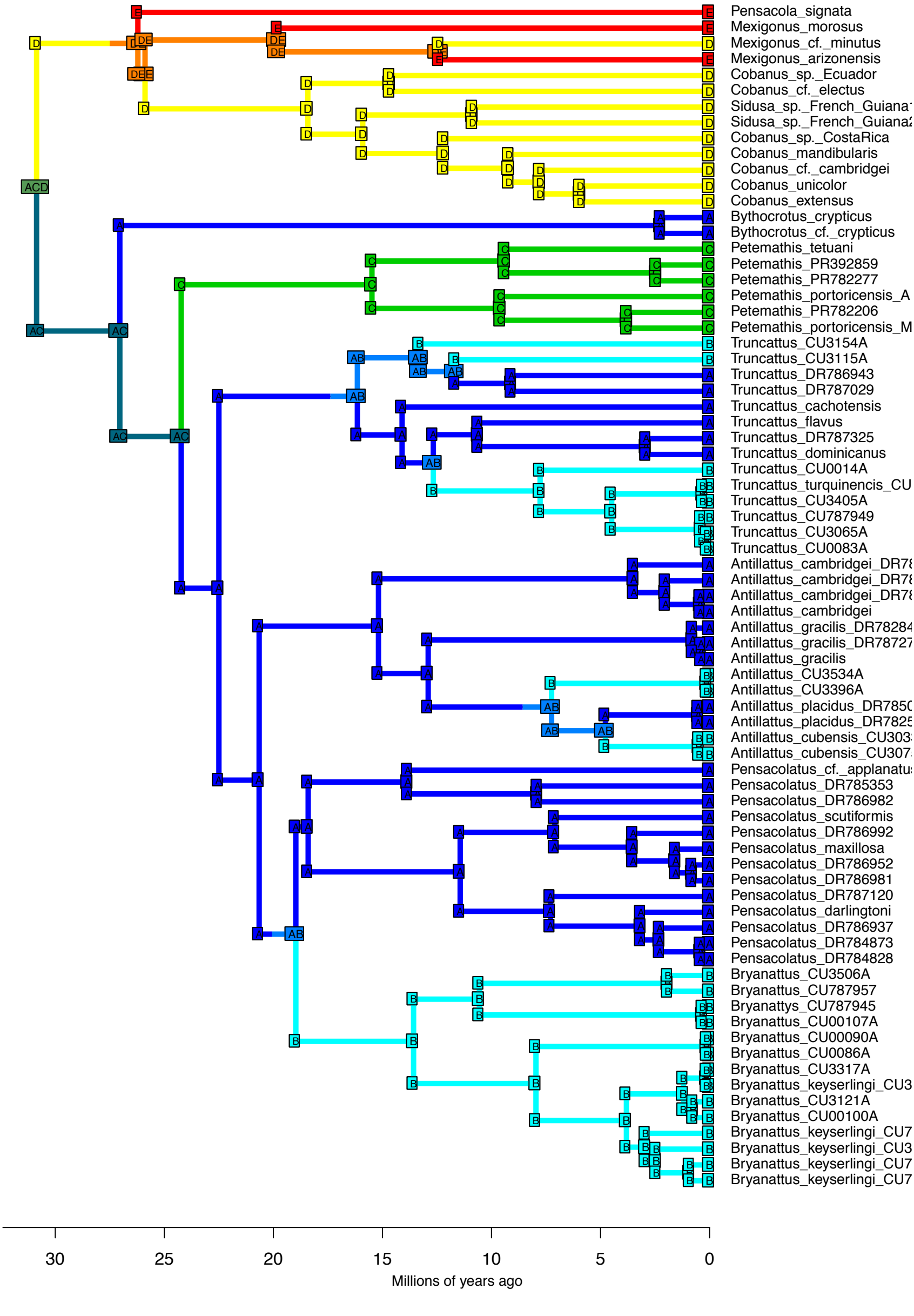

DEC – Stochastic Map #21/50
ancstates: global optim, 5 areas max. d=0.0017; e=0; j=0; LnL=–50.93

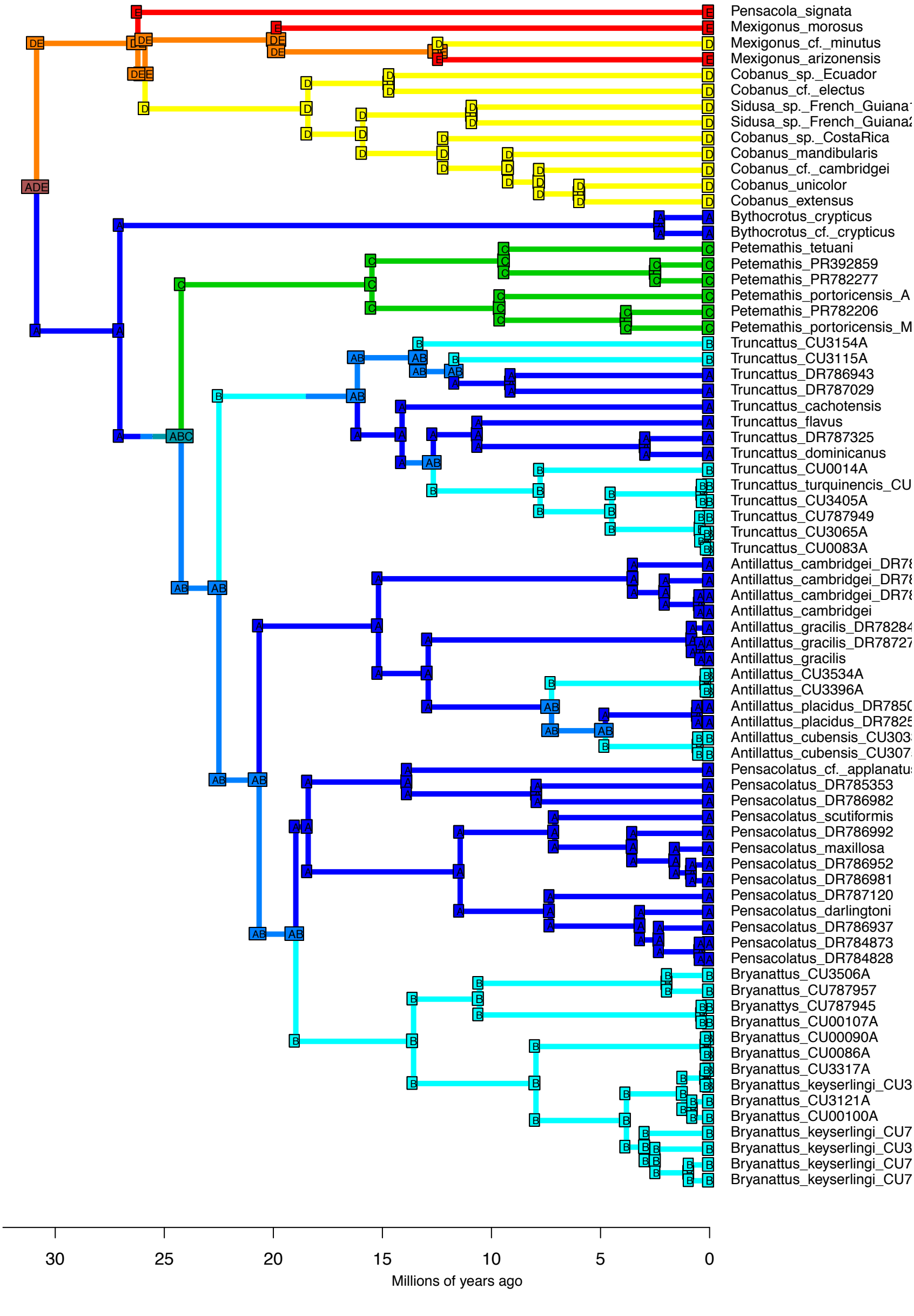

DEC – Stochastic Map #22/50
ancstates: global optim, 5 areas max. d=0.0017; e=0; j=0; LnL=–50.93

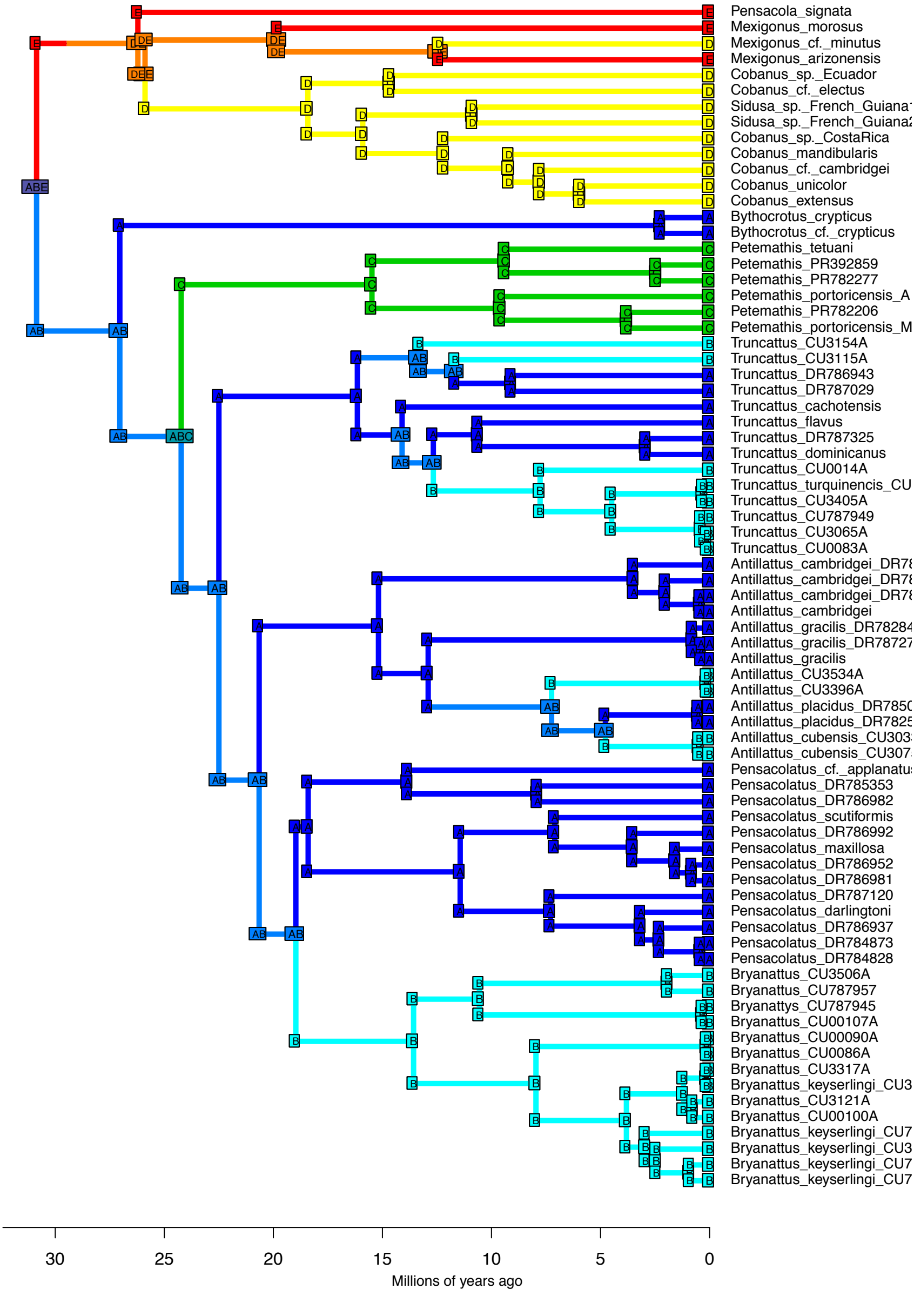

DEC – Stochastic Map #23/50
ancstates: global optim, 5 areas max. d=0.0017; e=0; j=0; LnL=–50.93

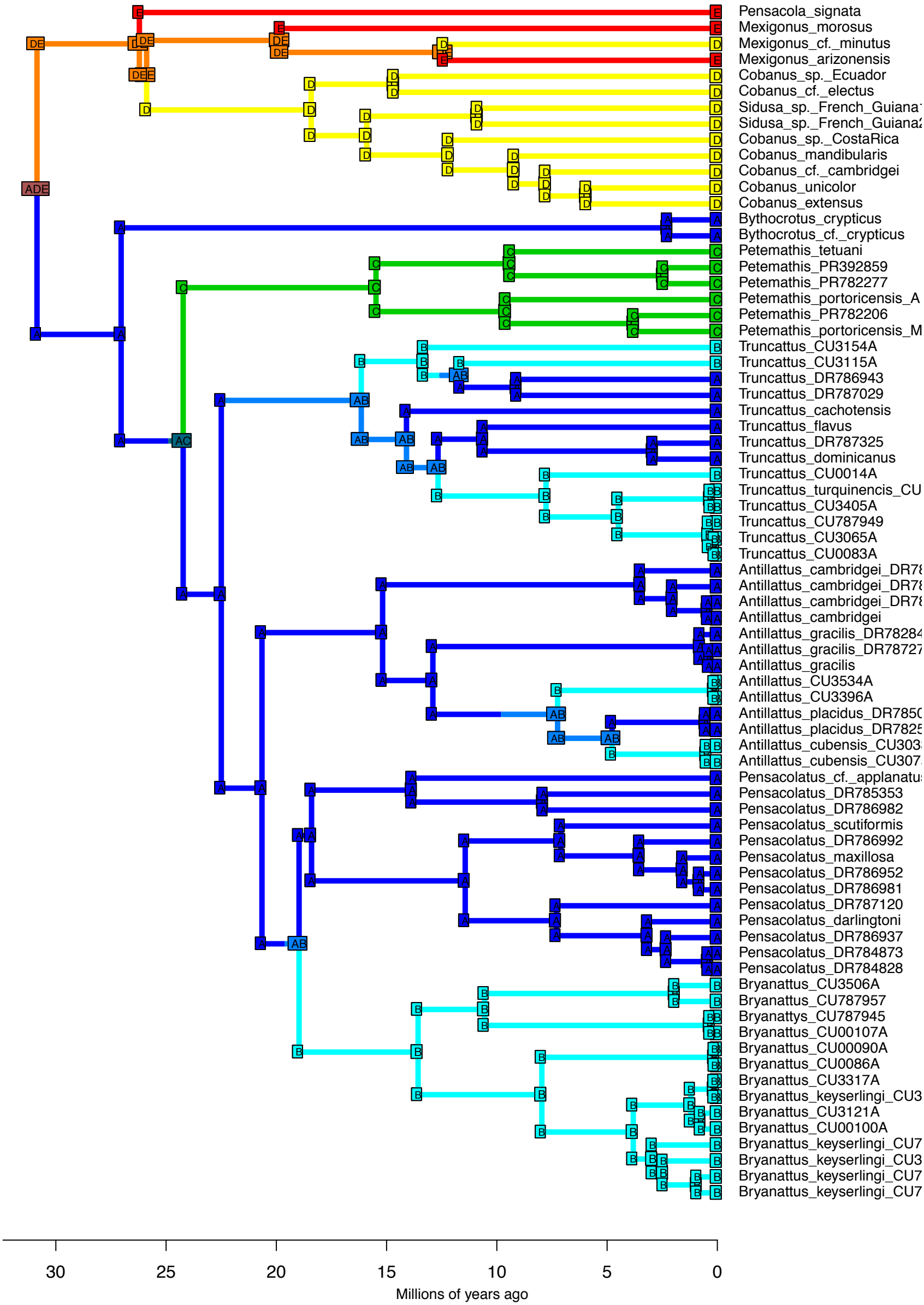

DEC – Stochastic Map #24/50
ancstates: global optim, 5 areas max. d=0.0017; e=0; j=0; LnL=–50.93

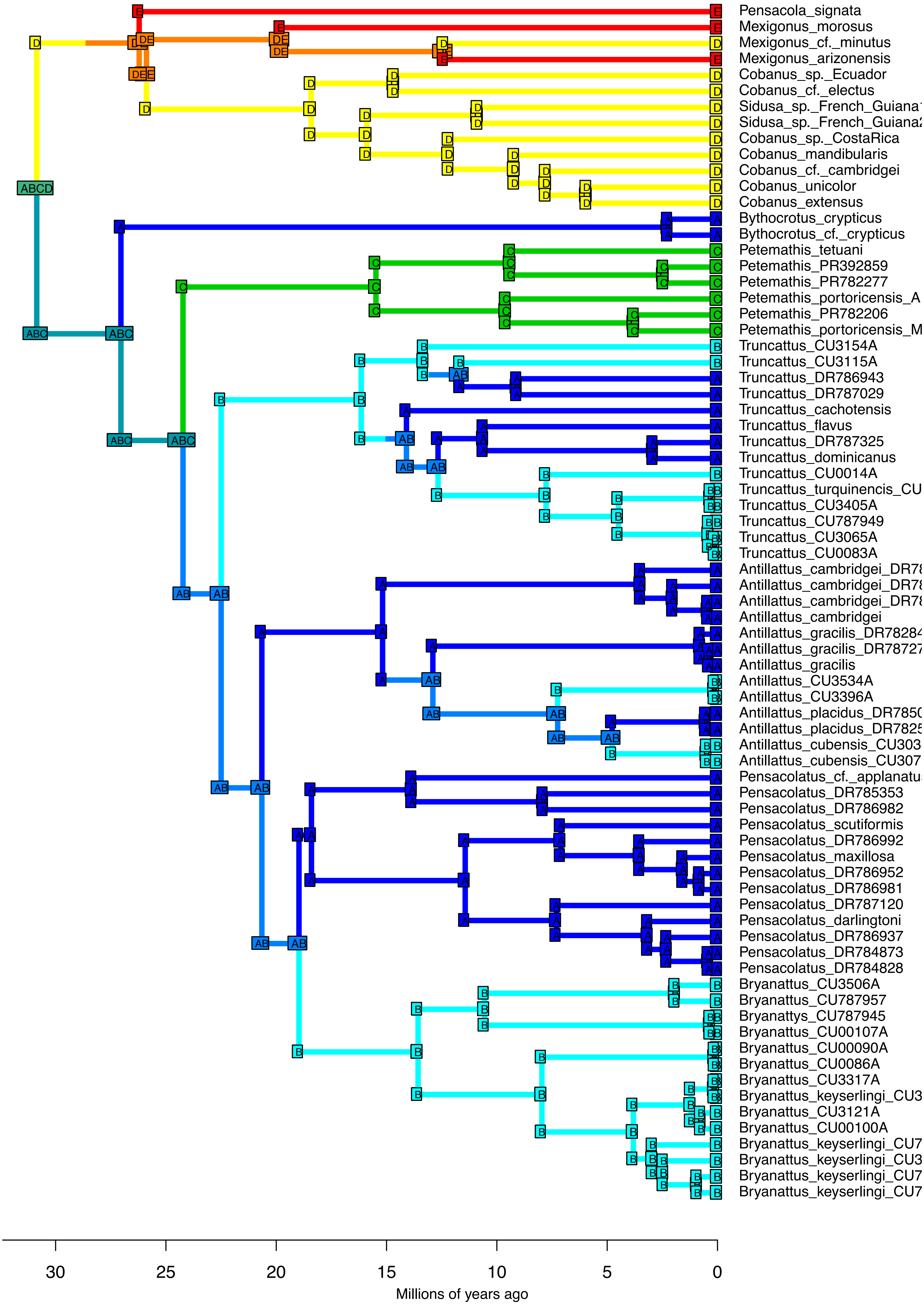

DEC – Stochastic Map #25/50
ancstates: global optim, 5 areas max. d=0.0017; e=0; j=0; LnL=–50.93

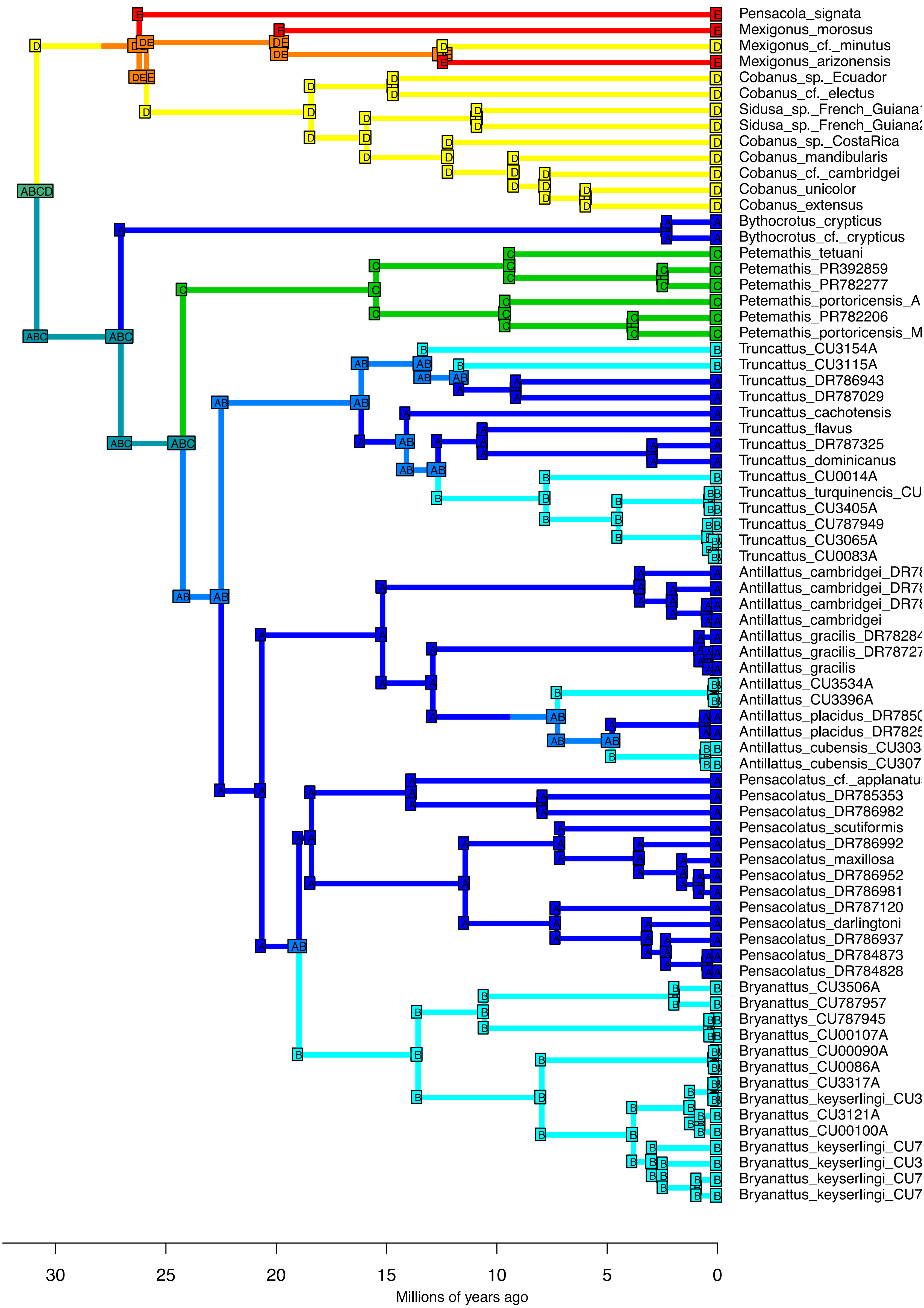

DEC – Stochastic Map #26/50
ancstates: global optim, 5 areas max. d=0.0017; e=0; j=0; LnL=–50.93

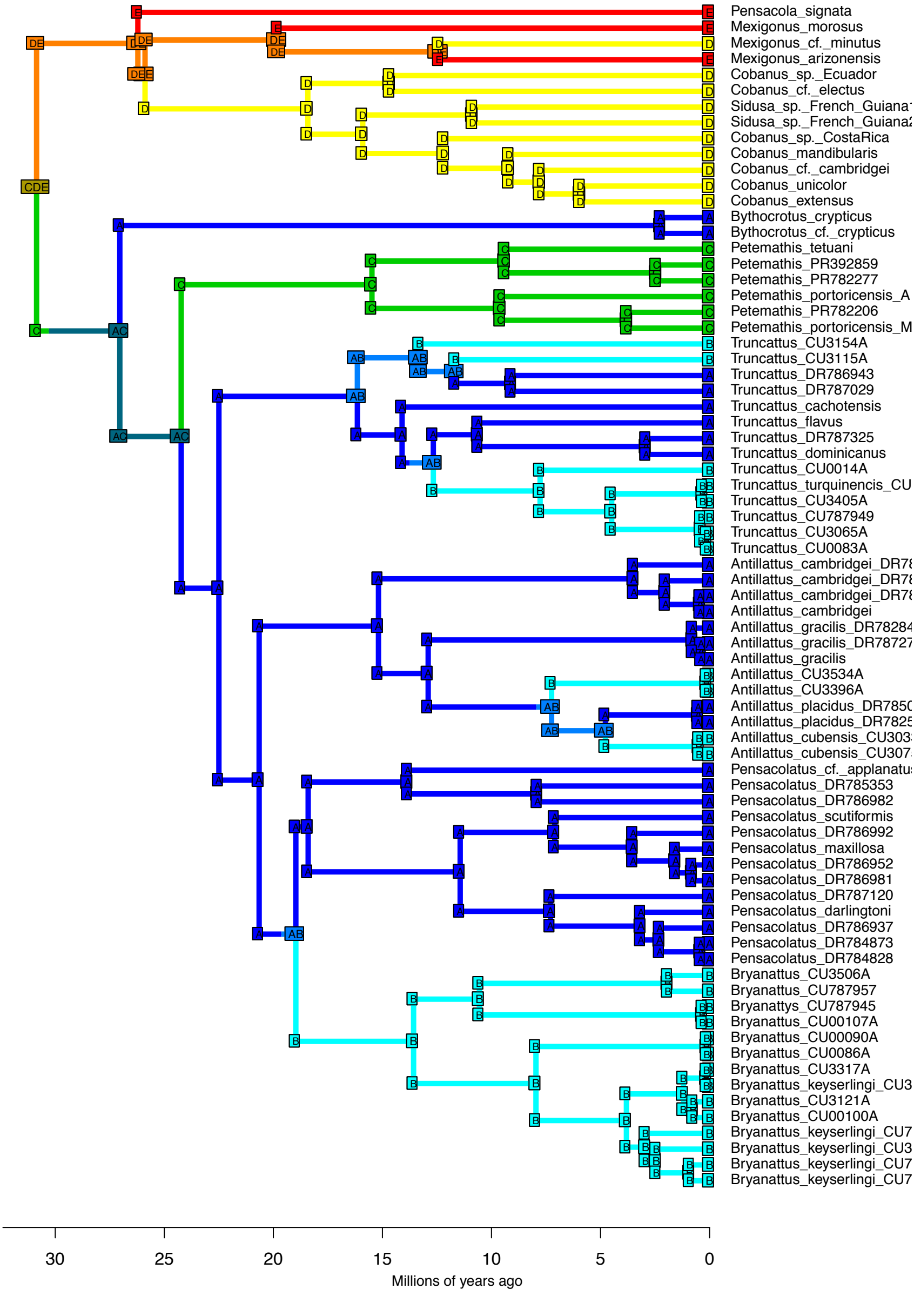

DEC – Stochastic Map #27/50
ancstates: global optim, 5 areas max. d=0.0017; e=0; j=0; LnL=–50.93

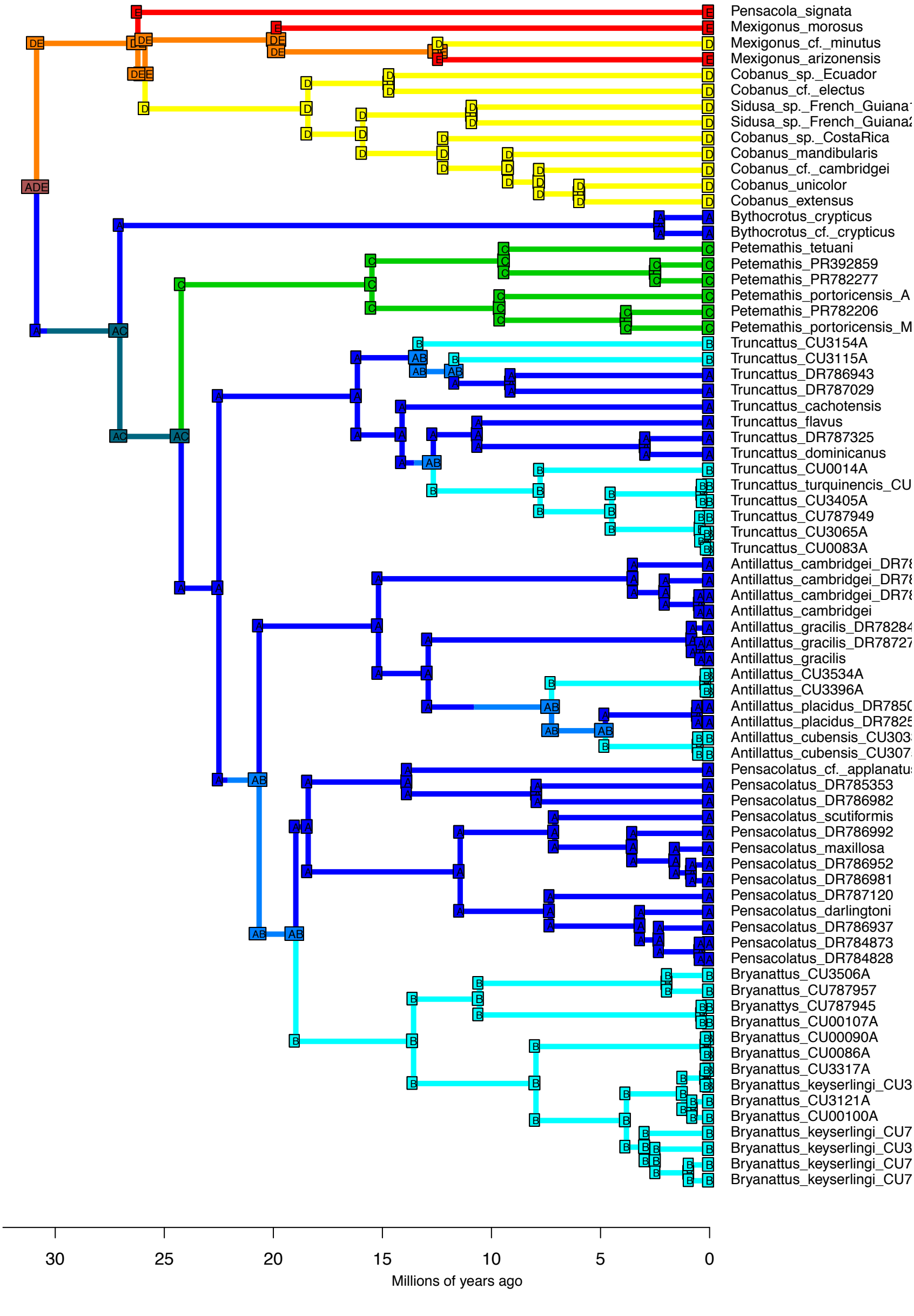

DEC – Stochastic Map #28/50
ancstates: global optim, 5 areas max. d=0.0017; e=0; j=0; LnL=–50.93

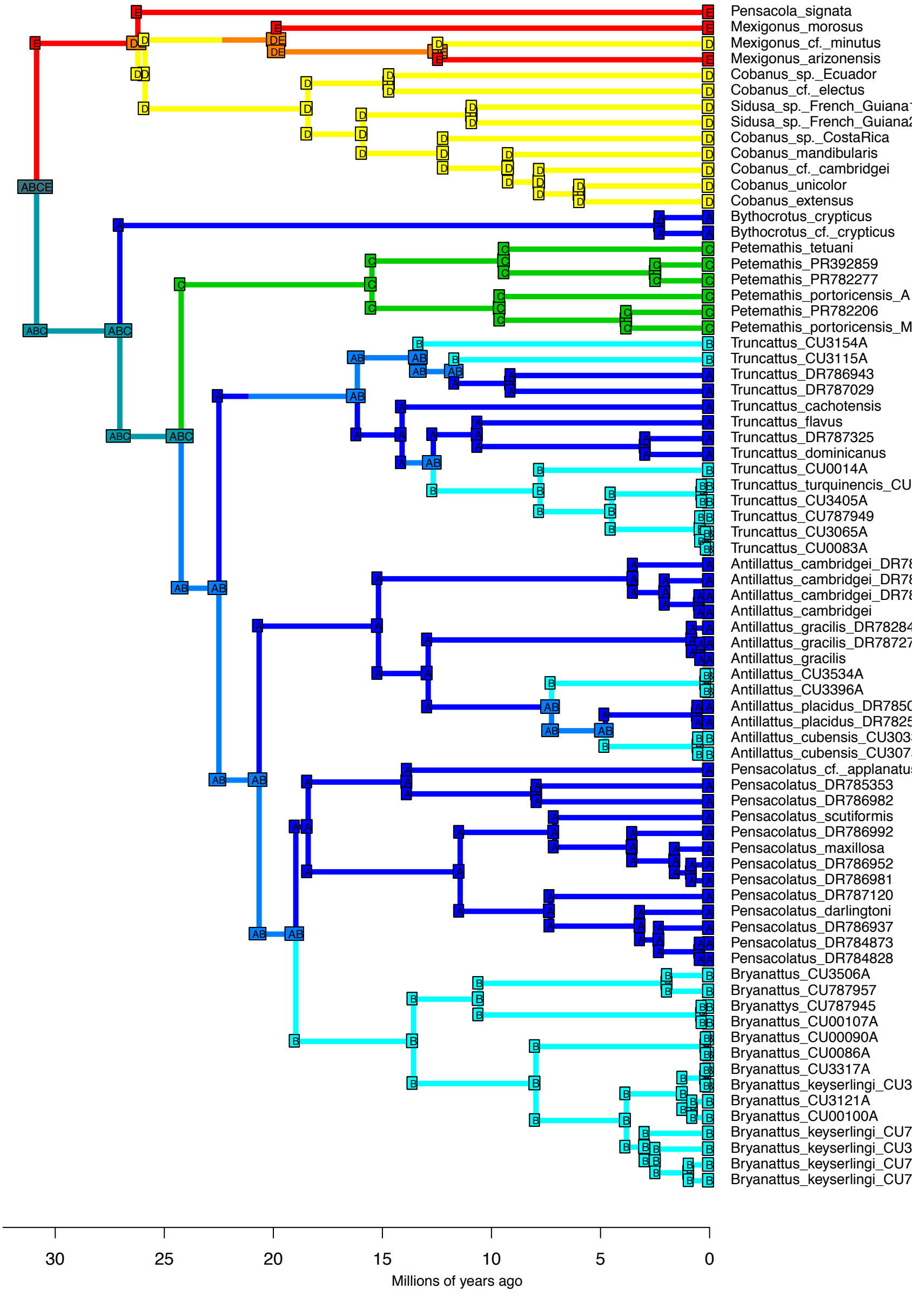

DEC – Stochastic Map #29/50
ancstates: global optim, 5 areas max. d=0.0017; e=0; j=0; LnL=–50.93

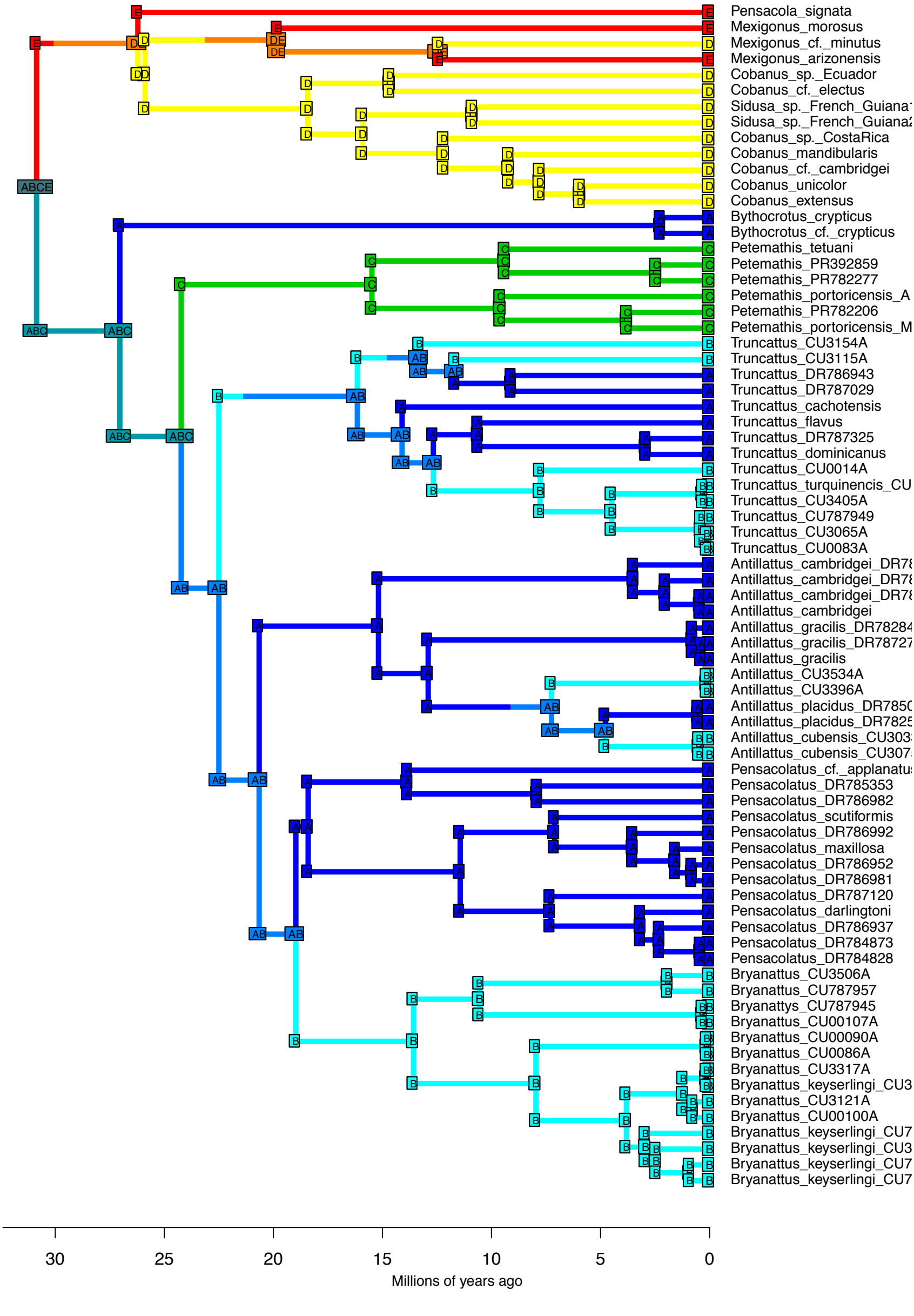

DEC – Stochastic Map #30/50
ancstates: global optim, 5 areas max. d=0.0017; e=0; j=0; LnL=–50.93

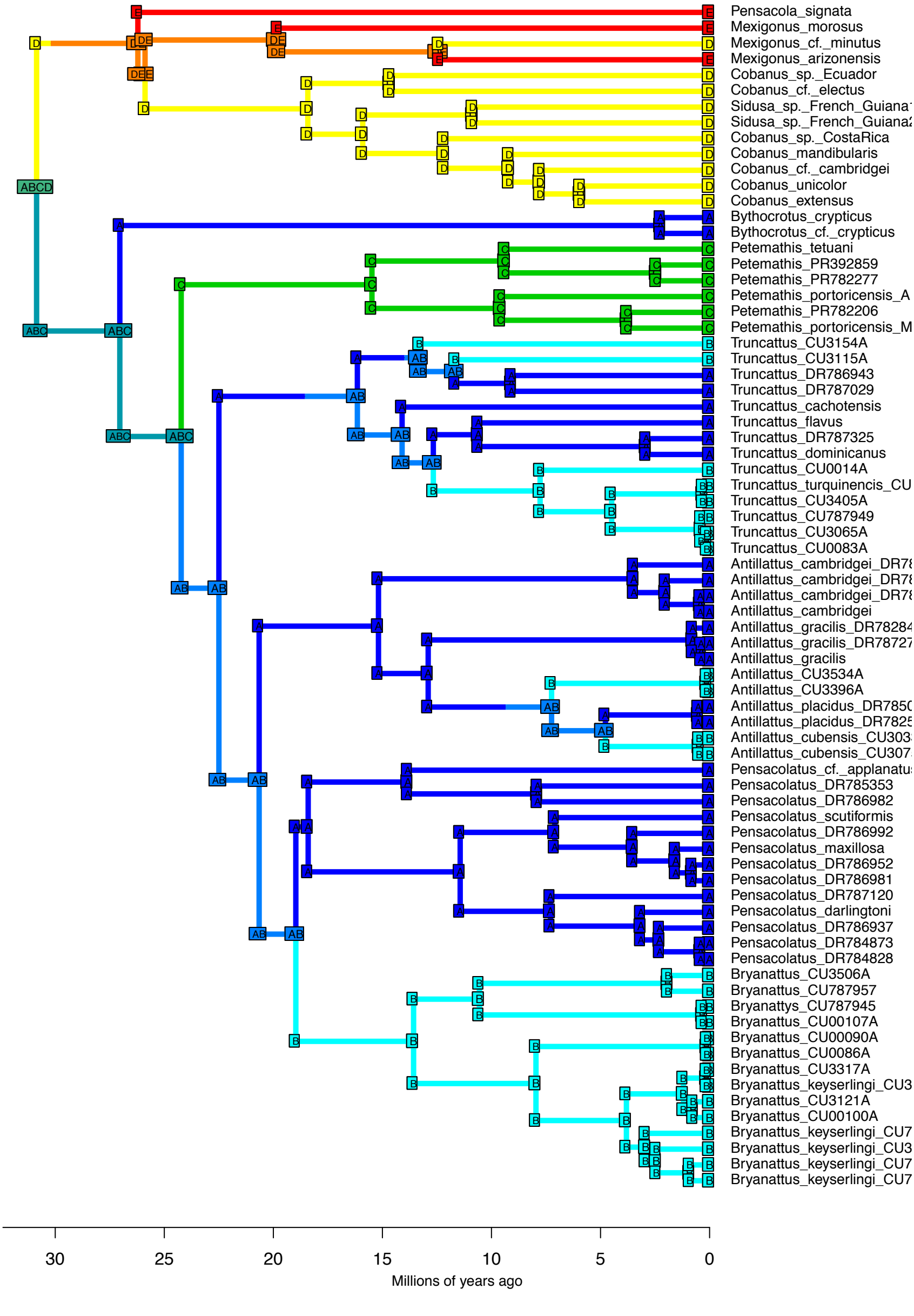

DEC – Stochastic Map #31/50
ancstates: global optim, 5 areas max. d=0.0017; e=0; j=0; LnL=–50.93

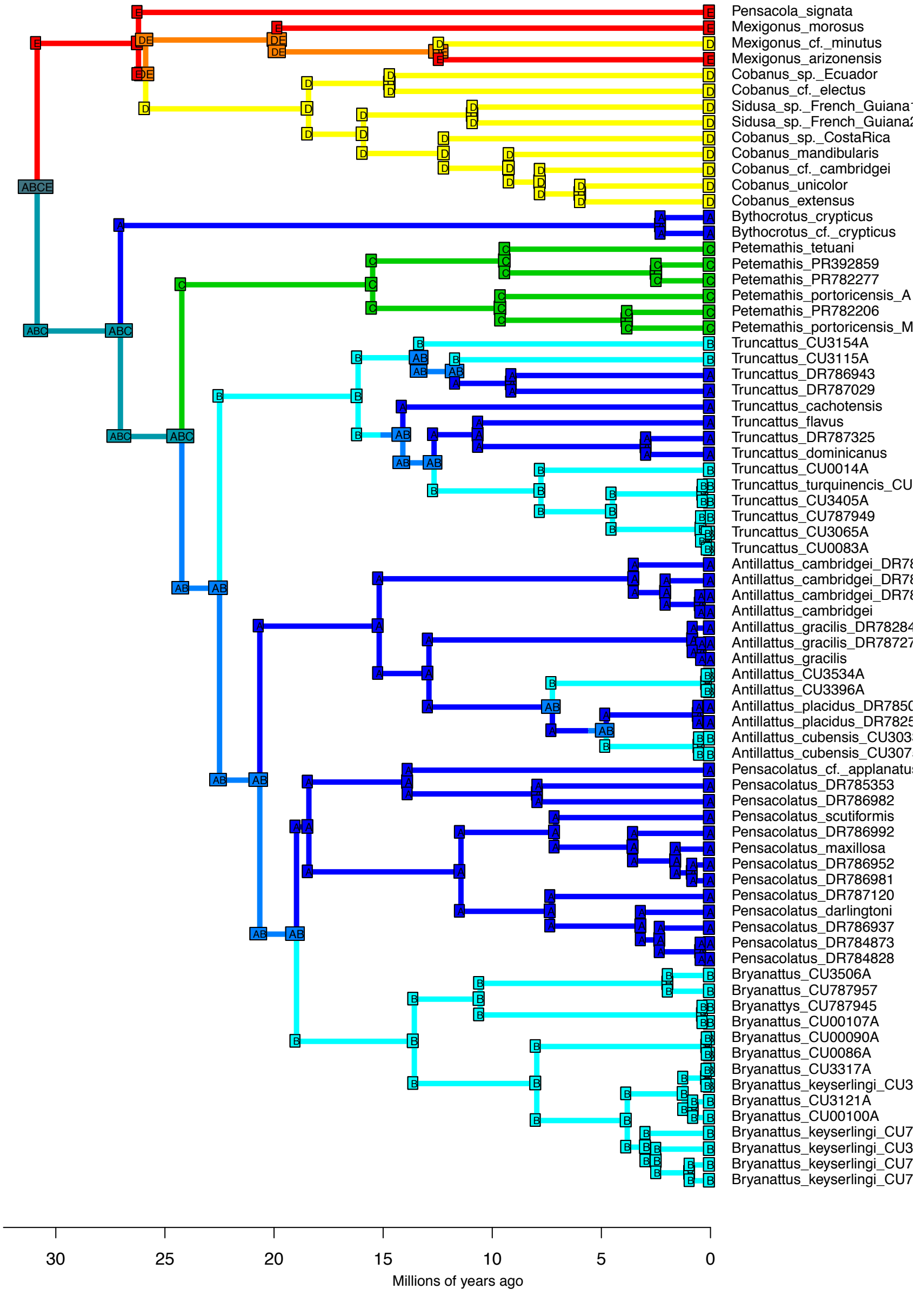

DEC – Stochastic Map #32/50
ancstates: global optim, 5 areas max. d=0.0017; e=0; j=0; LnL=–50.93

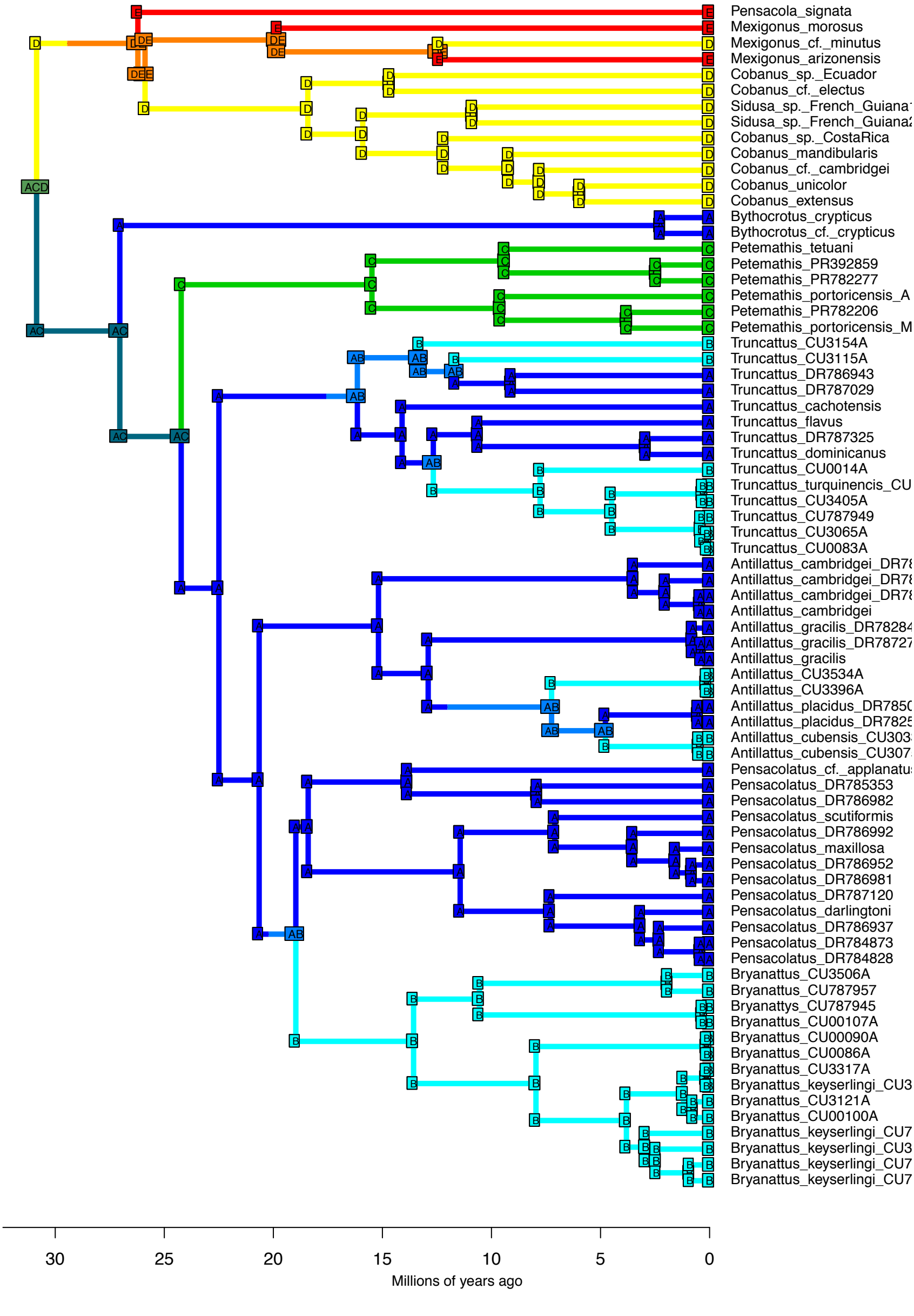

DEC – Stochastic Map #33/50
ancstates: global optim, 5 areas max. d=0.0017; e=0; j=0; LnL=–50.93

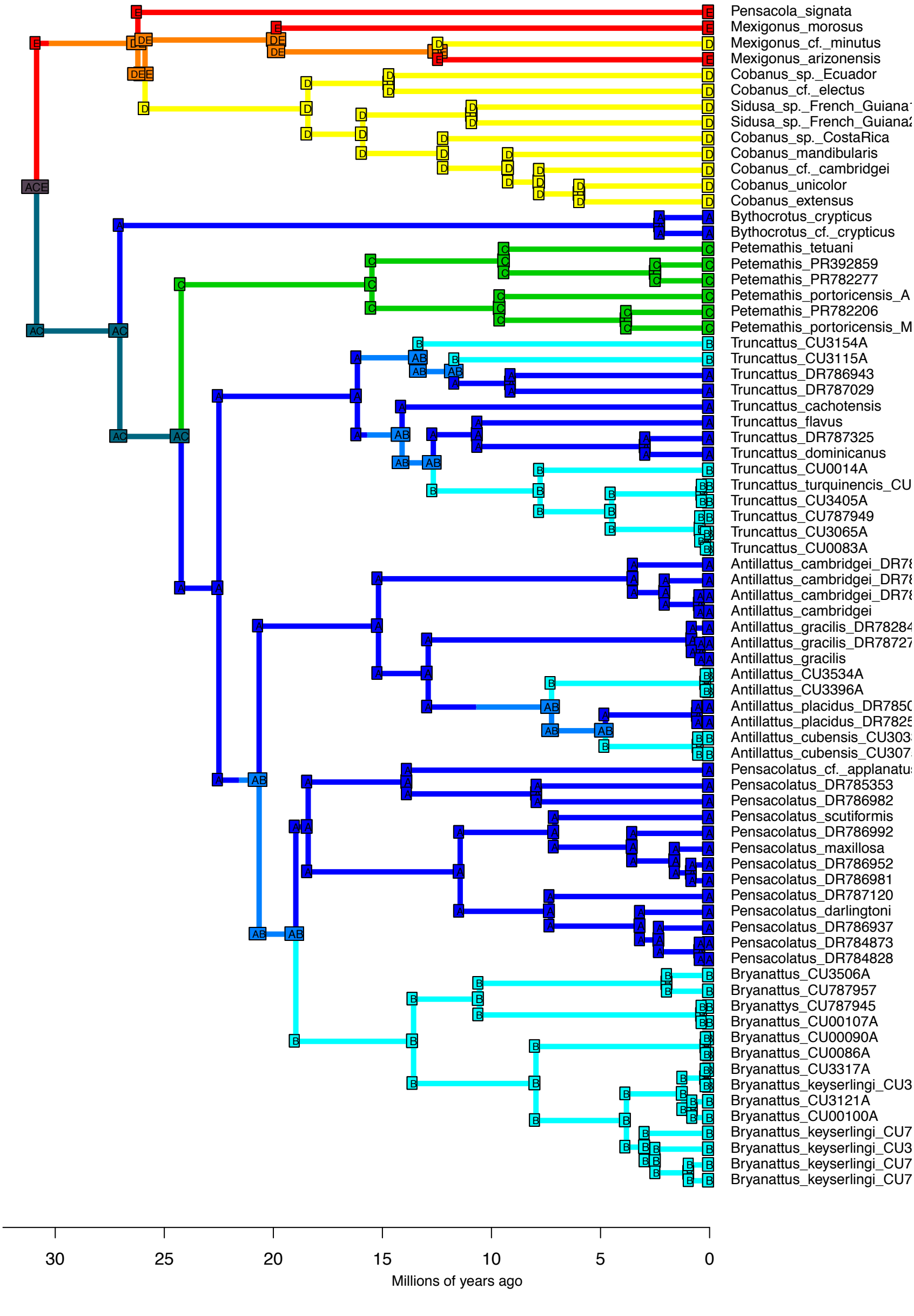

DEC – Stochastic Map #34/50
ancstates: global optim, 5 areas max. d=0.0017; e=0; j=0; LnL=–50.93

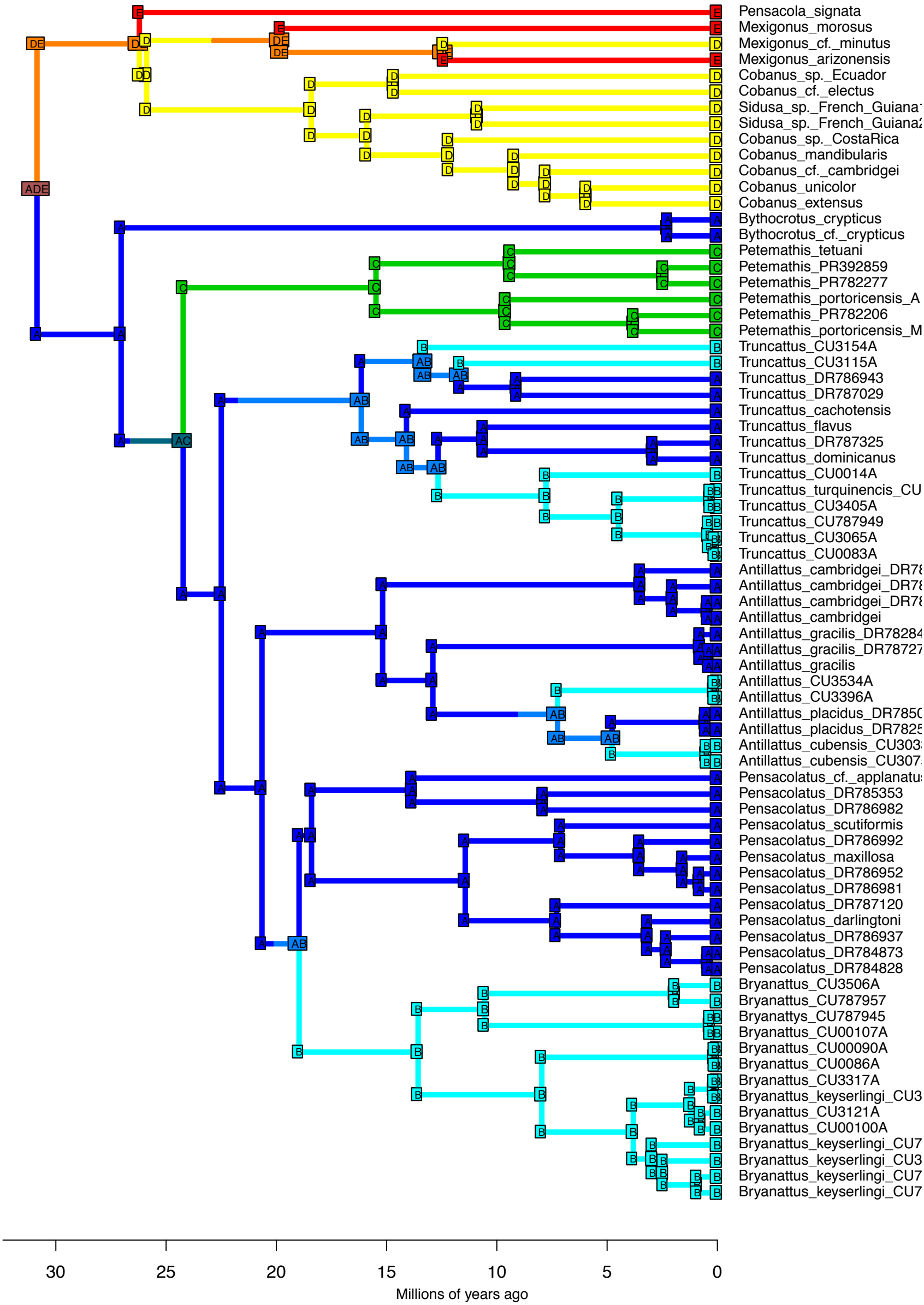

DEC – Stochastic Map #35/50
ancstates: global optim, 5 areas max. d=0.0017; e=0; j=0; LnL=–50.93

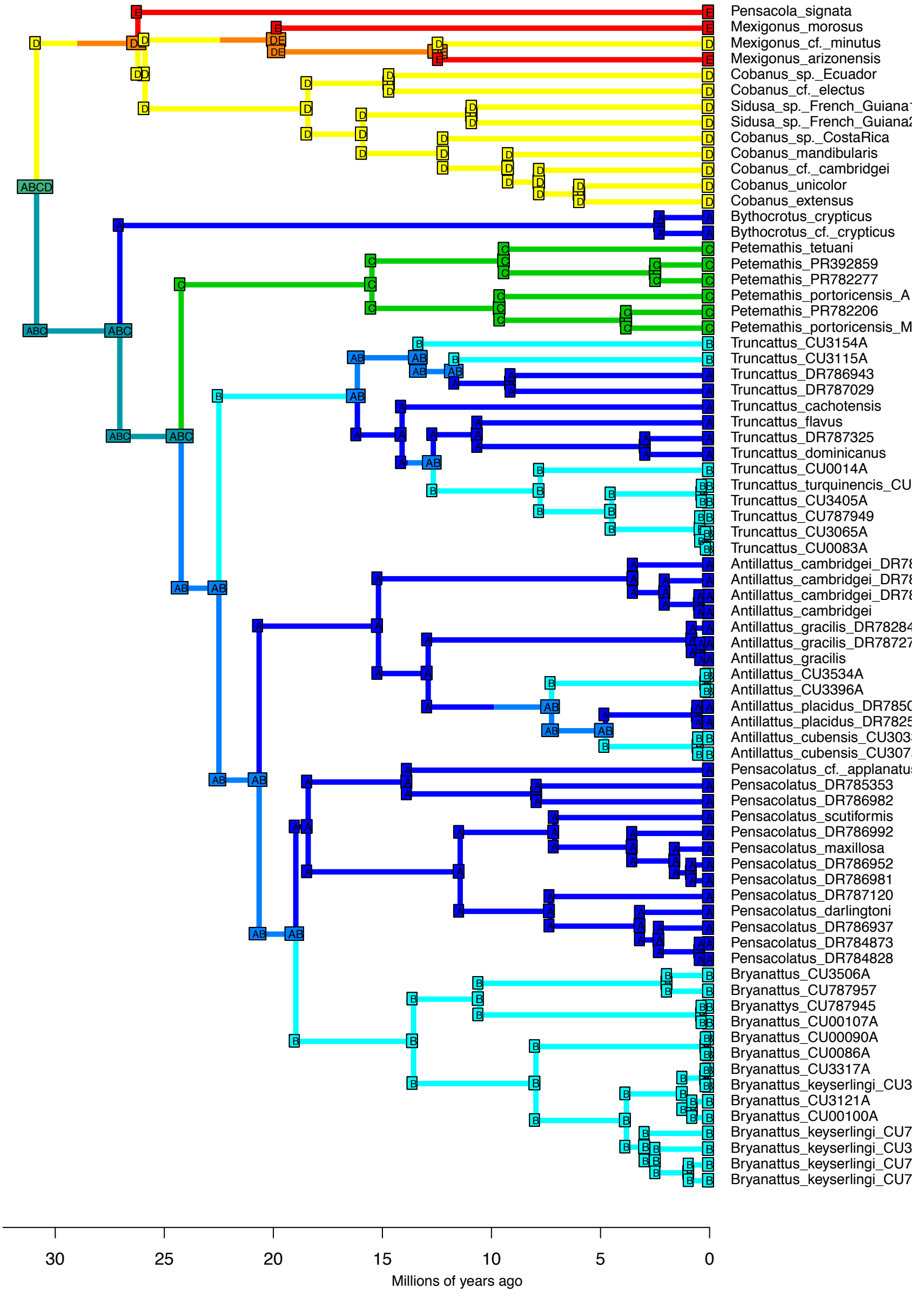

DEC – Stochastic Map #36/50
ancstates: global optim, 5 areas max. d=0.0017; e=0; j=0; LnL=–50.93

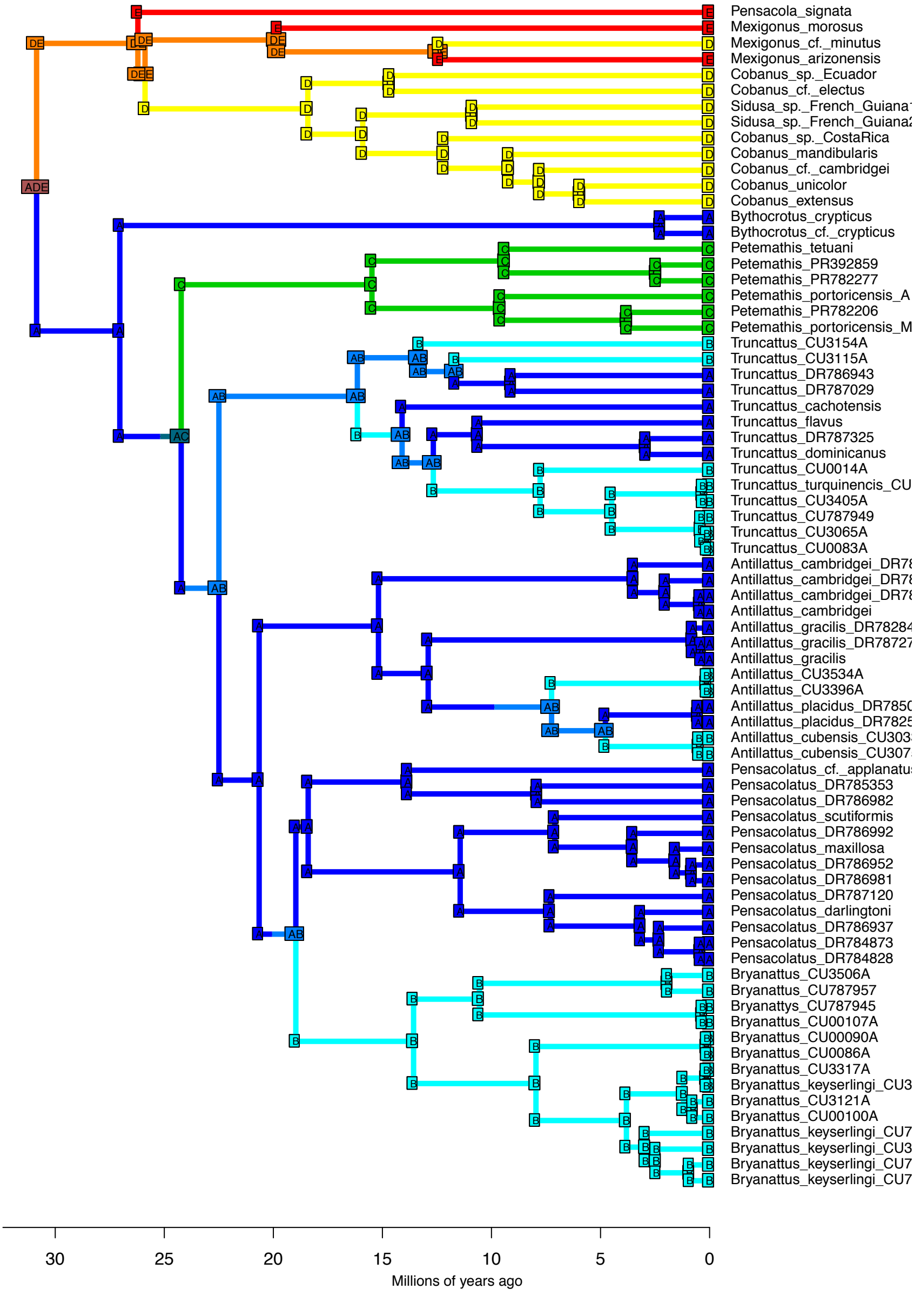

DEC – Stochastic Map #37/50
ancstates: global optim, 5 areas max. d=0.0017; e=0; j=0; LnL=–50.93

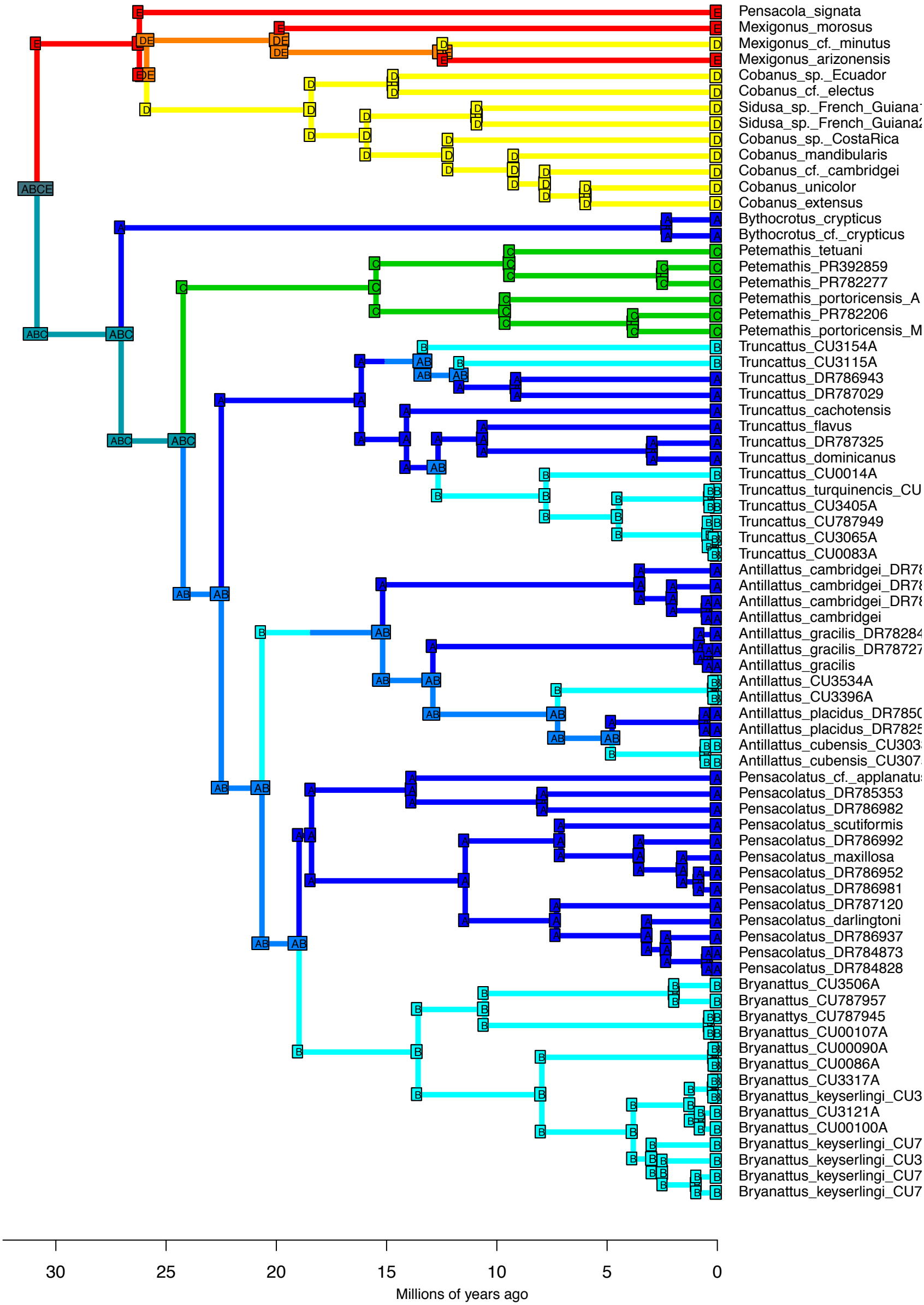

DEC – Stochastic Map #38/50
ancstates: global optim, 5 areas max. d=0.0017; e=0; j=0; LnL=–50.93

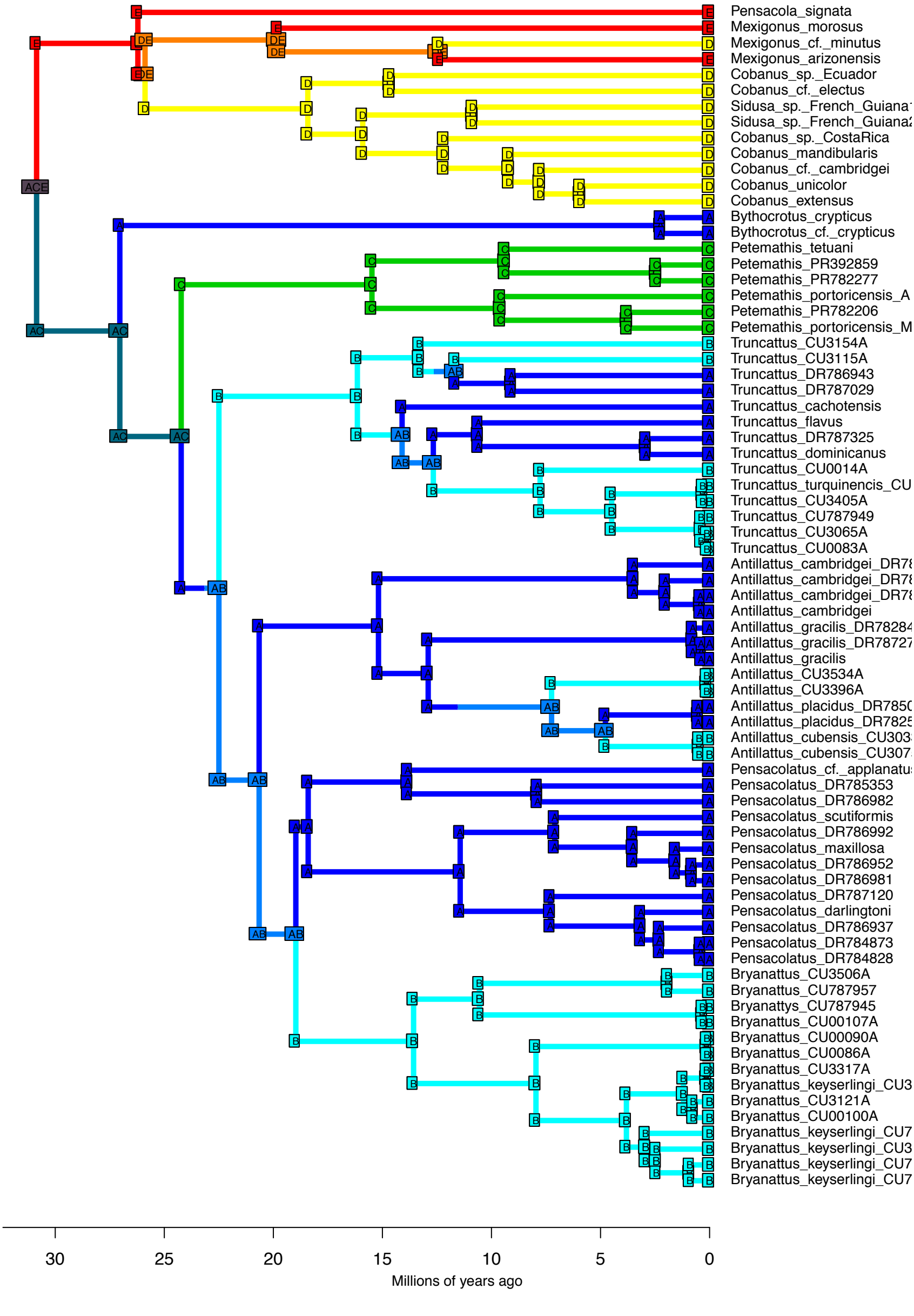

DEC – Stochastic Map #39/50
ancstates: global optim, 5 areas max. d=0.0017; e=0; j=0; LnL=–50.93

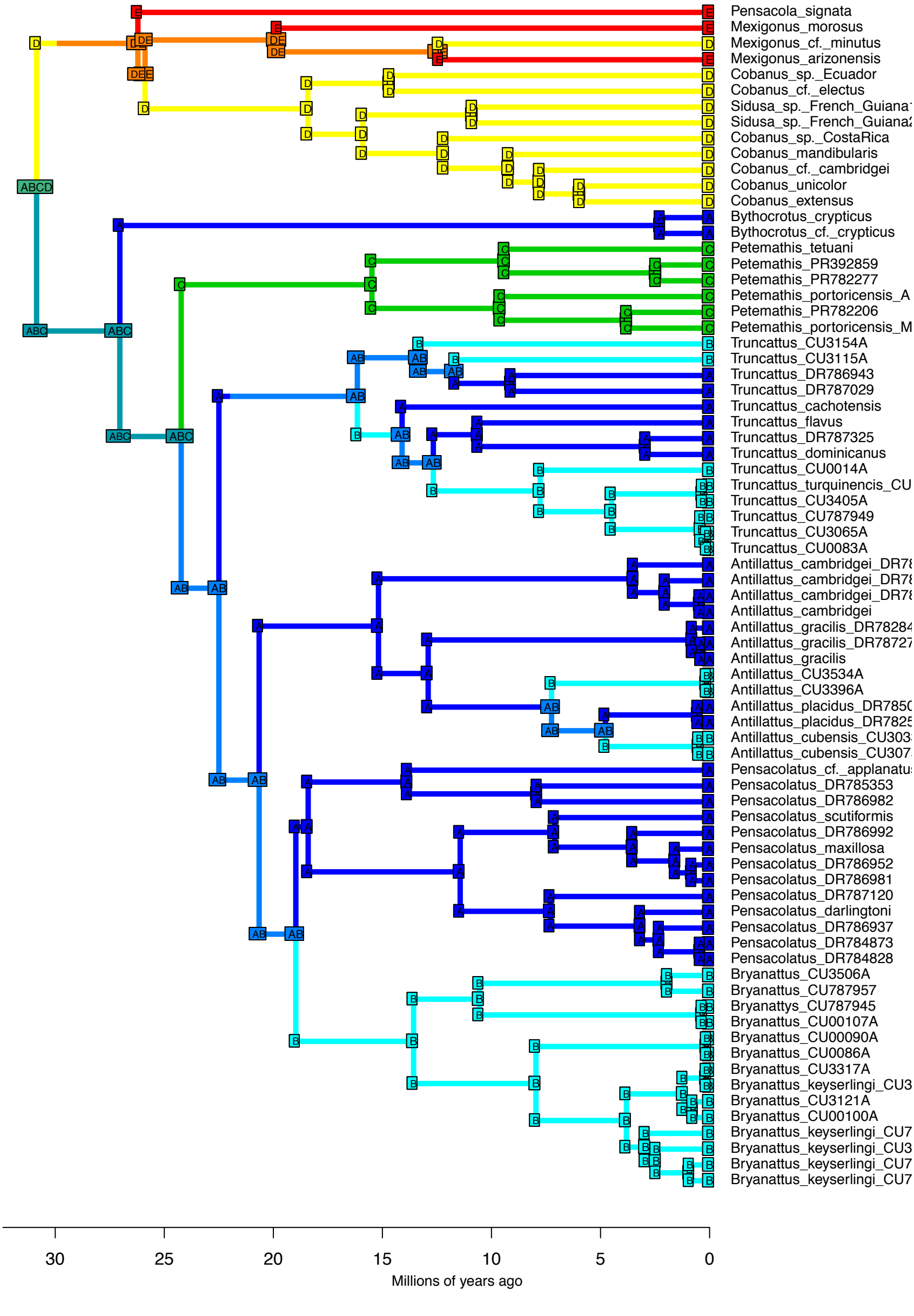

DEC – Stochastic Map #40/50
ancstates: global optim, 5 areas max. d=0.0017; e=0; j=0; LnL=–50.93

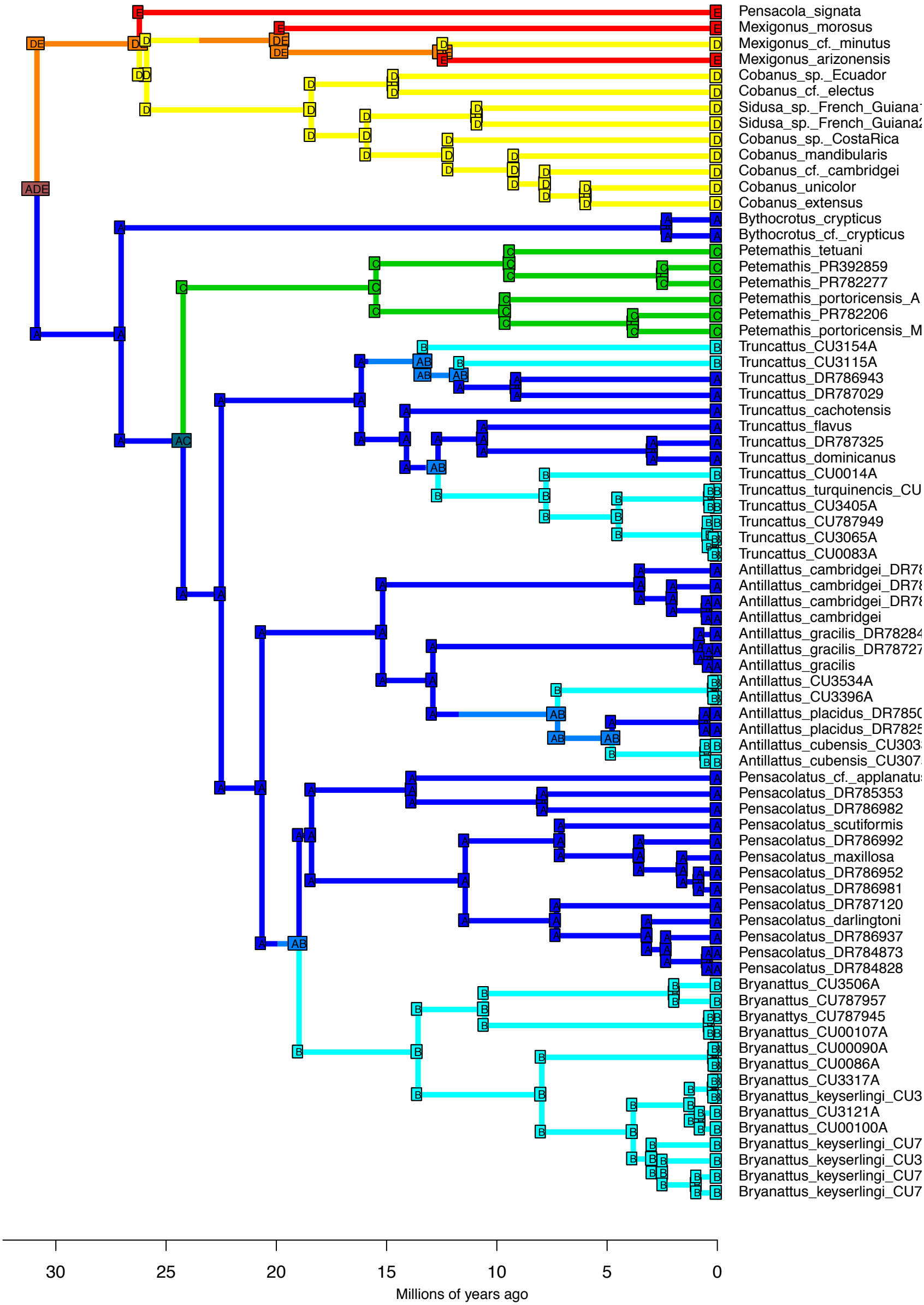

DEC – Stochastic Map #41/50
ancstates: global optim, 5 areas max. d=0.0017; e=0; j=0; LnL=–50.93

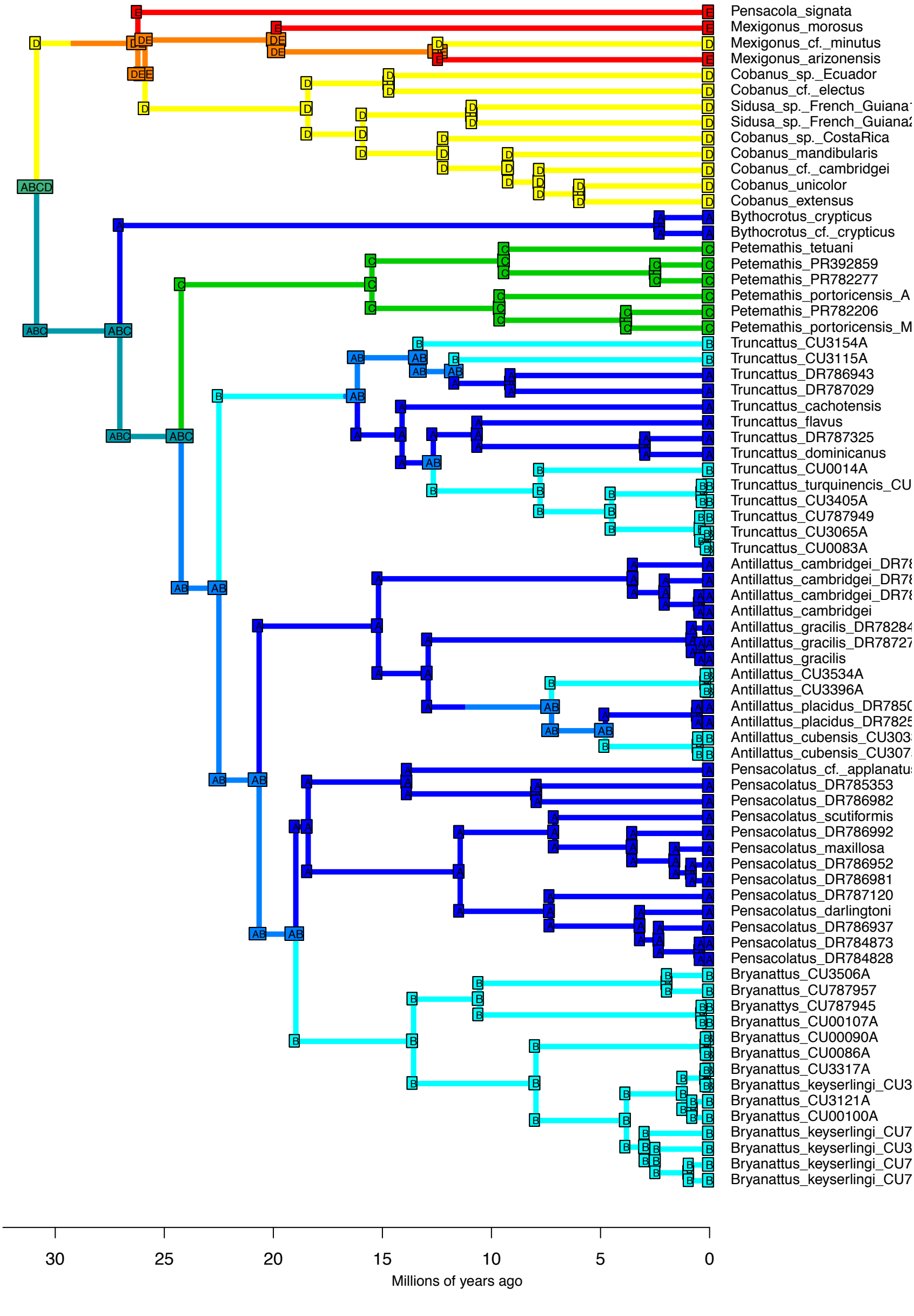

DEC – Stochastic Map #42/50
ancstates: global optim, 5 areas max. d=0.0017; e=0; j=0; LnL=–50.93

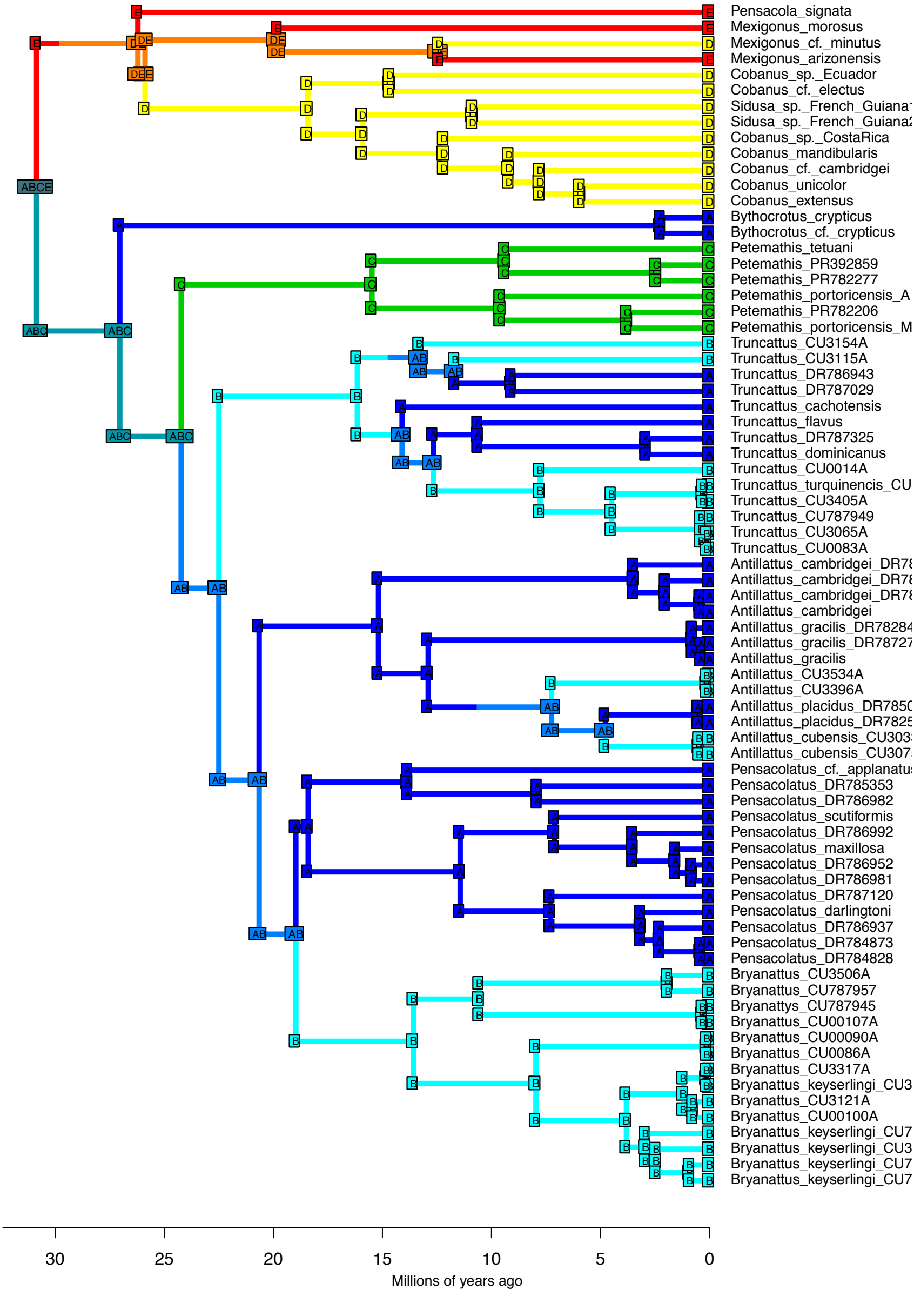

DEC – Stochastic Map #43/50
ancstates: global optim, 5 areas max. d=0.0017; e=0; j=0; LnL=−50.93

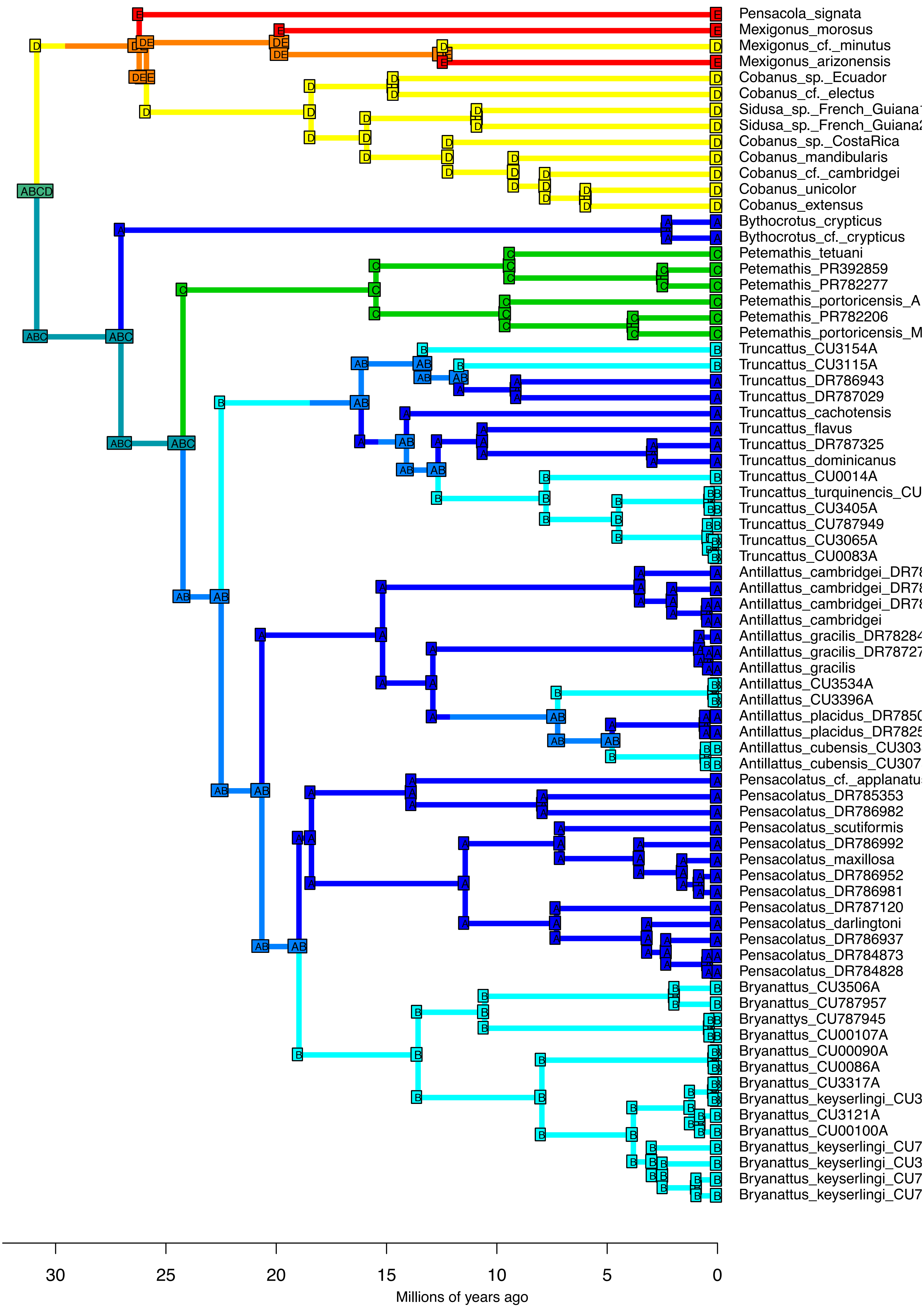

DEC – Stochastic Map #44/50
ancstates: global optim, 5 areas max. d=0.0017; e=0; j=0; LnL=–50.93

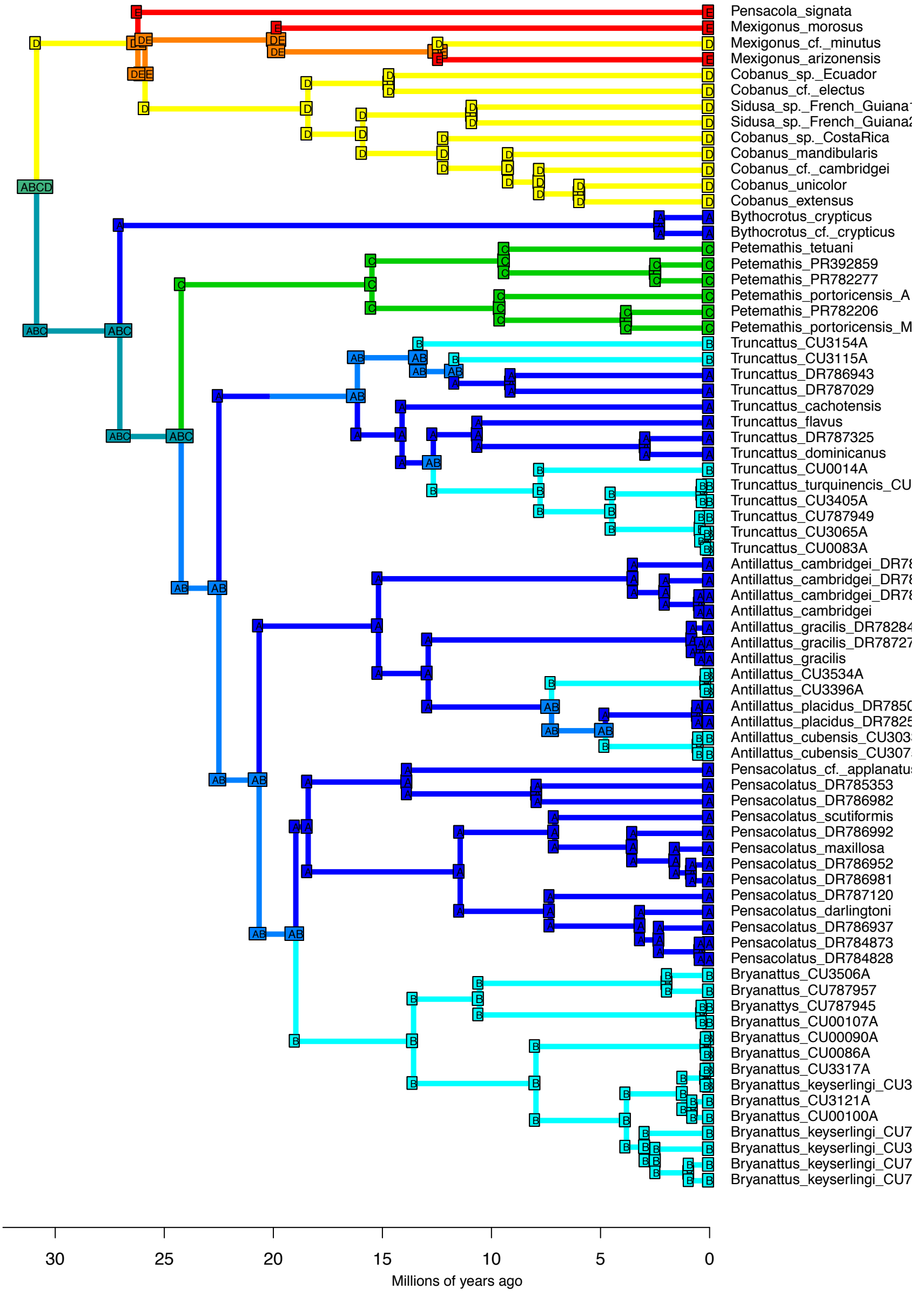

DEC – Stochastic Map #45/50
ancstates: global optim, 5 areas max. d=0.0017; e=0; j=0; LnL=–50.93

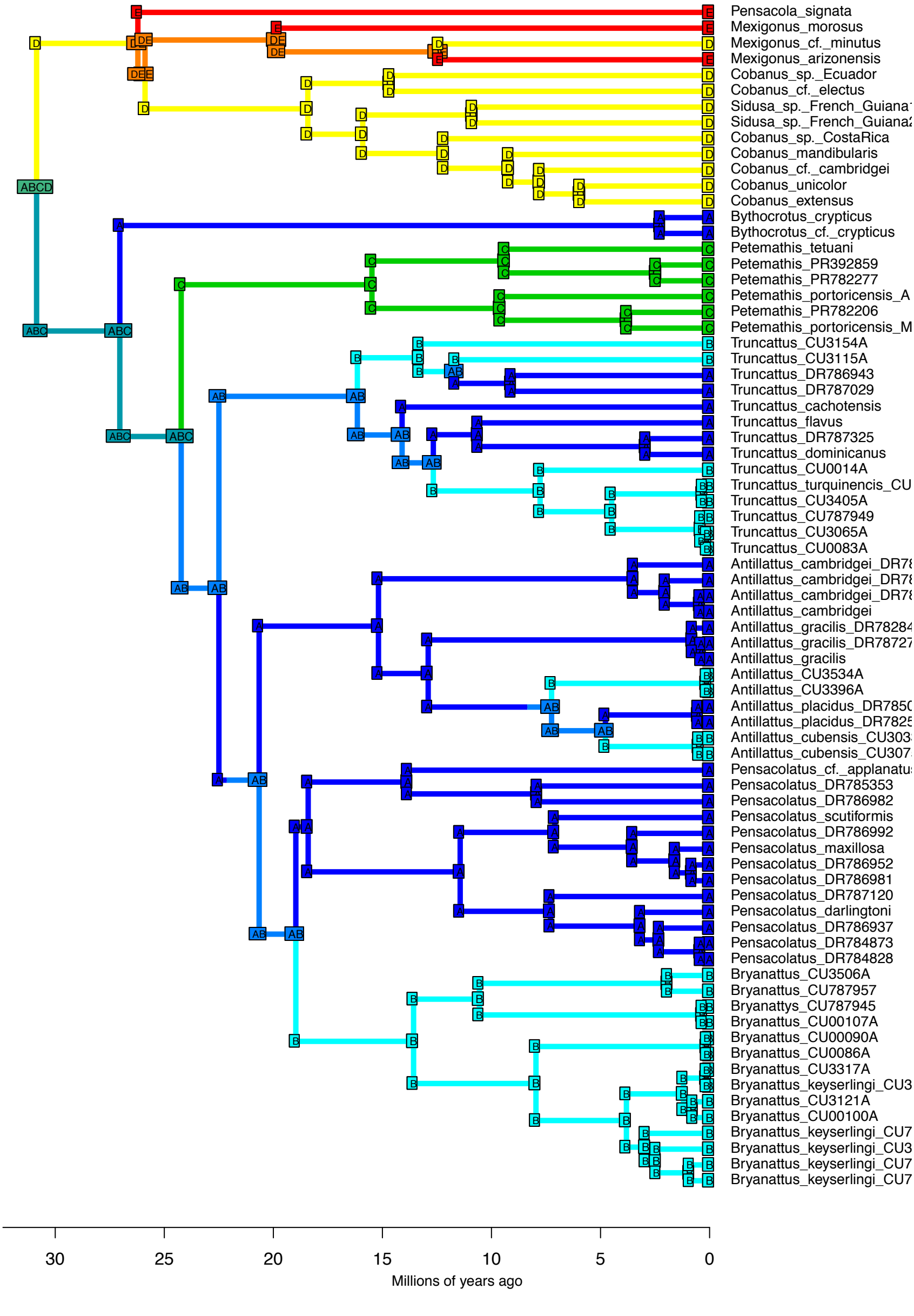

DEC – Stochastic Map #46/50
ancstates: global optim, 5 areas max. d=0.0017; e=0; j=0; LnL=–50.93

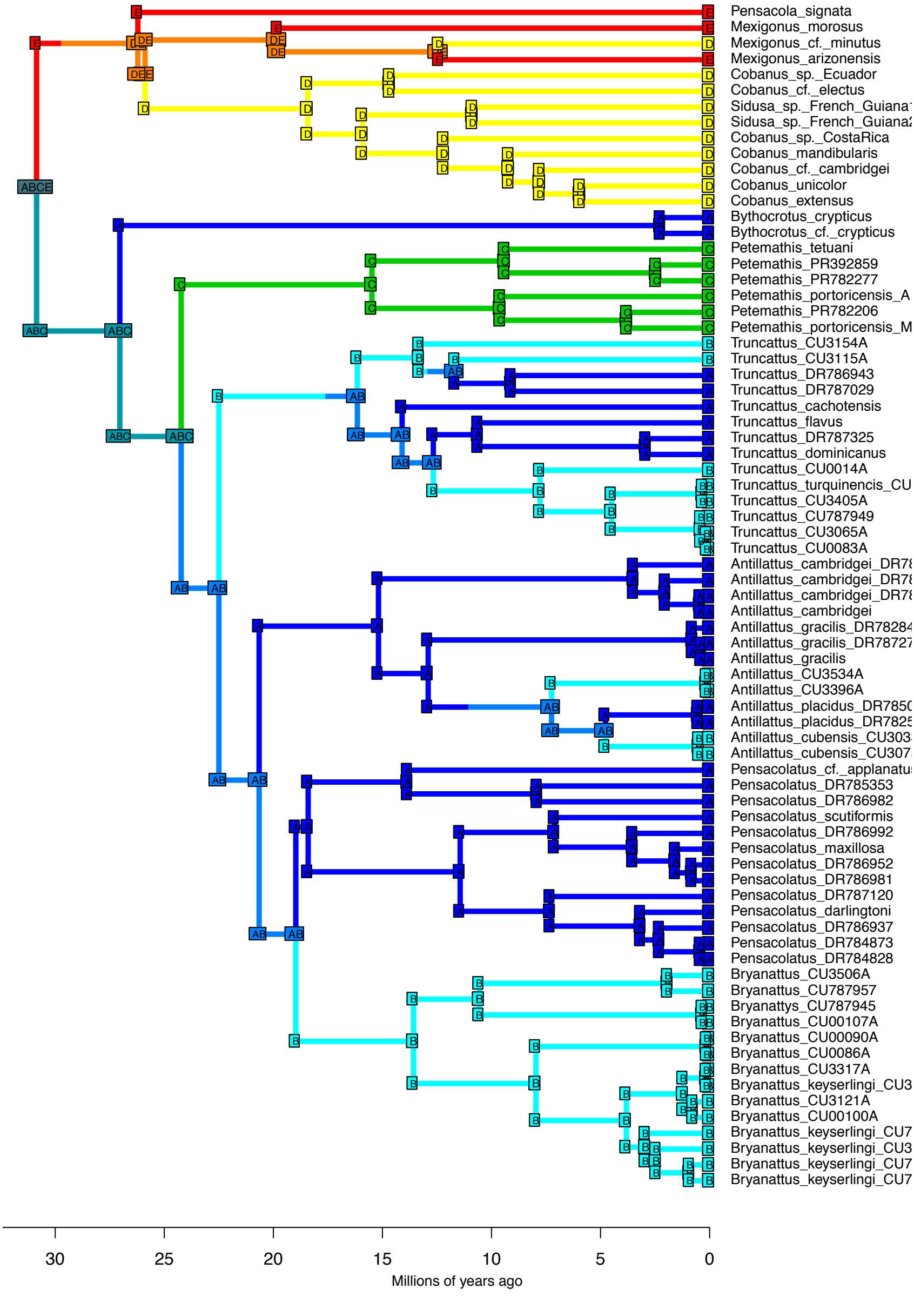

DEC – Stochastic Map #47/50
ancstates: global optim, 5 areas max. d=0.0017; e=0; j=0; LnL=–50.93

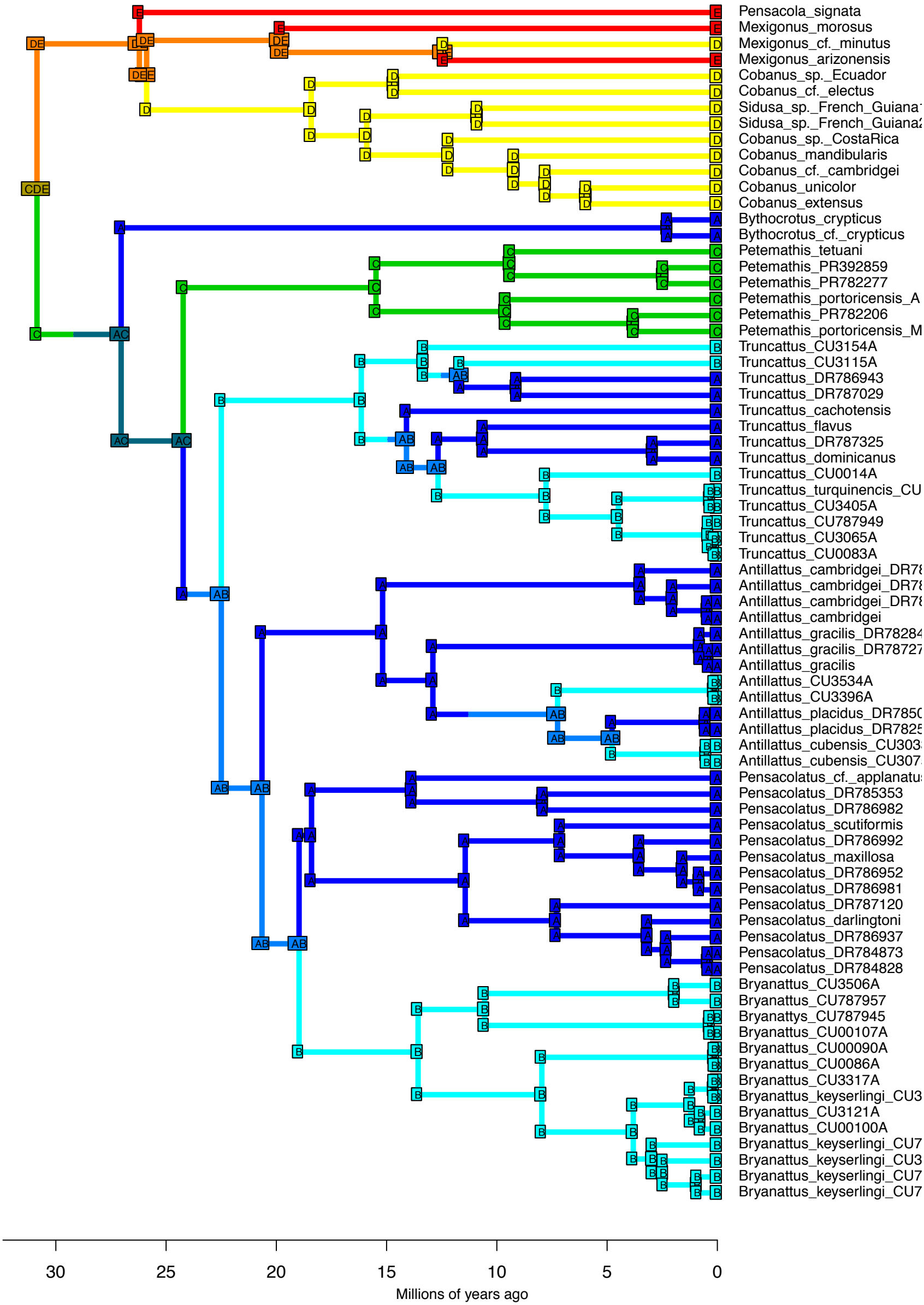

DEC – Stochastic Map #48/50
ancstates: global optim, 5 areas max. d=0.0017; e=0; j=0; LnL=–50.93

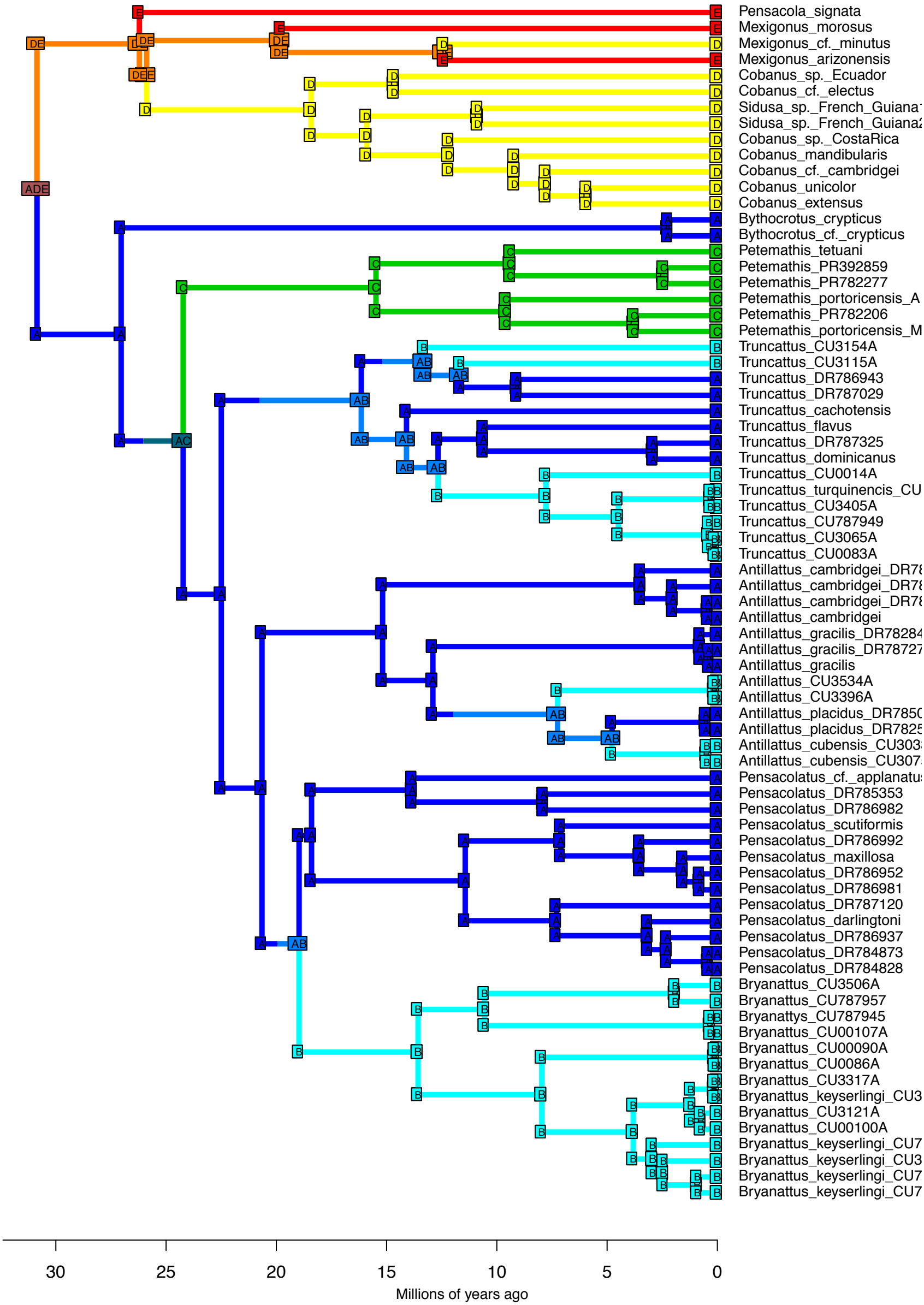

DEC – Stochastic Map #49/50
ancstates: global optim, 5 areas max. d=0.0017; e=0; j=0; LnL=–50.93

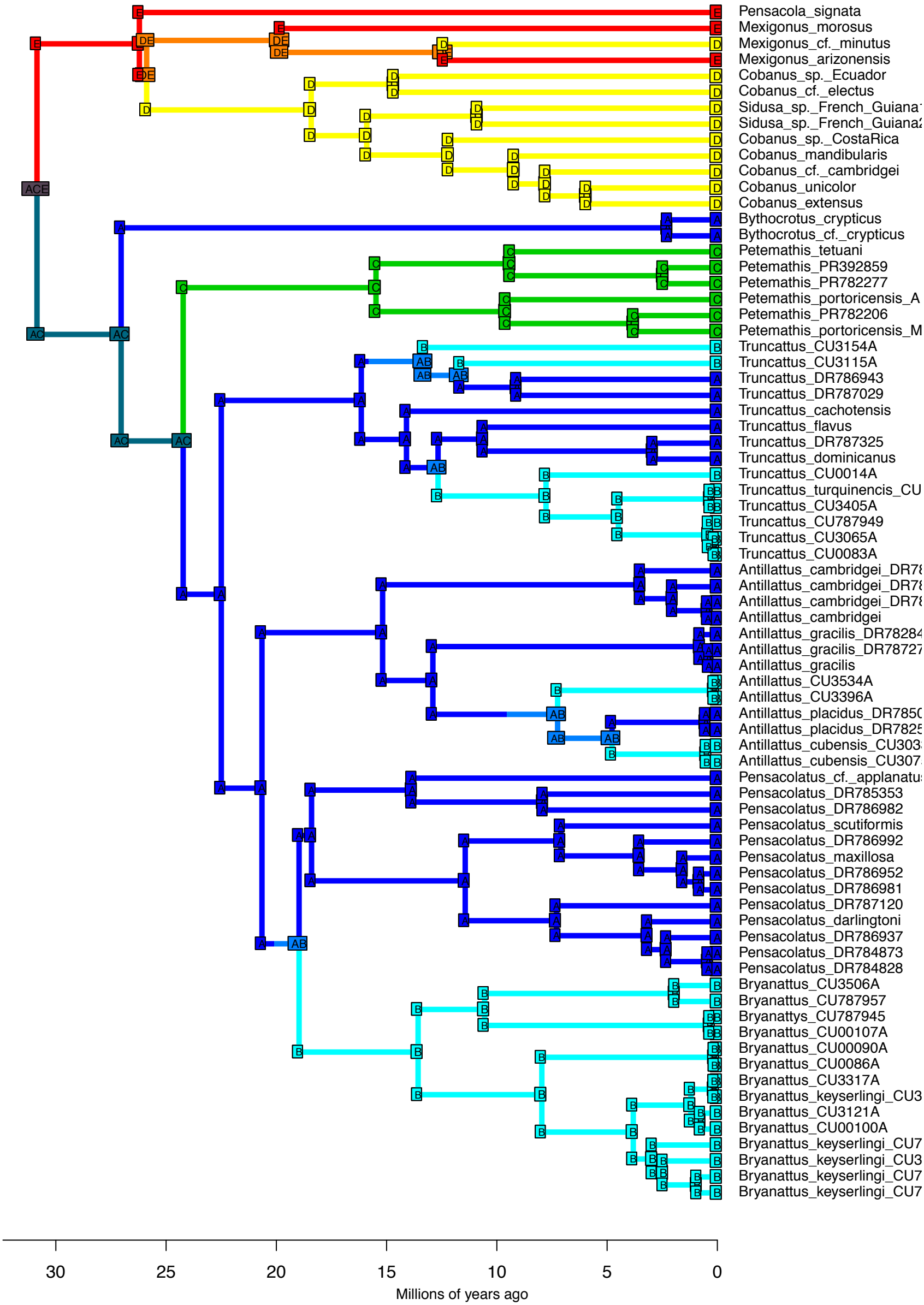

DEC – Stochastic Map #50/50
ancstates: global optim, 5 areas max. d=0.0017; e=0; j=0; LnL=–50.93

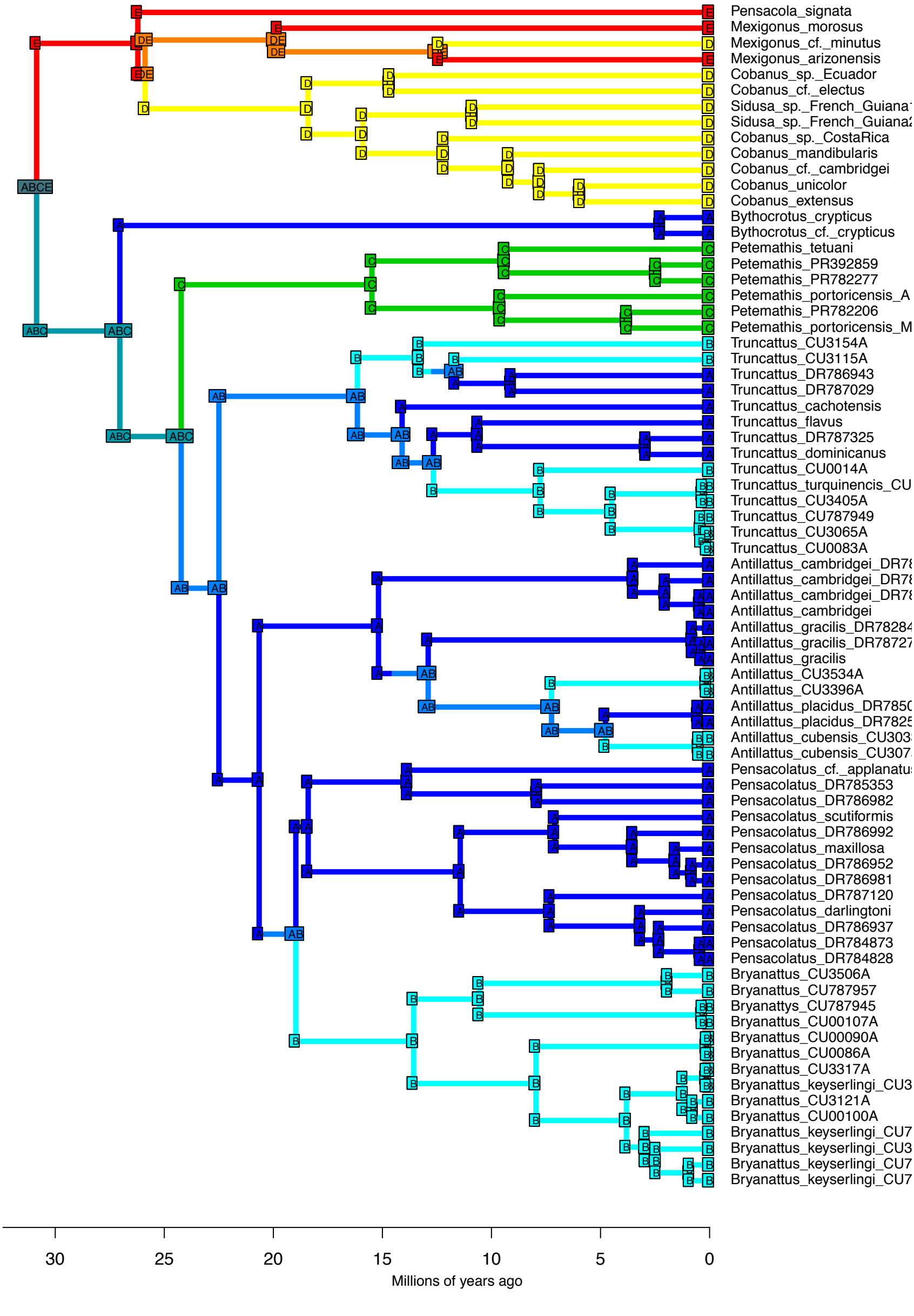

DEC_M3b_strat – Stochastic Map #1/50
ancstates: global optim, 5 areas max. d=0.0017; e=0; j=0; LnL=–50.93

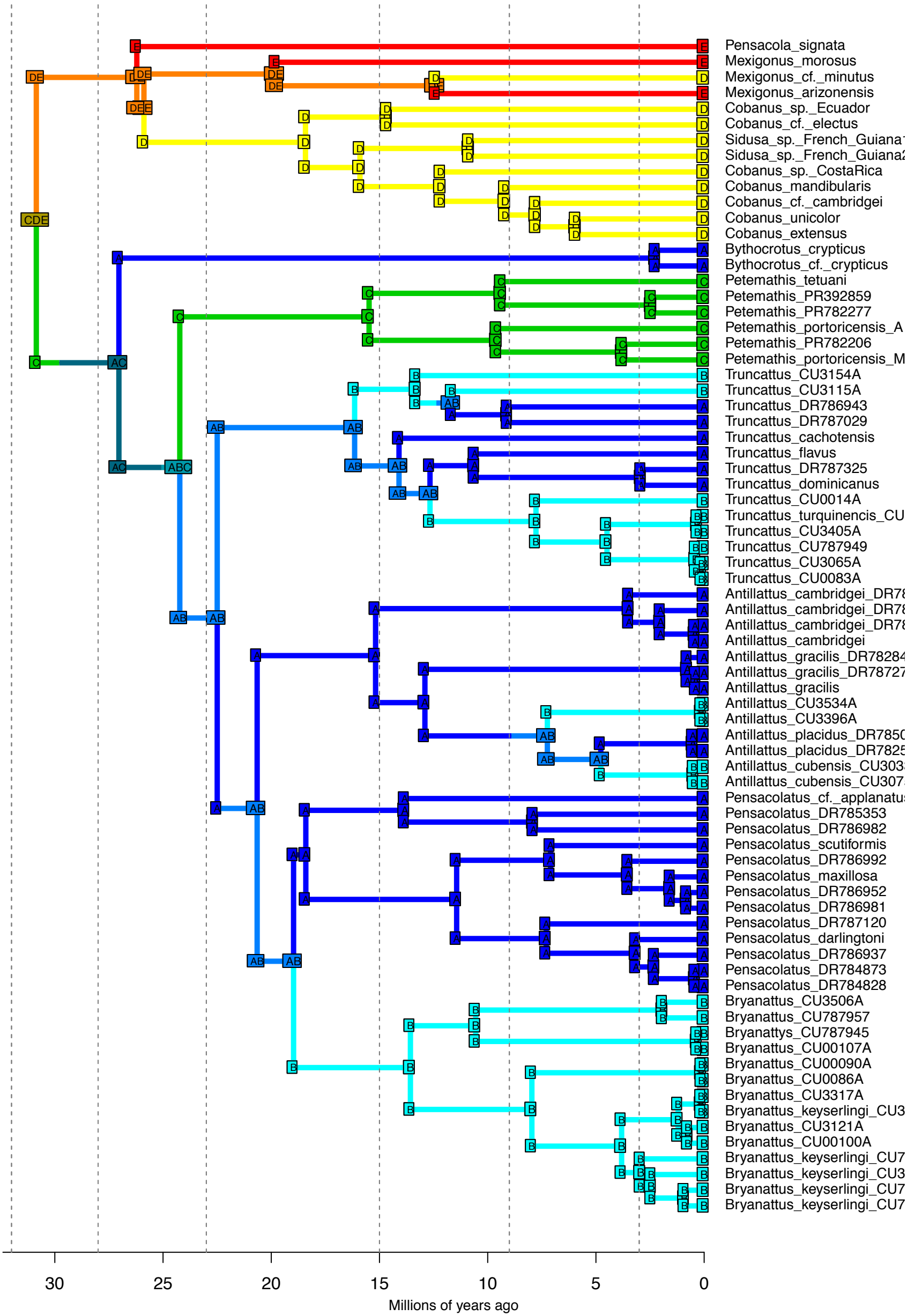

DEC_M3b_strat – Stochastic Map #2/50
ancstates: global optim, 5 areas max. d=0.0017; e=0; j=0; LnL=–50.93

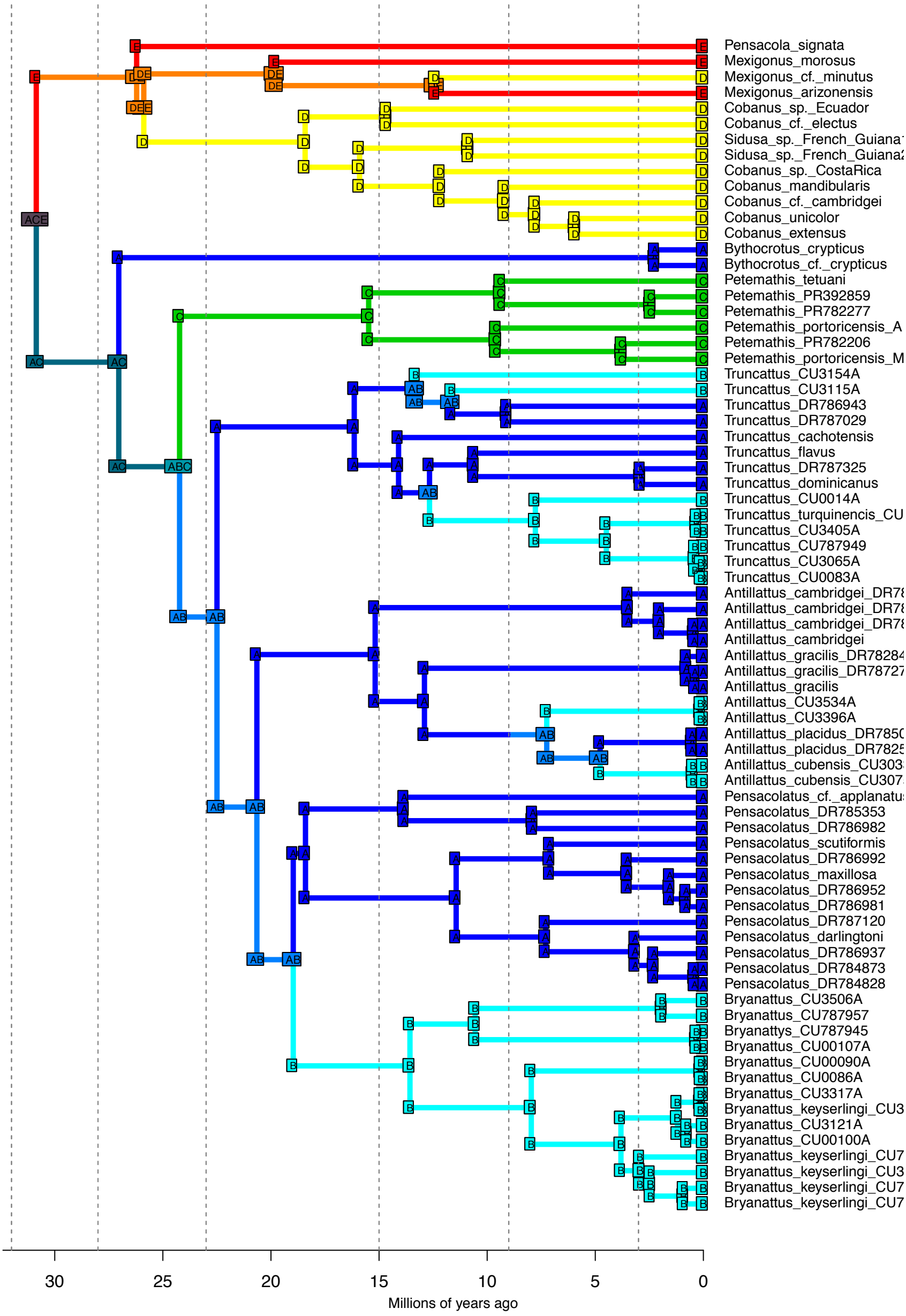

DEC_M3b_strat – Stochastic Map #3/50
ancstates: global optim, 5 areas max. d=0.0017; e=0; j=0; LnL=–50.93

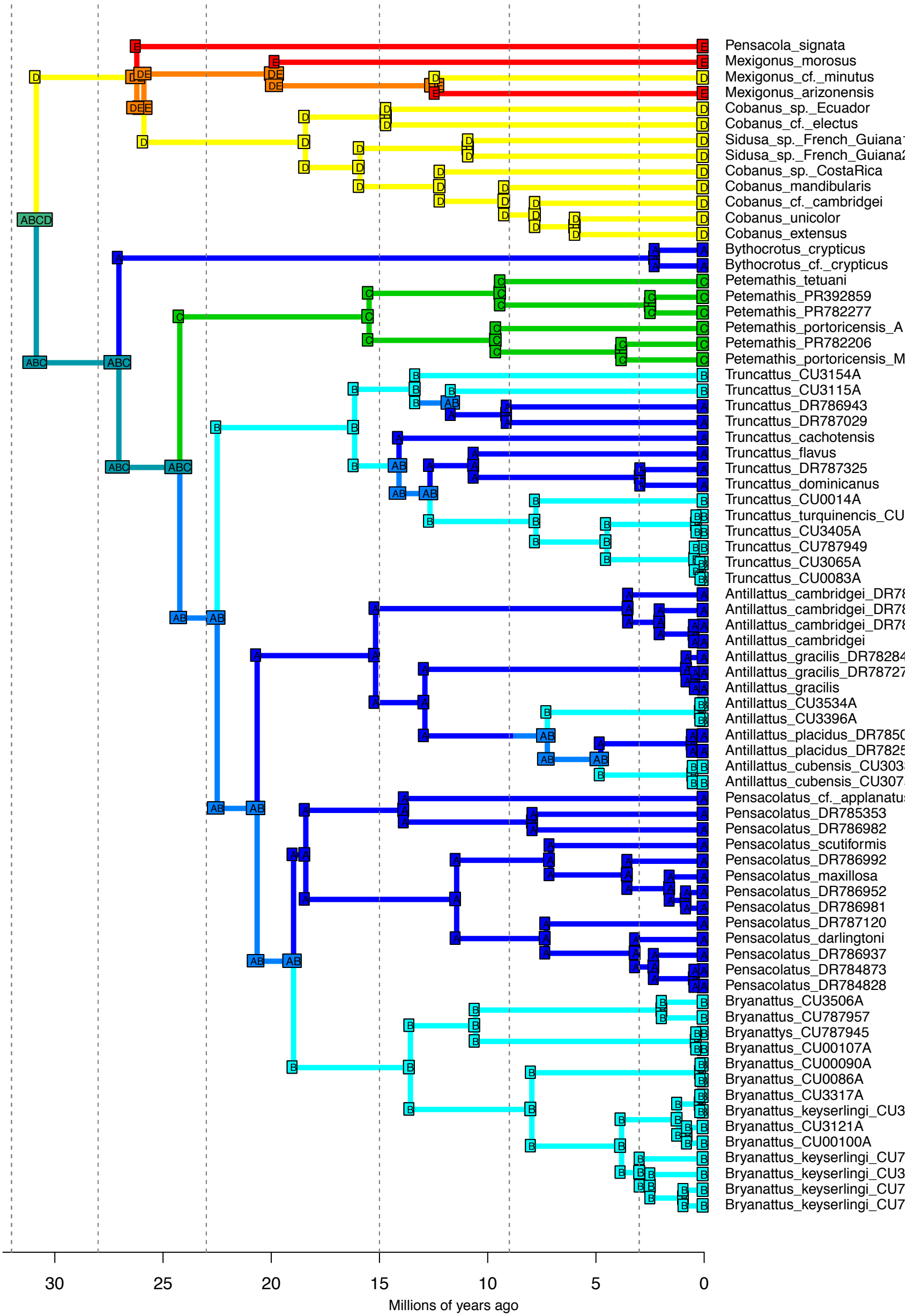

DEC_M3b_strat – Stochastic Map #4/50
ancstates: global optim, 5 areas max. d=0.0017; e=0; j=0; LnL=–50.93

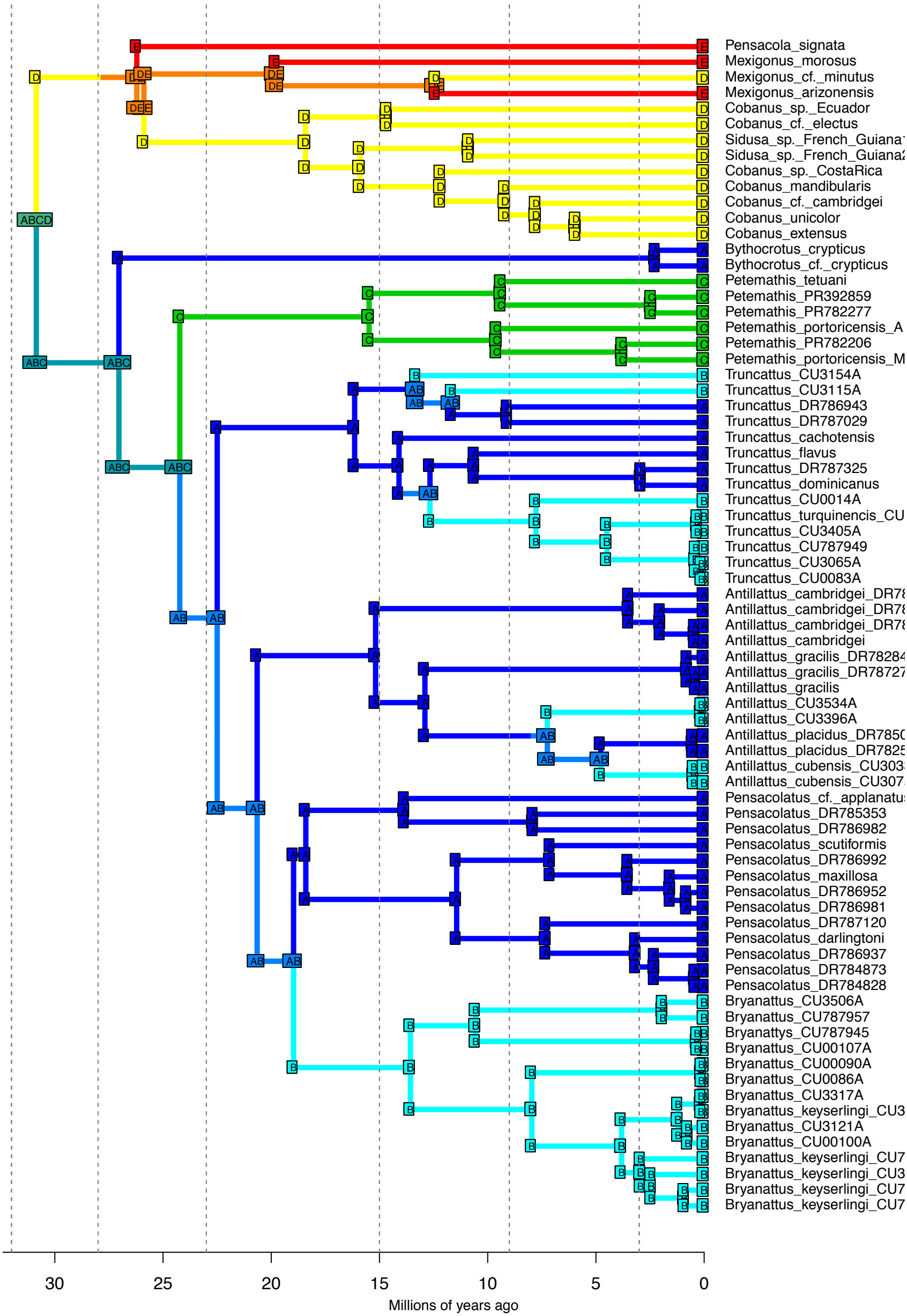

DEC_M3b_strat – Stochastic Map #5/50
ancstates: global optim, 5 areas max. d=0.0017; e=0; j=0; LnL=–50.93

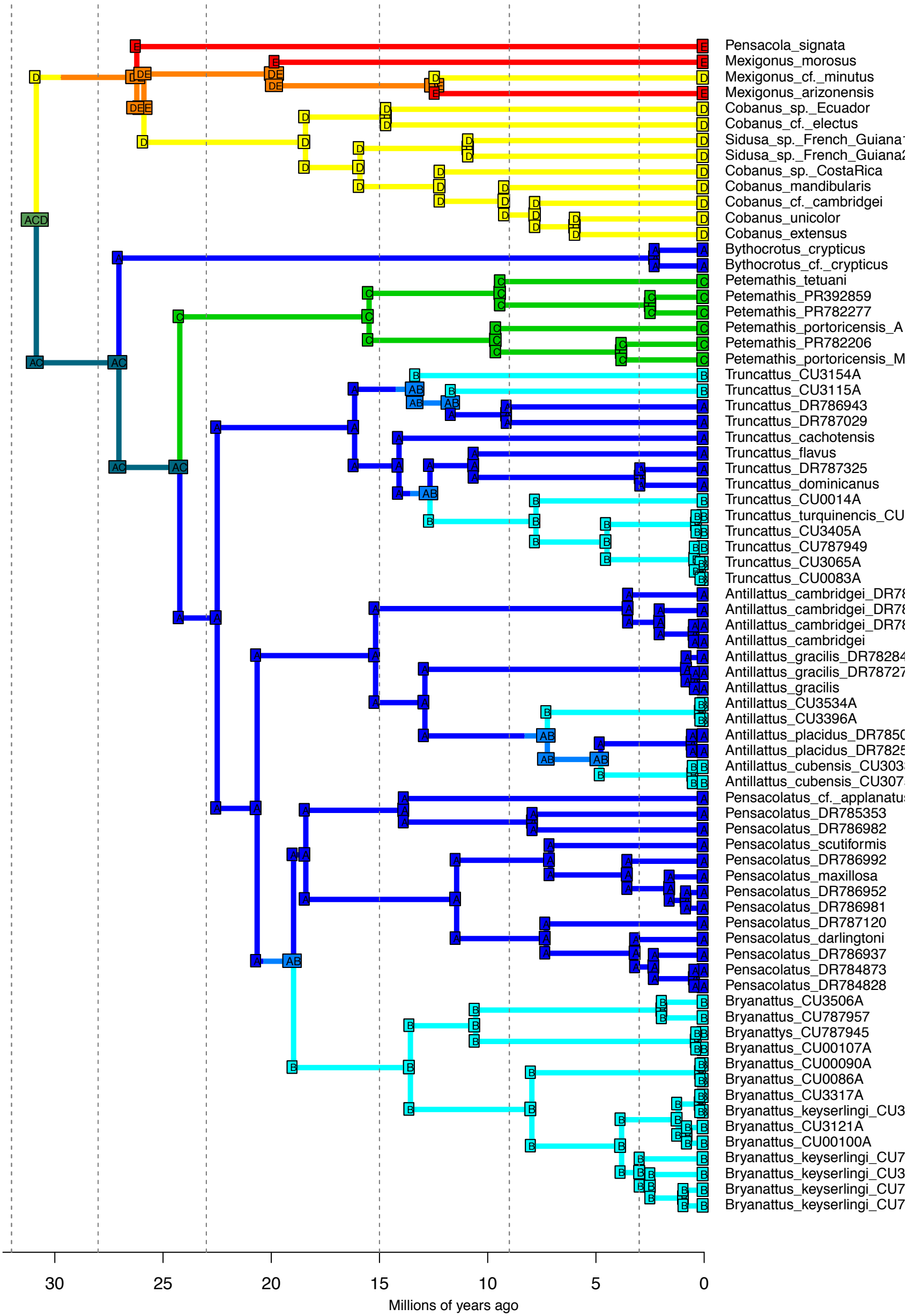

DEC_M3b_strat – Stochastic Map #6/50
ancstates: global optim, 5 areas max. d=0.0017; e=0; j=0; LnL=–50.93

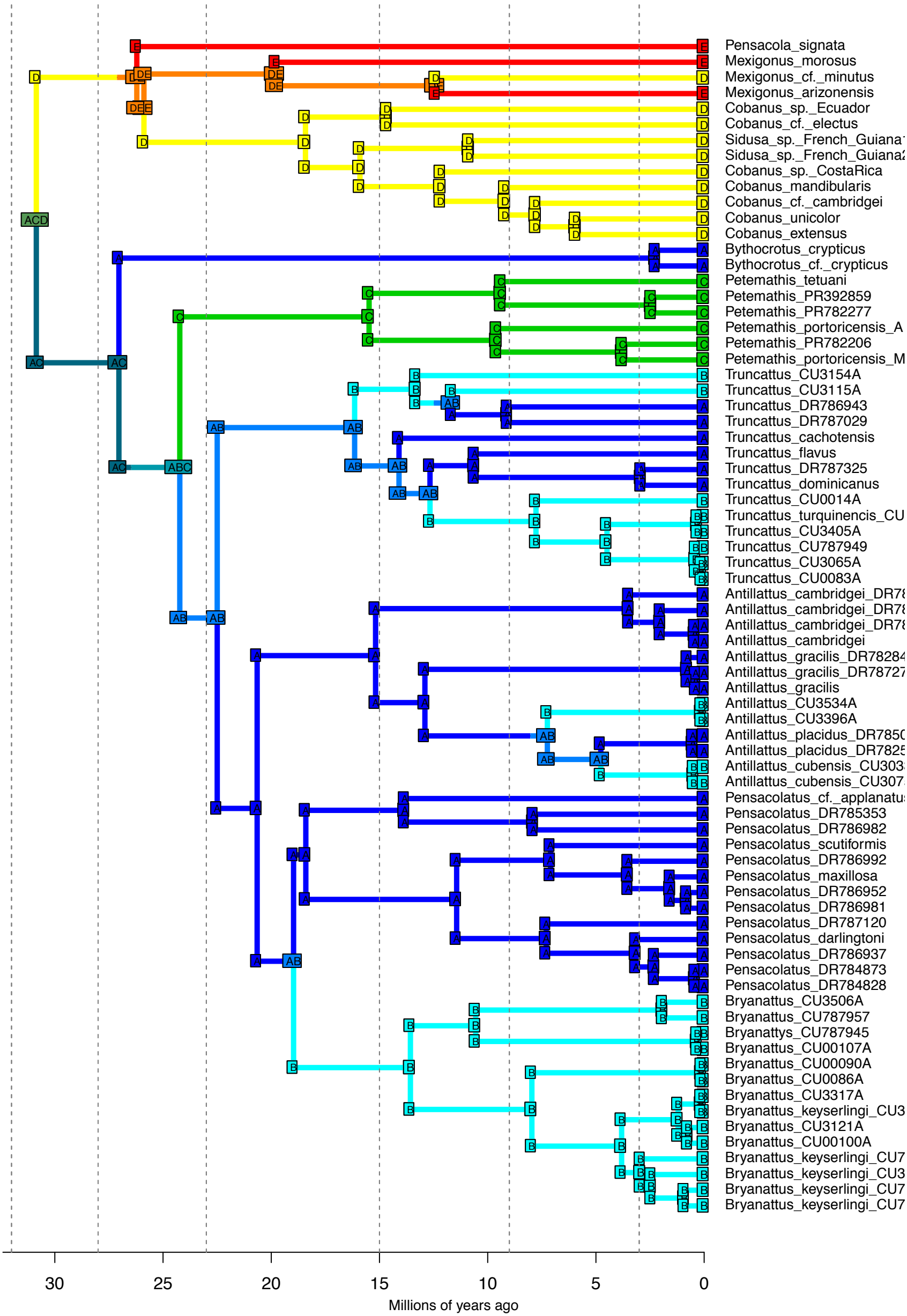

DEC_M3b_strat – Stochastic Map #7/50
ancstates: global optim, 5 areas max. d=0.0017; e=0; j=0; LnL=–50.93

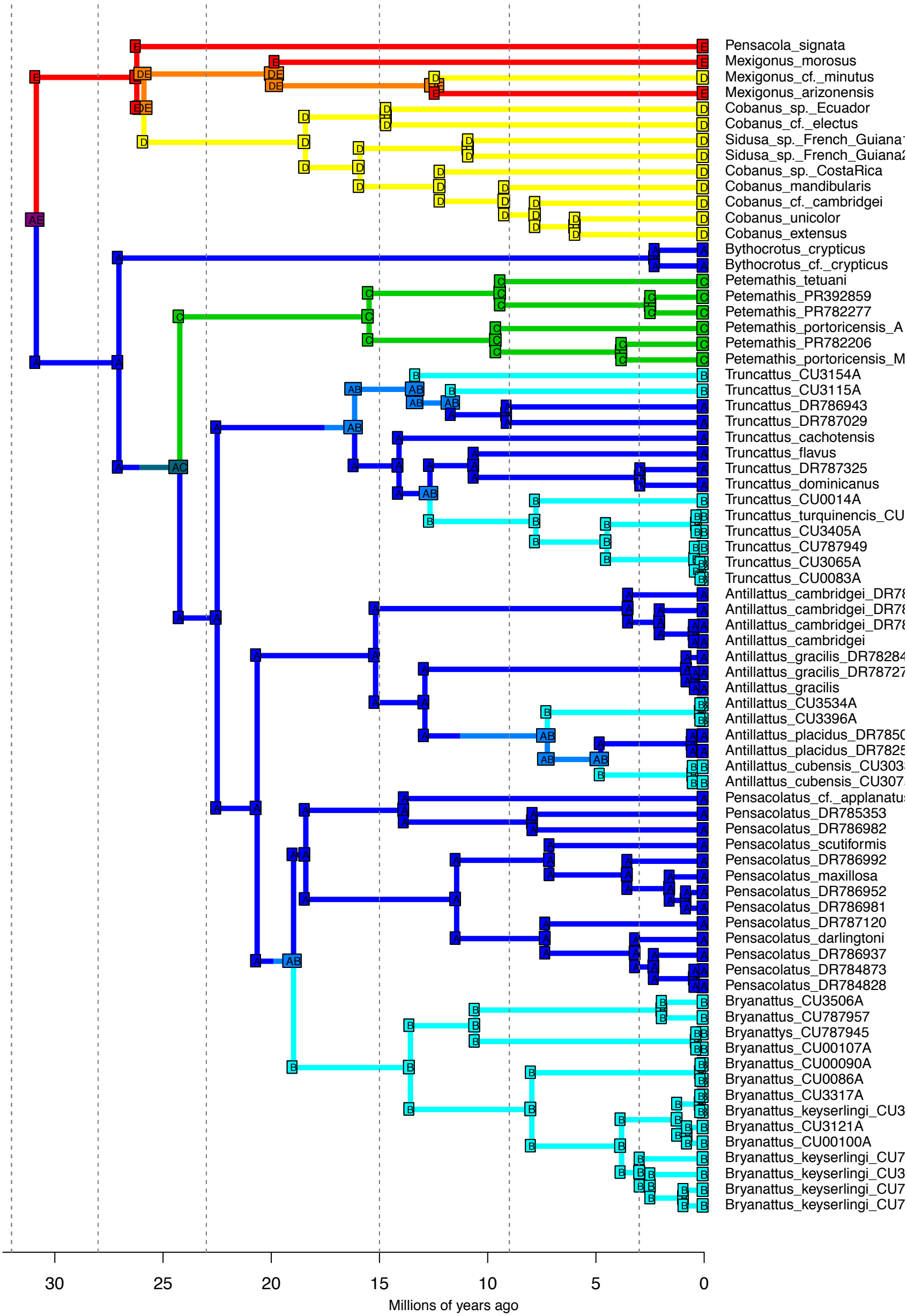

DEC_M3b_strat – Stochastic Map #8/50
ancstates: global optim, 5 areas max. d=0.0017; e=0; j=0; LnL=–50.93

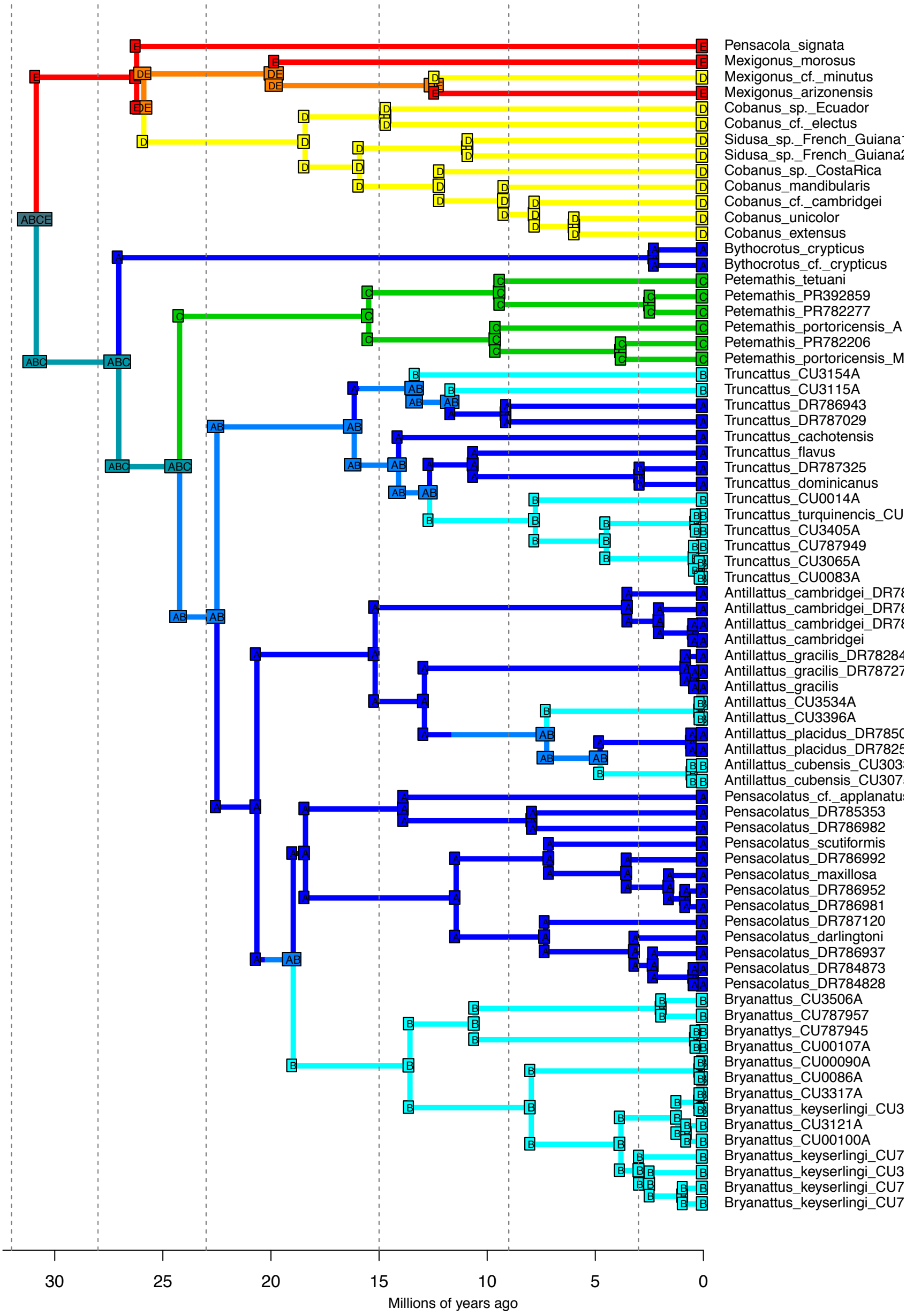

DEC_M3b_strat – Stochastic Map #9/50
ancstates: global optim, 5 areas max. d=0.0017; e=0; j=0; LnL=–50.93

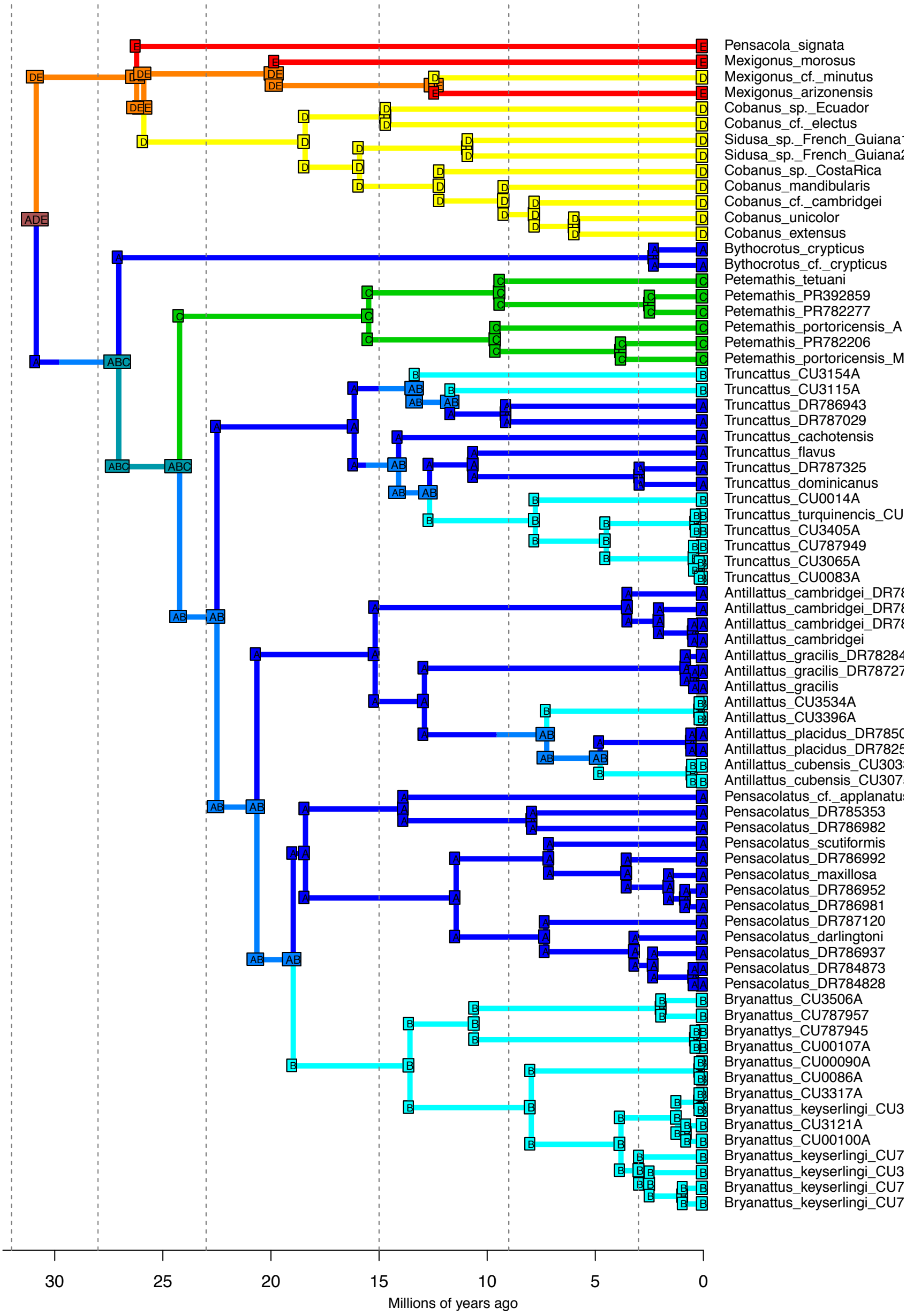

DEC_M3b_strat – Stochastic Map #10/50
ancstates: global optim, 5 areas max. d=0.0017; e=0; j=0; LnL=−50.93

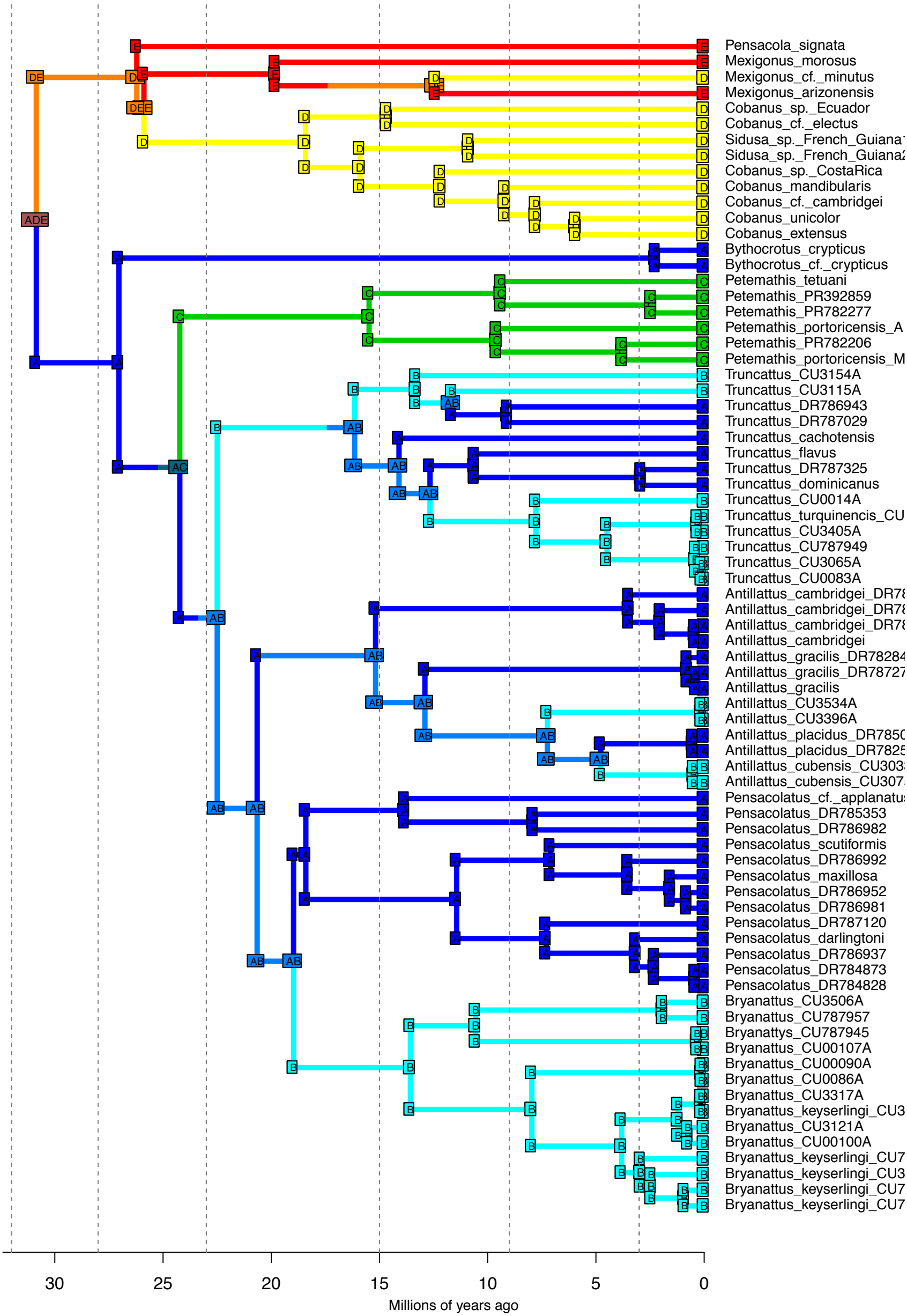

DEC_M3b_strat – Stochastic Map #11/50
ancstates: global optim, 5 areas max. d=0.0017; e=0; j=0; LnL=−50.93

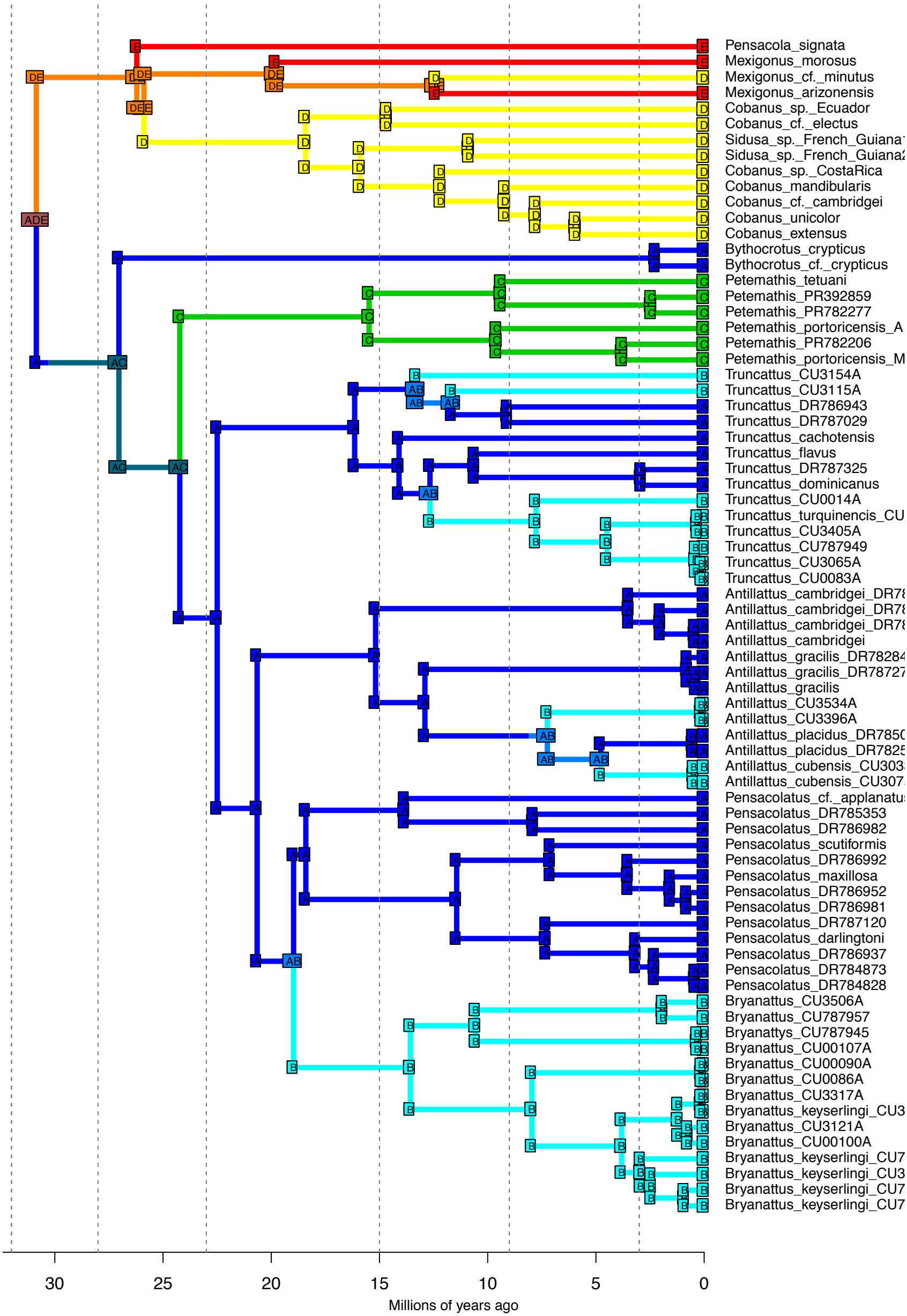

DEC_M3b_strat – Stochastic Map #12/50
ancstates: global optim, 5 areas max. d=0.0017; e=0; j=0; LnL=−50.93

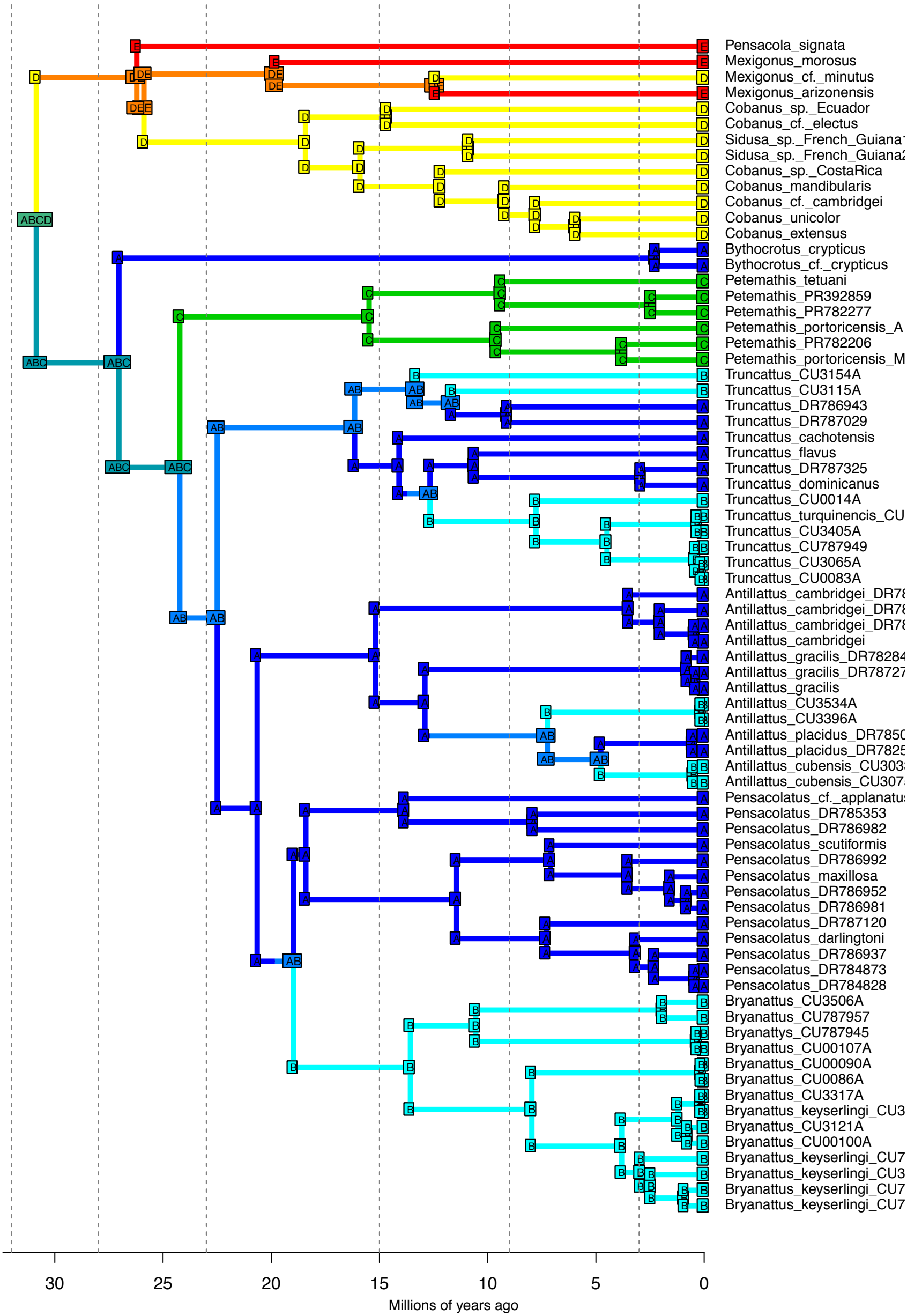

DEC_M3b_strat – Stochastic Map #13/50
ancstates: global optim, 5 areas max. d=0.0017; e=0; j=0; LnL=−50.93

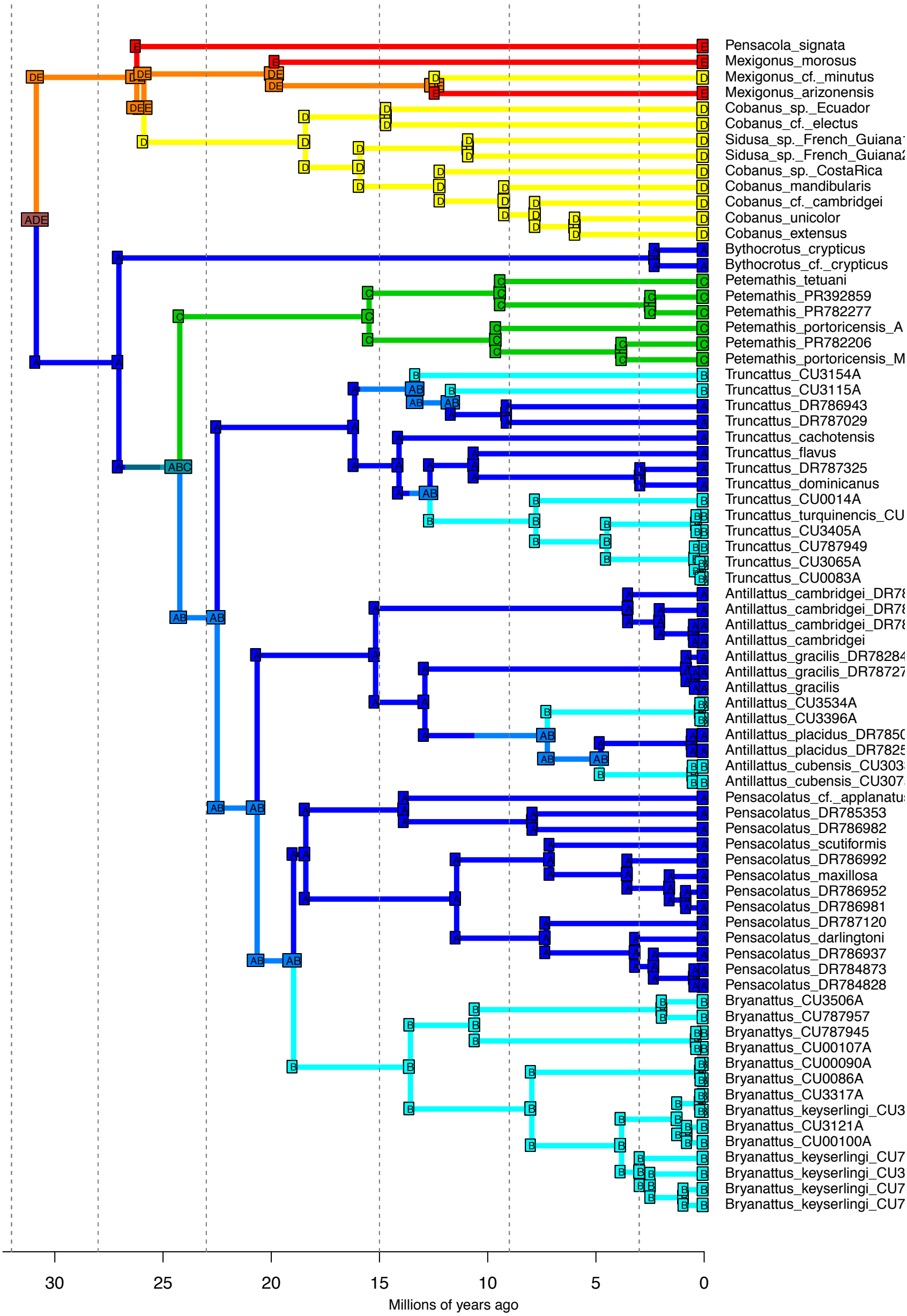

DEC_M3b_strat – Stochastic Map #14/50
ancstates: global optim, 5 areas max. d=0.0017; e=0; j=0; LnL=−50.93

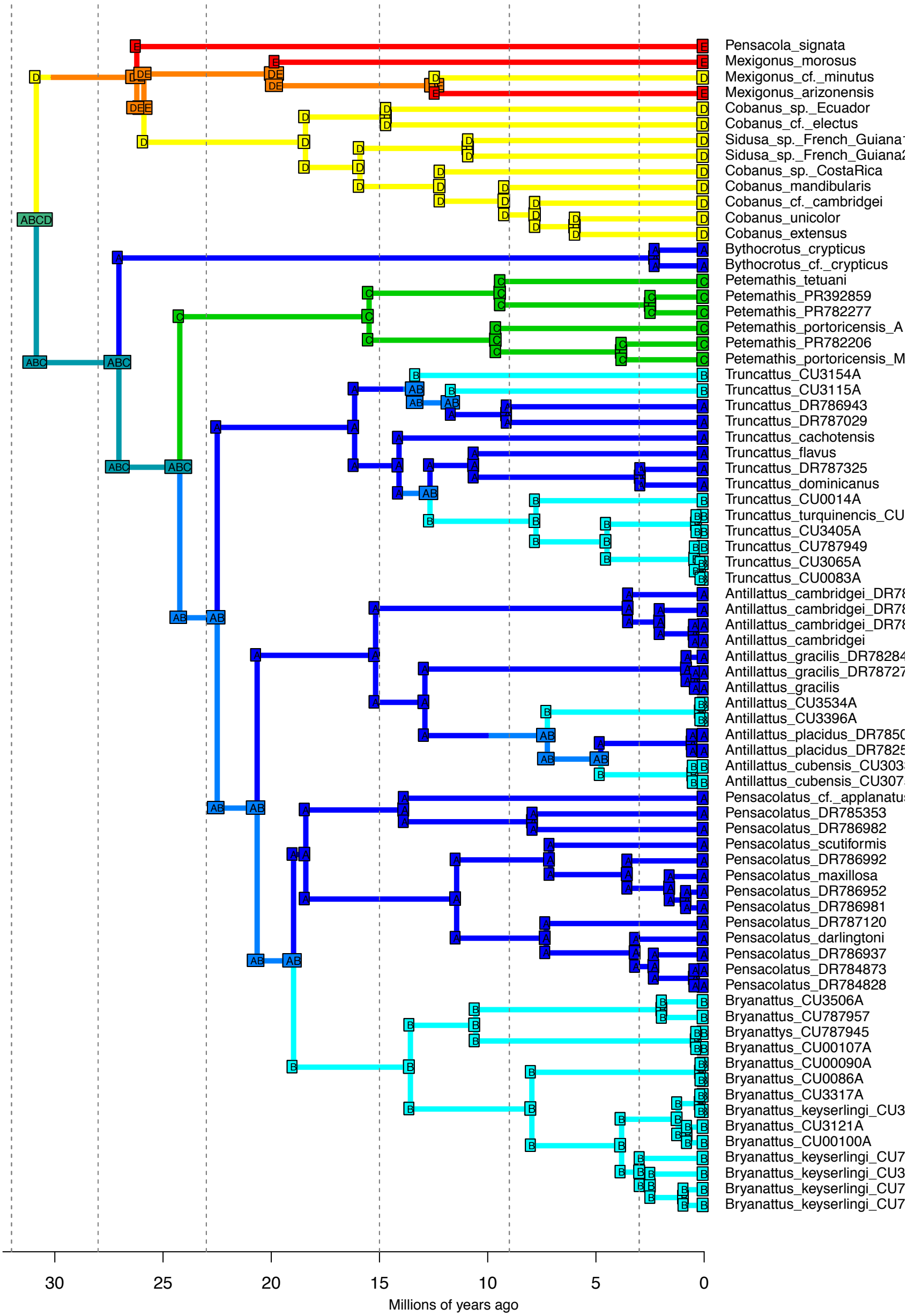

DEC_M3b_strat – Stochastic Map #15/50
ancstates: global optim, 5 areas max. d=0.0017; e=0; j=0; LnL=−50.93

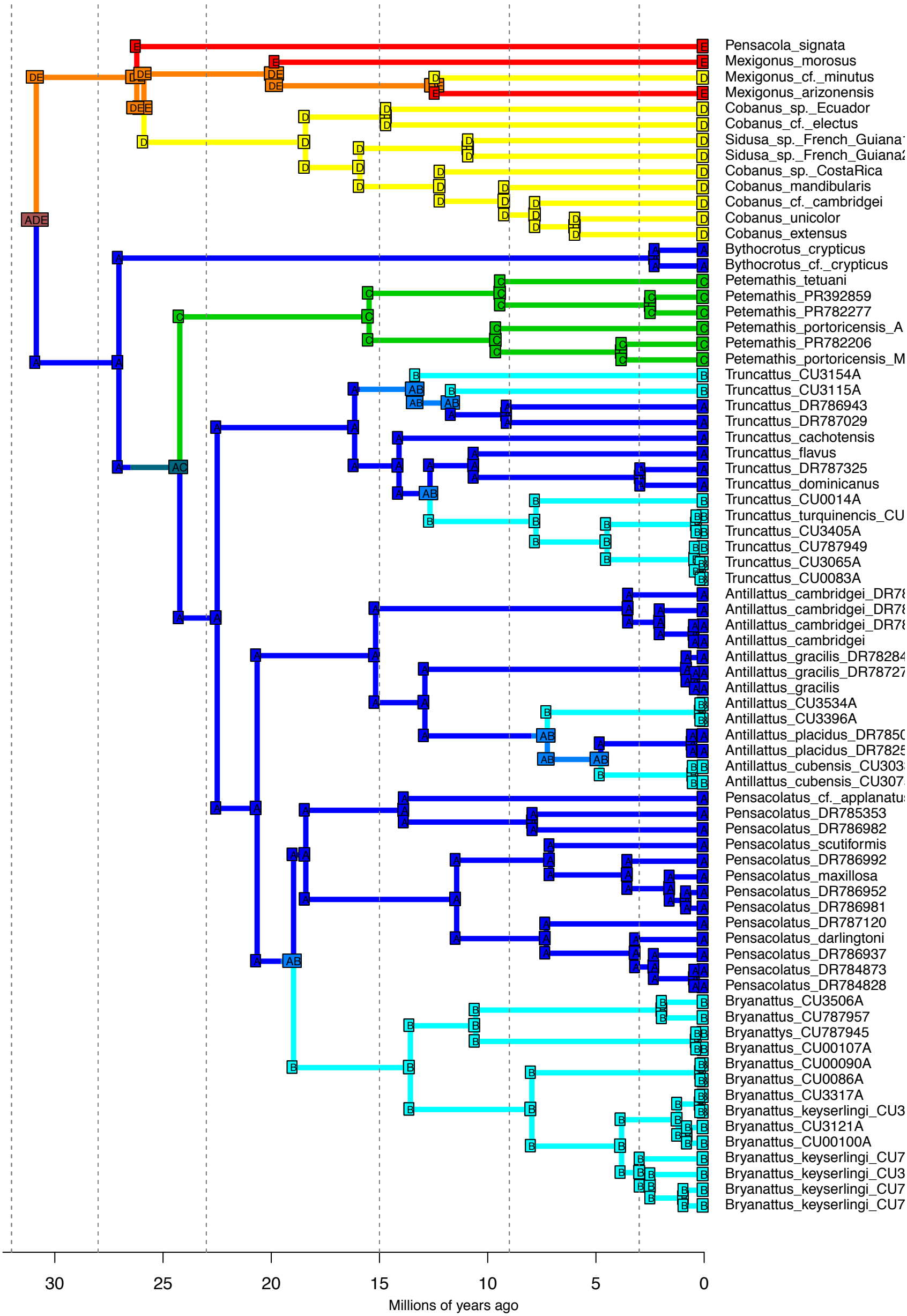

DEC_M3b_strat – Stochastic Map #16/50
ancstates: global optim, 5 areas max. d=0.0017; e=0; j=0; LnL=−50.93

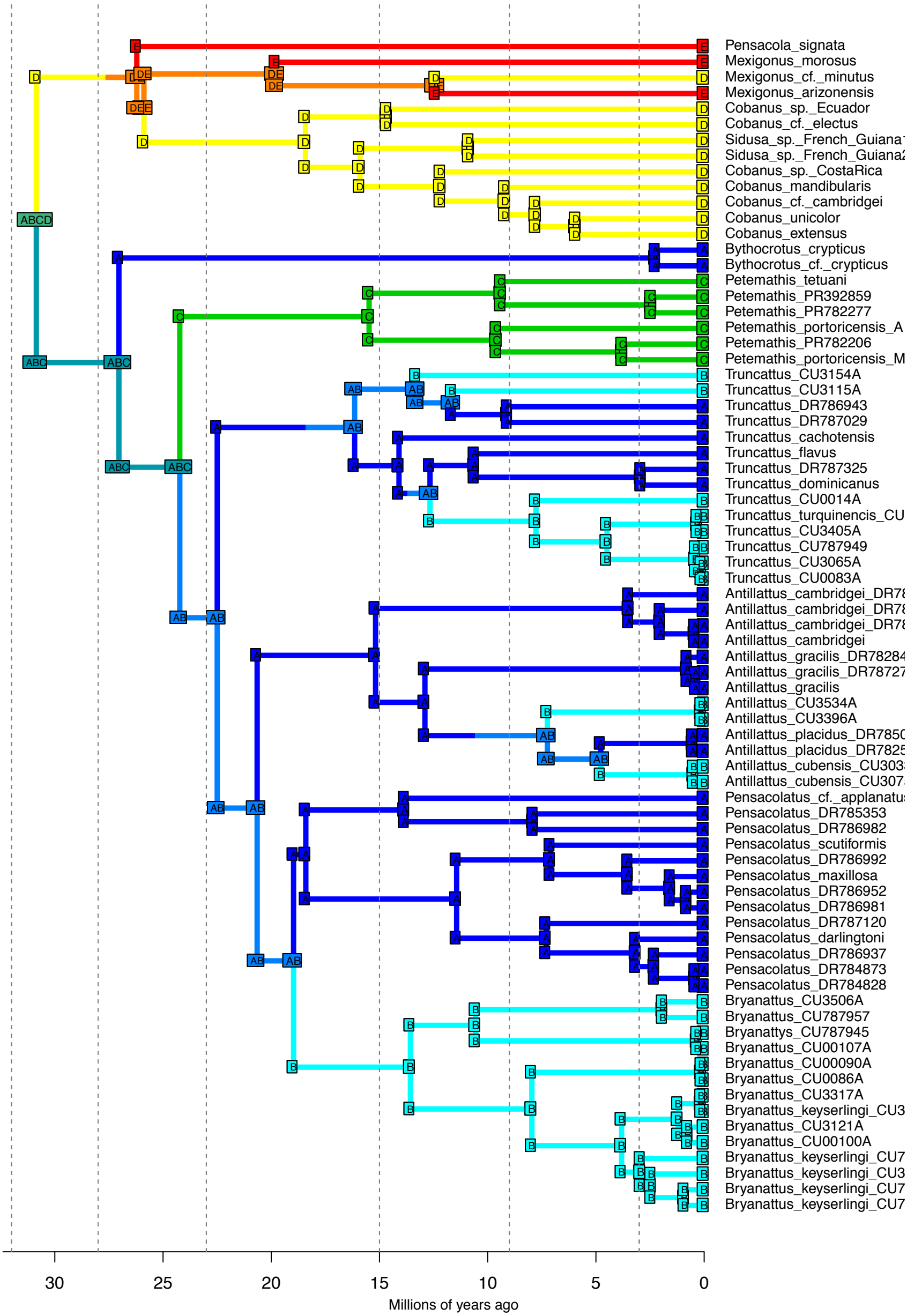

DEC_M3b_strat – Stochastic Map #17/50
ancstates: global optim, 5 areas max. d=0.0017; e=0; j=0; LnL=−50.93

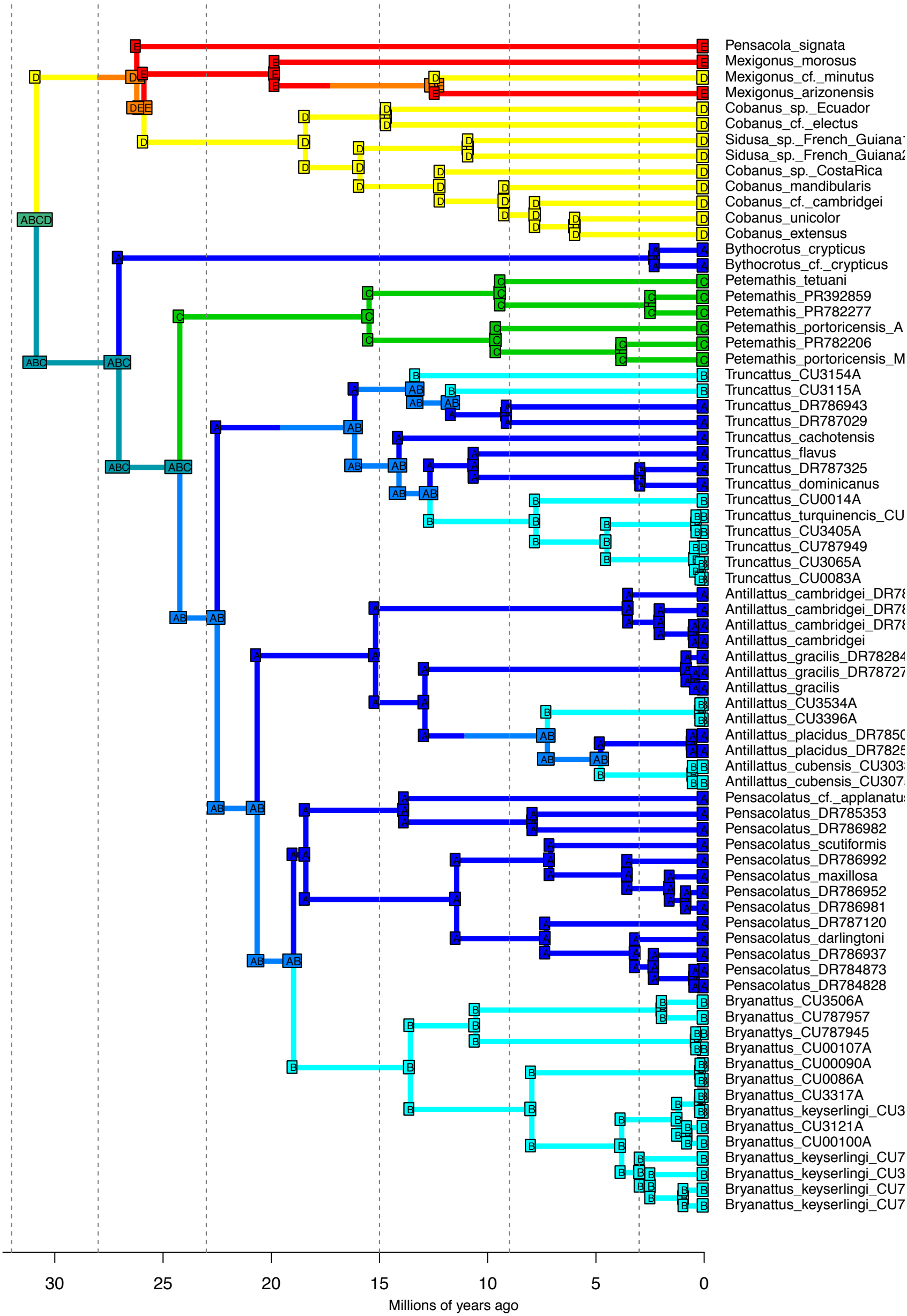

DEC_M3b_strat – Stochastic Map #18/50
ancstates: global optim, 5 areas max. d=0.0017; e=0; j=0; LnL=−50.93

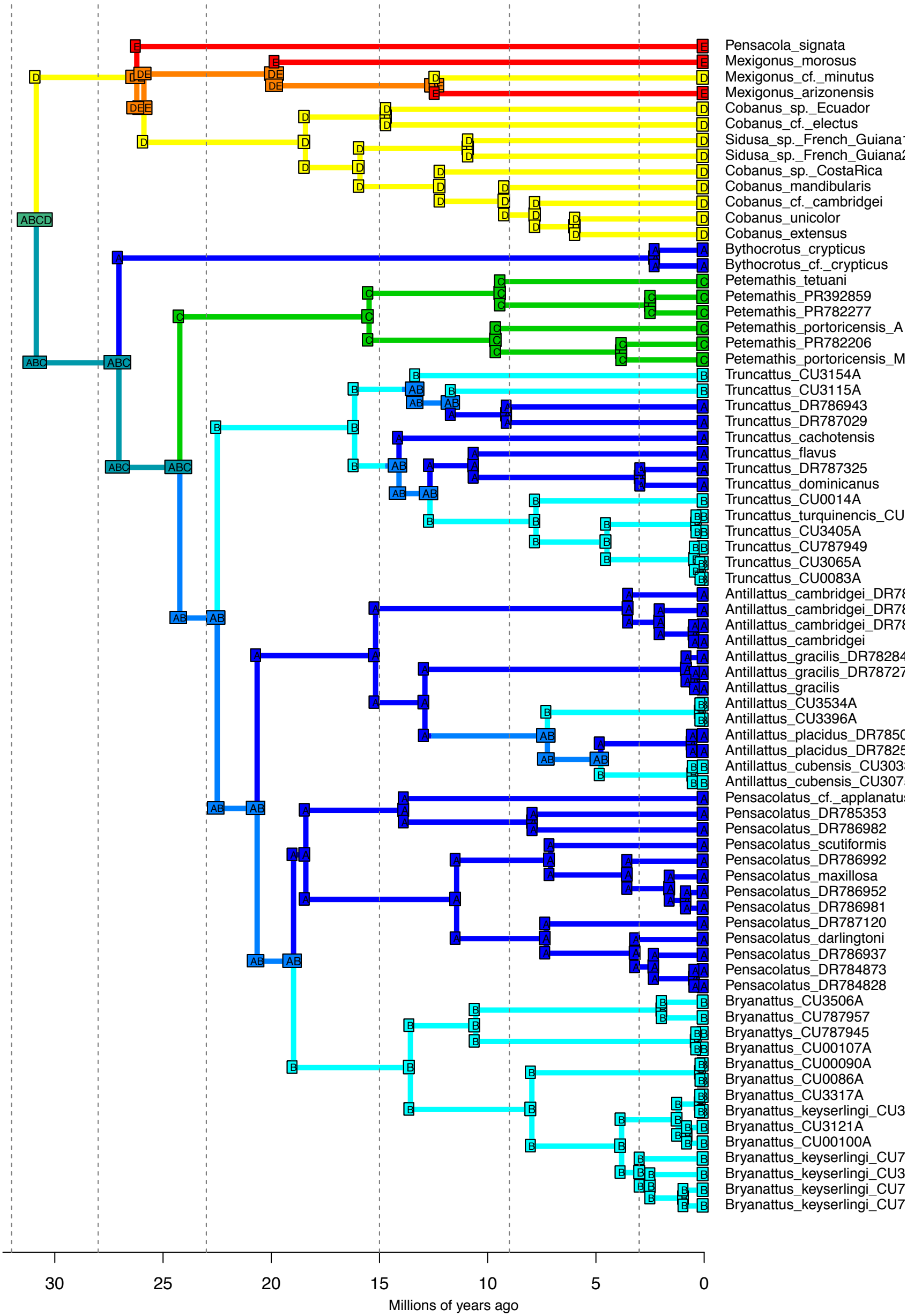

DEC_M3b_strat – Stochastic Map #19/50
ancstates: global optim, 5 areas max. d=0.0017; e=0; j=0; LnL=−50.93

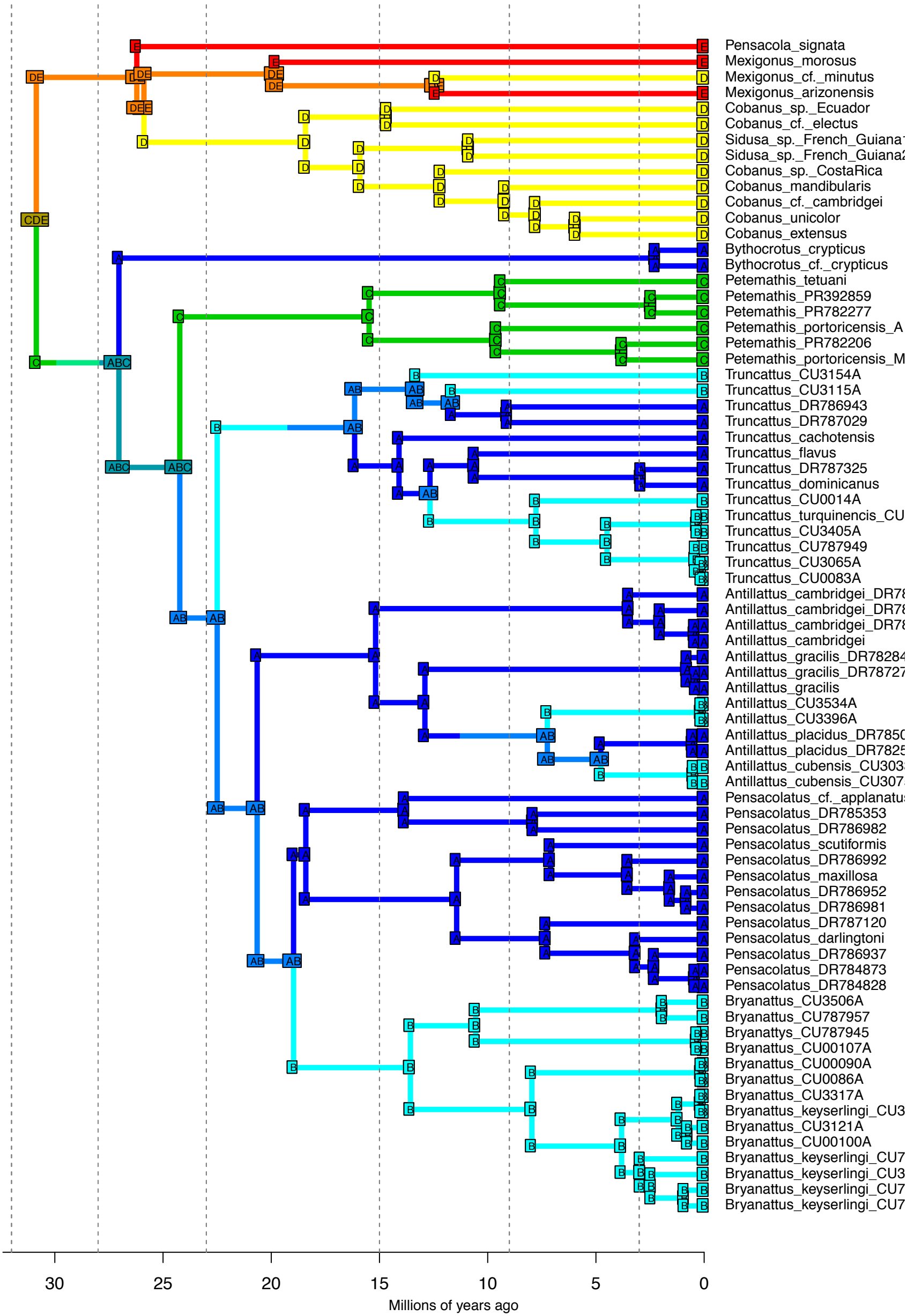

DEC_M3b_strat – Stochastic Map #20/50
ancstates: global optim, 5 areas max. d=0.0017; e=0; j=0; LnL=–50.93

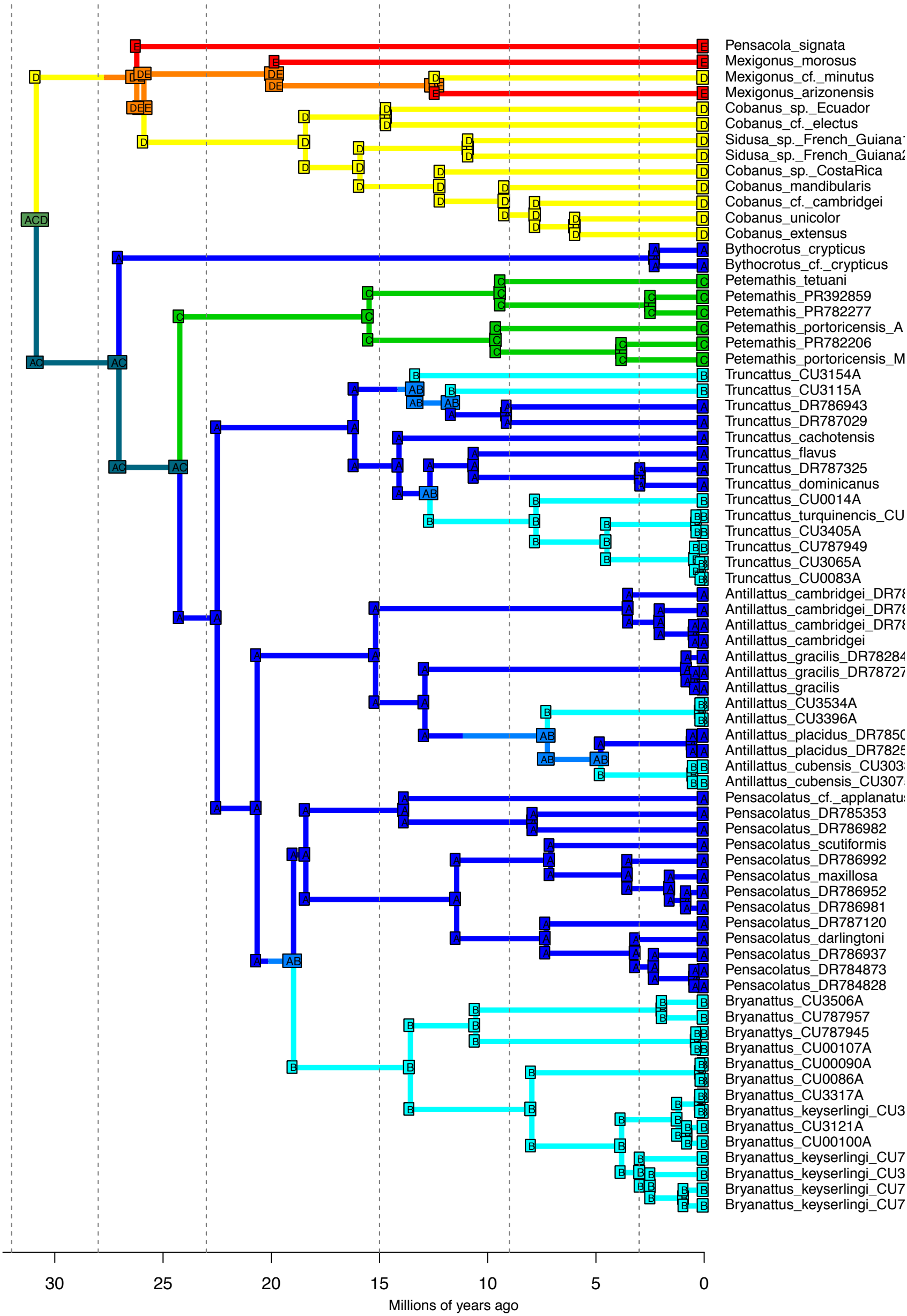

DEC_M3b_strat – Stochastic Map #21/50
ancstates: global optim, 5 areas max. d=0.0017; e=0; j=0; LnL=−50.93

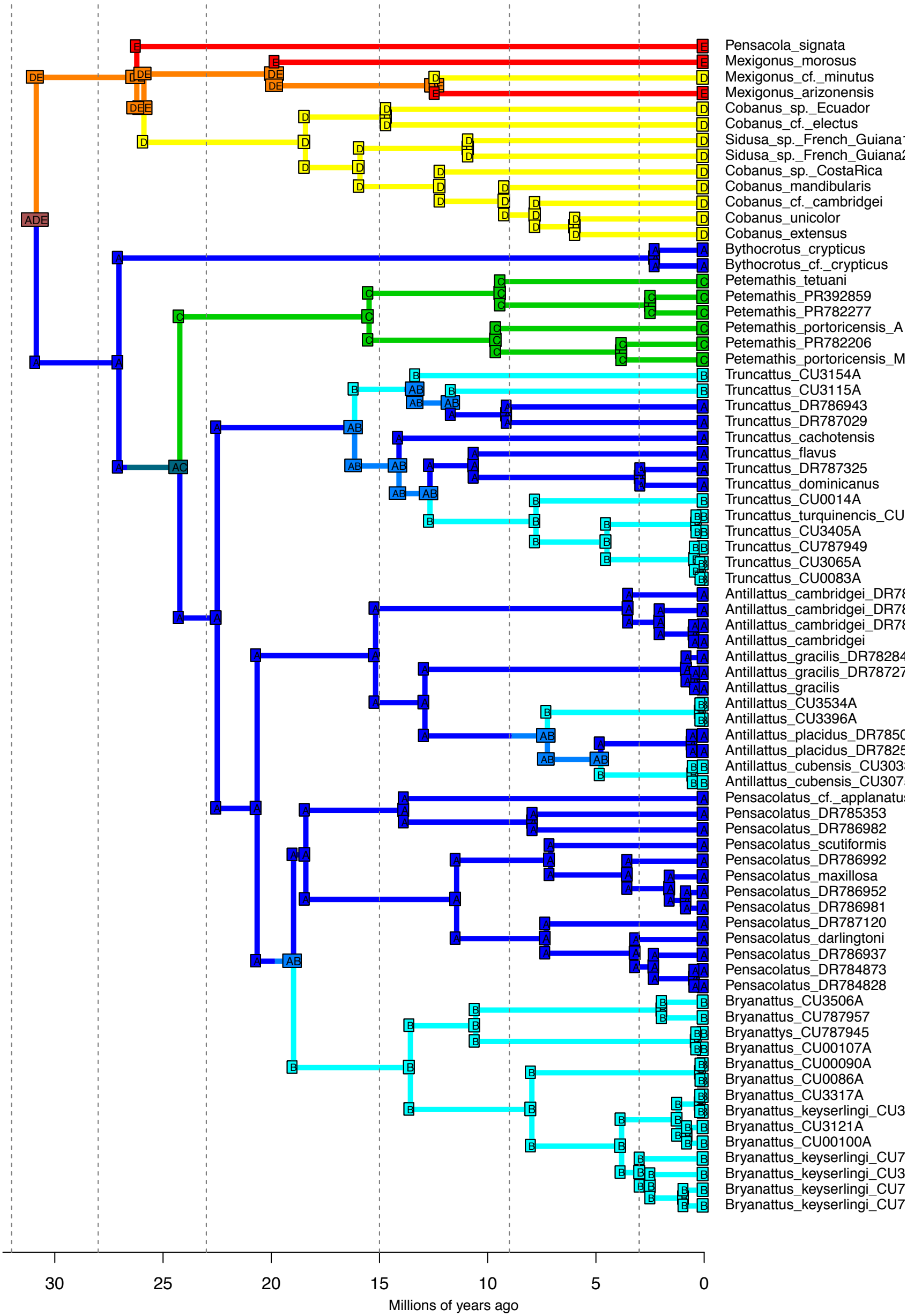

DEC_M3b_strat – Stochastic Map #22/50
ancstates: global optim, 5 areas max. d=0.0017; e=0; j=0; LnL=–50.93

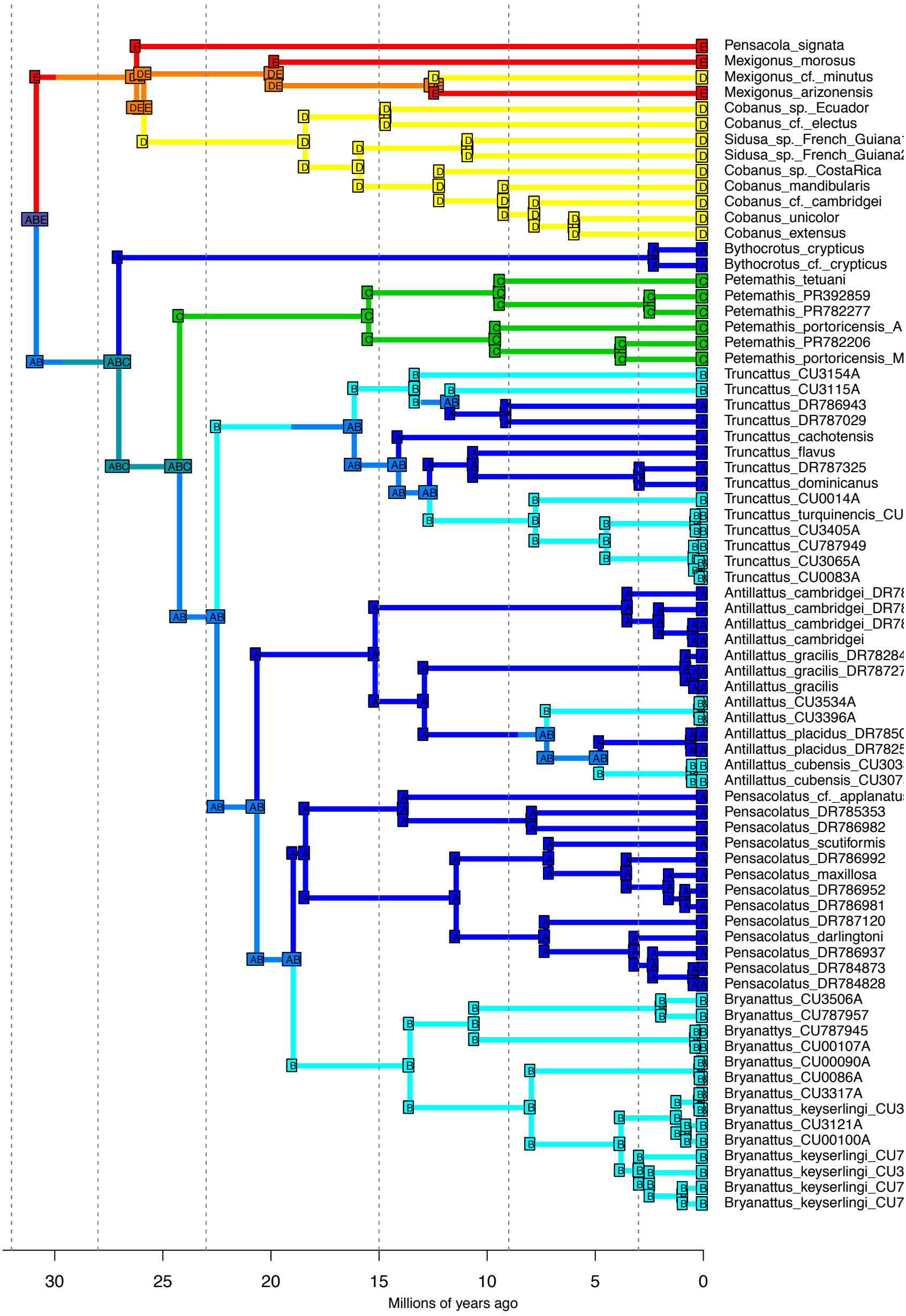

DEC_M3b_strat – Stochastic Map #23/50
ancstates: global optim, 5 areas max. d=0.0017; e=0; j=0; LnL=−50.93

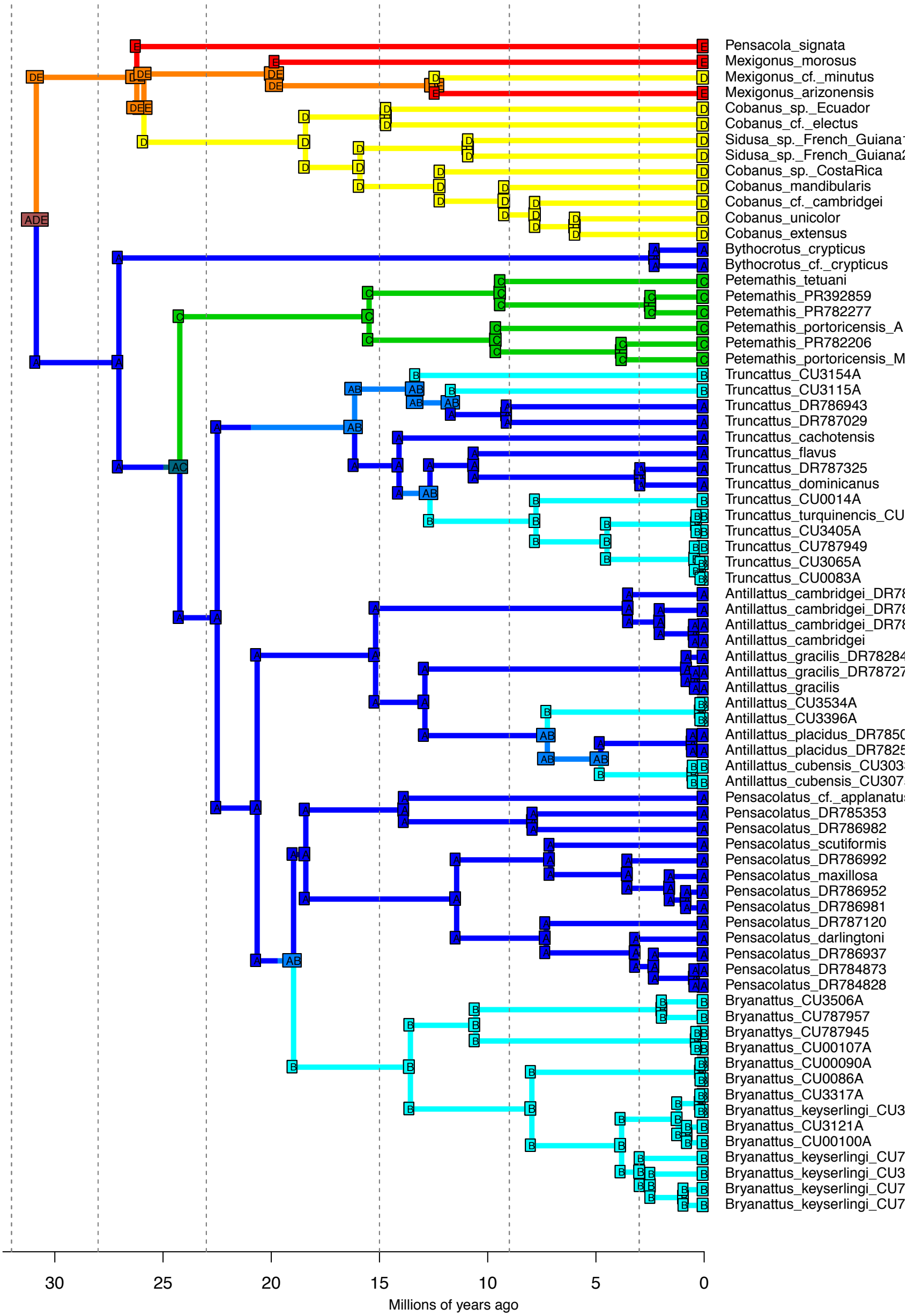

DEC_M3b_strat – Stochastic Map #24/50
ancstates: global optim, 5 areas max. d=0.0017; e=0; j=0; LnL=−50.93

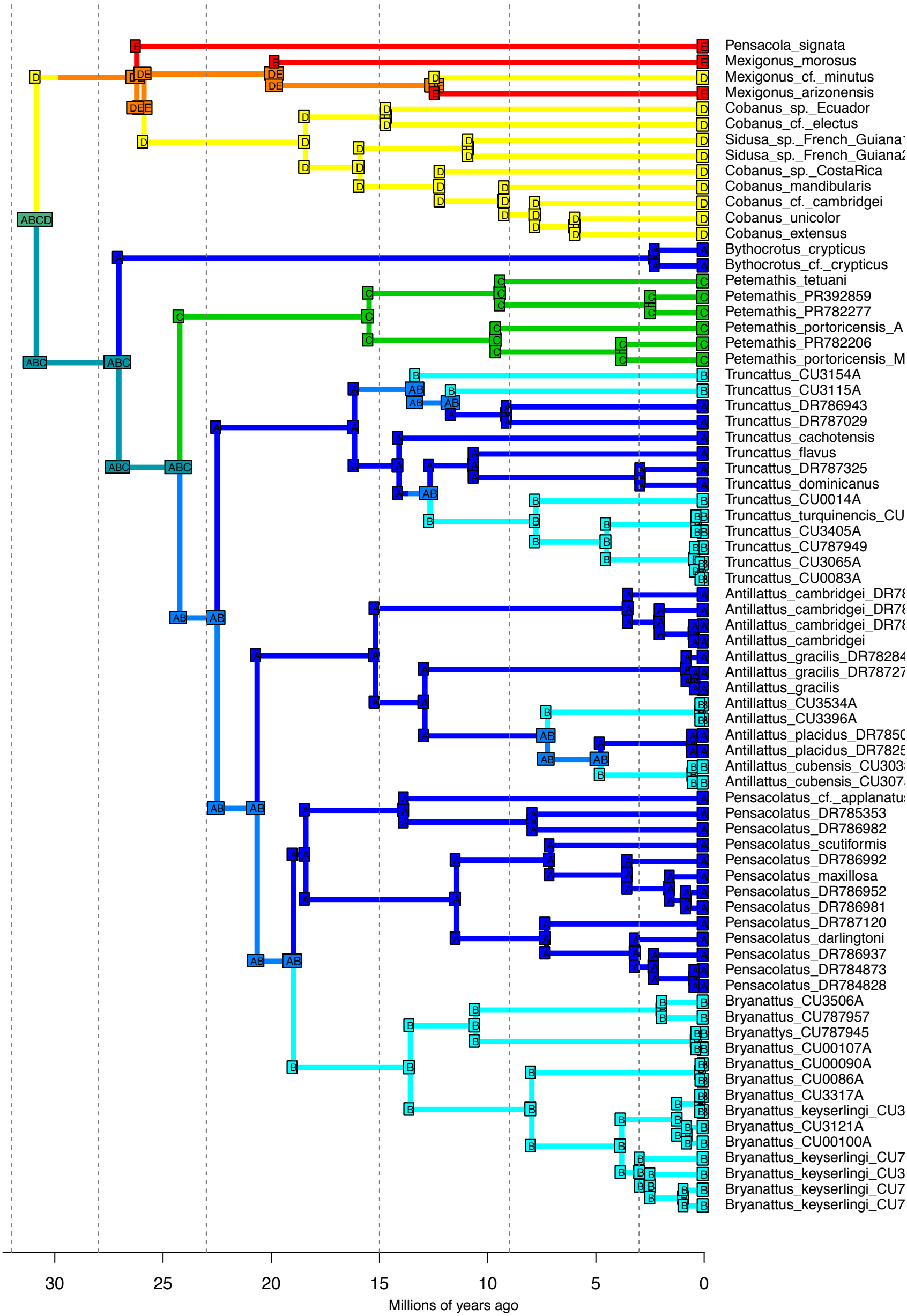

DEC_M3b_strat – Stochastic Map #25/50
ancstates: global optim, 5 areas max. d=0.0017; e=0; j=0; LnL=−50.93

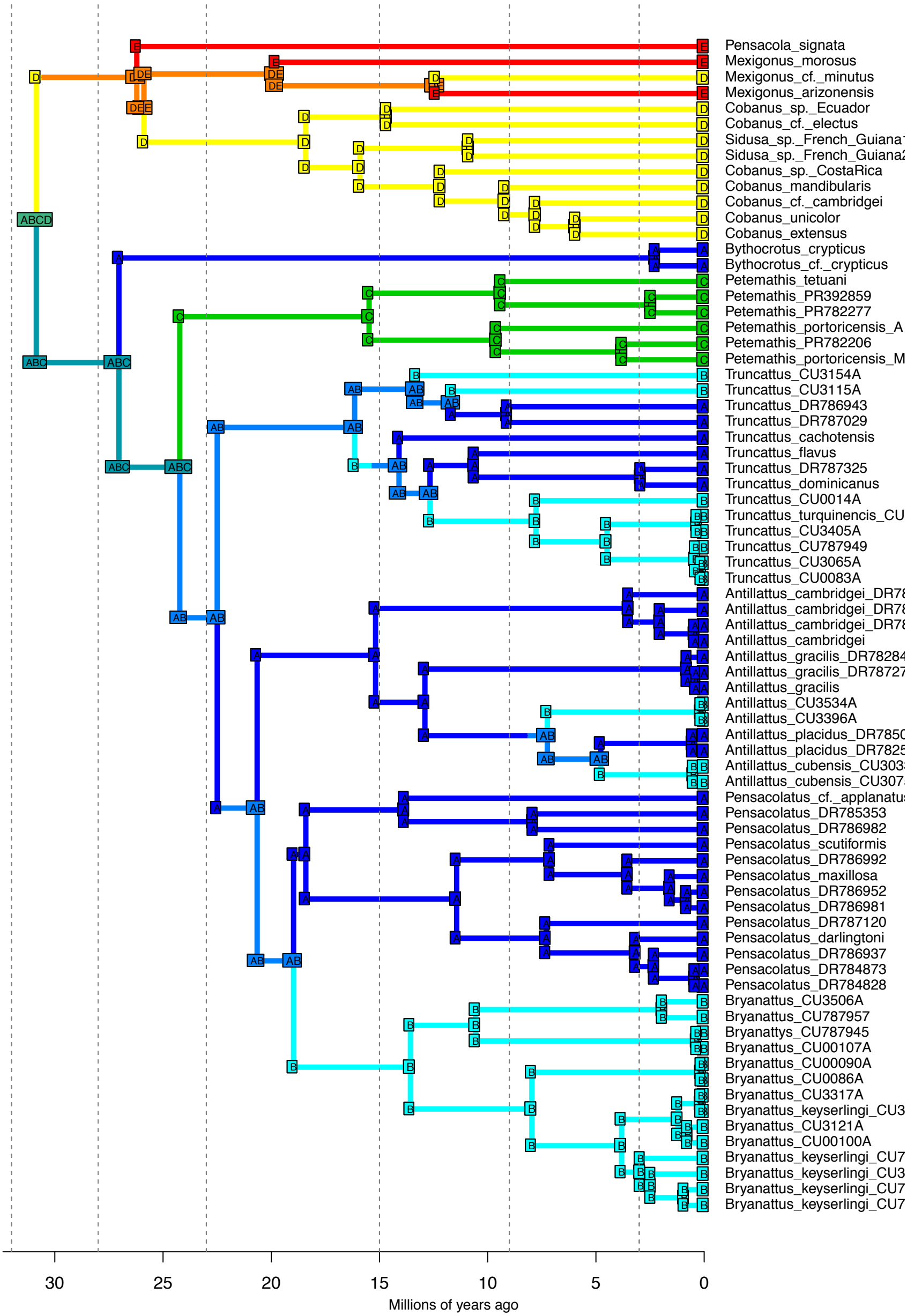

DEC_M3b_strat – Stochastic Map #26/50
ancstates: global optim, 5 areas max. d=0.0017; e=0; j=0; LnL=−50.93

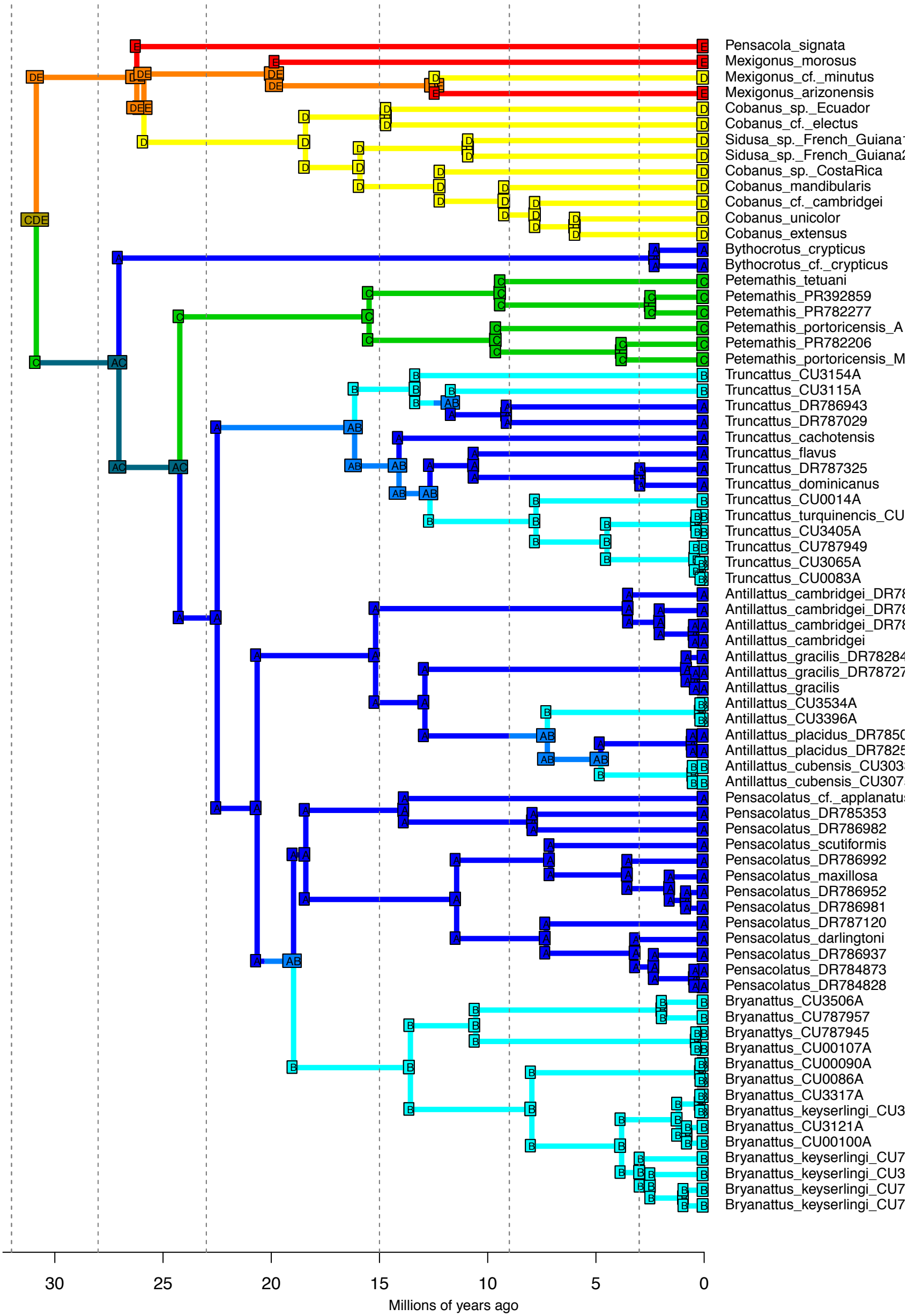

DEC_M3b_strat – Stochastic Map #27/50
ancstates: global optim, 5 areas max. d=0.0017; e=0; j=0; LnL=–50.93

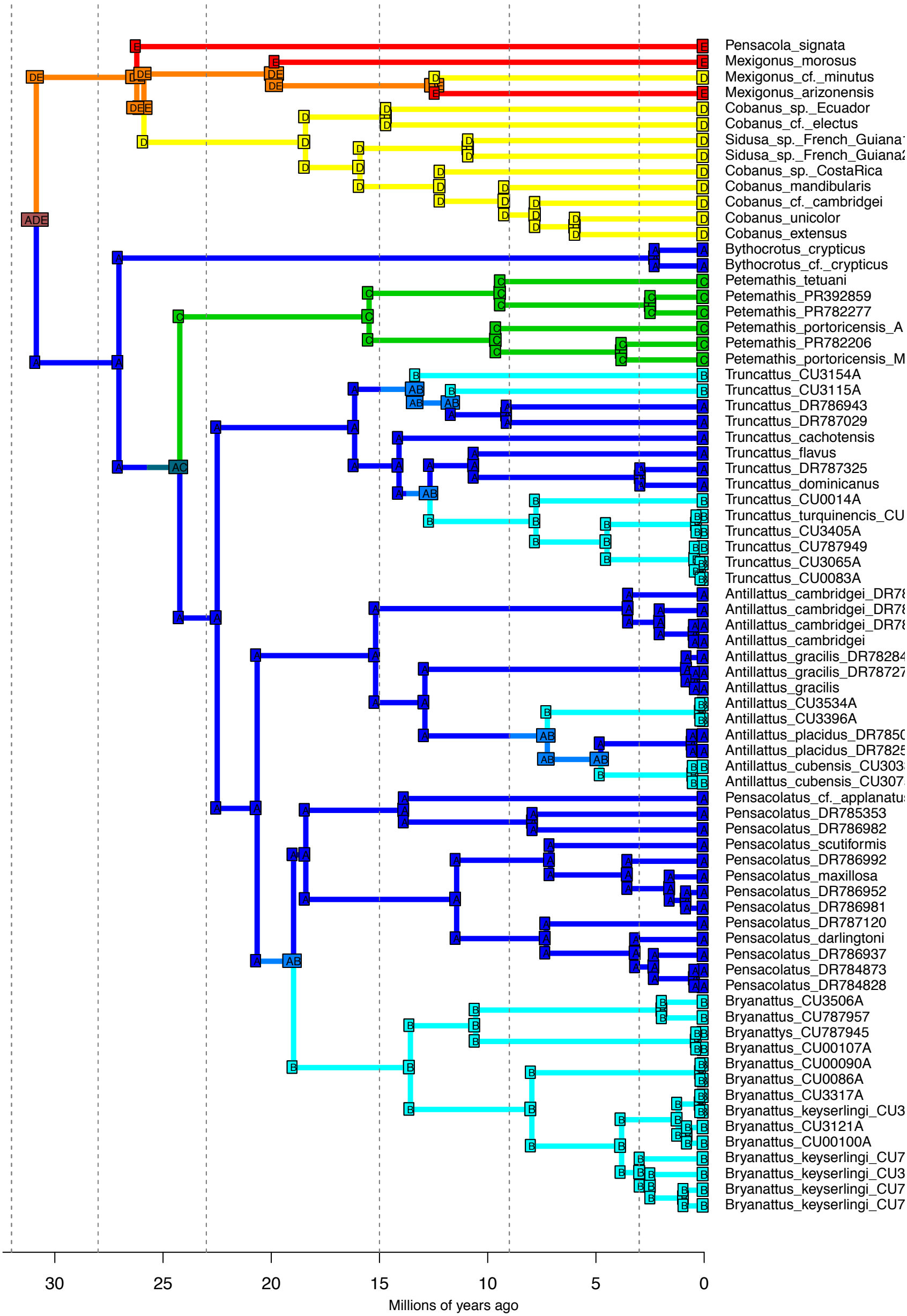

DEC_M3b_strat – Stochastic Map #28/50
ancstates: global optim, 5 areas max. d=0.0017; e=0; j=0; LnL=–50.93

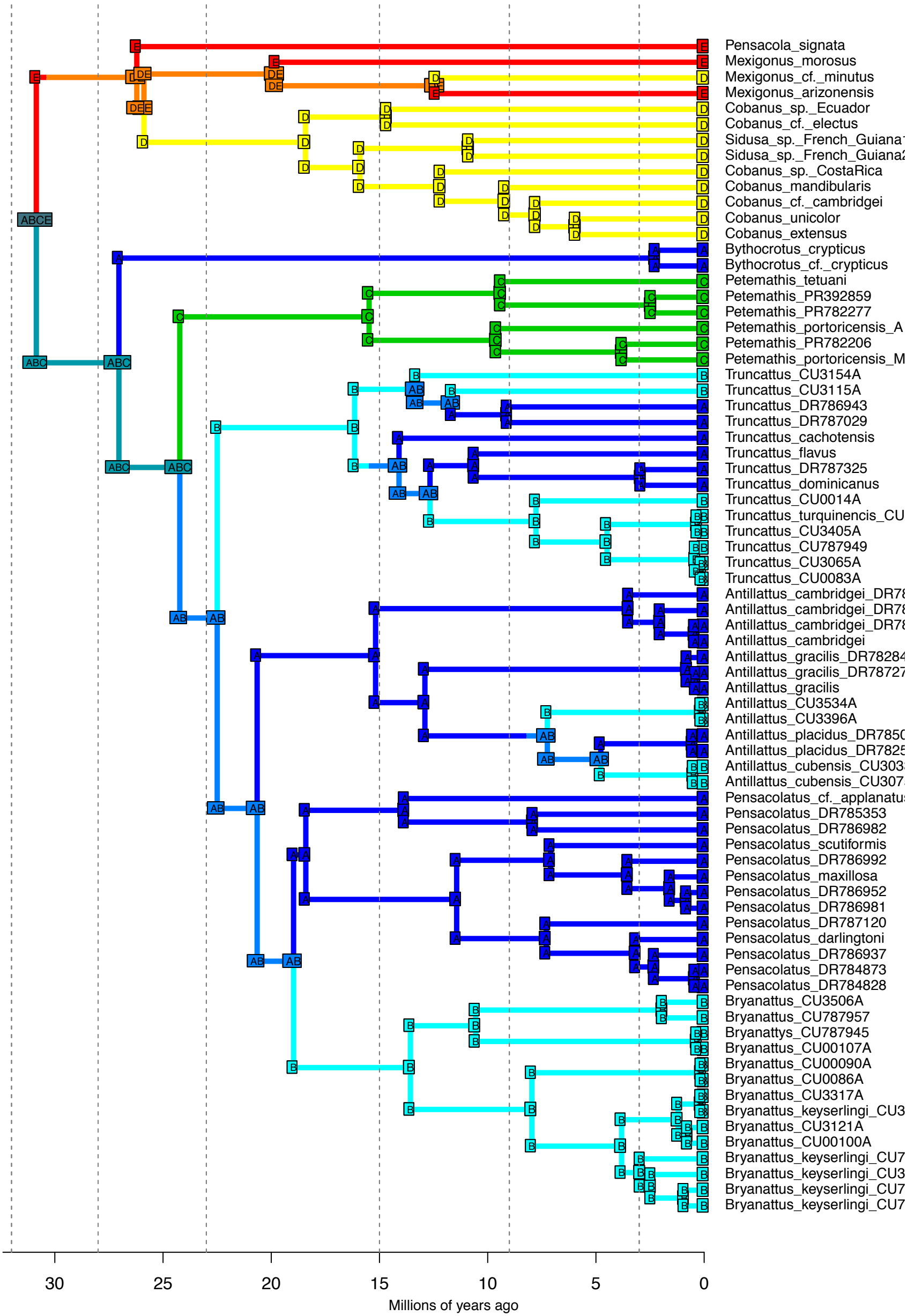

DEC_M3b_strat – Stochastic Map #29/50
ancstates: global optim, 5 areas max. d=0.0017; e=0; j=0; LnL=–50.93

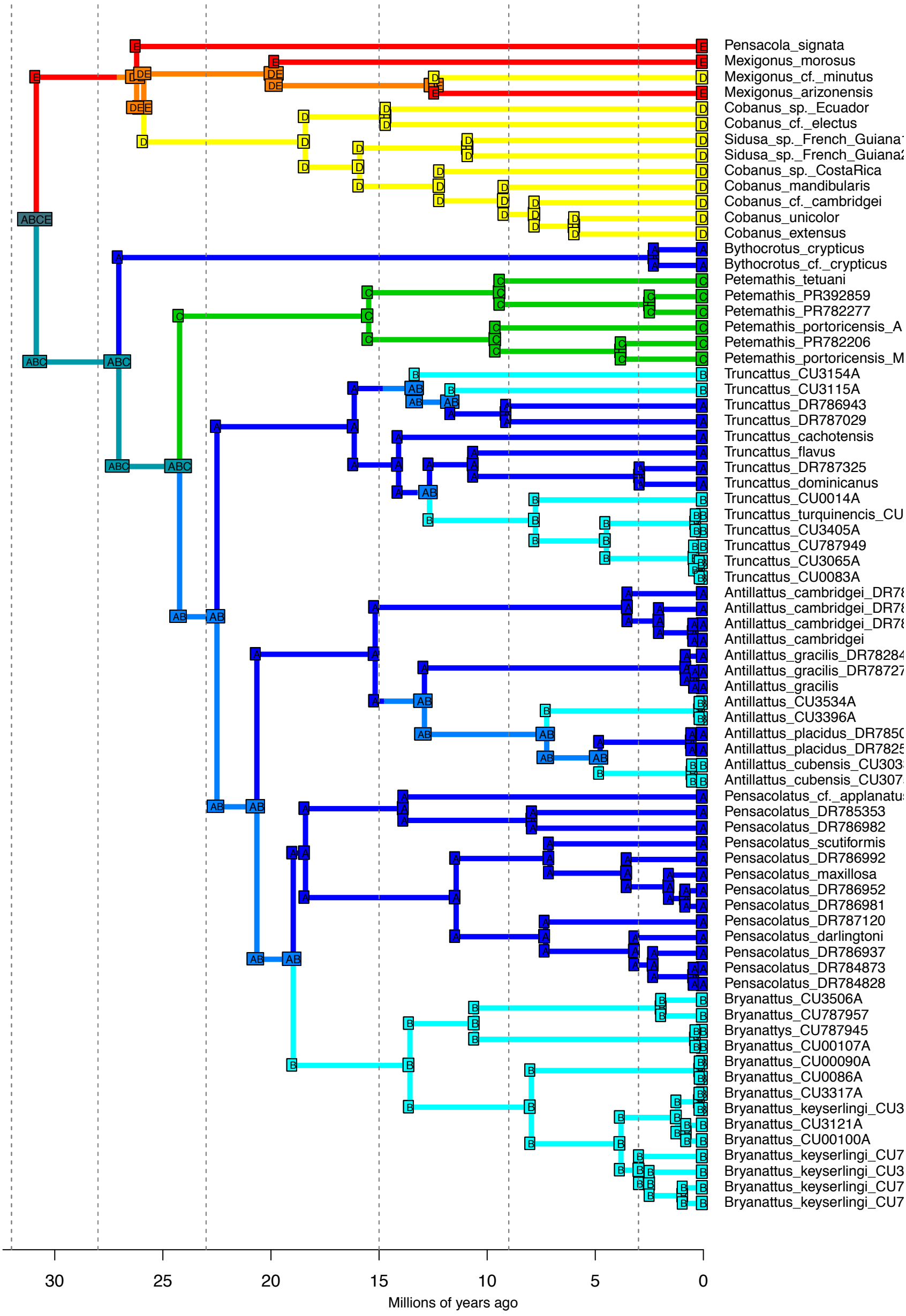

DEC_M3b_strat – Stochastic Map #30/50
ancstates: global optim, 5 areas max. d=0.0017; e=0; j=0; LnL=−50.93

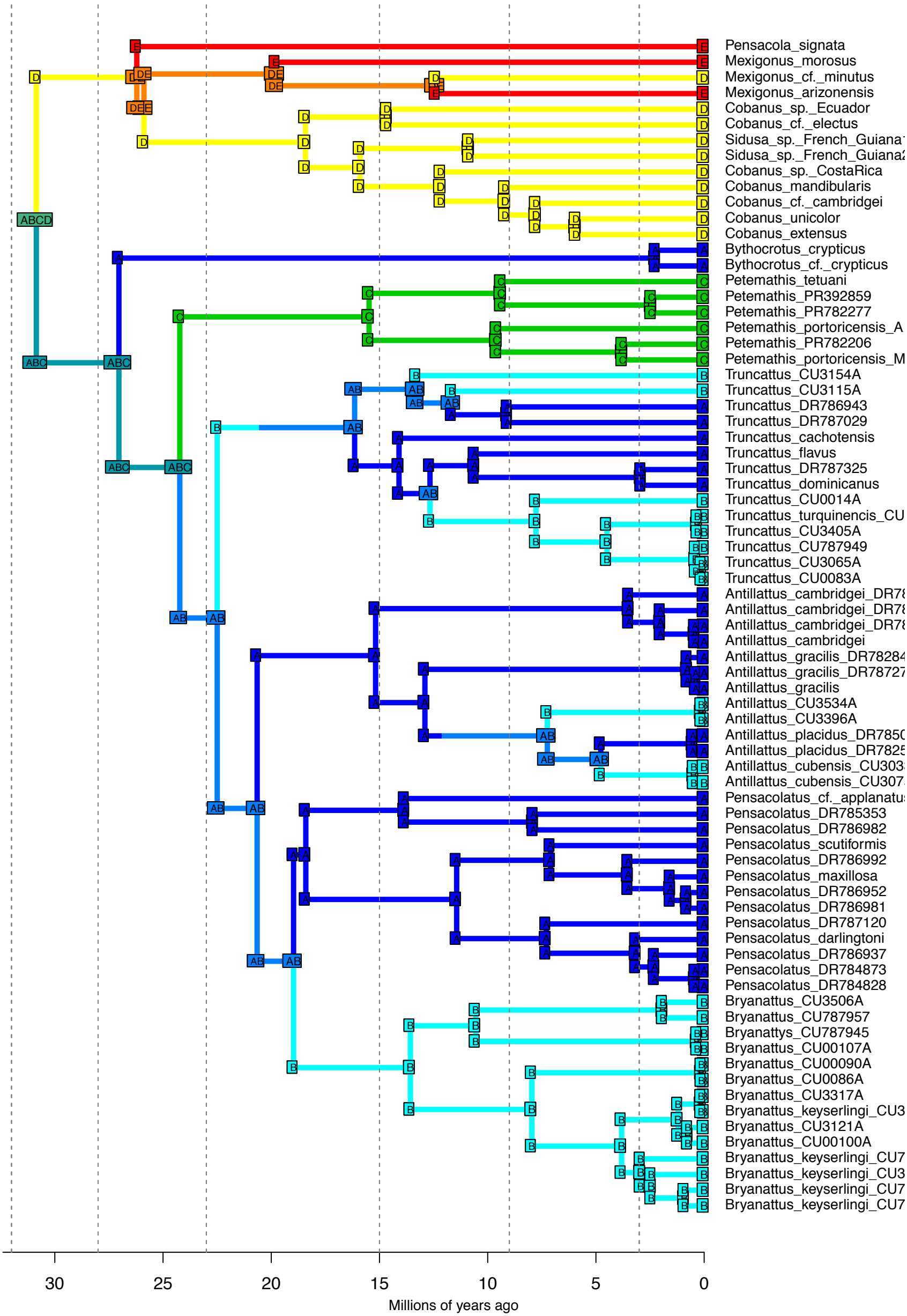

DEC_M3b_strat – Stochastic Map #31/50
ancstates: global optim, 5 areas max. d=0.0017; e=0; j=0; LnL=−50.93

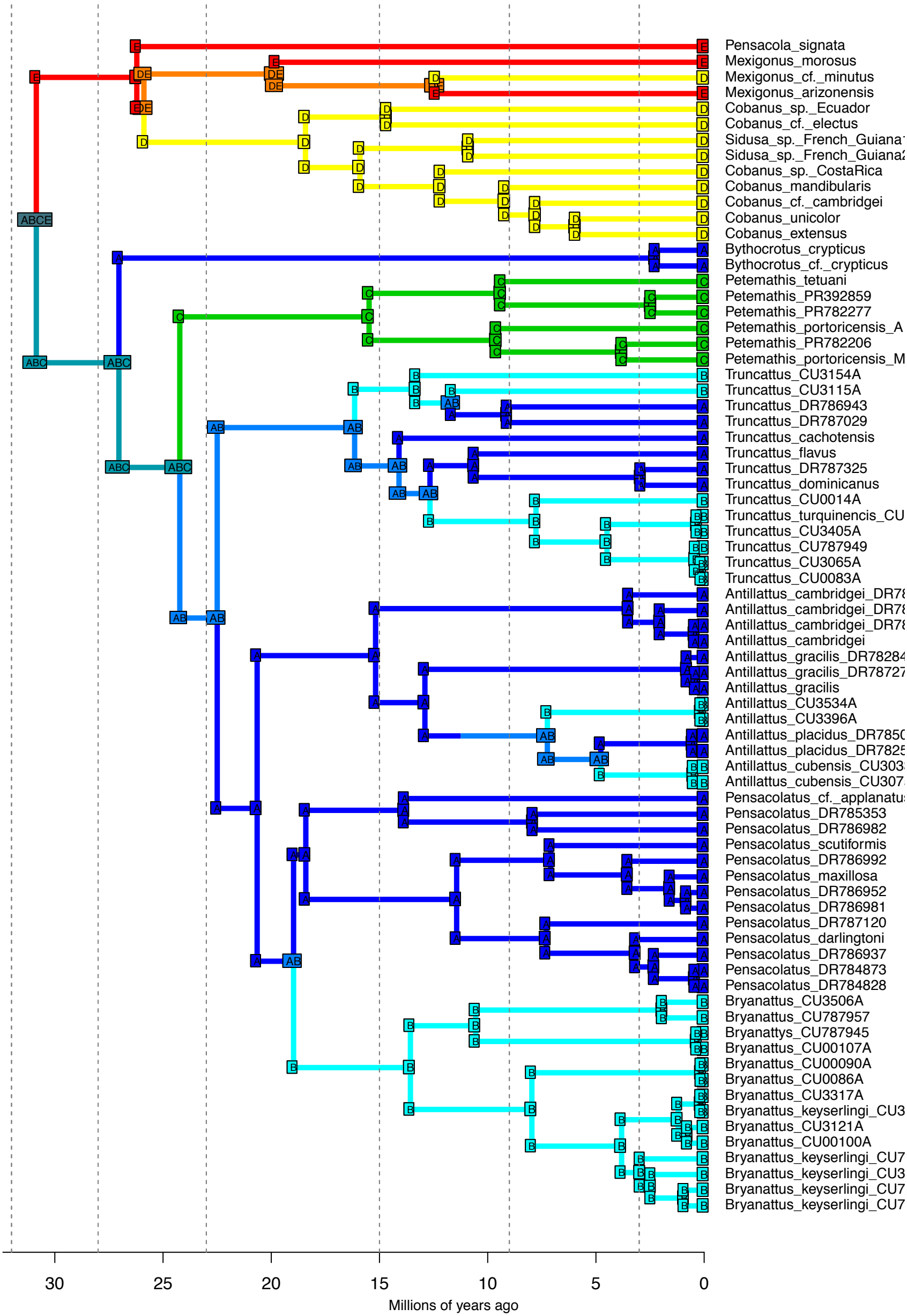

DEC_M3b_strat – Stochastic Map #32/50
ancstates: global optim, 5 areas max. d=0.0017; e=0; j=0; LnL=–50.93

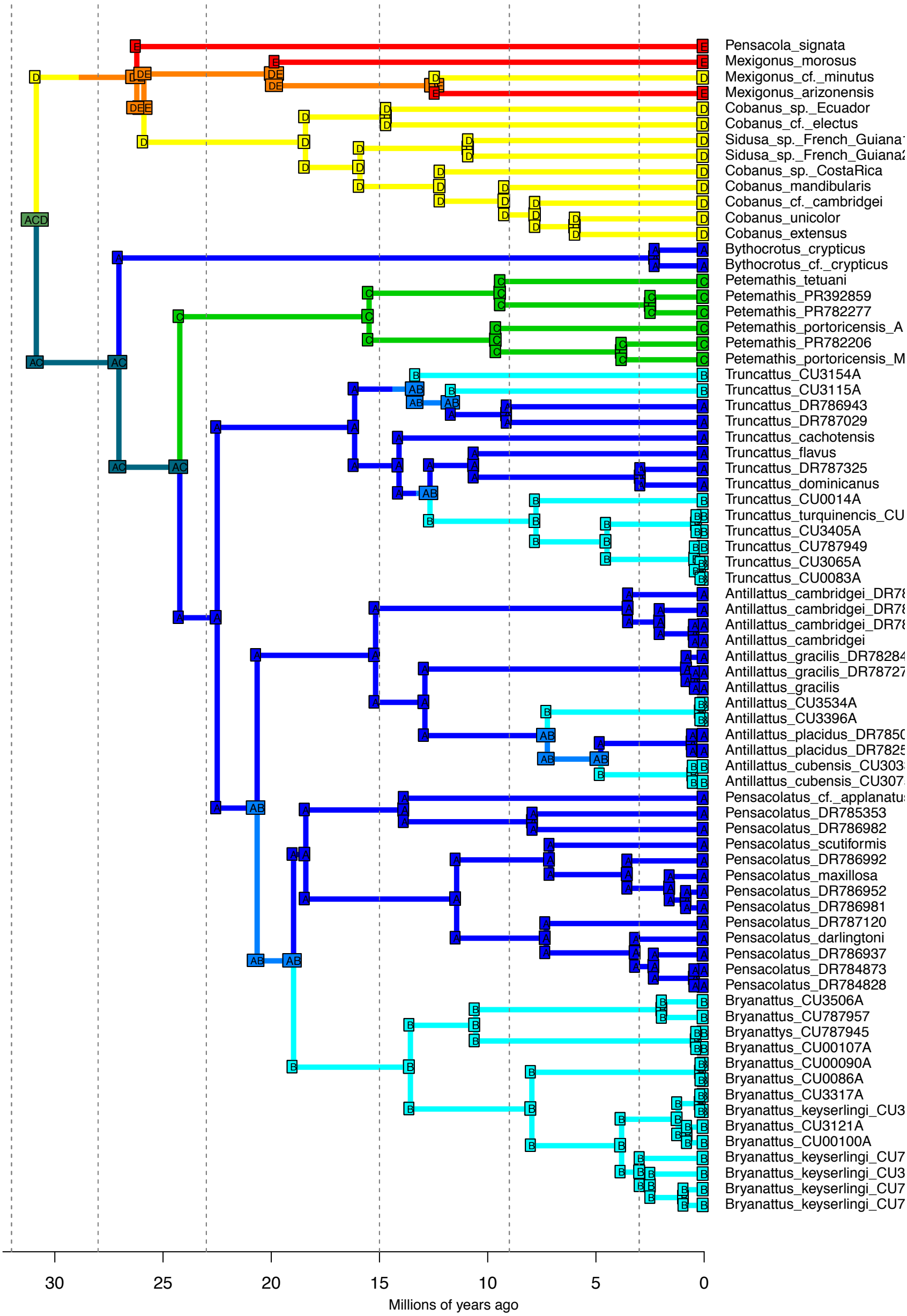

DEC_M3b_strat – Stochastic Map #33/50
ancstates: global optim, 5 areas max. d=0.0017; e=0; j=0; LnL=−50.93

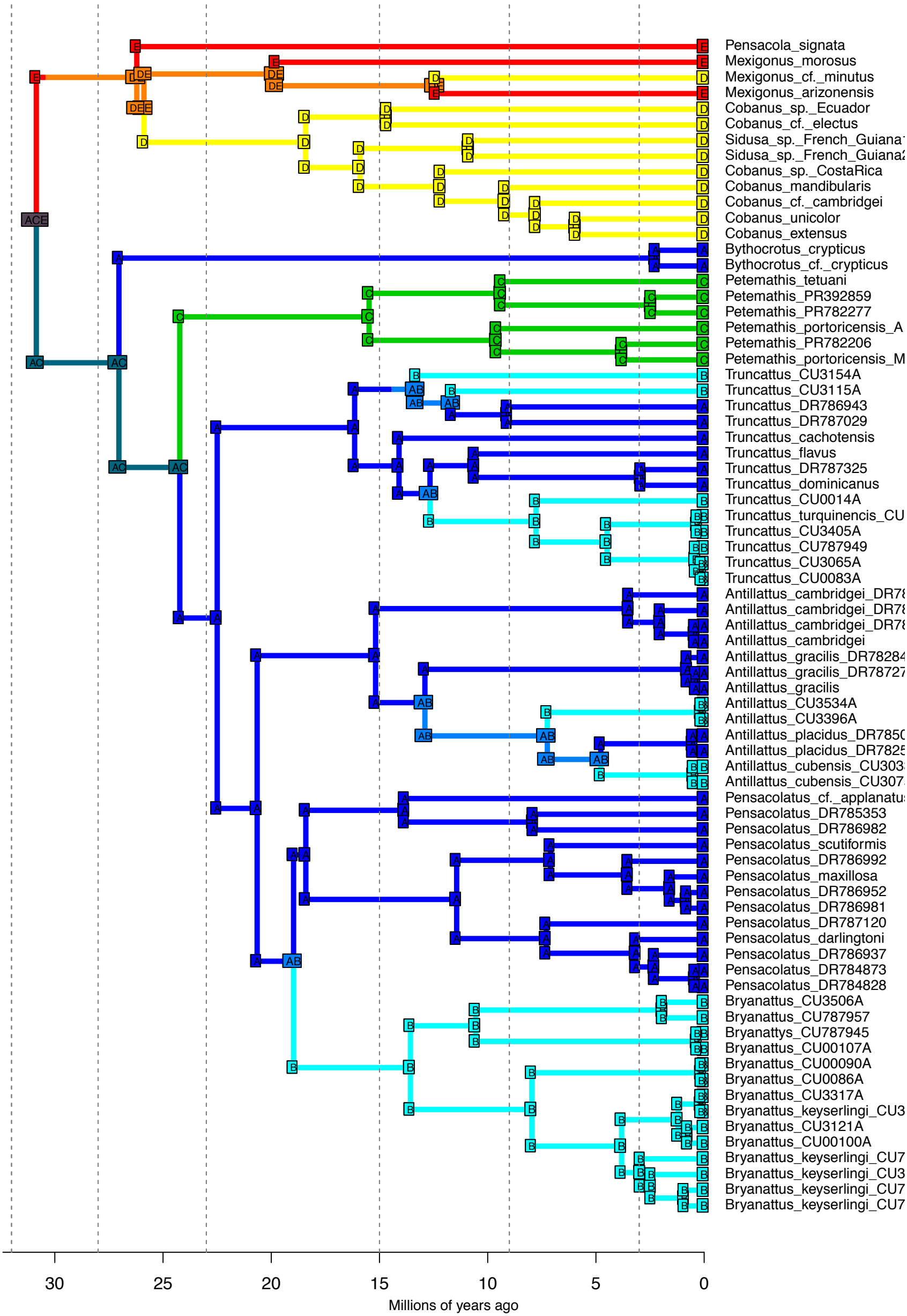

DEC_M3b_strat – Stochastic Map #34/50
ancstates: global optim, 5 areas max. d=0.0017; e=0; j=0; LnL=−50.93

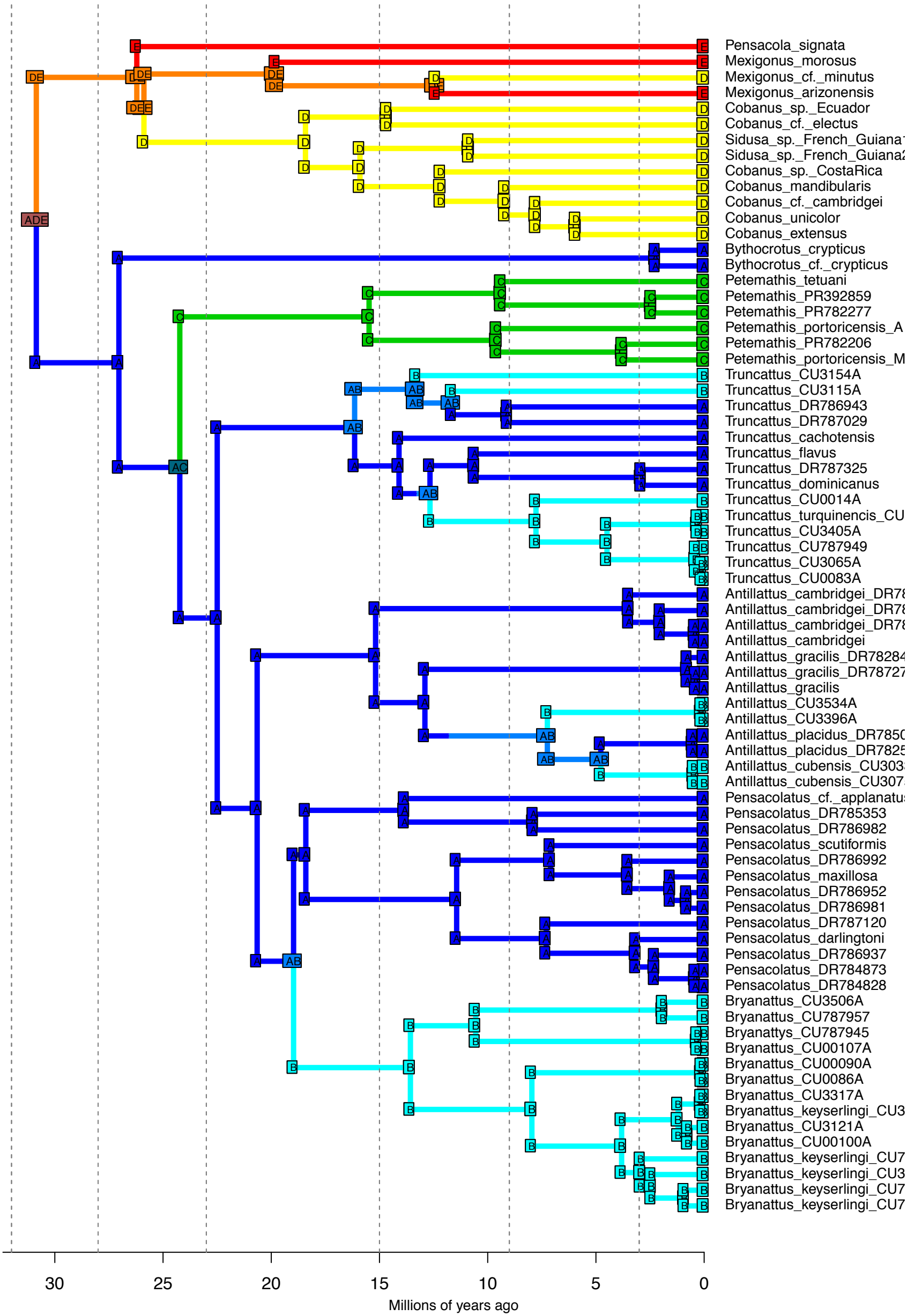

DEC_M3b_strat – Stochastic Map #35/50
ancstates: global optim, 5 areas max. d=0.0017; e=0; j=0; LnL=−50.93

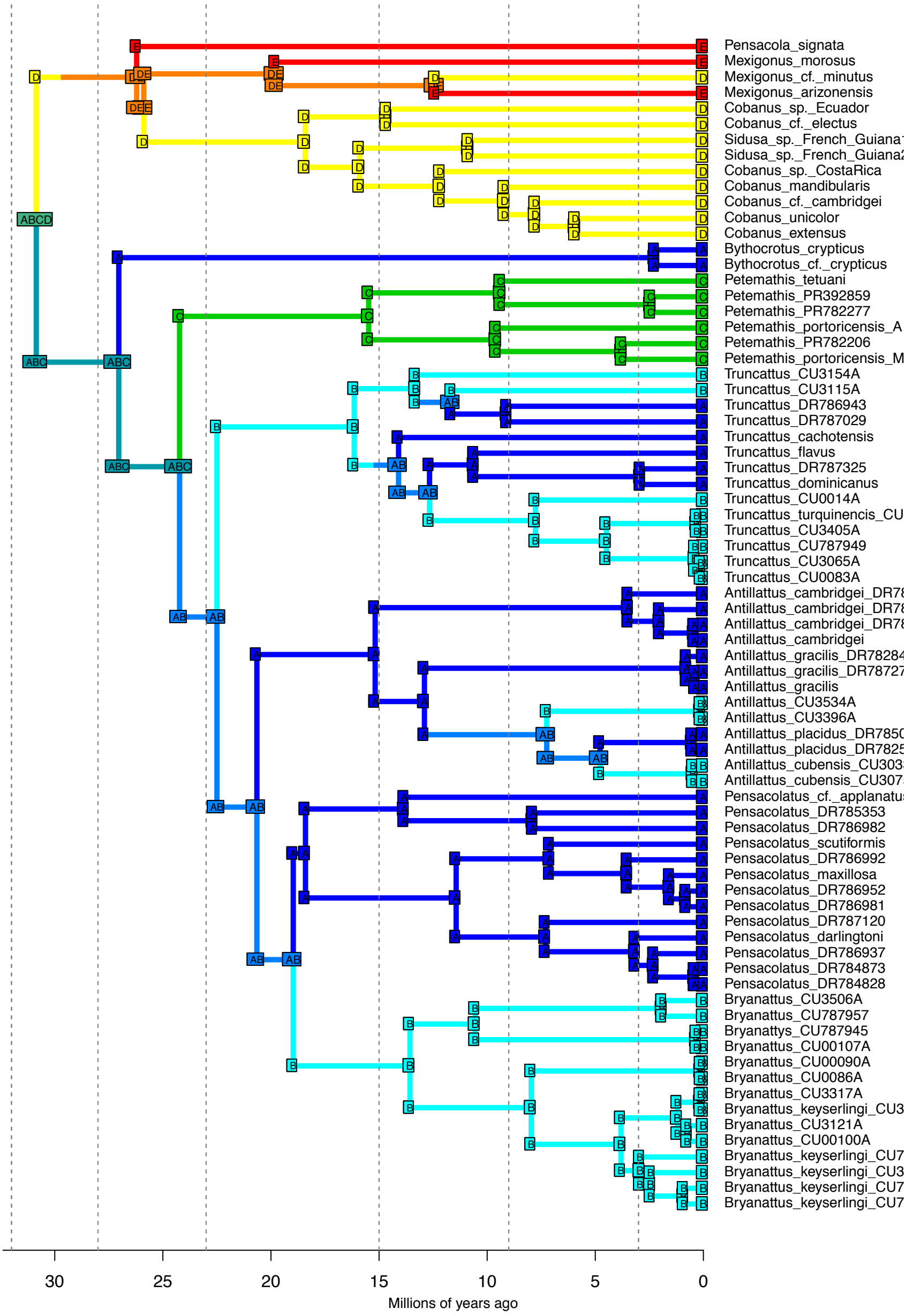

DEC_M3b_strat – Stochastic Map #36/50
ancstates: global optim, 5 areas max. d=0.0017; e=0; j=0; LnL=−50.93

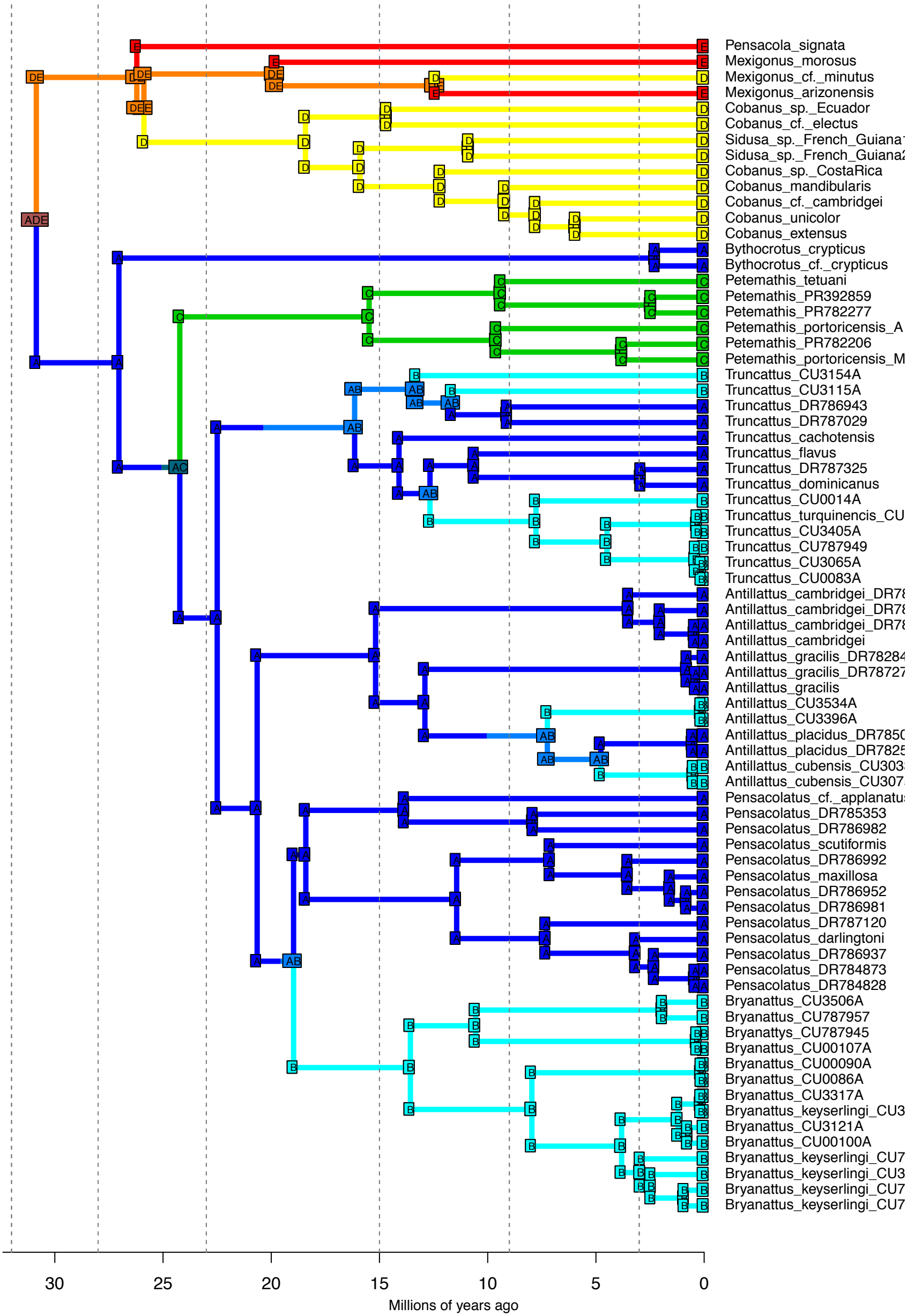

DEC_M3b_strat – Stochastic Map #37/50
ancstates: global optim, 5 areas max. d=0.0017; e=0; j=0; LnL=−50.93

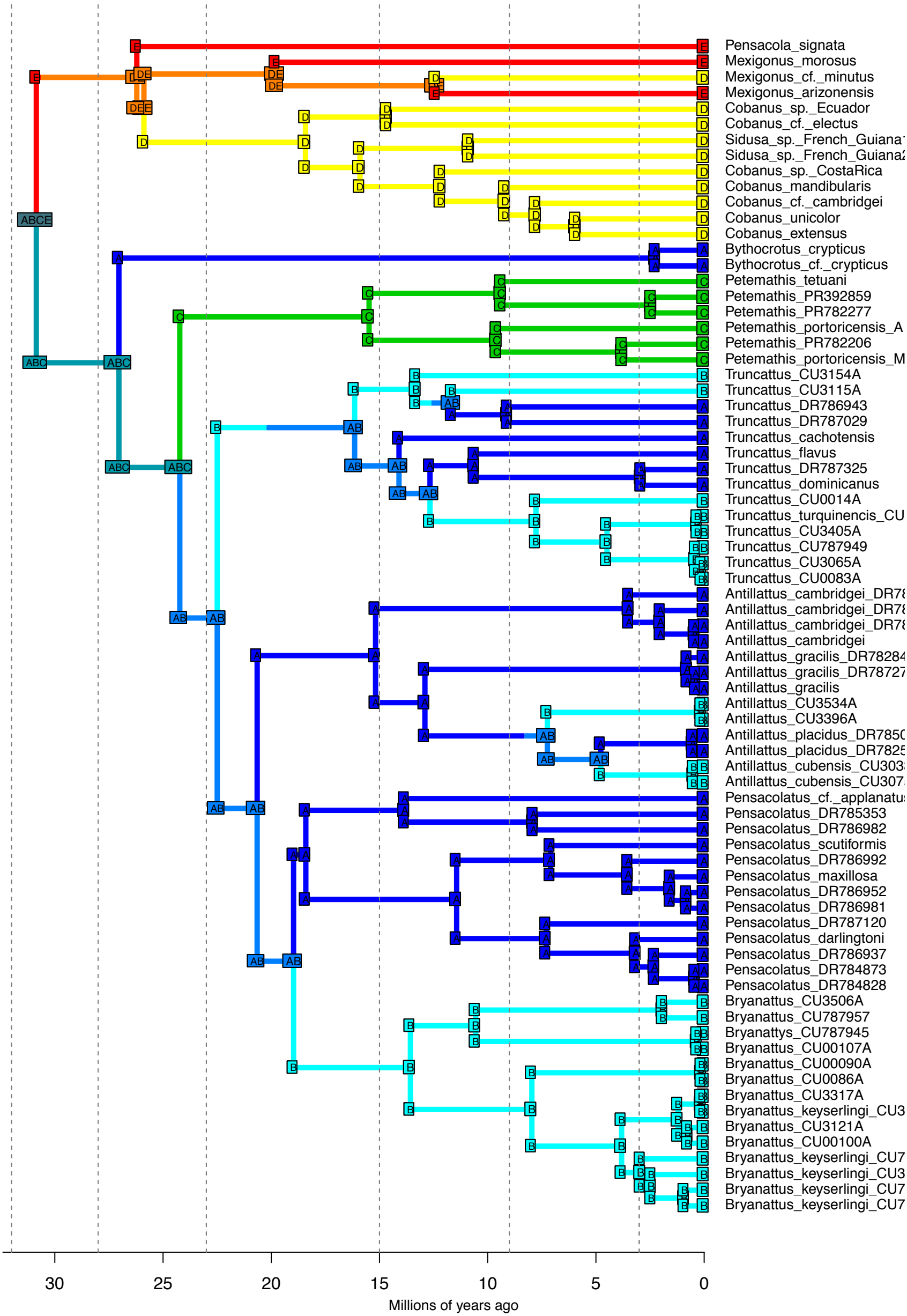

DEC_M3b_strat – Stochastic Map #38/50
ancstates: global optim, 5 areas max. d=0.0017; e=0; j=0; LnL=−50.93

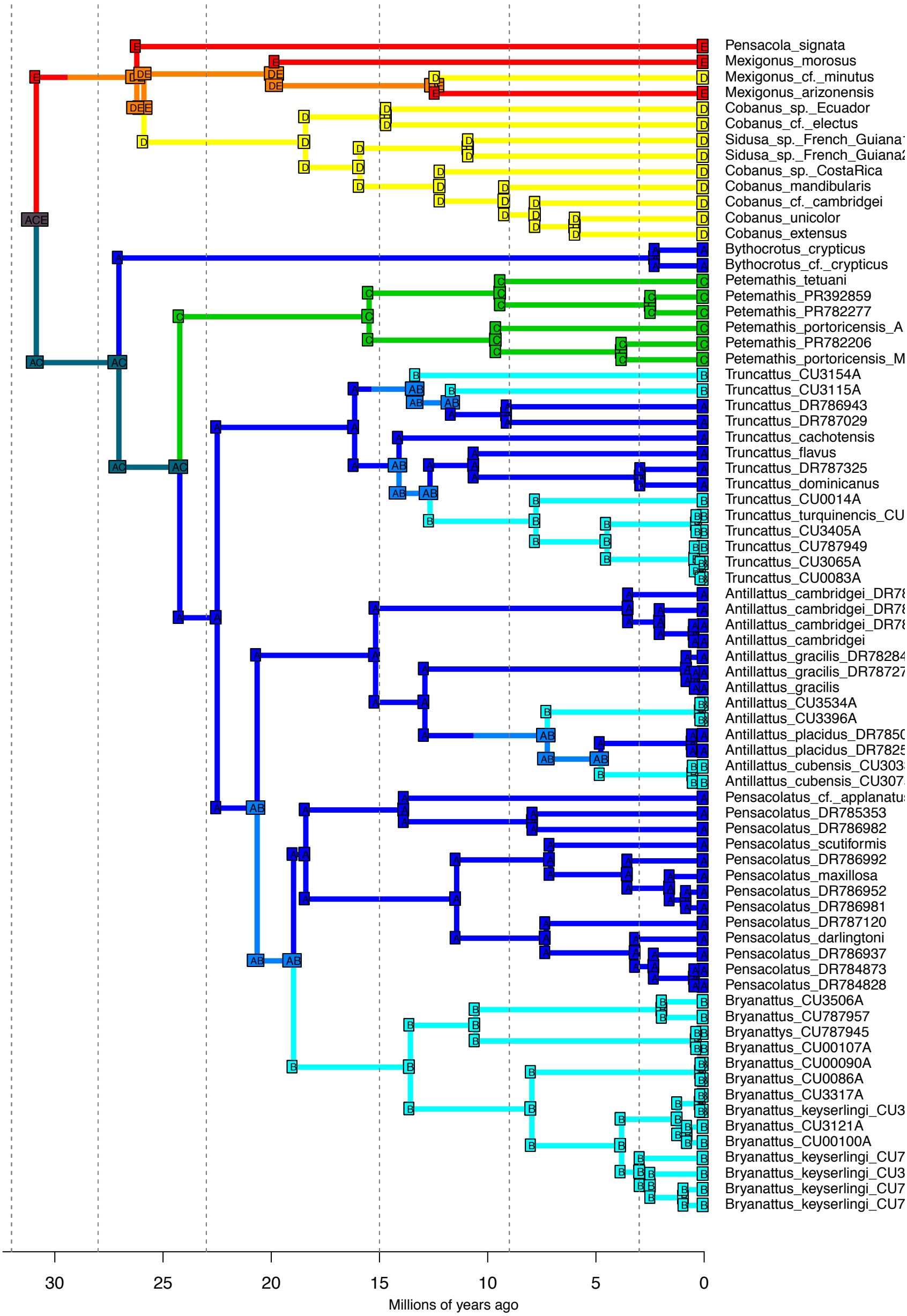

DEC_M3b_strat – Stochastic Map #39/50
ancstates: global optim, 5 areas max. d=0.0017; e=0; j=0; LnL=−50.93

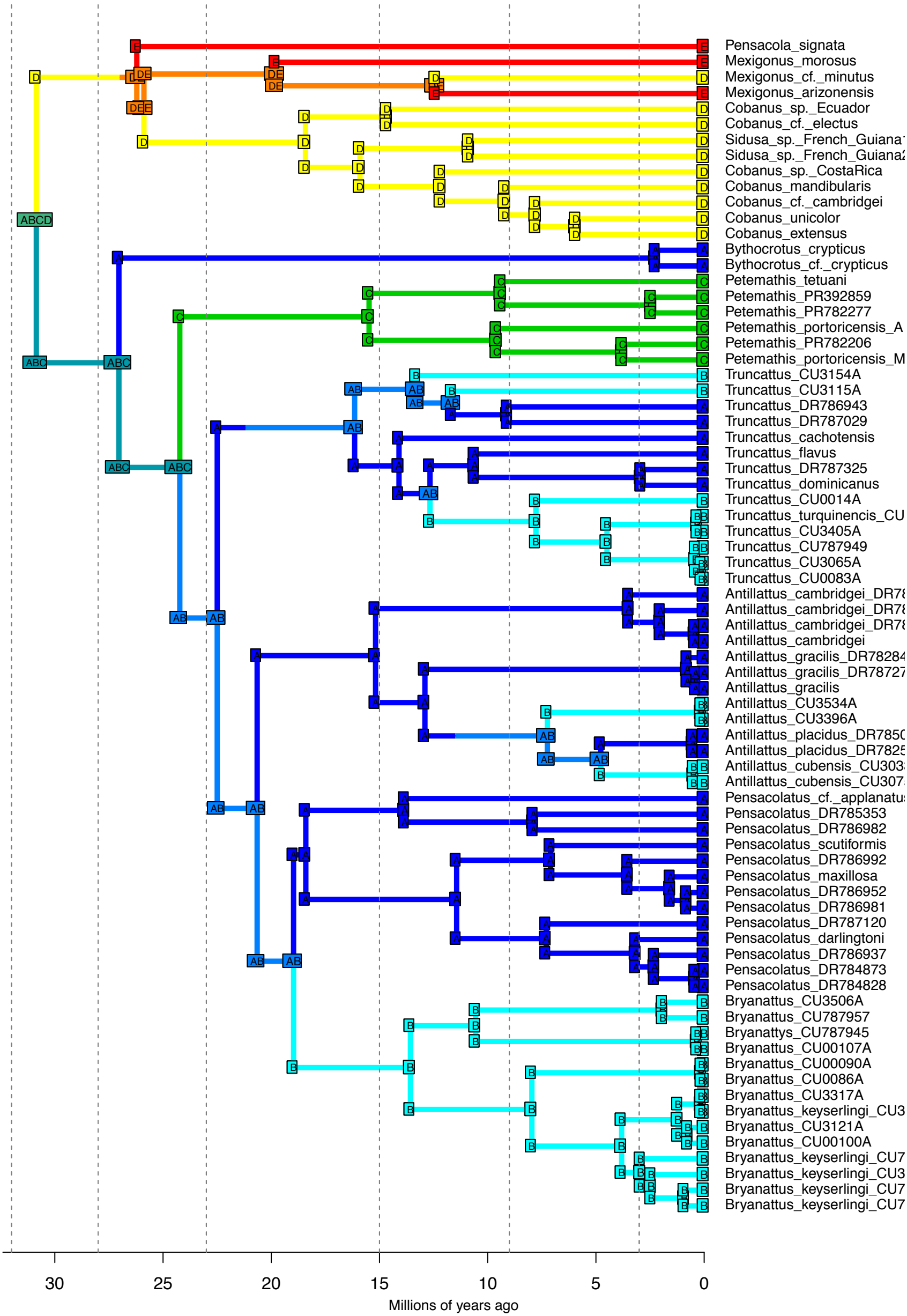

DEC_M3b_strat – Stochastic Map #40/50
ancstates: global optim, 5 areas max. d=0.0017; e=0; j=0; LnL=−50.93

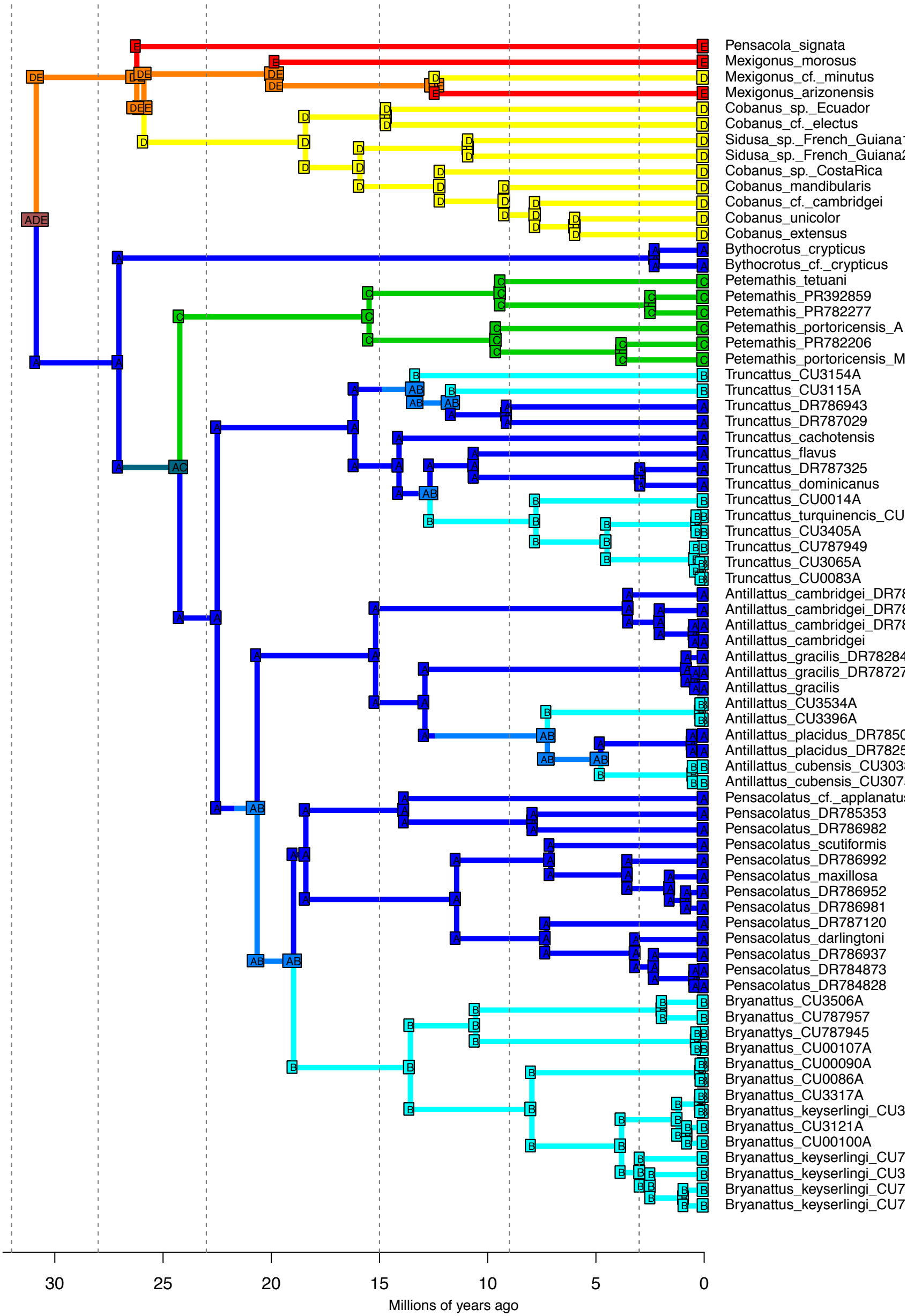

DEC_M3b_strat – Stochastic Map #41/50
ancstates: global optim, 5 areas max. d=0.0017; e=0; j=0; LnL=−50.93

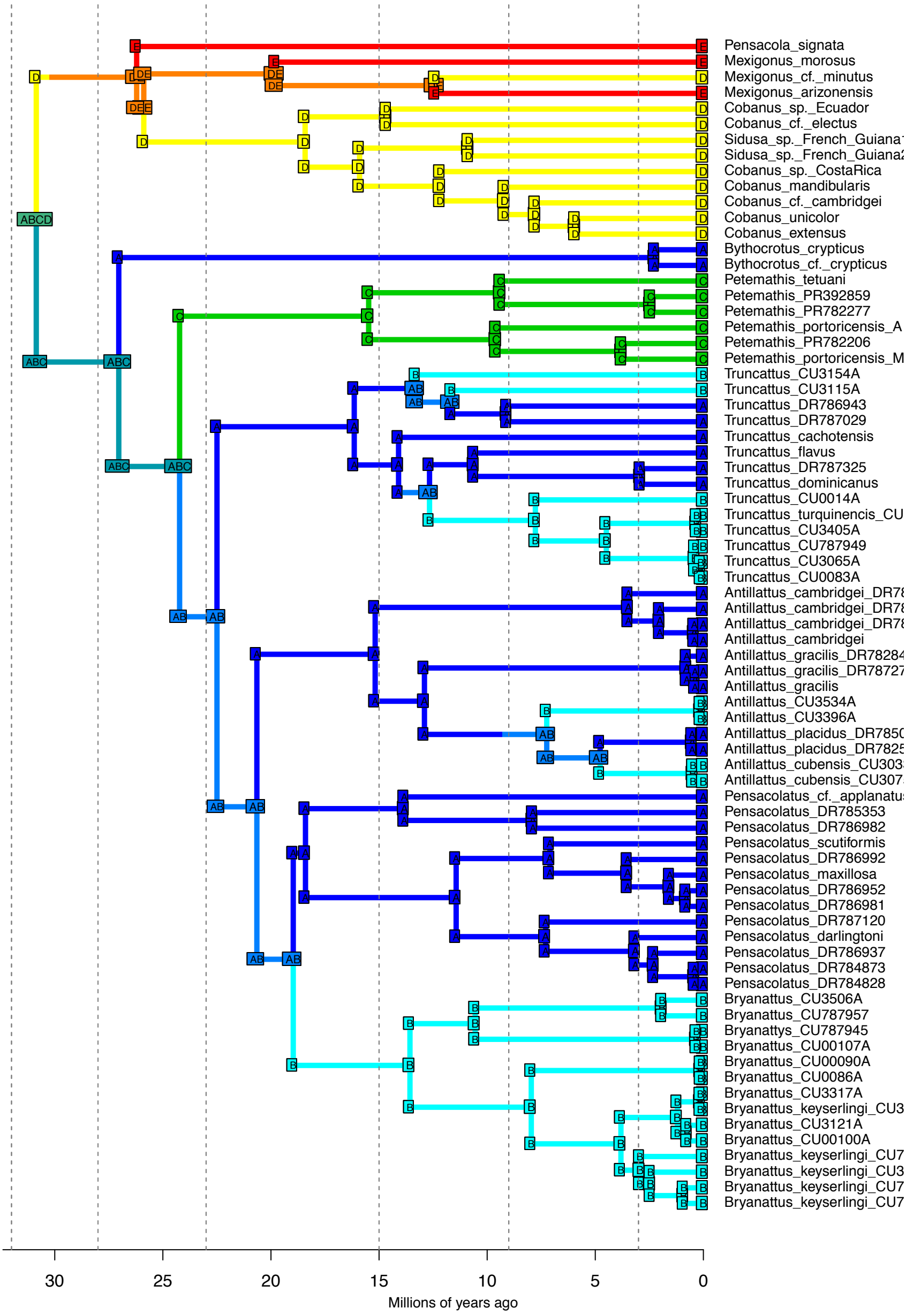

DEC_M3b_strat – Stochastic Map #42/50
ancstates: global optim, 5 areas max. d=0.0017; e=0; j=0; LnL=−50.93

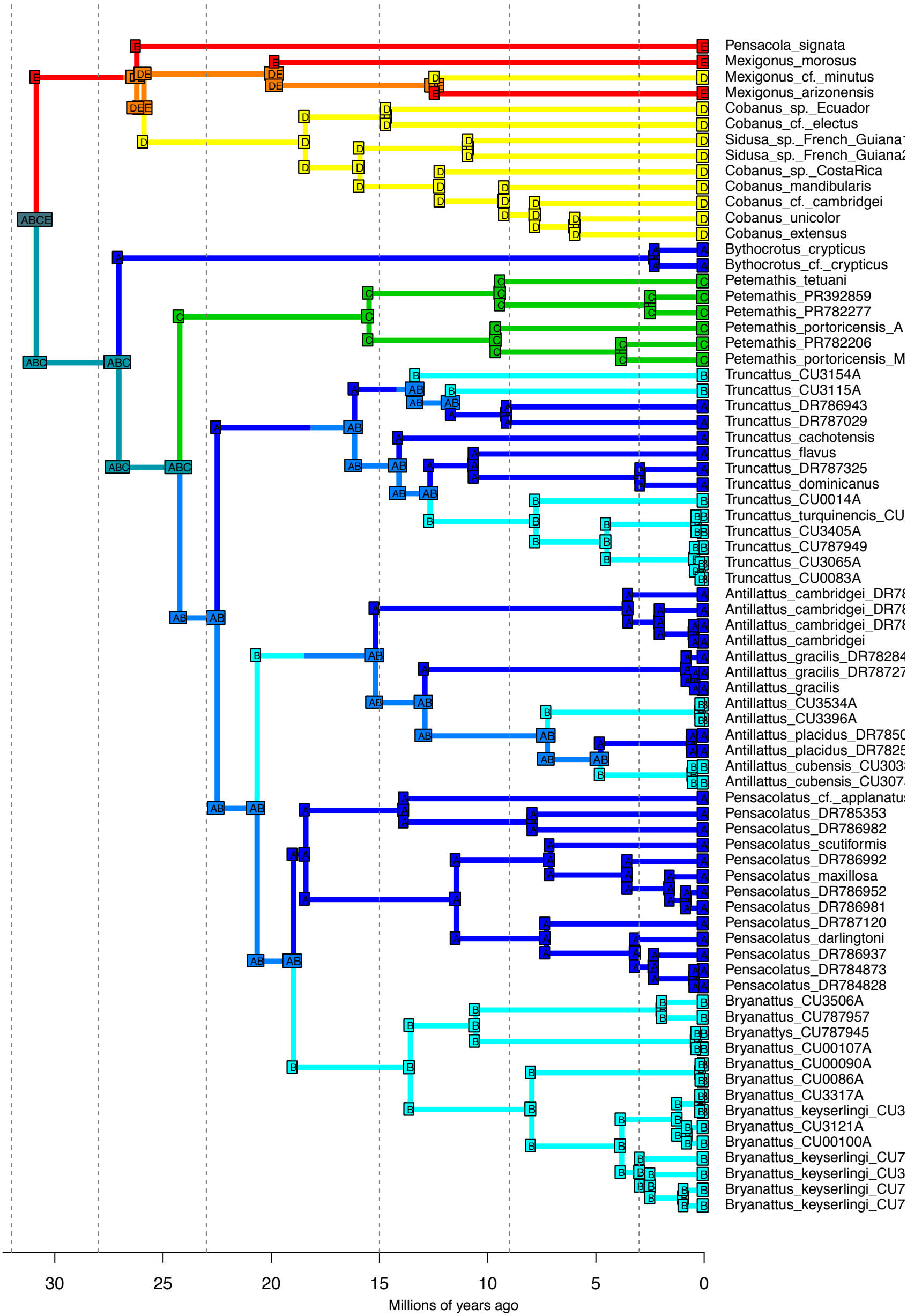

DEC_M3b_strat – Stochastic Map #43/50
ancstates: global optim, 5 areas max. d=0.0017; e=0; j=0; LnL=−50.93

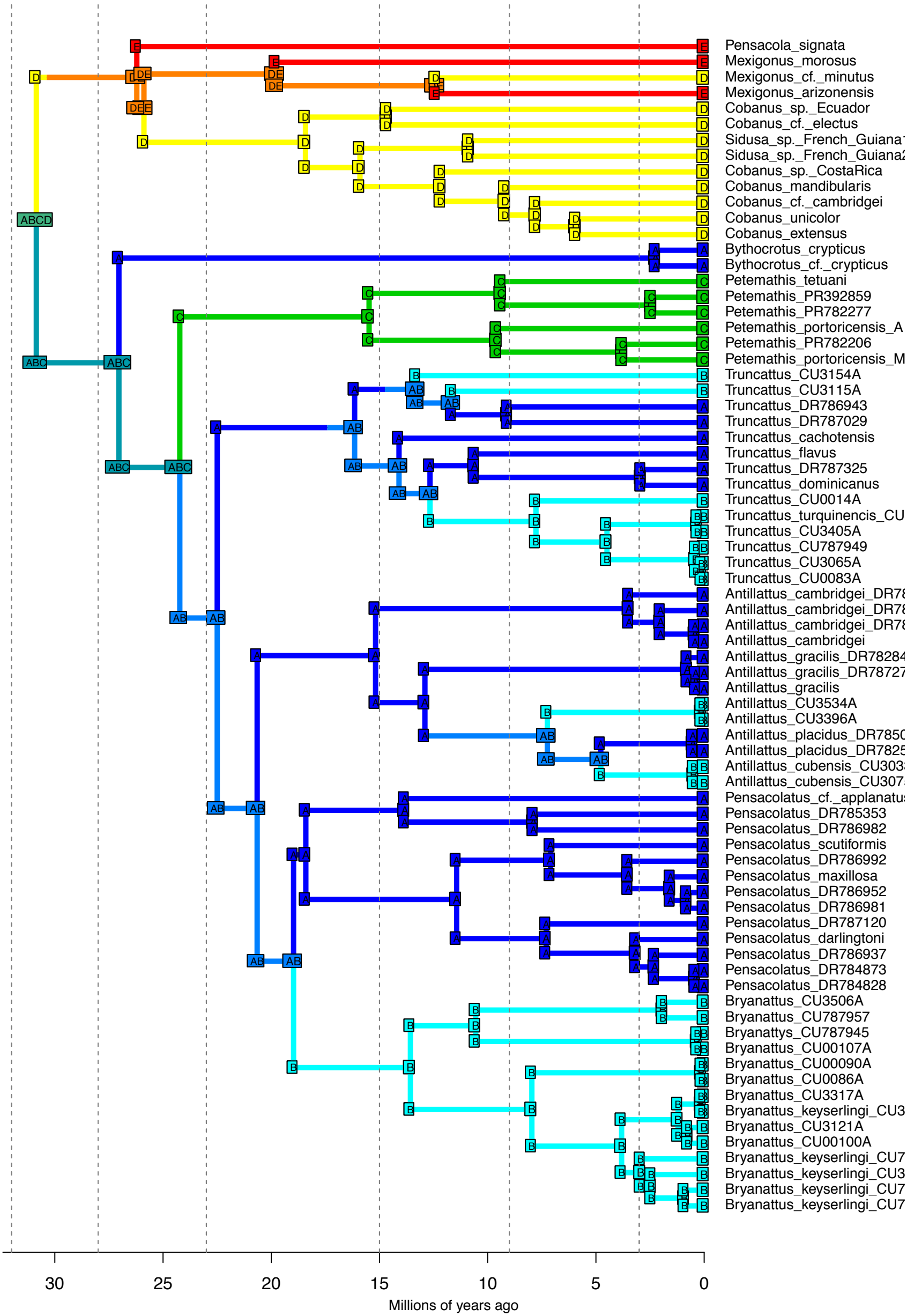

DEC_M3b_strat – Stochastic Map #44/50
ancstates: global optim, 5 areas max. d=0.0017; e=0; j=0; LnL=−50.93

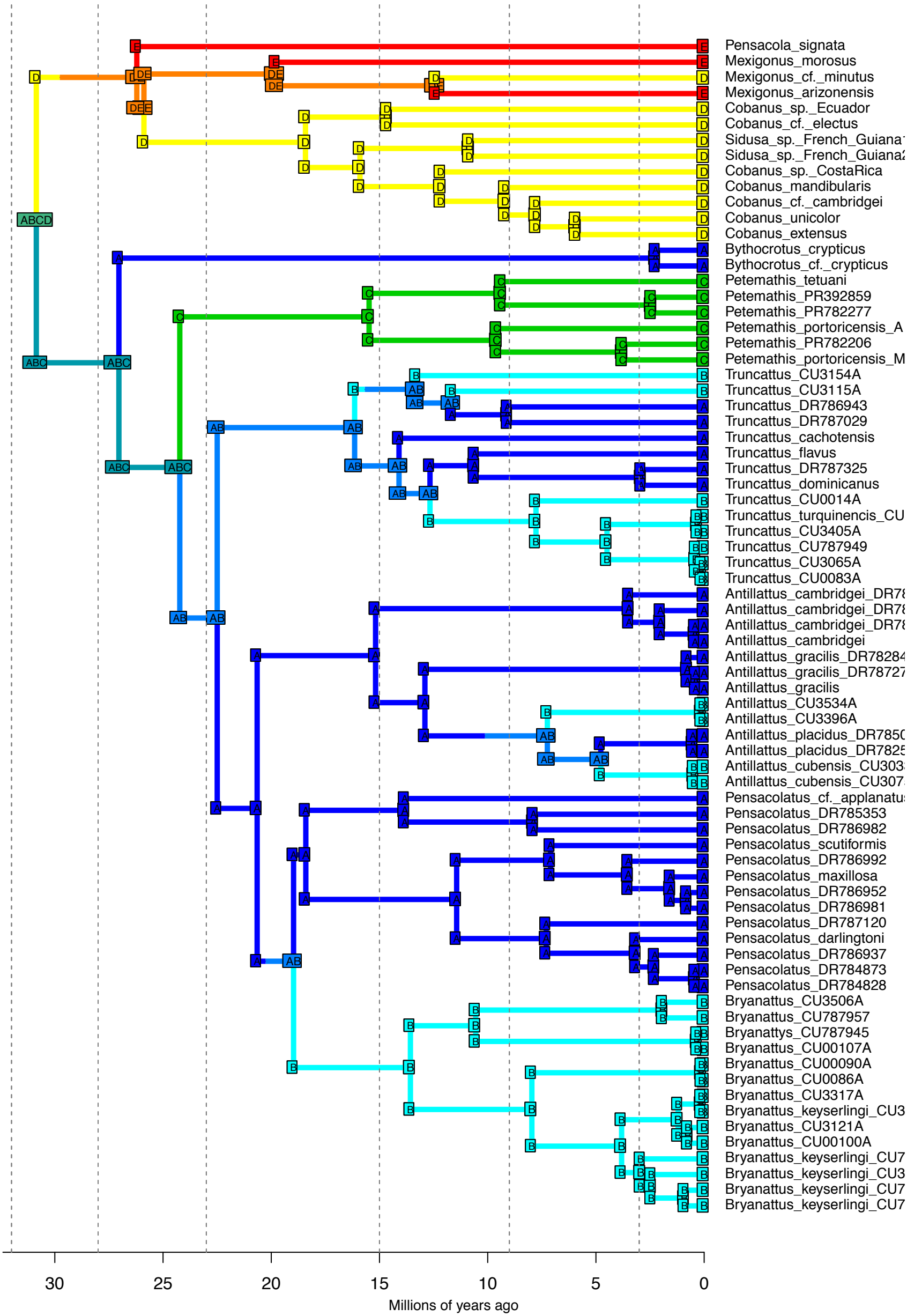

DEC_M3b_strat – Stochastic Map #45/50
ancstates: global optim, 5 areas max. d=0.0017; e=0; j=0; LnL=−50.93

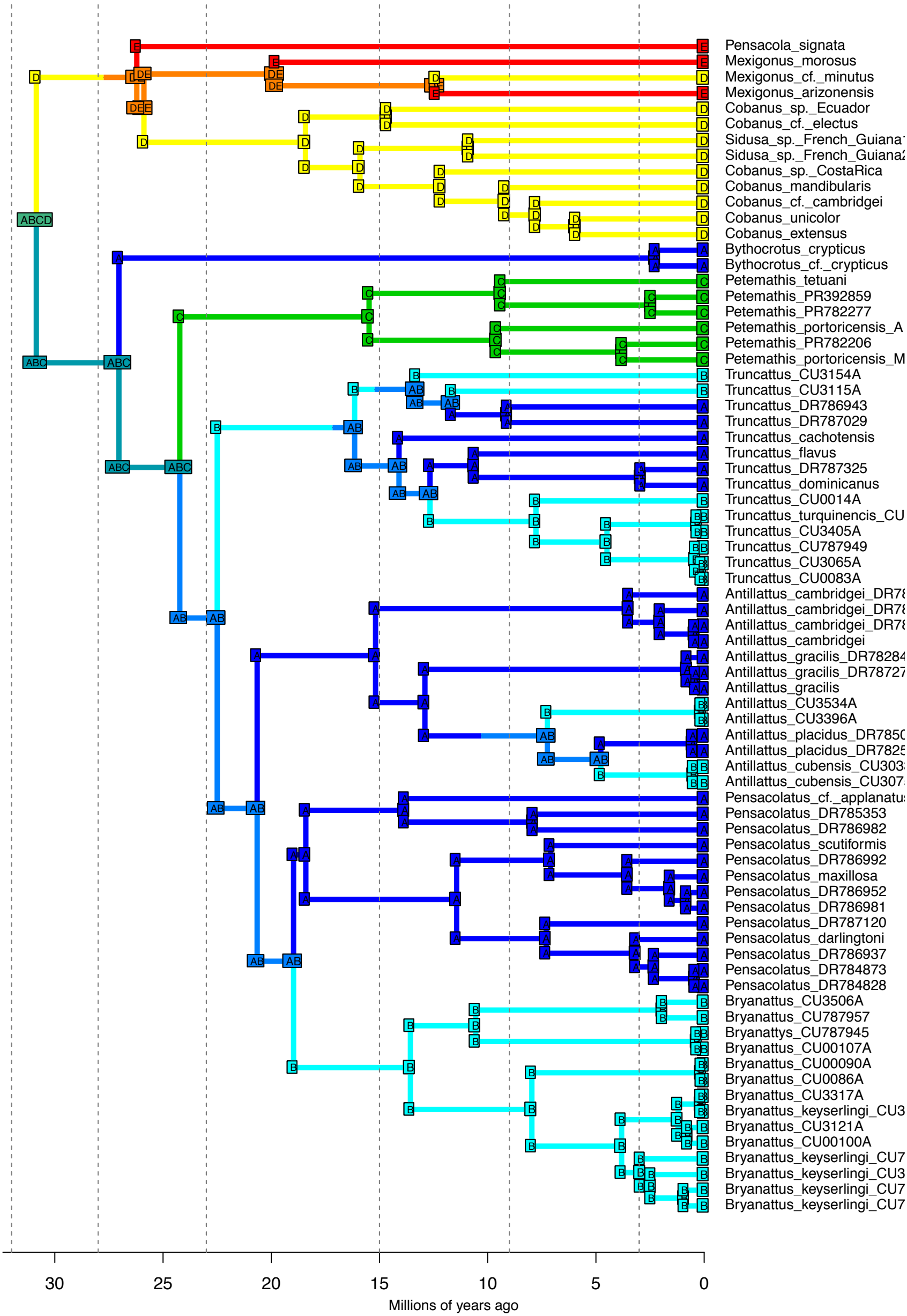

DEC_M3b_strat – Stochastic Map #46/50
ancstates: global optim, 5 areas max. d=0.0017; e=0; j=0; LnL=−50.93

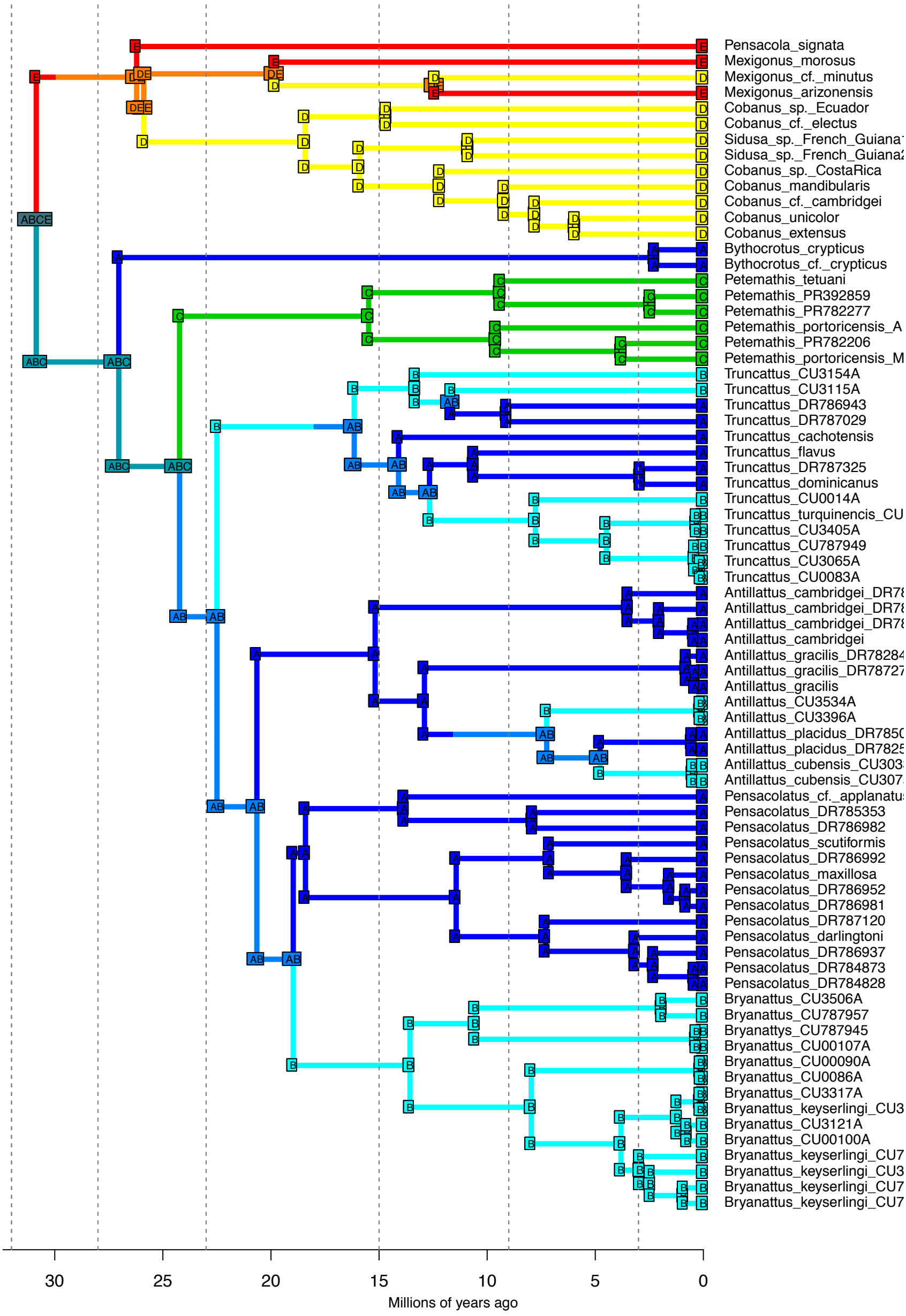

DEC_M3b_strat – Stochastic Map #47/50
ancstates: global optim, 5 areas max. d=0.0017; e=0; j=0; LnL=−50.93

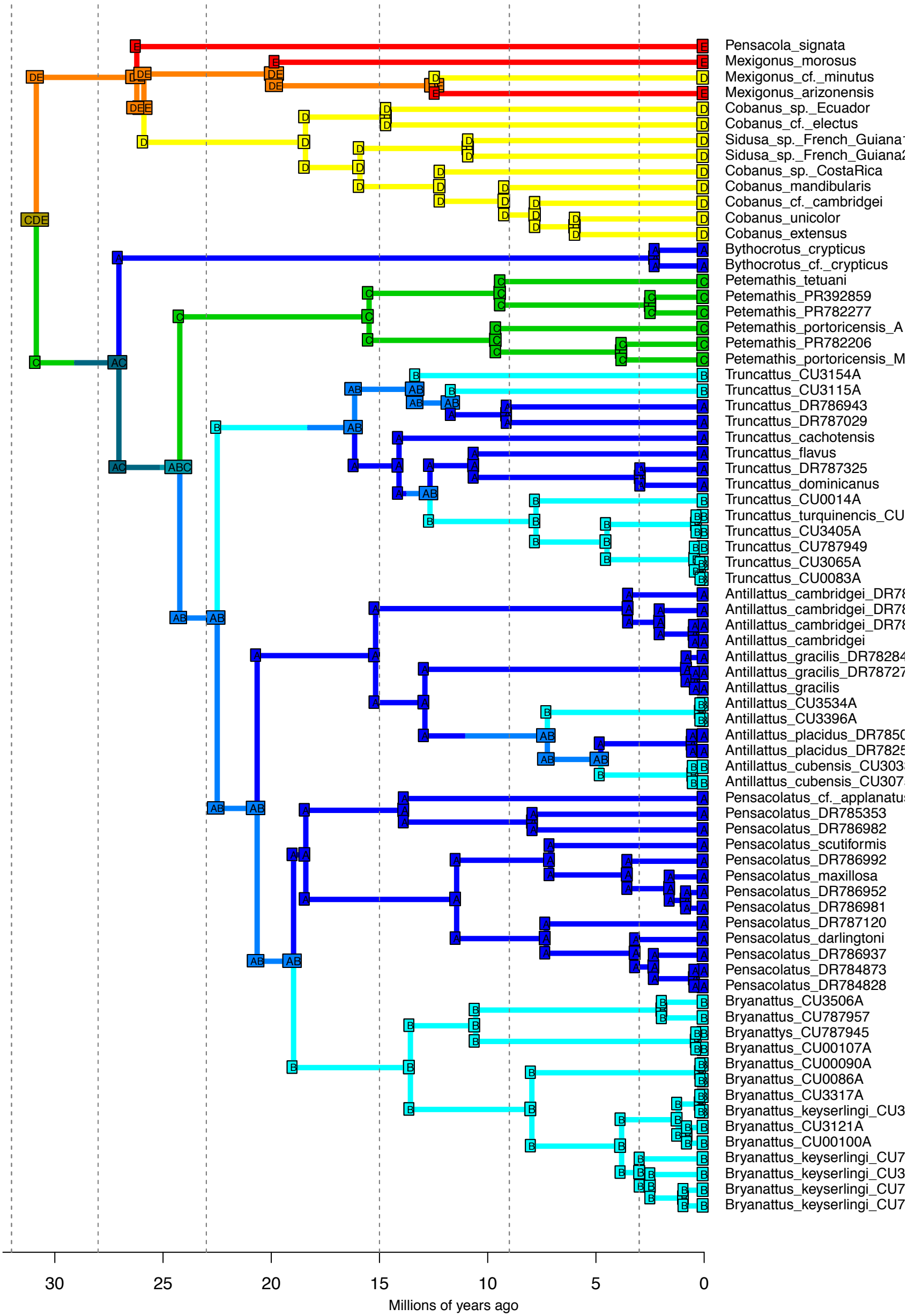

DEC_M3b_strat – Stochastic Map #48/50
ancstates: global optim, 5 areas max. d=0.0017; e=0; j=0; LnL=−50.93

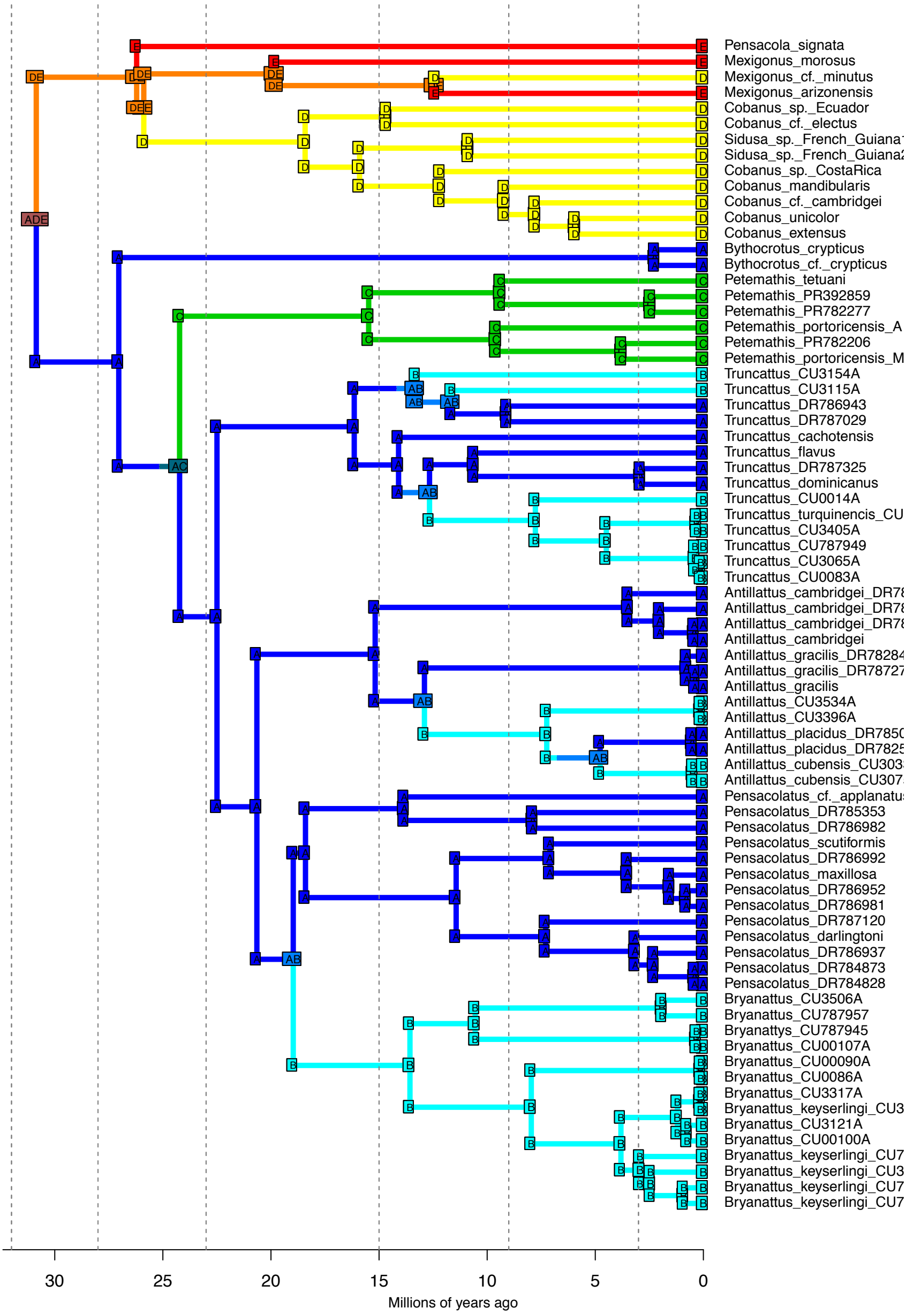

DEC_M3b_strat – Stochastic Map #49/50
ancstates: global optim, 5 areas max. d=0.0017; e=0; j=0; LnL=−50.93

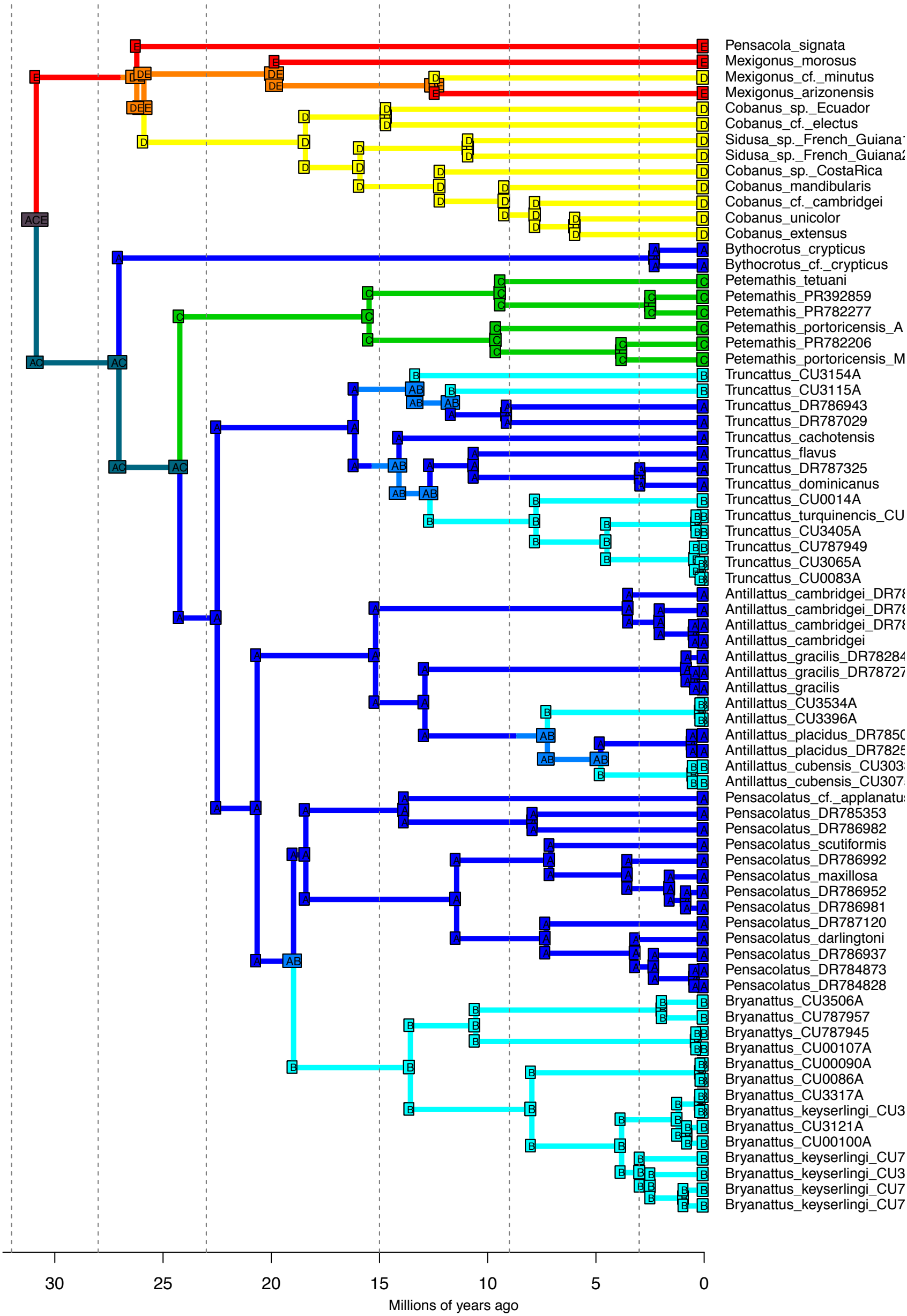

DEC_M3b_strat – Stochastic Map #50/50
ancstates: global optim, 5 areas max. d=0.0017; e=0; j=0; LnL=–50.93

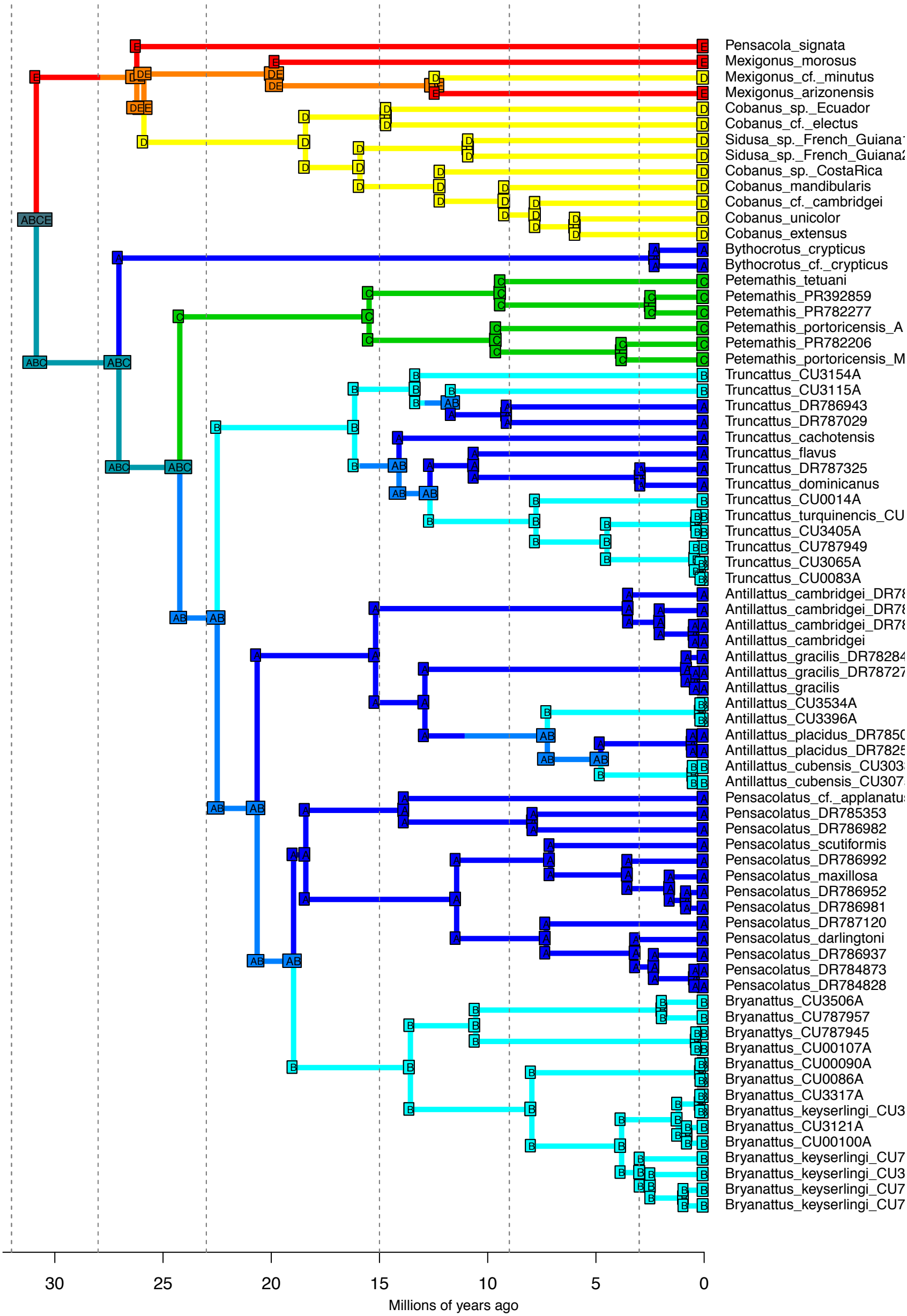

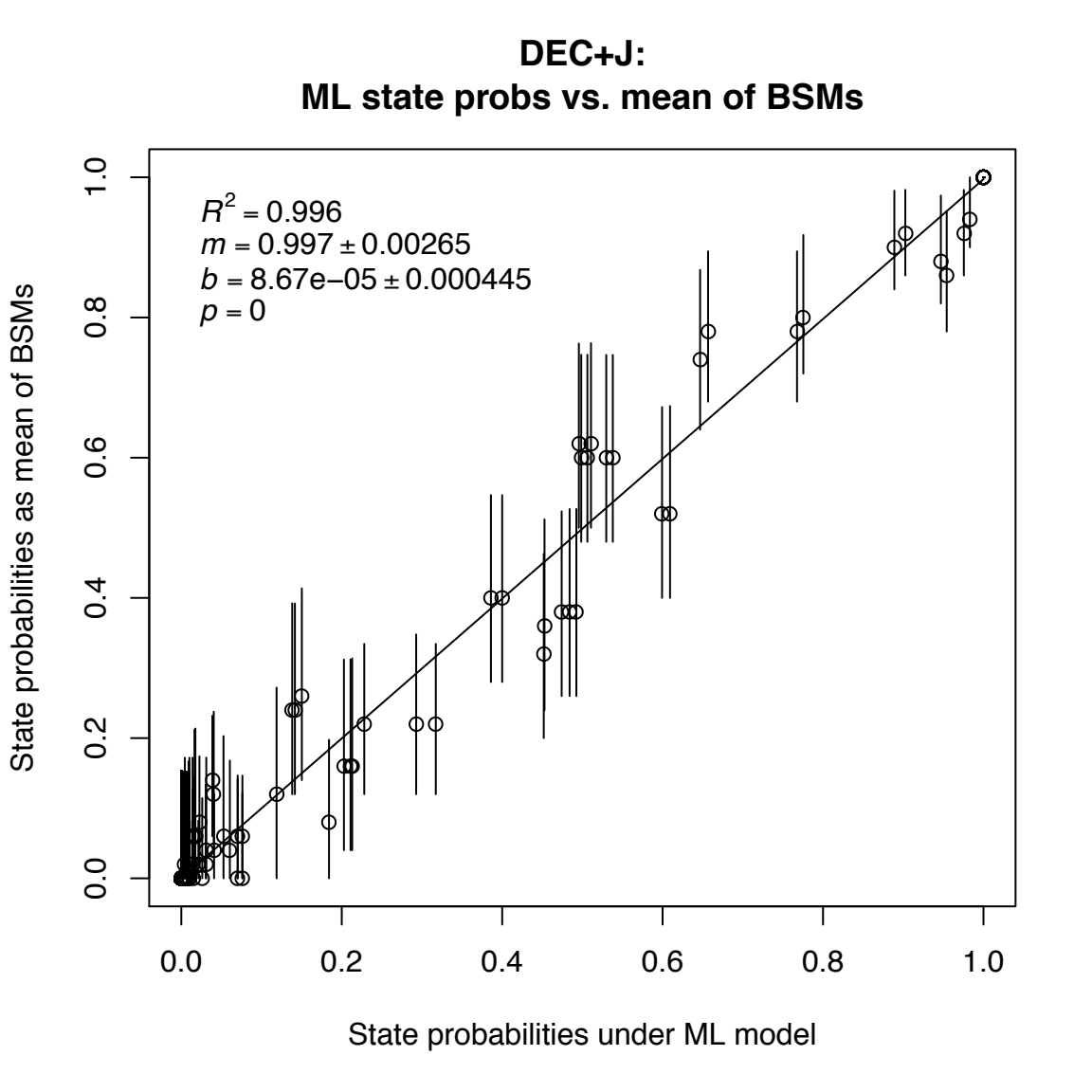
DEC+J:
ML state probs vs. mean of BSMs
$R^2 = 0.996$
$m = 0.997 \pm 0.00265$
$b = 8.67e{-}05 \pm 0.000445$
$p = 0$
State probabilities as mean of BSMs
State probabilities under ML model
0.0
0.2
0.4
0.6
0.8
1.0

DEC+J – Stochastic Map #1/50
ancstates: global optim, 5 areas max. d=0; e=0; j=0.0153; LnL=–44.20

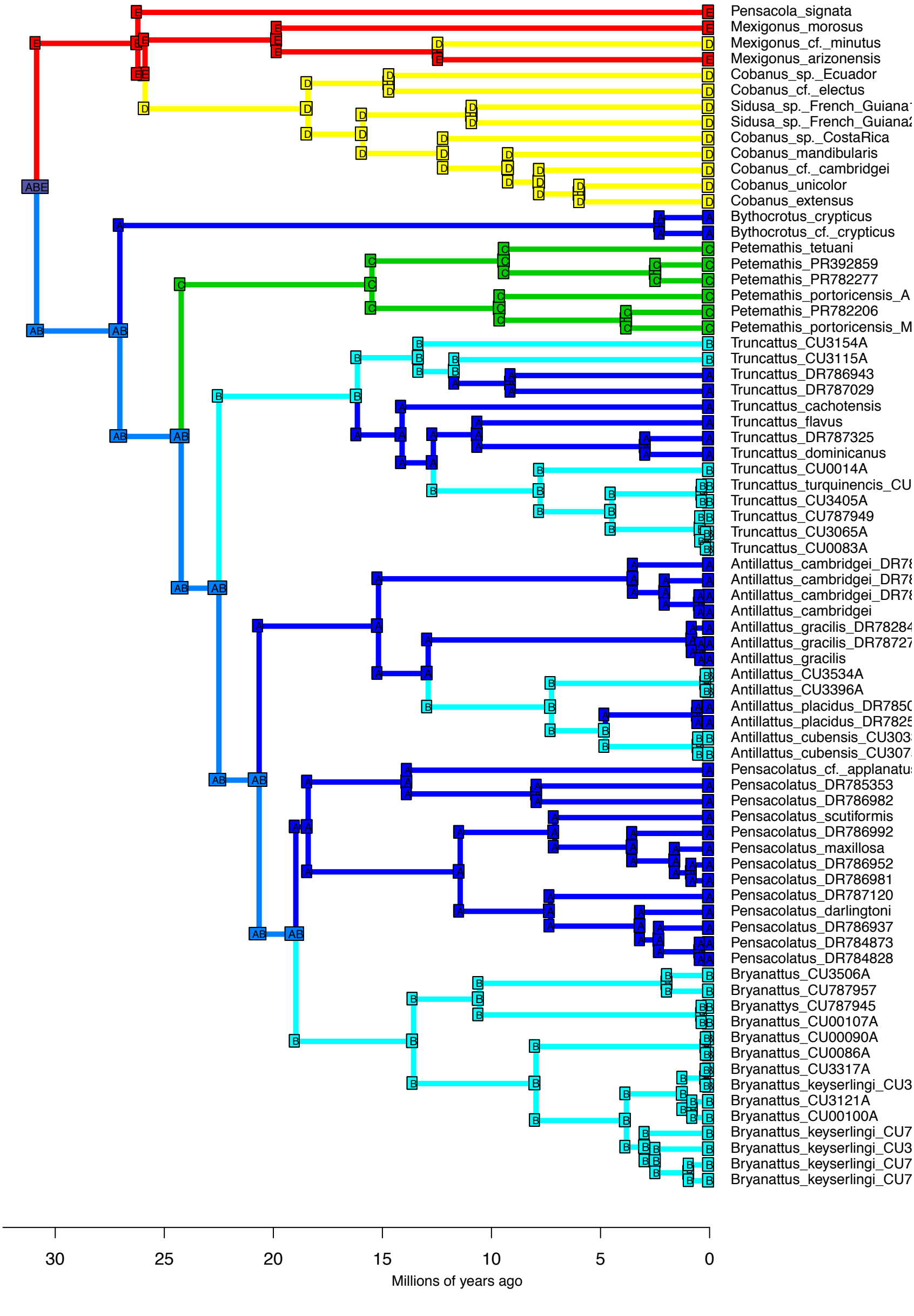

DEC+J – Stochastic Map #2/50
ancstates: global optim, 5 areas max. d=0; e=0; j=0.0153; LnL=–44.20

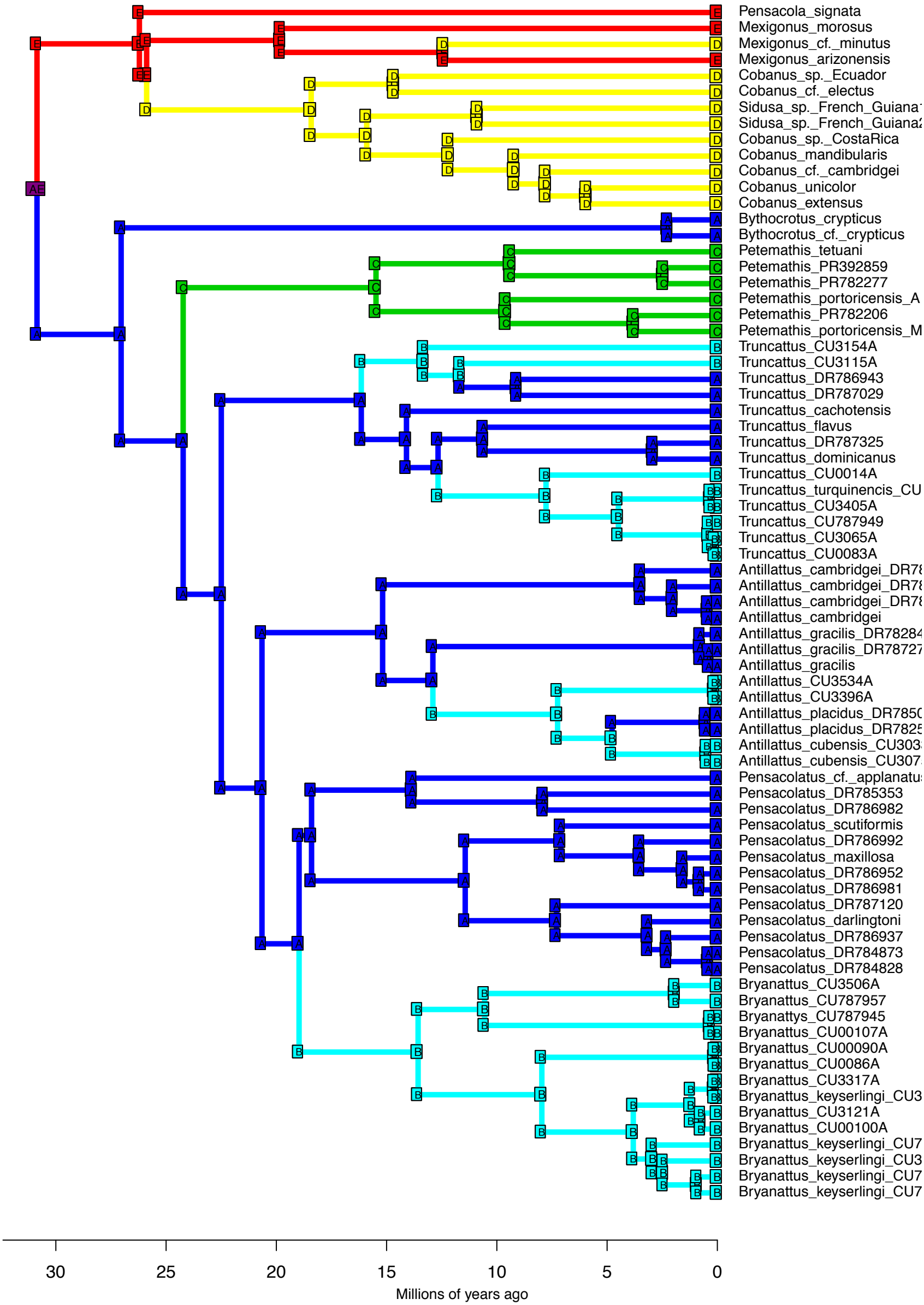

DEC+J – Stochastic Map #3/50
ancstates: global optim, 5 areas max. d=0; e=0; j=0.0153; LnL=–44.20

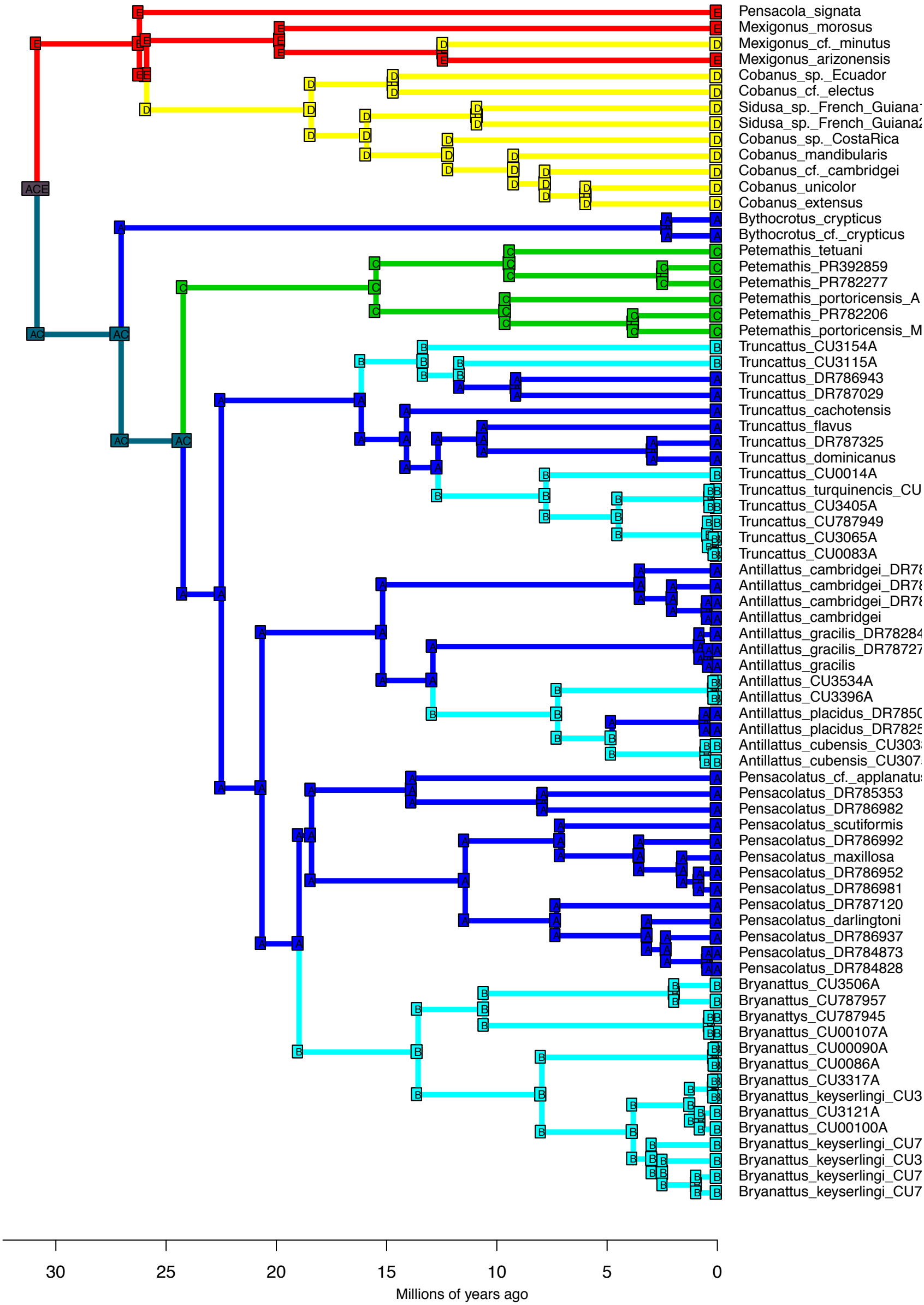

DEC+J – Stochastic Map #4/50
ancstates: global optim, 5 areas max. d=0; e=0; j=0.0153; LnL=–44.20

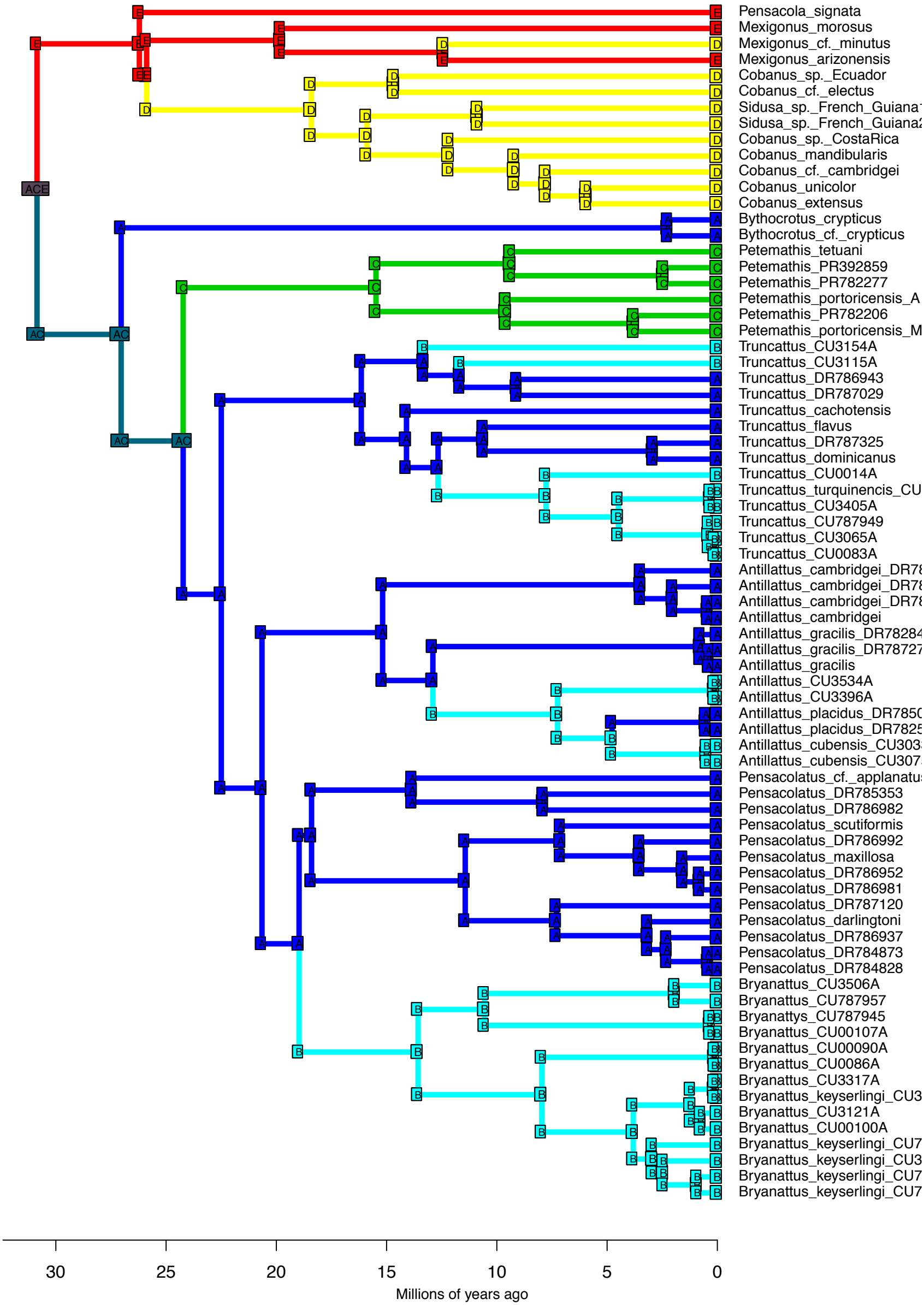

DEC+J – Stochastic Map #5/50
ancstates: global optim, 5 areas max. d=0; e=0; j=0.0153; LnL=–44.20

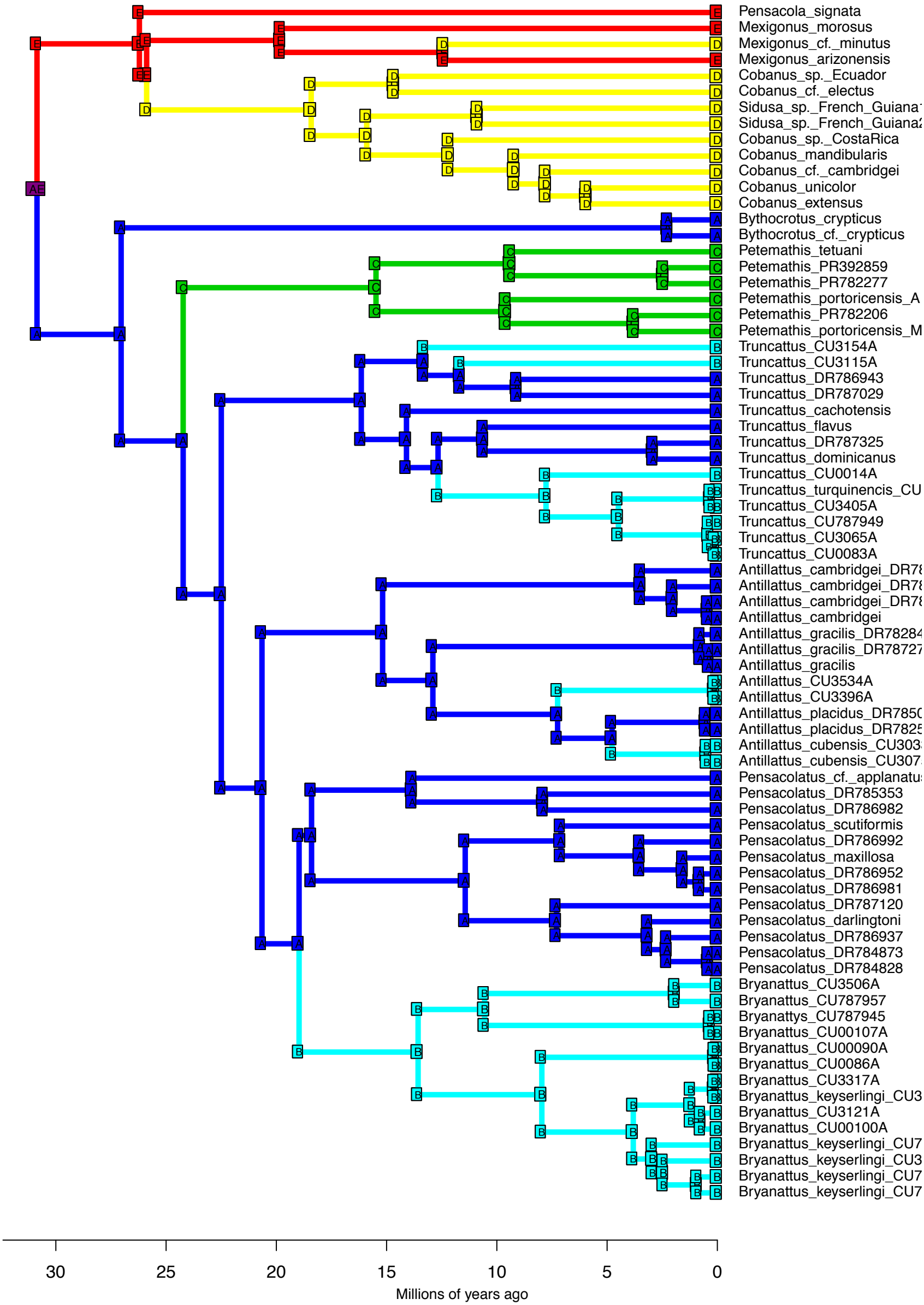

DEC+J – Stochastic Map #6/50
ancstates: global optim, 5 areas max. d=0; e=0; j=0.0153; LnL=–44.20

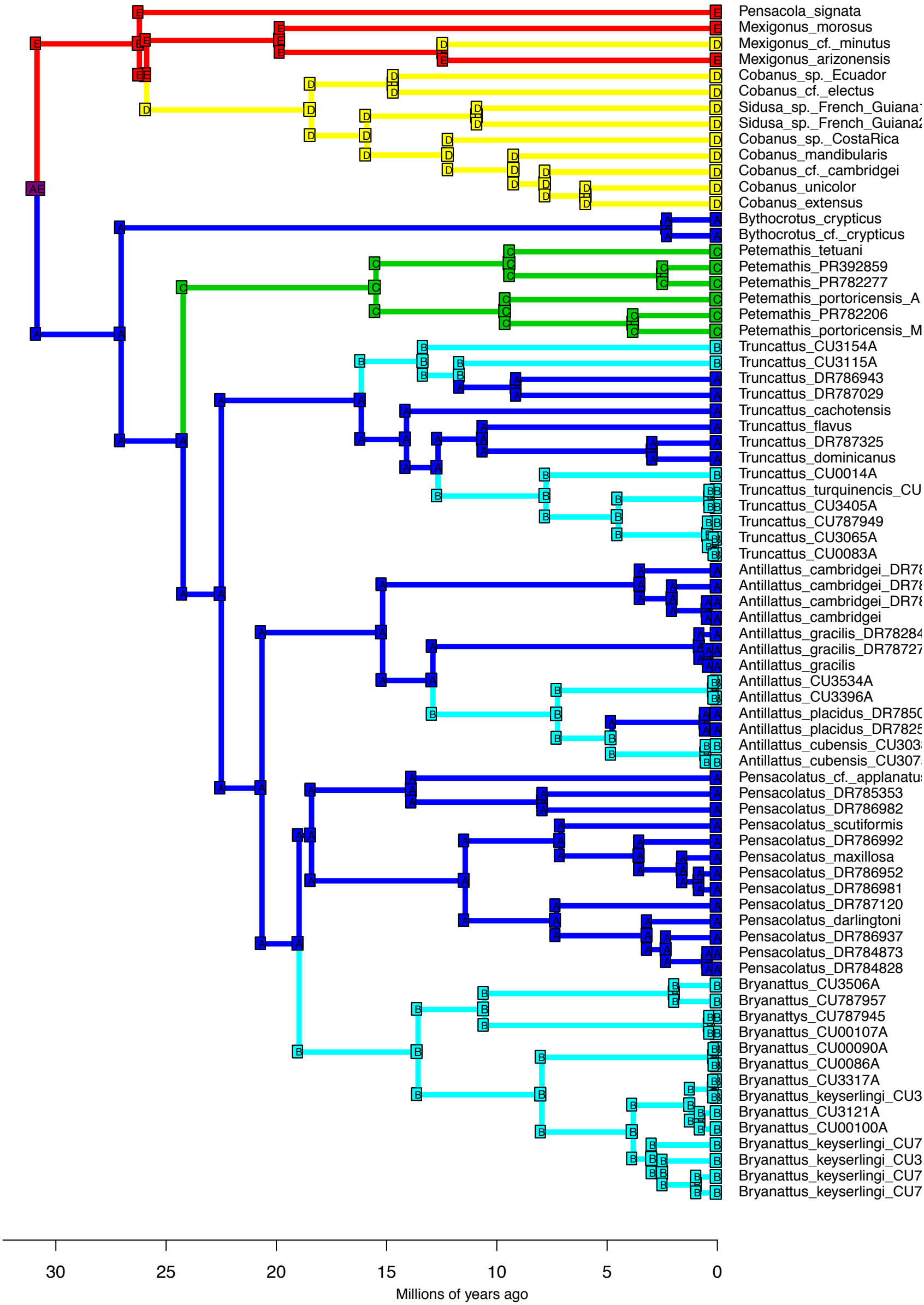

DEC+J – Stochastic Map #7/50
ancstates: global optim, 5 areas max. d=0; e=0; j=0.0153; LnL=–44.20

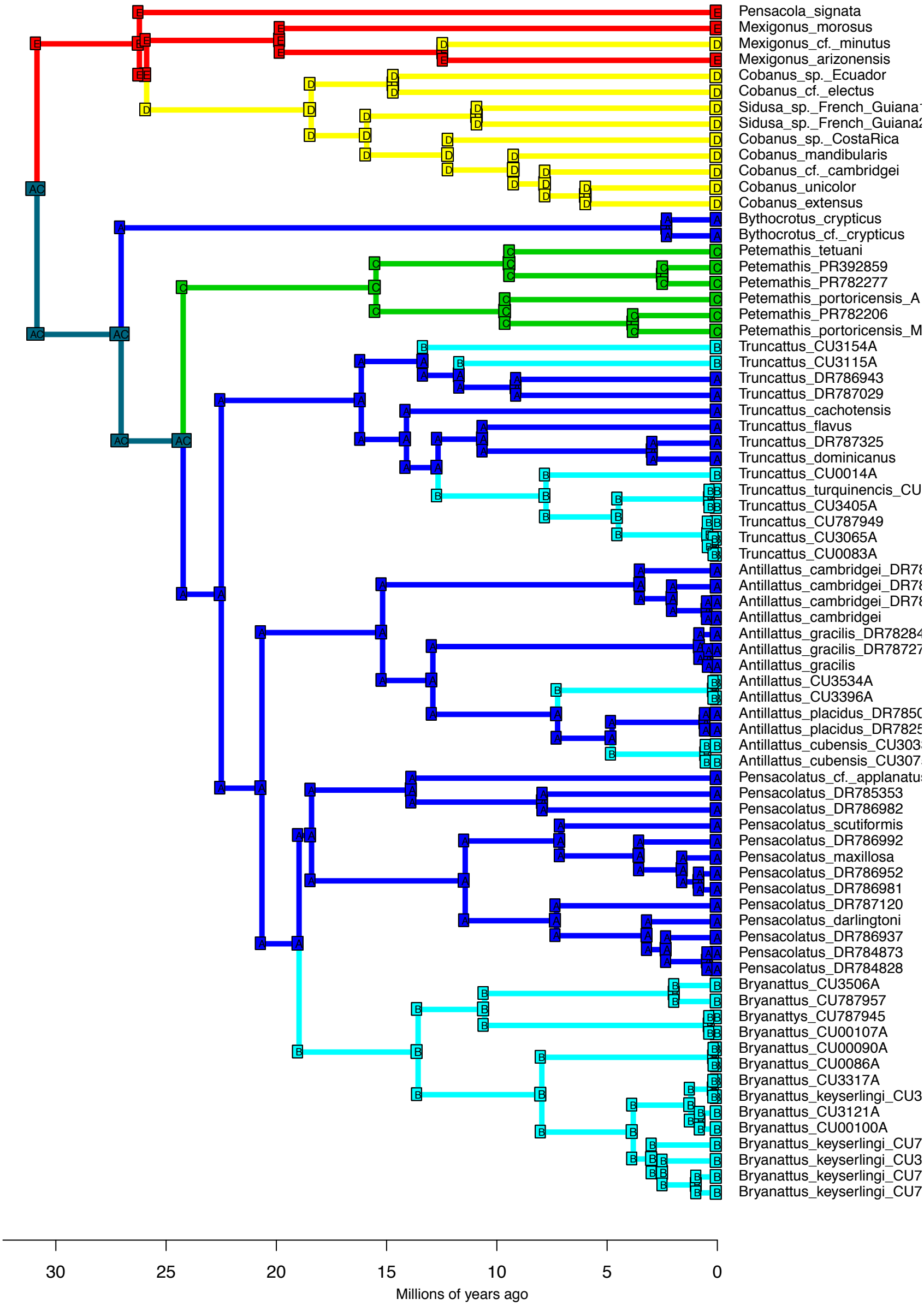

DEC+J – Stochastic Map #8/50
ancstates: global optim, 5 areas max. d=0; e=0; j=0.0153; LnL=–44.20

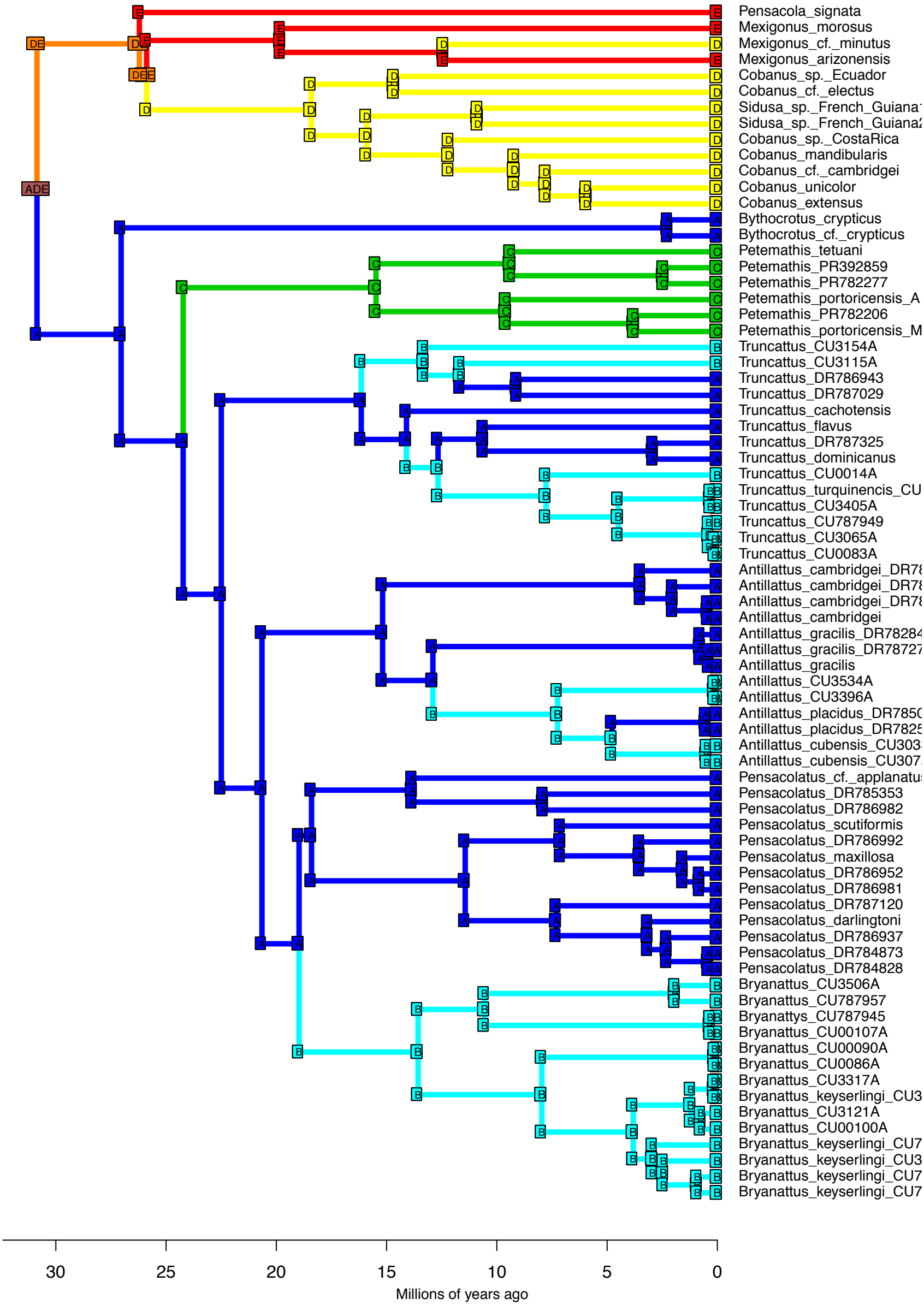

DEC+J – Stochastic Map #9/50
ancstates: global optim, 5 areas max. d=0; e=0; j=0.0153; LnL=−44.20

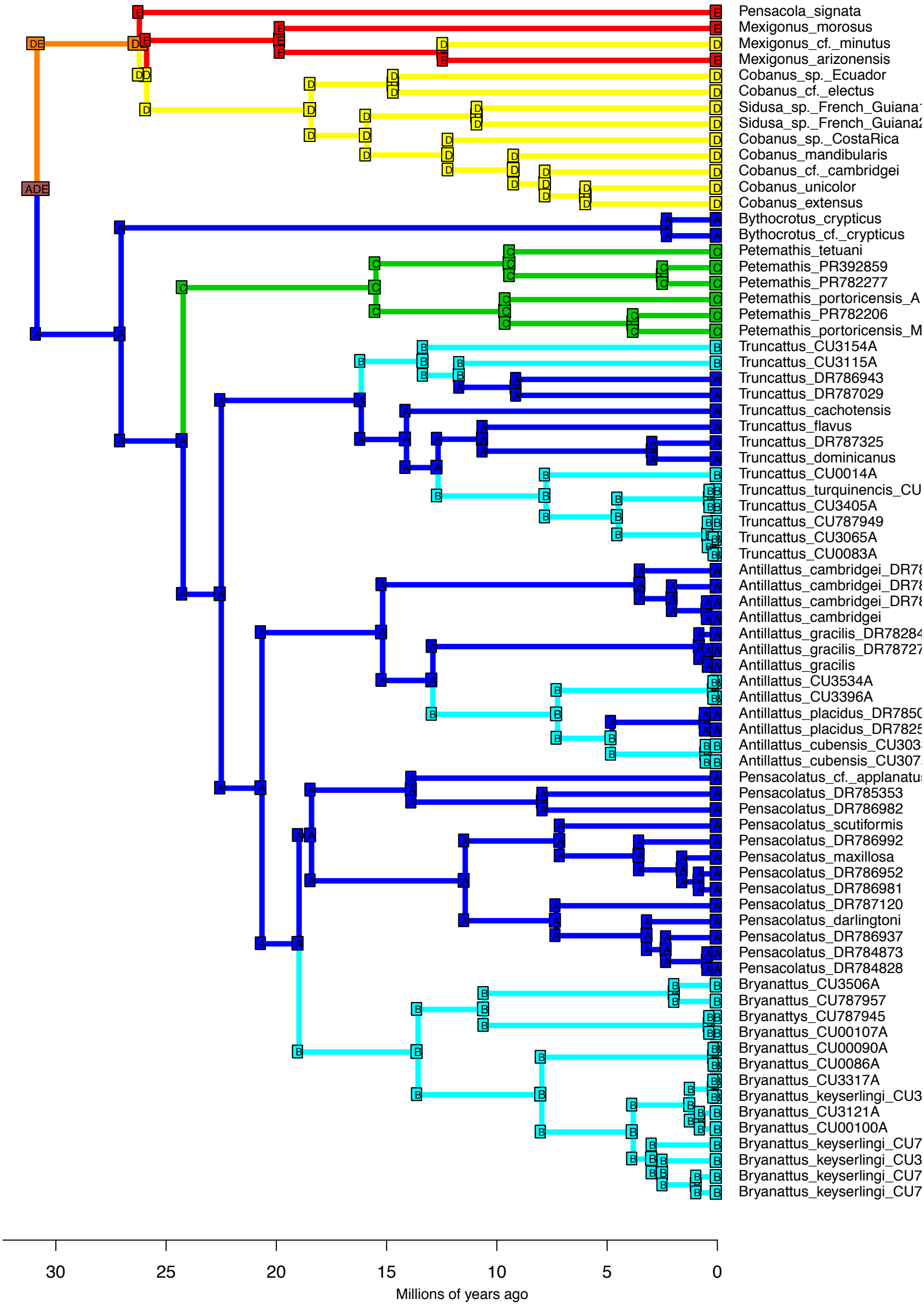

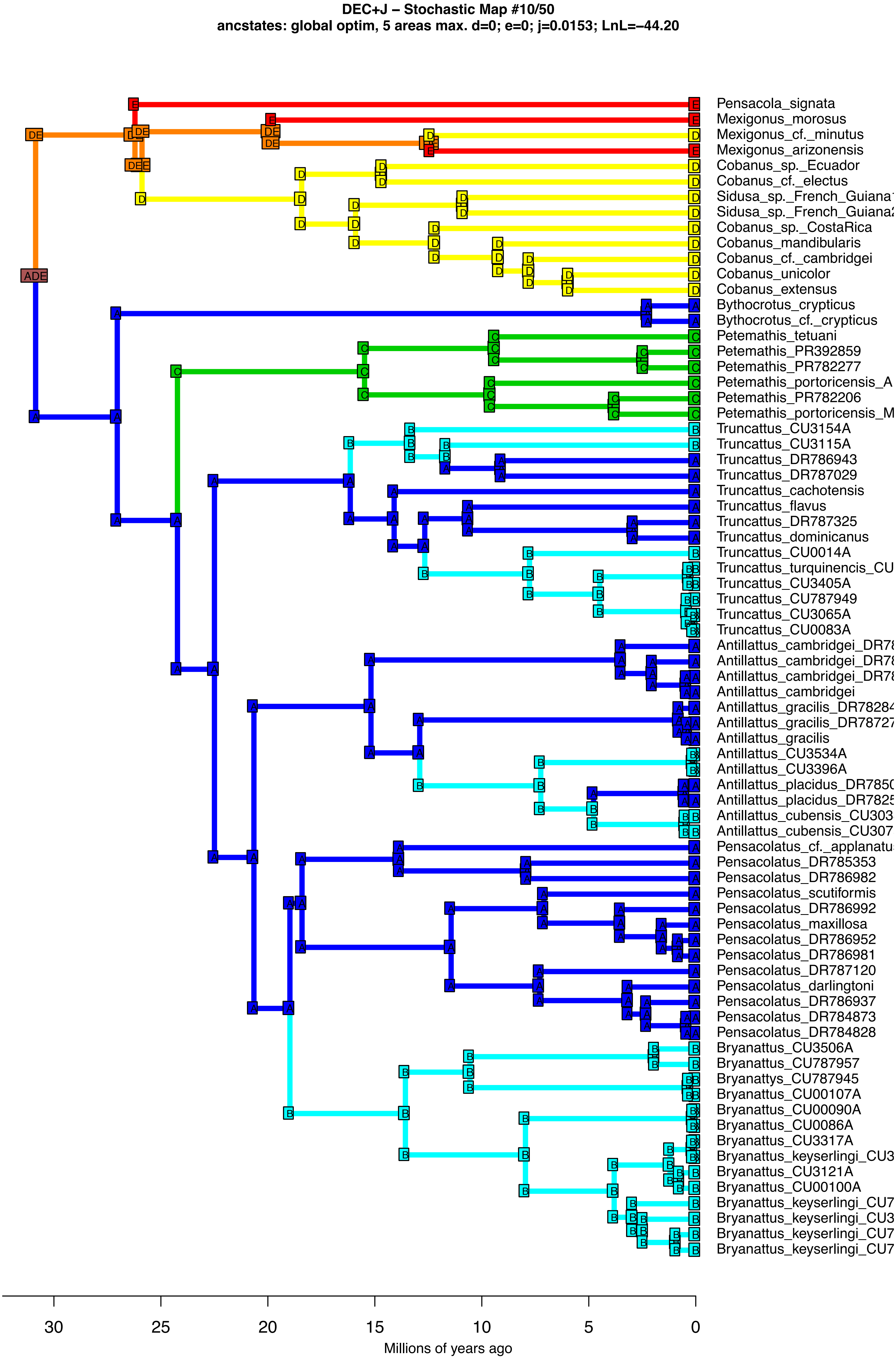
DEC+J – Stochastic Map #10/50
ancstates: global optim, 5 areas max. d=0; e=0; j=0.0153; LnL=–44.20
Pensacola_signata
Mexigonus_morosus
Mexigonus_cf._minutus
Mexigonus_arizonensis
Cobanus_sp._Ecuador
Cobanus_cf._electus
Sidusa_sp._French_Guiana
Sidusa_sp._French_Guiana
Cobanus_sp._CostaRica
Cobanus_mandibularis
Cobanus_cf._cambridgei
Cobanus_unicolor
Cobanus_extensus
Bythocrotus_crypticus
Bythocrotus_cf._crypticus
Petemathis_tetuani
Petemathis_PR392859
Petemathis_PR782277
Petemathis_portoricensis_A
Petemathis_PR782206
Petemathis_portoricensis_M
Truncattus_CU3154A
Truncattus_CU3115A
Truncattus_DR786943
Truncattus_DR787029
Truncattus_cachotensis
Truncattus_flavus
Truncattus_DR787325
Truncattus_dominicanus
Truncattus_CU0014A
Truncattus_turquinencis_CU
Truncattus_CU3405A
Truncattus_CU787949
Truncattus_CU3065A
Truncattus_CU0083A
Antillattus_cambridgei_DR7
Antillattus_cambridgei_DR7
Antillattus_cambridgei_DR7
Antillattus_cambridgei
Antillattus_gracilis_DR7828
Antillattus_gracilis_DR7872
Antillattus_gracilis
Antillattus_CU3534A
Antillattus_CU3396A
Antillattus_placidus_DR785
Antillattus_placidus_DR782
Antillattus_cubensis_CU303
Antillattus_cubensis_CU307
Pensacolatus_cf._applanatu
Pensacolatus_DR785353
Pensacolatus_DR786982
Pensacolatus_scutiformis
Pensacolatus_DR786992
Pensacolatus_maxillosa
Pensacolatus_DR786952
Pensacolatus_DR786981
Pensacolatus_DR787120
Pensacolatus_darlingtoni
Pensacolatus_DR786937
Pensacolatus_DR784873
Pensacolatus_DR784828
Bryanattus_CU3506A
Bryanattus_CU787957
Bryanattys_CU787945
Bryanattus_CU00107A
Bryanattus_CU00090A
Bryanattus_CU0086A
Bryanattus_CU3317A
Bryanattus_keyserlingi_CU3
Bryanattus_CU3121A
Bryanattus_CU00100A
Bryanattus_keyserlingi_CU7
Bryanattus_keyserlingi_CU3
Bryanattus_keyserlingi_CU7
Bryanattus_keyserlingi_CU7
30
25
20
15
10
5
0
Millions of years ago

DEC+J – Stochastic Map #11/50
ancstates: global optim, 5 areas max. d=0; e=0; j=0.0153; LnL=−44.20

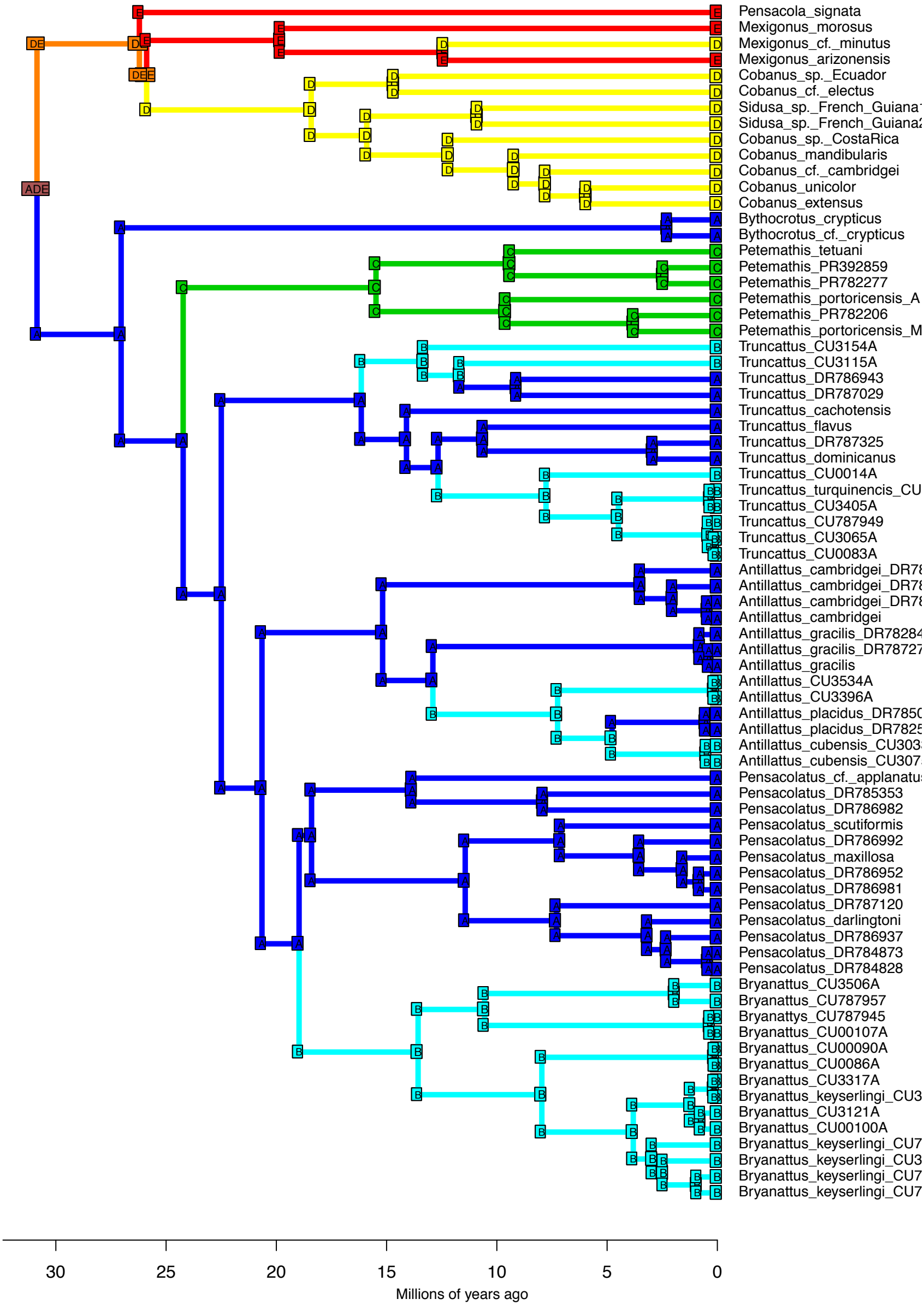

DEC+J – Stochastic Map #12/50
ancstates: global optim, 5 areas max. d=0; e=0; j=0.0153; LnL=−44.20

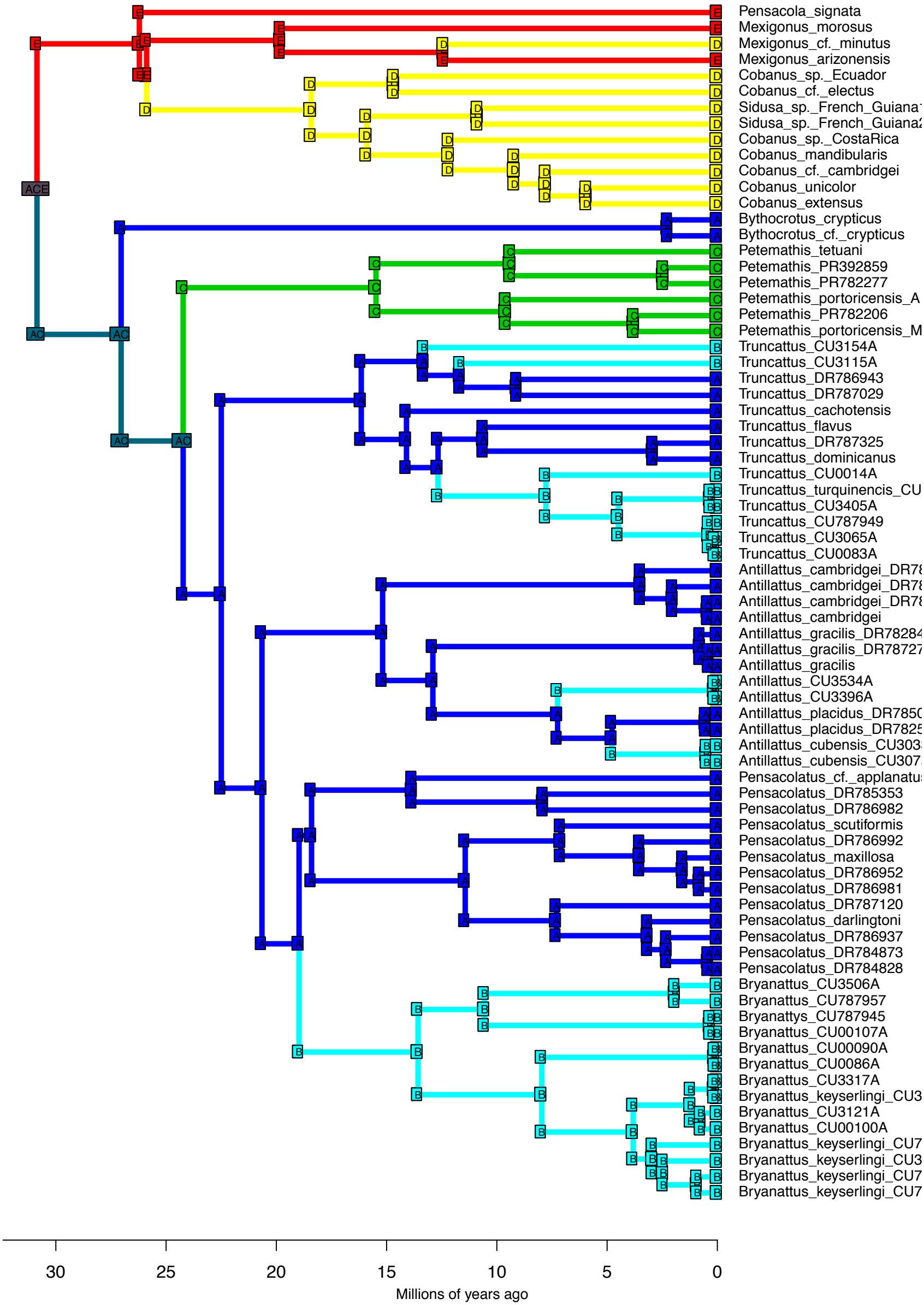

DEC+J – Stochastic Map #13/50
ancstates: global optim, 5 areas max. d=0; e=0; j=0.0153; LnL=−44.20

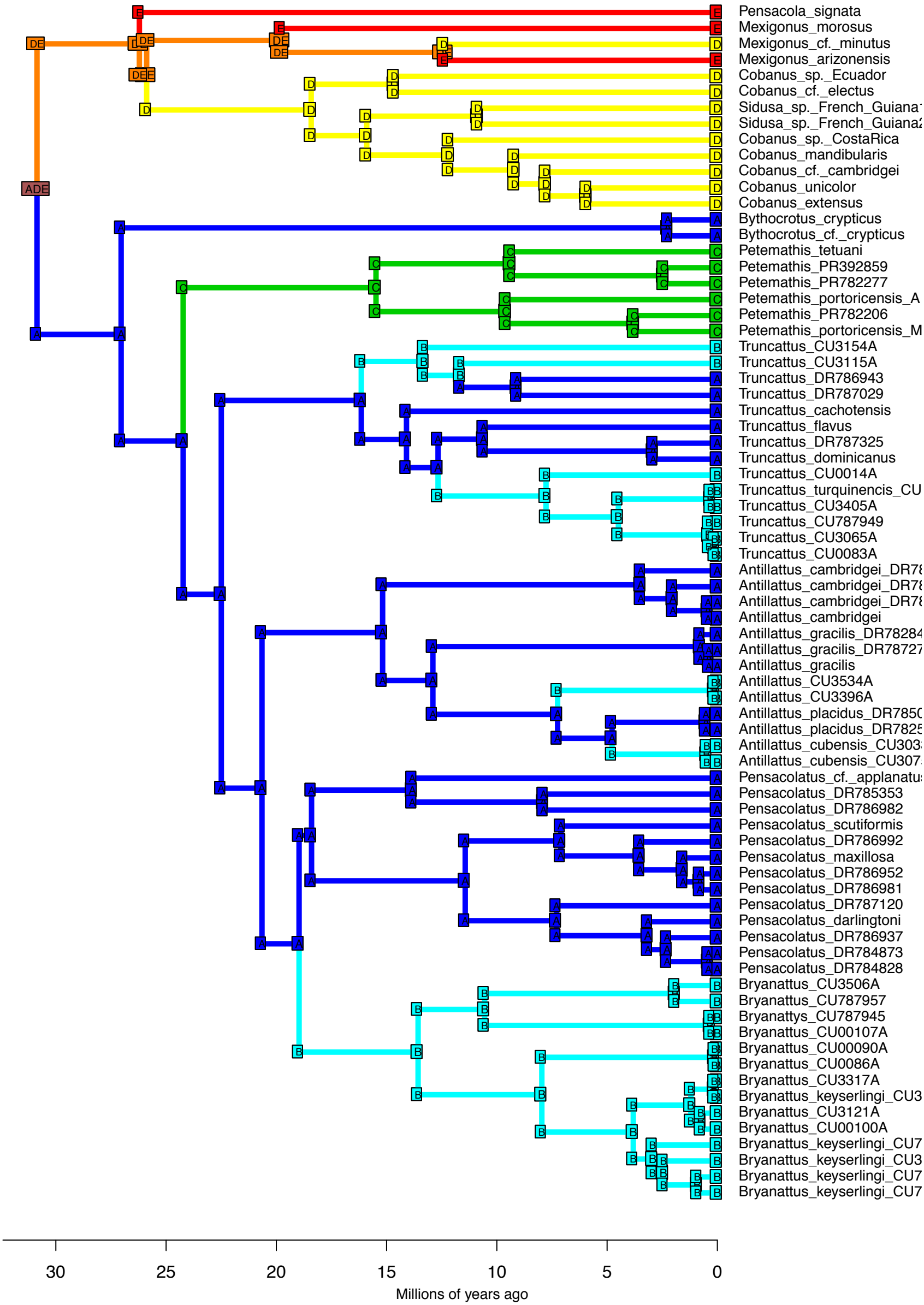

DEC+J – Stochastic Map #14/50
ancstates: global optim, 5 areas max. d=0; e=0; j=0.0153; LnL=−44.20

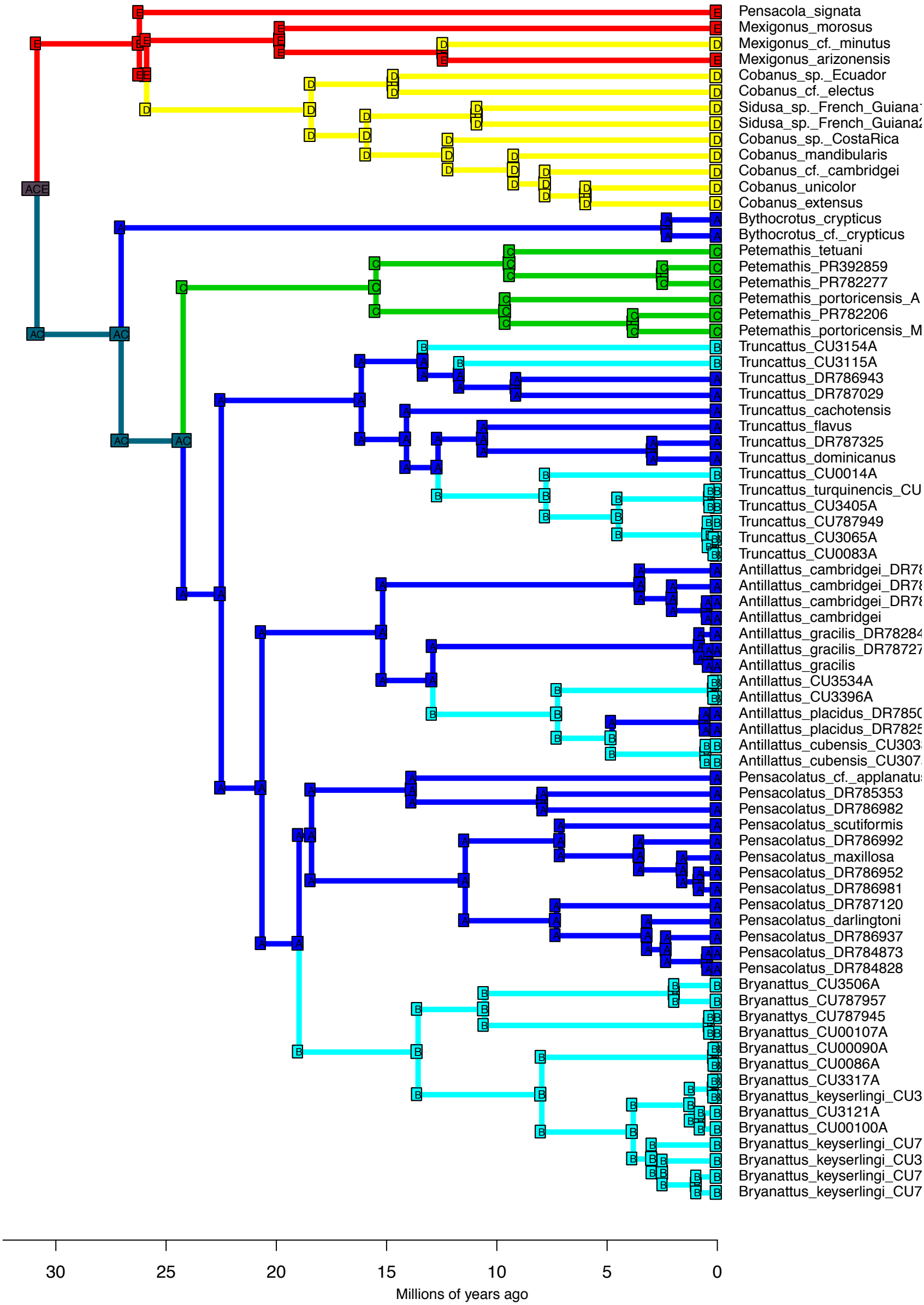

DEC+J – Stochastic Map #15/50
ancstates: global optim, 5 areas max. d=0; e=0; j=0.0153; LnL=−44.20

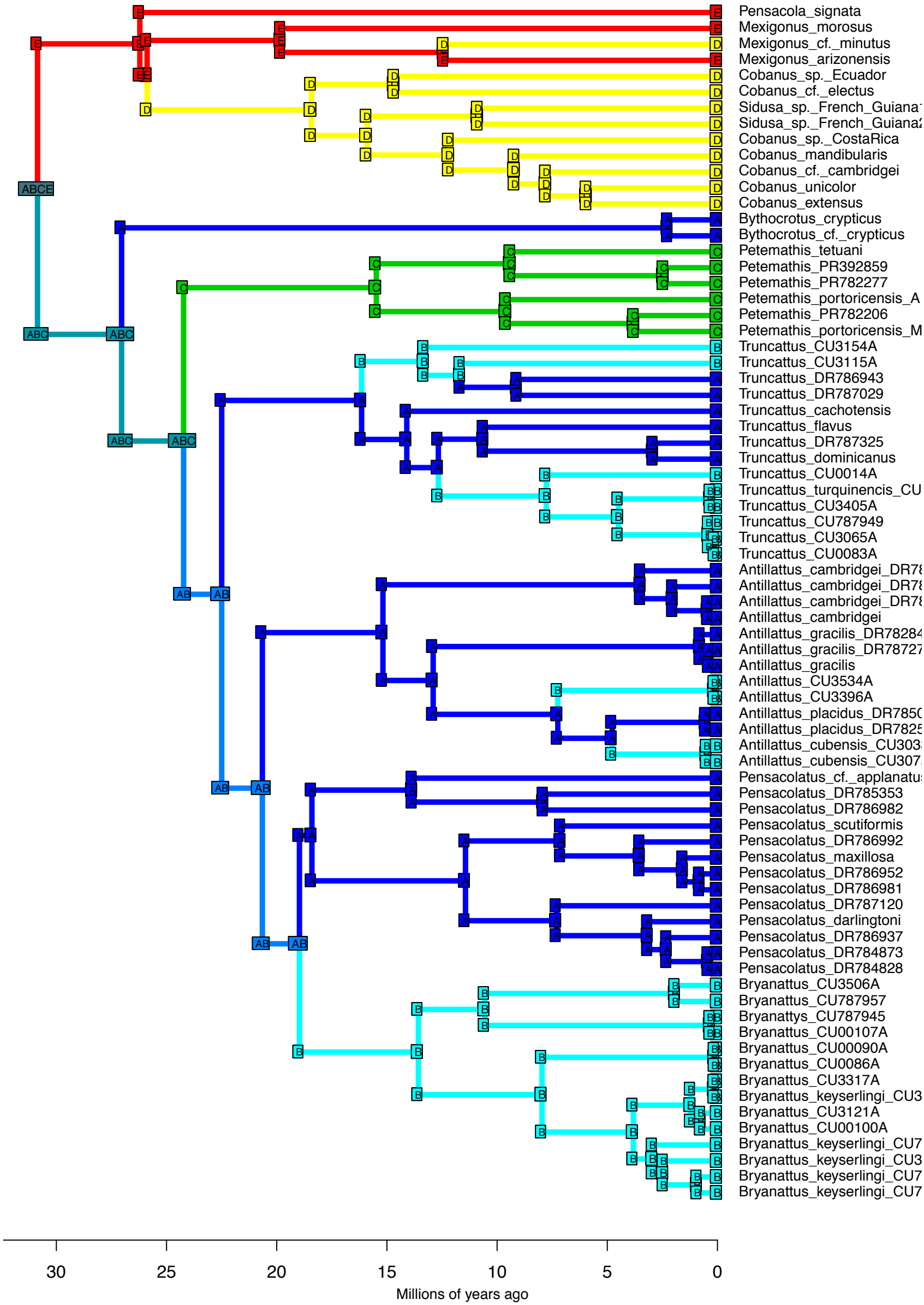

DEC+J – Stochastic Map #16/50
ancstates: global optim, 5 areas max. d=0; e=0; j=0.0153; LnL=−44.20

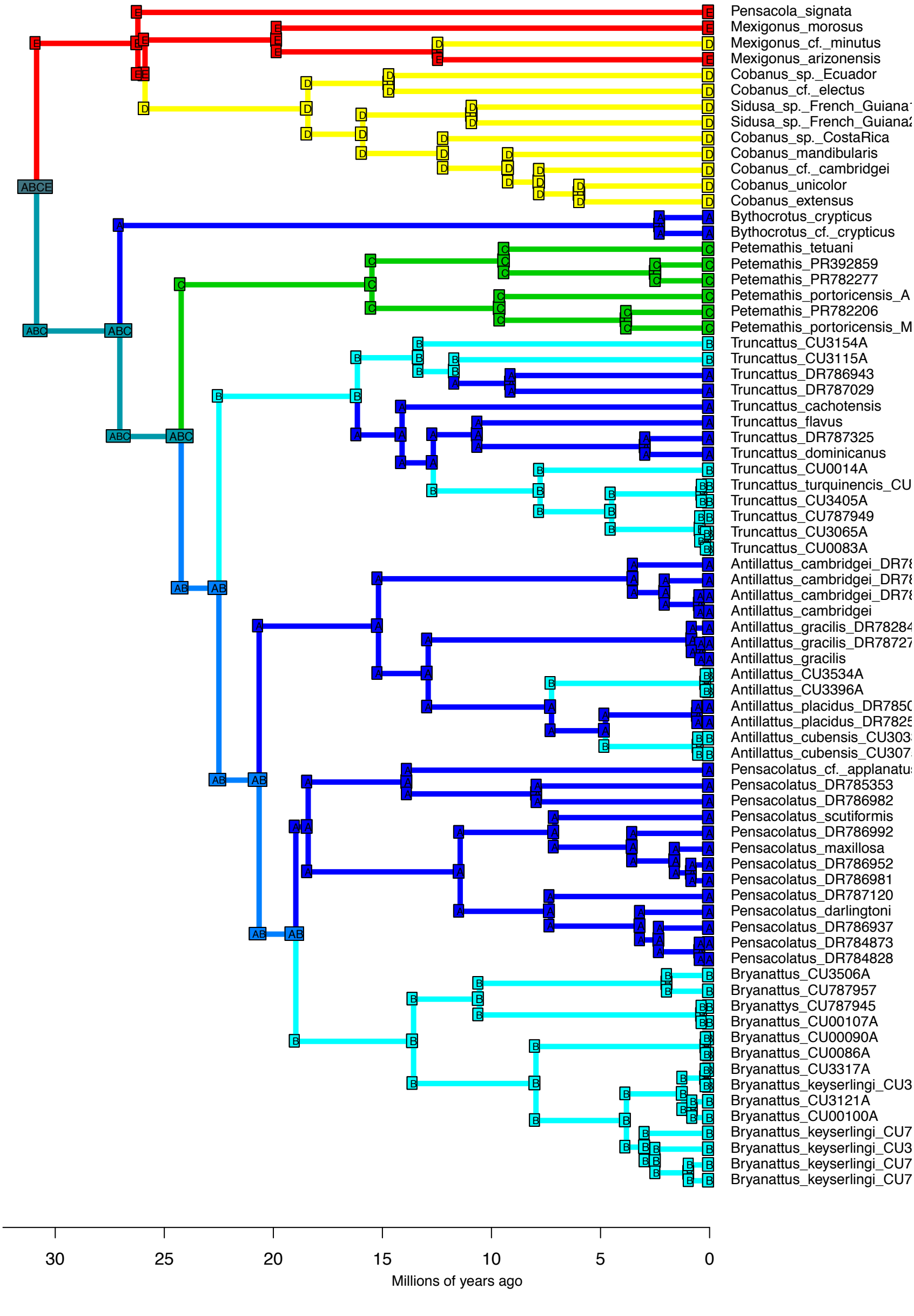

DEC+J – Stochastic Map #17/50
ancstates: global optim, 5 areas max. d=0; e=0; j=0.0153; LnL=−44.20

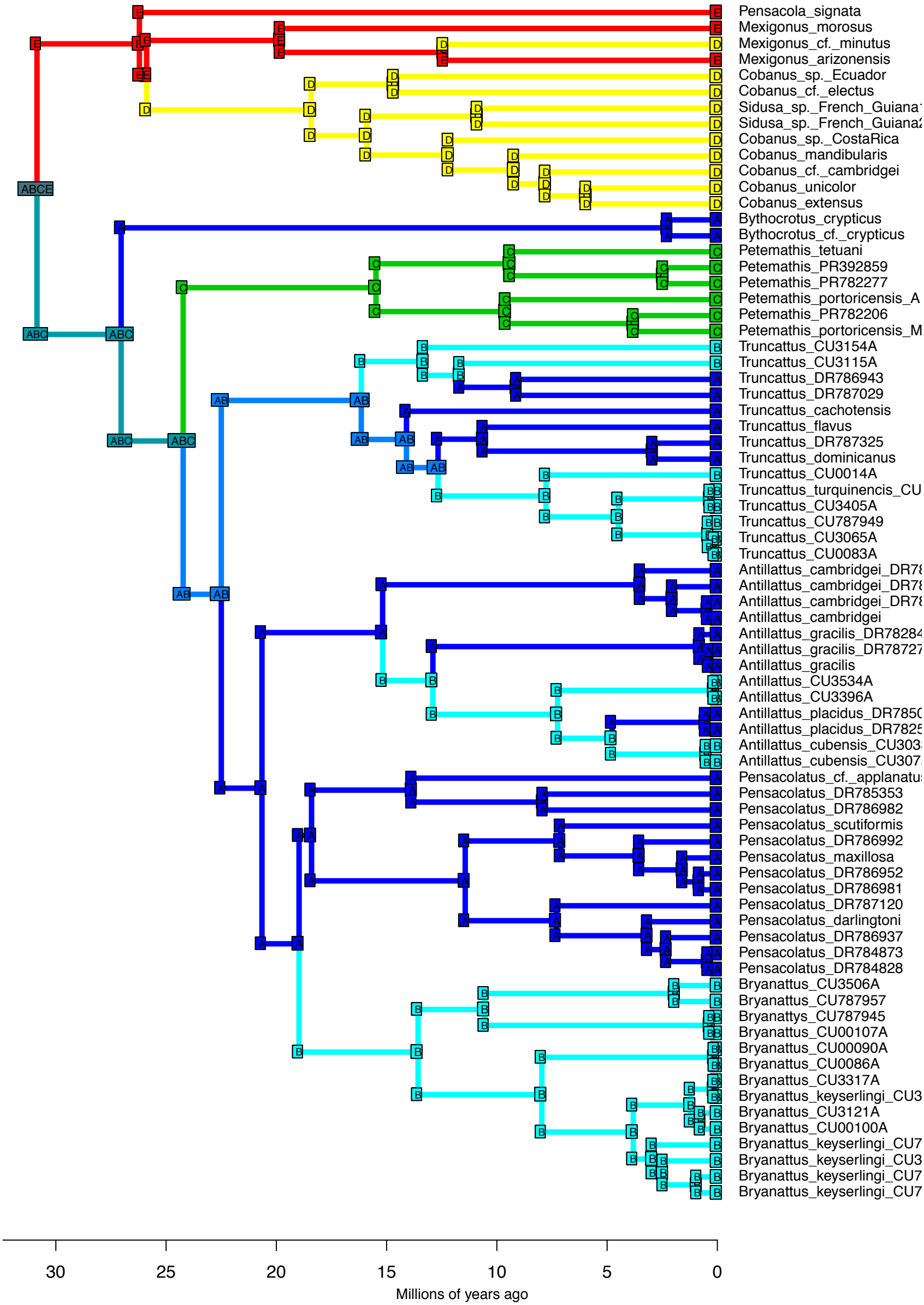

DEC+J – Stochastic Map #18/50
ancstates: global optim, 5 areas max. d=0; e=0; j=0.0153; LnL=−44.20

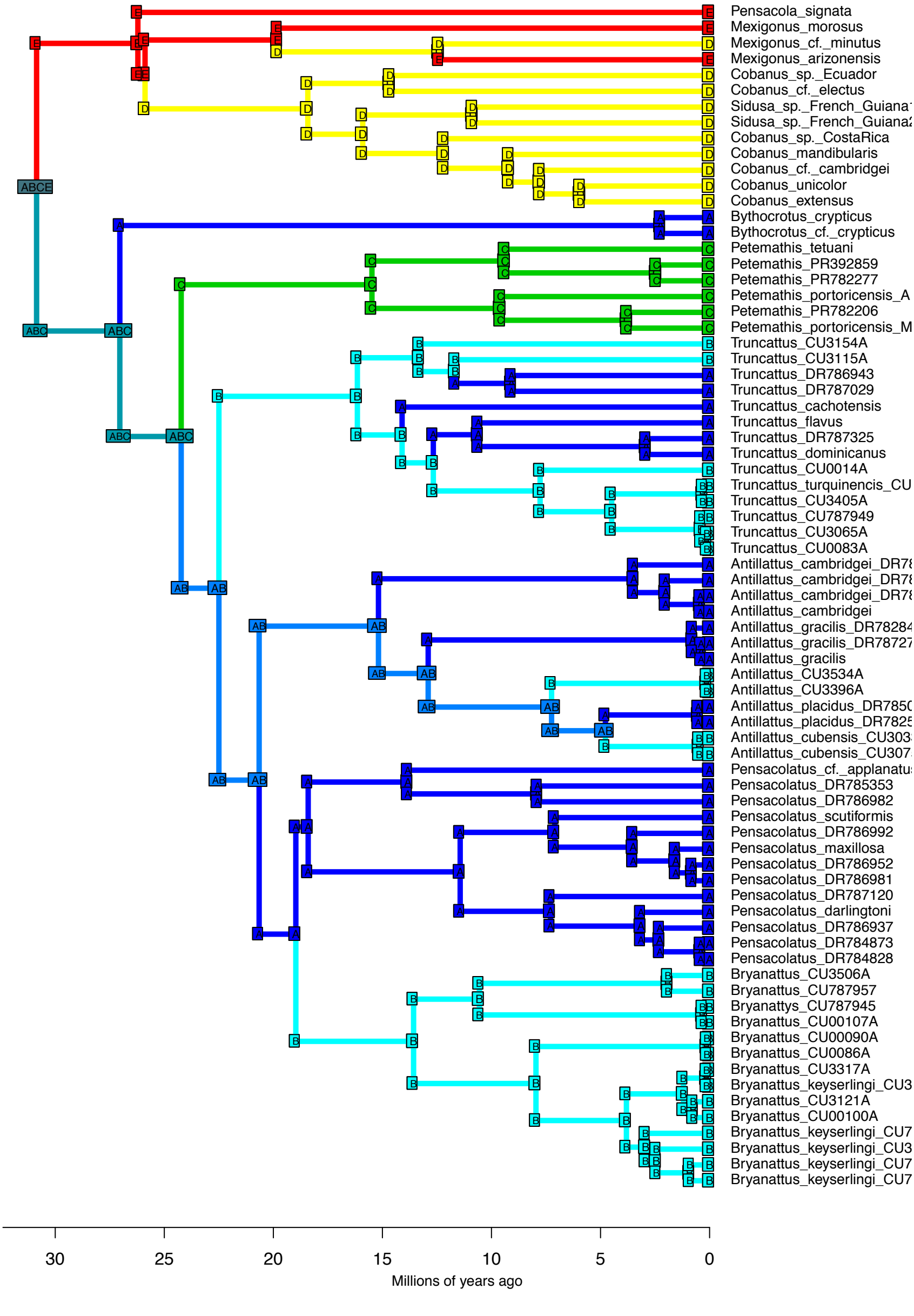

DEC+J – Stochastic Map #19/50
ancstates: global optim, 5 areas max. d=0; e=0; j=0.0153; LnL=−44.20

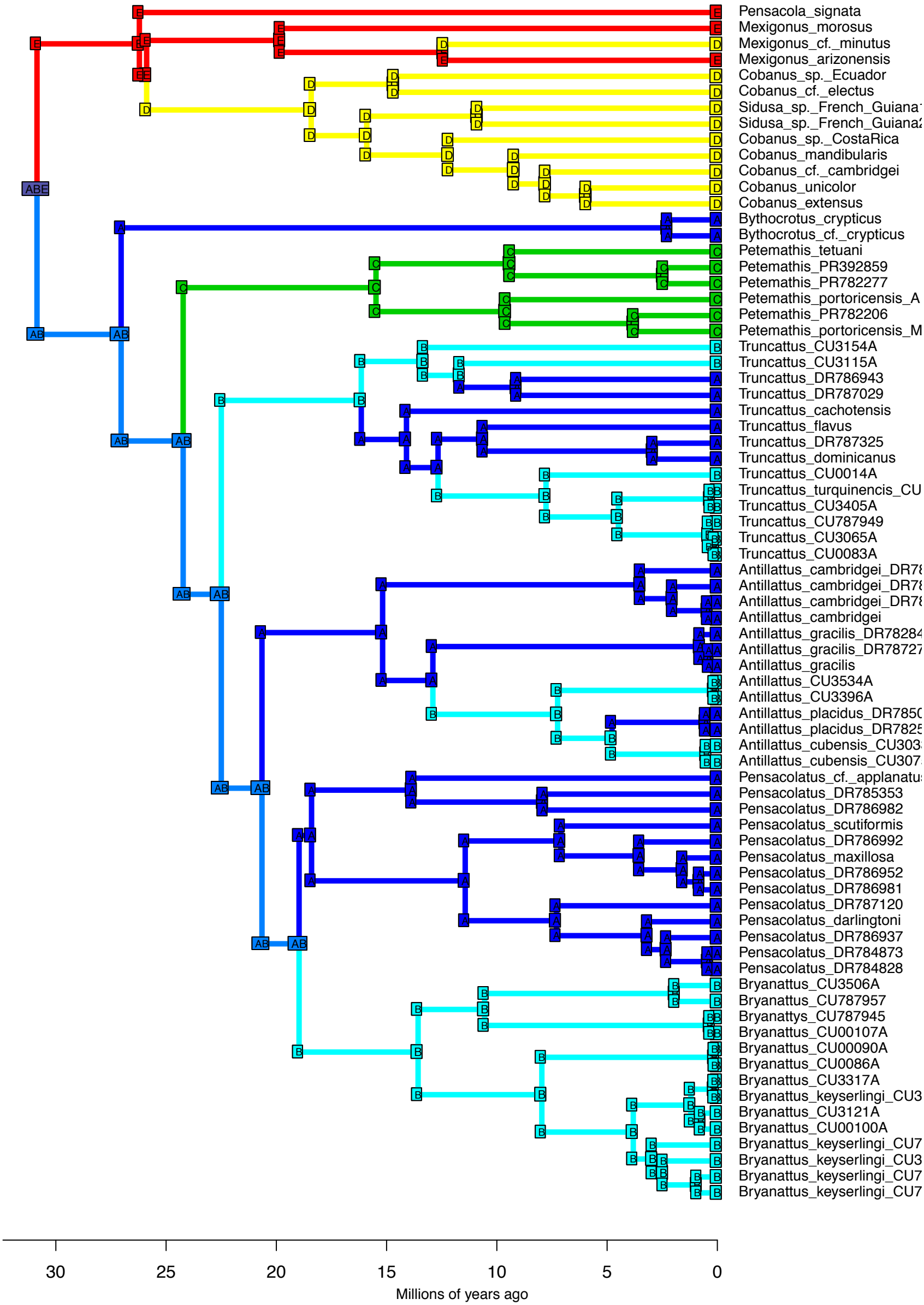

DEC+J – Stochastic Map #20/50
ancstates: global optim, 5 areas max. d=0; e=0; j=0.0153; LnL=−44.20

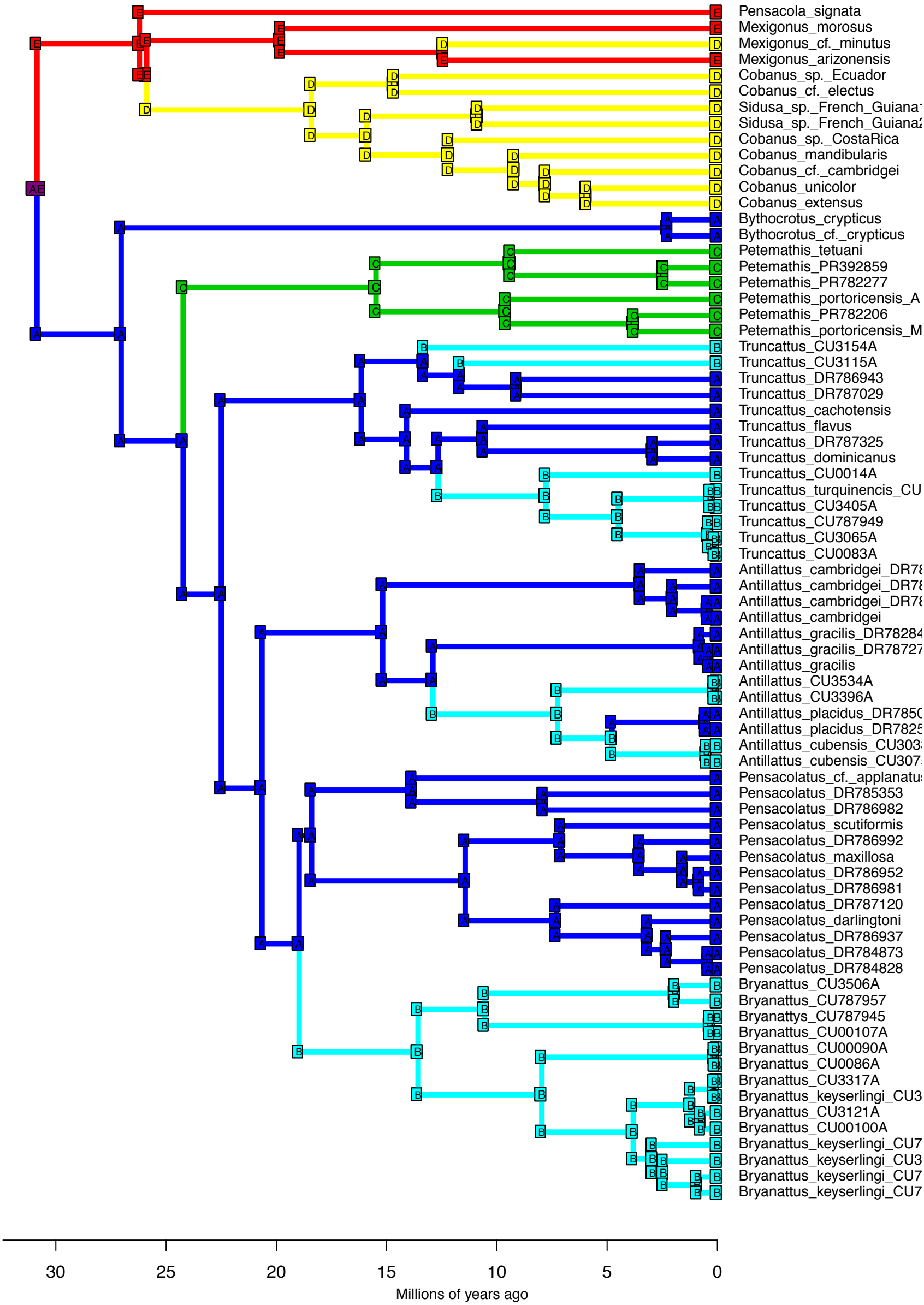

DEC+J – Stochastic Map #21/50
ancstates: global optim, 5 areas max. d=0; e=0; j=0.0153; LnL=−44.20

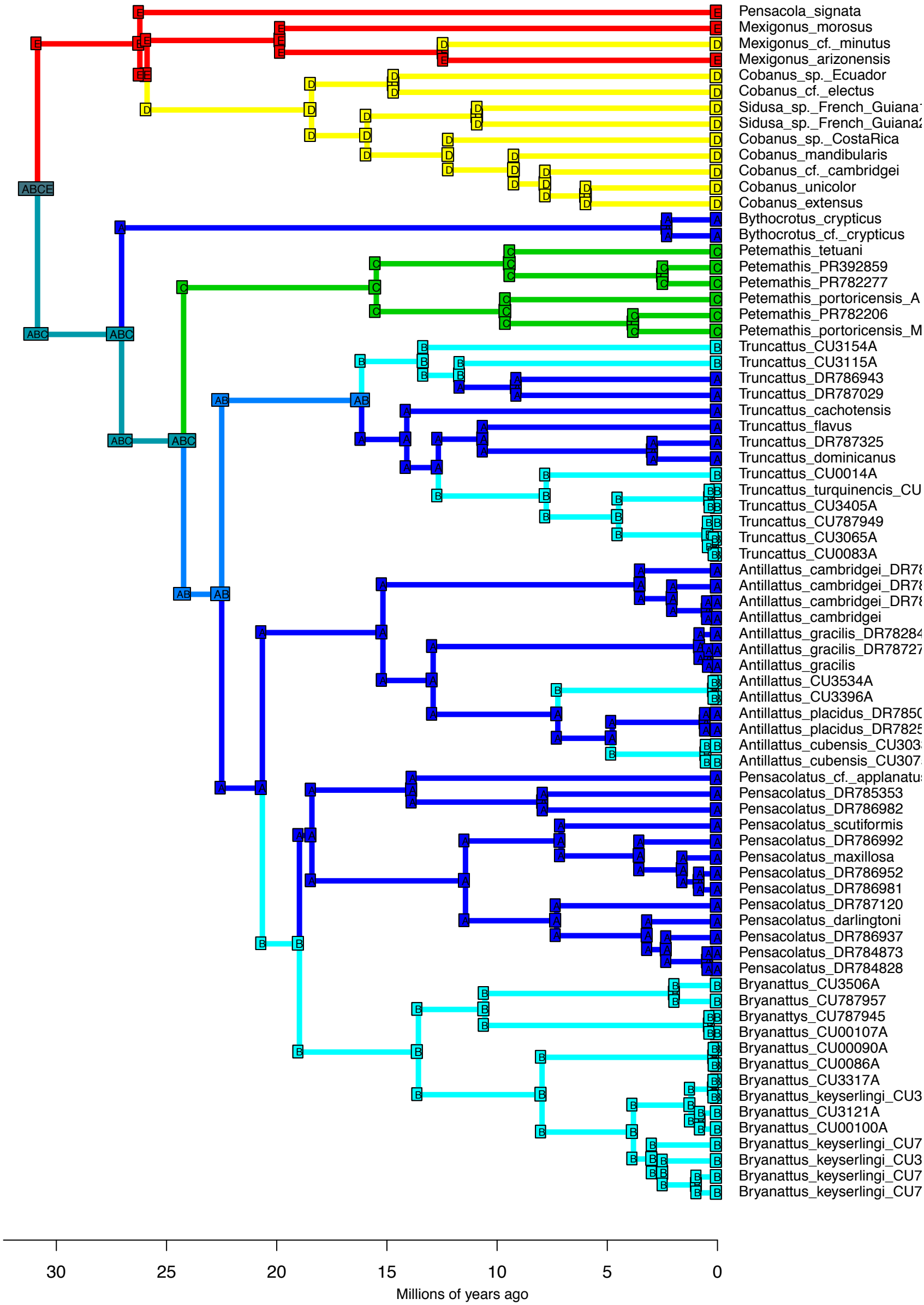

DEC+J – Stochastic Map #22/50
ancstates: global optim, 5 areas max. d=0; e=0; j=0.0153; LnL=−44.20

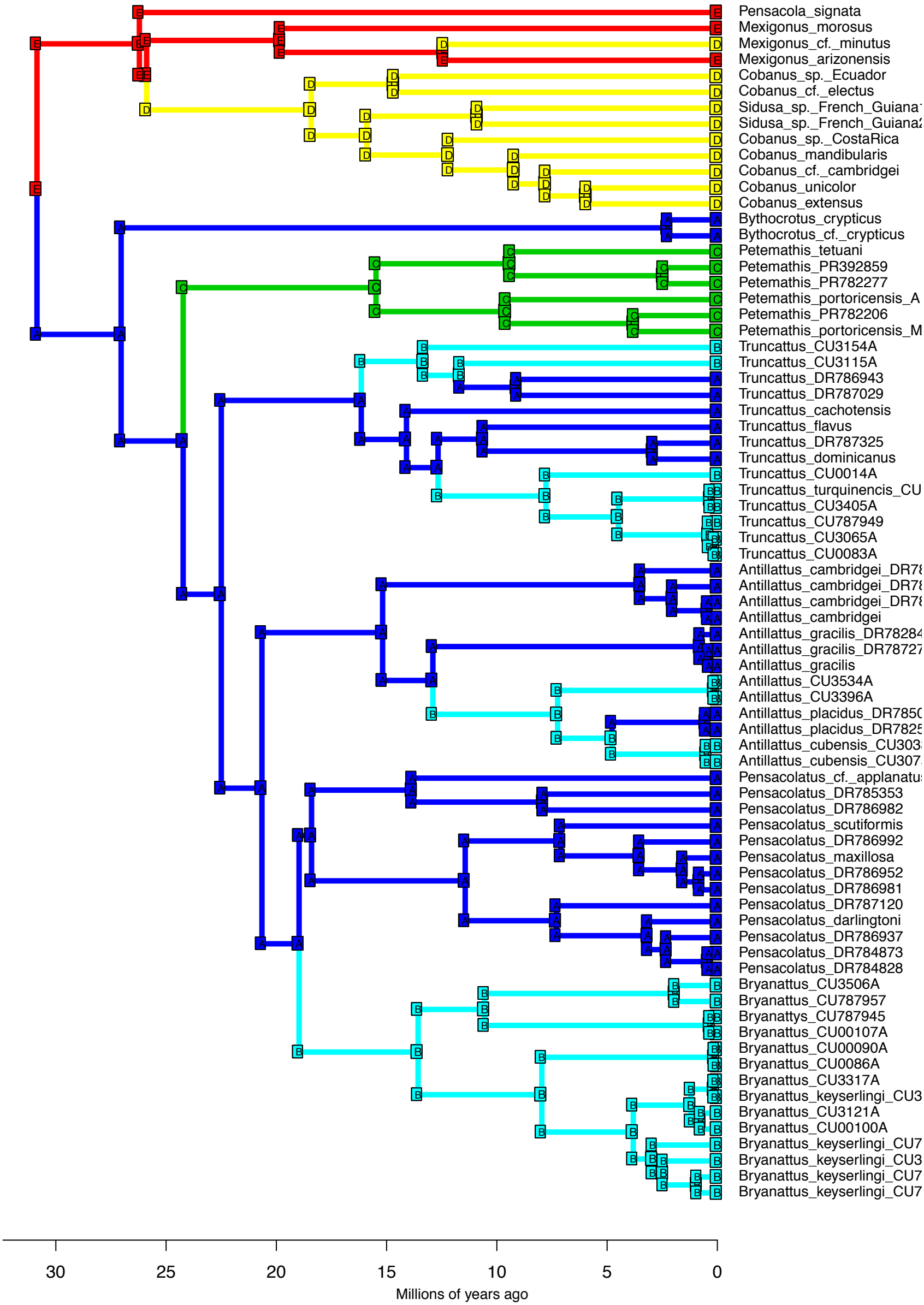

DEC+J – Stochastic Map #23/50
ancstates: global optim, 5 areas max. d=0; e=0; j=0.0153; LnL=−44.20

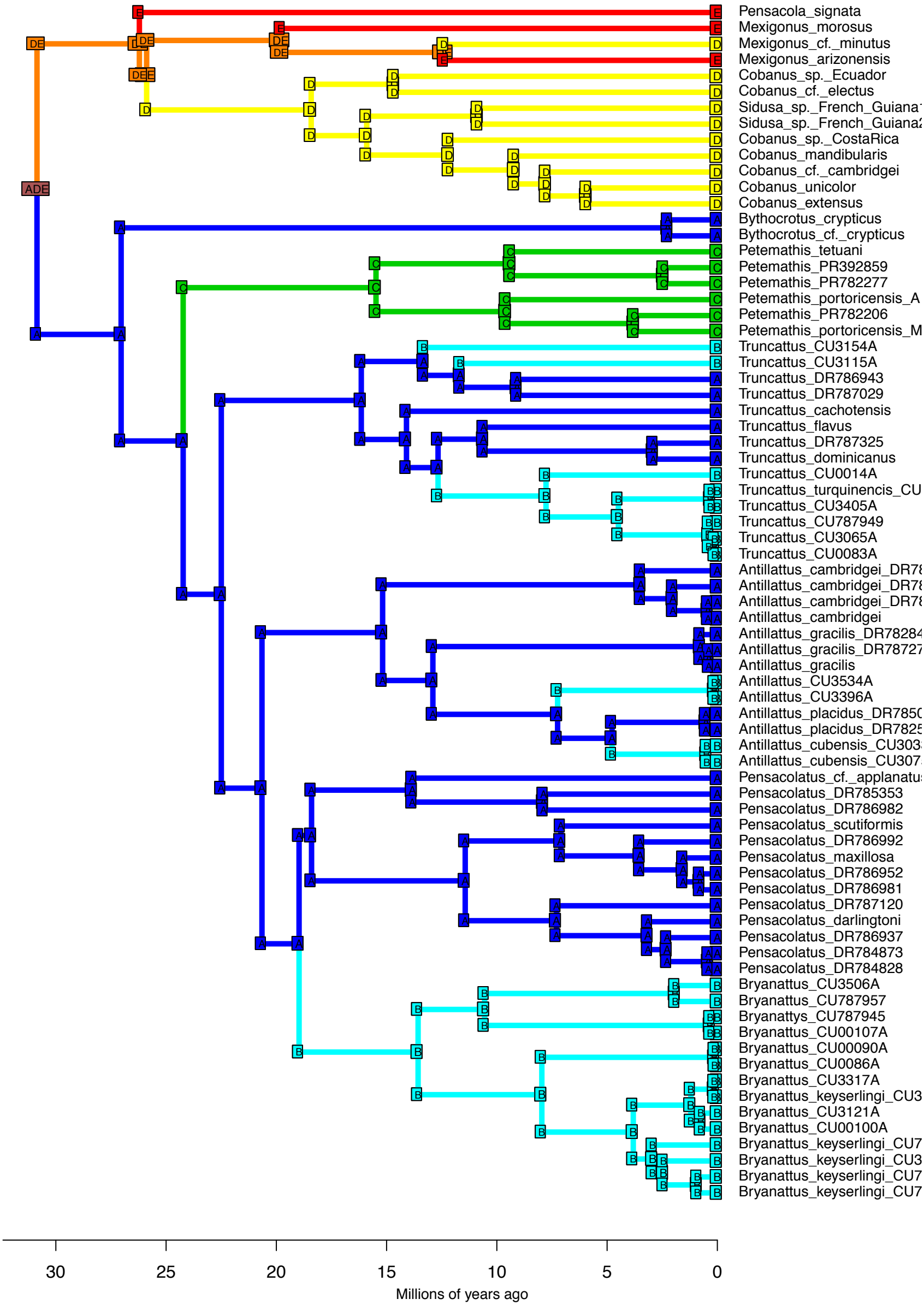

DEC+J – Stochastic Map #24/50
ancstates: global optim, 5 areas max. d=0; e=0; j=0.0153; LnL=−44.20

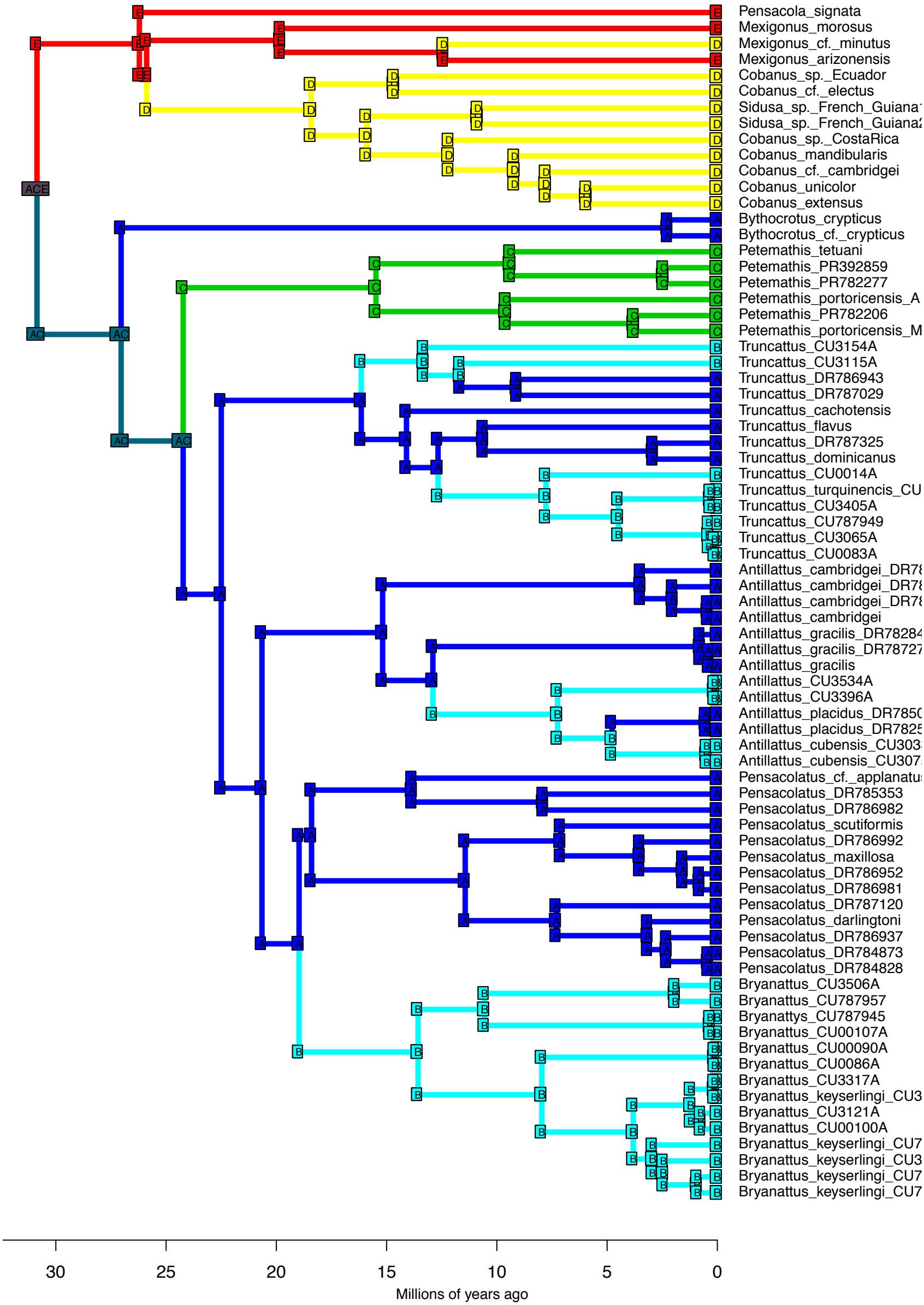

DEC+J – Stochastic Map #25/50
ancstates: global optim, 5 areas max. d=0; e=0; j=0.0153; LnL=−44.20

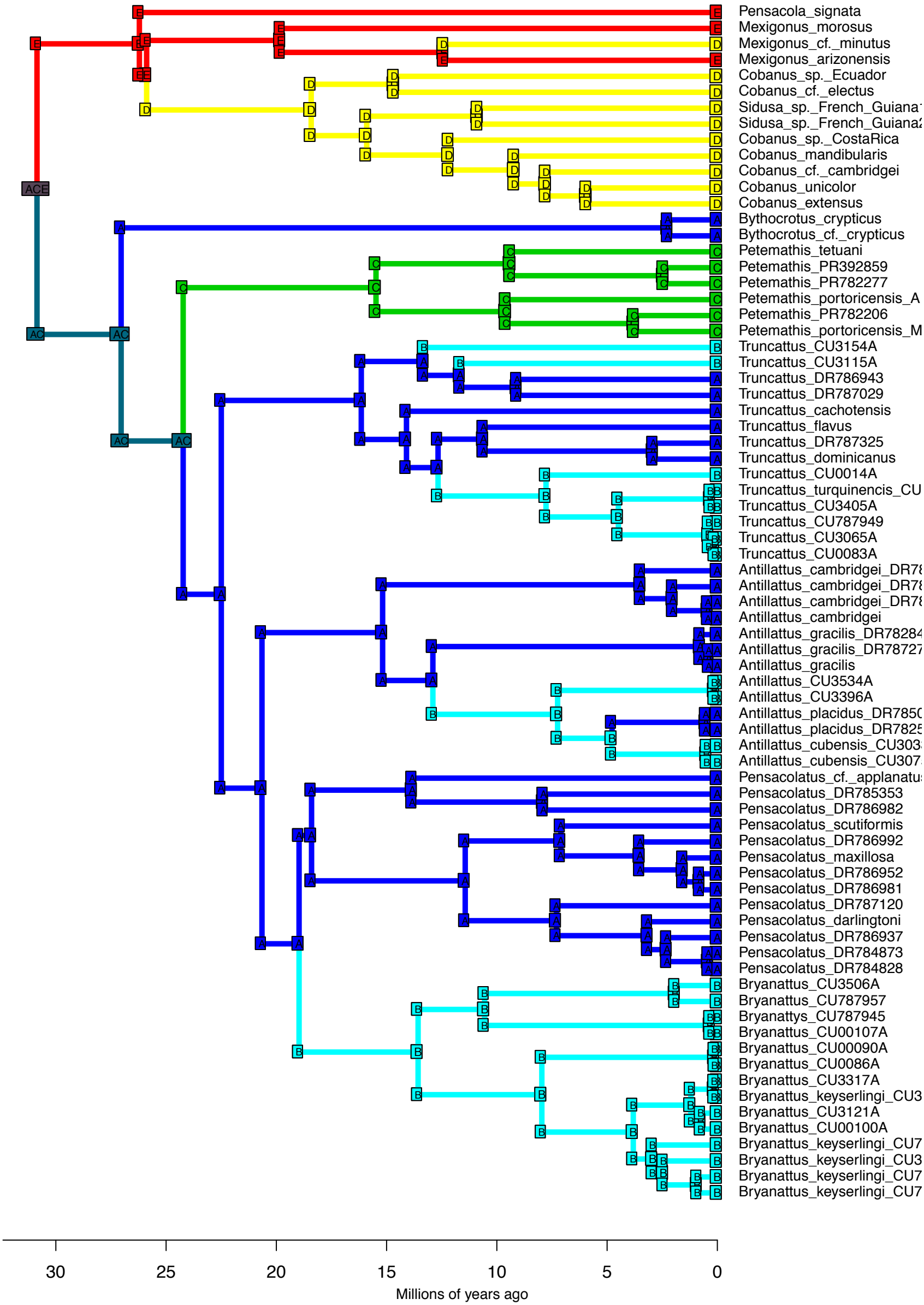

DEC+J – Stochastic Map #26/50
ancstates: global optim, 5 areas max. d=0; e=0; j=0.0153; LnL=−44.20

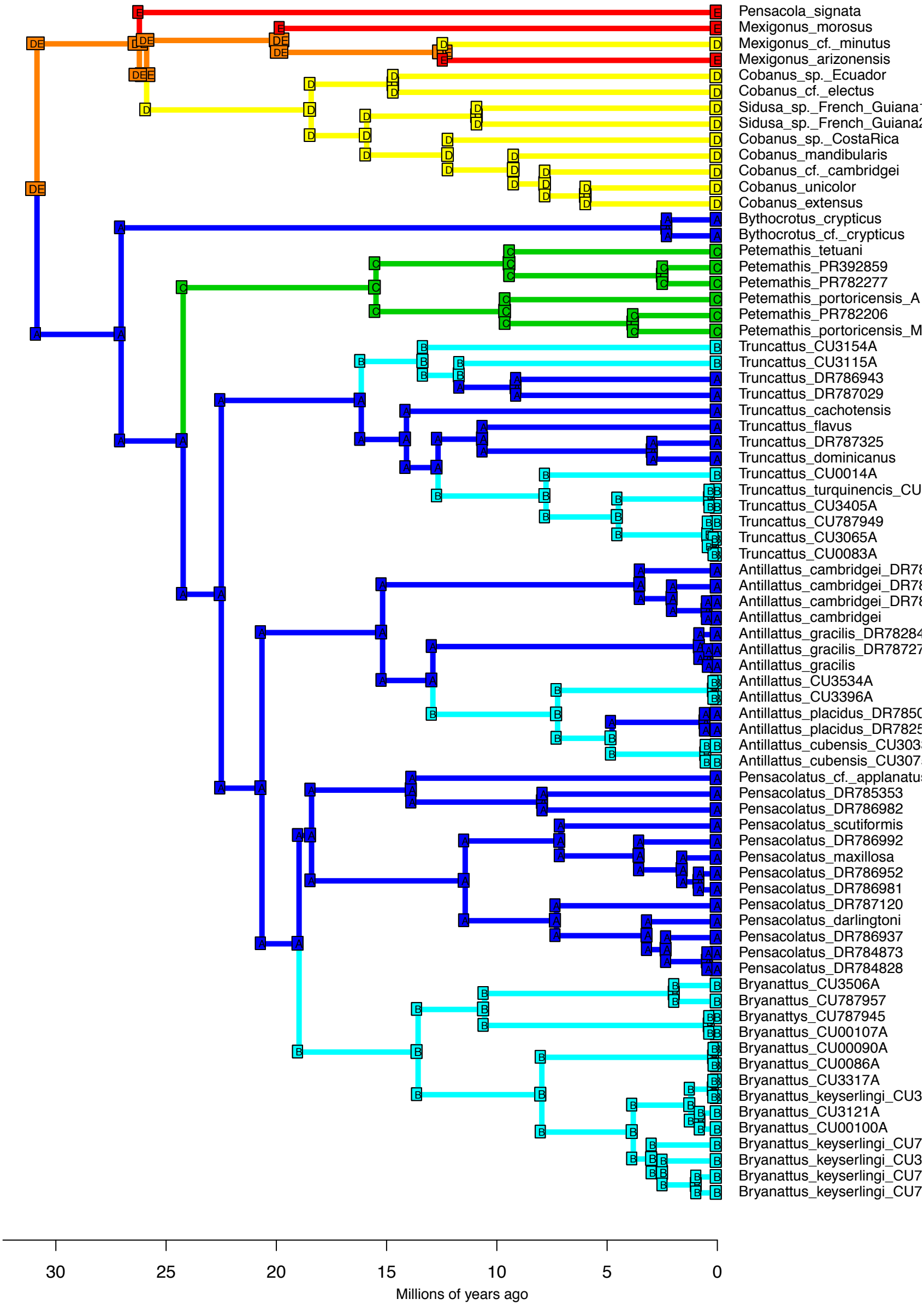

DEC+J – Stochastic Map #27/50
ancstates: global optim, 5 areas max. d=0; e=0; j=0.0153; LnL=−44.20

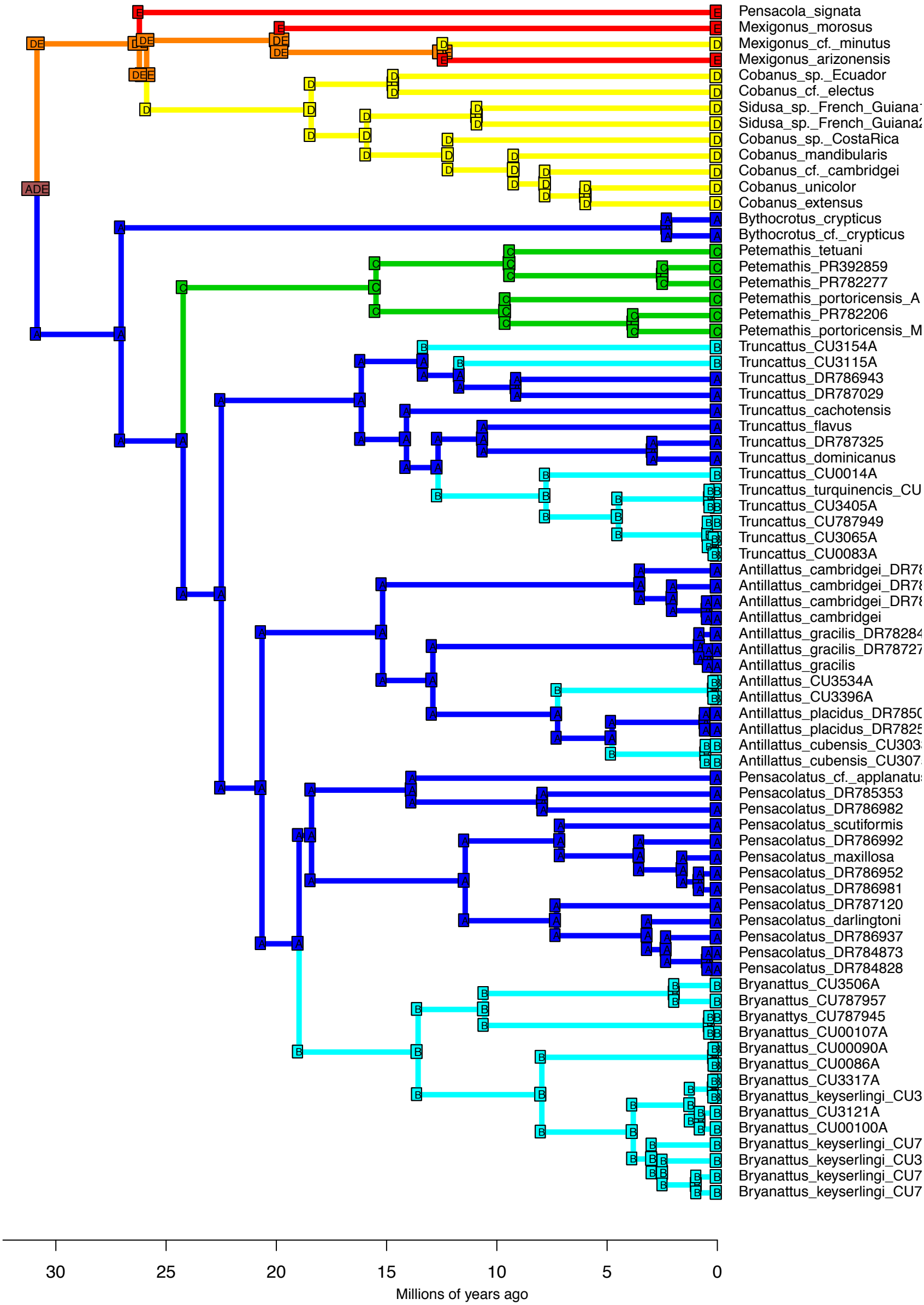

DEC+J – Stochastic Map #28/50
ancstates: global optim, 5 areas max. d=0; e=0; j=0.0153; LnL=−44.20

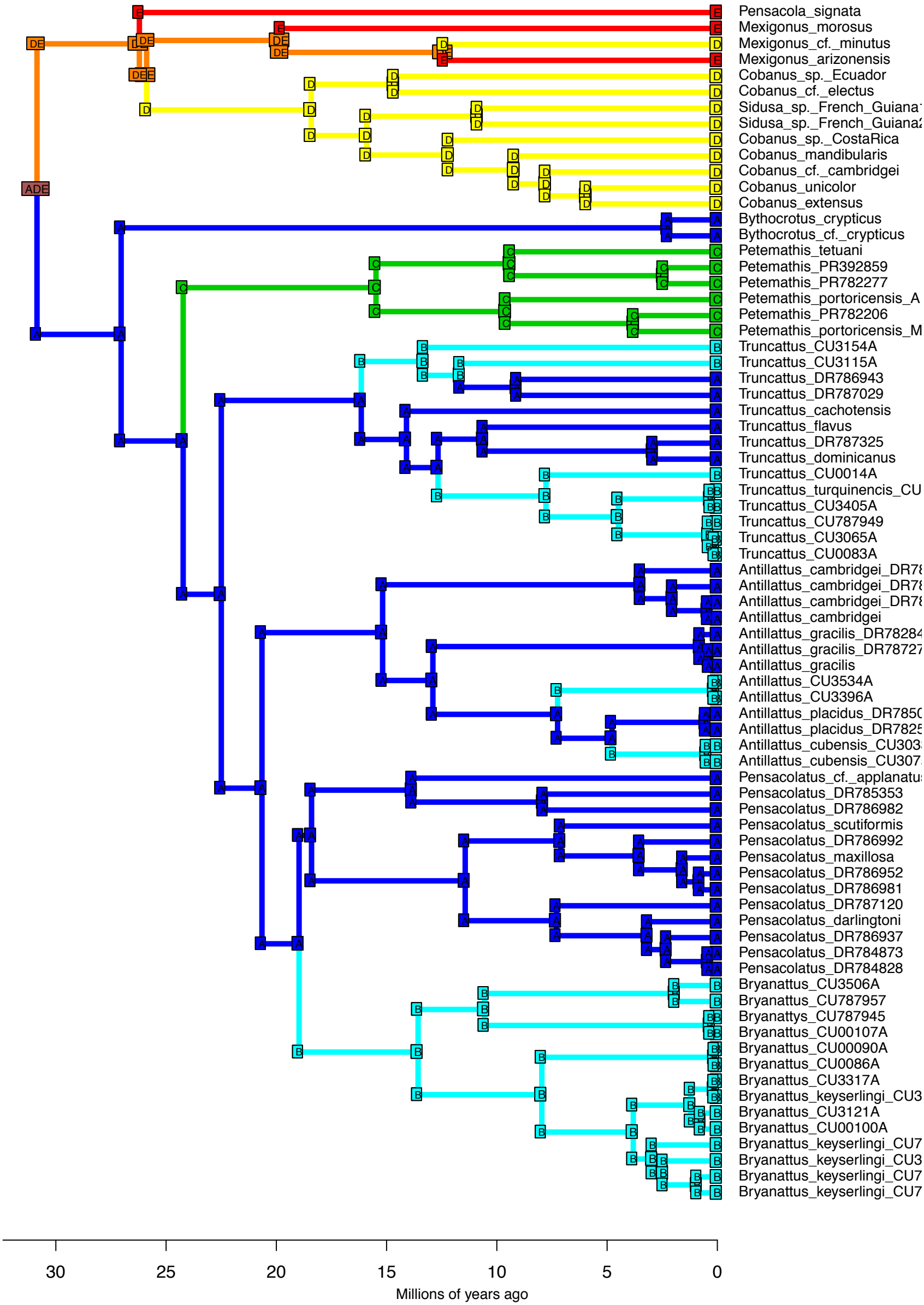

DEC+J – Stochastic Map #29/50
ancstates: global optim, 5 areas max. d=0; e=0; j=0.0153; LnL=−44.20

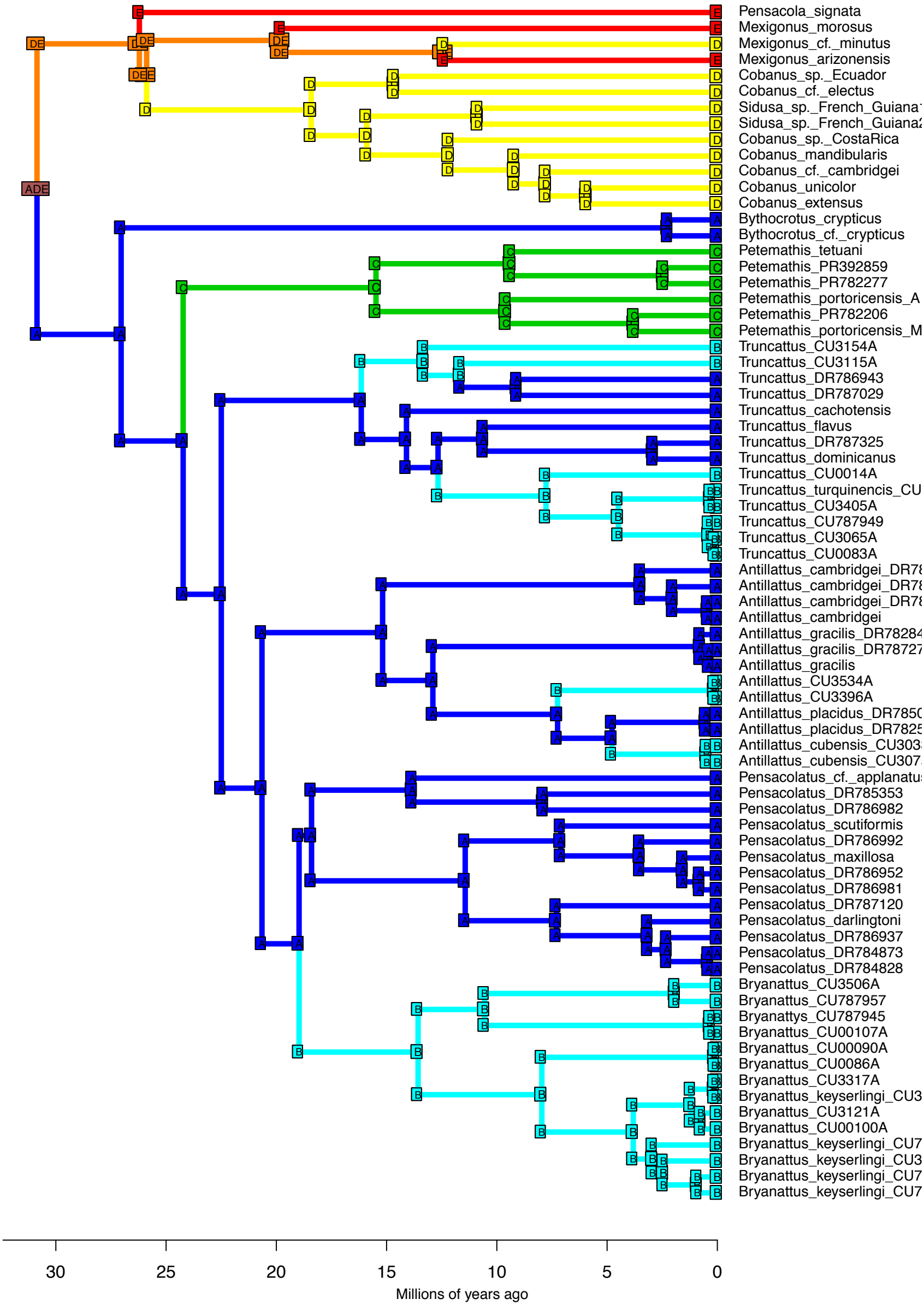

DEC+J – Stochastic Map #30/50
ancstates: global optim, 5 areas max. d=0; e=0; j=0.0153; LnL=−44.20

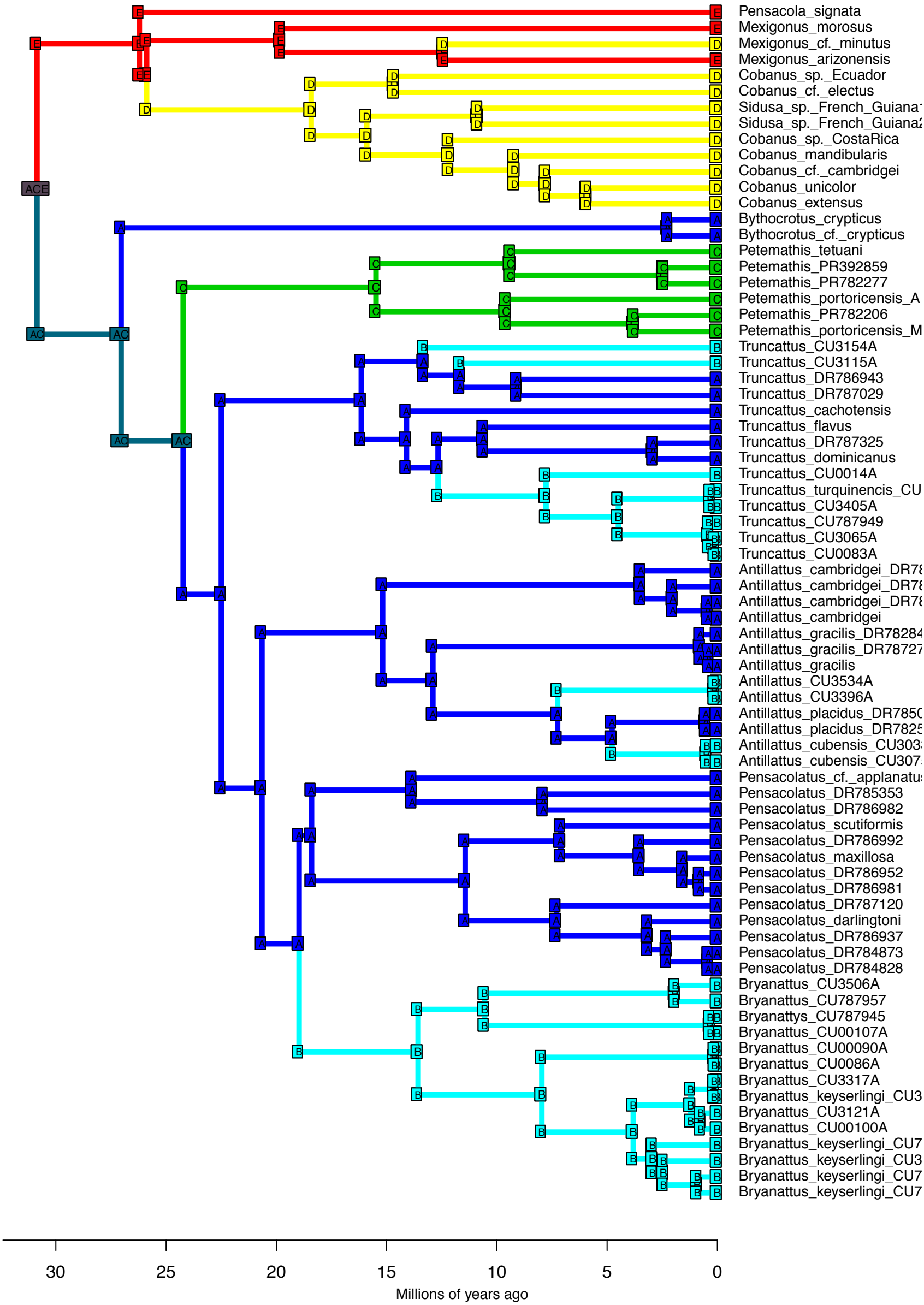

DEC+J – Stochastic Map #31/50
ancstates: global optim, 5 areas max. d=0; e=0; j=0.0153; LnL=−44.20

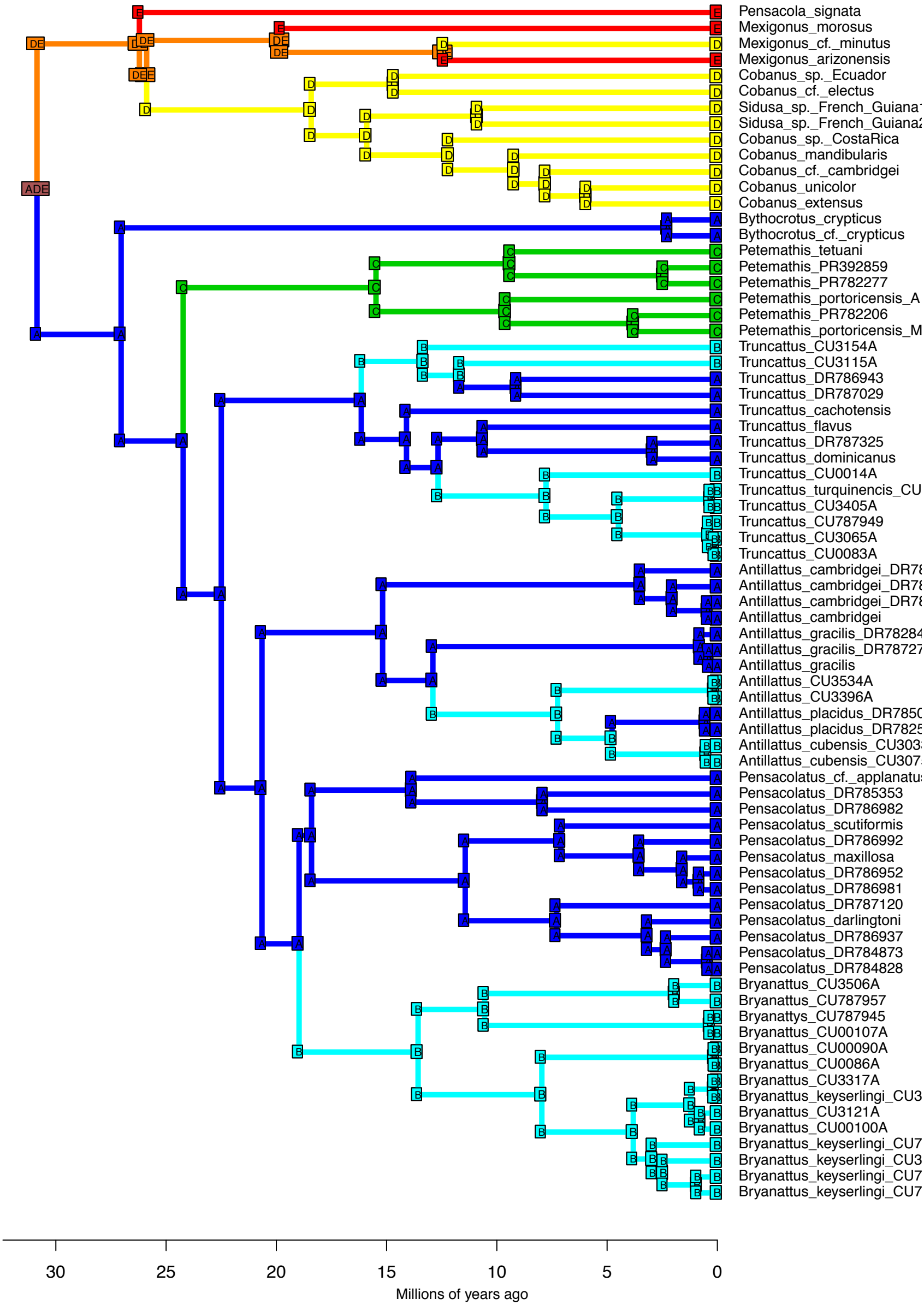

DEC+J – Stochastic Map #32/50
ancstates: global optim, 5 areas max. d=0; e=0; j=0.0153; LnL=−44.20

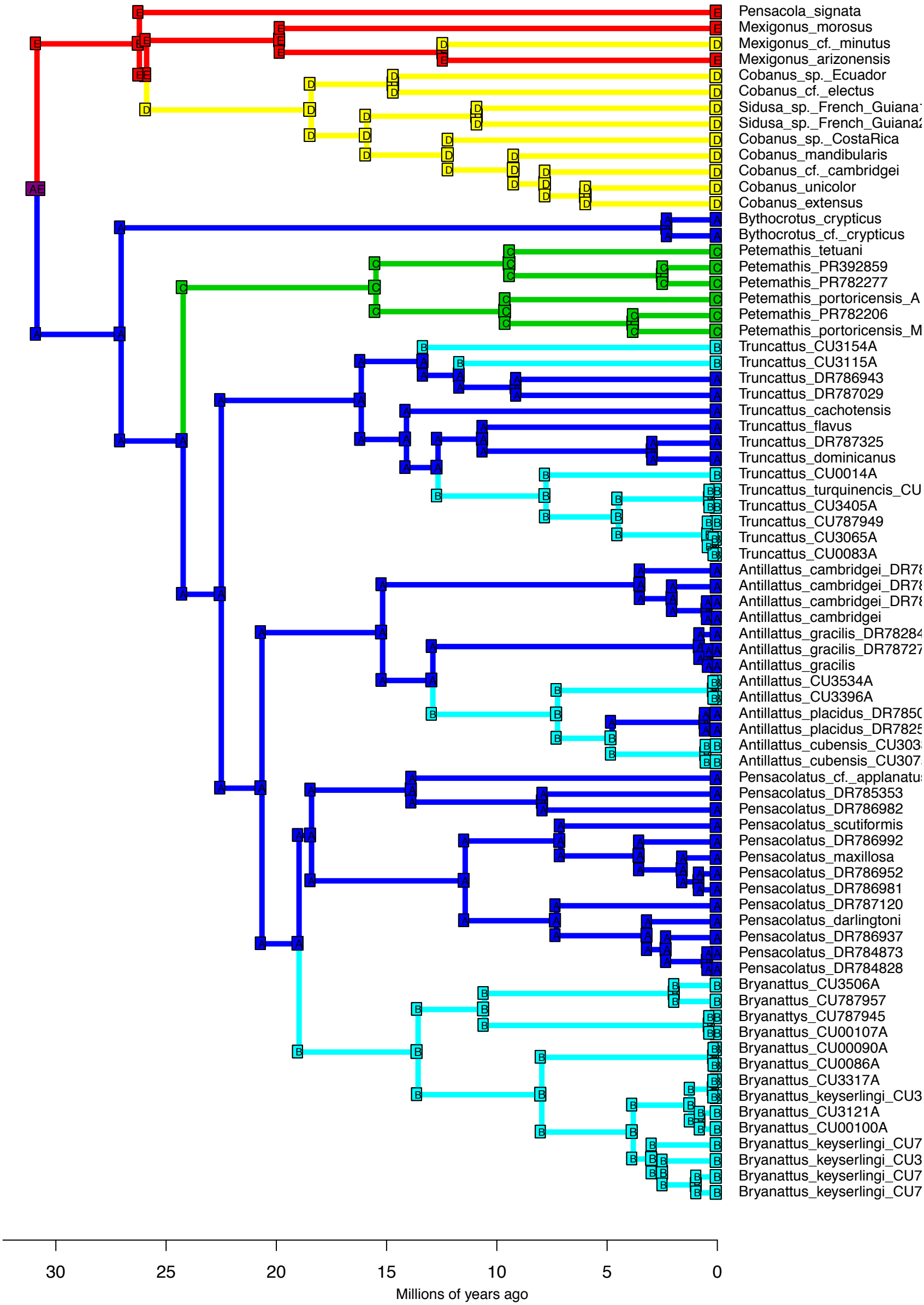

DEC+J – Stochastic Map #33/50
ancstates: global optim, 5 areas max. d=0; e=0; j=0.0153; LnL=−44.20

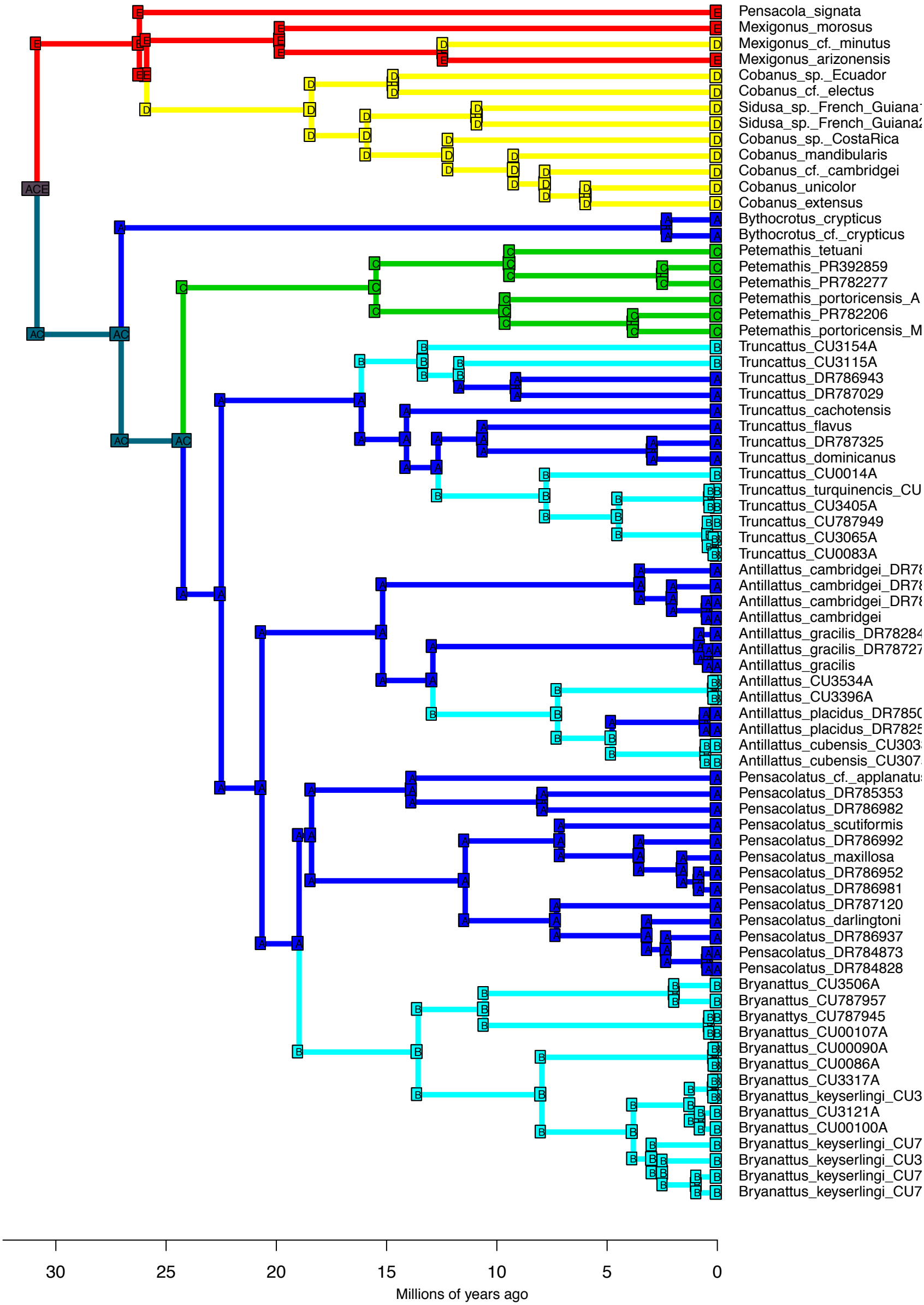

DEC+J – Stochastic Map #34/50
ancstates: global optim, 5 areas max. d=0; e=0; j=0.0153; LnL=−44.20

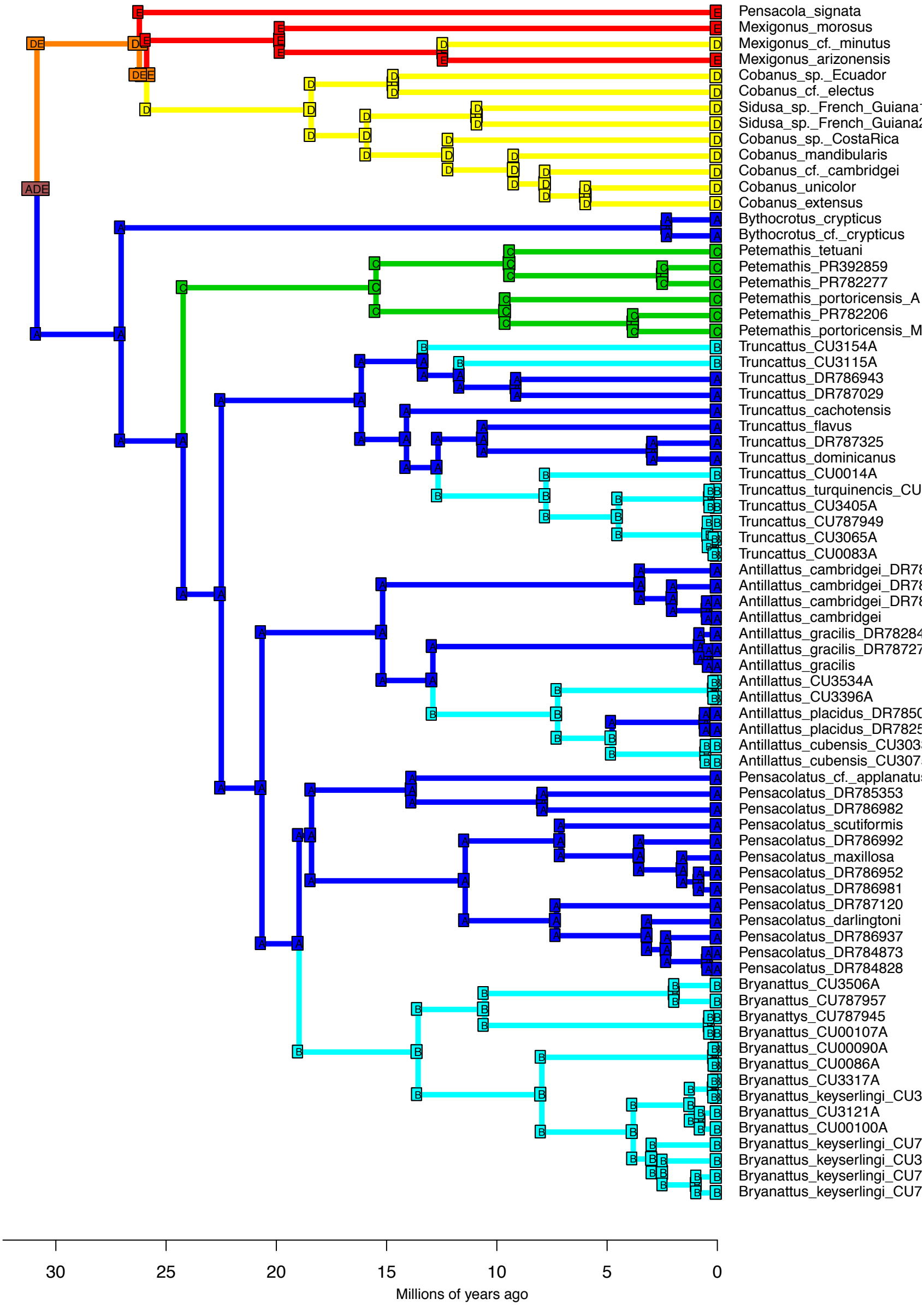

DEC+J – Stochastic Map #35/50
ancstates: global optim, 5 areas max. d=0; e=0; j=0.0153; LnL=−44.20

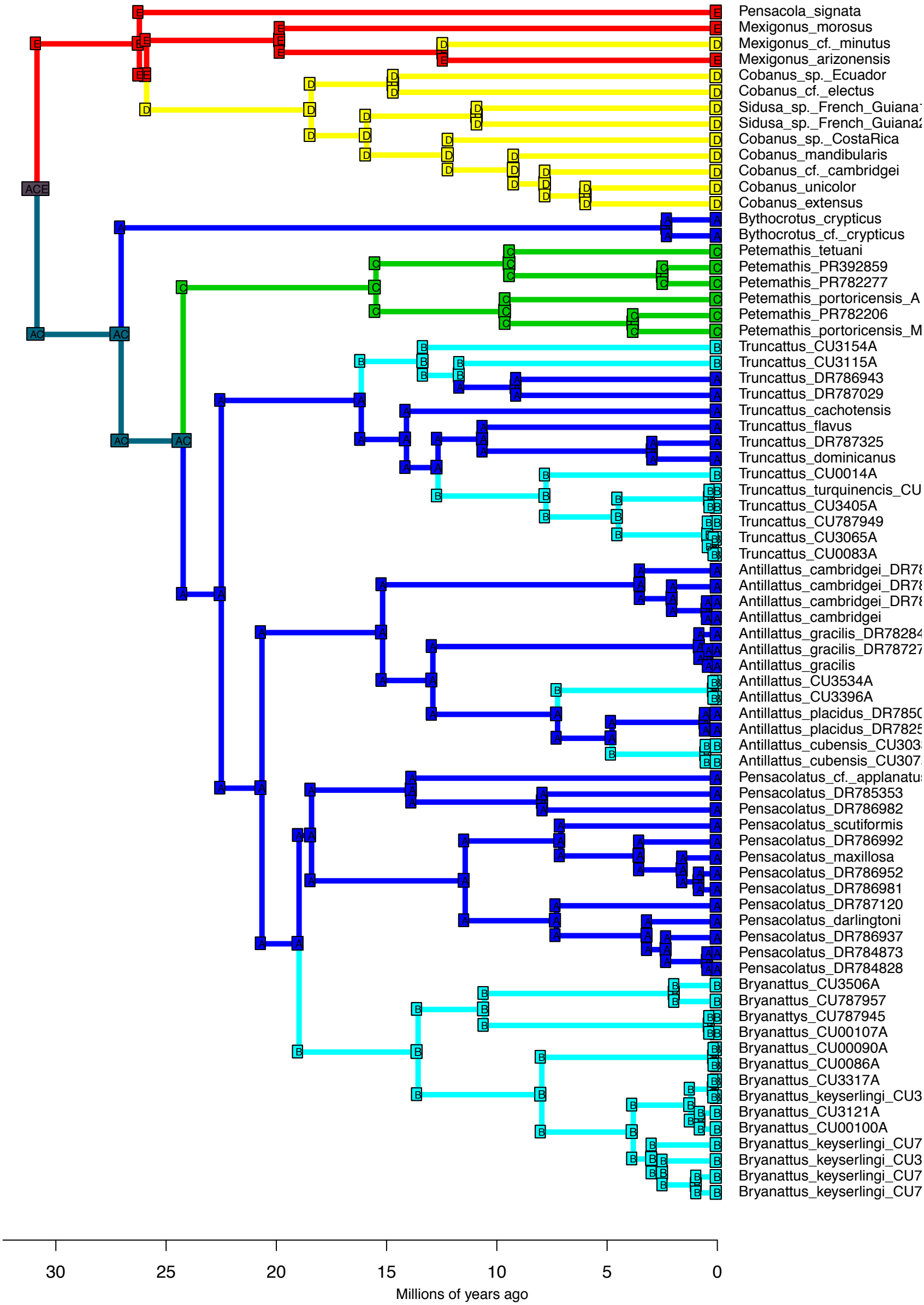

DEC+J – Stochastic Map #36/50
ancstates: global optim, 5 areas max. d=0; e=0; j=0.0153; LnL=−44.20

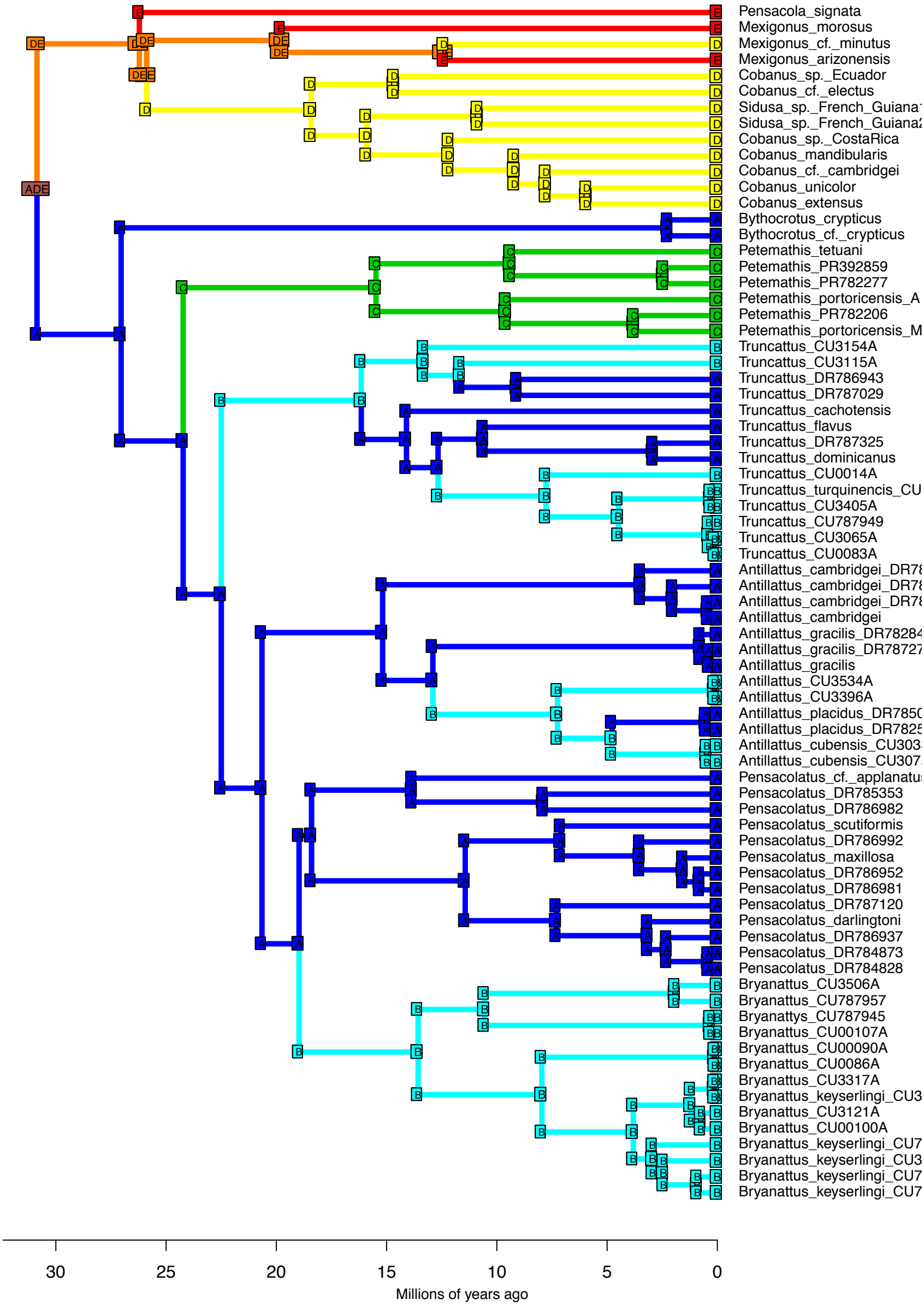

DEC+J – Stochastic Map #37/50
ancstates: global optim, 5 areas max. d=0; e=0; j=0.0153; LnL=−44.20

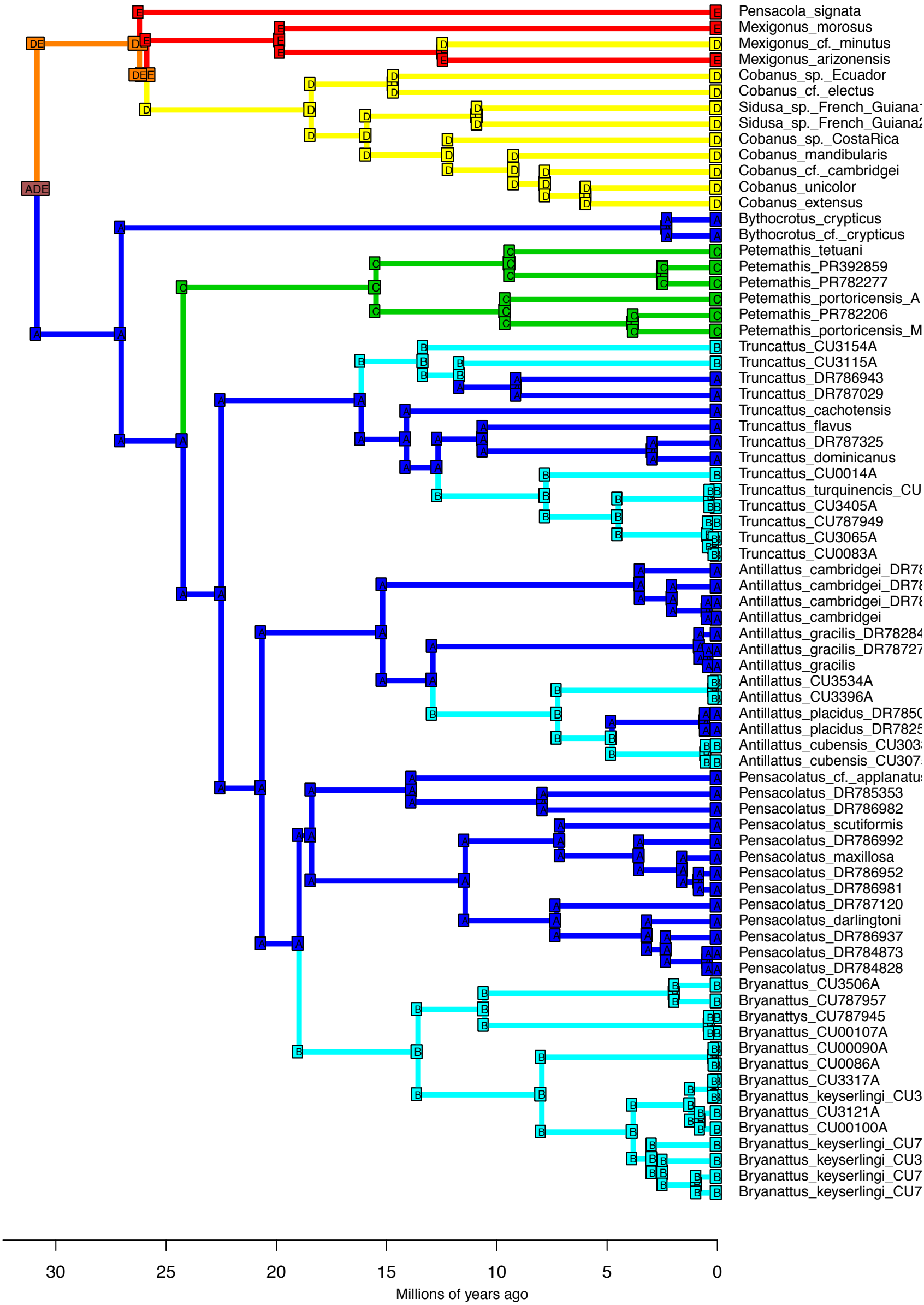

DEC+J – Stochastic Map #38/50
ancstates: global optim, 5 areas max. d=0; e=0; j=0.0153; LnL=−44.20

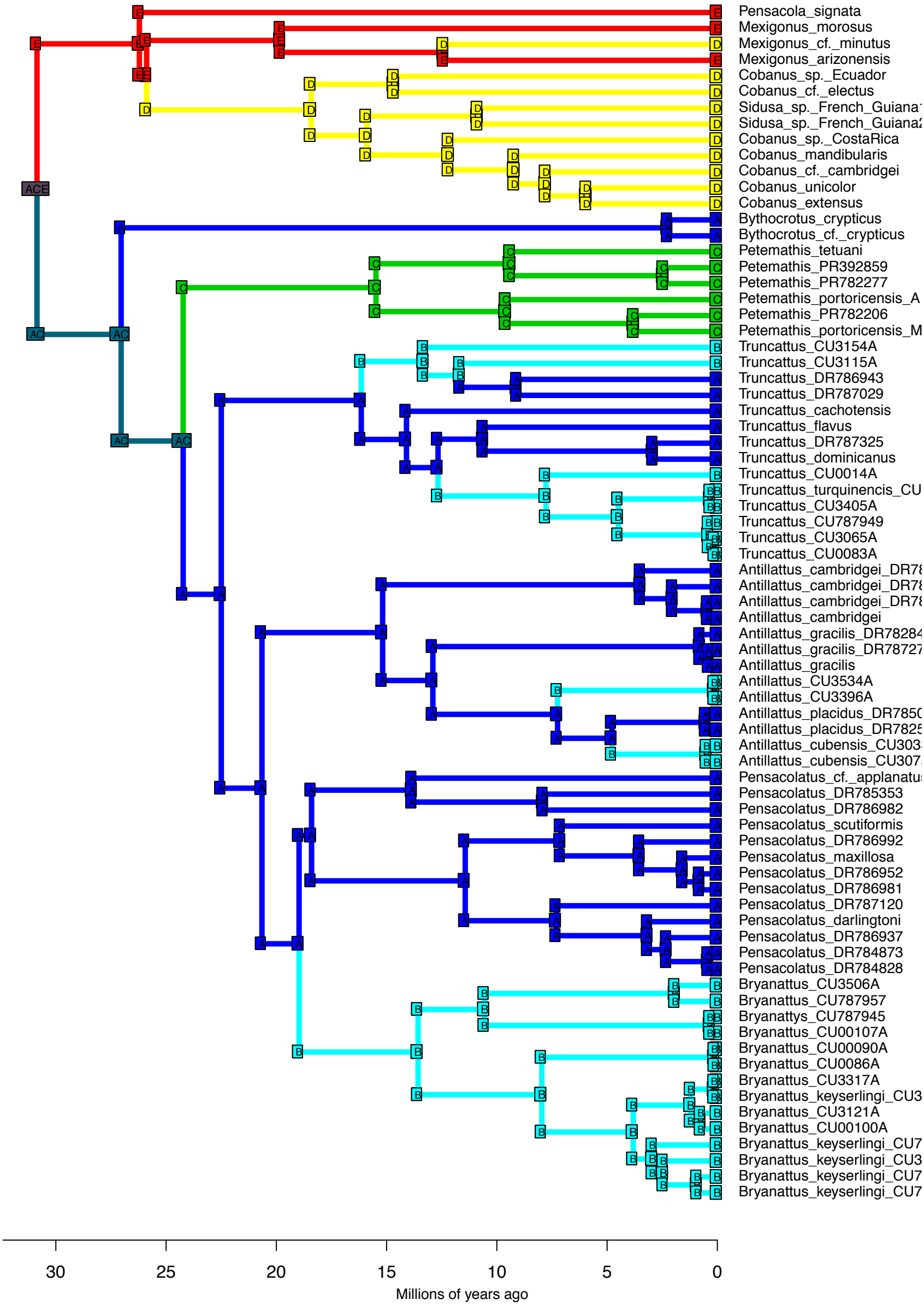

DEC+J – Stochastic Map #39/50
ancstates: global optim, 5 areas max. d=0; e=0; j=0.0153; LnL=−44.20

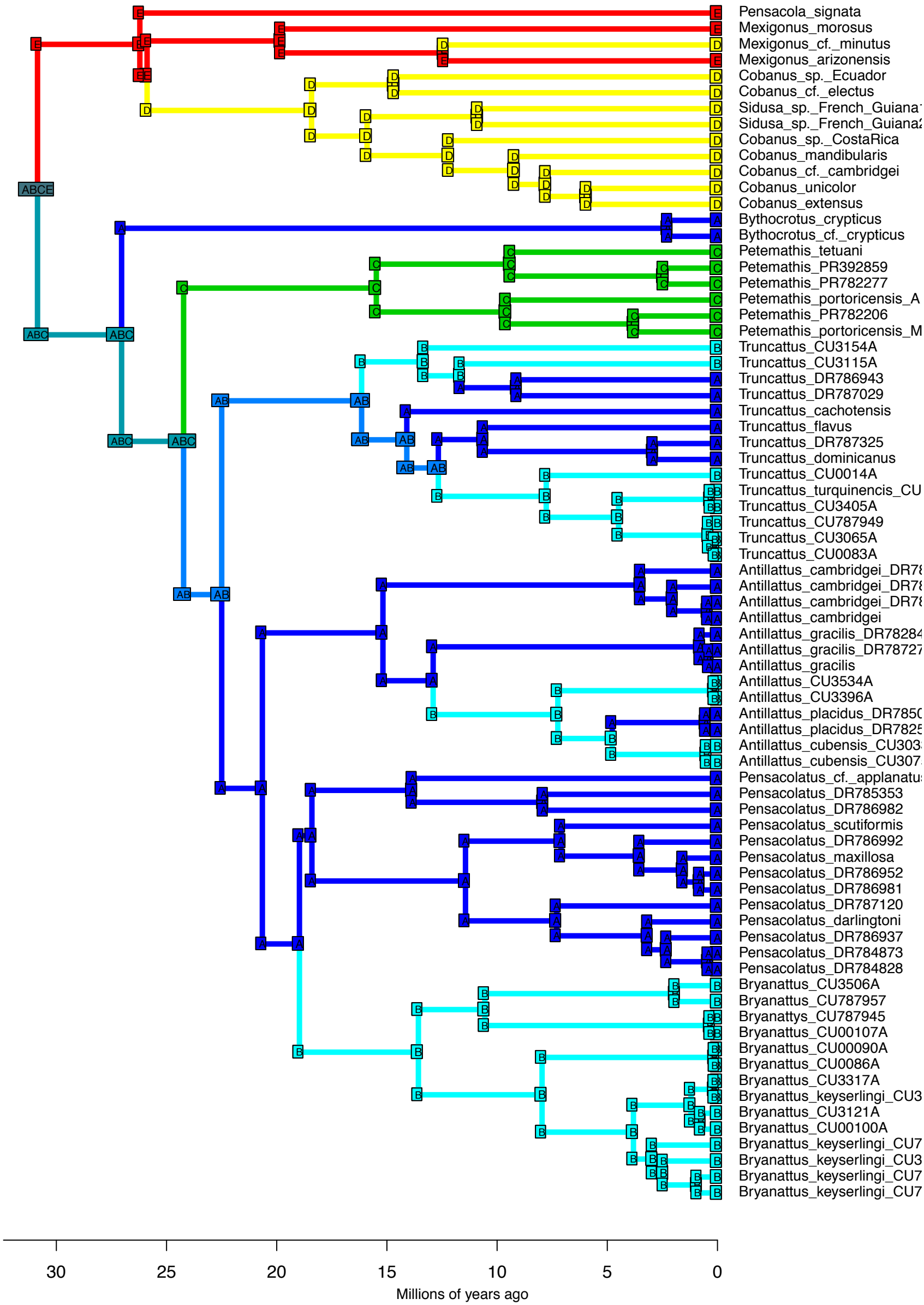

DEC+J – Stochastic Map #40/50
ancstates: global optim, 5 areas max. d=0; e=0; j=0.0153; LnL=−44.20

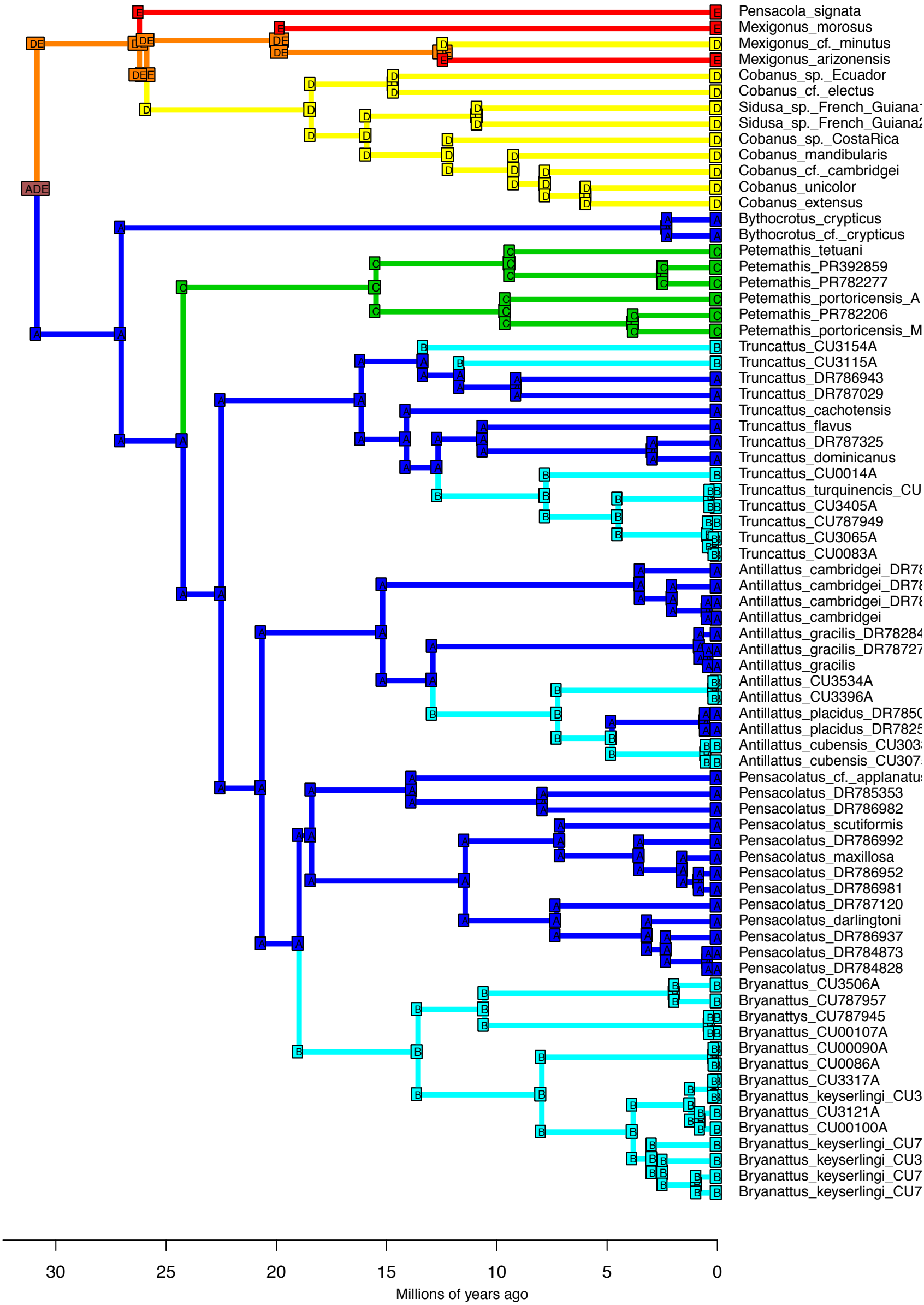

DEC+J – Stochastic Map #41/50
ancstates: global optim, 5 areas max. d=0; e=0; j=0.0153; LnL=−44.20

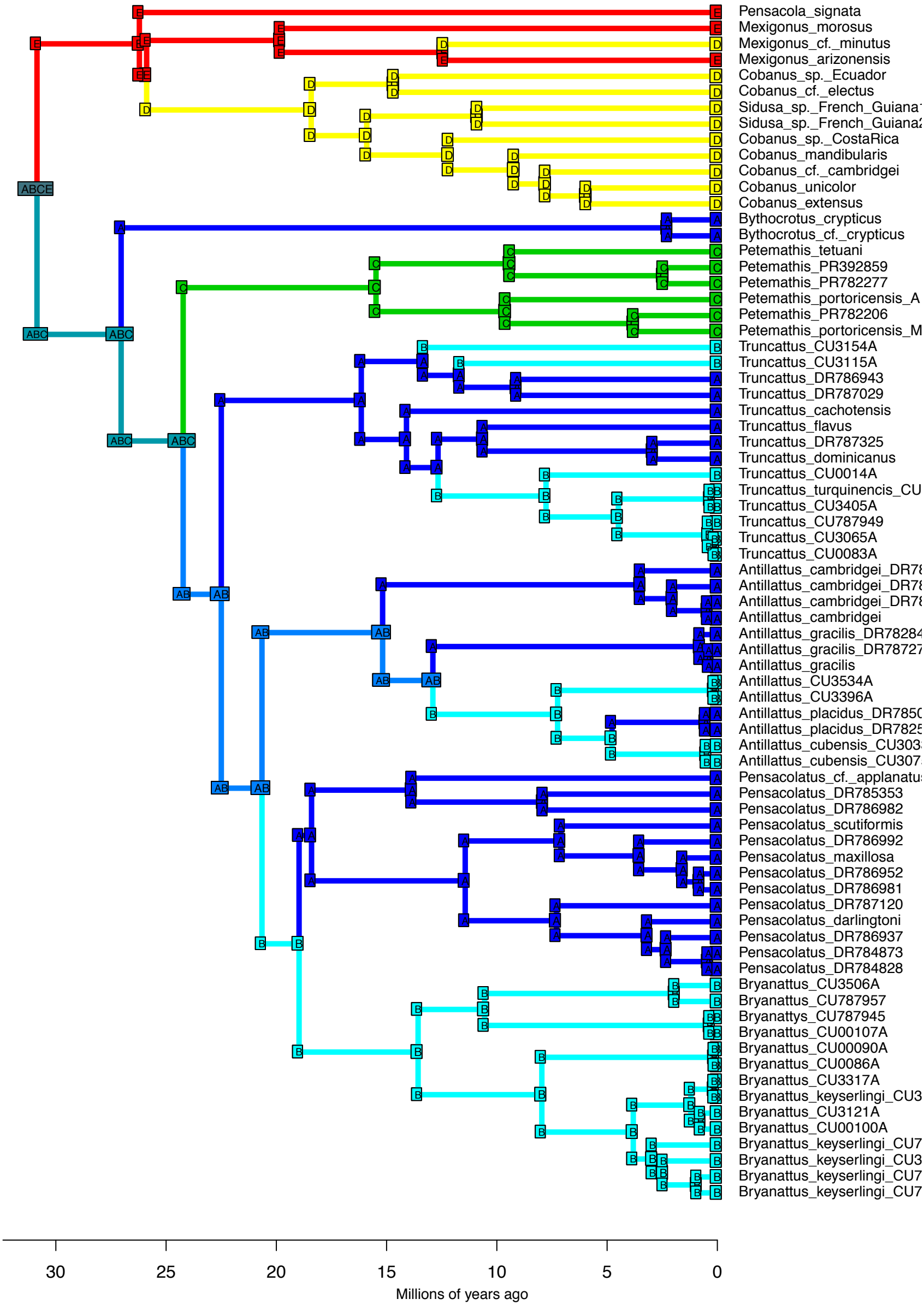

DEC+J – Stochastic Map #42/50
ancstates: global optim, 5 areas max. d=0; e=0; j=0.0153; LnL=−44.20

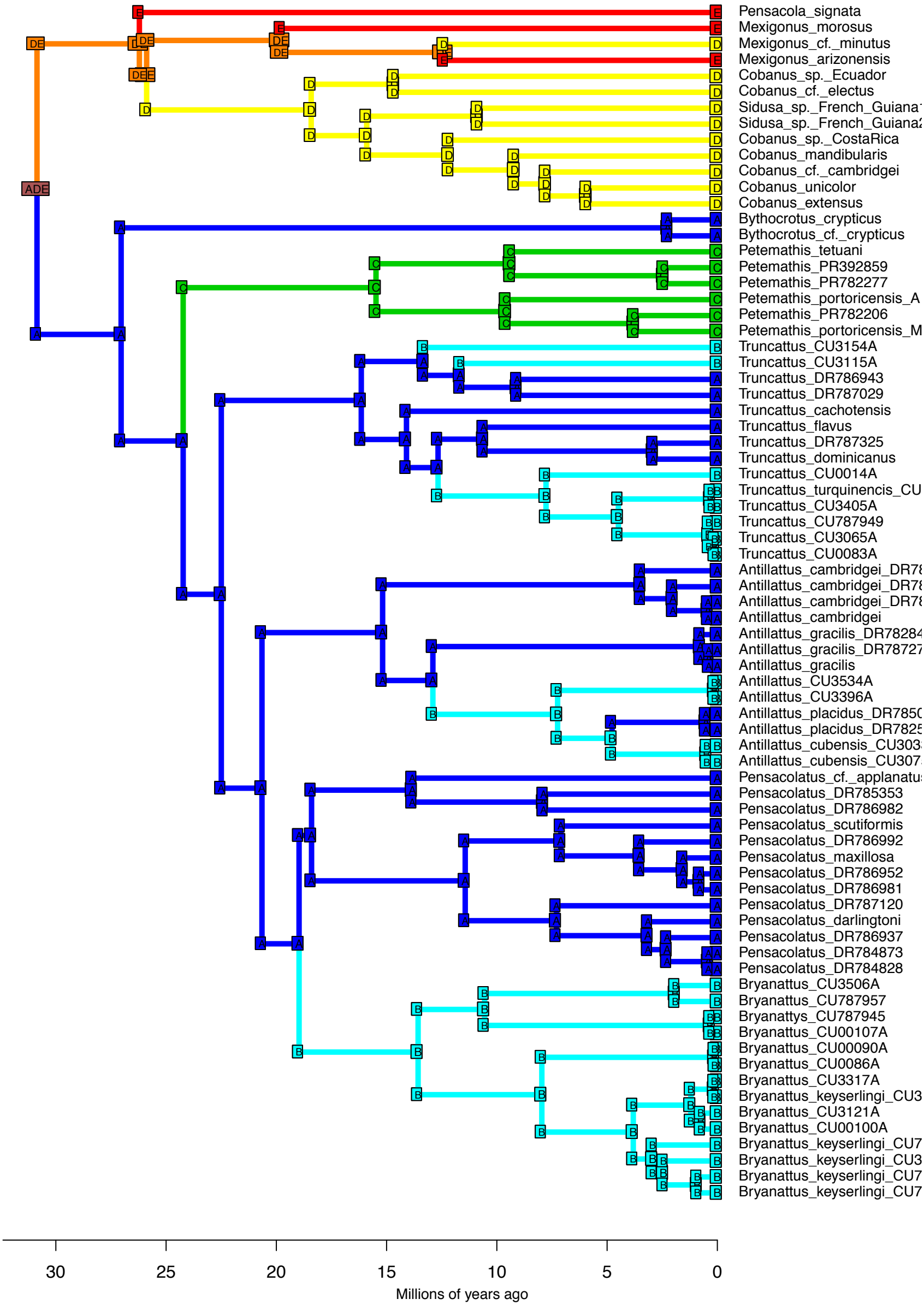

DEC+J – Stochastic Map #43/50
ancstates: global optim, 5 areas max. d=0; e=0; j=0.0153; LnL=−44.20

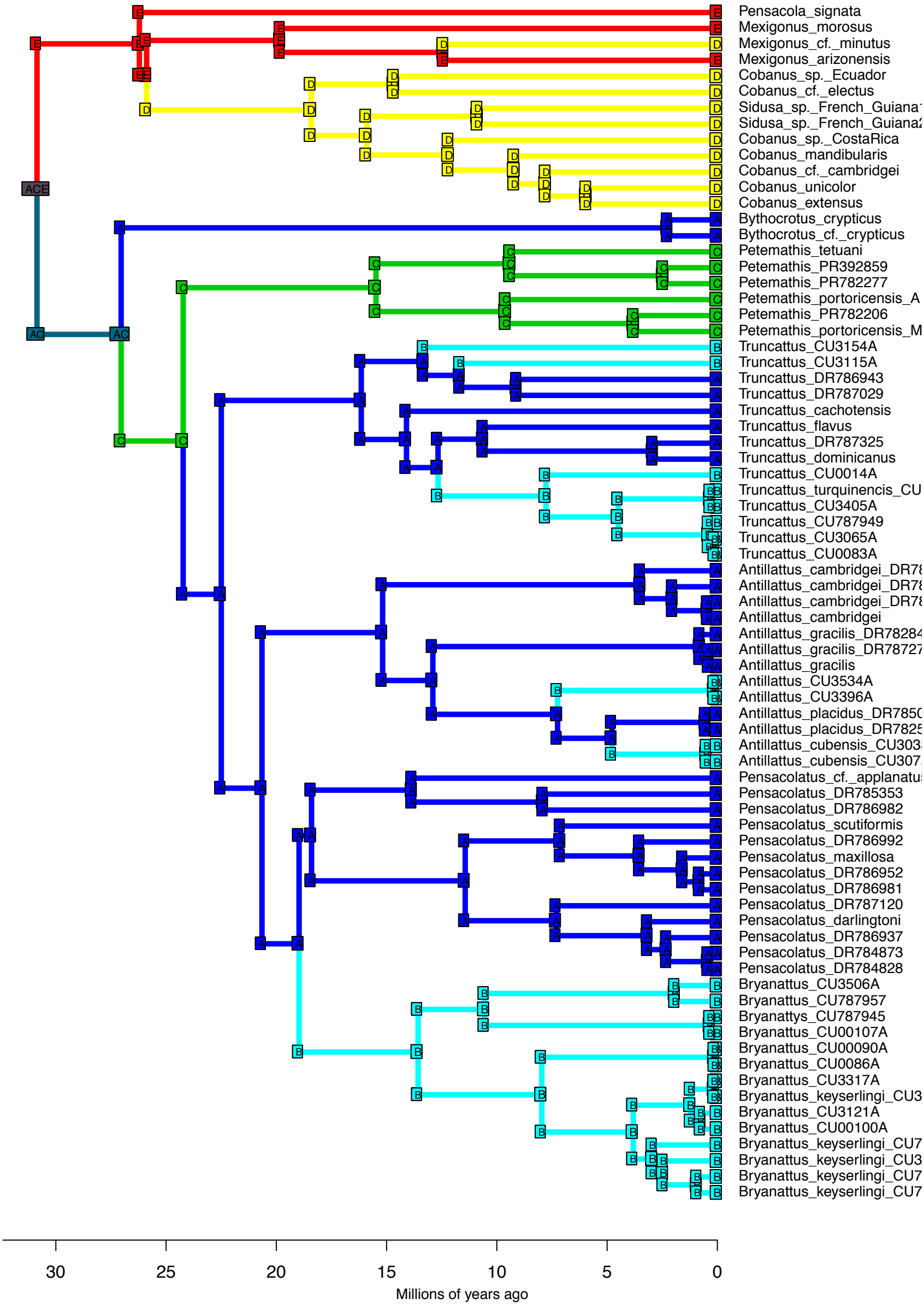

DEC+J – Stochastic Map #44/50
ancstates: global optim, 5 areas max. d=0; e=0; j=0.0153; LnL=−44.20

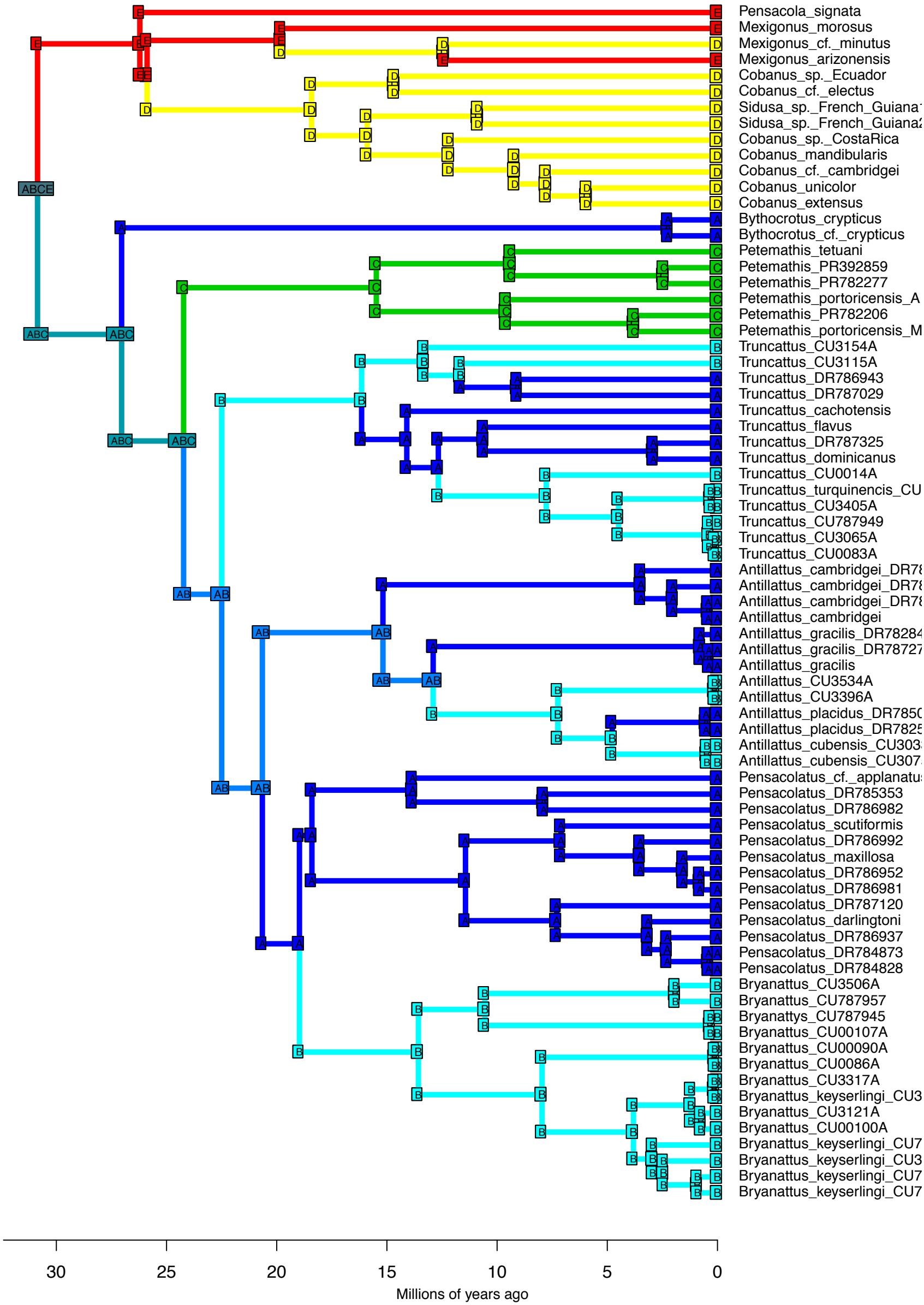

DEC+J – Stochastic Map #45/50
ancstates: global optim, 5 areas max. d=0; e=0; j=0.0153; LnL=−44.20

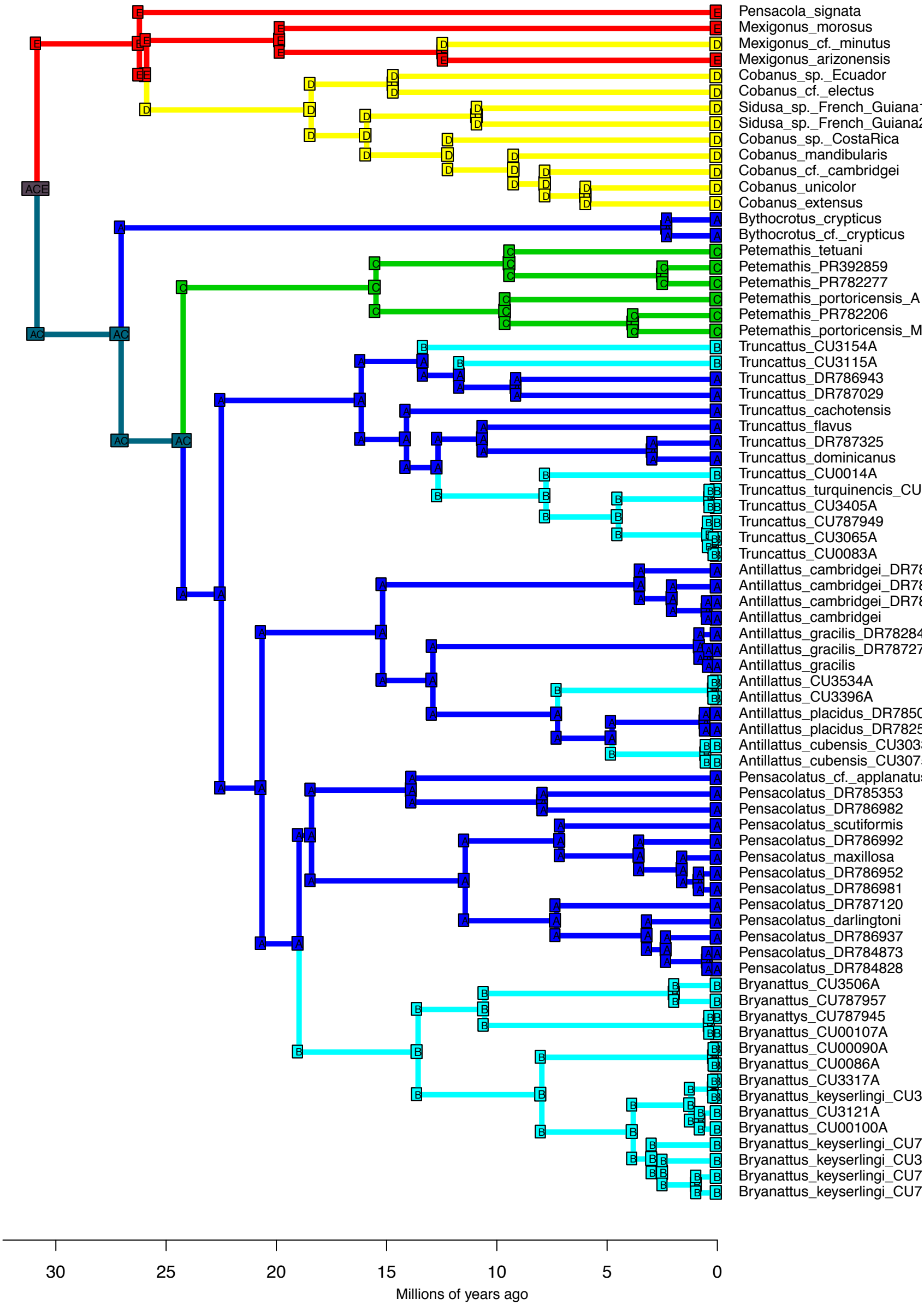

DEC+J – Stochastic Map #46/50
ancstates: global optim, 5 areas max. d=0; e=0; j=0.0153; LnL=−44.20

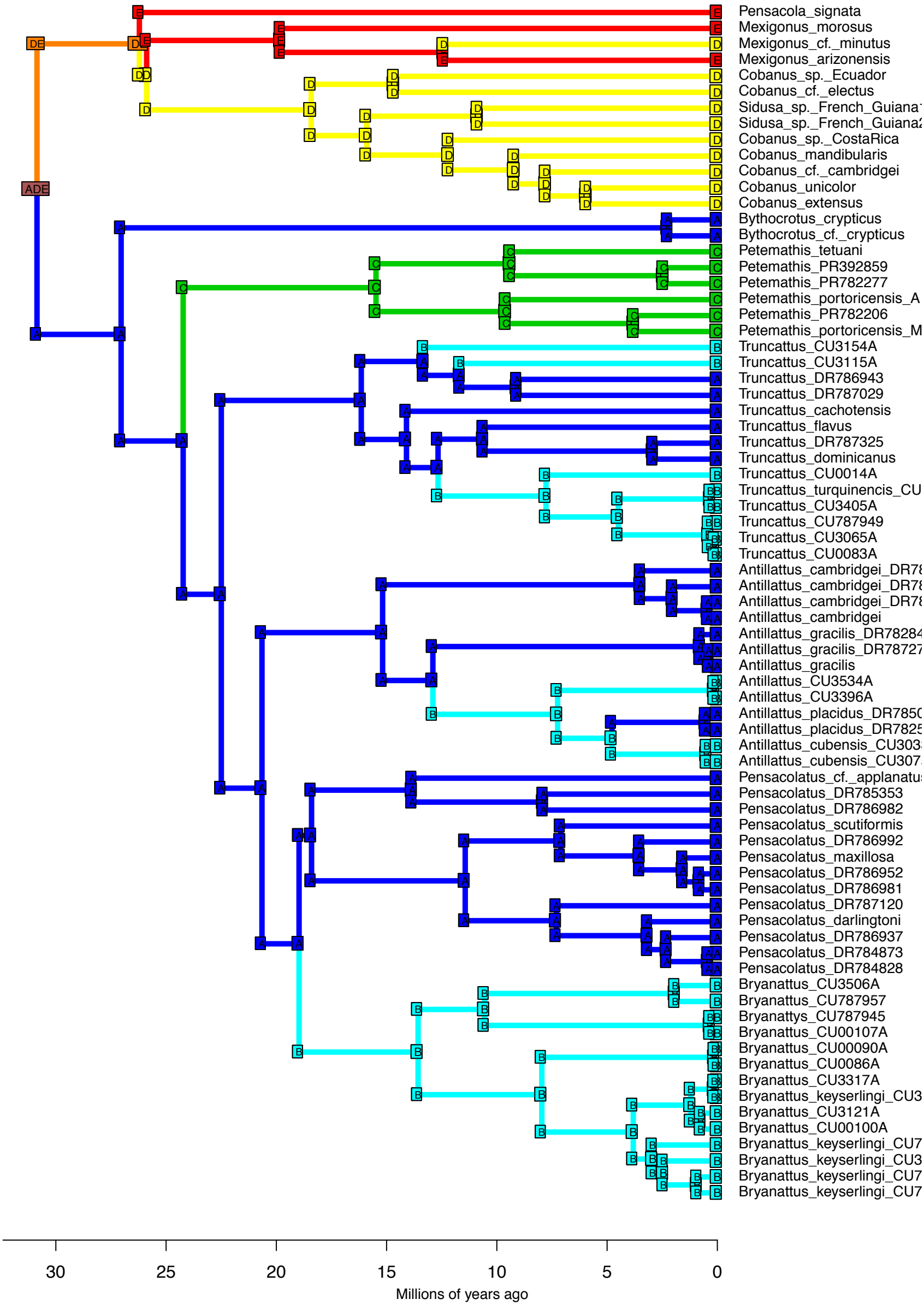

DEC+J – Stochastic Map #47/50
ancstates: global optim, 5 areas max. d=0; e=0; j=0.0153; LnL=−44.20

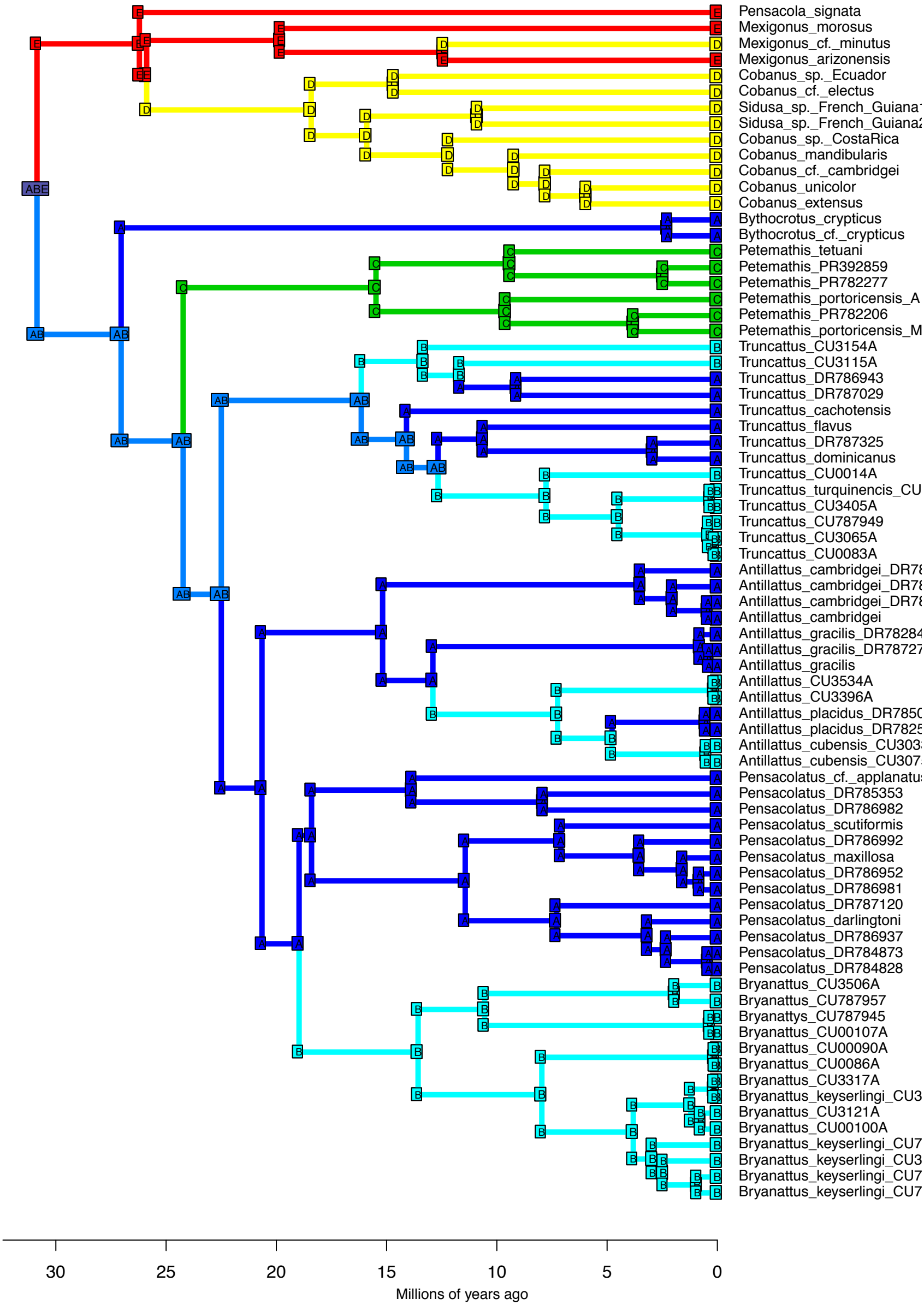

DEC+J – Stochastic Map #48/50
ancstates: global optim, 5 areas max. d=0; e=0; j=0.0153; LnL=−44.20

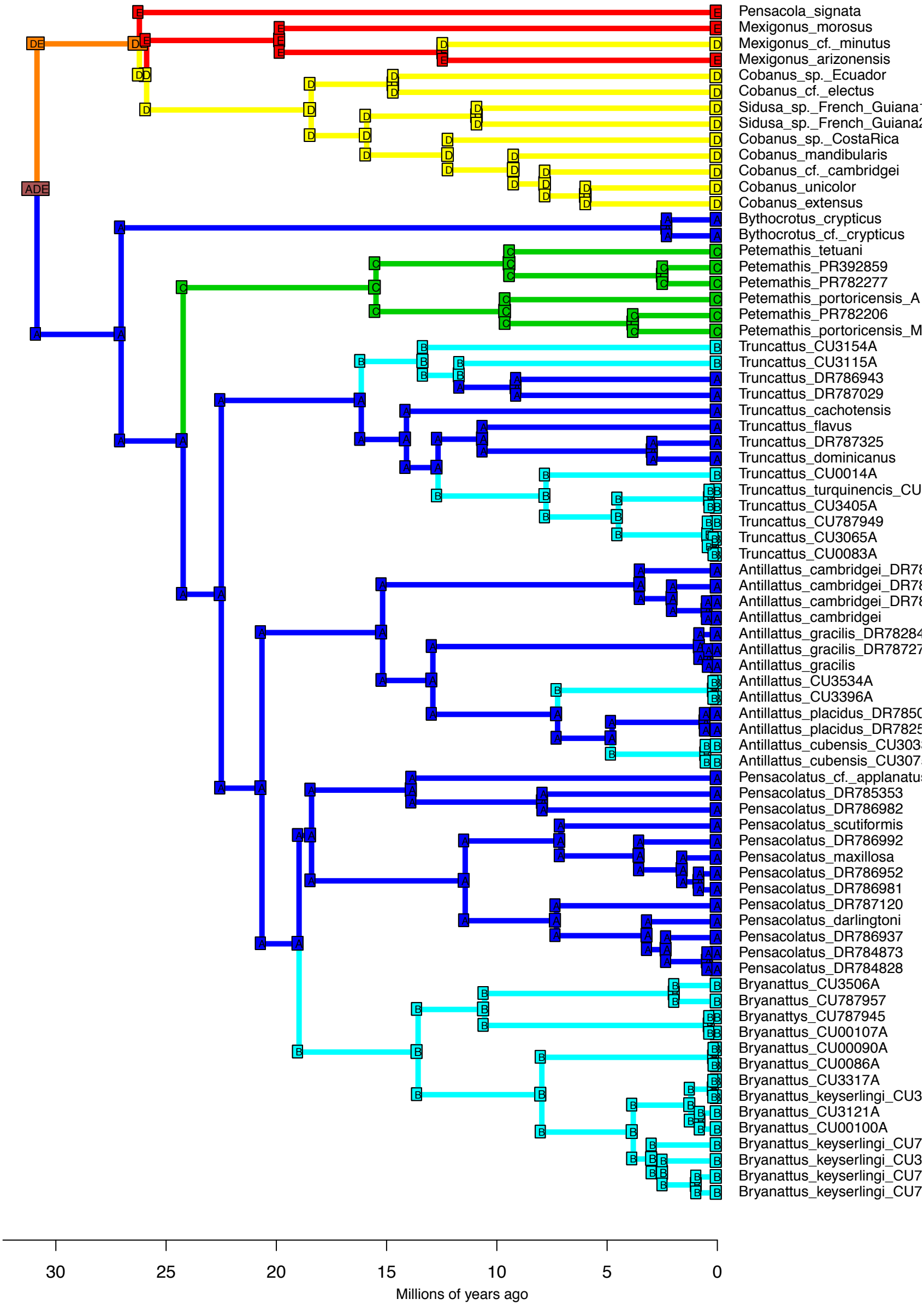

DEC+J – Stochastic Map #49/50
ancstates: global optim, 5 areas max. d=0; e=0; j=0.0153; LnL=−44.20

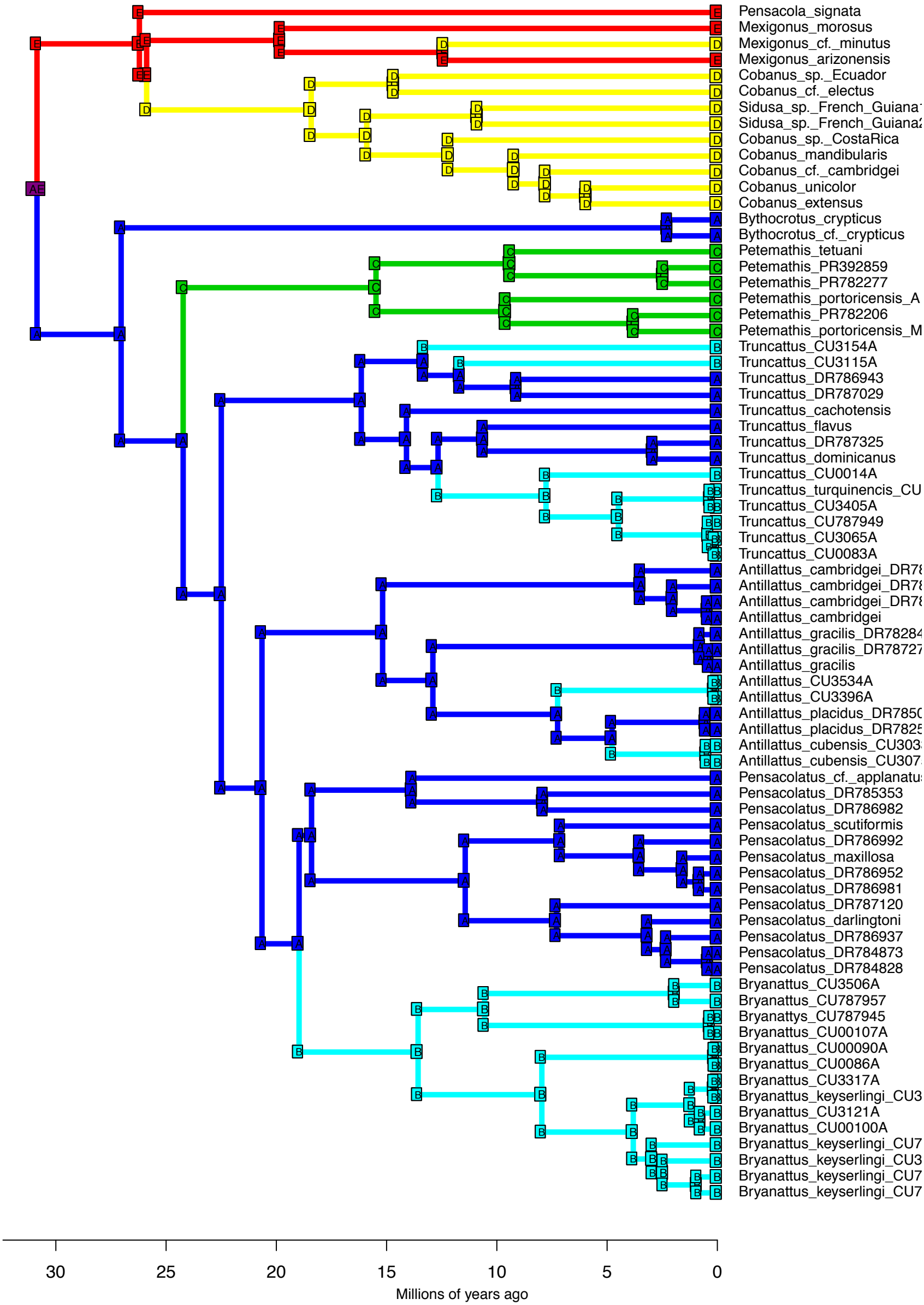

DEC+J – Stochastic Map #50/50
ancstates: global optim, 5 areas max. d=0; e=0; j=0.0153; LnL=−44.20

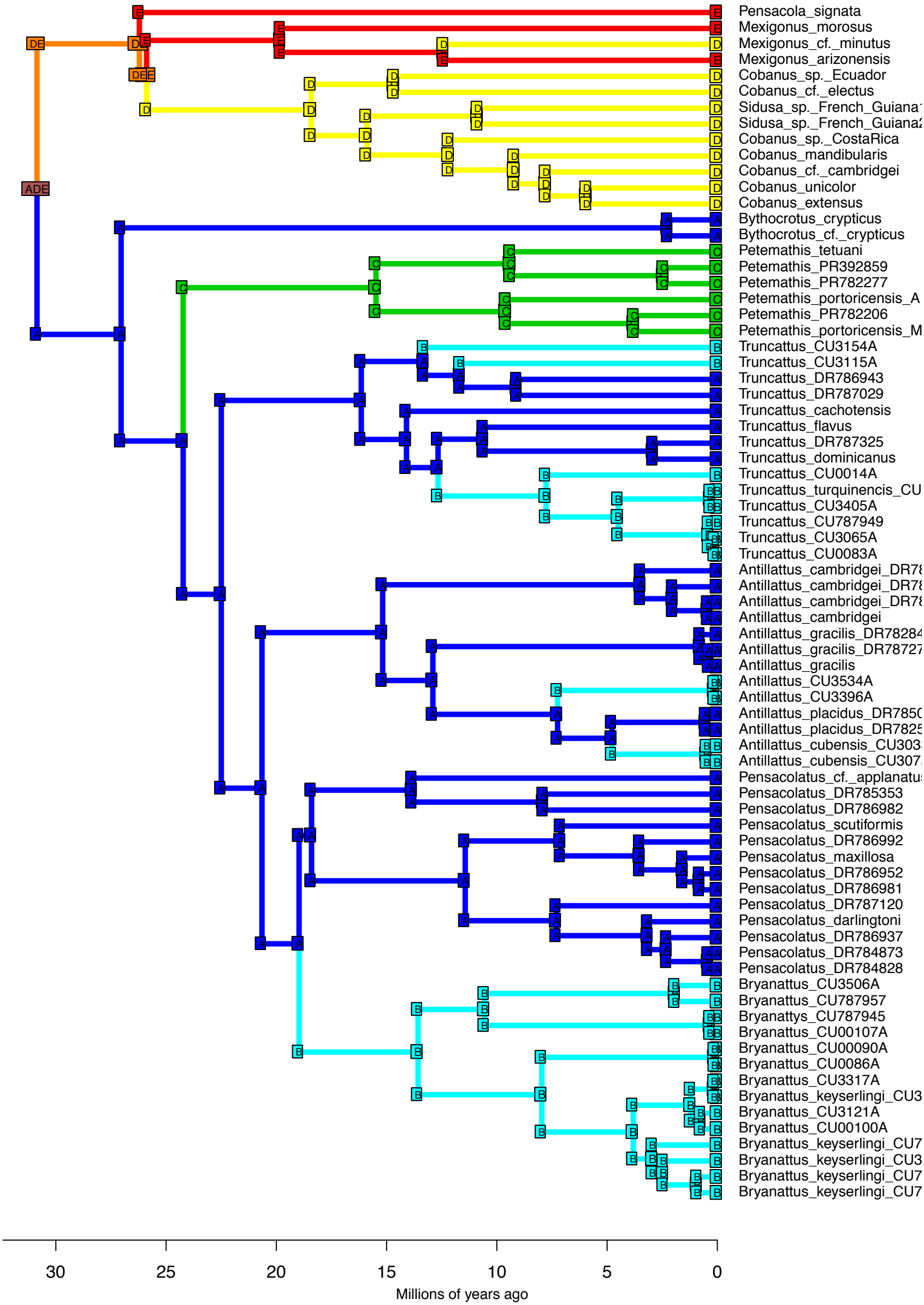

DEC+J_M3b_strat – Stochastic Map #1/50
ancstates: global optim, 5 areas max. d=0; e=0; j=0.0153; LnL=−44.20

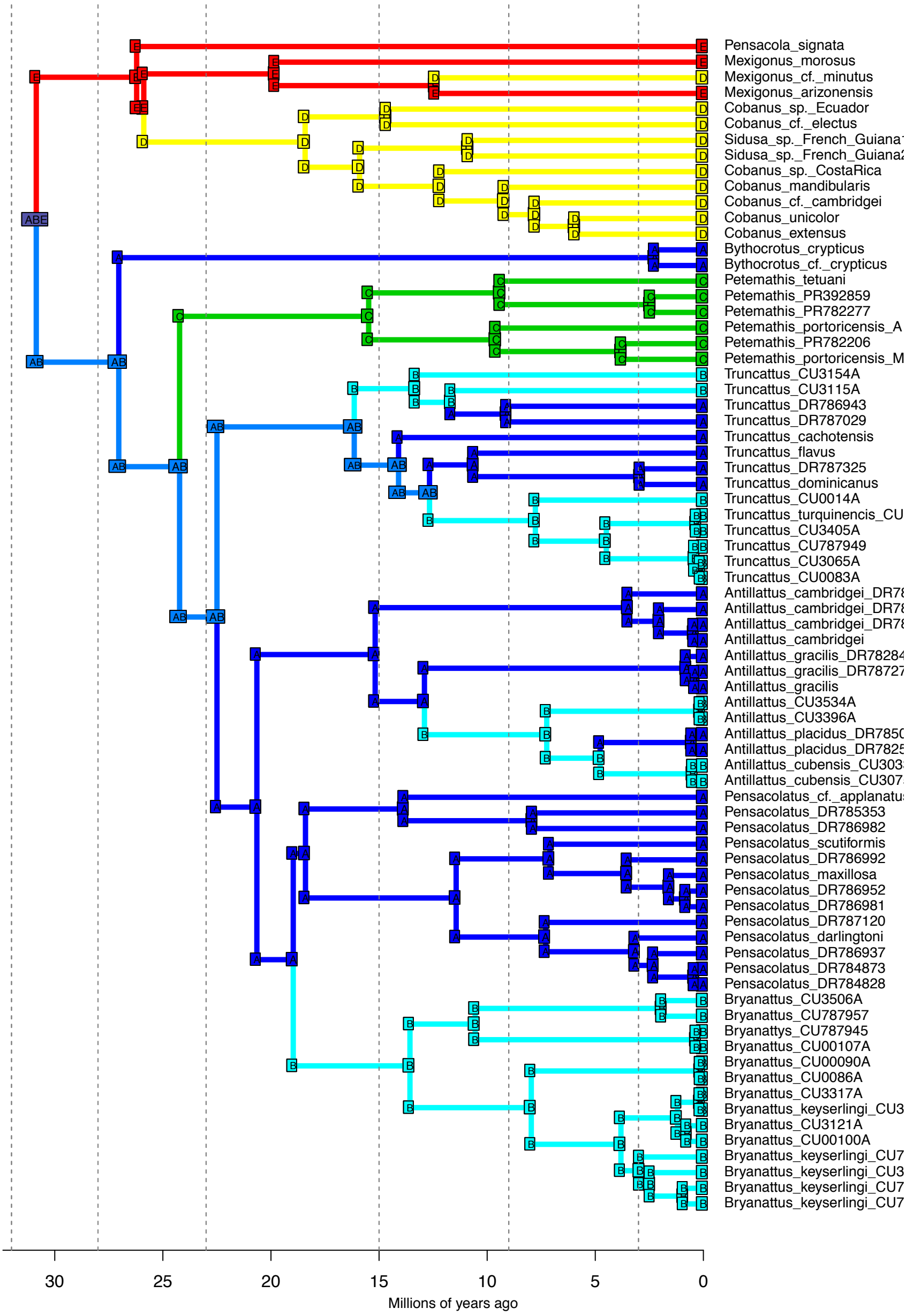

DEC+J_M3b_strat – Stochastic Map #2/50
ancstates: global optim, 5 areas max. d=0; e=0; j=0.0153; LnL=–44.20

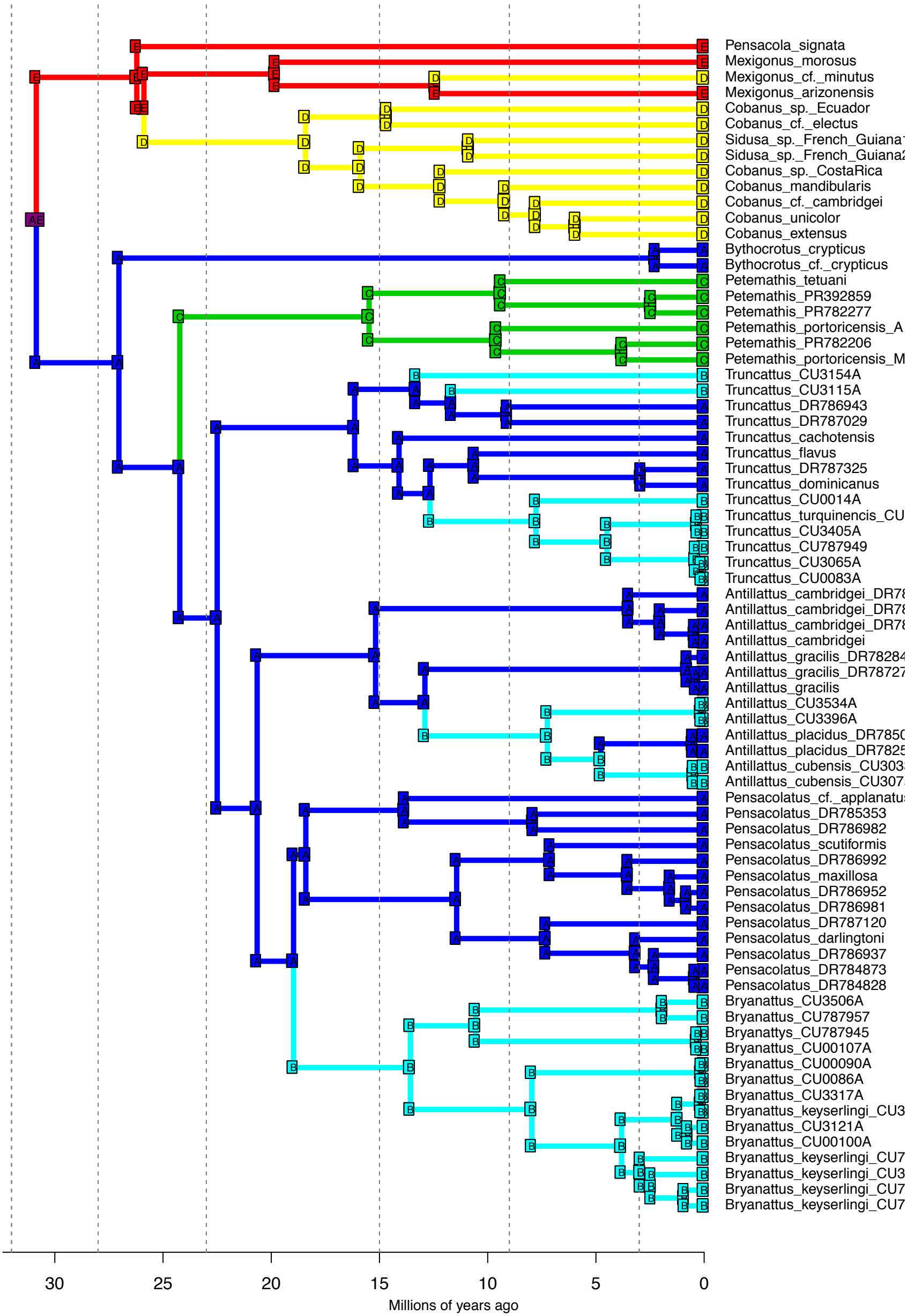

DEC+J_M3b_strat – Stochastic Map #3/50
ancstates: global optim, 5 areas max. d=0; e=0; j=0.0153; LnL=−44.20

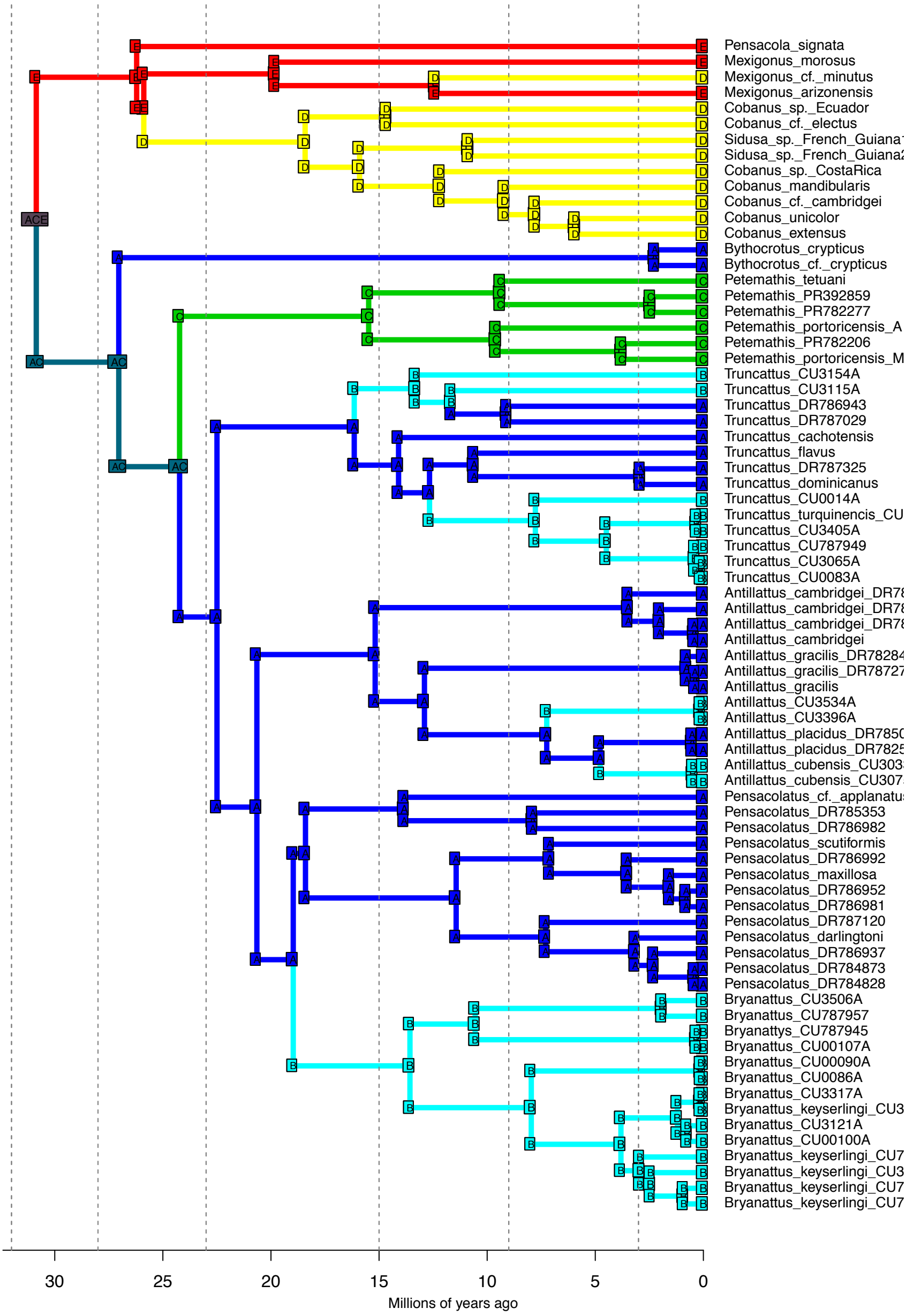

DEC+J_M3b_strat – Stochastic Map #4/50
ancstates: global optim, 5 areas max. d=0; e=0; j=0.0153; LnL=−44.20

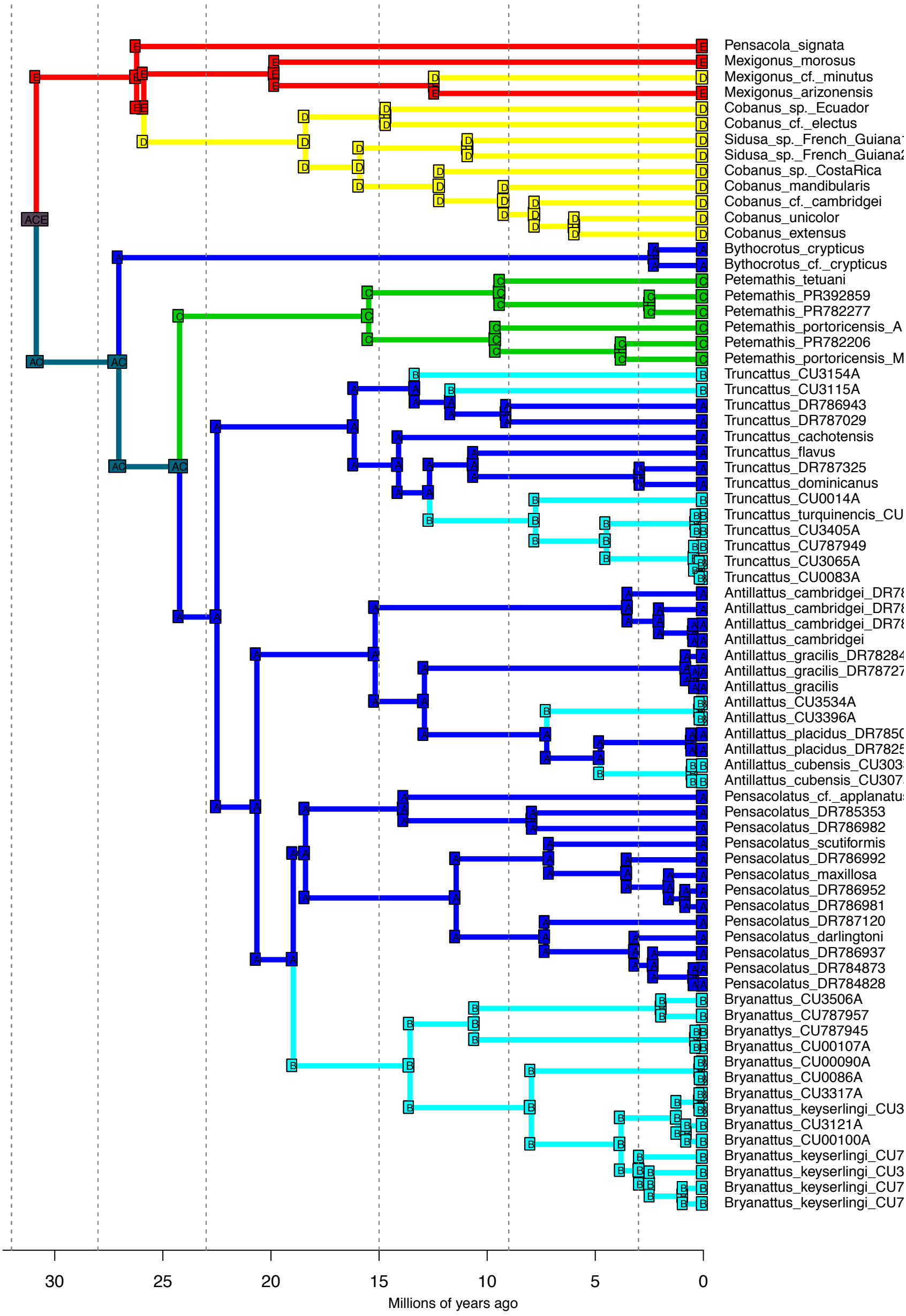

DEC+J_M3b_strat – Stochastic Map #5/50
ancstates: global optim, 5 areas max. d=0; e=0; j=0.0153; LnL=−44.20

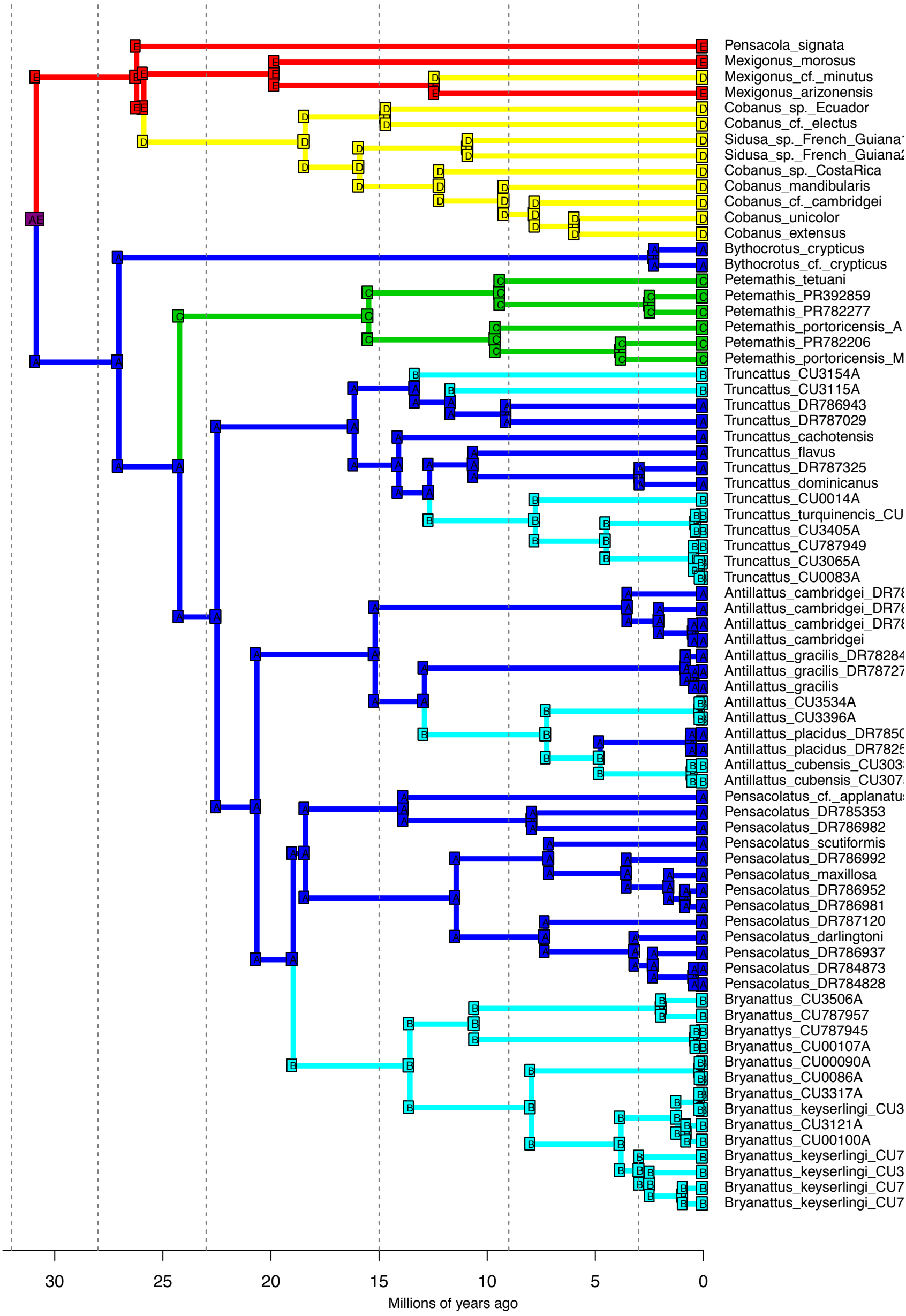

DEC+J_M3b_strat – Stochastic Map #6/50
ancstates: global optim, 5 areas max. d=0; e=0; j=0.0153; LnL=−44.20

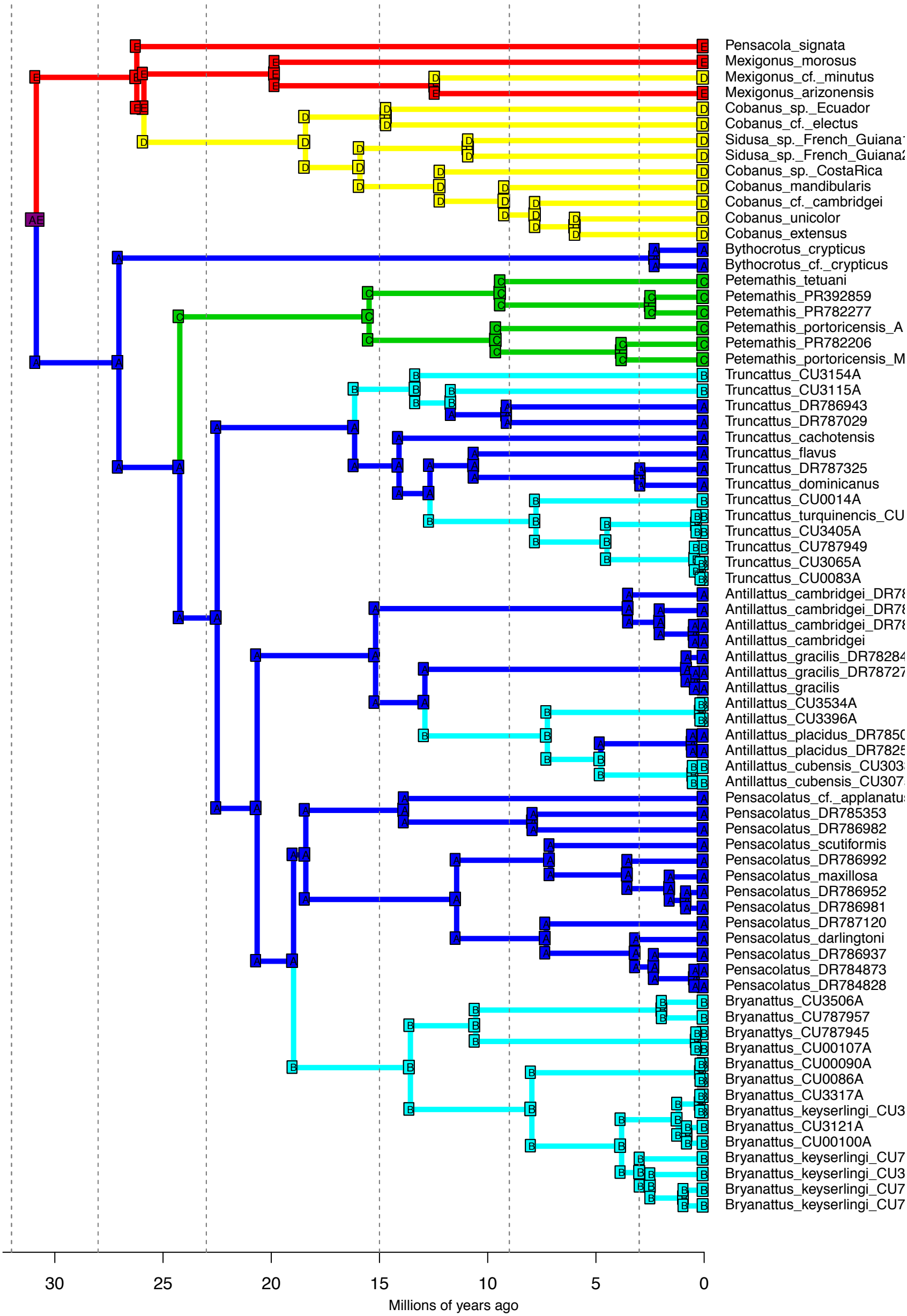

DEC+J_M3b_strat – Stochastic Map #7/50
ancstates: global optim, 5 areas max. d=0; e=0; j=0.0153; LnL=−44.20

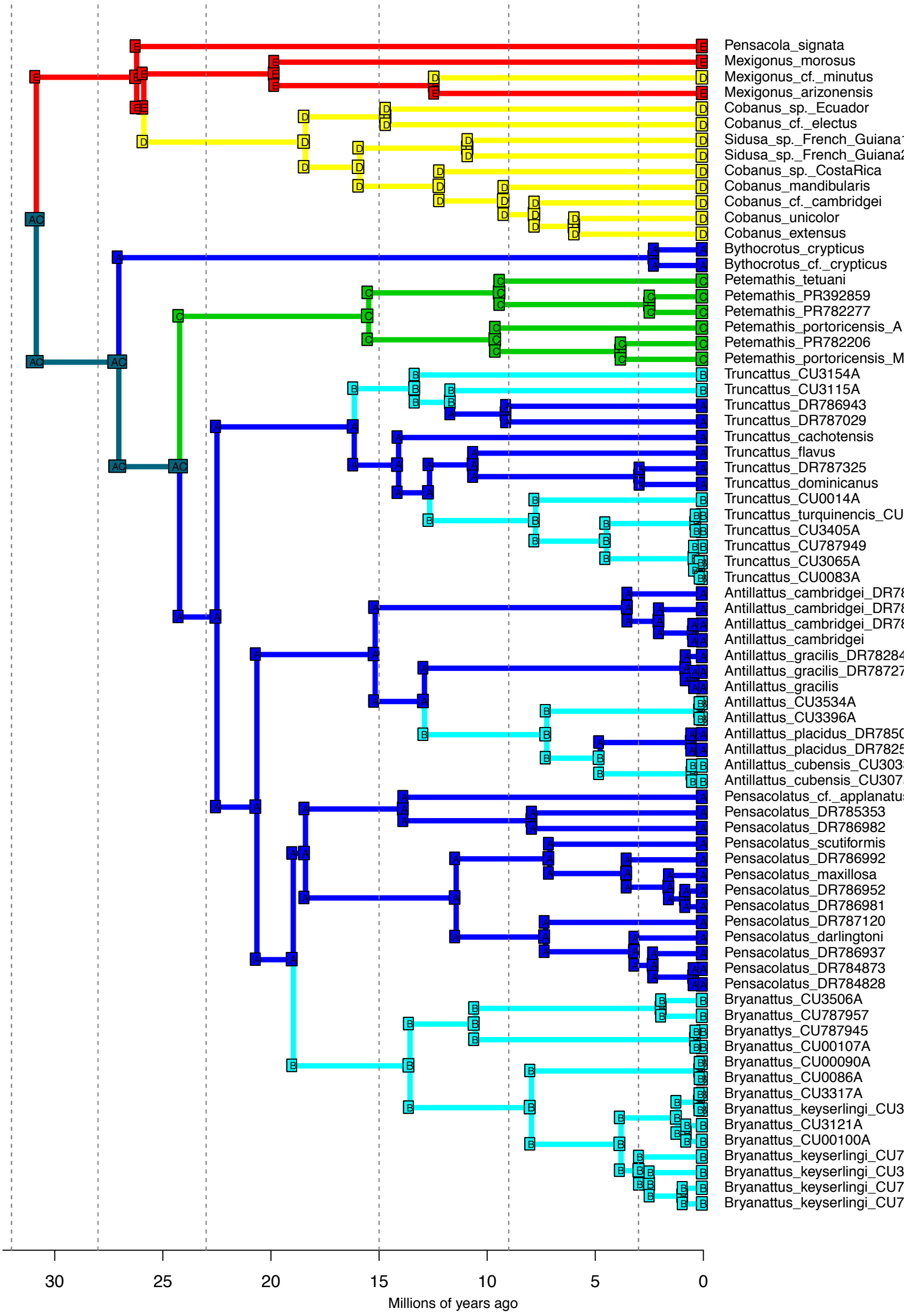

DEC+J_M3b_strat – Stochastic Map #8/50
ancstates: global optim, 5 areas max. d=0; e=0; j=0.0153; LnL=−44.20

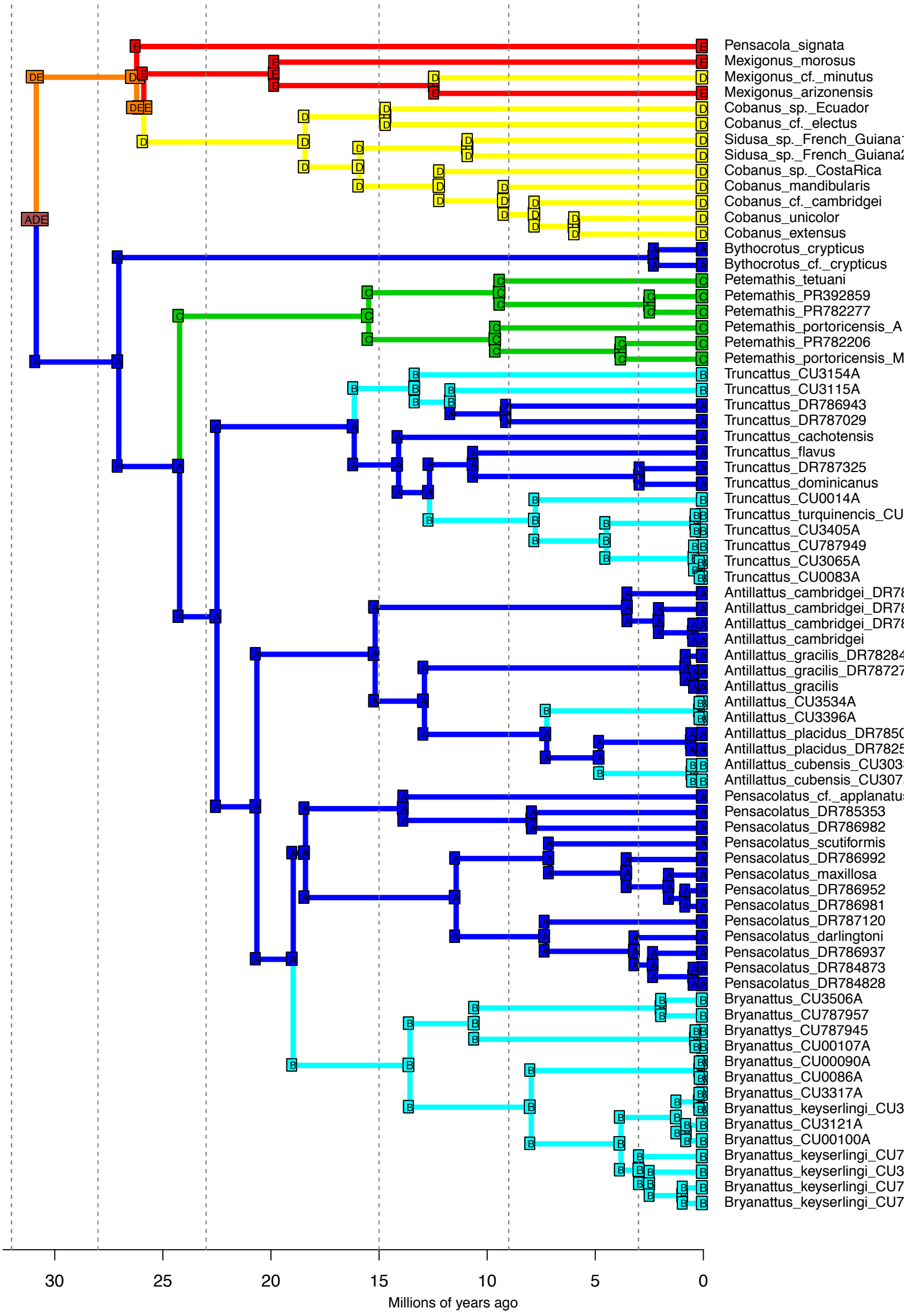

DEC+J_M3b_strat – Stochastic Map #9/50
ancstates: global optim, 5 areas max. d=0; e=0; j=0.0153; LnL=−44.20

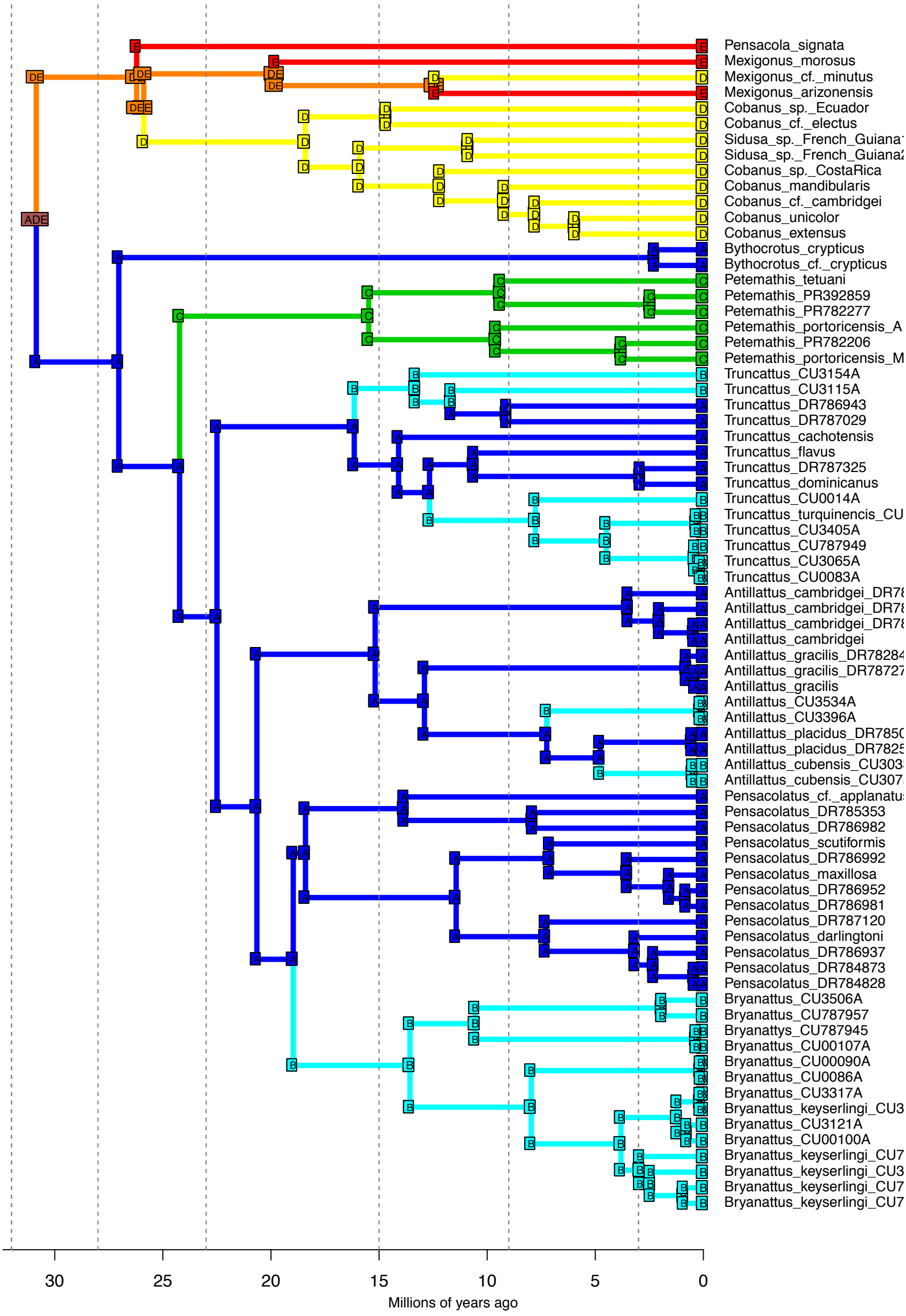

DEC+J_M3b_strat – Stochastic Map #10/50
ancstates: global optim, 5 areas max. d=0; e=0; j=0.0153; LnL=−44.20

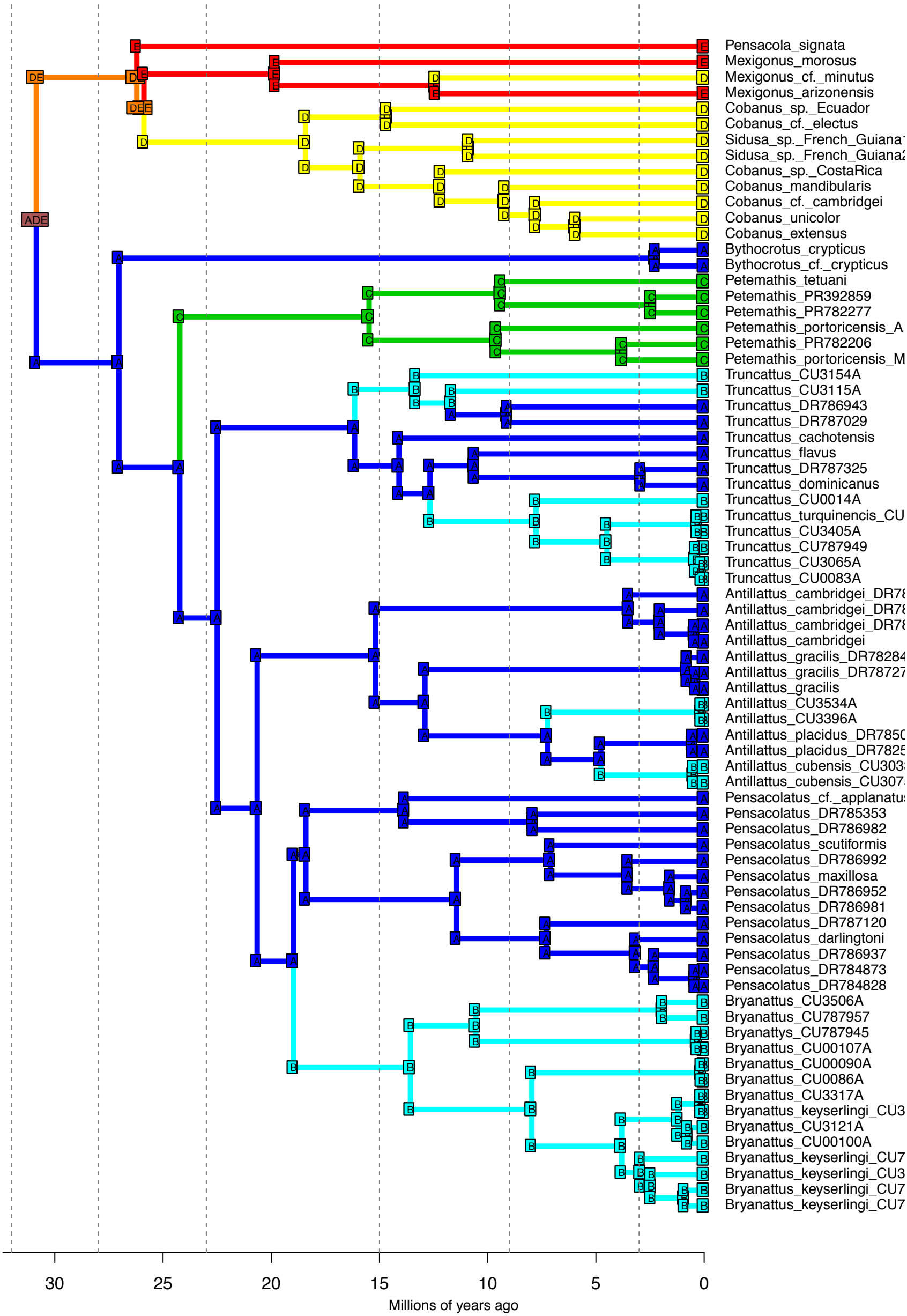

DEC+J_M3b_strat – Stochastic Map #11/50
ancstates: global optim, 5 areas max. d=0; e=0; j=0.0153; LnL=−44.20

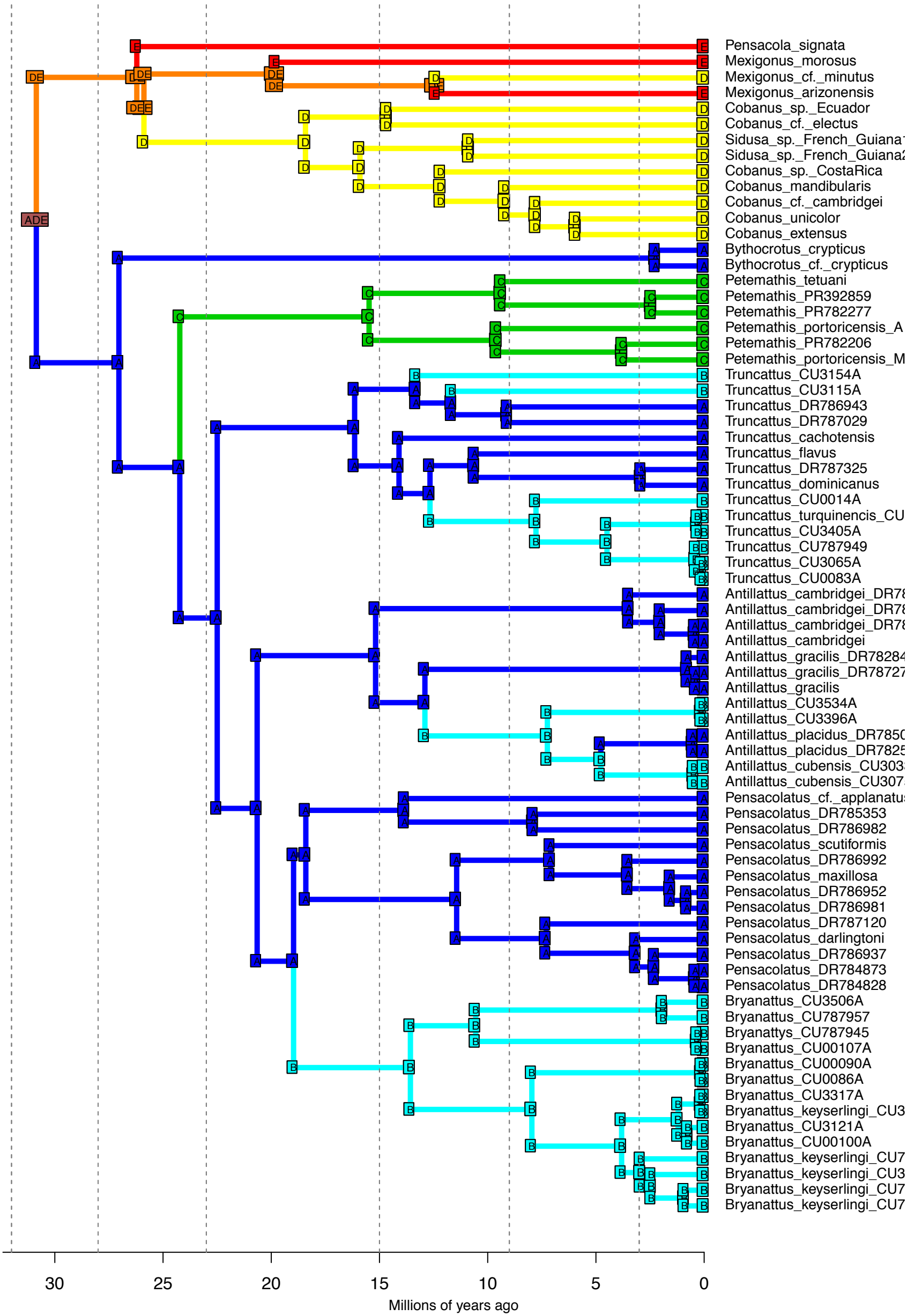

DEC+J_M3b_strat – Stochastic Map #12/50
ancstates: global optim, 5 areas max. d=0; e=0; j=0.0153; LnL=−44.20

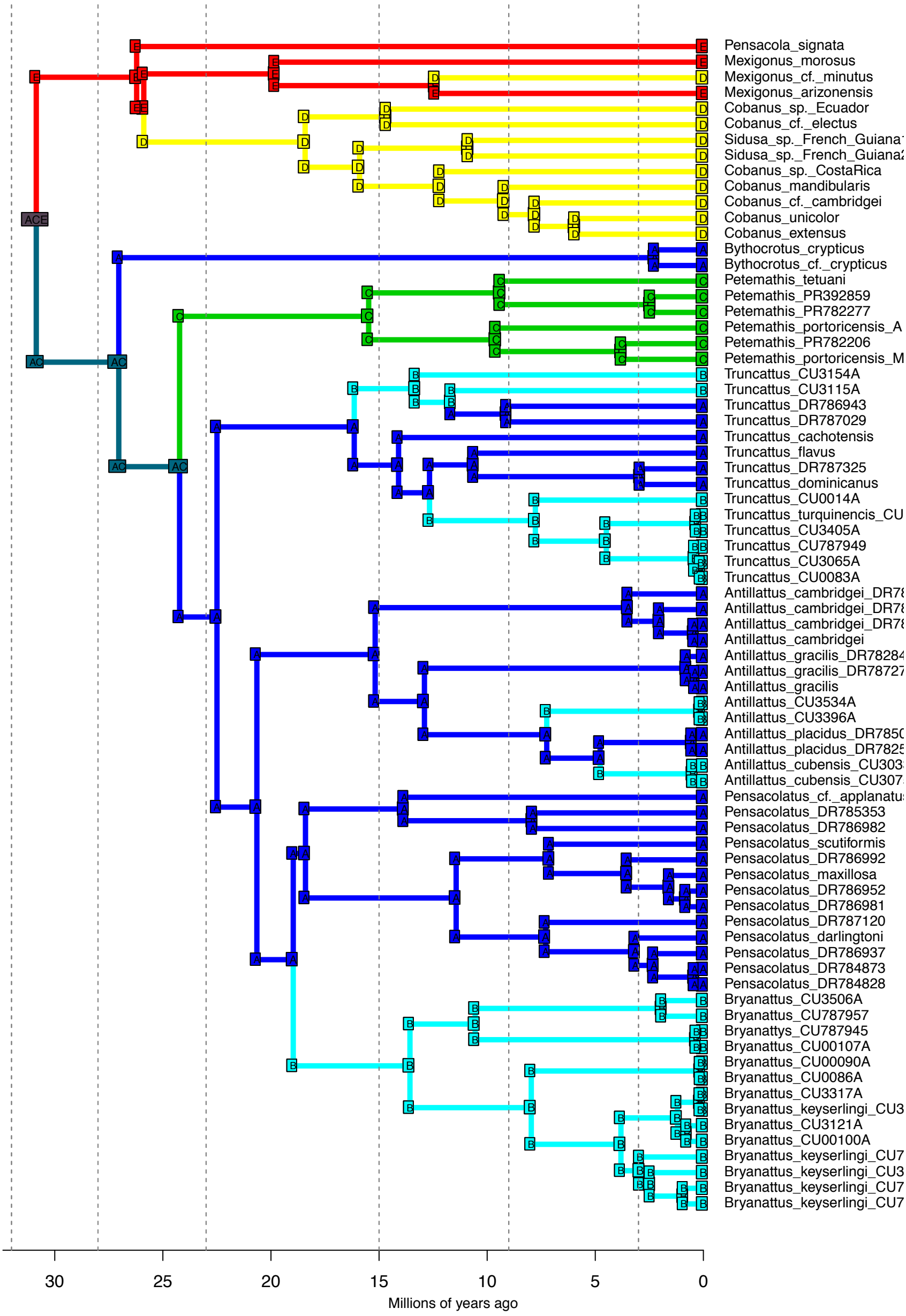

DEC+J_M3b_strat – Stochastic Map #13/50
ancstates: global optim, 5 areas max. d=0; e=0; j=0.0153; LnL=−44.20

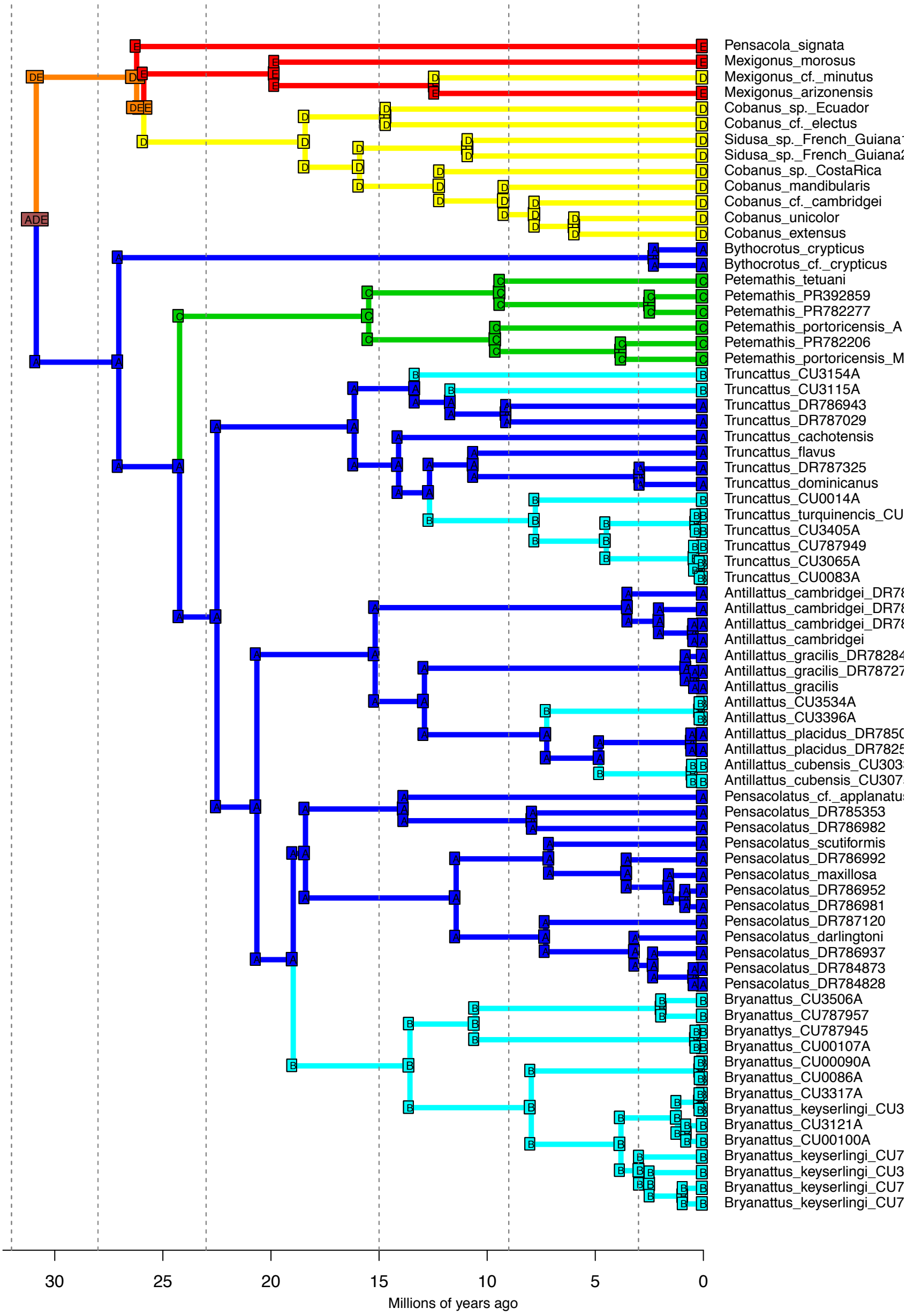

DEC+J_M3b_strat – Stochastic Map #14/50
ancstates: global optim, 5 areas max. d=0; e=0; j=0.0153; LnL=−44.20

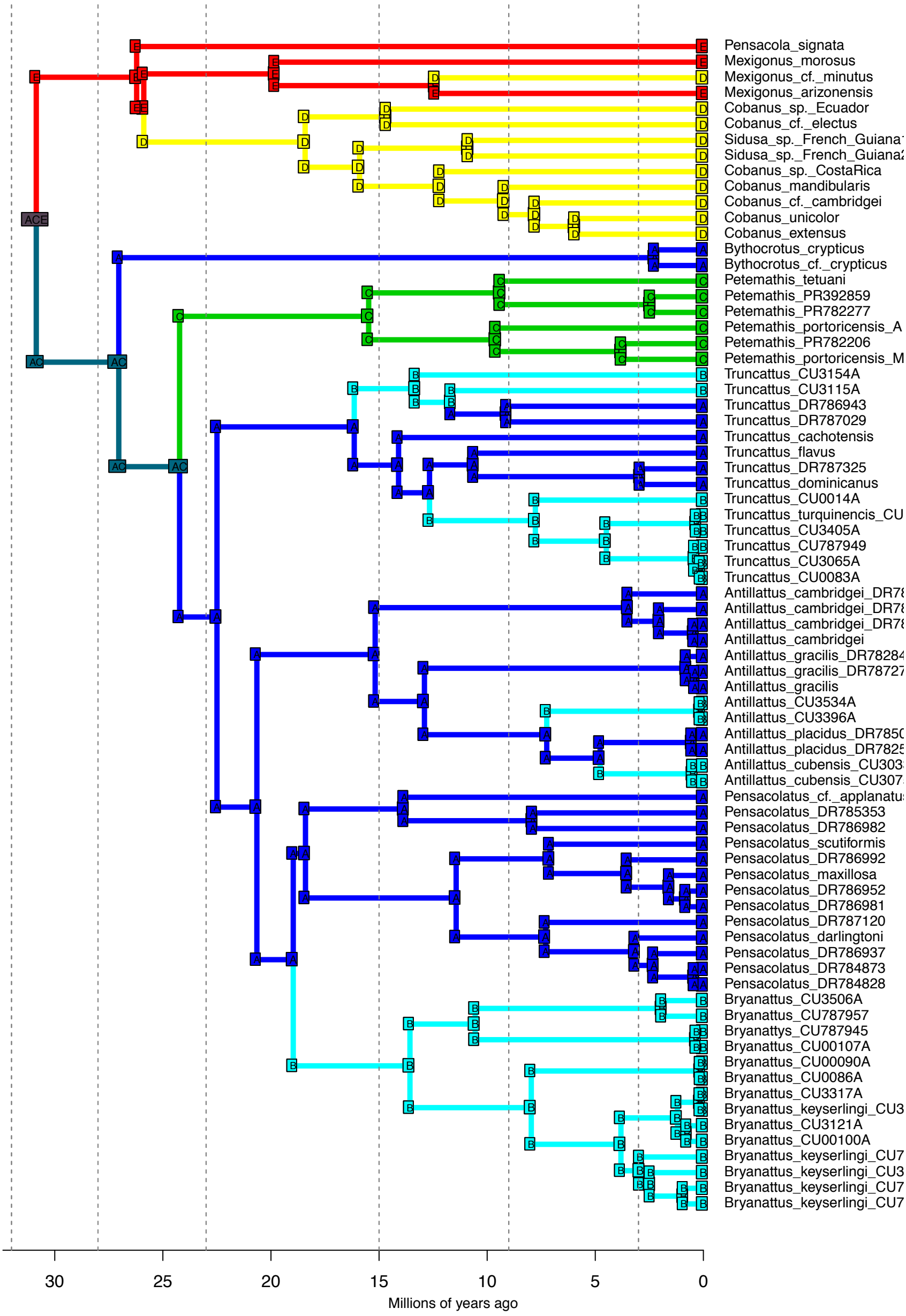

DEC+J_M3b_strat – Stochastic Map #15/50
ancstates: global optim, 5 areas max. d=0; e=0; j=0.0153; LnL=−44.20

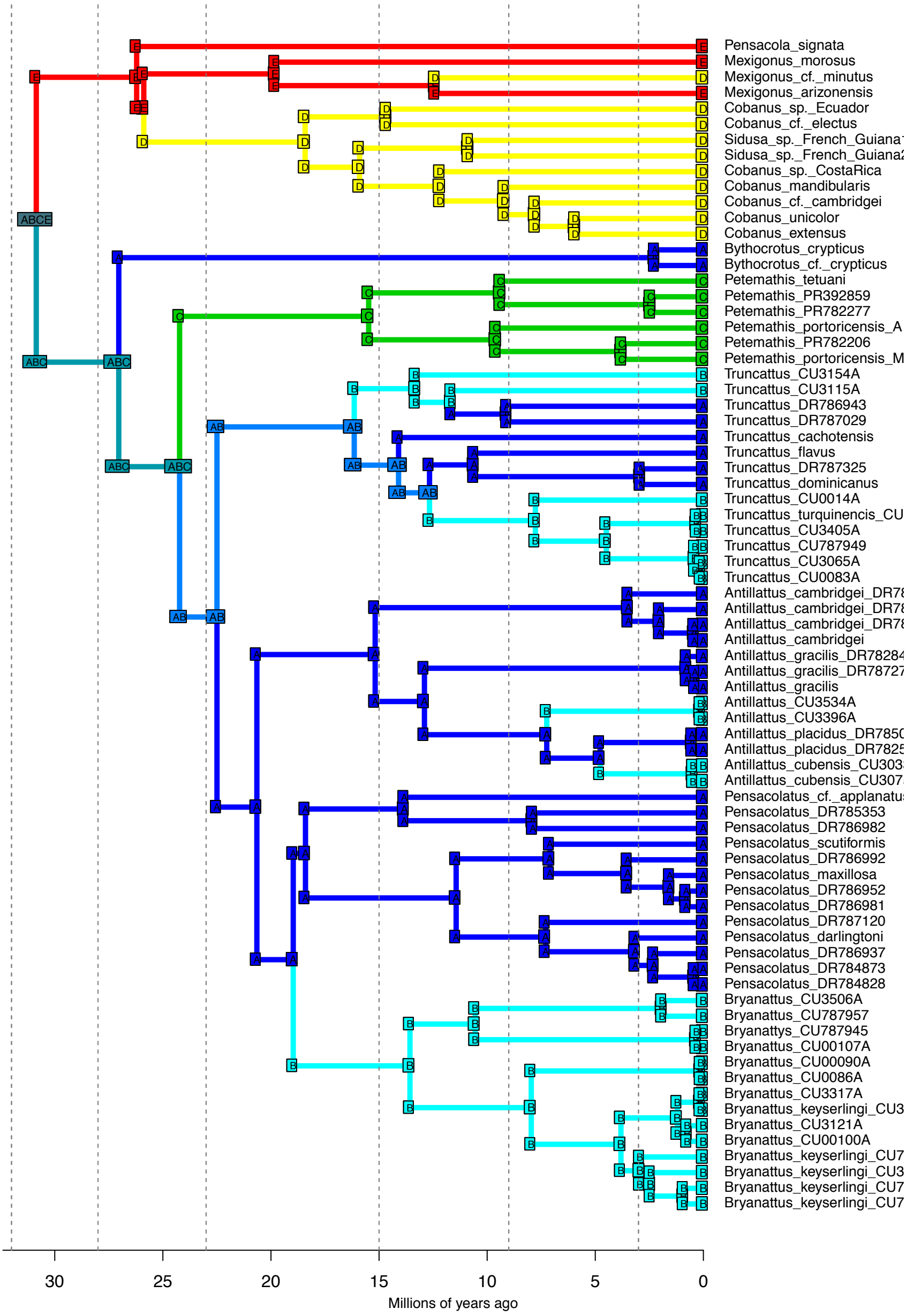

DEC+J_M3b_strat – Stochastic Map #16/50
ancstates: global optim, 5 areas max. d=0; e=0; j=0.0153; LnL=−44.20

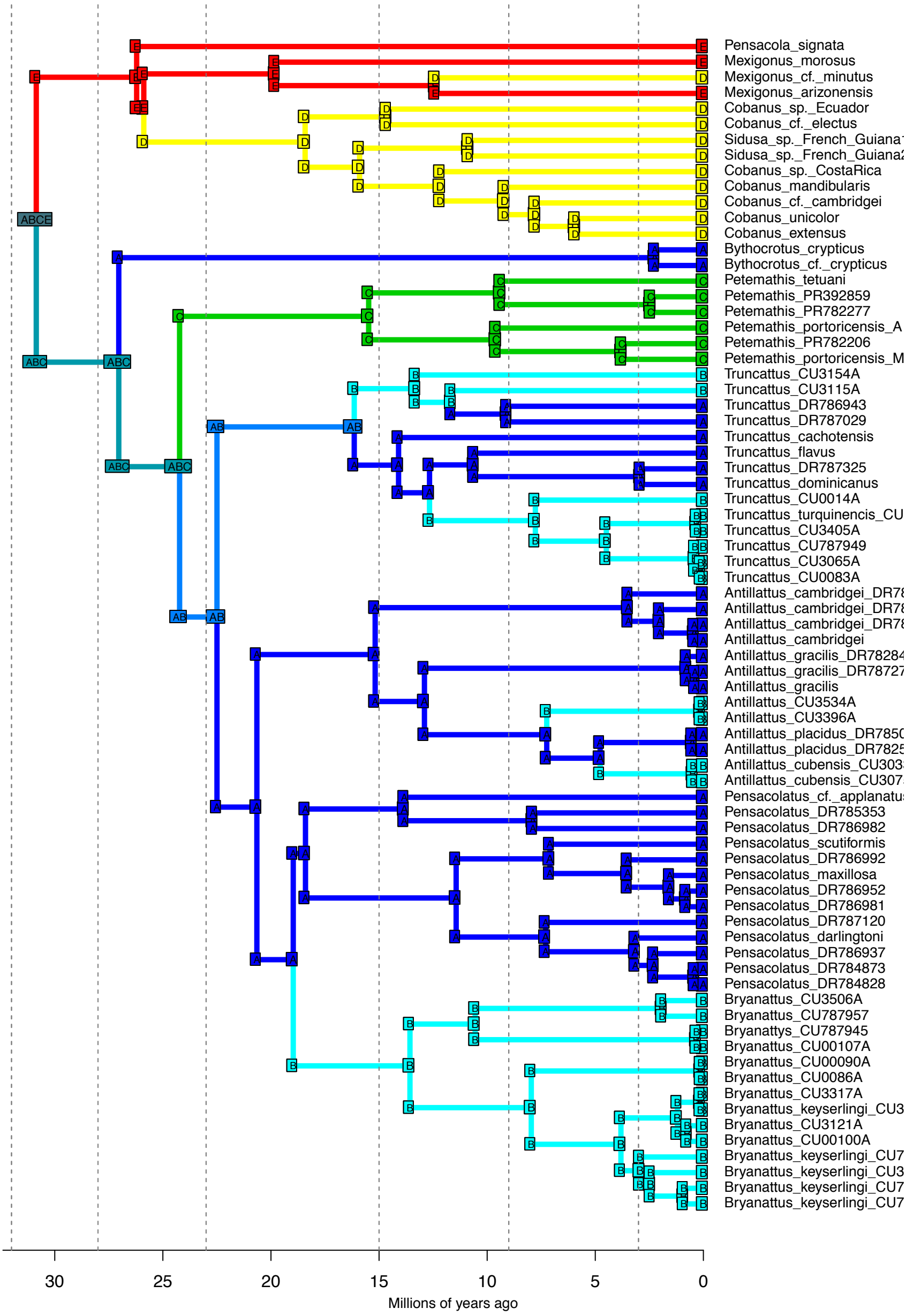

DEC+J_M3b_strat – Stochastic Map #17/50
ancstates: global optim, 5 areas max. d=0; e=0; j=0.0153; LnL=−44.20

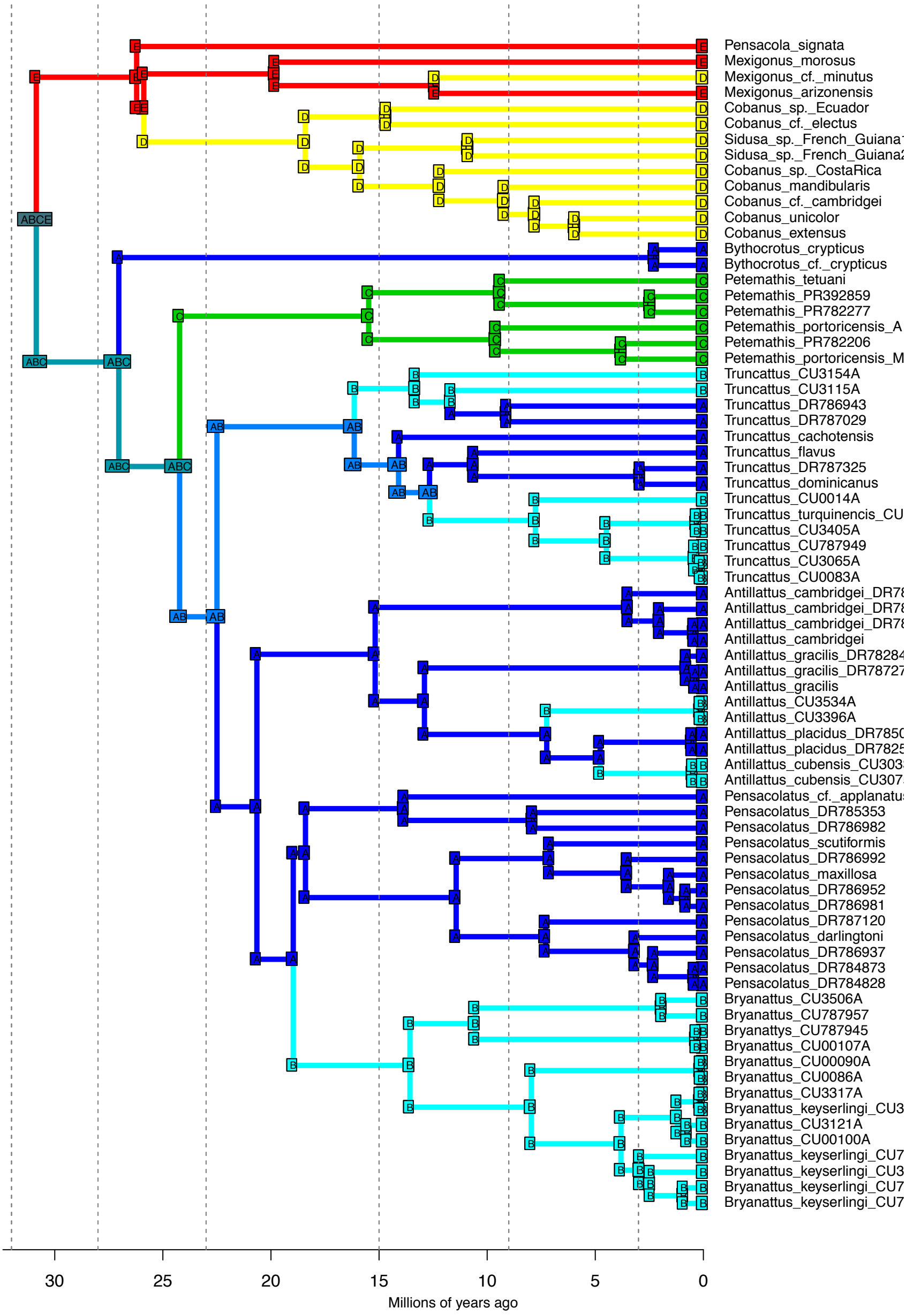

DEC+J_M3b_strat – Stochastic Map #18/50
ancstates: global optim, 5 areas max. d=0; e=0; j=0.0153; LnL=−44.20

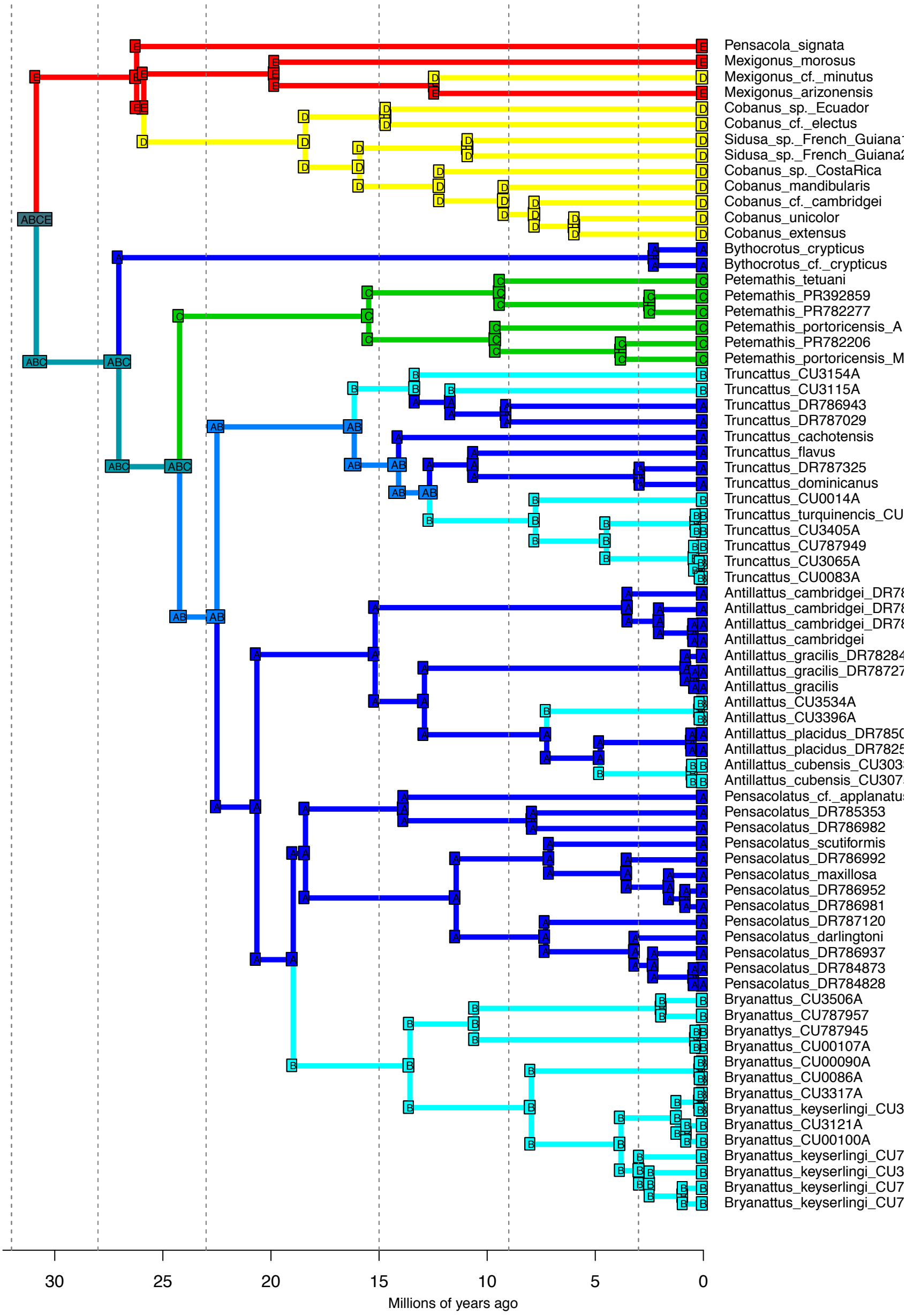

DEC+J_M3b_strat – Stochastic Map #19/50
ancstates: global optim, 5 areas max. d=0; e=0; j=0.0153; LnL=−44.20

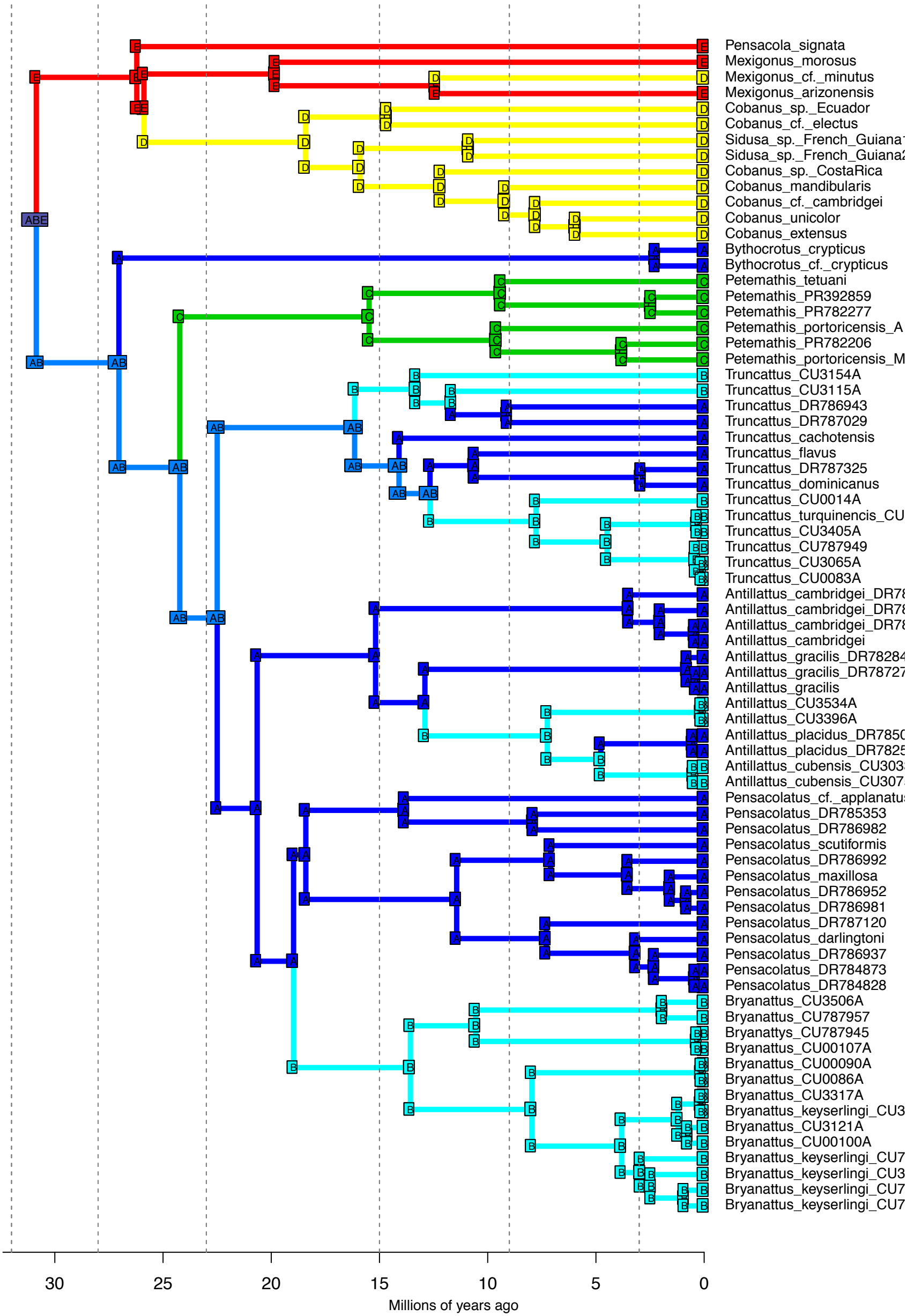

DEC+J_M3b_strat – Stochastic Map #20/50
ancstates: global optim, 5 areas max. d=0; e=0; j=0.0153; LnL=−44.20

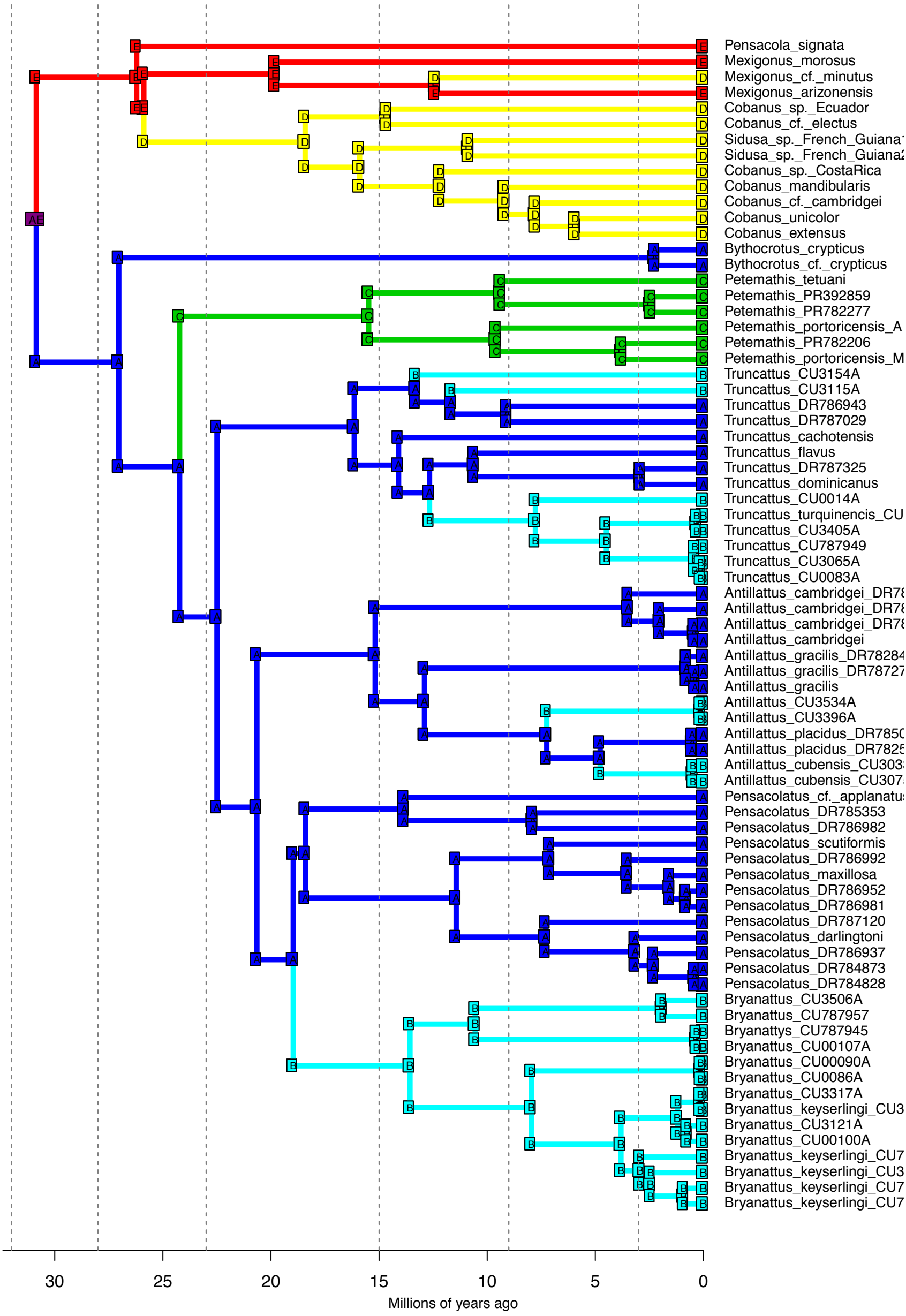

DEC+J_M3b_strat – Stochastic Map #21/50
ancstates: global optim, 5 areas max. d=0; e=0; j=0.0153; LnL=−44.20

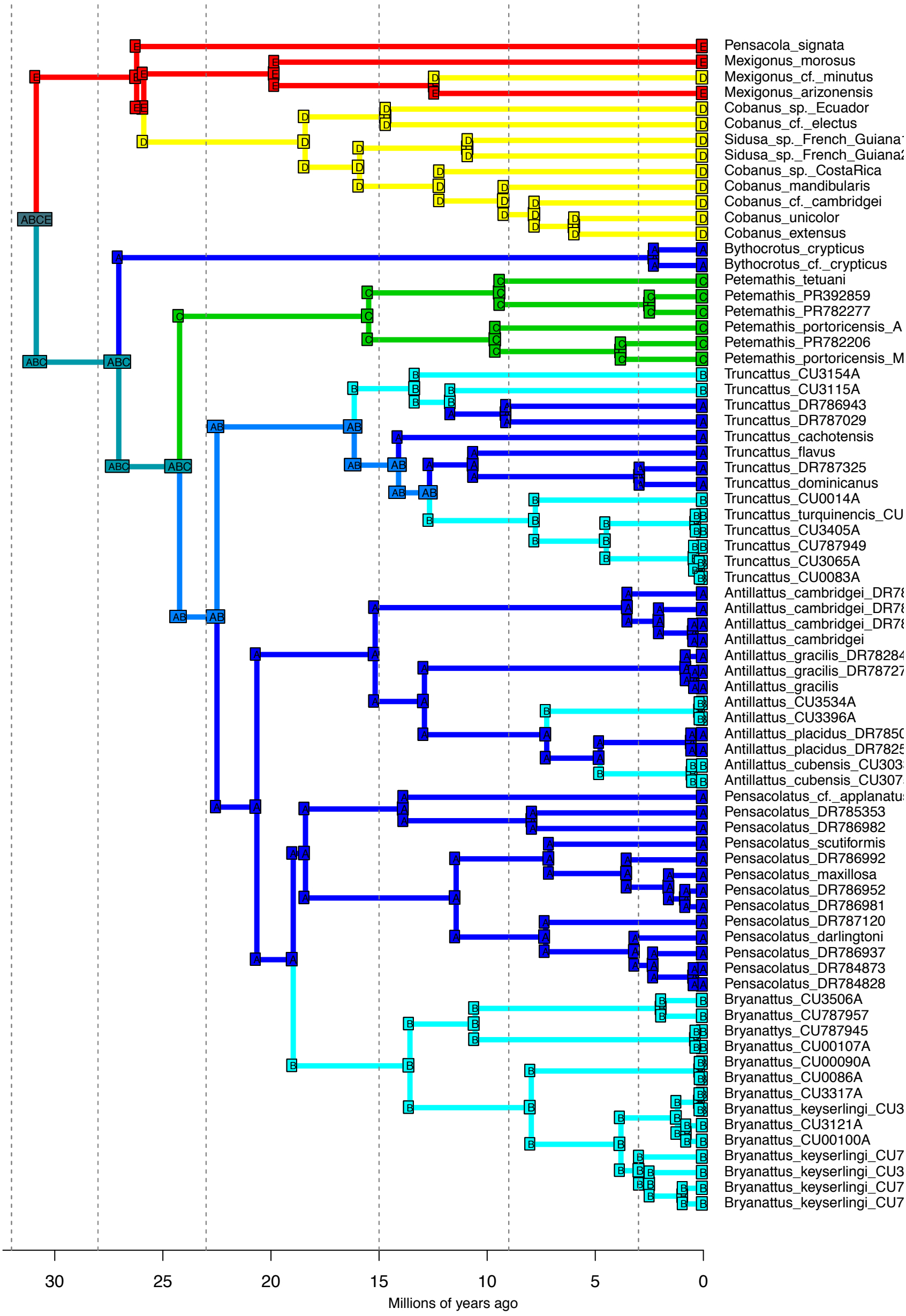

DEC+J_M3b_strat – Stochastic Map #22/50
ancstates: global optim, 5 areas max. d=0; e=0; j=0.0153; LnL=−44.20

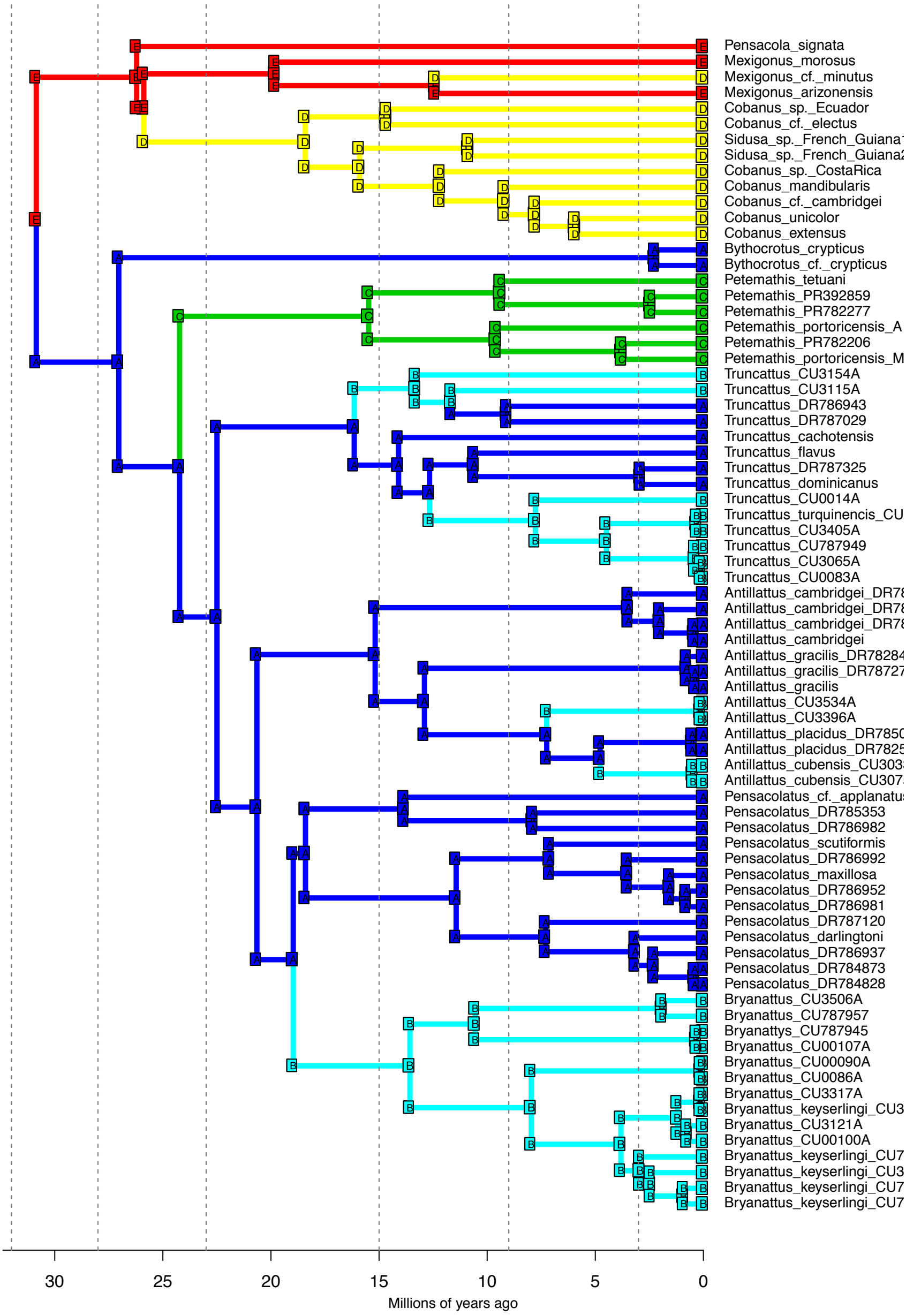

DEC+J_M3b_strat – Stochastic Map #23/50
ancstates: global optim, 5 areas max. d=0; e=0; j=0.0153; LnL=−44.20

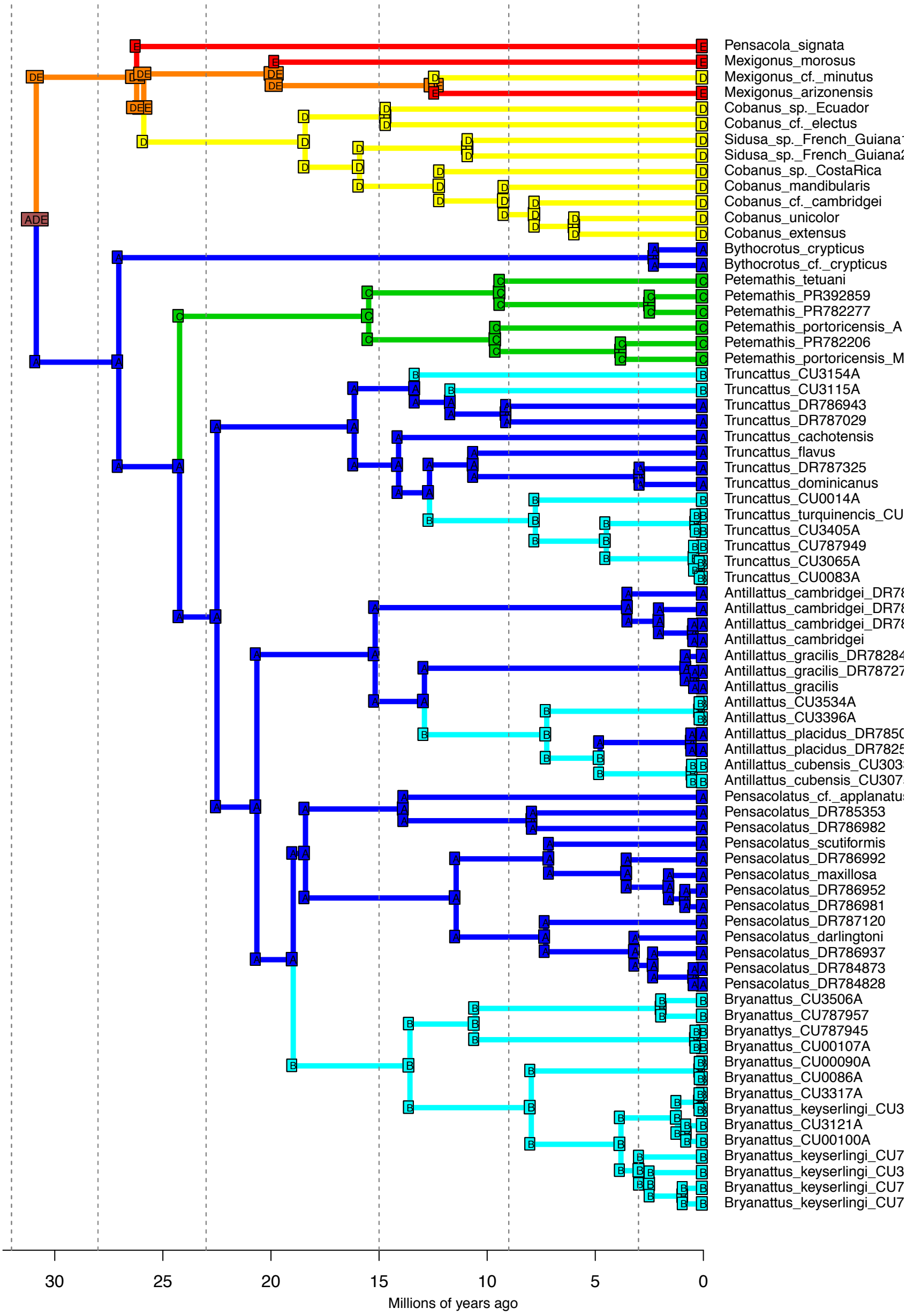

DEC+J_M3b_strat – Stochastic Map #24/50
ancstates: global optim, 5 areas max. d=0; e=0; j=0.0153; LnL=−44.20

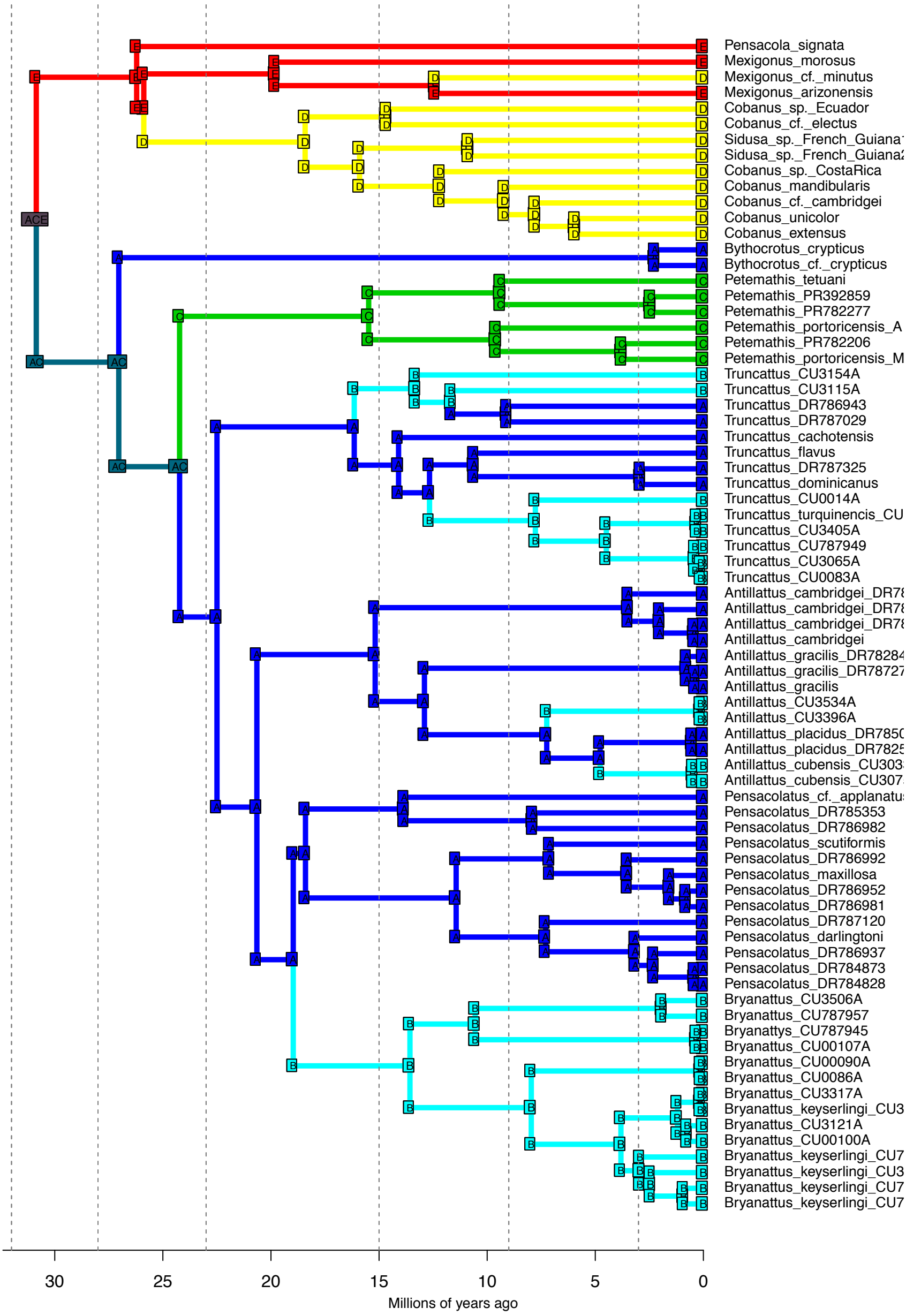

DEC+J_M3b_strat – Stochastic Map #25/50
ancstates: global optim, 5 areas max. d=0; e=0; j=0.0153; LnL=−44.20

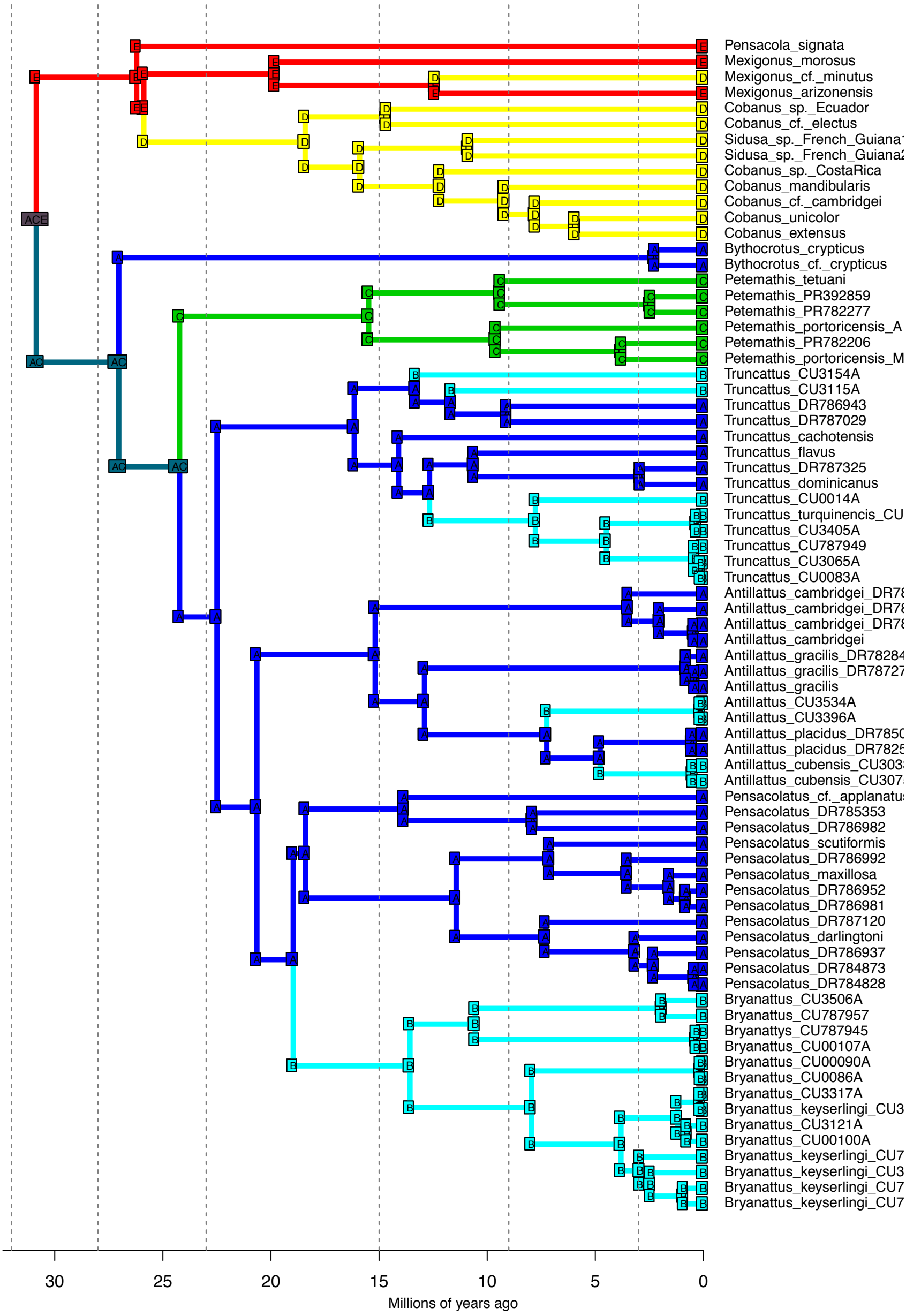

DEC+J_M3b_strat – Stochastic Map #26/50
ancstates: global optim, 5 areas max. d=0; e=0; j=0.0153; LnL=−44.20

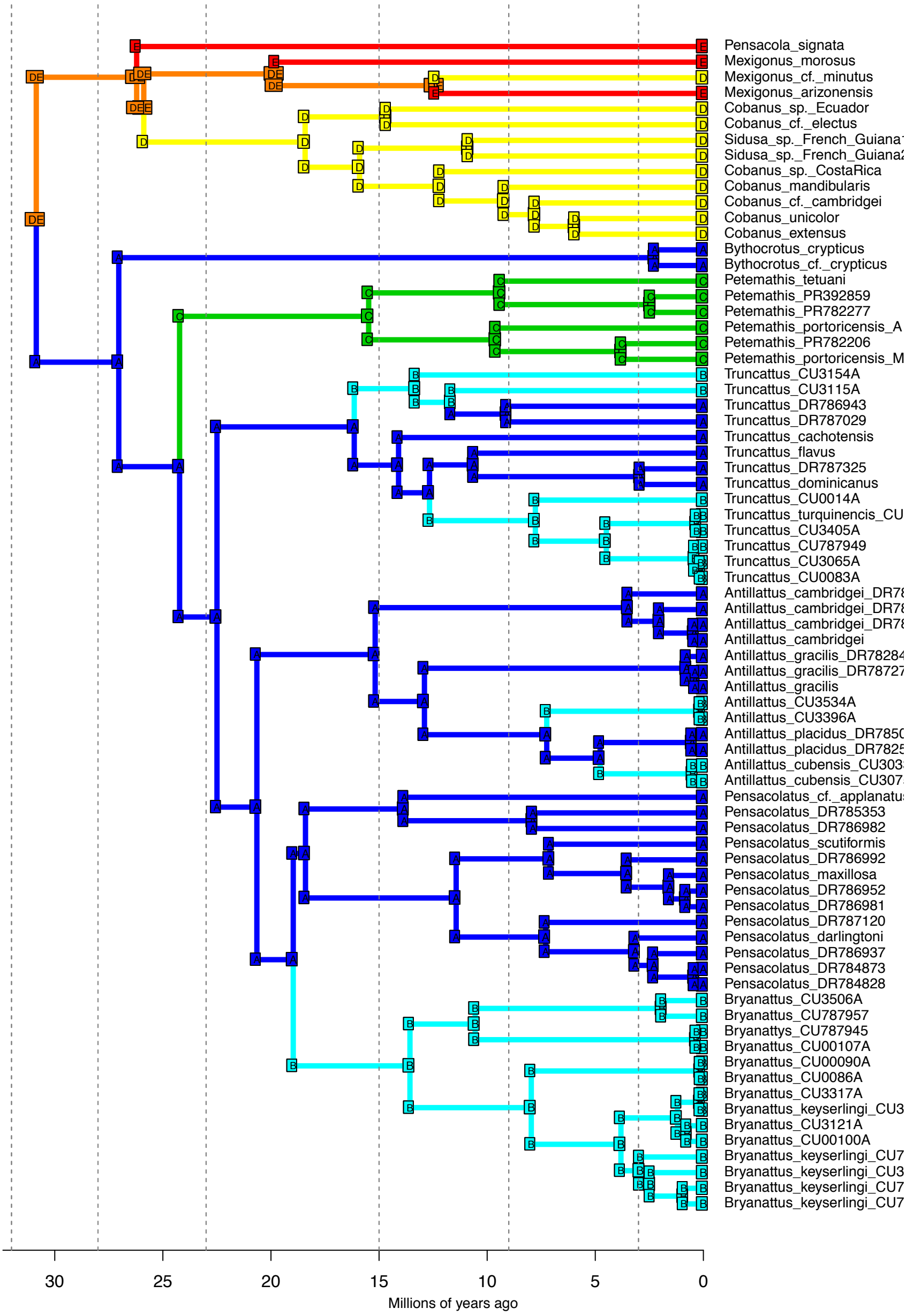

DEC+J_M3b_strat – Stochastic Map #27/50
ancstates: global optim, 5 areas max. d=0; e=0; j=0.0153; LnL=−44.20

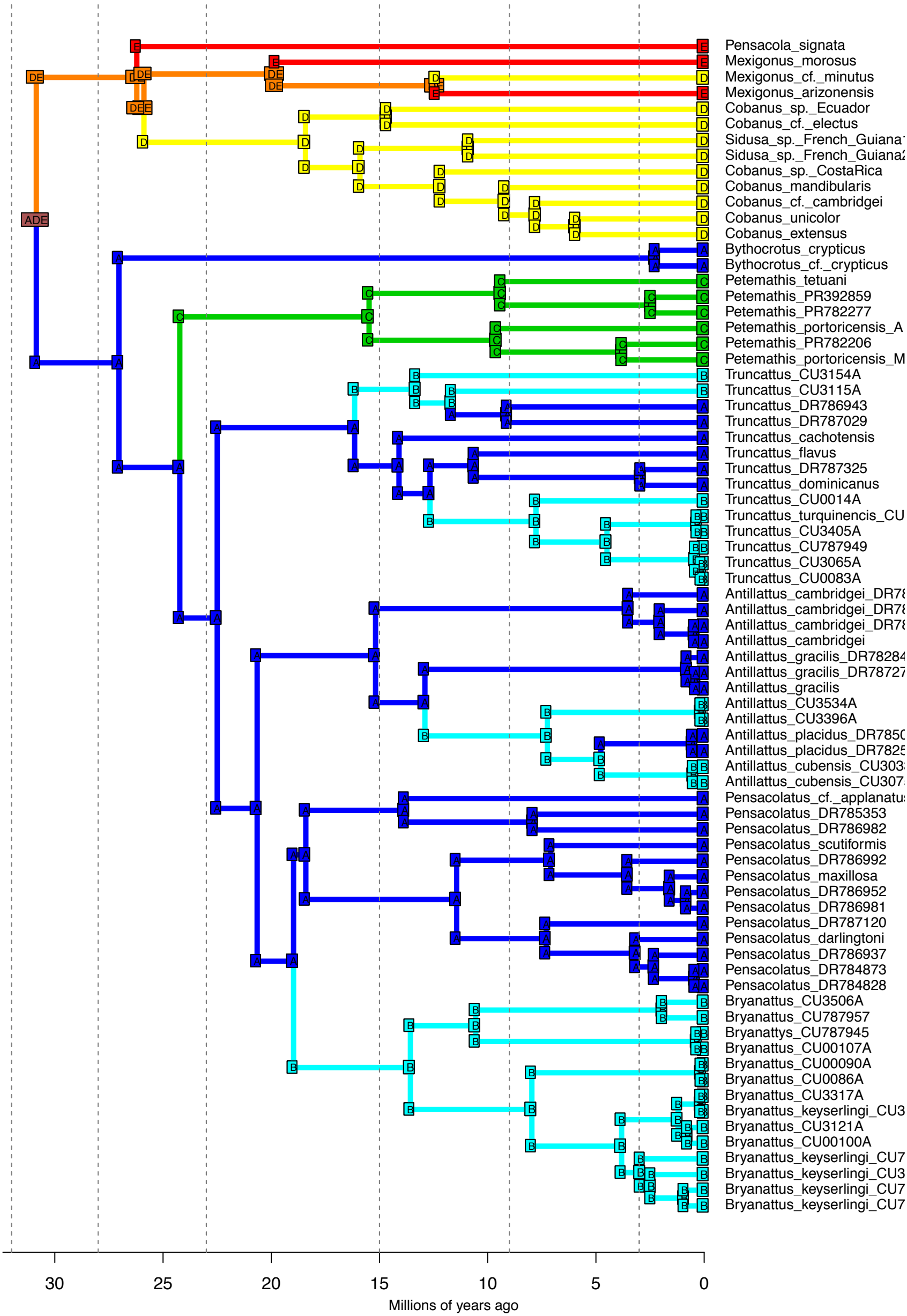

DEC+J_M3b_strat – Stochastic Map #28/50
ancstates: global optim, 5 areas max. d=0; e=0; j=0.0153; LnL=−44.20

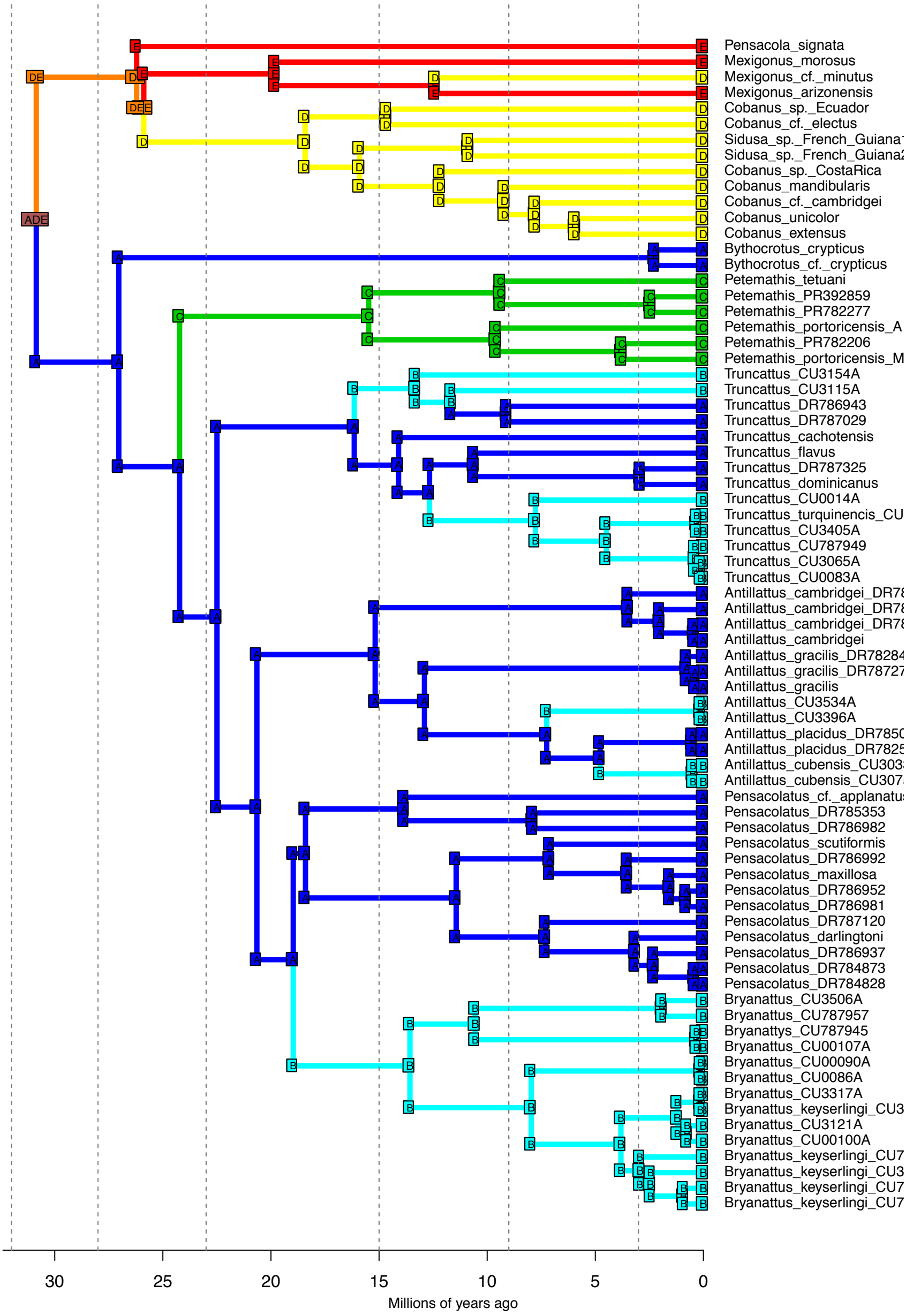

DEC+J_M3b_strat – Stochastic Map #29/50
ancstates: global optim, 5 areas max. d=0; e=0; j=0.0153; LnL=−44.20

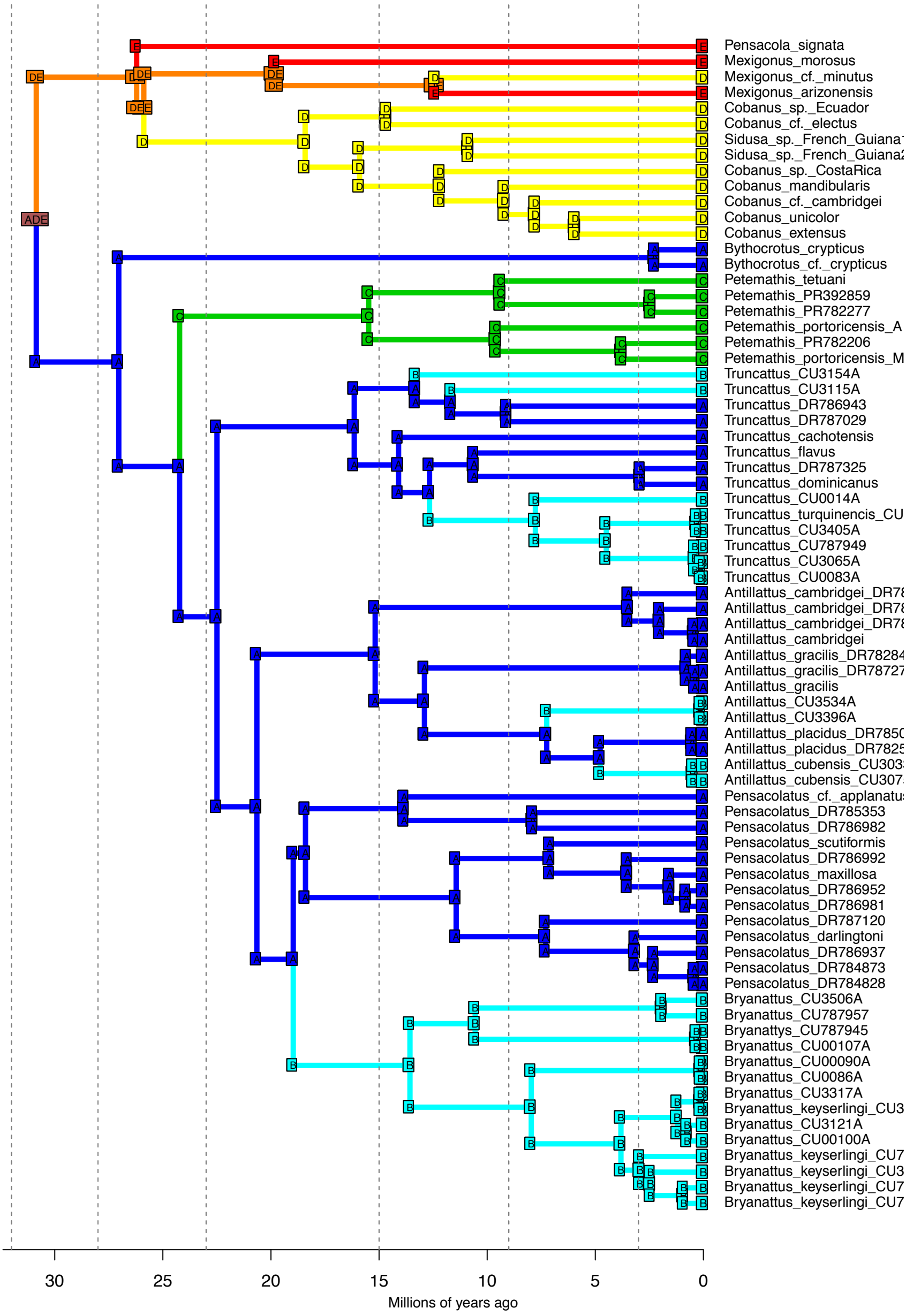

DEC+J_M3b_strat – Stochastic Map #30/50
ancstates: global optim, 5 areas max. d=0; e=0; j=0.0153; LnL=−44.20

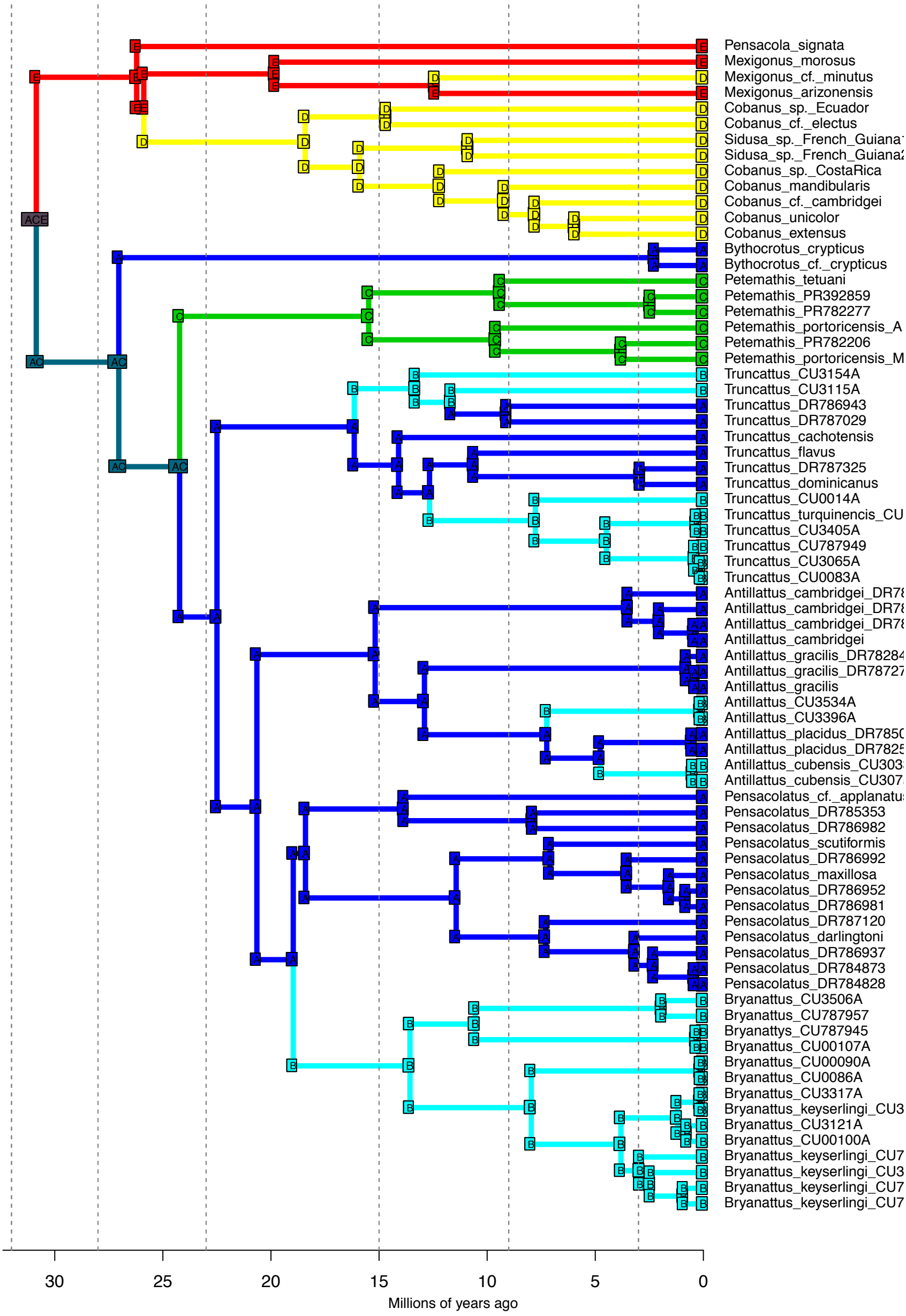

DEC+J_M3b_strat – Stochastic Map #31/50
ancstates: global optim, 5 areas max. d=0; e=0; j=0.0153; LnL=−44.20

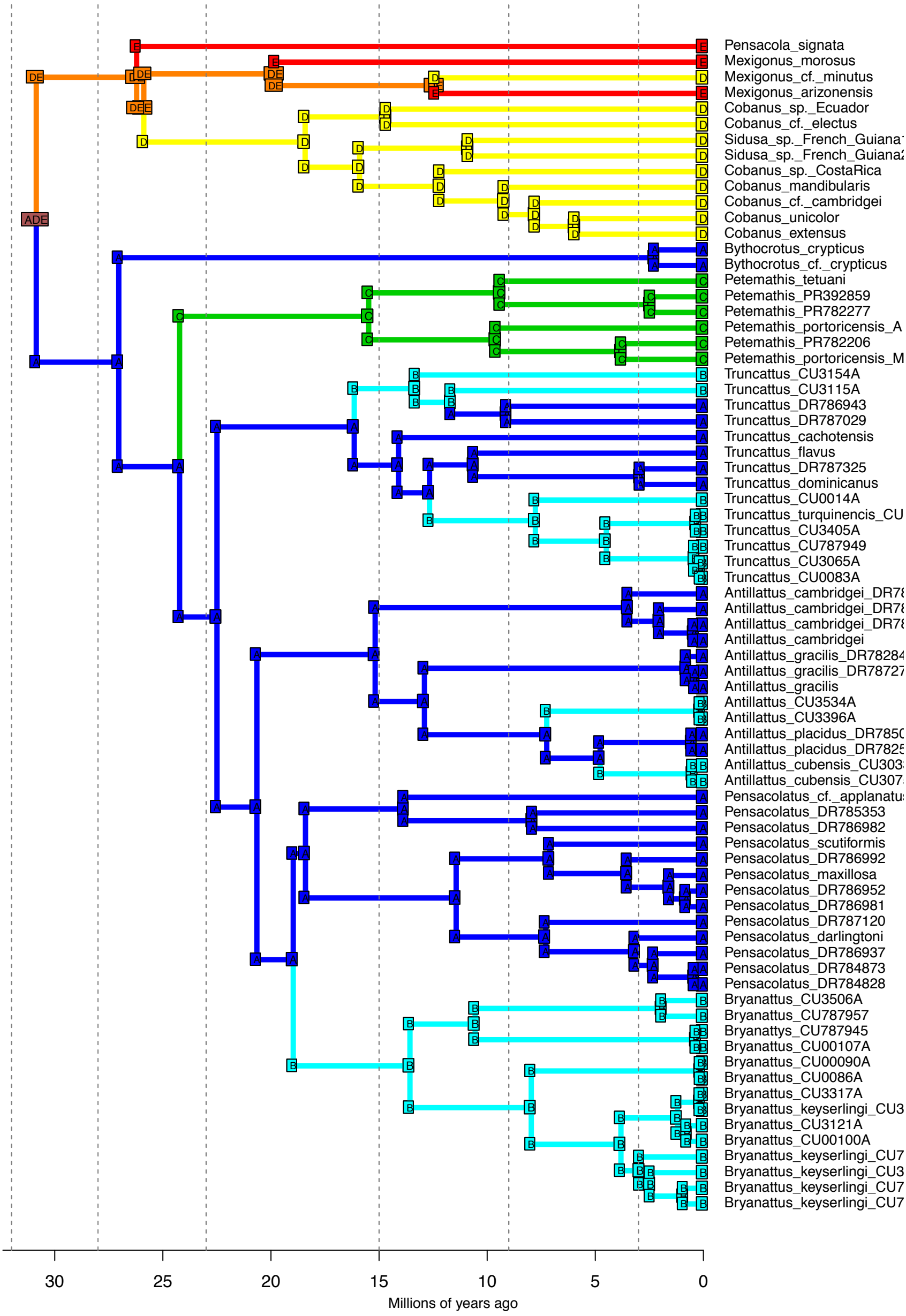

DEC+J_M3b_strat – Stochastic Map #32/50
ancstates: global optim, 5 areas max. d=0; e=0; j=0.0153; LnL=−44.20

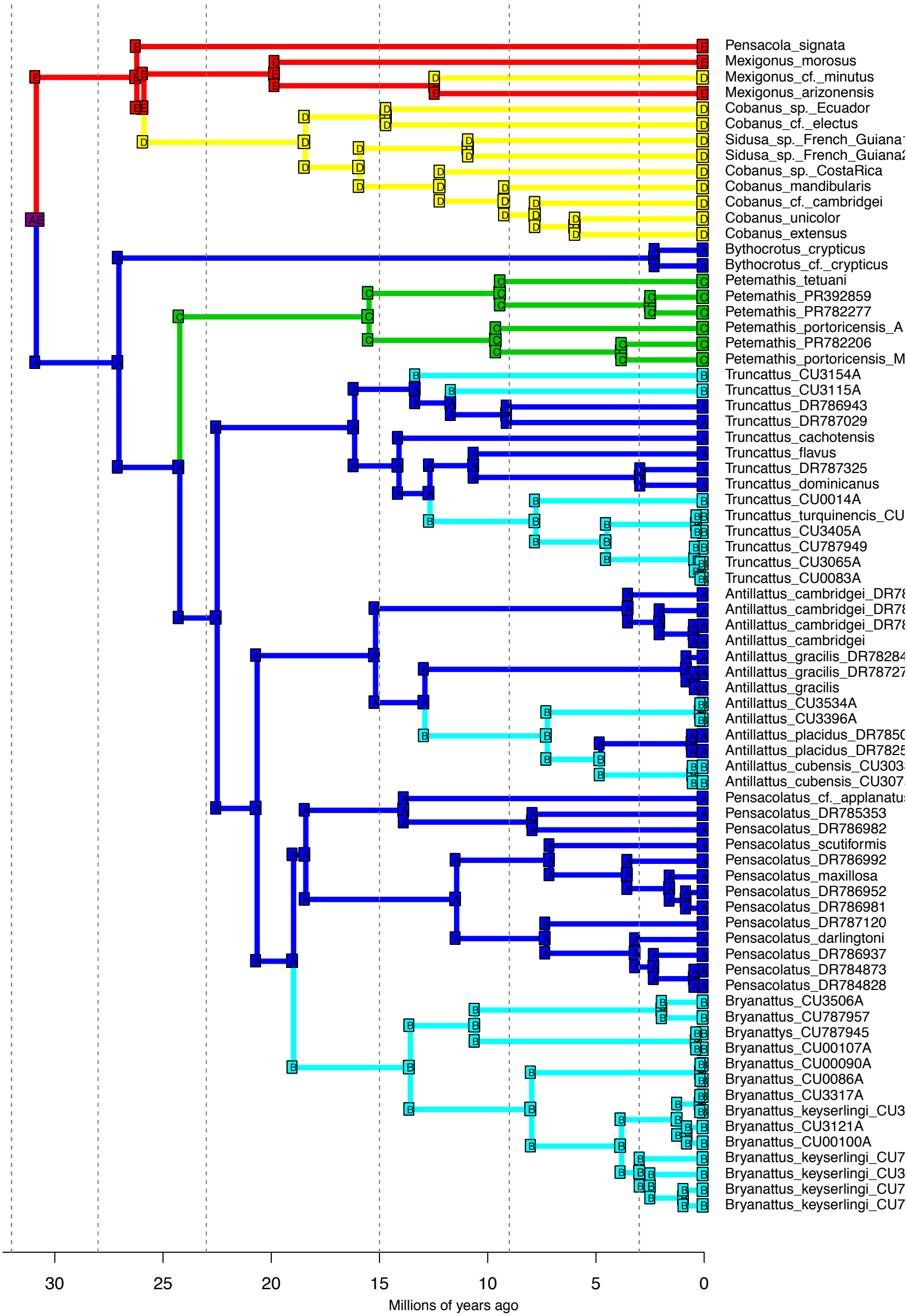

DEC+J_M3b_strat – Stochastic Map #33/50
ancstates: global optim, 5 areas max. d=0; e=0; j=0.0153; LnL=−44.20

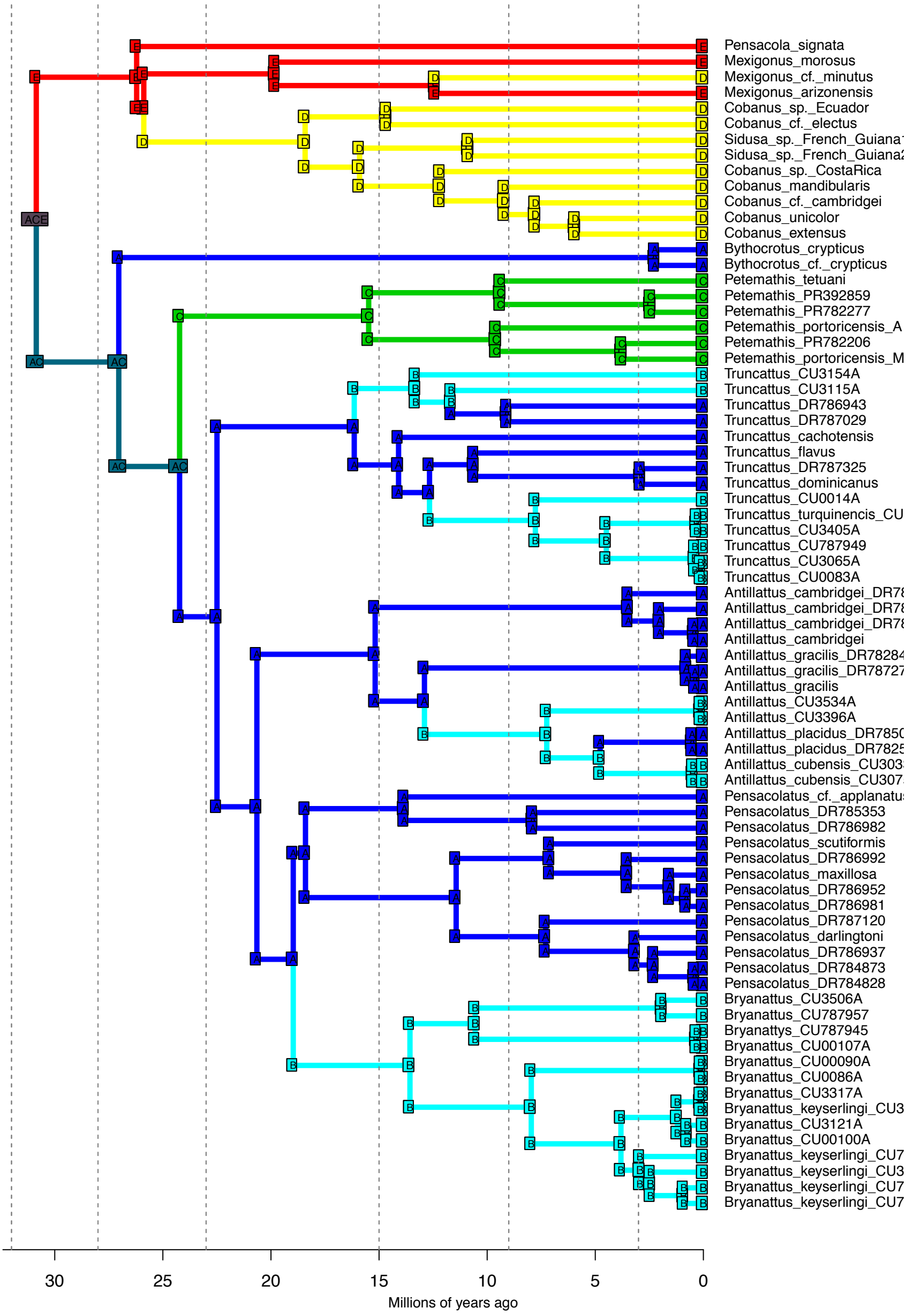

DEC+J_M3b_strat – Stochastic Map #34/50
ancstates: global optim, 5 areas max. d=0; e=0; j=0.0153; LnL=−44.20

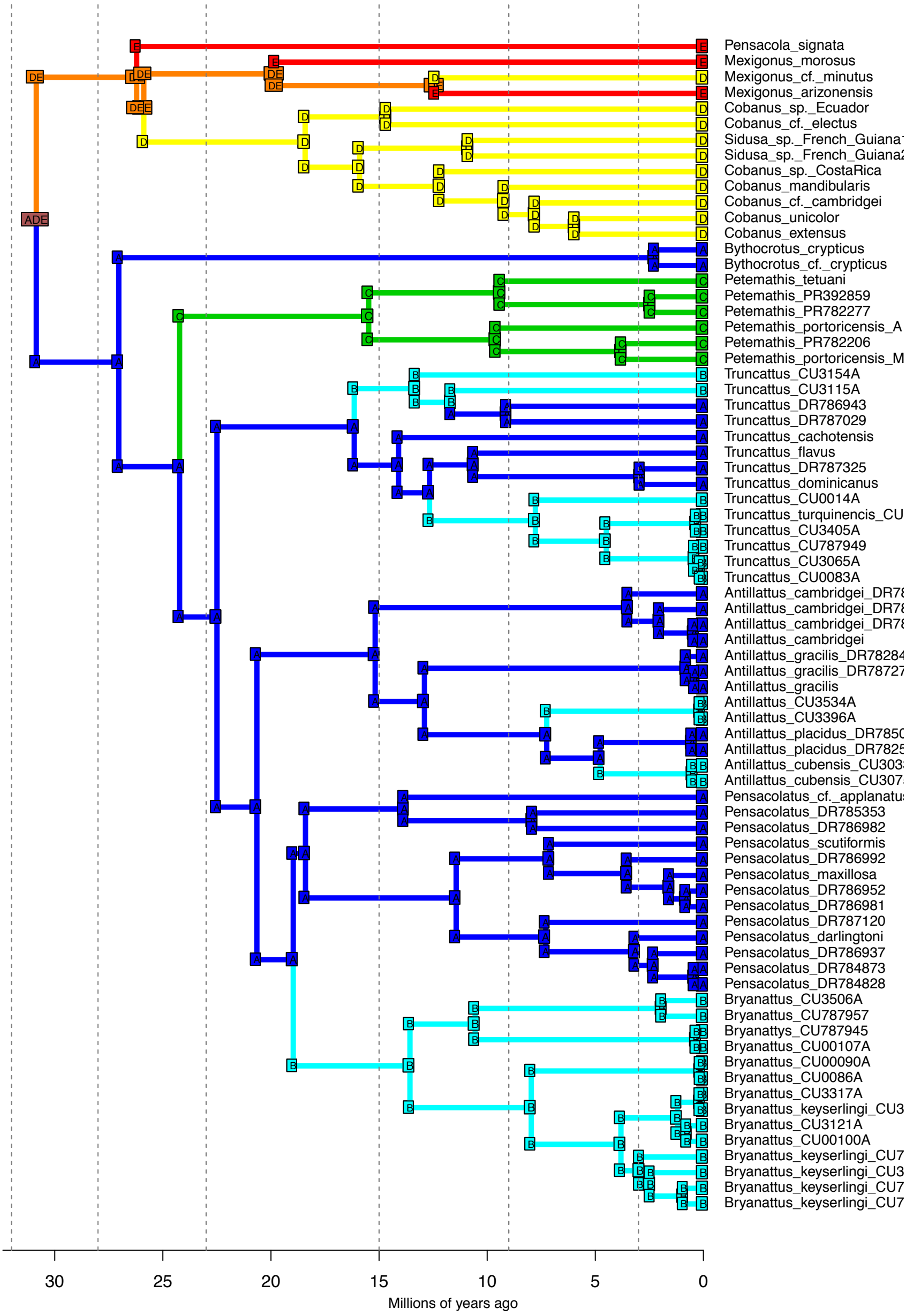

DEC+J_M3b_strat – Stochastic Map #35/50
ancstates: global optim, 5 areas max. d=0; e=0; j=0.0153; LnL=−44.20

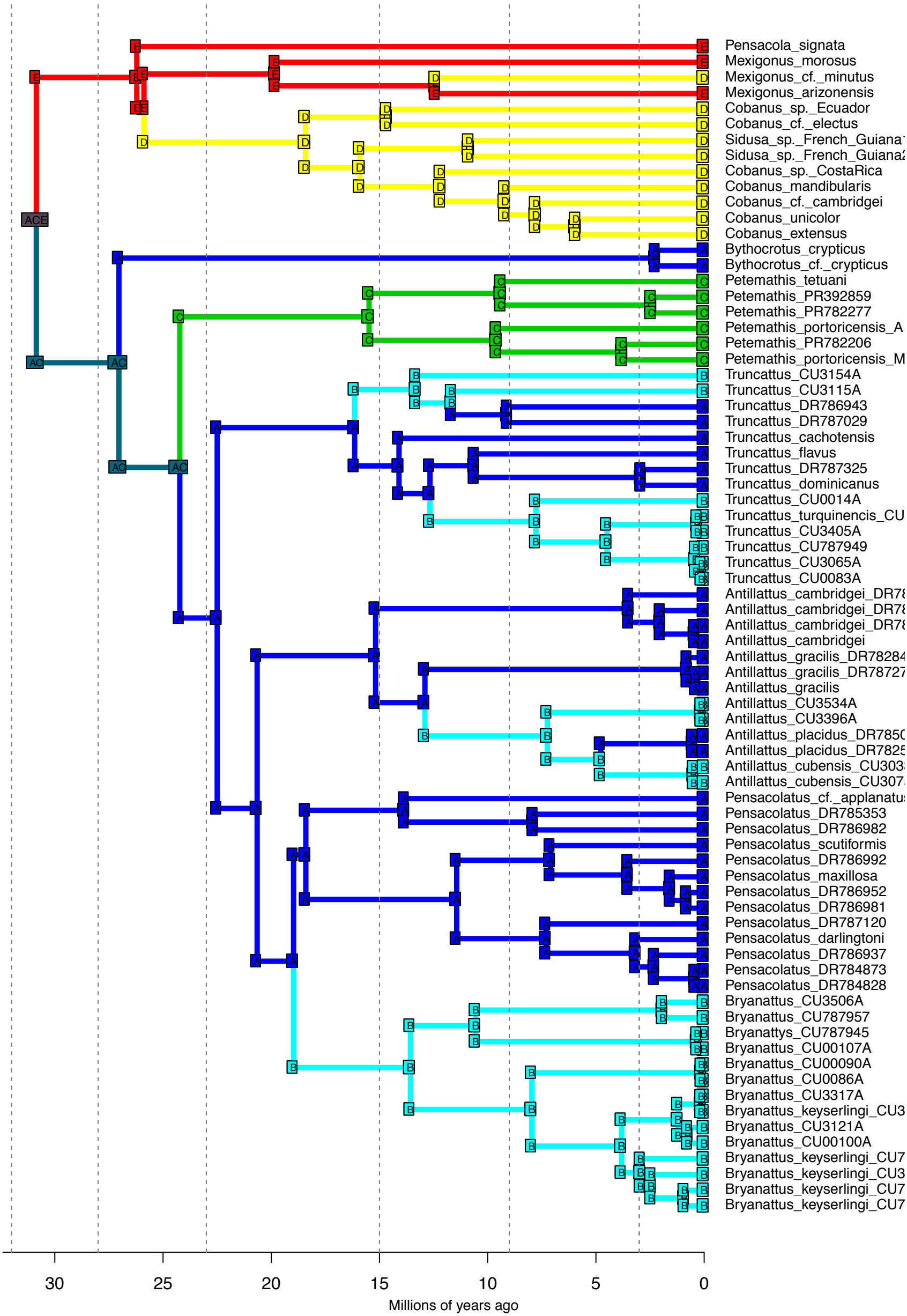

DEC+J_M3b_strat – Stochastic Map #36/50
ancstates: global optim, 5 areas max. d=0; e=0; j=0.0153; LnL=−44.20

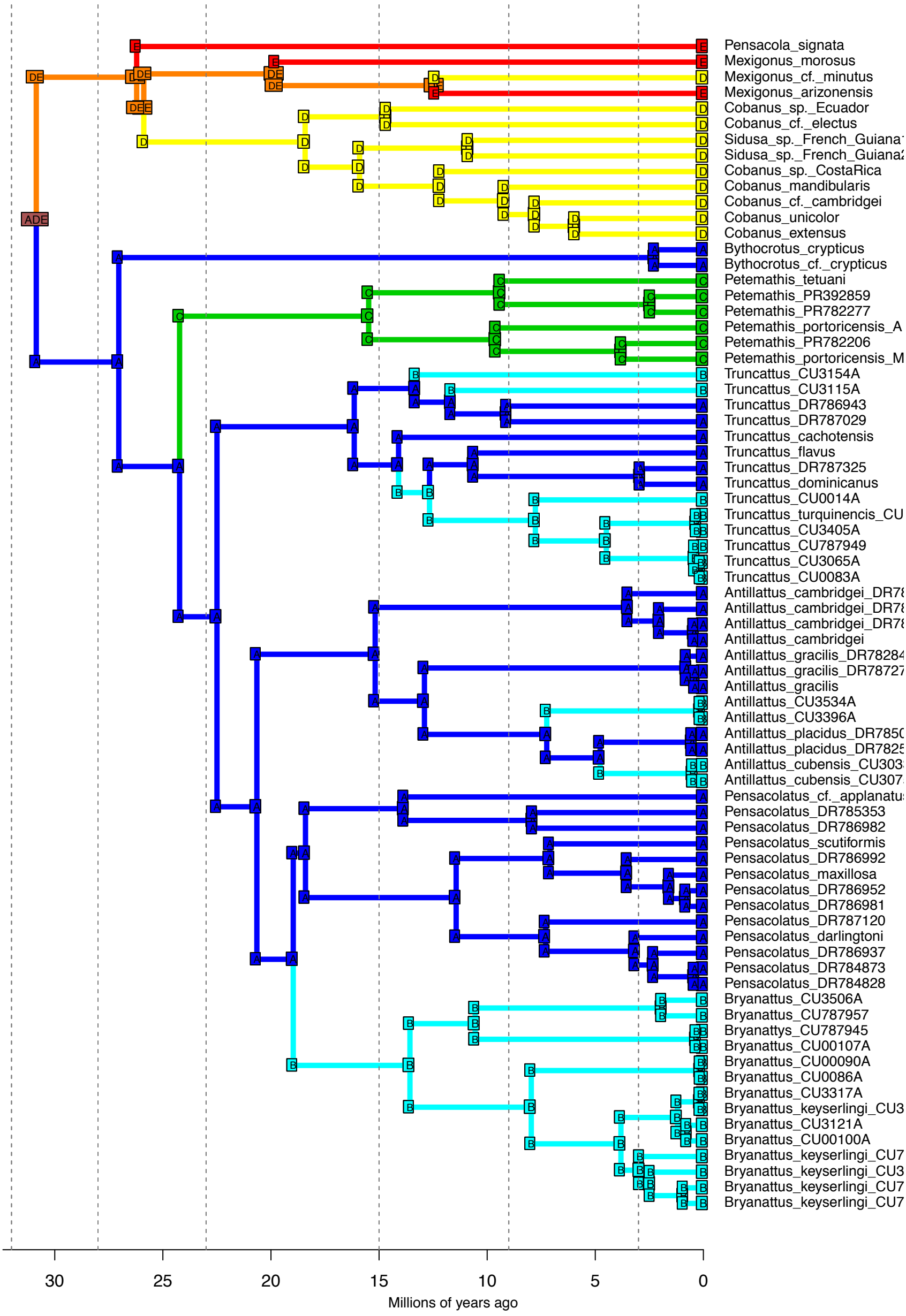

DEC+J_M3b_strat – Stochastic Map #37/50
ancstates: global optim, 5 areas max. d=0; e=0; j=0.0153; LnL=−44.20

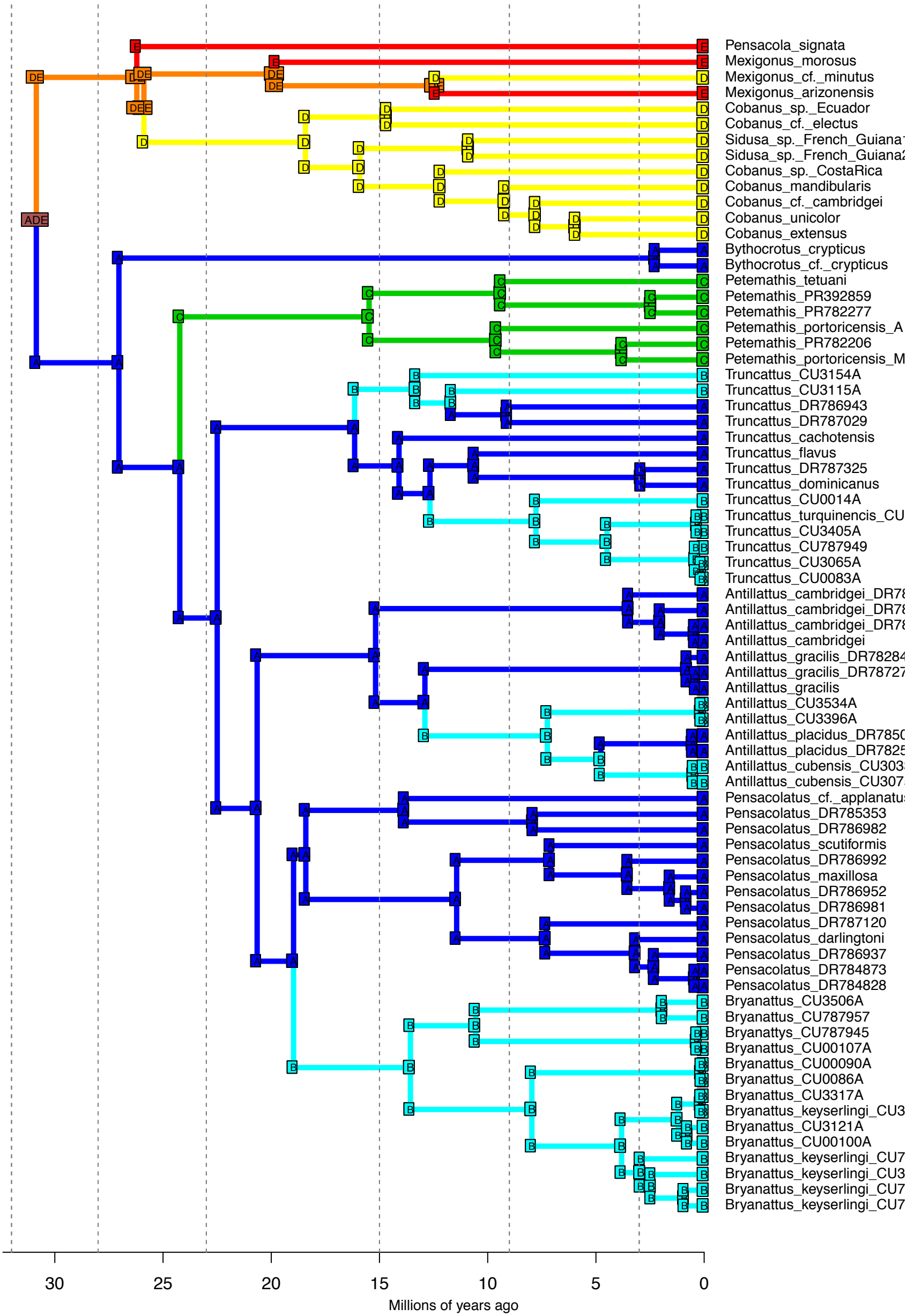

DEC+J_M3b_strat – Stochastic Map #38/50
ancstates: global optim, 5 areas max. d=0; e=0; j=0.0153; LnL=−44.20

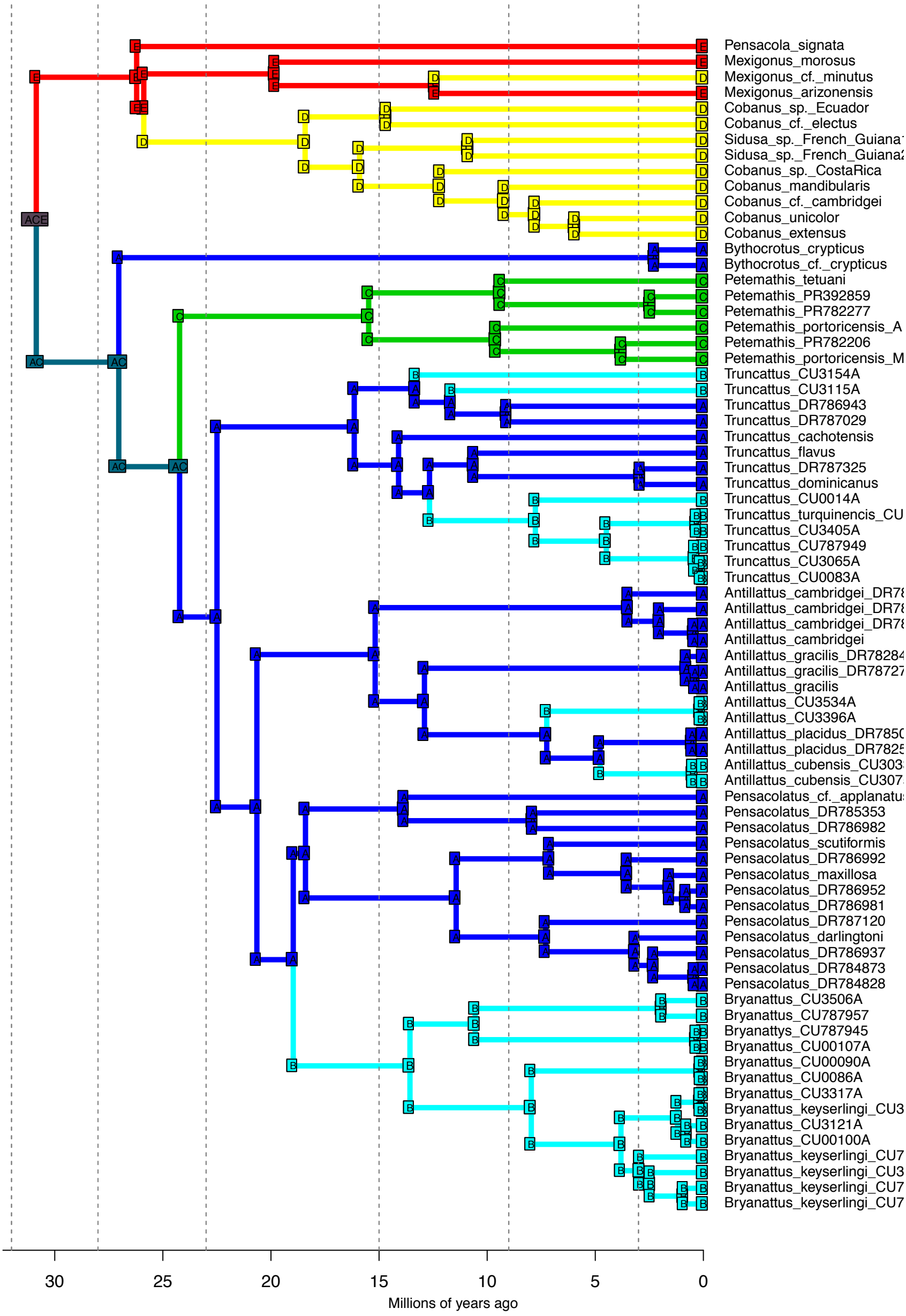

DEC+J_M3b_strat – Stochastic Map #39/50
ancstates: global optim, 5 areas max. d=0; e=0; j=0.0153; LnL=−44.20

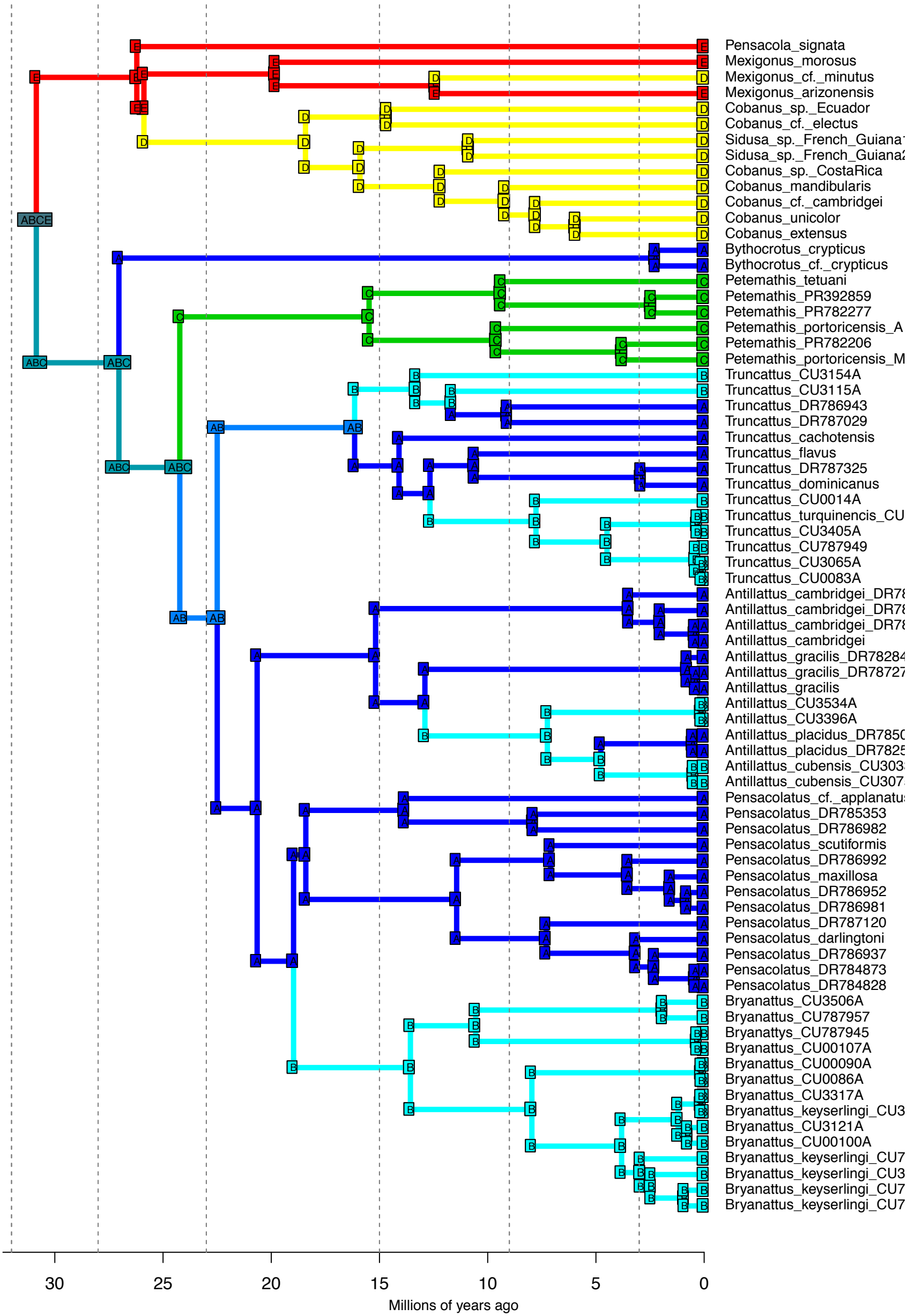

DEC+J_M3b_strat – Stochastic Map #40/50
ancstates: global optim, 5 areas max. d=0; e=0; j=0.0153; LnL=−44.20

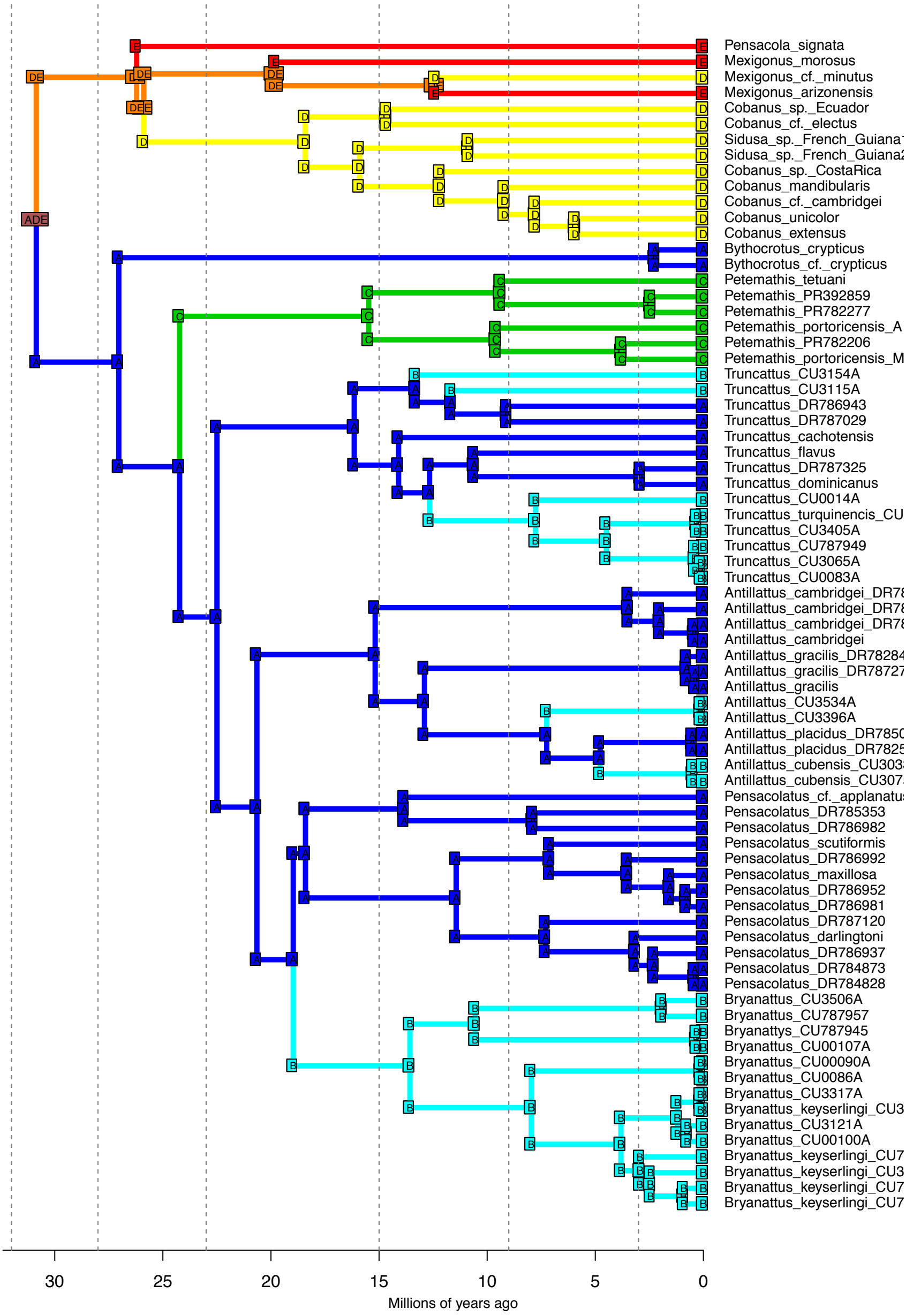

DEC+J_M3b_strat – Stochastic Map #41/50
ancstates: global optim, 5 areas max. d=0; e=0; j=0.0153; LnL=−44.20

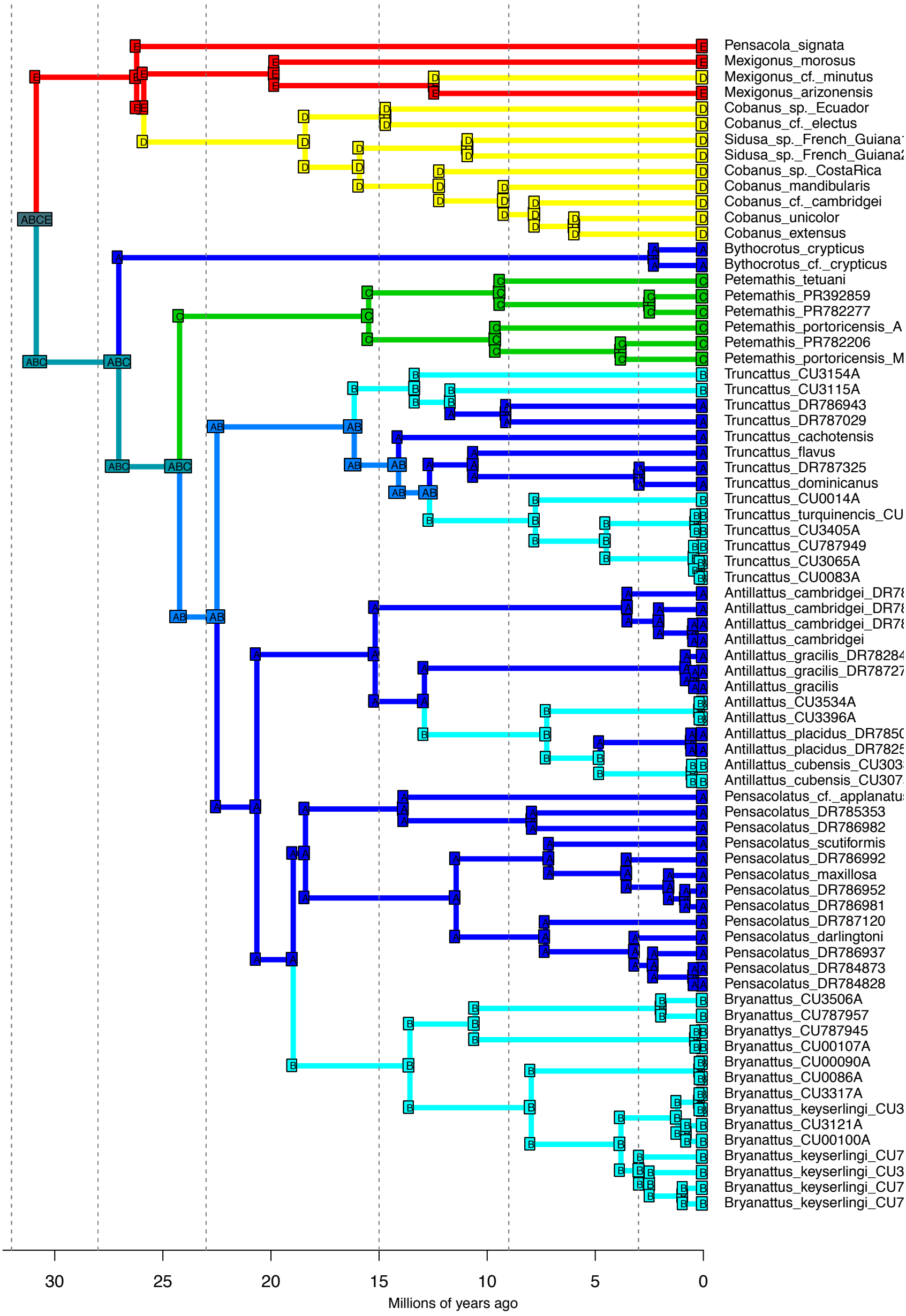

DEC+J_M3b_strat – Stochastic Map #42/50
ancstates: global optim, 5 areas max. d=0; e=0; j=0.0153; LnL=−44.20

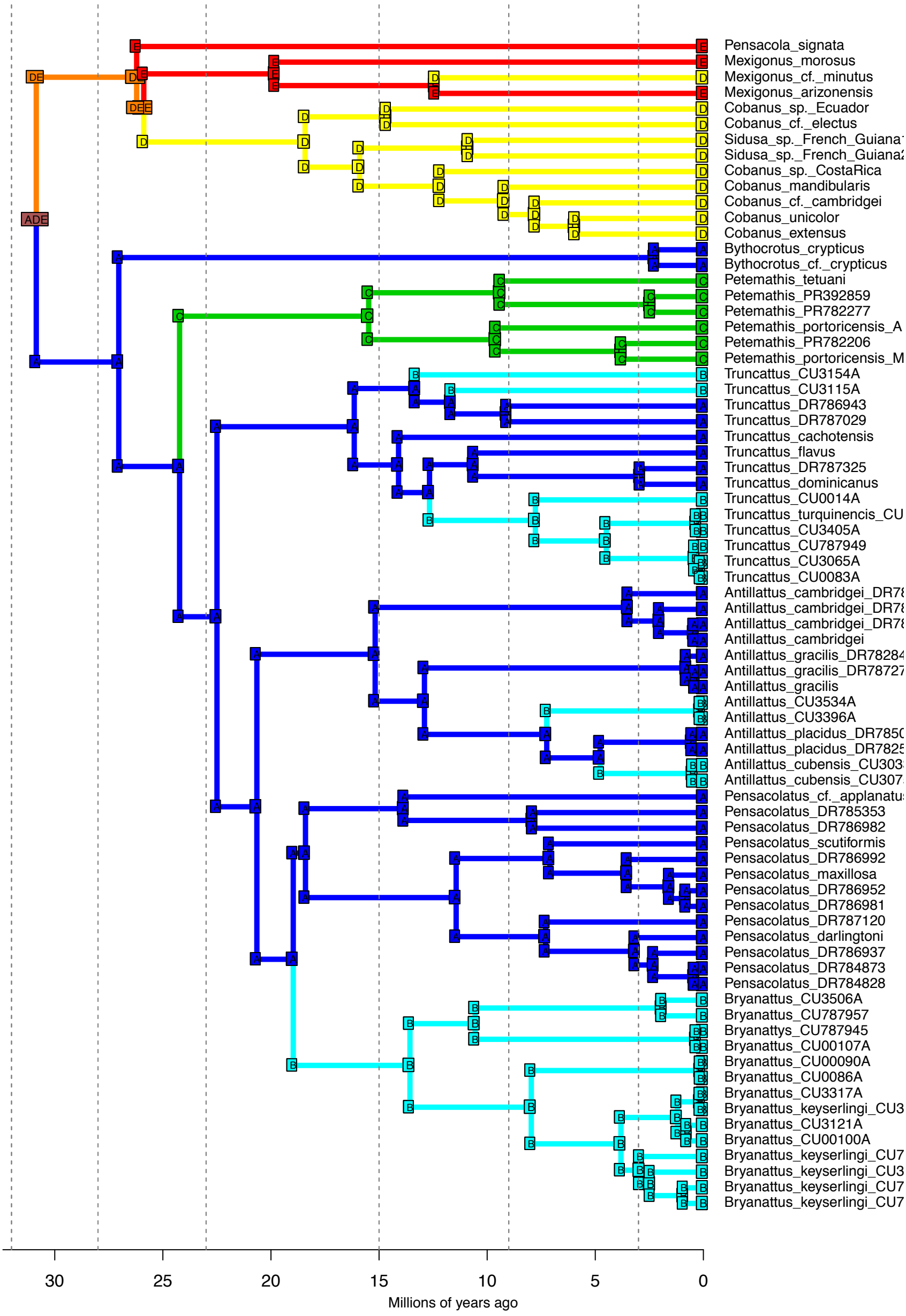

DEC+J_M3b_strat – Stochastic Map #43/50
ancstates: global optim, 5 areas max. d=0; e=0; j=0.0153; LnL=−44.20

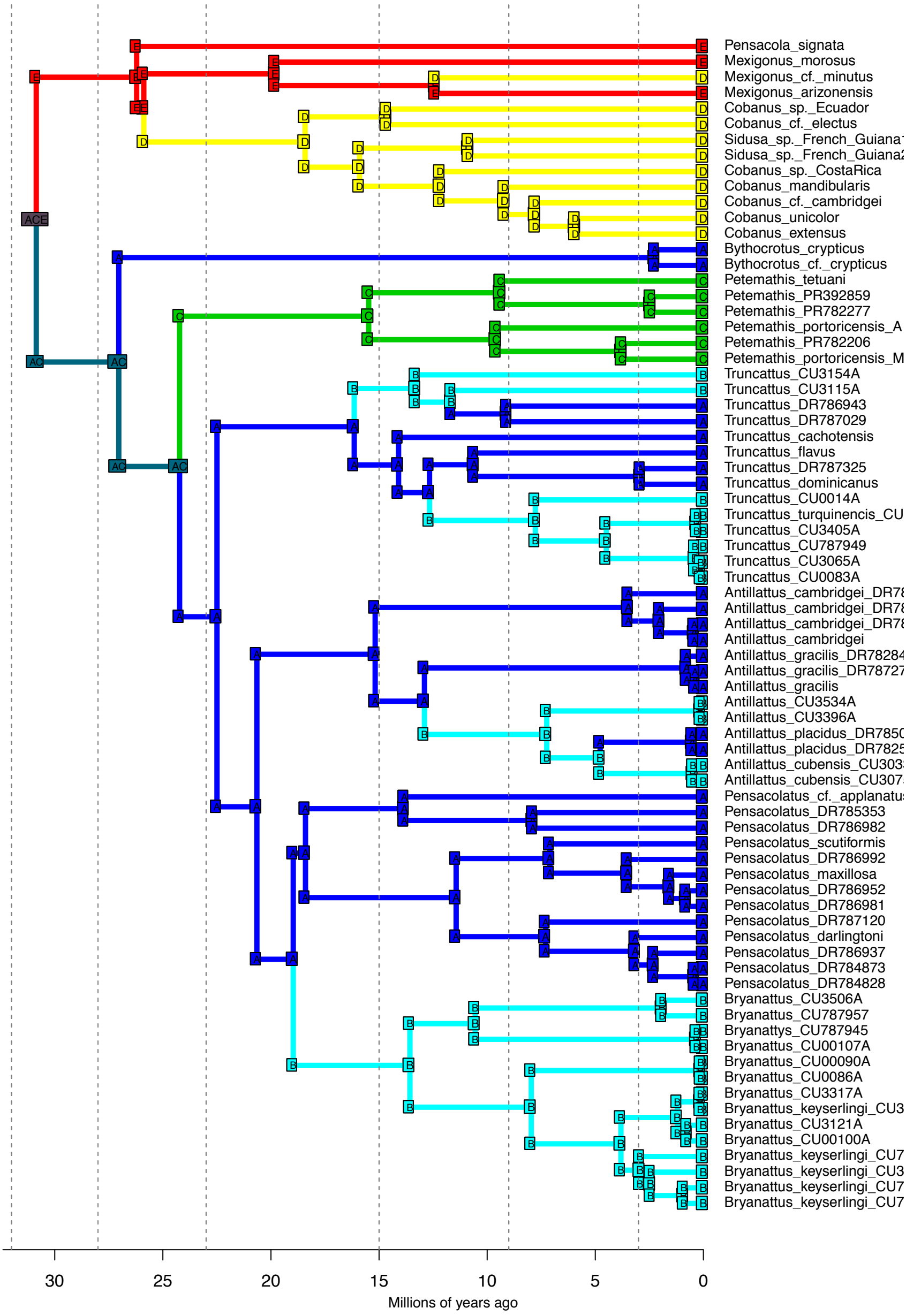

DEC+J_M3b_strat – Stochastic Map #44/50
ancstates: global optim, 5 areas max. d=0; e=0; j=0.0153; LnL=−44.20

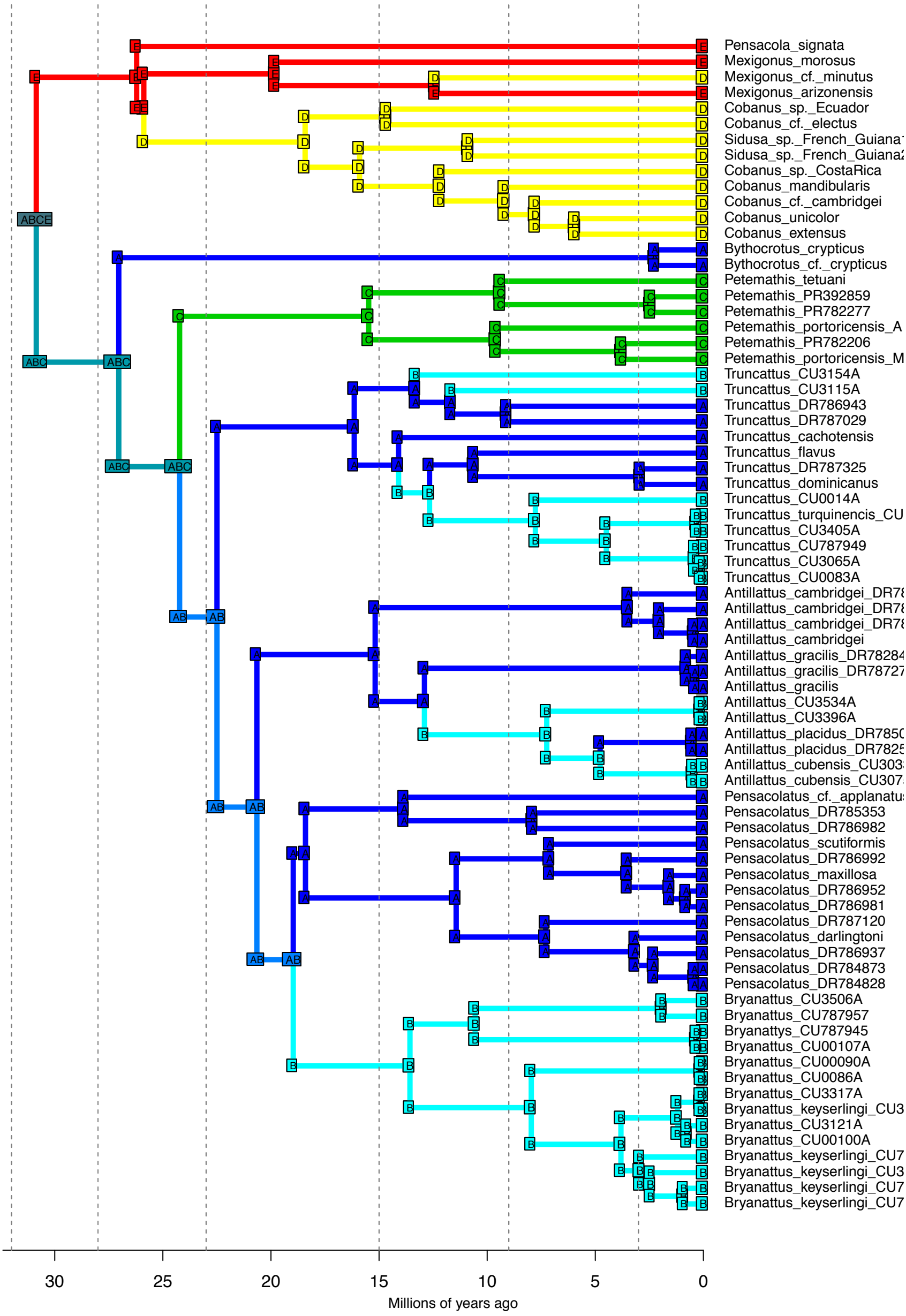

DEC+J_M3b_strat – Stochastic Map #45/50
ancstates: global optim, 5 areas max. d=0; e=0; j=0.0153; LnL=−44.20

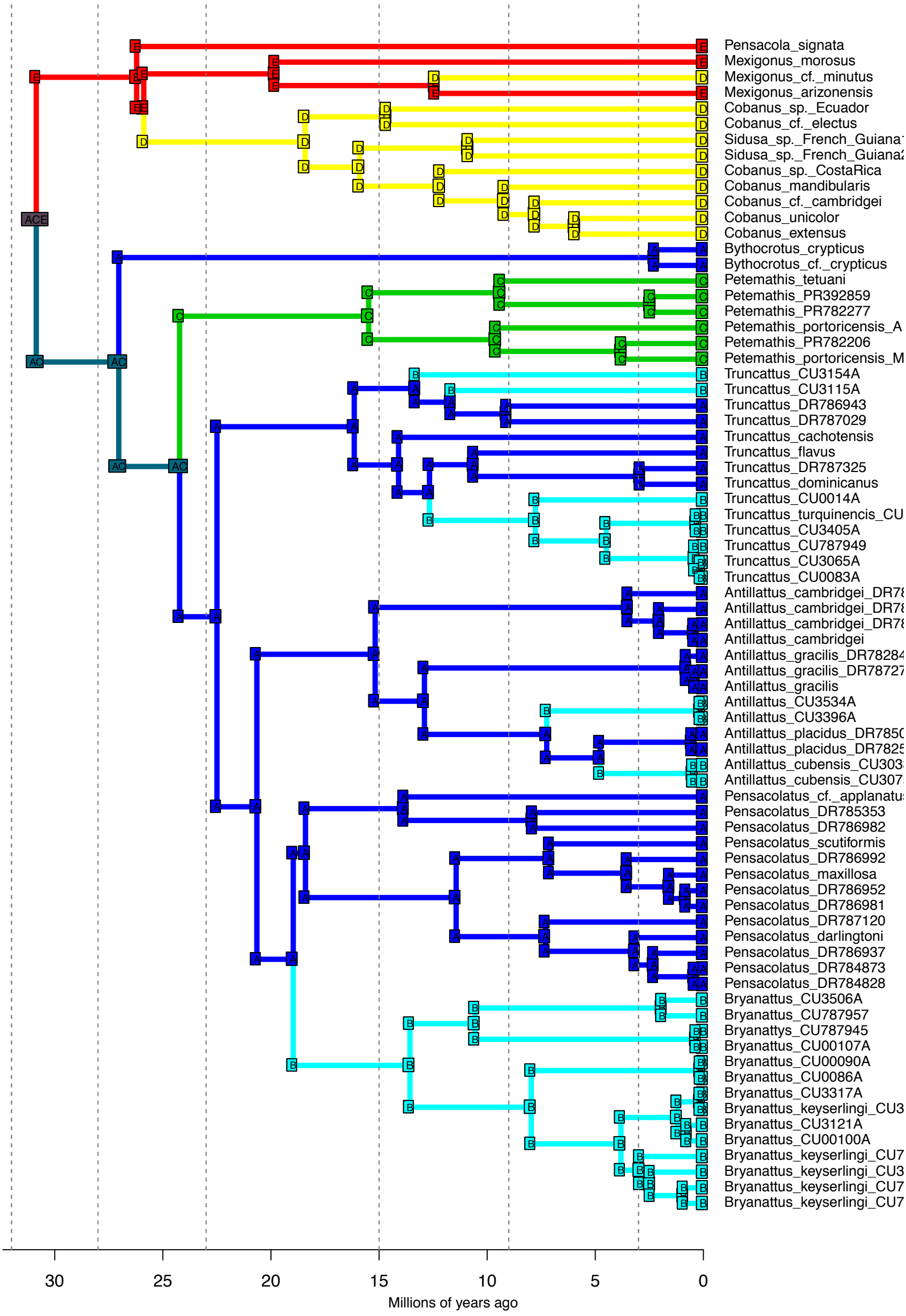

DEC+J_M3b_strat – Stochastic Map #46/50
ancstates: global optim, 5 areas max. d=0; e=0; j=0.0153; LnL=−44.20

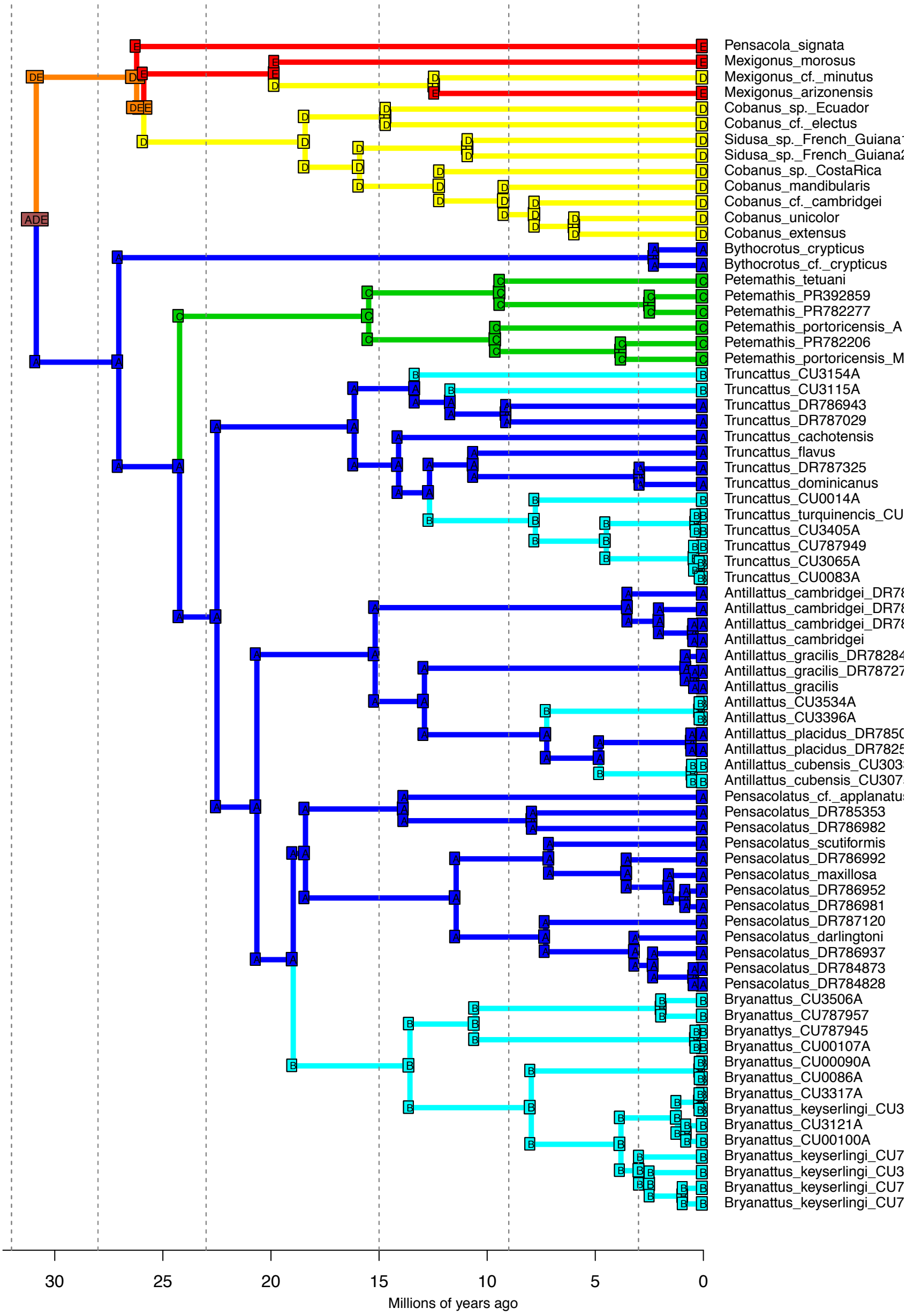

DEC+J_M3b_strat – Stochastic Map #47/50
ancstates: global optim, 5 areas max. d=0; e=0; j=0.0153; LnL=−44.20

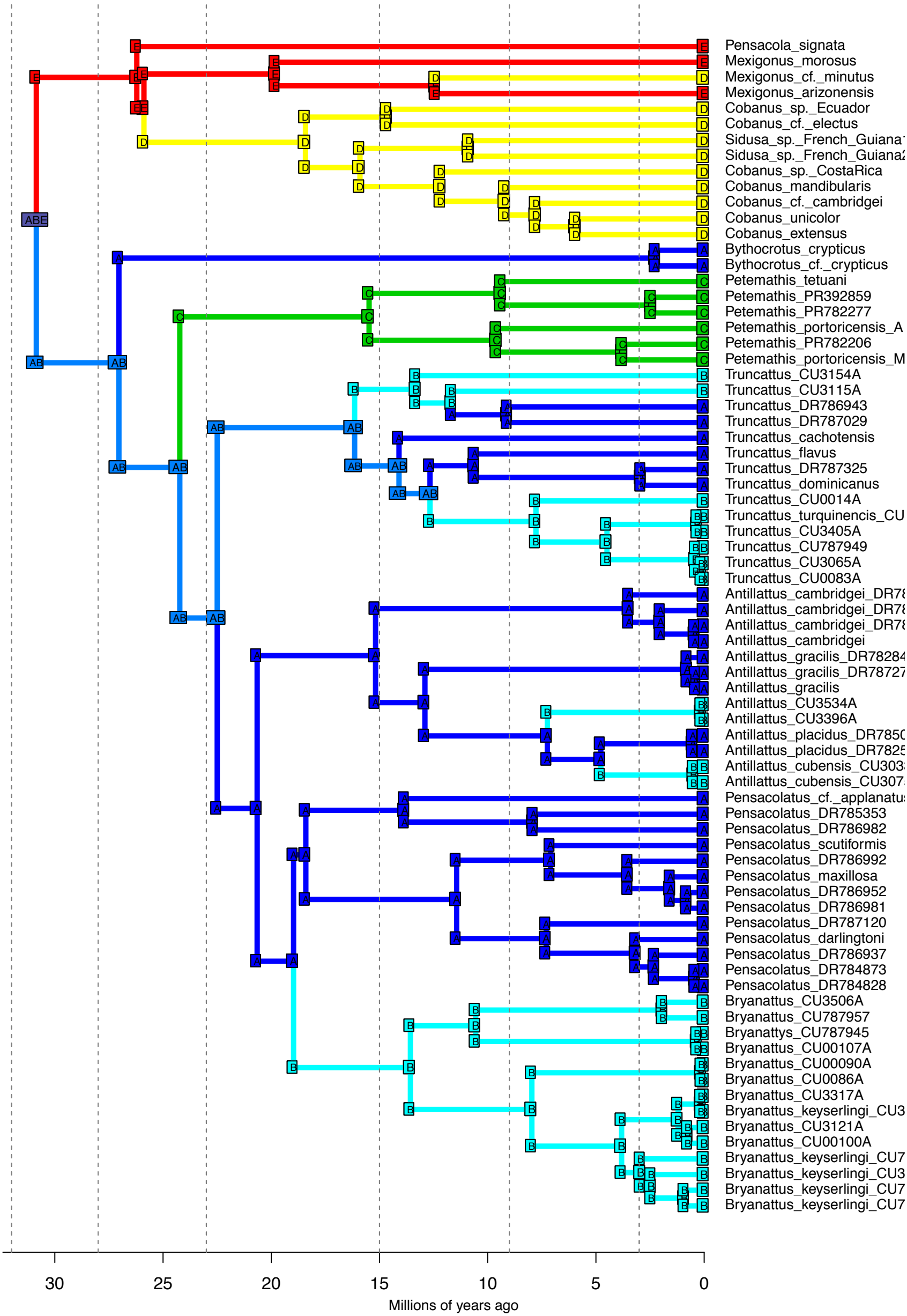

DEC+J_M3b_strat – Stochastic Map #48/50
ancstates: global optim, 5 areas max. d=0; e=0; j=0.0153; LnL=−44.20

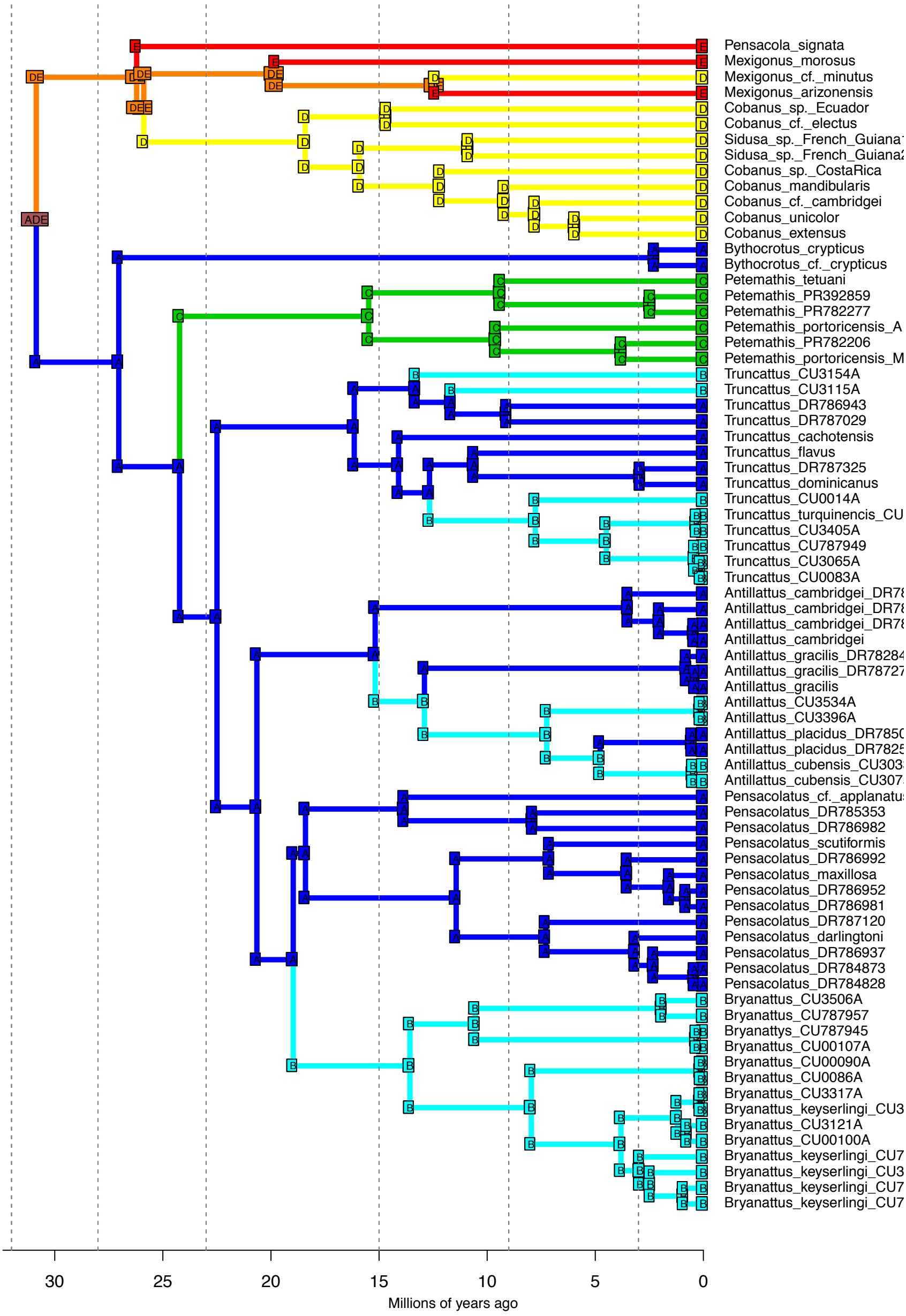

DEC+J_M3b_strat – Stochastic Map #49/50
ancstates: global optim, 5 areas max. d=0; e=0; j=0.0153; LnL=−44.20

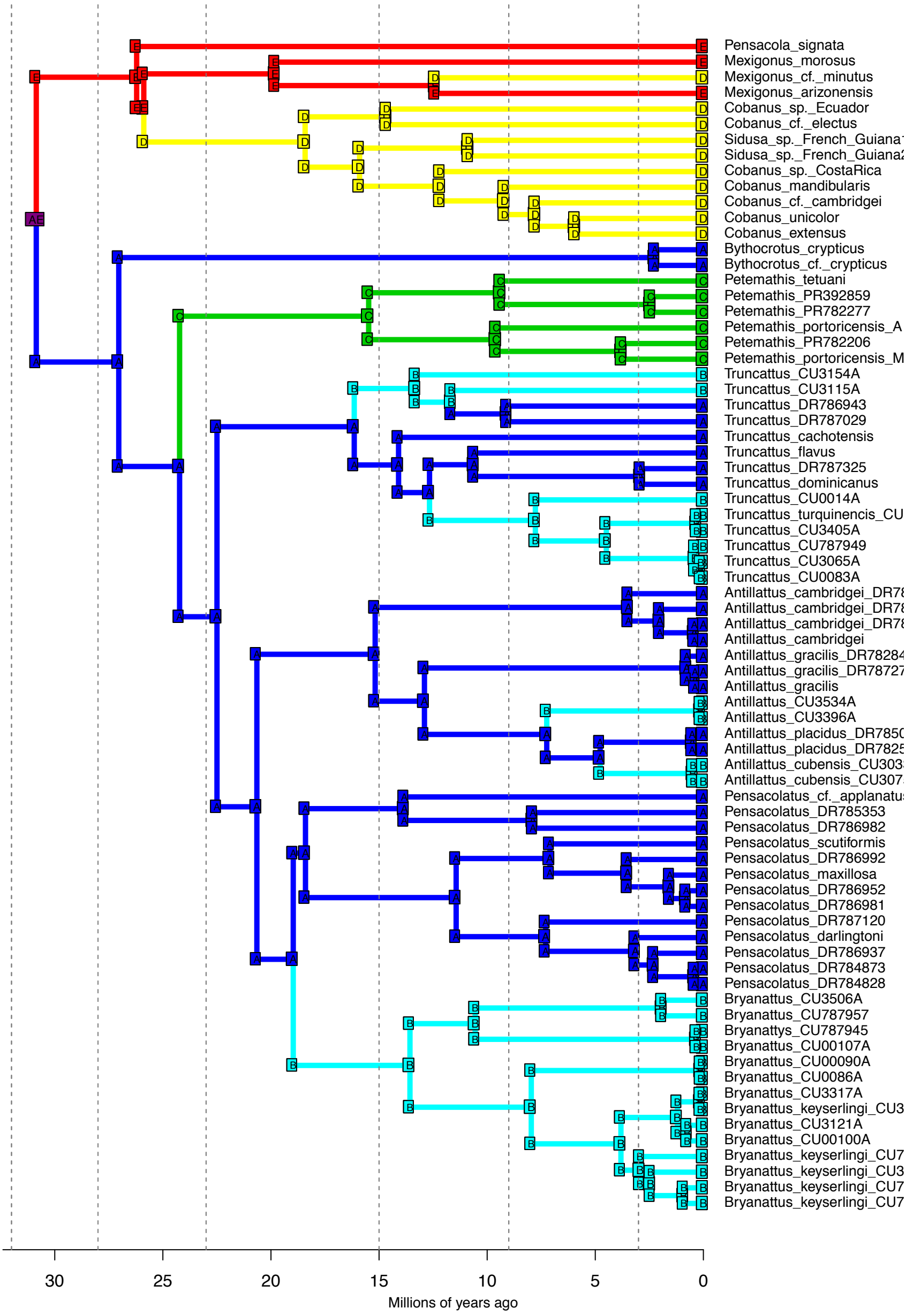

DEC+J_M3b_strat – Stochastic Map #50/50
ancstates: global optim, 5 areas max. d=0; e=0; j=0.0153; LnL=−44.20